Publication Year	2018
Acceptance in OA	2020-11-25T08:52:13Z
Title	Quasars at all Cosmic Epochs
Authors	MARZIANI, Paola, D'ONOFRIO, MAURO, del Olmo, Ascensión, Dultzin, Deborah
Publisher's version (DOI)	10.3389/978-2-88945-604-8
Handle	http://hdl.handle.net/20.500.12386/28523
Serie	FRONTIERS RESEARCH TOPICS

QUASARS AT ALL COSMIC EPOCHS

EDITED BY: Paola Marziani, Mauro D'Onofrio, Ascensión del Olmo and Deborah Dultzin

PUBLISHED IN: Frontiers in Astronomy and Space Sciences

frontiers Research Topics

Frontiers Copyright Statement

© Copyright 2007-2018 Frontiers Media SA. All rights reserved.

All content included on this site, such as text, graphics, logos, button icons, images, video/audio clips, downloads, data compilations and software, is the property of or is licensed to Frontiers Media SA ("Frontiers") or its licensees and/or subcontractors. The copyright in the text of individual articles is the property of their respective authors, subject to a license granted to Frontiers.

The compilation of articles constituting this e-book, wherever published, as well as the compilation of all other content on this site, is the exclusive property of Frontiers. For the conditions for downloading and copying of e-books from Frontiers' website, please see the Terms for Website Use. If purchasing Frontiers e-books from other websites or sources, the conditions of the website concerned apply.

Images and graphics not forming part of user-contributed materials may not be downloaded or copied without permission.

Individual articles may be downloaded and reproduced in accordance with the principles of the CC-BY licence subject to any copyright or other notices. They may not be re-sold as an e-book.

As author or other contributor you grant a CC-BY licence to others to reproduce your articles, including any graphics and third-party materials supplied by you, in accordance with the Conditions for Website Use and subject to any copyright notices which you include in connection with your articles and materials.

All copyright, and all rights therein, are protected by national and international copyright laws.

The above represents a summary only. For the full conditions see the Conditions for Authors and the Conditions for Website Use.

ISSN 1664-8714
ISBN 978-2-88945-604-8
DOI 10.3389/978-2-88945-604-8

About Frontiers

Frontiers is more than just an open-access publisher of scholarly articles: it is a pioneering approach to the world of academia, radically improving the way scholarly research is managed. The grand vision of Frontiers is a world where all people have an equal opportunity to seek, share and generate knowledge. Frontiers provides immediate and permanent online open access to all its publications, but this alone is not enough to realize our grand goals.

Frontiers Journal Series

The Frontiers Journal Series is a multi-tier and interdisciplinary set of open-access, online journals, promising a paradigm shift from the current review, selection and dissemination processes in academic publishing. All Frontiers journals are driven by researchers for researchers; therefore, they constitute a service to the scholarly community. At the same time, the Frontiers Journal Series operates on a revolutionary invention, the tiered publishing system, initially addressing specific communities of scholars, and gradually climbing up to broader public understanding, thus serving the interests of the lay society, too.

Dedication to Quality

Each Frontiers article is a landmark of the highest quality, thanks to genuinely collaborative interactions between authors and review editors, who include some of the world's best academicians. Research must be certified by peers before entering a stream of knowledge that may eventually reach the public - and shape society; therefore, Frontiers only applies the most rigorous and unbiased reviews.
Frontiers revolutionizes research publishing by freely delivering the most outstanding research, evaluated with no bias from both the academic and social point of view. By applying the most advanced information technologies, Frontiers is catapulting scholarly publishing into a new generation.

What are Frontiers Research Topics?

Frontiers Research Topics are very popular trademarks of the Frontiers Journals Series: they are collections of at least ten articles, all centered on a particular subject. With their unique mix of varied contributions from Original Research to Review Articles, Frontiers Research Topics unify the most influential researchers, the latest key findings and historical advances in a hot research area! Find out more on how to host your own Frontiers Research Topic or contribute to one as an author by contacting the Frontiers Editorial Office: researchtopics@frontiersin.org

QUASARS AT ALL COSMIC EPOCHS

Topic Editors:
Paola Marziani, National Institute for Astrophysics, Italy
Mauro D'Onofrio, University of Padova, Italy
Ascensión del Olmo, Instituto de Astrofísica de Andalucía, Spain
Deborah Dultzin, Universidad Naciónal Autónoma de México, Mexico

The wide-field image is centered around the bright Population A quasar HE0109-3518 (apparent visual magnitude 16.5), one of the most luminous quasars in the Universe (absolute B magnitude -29.6) at redshift 2.406 (J. W. Sulentic et al. 2017, Astron. Astroph. 608, A122). The image is a colour composite made from exposures from the Digitized Sky Survey 2 (DSS2). Within a field of view of 2.5 times 3 degrees (roughly corresponding to the size of the cover page), more than 600 quasars and quasar candidates are listed by the million quasars (Milliquas) catalog (V5.2; Flesch, 2017, originally published in: Flesch et al., 2015, Publ. Astron. Soc. Australia, 32, 10), from redshift 0.3 to 3 i.e., over cosmic epochs between 10 Gyr and 2 Gyr from the Big Bang.

Credits: ESO/Digitized Sky Survey 2, and Davide De Martin. The image is licensed under under a Creative Commons Attribution 4.0 International License.

The last 50 years have seen a tremendous progress in the research on quasars. From a time when quasars were unforeseen oddities, we have come to a view that considers quasars as active galactic nuclei, with nuclear activity a coming-of-age experienced by most or all galaxies in their evolution. We have passed from a few tens of known quasars of the early 1970s to the 500,000 listed in the catalogue of the Data Release 14 of the Sloan Digital Sky Survey. Not surprisingly, accretion processes on the central black holes in the nuclei of galaxies — the key concept in our understanding of quasars and active nuclei in general — have gained an outstanding status in present-day astrophysics. Accretion produces a rich spectrum of phenomena in all bands of the electromagnetic spectrum. The power output of highly-accreting quasars has impressive effects on their host galaxies. All the improvement in telescope light gathering and in computing power notwithstanding,

we still miss a clear connection between observational properties and theory for quasars, as provided, for example, by the H-R diagram for stars. We do not yet have a complete self-consistent view of nuclear activity with predictive power, as we do for main-sequence stellar sources. At the same time quasars offer many "windows open onto the unknown". On small scales, quasar properties depend on phenomena very close to the black hole event horizon. On large scales, quasars may effect evolution of host galaxies and their circum-galactic environments. Quasars' potential to map the matter density of the Universe and help reconstruct the Universe's spacetime geometry is still largely unexploited.

The times are ripe for a critical assessment of our present knowledge of quasars as accreting black holes and of their evolution across the cosmic time. The foremost aim of this research topic is to review and contextualize the main observational scenarios following an empirical approach, to present and discuss the accretion scenario, and then to analyze how a closer connection between theory and observation can be achieved, identifying those aspects of our understanding that are still on a shaky terrain and are therefore uncertain knowledge. This research topic covers topics ranging from the nearest environment of the black hole, to the environment of the host galaxies of active nuclei, and to the quasars as markers of the large scale structure and of the geometry of spacetime of the Universe. The spatial domains encompass the accretion disk, the emission and absorption regions, circum-nuclear starbursts, the host galaxy and its interaction with other galaxies. Systematic attention is devoted to some key problems that remain outstanding and are clearly not yet solved: the existence of two quasar classes, radio quiet and radio loud, and in general, the systematic contextualization of quasar properties the properties of the central black hole, the dynamics of the accretion flow in the inner parsecs and the origin of the accretion matter, the quasars' small and large scale environment, the feedback processes produced by the black hole into the host galaxy, quasar evolutionary patterns from seed black holes to the present-day Universe, and the use of quasars as cosmological standard candles. The timing is appropriate as we are now witnessing a growing body of results from major surveys in the optical, UV X, near and far IR, and radio spectral domains. Radio instrumentation has been upgraded to linear detector — a change that resembles the introduction of CCDs for optical astronomy — making it possible to study radio-quiet quasars at radio frequencies. Herschel and ALMA are especially suited to study the circum-nuclear star formation processes. The new generation of 3D magnetohydrodynamical models offers the prospective of a full physical modeling of the whole quasar emitting regions. At the same time, on the forefront of optical astronomy, applications of adaptive optics to long-slit spectroscopy is yielding unprecedented results on high redshift quasars. Other measurement techniques like 2D and photometric reverberation mapping are also yielding an unprecedented amount of data thanks to dedicated experiments and instruments. Thanks to the instrumental advances, ever growing computing power as well as the coming of age of statistical and analysis techniques, the smallest spatial scales are being probed at unprecedented resolution for wide samples of quasars. On large scales, feedback processes are going out of the realm of single-object studies and are entering into the domain of issues involving efficiency and prevalence over a broad range of cosmic epochs.

The Research Topic "Quasars at all Cosmic Epochs" collects a large fraction of the contributions presented at a meeting held in Padova, sponsored jointly by the National Institute for Astrophysics, the Padova Astronomical Observatory, the Department

of Physics and Astronomy of the University of Padova, and the Instito de Astrofísica de Andalucía (IAA) of the Consejo Superiór de Investigación Cientifica (CSIC). The meeting has been part of the events meant to celebrate the 250th anniversary of the foundation of the Padova Observatory.

Citation: Marziani, P., D'Onofrio, M., del Olmo, A., Dultzin, D., eds. (2018). Quasars at All Cosmic Epochs. Lausanne: Frontiers Media. doi: 10.3389/978-2-88945-604-8

Table of Contents

10 ***Editorial: Quasars at all Cosmic Epochs***
Paola Marziani, Ascensión Del Olmo, Mauro D'Onofrio and Deborah Dultzin

CHAPTER: OBSERVATIONAL PROPERTIES OF ACTIVE GALACTIC NUCLEI

SECTION: AGN CLASSES AND SPECTRAL ENERGY DISTRIBUTIONS

12 ***Active Galactic Nuclei at all Wavelengths and From all Angles***
Paolo Padovani

19 ***Gaia Space Mission and Quasars***
Tomaž Zwitter

24 ***Multi-Frequency Databases for AGN Investigation—Results and Perspectives***
Giovanni La Mura, Marco Berton, Sina Chen, Stefano Ciroi, Enrico Congiu, Valentina Cracco, Michele Frezzato and Piero Rafanelli

31 ***Pair-Matching of Radio-Loud and Radio-Quiet AGNs***
Dorota Kozieł-Wierzbowska, Grażyna Stasińska, Natalia Vale Asari, Marek Sikora, Elisa Goettems and Anna Wójtowicz

37 ***What we Talk About When we Talk About Blazars***
Luigi Foschini

43 ***An Optical View of Extragalactic γ-Ray Emitters***
Simona Paiano, Renato Falomo, Marco Landoni, Aldo Treves and Riccardo Scarpa

49 ***Probing the Diffuse Optical-IR Background With TeV Blazars Detected With the MAGIC Telescopes***
Elisa Prandini, Alberto Domínguez, Vandad Fallah Ramazani, Tarek Hassan, Daniel Mazin, Abelardo Moralejo, Mireia Nievas Rosillo, Gaia Vanzo and Monica Vazquez Acosta for the MAGIC Collaboration

54 ***An Orientation-Based Unification of Young Jetted AGN: The Case of 3C 286***
Marco Berton, Luigi Foschini, Alessandro Caccianiga, Stefano Ciroi, Enrico Congiu, Valentina Cracco, Michele Frezzato, Giovanni La Mura and Piero Rafanelli

61 ***SDSS J090152.05+624342.6: A NEW "OVERLAPPING-TROUGH" FeLoBAL QUASAR AT Z ~ 2***
Jing Wang, Dawei Xu and Jianyan Wei

66 ***The AGN Nature of LINER Nuclear Sources***
Isabel Márquez, Josefa Masegosa, Omaira González-Martin, Lorena Hernández-Garcia, Mirjana Pović, Hagai Netzer, Sara Cazzoli and Ascensión del Olmo

77 ***TeV Diffuse Emission From the Inner Galaxy***
Amid Nayerhoda, Francisco Salesa Greus and Sabrina Casanova for the HAWC collaboration

SECTION: VARIABILITY AND REVERBERATION MAPPING

82 ***Optical Variability of Active Galactic Nuclei***
Szymon Kozłowski

85 ***Changing-Look AGNs or Short-Lived Radio Sources?***
Aleksandra Wołowska, Magdalena Kunert-Bajraszewska, Kunal Mooley and Gregg Hallinan

89 ***The MEXSAS2 Sample and the Ensemble X-ray Variability of Quasars***
Roberto Serafinelli, Fausto Vagnetti, Elia Chiaraluce and Riccardo Middei

93 ***Long-Term Monitoring of the Broad-Line Region Properties in a Selected Sample of AGN***
Dragana Ilić, Alla I. Shapovalova, Luka Č. Popović, Vahram Chavushyan, Alexander N. Burenkov, Wolfram Kollatschny, Andjelka Kovačević, Sladjana Marčeta-Mandić, Nemanja Rakić, Giovanni La Mura and Piero Rafanelli

99 ***Exploring Possible Relations Between Optical Variability Time Scales and Broad Emission Line Shapes in AGN***
Edi Bon, Predrag Jovanović, Paola Marziani, Nataša Bon and Aleksandar Otašević

107 ***Multiwavelength Variability Analysis of 3C 279***
Víctor M. Patiño-Álvarez, Sunil Fernandes, Vahram Chavushyan, Erique López-Rodríguez, Jonathan León-Tavares, Eric M. Schlegel, Luis Carrasco, José R. Valdés and Alberto Carramiñana

112 ***Time-Evolving SED of MKN421: A Multi-Band View and Polarimetric Signatures***
Bernardo M. O. Fraga, Ulisses Barres de Almeida, Sargis Gasparyan, Paolo Giommi and Narek Sahakyan

117 ***AGN Broad Line Region Variability in the Context of Eigenvector 1: Case of NGC 5548***
Nataša Bon, Edi Bon and Paola Marziani

126 ***C IV Broad Absorption Line Variability in QSO Spectra From SDSS Surveys***
Demetra De Cicco, William N. Brandt, Catherine J. Grier and Maurizio Paolillo

133 ***Rapid BAL Variability: Re-Emerging Absorption***
Damla Erakuman and Nurten Filiz Ak

138 ***Reverberation Mapping of High-Luminosity Quasars***
Shai Kaspi, William N. Brandt, Dan Maoz, Hagai Netzer, Donald P. Schneider and Ohad Shemmer

144 ***Reverberation Mapping of High-z, High-Luminosity Quasars***
Paulina Lira, Ismael Botti, Shai Kaspi and Hagai Netzer

149 ***Continuum Reverberation Mapping of AGN Accretion Disks***
Michael M. Fausnaugh, Bradley M. Peterson, David A. Starkey, Keith Horne and the AGN STORM Collaboration

CHAPTER: ACCRETION PROCESSES ON SUPERMASSIVE BLACK HOLES

155 ***Self-Consistent Dynamical Model of the Broad Line Region***
Bozena Czerny, Yan-Rong Li, Justyna Sredzinska, Krzysztof Hryniewicz, Swayam Panda, Conor Wildy and Vladimir Karas

160 ***The Physical Driver of the Optical Eigenvector 1 in Quasar Main Sequence***
Swayamtrupta Panda, Bożena Czerny and Conor Wildy

168 ***The Physical Relation Between Disc and Coronal Emission in Quasars***
Elisabeta Lusso and Guido Risaliti

174 ***Jet Physics of Accreting Super-Massive Black Holes in the era of the*** **Fermi Gamma-ray Space Telescope**
Filippo D'Ammando on behalf of the Fermi Large Area Telescope Collaboration

180 ***The Correlation Between the Total Magnetic Flux and the Total Jet Power***
Elena E. Nokhrina

187 ***Confrontation of the Magnetically Arrested Disc Scenario With Observations of FR II Sources***
Katarzyna Rusinek and Marek Sikora

192 ***Dynamics and Formation of Obscuring Tori in AGNs***
Elena Yu. Bannikova and Alexey V. Sergeyev

198 ***Modeling the Broad-Band Emission From the Gamma-Ray Emitting Narrow-Line Seyfert-1 Galaxies 1H 0323+342 and B2 0954+25A***
Maialen Arrieta-Lobo, Catherine Boisson and Andreas Zech

CHAPTER: CONNECTION BETWEEN THEORY AND OBSERVATION

205 ***A Main Sequence for Quasars***
Paola Marziani, Deborah Dultzin, Jack W. Sulentic, Ascensión Del Olmo, C. A. Negrete, Mary L. Martínez-Aldama, Mauro D'Onofrio, Edi Bon, Natasa Bon and Giovanna M. Stirpe

225 ***The Virial Factor and Biases in Single Epoch Black Hole Mass Determinations***
Julián E. Mejía-Restrepo, Paulina Lira, Hagai Netzer, Benny Trakhtenbrot and Daniel Capellupo

233 ***Black Hole Mass Estimation in Type 1 AGN: Hβ vs. Mg II Lines and the Role of Balmer Continuum***
Jelena Kovačević-Dojčinović, Sladjana Marčeta-Mandić and Luka Č. Popović

239 ***Ultraviolet/Optical Emission of the Ionized Gas in AGN: Diagnostics of the Ionizing Source and Gas Properties***
Anna Feltre, Stephane Charlot, Marco Mignoli, Angela Bongiorno, Francesco Calura, Jacopo Chevallard, Emma Curtis-Lake, Roberto Gilli and Adele Plat

244 ***The Relationship Between Mg II Broad Emission and Quasar Inclination Angle***
Conor Wildy and Bozena Czerny

251 ***On the Intermediate Line Region in AGNs***
Tek P. Adhikari, Agata Różańska, Krzysztof Hryniewicz, Bozena Czerny and Gary J. Ferland

256 ***EW[OIII] as an Orientation Indicator for Quasars: Implications for the Torus***
Susanna Bisogni, Alessandro Marconi, Guido Risaliti and Elisabeta Lusso

262 ***New Constraints on Quasar Broad Absorption and Emission Line Regions From Gravitational Microlensing***
Damien Hutsemékers, Lorraine Braibant, Dominique Sluse, Timo Anguita and René Goosmann

268 ***Disentangling Accretion Disk and Dust Emissions in the Infrared Spectrum of Type 1 AGN***
Antonio Hernán-Caballero, Evanthia Hatziminaoglou, Almudena Alonso-Herrero and Silvia Mateos

274 ***NGC 1275: An Outlier of the Black Hole-Host Scaling Relations***
Eleonora Sani, Federica Ricci, Fabio La Franca, Stefano Bianchi, Angela Bongiorno, Marcella Brusa, Alessandro Marconi, Francesca Onori, Francesco Shankar and Cristian Vignali

281 ***Theoretical Re-evaluations of Scaling Relations Between SMBHs and Their Host Galaxies—1. Effect of Seed BH Mass***
Hikari Shirakata, Toshihiro Kawaguchi, Takashi Okamoto, Ryu Makiya, Tomoaki Ishiyama, Yoshiki Matsuoka, Masahiro Nagashima, Motohiro Enoki, Taira Oogi and Masakazu A. R. Kobayashi

285 ***Statistical Detection of the He II Transverse Proximity Effect: Evidence for Sustained Quasar Activity for >25 Million Years***
Tobias M. Schmidt, Gabor Worseck, Joseph F. Hennawi, J. Xavier Prochaska, Neil H. M. Crighton, Zarija Lukić and Jose Oñorbe

CHAPTER: FEEDBACK AND ENVIRONMENT OF ACTIVE GALAXIES AND QUASARS

SECTION: FEEDBACK

293 ***The Many Routes to AGN Feedback***
Raffaella Morganti

303 ***AGN Feedback and its Quenching Efficiency***
Francoise Combes

308 ***Probing the Gas Fueling and Outflows in Nearby AGN With ALMA***
Anelise Audibert, Françoise Combes, Santiago García-Burillo and Philippe Salomé

313 ***Negative and Positive Outflow-Feedback in Nearby (U)LIRGs***
Sara Cazzoli

318 ***Ionized Gas Outflows From the MAGNUM Survey: NGC 1365 and NGC 4945***
Giacomo Venturi, Alessandro Marconi, Matilde Mingozzi, Stefano Carniani, Giovanni Cresci, Guido Risaliti and Filippo Mannucci

324 ***Quasar Massive Ionized Outflows Traced by CIV λ1549 and [OIII] λλ4959,5007***
Paola Marziani, C. Alenka Negrete, Deborah Dultzin, Mary L. Martínez-Aldama, Ascensión Del Olmo, Mauro D'Onofrio and Giovanna M. Stirpe

330 ***Star Formation Quenching in Quasar Host Galaxies***
Stefano Carniani

336 ***Luminous and Obscured Quasars and Their Host Galaxies***
Agnese Del Moro, David M. Alexander, Franz E. Bauer, Emanuele Daddi, Dale D. Kocevski, Flora Stanley and Daniel H. McIntosh

341 ***Extended Narrow-Line Region in Seyfert Galaxies***
Enrico Congiu, Marcella Contini, Stefano Ciroi, Valentina Cracco, Francesco Di Mille, Marco Berton, Michele Frezzato, Giovanni La Mura and Piero Rafanelli

347 ***How Quasar Feedback May Shape the Co-evolutionary Paths***
Wako Ishibashi

351 ***Theoretical Re-evaluations of Scaling Relations Between SMBHs and Their Host Galaxies–2. Importance of AGN Feedback Suggested by Stellar Age–Velocity Dispersion Relation***
Hikari Shirakata, Toshihiro Kawaguchi, Takashi Okamoto and Tomoaki Ishiyama

SECTION: ENVIRONMENT

357 ***On the Role of the Environments and Star Formation for Quasar Activity***
Daniela Bettoni, Renato Falomo, Jari K. Kotilainen and Kalle Karhunen

363 *The Overdense Environments of* WISE-*Selected, Ultra-Luminous, High-Redshift AGN in the Submillimeter*
Suzy F. Jones

369 *Large-Scale Environment Properties of Narrow-Line Seyfert 1 Galaxies at z < 0.4*
Emilia Järvelä, A. Lähteenmäki and H. Lietzen

376 *Tracing the External Origin of the AGN Gas Fueling Reservoir*
Sandra I. Raimundo

379 *Direct HST Dust Lane Detection in Powerful Narrow-Line Radio Galaxies*
Edgar A. Ramírez, Itziar Aretxaga, Clive N. Tadhunter, Enrique Lopez-Rodriguez and Chris Packham

383 *Fast-Growing SMBHs in Fast-Growing Galaxies, at High Redshifts: The Role of Major Mergers as Revealed by ALMA*
Benny Trakhtenbrot, Paulina Lira, Hagai Netzer, Claudia Cicone, Roberto Maiolino and Ohad Shemmer

389 *Circum-Galactic Medium in the Halo of Quasars*
Riccardo Ottolina, Renato Falomo, Aldo Treves, Michela Uslenghi, Jari K. Kotilainen, Riccardo Scarpa and Emanuele Paolo Farina

CHAPTER: QUASAR EVOLUTION OVER COSMIC TIME AND QUASARS AS COSMOLOGICAL TOOLS

SECTION: EVOLUTION

393 *A Catalog of Active Galactic Nuclei From the First 1.5 Gyr of the Universe*
Krisztina Perger, Sándor Frey, Krisztina É. Gabányi and L. Viktor Tóth

399 *On the Selection of High-z Quasars Using LOFAR Observations*
Edwin Retana-Montenegro and Huub Röttgering

408 *Phylogenetic Analyses of Quasars and Galaxies*
Didier Fraix-Burnet, Mauro D'Onofrio and Paola Marziani

414 *Catalog of 3 < z < 5.5 Quasar Candidates Selected Among XMM-Newton Sources and its Spectroscopic Verification*
Georgii Khorunzhev, Sergey Sazonov, Rodion Burenin and Maxim Eselevich

SECTION: QUASARS AS DISTANCE INDICATORS

418 *A Hubble Diagram for Quasars*
Susanna Bisogni, Guido Risaliti and Elisabeta Lusso

424 *Quasars as Cosmological Standard Candles*
C. Alenka Negrete, Deborah Dultzin, Paola Marziani, Jack W. Sulentic, Donají Esparza-Arredondo, Mary L. Martínez-Aldama and Ascensión Del Olmo

429 *Highly Accreting Quasars at High Redshift*
Mary L. Martínez-Aldama, Ascensión Del Olmo, Paola Marziani, Jack W. Sulentic, C. Alenka Negrete, Deborah Dultzin, Jaime Perea and Mauro D'Onofrio

436 *HE0359-3959: An Extremely Radiating Quasar*
M. L. Martínez-Aldama, A. Del Olmo, P. Marziani, C. A. Negrete, D. Dultzin and M. A. Martínez-Carballo

CHAPTER: CONCLUDING REMARKS

441 *Meeting Summary: A 2017 View of Active Galactic Nuclei*
Hagai Netzer

frontiers in Astronomy and Space Sciences

EDITORIAL
published: 17 August 2018
doi: 10.3389/fspas.2018.00028

Editorial: Quasars at All Cosmic Epochs

Paola Marziani[1], Ascensión Del Olmo[2], Mauro D'Onofrio[3] and Deborah Dultzin[4]*

[1] National Institute for Astrophysics (INAF), Padua Astronomical Observatory, Padua, Italy, [2] Instituto de Astrofísica de Andalucía (CSIC), Granada, Spain, [3] Dipartimento di Fisica & Astronomia "Galileo Galilei," Università di Padova, Padua, Italy, [4] Instituto de Astronomía, UNAM, Mexico City, Mexico

Keywords: quasars, cosmology, massive and supermassive black holes, galaxies, galaxy evolution, active galactic nuclei, accretion processes

OPEN ACCESS

Edited and reviewed by:
Lee Samuel Finn, Pennsylvania State University, United States

****Correspondence:***
Paola Marziani
paola.marziani@inaf.it

Specialty section:
This article was submitted to Milky Way and Galaxies, a section of the journal Frontiers in Astronomy and Space Sciences

Received: *21 July 2018*
Accepted: *25 July 2018*
Published: *17 August 2018*

Citation:
Marziani P, Del Olmo A, D'Onofrio M and Dultzin D (2018) Editorial: Quasars at All Cosmic Epochs. Front. Astron. Space Sci. 5:28. doi: 10.3389/fspas.2018.00028

Editorial on the Research Topic

Quasars at All Cosmic Epochs

Accretion onto massive black holes—and its associated manifestation as nuclear activity in galaxies—is among the most remarkable phenomena occurring in the Universe, and likely a key factor in galaxy evolution over a broad range of cosmic epochs. From a time when it was believed that accreting black holes were isolated sources affecting their host only within a limited sphere of influence, we have just begun to appreciate the rich and complex phenomenology induced by active nuclei in their host galaxies due to their radiative and mechanical output. Nuclear activity also presents a unique opportunity to probe spatial scales that we cannot yet resolve, as accretion related phenomena provide an immensely rich phenomenology extending from the longest radio wavelengths to the hardest γ-rays within a few parsec from the central black hole. A world of accreting black holes completely hidden at present will emerge in the next few years from the development of gravitational wave observatories. In late 2016, the time was ripe for a critical assessment of our understanding of quasars as accreting black holes and of their evolution across the cosmic time, with an eye on future developments.

This Research Topic is based on contributions presented at a meeting held in Padova in April 2017. Close to 170 participants convened in Padova from research institutes and Universities around the world. The Padova meeting was one of the largest conferences on active galactic nuclei in recent years. With 159 contributions (88 talks), gender balance was achieved (within 2 σ confidence-level stochastic fluctuations expected from binomial statistics), as the percentage of women participant was 43%, the percentage of women first author in a contribution 48%, and the percentange of women speakers was 55%.

The meeting highlighted progress—both observational and theoretical—achieved over the last decade. At the same time, many shortcomings, wishful thinkings, and never critically-reanalyzed prejudices emerged in discussions among the participants about our view of quasars and nuclear activity in general.

The organization of the e-book produced from this Research Topic reflects the temporal sequence of the meeting sessions. Each day was organized around a broad theme, focused on one or more overarching questions. On the first day, we aimed at a comprehensive overview of the main observational aspects of active galactic nuclei (AGN), with a focus on several key questions (Chapter 1). Contributions from this first day, organized into Chapter 1, discuss the most relevant photometric, spectroscopic, polarimetric, and variability observations over the full spectral energy distribution (SED), together with their interpretation, with attention to both statistical results and case studies. Overarching issues are some still-enigmatic aspects of the SED, systematic organization, and contextualization of observational properties, radio properties of

jetted and non-jetted quasars, as well as selection effects that still affect major surveys. Chapter 2 contains contributions on accretion disk structure and wind and jet launching processes. The overarching theoretical issues (which remain open to-date) are the connections between disk structure, relativistic ejections, and continuum and line emitting regions. A satisfactory model of the broad line emitting region of quasars—to which almost 2,000 papers were dedicated over 40 years and to which a large part of the Conference was devoted—could pave the road to the use of quasars as distance indicators but remains as yet incomplete. The contributions in Chapter 3 attempt to connect theory and observation. The overarching questions remain, why do the radio properties of quasars divide the quasar population into the two categories radio quiet and radio loud? What is the connection between disk structure, relativistic ejections, and emitting regions structure? We think that one of the more remarkable outcomes of the conference was the realization of the many observational manifestations of accretion in quasars in a broad range of luminosity and cosmic epochs, and of their dependence on accretion parameters such as mass, dimensionless accretion rate, and spin. As the accreting black hole systems only possess axial symmetry and not spherical symmetry, many observational properties are affected by the viewing angle. Our ability to connect observational to physical and aspect parameters is still lacunose but, if filled, the importance could be comparable to the development of the Hertzspung-Russell diagrams for stars. We miss an equivalent for quasars, although prospective improvements are in sight. Significant attention was devoted to a promising approach, developed by Jack Sulentic, his collaborators, and other research groups, based on the analysis of the "first eigenvector" of a 4D correlation space of quasar properties.

Chapter 4 and in part Chapter 5 are devoted to the role of nuclear activity in shaping the evolution of galaxies. Feedback and environment of active nuclei are seen in the suggested black hole and host galaxy coevolution, but open issues still involve the interplay of black hole fueling (strongly influenced by the environment over cosmic ages), star formation and feedback. The overarching question posed at the meeting was: which are the strongest evidences and the state-of-the-art modeling, and which are the tests and surveys, both observational and theoretical, that can lead to progresses in our understanding of fueling and feedback processes on all scales?

Chapter 5 discussed some interesting developments having taken place in the last two years, as we seek to learn from the observations of the increasing number of high redshift quasars. An open issue remains the role of quasars at the epoch of re-ionization. A more basic question is the role of first seed quasars and their relation to galaxy formation. The overarching question remains whether we understand quasar evolution beyond selection effects.

The last contributions deal with the possibility to exploit quasars as helpful distance indicators, a possibility that was found closely linked to an improvement in our understanding of the quasar emitting region structure and dynamics. Major issues and the recent developments, including several research lines aimed at answering some of the overarching questions, are critically evaluated in the conference closing remarks by Hagai Netzer (Chapter 6).

DATA AVAILABILITY STATEMENT

Slides of most of the presentations are available at zenodo.org on the Quasars at all cosmic epochs page.

AUTHOR CONTRIBUTIONS

PM wrote the paper. The other authors gave significant contributions.

FUNDING

The conference was sponsored jointly by the National Institute for Astrophysics, the Padova Astronomical Observatory, the Department of Physics and Astronomy of the University of Padova, and the Instituto de Astrofísica de Andalucía (IAA) of the Consejo Superiór de Investigación Cientifica (CSIC) whose support is gratefully acknowldeged. We are very grateful for the facilitation and sponsorship (including the best poster contest) that was provided by the Journal Frontiers in Astronomy and Space Sciences. Sponsors Officina stellare and Springer Verlag provided conference material free-of-charge. The meeting has been part of the events meant to celebrate the 250th anniversary of the foundation of the Padova Observatory.

ACKNOWLEDGMENTS

The Editors wish to thank all participants, all members of the Scientific and Local Organizing Committee, and all speakers (see the conference website at https://indico.ict.inaf.it/event/338/ and the conference poster). A special thank goes to the authors who submitted their contributions to the Journal and for the Conference proceedings and to the reviewers of the submitted papers for their time, their careful work, and incredible patience.

We gratefully acknowledge the kindness and professionalism of the people with the Editorial Office of Frontiers who masterfully handled several issues during the reviews of the Research Topic contributions, and especially Daisy Hessenberger and Claudio Bogazzi. We thank the Chief Editor of Frontiers in Astronomy and Space Science, Sam Finn, for a careful reading of the Editorial.

Conflict of Interest Statement: The authors declare that the research was conducted in the absence of any commercial or financial relationships that could be construed as a potential conflict of interest.

Copyright © 2018 Marziani, Del Olmo, D'Onofrio and Dultzin. This is an open-access article distributed under the terms of the Creative Commons Attribution License (CC BY). The use, distribution or reproduction in other forums is permitted, provided the original author(s) and the copyright owner(s) are credited and that the original publication in this journal is cited, in accordance with accepted academic practice. No use, distribution or reproduction is permitted which does not comply with these terms.

frontiers in Astronomy and Space Sciences

REVIEW
published: 07 November 2017
doi: 10.3389/fspas.2017.00035

Active Galactic Nuclei at All Wavelengths and from All Angles

*Paolo Padovani**

European Southern Observatory, Garching bei München, Germany

AGN are quite unique astronomical sources emitting over more than 20 orders of magnitude in frequency, with different electromagnetic bands providing windows on different sub-structures and their physics. They come in a large number of flavors only partially related to intrinsic differences. I highlight here the types of sources selected in different bands, the relevant selection effects and biases, and the underlying physical processes. I then look at the "big picture" by describing the most important parameters one needs to describe the variety of AGN classes and by discussing AGN at all frequencies in terms of their sky surface density. I conclude with a look at the most pressing open issues and the main new facilities, which will flood us with new data to tackle them.

Keywords: quasars, active galactic nuclei, supermassive black holes, radio emission, infrared emission, X-ray emission, γ-ray emission

OPEN ACCESS

Edited by:
Paola Marziani, Osservatorio Astronomico di Padova (INAF), Italy

Reviewed by:
Alenka Negrete, Universidad Nacional Autónoma de México, Mexico
Dawei Xu, National Astronomical Observatories (CAS), China

***Correspondence:**
Paolo Padovani
ppadovan@eso.org

Specialty section:
This article was submitted to Milky Way and Galaxies, a section of the journal Frontiers in Astronomy and Space Sciences

Received: *14 September 2017*
Accepted: *23 October 2017*
Published: *07 November 2017*

Citation:
Padovani P (2017) Active Galactic Nuclei at All Wavelengths and from All Angles. Front. Astron. Space Sci. 4:35. doi: 10.3389/fspas.2017.00035

1. INTRODUCTION

AGN are, by definition, more powerful than the nuclei of normal galaxies. This "additional" component is now universally accepted to be due to an actively accreting central supermassive ($\gtrsim 10^6\ M_\odot$) black hole (SMBH). This implies a number of fascinating properties, which include very high luminosities (up to $L_{\rm bol} \approx 10^{48}$ erg s^{-1}), small emitting regions in most bands (of the order of a milliparsec), strong evolution of the luminosity functions, and broad-band emission covering the entire electromagnetic spectrum (see Padovani et al., 2017, for a review).

The latter property means that AGN have been discovered at all wavelengths. This is partly responsible for the very large number of classes and sub-classes AGN researchers have come up with (see **Table 1**), which appear to be overwhelming and very confusing, especially to astronomers working in other fields and particularly to physicists.

Different methods are employed to select AGN in the various bands, which also provide different views on AGN physics. I discuss this next. I refer to Padovani et al. (2017) for a more in-depth review of these (and other) topics.

2. THE RADIO BAND

One of the main results of the past few years has been the realization that the radio sky population undergoes major changes at low flux densities. Namely, while the bright radio sky ($f_{\rm r} \gtrsim 1$ mJy around 1 GHz, where 1 Jy is 10^{-23} erg cm^{-2} s^{-1} Hz^{-1}) is populated mostly by radio galaxies (RGs) and radio quasars, that is largely non-thermal sources, at faint radio flux densities we are now detecting mainly star-forming galaxies (SFGs) and the more common non-jetted AGN (see Padovani, 2016, for a review). This change is also apparent by looking at the Euclidean normalized 1.4 GHz source counts, which show an upturn around ≈ 0.1 mJy (see **Figure 1**). We therefore need to deal separately with the two flux density regimes.

TABLE 1 | The AGN zoo: list of AGN classes.

Class/Acronym	Meaning/Main properties
Quasar	Quasi-stellar radio source (originally)
Sey1	Seyfert 1, FWHM $\gtrsim$ 1,000 km s^{-1}
Sey2	Seyfert 2, FWHM $\lesssim$ 1,000 km s^{-1}
QSO	Quasi-stellar object
QSO2	Quasi-stellar object 2, high power Sey2
RQ AGN	Radio-quiet AGN
RL AGN	Radio-loud AGN
Jetted AGN	With strong relativistic jets
Non-jetted AGN	Without strong relativistic jets
Type 1	Sey1 and quasars
Type 2	Sey2 and QSO2
FR I	Fanaroff-Riley class I radio source
FR II	Fanaroff-Riley class II radio source
BL Lac	BL Lacertae object
Blazars	BL Lacs and FSRQs
BAL	Broad absorption line (quasar)
BLO	Broad-line object, FWHM $\gtrsim$ 1,000 km s^{-1}
BLAGN	Broad-line AGN, FWHM $\gtrsim$ 1,000 km s^{-1}
BLRG	Broad-line radio galaxy
CDQ	Core-dominated quasar
CSS	Compact steep spectrum radio source
CT	Compton-thick
FR 0	Fanaroff-Riley class 0 radio source
FSRQ	Flat-spectrum radio quasar
GPS	Gigahertz-peaked radio source
HBL/HSP	High-energy cutoff BL Lac/blazar
HEG	High-excitation galaxy
HPQ	High polarization quasar
Jet-mode	
IBL/ISP	Intermediate-energy cutoff BL Lac/blazar
LINER	Low-ionization nuclear emission-line regions
LLAGN	Low-luminosity AGN
LBL/LSP	Low-energy cutoff BL Lac/blazar
LDQ	Lobe-dominated quasar
LEG	Low-excitation galaxy
LPQ	Low polarization quasar
NLAGN	Narrow-line AGN, FWHM $\lesssim$ 1,000 km s^{-1}
NLRG	Narrow-line radio galaxy
NLS1	Narrow-line Seyfert 1
OVV	Optically violently variable (quasar)
Population A	
Population B	
Radiative-mode	
RBL	Radio-selected BL Lac
Sey1.5	Seyfert 1.5
Sey1.8	Seyfert 1.8
Sey1.9	Seyfert 1.9
SSRQ	Steep-spectrum radio quasar
USS	Ultra-steep spectrum source
XBL	X-ray-selected BL Lac
XBONG	X-ray bright optically normal galaxy

The top part of the table relates to major/classical classes. See Padovani et al. (2017) for a more complete version of this table, including more details and references.

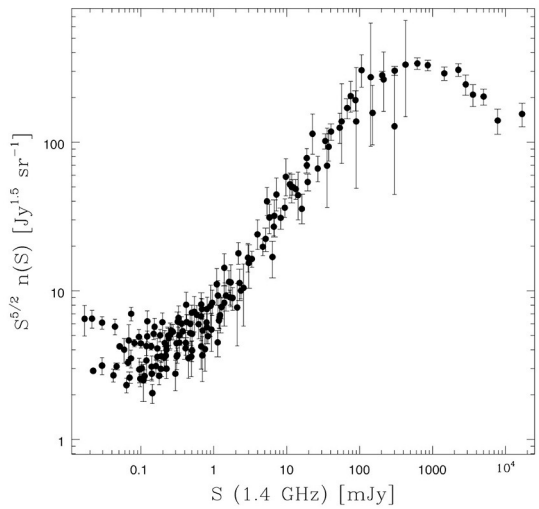

FIGURE 1 | The Euclidean normalized 1.4 GHz source counts derived from various radio surveys. See Figure 14 of Padovani (2016) for references.

2.1. The Bright Radio Sky: $f_r \gtrsim 1$ mJy

Sources include mostly jetted AGN, mainly blazars and RGs. Selection is done by just observing the high Galactic latitude sky as AGN are (basically) the only sources. This is helped by the fact that stars are extremely weak radio emitters. For example, out of the 527 sources with 5 GHz flux density > 1 Jy and Galactic latitude $|b_{\rm II}| \geq 10^\circ$ (Kühr et al., 1981) only M 82 is not an AGN (and only M 82 and NGC 1068 do not belong to the RG, radio quasar, or blazar classes; moreover, ∼51% of the classified sources are blazars). The radio band probes the jet and its emission is due to synchrotron radiation (ultra-relativistic electrons in a magnetic field). The only bias is that we are sampling the jetted AGN population, which is only a small fraction (<10%) of the total.

2.2. The Faint Radio Sky: $f_r \lesssim 1$ mJy

Sources include both non-jetted AGN and a quickly decreasing fraction of jetted AGN (see Figure 7 of Padovani, 2016); the former are the dominant type. Selection requires data in various bands to single out the AGN, especially the non-jetted ones, from the SFGs, as the optical counterparts are very faint (as detailed in section 5.1 of Padovani, 2016). Apart from probing the jet in jetted AGN, radio emission is mostly due to star formation (through synchrotron emission from relativistic plasma accelerated in supernova remnants) in non-jetted ones (at least for radio-selected sources: see discussion in section 6.2 of Padovani, 2016). There is some chance of contamination from SFGs (especially if no X-ray detection is available). But we are now reaching the most common non-jetted AGN with no obscuration bias.

I would also like to stress, once more (see also Padovani, 2016, 2017), that the differences between jetted and non-jetted AGN are *not* taxonomic but reflect intrinsic differences, with jetted AGN emitting a large fraction of their energy in association

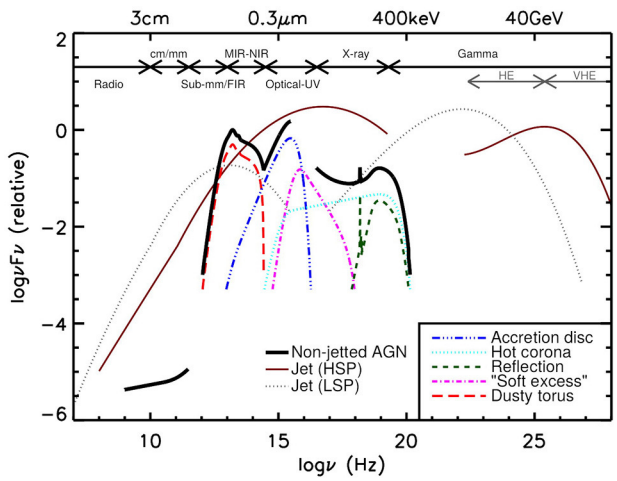

FIGURE 2 | A schematic representation of an AGN spectral energy distribution (SED), loosely based on the observed SEDs of non-jetted quasars (e.g., Elvis et al., 1994; Richards et al., 2006). The black solid curve represents the total emission and the various colored curves (shifted down for clarity) represent the individual components. The intrinsic shape of the SED in the mm-far infrared (FIR) regime is uncertain; however, it is widely believed to have a minimal contribution (to an overall galaxy SED) compared to star formation (SF), except in the most intrinsically luminous quasars and powerful jetted AGN. The primary emission from the AGN accretion disk peaks in the UV region. The jet SED is also shown for a high synchrotron peaked blazar (HSP, based on the SED of Mrk 421) and a low synchrotron peaked blazar (LSP, based on the SED of 3C 454.3). Adapted from Harrison (2014). Image credit: C. M. Harrison. Figure reproduced from Padovani et al. (2017), Figure 1, with permission of Springer.

with powerful relativistic jets and therefore non-thermally, while the multi-wavelength emission of non-jetted AGN is dominated by thermal emission related to the accretion disk, which forms around the SMBH. Because of this, only jetted AGN manage to emit in the hard X-ray to γ-ray bands (see also **Figure 2**). Furthermore, the 50-year-old "radio-loud/radio-quiet" labels are obsolete, misleading, and wrong and should be dropped (Padovani, 2016, 2017).

3. THE INFRARED BAND

Whatever its detailed distribution and properties, we know there is dust around most AGN outside the accretion disk and on scales larger than those of the broad line region (BLR). This dust has a temperature in the 100–1,000 K range and is located at a minimum distance determined by the sublimation temperature of the dust grains (Barvainis, 1987). Ultraviolet (UV)/optical emission from the accretion disk is absorbed by it and re-emitted in the infrared (IR) band where it dominates the AGN spectral energy distribution (SED) at $\lambda \gtrsim 1\ \mu$m up to a few tens of micron (**Figure 2**).

Dust plays a vital role in AGN unification schemes (e.g., Antonucci, 1993; Urry and Padovani, 1995). Thanks to polarization studies it was in fact realized that the difference between type 1 (broad-lined) and type 2 (narrow-lined) AGN was solely due to orientation with respect to the dust. In the latter objects our view of the accretion disk and the BLR is obscured by the dust and therefore we cannot see the UV bump and the broad lines typical of type 1 AGN but can only detect the narrow lines emitted by slower-moving clouds beyond the dust (but see Elitzur and Netzer, 2016 for a discussion about possible *real* type 2 AGN where the difference is not caused by dust obscuration; see also section 5.3 of Padovani et al., 2017).

Importantly, it now looks like the dust and the BLR are only present at high powers ($\gtrsim 10^{42}$ erg s^{-1})/high Eddington ratios ($L/L_{\rm Edd} \gtrsim 0.01$; see discussion in Padovani et al., 2017), which implies that dust-driven unification breaks down below these values. Jet-driven, low-power unification (linking BL Lacs with LEG RGs) is unaffected by this.

Based on all of the above, AGN selected in the IR band include mostly non-jetted AGN (because low-power/low accretion rate jetted sources do not have any dust) of the radiative-mode type (i.e., with high accretion rates and $L/L_{\rm Edd}$). The IR is sensitive to both obscured and unobscured AGN, providing an almost isotropic selection, and in particular to extremely obscured AGN (missed by optical and soft X-ray surveys). Selection is done by typically using IR colors with the aim of separating AGN from SFGs (see section 3.2 in Padovani et al., 2017, and specifically Figure 5 and Table 2). While for shallow surveys relatively high reliability and completeness can be obtained (see caption of **Table 2** for definitions) this is not the case for deeper ones, where high reliability can only be obtained by having low completeness (in other words, one can select mostly AGN only by missing a large fraction of them above a given flux limit).

4. THE OPTICAL/UV BAND

Optical/UV emission in AGN comes from the accretion disk and the BLR. Because of the presence of dust discussed in section 3 one can detect this emission only if our line of sight is unobstructed (which happens only for specific orientations) and therefore only in unobscured sources. The optical/UV band, therefore, provides a very biased view of the AGN phenomenon, although it was also thanks to their strong optical/UV emission that AGN were mostly discovered in the past.

AGN selected in the optical/UV band, therefore, include unobscured sources mostly of the non-jetted type [as only a small fraction of jetted AGN (radio quasars) have also a standard accretion disk and a BLR]; in short, type 1 AGN. Predictably, this band misses lots of obscured AGN (the type 2′s), although many of them are still selected through their narrow emission lines, and even the moderately obscured ones. Other biases are against low-luminosity AGN (where the host galaxy light swamps the AGN) and also AGN close to stellar loci (as stars are also strong optical/UV emitters) especially at $z \sim 2.6$ and 3.5.

The optical/UV band, however, makes up for these shortcomings in two ways: (1) by providing spectra which are vital to study AGN physics, e.g., the accretion disk, to estimate the mass of the central SMBH through "reverberation mapping", and to study the AGN spectral diversity; (2) by supplying us with huge optical catalogs. More details on these topics can be found in section 4 of Padovani et al. (2017).

TABLE 2 | A multi-wavelength overview of AGN highlighting the different selection biases (weaknesses) and key capabilities (strengths).

Band	Type	Physics	Selection biases/weaknesses	Key capabilities/strengths
Radio, $f_r \gtrsim 1$ mJy	Jetted	Jet	Non-jetted sources	High efficiency, no obscuration bias
Radio, $f_r \lesssim 1$ mJy	Jetted and non-jetted	Jet and SF	Host contamination	Completeness, no obscuration bias
IR	Type 1 and 2	Hot dust and SF	Completeness, reliability, host contamination, no dust	Weak obscuration bias, high efficiency
Optical	Type 1	Disk	Completeness, low-luminosity, obscured sources, host contamination	High efficiency, detailed physics from lines
X-ray	Type 1 and (most) 2	Corona	Very low-luminosity, heavy obscuration	Completeness, low host contamination
γ-ray	Jetted	Jet	Non-jetted, unbeamed sources	High reliability
Variability	All (in principle)	Corona, disk, jet	Host contamination, obscuration, cadence and depth of observations	Low-luminosity

The definitions of some of the terms used in the bias and capability columns are as follows: Efficiency, ability to identify a large number of AGN with relative small total exposure times (this is thus a combination of the nature of AGN emission and the capabilities of current telescopes in a given band). Reliability, the fraction of sources that are identified as AGN using typical criteria that are truly AGN. Completeness*: the ability to detect as much as possible of the full underlying population of AGN. Table reproduced from Padovani et al. (2017), Table 3, with permission of Springer.*

5. THE X-RAY BAND

X-ray emission appears to be one of the defining features of AGN and therefore the X-ray band has proven to be very important for AGN studies. X-rays are deemed to be due to inverse Compton scattering of the accretion-disk photons by an atmosphere above the accretion disk (referred to as the "corona" and whose geometry is still unknown). In jetted AGN the X-rays can have a major contribution from the jet as well. The X-rays then interact with matter by being reflected, scattered, and absorbed by the accretion disk and/or the dust discussed in section 3. X-ray spectra are sensitive to all of these components and, in particular, to the amount of absorbing material, which means they can be also used to classify sources into absorbed (type 2) and unabsorbed (type 1). This is because lower energy X-rays are more easily absorbed than higher energy ones and so the shape of the spectrum depends on the column density $N_{\rm H}$. When $N_{\rm H} > 1.5 \times 10^{24}$ cm^{-2} (in so-called Compton-thick [CT] sources) the source looks completely absorbed in the X-ray band.

X-ray selected AGN, then, include in theory all AGN. However, sources with progressively larger $N_{\rm H}$ will be systematically missed below an increasingly higher energy, until the CT value is reached when all AGN are undetectable in the X-ray band. Low-luminosity AGN with $L_{\rm x} \lesssim 10^{42}$ erg s^{-1} are also biased against as this is the power associated with host galaxy emission. For the same reason at very low soft X-ray fluxes ($f_{0.5-2{\rm keV}} \lesssim 6 \times 10^{-18}$ erg cm^{-2} s^{-1}) contamination from SFGs kicks in. Low-power RGs (i.e., of the LEG type) are also mostly missed since their X-ray jet emission is not very strong and they lack an accretion disk. More details on these topics can be found in section 5 of Padovani et al. (2017).

6. THE γ-RAY BAND

The γ-ray band is conventionally divided into the High Energy (HE) band, between 100 MeV (2.4×10^{22} Hz) and ∼100 GeV (2.4×10^{25} Hz), and the Very High Energy (VHE) band, covering the ∼50 GeV to ∼10 TeV (2.4×10^{27} Hz) range. Different detectors operate in the two bands: in the former we have electron pair-conversion telescopes in space characterized by a very large field of view (FoV; thousands of square degrees) (e.g., AGILE and *Fermi*: Atwood et al., 2009; Tavani et al., 2009); VHE γ-rays, on the other hand, are detected by Imaging Atmospheric Cherenkov Telescopes and Extensive Air Shower observatories on the ground[1] (e.g., Cangaroo, Hess, Magic, Veritas, and HAWC: de Naurois and Mazin, 2015; Abeysekara et al., 2017).

γ-ray astronomy is still a relatively young branch so its number of sources is much smaller compared to the other bands. The Third *Fermi* source catalog (Acero et al., 2015) has detected 3,033 sources all-sky above 100 MeV and up to 300 GeV. AGN make up ≈60%, and possibly ≲90% (including the still unclassified sources), of these. These include only jetted AGN, the large majority of them being blazars with only a handful of RGs. Therefore, the current γ-ray sky is quite similar to the radio-bright sky, which is also dominated by blazars (section 2.1). This is simply because both radio and γ-ray photons are sampling jet-related, non-thermal processes.

[1] These instruments observe at ground level the particle showers that are produced by the interaction of VHE γ-ray photons with the top layers of the atmosphere through the Cherenkov light they create or via the detection of the charged particles in the shower.

The VHE sky is even more sparsely populated, as only ∼200 sources have been detected at TeV energies[2]. Of those ∼35% are AGN, mostly blazars. Blazars, so far, make up ∼92% of the extragalactic γ-ray sky, with the remaining fraction including LEG RGs (∼6%) and SFGs (∼2%).

γ-ray selected AGN, therefore, include only jetted AGN, mostly blazars. There is then an obvious bias against non-jetted AGN, which is simply due, in my opinion, to the fact that these sources lack the engine to produce γ-ray photons (although they could still be *very* weak γ-ray sources through proton-proton collisions [via $pp \rightarrow \pi^0 \rightarrow 2\gamma$: the so-called "pion decay"] thanks to their outflows: Wang and Loeb, 2016; Lamastra et al., 2017).

Although it is clear that γ-rays are produced by relativistic jets, the exact process through which this happens is still not understood. Most researchers favor leptonic processes, where the electrons in the jet inverse Compton scatter their own synchrotron photons (synchrotron self-Compton) or an external photon field (external inverse Compton). In hadronic scenarios, on the other hand, γ-rays are instead thought to stem from high-energy protons either loosing energy through synchrotron emission or through pion decay. In the hadronic case blazars would also produce neutrinos (from charged pions decay) and possibly also cosmic rays becoming therefore multi-messenger sources (e.g., Padovani et al., 2016; Resconi et al., 2017).

7. PUTTING IT ALL TOGETHER

7.1. Making Order Out of Chaos: A Minimalistic Approach to AGN

Figure 2 brings home one of the main points of this paper: different AGN components emit in different bands and only by looking at the broad, multi-wavelength picture can we understand AGN. But different bands gives us also different perspectives and types of sources, which means we need to be fully aware of selection effects. The selection biases and key capabilities (i.e., the weaknesses and the strengths) of all bands discussed above are summarized in **Table 2**.

Based on our current understanding of AGN we can now look back at **Table 1** and see that the complexity it displays is only apparent. It has been known for quite some time that many of the different classes can be explained by taking orientation and the presence (or lack) of a relativistic jet into account. More recent evidence suggests that other parameters play a role, above all the accretion rate (or equivalently $L/L_{\rm Edd}$: see section 8.1 of Padovani et al., 2017 for references). This can change the structure of the accretion flow and thus the SED shape. I am convinced that these three parameters (i.e., orientation, relativistic jet, and accretion rate) explain most of the AGN variety. For example, BL Lacs are LEG RGs with their jets pointing toward the observer and also the radiatively inefficient version (with lower accretion rate and $L/L_{\rm Edd}$) of FSRQs. Additionally, possible second-order parameters include the galaxy environment (e.g., Chiaberge et al., 2015) and the host galaxy, which can also partially obscure the AGN (e.g., Buchner and Bauer, 2017).

[2]http://tevcat.uchicago.edu/

7.2. AGN at All Frequencies

AGN emit over the full electromagnetic spectrum (and possibly even beyond it). The ease with which AGN are detected in the various bands, however, depends essentially on three aspects: (1) astrophysics. As shown by **Figure 2** AGN do not emit at the same level in all bands and the SED is shaped by the various AGN components. The most manifest of these is the presence or absence of a strong relativistic jet, which leads to the distinction between jetted and non-jetted AGN but also modifies the SED substantially (the latter class is weaker in the radio and not present in the γ-ray band). Other effects include changes in the accretion rate (or $L/L_{\rm Edd}$), which can also modify the SED predominantly in the optical/UV and X-ray bands, and obviously obscuration by gas and dust that can absorb emission from the near-IR (NIR) to the soft X-rays; (2) selection effects. AGN selection techniques are not uniformly efficient in the various bands, resulting in (sometimes strong) biases. For example, the host galaxy in the optical, IR, and to some extent the radio band can be particularly luminous making the selection of faint AGN more challenging; host contamination is instead particularly low in the X-ray band; (3) technology. Not all astronomical detectors are equally efficient (it is much harder to catch a high-energy photon than a low-energy one) which means that observations in some wavebands are going to be more sensitive than others relative to the typical AGN SED. For example, contemporary radio telescopes can detect jetted AGN with much smaller bolometric fluxes compared to current γ-ray observatories.

This complex mix of physics, selection effects, and technology is behind the numbers in **Figure 3**, which shows the *largest* AGN surface density over the whole electromagnetic spectrum. Thanks to cutting-edge X-ray observatories and the low contamination from the host galaxy the AGN surface density is largest in the soft X-ray band. And the difficulty of detecting γ-ray photons combined with the fact that only a minority of AGN (the jetted ones) are γ-ray emitters result in a very low surface density in this band. Furthermore, despite being intrinsically radio faint, non-jetted AGN have a surface density in the radio band larger than that reached by the deepest optical surveys and at the same level as the NIR values, which highlights the sensitivity reached by present radio facilities. Since radio observations are unaffected by absorption they are also sensitive to all types of AGN, irrespective of their orientation (i.e., type 1s and type 2s), unlike soft X-ray ones.

Three more considerations (of the many more one could make!) are in order about **Figure 3**: (1) the actual number of *detected and identified* AGN has a wavelength dependence very different from that shown in the figure and is still heavily biased toward the optical/NIR bands, as most AGN were discovered through dedicated large-area spectroscopic surveys. The figure could then be thought of as describing the "detection potential" of the various bands; (2) the largest entry in the figure translates into *at least* ≈1 billion AGN in the Universe that could be detected with current technology. The comparison with the number of *currently known* AGN (of the order of a million: see Figure 6 of Padovani et al., 2017) shows that there is still a lot of room for discovery in future AGN surveys (see section 8); (3) it is worth reflecting on the large financial and human investment behind

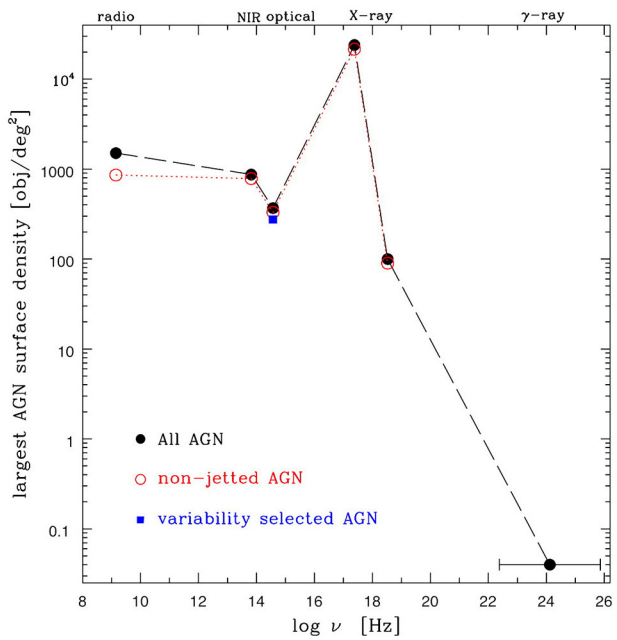

FIGURE 3 | The largest AGN surface density over the whole electromagnetic spectrum. Black filled points refer to all AGN, open red points are for non-jetted AGN. The latter are actually directly measured only in the radio band, while in the NIR to X-ray bands they have been derived by simply subtracting 10% from the total values. Non-jetted AGN have not been detected in the γ-ray band. The blue square indicates variability selected AGN. Updated from Figure 11 of Padovani (2016), where one can find the references to the relevant samples and facilities, to include variability selected AGN and the results of the CDFS 7 Ms sample (Luo et al., 2017). Figure reproduced from Padovani et al. (2017), Figure 21, with permission of Springer.

the figure, which could only be put together thanks to state-of-the-art ground- and space-based facilities (the ones listed in the caption of Figure 11 of Padovani, 2016 do not take into account the multi-wavelength data most of the surveys had to accumulate in order to be able to identify their targets) and the effort of many teams.

8. OPEN ISSUES AND THE NEAR FUTURE

We have learnt a lot about AGN since the discovery of the first quasar in 1963. However, there are still many open questions in AGN research, some of them quite important, to say the least, a comprehensive list of which is given in section 8.4 of Padovani et al. (2017). My favorite topics include:

- Why do a minority of AGN have jets? There are some hints, as jetted AGN *appear* to be more clustered, undergo mergers, reside in more massive, bulge-dominated galaxies (and perhaps spin faster) than non-jetted AGN. But the truth is this is still an unsolved issue.
- What is the composition, geometry, and morphology of the obscuring dust? Recent ground-based mid-IR interferometric observations have suggested that our "standard" (doughnut-like) picture of the so-called dusty torus might not be always valid and that a large fraction of the dust might instead reside in the walls of the ionization cone (e.g., López-Gonzaga et al., 2016, and references therein).
- How does the cosmic history of black hole accretion as traced by AGN compare to the history of star formation in galaxies? More generally, what is the physical connection between SMBH evolution and that of their host galaxies and halos, and are these driven by common processes? This is a very hot topic, which has attracted a lot of attention in the past few years and has important implications for galaxy evolution. Despite this, we still do not have definite answers to these questions.
- Are blazars multi-messenger emitters? Said otherwise, is there a connection between γ-ray emission from jetted AGN, neutrinos and cosmic rays? If so, this would have huge implications for astro-particle physics, solving at the same time the mystery of the origin of (at least some of) the IceCube neutrinos and ultra high-energy cosmic rays detected, amongst others, by the Pierre Auger Observatory and the Telescope Array. It would also constrain theoretical models for particle acceleration in AGN by proving beyond any doubt the existence of very energetic protons.

We will soon have plenty of data to tackle these and other open issues. Here I simply list some of the main future facilities, which we will be having at our disposal in the next few years, sorted by band. Many more details and relevant hyperlinks can be found in Padovani et al. (2017).

- Radio: ASKAP (Australia), MeerKAT (South Africa), e-MERLIN (UK), APERTIF (The Netherlands), and finally the Square Kilometre Array;
- IR: JWST (NASA/ESA), Tokyo Atacama Observatory (Japan), Euclid (ESA/NASA), WFIRST (NASA), SPICA;
- Optical/NIR: Zwicky Transient Facility (USA), LSST, and the giant telescopes namely GMT, TMT, and the ELT;
- X-ray: eROSITA (Germany/Russia), XIPE, and Athena;
- γ-ray: Cherenkov Telescope Array and the Large High Altitude Air Shower Observatory (China).

In terms of AGN science these facilities will open up entire new regions of parameter space, especially with regard to sensitivity and number of sources. Just to give a few numbers: the Evolutionary Map of the Universe, one of the ASKAP surveys, will detect approximately 30 million AGN in the radio band; Euclid will provide NIR spectra for ≈1 million AGN; the LSST will select more than 10 million AGN; eROSITA will provide X-ray data for ≈3 million AGN; and the Cherenkov Telescope Array will detect ∼10 times more blazars than are currently known at TeV energies.

In short, the future of AGN studies is very bright and we will soon be flooded with amazing new data. To take full advantage of them we need to ask the right questions and use the most appropriate and efficient tools.

9. MAIN MESSAGES

The main points of this paper can be thus summarized:

1. Different bands give us different perspectives, different physics, and different types of AGN: one needs to be aware of selection effects!

2. The "AGN zoo" is unnecessarily complex: most of the variety of AGN classes can be explained by three main parameters, namely orientation, presence or lack of relativistic jets, and accretion rate. Second-order parameters might include the environment and the host galaxy.
3. There are two main classes of AGN: jetted and non-jetted (not "radio-loud" and "radio-quiet")!
4. In the next few years we will be flooded with AGN data. We need to be ready for them by: (1) asking the right questions; (2) having the right tools to analyze them.

AUTHOR CONTRIBUTIONS

The author confirms being the sole contributor of this work and approved it for publication.

ACKNOWLEDGMENTS

Many of the concepts discussed here come from Padovani et al. (2017); I thank the co-authors of that paper for their work over many months in writing the review.

REFERENCES

Abeysekara, A. U., Albert, A., Alfaro, R., Alvarez, C., Álvarez, J. D., Arceo, R., et al. (2017). The 2HWC HAWC observatory gamma-ray catalog. *Astrophys. J.* 843:40. doi: 10.3847/1538-4357/aa7556

Acero, F., Ackermann, M., Ajello, M., Albert, A., Atwood, W. B., Axelsson, M., et al. (2015). Fermi large area telescope third source catalog. *Astrophys. J. Suppl.* 218:23. doi: 10.1088/0067-0049/218/2/23

Antonucci, R. (1993). Unified models for active galactic nuclei and quasars. *Ann. Rev. Astron. Astrophys.* 31, 473–521. doi: 10.1146/annurev.aa.31.090193.002353

Atwood, W. B., Abdo, A. A., Ackermann, M., Althouse, W., Anderson, B., Axelsson, M., et al. (2009). The large area telescope on the fermi gamma-ray space telescope mission. *Astrophys. J.* 697, 1071–1102. doi: 10.1088/0004-637X/697/2/1071

Barvainis, R. (1987). Hot dust and the near-infrared bump in the continuum spectra of quasars and active galactic nuclei. *Astrophys. J.* 320, 537–544. doi: 10.1086/165571

Buchner, J., and Bauer, F. E. (2017). Galaxy gas as obscurer - II. Separating the galaxy-scale and nuclear obscurers of active galactic nuclei. *Mon. Not. R. Astron. Soc.* 465, 4348–4362. doi: 10.1093/mnras/stw2955

Chiaberge, M., Gilli, R., Lotz, J. M., and Norman, C. (2015). Radio loud AGNs are mergers. *Astrophys. J.* 806:147. doi: 10.1088/0004-637X/806/2/147

de Naurois, M., and Mazin, D. (2015). Ground-based detectors in very-high-energy gamma-ray astronomy. *C. R. Phys.* 16, 610–627. doi: 10.1016/j.crhy.2015.08.011

Elitzur, M., and Netzer, H. (2016). Disc outflows and high-luminosity true type 2 AGN. *Mon. Not. R. Astron. Soc.* 459, 585–594. doi: 10.1093/mnras/stw657

Elvis, M., Wilkes, B. J., McDowell, J. C., Green, R. F., Bechtold, J., Willner, S. P., et al. (1994). Atlas of quasar energy distributions. *Astrophys. J. Suppl.* 95, 1–68. doi: 10.1086/192093

Harrison, C. (2014). *Observational Constraints on the Influence of Active Galactic Nuclei on the Evolution of Galaxies*. PhD Thesis, Durham University.

Kühr, H., Witzel, A., Pauliny-Toth, I. I. K., and Nauber, U. (1981). A catalogue of extragalactic radio sources having flux densities greater than 1 Jy at 5 GHz. *Astron. Astrophys. Suppl. Ser.* 45, 367–430.

Lamastra, A., Menci, N., Fiore, F., Antonelli, L. A., Colafrancesco, S., Guetta, D., et al. (2017). Extragalactic gamma-ray background from AGN winds and star-forming galaxies in cosmological galaxy formation models. *Astron. Astrophys.* 607:A18. doi: 10.1051/0004-6361/201731452

López-Gonzaga, N., Burtscher, L., Tristram, K. R. W., Meisenheimer, K., and Schartmann, M. (2016). Mid-infrared interferometry of 23 AGN tori: on the significance of polar-elongated emission. *Astron. Astrophys.* 591:A47. doi: 10.1051/0004-6361/201527590

Luo, B., Brandt, W. N., Xue, Y. Q., Lehmer, B., Alexander, D. M., Bauer, F. E., et al. (2017). The chandra deep field-south survey: 7 Ms source catalogs. *Astrophys. J. Suppl.* 228:2. doi: 10.3847/1538-4365/228/1/2

Padovani, P. (2016). The faint radio sky: radio astronomy becomes mainstream. *Astron. Astrophys. Rev.* 24:13. doi: 10.1007/s00159-016-0098-6

Padovani, P. (2017). On the two main classes of active galactic nuclei. *Nat. Astron.* 1, 0194. doi: 10.1038/s41550-017-0194

Padovani, P., Alexander, D. M., Assef, R. J., De Marco, B., Giommi, P., Hickox, R. C., et al. (2017). Active galactic nuclei: what's in a name? *Astron. Astrophys. Rev.* 25, 2. doi: 10.1007/s00159-017-0102-9

Padovani, P., Resconi, E., Giommi, P., Arsioli, B., and Chang, Y. L. (2016). Extreme blazars as counterparts of IceCube astrophysical neutrinos. *Mon. Not. R. Astron. Soc.* 457, 3582–3592. doi: 10.1093/mnras/stw228

Resconi, E., Coenders, S., Padovani, P., Giommi, P., and Caccianiga, L. (2017). Connecting blazars with ultrahigh-energy cosmic rays and astrophysical neutrinos. *Mon. Not. R. Astron. Soc.* 468, 597–606. doi: 10.1093/mnras/stx498

Richards, G. T., Lacy, M., Storrie-Lombardi, L. J., Hall, P. B., Gallagher, S. C., Hines, D. C., et al. (2006). Spectral energy distributions and multiwavelength selection of Type 1 Quasars. *Astrophys. J. Suppl.* 166, 470–497. doi: 10.1086/506525

Tavani, M., Barbiellini, G., Argan, A., Boffelli, F., Bulgarelli, A., Caraveo, P., et al. (2009). The AGILE mission. *Astron. Astrophys.* 502, 995–1013. doi: 10.1051/0004-6361/200810527

Urry, C. M., and Padovani, P. (1995). Unified Schemes for Radio-Loud Active Galactic Nuclei. *Publ. Astron. Soc. Pac.* 107:803. doi: 10.1086/133630

Wang, X., and Loeb, A. (2016). Contribution of quasar-driven outflows to the extragalactic gamma-ray background. *Nat. Phys.* 12, 1116–1118. doi: 10.1038/nphys3837

Conflict of Interest Statement: The author declares that the research was conducted in the absence of any commercial or financial relationships that could be construed as a potential conflict of interest.

Copyright © 2017 Padovani. This is an open-access article distributed under the terms of the Creative Commons Attribution License (CC BY). The use, distribution or reproduction in other forums is permitted, provided the original author(s) or licensor are credited and that the original publication in this journal is cited, in accordance with accepted academic practice. No use, distribution or reproduction is permitted which does not comply with these terms.

frontiers in Astronomy and Space Sciences

ORIGINAL RESEARCH
published: 15 November 2017
doi: 10.3389/fspas.2017.00041

Gaia Space Mission and Quasars

*Tomaž Zwitter**

Faculty of Mathematics and Physics, University of Ljubljana, Ljubljana, Slovenia

Quasars are often considered to be point-like objects. This is largely true and allows for an excellent alignment of the optical positional reference frame of the ongoing ESA mission Gaia with the International Celestial Reference Frame. But presence of optical jets in quasars can cause shifts of the optical photo-centers at levels detectable by Gaia. Similarly, motion of emitting blobs in the jet can be detected as proper motion shifts. Gaia's measurements of spectral energy distribution for around a million distant quasars is useful to determine their redshifts and to assess their variability on timescales from hours to years. Spatial resolution of Gaia allows to build a complete magnitude limited sample of strongly lensed quasars. The mission had its first public data release in September 2016 and is scheduled to have the next and much more comprehensive one in April 2018. Here we briefly review the capabilities and current results of the mission. Gaia's unique contributions to the studies of quasars are already being published, a highlight being a discovery of a number of quasars with optical jets.

Keywords: extragalactic astronomy, active galactic nuclei, quasars, quasar spectral energy distribution, extragalactic radio jets, strong gravitational lensing, astrometry, photometry

OPEN ACCESS

Edited by:
Paola Marziani, Osservatorio Astronomico di Padova (INAF), Italy

Reviewed by:
Maurizio Paolillo, Università degli Studi di Napoli Federico II, Italy
Mary Loli Martínez-Aldama, Instituto de Astrofísica de Andalucía (CSIC), Spain

***Correspondence:**
Tomaž Zwitter
tomaz.zwitter@fmf.uni-lj.si

Specialty section:
This article was submitted to Milky Way and Galaxies, a section of the journal Frontiers in Astronomy and Space Sciences

Received: *28 August 2017*
Accepted: *27 October 2017*
Published: *15 November 2017*

Citation:
Zwitter T (2017) Gaia Space Mission and Quasars. Front. Astron. Space Sci. 4:41. doi: 10.3389/fspas.2017.00041

1. THE GAIA MISSION

Gaia, an ongoing mission of ESA (gaia.esa.int), is conducting a massive all sky optical survey of sources with $0.0 \leq V \leq 20.9$ (for current review of mission properties and its status see Prusti et al., 2016). Brown et al. (2016) published an initial sky chart with 1,142,679,969 sources, which already makes Gaia the largest all-sky survey of celestial objects to date. Gaia is primarily an astrometric mission, positional accuracy at the end of the mission is expected to be between 5 and 400 μas (**Figure 1**), while the spatial resolution is ∼0.1 arc-second (as). This impressive accuracy of position of optical photo-center is mostly photon-noise limited and in many cases supersedes the accuracy of VLBI positions for radio emitting sources. Gaia is continuously scanning the skies. In 5 years of official mission lifetime it will observe each source in the sky transiting its focal plane from 50 to over 200 times, median is 72. Sampling is uneven, with the shortest separations corresponding to two observations within the 6-h spin period of the satellite. Gaia includes three main instruments: astrometry is done in white light (G band, between 330 and 1,050 nm), photometry is collected via weakly dispersed spectra in the blue (BP, blue photometer, 330–680 nm) and red (RP, red photometer, 640–1,050 nm) bands, each sampled in wavelength by 45 pixels. 76% of energy of a sharp line from a point source is spread in the wavelength direction over ∼1.6 pixels (BP) and ∼3.8 pixels (RP). Finally there is a spectroscopic instrument on-board which is collecting spectra in the 845–872 nm range for objects brighter than V ∼15.5 and at a resolving power of 10,500. The main goal of spectroscopic instrument is to determine radial velocities, but for the very bright stars ($V \leq 12$) it will also measure abundances of chemical elements with lines in wavelength range of the spectrograph. Magnitude and wavelength limitations of Gaia's spectroscopic instrument are being complemented by ground-based optical stellar spectroscopic surveys which are aimed to obtain stellar parameters and accurate radial velocities, as well as abundances of individual elements for

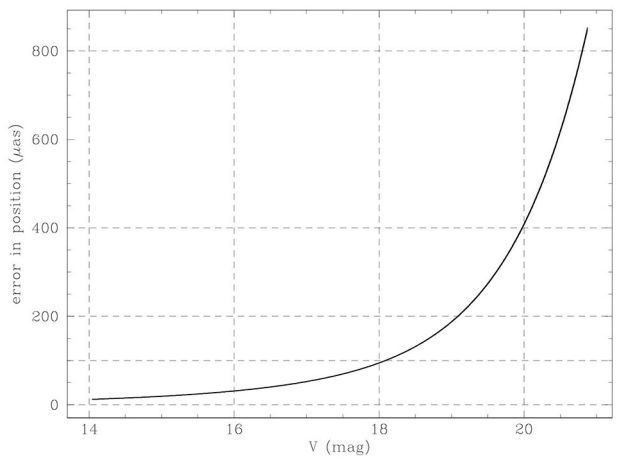

FIGURE 1 | Positional error after a 5-year mission as a function of V magnitude. The latter was derived from Gaia's intrinsic *G* magnitude using the relation $V = 1.02\,G - 0.24$, which is appropriate for quasars with $z \leq 4$ (Proft et al., 2015). Positional error estimate assumes a point-like source and follows Equations (4–7) from Prusti et al. (2016) with $0.54 < V - I < 0.98$.

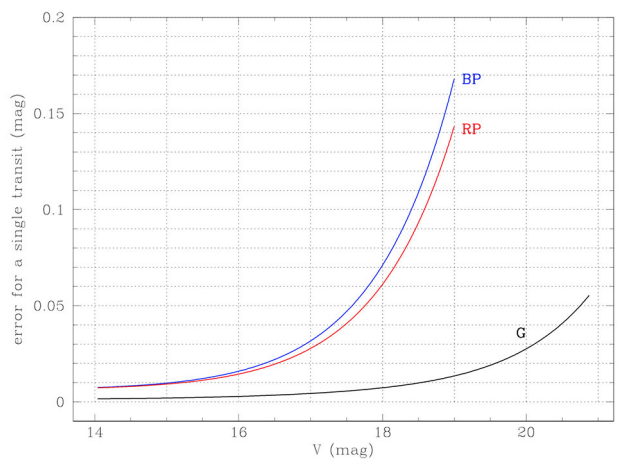

FIGURE 2 | Errors in integrated G (white light), RP (red photometer), and BP (blue photometer) magnitudes per transit, as a function of V magnitude, estimated from G magnitude as explained in **Figure 1**. Errors were estimated from Equations (9–13) in Prusti et al. (2016) using $N_{obs} = 1$. Combining blocks of N_{obs} transits obtained on timescales of days or weeks reduces the errors by $\sqrt{N_{obs}}$.

stars which are not within the reach of Gaia. They can however observe only a small fraction of such sources. The ongoing surveys include RAVE (Kunder et al., 2017, https://www.rave-survey.org/project/), LAMOST (Cui et al., 2012, http://www.lamost.org), Gaia-ESO (Gilmore et al., 2012, https://www.gaia-eso.eu/), and Galah (https://galah-survey.org, de Silva et al., 2015, see also Martell et al. 2017).

2. GAIA AND QUASARS

A vast majority of quasars are fainter than $V \sim 15.5$ so they are not observed by the spectroscopic instrument aboard Gaia, but the mission's astrometry and spectrophotometric BP and RP measurements are extremely relevant for quasar studies. **Figure 1** shows that one may expect a positional accuracy of $\sim$70 μas at $V \sim$17 and $\sim$400 μas at $V \sim$20 at the end of the official 5-year mission lifetime. These figures may actually be too pessimistic, as Gaia performs better than expected on the faint end, and the mission itself may be extended up to 2022 or beyond, therefore increasing the photon budget and time span of its observations. **Figure 2** shows accuracy of integrated magnitudes over the *G*, BP, and RP bands for each transit. It demonstrates the potential of Gaia's $\sim$72 observations of each quasar over a $\sim$5 year timeframe to assess temporal variability for a complete population of quasars down to $V \sim$20 in white light (*G* band). For bright sources ($V < 18$) one can also study color changes on timescales from hours to years, using their integrated BP and RP magnitudes.

BP and RP instruments do not collect only integrated magnitudes but also spectrophotometric information. **Figure 3** shows a typical quasar spectrum (black tracing), and its BP (blue) and RP (red) spectrophotometry collected by Gaia over a 5-year mission. The panels show the signal for objects with apparent magnitude $V = 20$ which have 4 different redshifts between 0.5 and 3.5. Vertical stripe at $\sim$8,600 Å is the wavelength range of Gaia's spectroscopic instrument. In our view the figure, which summarizes simulations of Proft et al. (2015), clearly demonstrates the ability of Gaia to determine photometric redshifts for a complete population of quasars down to $V \sim$20. For brighter objects even changes in their spectral energy distribution (SED) should be detectable. Proft et al. (2015) demonstrate that variability of SDSS 154757.71+060626.6, which has Sloan red magnitude $r' = 17.5$ and redshift $z = 2.03$, is clearly within the reach of Gaia.

Gaia mission observes any object bright enough to trigger its instruments. So the initial quasar catalog with 1,248,372 sources, which was prepared before the launch by Andrei et al. (2014), is only a lower limit of what we may expect to be observed. Properties of the catalog are summarized in **Table 1**. Note the relatively low astrometry precision for most of the quasars. Position is of course more accurately known for 4,866 VLBI sources which are part of the catalog and for additional 38,699 sources with available radio position, although of lower precision.

3. QUASARS IN GAIA'S FIRST DATA RELEASE

Gaia's first data release (Gaia DR1) was published in September 2016 (Brown et al., 2016). It contains

1. Positions, parallaxes (error $\sim$0.3 milli arc-second, hereafter mas) and proper motions (error $\sim$1 mas/yr) for 2 million Hipparcos and Tycho stars;
2. Positions (error $\sim$10 mas) and G magnitudes (error $<$0.03 mag) for 1.1 billion objects ($V \leq 20.9$);
3. G-band light curves and characterization for $\sim$3,000 Cepheids and RR Lyrae stars around the south ecliptic pole.

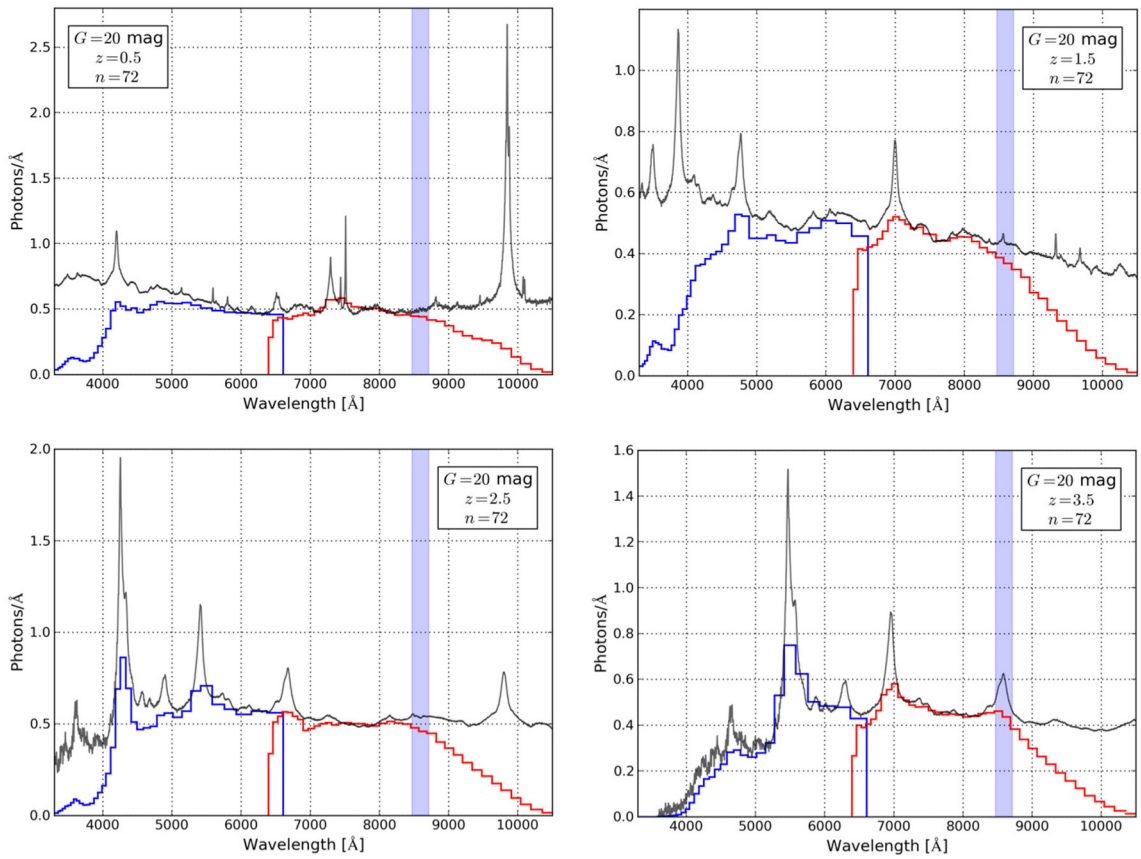

FIGURE 3 | Ability of Gaia to determine redshifts of quasars with $G = 20$ (corresponding to $V \approx 20.2$) after a median of 72 exposures collected over a 5-year mission. From Proft et al. (2015), with permission.

TABLE 1 | Properties of the Initial quasar catalog with numbers of different sources and their expected typical precision, adapted from Andrei et al. (2014).

Number of sources	1,248,372
Sources with magnitude	1,246,512
Sources with redshift	1,157,285
Sources with $G < 20$	371,098
Sources with $G > 21$	690,507
Sources with $z < 1.0$	250,405
Sources with $z > 2.0$	383,487
Astrometry precision (arc sec)	1
Magnitude precision	0.5
Redshift precision	0.01
Average density (sources/deg^2)	30.3
Average neighbor distance (arc sec)	220

Quasars observed within the first data release have been discussed by Lindegren et al. (2016) and Mignard et al. (2016). Main results can be summarized as follows: Some 135,000 quasars from the list of Andrei et al. (2014) were included in the astrometric solution, and their positions were determined with an (inflated) standard uncertainty of 1 mas. Accurately known positions from VLBI were used to align the Gaia DR1 reference frame with the extragalactic radio frame. A special astrometric solution has been computed for selected extragalactic objects with optical counterparts in Gaia DR1, including the ones from the second realization of the International Celestial Reference Frame (ICRF2). Formal standard error for 2,191 such quasars (with $17.6 < V < 20.7$) does not exceed 0.76 mas for 50% and 3.35 mas for 90% of the sources. Alignment of the Gaia DR1 reference frame with the ICRF2 is better than 0.1 mas at epoch 2015.0. The two frames do not rotate to within 0.03 mas/yr. There are now 11,444 objects with VLBI positions, i.e., 3.5-times more than in ICRF2 (Petrov and Kovalev, 2017).

4. OFFSETS BETWEEN GAIA AND VLBI POSITIONS AND EVIDENCE FOR OPTICAL JETS

Lindegren et al. (2016) note that for sources with good optical and radio astrometry they found no indication of physical optical vs. radio offsets exceeding a few tens of mas, in most cases they are less than 1 mas. This in encouraging, as it will permit to build a very accurate common Gaia+radio reference frame in the

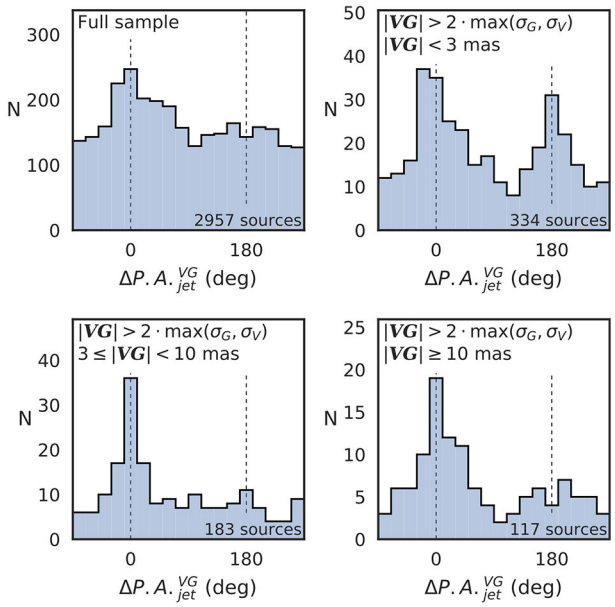

FIGURE 4 | Histograms of differences in position angle ($\Delta P.A.$) between the direction of the radio jet (*jet*) and the direction of the offset (*VG*) from radio to optical position of the source. All but the top-left panel plot only objects with the size of the offset *VG* being at least two times larger than the errors of their VLBI (σ_V) and Gaia (σ_G) positions. Vertical dashed lines indicate aligned and counter-aligned jets. From Kovalev et al. (2017), with permission.

future. But some objects may require further checks. In particular, Makarov et al. (2017) publish a list of 188 objects (out of 2,293 ICRF2 sources), most of them with $z < 0.5$, with offsets up to 1 arcsec, the latter corresponds to a distance of ∼7.5 kpc at z ∼0.5. They propose that 89 of them may be AGNs (quasars and BL Lac) dislodged from their host galaxies' centers.

In a much larger study Petrov and Kovalev (2017) used the whole 1.1 billion object dataset from Gaia DR1 and the VLBI absolute astrometry catalog RFC 2016c to find 6,055 secure matches with AGNs. Kovalev et al. (2017) used this large sample to check on offsets between radio and optical positions. In 2,957 AGNs they were able to determine the direction of the radio jet. They find a significant prevalence of optical and radio offsets in directions along or opposite the one of the radio jet (**Figure 4**). This suggests that strong, extended optical jet structures are present in many AGN. Position offsets along the jet require strong, extended parsec-scale optical jets, while small (<1 mas) offsets in direction opposite to the jet can be due to extended VLBI jet structure or a "core-shift" effect due to synchrotron opacity.

5. CONCLUSIONS

Gaia is living to its promise of revolutionizing virtually any field of astronomy. In case of quasars two of the instruments on board are of particular interest: spectrophotometric BP/RP instrument and astrometric instrument. The former allows studies of SED variability for a complete sample of sources with $V < 18$, and of general brightness variations and photometric redshift determination for all sources brighter than $V \sim 20$. The emphasis is on completeness, and on the ability to discover and characterize yet unknown quasars in this magnitude range. Both present a major advance to current lively research efforts to characterize quasar variability (e.g., Peters et al., 2016; Marziani et al., 2017; Rumbaugh et al., 2017). An obvious importance of astrometry of quasars is to harmonize optical and radio reference frames. Some 135,000 quasars, which were already analyzed within the first data release, already allowed to achieve an unprecedented accuracy of alignment of VLBI radio and optical Gaia reference frames. A small offset between optical and radio position, which is seen in some quasars with well determined directions of radio jets, points to presence of strong, extended optical jets on parsec scales. Spatial resolution of Gaia allows to discover large numbers of gravitationally lensed quasars (Lemon et al., 2017), especially when photometric and spectrophotometric measurements of Gaia are combined with mid-infrared selection, as enabled by the WISE mission (Agnello, 2017).

Gaia observations are ongoing, with the second public data release planned for April 2018. It will include a five-parameter astrometric solutions for all sources with acceptable formal standard errors ($>10^9$ are anticipated), and positions (R.A., Dec.) for sources for which parallaxes and proper motions cannot be derived. Next, it will include G and integrated BP and RP photometric magnitudes for all sources. For sources brighter than $G_{RVS} = 12$ also median radial velocities will be published. Finally for stars brighter than G = 17 there will be estimates of the effective temperature and, where possible, line-of-sight extinction, based on the above photometric data. Of less interest to quasar studies, a list of photometric data for a sample of variable stars and epoch astrometry for a pre-selected list of over 10,000 asteroids will be provided.

There are further planned intermediate public data releases, with the final database to be published some 3 years after the end of observations, which may happen anytime between 2019 and 2023. By then a complete magnitude limited sample of quasars, many of them new, together with their variability, redshift and in many cases optical jets or multiple gravitationally lensed images are bound to be discovered.

AUTHOR CONTRIBUTIONS

The author confirms being the sole contributor of this work and approved it for publication.

ACKNOWLEDGMENTS

The author acknowledges financial support of the Slovenian Research Agency (research core funding No. P1-0188). This research has been partially funded by the European Space Agency contract 4000111918.

REFERENCES

Agnello, A. (2017). Quasar lenses and galactic streams: outlier selection and Gaia multiplet detection. *Month. Notices R. Astron. Soc.* 471, 2013–2021. doi: 10.1093/mnras/stx1650

Andrei, A. H., Antón, S., Taris, F., Bourda, G., Souchay, J., Bouquillon, J., et al. (2014). "The gaia initial quasar catalog," in *Proceedings of the Journées 2013: "Systèmes de référence spatio-temporels*," ed N. Capitaine, 84–87.

Brown, A. G. A., Vallenari, A., Prusti, T., de Bruijne, J. H. J., Mignard, F., Drimmel, R., et al. (2016). Gaia data release 1. Summary of the astrometric, photometric, and survey properties. *Astron. Astrophys.* 595:23. doi: 10.1051/0004-6361/201629512

Cui, X. Q., Zhao, Y. H., Chu, Y. Q., Li, G. P., Li, Q., Zhang, L. P., et al. (2012). The large sky area multi-object fiber spectroscopic telescope (LAMOST). *Res. Astron. Astrophys.* 12, 1197–1242. doi: 10.1088/1674-4527/12/9/003

De Silva, G. M., Freeman, K. C., Bland-Hawthorn, J., Martell, S., de Boer, E. W., Asplund, M., et al. (2015). The GALAH survey: scientific motivation. *Month. Notices R. Astron. Soc.* 449, 2604–2617. doi: 10.1093/mnras/stv327

Gilmore, G., Randich, S., Asplund, M., Binney, J., Bonifacio, P., Drew, J., et al. (2012). The Gaia-ESO public spectroscopic survey. *Messenger* 147, 25–31.

Kovalev, Y. Y., Petrov, L. and Plavin, A. V. (2017). VLBI-Gaia offsets favor parsec-scale jet direction in active galactic nuclei. *Astron. Astrophys.* 598:4. doi: 10.1051/0004-6361/201630031

Kunder, A., Kordopatis, G., Steinmetz, M., Zwitter, T., McMillan, P. J., Casagrande, L., et al. (2017). The radial velocity experiment (RAVE): fifth data release. *Astron. J.* 153:30. doi: 10.3847/1538-3881/153/2/75

Lemon, C. A., Auger, M. W., McMahon, R. G., and Koposov, S. E. (2017). Gravitationally lensed quasars in gaia: I. Resolving small-separation lenses. arXiv:1709.08976.

Lindegren, L., Lammers, U., Bastian, U., Hernández, J., Klioner, S., Hobbs, D., et al. (2016). Gaia data release 1. Astrometry: one billion positions, two million proper motions and parallaxes. *Astron. Astrophys.* 595:32. doi: 10.1051/0004-6361/201628714

Makarov, V. V., Frouard, J., Berghea, C. T., Rest, A., Chambers, K. C., Kaiser, N., et al. (2017). Astrometric evidence for a population of dislodged AGNs. *Astrophys. J. Lett.* 835:6. doi: 10.3847/2041-8213/835/2/L30

Martell, S. L., Sharma, S., Buder, S., Duong, L., Schlesinger, K. J., Simpson, J., et al. (2017). The GALAH survey: observational overview and Gaia DR1 companion. *Month. Notices R. Astron. Soc.* 465:3203. doi: 10.1093/mnras/stw2835

Marziani, P., Bon, E., Grieco, A., Bon, N., Dultzin, D., Del Olmo, A., et al. (2017). "Optical variability patterns of radio-quiet and radio-loud quasars," in *New Frontiers in Black Hole Astrophysics*, *Proceedings of the IAU Symposium*, Vol. 324, 243–244.

Mignard, F., Klioner, S., Lindegren, L., Bastian, U., Bombrun, A., Hernández, J., et al. (2016). Gaia data release 1. Reference frame and optical properties of ICRF sources. *Astron. Astrophys.* 595:16. doi: 10.1051/0004-6361/201629534

Peters, C. M., Richards, G. T., Myers, A. D., Strauss, M. A., Schmidt, K. B., Ivezić, Ž., et al. (2016). Quasar classification using color and variability. *Astrophys. J.* 811:29.

Petrov, L., and Kovalev, Y. Y. (2017). On significance of VLBI/Gaia position offsets. *Month. Notices R. Astron. Soc.* 467, L71–L75. doi: 10.1093/mnrasl/slx001

Proft, S., and Wambsganss, J. (2015). Exploration of quasars with the Gaia mission. *Astron. Astrophys.* 574:11. doi: 10.1051/0004-6361/201323280

Prusti, T., de Bruijne, J. H. J., Brown, A. G. A., Vallenari, A., Babusiaux, C., Bailer-Jones, C. A. L., et al. (2016). The Gaia mission. *Astron. Astrophys.* 595:36.

Rumbaugh, N., Shen, Y., Morganson, E., Liu, X., Banerji, M., McMahon, R. G., et al. (2017). Extreme variability quasars from the Sloan Digital Sky Survey and the Dark Energy Survey. arXiv:1706.07875.

Conflict of Interest Statement: The author declares that the research was conducted in the absence of any commercial or financial relationships that could be construed as a potential conflict of interest.

Copyright © 2017 Zwitter. This is an open-access article distributed under the terms of the Creative Commons Attribution License (CC BY). The use, distribution or reproduction in other forums is permitted, provided the original author(s) or licensor are credited and that the original publication in this journal is cited, in accordance with accepted academic practice. No use, distribution or reproduction is permitted which does not comply with these terms.

frontiers in Astronomy and Space Sciences

PERSPECTIVE
published: 17 October 2017
doi: 10.3389/fspas.2017.00025

Multi-Frequency Databases for AGN Investigation—Results and Perspectives

Giovanni La Mura[1], Marco Berton[1,2], Sina Chen[1], Stefano Ciroi[1], Enrico Congiu[1,2], Valentina Cracco[1], Michele Frezzato[1] and Piero Rafanelli[1]*

[1] Department of Physics and Astronomy, University of Padua, Padua, Italy, [2] Astronomical Observatory of Brera, National Institute for Astrophysics, Milan, Italy

Active Galactic Nuclei (AGNs) are characterized by emission of radiation over more than 10 orders of magnitude in frequency. Therefore, the execution of extensive surveys of the sky, with different types of detectors, is providing the attractive possibility to identify and to investigate the properties of AGNs on very large statistical samples. Thanks to the large spectroscopic surveys that allow detailed investigation of many of these sources, we have the opportunity to place new constraints on the nature and evolution of AGNs and to investigate their relations with the host systems. In this contribution we present the results that can be obtained by using a new interactive catalog that we developed to investigate the range of AGN spectral energy distributions (SEDs). We present simple SED models based on data collected in the catalog and discuss their relations with optical spectra obtained by follow up observations. We compare our findings with the expectations based on the AGN Unification Model, and we discuss the perspectives of multi-wavelength approaches to address AGN related processes such as black hole accretion and acceleration of relativistic jets.

Keywords: galaxies: active, galaxies: nuclei, quasars: emission lines, quasars: supermassive black holes, galaxies: jets, catalogs, surveys

OPEN ACCESS

Edited by:
Deborah Dultzin, National Autonomous University of Mexico, Mexico

Reviewed by:
Andjelka Branislav Kovacevic, University of Belgrade, Serbia
Giovanna Maria Stirpe, Osservatorio Astronomico di Bologna (INAF), Italy

****Correspondence:***
Giovanni La Mura
giovanni.lamura@unipd.it

Specialty section:
This article was submitted to Milky Way and Galaxies, a section of the journal Frontiers in Astronomy and Space Sciences

Received: *07 August 2017*
Accepted: *02 October 2017*
Published: *17 October 2017*

Citation:
La Mura G, Berton M, Chen S, Ciroi S, Congiu E, Cracco V, Frezzato M and Rafanelli P (2017) Multi-Frequency Databases for AGN Investigation—Results and Perspectives. Front. Astron. Space Sci. 4:25. doi: 10.3389/fspas.2017.00025

1. INTRODUCTION

Since their first identification as sources of prominent emission lines from ionized gas in the core of galaxies with exceptionally bright centers (Seyfert, 1943), *Active Galactic Nuclei* (AGNs) became a primary source of discoveries and new challenges in Astrophysics. In addition to being the most energetic non-transient objects that we currently know, maintaining luminosities of the order of $L > 10^{41}\,\mathrm{erg\,s^{-1}}$ for timescales spanning from several thousands up to hundred millions years, they populate both the local and the remote Universe, suggesting that their existence must have a relevant impact on the evolution of cosmic structures. The well known paradigm that identifies their energy source as the conversion of gravitational binding energy of material accreted by a Super Massive Black Hole (SMBH) into radiative power accounts very well for most of their observational properties (Blandford and Znajek, 1977; Blandford, 1986) and it is largely supported by the strong evidence for the existence of SMBHs in the nuclei of all massive galaxies (Magorrian et al., 1998; Ferrarese and Merritt, 2000). It is well established that the process of matter accretion onto SMBHs can give raise to different mechanisms resulting in the production of a complex spectrum of electro-magnetic radiation that, depending on the characteristics of the source, may exhibit various emission and absorption components. Attempts to explain the resulting wealth of

observational features in a single physical picture led to the formulation of the *AGN Unification Model* (Antonucci, 1993; Urry and Padovani, 1995).

In spite of major advances in our understanding of the physics of AGNs, today we still seek the answer of some fundamental questions, such as how nuclear activity is triggered, what role does it play on the evolution of galaxies and which are the most relevant physical processes that govern the mass flow in the close vicinity of the SMBH, controlling the formation of structures like accretion disks and relativistic jets. While waiting for the deployment of instrumental facilities that might directly address part of these questions, such as the *James Webb Space Telescope* (JWST), the *Square Kilometer Array* (SKA), or the *European Extremely Large Telescope* (E-ELT), among others, the approach of testing the properties of AGNs taking advantage of the complexity and the extension of their spectral energy distribution (SED) on large statistical populations is providing very attractive results (Massaro et al., 2011; D'Abrusco et al., 2012).

With this contribution, it is our aim to present an innovative approach to collect multi-frequency information from astronomical databases, in order to identify different types of AGNs. The gathered information can be used in connection with spectroscopic surveys, monitoring experiments and follow-up observations in order to validate the predictions of AGN physical models and to clarify some of the issues that are currently under debate. In the following sections we shall therefore present our work on AGN databases (section 2), discuss its comparison with other existing services (section 3), and finally provide considerations on the results that have so far been achieved, with a mention on their possible development.

2. AN INTERACTIVE AGN MULTI-FREQUENCY OBSERVATION ARCHIVE

By identifying AGNs with objects where the central SMBH of a galaxy is persistently fed by an accretion flow, it can be roughly estimated that, from the highest power Quasi Stellar Object (QSO) to the much dimmer Low-Ionization Nuclear Emission Region (LINER), approximately 10% of all galaxies host some kind of nuclear activity. The task to collect into a single catalog the most fundamental information, such as position, distance, apparent magnitude and luminosity estimates, becomes itself a non trivial problem with the resulting numbers. The *Catalog of Quasars and Active Galactic Nuclei* (Véron-Cetty and Véron, 2010), in its 13th edition, represented a major attempt to assemble a systematic list of active galaxies, providing basic information. With its 168,480 main entries, however, it represents only a small fraction of the millions potentially detectable sources, as demonstrated by Flesch (2015). In addition to designing an effective scheme to handle the catalog contents, the large number of entries implies a coarse classification of objects with a non-negligible chance to overlook important features or to fail in spotting unreliable measurements.

It is now clear that in the case of AGNs a proper and physically meaningful classification is fundamental, both for our current understanding, as well as for its development perspectives. The execution of large survey and monitoring programs with publicly available spectroscopic observations, such as the Sloan Digital Sky Survey (York et al., 2000; Alam et al., 2015, SDSS) and the 6dF Galaxy Redshift Survey (Jones et al., 2004, 2009, 6dFGS), combined with the deployment of instruments able to explore the electromagnetic radiation with unprecedented sensitivity and resolution, especially in the energies of the X rays and above, now provide the possibility to probe the physics of many objects in very high detail. Taking advantage of the increase in the computational power and in the efficiency of data transmission networks available to final users, which characterized the technological progress of the last years, we explored the possibility to develop a new strategy to collect multi-frequency data and to use them for the investigation of AGNs. Due to the complex mechanisms that are involved in the emission of their radiation, generally resulting from the combination of both thermal and non-thermal processes, the SEDs of AGNs often span several orders of magnitude in frequency, effectively distinguishing these objects from quiescent and star-forming galaxies, whose emission is mostly confined in the IR-optical-UV range. The use of this property, however, is not always the best option to search for AGNs, since intrinsic or external absorption processes can lead to the loss of important frequency ranges. Limiting the analysis to very specific radiation bands, on the other hand, may lead to substantial selection effects and, therefore, restrict the scope of investigations to under-representative samples. Some additional methods to detect AGNs rely on variability investigations, but again they are prone to the observability constraints of the selected frequency and they can be considerably expensive, in terms of observational efforts, due to the necessity to monitor many targets on a regular schedule.

In order to overcome, at least in part, the difficulties listed above, we explored the possibility of building an interactive AGN observation catalog, named AGN Multi-Wavelength Catalog (AGNMWC), that users can tune with minimal effort to match their specific requirements. Because our aim has been to set up an instrument that can manage large sets of information, without losing the possibility to explore single objects in detail, we adopted a structured database architecture, as our strategy to store data, and we developed a client application, written in Java language, to grant compliance with any operating system hosting a Java Runtime Environment (JRE). The innovative aspect of this solution is that it is not constrained to access a specific data source, which might become outdated or unavailable, but it allows the user to build customized catalogs, using data from virtually any source, provided that the correct information on how to manage the input is given. The adopted strategy is to connect to an SQL database, presently managed either by *MySQL* or *SQL Server*, that must be available on the user's workstation or through network or Internet connection. The Java application is therefore used to import data selected by the user and to build a multi-frequency catalog in the database where every data source is associated with a set of customizable options that define what type of information is being stored. The application also connects

through the Internet to the SDSS and the 6dF spectroscopic databases, to visualize spectral previews, if available, and to the Digitized Sky Survey, to show maps of the sources in the optical *R* band.

3. COMPARISON WITH EXISTING CATALOGS AND ON-LINE SERVICES

One of the key features of scientific investigation is the repeatability of experiences. In the case of Astrophysics this requirement can hardly be matched, because many observations, especially those obtained by space-born detectors, are prone to a continuous deterioration of the instrument. Moreover, the study of variable sources, like many processes connected with AGN activity, is often related to unpredictable situations, which rarely repeat under similar conditions. For these reasons, the possibility to repeat experiences is generally replaced with an accurate knowledge of the observation target and of the conditions of instruments at the time of the observation. Holding such information is the main goal of the data archives maintained by most observatories and experiment collaborations. In general, each instrument has its own characteristics, which require different calibrating information and reduction approaches, in order to extract the final data products. Replicating such information to meet the requirements of different users, or communicating it upon request, usually leads to large costs in terms of data storage or transmission efficiency.

In recent times, thanks especially to a fast increase in the efficiency of data transmission networks, several tools have been developed, which connect different types of archives. These tools lead to the collection of high-level data products, offering selective and customizable output. Very well known examples are the Nasa Extragalactic Database (NED)[1] and the Vizier service[2], which, connecting different catalogs and data sources are able to plot SEDs and to connect to external spectroscopic servers (chiefly the SDSS and the 6dF databases). More recently, the *Virtual Observatory* project[3] attempted the creation of a more interactive environment, providing tools to inspect raw and calibrated data from various archives. Other mission specific tools to analyze data at various levels are provided, for instance, by the High Energy Astrophysic Science Archive Center (HEASARC)[4] and the Italian Space Agency Science Data Center (ASDC)[5], which additionally proposes powerful tools to fit analytical models to specific types of SEDs. The possibility to build a catalog of multi-frequency AGN observations based on the contemporary availability of data has also been thoroughly explored (Padovani et al., 1997).

All of the aforementioned solutions are particularly useful either to perform detailed investigations of single targets or to quickly manage large data samples, but they often cannot work as effectively in both modes, or provide a customizable and easy to update solution. The choice to set up a new archive interface, therefore, descends from the importance of collecting data from the large archives of AGN observations that we currently possess, while maintaining the ability to develop customizable access to advanced information, such as spectroscopy and time resolution. All such features should be combined with the ability to perform statistical studies of SEDs, fitted through combinations of thermal and non-thermal radiation sources.

4. RESULTS AND PERSPECTIVES

Due to the complex combination of thermal and non-thermal contributions that participate to their spectrum, involving black-body radiation from the accretion disk, synchrotron emission from relativistic plasmas and inverse Compton scattering of seed photons in the disk corona and possibly in jets, AGNs are commonly detected over a broad range of frequencies. As a result AGNs are often characterized by a high-energy radiation excess and X-ray surveys are very effective to identify them. Moreover they are the dominant population of extragalactic sources in the range of γ-ray emission (Acero et al., 2015). Taking advantage of the availability of spectroscopic surveys, we are able to investigate the SED properties of multi-frequency emitters, in connection with the optical spectroscopic properties that lead us to identify the existence of a specific type of nuclear activity. **Figure 1** illustrates an example application of AGNMWC to set up such kind of investigation. Starting from the 2nd ROSAT all sky survey catalog (2RXS, Boller et al., 2016) and requiring coincident detections in the WISE, GALEX, and USNO (Monet et al., 2003) at an angular separation of $r < 15$ arcsec (to account for the limited spatial resolution of ROSAT), we select 53,683 sources with multi-frequency detection, distributed at high galactic latitude. Using AGNMWC to import observations obtained from the data sources listed in **Table 1**, we are able to reconstruct the SED of targets and to model their features in terms of power-law and black-body components. By comparing the models of different types of sources, we can immediately appreciate how the transition from Type 1 to Type 2 objects occurs in a consistent way with the expected effects of an increasing amount of obscuration toward the central source. The case of 3C 273, a prototypical Type 1 QSO belonging to the Flat Spectrum Radio Quasar (FSRQ) blazar family, is a fair example of AGN SED with prominent non-thermal emission and a clear signature of a thermal excess, having an estimated temperature of $2.58 \cdot 10^4$ K, in very good agreement with the expectations for an AGN seen without significant obscuration toward the central engine. Conversely, in the SED of NGC 1068, a Type 2 source that has well established evidence for a hidden Broad Line Region (BLR, Antonucci and Miller, 1985), the non-thermal contribution is energetically overwhelmed by the thermal emission of an optically thick obscuring structure that absorbs most of the ionizing radiation of the central source, with just the exception of the highest energy, more penetrating photons, and radiates it back isotropically, in the form of an IR bump. The search of similar features in the SEDs of objects detected at various frequencies leads to the identification of AGN candidates located at high Galactic latitudes all over the sky.

[1] https://ned.ipac.caltech.edu/
[2] http://vizier.u-strasbg.fr/viz-bin/VizieR
[3] http://www.ivoa.net/index.html
[4] https://heasarc.gsfc.nasa.gov/
[5] https://tools.asdc.asi.it/

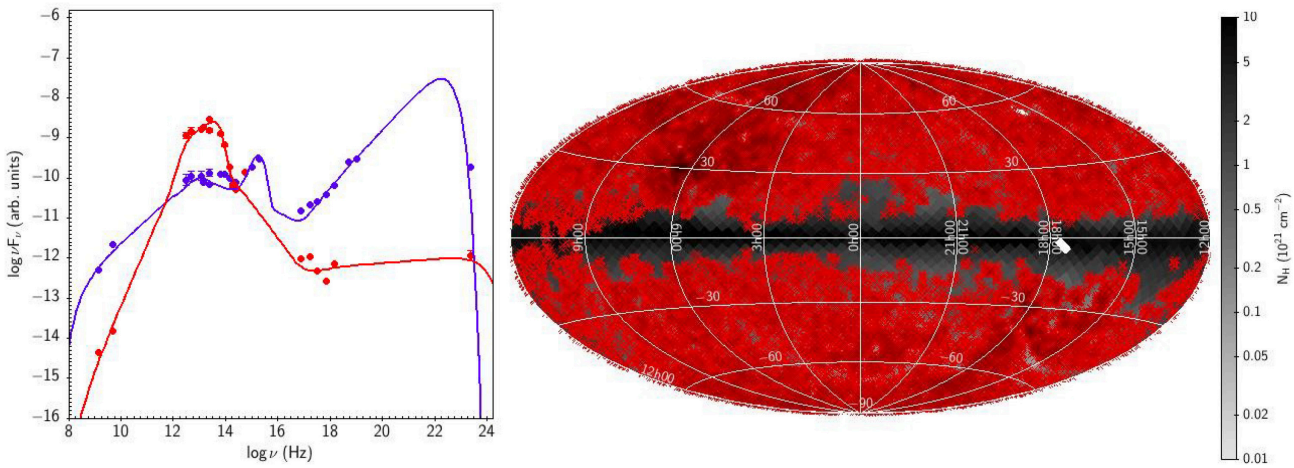

FIGURE 1 | (Left) Examples of SED models for proto-typical Type 1 (3C 273, blue points and continuous curve) and Type 2 (NGC 1068, red points and continuous curve) obtained from the cross-match of NVSS, WISE, IRAS, 2MASS, USNO B2, GALEX, XMM-Newton, INTEGRAL, and Fermi/LAT data. The SEDs have been modeled through the combination of three exponential cut-off power laws and a black-body contribution and normalized to the same optical flux. We note the energetically dominant non-thermal emission with a hot UV thermal contribution in the case of the Type 1 SED, compared to the IR thermal excess due to radiation reprocessing in the warm obscuring medium of the Type 2 source. **(Right)** Aitoff projected distribution of 53,683 sources, selected on the basis of detected emission over the frequency range spanning from IR to X rays, plotted in galactic coordinates over a gray-scale map of HI column density in the Milky Way. Absorption of radiation and source confusion are still the main issues affecting the detection of extragalactic objects close to the Galactic plane.

TABLE 1 | Data sources for the selection of multi-wavelength SED points.

Instr./catalog	log ν (Hz)	Band	References
SUMSS	8.93	Radio	Mauch et al., 2003
NVSS	9.15	Radio	Condon et al., 1998
IRAS	12.48 – 13.40	FIR	Helou and Walker, 1988
WISE	13.13 – 13.94	FIR	Cutri et al., 2012
2MASS	14.14 – 14.38	NIR	Skrutskie et al., 2006
GALEX	15.00 – 15.30	UV	Bianchi et al., 2011
ROSAT	16.86 – 17.23	Soft-X	Boller et al., 2016
XMM-Newton	16.86 – 18.16	X rays	Rosen et al., 2016
INTEGRAL	18.70 – 19.00	Soft γ rays	Bird et al., 2010
Fermi/LAT	23.00 – 26.00	γ rays	Acero et al., 2015

The distribution of such objects strongly argues in favor of their extragalactic origin and the AGN nature can be directly assessed, if the source lies in the footprint of a spectroscopic survey or it can be associated to an optical counterpart for spectroscopic follow-up. Looking at the sources located in the footprint of the SDSS-DR 12, we find 6,127 objects with spectra, out of which 5,901 are spectroscopically confirmed AGNs, while the remaining are mainly interacting star systems. By requiring that the X-ray spectra of the sources are dominated by a power-law contribution, we reduce to a total number of 2,389 sources, 2,300 out of which are confirmed active galaxies. Similar methods have been widely used in the literature (e.g., Massaro et al., 2014, 2015; Alvarez Crespo et al., 2016a,b,c), and they were specifically adapted in our catalogs to investigate the nature of unclassified γ-ray sources (Chiaro et al., 2016; La Mura et al., 2017).

An additional advantage of developing a customizable service to investigate the multi-wavelength properties of AGNs stems from the possibility to explore time domain properties. Indeed, one of the most striking properties of AGNs, particularly in the case of Type 1 sources and especially for blazars, is a strong and mostly irregular variability. The origin of this behavior is related to the details of the accretion process in the central engine and the influence of changes in one spectral component on the others may lead to unveil the structure of the source beyond the current limits of observational resolution (Blandford and McKee, 1982; Peterson, 1998). An example of such application is illustrated in **Figure 2**, for the case of the FSRQ blazar 3C 345 (Berton et al., 2017). During the period monitored by the Fermi/LAT γ-ray telescope between August 2008 and October 2016, this source showed a significant decrease of high-energy activity, which, in spite of the occurrence of strong outbursts, apparently involved its overall emission. Like many other blazars, its SED is energetically dominated by the non-thermal processes arising in the jet and the observed decrease in luminosity might be interpreted as a loss of jet power. The ejection of new relativistic plasma blobs, reported by VLBI radio observations in correspondence with some flares represents episodic breaks in this general trend, which, in some cases, appears to affect other spectral components, like the prominent broad Mg II λ2798 emission line. This line, which in general shows a well defined anti-correlation between equivalent width and continuum intensity (i.e., a Baldwin Effect, Baldwin, 1977; Pogge and Peterson, 1992), exhibited a strong variation shortly after a γ-ray flare without any evidence of changes in the underlying continuum, suggesting that the flare occurred very close to the central SMBH and within the BLR. A subsequent analysis of its spectrum and SED shows that, while moving from

the maximum activity to the minimum observed during the monitoring, the source featured a decrease of jet emission power, but a relevant enhancement in the relative importance of the thermal component, for which we also observe a slight increase of temperature. A possible explanation of such a behavior may reside in the fact that the processes, which feed power to the jet, are likely slowing the accretion rate. In such circumstances, it could be possible that the ejection of a plasma blob from very close to the black hole affects the coupling of jet and accretion disk, favoring the accretion flow with respect to the jet immediately after the outburst. Clearly much more investigation of similar processes in this and other sources is required to verify this possibility. A summary of the models that were used to reconstruct the illustrated SEDs is reported in **Table 2**.

In order to take full advantage of the opportunity to investigate AGN SEDs with the wealth of available observing

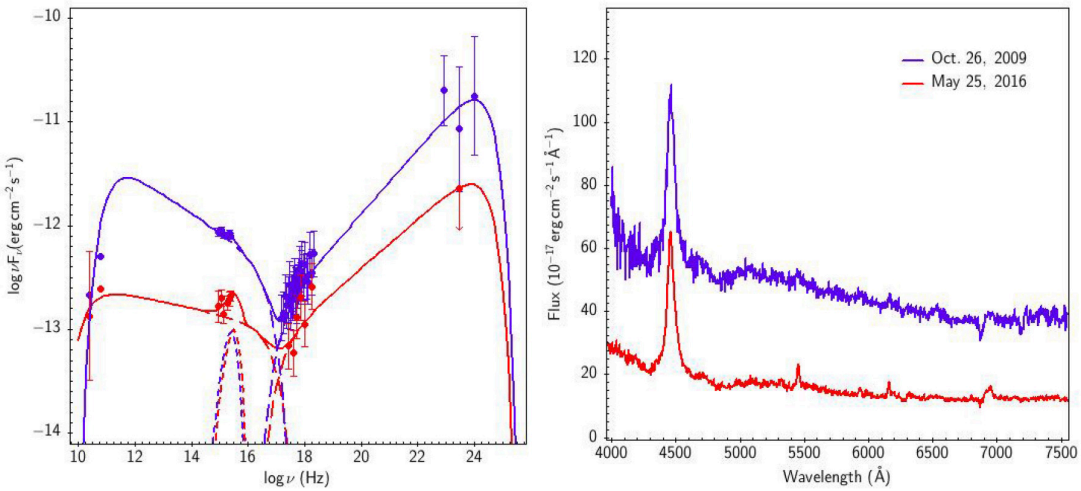

FIGURE 2 | SED fits **(left)** and corresponding optical spectra **(right)** of the FSRQ blazar 3C 345 observed during a high state (October 26, 2009; blue points and lines) and a low state (May 25, 2016; red points and line). Non-thermal power laws have been represented as long-dashed lines, while short-dashed curves are thermal contributions. Solid lines are used to show total models. The power-law dominance for this object suggests that the main source of radiation probably arises from the relativistically beamed contribution of the jet, as expected for blazars. In the low activity state, however, a slight but sensible increase in the relative importance of the thermal component can be appreciated, suggesting that a weaker jet activity is likely being associated with an increased accretion efficiency and a higher temperature of the accretion disk.

TABLE 2 | SED fitting models.

Object	Function	log $\nu^{(a)}_{min}$	log $\nu^{(a)}_{max}$	Norm.	Index$^{(b)}$	Temp.	χ^2_{red}
3C 273	Power law	8.6	13.1	$2.30 \cdot 10^{-18}$	0.60	–	
	Power law	13.1	17.6	$1.31 \cdot 10^{-6}$	−0.31	–	
	Power law	17.1	22.6	$1.26 \cdot 10^{-23}$	0.70	–	
	Black body	–	–	$1.03 \cdot 10^{-12}$	–	25,800 K	1.11
NGC 1068	Power law	8.5	13.0	$2.49 \cdot 10^{-28}$	1.52	–	
	Power law	12.8	17.5	$7.068 \cdot 10^{2}$	−0.85	–	
	Power law	17.0	24.0	$4.82 \cdot 10^{-13}$	0.05	–	
	Black body	–	–	$1.04 \cdot 10^{-4}$	–	540 K	1.17
3C 345 (high)	Power law	11.0	16.8	$5.193 \cdot 10^{-10}$	−0.19	–	
	Power law	17.0	24.5	$8.28 \cdot 10^{-19}$	0.31	–	
	Black body	–	–	$7.51 \cdot 10^{-17}$	–	31,340 K	1.05
3C 345 (low)	Power law	10.1	17.0	$1.096 \cdot 10^{-12}$	−0.06	–	
	Power law	17.0	24.5	$7.07 \cdot 10^{-18}$	0.24	–	
	Black body	–	–	$3.38 \cdot 10^{-17}$	–	38, 630 K	1.06

[(a)] *Logarithm of exponential cut-off frequency given in Hz.*
[(b)] *The power-law index is given according to the notation* $\nu F_\nu \propto \nu^\alpha$.

material, we are currently developing our interactive catalog tools in the framework of possible connections with an ever increasing number of online services and particularly matching the procedural strategies of the Virtual Observatory. Although several opportunities to improve AGNMWC can still be pursued, especially with the inclusion of more detailed physical models to fit the target SEDs and the introduction of more suitable stand-alone solutions that may rely on lighter requirements on the connection with SQL driven databases, we maintain a test suite of the tool at the URL address: https://1drv.ms/u/s!AngiMxTxSRoxgjnYsXm3-DuHub2u that is used for testing and development purposes. The online package includes the Java client application, the example catalog described in this study and a technical description illustrating the procedures to build a compliant database. Its system requirements are limited to the presence of a JRE v1.6 or above and to the possibility to connect to an SQL database managed either by MySQL v5.6.19 or by MS SQL Server 2008, or following releases.

AUTHOR CONTRIBUTIONS

GL is the developer of the AGN Multi-Wavelength Catalog, PI of AGN selection procedures in databases and author of the manuscript's text. MB is PI of the AGN monitoring programs that provided data on 3C 345. SCh contributed to source association and spectroscopic follow-up in the Southern Hemisphere, SC contributed as data reduction specialist, EC, VC, MF contributed multi-wavelength data analysis, target selection and SED modeling, while PR is the concept creator for the Multi-Wavelength Catalog and the scientific supervisor of the project. All authors contributed to text revision and improvement.

FUNDING

Funding for this research program has been provided by the Department of Physics and Astronomy of the University of Padua and by the European Space Agency (ESA), under Express Procurement Contract No. 4000111138/14/NL/CB/gp. Additional support from ASTROMUNDUS mobility grants is also gratefully acknowledged.

ACKNOWLEDGMENTS

We gratefully thank Dr. Stirpe and Dr. Kovačević for discussion and comments leading to the improvement of this work. This research has made use of the NASA/IPAC Extragalactic Database (NED) which is operated by the Jet Propulsion Laboratory, California Institute of Technology, under contract with the National Aeronautics and Space Administration.

Funding for the Sloan Digital Sky Survey IV has been provided by the Alfred P. Sloan Foundation, the U.S. Department of Energy Office of Science, and the Participating Institutions. SDSS acknowledges support and resources from the Center for High-Performance Computing at the University of Utah. The SDSS web site is www.sdss.org.

SDSS is managed by the Astrophysical Research Consortium for the Participating Institutions of the SDSS Collaboration including the Brazilian Participation Group, the Carnegie Institution for Science, Carnegie Mellon University, the Chilean Participation Group, the French Participation Group, Harvard-Smithsonian Center for Astrophysics, Instituto de Astrofísica de Canarias, The Johns Hopkins University, Kavli Institute for the Physics and Mathematics of the Universe (IPMU)/University of Tokyo, Lawrence Berkeley National Laboratory, Leibniz Institut für Astrophysik Potsdam (AIP), Max-Planck-Institut für Astronomie (MPIA Heidelberg), Max-Planck-Institut für Astrophysik (MPA Garching), Max-Planck-Institut für Extraterrestrische Physik (MPE), National Astronomical Observatories of China, New Mexico State University, New York University, University of Notre Dame, Observatório Nacional/MCTI, The Ohio State University, Pennsylvania State University, Shanghai Astronomical Observatory, United Kingdom Participation Group, Universidad Nacional Autónoma de México, University of Arizona, University of Colorado Boulder, University of Oxford, University of Portsmouth, University of Utah, University of Virginia, University of Washington, University of Wisconsin, Vanderbilt University, and Yale University.

This work is based on observations collected at Copernico telescope (Asiago, Italy) of the INAF - Osservatorio Astronomico di Padova and on observations collected with the 1.22 m *Galileo* telescope of the Asiago Astrophysical Observatory, operated by the Department of Physics and Astronomy "G. Galilei" of the University of Padova.

REFERENCES

Acero, F., Ackermann, M., Ajello, M., Albert, A., Atwood, W. B., Axelsson, M., et al. (2015). Fermi large area telescope third source catalog. *Astrophys. J. Suppl. Ser.* 218:23. doi: 10.1088/0067-0049/218/2/23

Alam, S., Albareti, F. D., Allende Prieto, C., Anders, F., Anderson, S. F., Anderton, T., et al. (2015). The eleventh and twelfth data releases of the sloan digital sky survey: final data from SDSS-III. *Astrophys. J. Suppl. Ser.* 219:12. doi: 10.1088/0067-0049/219/1/12

Alvarez Crespo, N., Masetti, N., Ricci, F., Landoni, M., Patiño-Alvarez, V., Massaro, F., et al. (2016a). Optical spectroscopic observations of gamma-ray blazar candidates. V. TNG, KPNO, and OAN observations of blazar candidates of uncertain type in the Northern Hemisphere. *Astron. J.* 151:32. doi: 10.3847/0004-6256/151/2/32

Alvarez Crespo, N., Massaro, F., D'Abrusco, R., Landoni, M., Masetti, N., Chavushyan, V., et al. (2016b). Optical archival spectra of blazar candidates of uncertain type in the 3rd Fermi Large Area Telescope Catalog. *Astrophys. Space Sci.* 361:316. doi: 10.1007/s10509-016-2902-1

Alvarez Crespo, N., Massaro, F., Milisavljevic, D., Landoni, M., Chavushyan, V., Patiño-Alvarez, V., et al. (2016c). Optical spectroscopic observations of gamma-ray blazar candidates. VI. Further observations from TNG, WHT, OAN, SOAR, and Magellan Telescopes. *Astron. J.* 151:95. doi: 10.3847/0004-6256/151/4/95

Antonucci, R. (1993). Unified models for active galactic nuclei and quasars. *Ann. Rev. Astron. Astrophys.* 31, 473–521. doi: 10.1146/annurev.aa.31.090193.002353

Antonucci, R. R. J., and Miller, J. S. (1985). Spectropolarimetry and the nature of NGC 1068. *Astrophys. J.* 297, 621–632. doi: 10.1086/163559

Baldwin, J. A. (1977). Luminosity indicators in the spectra of Quasi-Stellar objects. *Astrophys. J.* 214, 679–684. doi: 10.1086/155294

Berton, M., Liao, N. H., La Mura, G., Järvelä, E., Congiu, E., Foschini, L., et al. (2017). The FSRQ 3C 345 from the high to the low emission state. ArXiv e-prints.

Bianchi, L., Herald, J., Efremova, B., Girardi, L., Zabot, A., Marigo, P., et al. (2011). GALEX catalogs of UV sources: statistical properties and sample science applications: hot white dwarfs in the Milky Way. *Astrophys. Space Sci.* 335, 161–169. doi: 10.1007/s10509-010-0581-x

Bird, A. J., Bazzano, A., Bassani, L., Capitanio, F., Fiocchi, M., Hill, A. B., et al. (2010). The fourth IBIS/ISGRI soft gamma-ray survey catalog. *Astrophys. J. Suppl. Ser.* 186, 1–9. doi: 10.1088/0067-0049/186/1/1

Blandford, R. D. (1986). "Black hole models of quasars," in *Quasars*, volume 119 *of IAU Symposium*, eds G. Swarup and V. K. Kapahi, 359–368. doi: 10.1007/978-94-009-4716-0_87

Blandford, R. D., and McKee, C. F. (1982). Reverberation mapping of the emission line regions of Seyfert galaxies and quasars. *Astrophys. J.* 255, 419–439. doi: 10.1086/159843

Blandford, R. D., and Znajek, R. L. (1977). Electromagnetic extraction of energy from Kerr black holes. *Month. Notices RAS* 179, 433–456. doi: 10.1093/mnras/179.3.433

Boller, T., Freyberg, M. J., Trümper, J., Haberl, F., Voges, W., and Nandra, K. (2016). Second ROSAT all-sky survey (2RXS) source catalogue. *Astron. Astrophys.* 588:A103. doi: 10.1051/0004-6361/201525648

Chiaro, G., Salvetti, D., La Mura, G., Giroletti, M., Thompson, D. J., and Bastieri, D. (2016). Blazar flaring patterns (B-FlaP) classifying blazar candidate of uncertain type in the third Fermi-LAT catalogue by artificial neural networks. *Month. Notices RAS* 462, 3180–3195. doi: 10.1093/mnras/stw1830

Condon, J. J., Cotton, W. D., Greisen, E. W., Yin, Q. F., Perley, R. A., Taylor, G. B., et al. (1998). The NRAO VLA sky survey. *Astron. J.* 115, 1693–1716. doi: 10.1086/300337

Cutri, R. M., Wright, E. L., Conrow, T., Bauer, J., Benford, D., Brandenburg, H., et al. (2012). *Explanatory Supplement to the WISE All-Sky Data Release Products*. Technical report. Infrared Processing and Analysis Center IPAC-CalTech.

D'Abrusco, R., Massaro, F., Ajello, M., Grindlay, J. E., Smith, H. A., and Tosti, G. (2012). Infrared colors of the Gamma-Ray-detected blazars. *Astrophys. J.* 748:68. doi: 10.1088/0004-637X/748/1/68

Ferrarese, L., and Merritt, D. (2000). A fundamental relation between supermassive black holes and their host galaxies. *Astrophys. J. Lett.* 539, L9–L12. doi: 10.1086/312838

Flesch, E. W. (2015). The half million quasars (HMQ) catalogue. *Publ. Astron. Soc. Aust.* 32:e010. doi: 10.1017/pasa.2015.10

Helou, G., and Walker, D. W., (eds.). (1988). *Infrared Astronomical Satellite (IRAS) Catalogs and Atlases. Volume 7: The Small Scale Structure Catalog*. Washington, DC: NASA.

Jones, D. H., Read, M. A., Saunders, W., Colless, M., Jarrett, T., Parker, Q. A., et al. (2009). The 6dF galaxy survey: final redshift release (DR3) and southern large-scale structures. *Month. Notices RAS* 399, 683–698. doi: 10.1111/j.1365-2966.2009.15338.x

Jones, D. H., Saunders, W., Colless, M., Read, M. A., Parker, Q. A., Watson, F. G., et al. (2004). The 6dF galaxy survey: samples, observational techniques and the first data release. *Month. Notices RAS* 355, 747–763. doi: 10.1111/j.1365-2966.2004.08353.x

La Mura, G., Busetto, G., Ciroi, S., Rafanelli, P., Berton, M., Congiu, E., et al. (2017). Relativistic plasmas in AGN jets. From synchrotron radiation to γ-ray emission. *Eur. Phys. J. D* 71:95. doi: 10.1140/epjd/e2017-70745-2

Magorrian, J., Tremaine, S., Richstone, D., Bender, R., Bower, G., Dressler, A., et al. (1998). The demography of massive dark objects in galaxy centers. *Astron. J.* 115, 2285–2305. doi: 10.1086/300353

Massaro, F., D'Abrusco, R., Ajello, M., Grindlay, J. E., and Smith, H. A. (2011). Identification of the infrared non-thermal emission in blazars. *Astrophys. J. Lett.* 740:L48. doi: 10.1088/2041-8205/740/2/L48

Massaro, F., Landoni, M., D'Abrusco, R., Milisavljevic, D., Paggi, A., Masetti, N., et al. (2015). Optical spectroscopic observations of γ-ray blazar candidates. II. The 2013 KPNO campaign in the northern hemisphere. *Astron. J.* 575:A124. doi: 10.1051/0004-6361/201425119

Massaro, F., Masetti, N., D'Abrusco, R., Paggi, A., and Funk, S. (2014). Optical spectroscopic observations of blazars and γ-Ray blazar candidates in the sloan digital sky survey data release nine. *Astron. J.* 148:66. doi: 10.1088/0004-6256/148/4/66

Mauch, T., Murphy, T., Buttery, H. J., Curran, J., Hunstead, R. W., Piestrzynski, B., et al. (2003). SUMSS: a wide-field radio imaging survey of the southern sky - II. The source catalogue. *Month. Notices RAS* 342, 1117–1130. doi: 10.1046/j.1365-8711.2003.06605.x

Monet, D. G., Levine, S. E., Canzian, B., Ables, H. D., Bird, A. R., Dahn, C. C., et al. (2003). The USNO-B catalog. *Astron. J.* 125, 984–993. doi: 10.1086/345888

Padovani, P., Giommi, P., and Fiore, F. (1997). A multifrequency database of active galactic nuclei. *Mem. Soc. Astron. Ital.* 68:147.

Peterson, B. M. (1998). Reverberation mapping of active nuclei. *Adv. Space Res.* 21, 57–66. doi: 10.1016/S0273-1177(97)00614-5

Pogge, R. W., and Peterson, B. M. (1992). The intrinsic nature of the Baldwin effect. *Astron. J.* 103, 1084–1088. doi: 10.1086/116127

Rosen, S. R., Webb, N. A., Watson, M. G., Ballet, J., Barret, D., Braito, V., et al. (2016). The XMM-Newton serendipitous survey. VII. The third XMM-Newton serendipitous source catalogue. *Astron. Astrophys.* 590:A1. doi: 10.1051/0004-6361/201526416

Seyfert, C. K. (1943). Nuclear emission in spiral nebulae. *Astrophys. J.* 97:28. doi: 10.1086/144488

Skrutskie, M. F., Cutri, R. M., Stiening, R., Weinberg, M. D., Schneider, S., Carpenter, J. M., et al. (2006). The two micron all sky survey (2MASS). *Astron. J.* 131, 1163–1183. doi: 10.1086/498708

Urry, C. M., and Padovani, P. (1995). Unified schemes for radio-loud active galactic nuclei. *Publ. ASP* 107:803. doi: 10.1086/133630

Véron-Cetty, M.-P., and Véron, P. (2010). A catalogue of quasars and active nuclei: 13th edition. *Astron. Astrophys.* 518:A10. doi: 10.1051/0004-6361/201014188

York, D. G., Adelman, J., Anderson, J. E. Jr., Anderson, S. F., Annis, J., Bahcall, N. A., et al. (2000). The sloan digital sky survey: technical summary. *Astron. J.* 120, 1579–1587. doi: 10.1086/301513

Conflict of Interest Statement: The authors declare that the research was conducted in the absence of any commercial or financial relationships that could be construed as a potential conflict of interest.

Copyright © 2017 La Mura, Berton, Chen, Ciroi, Congiu, Cracco, Frezzato and Rafanelli. This is an open-access article distributed under the terms of the Creative Commons Attribution License (CC BY). The use, distribution or reproduction in other forums is permitted, provided the original author(s) or licensor are credited and that the original publication in this journal is cited, in accordance with accepted academic practice. No use, distribution or reproduction is permitted which does not comply with these terms.

frontiers in Astronomy and Space Sciences

ORIGINAL RESEARCH
published: 07 November 2017
doi: 10.3389/fspas.2017.00039

Pair-Matching of Radio-Loud and Radio-Quiet AGNs

Dorota Kozieł-Wierzbowska[1], Grażyna Stasińska[2], Natalia Vale Asari[3], Marek Sikora[4], Elisa Goettems[3] and Anna Wójtowicz[1]*

[1] Astronomical Observatory, Jagiellonian University, Krakow, Poland, [2] LUTH, Observatoire de Paris, Centre National de la Recherche Scientifique, Université Paris Diderot, Meudon, France, [3] Departamento de Física–CFM, Universidade Federal de Santa Catarina, Florianópolis, Brazil, [4] Nicolaus Copernicus Astronomical Center, Warsaw, Poland

Active galactic nuclei (AGNs) are known to cover an extremely broad range of radio luminosities and the spread of their radio-loudness is very large at any value of the Eddington ratio. This implies very diverse jet production efficiencies which can result from the spread of the black hole spins and magnetic fluxes. Magnetic fluxes can be developed stochastically in the innermost zones of accretion discs, or can be advected to the central regions prior to the AGN phase. In the latter case there could be systematic differences between the properties of galaxies hosting radio-loud (RL) and radio-quiet (RQ) AGNs. In the former case the differences should be negligible for objects having the same Eddington ratio. To study the problem we decided to conduct a comparison study of host galaxy properties of RL and RQ AGNs. In this study we selected type II AGNs from SDSS spectroscopic catalogs. Our RL AGN sample consists of the AGNs appearing in the Best and Heckman (2012) catalog of radio galaxies. To compare RL and RQ galaxies that have the same AGN parameters we matched the galaxies in black hole mass, Eddington ratio and redshift. We compared several properties of the host galaxies in these two groups of objects like galaxy mass, color, concentration index, line widths, morphological type and interaction signatures. We found that in the studied group RL AGNs are preferentially hosted by elliptical galaxies while RQ ones are hosted by galaxies of later type. We also found that the fraction of interacting galaxies is the same in both groups of AGNs. These results suggest that the magnetic flux in RL AGNs is advected to the nucleus prior to the AGN phase.

Keywords: active galaxies, radio galaxies, jetted and non-jetted AGNs, radio-loudness, galaxy morphology

OPEN ACCESS

Edited by:
Mauro D'Onofrio, Università degli Studi di Padova, Italy

Reviewed by:
Paolo Padovani, European Southern Observatory, Germany
Maurizio Paolillo, Università degli Studi di Napoli Federico II, Italy

****Correspondence:***
Dorota Kozieł-Wierzbowska
dorota.koziel@uj.edu.pl

Specialty section:
This article was submitted to Milky Way and Galaxies, a section of the journal Frontiers in Astronomy and Space Sciences

Received: *31 August 2017*
Accepted: *25 October 2017*
Published: *07 November 2017*

Citation:
Kozieł-Wierzbowska D, Stasińska G, Vale Asari N, Sikora M, Goettems E and Wójtowicz A (2017) Pair-Matching of Radio-Loud and Radio-Quiet AGNs. Front. Astron. Space Sci. 4:39. doi: 10.3389/fspas.2017.00039

1. INTRODUCTION

Active galactic nuclei (AGNs) are powered by accretion on a supermassive black hole (BH). Although the first discovered AGNs were radio-loud (RL), most of AGNs are radio-quiet (RQ). The radio-loudness of RL AGNs, defined as the ratio of the radio flux to the optical flux (Kellermann et al., 1989), covers several orders of magnitude (e.g., Sikora et al., 2007; Lal and Ho, 2010) which implies very diverse jet production efficiencies. For jets powered by rotating BHs (Blandford and Znajek, 1977), the efficiency of the jet production can be related to the spread of the BH spins and the amount of magnetic fluxes accumulated in the central AGNs.

Magnetic fluxes can be developed stochastically in the innermost zones of accretion discs (Begelman and Armitage, 2014), or can be advected to the central regions of a galaxy prior to the AGN phase (Sikora et al., 2013; Sikora and Begelman, 2013). In the latter case there could be

systematic differences between the properties of galaxies hosting radio-loud and radio-quiet AGNs. Our aim is to compare the properties of the host galaxies of radio-loud and radio-quiet AGNs to distinguish which of these two scenarios is more probable. If we find that RQ and RL are hosted by different galaxies, we could discard the scenario where radio jets are stochastic.

Radio-loud (jetted) and radio-quiet (non-jetted) AGNs have already been studied extensively and some systematic differences were found between these two groups of objects:

- The most radio-loud AGNs are found in galaxies with black hole masses $\geq 10^8\,M_\odot$ (Laor, 2000; Dunlop et al., 2003; Floyd et al., 2004; McLure and Jarvis, 2004; Best et al., 2005).
- The fraction of radio-loud objects and radio loudness increases with decreasing Eddington ratio, $\lambda = L_{\rm bol}/L_{\rm Edd}$ (e.g., Terashima and Wilson, 2003; Kratzer and Richards, 2015), but there is a large scatter in radio loudness for AGNs with similar Eddington ratio.
- The fraction of galaxies with disturbed morphology is larger in RL than in RQ AGNs (Bessiere et al., 2012; Chiaberge et al., 2015).
- RL AGNs are located in denser environments (e.g., Mandelbaum et al., 2009; Ramos Almeida et al., 2013).

However, the differences listed above concern entire families of objects, but not objects that have the same accretion properties. Moreover, in catalogs of AGNs there are many objects with properties characteristic of RL objects like very massive black holes, low Eddington ratios, and disturbed morphologies, but they are radio-quiet. Therefore, we ask the question why is the efficiency of the jet production very different among otherwise similar objects?

In our project we concentrate on Type 2 (i.e., obscured) objects, to be able to study the properties of the host galaxies, with Eddington ratios $\lambda \geq 0.003$, and we seek the differences between radio-loud and radio-quiet AGNs to check if there are any generic differences between the host galaxies of these two groups of objects that can indicate different evolution histories of jetted and non-jetted AGNs.

2. METHODS

2.1. Selection of the Samples

The samples of radio-loud and radio-quiet galaxies were selected from the SDSS DR7 spectroscopic catalogs (Abazajian et al., 2009). Only galaxies with S/N $\geq$ 10 Å^{-1} in the region around $\lambda_0 = 4{,}020$ Å were chosen. We also applied the redshift cuts, low velocity dispersion limit and S/N limits in emission line fluxes as

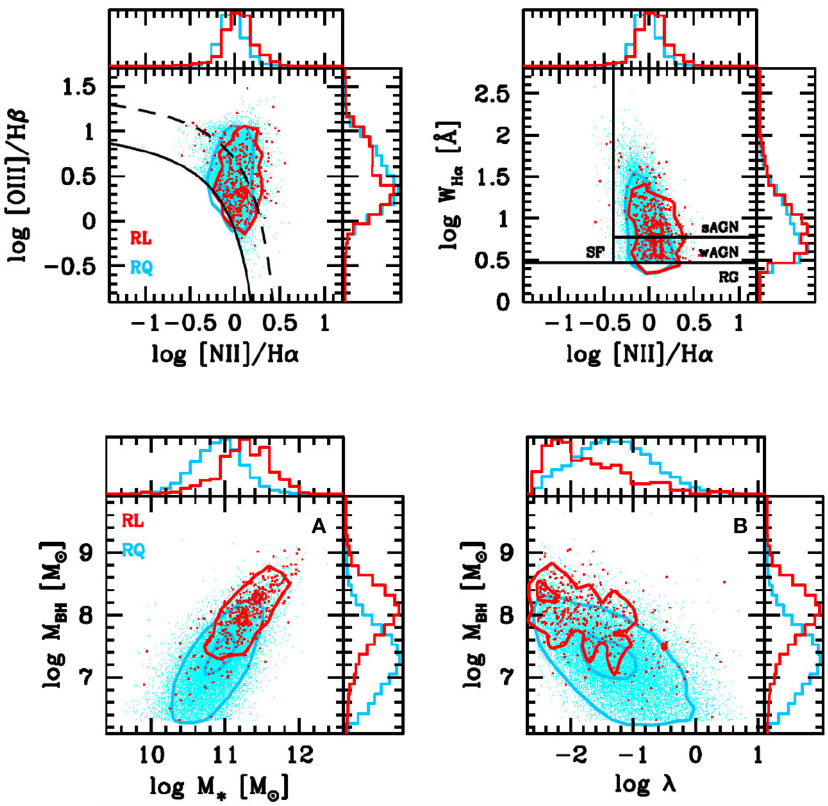

FIGURE 1 | Top: BPT and WHAN diagrams for RL and RQ AGNs (red and blue points, respectively). The solid black line in the BPT diagram is the Kewley et al. (2001) line, while the dashed line separates galaxies with line emission dominated by the AGN. In the WHAN diagram the solid lines separate SF galaxies, strong AGNs, weak AGNs and retired galaxies (Cid Fernandes et al., 2011). **Bottom:** M_{BH} vs. stellar mass and M_{BH} vs. Eddington ratio. The histograms of plotted parameters for RL and RQ galaxies are also shown. Updated version published in Kozieł-Wierzbowska et al. (2017).

in Kozieł-Wierzbowska et al. (2017). Galaxies with faulty pixels in the area of emission lines were eliminated. After this step, AGNs were selected based on the BPT diagram and the Kewley et al. (2001) line. Using the WHAN diagram (Cid Fernandes et al., 2011), we removed those galaxies in which the emission lines could be produced by hot, low-mass, evolved stars (the retired galaxies defined in Stasińska et al., 2008). This procedure selected 19883 optical AGNs.

Among this sample of optical AGNs, we searched those which belong to the Best and Heckman(2012; BH12) catalog of radio galaxies and whose radio emission is considered by them to be produced by an AGN. The BH12 catalog flux limit is 5 mJy.

After limiting ourselves to AGNs with Eddington ratio $\lambda \geq 0.003$[1], i.e., focusing mostly on sources with radiatively efficient accretion, we obtained our RL AGN sample of 376 objects, and our RQ AGN sample of 10,918 objects.

The host galaxy stellar masses, velocity dispersions (used to calculate $M_{\rm BH}$), nebular extinction, emission line fluxes and equivalent widths, and the Eddington ratios, λ, where obtained from the SDSS data after applying the STARLIGHT (Cid Fernandes et al., 2005) spectral model-fitting.

The upper panels of **Figure 1** show the BPT (Baldwin et al., 1981) and the WHAN (Cid Fernandes et al., 2011) diagrams for our RL and RQ samples. RL AGNs are shown in red and RQ AGNs in blue. On both axes the normalized histograms are presented. The black curve is the Kewley et al. (2001) line. The location of red and blue points is similar which shows that objects from both samples have similar ionization properties. The bottom panel in **Figure 1** shows M_{BH} as a function of the galaxy stellar mass M_*, and of the Eddington ratio, λ. In these diagrams RL and RQ galaxies are shifted relative to each other. On average, RL AGNs have higher black hole masses and higher stellar masses compared to RQ galaxies. RL objects have also lower λ. These observations are compatible with trends found by previous authors (see Introduction). These two panels clearly show that in order to compare RL and RQ AGNs it is necessary to match them in black hole mass and Eddington ratio.

2.2. Pair-Matching of RL and RQ Galaxies

To compare RL and RQ galaxies with the same AGN parameters, we applied a pair-matching technique. Galaxies were matched in redshift, black hole mass (M_{BH}) and Eddigton ratio (λ). In practice for each RL object we selected all RQ objects for which: $|\Delta z| \leq 0.01$, $|\Delta \log \lambda| \leq 0.09$, and $|\Delta \log M_{\rm BH}| \leq 0.1206$. We computed the distance as $d^2_{\rm match} = \sum \Delta^2$. For each RL AGN three RQ galaxies with the smallest d were included into the matched RQ sample (mRQ sample).

We defined the radio loudness parameter by $\mathcal{R} \equiv L_{1.4}[W\,Hz^{-1}]/L_{\rm H\alpha}[L_\odot]$, where $L_{1.4}$ is the radio luminosity at 1.4 GHz. The classical criterion for radio-loud AGN, $\mathcal{R}^{(K)} > 10$ (Kellermann et al., 1989), translates into $\log \mathcal{R} > 15.8$. From the matched RQ sample we excluded galaxies that were undetected in radio and for which the radio-loudness (estimated from the

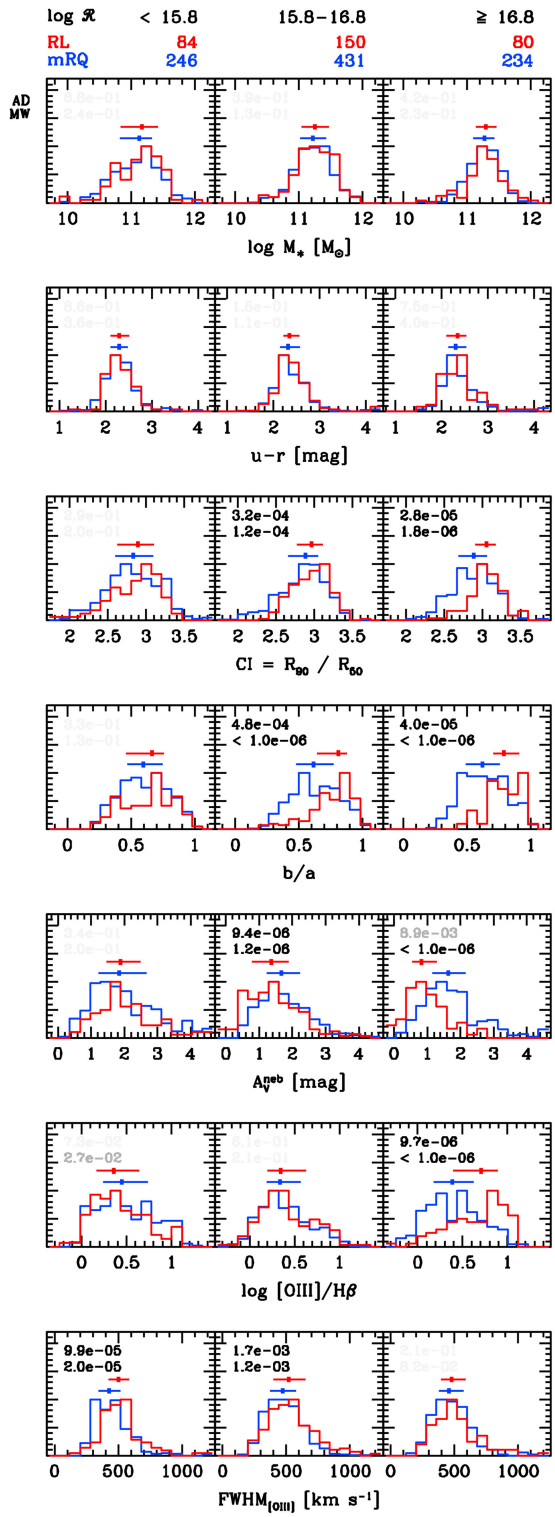

FIGURE 2 | Histograms of selected parameters of RL (red) and mRQ (blue) objects. In each panel we show the results of the Anderson-Darling and Mann-Whitney tests in terms of probabilities p that the samples could be drawn from the same population. Results with $p < 0.003$ are written in black, those with $p < 0.05$ are written in dark gray. Blue and red points at the top of each histogram indicate the median values and the horizontal lines indicate the quartiles. Published in Kozieł-Wierzbowska et al. (2017).

[1]This step ensures us that we calculate the bolometric luminosity consistently and correctly for all studied sources.

flux limit od 5 mJy in the BH12 catalog) is larger than 10 (log $\mathcal{R} > 15.8$).

3. RESULTS

We present our results in the form of histograms. **Figure 2** shows histograms of selected parameters of RL (red) and RQ (blue) galaxies. Results for RL AGNs and their matched RQ galaxies are presented separately for three bins in the value of the radio-loudness $\mathcal{R}$ of the parent RL object. $\mathcal{R}$ bins were chosen to represent classically radio-quiet (although jetted, log $\mathcal{R} < 15.8$) objects, intermediate radio-loud objects ($15.8 < \log \mathcal{R} < 16.8$), and the most radio-loud ones (log $\mathcal{R} > 16.8$). In each bin, the tick mark with horizontal line shown on the top of the histograms represents the median value and the quartiles. We used two statistical tests to study the difference between RL and mRQ samples. These are the Anderson-Darling (AD) and Mann-Whitney (MW) tests. These tests give the probability that both samples are drawn from the same population.

Among the studied parameters, the stellar galaxy masses, M_*, and the colors, u-r, have very similar distributions for RL and RQ AGNs. In the case of galaxy mass this result is expected since we matched our objects in M_{BH} which correlates with M_*. The concentration index, CI, and the galaxy axes ratio, b/a, the two parameters associated with galaxy shape and morphology, show significant differences. RL galaxies tend to have larger concentration index, and larger axes ratios in the two highest $\mathcal{R}$ bins. The lower values of CI and b/a ratio in the matched RQ sample indicate more disky galaxy morphology.

In the next two panels we present a comparison of the nebular extinction, $A_V^{\rm neb}$, and of the [O III] to Hβ line fluxes ratio. The values of $A_V^{\rm neb}$ decrease with increasing $\mathcal{R}$. [O III]/Hβ differs significantly in the bin of the highest $\mathcal{R}$. These results may suggest some contribution from the H II regions to the line emission. The last panel shows histograms of [O III] line widths. We see that the line widths in RL galaxies tend to be larger then in RQ AGNs in the lowest $\mathcal{R}$ bins. We speculate that this can result from having at low R less collimated jets. Forming wider outflows such jets may affect the motion of the gas clouds in the narrow line region, and hence broaden the emission line profiles.

To eliminate the contribution of H II regions from our studies we decided to use "cleaned" samples. In these samples only galaxies that lie above the dashed curve shown in BPT diagram from **Figure 1** are included. In these galaxies the contribution from H II regions can be neglected. The results for the cleaned samples (see Kozieł-Wierzbowska et al., 2017) confirm our findings for the whole RL and mRQ samples concerning morphological properties.

From the comparison of CI and of the b/a ratio we see that there is a difference in morphology between RL and

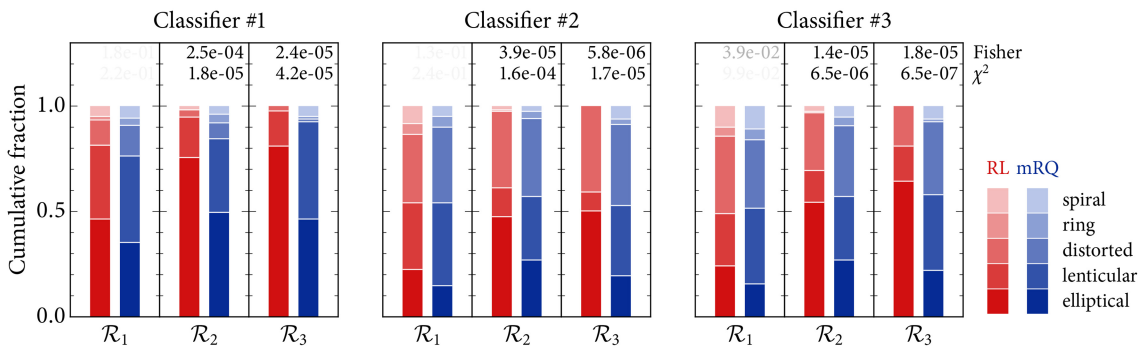

FIGURE 3 | Cumulative fraction of RL (shades of red) and RQ (shades of blue) classified as elliptical, lenticular, distorted, ring, or spiral galaxies. R_1 corresponds to $\log \mathcal{R} < 15.8$, R_2 to $15.8 < \log \mathcal{R} < 16.8$, and R_3 to $\log \mathcal{R} > 16.8$. Results are shown for three classifiers separately.

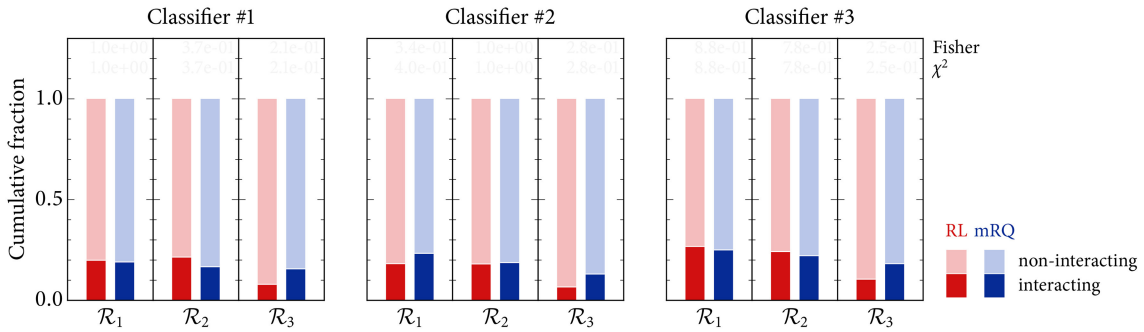

FIGURE 4 | Cumulative fraction of RL AGNs in three $\mathcal{R}$ bins, and their closest mRQ galaxies showing signs of the galaxy interaction. The layout is the same as for **Figure 3**.

mRQ galaxies. To confirm this result we decided to perform a morphological classification of all RL galaxies and the closest match from the RQ galaxies. Classifiers looked at the color SDSS images of these objects and attributed to each galaxy a morphological type. The results for the three classifiers are shown in **Figure 3**. The panels in this figure show in different shades of red (blue) the fraction of RL (mRQ) galaxies classified as elliptical, lenticular, distorted, ring, or spiral galaxies. As before, results are presented separately for three $\mathcal{R}$ bins. As we can see, the fraction of ellipticals among RL objects in all three radio-loudness bins is larger than among the matched RQ galaxies. Note that low-CI galaxies are not spirals, but lenticular or distorted galaxies. This result was confirmed using Galaxy ZOO data.

The classification scheme also included information about galaxy interactions like major or minor mergers, tail, or suspected interaction. **Figure 4** shows the results concerning the fraction of galaxies with interaction signatures considered as certain. Here, as interacting, we consider major or minor mergers and galaxies with a tail. In **Figure 4** we do not see any systematic difference between RL and RQ AGNs suggesting that galaxy interaction has no special effect on the radio activity of the AGN. Our result is in contradiction with Chiaberge et al. (2015) who found that all radio-loud galaxies in their sample are mergers, however their sample consisted of FRII radio galaxies at redshifts larger than 1, while in our sample we have only local AGNs mostly with compact morphologies.

4. SUMMARY

The results presented here clearly show that not only Eddington ratio and black hole mass determine the jet production efficiency. In the description of the jet production the accumulation of the magnetic flux in the AGN center and the BH spin have also to be taken into account. The fact that we find a higher fraction of ellipticals among RL galaxies than among the matched RQ ones suggest that elliptical galaxies have already a sufficient amount of magnetic flux accumulated in the center to produce and collimate radio jets in the Blandford and Znajek, 1977 scenario. This is in agreement with findings of Sikora et al. (2013) and Sikora and Begelman (2013) on the RL AGN pre-phase.

AUTHOR CONTRIBUTIONS

DK-W: data analysis, interpretation, writing. NV: data analysis, figure preparation. GS: data analysis, interpretation, writing. MS: theoretical interpretation. EG and AW: data analysis, morphological classification.

ACKNOWLEDGMENTS

This work was carried out within the framework of the Polish National Science Centre grant UMO-2013/09/B/ST9/00026. GS was partially supported by the National Research Centre, Poland, DEC-2013/08/M/ST9/00664, within the framework of the HECOLS International Associated Laboratory. GS and NVA acknowledge the support from the CAPES CSF–PVE project 88881.068116/2014-01. The Sloan Digital Sky Survey is a joint project of The University of Chicago, Fermilab, the Institute for Advanced Study, the Japan Participation Group, the Johns Hopkins University, the Los Alamos National Laboratory, the Max-Planck-Institute for Astronomy, the Max-Planck-Institute for Astrophysics, New Mexico State University, Princeton University, the United States Naval Observatory, and the University of Washington. Funding for the project has been provided by the Alfred P. Sloan Foundation, the Participating Institutions, the National Aeronautics and Space Administration, the National Science Foundation, the U.S. Department of Energy, the Japanese Monbukagakusho, and the Max Planck Society.

REFERENCES

Abazajian, K. N., Adelman-McCarthy, J. K., Agüeros, M. A., Allam, S. S., Allende Prieto, C., An, D., et al. (2009). The seventh data release of the sloan digital sky survey. *Astrophys. J. Suppl.* 182, 543–558. doi: 10.1088/0067-0049/182/2/543

Baldwin, J. A., Phillips, M. M., and Terlevich, R. (1981). Classification parameters for the emission-line spectra of extragalactic objects. *PASP* 93, 5–19. doi: 10.1086/130766

Begelman, M. C., and Armitage, P. J. (2014). A mechanism for hysteresis in black hole binary state transitions. *Astrophys. J. Lett.* 782:L18. doi: 10.1088/2041-8205/782/2/L18

Bessiere, P. S., Tadhunter, C. N., Ramos Almeida, C., and Villar Martín, M. (2012). The importance of galaxy interactions in triggering type II quasar activity. *Month. Notices R. Astron. Soc.* 426, 276–295. doi: 10.1111/j.1365-2966.2012.21701.x

Best, P. N., and Heckman, T. M. (2012). On the fundamental dichotomy in the local radio-AGN population: accretion, evolution and host galaxy properties. *Month. Notices R. Astron. Soc.* 421, 1569–1582. doi: 10.1111/j.1365-2966.2012.20414.x

Best, P. N., Kauffmann, G., Heckman, T. M., Brinchmann, J., Charlot, S., Ivezić, Ž., et al. (2005). The host galaxies of radio-loud active galactic nuclei: mass dependences, gas cooling and active galactic nuclei feedback. *Month. Notices R. Astron. Soc.* 362, 25–40. doi: 10.1111/j.1365-2966.2005.09192.x

Blandford, R. D., and Znajek, R. L. (1977). Electromagnetic extraction of energy from Kerr black holes. *Month. Notices R. Astron. Soc.* 179, 433–456. doi: 10.1093/mnras/179.3.433

Chiaberge, M., Gilli, R., Lotz, J. M., and Norman, C. (2015). Radio loud AGNs are mergers. *Astrophys. J.* 806:147. doi: 10.1088/0004-637X/806/2/147

Cid Fernandes, R., Mateus, A., Sodré, L., Stasińska, G., and Gomes, J. M. (2005). Semi-empirical analysis of Sloan Digital Sky Survey galaxies - I. Spectral synthesis method. *Month. Notices R. Astron. Soc.* 358, 363–378. doi: 10.1111/j.1365-2966.2005.08752.x

Cid Fernandes, R., Stasińska, G., Mateus, A., and Vale Asari, N. (2011). A comprehensive classification of galaxies in the Sloan Digital Sky Survey: how to tell true from fake AGN? *Month. Notices R. Astron. Soc.* 413, 1687–1699. doi: 10.1111/j.1365-2966.2011.18244.x

Dunlop, J. S., McLure, R. J., Kukula, M. J., Baum, S. A., O'Dea, C. P., and Hughes, D. H. (2003). Quasars, their host galaxies and their central black holes. *Month. Notices R. Astron. Soc.* 340, 1095–1135. doi: 10.1046/j.1365-8711.2003.06333.x

Floyd, D. J. E., Kukula, M. J., Dunlop, J. S., McLure, R. J., Miller, L., Percival, W. J., et al. (2004). The host galaxies of luminous quasars. *Month. Notices R. Astron. Soc.* 355, 196–220. doi: 10.1111/j.1365-2966.2004.08315.x

Kellermann, K. I., Sramek, R., Schmidt, M., Shaffer, D. B., and Green, R. (1989). VLA observations of objects in the Palomar Bright Quasar Survey. *Astron. J.* 98, 1195–1207. doi: 10.1086/115207

Kewley, L. J., Dopita, M. A., Sutherland, R. S., Heisler, C. A., and Trevena, J. (2001). Theoretical modeling of starburst galaxies. *Astrophys. J.* 556, 121–140. doi: 10.1086/321545

Kozieł-Wierzbowska, D., Vale Asari, N., Stasińska, G., Sikora, M., Goettems, E., and Wójtowicz, A. (2017). What distinguishes the host galaxies of radio-loud and radio-quiet AGNs? *Astrophys. J.* 846, 42–53. doi: 10.3847/1538-4357/aa8326

Kratzer, R. M., and Richards, G. T. (2015). Mean and extreme radio properties of quasars and the origin of radio emission. *Astron. J.* 149:61. doi: 10.1088/0004-6256/149/2/61

Lal, D. V., and Ho, L. C. (2010). The Radio Properties of Type 2 Quasars. *Astron. J.* 139, 1089–1105. doi: 10.1088/0004-6256/139/3/1089

Laor, A. (2000). On black hole masses and radio loudness in active galactic nuclei. *Astrophys. J. Lett.* 543, L111–L114. doi: 10.1086/317280

Mandelbaum, R., Li, C., Kauffmann, G., and White, S. D. M. (2009). Halo masses for optically selected and for radio-loud AGN from clustering and galaxy-galaxy lensing. *Month. Notices R. Astron. Soc.* 393, 377–392. doi: 10.1111/j.1365-2966.2008.14235.x

McLure, R. J., and Jarvis, M. J. (2004). The relationship between radio luminosity and black hole mass in optically selected quasars. *Month. Notices R. Astron. Soc.* 353, L45–L49. doi: 10.1111/j.1365-2966.2004.08305.x

Ramos Almeida, C., Bessiere, P. S., Tadhunter, C. N., Inskip, K. J., Morganti, R., Dicken, D., et al. (2013). The environments of luminous radio galaxies and type-2 quasars. *Month. Notices R. Astron. Soc.* 436, 997–1016. doi: 10.1093/mnras/stt1595

Sikora, M., and Begelman, M. C. (2013). Magnetic Flux Paradigm for Radio Loudness of Active Galactic Nuclei. *Astrophys. J. Lett.* 764:L24. doi: 10.1088/2041-8205/764/2/L24

Sikora, M., Stasińska, G., Kozieł-Wierzbowska, D., Madejski, G. M., and Asari, N. V. (2013). Constraining Jet Production Scenarios by Studies of Narrow-line Radio Galaxies. *Astrophys. J.* 765:62. doi: 10.1088/0004-637X/765/1/62

Sikora, M., Stawarz, Ł., and Lasota, J.-P. (2007). Radio loudness of active galactic nuclei: observational facts and theoretical implications. *Astrophys. J.* 658, 815–828. doi: 10.1086/511972

Stasińska, G., Vale Asari, N., Cid Fernandes, R., Gomes, J. M., Schlickmann, M., Mateus, A., et al. (2008). Can retired galaxies mimic active galaxies? Clues from the Sloan Digital Sky Survey. *Month. Notices R. Astron. Soc.* 391, L29–L33. doi: 10.1111/j.1745-3933.2008.00550.x

Terashima, Y., and Wilson, A. S. (2003). Chandra snapshot observations of low-luminosity active galactic nuclei with a compact radio source. *Astrophys. J.* 583, 145–158. doi: 10.1086/345339

Conflict of Interest Statement: The authors declare that the research was conducted in the absence of any commercial or financial relationships that could be construed as a potential conflict of interest.

Copyright © 2017 Kozieł-Wierzbowska, Stasińska, Vale Asari, Sikora, Goettems and Wójtowicz. This is an open-access article distributed under the terms of the Creative Commons Attribution License (CC BY). The use, distribution or reproduction in other forums is permitted, provided the original author(s) or licensor are credited and that the original publication in this journal is cited, in accordance with accepted academic practice. No use, distribution or reproduction is permitted which does not comply with these terms.

frontiers in Astronomy and Space Sciences

MINI REVIEW
published: 11 July 2017
doi: 10.3389/fspas.2017.00006

What We Talk about When We Talk about Blazars

Luigi Foschini *

INAF – Osservatorio Astronomico di Brera, Lecco, Italy

After the discovery of powerful relativistic jets from Narrow-Line Seyfert 1 Galaxies, and the understanding of their similarity with those of blazars, a problem of terminology was born. The word blazar is today associated to BL Lac Objects and Flat-Spectrum Radio Quasars, which are somehow different from Narrow-Line Seyfert 1 Galaxies. Using the same word for all the three classes of AGN could drive either toward some misunderstanding, or to the oversight of some important characteristics. I review the main characteristics of these sources, and finally I propose a new scheme of classification.

Keywords: relativistic jet, blazar, quasar, BL Lac Object, Narrow-Line Seyfert 1 galaxy, black hole, neutron star

OPEN ACCESS

Edited by:
Paola Marziani,
National Institute for Astrophysics (INAF), Italy

Reviewed by:
Vahram Chavushyan,
National Institute of Astrophysics, Optics and Electronics, Mexico
Daniela Bettoni,
Osservatorio Astronomico di Padova (INAF), Italy

***Correspondence:**
Luigi Foschini
luigi.foschini@brera.inaf.it

Specialty section:
This article was submitted to Milky Way and Galaxies, a section of the journal Frontiers in Astronomy and Space Sciences

Received: *29 May 2017*
Accepted: *23 June 2017*
Published: *11 July 2017*

Citation:
Foschini L (2017) What We Talk about When We Talk about Blazars. Front. Astron. Space Sci. 4:6. doi: 10.3389/fspas.2017.00006

1. INTRODUCTION

The title is borrowed from Haruki Murakami's *What we talk about when we talk about running*, who, in turn, borrowed it from Raymond Carver's *What we talk about when we talk about love*. Far from competing with those two outstanding authors, I just would like to draw the attention on some recent discoveries about relativistic jets, and how to include them into the unified model of active galactic nuclei (AGN) with jets. I would like to underline that this is not a challenge to the unified model, but rather the request of an evolution and an improvement.

It is not the first time that there is an evolution in the terminology of this type of cosmic sources. This should not be looked as a mere fashion about words. It is true that physical objects exist independently on how we name them, but it is also true that using the most proper words makes it easier to study them, by avoiding to remain stuck on a swamp of fake problems and misleading questions. When Gregorio Ricci Curbastro and Tullio Levi-Civita proposed the tensor calculus, many other mathematicians rejected it, because they thought it was just a mere rehash of old maths. When speaking about Ricci Curbastro, Luigi Bianchi told that he preferred to find new things with old methods, rather than to find old things with new methods (cited in Toscano, 2004). On the opposite, Henri Poincaré wrote that a proper notation in mathematics has the same importance of a good classification in natural science, because it allows us to connect each other many events without any apparent link (cited in Bottazzini, 1990).

Back to the topic of this essay, I would like to remind some past changes in terminology about relativistic jets. In 1978, Ed Spiegel proposed the term *blazar* as a contraction of the words BL Lac Objects and Optically Violently Variable Quasars (OVV) (Angel and Stockman, 1980); in 1994–1995, Paolo Padovani and Paolo Giommi proposed to rename radio-selected BL Lac Objects (RBL) as low-energy cutoff BL Lacs (LBL), and X-ray selected BL Lac Objects (XBL) changed to high-energy cutoff BL Lacs (HBL) (Giommi and Padovani, 1994; Padovani and Giommi, 1995); also the Fanaroff-Riley classes of radio galaxies changed to low- and high-excitation radio galaxies (LErG, HErG) (Hine and Longair, 1979; Laing et al., 1994; Buttiglione et al., 2010). In his opening talk at the conference *Quasar at all cosmic epochs* (Padova, April 2–7, 2017), Paolo Padovani proposed to stop using radio loud/quiet terms and to start speaking about jetted AGN or not. I was less severe

in my thoughts on radio loudness some years ago (Foschini, 2011), although I agreed with Padovani. It is time to be resolute in changing terminology. Also Martin Gaskell wrote: "I tell students that classification is one of the first step in science. As science progresses, however, I believe that we need to move toward physically meaningful classification schemes as soon as possible. To achieve this, we need to be willing to modify our definitions, or else we can impede progress" (cited in D'Onofrio et al., 2012). This means to move from a purely observational classification to a terminology with more physical grounds. It should be needless to say, but before establishing the type of a cosmic source, it is necessary to study it. A simple measure is the easy way, but it is also the most prone to errors.

Today, AGN with jets are unified according to the scheme by Urry and Padovani (1995, Table 1), which in turn summarizes many years of contributions from pioneers (see the historical review in D'Onofrio et al., 2012). Urry and Padovani's scheme has its pillars in three main factors: viewing angle, optical spectrum, radio emission. They also suggested a fourth factor, the black hole spin, which should be greater for jetted AGN.

With reference to jetted AGN only, the Urry and Padovani's unified model can be divided into two main classes and four subclasses on the basis of viewing angle and optical spectrum (Urry and Padovani, 1995):

1. Blazar (small viewing angle, beamed sources):
   (a) Flat-spectrum radio quasar (FSRQ), prominent emission lines in the optical spectrum;
   (b) BL Lac Object, weak emission lines or featureless continuum in the optical spectrum;
2. Radio galaxies (large viewing angles, unbeamed sources):
   (a) HErG, prominent emission lines in the optical spectrum;
   (b) LErG, weak emission lines or featureless continuum in the optical spectrum;

The mass of the central spacetime singularity was generally in the range $\sim 10^{8-10} M_{\odot}$ (Buttiglione et al., 2010; Ghisellini et al., 2010; Tadhunter, 2016), which seemed to fit well with the elliptical galaxies hosting this type of cosmic sources (Olguín-Iglesias et al., 2016). The limited range meant to neglect the mass when scaling the jet power. Therefore, the main factor regulating the electromagnetic emission became the electron cooling, which is the basis of the so-called *blazar sequence* (Fossati et al., 1998; Ghisellini et al., 1998). The observed blazar sequence indicated that the spectral energy distribution (SED) of high-power blazar (FSRQs) had the synchrotron and the inverse-Compton peaks at infrared and MeV-GeV energies, respectively, while that of low-power sources (BL Lac Objects) had the peaks shifted to greater energies (UV/X-rays and TeV, respectively) (Fossati et al., 1998). This was explained as different cooling of relativistic electrons due to different environment, rich of photons or not (physical blazar sequence, Ghisellini et al., 1998). In addition, since no other jetted AGN with smaller masses were known, it was thought that the generation of a relativistic jet required a minimum black hole mass (Laor, 2000; Chiaberge and Marconi, 2011).

Truly speaking, the lack of small-mass jetted AGN was a selection bias. For example, in Miley and Miller (1979) studied a sample of 34 quasars with $z < 0.7$: their sample included also objects with small black hole mass, which resulted to have compact radio morphology. In Wills and Browne (1986) studied a sample of 79 quasars with the same redshift range, but selecting only bright sources (mag < 17): small-mass objects disappeared. Therefore, jets from small-mass AGN were known at least since seventies, but they were disregarded, likely because of the poor instruments sensitivity. The recent technological improvements resulted in an increase of the cases of powerful jets hosted in spiral galaxies (hence, small mass of the central black hole) (Keel et al., 2006; Morganti et al., 2011). Also recent surveys showed that disk/spiral hosts are not just an exception, but they could be a significant fraction of jetted AGN (Inskip et al., 2010; Coziol et al., 2017). Particularly, Coziol et al. (2017) confirmed the results of Miley and Miller (1979): small-mass compact objects have generally weak, and compact radio jets.

2. HIGH-ENERGY GAMMA RAYS FROM NARROW-LINE SEYFERT 1 GALAXIES

The turning point occurred in 2009, with the detection of high-energy γ rays from Narrow-Line Seyfert 1 Galaxies (NLS1), thus providing evidence of powerful relativistic jets from small-mass AGN (Abdo et al., 2009a,b,c; Foschini et al., 2010) (see also Foschini, 2012b for a historical review). NLS1s do have small-mass central black holes ($\lesssim 10^8 M_{\odot}$), high accretion luminosity (close to the Eddington limit), prominent optical emission lines, but relatively weak jet power, comparable to BL Lac Objects (Foschini et al., 2015). Kinematics of radio components revealed superluminal motion ($\sim$10c Lister et al., 2016; see also Angelakis et al., 2015; Lähteenmäki et al., 2017 for more information about radio properties), while infrared colors indicated an enhanced star formation activity (Caccianiga et al., 2015). The host galaxy is not yet clearly defined: there is evidence that NLS1 without jets are hosted by spiral galaxies, but $\gamma-$ray NLS1 are still poorly known. However, early observations of a handful of sources point to disk galaxy hosts[1], the result of either a recent merger or a secular accretion (Zhou et al., 2007; Antón et al., 2008; Hamilton and Foschini, 2012; León Tavares et al., 2014; Kotilainen et al., 2016; Olguín-Iglesias et al., 2017).

All the observed characteristics of NLS1s suggested that this class of AGN could be the low-mass tail of the quasars distribution (Abdo et al., 2009a; Foschini et al., 2015). Indeed, as proved by Berton et al. (2016), the NLS1s luminosity function matches that of FSRQs. The parent population of jetted NLS1s could be that of Compact Steep Spectrum (CSS) HErG (Berton et al., 2016, in press). This fits well with the idea that NLS1s are quasars at the early stage of their evolution or rejuvenated by a recent merger (Mathur, 2000).

[1]Two opposite interpretation were proposed for FBQS J1644+2619, a spiral barred host (Olguín-Iglesias et al., 2017), and an elliptical galaxy (D'Ammando et al., 2017). However, the former observation seems to be more reliable, because done with a much better seeing than the latter.

However, I would like to underline that it is not a matter of NLS1s only, but of small-mass AGN. Recent surveys with *Fermi/LAT* (Shaw et al., 2012; Foschini et al., 2016) and the *Sloan Digital Sky Survey* (Best and Heckman, 2012) indicated that jetted AGN with small-mass black holes are not restricted to NLS1s-type AGN. The exact observational classification is not the point, but what is important is the relatively small mass of the central spacetime singularity. This confirms once again that the mass threshold to generate the relativistic jet in AGN was just an observational bias.

3. THE UNIFICATION OF RELATIVISTIC JETS

Removing the mass-threshold bias has the important consequence of the unification of relativistic jets from AGN and from Galactic X-ray binaries (XRBs) (Foschini, 2012a, 2014). In a jet power vs. disk luminosity graph (see Figure 7.4 of Foschini, 2017), NLS1s populate the previously missing branch of small-mass highly-accreting compact objects, the analogous of accreting neutron stars for the XRBs sample (see also Paliya et al., 2016 for a larger sample of AGN). By applying the scaling relationships elaborated by Heinz and Sunyaev (2003), it is possible to merge the AGN and XRBs populations. A residual dispersion of about three orders of magnitudes remain (see Foschini, 2012a, 2014): measurements errors could account for about one order of magnitude, while the remaining two could likely to be due to the spin of the compact object (Heinz and Sunyaev, 2003; Mościbrodzka et al., 2016), whose measure is still missing or largely unreliable (see also Foschini, 2017).

4. IMPLICATIONS OF THE UNIFICATION

Having proved the Heinz and Sunyaev's scaling theory (Heinz and Sunyaev, 2003), the jet power vs. disk luminosity graph could be used also to understand and to visualize some implications of the unification of relativistic jets (**Figure 1**). Each population has two branches, depending on the main factor driving the changes in the jet power. The dashed blue rectangle in **Figure 1A** summarizes the blazar sequence (Fossati et al., 1998; Ghisellini et al., 1998): the black hole masses of blazars are within about one, maximum two, orders of magnitudes, and, therefore, the main changes in the jet power are driven by the electron cooling in different environments. The red rectangle in **Figure 1A** refers to similar environments (FSRQs and NLS1s), but largely different masses ($\gtrsim 10^8 M_\odot$ vs. $\lesssim 10^8 M_\odot$, respectively), which in turn implies that the main change in the jet power is due to the mass of the central black hole (Heinz and Sunyaev, 2003). The relatively small-mass black hole ($\lesssim 10^8 M_\odot$) is necessary to explain the weak jet power of NLS1s, which is comparable with BL Lac Objects (Foschini et al., 2015): as the environment of NLS1s is rich of photons like FSRQs, a large black hole mass would mean that relativistic electrons of the jet do no cool efficiently with so many photons, thus contradicting a basic physical law. Indeed, BL Lac Objects have weak jet and large masses ($\gtrsim 10^8 M_\odot$), but their environment is photon-starving (see also Foschini, 2017). The NLS1s branch (red rectangle) also prove that the observational blazar sequence (the dashed blue rectangle only Fossati et al., 1998) was due to a bright-source selection bias, although the physical blazar sequence (Ghisellini et al., 1998) remains valid, as it simply refers to how relativistic electrons cool depending on photon availability.

When comparing the AGN with XRBs samples, one can note that the blazar sequence corresponds somehow to the stellar-mass black hole states, but on different time scales. Galactic black holes evolve on human time scales: it is possible to observe a state change of a black hole along months/years of observations. A quasar requires some billion of years to swallow most of the available interstellar gas and to become a BL Lac Object (Böttcher and Dermer, 2002; Cavaliere and D'Elia, 2002; Maraschi and Tavecchio, 2003). This opens another implication, namely the cosmological evolution (**Figure 1B**). The blazar evolutionary sequence (Cavaliere and D'Elia, 2002; Böttcher and Dermer, 2002; Maraschi and Tavecchio, 2003) suggested that quasar are young AGN, which become BL Lac Objects as they grow. This scenario has to be updated now by adding also NLS1s, which are thought to be a low-redshift analogous of the early quasars (Mathur, 2000; Berton et al., in press). Therefore, one could think at the sequence NLS1s → FSRQs → BL Lac Objects, going from small-mass highly-accreting to large-mass poorly-accreting black holes, as different stages of the cosmological evolution of the same type of source (young → adult → old, **Figure 1B**). This view implies that BL Lac Objects have the largest masses, being (perhaps) the final stage of the cosmic lifetime, at odds with the results of some surveys (Ghisellini et al., 2010). Again, if one removes the bright sources selection bias, it is possible to find that indeed BL Lacs/LErGs do have masses larger than FSRQs/HErGs (Best and Heckman, 2012).

On the other side of the evolution, it is worth noting the presence of strong star formation in NLS1s, with infrared properties similar to UltraLuminous InfraRed Galaxies (ULIRGs) (Caccianiga et al., 2015). This points also to some link to the very birth of a quasar and its jet, which in turn could be an essential angular momentum relief valve to enhance the accretion (Jolley and Kuncic, 2008). ULIRGs as early quasar stage were already studied by Sanders et al. (1988a,b) and it is interesting to note the presence in his sample of both the NLS1 and the quasar prototypes (I Zw 1, and 3C 273, respectively).

It is also worth noting the application of the same sequence to the XRBs population, which implies a transition from accreting neutron stars to stellar-mass black holes (Belczynski et al., 2012; Zdziarski et al., 2013; Neustroev et al., 2014).

5. CONCLUSION: A RENEWED UNIFIED SCHEME

The Urry and Padovani's scheme (Urry and Padovani, 1995) updated with the addition of NLS1s and their parent population of CSS/HErG is shown in **Figure 2A**. However, this generates

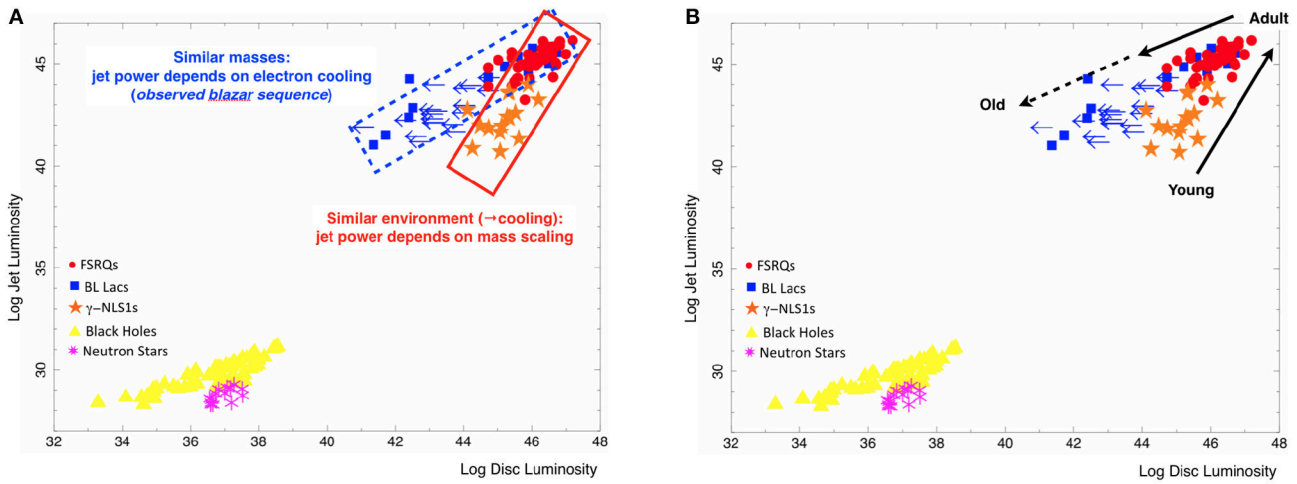

FIGURE 1 | Implications of the unification of relativistic jets. The AGN sample includes FSRQs (red circles), BL Lac Objects (blue squares or arrows for upper limits in disk luminosity), and NLS1s (orange stars). The XRB sample includes different states of some stellar-mass black holes (yellow triangles) and accreting neutron stars (magenta asterisks). HLX-1 is the only known jetted ultraluminous X-ray source with a reliable intermediate-mass black hole. See Foschini (2014) and references therein for details. **(A)** Different branches, different mechanisms. **(B)** Cosmological evolution.

A

AGN with Jets	Strong Emission Lines	Weak/No Emission Lines
Beamed (blazar?)	FSRQ + NLS1	BL Lac Obj
Unbeamed (radio galaxy?)	HErG + CSS	LErG

B

AGN with Jets	Fast Cooling	Slow Cooling
High Mass	**HMFC** (FSRQ, HErG)	**HMSC** (BL Lac Obj, LErG)
Low Mass	**LMFC** (NLS1, CSS)	**LMSC?**

FIGURE 2 | Changing terms in the unification scheme. **(A)** The updated Urry and Padovani's scheme. **(B)** Physical unification scheme.

some problem in terminology. The words blazar and radio galaxy indicate a certain type of cosmic source characterized by a high black hole mass and hosted by an elliptical galaxy. The easy addition of NLS1s and CSS to the above scheme risks to hide important information, as outlined in the previous section (different black hole mass, different host, ...). This is not a negligible detail: remind the misleading research directions caused by the bright sources selection bias, such as the threshold in the jet generation and the observed blazar sequence. Martin Gaskell wrote: "When you attach different classification to things, it is all too easy to get convinced that they are different things." (cited in D'Onofrio et al., 2012). On the opposite, if you attach the same name to different things, it is all too easy to get convinced that they are the same thing. Therefore, on one side, we need to unify jetted AGN, but, on the other side, we need to keep some information about the roots of this unification to understand the physical processes driving the observational characteristics. The jets of AGN and XRBs are similar, but their power depends on the mass of the compact object, its spin, and its accretion (environment). It is important to note that **Figures 1A,B** were built by using the jet power corrected for beaming. Indeed, it places on the same plane both beamed AGN and XRBs, which are not so beamed, as it is quite difficult for a Galactic jet to point toward the Earth, being both on the same equatorial Galactic plane[2]. The addition of HErG/LErG/CSS sources would not change the two-branches structure for each population. Therefore, it should be possible to drop also the distinction beamed/unbeamed. From a physical point of view, the two most important factors in scaling the jet power are the mass of the compact object and the nearby environment (for the electron cooling), which in turn depends on the accretion. As already stated, the spin determines a larger dispersion only (Heinz and Sunyaev, 2003; Mościbrodzka et al., 2016). Therefore, a more physical-based unification could be set up by dividing the sources depending on the mass and on the cooling only (**Figure 2B**). The dividing mass is $\sim 10^8 M_\odot$ not because of historical reasons, but because no BL Lac Object with small mass is known. Indeed, I have left a question mark on the LMSC (Low Mass Slow Cooling) cell. Current BL Lacs should be the latest stage of the cosmological evolution of jetted AGN, and, therefore, a small-mass BL Lac would mean that there was no evolution. Did such AGN have no matter enough for accretion? As there are other small-mass AGN, which are not necessarily NLS1-type (Best and Heckman, 2012; Shaw et al., 2012; Foschini et al., 2016), it would be interesting to understand if some of them have

[2]Galactic compact objects with jets are named microquasars, but there is no such thing as a microblazar, i.e., a Galactic jet pointed toward the Earth.

a photon-starving environment. Perhaps, one intriguing case could be PKS 2004−447 ($z = 0.24$) that showed observational characteristics somehow different from the other jetted NLS1s (Abdo et al., 2009c; Kreikenbohm et al., 2016; Schulz et al., 2016). There was also some disagreement on its classification as NLS1s, on the basis of the weakness of the FeII multiplets (Gallo et al., 2006; Komossa et al., 2006). It is interesting to point out that it is the only NLS1 (orange star) in the region of BL Lac Objects (blue squares or arrows) in **Figures 1A,B**.

The same terminology adapts well also to the XRB population: in this case, the dividing mass should be $\sim 3M_{\odot}$, which is the minimum for a Galactic black hole. Also in this case, the LMSC cell remains with a question mark, but the question is more intriguing, because of shorter time scales. Could it be filled by pulsars? Similar questions on AGN evolution apply here.

As a final remark I think it is important to stress the different view offered by a terminology change built on more physical ground, rather than to focus on observational details.

AUTHOR CONTRIBUTIONS

The author confirms being the sole contributor of this work and approved it for publication.

FUNDING

This work has been partially supported by PRIN INAF 2014 "Jet and astro-particle physics of gamma-ray blazars" (PI F. Tavecchio).

REFERENCES

Abdo, A. A., Ackermann, M., Ajello, M., Axelsson, M., Baldini, L., Ballet, J., et al. (2009a). Fermi/Large area telescope discovery of gamma-ray emission from a relativistic jet in the narrow-line quasar PMN J0948+0022. *Astrophys. J.* 699, 976–984. doi: 10.1088/0004-637X/699/2/976

Abdo, A. A., Ackermann, M., Ajello, M., Axelsson, M., Baldini, L., Ballet, J., et al. (2009b). Multiwavelength monitoring of the enigmatic narrow-line seyfert 1 PMN J0948+0022 in 2009 March-July. *Astrophys. J.* 707, 727–737. doi: 10.1088/0004-637X/707/1/727

Abdo, A. A., Ackermann, M., Ajello, M., Baldini, L., Ballet, J., Barbiellini, G., et al. (2009c). Radio-Loud narrow-line seyfert 1 as a new class of gamma-ray active galactic nuclei. *Astrophys. J.* 707, L142–L147. doi: 10.1088/0004-637X/707/2/L142

Angel, J. R. P., and Stockman, H. S. (1980). Optical and infrared polarization of active extragalactic objects. *Ann. Rev. Astron. Astrophys.* 18, 321–361. doi: 10.1146/annurev.aa.18.090180.001541

Angelakis, E., Fuhrmann, L., Marchili, N., Foschini, L., Myserlis, I., Karamanavis, V., et al. (2015). Radio jet emission from GeV-emitting narrow-line Seyfert 1 galaxies. *Astron. Astrophys.* 575:A55. doi: 10.1051/0004-6361/201425081

Antón, S., Browne, I. W. A., and Marchã, M. J. (2008). The colour of the narrow line Sy1-blazar 0324+3410. *Astron. Astrophys.* 490, 583–587. doi: 10.1051/0004-6361:20078926

Belczynski, K., Wiktorowicz, G., Fryer, C. L., Holz, D. E., and Kalogera, V. (2012). Missing Black Holes Unveil the Supernova Explosion Mechanism. *Astrophys. J.* 757:91. doi: 10.1088/0004-637X/757/1/91

Berton, M., Caccianiga, A., Foschini, L., Peterson, B. M., Mathur, S., Terreran, G., et al. (2016). Compact steep-spectrum sources as the parent population of flat-spectrum radio-loud narrow-line Seyfert 1 galaxies. *Astron. Astrophys.* 591:A98. doi: 10.1051/0004-6361/201628171

Berton, M., Foschini, L., Caccianiga, A., Ciroi, S., Congiu, E., Cracco, V., et al. (in press). An orientation-based unification of young jetted active galactic nuclei: the case of 3C 286. *Front. Astron. Space Sci.* 4:00008. doi: 10.3389/fspas.2017.00008

Best, P. N., and Heckman, T. M. (2012). On the fundamental dichotomy in the local radio-AGN population: accretion, evolution and host galaxy properties. *Mon. Not. R. Soc. Astron.* 421, 1569–1582. doi: 10.1111/j.1365-2966.2012.20414.x

Bottazzini, U. (1990). *Il Flauto di Hilbert*. Torino:UTET.

Böttcher, M., and Dermer, C. D. (2002). An evolutionary scenario for blazar unification. *Astrophys. J.* 564, 86–91. doi: 10.1086/324134

Buttiglione, S., Capetti, A., Celotti, A., Axon, D. J., Chiaberge, M., Macchetto, F. D., et al. (2010). An optical spectroscopic survey of the 3CR sample of radio galaxies with z < 0.3 . II. Spectroscopic classes and accretion modes in radio-loud AGN. *Astron. Astrophys.* 509:A6. doi: 10.1051/0004-6361/200913290

Caccianiga, A., Antón, S., Ballo, L., Foschini, L., Maccacaro, T., Della Ceca, R., et al. (2015). WISE colours and star formation in the host galaxies of radio-loud narrow-line Seyfert 1. *Mon. Not. R. Soc. Astron.* 451, 1795–1805. doi: 10.1093/mnras/stv939

Cavaliere, A., and D'Elia, V. (2002). The Blazar Main Sequence. *Astrophys. J.* 571, 226–233. doi: 10.1086/339778

Chiaberge, M., and Marconi, A. (2011). On the origin of radio loudness in active galactic nuclei and its relationship with the properties of the central supermassive black hole. *Mon. Not. R. Soc. Astron.* 416, 917–926. doi: 10.1111/j.1365-2966.2011.19079.x

Coziol, R., Andernach, H., Torres-Papaqui, J. P., Ortega-Minakata, R. A., and Moreno del Rio, F. (2017). What sparks the radio-loud phase of nearby quasars? *Mon. Not. R. Astron. Soc.* 466, 921–944. doi: 10.1093/mnras/stw3164

D'Ammando, F., Acosta-Pulido, J. A., Capetti, A., Raiteri, C. M., Baldi, R. D., Orienti, M., et al. (2017). Uncovering the host galaxy of the γ-ray-emitting narrow-line Seyfert 1 galaxy FBQS J1644+2619. *Mon. Not. R. Astron. Soc.* 469, L11–L15. doi: 10.1093/mnrasl/slx042

D'Onofrio, M., Marziani, P., and Sulentic, J. W. (2012). *Fifty Years of Quasars*. Heidelberg: Springer.

Foschini, L. (2011). Accretion and jet power in active galactic nuclei. *Res. Astron. Astrophys.* 11, 1266–1278. doi: 10.1088/1674-4527/11/11/003

Foschini, L. (2012a). "γ-ray emission from Narrow-Line Seyfert 1 galaxies and implications on the jets unification," in *American Institute of Physics Conference Series*, Volume 1505 of *American Institute of Physics Conference Series*, eds F. A. Aharonian, W. Hofmann, and F. M. Rieger (Melville, NY: American Institute of Physics), 574–577.

Foschini, L. (2012b). "Powerful relativistic jets in narrow-line Seyfert 1 glaxies (review)," in *Nuclei of Seyfert Galaxies and QSOs – Central Engine and Conditions of STAR Formation (Seyfert 2012), Proceedings of Science* (Bonn).

Foschini, L. (2014). The unification of relativistic jets. *Int. J. Mod. Phys. Conf. Ser.* 28:1460188. doi: 10.1142/S2010194514601884

Foschini, L. (2017). Yet another introduction to relativistic astrophysics. arXiv:1703.05575.

Foschini, L., Berton, M., Caccianiga, A., Ciroi, S., Cracco, V., Peterson, B. M., et al. (2015). Properties of flat-spectrum radio-loud narrow-line Seyfert 1 galaxies. *Astron. Astrophys.* 575:A13. doi: 10.1051/0004-6361/201424972

Foschini, L., Berton, M., Caccianiga, A., Ciroi, S., Cracco, V., Peterson, B. M., et al. (2016). "Broad-band properties of flat-spectrum radio-loud narrow-line Seyfert 1 galaxies," in *Proceedings 28th Texas Symposium on Relativistic Astrophysics*, (Geneva).

Foschini, L., for the Fermi/LAT Collaboration, Ghisellini, G., Maraschi, L., Tavecchio, F., and Angelakis, E. (2010). "Fermi/LAT discovery of gamma-ray emission from a relativistic jet in the narrow-line seyfert 1 quasar PMN J0948+0022," in *Accretion and Ejection in AGN: a Global View*, *Vol. 427* of *Astronomical Society of the Pacific Conference Series*, eds L. Maraschi, G. Ghisellini, R. Della Ceca, and F. Tavecchio (San Francisco, CA: Astronomical Society of the Pacific), 243–248.

Fossati, G., Maraschi, L., Celotti, A., Comastri, A., and Ghisellini, G. (1998). A unifying view of the spectral energy distributions of blazars. *Mon. Not. R. Soc. Astron.* 299, 433–448. doi: 10.1046/j.1365-8711.1998.01828.x

Gallo, L. C., Edwards, P. G., Ferrero, E., Kataoka, J., Lewis, D. R., Ellingsen, S. P., et al. (2006). The spectral energy distribution of PKS 2004-447: a compact

steep-spectrum source and possible radio-loud narrow-line Seyfert 1 galaxy. *Mon. Not. R. Soc. Astron.* 370, 245–254. doi: 10.1111/j.1365-2966.2006.10482.x

Ghisellini, G., Celotti, A., Fossati, G., Maraschi, L., and Comastri, A. (1998). A theoretical unifying scheme for gamma-ray bright blazars. *Mon. Not. R. Soc. Astron.* 301, 451–468. doi: 10.1046/j.1365-8711.1998.02032.x

Ghisellini, G., Tavecchio, F., Foschini, L., Ghirlanda, G., Maraschi, L., and Celotti, A. (2010). General physical properties of bright Fermi blazars. *Mon. Not. R. Astron. Soc.* 402, 497–518. doi: 10.1111/j.1365-2966.2009.15898.x

Giommi, P., and Padovani, P. (1994). BL Lac Reunification. *Mon. Not. R. Astron. Soc.* 268:L51. doi: 10.1093/mnras/268.1.L51

Hamilton, T. S., and Foschini, L. (2012). "Gamma-ray bright narrow line seyfert 1s: their host galaxies and origin," in *American Astronomical Society Meeting Abstracts #220*, *Vol. 220 of American Astronomical Society Meeting Abstracts* (Anchorage, AK), 335.07.

Heinz, S., and Sunyaev, R. A. (2003). The non-linear dependence of flux on black hole mass and accretion rate in core-dominated jets. *Mon. Not. R. Astron. Soc.* 343, L59–L64. doi: 10.1046/j.1365-8711.2003.06918.x

Hine, R. G., and Longair, M. S. (1979). Optical spectra of 3CR radio galaxies. *Mon. Not. R. Astron. Soc.* 188, 111–130. doi: 10.1093/mnras/188.1.111

Inskip, K. J., Tadhunter, C. N., Morganti, R., Holt, J., Ramos Almeida, C., and Dicken, D. (2010). A near-IR study of the host galaxies of 2 Jy radio sources at $0.03 \lesssim z \lesssim 0.5$ - I. The data. *Mon. Not. R. Astron. Soc.* 407, 1739–1766. doi: 10.1111/j.1365-2966.2010.17002.x

Jolley, E. J. D., and Kuncic, Z. (2008). Jet-enhanced accretion growth of supermassive black holes. *Mon. Not. R. Astron. Soc.* 386, 989–994. doi: 10.1111/j.1365-2966.2008.13082.x

Keel, W. C., White, III, R. E., Owen, F. N., and Ledlow, M. J. (2006). The spiral host galaxy of the double radio source 0313-192. *Astron. J.* 132, 2233–2242. doi: 10.1086/508340

Komossa, S., Voges, W., Xu, D., Mathur, S., Adorf, H.-M., Lemson, G., et al. (2006). Radio-loud narrow-line type 1 quasars. *Astrophys. J.* 132, 531–545. doi: 10.1086/505043

Kotilainen, J. K., León-Tavares, J., Olguín-Iglesias, A., Baes, M., Anórve, C., Chavushyan, V., et al. (2016). Discovery of a pseudobulge galaxy launching powerful relativistic jets. *Astrophys. J.* 832:157. doi: 10.3847/0004-637X/832/2/157

Kreikenbohm, A., Schulz, R., Kadler, M., Wilms, J., Markowitz, A., Chang, C. S., et al. (2016). The gamma-ray emitting radio-loud narrow-line Seyfert 1 galaxy PKS 2004-447. I. The X-ray View. *Astron. Astrophys.* 585:A91. doi: 10.1051/0004-6361/201424818

Lähteenmäki, A., Järvelä, E., Hovatta, T., Tornikoski, M., Harrison, D. L., López-Caniego, M., et al. (2017). 37 GHz observations of narrow-line Seyfert 1 galaxies. *Astron. Astrophys.* arXiv:1703.10365.

Laing, R. A., Jenkins, C. R., Wall, J. V., and Unger, S. W. (1994). "Spectrophotometry of a complete sample of 3CR radio sources: implications for unified models," in *The Physics of Active Galaxies*, *Vol. 54* of *Astronomical Society of the Pacific Conference Series*, eds G. V. Bicknell, M. A. Dopita, and P. J. Quinn (San Francisco, CA: Astronomical Society of the Pacific), 201.

Laor, A. (2000). On black hole masses and radio loudness in active galactic nuclei. *Astrophys. J.* 543, L111–L114. doi: 10.1086/317280

León Tavares, J., Kotilainen, J., Chavushyan, V., Añorve, C., Puerari, I., Cruz-González, I., et al. (2014). The host galaxy of the gamma-ray narrow-line seyfert 1 galaxy 1H 0323+342. *Astrophys. J.* 795:58. doi: 10.1088/0004-637X/795/1/58

Lister, M. L., Aller, M. F., Aller, H. D., Homan, D. C., Kellermann, K. I., Kovalev, Y. Y., et al. (2016). MOJAVE: XIII. Parsec-scale AGN Jet Kinematics Analysis Based on 19 years of VLBA Observations at 15 GHz. *Astron. J.* 152:12. doi: 10.3847/0004-6256/152/1/12

Maraschi, L., and Tavecchio, F. (2003). The Jet-Disk Connection and Blazar Unification. *Astrophys. J.* 593, 667–675. doi: 10.1086/342118

Mathur, S. (2000). Narrow-line Seyfert 1 galaxies and the evolution of galaxies and active galaxies. *Mon. Not. R. Astron. Soc.* 314, L17–L20. doi: 10.1046/j.1365-8711.2000.03530.x

Miley, G. K., and Miller, J. S. (1979). Relations between the emission spectra and radio structures of quasars. *Astrophys. J.* 228, L55–L58. doi: 10.1086/182902

Morganti, R., Holt, J., Tadhunter, C., Ramos Almeida, C., Dicken, D., Inskip, K., et al. (2011). PKS 1814-637: a powerful radio-loud AGN in a disk galaxy. *Astron. Astrophys.* 535:A97. doi: 10.1051/0004-6361/201117686

Mościbrodzka, M., Falcke, H., and Noble, S. (2016). Scale-invariant radio jets and varying black hole spin. *Astron. Astrophys.* 596:A13. doi: 10.1051/0004-6361/201629157

Neustroev, V. V., Veledina, A., Poutanen, J., Zharikov, S. V., Tsygankov, S. S., Sjoberg, G., et al. (2014). Spectroscopic evidence for a low-mass black hole in SWIFT J1753.5-0127. *Mon. Not. R. Astron. Soc.* 445, 2424–2439. doi: 10.1093/mnras/stu1924

Olguín-Iglesias, A., Kotilainen, J. K., León Tavares, J., Chavushyan, V., and Añorve, C. (2017). Evidence of bar-driven secular evolution in the gamma-ray narrow-line Seyfert 1 galaxy FBQS J164442.5+261913. *Mon. Not. R. Astron. Soc.* 467, 3712–3722. doi: 10.1093/mnras/stx022

Olguín-Iglesias, A., León-Tavares, J., Kotilainen, J. K., Chavushyan, V., Tornikoski, M., Valtaoja, E., et al. (2016). The host galaxies of active galactic nuclei with powerful relativistic jets. *Mon. Not. R. Astron. Soc.* 460, 3202–3220. doi: 10.1093/mnras/stw1208

Padovani, P., and Giommi, P. (1995). The connection between x-ray- and radio-selected BL Lacertae objects. *Astrophys. J.* 444, 567–581. doi: 10.1086/175631

Paliya, V. S., Parker, M. L., Fabian, A. C., and Stalin, C. S. (2016). Broadband Observations of High Redshift Blazars. *Astrophys. J.* 825:74. doi: 10.3847/0004-637X/825/1/74

Sanders, D. B., Soifer, B. T., Elias, J. H., Madore, B. F., Matthews, K., Neugebauer, G., et al. (1988a). Ultraluminous infrared galaxies and the origin of quasars. *Astrophys. J.* 325, 74–91. doi: 10.1086/165983

Sanders, D. B., Soifer, B. T., Elias, J. H., Neugebauer, G., and Matthews, K. (1988b). Warm ultraluminous galaxies in the IRAS survey - The transition from galaxy to quasar? *Astrophys. J.* 328, L35–L39. doi: 10.1086/185155

Schulz, R., Kreikenbohm, A., Kadler, M., Ojha, R., Ros, E., Stevens, J., et al. (2016). The gamma-ray emitting radio-loud narrow-line Seyfert 1 galaxy PKS 2004-447. II. The radio view. *Astron. Astrophys.* 588:A146. doi: 10.1051/0004-6361/201527404

Shaw, M. S., Romani, R. W., Cotter, G., Healey, S. E., Michelson, P. F., Readhead, A. C. S., et al. (2012). Spectroscopy of Broad-line Blazars from 1LAC. *Astrophys. J.* 748:49. doi: 10.1088/0004-637X/748/1/49

Tadhunter, C. (2016). Radio AGN in the local universe: unification, triggering and evolution. *Astron. Astrophys. Rev.* 24:10. doi: 10.1007/s00159-016-0094-x

Toscano, F. (2004). *Il Genio e il Gentiluomo*. Milano: Sironi.

Urry, C. M., and Padovani, P. (1995). Unified Schemes for Radio-Loud Active Galactic Nuclei. *Publ. Astron. Soc. Pacific* 107:803. doi: 10.1086/133630

Wills, B. J., and Browne, I. W. A. (1986). Relativistic beaming and quasar emission lines. *Astrophys. J.* 302, 56–63. doi: 10.1086/163973

Zdziarski, A. A., Mikołajewska, J., and Belczyński, K. (2013). Cyg X-3: a low-mass black hole or a neutron star. *Mon. Not. R. Astron. Soc.* 429, L104–L108. doi: 10.1093/mnrasl/sls035

Zhou, H., Wang, T., Yuan, W., Shan, H., Komossa, S., Lu, H., et al. (2007). A Narrow-Line Seyfert 1-Blazar Composite Nucleus in 2MASX J0324+3410. *Astrophys. J.* 658, L13–L16. doi: 10.1086/513604

Conflict of Interest Statement: The author declares that the research was conducted in the absence of any commercial or financial relationships that could be construed as a potential conflict of interest.

The reviewer DB and handling Editor declared their shared affiliation, and the handling Editor states that the process nevertheless met the standards of a fair and objective review.

Copyright © 2017 Foschini. This is an open-access article distributed under the terms of the Creative Commons Attribution License (CC BY). The use, distribution or reproduction in other forums is permitted, provided the original author(s) or licensor are credited and that the original publication in this journal is cited, in accordance with accepted academic practice. No use, distribution or reproduction is permitted which does not comply with these terms.

frontiers in Astronomy and Space Sciences

PERSPECTIVE
published: 23 November 2017
doi: 10.3389/fspas.2017.00045

An Optical View of Extragalactic γ-Ray Emitters

Simona Paiano[1,2]*, *Renato Falomo*[1], *Marco Landoni*[3], *Aldo Treves*[4] *and Riccardo Scarpa*[5,6]

[1] Osservatorio Astronomico di Padova (INAF), Padua, Italy, [2] Istituto Nazionale di Fisica Nucleare, Sezione di Padova, Padua, Italy, [3] Osservatorio Astronomico di Brera (INAF), Merate, Italy, [4] Università degli Studi dell'Insubria, Varese, Italy, [5] Instituto de Astrofísica de Canarias, Santa Cruz de Tenerife, Spain, [6] Departamento de Astrofsica, Universidad de La Laguna, San Cristóbal de La Laguna, Spain

The Fermi Gamma-ray Observatory discovered about a thousand extragalactic sources emitting energy from 100 MeV to 100 GeV. The majority of these sources belong to the class of blazars characterized by a quasi-featureless optical spectrum (BL Lac Objects). This hampers the determination of their redshift and therefore hinders the characterization of this class of objects. To investigate the nature of these sources and to determine their redshift, we are carrying out an extensive campaign using the 10 m Gran Telescopio Canarias to obtain high S/N ratio optical spectra. These observations allow us to confirm the blazar nature of the targets, to find new redshifts or to set stringent limits on the redshift based on the minimum equivalent width of specific absorption features that can be measured in the spectrum and are expected from their host galaxy, assuming it is a massive elliptical galaxy. These results are of importance for the multi-frequencies emission models of the blazars, to test their extreme physics, to shed light on their cosmic evolution and abundance in the far Universe. These gamma emitters are also of great importance for the characterization of the extragalactic background light through the absorption by the IR-optical background photons.

Keywords: blazars, BL Lac objects, optical spectroscopy, redshift, γ-ray astronomy

OPEN ACCESS

Edited by:
Paola Marziani, Osservatorio Astronomico di Padova (INAF), Italy

Reviewed by:
Brian Punsly, International Center for Relativistic Astrophysics, Italy
Dawei Xu, National Astronomical Observatories (CAS), China

***Correspondence:**
Simona Paiano
simona.paiano@oapd.inaf.it

Specialty section:
This article was submitted to Milky Way and Galaxies, a section of the journal Frontiers in Astronomy and Space Sciences

Received: *06 September 2017*
Accepted: *31 October 2017*
Published: *23 November 2017*

Citation:
Paiano S, Falomo R, Landoni M, Treves A and Scarpa R (2017) An Optical View of Extragalactic γ-Ray Emitters. Front. Astron. Space Sci. 4:45. doi: 10.3389/fspas.2017.00045

1. INTRODUCTION

A blazar is a jetted active galactic nucleus (AGN) with the relativistic jet that points along the line of sight of the observer. These kind of objects are bright emitters at all frequencies (from radio to TeV regime), are characterized by high variability at all frequencies and large polarization, and are often dominated by the γ-ray emission especially during the outbursts.

Their spectral energy distribution (SED) shows the typical doubled-humped structure with two broad peaks: the first bump is located at low energies, typically in the infrared to X-ray region, and is interpreted as due to synchrotron emission produced by electrons of the jet spiraling along the lines of force of the magnetic field, instead the second peak is placed at higher frequency, between the X-ray and the MeV-TeV energies, and as suggested in most leptonic models, can be due to Compton scattering of the same electrons (e.g., Maraschi et al., 1992; Dermer and Schlickeiser, 1993; Ghisellini and Tavecchio, 2009).

Blazars are commonly classified in two categories, BL Lac Objects (BLLs) and the Flat Spectrum Radio Quasars (FSRQs), and this classification depends on the strength of their broad emission lines respect to the continuum. A more physical distinction is based on to the comparison between

the luminosity of the broad line region (BLR) and the Eddington luminosity (e.g., Ghisellini et al., 2017): FSRQs have radially efficient accretion disk, while the BL Lac objects are not able to photoionise gas of the BLR, causing the absence of features in the majority of their optical spectra. This classification needs to know the mass of the accreting black hole and the redshift of the source, which for broad emission line AGNs can be determined by spectroscopy, while for the BLLs is arduous due to the faintness or absence of the emission/absorption lines, showing a completely featureless optical spectra (Falomo et al., 2014).

The advent of the *Fermi* γ-ray observatory, starting observations in 2008 (Atwood et al., 2009), with its systematic scanning of the entire sky every 3 h at the high energy band (HE; > 20 MeV), has revolutionized the blazar studies, previously performed with radio and X-ray surveys. The extragalactic γ-ray sky is dominated by blazars (Acero et al., 2015) and in the third AGN *Fermi*/LAT catalogue (Ackermann et al., 2015, 3LAC), 1738 blazars are reported, compared with the 3033 γ-ray detected sources:662 are classified as BLL, 491 as FSRQ, while the remaining blazars are as of uncertain type. It is worth to note that a growing sub-sample of the GeV blazars are also emitters at the TeV energies (VHE; E > 100 GeV), detected by the Cherenkov telescopes as MAGIC, VERITAS and the HESS arrays, that can sample energies down to 30–50 GeV. The majority of them are BLLs (in the TeVcat[1] there are 60 BLLs against 6 FSRQs), implying that the BLL class dominates the extragalactic TeV sky.

Although BLLs are the most numerous extragalactic class in the HE and VHE bands, for a large fraction of them the redshift is still unknown or highly uncertain, because contrarily to most AGNs, the BLLs are characterized by featureless (or quasi) featureless spectra. On the basis of the recent statistics, it was proposed that on average BLLs have lower redshift and smaller high energy γ-ray luminosity than FSRQs (Ghisellini et al., 2017). However, this could be due to a bias since the number of robustly detected high redshift BLLs is significantly limited due to the difficulty to measure their distance. Hence the determination of the blazar redshift is crucial to calculate their luminosity, to build and characterize realistic emission models and to allow us a sound comparison of the multi-frequency SEDs between the two blazar classes (see the *blazar sequence*, Fossati et al., 1998; Ghisellini et al., 2017).

The estimation of the BLL redshifts is also essential to determine the properties of the extragalactic background light (EBL). The BLL γ-rays of high energy can interact with the EBL infrared-optical photons and produce pairs e^-/e^+, resulting in an absorption in the GeV-TeV BLL spectrum starting at frequencies and with optical depth that depend on the redshift of the γ-ray source and is more pronounced in the $0.5 < z < 2$ interval (Franceschini et al., 2008). At higher z the absorption due to pair production moves to *Fermi* energies, completely extinguishing the source in the VHE regime. Although a significant number of FSRQ detections, up to $z > 4$ already exist (Ackermann et al., 2017), at the TeV energies, due to their Compton inverse peak position, only a small fraction of them are detected. Therefore the identification of high redshift BLLs at these energies is particularly challenging in order to study the earliest EBL components due to the first-light sources (Population III stars, galaxies or quasars) in the universe (e.g., Franceschini and Rodighiero, 2017).

These considerations motivated us to carry out an extensive campaign at the 10.4 m Gran Telescopio Canarias aimed to obtain high signal-to-noise ratio (SNR) optical spectra and to estimate the redshift of BLLs. The results of this project are shown in Landoni et al. (2015) for S20954+65, Paiano et al. (2016) for the TeV BLL S20109+22, Falomo et al. (2017) for the blazar B0218+357, Paiano et al. (2017b) for a sample of 15 TeV BLL and 7 TeV candidates with unknown or uncertain redshift and in Paiano et al. (2017a) focused on 10 BLLs detected by *Fermi* satellite suggested to be at relatively high redshift by previous works. Moreover, till now, we observed 40 unassociated γ-ray objects detected by *Fermi* and candidate to be blazars (Paiano et al., submitted), 20 BLLs optically selected among the SDSS blazars (Landoni et al., submitted) and 10 hard *Fermi* sources.

2. SAMPLE, DATA REDUCTION AND ANALYSIS

This spectroscopic program involved a conspicuous sample of BLLs, for a total of ∼100 objects and for which the selection followed different criteria (see details in Paiano et al., 2017a,b). All of these objects were also selected to have unknown or uncertain redshift for which conflicting estimates are published in the literature, mainly due to spectra with low S/N.

The observations were gathered at the GTC using the medium resolution spectrograph OSIRIS (Cepa et al., 2003), configured with the grisms R1000B and R1000R and covering the spectral range 4100-10000 Å. Details about the observational strategy, the data reduction and analysis procedure are reported in Paiano et al. (2017a,b), where all spectra, corrected for atmospheric extinction and flux calibrated, are reported. They are also reported in the website http://www.oapd.inaf.it/zbllac/. On average, the S/N ranges from 100 to 200 at 4500 and 8000 Å, to a peak of 300 at ∼6000 Å.

3. RESULTS

Our spectra allow us to confirm the blazar nature of the observed targets and, on the basis on the spectroscopic properties, they exhibit four characteristic features: (1) weak emission lines typical of low density gas; (2) spectral lines of stars from the host galaxy; (3) intervening absorption systems due to cold gas; and (4) a pure featureless continuum. While the first three types can co-exist and from them a redshift can be derived when emission and/or absorption lines are identified, in the latter case, thank to high SNR achieved, we can set a stringent redshift lower limit on the basis of the minimum Equivalent Width (EW) of absorption lines expected from the starlight emission of the blazar host galaxy.

[1] http://tevcat.uchicago.edu/

- **Spectra with emission lines characteristic of low-density gas**

Although the BLL optical spectra are mainly characterized by a featureless continuum, very weak emission lines can be seen, with an intrinsic luminosity lower than those observed in quasars. Owing to the weakness of these lines, their detectability depends on the state of the source, with faint state of the source that favors the detection of intrinsic emission lines, and on the quality of the observations, especially in terms of S/N ratio.

In particular from our spectra, we detect weak emission lines due to [O III] (5007 Å) in the spectrum of 1ES1215+303, W-Comae, MS1221.8+2452 and PKS1424+240, and the [O II] (3727 Å) emission in 1ES0033+595, 1ES1215+303, and PKS1424+240. For the first time, we are able to determine the spectroscopic redshift of $z = 0.467$ and $z = 0.6047$ for 1ES0033+595 and PKS1424+240 respectively (in **Figure 1** the spectrum of PKS1424+240, one of the farthest TeV BLLs).

- **Spectra with absorption lines due to the stellar population of the host galaxy**

BLLs are located in the nuclei of giant/massive elliptical galaxies with a prominent spheroidal component and with average luminosity in the R band of $M_R \sim 23$ (Falomo et al., 2014, and references therein). Their stellar population is composed by old stars and therefore the main observable absorption lines are Ca II (3934, 3967 Å) , G-band (4304 Å), H_β (4861 Å), Mg I (5175 Å) and Na I (5875 Å). These absorption features can be detected over the non-thermal component and this depends on the signal-to-noise ratio and the spectral resolution of the spectrum, and finally on the relative power of the non-thermal nucleus and the host galaxy. In very few cases, high quality spectroscopy with adequate high spatial resolution can probe star formation of the host galaxy and allow us to detect narrow emission lines from it.

In our sample, we were able to detect host galaxy absorption lines for W Comae ($z = 0.102$), MS 1221.8+2452 ($z = 0.218$), 3FGL J0505.5+0416 ($z = 0.423$), and 3FGL J0814.5+2943 ($z = 0.703$, see **Figure 2**).

- **Spectra with intervening absorption lines**

As for the high redshift quasars, gas along the BLL direction can produce systems of absorption at redshifts lower than the target redshift. Given that BLLs show quasi featureless continuous spectrum, they are ideal sources for studying absorptions from these intervening systems (Landoni et al., 2012, and references

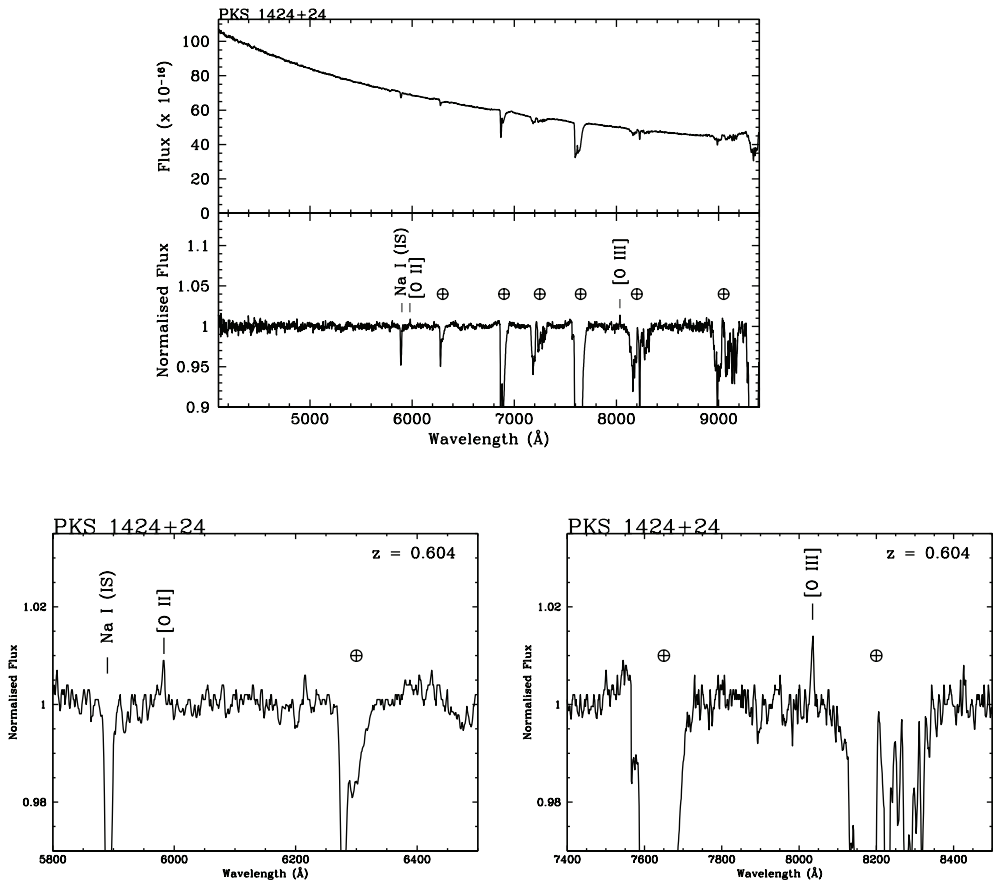

FIGURE 1 | Spectrum of the TeV source PKS 1424+240 ($z = 0.6047$) obtained at GTC. **Top**: Flux-calibrated and dereddered spectrum, and normalized spectrum. The main telluric bands are indicated by ⊕, the absorption features from interstellar medium of our galaxies are labeled as IS (Inter-Stellar). **Bottom**: Close-up of the normalized spectrum around the found emission spectral lines, marked by line identification.

therein). The redshift of the intervening systems yields a lower limit to the BLL redshift, while an upper limit can be set from the expected distribution of the absorbers (Zhu and Ménard, 2013).

For six of our targets, 3FGL J0008.0+4713, BZB J1243+3627, and 3FGL J1450.9+5200 with an uncertain redshift in literature, and BZB J1540+8155, 3FGL J1107.5+0222, and BZB J2323+4210 with unknown redshift, we detected intervening absorption systems that allow us to set spectroscopic redshift lower limits. In **Figure 3** two examples of spectra of our sample that exhibit Ly$_\alpha$ forest, C IV (1548 Å) and Mg II (2800 Å) absorption systems.

- **Featureless spectra**

In spite of the high quality of the optical spectra for 18 observed targets the spectrum appears very featureless. This occurs when the emission from the underlying nebulosity of the host galaxy is over-shined by the non-thermal continuum.

As example, **Figure 4** shows the featureless spectra of two TeV BLLs RGB J0136+391 and 3C 66A. For the latter, a previous redshift of 0.444 was proposed in literature (Miller et al., 1978) and reported in the NED. On the basis of our high S/N ratio and featureless spectrum, we cannot support this value and thus the redshift of 3C 66A is still unknown and the emission models of the source assuming the wrong redshift should be revised.

In the case of no detection of spectral lines, following the scheme outlined in Appendix A of Paiano et al. (2017b), we can set redshift lower limit using the minimum Equivalent Width method, based on the assumption that the BL Lac objects are hosted in massive elliptical galaxies and that hence the detection of their stellar absorption features depends on the

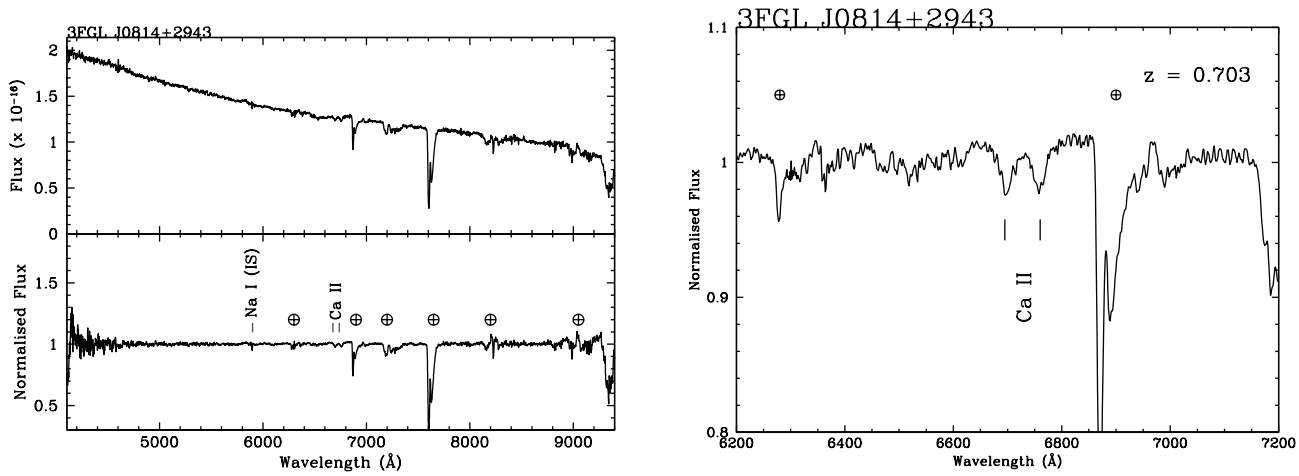

FIGURE 2 | Spectrum with S/N ∼ 160 of the 3FGL BLL J0814.5+2943. In the close-up image, the absorption doublet at 6699–6759 Å identified as Ca II (3934, 3967 Å) at $z = 0.703$ from the the host galaxy.

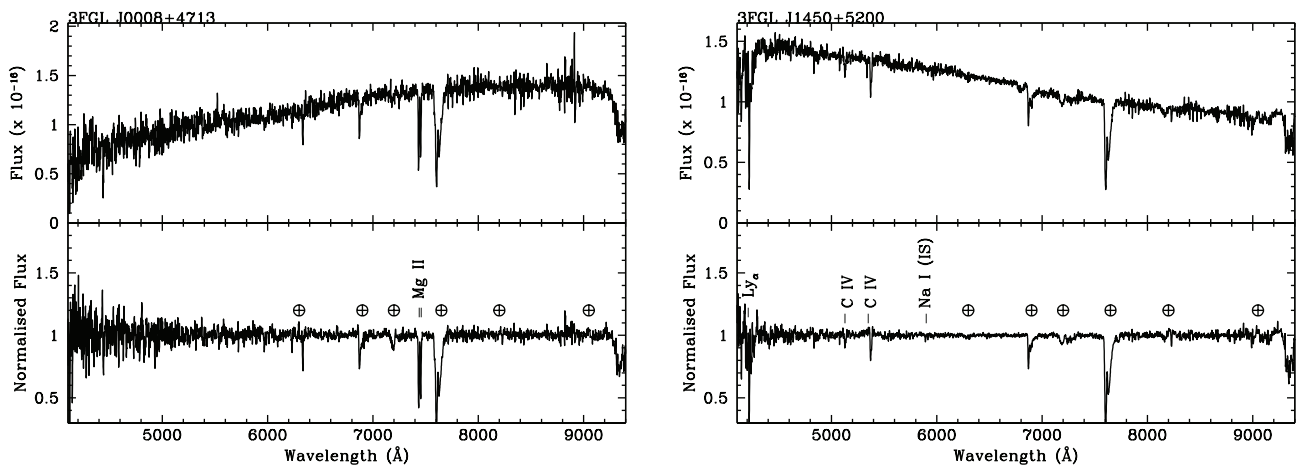

FIGURE 3 | Spectrum of the 3FGL BLLs J0008.0+4713, that shows an intervening doublet absorption system at 7440 Å identified as Mg II (2800 Å) at $z = 1.659$, and the spectrum of the 3FGL J1450.9+5200 that shows the absorption line at 5372 Å due to C IV (1548 Å) intervening gas and a strong Ly$_\alpha$ (1216 Å) absorption at the same redshift ($z = 2.470$). A second C IV intervening system at $z = 2.312$ is associated to the absorption feature detected at 5127 Å.

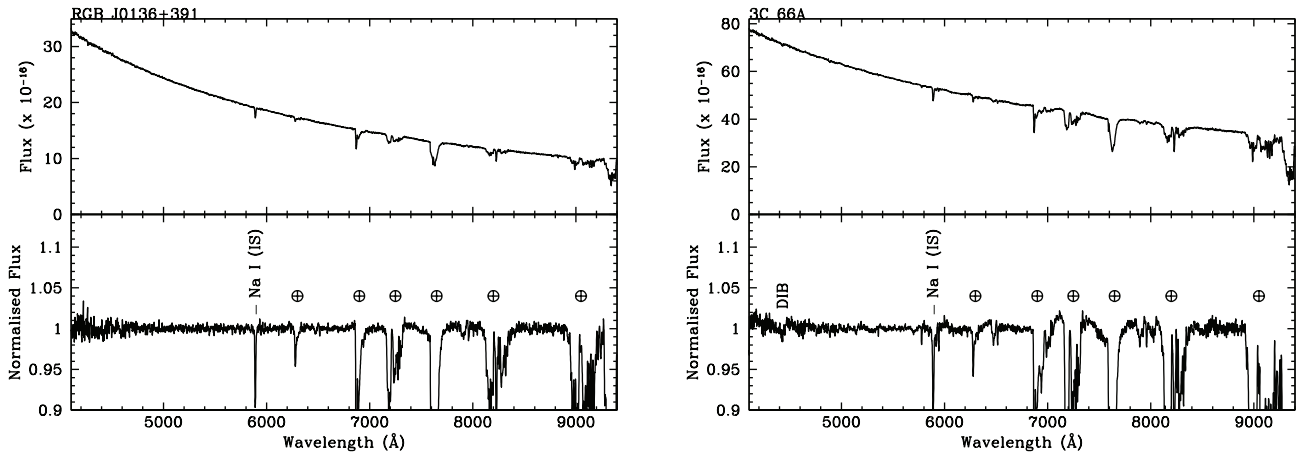

FIGURE 4 | Featureless spectra of the TeV BLL RGB J0136+391 and 3C 66A. No emission/absorption lines are identified, hence for these sources the redshift is still unknown.

SNR of their optical spectra, on the spectral resolution, and on the flux ratio between the nucleus and the host galaxy. The redshift lower limit found for 18 objects with featureless spectra are summarized in Table 3 of Paiano et al. (2017b) and Paiano et al. (2017a).

4. CONCLUSION

We secured high quality and S/N spectra for 32 γ-ray BL Lac objects, selected for being TeV sources, TeV candidates or high redshift *Fermi* objects, with unknown redshift or with conflicting redshift values in literature. We determined the redshift for 8 objects and spectroscopic redshift lower limit for 6 sources, including three of the farthest BLLs detected in the GeV and TeV regime, but for the remaining sources, in spite of the very high S/N and of the improvement of spectral resolution, their spectrum is featureless.

Although these observations represent the state of the art of the observing facilities (telescopes with large aperture and modern instrumentation) and the capabilities to perform the spectroscopy of BLLs, the redshift determination of this class of objects remains still rather arduous. For this reason, the detection of the spectral features in their spectra requires observations with very high SNR and an adequate resolution that seems feasible only with the next generation of extremely large (30–50 m class) telescopes, such as E-ELT (the European Extremely Large Telescope). An idea about the performances of these new class of telescopes is given in Landoni et al. (2014) where simulations of BLL spectra are made using an X-Shooter-like instrument (with an spectral resolution ∼3000) coupled to the E-ELT and including a moderate adaptive optics module. With these new facilities, it should be possible to measure the redshift of BLLs having extreme nucleus-to-host galaxy ratios between ∼300 to ∼2,500, depending on the redshift and the target brightness.

AUTHOR CONTRIBUTIONS

SP is the corresponding author of this contribution and presented the corresponding talk at the conference "QSO at all epochs 2017." All authors contributed to data analysis, text revision and improvement.

ACKNOWLEDGMENTS

The authors of this work thank the organizers of the "Quasars at All Cosmic Epoch" conference.

REFERENCES

Acero, F., Ackermann, M., Ajello, M., Albert, A., Atwood, W. B., Axelsson, M., et al. (2015). *Fermi* large area telescope third source catalog - *Fermi*-LAT collaboration. *Astrophys. J. Suppl.* 218:23. doi: 10.1088/0067-0049/218/2/23

Ackermann, M., Ajello, M., Atwood, W. B., Baldini, L., Ballet, J., Barbiellini, G., et al. (2015). The third catalog of active galactic nuclei detected by the fermi large area telescope. *Astrophys. J.* 810:4. doi: 10.1088/0004-637X/810/1/14

Ackermann, M., Ajello, M., Baldini, L., Ballet, J., and Barbiellini, G. (2017). Gamma-ray blazars within the first 2 billion years. *Astrophys. J. Lett.* 837:L5. doi: 10.3847/2041-8213/aa5fff

Atwood, W. B., Abdo, A. A., Ackermann, M., Althouse, W., Anderson, B., Axelsson, M., et al. (2009). The large area telescope on the fermi gamma-ray space telescope mission. *Astrophys. J.* 697, 1071–1102. doi: 10.1088/0004-637X/697/2/1071

Cepa, J., Aguiar-Gonzalez, M., Bland-Hawthorn, J., Castaneda, H., Cobos, F. J., Correa, S., et al. (2003). OSIRIS tunable imager and spectrograph for the GTC. Instrument status. *Proc. SPIE* 4841, 1739–1749. doi: 10.1117/12.460913

Dermer, C. D., and Schlickeiser, R. (1993). Model for the high-energy emission from blazars. *Astrophys. J.* 416:458. doi: 10.1086/173251

Falomo, R., Pian, E., and Treves, A. (2014). An optical view of BL Lacertae objects. *Astron. Astrophys. Rev.* 22:73. doi: 10.1007/s00159-014-0073-z

Falomo, R., Treves, A., Scarpa, R., Paiano, S., and Landoni, M. (2017). On the lensed blazar B0218+357. *Month. Notices R. Astron. Soc.* 470, 2814–2821. doi: 10.1093/mnras/stx1411

Fossati, G., Maraschi, L., Celotti, A., Comastri, A., and Ghisellini, G. (1998). A unifying view of the spectral energy distributions of blazars. *Month. Notices R. Astron. Soc.* 299, 433–448. doi: 10.1046/j.1365-8711.1998.01828.x

Franceschini, A., and Rodighiero, G. (2017). The extragalactic background light revisited and the cosmic photon-photon opacity. *Astron. Astrophys.* 603:A34. doi: 10.1051/0004-6361/201629684

Franceschini, A., Rodighiero, G., and Vaccari, M. (2008). Extragalactic optical-infrared background radiation, its time evolution and the cosmic photon-photon opacity. *Astron. Astrophys.* 487, 837–852. doi: 10.1051/0004-6361:200809691

Ghisellini, G., Righi, C., Costamante, L., and Tavecchio, F. (2017). The Fermi blazar sequence. *Month. Notices R. Astron. Soc.* 469, 255–266. doi: 10.1093/mnras/stx806

Ghisellini, G., and Tavecchio, F. (2009). Canonical high-power blazars. *Month. Notices R. Astron. Soc.* 397, 985–1002. doi: 10.1111/j.1365-2966.2009.15007.x

Landoni, M., Falomo, R., Treves, A., and Sbarufatti, B. (2014). Spectroscopy of BL Lacertae objects of extraordinary luminosity. *Astron. Astrophys.* 570:A126. doi: 10.1051/0004-6361/201424232

Landoni, M., Falomo, R., Treves, A., Sbarufatti, B., Decarli, R., Tavecchio, F., et al. (2012). On the redshift of the bright BL Lacertae object PKS 0048-097. *Astron. Astrophys.* 543:A116. doi: 10.1051/0004-6361/201219114

Landoni, M., Falomo, R., Treves, A., Scarpa, R., and Reverte Payá, D. (2015). What Is the Redshift of the Gamma-ray BL Lac Source S4 0954+65? *Astron. J.* 150:181. doi: 10.1088/0004-6256/150/6/181

Maraschi, L., Ghisellini, G., and Celotti, A. (1992). A jet model for the gamma-ray emitting blazar 3C 279. *Astrophys. J. Lett.* 397, L5–L9. doi: 10.1086/186531

Miller, J. S., French, H. B., and Hawley, S. A. (1978). "Optical spectra of BL Lacertae objects," in *BL Lac Objects*, ed A. M. Wolfe (Pittsburgh, PA: University of Pittsburgh), 176–187.

Paiano, S., Landoni, M., Falomo, R., Scarpa, R., and Treves, A. (2016). On the redshift of the very high-energy gamma-ray BL Lac object S2 0109+22. *Month. Notices R. Astron. Soc.* 458, 2836–2839. doi: 10.1093/mnras/stw472

Paiano, S., Landoni, M., Falomo, R., Treves, A., and Scarpa, R. (2017a). Spectroscopy of 10 γ-ray BL Lac objects at high redshift. *Astrophys. J.* 844:120. doi: 10.3847/1538-4357/aa7aac

Paiano, S., Landoni, M., Falomo, R., Treves, A., Scarpa, R., and Righi, C. (2017b). On the Redshift of TeV BL Lac Objects. *Astrophys. J.* 837:144. doi: 10.3847/1538-4357/837/2/144

Zhu, G., and Ménard, B. (2013). The JHU-SDSS metal absorption line catalog: redshift evolution and properties of Mg II absorbers. *Astrophys. J.* 770:130. doi: 10.1088/0004-637X/770/2/130

Conflict of Interest Statement: The authors declare that the research was conducted in the absence of any commercial or financial relationships that could be construed as a potential conflict of interest.

The handling Editor declared a shared affiliation, though no other collaboration, with the authors SP and RF.

Copyright © 2017 Paiano, Falomo, Landoni, Treves and Scarpa. This is an open-access article distributed under the terms of the Creative Commons Attribution License (CC BY). The use, distribution or reproduction in other forums is permitted, provided the original author(s) or licensor are credited and that the original publication in this journal is cited, in accordance with accepted academic practice. No use, distribution or reproduction is permitted which does not comply with these terms.

frontiers in Astronomy and Space Sciences

ORIGINAL RESEARCH
published: 22 November 2017
doi: 10.3389/fspas.2017.00050

Probing the Diffuse Optical-IR Background with TeV Blazars Detected with the MAGIC Telescopes

Elisa Prandini[1], Alberto Domínguez[2], Vandad Fallah Ramazani[3], Tarek Hassan[4], Daniel Mazin[5,6], Abelardo Moralejo[4], Mireia Nievas Rosillo[2], Gaia Vanzo[7,8], and Monica Vazquez Acosta[7,8] for the MAGIC Collaboration*

[1] Dipartimento di Fisica e Astronomia "G. Galilei", University of Padova, Padua, Italy, [2] Departamento de Física Atómica, Universidad Complutense, Madrid, Spain, [3] Tuorla observatory, University of Turku, Turku, Finland, [4] IFAE, The Barcelona Institute of Science and Technology, Bellaterra, Spain, [5] Max Planck Institute for Physics, Munich, Germany, [6] Institute for Cosmic Ray Research, University of Tokyo, Tokyo, Japan, [7] Instituto de Astrofísica de Canarias, Tenerife, Spain, [8] Departamento de Astrofisica, Universidad de La Laguna, Tenerife, Spain

OPEN ACCESS

Edited by:
Ascensión Del Olmo,
Instituto de Astrofísica de Andalucía (CSIC), Spain

Reviewed by:
Daniela Bettoni,
Osservatorio Astronomico di Padova (INAF), Italy
Milan S. Dimitrijevic,
Astronomical Observatory, Serbia

***Correspondence:**
Elisa Prandini
prandini@pd.infn.it

Specialty section:
This article was submitted to Milky Way and Galaxies, a section of the journal Frontiers in Astronomy and Space Sciences

Received: 22 October 2017
Accepted: 07 November 2017
Published: 22 November 2017

Citation:
Prandini E, Domínguez A, Fallah Ramazani V, Hassan T, Mazin D, Moralejo A, Nievas Rosillo M, Vanzo G and Vazquez Acosta M for the MAGIC Collaboration (2017) Probing the Diffuse Optical-IR Background with TeV Blazars Detected with the MAGIC Telescopes. Front. Astron. Space Sci. 4:50. doi: 10.3389/fspas.2017.00050

Blazars are radio loud quasars whose jet points toward the observer. The observed emission is mostly non-thermal, dominated by the jet emission, and in some cases extends up to the very high energy gamma rays (VHE; E > 100 GeV). To date, more than 60 blazars have been detected at VHE mainly with ground-based imaging atmospheric Cherenkov telescopes (IACTs) such as MAGIC, H.E.S.S., and VERITAS. Energetic photons from a blazar may interact with the diffuse optical and IR background (the extragalactic background light, EBL) leaving an imprint on the blazar energy spectrum. This effect can be used to constrain the EBL, with basic assumptions on the intrinsic energy spectrum. Current generation of IACTs is providing valuable measurements of the EBL density and energy spectrum from optical to infrared frequencies. In this contribution, we present the latest results obtained with the data taken with the MAGIC telescopes: using 32 spectra from 12 blazars, the scale factor of the optical density predicted by the EBL model from Domínguez et al. (2011) is constrained to be $0.95\ (+0.11,\ -0.12)_{stat}\ (+0.16,\ -0.07)_{sys}$, where a value of 1 means the perfect match with the model.

Keywords: Active Galactic Nuclei (AGN), blazars, Extragalactic Background Light (EBL), relativistic jets, MAGIC telescopes, gamma rays

1. THE EXTRAGALACTIC BACKGROUND LIGHT AND ITS IMPRINT IN BLAZAR SPECTRA

The optical-infrared diffuse background that permeates the Universe is also referred as the Extragalactic Background Light (EBL). The EBL consists of light emitted by stars directly (optical) and, in part, absorbed by dust in their host galaxies and re-emitted at longer wavelengths (IR) since the birth of the first stars.

A collection of current measurements of the EBL is described in Cooray (2016), a recent and detailed review on EBL measurements and applications. Direct measurements of the EBL are complex due to strong foreground radiations from our Galaxy, but mainly from our own Solar System. Solid lower limits on the EBL density are provided by galaxy counts. Different models which take into account the evolution of galaxies have been proposed to explain and predict this optical and IR background (e.g., Franceschini et al., 2008; Domínguez et al., 2011; Gilmore et al., 2012). They differ from the degree of complexity and approach, but all converge on a similar

spectral shape and intensity for the EBL. Yet, some differences persist in the cosmic evolution of the background.

A limited number of extragalactic sources (approximately 60) is known to emit electromagnetic radiation up to the so-called very high energies (VHE, E > 100 GeV). The large majority of these sources are blazars, active galaxies displaying a jet of ultra-relativistic particles almost aligned to the line of sight. Main engine of the activity is an accreting, supermassive black hole. Blazars emitting at VHE offer a unique opportunity to test EBL models. Gamma rays with energies of hundreds of GeV and above may be, in fact, absorbed due to the interaction with EBL photons via electron-positron pair creation (Salamon and Stecker, 1998). The absorption is not only a distance dependent effect but also an energy dependent effect. Due to the energy dependence of the pair production, we have an *imprint of the EBL* in the observed spectrum from a blazar. This imprint on the blazar spectra may be used to constrain the EBL itself, under some assumptions on the shape of the intrinsic spectra.

The study presented in this paper aims at testing the state-of-the-art EBL models by means of a sample of 32 blazar spectra spanning a redshift from 0.03 to 0.944 collected with the MAGIC telescopes.

TABLE 1 | List of 12 blazars observed with the MAGIC telescopes and used in this study, sorted from the lowest to the highest redshifts.

Source name	Source type	Redshift	Observation time [h]
Markarian 421	HBL	0.03	43.8
(15 spectra)			
1ES 1959+650	HBL	0.048	4.8
OT 546	HBL	0.055	6.4
BL Lacertae	IBL	0.069	1.0
1ES 0229+200	HBL	0.14	105.2
1ES 1011+496	HBL	0.212	11.8
PKS 1510−089	FSRQ	0.361	5.0
(2 spectra)			
PKS 1222+216	FSRQ	0.432	0.5
PG 1553+113	HBL	0.43–0.58	66.4
(5 spectra)			
PKS 1424+240	HBL	0.604	49.1
(2 spectra)			
PKS 1441+25	FSRQ	0.939	20.1
QSO B0218+35	FSRQ	0.944	2.1

2. THE MAGIC TELESCOPES

MAGIC (Major Atmospheric Gamma Imaging Cherenkov) is a system of two Imaging Atmospheric Cherenkov Telescopes (IACTs) designed to observe VHE gamma rays from 50 GeV up to tens of TeV (Aleksić et al., 2016a). It is located in the Canary island of La Palma, at ∼2,200 m above the sea level. Since 2004, MAGIC has been used to observe and detect a significant signal from tens of blazars located in the Northern hemisphere. For a recent review, see Sitarek (2017).

MAGIC achieved his best performances after 2012, when the last major upgrade of the system took place. The current integral sensitivity above 220 GeV is (0.66 ± 0.03)% of the Crab Nebula flux in 50 h of observations, when assuming point-like sources with Crab Nebula-like spectrum. The angular resolution at those energies, defined as the sigma of a 2-dimensional Gaussian distribution, is <0.07 degree. The energy resolution is 16% and is defined as the standard deviation obtained from a Gaussian fit to the distribution of (Eest - Etrue)/Etrue, where Eest is the *reconstructed energy* and Etrue is the *true energy* simulated with Monte Carlo data. More details on the data analysis and the MAGIC performance can be found in Aleksić et al. (2016b).

3. METHODS

The purpose of this study is to use the largest available dataset collected with the MAGIC telescopes and set new limits on the EBL energy density. In particular, we adopt the method proposed

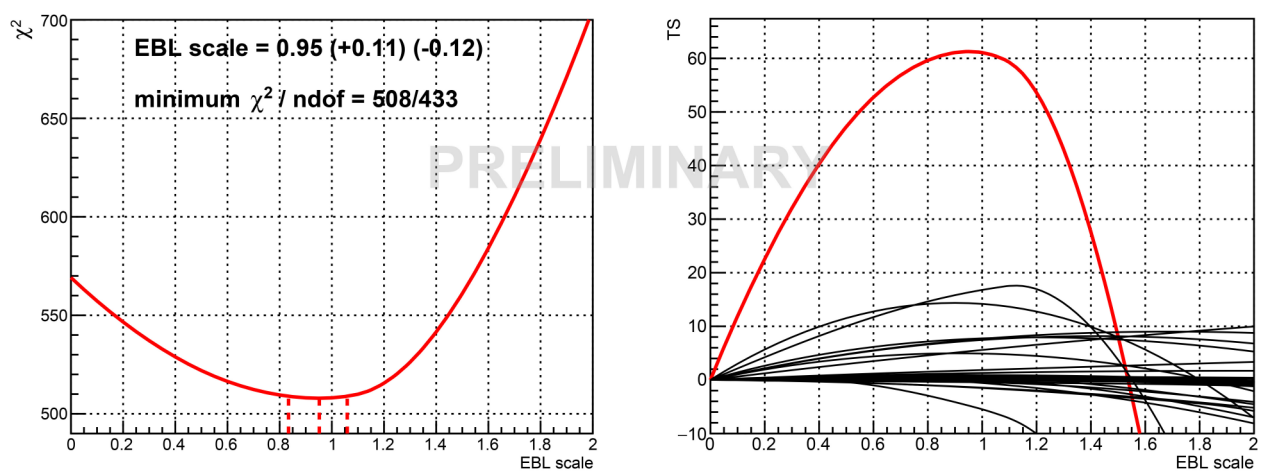

FIGURE 1 | Left: Total χ^2 from the maximum likelihood fit. **Right:** Total (red) and spectrum-wise (black) Test Statistics TS = $\chi^2(0) - \chi^2$ vs. EBL scale relative to the Domínguez model.

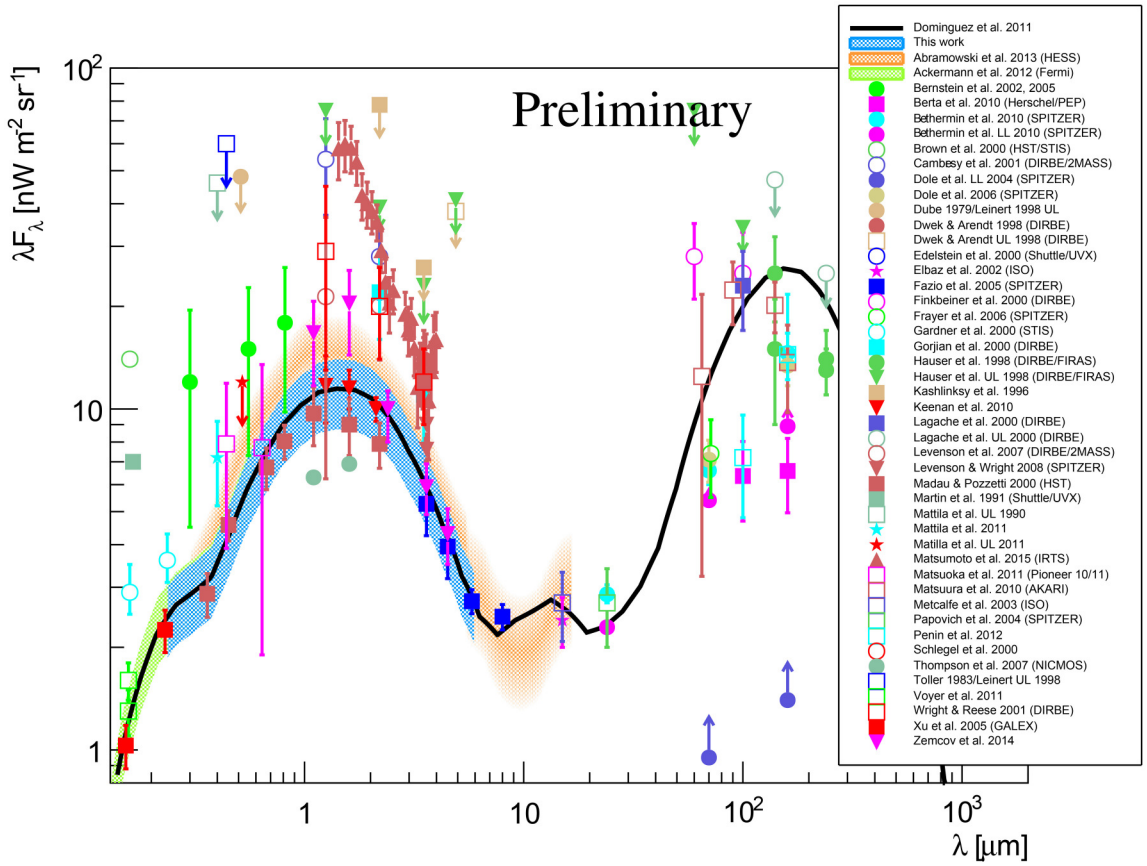

FIGURE 2 | A collection of EBL measurements with our measurements (blue area). The reported uncertainties are statistical only.

in Abramowski et al. (2013) which consists in estimating a scale factor for the EBL energy density, and can be outlined as follows:

1. Assume a particular *EBL spectral shape and its evolution over redshift*. For this work we have considered the model from Domínguez et al. (2011);
2. Assume an *instrinsic shape* that could describe the blazar spectrum before any interaction with the EBL. To this purpose, we have taken into account the following shapes: log-parabola, power-law with exponential cut-off, log-parabola with exponential cut-off, and power-law with sub/super exponential cut-off;
3. In order to estimate the most likely EBL scale factor, we have then adopted the *poissonian maximum likelihood approach*. We have compared the measured number of events in bins of estimated energy with the expected number of events estimated by assuming a particular instrinsic spectrum folded with the MAGIC instrument response function and corrected for the EBL absorption effect ($dF/dE_{observed} = dF/dE_{intrinsic} \cdot e^{-\alpha\tau(E,z)}$). Free parameters are the EBL scale factor (alpha) and the intrinsic spectral parameters. The cosmic-ray background rates vs. estimated energy are treated as nuisance parameters.
4. The previous step has been iteratively repeated in order to scan the EBL scale factor and the different instrinsic spectral shapes. In each step the fit probability has been used to decide among the 4 spectral shape options and the best fit χ^2 was estimated. The scale α_0 for which the χ^2 reaches its minimum (χ^2_{min}) is the value which best fits the data, and the condition $\Delta\chi^2 = 1$ relative to the minimum indicates the $1\,\sigma$ statistical uncertainty range.

4. DATASET

To perform this study, we have used 32 spectra from 12 sources, summarized in **Table 1**. The use, in some cases, of multiple spectra from the same source is due to the variability of the observed spectrum. The sources considered belong to two different blazar classes (second column, from TeVCat[1]): flat spectrum radio quasars (FSRQs) and high frequency peaked BL Lac objects (HBL). They span a redshift range from 0.03 to 0.944, third column. The observation time of MAGIC is reported in the last column of the Table.

[1]http://tevcat2.uchicago.edu

5. RESULTS

The results of our study are displayed in **Figure 1**. On the left panel the total χ^2, which is the linear combination of the best χ^2 values from the individual spectra, from the maximum likelihood fit procedure applied to each spectrum is reported. The minimum χ^2 corresponds to a scale factor $\alpha_0 = 0.95^{+0.11}_{-0.12}$.

The right panel of **Figure 1** displays the corresponding Test Statistics (TS $= \chi^2(0) - \chi^2$) of the total and for each individual spectrum curves as a function of the EBL scale relative to the Domínguez model.

Figure 2 shows a compilation of EBL data and models, plus the results of our analysis. This figure also shows the model proposed by Domínguez et al. (2011) whose spectral intensity is multiplied by our scale factor $\alpha_0 = 0.95^{+0.11}_{-0.12}$. It is in good agreement with recent EBL measurements (Abramowski et al., 2013; Sitarek, 2017).

5.1. Systematic Uncertainties

In order to evaluate the systematic uncertainties affecting our estimate, we have allowed for a maximum average deviation of $\pm$ 15% between data and Monte Carlo simulations of the gamma-ray showers and the detector in terms of deviation in the light throughput (atmosphere and telescopes), and tested its effect on the EBL estimate. Moreover, we have also considered the effect introduced by the different assumptions of the intrinsic spectral function. Our result is the best-fit EBL scale, $\alpha_0 = 0.95(^{+0.11}_{-0.12})_{stat}(^{+0.19}_{-0.15})_{sys}$.

6. CONCLUSIONS

Observations of blazars with the MAGIC telescopes have been used to estimate new constraints on the EBL energy density. The strategy adopted is based on the maximum-likelihood fit to 32 VHE spectra taken with the MAGIC telescopes, in analogy with similar studies carried out using the High Energy Stereoscopic System, H.E.S.S. (Abramowski et al., 2013), and *Fermi*-Large Area Telescope (LAT) data (Ackermann et al., 2012). The method consists in estimating the most likely EBL scale factor, once an evolving EBL spectral shape, and an intrinsic blazar spectrum are assumed.

In this work, we have assumed the EBL model from Domínguez et al. (2011), and allowed different possible shapes for the intrinsic spectrum (log-parabola, power-law with exponential cut-off, log-parabola with exponential cut-off, and power-law with sub/super exponential cut-off). For the EBL scale factor we have obtained $\alpha_0 = 0.95(^{+0.11}_{-0.12})_{stat}(^{+0.19}_{-0.15})_{sys}$, which is fully consistent with other constraints and with state-of-the-art EBL models.

AUTHOR CONTRIBUTIONS

EP contributed to the data analysis and wrote the manuscript. AM and DM initiated and coordinated the project, contributed to the data analysis, and provided a critical review of the manuscript. AD, VF, TH, MN, GV, and MV contributed to the data analysis and provided a critical review of the manuscript.

FUNDING

This work has been partially supported by University of Padova.

ACKNOWLEDGMENTS

We would like to thank the Instituto de Astrofísica de Canarias for the excellent working conditions at the Observatorio del Roque de los Muchachos in La Palma. The financial support of the German BMBF and MPG, the Italian INFN and INAF, the Swiss National Fund SNF, the ERDF under the Spanish MINECO (FPA2015-69818-P, FPA2012-36668, FPA2015-68378-P, FPA2015-69210-C6-2-R, FPA2015-69210-C6-4-R, FPA2015-69210-C6-6-R, AYA2015-71042-P, AYA2016-76012-C3-1-P, ESP2015-71662-C2-2-P, CSD2009-00064), and the Japanese JSPS and MEXT is gratefully acknowledged. This work was also supported by the Spanish Centro de Excelencia "Severo Ochoa" SEV-2012-0234 and SEV-2015-0548, and Unidad de Excelencia "María de Maeztu" MDM-2014-0369, by the Croatian Science Foundation (HrZZ) Project 09/176 and the University of Rijeka Project 13.12.1.3.02, by the DFG Collaborative Research Centers SFB823/C4 and SFB876/C3, the Polish National Research Centre grant UMO-2016/22/M/ST9/00382 and by the Brazilian MCTIC, CNPq, and FAPERJ.

REFERENCES

Abramowski, A., Acero, F., Aharonian, F., Akhperjanian, A. G., Anton, G., Balenderan, S., et al. (2013). Measurement of the extragalactic background light imprint on the spectra of the brightest blazars observed with H.E.S.S. *Astron. Astrophys.* 550:A4. doi: 10.1051/0004-6361/201220355

Ackermann, M., Ajello, M., Allafort, A., Schady, P., Baldini, L., Ballet, J., et al. (2012). The imprint of the extragalactic background light in the gamma-ray spectra of blazars. *Science* 338:1190. doi: 10.1126/science.1227160

Aleksić, J., Ansoldi, S., Antonelli, L. A., Antoranz, P., Babic, A., Bangale, P., et al. (2016a). The major upgrade of the MAGIC telescopes, Part I: The hardware improvements and the commissioning of the system. *Astropart. Phys.* 72, 61–75. doi: 10.1016/j.astropartphys.2015.04.004

Aleksić, J., Ansoldi, S., Antonelli, L. A., Antoranz, P., Babic, A., Bangale, P., et al. (2016b). The major upgrade of the MAGIC telescopes, Part II: A performance study using observations of the Crab Nebula. *Astropart. Phys.* 72, 76–94. doi: 10.1016/j.astropartphys.2015.02.005

Cooray, A. (2016). Extragalactic background light measurements and applications. *Roy. Soc. Open Sci.* 3:150555. doi: 10.1098/rsos.150555

Domínguez, A., Primack, J. R., Rosario, D. J., Prada, F., Gilmore, R. C., Faber, S. M., et al. (2011). Extragalactic background light inferred from AEGIS galaxy-SED-type fractions. *Month. Notices R. Astron. Soc.* 410, 2556–2578. doi: 10.1111/j.1365-2966.2010.17631.x

Franceschini, A., Rodighiero, G., and Vaccari, M. (2008). Extragalactic optical-infrared background radiation, its time evolution and the

cosmic photon-photon opacity. *Astron. Astrophys.* 487, 837–852. doi: 10.1051/0004-6361:200809691

Gilmore, R. C., Somerville, R. S., Primack, J. R., and Domínguez, A. (2012). Semi-analytic modelling of the extragalactic background light and consequences for extragalactic gamma-ray spectra. *Month. Notices R. Astron. Soc.* 422, 3189–3207. doi: 10.1111/j.1365-2966.2012.20841.x

Salamon, M. H., and Stecker, F. W. (1998). Absorption of high-energy gamma rays by interactions with extragalactic starlight photons at high redshifts and the high-energy gamma-ray background. *Astrophys. J.* 493, 547–554. doi: 10.1086/305134

Sitarek, J. (2017). Highlights of the MAGIC AGN program. ArXiv e-prints.

Conflict of Interest Statement: The authors declare that the research was conducted in the absence of any commercial or financial relationships that could be construed as a potential conflict of interest.

Copyright © 2017 Prandini, Domínguez, Fallah Ramazani, Hassan, Mazin, Moralejo, Nievas Rosillo, Vanzo, and Vazquez Acosta for the MAGIC Collaboration. This is an open-access article distributed under the terms of the Creative Commons Attribution License (CC BY). The use, distribution or reproduction in other forums is permitted, provided the original author(s) or licensor are credited and that the original publication in this journal is cited, in accordance with accepted academic practice. No use, distribution or reproduction is permitted which does not comply with these terms.

frontiers in Astronomy and Space Sciences

PERSPECTIVE
published: 25 July 2017
doi: 10.3389/fspas.2017.00008

An Orientation-Based Unification of Young Jetted AGN: The Case of 3C 286

Marco Berton[1,2], Luigi Foschini[2], Alessandro Caccianiga[2], Stefano Ciroi[1], Enrico Congiu[1,2], Valentina Cracco[1], Michele Frezzato[1], Giovanni La Mura[1] and Piero Rafanelli[1]*

[1] Dipartimento di Fisica e Astronomia "G. Galilei," Università di Padova, Padova, Italy, [2] Brera Astronomical Observatory (INAF), Merate, Italy

In recent years, the old paradigm according to which only high-mass black holes can launch powerful relativistic jets in active galactic nuclei (AGN) has begun to crumble. The discovery of γ-rays coming from narrow-line Seyfert 1 galaxies (NLS1s), usually considered young and growing AGN harboring a central black hole with mass typically lower than 10^8 $M_\odot$, indicated that also these low-mass AGN can produce powerful relativistic jets. The search for parent population of γ-ray emitting NLS1s revealed their connection with compact steep-spectrum sources (CSS). In this proceeding we present a review of the current knowledge of these sources, we present the new important case of 3C 286, classified here for the fist time as NLS1, and we finally provide a tentative orientation based unification of NLS1s and CSS sources.

Keywords: Active Galactic Nuclei (AGN), narrow-line Seyfert 1 galaxies, compact steep-spectrum sources, relativistic jets, unification models

OPEN ACCESS

Edited by:
Paola Marziani, Astronomical Observatory of Padua, National Institute for Astrophysics (INAF), Italy

Reviewed by:
Alenka Negrete, National Autonomous University of Mexico, Mexico
Víctor Manuel Patiño Álvarez, National Institute of Astrophysics, Optics and Electronics, Mexico

****Correspondence:***
Marco Berton
marco.berton@unipd.it

Specialty section:
This article was submitted to Cosmology, a section of the journal Frontiers in Astronomy and Space Sciences

Received: *22 May 2017*
Accepted: *05 July 2017*
Published: *25 July 2017*

Citation:
Berton M, Foschini L, Caccianiga A, Ciroi S, Congiu E, Cracco V, Frezzato M, La Mura G and Rafanelli P (2017) An Orientation-Based Unification of Young Jetted AGN: The Case of 3C 286. Front. Astron. Space Sci. 4:8. doi: 10.3389/fspas.2017.00008

1. OVERVIEW

Relativistic jets are usually thought to be a product of accretion onto a central supermassive black hole (SMBH) (e.g., Blandford and Znajek, 1977; Blandford and Payne, 1982). In active galactic nuclei (AGN), the interplay between the accretion disk and the SMBH is likely to produce powerful and collimated bipolar outflows. According to the unified model of jetted-AGN (Urry and Padovani, 1995), the two classes of blazars, BL Lacertae objects (BL Lacs) and flat-spectrum radio quasars (FSRQs), are double-lobed radio galaxies, with Fanaroff-Riley (FR) morphological types I and II, respectively, in which the line of sight falls inside the relativistic jet aperture cone. In recent years, this scenario has been slightly revised in a more physical way. BL Lacs and FSRQs indeed seem to reflect two different accretion modes. While BL Lacs have an inefficient accretion onto their central SMBH and a low density environment, FSRQs have instead a strong disk accreting efficiently and a photon- and matter-rich environment (Best and Heckman, 2012). This dichotomy led to the distinction between high-excitation radio galaxies and low-excitation radio galaxies (HERGs and LERGs, respectively) classified according, for example, to the [O III]/Hα flux ratio (Laing et al., 1994), and corresponding, respectively, to FSRQ and BL Lac objects when observed at small angles (although exceptions are known, Giommi et al., 2012, see also the review by Foschini, 2017).

Another important aspect of jetted-AGN is that for many years they were thought to be produced only by the most massive black holes harbored in giant passive elliptical galaxies (Laor, 2000; Böttcher and Dermer, 2002; Marscher, 2009). However, the discovery of gamma-ray emission coming from the AGN class known as narrow-line Seyfert 1 galaxies (NLS1s) proved this paradigm

to be wrong (Abdo et al., 2009a,b; Foschini et al., 2015). Low mass AGN, indeed, are also able to launch relativistic jets, whose power is lower because of the well-known scaling of the black hole mass (Heinz and Sunyaev, 2003; Foschini, 2011). This result was confirmed by the identification of low-mass sources among flat-spectrum radio quasars (FSRQs, Ghisellini, 2016), and by the discovery of relativistic jets associated with spiral galaxies (e.g., Keel et al., 2006; Mao et al., 2015).

NLS1s are the most prominent class of low-mass AGN. Classified according to the FWHM(Hβ) $<$ 2,000 km s^{-1} and the ratio between [O III]/Hβ $<$ 3, they are unobscured AGN with relatively low black hole mass ($\lesssim 10^8$ M$_\odot$) and high Eddington ratio, which accounts for the narrowness of the permitted lines and other observational properties (for a review, see Komossa, 2008). A well-known interpretation for these peculiar features is that NLS1s are young AGN still growing and evolving (Mathur, 2000), or sources rejuvenated by a recent merger (Mathur et al., 2012). While a large fraction of NLS1s is radio-quiet, some of them are radio-loud and, as previously mentioned, harbor powerful relativistic jets (Yuan et al., 2008). These radio-loud NLS1s (RLNLS1s) are characterized by a strong and very fast variability consistent with the low-mass scenario, and particularly evident in those with a flat radio spectrum (Foschini et al., 2015).

Another class of radio-loud AGN is known as compact steep-spectrum sources (CSS, see the review by O'Dea, 1998). The radio morphology of these objects is typically characterized by fully developed radio lobes and by a small linear size, with jets confined within the host galaxy. Many authors interpret these properties as signs of young age (Fanti et al., 1995): different estimates of this parameter indeed revealed that they could be radio sources younger than 10^5 years (Owsianik and Conway, 1998; Murgia et al., 1999). CSS sources might eventually evolve to giant double-lobed radio galaxies, or simply switch off because of disk instabilities, going through multiple activity phases during their lifetime (e.g., Czerny et al., 2009; Orienti, 2015). As regular radio galaxies, CSS sources can also be divided in HERGs and LERGs according to their optical spectrum (Kunert-Bajraszewska and Labiano, 2010; Kunert-Bajraszewska et al., 2010).

2. CSS SOURCES AND NLS1S

A possible link between NLS1s and CSS was first suggested by Oshlack et al. (2001), who remarked how the RLNLS1 PKS 2004-447 radio morphology was consistent with that of a CSS source. In the following years, many authors reached the same conclusion (Gallo et al., 2006; Komossa et al., 2006; Yuan et al., 2008; Caccianiga et al., 2014; Schulz et al., 2015). In particular Gu et al. (2015) carried out a VLBA survey on 14 NLS1s at 5 GHz, finding that essentially all RLNLS1s with a steep radio spectrum have a compact morphology, just like CSS. Caccianiga et al. (2017), focusing on the steep-spectrum RLNLS1 SDSS J143244.91+301435.3, found a spectral turnover at low frequency and a small linear size, confirming that this object can be classified as CSS as well.

Beside the morphological similarities, there are other hints that point toward a unification between CSS sources and RLNLS1s. This was investigated under three different points of view in Berton et al. (2016a), using two complete samples of CSS/HERGs and flat-spectrum RLNLS1s (F-NLS1s) limited to $z = 0.6$. A first indication of similarity between these two samples was provided by the V/V$_{max}$ test, which revealed that both of them are consistent with no evolution up to their redshift limit. Moreover, the 1.4 GHz luminosity function (LF) of both samples was derived. Following Urry and Padovani (1995), the effect of relativistic beaming was applied to the observed LF of CSS/HERG to predict the expected shape of the LF of the sources observed along the jet direction. The resulting LF was in good agreement with the observed LF of F-NLS1 thus indicating that at least some CSS/HERGs might be RLNLS1s observed at large angles.

Finally, a comparison between the black hole mass distributions of both samples unveiled again a very good agreement. We repeated here the analysis on the black hole mass distributions on a larger sample of 60 NLS1s. In **Figure 1** we show the distribution of the CSS/HERGs sample by Berton et al. (2016a), compared to all of the masses derived for flat- and steep-spectrum RLNLS1s in Foschini et al. (2015) (42 objects) and Berton et al. (2015) (17 sources), and to that of 3C 286 (see Section 3). It is immediately evident from the plot that 3C 286 is located in the same region as NLS1s. To test the similarity of the distributions, we applied the Kolmogorov-Smirnov test (K-S). The null hypothesis is that the two distributions are originated by the same population. As a rejection threshold, we used a p-value lower than 0.10. Considering CSS/HERGs, the null hypothesis cannot be rejected when comparing them to both flat- and steep-spectrum RLNLS1s, with p-values 0.82 and 0.39, respectively. Testing RLNLS1s as a whole, the p-value is 0.68, again too high to reject the null hypothesis. The mass distribution of CSS/HERGs is therefore statistically consistent

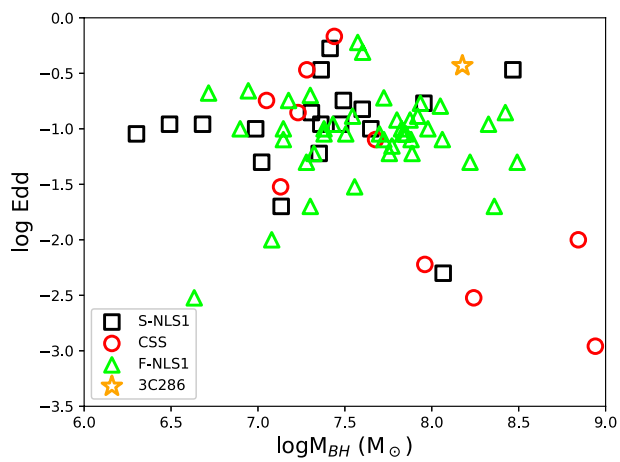

FIGURE 1 | Black hole mass vs. Eddington ratio distribution. Flat-spectrum RLNLS1s are indicated by green triangles, the red circles indicate CSS/HERG sources, the black squares indicate steep-spectrum RLNLS1s, and the orange star represents 3C 286.

with that of RLNLS1s, in agreement with the previously shown results.

3. 3C 286

We present here another interesting case of CSS/HERG, that of 3C 286 ($z = 0.85$). This object is a well-known CSS classified for the first time by Peacock and Wall (1982). It is often used as a calibrator at centimeter wavelengths for both total flux and linear polarization. It shows both the turnover in the radio spectrum around 300 MHz, a spectral index between 1.4 and 50 GHz of $\alpha = -0.61$. It also exhibits the compact morphology typical of CSS: while it remains unresolved at kpc scales, a core-jet structure is visible on pc scale. The jet inclination has been estimated of 48° with respect to the line of sight (e.g., see An et al., 2017, and references therein).

The first optical spectrum of this radio source was obtained by Schmidt (1962), who did not recognize the strongly redshifted Mg II λ2798 line. Since its redshift determination (Burbidge and Burbidge, 1969), a significant improvement has been made in optical with the SDSS-BOSS survey (Dawson et al., 2013), which obtained a new spectrum extended up to 10000Å. The Hβ line, now visible, has a FWHM of (1811±169) km s^{-1}, a ratio [O III]/Hβ of 1.03±0.05, and Fe II multiplets are clearly visible in the spectrum (see **Figure 2**). The corresponding uncertainties were calculated with a Monte Carlo method described by Berton et al. (2016b). These parameters clearly indicate that 3C 286 can be classified as NLS1.

We derived its black hole mass following the method described by Foschini et al. (2015). After correcting for redshift, we subtracted the continuum emission by fitting it with a power law, plus the Fe II multiplets using an online software (Kovačević et al., 2010; Shapovalova et al., 2012)[1] as shown in top panel of **Figure 2**. We then fitted Hβ profile using three Gaussians, one to reproduce the narrow component and two to reproduce the broad component (see bottom panel of **Figure 1**). The narrow component flux was fixed to be 1/10 of [O III] λ5007 (Véron-Cetty et al., 2001) and its FWHM to be the same as [O II] λ3727 (∼600 km s^{-1}). After subtracting the Hβ narrow component, we derived the second-order moment of the broad component σ as a proxy for velocity (Peterson et al., 2004), we obtained the broad-line region (BLR) radius by means of Hβ luminosity. Under the hypothesis of virialized system, the black hole mass is 1.5×10^8 $M_\odot$ and the Eddington ratio, defined as the ratio between the bolometric luminosity and the Eddington luminosity of the black hole, is 0.37. Both of these values are consistent with those derived for other radio-loud NLS1s (Foschini et al., 2015, see **Figure 1**).

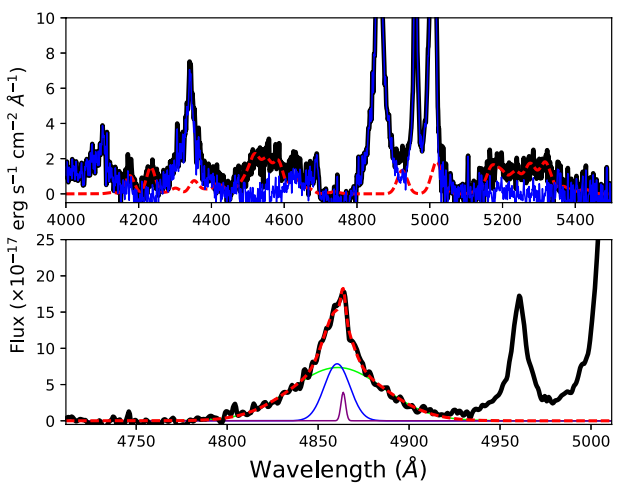

FIGURE 2 | Section of the optical spectrum of 3C 286, obtained from the SDSS-BOSS survey. **Top panel:** black solid line is the region between 4,000 and 5,500 Å restframe continuum subtracted, the red dashed line represents the Fe II template, while the blue solid line is the spectrum after the iron subtraction. **Bottom panel:** black solid line indicates the Hβ region, the three Gaussians used to reproduce the line profile are indicated by the green, blue and purple solid line, and the red dashed line represents their sum.

Interestingly, this object is a γ-ray emitter, identified in the 3rd Fermi catalog with the source 3FGL J1330.5+3023 (Ackermann et al., 2015)[2]. 3C 286 is therefore the third γ-ray detected steep-spectrum RLNLS1 after RX J2314.9+2243 (Komossa et al., 2015) and B3 1441+476 (Liao et al., 2015). This is a very interesting result, since the number of misaligned NLS1s detected in γ-rays appears to be significantly higher than in other AGN classes. Indeed, only ∼10 radiogalaxies are known to be γ-ray emitters (Rieger, 2016), and their corresponding beamed population of FSRQs and BL Lacs is made of 1144 sources. Conversely, among NLS1s, currently three misaligned γ-ray sources are known, out of nine oriented objects. The physical interpretation of this phenomenon is not clear yet, but interaction between the jet and the interstellar medium inside the host galaxy could in principle produce the observed γ-ray emission (Migliori et al., 2014).

The classification of this source has another important implication on NLS1s nature. Some authors (e.g., Decarli et al., 2008) suggested that NLS1s are not objects with a low-mass black hole and a high accretion rate. If their BLR had a disk-like shape, when observed pole-on the permitted lines would appear as narrow because of the lack of Doppler broadening. NLS1 would be just low-inclination sources rather AGN with a low-mass central SMBH. The large observing angle (48°) estimated by An et al. (2017) for 3C 286 seems to contradict this hypothesis, at least for this particular object and other RLNLS1s sharing the same property (e.g., Mrk 783, Congiu et al., 2017).

4. YOUNG JETTED-AGN UNIFICATION

As previously mentioned, CSS sources are usually considered as young radiogalaxies still growing (Fanti et al., 1995). The previous results seem to point out that these objects can often be jetted-NLS1s observed at large angles. Of course, this does not mean that all CSS sources are misaligned NLS1s, because some objects probably have a larger black hole mass. The opposite instead might be true, since many of the jetted-NLS1 observed at large angles studied so far appear as CSS/HERGs. An important conclusion can be inferred from this result. If CSS/HERGs are

[1] http://servo.aob.rs/FeII_AGN/,
[2] http://www.asdc.asi.it/fermi3fgl/.

young sources, and RLNLS1s are CSS sources, they should be young objects as well. This result, just like the high inclination of 3C 286, is in contrast with the vision of NLS1s as a pole-on view of a type 1 AGN.

According to the unified model of radio-loud AGN (Urry and Padovani, 1995), the parent population of FSRQs are FR II radio galaxies, that is when an FR II is observed along its relativistic jet, it appears as a FSRQ. In a similar way, FR I radio galaxies constitute the parent population of BL Lacs. This interpretation might not be completely appropriate, since there are FR I sources that can be associated with FSRQs, and FR II which appear as BL Lacs. Recently it was suggested that a more accurate unification is between FSRQs and all the FR radio galaxies optically classified as HERG (FR_{HERG}), while BL Lacs should be associated to FR with a LERG-type optical spectrum (FR_{LERG}, Giommi et al., 2012). This revised unification is more physics-based, since it accounts for the different accretion mechanisms (strong disk for FSRQs, weak disk for BL Lacs, Best and Heckman, 2012). CSS/HERGs, in this picture, are the young stage of FR_{HERG} objects. Therefore, if flat-spectrum RLNLS1s are beamed CSS/HERGs, and FSRQs are beamed FR_{HERG}, F-NLS1s could be the young stage of FSRQs (Foschini et al., 2015; Berton et al., 2016a, see **Figure 3**).

This is in agreeement with the finding that flat-spectrum RLNLS1s are the low-mass tail of FSRQs (Foschini et al., 2015; Paliya et al., 2016). Indeed, the jet power scales with the black hole mass (Heinz and Sunyaev, 2003; Foschini, 2011) and, as expected, the jet power of RLNLS1s is lower than that observed in FSRQs. Once rescaled for the central mass, though, the normalized power is essentially the same, indicating that the launching mechanism is the same (Foschini et al., 2015). Finally, as shown in Berton et al. (2016a), the radio luminosity function of flat-spectrum RLNLS1s suggests that they might be the low-luminosity tail of FSRQs, indicating again an evolutionary link between these two classes.

All these results can be summarized in the scheme of **Figure 3**. A young jetted-AGN with a strong accretion disk and a photon-rich environment in the central engine surroundings, when observed along its relativistic jets, can appear as a flat-spectrum RLNLS1, characterized by a low black hole mass and a low jet luminosity and power. When the inclination angle increases, the object appears first as a steep-spectrum RLNLS1, with an extended radio emission and a relatively small linear size, that can be classified as a CSS/HERG. Finally, when the line of sight intercepts the molecular torus surrounding the nucleus, the object appears as a type 2 AGN in optical and as a CSS in radio. For older jetted-AGN, instead, the usual unified model holds, with FR_{HERG} (type 1 or 2 quasars in optical, according to the inclination) as parent population of FSRQs.

Such a scheme is probably true only in a statistical sense. Objects like 3C 286 are still fairly rare, and might represent an exception. Moreover, it is unlikely that all type 1 (unobscured) young AGN fit the NLS1 classification. Several other non-NLS1 unobscured AGN with a low-mass black hole exist and were found among γ-ray emitting sources (e.g., Shaw et al., 2012; Ghisellini, 2016). These objects do not appear as NLS1s even when observed at larger angles and in fact, as expected, not all type 1 CSS/HERGs can be classified as NLS1s. However, despite these notable exceptions, the scheme of **Figure 3** seems to be consistent with several observations.

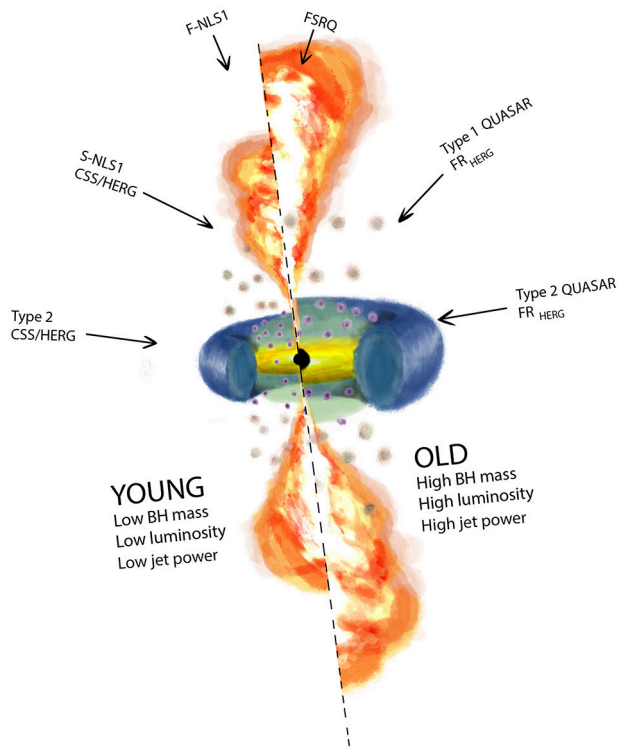

FIGURE 3 | Unification scheme of jetted-AGN with high accretion rate with respect to the Eddington limit and a high-density photon-rich environment. On the left side, young and smaller sources (NLS1s and CSS sources), compared to older and larger objects (FSRQs and FR_{HERG}).

This orientation-based unification could be confirmed by means of RLNLS1s and CSS/HERGs host galaxy observations. NLS1s usually have a late-type host galaxy (Crenshaw et al., 2003), and some RLNLS1s indeed seem to share the same property (Antón et al., 2008; Caccianiga et al., 2015; Kotilainen et al., 2016; Olguín-Iglesias et al., 2017). CSS sources in general are believed to be instead hosted by early-type hosts (e.g., Best et al., 2005). However, some studies pointed out that their host galaxy can be a spiral as well (Morganti et al., 2011), and that HERGs and LERGs can live in different morphological types, with HERGs showing more late-type hosts (Best and Heckman, 2012). Further observations are needed to better investigate this crucial aspect of young AGN.

5. SUMMARY

In this proceeding we presented a review of the current knowledge about young jetted-AGN, showing as well new results strictly connected to this topic and a tentative orientation-based unification model of these sources. We provided a new classification for the well-known CSS source 3C 286 which, thanks to new observations in the near-infrared, can be now

classified as a NLS1 galaxy. This result confirms that RLNLS1s can often appear, in radio, as CSS sources. Moreover, we confirmed that the black hole mass distribution of CSS/HERGs is very similar to that of RLNLS1s. Along with other results already published in the literature, these findings seem to strengthen the scheme according to which flat-spectrum RLNLS1s are CSS/HERGs observed along their relativistic jet, that can appear as a steep-spectrum RLNLS1 when observed at intermediate angles, and as a type 2 radio galaxy when obscured. RLNLS1s and CSS/HERGs then might represent the young and growing stage of FSRQs and FR_{HERG} radio galaxies, respectively, and constitute a part of the young AGN population. New observations on larger samples, particularly aimed at determining the host galaxy morphology, are needed to provide a final confirmation to this unification model.

FUNDING

This work has been partially supported by PRIN INAF 2014 *Jet and astro-particle physics of gamma-ray blazars* (PI F. Tavecchio).

AUTHOR CONTRIBUTIONS

MB coordinated the project, analyzed the spectroscopic data, contributed to the development of the model, and wrote the manuscript. LF initiated the project, contributed to the development of the model, and provided a critical review of the manuscript. AC contributed to the development of the model, and provided a critical review of the manuscript. SC, EC, VC, MF, GL, and PR helped collecting the data and provided a critical review of the manuscript.

ACKNOWLEDGMENTS

We are grateful to Mrs. Lucia Zarantonello for drawing the sketch of the young unification scheme. This research has made use of the NASA/IPAC Extragalactic Database (NED) which is operated by the Jet Propulsion Laboratory, California Institute of Technology, under contract with the National Aeronautics and Space Administration. Funding for the Sloan Digital Sky Survey has been provided by the Alfred P. Sloan Foundation, and the U.S. Department of Energy Office of Science. The SDSS web site is http://www.sdss.org. SDSS-III is managed by the Astrophysical Research Consortium for the Participating Institutions of the SDSS-III Collaboration including the University of Arizona, the Brazilian Participation Group, Brookhaven National Laboratory, Carnegie Mellon University, University of Florida, the French Participation Group, the German Participation Group, Harvard University, the Instituto de Astrofisica de Canarias, the Michigan State/Notre Dame/JINA Participation Group, Johns Hopkins University, Lawrence Berkeley National Laboratory, Max Planck Institute for Astrophysics, Max Planck Institute for Extraterrestrial Physics, New Mexico State University, University of Portsmouth, Princeton University, the Spanish Participation Group, University of Tokyo, University of Utah, Vanderbilt University, University of Virginia, University of Washington, and Yale University.

REFERENCES

Abdo, A. A., Ackermann, M., Ajello, M., Axelsson, M., Baldini, L., Ballet, J., et al. (2009a). Fermi/Large Area Telescope Discovery of Gamma-Ray Emission from a Relativistic Jet in the Narrow-Line Quasar PMN J0948+0022. *Astrophys. J.* 699, 976–984. doi: 10.1088/0004-637X/699/2/976

Abdo, A. A., Ackermann, M., Ajello, M., Axelsson, M., Baldini, L., Ballet, J., et al. (2009b). Multiwavelength Monitoring of the Enigmatic Narrow-Line Seyfert 1 PMN J0948+0022 in 2009 March-July. *Astrophys. J.* 707, 727–737. doi: 10.1088/0004-637X/707/1/727

Ackermann, M., Ajello, M., Atwood, W. B., Baldini, L., Ballet, J., Barbiellini, G., et al. (2015). The Third Catalog of Active Galactic Nuclei Detected by the Fermi Large Area Telescope. *Astrophys. J.* 810:14. doi: 10.1088/0004-637X/810/1/14

An, T., Lao, B.-Q., Zhao, W., Mohan, P., Cheng, X.-P., Cui, Y.-Z., et al. (2017). Parsec-scale jet properties of the gamma-ray quasar 3C 286. *Mon. Not R. Astron. Soc.* 466, 952–959. doi: 10.1093/mnras/stw2887

Antón, S., Browne, I. W. A., and Marchã, M. J. (2008). The colour of the narrow line Sy1-blazar 0324+3410. *Astron. Astrophys.* 490, 583–587. doi: 10.1051/0004-6361:20078926

Berton, M., Caccianiga, A., Foschini, L., Peterson, B. M., Mathur, S., Terreran, G., et al. (2016a). Compact steep-spectrum sources as the parent population of flat-spectrum radio-loud narrow-line Seyfert 1 galaxies. *Astron. Astrophys.* 591:A98. doi: 10.1051/0004-6361/201628171

Berton, M., Foschini, L., Ciroi, S., Cracco, V., La Mura, G., Di Mille, F., et al. (2016b). [O III] line properties in two samples of radio-emitting narrow-line Seyfert 1 galaxies. *Astron. Astrophys.* 591:A88. doi: 10.1051/0004-6361/201527056

Berton, M., Foschini, L., Ciroi, S., Cracco, V., La Mura, G., Lister, M. L., et al. (2015). Parent population of flat-spectrum radio-loud narrow-Line Seyfert 1 galaxies. *Astron. Astrophys.* 578:A28. doi: 10.1051/0004-6361/201525691

Best, P. N., and Heckman, T. M. (2012). On the fundamental dichotomy in the local radio-AGN population: accretion, evolution and host galaxy properties. *Mon. Not R. Astron. Soc.* 421, 1569–1582. doi: 10.1111/j.1365-2966.2012.20414.x

Best, P. N., Kauffmann, G., Heckman, T. M., Brinchmann, J., Charlot, S., Ivezić, Ž., et al. (2005). The host galaxies of radio-loud active galactic nuclei: mass dependences, gas cooling and active galactic nuclei feedback. *Mon. Not R. Astron. Soc.* 362, 25–40. doi: 10.1111/j.1365-2966.2005.09192.x

Blandford, R. D., and Payne, D. G. (1982). Hydromagnetic flows from accretion discs and the production of radio jets. *Mon. Not. Roy. Astron. Soc.* 199, 883–903. doi: 10.1093/mnras/199.4.883

Blandford, R. D., and Znajek, R. L. (1977). Electromagnetic extraction of energy from Kerr black holes. *Mon. Not. Roy. Astron. Soc.* 179, 433–456.

Böttcher, M., and Dermer, C. D. (2002). An evolutionary scenario for blazar unification. *Astrophys. J.* 564, 86–91. doi: 10.1093/mnras/179.3.433

Burbidge, G. R., and Burbidge, E. M. (1969). Red-shifts of Quasi-stellar Objects and Related Extragalactic Systems. *Nature* 222, 735–741. doi: 10.1038/222735a0

Caccianiga, A., Antón, S., Ballo, L., Dallacasa, D., Della Ceca, R., Fanali, R., et al. (2014). SDSS J143244.91+301435.3: a link between radio-loud narrow-line Seyfert 1 galaxies and compact steep-spectrum radio sources? *Mon. Not R. Astron. Soc.* 441, 172–186. doi: 10.1093/mnras/stu508

Caccianiga, A., Antón, S., Ballo, L., Foschini, L., Maccacaro, T., Della Ceca, R., et al. (2015). WISE colours and star formation in the host galaxies of radio-loud narrow-line Seyfert 1. *Mon. Not R. Astron. Soc.* 451, 1795–1805. doi: 10.1093/mnras/stv939

Caccianiga, A., Dallacasa, D., Antón, S., Ballo, L., Berton, M., Mack, K.-H., et al. (2017). SDSSJ143244.91+301435.3 at VLBI: a compact radio galaxy in a narrow-line Seyfert 1. *Mon. Not R. Astron. Soc.* 464, 1474–1480. doi: 10.1093/mnras/stw2471

Congiu, E., Berton, M., Giroletti, M., Antonucci, R., Caccianiga, A., Kharb, P., et al. (2017). Kiloparsec-scale emission in the narrow-line Seyfert 1 galaxy Mrk 783. *Astrono. Astrophys.* 603:A32. doi: 10.1051/0004-6361/201730616

Crenshaw, D. M., Kraemer, S. B., and Gabel, J. R. (2003). The host galaxies of narrow-line seyfert 1 galaxies: evidence for bar-driven fueling. *Astron. J.* 126, 1690–1698. doi: 10.1086/377625

Czerny, B., Siemiginowska, A., Janiuk, A., Nikiel-Wroczyński, B., and Stawarz, Ł. (2009). Accretion disk model of short-timescale intermittent activity in young radio sources. *Astrophys. J.* 698, 840–851. doi: 10.1088/0004-637X/698/1/840

Dawson, K. S., Schlegel, D. J., Ahn, C. P., Anderson, S. F., Aubourg, É., Bailey, S., et al. (2013). The Baryon oscillation spectroscopic survey of SDSS-III. *Astron. J.* 145:10. doi: 10.1088/0004-6256/145/1/10

Decarli, R., Dotti, M., Fontana, M., and Haardt, F. (2008). Are the black hole masses in narrow-line Seyfert 1 galaxies actually small? *Mon. Not R. Astron. Soc.* 386, L15–L19. doi: 10.1111/j.1745-3933.2008.00451.x

Fanti, C., Fanti, R., Dallacasa, D., Schilizzi, R. T., Spencer, R. E., and Stanghellini, C. (1995). Are compact steep-spectrum sources young? *Astron. Astrophys.* 302:317.

Foschini, L. (2011). Accretion and jet power in active galactic nuclei. *Res. Astron. Astrophys.* 11, 1266–1278. doi: 10.1088/1674-4527/11/11/003

Foschini, L. (2017). What we talk about when we talk about blazars? *Front. Astron. Space Sci.* 4:6. doi: 10.3389/fspas.2017.00006

Foschini, L., Berton, M., Caccianiga, A., Ciroi, S., Cracco, V., Peterson, B. M., et al. (2015). Properties of flat-spectrum radio-loud narrow-line Seyfert 1 galaxies. *Astron. Astrophys.* 575:A13. doi: 10.1051/0004-6361/201424972

Gallo, L. C., Edwards, P. G., Ferrero, E., Kataoka, J., Lewis, D. R., Ellingsen, S. P., et al. (2006). The spectral energy distribution of PKS 2004-447: a compact steep-spectrum source and possible radio-loud narrow-line Seyfert 1 galaxy. *Mon. Not R. Astron. Soc.* 370, 245–254. doi: 10.1111/j.1365-2966.2006.10482.x

Ghisellini, G. (2016). The Blazar Sequence 2.0. *Galaxies* 4:36. doi: 10.3390/galaxies4040036

Giommi, P., Padovani, P., Polenta, G., Turriziani, S., D'Elia, V., and Piranomonte, S. (2012). A simplified view of blazars: clearing the fog around long-standing selection effects. *Mon. Not R. Astron. Soc.* 420, 2899–2911. doi: 10.1111/j.1365-2966.2011.20044.x

Gu, M., Chen, Y., Komossa, S., Yuan, W., Shen, Z., Wajima, K., et al. (2015). The radio properties of radio-loud narrow-line Seyfert 1 galaxies on parsec scales. *Astrophys. J.* 221:3. doi: 10.1088/0067-0049/221/1/3

Heinz, S., and Sunyaev, R. A. (2003). The non-linear dependence of flux on black hole mass and accretion rate in core-dominated jets. *Mon. Not. R. Astron. Soc.* 343, L59–L64. doi: 10.1046/j.1365-8711.2003.06918.x

Keel, W. C., White, R. E. III, Owen, F. N., and Ledlow, M. J. (2006). The spiral host galaxy of the double radio source 0313-192. *Astron. J.* 132, 2233–2242. doi: 10.1086/508340

Komossa, S. (2008). "Narrow-line Seyfert 1 Galaxies," in *Revista Mexicana de Astronomia y Astrofisica Conference Series*, Vol. 32 of *Revista Mexicana de Astronomia y Astrofisica Conference Series* (Huatulco, MX), 86–92.

Komossa, S., Voges, W., Xu, D., Mathur, S., Adorf, H.-M., Lemson, G., et al. (2006). Radio-loud Narrow-Line Type 1 Quasars. *Astron. J.* 132, 531–545. doi: 10.1086/505043

Komossa, S., Xu, D., Fuhrmann, L., Grupe, D., Yao, S., Fan, Z., et al. (2015). What powers the radio-loud narrow-line Seyfert 1 galaxy RX J2314.9+2243?. a view onto its central engine from radio to X-rays. *Astron. Astrophys.* 574:A121. doi: 10.1051/0004-6361/201424814

Kotilainen, J. K., León-Tavares, J., Olguín-Iglesias, A., Baes, M., Anórve, C., Chavushyan, V., et al. (2016). Discovery of a pseudobulge galaxy launching powerful relativistic jets. *Astrophys. J.* 832:157. doi: 10.3847/0004-637X/832/2/157

Kovačević, J., Popović, L. Č., and Dimitrijević, M. S. (2010). Analysis of Optical Fe II Emission in a Sample of Active Galactic Nucleus Spectra. *Astrophys. J.* 189, 15–36. doi: 10.1088/0067-0049/189/1/15

Kunert-Bajraszewska, M., Gawroński, M. P., Labiano, A., and Siemiginowska, A. (2010). A survey of low-luminosity compact sources and its implication for the evolution of radio-loud active galactic nuclei - I. Radio data. *Mon. Not R. Astron. Soc.* 408, 2261–2278. doi: 10.1111/j.1365-2966.2010.17271.x

Kunert-Bajraszewska, M., and Labiano, A. (2010). A survey of low-luminosity compact sources and its implication for the evolution of radio-loud active galactic nuclei - II. Optical analysis. *Mon. Not R. Astron. Soc.* 408, 2279–2289. doi: 10.1111/j.1365-2966.2010.17300.x

Laing, R. A., Jenkins, C. R., Wall, J. V., and Unger, S. W. (1994). "Spectrophotometry of a complete sample of 3CR radio sources: implications for unified models," in *The Physics of Active Galaxies*, Vol. 54 of *Astronomical Society of the Pacific Conference Series* (Canberra), 201.

Laor, A. (2000). On Black Hole Masses and Radio Loudness in Active Galactic Nuclei. *Astrophys. J.* 543, L111–L114. doi: 10.1086/317280

Liao, N.-H., Liang, Y.-F., Weng, S.-S., Gu, M.-F., and Fan, Y.-Z. (2015). Discovery of γ-ray emission from a steep radio spectrum NLS1 B3 1441+476. *ArXiv e-prints*. arXiv:1510.05584

Mao, M. Y., Owen, F., Duffin, R., Keel, B., Lacy, M., Momjian, E., et al. (2015). J1649+2635: a grand-design spiral with a large double-lobed radio source. *Mon. Not. R. Astron. Soc.*, 446, 4176–4185. doi: 10.1093/mnras/stu2302

Marscher, A. P. (2009). Jets in active galactic nuclei. *ArXiv e-prints*. arXiv:0909.2576

Mathur, S. (2000). Narrow-line Seyfert 1 galaxies and the evolution of galaxies and active galaxies. *Mon. Not R. Astron. Soc.* 314, L17–L20. doi: 10.1046/j.1365-8711.2000.03530.x

Mathur, S., Fields, D., Peterson, B. M., and Grupe, D. (2012). Supermassive Black Holes, Pseudobulges, and the Narrow-line Seyfert 1 Galaxies. *Astrophys. J.* 754:146. doi: 10.1088/0004-637X/754/2/146

Migliori, G., Siemiginowska, A., Kelly, B. C., Stawarz, Ł., Celotti, A., and Begelman, M. C. (2014). Jet Emission in Young Radio Sources: A Fermi Large Area Telescope Gamma-Ray View. *Astrophys. J.* 780:165. doi: 10.1088/0004-637X/780/2/165

Morganti, R., Holt, J., Tadhunter, C., Ramos Almeida, C., Dicken, D., Inskip, K., et al. (2011). PKS 1814-637: a powerful radio-loud AGN in a disk galaxy. *Astron. Astrophys.* 535:A97. doi: 10.1051/0004-6361/201117686

Murgia, M., Fanti, C., Fanti, R., Gregorini, L., Klein, U., Mack, K.-H., et al. (1999). Synchrotron spectra and ages of compact steep spectrum radio sources. *Astron. Astrophys.* 345, 769–777.

O'Dea, C. P. (1998). The Compact Steep-Spectrum and Gigahertz Peaked-Spectrum Radio Sources. *Astron. Soc. Pacific.* 110, 493–532. doi: 10.1086/316162

Olguín-Iglesias, A., Kotilainen, J. K., León Tavares, J., Chavushyan, V., and Añorve, C. (2017). Evidence of bar-driven secular evolution in the gamma-ray narrow-line Seyfert 1 galaxy FBQS J164442.5+261913. *Mon. Not R. Astron. Soc.* 467, 3712–3722. doi: 10.1093/mnras/stx022

Orienti, M. (2015). Radio properties of Compact Steep Spectrum and GHz-Peaked Spectrum radio sources. *ArXiv e-prints*. arXiv:1511.00436

Oshlack, A. Y. K. N., Webster, R. L., and Whiting, M. T. (2001). A Very Radio Loud Narrow-Line Seyfert 1: PKS 2004-447. *Astrophys. J.* 558, 578–582. doi: 10.1086/322299

Owsianik, I., and Conway, J. E. (1998). First detection of hotspot advance in a Compact Symmetric Object. Evidence for a class of very young extragalactic radio sources. *Astron. Astrophys.* 337, 69–79.

Paliya, V. S., Rajput, B., Stalin, C. S., and Pandey, S. B. (2016). Broadband Observations of the Gamma-Ray Emitting Narrow Line Seyfert 1 Galaxy SBS 0846+513. *Astrophys. J.* 819:121. doi: 10.3847/0004-637X/819/2/121

Peacock, J. A., and Wall, J. V. (1982). Bright extragalactic radio sources at 2.7 GHz. II - Observations with the Cambridge 5-km telescope. *Mon. Not R. Astron. Soc.* 198, 843–860. doi: 10.1093/mnras/198.3.843

Peterson, B. M., Ferrarese, L., Gilbert, K. M., Kaspi, S., Malkan, M. A., Maoz, D., et al. (2004). Central Masses and Broad-Line Region Sizes of Active Galactic Nuclei. II. A Homogeneous Analysis of a Large Reverberation-Mapping Database. *Astrophys. J.* 613, 682–699. doi: 10.1086/423269

Rieger, F. M. (2016). Gamma-Rays from Non-Blazar AGN. *ArXiv e-prints*. arXiv:1611.02986

Schmidt, M. (1962). Spectrum of a Stellar Object Identified with the Radio Source 3c 286. *Astrophys. J.* 136:684. doi: 10.1086/147424

Schulz, R., Kreikenbohm, A., Kadler, M., Ojha, R., Ros, E., Stevens, J., et al. (2015). The Gamma-Ray Emitting Radio-Loud Narrow-Line Seyfert 1 Galaxy PKS 2004-447 II. The Radio View. *ArXiv e-prints*. arXiv:1511.02631

Shapovalova, A. I., Popović, L. Č., Burenkov, A. N., Chavushyan, V. H., Ilić, D., Kovačević, A., et al. (2012). Spectral Optical Monitoring of the Narrow-line Seyfert 1 Galaxy Ark 564. *Astrophys. J.* 202:10. doi: 10.1088/0067-0049/202/1/10

Shaw, M. S., Romani, R. W., Cotter, G., Healey, S. E., Michelson, P. F., Readhead, A. C. S., et al. (2012). Spectroscopy of Broad-line Blazars from 1LAC. *Astrophys. J.* 748:49. doi: 10.1088/0004-637X/748/1/49

Urry, C. M., and Padovani, P. (1995). Unified Schemes for Radio-Loud Active Galactic Nuclei. *Publ. Astron. Soc. Pacific* 107:803. doi: 10.1086/133630

Véron-Cetty, M.-P., Véron, P., and Gonçalves, A. C. (2001). A spectrophotometric atlas of Narrow-Line Seyfert 1 galaxies. *Astron. Astrophys.* 372, 730–754. doi: 10.1051/0004-6361:20010489

Yuan, W., Zhou, H. Y., Komossa, S., Dong, X. B., Wang, T. G., Lu, H. L., et al. (2008). A Population of Radio-Loud Narrow-Line Seyfert 1 Galaxies with Blazar-Like Properties? *Astrophys. J.* 685:801. doi: 10.1086/591046

Conflict of Interest Statement: The authors declare that the research was conducted in the absence of any commercial or financial relationships that could be construed as a potential conflict of interest.

Copyright © 2017 Berton, Foschini, Caccianiga, Ciroi, Congiu, Cracco, Frezzato, La Mura and Rafanelli. This is an open-access article distributed under the terms of the Creative Commons Attribution License (CC BY). The use, distribution or reproduction in other forums is permitted, provided the original author(s) or licensor are credited and that the original publication in this journal is cited, in accordance with accepted academic practice. No use, distribution or reproduction is permitted which does not comply with these terms.

frontiers in Astronomy and Space Sciences

ORIGINAL RESEARCH
published: 22 November 2017
doi: 10.3389/fspas.2017.00040

SDSS J090152.05+624342.6: A NEW "OVERLAPPING-TROUGH" FeLoBAL QUASAR AT Z ∼ 2

Jing Wang[1,2]*, *Dawei Xu*[1,2] *and Jianyan Wei*[1,2]

[1] *Key Laboratory of Space Astronomy and Technology, National Astronomical Observatories, Chinese Academy of Sciences, Beijing, China,* [2] *School of Astronomy and Space Science, University of Chinese Academy of Sciences, Beijing, China*

We here report an identification of SDSS J090152.04+624342.6 as a new "overlapping-trough" iron low-ionization broad absorption line quasar at redshift of $z \sim 2.1$. No strong variation of the broad absorption lines can be revealed through the two spectra taken by the Sloan Digital Sky Survey with a time interval of ∼6 yr. Further optical and infrared spectroscopic study on this object is suggested.

Keywords: quasars, broad absorption lines, spectroscopy, line identification, variability

OPEN ACCESS

Edited by:
Mauro D'Onofrio,
Università degli Studi di Padova, Italy

Reviewed by:
Giovanna Maria Stirpe,
Osservatorio Astronomico di Bologna (INAF), Italy
Daniela Bettoni,
Osservatorio Astronomico di Padova (INAF), Italy

****Correspondence:***
Jing Wang
wj@bao.ac.cn

Specialty section:
This article was submitted to Milky Way and Galaxies, a section of the journal Frontiers in Astronomy and Space Sciences

Received: *18 September 2017*
Accepted: *25 October 2017*
Published: *22 November 2017*

Citation:
Wang J, Xu D and Wei J (2017) SDSS J090152.05+624342.6: A NEW "OVERLAPPING-TROUGH" FeLoBAL QUASAR AT Z ∼ 2. Front. Astron. Space Sci. 4:40. doi: 10.3389/fspas.2017.00040

1. INTRODUCTION

Broad absorption line (BAL) quasars are the objects whose spectra show gas absorptions with a blueshfited outflow velocity from 2,000 km s^{-1} up to $0.1c$ (Weymann et al., 1991). Although the detailed physics of the outflow is still an open issue (e.g., Fabian, 2012), the outflow is believed to play an important role in the coevolution of the supermassive blackhole (SMBH) and its host galaxy, which is firmly established in local AGNs (see Heckman and Best, 2014 for a review) by either expelling circumnuclear gas (e.g., Kormendy and Ho, 2013; Woo et al., 2017) or triggering star formation through gas compressing (e.g., Zubovas et al., 2013; Ishibashi and Fabian, 2014).

Previous studies, especially the ones based on the Sloan Digital Sky Survey (SDSS, York et al., 2000), indicate that at low and intermediate redshift the fraction of BAL quasars is about 20–40% (e.g., Hewett and Foltz, 2003; Reichard et al., 2003; Trump et al., 2006; Dai et al., 2008; Knigge et al., 2008; Scaringi et al., 2009; Urrutia et al., 2009), depending on the selection method. About 90% of the BAL quasars are characterized by only high-ionized broad absorptions lines (HiBALs, e.g., CIV, SiIV, NV, OVI). The low-ionized absorption lines, such as MgII and AlIII, are identified in the so-called LoBAL quasars with a fraction of ∼10%. Among the LoBAL quasars, a small subset (∼ 1% of BAL quasars) of objects are classified as FeLoBAL quasars according to their FeII and/or FeIII absorption lines (Hazard et al., 1987; Hall et al., 2002; Brunner et al., 2003; Gibson et al., 2009; Zhang et al., 2010; Yi et al., 2017).

Although the physical origin of BAL quasars is originally ascribed to the orientation effect (e.g., Weymann et al., 1991; Goodrich and Miller, 1995; Gallagher et al., 2007), the higher reddening in BAL quasars than in non-BAL quasars motivate a lot of studies to try to understand if BAL quasars are young AGNs, in which the FeLoBAL quasars with the highest reddening and column density are possible transitional quasars from a dust-obscured AGN to a unobscured one. Mudd et al. (2017) recently identified the first post-starburst FeLoBAL quasar DES QSO J0330-28 at a redshift of 0.65.

In this paper, we report an identification of SDSS J090152.04+624342.6 as a new unusual FeLoBAL quasar with "overlapping-trough" (OFeLoBAL quasars) at $z \sim 2.1$.

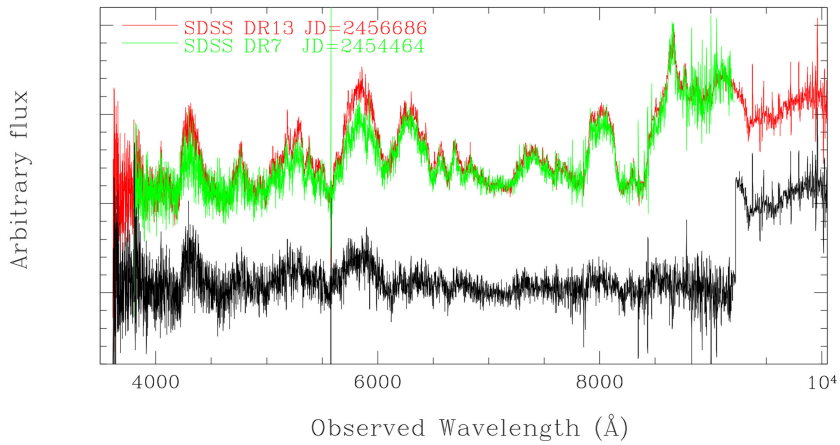

FIGURE 1 | The spectra taken from SDSS DR13 and that from SDSS DR7. Both spectra are shown in observer frame. The bottom black curve shows the differential spectrum that is vertically shifted by an arbitrary amount for visibility.

2. SPECTROSCOPIC IDENTIFICATION

2.1. History of SDSS J090152.04+624342.6

SDSS J090152.04+624342.6 was serendipitously extracted from the Sloan Digital Sky Survey (SDSS, York et al., 2000) Data Release 7 spectroscopic catalog, when we examined the spectrum of the "unknown" objects one by one **by eye.** The object was then classified as a quasar at $z = 2.09$ in the 7th SDSS Quasar Catalog (Schneider et al., 2010; Shen et al., 2011) by identifying the broad emission line at the red end as **MgII**λ2800. With a new spectroscopic observation, the redshift was recently (and improperly) updated to $z = 6.389420 \pm 0.000594$ by the pipelines of SDSS Data Release 13[1] through an identification of the peak as Lyα emission line. **Figure 1** shows the observer-frame spectrum of SDSS DR13 and that of DR7. In fact, by assuming a redshift of $z \sim 6$, the object shows abnormally significant emission blueward of the Lyman limit at observer frame wavelength of ∼6,500Å (see the typical spectra of the high-redshift quasars at $z \sim 6$ in Fan et al., 2006, Wu et al., 2015, Wang et al., 2017, Yang et al., 2017 and references therein).

2.2. Data Reduction

The spectral analysis is performed as follows by the IRAF packages[2]. The 1-Dimensional spectra of the object taken from SDSS DR13 is corrected for the Galactic extinction basing upon the V-band extinction taken from Schlafly and Finkbeiner (2011). An $R_V = 3.1$ extinction law (Cardelli et al., 1989) of the MilkyWay is adopted in the correction.

2.3. Identification of a New OFeLoBAL Quasar

Both spectra of the object taken from SDSS show an abrupt drops in flux at around the observer frame wavelength of $\lambda \sim 8,000$Å and many "features" blueward of the drop, which closely resemble the spectra of the unusual OFeLoBAL quasars discovered in previous studies, such as SDSS J0300+0048 ($z = 0.89$), SDSS J1154+0300 ($z = 1.458$), Mark 231, FIRST 1556+3517 and FBQS 1408+3054 (e.g., Smith et al., 1995; Becker et al., 1997, 2000; White et al., 2000; Hall et al., 2002). In the OFeLoBAL quasars, the abrupt drops are caused by a blueshifted absorptions due to MgII$\lambda\lambda$2796, 2803 and MgIλ2852, and almost no continuum windows can be identified blueward of the MgII emission because of the overlapping troughs mainly due to the FeII and FeIII absorptions.

Figure 2 shows the rest-frame spectrum of the object, along with our identification of both emission and absorption features. By ascribing the peak at the red end of spectrum as an emission from the MgII$\lambda\lambda$2796, 2803 doublets, the systematic redshift of the object is inferred to be $z = 2.09$ which is consistent with the previous claims in SDSS DR7 quasar catalog (e.g., Schneider et al., 2010; Shen et al., 2011; Wu et al., 2012). In fact, this redshift allows us to accurately **predict** the wavelength of not only the broad emission redward of the MgII emission, but also the CIVλ1549 and possible NeVλ1240 emission features, although the CIII]λ1909 emission commonly appearing in the quasar's spectra is hard to be identified in this object. The two bumps redward of the MgII emission are identified to be a blend of the HeIλ2945+FeIIλ2950 (UV60 and UV78) complex and a blend of the optical FeII complex at around 3,200Å (i.e., Opt7 and Opt6).

The spectrum blueward of the MgII emission is dominated by multiple overlapping troughs with a redshift of ∼1.98. Again, the redshift accurately predicts the wavelength of the absorptions blueward of the MgII emission. The onset of the troughs is a strong MgIλ2857 absorption followed by damped MgII$\lambda\lambda$2796, 2803 absorptions. An evident residual flux at high-velocity end of the MgII trough enables us to argue a presence of FeIIλ2750 (UV62 and UV63) absorptions, which is followed by the absorption features of FeII UV1 and UV2. With the redshift of ∼1.98, the troughs at middle of the spectrum

[1] http://www.sdss.org/dr13/data_access/bulk/

[2] IRAF is distributed by the National Optical Astronomy Observatory, which is operated by the Association of Universities for Research in Astronomy, Inc., under cooperative agreement with the National Science Foundation.

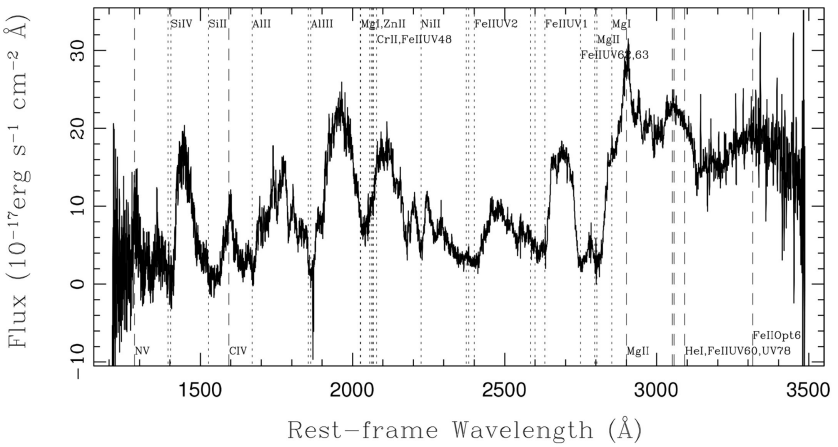

FIGURE 2 | The SDSS DR13 rest-frame spectrum of the object based on the redshift of the absorption features of $z = 1.98$. The long dashed lines from top to bottom marks the predicted wavelengths of the identified emission features, and the short dashed lines the wavelengths of the absorptions. The emission and absorption features are labeled at bottom and top of the figure, respectively.

are identified as the absorptions due to MgI+ZnII+CrII+FeII UV48, AlIIIλλ1854,1862 and AlIIλ1671, which are all common in the spectra of FeLoBAL quasars. Finally, two troughs due to SiIIλ1527 (UV2) and SiIVλλ1394,1402 absorptions can be identified at the predicted wavelengths at the blue end of the spectrum.

3. NON-VARIATION OF THE NEW OFELOBAL QUASAR

Significant variation of BALs, including a complete disappearance, with a time scale of 1–10 year in the quasar rest-frame have been reported in the previous studies (e.g., Hall et al., 2011; Zhang et al., 2011, 2015; Filiz Ak et al., 2012, 2013; Vivek et al., 2012, 2014; Joshi et al., 2014). The significant variation can be explained by a variation of either the ionizing power (e.g., Trevese et al., 2013) or the covering factor due to a cloud transiting the line-of-sight (e.g., Hall et al., 2011). By comparing the variability of OFeLoBAL and non-OFeLoBAL quasars, Zhang et al. (2015) claimed a prevalence of strong BAL variation in the OFeLoBAL quasars rather than in the non-OFeLoBAL ones, which allows the authors to argue that the troughs in OFeLoBAL quasars are resulted from dense outflow gas closer to the central SMBH.

SDSS J090152.04+624342.6 has been observed twice by SDSS with a time interval of ∼6 yr, which corresponds to a rest-frame time of ∼2 yr. The two spectra are compared in **Figure 1**, along with a difference spectrum. The difference spectrum is obtained by a direct subtraction of the two spectra at the different epochs, since they are matched very well redward of the MgII line emission. One can see from the figure that no significant variation can be identified in the object through a comparison of the two SDSS spectroscopic observations. The invariant of the spectra of the object suggests a rest-frame life time of its BAL structure being no shorter than 2 yr. The knife-edge model in Capellupo et al. (2013) gives a simple relation of the crossing velocity υ of the absorber of $\upsilon_{\rm cross} = \Delta AD/\Delta t$, where ΔA is the fraction of the continuum region crossed by the absorber, and D the diameter of the continuum region. With the typical values of $\Delta A = 0.1$ and $D = 10^{-3}$pc (e.g., Capellupo et al., 2013; McGraw et al., 2015), the invariant of the BAL structure of the object within a rest-frame time of 2 yr suggests a crossing velocity $\upsilon_{\rm cross} < 5 \times 10^3$km s^{-1}.

4. CONCLUSION AND FUTURE STUDY

SDSS J090152.04+624342.6 is identified as a new OFeLoBAL quasar at $z \sim 2.1$. The spectra taken by SDSS at two epochs with a time interval of 6 yr do not show significant variation of its BAL. Further infrared spectroscopic observation is necessary for confirming the redshift determination, studying the host galaxy stellar population and estimating BH viral mass through Balmer emission lines. Based on the redshift of $z \sim 2.1$, the Hβ line which is traditionally used for BH mass estimation, is redshifted to 1.5μm at observer frame. And also, further optical spectroscopic and photometric monitor is useful for revealing significant BAL variation in the object.

AUTHOR CONTRIBUTIONS

JW initiated the study, conducted data reductions, and wrote the manuscript. DX and JYW contributed to the discussions and manuscript preparation.

FUNDING

This study is supported by the National Natural Science Foundation of China under grants 11473036 and 11773036, and by the National Basic Research Program of China (grant 2009CB824800).

ACKNOWLEDGMENTS

The authors would like to thank the referees for very useful comments and suggestions for improving the manuscript. This study uses the SDSS archive data that was created and distributed by the Alfred P. Sloan Foundation. The author would like to thank the referee from journal of ApJ letter who pointed out our initial mistake and gave us very useful suggestions.

REFERENCES

Becker, R. H., Gregg, M. D., Hook, I. M., McMahon, R. G., White, R. L., and Helfand, D. J. (1997). The FIRST radio-loud broad absorption line QSO and evidence for a hidden population of quasars. *Astrophys. J. Lett.* 479, 93–96. doi: 10.1086/310594

Becker, R. H., White, R. L., Gregg, M. D., Brotherton, M. S., Laurent-Muehleisen, S., and Arav, N. (2000). Properties of radio-selected broad absorption line quasars from the first bright quasar survey. *Astrophys. J.*, 538, 72–82. doi: 10.1086/309099

Brunner, R. J., Hall, P. B., Djorgovski, S. G., Gal, R. R., Mahabal, A. A., Lopes, P. A. A., et al. (2003). Peculiar broad absorption line quasars found in the digitized palomar observatory sky survey. *Astron. J.* 126, 53–62. doi: 10.1086/375763

Capellupo, D. M., Hamann, F., Shields, J. C., Halpern, J. P., and Barlow, T. A. (2013). Variability in quasar broad absorption line outflows - III. What happens on the shortest time-scales? *Month. Notices R. Astron. Soc.* 429, 1872–1886. doi: 10.1093/mnras/sts427

Cardelli, J. A., Clayton, G. C., and Mathis, J. S. (1989). The relationship between infrared, optical, and ultraviolet extinction. *Astrophys. J.* 345, 245–256. doi: 10.1086/167900

Dai, X. Y., Shankar, F., and Sivakoff, G. R. (2008). 2MASS reveals a large intrinsic fraction of BALQSOs. *Astrophys. J.* 672, 108–114. doi: 10.1086/523688

Fabian, A. C. (2012). Observational evidence of active galactic nuclei feedback. *Annu. Rev. Astron. Astrophys.* 50, 455–489. doi: 10.1146/annurev-astro-081811-125521

Fan, X. H., Carilli, C. L., Keating, B. (2006). Observational constraints on cosmic reionization. *Annu. Rev. Astron. Astrophys.* 44, 415–462. doi: 10.1146/annurev.astro.44.051905.092514

Filiz Ak, N., Brandt, W. N., Hall, P. B., Schneider, D. P., Anderson, S. F., Gibson, R. R., et al. (2012). Broad absorption line disappearance on multi-year timescales in a large quasar sample. *Astrophys. J.* 757, 114–133. doi: 10.1088/0004-637X/757/2/114

Filiz Ak, N., Brandt, W. N., Hall, P. B., Schneider, D. P., Anderson, S. F., Hamann, F., et al. (2013). Broad absorption line variability on multi-year timescales in a large quasar sample. *Astrophys. J.* 777, 168–197. doi: 10.1088/0004-637X/777/2/168

Gallagher, S. C., Hines, D. C., Blaylock, M., Priddey, R. S., Brandt, W. N., and Egami, E. E. (2007). Radio through X-ray spectral energy distributions of 38 broad absorption line quasars. *Astrophys. J.* 665, 157–173. doi: 10.1086/519438

Gibson, R. R., Jiang, L., Brandt, W. N., Hall, P. B., Shen, Y., Wu, J., Anderson, S. F., et al. (2009). A catalog of broad absorption line quasars in sloan digital sky survey data release 5. *Astrophys. J.* 692, 758–777. doi: 10.1088/0004-637X/692/1/758

Goodrich, R. W., and Miller, J. S. (1995). Polarization clues to the structure of broad absorption line quasi-stellar objects. *Astrophys. J. Lett.* 448, 73–76. doi: 10.1086/309600

Hall, P. B., Anderson, S. F.; Strauss, M. A., York, D. G., Richards, G. T., Fan, X., et al., (2002). Unusual broad absorption line quasars from the sloan digital sky survey. *Astrophys. J. Suppl.* 141, 267–309. doi: 10.1086/340546

Hall, P. B., Anosov, K., White, R. L., Brandt, W. N., Gregg, M. D., Gibson, R. R., et al. (2011). Implications of dramatic broad absorption line variability in the quasar FBQS J1408+3054. *Month. Notices R. Astron. Soc.* 411, 2653–2666. doi: 10.1111/j.1365-2966.2010.17870.x

Hazard, C., McMahon, R. G., Webb, J. K., and Morton, D. C. (1987). The remarkable broad absorption line QSO 0059-2735 with extensive Fe II absorption. *Astrophys. J.* 323, 263–270. doi: 10.1086/165823

Heckman, T. M., and Best, P. N. (2014). The coevolution of galaxies and supermassive black holes: insights from surveys of the contemporary universe. *Annu. Rev. Astron. Astrophys.* 52, 589–660. doi: 10.1146/annurev-astro-081913-035722

Hewett, P. C., and Foltz, C. B. (2003). The frequency and radio properties of broad absorption line quasars. *Astron. J.* 125, 1784–1794. doi: 10.1086/368392

Ishibashi, W., and Fabian, A. C. (2014). How the central black hole may shape its host galaxy through AGN feedback. *Month. Notices R. Astron. Soc.* 441, 1474–1478. doi: 10.1093/mnras/stu672

Joshi, R., Chand, H., Srianand, R., and Majumdar, J. (2014). CIV absorption-line variability in X-ray-bright broad absorption-line quasi-stellar objects. *Month. Notices R. Astron. Soc.* 442, 862–869. doi: 10.1093/mnras/stu840

Knigge, C., Scaringi, S., Goad, M. R., and Cottis, C. E. (2008). The intrinsic fraction of broad-absorption line quasars. *Month. Notices R. Astron. Soc.* 386, 1426–1435. doi: 10.1111/j.1365-2966.2008.13081.x

Kormendy, J., and Ho, L. C. (2013). Coevolution (or not) of supermassive black holes and host galaxies. *Annu. Rev. Astron. Astrophys.* 51, 511–653. doi: 10.1146/annurev-astro-082708-101811

McGraw, S. M., Shields, J. C., Hamann, F. W., Capellupo, D. M., Gallagher, S. C., and Brandt, W. N. (2015). Constraining FeLoBAL outflows from absorption line variability. *Month. Notices R. Astron. Soc.* 453, 1379–1395. doi: 10.1093/mnras/stv1697

Mudd, D., Martini, P., Tie, S. S., Lidman, C., McMahon, R., Banerji, M., Davis, T., et al., (2017). Discovery of a z = 0.65 post-starburst BAL quasar in the DES supernova fields. *Month. Notices R. Astron. Soc.* 468, 3682–3688. doi: 10.1093/mnras/stx708

Reichard, T. A., Schneider, D. P., Hall, P. B., Schneider, D. P., Vanden Berk, D. E., Fan, X., et al., (2003). Continuum and emission-line properties of broad absorption line quasars. *Astron. J.* 126, 2594–2607. doi: 10.1086/379293

Scaringi, S., Cottis, C. E., Knigge, C., and Goad, M. R. (2009). Classifying broad absorption line quasars: metrics, issues and a new catalogue constructed from SDSS DR5. *Month. Notices R. Astron. Soc.* 399, 2231–2238. doi: 10.1111/j.1365-2966.2009.15426.x

Schlafly, E. F., and Finkbeiner, D. P. (2011). Measuring reddening with sloan digital sky survey stellar spectra and recalibrating SFD. *Astrophys. J.* 737, 103–116. doi: 10.1088/0004-637X/737/2/103

Schneider, D. P., Richards, G. T., Hall, P. B., Strauss, M. A., Anderson, S. F., Boroson, T. A., Ross, N. P., et al. (2010). The sloan digital sky survey quasar catalog. V. Seventh data release. *Astron. J.* 139, 2360–2370. doi: 10.1088/0004-6256/139/6/2360

Shen, Y., Richards, G. T., Strauss, M. A., Hall, P. B., Schneider, D. P., Snedden, S., et al. (2011). A catalog of quasar properties from sloan digital sky survey data release 7. *Astrophys. J.* 194, 45–66. doi: 10.1088/0067-0049/194/2/45

Smith, P. S., Schmidt, G. D., Allen, R. G., and Angel, J. R. P. (1995). The polarization and ultraviolet spectrum of Markarian 231. *Astrophys. J.* 444, 146–156. doi: 10.1086/175589

Trevese, D., Saturni, F. G., Vagnetti, F., Perna, M., Paris, D., and Turriziani, S. (2013). A multi-epoch spectroscopic study of the BAL quasar APM 08279+5255. I. C IV absorption variability. *Astron. Astrophys* 557, 91–101. doi: 10.1051/0004-6361/201321864

Trump, J. R., Hall, P. B., Reichard, T. A., Richards, G. T., Schneider, D. P., Vanden Berk, D. E., et al., (2006). A catalog of broad absorption line quasars from the sloan digital sky survey third data release. *Astrophys. J. Suppl.*, 165, 1–18. doi: 10.1086/503834

Urrutia, T., Becker, R. H., White, R. L., Glikman, E., Lacy, M., Hodge, J., et al. (2009). The FIRST-2MASS red quasar survey. II. An anomalously high fraction of LoBALs in searches for dust-reddened quasars. *Astrophys. J.* 698, 1095–1109. doi: 10.1088/0004-637X/698/2/1095

Vivek, M., Srianand, R., Petitjean, P., Noterdaeme, P., Mohan, V., Mahabal, A., et al. (2012). Probing the time variability of five Fe low broad absorption-line quasars. *Month. Notices R. Astron. Soc.* 423, 2879–2892. doi: 10.1111/j.1365-2966.2012.21098.x

Vivek, M., Srianand, R., Petitjean, P., Mohan, V., Mahabal, A., and Samui, S. (2014). Variability in low ionization broad absorption line outflows. *Month. Notices R. Astron. Soc.* 440, 799–820. doi: 10.1093/mnras/stu288

Wang, F. G., Fan, X. H., Yang, J. Y., Wu, X. B., Yang, Q., Bian, F. Y., et al. (2017). First Discoveries of z > 6 Quasars with the DECam Legacy Survey and UKIRT Hemisphere Survey. *Astrophys. J.* 839, 27–35. doi: 10.3847/1538-4357/aa689f

Weymann, R. J., Morris, S. L., Foltz, C. B., and Hewett, P. C. (1991). Comparisons of the emission-line and continuum properties of broad absorption line and normal quasi-stellar objects. *Astrophys. J.* 373, 23–53. doi: 10.1086/170020

White, R. L., Becker, R. H., Gregg, M. D., Laurent-Muehleisen, S. A., Brotherton, M. S., Impey, C. D., et al. (2000). The FIRST Bright Quasar Survey. II. 60 Nights and 1200 Spectra Later. *Astrophys. J. Suppl.* 126, 133–207. doi: 10.1086/313300

Woo, J. H., Son. D., and Bae, H. J. (2017). Delayed or no feedback? Gas outflows in type 2 AGNs. III. . *Astrophys. J.* 839, 120–133. doi: 10.3847/1538-4357/aa6894

Wu, X. B., Hao, G. Q., Jia, Z. D., Zhang, Y. X., and Peng, N. B. (2012). SDSS quasars in the WISE preliminary data release and quasar candidate selection with optical/infrared colors. *Astron. J.* 144, 49–60. doi: 10.1088/0004-6256/144/2/49

Wu, X. B., Wang, F. G., Fan, X. H., Yi, W. M., Zuo, W. W., Bian, F. Y., et al. (2015). An ultraluminous quasar with a twelve-billion-solar-mass black hole at redshift 6.30, *Nature* 518, 512–515. doi: 10.1038/nature14241

Yang, J. Y., Fan, X. H., Wu, X. B., Wang, F. G., Bian, F. Y., Yang, Q., et al. (2017). Discovery of 16 New z 5.5 quasars: filling in the redshift gap of quasar color selection. *Astron. J.* 153, 184–194. doi: 10.3847/1538-3881/aa6577

Yi, W. M., Green, R., Bai, J. M., Wang, T. G., Grier, C. J., Trump, J. R., et al., (2017). The physical constraints on a new LoBAL QSO at z = 4.82. *Astrophys. J.* 838, 135–147. doi: 10.3847/1538-4357/aa65d6

York, D. G., Adelman, J.; Anderson, Jr. J. E., Anderson, S. F., Annis, J., Bahcall, N. A., et al., (2000). The sloan digital sky survey: technical summary. *Astron. J.* 120, 1579–1587. doi: 10.1086/301513

Zhang, S. H., Wang, T. G., Wang, H. Y., Zhou, H. Y., Dong, X. B., and Wang, J. G. (2010). Low-z Mg II broad absorption-line quasars from the sloan digital sky survey. *Astrophys. J.* 714, 367–383. doi: 10.1088/0004-637X/714/1/367

Zhang, S.-H, Wang, H.-Y., Zhou, H.-Y., Wang, T.-G., and Jiang, P. (2011). Discovery of a variable broad absorption line in the BL Lac object PKS B0138-097. *Res. Astron. Astrophys.* 11, 1163–1170. doi: 10.1088/1674-4527/11/10/005

Zhang, S. H., Zhou, H. Y., Wang, T. G., Wang, H. Y., Shi, X. H., Liu, B., et al. (2015). Strong variability of overlapping iron broad absorption lines in five radio-selected quasars. *Astrophys. J.* 803, 58–68. doi: 10.1088/0004-637X/803/2/58

Zubovas, K., Nayakshin, S., King, A., and Wilkinson, M. (2013). AGN outflows trigger starbursts in gas-rich galaxies. *Month. Notices R. Astron. Soc.* 433, 3079–3090. doi: 10.1093/mnras/stt952

Conflict of Interest Statement: The authors declare that the research was conducted in the absence of any commercial or financial relationships that could be construed as a potential conflict of interest.

Copyright © 2017 Wang, Xu and Wei. This is an open-access article distributed under the terms of the Creative Commons Attribution License (CC BY). The use, distribution or reproduction in other forums is permitted, provided the original author(s) or licensor are credited and that the original publication in this journal is cited, in accordance with accepted academic practice. No use, distribution or reproduction is permitted which does not comply with these terms.

frontiers in Astronomy and Space Sciences

REVIEW
published: 16 November 2017
doi: 10.3389/fspas.2017.00034

The AGN Nature of LINER Nuclear Sources

Isabel Márquez[1], Josefa Masegosa[1], Omaira González-Martin[2], Lorena Hernández-Garcia[3], Mirjana Pović[1,4], Hagai Netzer[5], Sara Cazzoli[1] and Ascensión del Olmo[1]*

[1] Instituto de Astrofisica de Andalucia (CSIC), Granada, Spain, [2] Instituto de Radioastronomía y Astrofísica, Universidad Nacional Autónoma de México, Morelia, Mexico, [3] Istituto di Astrofisica e Planetologia Spaziali, Rome, Italy, [4] Ethiopian Space Science and Technology Institute and Entoto Observatory and Research Center, Addis Ababa, Ethiopia, [5] Raymond and Beverly Sackler Faculty of Exact Sciences, School of Physics and Astronomy and the Wise Observatory, Tel-Aviv University, Tel Aviv, Israel

OPEN ACCESS

Edited by:
Fabio La Franca,
Roma Tre University, Italy

Reviewed by:
Daniela Bettoni,
Osservatorio Astronomico di Padova (INAF), Italy
Viviana Casasola,
Osservatorio Astrofisico di Arcetri (INAF), Italy
Simonetta Puccetti,
Agenzia Spaziale Italiana, Italy

***Correspondence:**
Isabel Márquez
isabel@iaa.es

Specialty section:
This article was submitted to Milky Way and Galaxies, a section of the journal Frontiers in Astronomy and Space Sciences

Received: 25 August 2017
Accepted: 23 October 2017
Published: 16 November 2017

Citation:
Márquez I, Masegosa J, González-Martin O, Hernández-Garcia L, Pović M, Netzer H, Cazzoli S and del Olmo A (2017) The AGN Nature of LINER Nuclear Sources. Front. Astron. Space Sci. 4:34. doi: 10.3389/fspas.2017.00034

Low-ionization nuclear emission-line regions (LINERs) are specially interesting objects since not only they represent the most numerous local Active Galactic Nuclei population, but they could be the link between normal and active galaxies as suggested by their low X-ray luminosities. The origin of LINER nuclei being still controversial, our works, through a multiwavelength approach, have contributed, firstly, to confirm that a large number of nuclear LINERs in the local universe are AGN powered. Secondly, from the study of X-ray spectral variability, we found that long term variations are very common, and they are mostly related to hard energies (2–10keV). These variations might be due to changes in the absorber and/or intrinsic variations of the source. Thirdly, Mid-infrared (MIR) imaging also indicates that LINERs are the low luminosity end of AGN toward lower luminosities, and MIR spectroscopy shows that the average spectrum of AGN-dominated LINERs with X-ray luminosities L_X(2–10 keV) $> 10^{41}$ erg/s is similar to the average mid-IR spectrum of AGN-dominated Seyfert 2s; for fainter LINERS, their spectral shape suggests that the dusty-torus may disappear. Fourth, the extended Hα emission of LINERs at HST resolution indicates that they follow remarkably well the Narrow Line Region morphology and the luminosity-size relation obtained for Seyfert and QSOs; HST Hα morphology may suggest the presence of outflows, which could contribute to the line broadening, with the resulting consequences on the percentage of LINERs where the Broad Line Region is detected. This issue is being revisited by our group with a high spectral resolution set of optical data for nearby type-1 LINERs. Finally, concerning systematic studies on the role of star formation in LINERs, which are scarce, our contribution deals with the study of a sample of the most luminous, highest star formation rate LINERs in the local Universe (at z from 0.04 to 0.11), together with its comparison with both lower-redshift LINERs and luminous LINERs previously detected at z $\sim$ 0.3. Most of our sources have $L_{AGN} \sim L_{SF}$, suggesting co-evolution of black hole and stellar mass. The AGN luminosity of local LINERs generally is related to the position they occupy on the main-sequence traced by Star Forming galaxies.

Keywords: active galactic nuclei, ionization, morphology, star formation, galaxies

1. INTRODUCTION

LINERs (Low Ionization Nuclear Emission Line Regions) were initially classified among Active Galactic Nuclei (AGN) since their emission line ratios could not be explained as produced by star forming processes (Heckman, 1980); they show optical spectra dominated by emission lines from low ionization species [(OI), (NII), (SII)] and faint high-ionization emission lines. The quantification of these properties is given by the position they occupy in diagnostic diagrams using optical (Veilleux and Osterbrock, 1987; Kewley et al., 2006) or Mid-infrared emission line ratios (Sturm et al., 2005, 2006; Bendo et al., 2006; Dale et al., 2006; Rupke et al., 2007; Smith et al., 2007). AGN were widely recognized as sources photo-ionized by a power-law continuum (Halpern and Steiner, 1983). Nevertheless, already pioneering works showed that the spectra of LINERs could also be explained by shock ionization models (Dopita and Sutherland, 1995; Franceschini et al., 2005) and photoionization by post-AGB stars, specially in the case of weak LINERs in ellipticals (Binette et al., 1994). Some LINER nuclei show broad permitted emission lines (type-1 LINERs, about 25% of all local LINERs, see Ho 2002) that, if confirmed as being produced by the Broad Line Region (BLR), would unambiguously connect type-1 LINERs to the AGN family. In the case of type-2 LINERs, the debate is still open, with the interpretation of all type-2 LINERs as low-luminosity AGN beeing still controversial, since the contribution from evolved (post-AGB) stars, low mass X-ray binaries or diffuse thermal plasma may have an important role (see Ho et al. 1997a for a full discussion on the topic; see also Eracleous et al. 2002; Stasińska et al. 2008; McKernan et al. 2010).

Already in Heckman's seminal work, LINERs were found to have lower luminosities that Seyfert nuclei and were generally identified in early-type hosts, a result which is irrespective of the interaction class, in the sense of finding the same morphologies in isolated and interacting LINER galaxies (Márquez and Masegosa, 2010; Márquez et al., 2010). LINERs are frequently found among nearby galaxies. For instance, around 40% of the galaxies in the Palomar Spectroscopic Survey (Ho et al., 1997a, and references therein) fall in this category. In the recent work by Leslie et al. (2016), 6.5% of the 202708 galaxies in their sample are classified as LINERs. Evidence is also compelling on LINERs probaly hosting heavily obscured (Compton-thick) AGN (González-Martín et al., 2009a, and references therein) which may imply that they may be even more numerous than previously deduced from optical selections. Therefore, their study seems relevant for understanding the demography of nearby AGN. AGN LINERs are found to be located at the faintest end of the fundamental correlation between star formation rate and accretion, representing very inefficient accreting systems (Satyapal et al. 2004; Dudik et al. 2005; Satyapal et al. 2005; Ho 2008; but see Netzer 2009). Ho (2009) places them in a sequence of decreasing L_{bol}/L_{Edd} which goes from Seyferts to LINERs, and transition objects, down to passive absorption-line systems. Understanding LINERs would therefore be important for a better understanding of low-efficiency accretion processes and their connection with higher power AGN activity. Provided that the mass of the central supermassive black hole and the mass of the hosting galaxy bulge are correlated and that there exists the expected connection between AGN with galaxy formation and evolutionary processes (e.g., Leslie et al. 2016), the study of LINERs is relevant for inferring their role as eventual end-products in the evolution of galaxies (see for instance Wang et al. 2008).

Together with the host contamination, the presence of eventual extinction and circumnuclear star formation hamper the detection and characterization of such faint sources, still today. After more than 30 years of research, it is clear that the nature of the ionizing source in LINERs have to be studied through a multi-wavelength approach (review by Ho, 2008 and references therein).

This paper is focused on the contributions from our group on the multi-wavelength research on LINERs that we started more than a decade ago, and that mainly refer to (i) the study of the X-ray properties and variability of LINERs, (ii) the analysis of their mid-infrared *Spitzer* spectroscopy, (iii) the morphology of the ionized galaxies in the nuclear regions with high spatial resolution HST imaging, (iv) the study of optical emission lines in local type-1 LINERs and (v) the determination of the star formation properties of LINERs at low redshifts (from 0.04 to 0.11). Before going deeper into the details, we want to emphasize that we use the available information to minimize in our samples the contamination from those LINERs that could not belong to the AGN family, as explained in the following section.

2. AGN LINERS

Previous works have shown that LINER-like spectra can also arise in a galactic disc (see for example González-Martín et al. 2009b). In fact the contribution from fast shocks in extra-nuclear spectra, the so-called Low Ionization Emission Region (LIER), can produce the observed optical line ratios (Dopita et al., 1997) as can ejecta from starburst driven winds (Armus et al., 1990) or even a diffuse ionized plasma (Collins and Rand, 2001). An example for the LINER galaxy NGC5966 is given in **Figure 1**.

The challenge is to determine which sources with a LIER-like spectrum actually harbor a LINER powered by an AGN. To make this determination, a number of diagnostics exist at different wavelengths (Baldwin et al., 1981; Veilleux and Osterbrock, 1987; Sturm et al., 2005, 2006; Bendo et al., 2006; Dale et al., 2006; Kewley et al., 2006; Rupke et al., 2007; Smith et al., 2007). In addition to the traditional diagrams by Baldwin et al. (1981) BPT, the use of the WHAN diagnostics (which use the width of Hα, WHα, vs. [N II]/Hα) by Cid Fernandes et al. (2011) has been recently added to discriminate between weak AGN and retired galaxies where the process of forming stars has stopped and hot low-mass evolved stars are the ionizing source. Even if a great proportion of galaxies belonging to the initial LINER class are reclassified as retired galaxies, all LINERs with WH$\alpha > 3$ Å are considered as weak AGN (see **Figures 1**, **6** in Cid Fernandes et al., 2011).

The detection of broad permitted lines (type-1 LINERs) is another indication of an AGN, as they are the detection of point like sources with AGN-like spectral properties at X-ray, UV and radio frequencies, and which are more secure indicators in

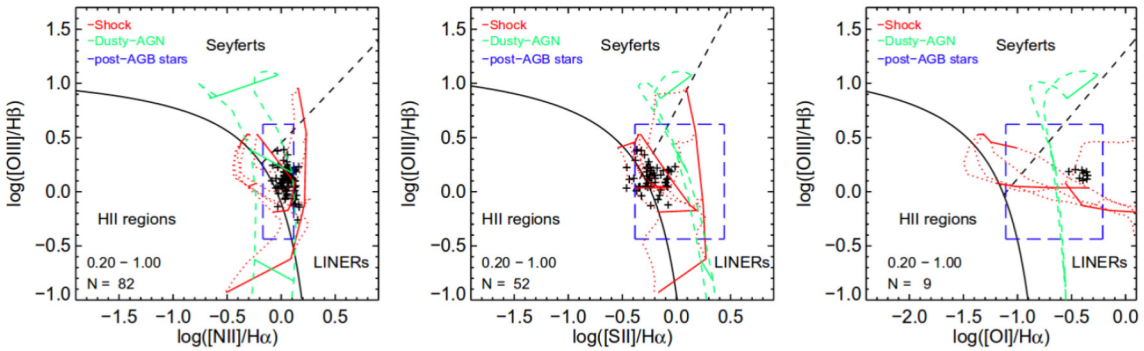

FIGURE 1 | Diagnostic BPT diagrams for the LINER galaxy NGC 5966. The crosses correspond to the different locations across the galaxy provided by integral field spectroscopic data. The black solid curve is the theoretical maximum starburst model (Kewley et al., 2001). The black-dashed curves represent the Seyfert-LINER dividing line (Kewley et al., 2006; Schawinski et al., 2007). The red lines represent shock grids models (Allen et al., 2008). Green curves indicate grids of photoionization by an AGN (Groves et al., 2004). The blue boxes correspond to the predictions of photoionization models by pAGB stars (Binette et al., 1994). Adapted from Figure 9 in Kehrig et al. (2012). A&A 540, A11, 2012, reproduced with permission © ESO.

the case of such sources showing variability. All the available indicators above have been used when selecting our sample galaxies in order to secure their AGN nature.

2.1. X-ray Properties and Variability

X-ray data offer the most reliable probe of the high energy spectrum for luminosity AGN. Additionally, the X-ray domain provides many AGN signatures, and therefore studies at X-rays frequencies become one of the most important for determining the AGN nature of LINERs. The advent of *Chandra* and *XMM-Newton* resulted in much progress on the field. Different studies carried out in the last decade show that an AGN is present in at least 50% of LINERs (Ho et al., 2001; Satyapal et al., 2004, 2005; Dudik et al., 2005), unless the AGN contribution to the 0.5–10 keV luminosity may be 60% (Flohic et al., 2006). Bolometric luminosities, L_{bol}, can be estimated from X-ray luminosities, L_X, by considering an universal bolometric correction for LINERs, $L_{bol} \sim L_X$. The derived Eddington ratios would imply that LINERs are the faintest end of the correlation between star formation rates and mass accretion, hosting very inefficient accretion processes (Eracleous et al., 2002; Dudik et al., 2005; Flohic et al., 2006; Ho, 2009).

Our first effort in this field was focused on the analysis of the X-ray properties of 51 LINERs with Chandra data (González-Martín et al., 2006). We found that their X-ray morphologies, spectra, and color-color diagrams together imply that a high percentage of LINER galaxies may host an AGN (González-Martín et al., 2006). We then updated our sample, including all LINERs from the catalog by Carrillo et al. (1999) with useful observations from Chandra and/or XMM-Newton; the resulting sample was the largest of LINERs (82 galaxies) with such data to date (González-Martín et al., 2009b,a). We first considered as AGN-candidates as those with a nuclear point-like source at the hard X-ray energy range (4.5–8.0 keV); at least ∼60% of the studied LINERs were class as AGN-candidate (see **Figure 2**). HST optical images and literature data on emission lines, radio compactness, and stellar population results were compiled, and their study allowed us to conclude that an AGN might be present in 90% of the sample. The spectral analysis at X-rays indicates that best fits involve a composite model: (1) an absorbed primary power-law continuum and (2) a soft component below 2 keV described by an absorbed, scattered and/or thermal component (González-Martín et al., 2009b). According to the most common tracers for Compton-thickness, i.e., the X-ray spectral index (Maiolino et al., 1998; Cappi et al., 2006), the F_X(2–10 keV) / F([OIII]) ratio (Panessa et al., 2006, and references therein), and the equivalent width of FeKα emission line (Matt, 1997; Bassani et al., 1999), about 50% of the studied LINERs showed evidence of being Compton-thick, a property more commonly found among LINERs than among Seyferts (González-Martín et al., 2009a, and references therein). Compared to Seyfert galaxies, LINERS have larger black hole masses and lower Eddington ratios, consistent with LINERs preferring early-type hosts. However note that, once X-ray luminosities were corrected for Compton-thickness, LINERs appeared to have lower X-ray luminosities and Eddington ratios, but somewhat overlapping the range of type-2 Seyferts, as further confirmed by Hernández-García et al. (2016) (see **Figure 3**).

In addition to a number of studies devoted to individual sources, the variability of LINERs as a family was studied at X-rays (Ptak and Griffiths, 1998; Pian et al., 2010) (see also Younes et al. 2011, 2012 but only for type 1 LINERs) and at UV (Maoz et al., 2005). Other works have considered LINERs but within the group of low luminosity AGN, where some Seyferts are also considered (González-Martín and Vaughan, 2012; Young et al., 2012, for example).

Starting with the finding of X-ray variability in the type-2 LINER NGC 4102 (González-Martín et al., 2011), and with the aim of contributing to the study of variability in LINERs in an homogeneous way, we extended our analysis to a sample of 17 AGN-LINERs with multi-epoch *XMM-Newton* and/or *Chandra* observations, to study both long and short-term variations. Variability is detected on timescales from days to years in 50% of the targets, but no short-term variations are detected. Flux

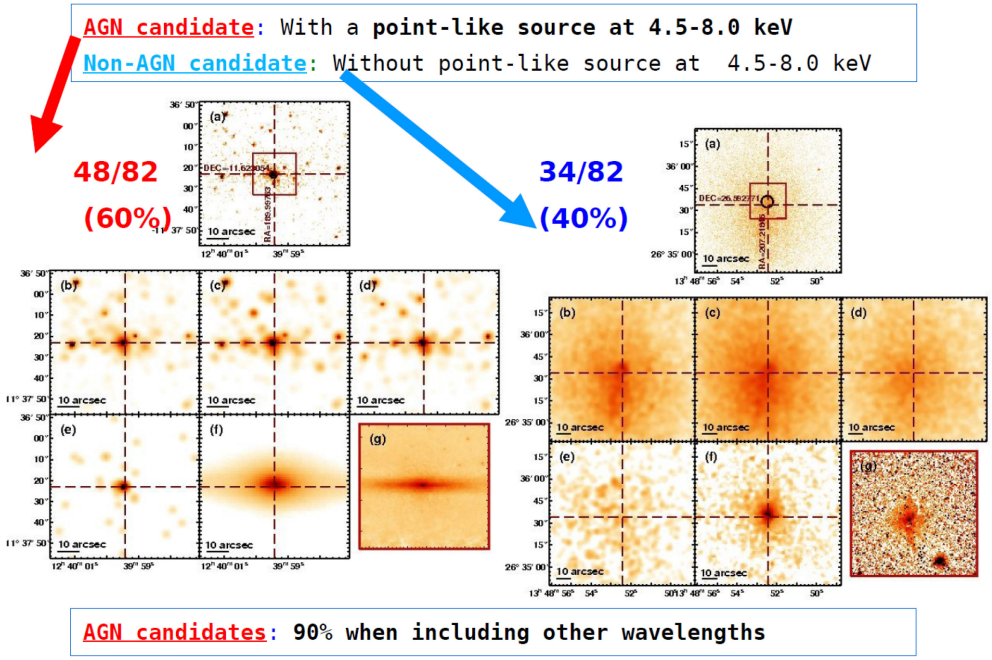

FIGURE 2 | This figure summarizes the results of the classification of the 82 LINERS in our sample based on X-ray imaging, where AGN-candidates were defined as those with a nuclear point-like source at the hard X-ray energy range (4.5–8.0 keV). An example of an AGN candidate is given in the **left (NGC 4594)** and for an non-AGN candidate in the **right (CGCG 162–010)**. In both columns we represent: Top: 0.6–8.0 keV band without smoothing. **Center-left**: 0.6–0.9 keV band. **Center-center**: 1.6–2.0 keV band. **Center-right**: 4.5–8.0* keV band. **Bottom left**: 6.0–7.0 keV band. **Center-bottom**: 2MASS image in Ks band. **Bottom-right**: sharp-divided HST optical image in the filter F814 W of the region marked as a rectangle in the top image. The sharp-dividing technique consists on dividing the original image by a smoothed version, and is aimed at better showing the internal structure (Márquez et al., 2003). The initial percentage of 60% AGN-candidates when only using X-ray imaging rises to 90% when the information at other wavelengths is considered (González-Martín et al., 2009b).

variations are generally due to changes in the normalization of the power-law component at hard energies (Hernández-García et al., 2013, 2014, 2016).

When LINERs are compared to Seyfert 2 galaxies, we find that changes are mostly related to variations in the nuclear continuum, with variations in the absorbers and at soft energies in a few cases in both families. Compton-thick sources do not show variability, most probably because the AGN is not accessible in the 0.5–10 keV energy band. We find that the X-ray variations may occur similarly in the two families, LINERs and Seyfert 2s, in the sense that they are related to the nuclear continuum, although they might have different accretion mechanisms. Variability at UV wavelengths is detected in LINERs but not in Seyfert 2s, suggesting that some LINERs may have an unobstructed view of the inner disk where the UV, sometimes variable, emission may take place. This result appears to be compatible with the disappearance of the torus and/or the broad-line region in at least some LINERs (Hernández-García et al., 2016).

2.2. Mid Infrared Spectroscopy

At Mid Infrared (MIR) frequencies, among arguments to reinforce for the existence of a non-thermal component in LINERs are the overall shape of the continuum and the detection and line ratios of emission lines. As shown by Lawrence et al. (1997), LINERs are dominated by the stellar host in the range 1–5 μm but a strong excess is observed in the range between 10 and 20 μm, which may indicate the presence of less hot dust than in Seyferts. The unique study done so far at MIR frequencies by Sturm et al. (2005) has shown that two different LINER populations exist: infrared-bright and infrared-faint LINERs. The LINER emission in the former often show spatially extended (non-AGN) LINER emission and show MIR Spectral Energy Distributions (SED) typical of starburst galaxies. Emission in infrared-faint LINERs mostly arise from compact nuclear regions, and their MIR SEDs are much bluer. Fine-structure emission lines from highly excited gas, such as [OIV], suggesting the presence of an AGN, is detected in both populations.

Our study of LINERs in the MIR, low spectral-resolution *Spitzer* data, complemented with QSOs, Seyferts 1 and 2 and starburst galaxies, allows us to conclude that the spectrum of faint LINERs (those with $L_X < 10^{41}$ erg/s) is different from the average spectra of any of the other optical classes (see **Figure 4**). We suggest that their dominant emission might be a combination of an elliptical galaxy host, a starburst, a jet, and/or Advection-dominated Accretion Flow emission (González-Martín et al., 2015). Concerning the analysis of the existing correlation between the emissions at MIR and X-rays in AGN (Gandhi et al., 2010; Asmus et al., 2014), our analysis of the galaxy NGC 835 (González-Martín et al., 2016) has pointed out that the knots

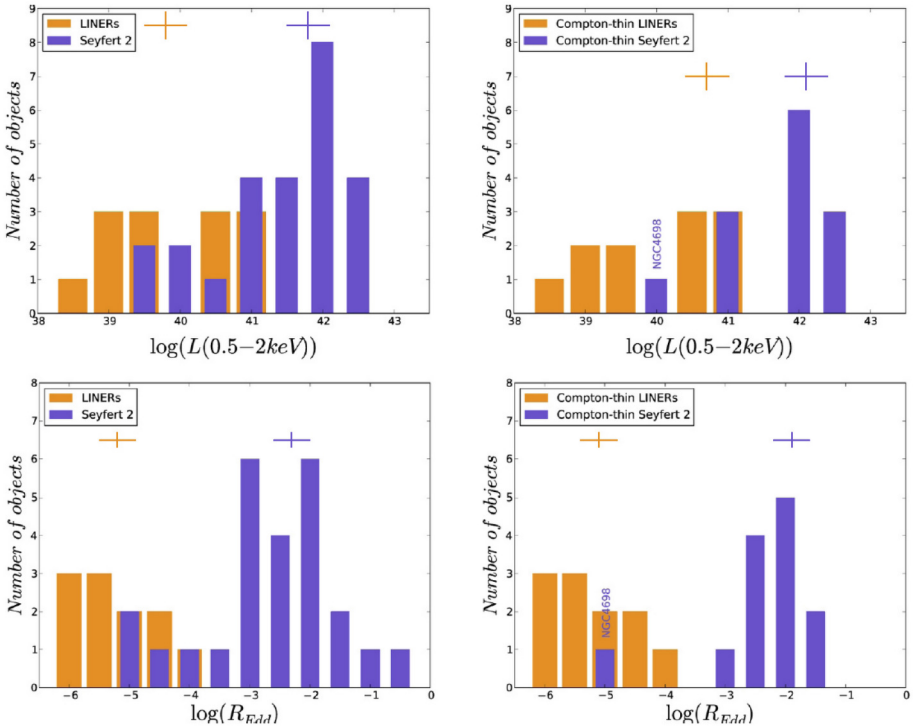

FIGURE 3 | Histograms of the hard X-ray luminosities **(top)** and Eddington ratios **(bottom)** of LINER and Seyfert 2 nuclei analyzed in Hernández-García et al. (2016), for the entire sample of LINERs and Seyfert 2s **(left)**, and Compton-thin LINERs and Seyfert 2s **(right)**. The crosses represent the median values. Adapted from Figure 3 in Hernández-García et al. (2016).

seen at X-rays are mostly located in the inner side of this MIR emission, which may suggest that outflows are present in the circumnuclear region.

Several authors have claimed that less luminous AGN are not capable of sustaining a dusty torus structure (Elitzur and Shlosman 2006, also reviewed by Heckman and Best 2014 and references therein). In order to study the gradual re-sizing and disappearance of the torus, we examined MIR *Spitzer*/IRS spectra of a sample of ∼ local AGN of different luminosities, from low-luminosity AGN and powerful Seyferts. A decomposition method was applied to decontaminate the torus component from other contributors (Hernán-Caballero et al., 2015); the nuclear fluxes provided by high spatial resolution MIR (or X-ray images and the Asmus' relation) were used to anchor the torus component. Starburst objects were included to ensure secure decomposition of the *Spitzer*/IRS spectra. Five groups were defined according to the torus contribution to the 5–15 μm range (C_{torus}) and L_{bol}, with a progressively higher C_{torus} and an increase of L_{bol} from Group 1 (no torus contribution, $\log(L_{bol}) \sim 41$) up to Group 5 ($C_{torus} \sim 80\%$ and $\log(L_{bol}) \sim 44$). The fit of clumply models to the average spectra of each group indicated that, in Group 1, the torus is no longer present, supporting that the torus disappears at low luminosities. For Groups 3, 4, and 5, higher outer radii of the torus were found for higher luminosities, consistent with a re-sizing of the torus according to AGN luminosity (González-Martín et al., 2017).

2.3. HST Hα Imaging

To get additional clues on the nature of LINERs in the absence of high resolution X-ray data, indirect information can be obtained from correlations between X-ray properties at lower resolution and optical/NIR properties at higher resolution. In particular, the study of the properties of the ionized gas and its relation to those at X-rays may be enlightening. The Hα morphology of LINERs has been shown to consist on a point source embedded in an extended structure; this structure is sometimes clumpy and filamentary, and with clear indications of nuclear obscuration in some particular cases (similarly to what is found in low luminosity Seyferts) (Pogge et al., 2000; Chiaberge et al., 2005; Dai and Wang, 2008). Walsh et al. (2008) use STIS spectroscopy to demonstrate that the energy source at scales of tens of parsecs of 13 LINERs is consistent with photo-ionization by a central nuclear source, but outflows dominate their NLR kinematics.

We made use of the high spatial resolution provided by HST Hα imaging for 32 LINERs (Masegosa et al., 2011), with the aim of characterizing the ionized gas in the nuclear regions. An unresolved nuclear component can be identified in 84% of the sources. Extended emission with equivalent sizes ranging from a few tens to hundreds of parsecs is also seen, with morphologies that can be grouped into three classes: nuclear outflow candidates (42%, see an example in **Figure 5**), core-halo morphologies (25%) and nuclear spiral disks (14%). The equivalent radius of the Hα emission and the (2-10 keV) X-ray luminosities show a size-luminosity relation. Both the morphologies of the

ionized gas and the relation between size and luminosity are completely equivalent to those found in low luminosity Seyferts, what indicated a common origin for the NLR of LINERs and Seyferts. We suggested for the first time a relation between the morphologies of the ionized gas and the soft X-rays in LINERs (Masegosa et al., 2011) similar to what was obtained for Seyferts (Schmitt and Kinney, 1996).

2.4. The BLR in LINERs 1.9 Revisited

Spectropolarimetric observations at the Keck 10 m telescope of 14 LINERs have shown that the BLR is detected in polarized light in only three of them (Ho, 2008). But models based on a clumpy torus, suggest that the BLR cannot survive for bolometric luminosities $L_{bol} < 10^{42} ergs^{-1}$, in clear contradiction with the existence of type-1 LINER nuclei in general, and with the particular 22 cases in the Palomar Spectroscopic survey by Ho et al. (1997b). The properties of the BLR in these objects are hence far from being well understood.

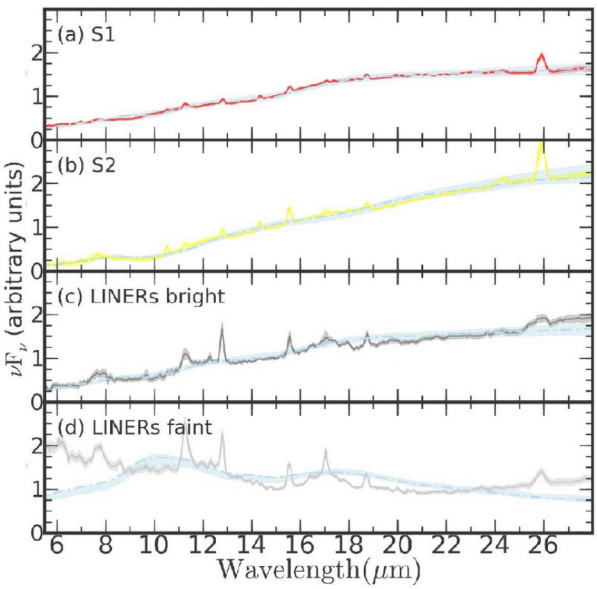

FIGURE 4 | Best fit to clumpy models (dot-dashed light-blue line) for the average spectra of Seyfert 1s **(a)**, Seyfert 2s **(b)**, bright LINERs **(c)**, and faint LINERs (those with $L_X < 10^{41}$ erg/s). **(d)**, From Figure 9 in González-Martín et al. A&A 578, A74, 2015, reproduced with permission © ESO.

Except for individual discoveries of type 1 LINERs (Storchi-Bergmann et al., 1993; Bower et al., 1996; Ho et al., 1997b; Eracleous and Halpern, 2001; Martínez et al., 2008), the only systematic work is Ho et al. (2003). They use an homogeneous detection method on a magnitude limited spectroscopic catalogue, so theirs is the best defined sample of type 1 LINERs. Unfortunately, their spectra quite often lack the required S/N for a precise measurement of the width of the broad Hα component. This could in principle be circumvented by using STIS-HST spectra, available for 14 out the 22 type 1 LINERs (Shields et al., 2007; Walsh et al., 2008; Balmaverde and Capetti, 2014). Nevertheless, as our analysis of the HST Hα imaging demonstrated, most objects show a morphology indicating the presence of outflows (Masegosa et al., 2011), which could contribute to the line broadening and consequently result in a wrong estimation of the BLR line width. Measuring the width of the low ionization line [OI]6300[1], which is not covered by the STIS-HST spectra (Balmaverde and Capetti, 2015; Constantin et al., 2015; Balmaverde et al., 2016), may help constrain whether outflows are relevant and estimate their contribution to the width of Hα.

We have observed, with the TWIN spectrograph attached to the 3.5 m telescope in Calar Alto, the 22 type 1 LINER galaxies in Ho's sample. The spectra covering the regions around both Hα and Hβ, with 0.54 A/pixel spectral resolution, have S/N $\sim$ 50 for the former. Our aim was to analyze whether the presence of outflows may have an impact on the line-widths and therefore on the identification of type 1 LINERs. A careful subtraction of the underlying stellar component was performed, using both Starlight (Cid Fernandes et al., 2005) and Ppfx

[1] A single, unblended line, contrary to [NII] and [SII].

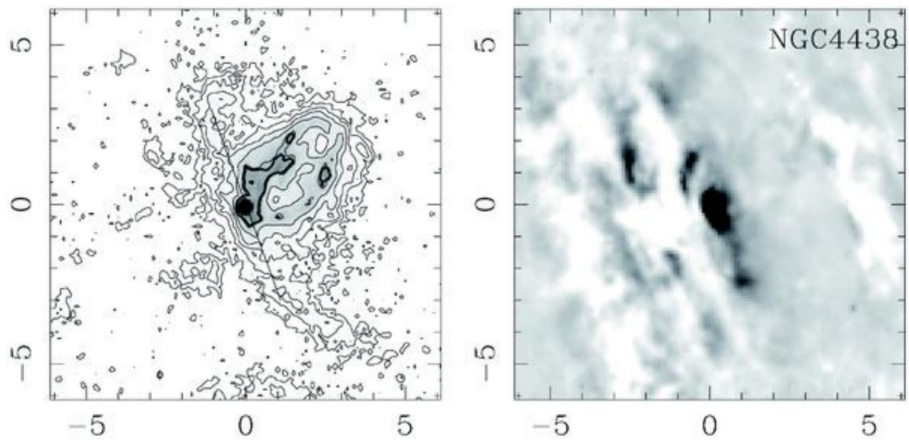

FIGURE 5 | HST Hα (left) and sharp-divided images of NGC 4438, one of the objects with a morphology suggestive on hosting an outflow. We note that this galaxy hosts a type-1 LINER nucleus. From Figure 2 in Masegosa et al. A&A 527, A23, 2011, reproduced with permission © ESO.

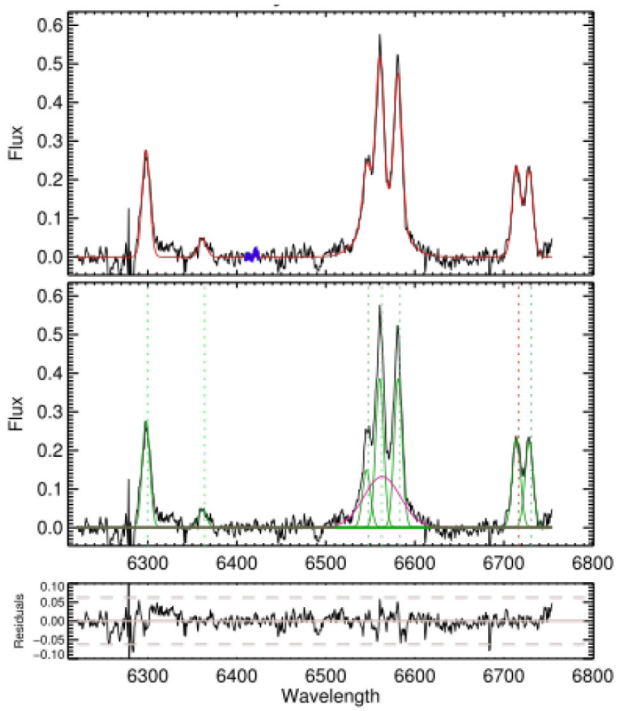

FIGURE 6 | Top: Stellar population subtracted spectrum of NGC 3718 (black), together with the final model with single Gaussian components for the narrow lines and an additional very broad component for Hα. **Middle**: Narrow line fitting in green and very broad Hα in magenta. **Bottom:** Residual spectrum.

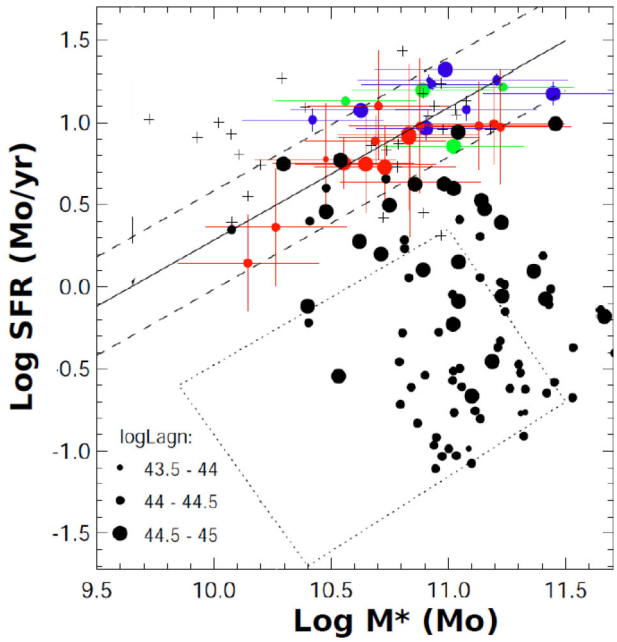

FIGURE 7 | The relationship between SFR and total stellar mass. SFRs were measured either with *Herschel*/PACS FIR data (big green filled circles), with IRAS data (big dark blue filled circles), or through Dn4000 index from optical spectroscopic data (big red filled circles). The solid black line shows the Main Sequence for SF at $z = 0.07$ (Whitaker et al., 2012), and the dashed lines its typical width. Together with our MLLINERs, the entire sample of luminous LINERs (black dots), and the most luminous LINERs at z ∼ 0.3 from Tommasin et al. (2012) (black crosses) are included. The dotted polygon represents the typical location of 60% of all LINERs at low redshifts (Leslie et al., 2016). AGN luminosity bins are represented with symbols of different sizes. Reproduced with permission from Figure 12. M. Povic et al. Star formation and AGN activity in the most luminous LINERs in the local universe. MNRAS (2016) 462 (3): 2878–2903. Published by Oxford University Press on behalf of The Royal Astronomical Society. Available online at: https://academic.oup.com/mnras/article/462/3/2878/2589850?searchresult=1. This figure is not covered by the Open-Access licence of this publication. For permissions contact Journals.permissions@OUP.com.

(Cappellari and Emsellem, 2004). The resulting narrow emission lines [SII] and [OI] were fitted by means of Gaussian single or double components, both providing in general different results for the line-widths. The line-widths and shifts of [NII] lines and Hα are fixed either to those from [SII] to [OI]; the best fit is determined from that with the smallest residuals. An additional broad component, indicative of a BLR, is also required only in eight cases (see for instance **Figure 6**). We find that outflows may explain the broad lines found in a number of these LINERs. A full discussion with these results and the comparison with those from previous works will be provided elsewhere (Marquez et al., 2017, in preparation).

3. MOST LUMINOUS LINERS AT REDSHIFTS FROM 0.04 TO 0.11

The best studied nearby LINERs are found in the nuclei of galaxies with little or no evidence of active star formation (SF). They are usually hosted by massive early-type galaxies (rarely spirals), with massive Super Massive Black Holes, old stellar populations and small amounts of gas and dust (e.g., Kauffmann et al. 2003; Cid Fernandes et al. 2004; Ho 2008; Leslie et al. 2016). Recently, a population of LINERs has been detected at z∼0.3 (Tommasin et al., 2012), showing higher SF and AGN luminosities than those typical of nearby LINERs (Ho et al., 1997a).

Aimed at searching for similar objects at lower redshifts, we have studied a sample of 42 of these most luminous LINERs in terms of both AGN and Star Formation luminosities (log(L_{AGN}) > 44.3 and log(L_{SF}) > 44.3, hereafter MLLINERs) but in the local universe, at z = 0.04–0.11, through the analysis of our own spectroscopic data (long-slit spectroscopy with the TWIN and ALFOSC spectrographs attached to the 3.5 m telescope in Calar Alto and the NOT in La Palma, respectively) and FIR data (Herschel and IRAS). We find that local MLLINERs show considerable differences in comparison to other low-redshift LINERs, in terms of higher extinctions, higher star-formation rates and AGN luminosities. They are hosted by galaxies of all morphological types, including 25% of peculiar galaxies (with clear asymmetries, substructures and/or distortions). Our MLLINERs are located on the main sequence (MS) of star-forming galaxies (see **Figure 7**), again in contrast to nearby LINERs that usually lye below the MS (Leslie et al., 2016).

MLLINERs have the same stellar masses (M_*), star forming rates and L_{AGN} than those previously detected at z ∼ 0.3

(Tommasin et al., 2012); hence we confirm the existence of such luminous LINERs in the local universe, and therefore discard an eventual evolutionary scenario with higher luminosity objects for higher redshifts. The median stellar mass of these MLLINERs corresponds to 6–7 $\times$ 10^{10} M$\odot$ which was found in previous work to correspond to the peak of relative growth rate of stellar populations and therefore for the highest SFRs. Other LINERs although showing similar AGN luminosities have lower SFR. We find that most of MLLINERs have $L_{AGN} \sim L_{SF}$ suggesting co-evolution of black hole and stellar mass. The fraction of z = 0.04–0.11 LINERs located on the MS is 2, 3, 11, and 37% in the bins of log(L_{AGN}) of (43–43.5), (43.5–44), (44–44.5), and (44.5–45), respectively (see **Figure 7**). Thus, we can safely conclude that the fraction of local LINERs on the main sequence of star-forming galaxies is related to their AGN luminosity. All these results are published in Pović et al. (2016).

4. CONCLUSIONS

The main conclusions of our contributions to the study of LINER AGN can be summarized as follows:

- From 60% to 90% of the studied LINERs in our initial sample of 82 objects with X-ray data can be considered as genuine AGN. The percentage of Compton-thick nuclei may be higher in LINERs than in Seyferts. Variability in X-rays is a common property in LINERs, with timescales from days to years. X-ray variations may occur similarly in LINERs and Seyfert 2s, i.e., they are related to the nuclear continuum, although they might have different accretion mechanisms, which may be related to the expected disappearance of the torus at low bolometric luminosities.
- Bright LINERs are similar to Seyfert 2s concerning MIR spectroscopic properties, whereas faint LINERs form a separate family. A refined decomposition of MIR spectra indicates that the torus contribution is negligible for $L_{BOL} < 10^{41}$ erg/s.
- The high spatial resolution HST imaging indicates that most LINERs show a broad-cone or core-halo Hα morphology, which may indicate the presence of outflows, specially in the former case.
- The study of new optical spectroscopic data around Hα of LINERs previously classified as type 1, allow a careful subtraction of the stellar component and the fitting to the resulting emission line spectra. Single/double Gaussian fitting results in the need of very broad Hα components only in 8 out of the 22 observed objects. The presence of such very broad lines being indicative of the detection of the BLR, the percentage of type 1 LINERs might be much smaller ($\sim$ 8%) than previously estimated (25%).
- The analysis of a sample of most luminous LINERs (with log(L_{AGN}) > 44.3 and log(L_{SF}) > 44.3, MLLINERs) at $z = 0.04 - 0.11$ results in such objects having the same stellar masses (M_*), star forming rates and L_{AGN} than luminous LINERs previously found at $z = 0.3$. Our MLLINERs are located along the line of $L_{AGN} = L_{SF}$. Most of them, with $M_* > 10^{10}$ M$\odot$, are located along the main sequence of star forming galaxies. Considering the whole population of LINERs [with log(L_{AGN}) from 43 to 45], the fraction of LINERs on the MS depends on L_{AGN}.

Still today LINERs remain interesting objects to be studied, and new data are needed to deepen in their knowledge. In particular, on one hand integral field spectroscopy will be of paramount importance to analyse the presence and relevance of shocks. On the other hand, MIR spectroscopy, with the required sensitivity and resolution with the advent of the JWST in the coming future, will provide an unprecedent approach to the hypothesis of the torus disapearence in such low luminous AGN.

AUTHOR CONTRIBUTIONS

All authors have contributed to the text. The analysis of LINERs at X-rays made within our group mainly comes from the PhD theses by OG-M and LH-G. JM, and IM led the analysis of HST Hα imaging. MIR spectroscopic studies were led by OG-M. The recently acquired optical spectroscopy of type 1 LINERs is led by IM, SC, and AdO being responsible for the spectral fittings. The study of MLLINERs was led by MP, IM, HN, and JM.

FUNDING

These works were supported by Spanish grants AYA2001-2089, AYA2003-00128, AYA2006-01325, AYA2007-62190, AYA2010-15169, AYA2013-42227P, and AYA2016-76682C3-1-P. Regional funding from the Junta de Andalucia was obtained through the grant TIC-114 and the Excellence Project P08-TIC-03531. MP acknowledges support from the Ethiopian Space Science and Technology Institute (ESSTI) under the Ethiopian Ministry of Science and Technology (MoST).

ACKNOWLEDGMENTS

We are grateful to our collaborators in the different papers produced within our group that are summarized in this contribution. IM acknowledges the kind invitation of the organizers of the meeting "QSO at All Cosmic Epochs." We acknowledge the comments provided by the referees, who helped to improve the paper.

REFERENCES

Allen, M., Groves, B., Dopita, M., Sutherland, R., and Kewley, L. (2008). The mappings iii library of fast radiative shock models. *Astrophys. J. Suppl. Ser.* 178, 20–55. doi: 10.1086/589652

Armus, L., Heckman, T., and Miley, G. (1990). The optical emission-line nebulae of powerful far-infrared galaxies. *Astrophys. J.* 364:471. doi: 10.1086/169431

Asmus, D., Hönig, S., Gandhi, P., Smette, A., and Duschl, W. (2014). The subarcsecond mid-infrared view of local active galactic nuclei - i.

the n- and q-band imaging atlas. *Mon. Not. R. Astron. Soc.* 439:1648. doi: 10.1093/mnras/stu041

Baldwin, A., Phillips, M. M., and Terlevich, R. (1981). Classification parameters for the emission-line spectra of extragalactic objects. *Publ. Astron. Soc. Pac.* 93:5. doi: 10.1086/130766

Balmaverde, B., and Capetti, A. (2014). The hst view of the broad line region in low luminosity agn. *Astron. Astrophys.* 563, A119. doi: 10.1051/0004-6361/201321989

Balmaverde, B., and Capetti, A. (2015). The naked nuclei of low ionization nuclear emission line regions. *Astron. Astrophys.* 581, A76. doi: 10.1051/0004-6361/201526496

Balmaverde, B., Capetti, A., Moisio, D., Baldi, R., and Marconi, A.(2016). The hst view of the innermost narrow line region. *Astron. Astrophys.* 586, A48. doi: 10.1051/0004-6361/201526927

Bassani, L., Dadina, M., Maiolino, R., Salvati, M., Risaliti, G., Ceca, R. D., et al. (1999). A three-dimensional diagnostic diagram for seyfert 2 galaxies: Probing x-ray absorption and compton thickness. *Astrophys. J. Suppl. Ser.* 121:473. doi: 10.1086/313202

Bendo, G., Buckalew, B., Dale, D., Draine, B., Joseph, R. R. K. Jr. Sheth, K., et al. (2006). Spitzer and jcmt observations of the active galactic nucleus in the sombrero galaxy (ngc 4594). *Astrophys. J.* 645:134. doi: 10.1086/504033

Binette, L., Magris, C., Stasińska, G., and Bruzual, A. (1994). Photoionization in elliptical galaxies by old stars. *Astron. Astrophys.* 292:13.

Bower, G., Wilson, A., Heckman, T., and Richstone, D. (1996). Double-peaked broad emission lines in the nucleus of m81. *Astron. J.* 111:1901. doi: 10.1086/117928

Cappellari, M., and Emsellem, E. (2004). Parametric recovery of line-of-sight velocity distributions from absorption-line spectra of galaxies via penalized likelihood. *Publ. Astron. Soc. Pac.* 116:138. doi: 10.1086/381875

Cappi, M., Panessa, F., Bassani, L., Dadina, M., Cocco, G. D., Comastri, A., et al. (2006). X-ray spectral survey with xmm-newton of a complete sample of nearby seyfert galaxies. *Astron. Astrophys.* 446:459. doi: 10.1051/0004-6361:20053893

Carrillo, R., Masegosa, J., Dultzin-Hacyan, D., and Ordoñez, R. (1999). A multifrequency catalog of liners. *Rev. Mex. Astron. Astrofis.* 35:187.

Chiaberge, M., Capetti, A., and Macchetto, F. (2005). The *hubble space telescope* view of liner nuclei: evidence for a dual population? *Astrophys. J.* 625:716. doi: 10.1086/429612

Cid Fernandes, R., Delgado, R. G., Schmitt, H., Storchi-Bergmann, T., Martins, L., Pérez, E., et al. (2004). The stellar populations of low-luminosity active galactic nuclei. i. ground-based observations. *Astrophys. J.* 605:105. doi: 10.1086/382217

Cid Fernandes, R., Mateus, A., Sodré, L., Stasińska, G., and Gomes, J. M. (2005). Semi-empirical analysis of sloan digital sky survey galaxies - i. spectral synthesis method. *Mon. Not. R. Astron. Soci.* 358:363. doi: 10.1111/j.1365-2966.2005.08752.x

Cid Fernandes, R., Stasińska, G., Mateus, A., and Asari, N. V. (2011). A comprehensive classification of galaxies in the sloan digital sky survey: how to tell true from fake agn? *Mon. Not. R. Astron. Soc.* 413:1687. doi: 10.1111/j.1365-2966.2011.18244.x

Collins, J., and Rand, R. (2001). Ionization sources and physical conditions in the diffuse ionized gas halos of four edge-on galaxies. *Astrophys. J.* 551:57. doi: 10.1086/320072

Constantin, A., Shields, J., Ho, L., Barth, A., Filippenko, A., and Castillo, C. (2015). Dissecting the power sources of low-luminosity emission-line galaxy nuclei via comparison of hst-stis and ground-based spectra. *Astrophys. J.* 814:149. doi: 10.1088/0004-637X/814/2/149

Dai, H., and Wang, T.-G. (2008). The structure of narrow-line region in liners. *Chin. J. Astron. Astrophys.* 8:245. doi: 10.1088/1009-9271/8/3/01

Dale, D., Smith, J., Armus, L., Buckalew, B., Helou, G., Kennicutt, R. C. Jr., et al. (2006). Mid-infrared spectral diagnostics of nuclear and extranuclear regions in nearby galaxies. *Astrophys. J.* 646:161. doi: 10.1086/504835

Dopita, M., Koratkar, A., Allen, M. G., Tsvetanov, Z., Ford, H., Bicknell, G., and Sutherland, R. (1997). The liner nucleus of m87: a shock-excited dissipative accretion disk. *Astrophys. J.* 490:202. doi: 10.1086/304862

Dopita, M., and Sutherland, R. (1995). Spectral signatures of fast shocks. ii. optical diagnostic diagrams. *Astrophys. J.* 455:468. doi: 10.1086/176596

Dudik, R. P., Satyapal, S., Gliozzi, M., and Sambruna, R. (2005). A chandra snapshot survey of infrared-bright liners: A possible link between star formation, active galactic nucleus fueling, and mass accretion. *Astrophys. J.* 620:113. doi: 10.1086/426856

Elitzur, M., and Shlosman, I. (2006). The agn-obscuring torus: the end of the "doughnut" paradigm? *Astrophys. J.* 648, L101. doi: 10.1016/j.newar.2006.06.027

Eracleous, M., and Halpern, J. (2001). Ngc 3065: a certified liner with broad, variable balmer lines. *Astrophys. J.* 554:240. doi: 10.1086/321331

Eracleous, M., Shields, J., Chartas, G., and Moran, E. (2002). Three liners under the chandra x-ray microscope. *Astrophys. J.* 565:108. doi: 10.1086/324394

Flohic, H., Eracleous, M., Chartas, G., Shields, J., and Moran, E. (2006). The central engines of 19 liners as viewed by chandra. *Astrophys. J.* 647:140. doi: 10.1086/505296

Franceschini, A., Manners, J., Polletta, M., Lonsdale, C., Gonzalez-Solares, E., Surace, J., et al. (2005). A complete multiwavelength characterization of faint chandra x-ray sources seen in the spitzer wide-area infrared extragalactic (swire) survey. *Astron. J.* 129:2074. doi: 10.1086/428004

Gandhi, P., Horst, H., Smette, A., Hönig, S., Comastri, A., Gilli, R., et al. (2010). "Resolved mid-infrared imaging of agn: an isotropic measure of intrinsic power," in *X-ray Astronomy 2009; Present Status, Multi-Wavelength Approach and Future Perspectives* (Bologna), Vol. 1248:431.

González-Martín, O., Hernández-García, L., Masegosa, J., Márquez, I., Rodríguez-Espinosa, J., Acosta-Pulido, J., et al. (2016). X-ray long-term variations in the low-luminosity agn ngc 835 and its circumnuclear emission. *Astron. Astrophys.* 587, A1. doi: 10.1051/0004-6361/201526990

González-Martín, O., Masegosa, J., Hernán-Caballero, A., Márquez, I., Almeida, C. R., Alonso-Herrero, A., et al. (2017). Hints on the gradual resizing of the torus in agns through decomposition of spitzer/irs spectra. *Astrophys. J.* 841:37. doi: 10.3847/1538-4357/aa6f16

González-Martín, O., Masegosa, J., Márquez, I., and Guainazzi, M. (2009a). Fitting liner nuclei within the active galactic nucleus family: a matter of obscuration? *Astrophys. J.* 704:1570. doi: 10.1088/0004-637X/704/2/1570

González-Martín, O., Masegosa, J., Márquez, I., Guainazzi, M., and Jiménez-Bailón, E. (2009b). An x-ray view of 82 liners with chandra and xmm-newton data. *Astron. Astrophys.* 506:1107. doi: 10.1051/0004-6361/200912288

González-Martín, O., Masegosa, J., Márquez, I., Guerrero, M., and Dultzin-Hacyan, D. (2006). X-ray nature of the liner nuclear sources. *Astron. Astrophys.* 460:45. doi: 10.1051/0004-6361:20054756

González-Martín, O., Masegosa, J., Márquez, I., Rodríguez-Espinosa, J., Acosta-Pulido, J., Almeida, C. R., et al. (2015). Nuclear obscuration in liners. clues from spitzer/irs spectra on the compton thickness and the existence of the dusty torus. *Astron. Astrophys.* 578, A74. doi: 10.1051/0004-6361/201425254

González-Martín, O., Papadakis, I., Braito, V., Masegosa, J., Márquez, I., Mateos, S., et al. (2011). Suzaku observation of the LINER NGC 4102. *Astron. Astrophys.* 527, A142. doi: 10.1051/0004-6361/201016097

González-Martín, O., and Vaughan, S. (2012). X-ray variability of 104 active galactic nuclei. xmm-newton power-spectrum density profiles. *Astron. Astrophys.* 544, A80. doi: 10.1051/0004-6361/201219008

Groves, B., Dopita, M., and Sutherland, R. (2004). Dusty, radiation pressure-dominated photoionization. i. model description, structure, and grids. *Astrophys. J. Suppl. Ser.* 153:9. doi: 10.1086/421113

Halpern, J., and Steiner, J. (1983). Low-ionization active galactic nuclei - x-ray or shock heated? *Astrophys. J.* 269, L37.

Heckman, T. (1980). An optical and radio survey of the nuclei of bright galaxies - stellar populations and normal hii regions. *Astron. Astrophys.* 87:142.

Heckman, T. M., and Best, P. N. (2014). The coevolution of galaxies and supermassive black holes: Insights from surveys of the contemporary universe. *Ann. Rev. Astron. Astrophys.* 52:589. doi: 10.1146/annurev-astro-081913-035722

Hernán-Caballero, A., Alonso-Herrero, A., Hatziminaoglou, E., Spoon, H., Almeida, C. R., Santos, T. D., et al. (2015). Resolving the agn and host emission in the mid-infrared using a model-independent spectral decomposition. *Astrophys. J.* 803:109. doi: 10.1088/0004-637X/803/2/109

Hernández-García, L., González-Martín, O., Márquez, I., and Masegosa, J. (2013). X-ray spectral variability of seven liner nuclei with xmm-newton and chandra data. *Astron. Astrophys.* 556, A47. doi: 10.1051/0004-6361/201321563

Hernández-García, L., González-Martín, O., Masegosa, J., and Márquez, I. (2014). X-ray spectral variability of liners selected from the palomar sample. *Astron. Astrophys.* 569, A26. doi: 10.1051/0004-6361/201424140

Hernández-García, L., Masegosa, J., González-Martín, O., Márquez, I., and Perea, J. (2016). Unveiling the physics of low-luminosity agns through x-ray variability: liner versus seyfert 2. *Astrophys. J.* 824:7. doi: 10.3847/0004-637X/824/1/7

Ho, L. (2002). "Nonstandard Central Engines in Nearby Galaxies," in *Astronomical Society of the Pacific Conference Series* (San Francisco, CA).

Ho, L. (2008). Nuclear activity in nearby galaxies. *Ann. Rev. Astron. Astrophys.* 46:475. doi: 10.1146/annurev.astro.45.051806.110546

Ho, L. (2009). Radiatively inefficient accretion in nearby galaxies. *Astrophys. J.* 699:626. doi: 10.1088/0004-637X/699/1/626

Ho, L., Feigelson, E., Townsley, L., Sambruna, R., Garmire, G., Brandt, W., et al. (2001). Detection of nuclear x-ray sources in nearby galaxies with chandra. *Astrophys. J.* 549, L51. doi: 10.1086/319138

Ho, L., Filippenko, A., and Sargent, W. (1997a). A search for "dwarf" seyfert nuclei. v. demographics of nuclear activity in nearby galaxies. *Astrophys. J.* 487:568.

Ho, L., Filippenko, A., and Sargent, W. (2003). A search for "dwarf" seyfert nuclei. vi. properties of emission-line nuclei in nearby galaxies. *Astrophys. J.* 583:159. doi: 10.1086/345354

Ho, L., Filippenko, A., Sargent, W., and Peng, C. (1997b). A search for "dwarf" seyfert nuclei. iv. nuclei with broad hα emission. *Astrophys. J. Suppl. Ser.* 112:391.

Kauffmann, G., Heckman, T., White, S., Charlot, S., Tremonti, C., Brinchmann, J., et al. (2003). Stellar masses and star formation histories for 10^5 galaxies from the sloan digital sky survey. *Mon. Not. R. Astron. Soc.* 341:33. doi: 10.1046/j.1365-8711.2003.06291.x

Kehrig, C., Monreal-Ibero, A., Papaderos, P., Vílchez, J. M., Gomes, J. M., Masegosa, J., et al. (2012). The ionized gas in the CALIFA early-type galaxies I. Mapping two representative cases: NGC 6762 and NGC 5966. *Astron. Astrophys.* 540:A11. doi: 10.1051/0004-6361/201118357

Kewley, L., Dopita, M., Sutherland, R., Heisler, C., and Trevena, J. (2001). Theoretical modeling of starburst galaxies. *Astrophys. J.* 556:121. doi: 10.1086/321545

Kewley, L., Groves, B., Kauffmann, G., and Heckman, T. (2006). The host galaxies and classification of active galactic nuclei. *Mon. Not. R. Astron. Soc.* 372:961. doi: 10.1111/j.1365-2966.2006.10859.x

Lawrence, A., Elvis, M., Wilkes, B., McHardy, I., and Brandt, N. (1997). X-ray and optical continua of active galactic nuclei with extreme fe ii emission. *Mon. Not. R. Astron. Soc.* 285:879. doi: 10.1093/mnras/285.4.879

Leslie, S., Kewley, L., Sanders, D., and Lee, N. (2016). Quenching star formation: insights from the local main sequence. *Mon. Not. R. Astron. Soc.* 455, L82. doi: 10.1093/mnrasl/slv135

Maiolino, R., Salvati, M., Bassani, L., Dadina, M., della Ceca, R., Matt, G., et al. (1998). Heavy obscuration in x-ray weak agns. *Astron. Astrophys.* 338:781.

Maoz, D., Nagar, N. M., Falcke, H., and Wilson, A. S. (2005). The murmur of the sleeping black hole: Detection of nuclear ultraviolet variability in liner galaxies. *Astrophys. J.* 625:699. doi: 10.1086/429795

Márquez, I., and Masegosa, J. (2010). Galaxies hosting agn activity and their environments. *Astrophys. Space Sci. Proc.* 14:119. doi: 10.1007/978-3-642-11250-8_11

Márquez, I., Masegosa, J., Durret, F., Delgado, R. M. G., Moles, M., Maza, J., et al. (2003). The detection of stellar velocity dispersion drops in the central regions of five isolated seyfert spirals. *Astron. Astrophys.* 409:459. doi: 10.1051/0004-6361:20031059

Márquez, I., Varela, J., Masegosa, J., and del Olmo, A. (2010). "Agn in isolated and interacting galaxies in the palomar spectroscopic survey," in *Galaxies in Isolation: Exploring Nature Versus Nurture* (Granada), Vol. 421:266.

Martínez, M., del Olmo, A., Coziol, R., and Focardi, P. (2008). Deficiency of broad-line agns in compact groups of galaxies. *Astrophys. J.* 678, L9. doi: 10.1086/588498

Masegosa, J., Márquez, I., Ramirez, A., and González-Martín, O. (2011). The nature of nuclear $h_{\alpha;}$ emission in liners. *Astron. Astrophy.* 527, A23. doi: 10.1051/0004-6361/201015047

Matt, G. (1997). The x-ray spectrum of compton-thick seyfert 2 galaxies. *Mem. Della Soc. Astron. Ital.* 68:127.

McKernan, B., Ford, K., and Reynolds, C. (2010). Black hole mass, host galaxy classification and agn activity. *Mon. Not. R. Astron. Soc.* 407:2399. doi: 10.1111/j.1365-2966.2010.17068.x

Netzer, H. (2009). Accretion and star formation rates in low-redshift type ii active galactic nuclei. *Mon. Not. R. Astron. Soc.* 399:1907. doi: 10.1111/j.1365-2966.2009.15434.x

Panessa, F., Bassani, L., Cappi, M., Dadina, M., Barcons, X., Carrera, F. J., et al. (2006). On the x-ray, optical emission line and black hole mass properties of local seyfert galaxies. *Astron. Astrophys.* 455:173. doi: 10.1051/0004-6361:20064894

Pian, E., Romano, P., Maoz, D., Cucchiara, A., Pagani, C., and Parola, V. L. (2010). Variability and spectral energy distributions of low-luminosity active galactic nuclei: a simultaneous x-ray/uv look with swift. *Mon. Not. R. Astron. Soc.* 401:677. doi: 10.1111/j.1365-2966.2009.15689.x

Pogge, R., Maoz, D., Ho, L., and Eracleous, M. (2000). The narrow-line regions of liners as resolved with the hubble space telescope. *Astrophys. J.* 532:323. doi: 10.1086/308567

Pović, M., Márquez, I., Netzer, H., Masegosa, J., Nordon, R., Pérez, E., and Schoenell, W. (2016). Star formation and agn activity in the most luminous liners in the local universe. *Mon. Not. R. Astron. Soc.* 462:2878. doi: 10.1093/mnras/stw1842

Ptak, A., Yaqoob, T., Mushotzky, R., Serlemitsos, P., and Griffiths, R. (1998). X-ray variability as a probe of advection-dominated accretion in low-luminosity active galactic nuclei. *Astrophys. J.* 501, L37. doi: 10.1086/311444

Rupke, D., Veilleux, S., Kim, D.-C., Sturm, E., Contursi, A., Lutz, D., et al. (2007). "Uncovering the active galactic nuclei in low-ionization nuclear emission-line regions with spitzer," in *Central Engine of Active Galactic Nuclei*, Vol. 373:525.

Satyapal, S., Dudik, R., O'Halloran, B., and Gliozzi, M. (2005). The link between star formation and accretion in liners: a comparison with other active galactic nucleus subclasses. *Astrophys. J.* 633:86. doi: 10.1086/449304

Satyapal, S., Sambruna, R., and Dudik, R. (2004). A joint mid-infrared spectroscopic and x-ray imaging investigation of liner galaxies. *Astron. Astrophys.* 414:825. doi: 10.1051/0004-6361:20031609

Schawinski, K., Thomas, D., Sarzi, M., C.Maraston, Kaviraj, S., Joo, S.-J., Yi, S., and Silk, J. (2007). Observational evidence for agn feedback in early-type galaxies. *Mon. Not. R. Astron. Soc.* 382:1415. doi: 10.1111/j.1365-2966.2007.12487.x

Schmitt, H., and Kinney, A. (1996). A comparison between the narrow-line regions of seyfert 1 and seyfert 2 galaxies. *Astrophys. J.* 463:498. doi: 10.1086/177264

Shields, J., Rix, H.-W., Sarzi, M., Barth, A., Filippenko, A., Ho, L., et al. (2007). The survey of nearby nuclei with the space telescope imaging spectrograph: Emission-line nuclei at hubble space telescope resolution. *Astrophys. J.* 654:125. doi: 10.1086/509059

Smith, J., Draine, B., Dale, D., Moustakas, J., Kennicutt, R. C. Jr. Helou, G., et al. (2007). The mid-infrared spectrum of star-forming galaxies: global properties of polycyclic aromatic hydrocarbon emission. *Astrophys. J.* 656:770. doi: 10.1086/510549

Stasińska, G., Asari, N. V., Fernandes, R. C., Gomes, J., Schlickmann, M., Mateus, A., et al. (2008). Can retired galaxies mimic active galaxies? clues from the sloan digital sky survey. *Mon. Not. R. Astron. Soc.* 391, L29. doi: 10.1111/j.1745-3933.2008.00550.x

Storchi-Bergmann, T., Baldwin, J., and Wilson, A. (1993). Double-peaked broad line emission from the liner nucleus of ngc 1097. *Astrophys. J.* 410, L11. doi: 10.1086/186867

Sturm, E., Rupke, D., Contursi, A., Kim, D.-C., Lutz, D., Netzer, H., et al. (2006). Mid-infrared diagnostics of liners. *Astrophys. J.* 653, L13. doi: 10.1086/510381

Sturm, E., Schweitzer, M., Lutz, D., Contursi, A., Genzel, R., Lehnert, M., et al. (2005). Silicate emissions in active galaxies: from liners to qsos. *Astrophys. J.* 629, L21. doi: 10.1086/444359

Tommasin, S., Netzer, H., Sternberg, A., Nordon, R., Lutz, D., ongiorno, A., et al. (2012). Star formation in liner host galaxies at z ˜ 0.3. *Astrophys. J.* 753:155. doi: 10.1088/0004-637X/753/2/155

Veilleux, S., and Osterbrock, D. (1987). Spectral classification of emission-line galaxies. *Astrophys. J. Suppl. Ser.* 63:295. doi: 10.1086/191166

Walsh, J., Barth, A., Ho, L., Filippenko, A., Rix, H.-W., Shields, J., et al. (2008). Hubble space telescope spectroscopic observations of the narrow-line region in nearby low-luminosity active galactic nuclei. *Astron. J.* 136:1677. doi: 10.1088/0004-6256/136/4/1677

Wang, L., Mao, J., Xiang, S., and Yuan, Y. (2008). The effect of agn and sne feedback on star formation, reionization and the near infrared background. *Chin. J. Astron. Astrophys.* 8:631. doi: 10.1088/1009-9271/8/6/02

Whitaker, K. E., van Dokkum, P., Brammer, G., and Franx, M. (2012). The star formation mass sequence out to z = 2.5. *Astrophys. J.* 754, L29. doi: 10.1088/2041-8205/754/2/L29

Younes, G., Porquet, D., Sabra, B., and Reeves, J. N. (2011). Study of LINER sources with broad Hα emission. X-ray properties and comparison to luminous AGN and X-ray binaries. *Astron. Astrophys.* 530, A149. doi: 10.1051/0004-6361/201116806

Younes, G., Porquet, D., Sabra, B., Reeves, J. N., and Grosso, N. (2012). Study of liner sources with broad hα emission. spectral energy distribution and multiwavelength correlations. *Astron. Astrophys.* 539, A104. doi: 10.1051/0004-6361/201118299

Young, M., Brandt, W. N., Xue, Y. Q., Paolillo, M., Alexander, D. M., Bauer, F. E., et al. (2012). Variability-selected low-luminosity active galactic nuclei in the 4 ms chandra deep field-south. *Astrophys. J.* 748:124. doi: 10.1088/0004-637X/748/2/124

Conflict of Interest Statement: The authors declare that the research was conducted in the absence of any commercial or financial relationships that could be construed as a potential conflict of interest.

Copyright © 2017 Márquez, Masegosa, González-Martin, Hernández-Garcia, Pović, Netzer, Cazzoli and del Olmo. This is an open-access article distributed under the terms of the Creative Commons Attribution License (CC BY). The use, distribution or reproduction in other forums is permitted, provided the original author(s) or licensor are credited and that the original publication in this journal is cited, in accordance with accepted academic practice. No use, distribution or reproduction is permitted which does not comply with these terms.

frontiers in Astronomy and Space Sciences

PERSPECTIVE
published: 23 April 2018
doi: 10.3389/fspas.2018.00008

TeV Diffuse Emission From the Inner Galaxy

Amid Nayerhoda[1], Francisco Salesa Greus[2], and Sabrina Casanova[3] for the HAWC collaboration*

[1] Institute of Nuclear Physics PAN, Kraków, Poland, [2] Max Planck Institute for Nuclear Physics, Heidelberg, Germany, [3] Institute of Nuclear Physics PAN, Kraków, Poland

The TeV diffuse emission from the Galactic plane is produced by multi TeV electrons and nuclei interacting with radiation fields and ambient gas, respectively. Measurements of the TeV diffuse emission help constrain CR origin and transport properties. We present a preliminary analysis of HAWC diffuse emission data from the inner Galaxy. The HAWC measurements will be used to constrain particle transport properties close to the Galaxy center correlating the HAWC maps with predictions of the DRAGON code.

Keywords: high energy astrophysics, inner galaxy, gamma rays, diffuse emission, cosmic rays, interstellar medium

OPEN ACCESS

Edited by:
Mauro D'Onofrio, Università degli Studi di Padova, Italy

Reviewed by:
Aldo Morselli, Istituto Nazionale di Fisica Nucleare (INFN), Italy
Milan S. Dimitrijevic, Astronomical Observatory, Serbia

****Correspondence:***
Amid Nayerhoda
amid.nayerhoda@gmail.com

Specialty section:
This article was submitted to Milky Way and Galaxies, a section of the journal Frontiers in Astronomy and Space Sciences

Received: *10 September 2017*
Accepted: *28 February 2018*
Published: *23 April 2018*

Citation:
Nayerhoda A, Salesa Greus F and Casanova S (2018) TeV Diffuse Emission From the Inner Galaxy. Front. Astron. Space Sci. 5:8. doi: 10.3389/fspas.2018.00008

1. INTRODUCTION

Cosmic rays (CRs) are the highly energetic nuclei and protons which carry, at least close to the Solar System, an energy density of about 1 eV/cm^3. This is comparable to the Galactic magnetic fields, energy density of the radiation fields, and turbulent motions of the interstellar gas. Thus CRs are an energetically important component of the interstellar medium (ISM). They play an important role in the dynamical balance of our Galaxy, and have an important effect on interstellar chemistry through the heating and ionization of the ISM, particularly in its denser regions. Being charged particles, CRs are also strongly coupled to the magnetic fields by Lorentz forces and by strong scattering off field irregularities (MHD waves).

CRs up to at least 10^{15} eV are believed to be accelerated through diffusive shock acceleration (DSA) in young supernova remnants (SNRs). In the shells of SNRs suprathermal particles would be injected into the acceleration process at the shock propagating into the ISM where collisionless processes transfer to them the kinetic energy of the magnetohydrodynamic shocks Krymskii (1977); Axford (1981); Blandford and Eichler (1987); Bell and Lucek (2001); Malkov (2001). The SNR paradigm for the CR origin is based upon energetic considerations. At least one supernovae explosion event is expected in every 30 years, and considering that, the non thermal energy release at each supernovae event should be 10^{50} ergs, (which is almost ten percent of total energy release at each SN explosion event), in order to explain the energy density of cosmic ray (which is about 1 ev/cm^3) Ginzburg and Syrovatskii (1964) in the Galaxy. This is in good agreement with the typical amount of energy predicted to be created during the acceleration of relativistic particles in supernovae remnant shocks within a DSA scenario Voelk and Biermann (1988); Drury et al. (1989).

Cosmic rays runaway the acceleration sites and finally propagate into the galactic magnetic field, so it is impossible to observe cosmic rays from the candidate injection sites directly.

The information on the cosmic ray spectra at the acceleration sites cannot be traced back, because of the unknown propagation mechanisms of cosmic ray spectra. Secondary CR data suggest that cosmic ray protons and nuclei diffuse in the magnetic fields for times of the order of $\tau_{escape} = 1.4 \times 10^7 (E/10GeV)^{-0.65}$ years, E being the particle energy, before escaping the Galaxy. During this time the particles accelerated by individual

sources diffuse into the Galaxy, mix together, get isotropized by the galactic magnetic fields and contribute to the bulk of Galactic cosmic rays known as *cosmic ray background* or cosmic ray *sea*, the information on the CR source and CR energy distribution at the source is lost.

However, while cosmic rays scape injection sources and diffuse in the Galaxy, they interact inelastically with ambient molecules and atoms of the interstellar gas and create gamma rays by decay of neutral pions. Electrons produce gamma-rays through inverse Compton scattering and also by bremsstrahlung processes. In contrast to CRs, the gamma rays produced by these accelerated particles, are neutral and travel in straight lines from the site where they were produced to the detector. The gamma ray energy flux from the different directions on the sky provides thus direct information about the parental cosmic ray flux in different locations in the Galaxy. This emission, extending from GeV to hundreds of TeV, is thus the most powerful tool to probe the origin and propagation mechanisms of CRs in the Galaxy and to investigate the extreme astrophysical environments in which these particles are accelerated.

Observational evidences show that the cosmic ray energy density varies strongly in different locations of the Galaxy, in particularly in leactive regions of the Galaxy, such as the MCs (Molecular clouds) close to young and middle aged SNRs and in active star forming regions. These regions, where the CR spectrum is also expected to be harder than the background CR spectrum, are the candidate sites for CR acceleration, which we will investigate deeply in our analysis.

2. HAWC

HAWC (High Altitude Water-Cherenkov) Telescope is well-designed to study cosmic rays and TeV gamma rays between 100 GeV and 100 TeV by observing the air-shower particles created by the primary particles in the high atmosphere which get in the detector. HAWC is placed on the side of the Sierra Negra volcano near Puebla, Mexico at an altitude of 4,100 meters.

Thanks to its wide field-of-view, with an instantaneous field of view which covers fifteen percent of the sky, within each 24 h period, HAWC observes two-third of the sky. Applying the HAWC observatory, we are performing a high-sensitivity synoptic survey of the gamma rays from the Northern Hemisphere. The detector contains 300 similar water Cherenkov detectors (WCDs) with 7.32 m diameter, 5 m high. Each tank comprises 190,000 L of purified water. Four skyward facing photomultiplier tubes (PMTs) are mounted at the base of each tank, a 10" Hamamatsu PMT located at the center and three 8" Hamamatsu PMTs which are located halfway between the tank center and rim. A trigger is produced when a big enough number of PMTs record a hit in a 150 Nanosecond time interval (see **Figure 1**).

Parameters of the air shower, such as, the direction, the size, and some gamma/hadron separation variables (for each triggered event), are calculated from the recorded hit times and amplitudes, using a shower model developed through the study of Monte Carlo simulations and calibrated using observations of the Crab Nebula.

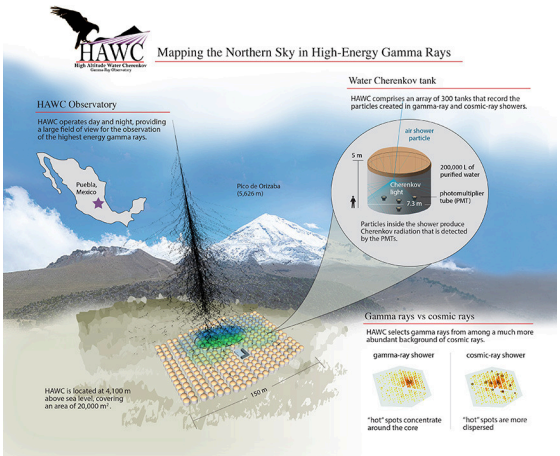

FIGURE 1 | The HAWC Observatory is a next-generation gamma-ray detector placed at an altitude of 4,100 m on the slope of the dormant volcano Pico de Orizaba in Mexico[1].

HAWC is an ideal tool to study Galactic gamma-ray sources. In the following we will review the HAWC map of the sky at 10s TeV after collecting one year of data.

3. DATA AND ANALYSIS

The analysis presented here is based on a dataset which contains 275 ± 1 source transits of the inner Galaxy taken between August 2, 2013, and July 9, 2014, While the HAWC array was partially constructed. Since the sensitivity of HAWC is related to the source declination, for the sources which transit via the detector vertex, the best sensitivity is gained. For the analysis presented here a zenith angle cut of 45° and declination between −26° and +64° is applied. The background rejection, energy and angular resolution of the detected gamma rays are associated with the shower size detected in the array, So the data are categorized into 10 bins corresponding to the ratio h of PMTs triggered out of the sum of the active PMTs.

In order to detach the cosmic-ray background from the gamma-ray signal, we apply cuts to three parameters (the fraction of the chi-square and reduced chi-square of the fit and a topological cut according to the compactness of the charge distribution) in each h bin Abeysekara et al. (2015a):

4. SKY MAPS AND MAXIMUM LIKELIHOOD METHOD

The air shower simulation program *CORSIKA* Heck (1998) and the detector simulation package *GEANT*4 Agostinelli et al. (2003) generate the detector response file which describes the PSF (Point Source Function) and energy distribution as a function of source declination and fraction of hit h bins. In order to simulate

[1]The High-Altitude Water Cherenkov Observatory (HAWC). HAWC Collaboration. Available online at: http://www.hawc-observatory.org/

flux from the gamma ray, we use a simulation model which turns the detector response to source of gamma rays.

Constructing a source model determined by spectrum and position of the source is the preliminary step of the maximum likelihood fit. The source spectrum in the following analysis is assumed to obey a power law:

$$\frac{dN}{dE} = I_0\left(\frac{E}{E_0}\right)^{-\Gamma} \tag{1}$$

where Γ is the spectral index. It has been assumed here a fixed index of 2.3 because of the limited sensitivity in this data set. The index of 2.3 is indicative of observed values for known Galactic objects, and I_0 is the differential flux normalization, E_0 is the pivot energy which is picked where the differential flux normalization is least dependent on the spectral index. Right ascension (R.A.) α and Declination (Dec.) δ are used to describe the source position.

The region of interest (ROI) which is applied for a likelihood fit should contain most photons from a given source so it must be wider than the angular resolution of the detector, and because of the high possibility of source confusion in the Galactic plane data, it is not usually easy to find an ROI which contains only photons from one single source.

Thus, the source model likely should contain more than one source, and in this case, the expected count is:

$$\lambda_{ij} = \beta_{ij} + \sum_k \gamma_{ijk}, \tag{2}$$

where γ_{ijk} and β_{ij} are the expected number of gamma rays and the background events respectively, in the jth pixel of ith h bin, correlated to the kth source. The event entwine with detector response.

since the detected event counts distribution obeys Poisson distribution in each pixel, one can assumes the probability of measuring N number of events given an expected count λ of the source model be:

$$\mathbf{P}(N;\lambda) = \frac{\lambda^N e^{-\lambda}}{N!}, \tag{3}$$

The product the likelihood in each h bin and of each pixel (in an ROI) is the likelihood in the source model (given parameter set $\boldsymbol{\theta} = (\alpha, \delta, I_0)$)

$$\mathcal{L}(\overrightarrow{\theta}, \overrightarrow{N}) = \prod_i^{fbins} \prod_j^{ROI} \mathbf{P}(N_{ij};\lambda_{ij}), \tag{4}$$

Where N_{ij} is detected and λ_{ij} is expected event counts in the jth pixel of the ith h bin. The logarithm of the likelihood is applied for ease of calculation:

$$\mathcal{L}(\overrightarrow{\theta}, \overrightarrow{N}) = \sum_i^{fbins} \sum_j^{ROI} (N_{ij}\lambda_{ij} - \lambda_{ij}). \tag{5}$$

Using the MINUIT package Brun and Rademakers (1997), The log likelihood became maximized with respect to the parameter set $\boldsymbol{\theta}$ in the source model. Since N_{ij} is not dependent of the parameters in the source model, it is discarded from Equation (5).

In order to determine how many sources are required to properly model an ROI a likelihood ratio test is performed.

In choose the preferred model over the background-only model first we calculate the log likelihood of the background-only model ln $\mathcal{L}_0$. Afterward we compute the log likelihood ln $\mathcal{L}_1$ of the one-source model. The test statistic (TS) defined by:

$$TS = -2(ln\mathcal{L}_{\prime} - ln\mathcal{L}_{\infty}) \tag{6}$$

the test statistics is applied to compare the advantage of the fit between the two models. In order to to compare between two models with N and N+1 sources, similar method of likelihood ratio test is used, in an iterative process; one source with three free parameters (α, δ, I_0) is added to the model step by step with the amplitude and position of the current sources free to change in respect to the new source. Finally the TS and differential flux of each source are calculated by fitting one source and considering other sources as a part of the background while parameters are fixed(differential fluxes and positions).

Figures 2–4 present the significance map of the inner Galaxy region investigated here. The map is made by moving a supposed point like source through each pixel, presenting a maximum likelihood fit of differential flux normalization with the fixed spectral index at 2.3. As it is shown in **Figure 2**.

There are multiple $> \sigma$ hot spots in the studied region. The area is divided into five region of interests. The method explained above is used to simultaneously account for the flux contributions of neighboring sources in each of divided region.

5. DRAGON

DRAGON is a code to solve the equation of CR transport in the Galaxy, it is implemented to simulate all the related processes relevant to Galactic CR propagation, in particular: diffusion, re-acceleration,cooling convection, (due to bremsstrahlung, synchrotron, Coulomb, inverse-Compton, and ionization), catastrophic losses (annihilation), and spallation). The code numerically solves the interstellar CR transport equation, including inhomogeneous and anisotropic diffusion emission. Evoli et al. (2008).

After solving the equation, the code provides the cosmic ray spectra in all regions of the Galaxy. With such information the code derives the gamma ray spectra. The DRAGON predicted gamma ray spectra from the Galactic plane will be compared to the observed spectra, measured by HAWC. In this way the CR transport propagation will be fine-tuned.

6. FORTHCOMING RESEARCH AND CONCLUSIONS

We showed a preliminary analysis of gamma-ray diffuse emission from the inner galaxy using data from HAWC detector. This analysis will serve to calibrate the dragon

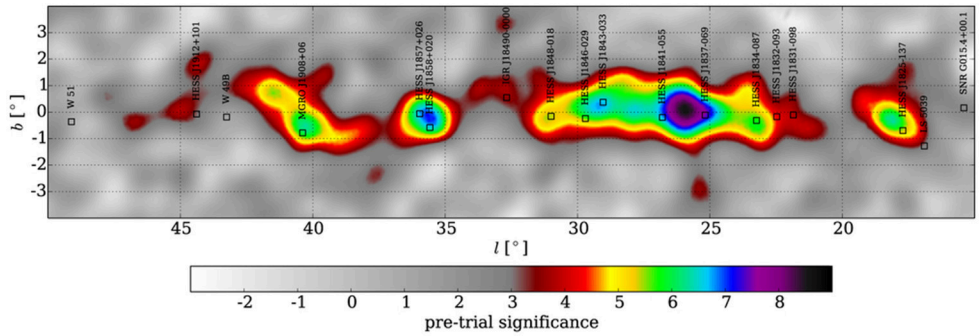

FIGURE 2 | Significance map.

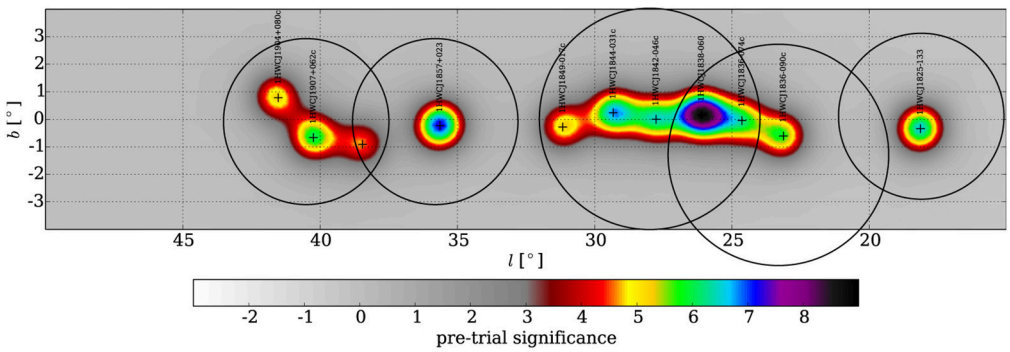

FIGURE 3 | A model with eleven sources Black circles demonstrate the five regions of interest (ROI).

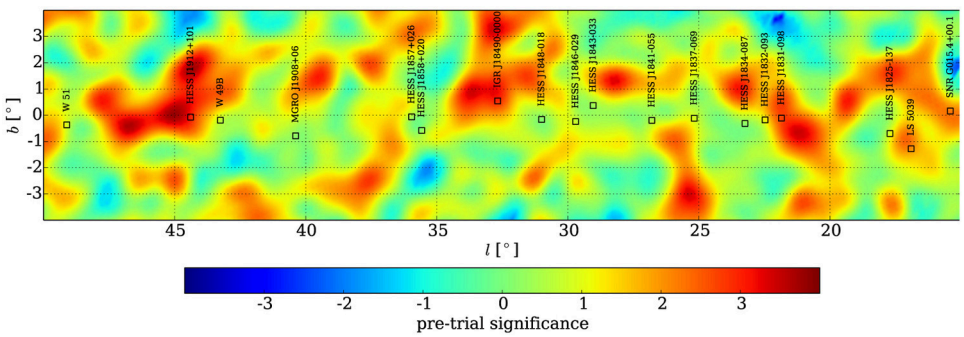

FIGURE 4 | Residual significance map.

code. We will use the results to constrain particle transport properties in that region using the Dragon code in order to understand whether particle transport there proceeds through isotropic diffusion, anisotropic diffusion or maybe through advection.

AUTHOR CONTRIBUTIONS

AN student, Has written this manuscript and also has presented it in Quasars at all cosmic epochs 2017, all the results have been gotten under supervision FS as a member of the group and also under the supervision of SC as a supervisor and head of the group.

ACKNOWLEDGMENTS

We acknowledge the support from: the US Department of Energy Office of High-Energy Physics; the US National Science Foundation (NSF); the Laboratory Directed Research and Development (LDRD) program of Los Alamos National

Laboratory; L'OREAL Fellowship for Women in Science 2014; the University of Wisconsin Alumni Research Foundation; Red HAWC, México; DGAPA-UNAM (grants IG100317, IN111315, IN111716-3, IA102715, 109916, IA102917); VIEP-BUAP; PIFI 2012, 2013, PROFOCIE 2014, 2015; the Institute of Geophysics, Planetary Physics, and Signatures at Los Alamos National Laboratory; AN, SC, and FS acknowledge the Polish Science Centre under grant DEC-2014/13/B/ST9/945; Coordinación de la Investigación Científica de la Universidad Michoacana. Consejo Nacional de Ciencia y Tecnología (CONACyT), México (grants 271051, 232656, 260378, 179588, 239762, 254964, 271737, 258865, 243290, 132197), Laboratorio Nacional HAWC de rayos gamma; Thanks to Luciano Díaz and Eduardo Murrieta for technical support.

REFERENCES

Abeysekara, A. U., Alfaro, R., Alvarez, C., Álvarez, J. D., Arceo, R., Arteaga-Velázquez, J. C., et al. (2015a). *HAWC Contributions to the 34th International Cosmic Ray Conference (ICRC2015)*. (The Hague).

Agostinelli, S., Allison, J., Amako, K., Apostolakis, J., Araujo, H., Arce, P., et al. (2003). GEANT4—a simulation tool kit. *Nucl. Instrum. Methods* A506, 250–303. doi: 10.1016/S0168-9002(03)01368-8

Axford, W. I. (1981). The acceleration of cosmic rays by shock waves. *NYASA*. 375, 297A

Bell, A. R., and Lucek, S. G. (2001). Cosmic ray acceleration to very high energy through the non-linear amplification by cosmic rays of the seed magnetic field. *MNRAS* 321, 433B.

Brun, R., and Rademakers, F. (1997). ROOT—an object oriented data analysis framework, in proceedings AIHENP'96 workshop. *Nucl. Inst. & Meth. Phys. Res.* A389, 81–86. Available online at: http://root.cern.ch

Blandford, R., and Eichler, D. (1987). Particle acceleration at astrophysical shocks: a theory of cosmic ray origin. *Phys. Rep.* 154:1.

Drury, L. O'. C., Markiewicz, W. J. and Voelk, H. J. (1989). Simplified models for the evolution of supernova remnants including particle acceleration. *Astron. Astrophys.* 225:179D

Evoli, C., Gaggero, D., Grasso, D., and Maccione, L. (2008). Cosmic-ray nuclei, antiprotons and gamma-rays in the galaxy: a new diffusion model. *JCAP arXiv:0807.4730 [astro-ph]*. doi: 10.1088/1475-7516/2008/10/018

Ginzburg, L. V., and Syrovatskii, S. I. (1964). *Origin of Cosmic Rays*. London: Pergamon Press.

Heck, D., Schatz, G., Thouw, T., Knap, J., and Capdevielle, J. N. (1998). CORSIKA: a monte carlo code to simulate extensive air showers. *Tech. Rep.* FZKA-6019:95.

Krymskii, G. F. (1977). A regular mechanism for the acceleration of charged particles on the front of a shock wave. *Akademiia Nauk SSSR*. 234, 1306–1308.

Malkov, M. A., and Drury, L. O'. C. (2001). Nonlinear theory of diffusive acceleration of particles by shock waves. *Rept. Prog. Phys.* 64, 429–481.

Voelk, H. J., and Biermann, P. L. (1988). Maximum energy of cosmic-ray particles accelerated by supernova remnant shocks in stellar wind cavities. *ApJ*. 333, L65–L68.

Conflict of Interest Statement: The authors declare that the research was conducted in the absence of any commercial or financial relationships that could be construed as a potential conflict of interest.

Copyright © 2018 Nayerhoda, Salesa Greus and Casanova. This is an open-access article distributed under the terms of the Creative Commons Attribution License (CC BY). The use, distribution or reproduction in other forums is permitted, provided the original author(s) and the copyright owner are credited and that the original publication in this journal is cited, in accordance with accepted academic practice. No use, distribution or reproduction is permitted which does not comply with these terms.

frontiers in Astronomy and Space Sciences

OPINION
published: 21 September 2017
doi: 10.3389/fspas.2017.00014

Optical Variability of Active Galactic Nuclei

*Szymon Kozłowski**

Astronomical Observatory, University of Warsaw, Warsaw, Poland

Keywords: accretion, accretion disks, galaxies: active, methods: data analysis, quasars: general

OPEN ACCESS

Edited by:
Mauro D'Onofrio,
University of Padua, Italy

Reviewed by:
Maurizio Paolillo,
Dipartimento di Fisica Ettore Pancini,
Università degli Studi di Napoli
Federico II, Italy

***Correspondence:**
Szymon Kozłowski
simkoz@astrouw.edu.pl

Specialty section:
This article was submitted to
Milky Way and Galaxies,
a section of the journal
Frontiers in Astronomy and Space
Sciences

Received: *04 August 2017*
Accepted: *31 August 2017*
Published: *21 September 2017*

Citation:
Kozłowski S (2017) Optical Variability
of Active Galactic Nuclei.
Front. Astron. Space Sci. 4:14.
doi: 10.3389/fspas.2017.00014

1. INTRODUCTION

Variability studies of active galactic nuclei (AGNs) typically use either power spectral density (PSD) and structure function (SF) analyses or direct modeling of light curves with the damped random walk (DRW) and the continuous autoregressive moving average (CARMA) models. A fair fraction of research publications on the subject are flawed, and simply report incorrect results, because they lack a deep understanding of where these methods originate from and what their limitations are. For example, SF analyses typically lack or use a wrong noise subtraction procedure, leading to flat SFs. DRW, on the other hand, can only be used if the experiment length is sufficient, at least ten times the signal decorrelation time scale τ, and if the data show the power-law SF slope of $\gamma \equiv 0.5$.

2. STRUCTURE FUNCTIONS

The structure function (SF) analysis is a model-independent technique of converting an active galactic nucleus (AGN) light curve into a different space, the variability amplitude–timescale space. The basic approach behind the SF analysis is as follows. Data points y_i in an AGN light curve are, in the simplest case, a sum of the variable signal s_i (with the variance σ_s^2) and the observational noise n_i (with the variance σ_n^2), so $y_i = s_i + n_i$. SF originates from simple mathematical properties of the covariance of the light curve (index i) with a shifted copy of itself (index j) by the timelag $\Delta t = t_i - t_j$, via (MacLeod et al., 2010; Kozłowski, 2016b)

$$\mathrm{SF}(\Delta t)^2 = 2\left(\sigma_s^2 - \mathrm{cov}(s_i, s_j)\right) + 2\sigma_n^2, \tag{1}$$

where $\mathrm{SF}(\Delta t)$ is typically measured from data as

$$\mathrm{SF}(\Delta t)^2 = \frac{1}{N_{\Delta \mathrm{t\ pairs}}} \sum_{i=1}^{N_{\Delta \mathrm{t\ pairs}}} (y_i - y_j)^2. \tag{2}$$

In order to measure the true AGN variability, so in fact $\mathrm{cov}(s_i, s_j)$ in Equation (1), one needs to subtract the full noise term ($2\sigma_n^2$) from the SF in Equation (2). This is either rarely done in recent works or done incorrectly, as commonly only a fraction of the noise term (σ_n^2) is subtracted. This leads to flat power-law SF slopes of $\gamma = 0.1$–0.4 at short timescales Δt ($\mathrm{SF}(\Delta t) \propto \Delta t^{\gamma}$) (e.g., Vanden Berk et al., 2004; de Vries et al., 2005), but when correctly measured, the SF slope in optical is significantly steeper $\gamma = 0.55 \pm 0.08$, based on ~9,200 SDSS AGN from Stripe 82 (Kozłowski, 2016b) and $\gamma \approx 0.45$ in mid-IR (Kozłowski et al., 2010a, 2016). An equally important variability

observable to the SF slope is the decorrelation timescale τ, a timescale at which the SF changes slope from the red noise ($\gamma = 0.5$) to the white noise ($\gamma = 0.0$). It seems to be about one year rest-frame, again based on ∼9,200 SDSS AGN from Stripe 82 (Kozłowski, 2016b). I recently proposed a new method of the measurement of the unbiased decorrelation timescale τ from SFs (Kozłowski, 2017a). Another SF observable is the AGN variability amplitude measured at 1 year (rest-frame) with the value of 0.20 ± 0.06 mag in optical bands, while the asymptotic variability amplitude at long timescales ($\Delta t \gg \tau$, so $\Delta t \gg 1$ year rest-frame) is 0.25 ± 0.06 mag (Kozłowski, 2016b). The SF amplitude at 1 year may be affected, while the asymptotic variability amplitude is not, by the bias due to the unknown underlying stochastic process for short datasets (Kozłowski, 2017a).

3. THE DAMPED RANDOM WALK

AGN light curves can be modeled and interpolated using the damped random walk (DRW) stochastic process. DRW modeling (Kelly et al., 2009; Kozłowski et al., 2010b; MacLeod et al., 2010) by definition assumes an exponential covariance matrix of the signal of the form

$$\mathrm{cov}(s_i, s_j) = \sigma_s^2 e^{-\frac{|t_i - t_j|}{\tau}}, \tag{3}$$

that again by definition produces a fixed SF power-law slope of $\gamma \equiv 0.5$ at timelags $\Delta t = t_i - t_j$ shorter than the signal decorrelation timescale τ (Kozłowski, 2016b). If the variability signal is due to a different stochastic process, where the SF slope is shallower/steeper than $\gamma = 0.5$, DRW will obtain a reasonable fit, however, it will report biased measurements (Kozłowski, 2016a). As of now, there is no statistical correction available to this problem, however, using the information on the SF/PSD slope one can modify the DRW model covariance matrix (Equation 3) and model the light curves with the modified DRW model to obtain correct parameters. DRW should be used to model an AGN light curve if one is convinced that the SF slope for a light curve is $\gamma = 0.5$ (or equivalently the PSD slope is -2). There is another issue with DRW: if the light curve is shorter than 10τ (∼10 years rest-frame), it will simply report meaningless variability parameters (Kozłowski, 2017b). DRW is the simplest of the CARMA models [i.e., DRW $\equiv$ CARMA$(1, 0)$], therefore the whole CARMA model family is plausibly affected by biases or problems reported above.

4. CONCLUSIONS

Constraining the SF, PSD, and DRW (or more generally the Gaussian processes) parameters typically require long and well-sampled AGN light curves. Such tight constraints may soon be available from the OGLE Sky Survey (Udalski et al., 2015), that has been monitoring the sky for 25 years, and in particular from its 20-year-long monitoring of nearly 1,000 AGNs (each with ∼1,000 epochs), discovered mostly by the Magellanic Quasars Survey (Kozłowski et al., 2013). Similarly to the results from the SDSS Stripe 82, preliminary results from OGLE point to the mean SF slope $\gamma \gtrsim 0.5$. For sparsely sampled or short light curves some corrections to improve biases in PSD/SF/excess variance measurements are available (Vaughan et al., 2003; Allevato et al., 2013), although in a statistical (ensemble) sense, rather than for individual objects.

AUTHOR CONTRIBUTIONS

The author confirms being the sole contributor of this work and approved it for publication.

FUNDING

SK acknowledges the financial support of the Polish National Science Center through the OPUS grant 2014/15/B/ST9/00093 and MAESTRO grant 2014/14/A/ST9/00121.

REFERENCES

Allevato, V., Paolillo, M., Papadakis, I., and Pinto, C. (2013). Measuring X-ray variability in faint/sparsely sampled active galactic nuclei. *Astrophys. J.* 771:9. doi: 10.1088/0004-637X/771/1/9

de Vries, W. H., Becker, R. H., White, R. L., and Loomis, C. (2005). Structure function analysis of long-term quasar variability. *Astron. J.* 129, 615–629. doi: 10.1086/427393

Kelly, B. C., Bechtold, J., and Siemiginowska, A. (2009). Are the variations in quasar optical flux driven by thermal fluctuations? *Astrophys. J.* 698, 895–910. doi: 10.1088/0004-637X/698/1/895

Kozłowski, S. (2016a). A degeneracy in DRW modelling of AGN light curves. *Mon. Not. R. Astron. Soc.* 459, 2787–2789. doi: 10.1093/mnras/stw819

Kozłowski, S. (2016b). Revisiting stochastic variability of AGNs with structure functions. *Astrophys. J.* 826:118. doi: 10.3847/0004-637X/826/2/118

Kozłowski, S. (2017a). A method to measure the unbiased decorrelation timescale of the AGN variable signal from structure functions. *Astrophys. J.* 835:250. doi: 10.3847/1538-4357/aa56c0

Kozłowski, S. (2017b). Limitations on the recovery of the true AGN variability parameters using damped random walk modeling. *Astron. Astrophys.* 597:A128. doi: 10.1051/0004-6361/201629890

Kozłowski, S., Kochanek, C. S., Ashby, M. L. N., Assef, R. J., Brodwin, M., Eisenhardt, P. R., et al. (2016). Quasar variability in the mid-infrared. *Astrophys. J.* 817:119. doi: 10.3847/0004-637X/817/2/119

Kozłowski, S., Kochanek, C. S., Stern, D., Ashby, M. L. N., Assef, R. J., Bock, J. J., et al. (2010a). Mid-infrared variability from the spitzer deep wide-field survey. *Astrophys. J.* 716, 530–543. doi: 10.1088/0004-637X/716/1/530

Kozłowski, S., Kochanek, C. S., Udalski, A., Wyrzykowski, Ł., Soszyński, I., Szymański, M. K., et al. (2010b). Quantifying quasar variability as part of a general approach to classifying continuously varying sources. *Astrophys. J.* 708, 927–945. doi: 10.1088/0004-637X/708/2/927

Kozłowski, S., Onken, C. A., Kochanek, C. S., Udalski, A., Szymański, M. K., Kubiak, M., et al. (2013). The magellanic quasars survey. III. Spectroscopic confirmation of 758 active galactic nuclei behind the magellanic clouds. *Astrophys. J.* 775:92. doi: 10.1088/0004-637X/775/2/92

MacLeod, C. L., Ivezić, Ž., Kochanek, C. S., Kozłowski, S., Kelly, B., Bullock, E., et al. (2010). Modeling the time variability of SDSS stripe

82 quasars as a damped random walk. *Astrophys. J.* 721, 1014–1033. doi: 10.1088/0004-637X/721/2/1014

Udalski, A., Szymański, M. K., and Szymański, G. (2015). OGLE-IV: fourth phase of the optical gravitational lensing experiment. *Acta Astron.* 65, 1–38.

Vanden Berk, D. E., Wilhite, B. C., Kron, R. G., Anderson, S. F., Brunner, R. J., Hall, P. B., et al. (2004). The ensemble photometric variability of ∼25,000 quasars in the sloan digital sky survey. *Astrophys. J.* 601, 692–714. doi: 10.1086/380563

Vaughan, S., Edelson, R., Warwick, R. S., and Uttley, P. (2003). On characterizing the variability properties of X-ray light curves from active galaxies. *Mon. Not. R. Astron. Soc.* 345, 1271–1284. doi: 10.1046/j.1365-2966.2003.07042.x

Conflict of Interest Statement: The author declares that the research was conducted in the absence of any commercial or financial relationships that could be construed as a potential conflict of interest.

Copyright © 2017 Kozłowski. This is an open-access article distributed under the terms of the Creative Commons Attribution License (CC BY). The use, distribution or reproduction in other forums is permitted, provided the original author(s) or licensor are credited and that the original publication in this journal is cited, in accordance with accepted academic practice. No use, distribution or reproduction is permitted which does not comply with these terms.

frontiers in Astronomy and Space Sciences

MINI REVIEW
published: 17 November 2017
doi: 10.3389/fspas.2017.00038

Changing-Look AGNs or Short-Lived Radio Sources?

Aleksandra Wołowska[1], Magdalena Kunert-Bajraszewska[1], Kunal Mooley[2] and Gregg Hallinan[3]*

[1] Toruń Centre for Astronomy, Faculty of Physics, Astronomy and Informatics, Nicolaus Copernicus University, Toruń, Poland, [2] Centre for Astrophysical Surveys, University of Oxford, Oxford, United Kingdom, [3] Cahill Center for Astronomy, California Institute of Technology, Pasadena, CA, United States

The evolution of extragalactic radio sources has been a fundamental problem in the study of active galactic nuclei for many years. A standard evolutionary model has been created based on observations of a wide range of radio sources. In the general scenario of the evolution, the younger and smaller Gigahertz-Peaked Spectrum (GPS) and Compact Steep Spectrum (CSS) sources become large-scale FRI and FRII objects. However, a growing number of observations of low power radio sources suggests that the model cannot explain all their properties and there are still some aspects of the evolutionary path that remain unclear. There are indications, that some sources may be short-lived objects on timescales of 10^4–10^5 years. Those objects represent a new population of active galaxies. Here, we present the discovery of several radio transient sources on timescales of 5–20 yrs, largely associated with renewed AGN (Active Galactic Nucleus) activity. These changing-look AGNs possibly represent behavior typical for many active galaxies.

Keywords: galaxies, active-galaxies, evolution, quasars, recurrent-activity

OPEN ACCESS

Edited by:
Paola Marziani, Osservatorio Astronomico di Padova (INAF), Italy

Reviewed by:
Brian Punsly, International Center for Relativistic Astrophysics, Italy
Nicolae Sebastian Zamfir, University of Wisconsin-Stevens Point, United States

****Correspondence:***
Aleksandra Wołowska
ola@astro.umk.pl

Specialty section:
This article was submitted to Milky Way and Galaxies, a section of the journal Frontiers in Astronomy and Space Sciences

Received: *31 August 2017*
Accepted: *25 October 2017*
Published: *17 November 2017*

Citation:
Wołowska A, Kunert-Bajraszewska M, Mooley K and Hallinan G (2017) Changing-Look AGNs or Short-Lived Radio Sources? Front. Astron. Space Sci. 4:38. doi: 10.3389/fspas.2017.00038

1. INTRODUCTION

The radio emission of extragalactic sources is usually explained by the existence of strong jets emitting non-thermal synchrotron radiation. However, AGNs with powerful jets represent only a small fraction of the entire population (Kellerman et al., 1989). The vast majority of sources are much less powerful in radio domain or even defined as radio-quiet. But even then they still emit radio waves at very small fluxes, compared to radio-loud AGNs. The relatively small amount of radio emission in some AGNs may be due the presence of less powerful jets (Ulvestad et al., 2005). This in turn connects the phenomena with the accretion process which can be radiatively inefficient in low radio luminosity AGNs (Merloni et al., 2003; Best and Heckman, 2012).

In the general scenario of the evolution of powerful radio-loud AGNs (Fanti et al., 1995), the younger and smaller Gigahertz-Peaked Spectrum (GPS) and Compact Steep Spectrum (CSS) sources become high luminosity large-scale FR II objects (Fanaroff and Riley, 1974; **Figure 1**). It seems reasonable to suspect that the compact AGNs with lower radio luminosity could be the progenitors of less luminous FR IIs and FR Is. However, the growing number of observations of low power radio sources and results of their analysis indicates that in their case the evolution can be more complicated or even halted at parsec scale. In order for the radio source to become a large-scale FR II or FR I object, the active phase needs to last longer than 10^4–10^5 years. The shorter active phase, which is probably caused by the low accretion rate, will result in poorly developed, sometimes disrupted, compact radio morphology. Some AGNs may undergo numerous short phases during their lifetime (Reynolds and Begelman, 1997; Czerny et al., 2009; Kunert-Bajraszewska et al., 2010). In this sense a "young" GPS or CSS source means ongoing episode of the

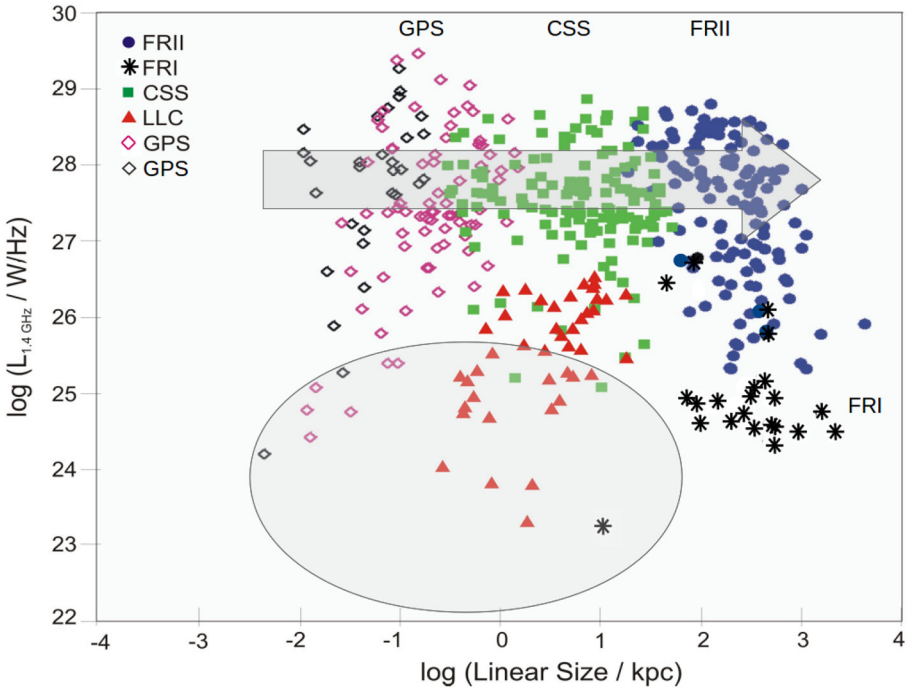

FIGURE 1 | Radio power vs. linear size evolutionary scheme for radio-loud AGN (Kunert-Bajraszewska, 2016, Copyright Wiley-VCH Verlag GmbH & Co. KGaA. Reproduced with permission). Squares represent CSS sources (Laing et al., 1983; Fanti et al., 2001; Marecki et al., 2003). Diamonds indicate GPS objects (Labiano et al., 2007). Stars indicate FRI and FRII objects (Laing et al., 1983). Red triangles represent low luminosity compact (LLC) sources previously studied by (Kunert-Bajraszewska et al., 2010, 2014; Kunert-Bajraszewska and Labiano, 2014). The gray arrow indicates the main evolutionary trend of radio-loud AGNs. The oval indicates the boundaries of the area in which the new radio transient sources are located and where, as we expect, the whole population of short-lived objects can be found.

accretion disk outburst. This indicates the temporary existence of many weak CSS and GPS sources with compact or slightly resolved radio morphologies (core-jet) similar to that observed in radio-quiet objects (Giroletti and Panessa, 2009; Sadler et al., 2014). They are called short-lived radio objects on timescales 10^4–10^5 years. Interestingly, the enhancement and cessation of the accretion process is one of the postulated explanation for the origin of changing-look behavior in the so-called "changing look AGNs" (Elitzur et al., 2014; Schawinski et al., 2015). Such objects are rare and their first discoveries were made based on the X-ray variability. However, Koay et al. (2016) recently reported the changing-look behavior in radio domain in one of such sources. This, in our opinion, links the discussion about the changing-look AGNs with the subject of short term radio activity.

To this day, only a handful of radio-loud short-lived AGN candidates have been found and studied (Kunert-Bajraszewska et al., 2010, 2014). However, the analysis of the radio, optical and X-ray proper- ties of a sample of low-luminosity compact (LLC) radio sources carried out by our group over the last few years (**Figure 1**) suggests that a much larger population of such radio sources exist, and need to be explored. The first unbiased study of these sources has been recently carried out with the Jansky VLA. The multi-year Caltech-NRAO Stripe 82 Survey (CNSS), revealed twelve transient sources on timescales of 5–20 yrs, largely associated with renewed AGN activity. The rates of such AGN possibly imply episodes of enhanced accretion and jet activity occurring once every 40,000 years in these galaxies. The whole CNSS consist of five epochs of observations over the entire ∼270 deg^2 of Stripe 82 and they will be published soon. The results from an initial pilot survey of a ∼50 deg^2 of Stripe 82 has been already published by Mooley et al. (2016).

2. NEW RADIO TRANSIENTS

The CNSS is a dedicated radio transient survey carried out with the Jansky VLA between December 2012 and May 2015. It was designed for systematically exploring the radio sky for slow transient phenomena on timescales between one day and several years. Observations of the 270 deg^2 of the SDSS Stripe 82 region were carried out over 5 epochs at 3 GHz and with a uniform rms noise of 80 μJy per epoch. The CNSS survey has facilitated an unbiased study of short-lived sources for the first time.

In this survey, 50 radio transients were discovered, among which are AGN, candidates of tidal disruption events and stellar explosions, flare stars, and active binary star systems (Mooley et al., 2016). Although the majority of radio flaring phenomena in AGN are due to shocks propagating down the jets (e.g., Marscher and Gear, 1985), properties of some AGNs discovered as radio transients are distinct from this flaring population.

This distinct population comprises AGNs that were not detected in radio in any previous survey of Stripe 82. They

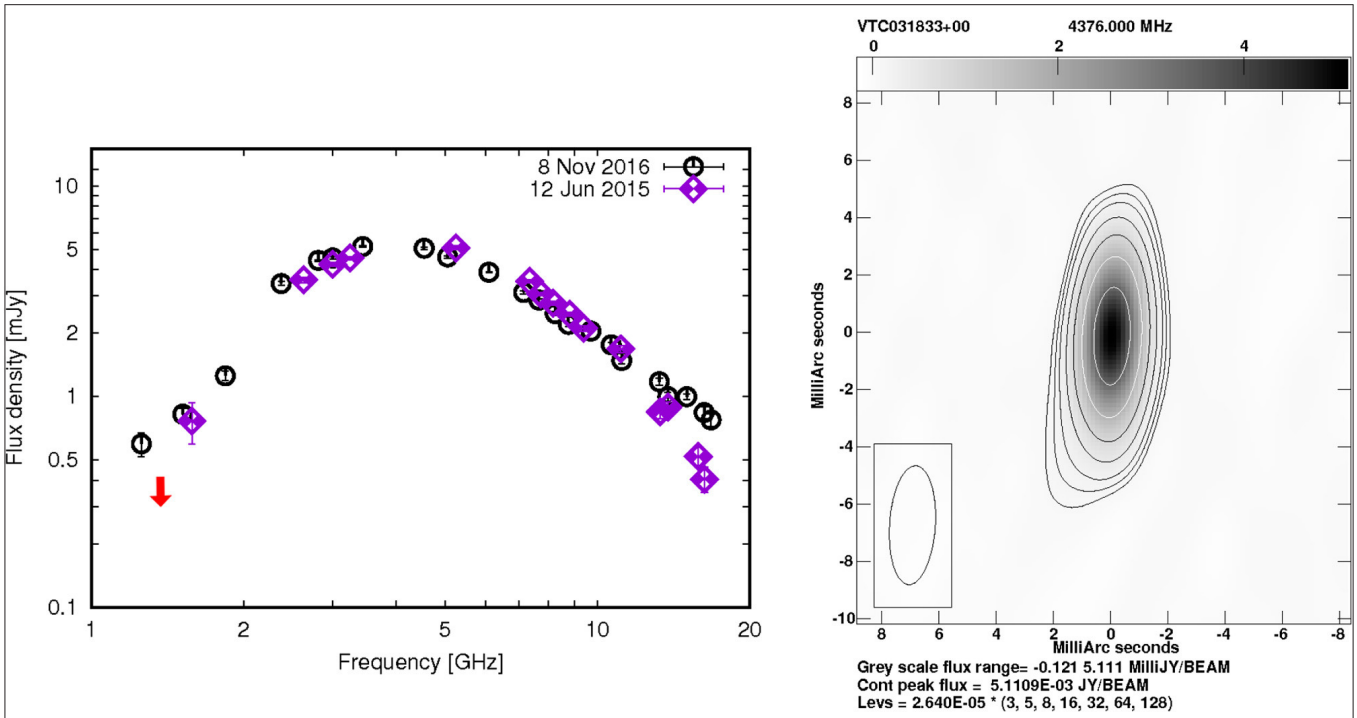

FIGURE 2 | The 1–20 GHz VLA spectrum and 4.5 GHz VLBA image of VTC031833+00. The sensitivity limit of the FIRST survey (1.4 GHz, mean epoch 1999.2) is shown as a red arrow on the spectrum plot.

have been radio-quiet sources so far. After the outburst, the new radio sources are characterised by convex radio spectra peaking at a few GHz, which is typical for young AGNs–GPS sources. From our set of optical observations, we have determined the spectral types of these objects to be the second kind. In the type-II objects the central nucleus is obscured by a molecular-dusty torus, which means that the direction of view is close to the plane of the disk. This significantly reduces the possibility of the Doppler enhancing of the jet flux fluctuations which can mimic the birth of new jet activity.

One such AGN, the type II quasar VTC233002-00 at redshift $z = 1.65$ has been recently reported by Mooley et al. (2016). VTC233002-00 was detected at ∼5.5 mJy at 3 GHz in the CNSS, while the 3σ upper limit at 1.4 GHz is 0.4 mJy (mean epoch 1999.2). The order-of-magnitude increase in flux density could be indicative of an enhanced accretion phenomenon leading to the production of a new jet. A comparison between the radio and optical flux densities indicates that this is a radio loud quasar. However, the value of the radio-loudness parameter (logR) calculated before and after the outburst changed from logR < 1 to logR $= 2.1$, respectively. This indicates that VTC233002-00 has changed its status (look) from radio-quiet to radio-loud source[1].

[1]We adopted radio-loudness definition from Kimball et al. (2011): logR $= (M_{radio} - M_i)/-2.5$, where M_{radio} is a K-corrected radio absolute magnitude and M_i is a Galactic reddening corrected and K-corrected i-band absolute magnitude. Source is considered to be radio-loud if logR > 1.

Finally, 12 such objects have been identified and we have undertaken a multi-frequency follow up campaign for those transient objects. New radio and X-ray observations and their analysis will be published soon. The latest preliminary results of our follow up VLA and VLBA observations of another of these objects are presented in **Figure 2**. VTC031833+00 has been discovered in 2015 in the CNSS survey and the Jansky VLA observations at 1–20 GHz carried by us in 2016 confirmed it is a GPS source peaking at 5GHz with a flux density of 5.1 mJy. The peak seems to slightly move towards lower frequency, when comparing the spectrum from June 2015 and the 2016 spectrum. That process could be due to propagating of the jet and its interaction with the circum-nuclear material in the host galaxy. The 4.5 GHz VLBA image of VTC031833+00 shows slightly resolved radio structure, with a flux density of 5.1 mJy, consistent with published VLA results. This radio morphology is similar to those of the radio-quiet AGNs probably indicative of weak jets that are not able to develop large-scale structure (Ulvestad et al., 2005).

3. SUMMARY

Our sample represents a special class of radio-loud AGNs that harbor jets switched on within the past few decades. These are, thus, the youngest radio sources that can provide information about the accretion state of supermassive black holes shortly after the onset of the jet formation. Furthermore,

studies of interactions between the young radio source and interstellar medium can provide information about the energy that is deposited into the ISM by the expanding radio source. This is important to our understanding of the feedback process. Taking this into account, we have undertaken a multi-frequency follow up campaign for the discovered transient objects. The detailed studies of their morphology and the jet evolution as well as the discussion about the postulated short term activity of AGNs will be published in forthcoming papers.

AUTHOR CONTRIBUTIONS

All authors participated in acquisition, analysis and interpretation of data as well as the preparation of the manuscript.

ACKNOWLEDGMENTS

This is the contribution to the proceedings of the conference "Quasars at all cosmic epochs," held in Padua (Italy) in April 2017.

REFERENCES

Best, P. N., and Heckman, T. M. (2012). On the fundamental dichotomy in the local radio-AGN population: accretion, evolution and host galaxy properties. *Month. Notices R. Astron. Soc.* 421, 1569–1582. doi: 10.1111/j.1365-2966.2012.20414.x

Czerny, B., Siemiginowska, A., Janiuk, A., Nikiel-Wroczyński, B., and Stawarz, Ł. (2009). Accretion disk model of short-timescale intermittent activity in young radio Sources. *Astrophys. J.* 698, 840–851. doi: 10.1088/0004-637X/698/1/840

Elitzur, M., Ho, L. C., and Trump, J. R. (2014). Evolution of broad-line emission from active galactic nuclei. *Month. Notices R. Astron. Soc.* 438, 3340–3351. doi: 10.1093/mnras/stt2445

Fanaroff, B. L., and Riley, J. M. (1974). The morphology of extragalactic radio sources of high and low luminosity. *Month. Notices R. Astron. Soc.* 167, 31P–36P. doi: 10.1093/mnras/167.1.31P

Fanti, C., Fanti, R., Dallacasa, D., Schilizzi, R. T., Spencer, R. E., and Stanghellini, C. (1995). Are compact steep-spectrum sources young? *Astron. Astrophys.* 302, 317–326.

Fanti, C., Pozzi, F., Dallacasa, D., Fanti, R., Gregorini, L., Stanghellini, C., et al. (2001). Multi-frequency VLA observations of a new sample of CSS/GPS radio sources. *Astron. Astrophys.* 369, 380–420. doi: 10.1051/0004-6361:20010051

Giroletti, M., and Panessa, F. (2009). The faintest seyfert radio cores revealed by VLBI. *Astrophys. J. Lett.* 706, L260–L264. doi: 10.1088/0004-637X/706/2/L260

Kellerman, K. I., Sramek, R., Schmidt, M., Shaffer, D. B., and Green, R. (1989). VLA Observations of objects in the palomar bright quasar survey. *Astron. J.* 98, 1195–1207.

Kimball, A. E., Ivezić, Ž., Wiita, P. J., and Schneider, D. P. (2011). Correlations of quasar optical spectra with radio morphology. *Astron. J.* 141:182. doi: 10.1088/0004-6256/141/6/182

Koay, J. Y., Vestergaard, M., Bignall, H. E., Reynolds, C., and Peterson, B. M. (2016). Parsec-scale radio morphology and variability of a changing-look AGN: the case of Mrk 590. *Month. Notices R. Astron. Soc.* 460, 304–316. doi: 10.1093/mnras/stw975

Kunert-Bajraszewska, M. (2016). Dichotomy in the population of young AGN: optical, radio, and X-ray properties. *Astron. Nachr.* 337, 27–30. doi: 10.1002/asna.201512259

Kunert-Bajraszewska, M., Gawroński, M. P., Labiano, A., and Siemiginowska, A. (2010). A survey of low-luminosity compact sources and its implication for the evolution of radio-loud active galactic nuclei - I. Radio data. *Month. Notices R. Astron. Soc.* 408, 2261–2278. doi: 10.1111/j.1365-2966.2010.17271.x

Kunert-Bajraszewska, M., and Labiano, A. (2014). A survey of low-luminosity compact sources and its implication for the evolution of radio-loud active galactic nuclei - II. Optical analysis. *Month. Notices R. Astron. Soc.* 408, 2279–2289. doi: 10.1111/j.1365-2966.2010.17300.x

Kunert-Bajraszewska, M., Labiano, A., Siemiginowska, A., and Guainazzi, M. (2014). First X-ray observations of low-power compact steep spectrum sources. *Month. Notices R. Astron. Soc.* 437, 3063–3071. doi: 10.1093/mnras/stt1978

Labiano, A., Barthel, P. D., O'Dea, C. P., de Vries, W. H., Prez, I., and Baum, S. A. (2007). GPS radio sources: new optical observations and an updated master list. *Astron. Astrophys.* 463, 97–104. doi: 10.1051/0004-6361:20066183

Laing, R. A., Riley, J. M., and Longair, M. S. (1983). Bright radio sources at 178 MHz - Flux densities, optical identifications and the cosmological evolution of powerful radio galaxies. *Month. Notices R. Astron. Soc.* 204, 151–187. doi: 10.1093/mnras/204.1.151

Marecki, A., Spencer, R. E., and Kunert, M. (2003). Location of Weak CSS Sources on the Evolutionary path of radio-loud AGN. *Astron. Soc. Aust.* 20, 46–49. doi: 10.1071/AS02051

Marscher, A. P., and Gear, W. K. (1985). Models for high-frequency radio outbursts in extragalactic sources, with application to the early 1983 millimeter-to-infrared flare of 3C 273. *Astron. J.* 298, 114–127. doi: 10.1086/163592

Merloni, A., Heinz, S., and di Matteo, T. (2003). A Fundamental Plane of black hole activity. *Month. Notices R. Astron. Soc.* 345, 1057–1076. doi: 10.1046/j.1365-2966.2003.07017.x

Mooley, K. P., Hallinan, G., Bourke, S., Horesh, A., Myers, S. T., Frail, D. A., et al. (2016). The Caltech-NRAO Stripe 82 Survey (CNSS). I. The pilot radio transient survey in 50 deg^2. *Astrophys. J.* 818:105. doi: 10.3847/0004-637X/818/2/105

Reynolds, C. S., and Begelman, M. C. (1997). Intermittant radio galaxies and source statistics. *Astrophys. J.* 487, L135–L138.

Sadler, E. M., Ekers, R. D., Mahony, E. K., Mauch, T., and Murphy, T. (2014). The local radio-galaxy population at 20 GHz. *Month. Notices R. Astron. Soc.* 438, 796–824. doi: 10.1093/mnras/stt2239

Schawinski, K., Koss, M., Berney, S., and Sartori, L. F. (2015). Active galactic nuclei flicker: an observational estimate of the duration of black hole growth phases of 10^5yr. *Month. Notices R. Astron. Soc.* 451, 2517–2523. doi: 10.1093/mnras/stv1136

Ulvestad, J. S., Antonucci, R. R. J., and Barvainis, R. (2005). VLBA imaging of central engines in radio-quiet quasars. *Astrophys. J.* 621, 123–129. doi: 10.1086/427426

Conflict of Interest Statement: The authors declare that the research was conducted in the absence of any commercial or financial relationships that could be construed as a potential conflict of interest.

Copyright © 2017 Wołowska, Kunert-Bajraszewska, Mooley and Hallinan. This is an open-access article distributed under the terms of the Creative Commons Attribution License (CC BY). The use, distribution or reproduction in other forums is permitted, provided the original author(s) or licensor are credited and that the original publication in this journal is cited, in accordance with accepted academic practice. No use, distribution or reproduction is permitted which does not comply with these terms.

frontiers in Astronomy and Space Sciences

PERSPECTIVE
published: 11 October 2017
doi: 10.3389/fspas.2017.00021

The MEXSAS2 Sample and the Ensemble X-ray Variability of Quasars

Roberto Serafinelli[1,2]*, *Fausto Vagnetti*[1], *Elia Chiaraluce*[1] and *Riccardo Middei*[3]

[1] Dipartimento di Fisica, Università di Roma Tor Vergata, Rome, Italy, [2] Dipartimento di Fisica, Università di Roma Sapienza, Rome, Italy, [3] Dipartimento di Matematica e Fisica, Università Roma Tre, Rome, Italy

We present the second Multi-Epoch X-ray Serendipitous AGN Sample (MEXSAS2), extracted from the 6th release of the XMM Serendipitous Source Catalog (XMMSSC-DR6), cross-matched with Sloan Digital Sky Survey quasar catalogs DR7Q and DR12Q. Our sample also includes the available measurements for masses, bolometric luminosities, and Eddington ratios. Analyses of the ensemble structure function and spectral variability are presented, together with their dependences on such parameters. We confirm a decrease of the structure function with the X-ray luminosity, and find a weak dependence on the black hole mass. We introduce a new spectral variability estimator, taking errors on both fluxes and spectral indices into account. We confirm an ensemble softer when brighter trend, with no dependence of such estimator on black hole mass, Eddington ratio, redshift, X-ray and bolometric luminosity.

Keywords: catalogs, quasars, spectral variability, structure function, X-rays

OPEN ACCESS

Edited by:
Paola Marziani, Osservatorio Astronomico di Padova (INAF), Italy

Reviewed by:
Edi Bon, Belgrade Astronomical Observatory, Serbia
Isabel Marquez Perez, Instituto de Astrofísica de Andalucía (CSIC), Spain

***Correspondence:**
Roberto Serafinelli
roberto.serafinelli@roma2.infn.it

Specialty section:
This article was submitted to Milky Way and Galaxies, a section of the journal Frontiers in Astronomy and Space Sciences

Received: *17 July 2017*
Accepted: *26 September 2017*
Published: *11 October 2017*

Citation:
Serafinelli R, Vagnetti F, Chiaraluce E and Middei R (2017) The MEXSAS2 Sample and the Ensemble X-ray Variability of Quasars. Front. Astron. Space Sci. 4:21. doi: 10.3389/fspas.2017.00021

1. THE MEXSAS2 CATALOG

We present here the MEXSAS2 catalog, obtained from the sixth release of the XMM Newton Serendipitous Source Catalog (XMMSSC-DR6, Rosen et al., 2016), combined with both SDSS-DR7Q (Schneider et al., 2010) and SDSS-DR12Q quasar catalogs (Pâris et al., 2017). The MEXSAS2 catalog is the updated version of MEXSAS (Multi-Epoch XMM Serendipitous AGN Sample), published by Vagnetti et al. (2016). It contains 9,735 X-ray observations for 3,366 quasars, which increases by about 25% the numbers of the previous version (7,837 observations, 2,700 quasars). It only contains sources with more than one observation, and it is therefore ideal for variability studies.

We complement the catalog with measurements of black hole masses, bolometric luminosities and Eddington ratios, which are available for 3,138 quasars (93%) from the catalogs by Shen et al. (2011) for the sources listed in SDSS-DR7Q, and by Kozłowski (2017) for SDSS-DR12Q. We use homogeneous criteria to derive the masses and bolometric luminosities from the two catalogs, adapting their criteria, which are slightly different for the redshift intervals where two different broad lines and two continuum luminosities are available. In fact, Shen et al. (2011) adopts different single-epoch virial estimates sharply dividing at redshift $z = 0.7$ for choosing between Hβ and MgII(2,798Å) relations, and at $z = 1.9$ for Mg II(2,798Å) and C IV(1,549Å). A similar option is adopted for computing bolometric luminosities from the continua at 5,100Å or 3,000Å dividing at $z = 0.7$, and at 3,000Å or 1,350Å dividing at $z = 1.9$. The criteria adopted by Kozłowski (2017) are instead to prefer the Mg II black hole mass estimate when available, rather than that from C IV, which is biased from various effects, and to compute bolometric luminosity as a weighted average of those derived from two different available continua. However, Kozłowski (2017) also find that the DR7Q line widths (which are derived from detailed fits of spectral components) are generally

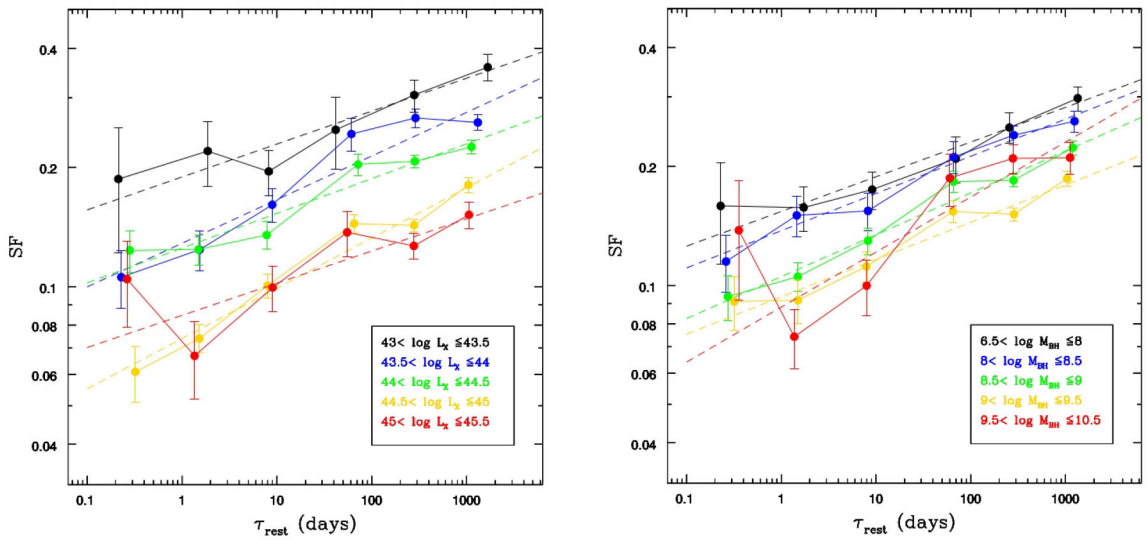

FIGURE 1 | The structure function in bins of X-ray luminosity L_X and black hole mass M_{BH} (data and continuous lines) with power-law fits (dashed lines). **Left panel:** Black, $43 < \log L_X \leq 43.5$; blue, $43.5 < \log L_X \leq 44$; green, $44 < \log L_X \leq 44.5$; yellow, $44.5 < \log L_X \leq 45$; red, $45 < \log L_X \leq 45.5$. **Right panel:** Black, $6.5 \lesssim \log M_{BH} \leq 8$; blue, $8 < \log M_{BH} \leq 8.5$; green, $8.5 < \log M_{BH} \leq 9$; yellow, $9 < \log M_{BH} \leq 9.5$; red, $9.5 < \log M_{BH} \lesssim 10.5$.

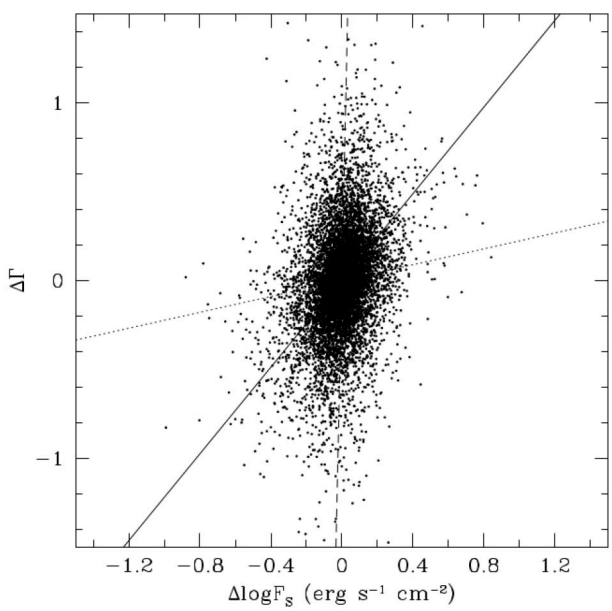

FIGURE 2 | The ensemble correlation between the variations of the photon index $\Delta\Gamma$ and the variations of the logarithmic flux $\Delta \log F$ are shown. The dotted line represents β_{xy}, the dashed line represents β_{yx}, while the bisector β_{bis} is shown as a continuous line.

more reliable than the DR12Q ones (which are derived from principal component analysis), thus they are to be preferred, when available. To apply the same criteria to the mass and luminosity data from both DR7Q and DR12Q, we adopt the following choice: (i) for quasars included only in DR12Q and not in DR7Q, we take the estimates by Kozłowski (2017) (2178 objects); (ii) for quasars included in both catalogs or only in DR7Q, and in redshift intervals with only one broad line and one continuum luminosity available ($z \lesssim 0.35$, $0.9 \lesssim z \lesssim 1.5$, $z \gtrsim 2.25$), we take the estimates by Shen et al. (2011) (442 objects); (iii) for quasars included in both catalogs or only in DR7Q, in redshift intervals with two broad lines and continua ($0.35 \lesssim z \lesssim 0.9$, $1.5 \lesssim z \lesssim 2.25$), we apply the Kozłowski (2017) criteria to the DR7Q data, deriving new estimates (518 objects).

The catalog, including X-ray measurements from XMMSSC and quasar data from SDSS and from our elaboration, will be published elsewhere (Vagnetti et al, in preparation). Here we provide preliminary results of our ensemble analyses of the X-ray variability.

2. FLUX VARIABILITY AND STRUCTURE FUNCTION

We compute the structure function according to Vagnetti et al. (2016), as a r.m.s. difference of the X-ray flux measured at two epochs differing by τ in the rest-frame, and corrected for the noise contribution,

$$SF(\tau) \equiv \sqrt{\langle [\log f_X(t+\tau) - \log f_X(t)]^2 \rangle - \sigma^2_{noise,SF}}, \qquad (1)$$

where $\sigma^2_{noise,SF} = \langle \sigma_n^2(t) + \sigma_n^2(t+\tau) \rangle$ is the quadratic contribution of the photometric noise to the observed variations, σ_n being the error on $\log f_X$ at each given time.

We use mainly EPIC X-ray fluxes in the XMM-Newton band 9 (0.5–4.5 KeV), as in our previous papers (Vagnetti et al., 2011, 2016).

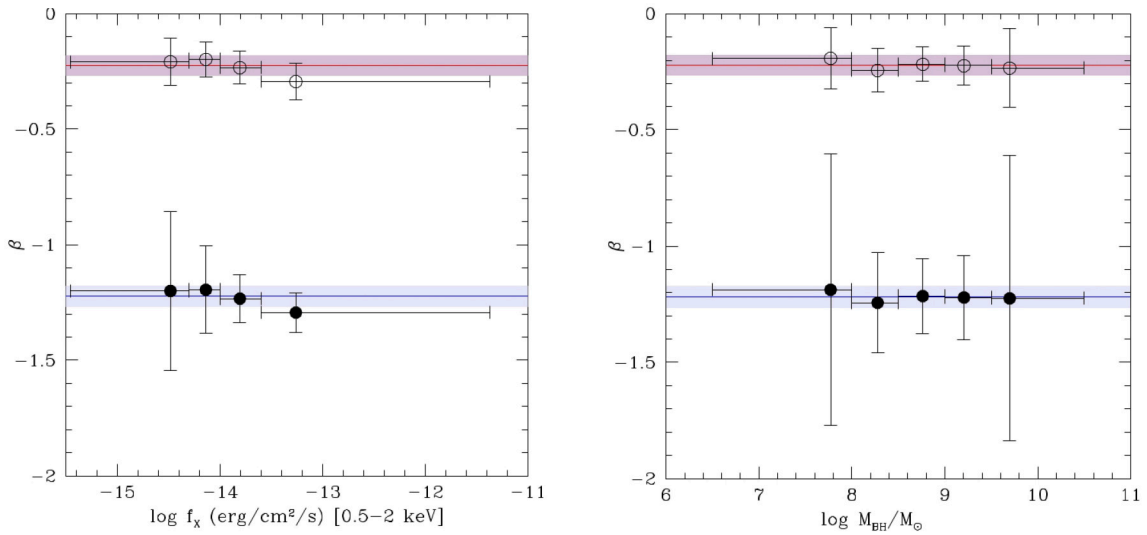

FIGURE 3 | The dependence of β_{xy} and β_{bis} in bins of soft X-ray flux **(Left panel)** and black hole mass **(Right panel)**. No dependence is found, and all the values of β_{xy} (empty circles) and β_{bis} (filled circles) are compatible with the corresponding ensemble values $\beta_{xy} = -0.22 \pm 0.04$ and $\beta_{bis} = -1.22 \pm 0.05$, which are indicated respectively by the red and blue lines, and by the lighter bands for the uncertainties. The horizontal bars indicate bin widths, not errors.

The SF can be fitted by a power-law SF $\propto \tau^b$. For the whole sample we find a slope $b = 0.11 \pm 0.01$. The SFs in bins of X-ray luminosity and black hole mass are shown in **Figure 1**. We confirm a strong anti-correlation with X-ray luminosity, approximately as $L_X^{-0.22}$, with correlation coefficient $r = -0.92$ and null probability $p(>r) = 0.04$, and no dependence on redshift, similarly to Vagnetti et al. (2016). There is an apparent decrease of the SF with black hole mass, approximately as $M_{BH}^{-0.15}$, with $r = -0.97$ and $p(>r) = 0.03$, but partial correlation analysis suggests that this is due to the strong correlation of mass with X-ray luminosity. Limiting the analysis to the luminosity interval 10^{44}erg/s $< L_X < 10^{45}$erg/s, the mass-luminosity correlation reduces ($r = -0.83$, $p(>r) = 0.06$), and the dependence of the SF on black hole mass is weaker, $\propto M_{BH}^{-0.06}$. We find neither dependence on bolometric luminosity nor on Eddington ratio.

3. SPECTRAL VARIABILITY

We update the analysis of the spectral variability parameter, initially introduced by Trevese and Vagnetti (2002) and recently adapted to the X-ray band by Serafinelli et al. (2017)

$$\beta = -\frac{\Delta\Gamma}{\Delta \log f_X}, \tag{2}$$

relating variations of the photon index Γ with those of the X-ray flux in a given band.

The spectra of most Seyfert galaxies with Eddington ratios above 0.01 typically become steeper in their brighter phases (e.g., Markowitz et al., 2003; Sobolewska and Papadakis, 2009; Connolly et al., 2016), as well as for many galactic black hole binary systems (e.g., Remillard and McClintock, 2006; Done et al., 2007; Dong et al., 2014). This is known as "softer when brighter" behavior and translates to a negative β value according to Equation 2. We also found this "softer when brighter" behavior, obtaining $\beta = -0.69 \pm 0.03$ in our ensemble analysis, for the previous version of the MEXSAS sample, using fluxes in the soft X-ray band 0.5–2 keV, and computing variations with respect to the mean values of each source (Serafinelli et al., 2017).

Since the ensemble correlation between $\Delta\Gamma$ and $\Delta \log f_X$ contains a large scatter, also due to the large measurement errors for the fainter sources, we fit a linear relation $\Delta\Gamma \propto \Delta \log f_X$ to the MEXSAS2 data set taking the uncertainties in both variables into account. We run a high number of linear fits replacing original data with Gaussian distributed values within the associated error box. Moreover, following Isobe et al. (1990), we computed both ordinary least squares regressions OLS($Y|X$) of the dependent variable Y on the independent variable X (which result we call for brevity β_{xy}), the inverse regression OLS($X|Y$) (β_{yx}), and the bisector:

$$\beta_{bis} = \frac{\beta_{xy}\beta_{yx} - 1 + \sqrt{(1+\beta_{xy}^2)(1+\beta_{yx}^2)}}{\beta_{xy} + \beta_{yx}}. \tag{3}$$

For the whole sample, we find ensemble values $\beta_{xy} = -0.22 \pm 0.04$ and $\beta_{bis} = -1.22 \pm 0.05$, confirming the "softer when brighter" behavior for both spectral variability parameters (see **Figure 2**).

We then divide our sample in bins of soft X-ray flux, to show that the resulting β does not change within the errors (see **Figure 3**). In fact this was expected, because measurement errors do affect the estimate of β, but this must reflect an intrinsic relation between the flux and slope variations which should not change with an observational parameter like the average flux of the sources.

We also divide our sample in bins of black hole mass, M_{BH}, and show the result in **Figure 3**. Both β_{xy} and β_{bis} are independent of M_{BH} within the errors, and always compatible with their overall ensemble values.

We similarly analyse possible dependencies on Eddington ratio, redshift, X-ray and bolometric luminosities, finding no evidence of change. This analysis will be reported in an upcoming paper (Vagnetti et al., in preparation).

4. SUMMARY

- We have updated our X-ray quasar catalog MEXSAS to MEXSAS2.
- We have confirmed our previous results for the structure function dependence on X-ray luminosity, and no dependence on redshift; we find a weak dependence on black hole mass, and no dependence on bolometric luminosity and Eddington ratio.
- We have developed new spectral variability estimators, by computing ordinary least squares and bisector fits with errors in both variables.
- We obtain "softer when brighter" trends for the new MEXSAS2 sample using both estimators.
- Our spectral variability estimates, that also take errors on both fluxes and spectral indices into account, do not present a dependence on the flux.
- No trend with black hole mass, Eddington ratio, redshift, X-ray and bolometric luminosities is found, in agreement with our previous results (Serafinelli et al., 2017).

AUTHOR CONTRIBUTIONS

RS performed the spectral variability analysis and wrote part of the text, FV was responsible for the idea that resulted in the paper and also contributed to the text, EC built the dataset of the MEXSAS2 catalog, RM performed the structure function analysis.

REFERENCES

Connolly, S. D., McHardy, I. M., Skipper, C. J., and Emmanoulopoulos, D. (2016). Long-term X-ray spectral variability in AGN from the Palomar sample observed by Swift. *Month. Notices R. Astron. Soc.* 459, 3963–3985. doi: 10.1093/mnras/stw878

Done, C., Gierliński, M., and Kubota, A. (2007). Modelling the behaviour of accretion flows in X-ray binaries. Everything you always wanted to know about accretion but were afraid to ask. *Astron. Astrophys. Rev.* 15, 1–66. doi: 10.1007/s00159-007-0006-1

Dong, A.-J., Wu, Q., and Cao, X.-F. (2014). A New Fundamental Plane for Radiatively Efficient Black-hole Sources. *Astrophys. J. Lett.* 787:L20. doi: 10.1088/2041-8205/787/2/L20

Isobe, T., Feigelson, E. D., Akritas, M. G., and Babu, G. J. (1990). Linear regression in astronomy. *Astrophys. J.* 364, 104–113. doi: 10.1086/169390

Kozłowski, S. (2017). Virial Black Hole Mass Estimates for 280,000 AGNs from the SDSS Broadband Photometry and Single-epoch Spectra. *Astrophys. J. Suppl.* 228:9. doi: 10.3847/1538-4365/228/1/9

Markowitz, A., Edelson, R., and Vaughan, S. (2003). Long-Term X-Ray Spectral Variability in Seyfert 1 Galaxies. *Astrophys. J.* 598, 935–955. doi: 10.1086/379103

Pâris, I., Petitjean, P., Ross, N. P., Myers, A. D., Aubourg, É., Streblyanska, A., et al. (2017). The sloan digital sky survey quasar catalog: twelfth data release. *Astron. Astrophys.* 597:A79. doi: 10.1051/0004-6361/201527999

Remillard, R. A., and McClintock, J. E. (2006). X-Ray Properties of black-hole binaries. *Annu. Rev. Astron. Astrophys.* 44, 49–92. doi: 10.1146/annurev.astro.44.051905.092532

Rosen, S. R., Webb, N. A., Watson, M. G., Ballet, J., Barret, D., Braito, V., Carrera, F. J., et al. (2016). The XMM-Newton serendipitous survey. VII. The third XMM-Newton serendipitous source catalogue. *Astron. Astrophys.* 590:A1. doi: 10.1051/0004-6361/201526416

Schneider, D. P., Richards, G. T., Hall, P. B., Strauss, M. A., Anderson, S. F., Boroson, T. A., et al. (2010). The sloan digital sky surveyquasar catalog. V. Seventh data release. *Astron. J.* 139, 2360–2373. doi: 10.1088/0004-6256/139/6/2360

Serafinelli, R., Vagnetti, F., and Middei, R. (2017). Quasar spectral variability from the XMM-Newton serendipitous source catalogue. *Astron. Astrophys.* 600:A101. doi: 10.1051/0004-6361/201629885

Shen, Y., Richards, G. T., Strauss, M. A., Hall, P. B., Schneider, D. P., Snedden, S., et al. (2011). A catalog of quasar properties from sloan digital sky survey data release 7. *Astrophys. J. Suppl.* 194:45. doi: 10.1088/0067-0049/194/2/45

Sobolewska, M. A., and Papadakis, I. E. (2009). The long-term X-ray spectral variability of AGN. *Month. Notices R. Astron. Soc.* 399, 1597–1610. doi: 10.1111/j.1365-2966.2009.15382.x

Trevese, D., and Vagnetti, F. (2002). Quasar spectral slope variability in the optical band. *Astrophys. J.* 564, 624–630. doi: 10.1086/324541

Vagnetti, F., Middei, R., Antonucci, M., Paolillo, M., and Serafinelli, R. (2016). Ensemble X-ray variability of active galactic nuclei. II. Excess variance and updated structure function. *Astron. Astrophys.* 593:A55. doi: 10.1051/0004-6361/201629057

Vagnetti, F., Turriziani, S., and Trevese, D. (2011). Ensemble X-ray variability of active galactic nuclei from serendipitous source catalogues. *Astron. Astrophys.* 536:A84. doi: 10.1051/0004-6361/201118072

Conflict of Interest Statement: The authors declare that the research was conducted in the absence of any commercial or financial relationships that could be construed as a potential conflict of interest.

Copyright © 2017 Serafinelli, Vagnetti, Chiaraluce and Middei. This is an open-access article distributed under the terms of the Creative Commons Attribution License (CC BY). The use, distribution or reproduction in other forums is permitted, provided the original author(s) or licensor are credited and that the original publication in this journal is cited, in accordance with accepted academic practice. No use, distribution or reproduction is permitted which does not comply with these terms.

frontiers in Astronomy and Space Sciences

ORIGINAL RESEARCH
published: 14 September 2017
doi: 10.3389/fspas.2017.00012

Long-Term Monitoring of the Broad-Line Region Properties in a Selected Sample of AGN

Dragana Ilić [1], Alla I. Shapovalova [2], Luka Č. Popović [1,3], Vahram Chavushyan [4], Alexander N. Burenkov [2], Wolfram Kollatschny [5], Andjelka Kovačević [1], Sladjana Marčeta-Mandić [1,3], Nemanja Rakić [1,6], Giovanni La Mura [7] and Piero Rafanelli [7]*

[1] Department of Astronomy, Faculty of Mathematics, University of Belgrade, Belgrade, Serbia, [2] Special Astrophysical Observatory, Russian Academy of Sciences, Nizhnii Arkhyz, Russia, [3] Astronomical Observatory, Belgrade, Serbia, [4] Instituto Nacional de Astrofísica, Óptica y Electrónica, Puebla, Mexico, [5] Institut fuer Astrophysik, Universitaet Goettingen, Göttingen, Germany, [6] Faculty of Science, University of Banjaluka, Banjaluka, Republic of Srpska, Bosnia and Herzegovina, [7] Department of Physics and Astronomy, University of Padova, Padova, Italy

OPEN ACCESS

Edited by:
Paola Marziani,
National Institute for Astrophysics (INAF), Italy

Reviewed by:
Shai Kaspi,
Tel Aviv University, Israel
Anna Lia Longinotti,
National Institute of Astrophysics, Optics and Electronics, Mexico

***Correspondence:**
Dragana Ilić
dilic@math.rs

Specialty section:
This article was submitted to Milky Way and Galaxies, a section of the journal Frontiers in Astronomy and Space Sciences

Received: 10 July 2017
Accepted: 21 August 2017
Published: 14 September 2017

Citation:
Ilić D, Shapovalova AI, Popović LČ, Chavushyan V, Burenkov AN, Kollatschny W, Kovačević A, Marčeta-Mandić S, Rakić N, La Mura G and Rafanelli P (2017) Long-Term Monitoring of the Broad-Line Region Properties in a Selected Sample of AGN. Front. Astron. Space Sci. 4:12. doi: 10.3389/fspas.2017.00012

We present the results of the long-term optical monitoring campaign of active galactic nuclei (AGN) coordinated by the Special Astrophysical Observatory of the Russian Academy of Science. This campaign has produced a remarkable set of optical spectra, since we have monitored for several decades different types of broad-line (type 1) AGN, from a Seyfert 1, double-peaked line, radio loud and radio quiet AGN, to a supermassive binary black hole candidate. Our analysis of the properties of the broad line region (BLR) of these objects is based on the variability of the broad emission lines. We hereby give a comparative review of the variability properties of the broad emission lines and the BLR of seven different type 1 AGNs, emphasizing some important results, such as the variability rate, the BLR geometry, and the presence of the intrinsic Baldwin effect. We are discussing the difference and similarity in the continuum and emission line variability, focusing on what is the impact of our results to the supermassive black hole mass determination from the BLR properties.

Keywords: galaxies:active-galaxies, quasar:individual (Arp 102B, 3C 390.3, NGC 5548, NGC 4151, NGC 7469, Ark 564, E1821+643), quasars: supermassive black holes, quasar:emission lines, line:profiles

1. INTRODUCTION

The broad line region (BLR) in active galactic nuclei (AGN) is responsible for the emission of intensive broad lines, seen in the optical spectra of type 1 AGN. We use these lines to probe the physics and kinematics of the BLR, aiming to study in more details the central engine and the supermassive black hole (SMBH) properties. This is because, on one hand the BLR is photoionized by the central continuum source, and on the other, it is gravitationally bound to the SMBH (Osterbrock and Ferland, 2006).

One way to do this is by using the variability of the broad emission lines, as they are known to be strongly variable in flux and profile. From the long-term monitoring campaign of optical broad emission lines in different type 1 AGN, it is possible to estimate the size of the BLR (reverberation analysis Lyutyi and Cherepashchuk, 1972; Blandford and McKee, 1982; Gaskell and Sparke, 1986) and the mass of the SMBH (Gaskell, 1988), and test the photoionization hypothesis by studying the line and continuum flux correlations (Osterbrock and Ferland, 2006). One particularly interesting

correlation, first detected in the broad C IV line, is the Baldwin effect, i.e., the anti-correlation between the emission line equivalent width and the near-by continuum luminosity (Baldwin, 1977). There are two different types of Baldwin effect: (i) global Baldwin effect which shows the above anti-correlation on single-epoch observations of a large number of AGN; and (ii) intrinsic Baldwin effect which is the same anti-correlation detected in an individual variable AGN. It is well known that the global Baldwin effect is not detected in case of the broad Hβ line. However, when testing this correlation in case of a single object monitoring data, i.e., the intrinsic Baldwin effect, it has been seen that the anti-correlation exists even in the case of Hβ (Pogge and Peterson, 1992; Rakić et al., 2017).

Here we present some interesting findings of the long-term (more than a decade) optical monitoring campaign of a sample of seven type 1 AGN of different spectral types: Seyfert 1 galaxies (NGC 5548, NGC 4151, NGC 7469), Narrow-line Seyfert 1 galaxy - NLSy 1 (Ark 564), double-peaked line radio loud (3C 390.3) and radio quiet (Arp 102B) galaxy, and a luminous quasar (E1821+643), a supermassive binary black hole candidate. All spectral data for each objects have been first presented and analyzed separately in Shapovalova et al. (2001, 2004, 2008, 2010a, 2012, 2013, 2016, 2017). However, since the obtained spectra are observed, reduced and analyzed in the same manner, the final result is a uniform set of data, which can be compared and discussed. Here we continue the discussion given in Ilić et al. (2015), where we first tried to give a comparative review of the variability properties of type 1 AGN in our sample, only that now our sample consist of seven objects, including one high-luminosity local quasar, which makes our sample more diverse. Here we focus on discussing the possible BLR geometry and the presence of the intrinsic Baldwin effect. The paper is organized as follows: in Section 2 we briefly describe the observations, the obtained data and performed analysis; in Section 3 we present the results, and in Section 4 we give the discussion and outline our conclusions.

2. OBSERVATIONS AND DATA ANALYSIS

The long-term monitoring campaign was coordinated by the Special Astrophysical Observatory of the Russian Academy of Science (SAO), using their 1-m and 6-m telescopes. Additionally, the campaign made use of the 2.1-m telescope of Guillermo Haro Astrophysical Observatory (Mexico), 2.1-m telescope of the Observatorio Astronomico Nacional at San Pedro Martir (Mexico), and the 3.5-m and 2.2-m telescopes of Calar Alto Observatory (Spain). The spectral data have been collected for several decades (since 1987 until 2015) and have been reduced and calibrated using the same procedures and methods, thus producing a homogeneous set of data. The information about the observations and the description of all procedures for each object are given in Shapovalova et al. (2001, 2004, 2008, 2010a, 2012, 2013, 2016, 2017). Here we outline some of the important line parameter measurements. In order to measure the broad line fluxes and full width half maximum (FWHM), we needed to subtract the underlying continuum emission, and the narrow and other near-by satellite lines, for which we performed the multi-Gaussian fittings (Popović et al., 2004). In case of Hβ line region, it is important to carefully model the Fe II multiplet emission, and this was done using a template[1] described in details in Kovačević et al. (2010) and Shapovalova et al. (2012).

In **Table 1** we list the spectral characteristics of the sample, together with the basic information (see caption of **Table 1**). The $R_{\rm BLR}$ comes from the time-lags calculated using the Z-transformed Discrete Correlation Function (Alexander, 1997), which was applied on continuum and line flux light-curves. Depending on the sampling of light curves we used either observed or simulated light-curves in order to get the most reliable result (for details see references in column 9, **Table 1**). The listed masses are taken from the monitoring results (see column 8 in **Table 1**), and for details on how the mass was calculated see given references (column 9 in **Table 1**). In case of NGC 5548 and NGC 4151 the mass was not derived in the original monitoring campaign, so we calculated in this work their SMBH masses, using the equation $M_{\rm BH} = f\Delta R_{\rm BLR} V^2_{\rm FWHM}/G$, where $\Delta V_{\rm FWHM}$ is the orbital velocity estimated from the width of the variable part of Hβ (taken from references given in **Table 1**), and f is the virial factor taken to be 5.5 (Onken et al., 2004). The variability parameter $F_{\rm var}$ gives the level of flux variability and is calculated using equation from O'Brien et al. (1998). For the luminosity at 5100 Å we calculated the luminosity distances with the online calculator of Wright (2006), taking the same cosmological parameters as in Ilić et al. (2015): $\Omega = 0.286$, $\Omega_\Lambda = 0.714$, and $\Omega_k = 0$, and a Hubble constant, $H_0 = 69.6\,{\rm km/s\,Mpc^{-1}}$.

3. RESULTS

In this paper we present a sample of 7 type 1 AGN with different broad line profiles (**Table 1**, columns 3–4) and different variability rate (**Table 1**, column 6). **Figure 1** shows the Hβ line flux light curves for all 7 objects, where the line flux and the errors-bars are shown normalized to the maximal flux for comparison. In all 7 objects, for which we have been collecting spectra for more than a decade and in some cases two decades, the line and continuum flux are varying. From **Table 1** and **Figure 1**, we can see that: NGC 4151 and NGC 5548 are strongly variable Seyfert 1.5, NGC 7469 is also a Seyfert 1 but with lower variability in line fluxes and profiles, Arp 102B and 3C 390.3 have broad double-peaked lines, Ark 564 is a NLSy1, and E1821+643 is a quasar with strong red-asymmetry in line profiles, but almost no variability.

One important prerequisite for the estimates of the radius of the BLR using the reverberation monitoring data, is the fact that the BLR is photoionized by the central continuum source (see e.g., Peterson and Horne, 2006). The simplest way to test this is by plotting the line luminosity as a function of the continuum luminosity. In **Figure 2** we thus

[1]For Fe II modeling and subtraction see the page of the Serbian Virtual Observatory, http://servo.aob.rs.

TABLE 1 | Spectral characteristics of the sample.

Object period [years] (1)	z (2)	AGN type (3)	Line Profile Shape FWHM [km/s] (4)	$c\tau_{BLR}$ Hβ [ld] (5)	F_{var} Hβ (6)	λL_λ (5100) [10^{44} erg/s] (7)	M_{BH} [$M_\odot$] (8)	References (9)
NGC 5548 (1996–2002)	0.0172	Sy 1.0–1.8	Strong shoulders 6,300	49^{+19}_{-8}	0.33	0.40 ± 0.12	2.1×10^9	Shapovalova et al., 2004; Kovačević et al., 2014
NGC 4151 (1996–2006)	0.0033	Sy 1.5–1.8	Absorption,bumps 6,110	5^{+28}_{-5}	0.42	0.05 ± 0.03	1.6×10^8	Shapovalova et al., 2008, 2010b; Rakić et al., 2017
3C390.3 (1995–2007)	0.0561	Radio loud	Double-peaked 11,900	96^{+28}_{-47}	0.38	0.90 ± 0.42	2.1×10^9	Shapovalova et al., 2001, 2010a; Jovanović et al., 2010; Popović et al., 2011
Ark 564 (1999–2010)	0.0247	NLSy1	Strong FeII 960	4^{+27}_{-4}	0.07	0.36 ± 0.04	1.0×10^6	Shapovalova et al., 2012
Arp 102B (1987–2013)	0.0242	LINER	Double-peaked 15,900	15^{+20}_{-15}	0.21	0.11 ± 0.01	1.1×10^8	Shapovalova et al., 2013; Popović et al., 2014
NGC 7469 (1996–2015)	0.0163	Sy 1.0	Narrower 2,000	21^{+7}_{-0}	0.23	0.52 ± 0.0.08	1.1×10^7	Shapovalova et al., 2017
E1821+643 (1990–2014)	0.297	Quasar	Red-asymmetry 5,610	$118^{+0.1}_{-0.0}$	0.07	104.4 ± 19.9	2.6×10^9	Shapovalova et al., 2016; Kovačević et al., 2017

The columns are: (1) object name and monitoring period, (2) redshift, (3) AGN type, (4) shape of line profile and FWHM of the mean Hβ, (5) BLR radius $R_{BLR} = c\tau_{BLR}$ of Hβ, (6) variability parameter F_{var} of Hβ, (7) mean continuum luminosity at 5100Å, (8) the mass of the SMBH M_{BH}, and (9) references.

show the Hβ line luminosity for all 7 objects (shown with dots) vs. the continuum luminosity at 5100 Å. Moreover, the mean value is also shown (filled circle) with the object name denoted next to it. The important finding is the fact that the luminosity of the Hβ line is following the same trend with the continuum luminosity for all objects, from the low-luminosity Seyfert up to the high-luminosity quasar (**Figure 2**).

On the other hand, it was shown that the intrinsic Baldwin effect is detected in the Balmer lines (Hα and Hβ) in 6 objects from this sample (see the results and discussion in Rakić et al., 2017). Here we show as an example the presence of the intrinsic Baldwin effect, an anti-correlation between the Hβ line equivalent width and the continuum flux[2] measured at 5100 Å) in case of Hβ of NGC 4151 (**Figure 3**), for which this effect is of high significance (see Rakić et al., 2017).

Figure 4 shows the radius of the broad Hβ line emitting-region as a function of the continuum luminosity at 5100 Å for our sample (**Table 1**, columns 5 and 7, respectively). Data are fitted with the scaling relation from Bentz et al. (2006) in the form of $\log R_{\rm BLR} = K + \alpha \log[\lambda L_\lambda(5100)/10^{44}]$, where α is the slope of the BLR radius-luminosity relationship and K is the scaling factor. The dashed line is plotted with the coefficients $\alpha = 0.533$ and $K = 1.527$, given by Bentz et al. (2013), and the solid line is a simple linear best-fitting of the above equation (not considering the error-bars) through all 7 objects, obtaining the fitting parameters of $\alpha = 0.226$ and $K = 1.639$. The linear regression fit was done using a nonlinear least-squares Marquardt-Levenberg algorithm available in gnuplot.

[2]Since the intrinsic Baldwin effect is detected in a single object, we can use a flux instead of luminosity.

4. DISCUSSION AND CONCLUSIONS

Here we have analyzed and compared the optical spectra for seven type 1 AGN which have different variability properties and characteristics of the broad emission line profiles. This remarkable set of spectral data has been collected for several decades (**Table 1**, column 1) within the SAO RAS long-term monitoring campaign. Following the comparative study given in Ilić et al. (2015), we extend here our sample to 7 objects and outline the most important results. We repeat again that all observational data sets were uniformly processed, and in that way could be compared.

If we compare the normalized light-curves shown in **Figure 1**, the strongest variable objects are NGC 5548, NGC 4151, and 3C 390.3 (see also in **Table 1** the variability parameter $F_{\rm var}$ which is ∼40%), followed by Arp 102B and NGC 7469 ($F_{\rm var}$ ∼20%). The least variable objects are the NLSy1 Ark 564 and the highly luminous quasar E1821+643, for which the line and continuum flux are almost constant for decades (for the Hβ line, $F_{\rm var}$ ∼7%). The case of the quasar E1821+643 is specially puzzling since its broad emission lines show a peak shift (of the order ∼1,000 km/s) and a strong asymmetry in the red wing, extended up to ∼15,000 km/s (see Shapovalova et al., 2016, and their Figure 15). This object was suggested to be a candidate for a binary SMBH or a recoiling black hole after the collision of two SMBH (Robinson et al., 2010), however Shapovalova et al. (2016) found it difficult to explain the unchanging line-profiles on such a long time-scales with the binary SMBH hypothesis, suggesting that the broad-line emitting region may be connected with some sort of gas-rich clouds that are orbiting around the recoiling SMBH.

Interestingly, the rate of variability shows no trend with the SMBH mass (**Table 1**, column 8), i.e., the low variability is detected in case of AGN with small and large SMBH mass (see

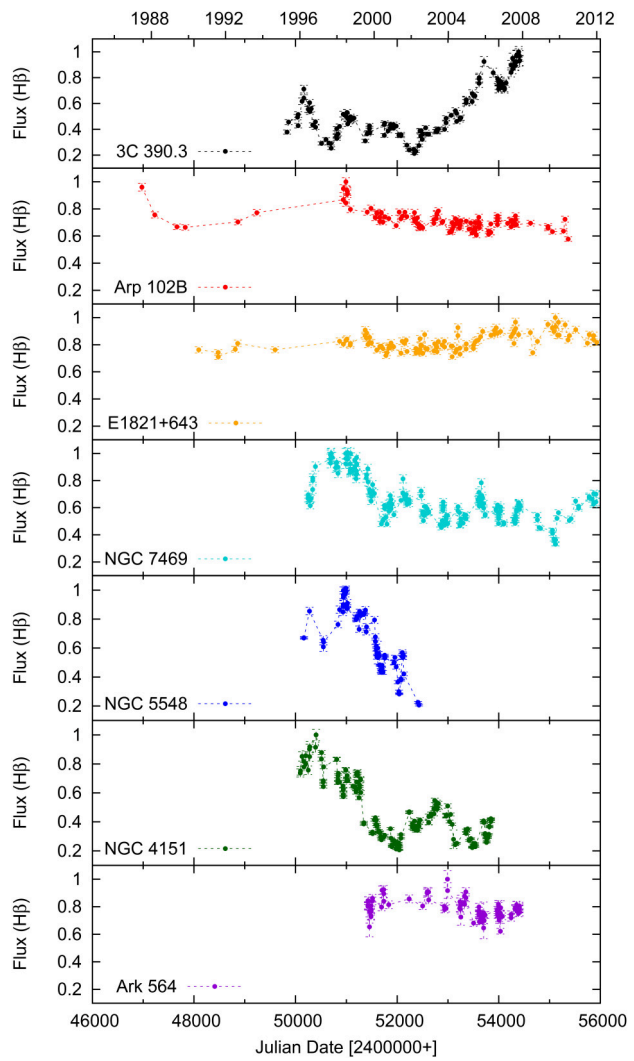

FIGURE 1 | Light curves of the Hβ line flux of all object in the sample (object name given in the bottom-left), normalized to the maximal flux for better comparison.

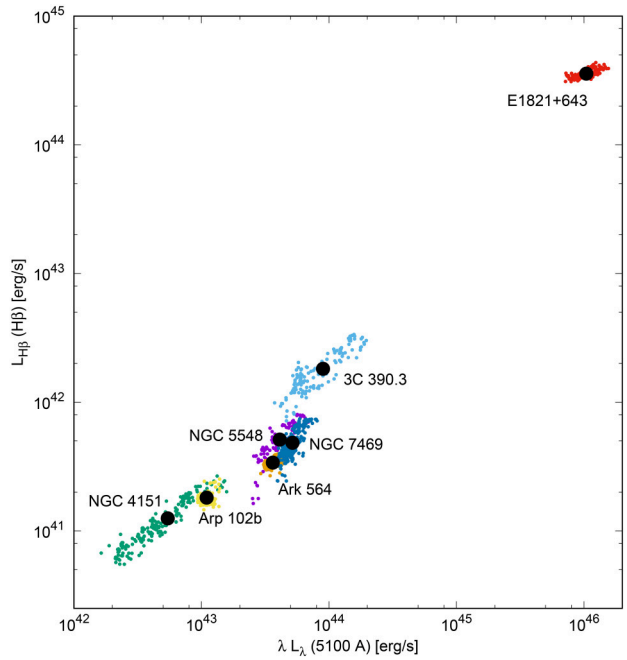

FIGURE 2 | Hβ line luminosity for all 7 objects vs. the continuum luminosity at 5100 Å (dots). The mean value is also shown (filled circle) with the object name denoted next to it.

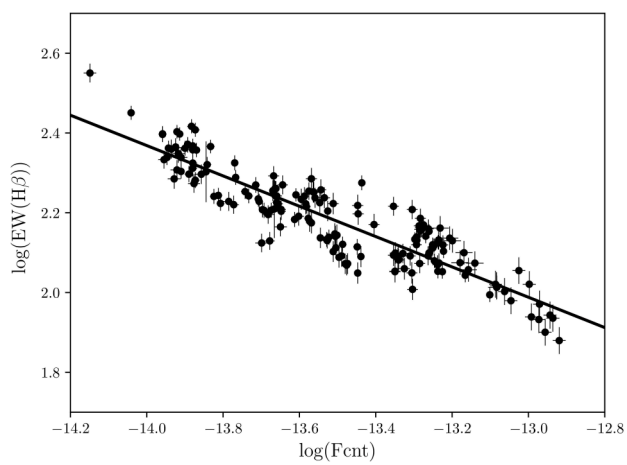

FIGURE 3 | The intrinsic Baldwin effect, i.e., the Hβ line equivalent width vs. the continuum flux at 5100 Å, in case of Seyfert 1 galaxy NGC 4151.

Table 1). This may be a result of the small number of objects in our sample, since it is well known that Seyfert galaxies, which are low luminosity type 1 AGNs have lower SMBH mass and stronger variability than quasars, which are high luminosity type 1 AGNs with much higher SMBH mass and much lower variability.

The luminosity of Hβ is following the same trend with the continuum luminosity for all objects, regardless of the luminosity. This is in support of the prediction that the photoionization by the central continuum source is mainly responsible for the heating and line production, which is one of the assumptions needed when calculating the BLR radius from reverberation mapping. However, if considering a single object, the correlation between the line and continuum emission can be violated, which is seen in the case of NGC 4151 and Ark 564 (see for details Shapovalova et al., 2008, 2012, respectively). Another correlation that is present and significant is the intrinsic Baldwin effect in the Hβ line. The physical origin of this effect is still unknown (see Rakić et al., 2017, for discussion), but some lines of evidence suggest the possibility that an additional optical continuum component, not related to the ionizing continuum, can be originated either in the BLR or in nuclear outflows, thus influencing the slope of the Hβ - continuum flux relation.

However, what is intriguing is the fact that all presented objects have different line profiles (**Table 1**, column 4), indicating that the geometry of the broad line-emitting region is probably

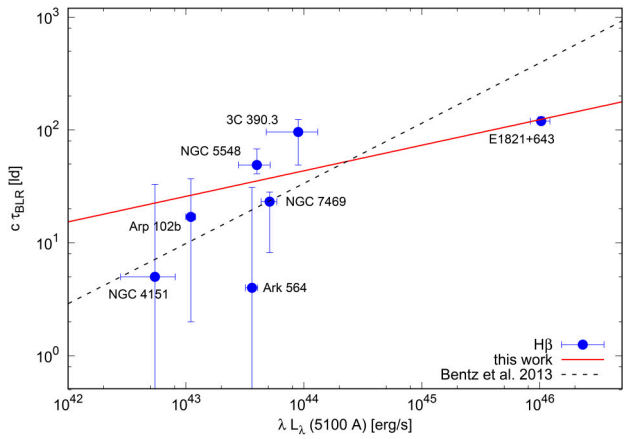

FIGURE 4 | The radius of the broad Hβ line emitting-region vs. the continuum luminosity at 5100 Å. The dashed line gives the BLR radius-luminosity scaling relation from Bentz et al. (2013) with $R_{\rm BLR} \sim L^{0.533}$, whereas the solid line is the fit through seven objects from this study, with $R_{\rm BLR} \sim L^{0.226}$. We note that the fit is strongly influenced from the one point, the luminous quasar E1821+643, and without that point the relation is consistent with the Bentz et al. (2013) result.

different. For example, in case of 3C 390.3 it is clear that the BLR is following the accretion disk geometry (Popović et al., 2011), whereas in case of the other double-peak line emitter Arp 102B this is maybe not the case (Popović et al., 2014). Also, the Seyfert galaxies NGC 4151 and NGC 5548 could host a binary SMBH with two separate BLR (Bon et al., 2012, 2016; Li et al., 2016), which puts more uncertainty on their mass estimates from reverberation mapping. Finally, the quasar E1821+643 is much below the theoretical radius-luminosity relation predicted by the photoionization theory ($R_{\rm BLR} \propto L^{0.5}$), and very low-variable AGN in the optical lines and continuum, therefore this SMBH mass estimate is also more uncertain. The peculiarity of the BLR of this quasar is probably the reason why the slope of the radius-luminosity scaling relation is much smaller than Bentz et al. (2006) relation. It is worth noticing that in **Figure 4**, if we discard Ark 564 (with very narrow lines that are not typical for type 1 AGNs and with a very large error-bars in estimated time-delays) and E1821+643 (a quasar with an outstanding luminosity), the remaining objects will apparently closely follow the dependence of Bentz et al. (2013).

We summarize here the main conclusions of this study:

(i) the rate of variability is not connected with the geometry of the BLR and mass of the SMBH (e.g., Arp 102B and 3C390.3), however in case of the SMBH mass this may be a result of the small number of objects in our sample;
(ii) the luminosity of Hβ is correlated with the continuum luminosity for all AGN in our sample, and the intrinsic Baldwin effect is present;
(iii) the photoionization is in general the main line-production mechanism, however in some AGN (e.g., NGC 4151) there are some additional mechanism which contribute to the line (continuum) emission.

Finally we can conclude that the long-term spectroscopic monitoring campaigns are very important for the investigation of the BLR structure and the SMBH mass estimates.

AUTHOR CONTRIBUTIONS

All authors listed have made a substantial, direct and intellectual contribution to the work, and approved it for publication.

FUNDING

RFBR (grants N97-02-17625 N00-02-16272, N03-02-17123, 06-02-16843, N09-02-01136, 12-02-00857a, 12-02-01237a, N15-02-02101); Ministry of Education, Science, Technology and Development, Republic of Serbia (project 176001 "Astrophysical Spectroscopy of Extragalactic Objects"); INTAS (grant N96-0328); DFG grants Ko857/32-2 and Ko857/33-1; Ministry of Science and Technology of R. Srpska (project "Investigation of supermassive binary black holes in the optical and X-ray spectra").

REFERENCES

Alexander, T. (1997). "Is AGN variability correlated with other AGN properties? ZDCF analysis of small samples of sparse light curves," in *Astronomical Time Series, Vol. 218 of Astrophysics and Space Science Library*, eds D. Maoz, A. Sternberg, and E. M. Leibowitz, (Dordrecht: Springer), 163.

Baldwin, J. A. (1977). Luminosity indicators in the spectra of quasi-stellar objects. *Astrophys. J.* 214, 679–684. doi: 10.1086/155294

Bentz, M. C., Denney, K. D., Grier, C. J., Barth, A. J., Peterson, B. M., Vestergaard, M., et al. (2013). The low-luminosity end of the radius-luminosity relationship for active galactic nuclei. *Astrophys. J.* 767:149. doi: 10.1088/0004-637X/767/2/149

Bentz, M. C., Peterson, B. M., Pogge, R. W., Vestergaard, M., and Onken, C. A. (2006). The radius-luminosity relationship for active galactic nuclei: the effect of host-galaxy starlight on luminosity measurements. *Astrophys. J.* 644, 133–142. doi: 10.1086/503537

Blandford, R. D., and McKee, C. F. (1982). Reverberation mapping of the emission line regions of seyfert galaxies and quasars. *Astrophys. J.* 255, 419–439. doi: 10.1086/159843

Bon, E., Jovanović, P., Marziani, P., Shapovalova, A. I., Bon, N., Borka Jovanović, V., et al. (2012). The first spectroscopically resolved sub-parsec orbit of a supermassive binary black hole. *Astrophys. J.* 759:118. doi: 10.1088/0004-637X/759/2/118

Bon, E., Zucker, S., Netzer, H., Marziani, P., Bon, N., Jovanović, P., et al. (2016). Evidence for periodicity in 43 year-long monitoring of NGC 5548. *Astrophys. J. Suppl. Ser.* 225:29. doi: 10.3847/0067-0049/225/2/29

Gaskell, C. M. (1988). Direct evidence for gravitational domination of the motion of gas Within one light-week of the central object in NGC 4151 and the determination of the mass of the probable black hole. *Astrophys. J.* 325, 114–118. doi: 10.1086/165986

Gaskell, C. M., and Sparke, L. S. (1986). Line variations in quasars and Seyfert galaxies. *Astrophys. J.* 305, 175–186. doi: 10.1086/164238

Ilić, D., Popović, L. Č., Shapovalova, A. I., Burenkov, A. N., Chavushyan, V. H., and Kovačević, A. (2015). Line shape variability in a sample of AGN with broad lines. *J. Astrophys. Astron.* 36, 433–445. doi: 10.1007/s12036-015-9360-y

Jovanović, P., Popović, L. Č., Stalevski, M., and Shapovalova, A. I. (2010). Variability of the Hβ line profiles as an indicator of orbiting bright spots in

accretion disks of quasars: a case study of 3C 390.3. *Astrophys. J.* 718, 168–176. doi: 10.1088/0004-637X/718/1/168

Kovačević, J., Popović, L. Č., and Dimitrijević, M. S. (2010). Analysis of optical Fe II emission in a sample of active galactic nucleus spectra. *Astrophys. J. Suppl.* 189, 15–36. doi: 10.1088/0067-0049/189/1/15

Kovačević, A., Popović, L. Č., Shapovalova, A. I., and Ilić, D. (2017). Periodicity in the continua and broad line curves of a quasar E1821+643. *Astrophys. Space Sci.* 362:31. doi: 10.1007/s10509-017-3009-z

Kovačević, A., Popović, L. Č., Shapovalova, A. I., Ilić, D., Burenkov, A. N., and Chavushyan, V. H. (2014). Time series analysis of active galactic nuclei: the case of Arp 102B, 3C 390.3, NGC 5548 and NGC 4051. *Adv. Space Res.* 54, 1414–1428. doi: 10.1016/j.asr.2014.06.025

Li, Y.-R., Wang, J.-M., Ho, L. C., Lu, K.-X., Qiu, J., Du, P., et al. (2016). Spectroscopic indication of a centi-parsec supermassive black hole binary in the galactic center of ngc 5548. *Astrophys. J.* 822:4. doi: 10.3847/0004-637X/822/1/4

Lyutyi, V. M., and Cherepashchuk, A. M. (1972). Narrow-band photoelectric observations of Hα-line variability in the nuclei of Seyfert galaxies NGC 4151, 3516, 1068. *Astronomicheskij Tsirkulyar* 688.

O'Brien, P. T., Dietrich, M., Leighly, K., Alloin, D., Clavel, J., Crenshaw, D. M., et al. (1998). Steps toward determination of the size and structure of the broad-line region in active galactic nuclei. XIII. ultraviolet observations of the broad-line radio galaxy 3C 390.3. *Astrophys. J.* 509, 163–176. doi: 10.1086/306464

Onken, C. A., Ferrarese, L., Merritt, D., Peterson, B. M., Pogge, R. W., Vestergaard, M., et al. (2004). Supermassive black holes in active galactic nuclei. II. calibration of the black hole mass-velocity dispersion relationship for active galactic nuclei. *Astrophys. J.* 615, 645–651. doi: 10.1086/424655

Osterbrock, D. E., and Ferland, G. J. (2006). *Astrophysics of Gaseous Nebulae and Active Galactic Nuclei*. Sausalito, CA: University Science Books.

Peterson, B. M., and Horne, K. (2006). "Reverberation mapping of active galactic nuclei," in *Planets to Cosmology*, eds M. Livio and S. Casertano (Cambridge, UK: Cambridge University Press), 89.

Pogge, R. W., and Peterson, B. M. (1992). The intrinsic nature of the Baldwin effect. *Astronom. J.* 103, 1084–1088. doi: 10.1086/116127

Popović, L. Č., Mediavilla, E., Bon, E., and Ilić, D. (2004). Contribution of the Disk Emission to the Broad Emission Lines in AGNs: Two-component model. *Astron. Astrophys.* 423, 909–918. doi: 10.1051/0004-6361:20034431

Popović, L. Č., Shapovalova, A. I., Ilić, D., Burenkov, A. N., Chavushyan, V. H., Kollatschny, W., et al. (2014). Spectral optical monitoring of the double-peaked emission line AGN Arp 102B. II. Variability of the broad line properties. *Astron. Astrophys.* 572:A66. doi: 10.1051/0004-6361/201423555

Popović, L. Č., Shapovalova, A. I., Ilić, D., Kovačević, A., Kollatschny, W., Burenkov, A. N., et al. (2011). Spectral optical monitoring of 3C 390.3 in 1995-2007. II. Variability of the spectral line parameters. *Astron. Astrophys.* 528:A130. doi: 10.1051/0004-6361/201016317

Rakić, N., La Mura, G., Ilić, D., Shapovalova, A. I., Kollatschny, W., Rafanelli, P., et al. (2017). The intrinsic Baldwin effect in broad Balmer lines of six long-term monitored AGNs. *Astron. Astrophys.* 603:A49. doi: 10.1051/0004-6361/201630085

Robinson, A., Young, S., Axon, D. J., Kharb, P., and Smith, J. E. (2010). Spectropolarimetric evidence for a kicked supermassive black hole in the Quasar E1821+643. *Astrophys. J. lett.* 717, L122–L126. doi: 10.1088/2041-8205/717/2/L122

Shapovalova, A. I., Burenkov, A. N., Carrasco, L., Chavushyan, V. H., Doroshenko, V. T., Dumont, A. M., et al. (2001). Intermediate resolution Hβ spectroscopy and photometric monitoring of 3C 390.3. I. Further evidence of a nuclear accretion disk. *Astron. Astrophys.* 376, 775–792. doi: 10.1051/0004-6361:20011011

Shapovalova, A. I., Doroshenko, V. T., Bochkarev, N. G., Burenkov, A. N., Carrasco, L., Chavushyan, V. H., et al. (2004). Profile variability of the Hα and Hβ broad emission lines in NGC 5548. *Astron. Astrophys.* 422, 925–940. doi: 10.1051/0004-6361:20035652

Shapovalova, A. I., Popović, L. Č., Burenkov, A. N., Chavushyan, V. H., Ilić, D., Kollatschny, W., et al. (2010a). Spectral optical monitoring of 3C 390.3 in 1995-2007. I. Light curves and flux variation in the continuum and broad lines. *Astron. Astrophys.* 517:A42. doi: 10.1051/0004-6361/201014118

Shapovalova, A. I., Popović, L. Č., Burenkov, A. N., Chavushyan, V. H., Ilić, D., Kollatschny, W., et al. (2013). Spectral optical monitoring of a double-peaked emission line AGN Arp 102B. Variability of spectral lines and continuum. *Astron. Astrophys.* 559:A10. doi: 10.1051/0004-6361/201321781

Shapovalova, A. I., Popović, L. Č., Burenkov, A. N., Chavushyan, V. H., Ilić, D., Kovačević, A., et al. (2010b). Long-term variability of the optical spectra of NGC 4151. II. Evolution of the broad Hα and Hβ emission-line profiles. *Astron. Astrophys.* 509:A106. doi: 10.1051/0004-6361/200912311

Shapovalova, A. I., Popović, L. Č., Burenkov, A. N., Chavushyan, V. H., Ilić, D., Kovačević, A., et al. (2012). Spectral Optical Monitoring of the Narrow-line Seyfert 1 Galaxy Ark 564. *Astron. Astrophys. Suppl. Ser.* 202:10. doi: 10.1088/0067-0049/202/1/10

Shapovalova, A. I., Popović, L. Č., Chavushyan, V. H., Afanasiev, V. L., Ilić, D., Kovačević, A., et al. (2017). Long-term optical spectral monitoring of NGC 7469. *Month. Notices R. Astronom. Soc.* 466, 4759–4775. doi: 10.1093/mnras/stx025

Shapovalova, A. I., Popović, L. Č., Chavushyan, V. H., Burenkov, A. N., Ilić, D., Kollatschny, W., et al. (2016). First long-term optical spectral monitoring of a binary black hole candidate E1821+643. I. Variability of spectral lines and continuum. *Astron. Astrophys. Suppl. Ser.* 222:25. doi: 10.3847/0067-0049/222/2/25

Shapovalova, A. I., Popović, L. Č., Collin, S., Burenkov, A. N., Chavushyan, V. H., Bochkarev, N. G., et al. (2008). Long-term variability of the optical spectra of NGC 4151. I. Light curves and flux correlations. *Astron. Astrophys.* 486, 99–111. doi: 10.1051/0004-6361:20079111

Wright, E. L. (2006). A cosmology calculator for the World Wide Web. *Astronom. Soc. Pacific* 118, 1711–1715. doi: 10.1086/510102

Conflict of Interest Statement: The authors declare that the research was conducted in the absence of any commercial or financial relationships that could be construed as a potential conflict of interest.

The reviewer ALL declared a shared affiliation, with no collaboration, with one of the authors, VC, to the handling Editor.

Copyright © 2017 Ilić, Shapovalova, Popović, Chavushyan, Burenkov, Kollatschny, Kovačević, Marčeta-Mandić, Rakić, La Mura and Rafanelli. This is an open-access article distributed under the terms of the Creative Commons Attribution License (CC BY). The use, distribution or reproduction in other forums is permitted, provided the original author(s) or licensor are credited and that the original publication in this journal is cited, in accordance with accepted academic practice. No use, distribution or reproduction is permitted which does not comply with these terms.

frontiers in Astronomy and Space Sciences

ORIGINAL RESEARCH
published: 01 June 2018
doi: 10.3389/fspas.2018.00019

Exploring Possible Relations Between Optical Variability Time Scales and Broad Emission Line Shapes in AGN

Edi Bon [1], Predrag Jovanović [1], Paola Marziani [2], Nataša Bon [1] and Aleksandar Otašević [1]*

[1] Astronomical Observatory, Belgrade, Serbia, [2] Osservatorio Astronomico di Padova (INAF) Padua, Padova, Italy

Here we investigate the connection of broad emission line shapes and continuum light curve variability time scales of type-1 Active Galactic Nuclei (AGN). We developed a new model to describe optical broad emission lines as an accretion disk model of a line profile with additional ring emission. We connect ring radii with orbital time scales derived from optical light curves, and using Kepler's third law, we calculate mass of central supermassive black hole (SMBH). The obtained results for central black hole masses are in a good agreement with other methods. This indicates that the variability time scales of AGN may not be stochastic, but rather connected to the orbital time scales which depend on the central SMBH mass.

Keywords: galaxies, active-galaxies, quasar, supermassive black holes, quasar, emission lines, line, profiles

OPEN ACCESS

Edited by:
Deborah Dultzin, Universidad Nacional Autónoma de México, Mexico

Reviewed by:
Omaira Gonzàlez Martín, Instituto de Radioastronomía y Astrofísica, Mexico
Milan S. Dimitrijevic, Astronomical Observatory, Serbia

****Correspondence:***
Edi Bon
ebon@aob.bg.ac.rs

Specialty section:
This article was submitted to Milky Way and Galaxies, a section of the journal Frontiers in Astronomy and Space Sciences

Received: *29 November 2017*
Accepted: *11 May 2018*
Published: *01 June 2018*

Citation:
Bon E, Jovanović P, Marziani P, Bon N and Otašević A (2018) Exploring Possible Relations Between Optical Variability Time Scales and Broad Emission Line Shapes in AGN. Front. Astron. Space Sci. 5:19. doi: 10.3389/fspas.2018.00019

1. INTRODUCTION

Type-1 Active Galactic Nuclei (AGN) are very powerful and variable emitters. The continuum emission in radio-quiet AGN is assumed to originate mainly from an accretion disk (AD) around a central supermassive black hole (SMBH) (Lynden-Bell, 1969; Shakura and Sunyaev, 1973). There is consensus that the accretion disk can be represented as virialized (rotating) gas in a flattened distribution following a Keplerian velocity field.

The optical broad emission lines (BELs) are assumed to be produced with photoionization processes (Netzer, 2013), as they respond to the variations of UV continuum. The accretion disk itself may be a low-ionization line emitter (see e.g., Chen and Halpern, 1989; Chen et al., 1989; Eracleous and Halpern, 1994; Popović et al., 2004; Bon et al., 2006, 2009a,b, 2015; Gavrilović et al., 2007; Bon, 2008), if part of the continuum radiation is scattered toward it. The optical broad line light curves (like for e.g., Hα) are highly correlated with the optical continuum light curves (e.g., Kaspi et al., 2000). The time lags between correlated patterns in the continuum and Hα flux are of the order of days, up to months, defining the size of broad line region (BLR). Reverberation mapping campaigns are based on this fact, and they measure time lags of correlated light curves in order to determine the sizes of reverberating region (which are after used for determination of central BH masses) in AGN (see e.g., Peterson, 1997; Kaspi et al., 2000; Peterson et al., 2002; Denney et al., 2009). The correlation of light curves might indicate that the signature of the main driver of the variability could be detected in the shape of the broad emission line profiles. This could give us the velocity resolved information about processes that drive the variability.

The shape of Balmer emission lines, particularly Hα and Hβ line profile, in many AGN could be described as similar to the shape of an AD line profile expected to originate from flattened distribution of rotating emitting gas. Characteristic double peaked very broad profile, are usually seen in simulated emission line profiles (see for e.g., Chen and Halpern, 1989; Chen et al., 1989; Eracleous and Halpern, 1994; Newman et al., 1997; Čadež et al., 1998; Popović et al., 2003, 2004; Bon et al., 2006, 2009a,b; Bon, 2008; Jovanović et al., 2010) but are observed only in one percent of AGN (Eracleous and Halpern, 1994; Strateva et al., 2003; Netzer, 2013). In typical, single peaked BEL profiles, the AD contributions could be blended by surrounding isotropic velocity component in the BLR (Popović et al., 2003, 2004; Bon et al., 2006, 2009a; Collin et al., 2006; Gavrilović et al., 2007; Bon, 2008). In some cases, broad Hα and Hβ line profiles show a red side more broadened and extended further into the red part of the spectrum, that could be associated with gravitational redshift (see e.g., Bon et al., 2015, and references therein). In case the blue side of a line is more extended, the contribution is usually assumed to be from the winds or outflows (see Marziani et al., 1996; Czerny, 2006; Collin et al., 2006; Sulentic et al., 2007).

Even though long term monitoring campaigns of AGN may still not be long enough to search for periodic variability (Bon et al., 2017), there are some highly monitored cases for which some claims of detecting significant periodicity have been made (see for example Bon et al., 2012, 2016, 2017; Graham et al., 2015a,b; Bhatta et al., 2016; Charisi et al., 2016). Currently, there are some ongoing campaigns of extensive monitoring programs (see e.g., Peterson et al., 2002; Gezari et al., 2007; Sergeev et al., 2007; Ilić et al., 2017) that may provide valuable light curves for the future variability investigations.

Here we explore a possibility that ripples in the observed broad optical emission line profiles may be in connection with variability time scales observed in optical continuum light curves. We present a case study of Arp 102B, using spectra and light curves from Shapovalova et al. (2013). Our hypothesis is that the variability patterns in the light curves may be induced by the orbiting of perturbers "perturbation" (a hot spot, a spiral arm, a compact body such as a stellar mass object or even up to intermediate mass black hole) within the accretion disk (see more i, for e.g., Chakrabarti and Wiita, 1994; Lin and Papaloizou, 1996; Newman et al., 1997; Gezari et al., 2007; Flohic and Eracleous, 2008; Jovanović et al., 2010; McKernan et al., 2012). Using the AD model with additional emitting rings (separated with gaps), developed specially for this purpose, we match the synthetic broad emission line profiles to the observed Hα line, in order to measure the ring radii. We connect variability time scales, with radii, and calculate the central BH mass.

The paper is organized as follows: first, we present the method (section 2) of measuring the radii that could be paired with variability time scales from light curves. For that purpose we developed a model of an AD emission with additional enhanced thin rings (section 2.1). We used data (spectra and light curves) available in Shapovalova et al. (2013). We match the AD model to the observed Hα broad emission line and measure the ring radii that we connect to optical variability time scales. We analyze optical light curves, find variability time scales that we match with measure ring radii, and calculate the mass of the SMBH as a test of our hypothesis (section 3). We discuss possible mechanisms in section 4. In the last section 5, we point out the main conclusions of our investigation.

2. METHOD

Light curves of an optical continuum and broad emission line flux are highly correlated (Kaspi et al., 2000). This may indicate the same origin of their variability source. Therefore, one could expect that the source of variability could leave a trace in the shapes of their broad line profile shape. Analysis of variation time scales may give us valuable information about why they vary the way they do, while the line profiles could provide us with the information about the kinematic parameters of the variability drive (like the radii where the source of variation is located).

In order to investigate the variability time scales of optical continuum light curves, we use standard methods like Lomb-Scargle (Lomb, 1976; Scargle, 1982), and sine function fitting, that we use here to determine variability time scales. Here we assume that the variability time scales corresponds to the orbital time scales within the region of AD where the optical light could be originating from (see e.g., Bon et al., 2012, 2016). Ripples in the broad emission line profiles could be produced by the effects of the same phenomena that drives the variability (Eracleous and Halpern, 1994; McKernan et al., 2013). If we detect them, we would then be able to determine some dynamical properties (see for e.g., Newman et al., 1997; Gezari et al., 2007). In case we could identify more then one variability time scale period in the light curves that could be linked to the radius of an emitting ring in the broad emission line profile, then for each ring-radius pair we should expect to obtain the same mass (or at least very close value) of the central SMBH using Kepler's laws.

In order to test these assumptions, as a first step we model synthetic line emission of an orbiting gas in the flat, disk like gas distribution, assuming that photo ionization process produces the emission line from that region, that we could approximate with the accretion disk emission model (Chen and Halpern, 1989; Chen et al., 1989; Eracleous and Halpern, 1994; Čadež et al., 1998; Jovanović and Popović, 2008; Jovanović et al., 2010; Bon et al., 2015).

By matching the AD model to the H_α broad emission line profile, we determine the inclination, inner and outer radii and additional ring radii. The inner radius is defined by matching the far red and blue wings of the observed line profile to the red wing of AD model line shape. The red wing part is most sensitive to the and gravitational redshift effect (see e.g., Bon et al., 2015), and therefore the extension of the red side of the line wing determines how close to the BH the gas is emitting the optical Balmer lines. We note that we determine the inner radius of an AD of the Hα broad line from the fit of the model, and that the inner radius in gravitational units is usually $\gtrsim 100$, much larger than the inner

radius derived from X-ray lines (like Fe K_α), usually close to the innermost stable circular orbit, 1 to 6 gravitational radii (for AD size of the optical emission lines, see for e.g., Chen and Halpern, 1989; Chen et al., 1989; Eracleous and Halpern, 1994; Popović et al., 2004; Bon et al., 2006, 2009a,b, 2015; Gavrilović et al., 2007; Bon, 2008). The part of the disk that contributes to the thermal continuum emission is the one of highest temperature, also close to the the innermost stable circular orbit (Lynden-Bell, 1969; Shakura and Sunyaev, 1973). This region is expected to be much closer to the black hole than the AD region suitable for the optical emission line emission. From the fit of the model to the observed broad line we determine inner and outer radius of the AD and each ring as well as the inclination and emissivity law that is common parameter for the complete model.

Simulated profiles of AD emission usually have characteristic two peaks in the core of the line, are broadened due to virial motion and made asymmetric by relativistic effects. The two peaks are usually blended by the isotropic emission component in the core of the line profile, originated further away from the AD, which is observed in majority of AGN spectra (Popović et al., 2003, 2004; Popovic et al., 2008; Bon et al., 2006, 2009a; Bon, 2008). Only in a very small number (less then 1%) of objects the two peaks are clearly recognized (see e.g., Strateva et al., 2003).

Small bump-like features can be found on the BEL profiles. They cannot be immediately modeled by smooth AD profiles.

2.1. Model of AD With Additional Ring Emission or AD With Ring Gaps

The AD model is an idealization of emission with assumption of an homogeneous AD. This may not be the case, and therefore the AD profile may not sufficient to describe all features in observed profiles like e.g., small bumps on the wings which are often present.

Assuming that the time scale of perturbed disk (cooling time, shock wave progression, or anything that produced additional emission from that ring) is significantly longer then the orbital time scale, then we could approximate that the time scale of variations measured in optical light curves correspond to the orbiting of some features within the AD at radii that could be associated to narrow rings that we located in AD by matching the observed emission lines with synthetic modeled profiles. Their radii are measured in units of gravitational radii Rg, since from the AD model we cannot obtain the information about the central mass. By connecting each variability time scale to some radii in the AD, with an assumption that the shorter variability time scale corresponds to a closer ring, while the outer radii correspond to a longer variability time scale, we could be able to calculate the mass of the central SMBH[1] using the Kepler's third law for a circular orbit:

$$P = 2\pi\sqrt{\frac{r^3}{GM}} = \frac{2\pi GM\xi^{3/2}}{c^3}, \quad (1)$$

[1]This is similar as in the case of planetary system where all orbiting objects radii and periods correspond to the same mass of the central body.

where $r = \xi(r_g)$ is the ring radius in gravitational radii and P is the circular orbital period of the orbiting region at such radii (as prposed in Newman et al., 1997; Gezari et al., 2007). We note here that regardless of the formula, our method is different then the method of Newman et al. (1997). These authors used monitoring spectra to determine the radius of a hot spot, which they then connected to the orbiting period. Here we use single epoch spectra and variability time scales measured from photometric data.

We use different AD model than in previous papers (Chen and Halpern, 1989; Chen et al., 1989; Antonucci et al., 1996; Newman et al., 1997; Gezari et al., 2007), even though we obtain similar values of parameters for the inclinations and the inner and outer radius. Here we use the relativistic ray tracing AD model[2] We propose that the origin of the variability patterns, could be traced to the ripples in the shape of broad line profiles. Making a connection of variability time scales and radii, Equation (1) can be used to determine dynamical properties of AGN.

We construct our model assuming the emission of an AD and each ring contributions to the line profiles with the same inclination and emissivity law as in the parent AD, which is preserved in ring models. The code includes both special relativistic and general relativistic effects on radiation from the accretion disk around SMBH (see e.g., Jovanović, 2012). This AD model is based on ray-tracing method in the Kerr metric (Fanton et al., 1997; Čadež et al., 1998), for different values of inner and outer radii and inclinations of rings in AD. The emissivity index was kept to be close as possible to the value $q = -2$, assuming the emissivity law to be $\sim r^q$, as expected for the case of photo-ionization mechanism. The model is then constructed using a previous match of the AD profile to the emission line, as a starting point. The scaled contributions of the ring profiles are added to the AD profile until bumpy features in observed spectra are described with the synthetic spectrum. Beside the fact that the shape of the line is fitted more realistic then with a simple AD model, we are also obtaining a valuable information about the radii in the disk plane where the emission is emitted from.

We considered our model as analogy to AD in which the emission is not continuous from R_{min} to R_{max}, but instead is restricted to emission emission annuli. The physical justification of disk gaps can reside on the removal of the gas disk in systems in which the the emission is not contributing to the emission line shape due to obscuration by dust in the outscirt of BLR (Bon et al., 2016) or by voids produced due to accreting secondary object within the AD plane (Lin and Papaloizou, 1996; Lin, 1997), or in case where gas was originally counterrotating with respect to the black hole spin (Vorobyov et al., 2016), or by an accreting object in the disk plane (Artymowicz et al., 1993). In this case, the disk profile is modeled by the addition of several emission annuli (assuming the same AD model and one inclination value). The

[2]We tested several different AD models (Fanton et al., 1997; Čadež et al., 1998; Jovanović and Popović, 2008; Jovanović, 2012; Bon et al., 2015) for a line fit, and find that obtained inclinations were practically the same regardless of the model used and also if we adopt more complex model, assuming the additional rings with the same AD parameters (inclination and emissivity law).

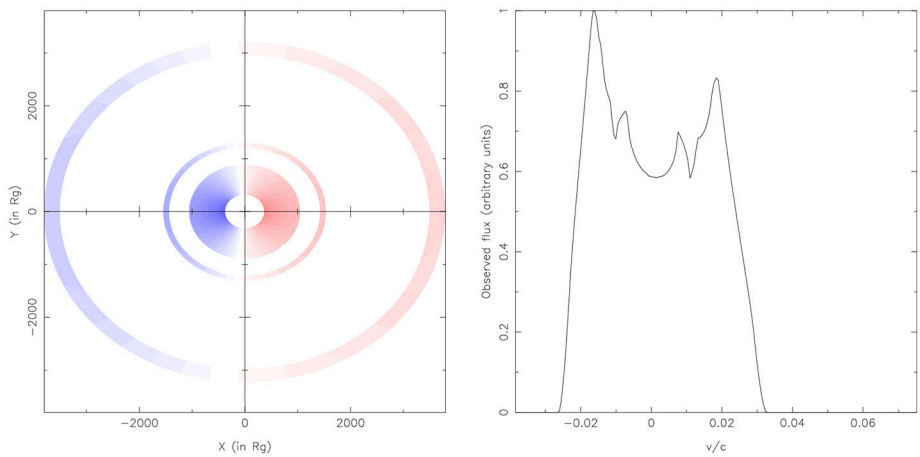

FIGURE 1 | An examples of AD + 2 outer rings (left panel) with corresponding shape of broad line profile, matched to Hα line of Arp 102B in 2.

analysis of the line profile is otherwise analogous to the excess ring emission model.

3. RESULTS

In order to test this our model interpretation of the BEL profiles, we performed a case study of Arp 102B because it is well-known for its broad emission lines with double peaked shape that was already proposed to correspond to the AD emission profile (Chen and Halpern, 1989; Chen et al., 1989; Sulentic et al., 1990; Eracleous and Halpern, 1994; Antonucci et al., 1996; Newman et al., 1997; Sergeev et al., 2000; Gezari et al., 2007; Jovanović et al., 2010; Popović et al., 2014).

Using the line profile matching to the model, we measure the ring radii that we connect to the variability time scales.

Assuming that the orbital time scale is the only match to time scale of variability patterns seen in these light curves, we combine measured radii ξ and variability scale periods, and derive mass assuming circular Keplerian orbit of this variable region positioned within the AD[3].

We measured ξ radii with an AD model in units of gravitational radii (R_g) from the broad emission line profiles. If two or more significant periods were detected, assuming a low cut taken to be at 400 days period (in order to avoid effects of Earth's orbital period of 1 year), then we try to pair the to the parts of an AD which could be perturbed, like inner and outer radius of a ring or a main part of AD, where the interaction with different state medium could be expected[4]. We test the assumption by calculating the mass of the central BH following Equation (1), with expectation that the obtained results for masses, for each pair of variability time scale and the ring radius, should be equal, or at least to be of similar values.

The example of the model (**Figure 1**) matched to the observed spectrum of the object Arp 102B is presented in **Figure 2**. The inclination is 32 degrees, and the AD is truncated in the following rings: 370–1050, 1430–1540, and 3500–3800 Rg, with the emissivity parameter q = −2.1 over the whole model. We note that the result is very similar to other fits of this object (Chen and Halpern, 1989; Chen et al., 1989; Newman et al., 1997), who obtained the same inclination while the complete disk was assumed to correspond to main part of AD in our model, with Rinn =350 Rg, and Rout =1000 Rg[5]. The measurement of variability time scales of light curves is shown in the **Figure 3**. We find the longer time scale to be about 14 years period (intrinsically 5250 days, after correction for the systematic redshift), while the shorter time scale is taken from earlier variability analysis (Newman et al., 1997; Sergeev et al., 2000; Shapovalova et al., 2013), where the variability time scale was found to be of about 700 days (in the interval 650–750 days, here taken as 680 after scaling for the redshift).

We assume that the variability is produced sharp edges of gaps and emitting rings. By matching the inner radius of AD to the corresponding variability time scale (370 Rg with 680 days), and 1500 Rg with 5255 days variability time scale), we obtain the mass of about 2.7 $\cdot 10^8$ M$\odot$ (as an average of these two values: 2.68 $\cdot 10^8$ and 2.71 $\cdot 10^8$ M$\odot$). This value is very close to the value of with 2.1 $\cdot 10^8$ M$\odot$ in Newman et al. (1997, obtained from the orbiting hotspot assumption) and not so different from 3.5 $\cdot 10^8$ M$\odot$ suggested in Sergeev et al. (2000, obtained with the model of thousands randum orbiting clouds, mached to the radial velocity maps of broad line variability), and about two times higher then the mass value of 1.1 $\cdot 10^8$ M$\odot$ as suggested in Shapovalova et al. (2013).

[3]It is important to stress that emission lines do respond to continuum changes on a timescale that is $\tau \ll P$ (months vs. 10 years), but this should not invalidate our argument right because the reverberation response τ is much smaller than P, which is the orbital period at radius ξ.

[4]We note that the expected orbital periods in optical part of the AD for typical AGN of M $\sim 10^8$ $M_\odot$ should be about 1 year (see for e.g., Gaskell, 2008), but this should not be a problem since also longer periods are detected.

[5]We note that at about the same radius was obtained as outer radius of AD in previous disk models (Chen and Halpern, 1989; Chen et al., 1989; Newman et al., 1997).

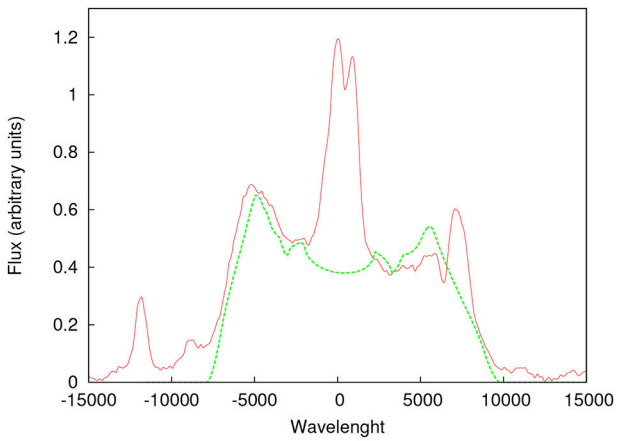

FIGURE 2 | An example of AD + rings model matching the observed broad Hα emission line profiles. Here is presented the case of Arp 102B.

The virial product $r\delta v_r{}^2/G$ can then be obtained from the 20 day lag of line flux to continuum Shapovalova et al. (2013), and following the formula form Collin et al. (2006) for radial velocity dispersion in case of rectangular shape[6] line profile δv_r = 14500 / 3.46 ≈ 4,190 km s^{-1}. The virial factor f can then be estimated by computing $r\delta v_r{}^2/G/M_{BH,P} = 1/f$, where $M_{BH,P}$ is the black hole mass computed from the P following Equation 1. Using these values we derive $1/f = 7.36 \cdot 10^7/(2.7 \cdot 10^8) \approx 0.287$. The $1/f$ should be equal to ratio of virial product and the mass[7] obtained from the period by definition, and f depends on inclination as $f \approx (sin(i))^{-2}$, resulting the inclination of 32°, which is consistent with the value from the AD model fitted to the Hα broad emission line (with our model and earlier fits as well). Therefore, not only that the model gives the consistent mass with the three different period-radii pairs, but also the retrieved inclination from the virial product gives a consistent value of inclination as the AD model fit to the Hα broad emission line.

Admittedly, our model follow from a very strong assumption: the use of variability time scale P (derived from the continuum variation) for estimating the black hole mass and the use of ξ derived from the profile ring should be consistent. The assumption may not be correct in principle, since the P obtained from the continuum may not refer to the same ξ of the profile rings. It requires *in-situ* emission at the ξ deduced from the ring.

4. POSSIBLE INTERPRETATIONS

Here we do not consider any details about what produces the hot ring regions or the dips in the AD, and we are fully aware that the measured periods are significant above the white noise levels, but may not appear significant compared to the red noise AR curves (Vaughan and Uttley, 2006; Vaughan et al., 2016). We were mainly interested in measuring time scales of orbital periods assuming that the variability patterns (Marziani et al., 2017a,b) in the light curves could be induced by the orbital time scales. Some interpretations of possible periodicities are discussed in many works (Chakrabarti and Wiita, 1994; Eracleous and Halpern, 1994; Newman et al., 1997; Gezari et al., 2007; Popović, 2012; Graham et al., 2015a,b; Bon et al., 2016, 2017; Charisi et al., 2016; Li et al., 2016; Liu et al., 2016). Assuming circular orbits in the disk as we did here, we suggest that possible source of optical variability should be located in the AD, amplifying emission at that radius. We are aware that at such radii, the standard models of thermal emission of AD (Shakura and Sunyaev, 1973) shows that the temperature of the disk is relatively low, under 1,000 K (according to the standard disk model, Shakura and Sunyaev, 1973), which is not sufficient enough for the photo ionization mechanism to produce optical broad emission lines, or to significantly contribute to the optical continuum flux, without additional emission mechanism, like shocks (Chakrabarti and Wiita, 1994; Eracleous and Halpern, 1994; Gezari et al., 2007), hot spot (Newman et al., 1997; Flohic and Eracleous, 2008; Jovanović et al., 2010), secondary orbiting object on a circular orbit around the central SMBH with additional accretion mechanism that is sufficient to produce significant contribution to the continuum and the line emission (see e.g., Lin and Papaloizou, 1996; Lin, 1997; McKernan et al., 2014, where they show a fast forming of intermediate mass BH's in AD with circular orbits arround the cetral SMBH). It is expected that in such cases the voids or gaps would be formed (see for e.g., McKernan et al., 2012, 2013, 2014) in the AD (similar to the planet formation in the stellar disks), with piling up of matter at the outer border of the gap ring (see, McKernan et al., 2013, and the references therein), that may represent the region that could be associated with the ring emission that we modeled here.

5. CONCLUSIONS

We simulated an AD emission profiles with additional ring regions and compared them with the observed profiles of the broad Hα emission lines. We measured variability time scales from available optical light curves. We pair each ring profile with the variability time scale. Using Kepler's third law, we then calculate central SMBH masses.

Our results show that:

1) The model of an AD with additional emitting rings or by a sequence of emission annuli separated by gaps could well describe the observed Hα emission line profiles in the case of Arp 102B.
2) Masses calculated from each pair of variability time scale and narrow ring with enhanced emission, result with very similar values providing support for the model and initial hypothesis, indicating that the features fitted in the line profiles are probably emitted in an AD (virial velocity field).

[6]line $FWHM/\sigma = 2 \times \sqrt{3} = 3.46$.

[7]$f = ((\sin(i))^2 + (H/R)^2)^{-1}$ as suggested in Netzer (2013), were H/R represents the contribution of isotropic velocity component as a ratio between the width of a disk and the radius of AD. Assuming H/R ≈ 0 the formula transforms into $f = (sin(i))^{-2}$.

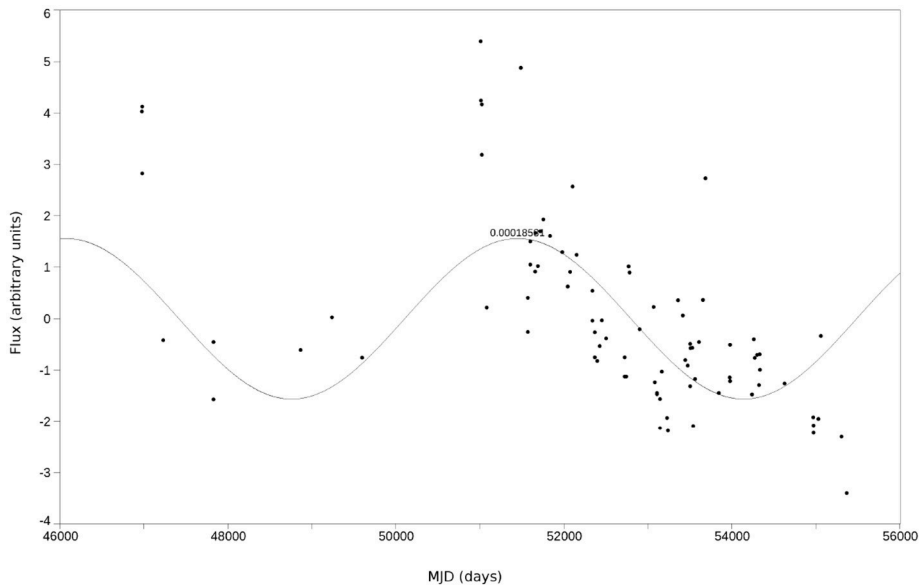

FIGURE 3 | Long term variability analysis of Arp 102B light curve after trend removal correction fitted with the sine function with the period of about 14 years.

3) We also test our model prediction from the fact that the virial factor depends on the inclination. Since, from the ratio of VP and the mass obtained with our model using Keplerian velocity, we obtain practically identical value of inclination as from the AD fit to the line profile. Therefore this gives another justification of our model.

This result may indicate that the variability time scales of AGN may be connected to the orbiting time scales which depend on the central SMBH mass.

In near future, we plan to extend the sample (Bon et al. 2018, in preparation), selecting more AGN with long term monitoring data.

AUTHOR CONTRIBUTIONS

EB is responsible for developing the idea and writing the text of the manuscript. PJ developed the code for the model. EB, NB, PJ, PM, and AO worked on analyses and discussions.

ACKNOWLEDGMENTS

This research is part of projects 176003 Gravitation and the large scale structure of the Universe and 176001 Astrophysical spectroscopy of extragalactic objects supported by the Ministry of Education and Science of the Republic of Serbia.

REFERENCES

Antonucci, R., Hurt, T., and Agol, E. (1996). Spectropolarimetric test of the relativistic disk model for the broad H alpha line of ARP 102B. *Astrophys. J. Lett.* 456:L25.

Artymowicz, P., Lin, D. N. C., and Wampler, E. J. (1993). Star trapping and metallicity enrichment in quasars and active galactic nuclei. *Astrophys. J.* 409, 592–603. doi: 10.1086/172690

Bhatta, G., Zola, S., Stawarz, Ł., Ostrowski, M., Winiarski, M., Ogłoza, W., et al. (2016). Detection of possible quasi-periodic oscillations in the long-term optical light curve of the BL Lac object OJ 287. *Astrophys. J.* 832:47. doi: 10.3847/0004-637X/832/1/47

Bon, E. (2008). The disk emission in single peaked lines for 12 AGNs. *Serbian Astron. J.* 177, 9–13. doi: 10.2298/SAJ0877009B

Bon, E., Gavrilović, N., La Mura, G., and Popović, L. Č. (2009a). Complex broad emission line profiles of AGN - Geometry of the broad line region. *New Astron. Rev.* 53, 121–127. doi: 10.1016/j.newar.2009.09.007

Bon, E., Jovanović, P., Marziani, P., Shapovalova, A. I., Bon, N., Borka Jovanović, V., et al. (2012). The first spectroscopically resolved sub-parsec orbit of a supermassive binary black hole. *Astrophys. J.* 759:118. doi: 10.1088/0004-637X/759/2/118

Bon, E., Marziani, P., and Bon, N. (2017). "Periodic optical variability of AGN," in *New Frontiers in Black Hole Astrophysics, Vol. 324 IAU Symposium*, eds A. Gomboc (Ljubljana), 176–179.

Bon, E., Popović, L. Č., Gavrilović, N., La Mura, G., and Mediavilla, E. (2009b). Contribution of a disc component to single-peaked broad lines of active galactic nuclei. *Mon. Not. R. Astron. Soc.* 400, 924–936. doi: 10.1111/j.1365-2966.2009.15511.x

Bon, E., Popović, L. Č., Ilić, D., and Mediavilla, E. (2006). Stratification in the broad line region of AGN: The two-component model. *New Astron. Rev.* 50, 716–719. doi: 10.1016/j.newar.2006.06.015

Bon, E., Zucker, S., Netzer, H., Marziani, P., Bon, N., Jovanović, P., et al. (2016). Evidence for Periodicity in 43 year-long Monitoring of NGC 5548. *Astrophys. J. Suppl.* 225:29. doi: 10.3847/0067-0049/225/2/29

Bon, N., Bon, E., Marziani, P., and Jovanović, P. (2015). Gravitational redshift of emission lines in the AGN spectra. *Astrophys. Space Sci.* 360:7. doi: 10.1007/s10509-015-2555-5

Čadež, A., Fanton, C., and Calvani, M. (1998). Line emission from accretion discs around black holes: the analytic approach. *New Astron.* 3, 647–654.

Chakrabarti, S. K. and Wiita, P. J. (1994). Variable emission lines as evidence of spiral shocks in accretion disks around active galactic nuclei. *Astrophys. J.* 434, 518–522. doi: 10.1086/174753

Charisi, M., Bartos, I., Haiman, Z., Price-Whelan, A. M., Graham, M. J., Bellm, E. C., et al. (2016). A population of short-period variable quasars from PTF as supermassive black hole binary candidates. *Mon. Not. R. Astron. Soc.* 463, 2145–2171. doi: 10.1093/mnras/stw1838

Chen, K. and Halpern, J. P. (1989). Structure of line-emitting accretion disks in active galactic nuclei - ARP 102B. *Astrophys. J.* 344, 115–124.

Chen, K., Halpern, J. P., and Filippenko, A. V. (1989). Kinematic evidence for a relativistic Keplerian disk - ARP 102B. *Astrophys. J.* 339, 742–751.

Collin, S., Kawaguchi, T., Peterson, B. M., and Vestergaard, M. (2006). Systematic effects in measurement of black hole masses by emission-line reverberation of active galactic nuclei: eddington ratio and inclination. *Astron. Astrophys.* 456, 75–90. doi: 10.1051/0004-6361:20064878

Czerny, B. (2006). "The role of the accretion disk in AGN variability," in *Astronomical Society of the Pacific Conference Series, Astronomical Society of the Pacific Conference Series, Vol. 360*, eds C. M.Gaskell, I. M. McHardy, B. M. Peterson, and S. G. Sergeev (San Francisco, CA), 265.

Denney, K. D., Peterson, B. M., Pogge, R. W., Adair, A., Atlee, D. W., Au-Yong, K., et al. (2009). Diverse kinematic signatures from reverberation mapping of the broad-line region in AGNs. *Astrophys. J. Lett.* 704, L80–L84. doi: 10.1088/0004-637X/704/2/L80

Eracleous, M. and Halpern, J. P. (1994). Doubled-peaked emission lines in active galactic nuclei. *Astrophys. J. Suppl.* 90, 1–30.

Fanton, C., Calvani, M., de Felice, F., and Cadez, A. (1997). Detecting accretion disks in active galactic nuclei. *Publ. Astron. Soc. Jpn.* 49, 159–169.

Flohic, H. M. L. G. and Eracleous, M. (2008). Interpreting the variability of double-peaked emission lines in active galactic nuclei with stochastically perturbed accretion disk models. *Astrophys. J.* 686, 138–147. doi: 10.1086/590547

Gaskell, C. M. (2008). "Accretion disks and the nature and origin of AGN continuum variability," in *Revista Mexicana de Astronomia y Astrofisica Conference Series, Vol. 32* (Huatulco), 1–11.

Gavrilović, N., Bon, E., Popović, L. Č., and Prugniel, P. (2007). "Determination of accretion disc parameters in the case of five AGN with double-peaked lines," in *Spectral Line Shapes in Astrophysics, American Institute of Physics Conference Series, Vol. 938*, eds L. C. Popovic and M. S. Dimitrijevic, 94–97.

Gezari, S., Halpern, J. P., and Eracleous, M. (2007). Long-term profile variability of double-peaked emission lines in active galactic nuclei. *Astrophys. J. Suppl.* 169, 167–212. doi: 10.1086/511032

Graham, M. J., Djorgovski, S. G., Stern, D., Drake, A. J., Mahabal, A. A., Donalek, C., et al. (2015a). A systematic search for close supermassive black hole binaries in the Catalina Real-time Transient Survey. *Mon. Not. R. Astron.Soc.* 453, 1562–1576. doi: 10.1093/mnras/stv1726

Graham, M. J., Djorgovski, S. G., Stern, D., Glikman, E., Drake, A. J., Mahabal, A. A., et al. (2015b). A possible close supermassive black-hole binary in a quasar with optical periodicity. *Nature* 518, 74–76. doi: 10.1038/nature14143

Ilić, D., Shapovalova, A. I., Popović, L. Č., Chavushyan, V., Burenkov, A. N., Kollatschny, W., et al. (2017). Long-term monitoring of the broad-line region properties in a selected sample of AGN. *Front. Astron. Space Sci.* 4:12. doi: 10.3389/fspas.2017.00012

Jovanović, P. (2012). The broad Fe Kα line and supermassive black holes. *New Astron. Rev.* 56, 37–48. doi: 10.1016/j.newar.2011.11.002

Jovanović, P. and Popović, L. Č. (2008). Observational effects of strong gravity in vicinity of supermassive black holes. *Fortschr. Phys.* 56, 456–461. doi: 10.1002/prop.200710519

Jovanović, P., Popović, L. Č., Stalevski, M., and Shapovalova, A. I. (2010). Variability of the Hβ line profiles as an indicator of orbiting bright spots in accretion disks of quasars: a case study of 3C 390.3. *Astrophys. J.* 718, 168–176. doi: 10.1088/0004-637X/718/1/168

Kaspi, S., Smith, P. S., Netzer, H., Maoz, D., Jannuzi, B. T., and Giveon, U. (2000). Reverberation measurements for 17 quasars and the size-mass-luminosity relations in active galactic nuclei. *Astrophys. J.* 533, 631–649. doi: 10.1086/308704

Li, Y.-R., Wang, J.-M., Ho, L. C., Lu, K.-X., Qiu, J., Du, P., et al. (2016). Spectroscopic indication of a centi-parsec supermassive black hole binary in the galactic center of NGC 5548. *Astrophys. J.* 822:4. doi: 10.3847/0004-637X/822/1/4

Lin, D. N. C. (1997). "Star/disk interaction in the nuclei of active galaxies," in *IAU Colloq. 159: Emission Lines in Active Galaxies: New Methods and Techniques, Astronomical Society of the Pacific Conference Series, Vol. 113*, eds B. M. Peterson, F.-Z. Cheng, and A. S. Wilson (Shanghai), 64.

Lin, D. N. C. and Papaloizou, J. C. B. (1996). Theory of accretion disks II: application to observed systems. *Annu. Rev. Astron. Astrophys.* 34, 703–748.

Liu, T., Gezari, S., Burgett, W., Chambers, K., Draper, P., Hodapp, K., et al. (2016). A Systematic Search for Periodically Varying Quasars in Pan-STARRS1: An Extended Baseline Test in Medium Deep Survey Field MD09. *Astrophys. J.* 833:6. doi: 10.3847/0004-637X/833/1/6

Lomb, N. R. (1976). Least-squares frequency analysis of unequally spaced data. *Astrophys. Space Sci.* 39, 447–462.

Lynden-Bell, D. (1969). Galactic nuclei as collapsed old quasars. *Nature* 223, 690–694.

Marziani, P., Bon, E., Grieco, A., Bon, N., Dultzin, D., Del Olmo, A., et al. (2017a). "Optical variability patterns of radio-quiet and radio-loud quasars," in *New Frontiers in Black Hole Astrophysics, IAU Symposium, Vol. 324*, ed A. Gomboc (Ljubljana), 243–244.

Marziani, P., Negrete, C. A., Dultzin, D., Martinez-Aldama, M. L., Del Olmo, A., Esparza, D., Sulentic, J. W., D'Onofrio, M., Stirpe, G. M., Bon, E., and Bon, N. (2017b). "Highly accreting quasars: a tool for cosmology?," in *New Frontiers in Black Hole Astrophysics, IAU Symposium, Vol. 324*, eds A. Gomboc (Ljubljana), 245–246.

Marziani, P., Sulentic, J. W., Dultzin-Hacyan, D., Calvani, M., and Moles, M. (1996). Comparative analysis of the high- and low-ionization lines in the broad-line region of active galactic nuclei. *Astrophys. J. Suppl.* 104:37.

McKernan, B., Ford, K. E. S., Kocsis, B., and Haiman, Z. (2013). Ripple effects and oscillations in the broad Fe Kα line as a probe of massive black hole mergers. *Mon. Not. R. Astron. Soc.* 432, 1468–1482. doi: 10.1093/mnras/stt567

McKernan, B., Ford, K. E. S., Kocsis, B., Lyra, W., and Winter, L. M. (2014). Intermediate-mass black holes in AGN discs - II. Model predictions and observational constraints. *Mon. Not. R. Astron. Soc.* 441, 900–909. doi: 10.1093/mnras/stu553

McKernan, B., Ford, K. E. S., Lyra, W., and Perets, H. B. (2012). Intermediate mass black holes in AGN discs - I. Production and growth. *Mon. Not. R. Astron. Soc.*, 425, 460–469. doi: 10.1111/j.1365-2966.2012.21486.x

Netzer, H. (2013). *The Physics and Evolution of Active Galactic Nuclei*. Cambridge, UK: Cambridge University Press.

Newman, J. A., Eracleous, M., Filippenko, A. V., and Halpern, J. P. (1997). Measurement of an active galactic nucleus central mass on centiparsec scales: results of long-term optical monitoring of Arp 102B. *Astrophys. J.* 485, 570–580.

Peterson, B. M. (1997). *An Introduction to Active Galactic Nuclei*. Cambridge; New York, NY: Cambridge University Press.

Peterson, B. M., Berlind, P., Bertram, R., Bischoff, K., Bochkarev, N. G., Borisov, N., et al. (2002). Steps toward determination of the size and structure of the broad-line region in active galactic nuclei. XVI. A 13 year study of spectral variability in NGC 5548. *Astrophys. J.* 581, 197–204. doi: 10.1086/344197

Popović, L. Č. (2012). Super-massive binary black holes and emission lines in active galactic nuclei. *New Astronomy Reviews*, 56:74–91.

Popovic, L. C., Bon, E., and Gavrilovic, N. (2008). "The broad emission lines in AGN: hidden disk Emission," in *Revista Mexicana de Astronomia y Astrofisica Conference Series,* Vol. 32 (Mexico city), 99–101.

Popović, L. Č., Mediavilla, E., Bon, E., and Ilić, D. (2004). Contribution of the disk emission to the broad emission lines in AGNs: two-component model. *Astron. Astrophys.* 423, 909–918. doi: 10.1051/0004-6361:20034431

Popović, L. Č., Mediavilla, E. G., Bon, E., Stanić, N., and Kubičela, A. (2003). The line emission region in III Zw 2: kinematics and variability. *Astrophys. J.* 599, 185–192. doi: 10.1086/379277

Popović, L. Č., Shapovalova, A. I., Ilić, D., Burenkov, A. N., Chavushyan, V. H., Kollatschny, W., et al. (2014). Spectral optical monitoring of the double-peaked emission line AGN Arp 102B. II. Variability of the broad line properties. *Astron. Astrophys.* 572:A66. doi: 10.1051/0004-6361/201423555

Scargle, J. D. (1982). Studies in astronomical time series analysis. II - Statistical aspects of spectral analysis of unevenly spaced data. *Astrophys. J.* 263, 835–853.

Sergeev, S. G., Doroshenko, V. T., Dzyuba, S. A., Peterson, B. M., Pogge, R. W., and Pronik, V. I. (2007). Thirty years of continuum and emission-line variability in NGC 5548. *Astrophys. J.* 668, 708–720. doi: 10.1086/520697

Sergeev, S. G., Pronik, V. I., and Sergeeva, E. A. (2000). Arp 102B: variability patterns of the Hα line profile as evidence for gas rotation in the broad-line region. *Astron. Astrophys.* 356, 41–49.

Shakura, N. I. and Sunyaev, R. A. (1973). Black holes in binary systems. Observational appearance. *Astron. Astrophys.* 24, 337–355.

Shapovalova, A. I., Popović, L. Č., Burenkov, A. N., Chavushyan, V. H., Ilić, D., Kollatschny, W., et al. (2013). Spectral optical monitoring of a double-peaked emission line AGN Arp 102B. Variability of spectral lines and continuum. *Astron. Astrophys.* 559:A10. doi: 10.1051/0004-6361/201321781

Strateva, I. V., Strauss, M. A., Hao, L., Schlegel, D. J., Hall, P. B., Gunn, J. E., et al. (2003). Double-peaked low-ionization emission lines in active galactic nuclei. *Astron. J.* 126, 1720–1749. doi: 10.1086/378367

Sulentic, J. W., Bachev, R., Marziani, P., Negrete, C. A., and Dultzin, D. (2007). C IV λ1549 as an eigenvector 1 parameter for active galactic nuclei. *Astrophys. J.* 666:757–777. doi: 10.1086/519916

Sulentic, J. W., Zheng, W., Calvani, M., and Marziani, P. (1990). Implications of ARP 102B - Line emission from an accretion disk? *Astrophys. J. Lett.* 355, L15–L18.

Vaughan, S. and Uttley, P. (2006). Detecting X-ray QPOs in active galaxies. *Adv. Space Res.* 38, 1405–1408. doi: 10.1016/j.asr.2005.02.064

Vaughan, S., Uttley, P., Markowitz, A. G., Huppenkothen, D., Middleton, M. J., Alston, W. N., et al. (2016). False periodicities in quasar time-domain surveys. *Mon. Not. R. Astron. Soc.* 461, 3145–3152. doi: 10.1093/mnras/stw1412

Vorobyov, E. I., Regaly, Z., Guedel, M., and Lin, D. N. C. (2016). An alternative model for the origin of gaps in circumstellar disks. *Astron. Astrophys.* 587:A146. doi: 10.1051/0004-6361/201527701

Conflict of Interest Statement: The authors declare that the research was conducted in the absence of any commercial or financial relationships that could be construed as a potential conflict of interest.

The reviewer MD declared a shared affiliation, with no collaboration, with several of the authors, EB, PJ, NB and AO, to the handling editor.

Copyright © 2018 Bon, Jovanović, Marziani, Bon and Otašević. This is an open-access article distributed under the terms of the Creative Commons Attribution License (CC BY). The use, distribution or reproduction in other forums is permitted, provided the original author(s) and the copyright owner are credited and that the original publication in this journal is cited, in accordance with accepted academic practice. No use, distribution or reproduction is permitted which does not comply with these terms.

frontiers in Astronomy and Space Sciences

ORIGINAL RESEARCH
published: 23 November 2017
doi: 10.3389/fspas.2017.00047

Multiwavelength Variability Analysis of 3C 279

Víctor M. Patiño-Álvarez[1], Sunil Fernandes[2], Vahram Chavushyan[3], Erique López-Rodríguez[4], Jonathan León-Tavares[5], Eric M. Schlegel[2], Luis Carrasco[3], José R. Valdés[3] and Alberto Carramiñana[3]*

[1] Max-Planck-Institut für Radioastronomie, Bonn, Germany, [2] Department of Physics and Astronomy, University of Texas at San Antonio, San Antonio, TX, United States, [3] Instituto Nacional de Astrofísica Óptica y Electrónica, Puebla, Mexico, [4] SOFIA Science Center, NASA Ames Center, Mountain View, CA, United States, [5] Centre for Remote Sensing and Earth Observation Processes (TAP), Flemish Institute for Technological Research (VITO), Mol, Belgium

OPEN ACCESS

Edited by:
Deborah Dultzin, Universidad Nacional Autónoma de México, Mexico

Reviewed by:
Giovanna Maria Stirpe, Osservatorio Astronomico di Bologna (INAF), Italy
Daniela Bettoni, Osservatorio Astronomico di Padova (INAF), Italy

***Correspondence:**
Víctor M. Patiño-Álvarez
patinoavm@mpifr-bonn.mpg.de

Specialty section:
This article was submitted to Milky Way and Galaxies, a section of the journal Frontiers in Astronomy and Space Sciences

Received: *01 July 2017*
Accepted: *03 November 2017*
Published: *23 November 2017*

Citation:
Patiño-Álvarez VM, Fernandes S, Chavushyan V, López-Rodríguez E, León-Tavares J, Schlegel EM, Carrasco L, Valdés JR and Carramiñana A (2017) Multiwavelength Variability Analysis of 3C 279. Front. Astron. Space Sci. 4:47. doi: 10.3389/fspas.2017.00047

We present a multifrequency analysis of the variability in the flat-spectrum radio quasar 3C 279 from 2008 to 2014. Our multiwavelength datasets range from 1 mm to gamma-rays, with additional optical polarimetry. Cross-correlation analysis shows a significant correlation between the UV continuum emission, the optical and NIR bands, at a delay consistent with zero, implying co-spatial emission regions. We also find a correlation between the UV continuum and the 1 mm data, which implies that the dominant process in producing the UV continuum is synchrotron emission. Based on the behavior of the gamma-ray light curve with respect to other bands, we identified three different activity periods. During period A we find a significant correlation at zero delay between the UV continuum and the gamma-rays, implying co-spatial emission regions which points toward synchrotron self-Compton as dominant gamma-ray emission mechanism. During period C we find a delay between the UV continuum and the gamma-rays, as well as a correlation at zero delay between X-rays and gamma-rays, both results implying that external inverse Compton is the dominant gamma-ray emission mechanism. During period B there are multiple flares in the bands from 1 mm to UV, however, none of these show a counterpart in the gamma-rays band. We propose that this is caused by an increase in the gamma-ray opacity due to electron-positron pair production.

Keywords: multiwavelength, blazar, 3C 279, gamma-rays, emission mechanism, FSRQ

1. CONTEXT

Blazars are one class of jetted active galactic nuclei, with small viewing angle, thus the relativistic jet points almost directly to our line of sight (Urry and Padovani, 1995). Blazars are known for their for their variability at all frequencies with a dominant component of non-thermal emission. They can be classified as Flat Spectrum Radio Quasars (FSRQ) or BL Lac type, depending on the visible features in their optical spectrum. 3C 279 is an FSRQ at $z = 0.536$, and was among the first quasars discovered to emit gamma-rays via observations by the Compton Gamma-Ray Observatory (Hartman et al., 1992). In this proceeding, we present the preliminary results of a multiwavelength variability study on the source 3C 279.

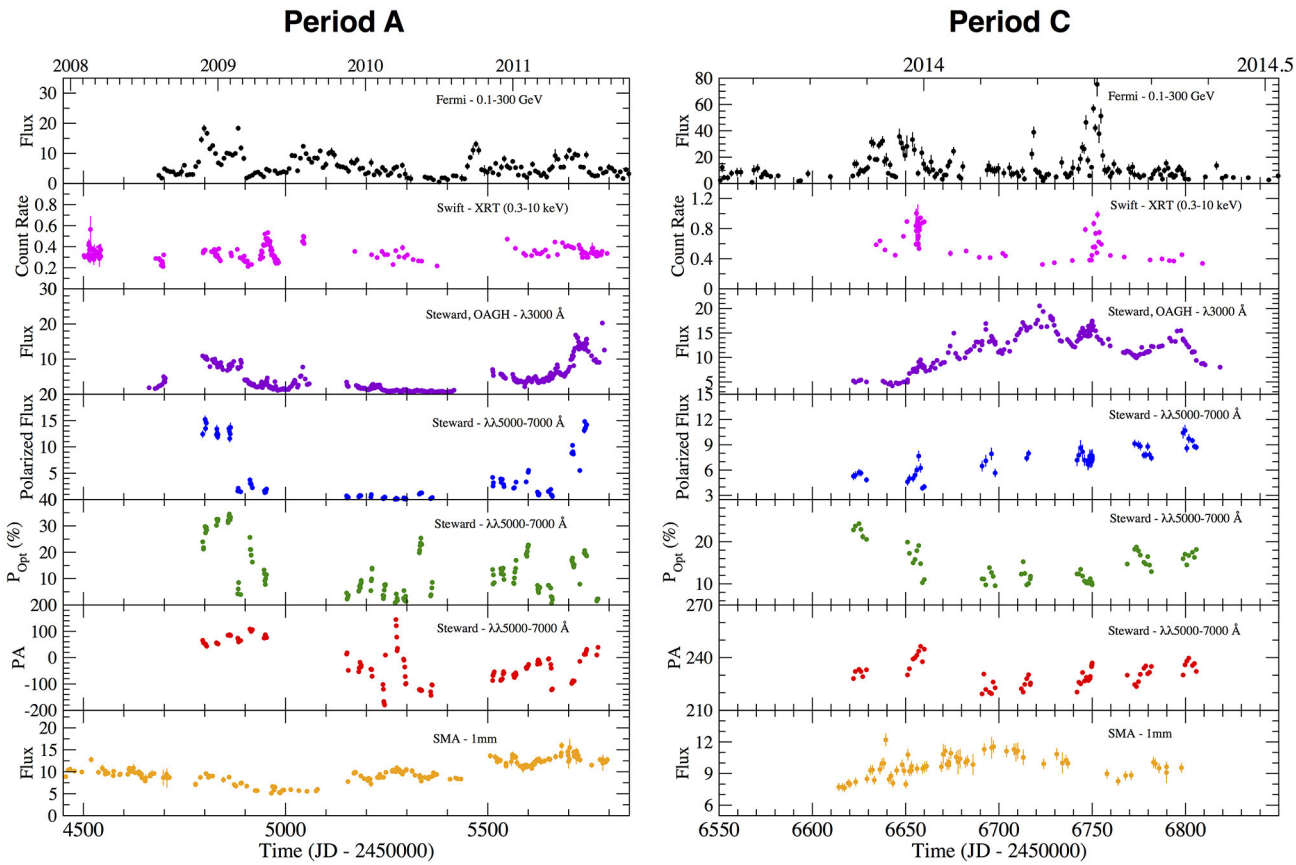

FIGURE 1 | Left: Light Curves for 3C 279 during Period A. **Right:** Light Curves for 3C 279 during Period C. These are the two different epochs where we found different delays between the UV continuum and the gamma-rays. This difference in the delay suggests a change in the dominant gamma-ray emission mechanism. From top to bottom, the vertical axes units are: [ph cm^{-2} s^{-1}], [c/s], [$\times 10^{-15}$ erg cm^{-2} s^{-1} Å^{-1}], [$\times 10^{-13}$ erg cm^{-2} s^{-1}], [%], [degrees], [Jy].

2. OBSERVATIONS

Our multiwavelength datasets include data from different public databases as well as our own observations. The gamma-ray data was retrieved from the Fermi Science Support Center database[1], which was observed by the Fermi Large Area Telescope (Fermi/LAT, Abdo et al., 2009). The X-rays was observed by the Swift X-Ray Telescope (Swift/XRT, Stroh and Falcone, 2013), 1mm observations were taken with the submillimeter Array[2] (SMA, Gurwell et al., 2007), Near Infrared photometry from the Observatorio Astrofísico Guillermo Haro (OAGH) and the SMARTS project[3] (Bonning et al., 2012); optical V Band from the Steward Observatory[4] (Smith et al., 2009) and SMARTS; optical spectra from OAGH (Patiño-Álvarez et al., 2013) and the Steward Observatory; and polarization spectra from the Steward Observatory as well. Details on data reduction can be found in the references given.

[1]https://fermi.gsfc.nasa.gov/ssc/data/access/
[2]http://sma1.sma.hawaii.edu/callist/callist.html
[3]http://www.astro.yale.edu/smarts/glast/home.php
[4]http://james.as.arizona.edu/~psmith/Fermi/

3. ACTIVITY PERIODS

Based on the behavior of the gamma-rays with respect to the UV, optical and NIR, we separated the entire time range into three different periods: A flaring period in multiple bands, with counterparts in gamma-rays; a flaring period in multiple bands with no counterparts in gamma-rays; and another flaring period in multiple bands with apparent counterparts in gamma-rays. We also performed cross-correlation analysis on these activity periods of the light curves.

Period A ranges from $JD_{245} = 4,650 - 5,850$ (see **Figure 1** left panel). During this period, we observed multiple flares in the gamma-ray emission, as well as counterparts in the optical (*V*-band), UV continuum, and NIR emission (*J*-, *H*- and *K*-bands). In the 1 mm light curve we observed a response to each of these flares, however, the amplitude of the 1 mm flares is not as high as in the other wavelengths.

Period B ranges from $JD_{245} = 5,850 - 6,400$ (see **Figure 2**). During this time period, we observed multiple flares in the optical *V*-band, with clear counterparts in the UV spectral continuum and NIR bands. We also observed an increase in

the 1 mm emission responding to each of these flares. The highest levels of 1 mm emission over the entire time-frame of our observations occur during this activity period. There are increases in polarization degree coincident with these flares; this might indicate that these flares have a non-thermal origin.

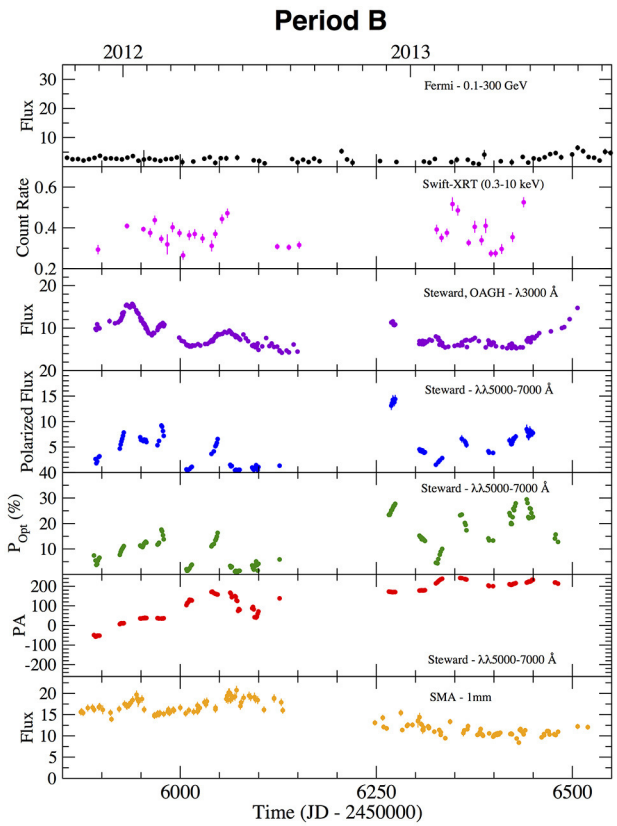

FIGURE 2 | Light Curves for 3C 279 during period B. Units are the same as in **Figure 1**.

However, there are no counterparts to any of these flares in the gamma-rays.

Period C ranges from $JD_{245} = 6{,}400 - 6{,}850$ (see **Figure 1** right panel). During this time period, we observed the highest levels of gamma-ray emission in our time-frame of study. At the start of this time period we observe a very intense flare in the gamma-rays with a clear counterpart in the 1 mm emission, and high levels of degree of polarization, however, we do not see any response in the wavelength range from UV to NIR.

4. CORRELATION ANALYSIS

In order to discern if the emission at different wavelengths are correlated, we applied Cross-Correlation analysis, by using three different methods: The Interpolated Cross-Correlation Function (ICCF, Gaskell and Sparke, 1986), the Discrete Cross-Correlation Function (DCCF, Edelson and Krolik, 1988), and the Z-Transformed Discrete Correlation Function (ZDCF, Alexander, 1997). The significance was calculated via Montecarlo simulations, and a correlation is only considered as significant if the signal is above 3-sigma, and we only state a delay when there is not more than one peak in the cross-correlation function.

With the results from the cross-correlation analysis, we have identified the simultaneity ($|\Delta t| < 1$ day) of the UV λ3000 Å continuum emission, the optical V Band, and the NIR J, H, and K bands. This correlation allows us to infer that the emissions from the middle UV range to the NIR are co-spatial. We report the finding of a significant correlation between the V Band and 1 mm emission in our entire observation time range. By interpolating the V Band observations to the times of the 1 mm observations, we obtain a Spearman correlation coefficient of 0.65, and a probability of obtaining this correlation by chance of $P \ll 0.01$. This strongly suggests that the optical V Band emission should be dominated by non-thermal emission from the jet. These results also imply that the emission from the middle UV range to the NIR is dominated by synchrotron emission.

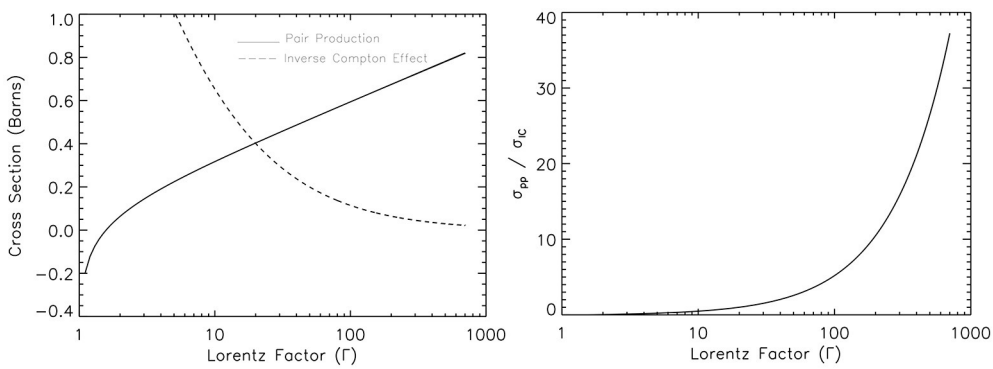

FIGURE 3 | Left: Theoretical cross sections obtained from our analytical model, for the inverse Compton effect and the electron-positron pair production as a function of the Lorentz factor. **Right:** Ratio of the cross sections of the two processes mentioned above as a function of the Lorentz factor. The model predicts that as the Lorentz factor increases significantly, there is a much higher probability of a pair production transition that can cause absorption of gamma-rays within a region of increasing Lorentz factor.

5. GAMMA-RAY EMISSION MECHANISM

Figure 1 (left panel) shows the light curves for Period A, which is noteworthy because we have a response in the gamma-rays every time we have a flare or flux increase in the other bands. The cross-correlation analysis between the UV continuum and the gamma-rays shows a delay of -0.7 ± 5.0 days (consistent with zero delay), implying that the emission regions are co-spatial. This, added to the low activity in the X-rays (which come mainly from the inner accretion disk and hot corona), strongly suggests that the dominant gamma-ray emission mechanism during this activity period is Synchrotron Self-Compton.

We also show in **Figure 1** (right panel) the light curves for Period C. This period comes after a quiescent state in the gamma-rays (see **Figure 2**, left panel), and is noteworthy for having the brightest gamma-ray flare observed in this source during our time-frame of observation. The cross-correlation analysis between the UV continuum and the gamma-rays shows a delay of 28.6 ± 4.8 days, indicating a separation between the UV continuum emission region and the gamma-ray emission region (in contrast to Period A). There is a delay between X-rays and gamma-rays of -0.1 ± 3.0 days (consistent with zero delay). Added to the delay obtained between the gamma-rays and UV continuum, points to the dominant gamma-ray emission mechanism being External Inverse Compton. We present for the first time observational evidence of a change with time in the dominant gamma-ray emission mechanism for a single source. This is an important result due to its implications for SED modeling of blazars and high-energy physics. The result could also imply that the gamma-ray emission zone is changing locations over time.

6. ANOMALOUS GAMMA-RAY ACTIVITY

We report the finding of an anomalous activity period on 3C 279. In this period we have multiple flares in the λ3000 Å continuum with counterparts in the optical V and NIR bands. We also observe coincident increases in the polarized flux and optical polarization degree, as well as the highest flux levels of 1mm emission during our entire observational time range. However, there is no counterpart in the gamma-ray band to any of this activity. The light curves for this period are shown in **Figure 2**.

We propose that this anomalous behavior is caused by an increase in the gamma-ray opacity in the flaring region, due to an increase in the Lorentz factor in the flaring region. In order to test if this scenario is plausible, we performed analytical calculations of the cross sections for the inverse Compton scattering and the electron-positron pair production. By performing the full quantum mechanical calculations we were able to calculate the cross sections for the aforementioned processes as a function of the Lorentz factor. The results of these calculations can be seen in **Figure 3**. The full calculations will be available in Patiño-Álvarez et al. (submitted).

AUTHOR CONTRIBUTIONS

VP-Á analyzed multiwavelength data and spectra, spectroscopic observations, statistical analysis, the explanation for lack of gamma-ray emission, as well as the analytical model, and writing of the paper. SF analyzed spectroscopic and polarimetric data and writing of the paper. VC is the group leader, establishment of scientific objectives, general direction, and scientific discussion. EL-R participated in the polarimetric analysis as well as general reviewing and scientific discussion. JL-T discussion about statistical methods as well as general reviewing and discussion. ES general reviewing and scientific discussion. LC NIR observations. JV spectroscopic observations. AC general reviewing and scientific discussion.

FUNDING

This work was supported by CONACyT research grant 151494 (México). VP-Á acknowledges support from the CONACyT program for Ph.D. studies. SF acknowledges support from the University of Texas at San Antonio (UTSA) and the Vaughan family, support from the NSF grant 0904421, as well as the UTSA Mexico Center Research Fellowship funded by the Carlos and Malu Alvarez Fund. This work has received computational support from Computational System Biology Core, funded by the National Institute on Minority Health and Health Disparities (G12MD007591) from the National Institutes of Health.

ACKNOWLEDGMENTS

We are thankful to P. Smith for his help on the polarimetry analysis. VP-Á and VC are grateful to UTSA for their hospitality during their stay. Data from the Steward Observatory spectro-polarimetric monitoring project were used; this program is supported by Fermi Guest Investigator grants NNX08AW56G, NNX09AU10G, and NNX12AO93G. 1 mm flux density light curve data from the Submillimeter Array was provided by Mark A. Gurwell. The Submillimeter Array is a joint project between the Smithsonian Astrophysical Observatory and the Academia Sinica Institute of Astronomy and Astrophysics and is funded by the Smithsonian Institution and the Academia Sinica.

REFERENCES

Abdo, A. A., Ackermann, M., Ajello, M., Atwood, W. B., Axelsson, M., Baldini, L., et al. (2009). Fermi/large area telescope bright gamma-ray source list. *Astrophys. J. Suppl.* 183:46. doi: 10.1088/0067-0049/183/1/46

Alexander, T. (1997). "Is AGN variability correlated with other AGN properties? ZDCF analysis of small samples of sparse light curves," in *Astronomical Time Series*, Vol. 218 of *Astrophysics and Space Science Library*, eds D. Maoz, A. Sternberg, and E. M. Leibowitz (Berlin: Springer), 163. doi: 10.1007/978-94-015-8941-3_14

Bonning, E., Urry, C. M., Bailyn, C., Buxton, M., Chatterjee, R., Coppi, P., et al. (2012). SMARTS optical and infrared monitoring of 12 gamma-ray bright blazars. *Astrophys. J.* 756:13. doi: 10.1088/0004-637X/756/1/13

Edelson, R. A., and Krolik, J. H. (1988). The discrete correlation function - A new method for analyzing unevenly sampled variability data. *Astrophys. J.* 333, 646–659. doi: 10.1086/166773

Gaskell, C. M., and Sparke, L. S. (1986). Line variations in quasars and Seyfert galaxies. *Astrophys. J.* 305, 175–186. doi: 10.1086/164238

Gurwell, M. A., Peck, A. B., Hostler, S. R., Darrah, M. R., and Katz, C. A. (2007). "Monitoring phase calibrators at submillimeter wavelengths," in *From Z-Machines to ALMA: (Sub)Millimeter Spectroscopy of Galaxies*, *Vol. 375 of Astronomical Society of the Pacific Conference Series*, eds A. J. Baker, J. Glenn, A. I. Harris, J. G. Mangum, and M. S. Yun (San Francisco, CA: Astronomical Society of the Pacific), 234.

Hartman, R. C., Bertsch, D. L., Fichtel, C. E., Hunter, S. D., Kanbach, G., Kniffen, D. A., et al. (1992). Detection of high-energy gamma radiation from quasar 3C 279 by the EGRET telescope on the Compton Gamma Ray Observatory. *Astrophys. J. Lett.* 385, L1–L4. doi: 10.1086/186263

Patiño-Álvarez, V., Chavushyan, V., León-Tavares, J., Valdés, J. R., Carramiñana, A., Carrasco, L., et al. (2013). Optical spectrophotometric monitoring of Fermi/LAT bright sources. *ArXiv e-prints*. ArXiv: 1303.1893.

Smith, P. S., Montiel, E., Rightley, S., Turner, J., Schmidt, G. D., and Jannuzi, B. T. (2009). Coordinated fermi/optical monitoring of blazars and the great 2009 september gamma-ray flare of 3C 454.3. *ArXiv e-prints* ArXiv: 0912.3621.

Stroh, M. C., and Falcone, A. D. (2013). Swift X-ray telescope monitoring of fermi-LAT gamma-ray sources of interest. *Astrophys. J. Suppl.* 207:28. doi: 10.1088/0067-0049/207/2/28

Urry, C. M., and Padovani, P. (1995). Unified schemes for radio-loud active galactic nuclei. *PASP* 107:803. doi: 10.1086/133630

Conflict of Interest Statement: The authors declare that the research was conducted in the absence of any commercial or financial relationships that could be construed as a potential conflict of interest.

Copyright © 2017 Patiño-Álvarez, Fernandes, Chavushyan, López-Rodríguez, León-Tavares, Schlegel, Carrasco, Valdés and Carramiñana. This is an open-access article distributed under the terms of the Creative Commons Attribution License (CC BY). The use, distribution or reproduction in other forums is permitted, provided the original author(s) or licensor are credited and that the original publication in this journal is cited, in accordance with accepted academic practice. No use, distribution or reproduction is permitted which does not comply with these terms.

frontiers in Astronomy and Space Sciences

ORIGINAL RESEARCH
published: 24 January 2018
doi: 10.3389/fspas.2018.00001

Time-Evolving SED of MKN421: A Multi-Band View and Polarimetric Signatures

Bernardo M. O. Fraga [1], Ulisses Barres de Almeida [1], Sargis Gasparyan [2], Paolo Giommi [3] and Narek Sahakyan [2]*

[1] COHEP - Centro Brasileiro de Pesquisas Físicas, Rio de Janeiro, Brazil, [2] ICRANet-Armenia, Yerevan, Armenia, [3] Agenzia Spaziale Italiana, Rome, Italy

The most detailed temporal studies of the emission from blazars are usually done by trying to obtain a dense, simultaneous coverage of the source over a large multi-wavelength observational campaign. Although it is well know that correlations between multi-band emission present sizeable temporal lags in their correlated variability, such properties are usually neglected in the majority of observational studies, which model the evolution of source parameters over time by either building time-averaged SEDs (when data is scarce) or considering strictly simultaneous snapshots of the source along the spectrum. By making use of the resources and large database made available through the ASI Science Data Center (ASDC), we present a novel approach to the modeling of blazar emission whereby the multi-epoch SEDs for Mkn 421 are modeled considering the temporal lags between bands (both in short and long-timescales), as obtained by a detailed cross-correlation analysis, spanning data from radio to Very High Energy (VHE) gamma-rays from 2008 to 2014. In addition to that, long-term optical polarization data are used to aid and complement our physical interpretation of the state and evolution of the source.

Keywords: blazars, MKN421, multiwavelength, time-evolution, SED modeling

OPEN ACCESS

Edited by:
Mauro D'Onofrio, Università degli Studi di Padova, Italy

Reviewed by:
Giovanna Maria Stirpe, Osservatorio Astronomico di Bologna (INAF), Italy
Daniela Bettoni, Osservatorio Astronomico di Padova (INAF), Italy

****Correspondence:***
Bernardo M. O. Fraga
bernardo@cbpf.br

Specialty section:
This article was submitted to Milky Way and Galaxies, a section of the journal Frontiers in Astronomy and Space Sciences

Received: *29 September 2017*
Accepted: *08 January 2018*
Published: *24 January 2018*

Citation:
Fraga BMO, Barres de Almeida U, Gasparyan S, Giommi P and Sahakyan N (2018) Time-Evolving SED of MKN421: A Multi-Band View and Polarimetric Signatures. Front. Astron. Space Sci. 5:1. doi: 10.3389/fspas.2018.00001

1. INTRODUCTION

Blazars are a class of Active Galactic Nuclei where the jet is pointed at a very small angle relative to the line of sight (see e.g., Urry and Padovani, 1995). Their emission is non-thermal across most of (or the entire) electromagnetic spectrum, from radio to γ-rays, sometimes reaching into the TeV domain. Furthermore, since the jet is pointing at a small angle with respect to the line of sight, the emission of blazars is affected by relativistic beaming, which could increase the observed luminosity by a large factor.

The Spectral Energy Distribution (SED) of these objects shows two bumps, one located in the infrared to the soft X-ray band, the other in the hard X-rays to γ-rays. According to the standard picture (see e.g., Abdo et al., 2010; Giommi et al., 2012), the first peak is due to the synchrotron emission of relativistic electrons moving in a magnetic field, while the second peak is due to the inverse-Compton (IC) scattering of the synchrotron photons by the same relativistic electron population that produced them (the Synchrotron self-Compton model, SSC). In some cases the seed photons undergoing IC scattering come from regions outside the nucleus, like the accretion disk or the broad line region (EC, external Compton).

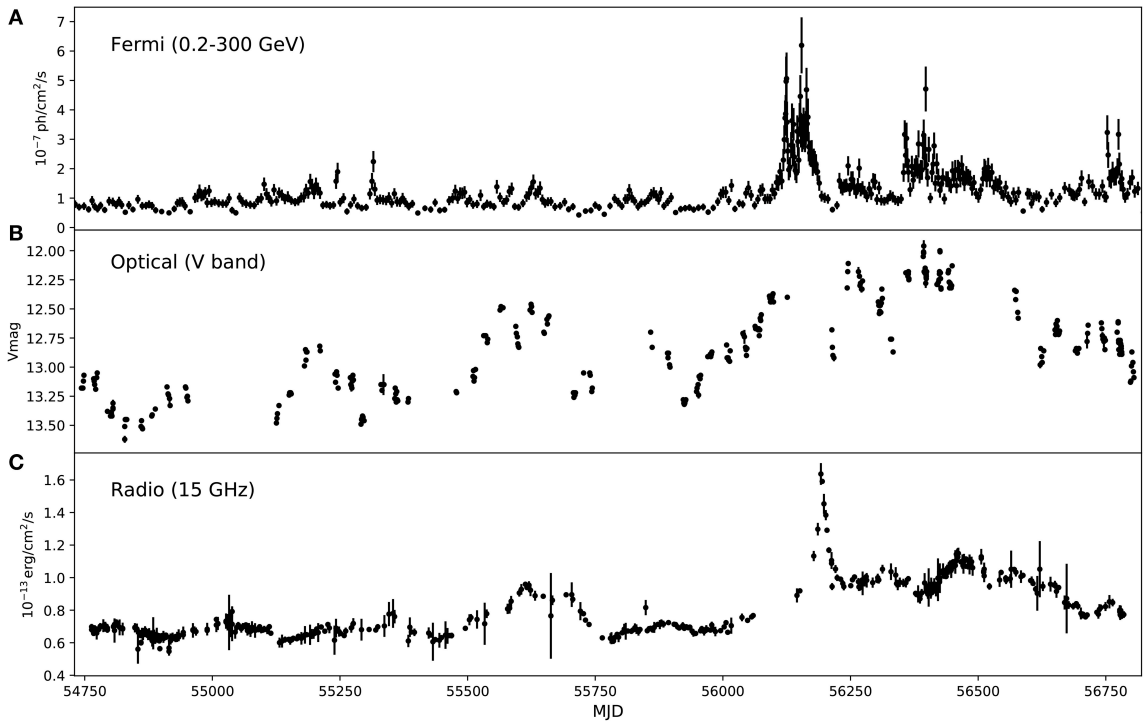

FIGURE 1 | γ-rays, **(A)**, optical **(B)**, and radio **(C)** light curves for Mkn421 from 2008 to 2014.

Since blazars emit all over the spectrum, the most efficient way to study their emission is through multiwavelength data; furthermore, since blazars often present short- and long-scale variability, simultaneous observations are desired. In order to attain these goals, multifrequency observation campaigns have been done for some blazars usually following a very bright flaring period, for example 3C454.3 (Vercellone et al., 2009), PKS2155-304 (Aharonian et al., 2009), and Mkn421 (Donnarumma et al., 2009).

Mkn 421 was the first extragalactic TeV object detected (Punch et al., 1992) and remains one of the brightest and most studied γ-ray blazars to date. It has been intensely monitored by several instruments in different frequencies and for a long period; thus, the amount of data available is quite large and with overlapping periods on several wavelengths. This makes Mkn421 a good source for a comprehensive study of the multi-band correlations and consequently the time evolution of the emission.

2. DATA

We obtained long term multiwavelength light curves for Mkn421 for a period of 6 years, from 2008 to 2014. The only continuous observations were done by the OVRO observatory (at 15 GHz), the Steward observatory (Smith et al., 2009) (V band) and the Fermi satellite. X-ray and UV data are also available from Swift but with long gaps (of approximately 6 months) due to the source proximity to the sun.

We obtained the radio light curve from the ASDC SED tool[1], while the optical data was taken directly from the observatory and checked for galaxy contamination. The Fermi light curve for the period was calculated using an adaptive binning method, where the size of the bins is flexible and chosen to produce constant flux uncertainties, so that they are narrower at higher states (Sahakyan and Gasparyan, 2017). In this way rapid changes of flux can be found. In **Figure 1** we show the three long term light curves; it is interesting to note that both in the γ-ray and the radio light curve the source appears to undergo a change of state sometime before MJD 56000 (beginning of 2012). While before there were only small flares, after 2012 it underwent a series of intense ones and the continuum emission increased. Due to this change of behavior, we consider both periods separately (before and after 2012) in calculating the cross-correlation functions.

3. TIME LAGS

Since AGN light curves are very often unevenly sampled, we used the Z-transformed discrete correlation function (ZDCF, Alexander, 1997) to calculate the cross-correlation functions. Simulations show that the use of Fischer's Z transform improve the performance in sparse light curves over the traditionally used discrete correlation function (DCF, Edelson and Krolik, 1988).

[1] tools.asi.asdc.it/SED/

We calculated the cross-correlation functions between all three lightcurves shown in **Figure 1**, before and after 2012. By using a maximum likelihood analysis (Alexander, 2013), we could find the maximum of the correlation function and the fiducial interval. For the period from 2008 to 2012, the only indication of a correlation is between optical and radio:

$$\tau_{o-r} = -35.8^{+9.91}_{-20.5} \text{ days}, \quad (1)$$

while for the period after 2012

$$\tau_{o-r} = -48.5^{+9.70}_{-20.2} \text{ days}, \quad (2)$$

$$\tau_{\gamma-r} = -45.3^{+7.00}_{-20.7} \text{ days} \quad (3)$$

$$\tau_{\gamma-o} = -5.06^{+10.7}_{-8.69} \text{ days} \quad (4)$$

where a negative lag means that the lower energy band comes after the higher energy one. All these lags are consistent with each other and the γ - optical lag is consistent with a zero day lag. In **Figure 2** we show all the cross-correlation functions.

With the exception of the Fermi–Optical correlation, all others present a clear and sharp maximum. The lag between Fermi and Radio is especially evident considering the very large flare present in both curves and their behavior afterwards. Given the absence of any other flares of this magnitude in the Radio light curve, it is unlikely that the two are unrelated; a more profound analysis is needed to confirm this.

4. SED FITTING

With the lags between different energy bands calculated, we proceeded to build the SEDs for each period. We shifted the Fermi and optical light curves by the values indicated above (considering a zero day lag between them). In addition to the data we had, we added also x-ray and UV data from Swift XRT and UVOT, respectively, taken from the ASDC website. The coverage from Swift is not continuous however; during the period our data covers, there are six windows of observation from Swift, which we

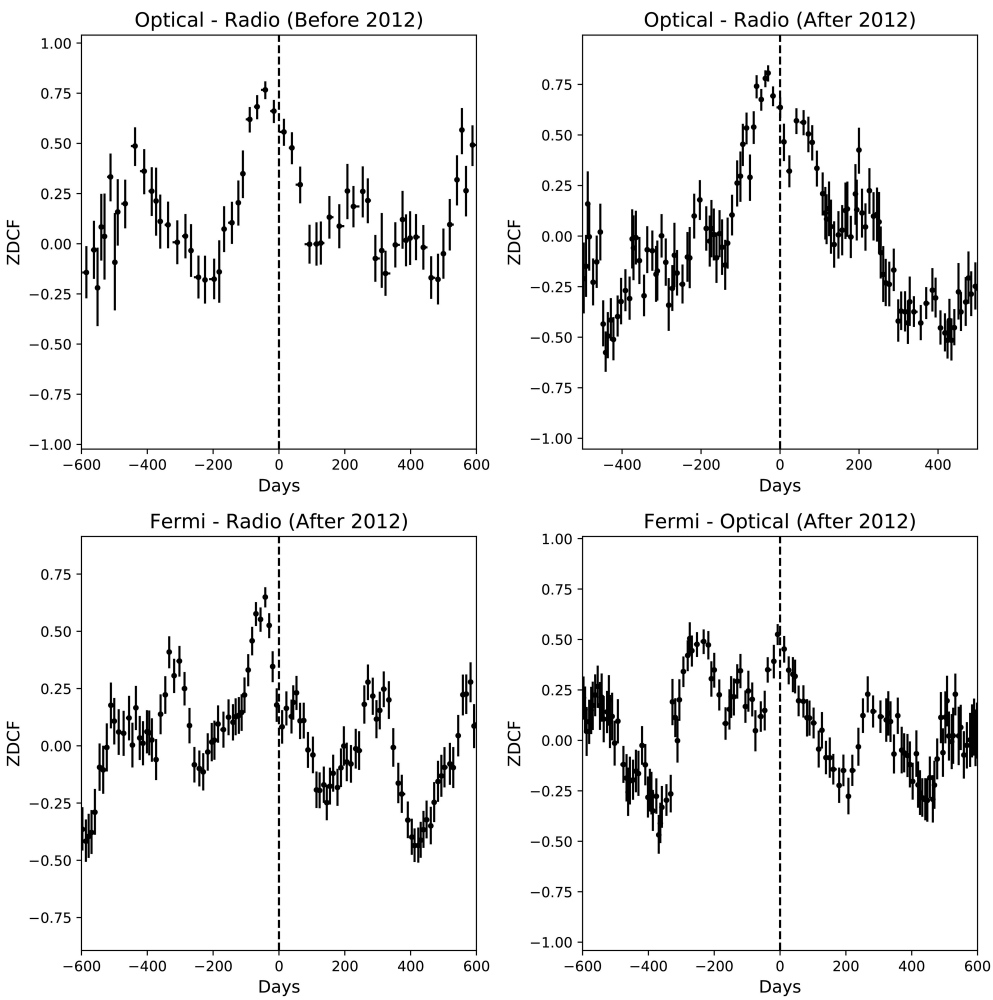

FIGURE 2 | The significant correlation functions between all light curves. **(Top left)** Optical-Radio before 2012; **(Top right)** Optical-Radio after 2012; **(Bottom left)** Fermi-Radio after 2012; **(Bottom right)** Fermi-optical after 2012. A negative lag indicates that the lower energy band comes after.

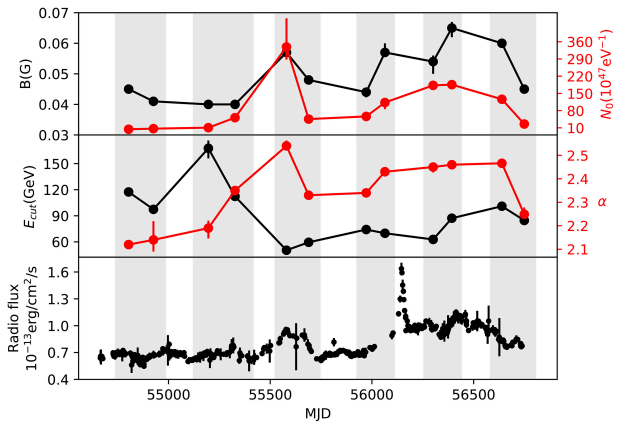

FIGURE 3 | The evolution of the parameters of the SED, with the periods chosen in gray, with the radio lightcurve (shifted by the lags found in section 3) on the bottom for comparison.

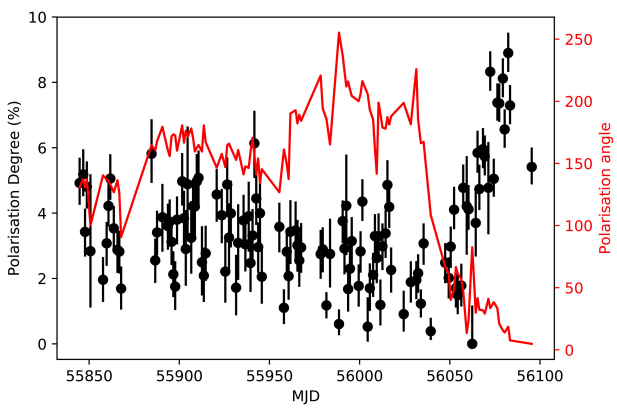

FIGURE 4 | Polarization angle and degree. The rotation of the angle can be seen around MJD 56040, right before the rise in the degree.

divided in two each (for a total of 12) to constrain the variability and make the fitting procedure easier.

We used a single-zone SSC model with the distribution of the electrons given by a power law with an exponential cut-off:

$$N_e(E_e) = N_0 \left(\frac{E_e}{m_e c^2}\right)^{-\alpha} \exp\left(-\frac{E_e}{E_{cut}}\right), \quad (5)$$

where E_{cut} is the cutoff energy, N_0 the normalization and m_e the electron mass

The fit was done numerically using a Markov Chain Monte Carlo (MCMC) code, deriving the best-fit and uncertainty distributions of the parameters through a sampling of their likelihood functions (Sahakyan and Gasparyan, 2017). In **Figure 3** we can see the evolution of the parameters for each period compared to the Radio light curve (already shifted by the lags found in the previous section). It is interesting to notice that the strong increase of N_0 and the magnetic field correlates with the presence of a small flare.

5. POLARIZATION MEASUREMENTS

From 2008 to 2012, a large polarization campaign was undertaken using the Liverpool Telescope and data from the Tuorla blazar monitoring program (Jermak et al., 2016). We present the data for MKN421 in **Figure 4**, with data from the end of 2011 to the middle of 2012.

It can be seen that in the beginning of 2012, the degree of polarization increases strongly (reaching an all-time maximum), while the polarization angle rotates by 180°; this change of behavior is just before the intense flare in γ-rays in 2012 (see **Figure 1**). Unfortunately, due to visibility, there isn't any optical data during the flare. However, this could be an indication that changes in the polarization are related to flaring activity.

6. DISCUSSION

Mkn421 is one of the brightest and most observed blazars to date. We collected long term data for the source in several energies in order to study the time evolution of the emission. From the long term light curves, we detected a change of state in γ-rays in the beginning of 2012, from a more quiescent state to a series of intense flares and an overall increase in the continuum emission. This prompted us to consider both periods separately when calculating the multi-bands correlation.

We calculated the cross-correlation function for each period between the three different long term light curves: overall, the radio lags behind the higher energy bands, while optical and γ-rays are simultaneous. We performed a fit of the SED for each period, already considering the time lags calculated before, using a single-zone SSC model.

We also obtained optical polarimetric data from the end of 2011 to the beginning of 2012. Mkn421 shows an all-time maximum of the polarization degree, and a flip of the polarization angle of 180°; this comes just before the intense flare in γ-rays.

Since we have also X-ray and UV data (with a 6 month gap in the coverage) we can start to calculate the short scale time lags including both. Observation campaigns including VHE instruments such as VERITAS and MAGIC have also been carried out, and we will include these in our analysis. This will help us understand both the long and short term effects of the variability and disentangle the different emission zones. From this initial results, we obtained some hints of correlation on a long time period between radio, γ-rays and optical. As expected, radio lags behind both others in the two periods considered. Besides that, there is some evidence that big rotations in the polarization angle could be related with flares in high energies.

AUTHOR CONTRIBUTIONS

BF made all the cross correlation and light curve analysis, and was the main writer of the work. UBdA obtained the polarization data and helped analyzing the results. PG helped with the gathering of the data through the SSDC web service and with the conclusions. NS gave performed the adaptive binning procedure to obtain the Fermi light curves and with the SED fitting. SG was also responsible for the SED fitting and results.

FUNDING

This research has made use of data from the OVRO 40-m monitoring program (Richards et al., 2011) which is supported in part by NASA grants NNX08AW31G, NNX11A043G, and NNX14AQ89G and NSF grants AST-0808050 and AST-1109911.

UBdA acknowledges the receipt of FAPERJ Jovem Cientista Fellowship 226465. This project was partly funded by CNPq Projeto Universal 426753/2016-0.

ACKNOWLEDGMENTS

NS and SG acknowledges the support of the RA MES State Committee of Science, in the frames of the research project No 15T-1C375.

REFERENCES

Abdo, A. A., Ackermann, M., Agudo, I., Ajello, M., Aller, H. D., Aller, M. F., et al. (2010). The spectral energy distribution of fermi bright blazars. *Astrophys. J.* 716, 30–70. doi: 10.1088/0004-637X/716/1/30

Aharonian, F., Akhperjanian, A. G., Anton, G., Barres de Almeida, U., Bazer-Bachi, A. R., Becherini, Y., et al. (2009). Simultaneous observations of PKS 2155-304 with HESS, Fermi, RXTE, and atom: spectral energy distributions and variability in a low state. *Astrophys. J. Lett.* 696, L150–L155. doi: 10.1088/0004-637X/696/2/L150

Alexander, T. (1997). *Astronomical Time Series, volume 218 of Astrophysics and Space Science Library*, eds D. Maoz, A. Sternberg, and E. M. Leibowitz (Dordrecht: Springer), 163.

Alexander, T. (2013). Improved AGN light curve analysis with the z-transformed discrete correlation function. arXiv:1302.1508.

Donnarumma, I., Vittorini, V., Vercellone, S., del Monte, E., Feroci, M., D'Ammando, F., et al. (2009). The june 2008 Flare of Markarian 421 from optical to TeV energies. *Astrophys. J. Lett.* 691, L13–L19. doi: 10.1088/0004-637X/691/1/L13

Edelson, R. A., and Krolik, J. H. (1988). The discrete correlation function - a new method for analyzing unevenly sampled variability data. *Astrophys. J.* 333, 646–659. doi: 10.1086/166773

Giommi, P., Padovani, P., Polenta, G., Turriziani, S., D'Elia, V., and Piranomonte, S. (2012). A simplified view of blazars: clearing the fog around long-standing selection effects. *Month. Notices R. Astron. Soc.* 420, 2899–2911. doi: 10.1111/j.1365-2966.2011.20044.x

Jermak, H., Steele, I. A., Lindfors, E., Hovatta, T., Nilsson, K., Lamb, G. P., et al. (2016). The RINGO2 and DIPOL optical polarization catalogue of blazars. *Month. Notices R. Astron. Soc.* 462, 4267–4299. doi: 10.1093/mnras/stw1770

Punch, M., Akerlof, C. W., Cawley, M. F., Chantell, M., Fegan, D. J., Fennell, S., et al. (1992). Detection of TeV photons from the active galaxy Markarian 421. *Nature* 358:477. doi: 10.1038/358477a0

Richards, J. L., Max-Moerbeck, W., Pavlidou, V., King, O. G., Pearson, T. J., Readhead, A. C. S., et al. (2011). Blazars in the Fermi era: the OVRO 40 m telescope monitoring program. *Astrophys. J. Suppl.* 194:29. doi: 10.1088/0067-0049/194/2/29

Sahakyan, N., and Gasparyan, S. (2017). High energy gamma-ray emission from PKS 1441+25. *Month. Notices R. Astron. Soc.* 470, 2861–2869. doi: 10.1093/mnras/stx1402

Smith, P. S., Montiel, E., Rightley, S., Turner, J., Schmidt, G. D., and Jannuzi, B. T. (2009). "Coordinated fermi/optical monitoring of blazars and the great 2009 september gamma-ray flare of 3C 454.3" in *2009 Fermi Symposium, eConf Proceedings C091122*. arXiv:0912.3621

Urry, C. M., and Padovani, P. (1995). Unified schemes for radio-loud active galactic nuclei. *Publ. Astron. Soc. Pacific* 107:803. doi: 10.1086/133630

Vercellone, S., Chen, A. W., Vittorini, V., Giuliani, A., D'Ammando, F., Tavani, M., et al. (2009). Multiwavelength observations of 3C 454.3. I. The AGILE 2007 november Campaign on the "Crazy Diamond". *Astrophys. J.* 690, 1018–1030. doi: 10.1088/0004-637X/690/1/1018

Conflict of Interest Statement: The authors declare that the research was conducted in the absence of any commercial or financial relationships that could be construed as a potential conflict of interest.

Copyright © 2018 Fraga, Barres de Almeida, Gasparyan, Giommi and Sahakyan. This is an open-access article distributed under the terms of the Creative Commons Attribution License (CC BY). The use, distribution or reproduction in other forums is permitted, provided the original author(s) or licensor are credited and that the original publication in this journal is cited, in accordance with accepted academic practice. No use, distribution or reproduction is permitted which does not comply with these terms.

frontiers in Astronomy and Space Sciences

ORIGINAL RESEARCH
published: 31 January 2018
doi: 10.3389/fspas.2018.00003

AGN Broad Line Region Variability in the Context of Eigenvector 1: Case of NGC 5548

Nataša Bon[1]*, *Edi Bon*[1] *and Paola Marziani*[2]

[1] *Astronomical Observatory, Belgrade, Serbia,* [2] *Osservatorio Astronomico di Padova (INAF), Padua, Italy*

Many active galactic nuclei (AGN) show strong variability of the optical continuum. Since the line flux, profile shapes and intensity ratios are changing, we analyze the variability patterns and possible periodicity of Type 1 AGN NGC 5548, using the Eigenvector 1 (EV1) diagram in different variability states, taking advantage of very long term monitoring campaign data. The preliminary results suggest that NGC 5548—a highly variable object that over several decades has shown large amplitude continuum fluctuations and flaring behavior—remains Pop B. This means that the range in Eddington ratio, even when the source is in a bright state, remains consistent with the value of the low accreting Pop B. We inspected EV 1 parameters of a single object though long term monitoring, assuming an inclination and black hole mass to be constant during the observational time. Our results imply that the main driver for the variations along the EV 1 diagram could be dimensionless accretion rate. If so, then it appears that the source never crossed the boundary for structural changes, indicatively placed at L/LEdd $\sim$ 0.2.

Keywords: galaxies:active-galaxies, quasar:supermassive black holes, quasar:emission lines, line:profiles, quasar: individual (NGC 5548)

OPEN ACCESS

Edited by:
Fabio La Franca,
Università degli Studi Roma Tre, Italy

Reviewed by:
Milan S. Dimitrijevic,
Astronomical Observatory, Serbia
Michael Fausnaugh,
Independent Researcher,
United States

****Correspondence:***
Nataša Bon
nbon@aob.bg.ac.rs

Specialty section:
This article was submitted to Milky Way and Galaxies, a section of the journal Frontiers in Astronomy and Space Sciences

Received: *31 October 2017*
Accepted: *12 January 2018*
Published: *31 January 2018*

Citation:
Bon N, Bon E and Marziani P (2018) AGN Broad Line Region Variability in the Context of Eigenvector 1: Case of NGC 5548. Front. Astron. Space Sci. 5:3. doi: 10.3389/fspas.2018.00003

1. INTRODUCTION

Differences between Type 1 and Type 2 spectra of AGNs, mainly described by the different viewing angle at the nuclear region of the galaxy, are already well known. On the other hand, there is a vast number of spectral characteristics, such as shift, width of the line, line ratios, Fe II blends, and many others that create diversity between different Type 1 spectra. One could expect that diversity also depends to some extend on the viewing angle.

There were many efforts to systematize Type 1 spectral diversity in a parameter space called the Eigenvector 1 (EV1), that represents the linear combination of several parameters, in order to introduce some order in spectral properties. The EV1 could be seen as an equivalent to the well-known Hertzsprung-Russell diagram for stars, and therefore capable to organize Type 1 AGN into a "main sequence" of quasars. This kind of systematization allows to set observational constrains on dynamics and physical properties of broad line region. The principal component analysis of Boroson and Green (1992) showed that there is a hidden single parameter responsible for the vast majority of spectral differences— R_{Fe}—the ratio of the optical Fe II pseudo continuum to the $H\beta$ flux. This idea was later on developed by Sulentic et al. (2000), and Shen and Ho (2014), among others.

The relation between EV1 and some theoretically motivated parameters, such as Eddington ratio, black hole mass, chemical composition, black hole spin, orientation etc., is still not clear.

Most favored parameter that drives EV1 is Eddington ratio (Boroson and Green, 1992; Sulentic et al., 2000; Marziani et al., 2001; Shen and Ho, 2014). Sniegowska et al. (2017) proposed that besides Eddington ratio the EV 1 is driven by the position of the maximum of the quasar spectral energy distribution, that is connected with the maximum of the accretion disk temperature, for the case of a Shakura and Sunyaev (1973) accretion disk model. Shen and Ho (2014) argued that the viewing angle in Type 1 sources represents just a dispersion to the quasar "main sequence."

In addition to the measurements of Boroson and Green (1992) and Sulentic et al. (2000) measured also the soft X-ray

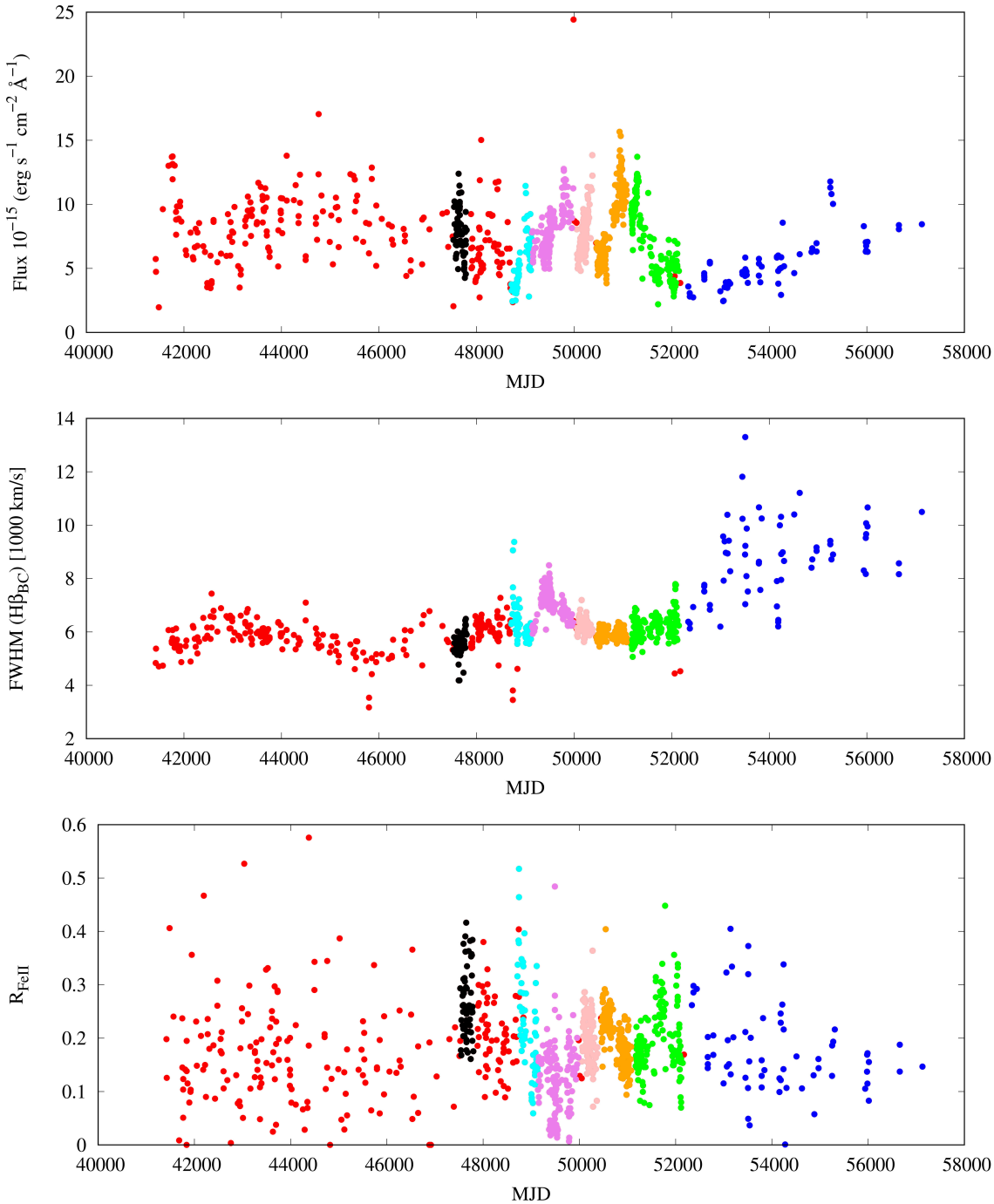

FIGURE 1 | Variability in the NGC 5548 spectra: (**top**) The light curve of the continuum measured at 5100 Å; (**middle**) FWHM Hβ variations; (**bottom**) R_{FeII} change with the time. Colors correspond to different time intervals.

photon index and a measure of CIV λ 1549 broad line profile velocity displacement at half maximum, in order to analyze 4D Eigenvector 1 parameter space. They showed that the "main sequence" of quasars follows some physical trends involving dimensionless accretion rate, as well as electron density which are increasing down the sequence toward strong FeII emitter, while ionization parameter is decreasing (Marziani et al., 2001). Black hole mass decreases from Pop. B to A in low-z, moderate luminosity samples (Fraix-Burnet et al., 2017). Besides, Sulentic et al. (2000) proposed a quasars dichotomy onto Pop A and Pop B according to their spectral properties. Pop B corresponds to more massive quasars (Zamfir et al., 2010) and is characterized by FWHM of Hβ higher than 4,000 km/s and higher red asymmetry.

With very long term monitoring campaign data, in this work we try to analyze the variability patterns on a Type 1 AGN using EV 1 diagrams in different variability states. We focus our analysis on the nearby and frequently observed galaxy NGC 5548, for which data from extensive monitoring campaigns are available.

2. EIGENVECTOR 1 DIAGRAM FOR A SINGLE OBJECT MULTI-EPOCH OBSERVATIONS

Variability of spectra both in the continuum and in emission lines is one of the main characteristic of an active galaxy. During this time, AGN spectra changed slope and shape of the continuum, as well as emission line profiles (their widths and shifts) and strength and relative intensity ratios. In a case study of a archetype of active galaxy -NGC 5548—that has been monitored through several decades, it is possible to follow these changes, and search for a connection between spectral properties. The EV1 parameter space represents a suitable tool to analyze the AGN spectral properties though time.

2.1. Variability of AGN Emission Lines—43 Years of Monitoring Campaigns of NGC 5548

Recently, Bon et al. (2016) presented the *uniform* analysis of NGC 5548 Seyfert 1 type spectra compiled from several monitoring campaigns obtained on different telescopes spanning over 43 years. Since different telescopes provide spectra with different resolution and calibration, as well as inhomogeneous aperture geometries used in different observation sets, a uniform analysis of all spectra was required. Bon et al. (2016) used ULySS—full spectrum fitting technique (Koleva et al., 2009; Bon et al., 2014) to calibrate the flux from all spectra in the same manner and to analyze *simultaneously* all components that contribute to the spectrum, in order to minimize dependencies between parameters of the model. Long-term spectral variations of the continuum at 5100 Å and of the Hβ line were investigated in that work. It was found that the light and radial velocity curves show periodic variation with the periodicity of nearly 16 years. Also, NGC 5548 was noticed before to be a changing look AGN (see for e.g., Sergeev et al., 2007), with the clear appearance and disappearance of broad Hβ component through time: the spectral type changed from Seyfert 1 to Seyfert 1.8.

Using the same technique as presented in Bon et al. (2016), here we measured EV1 diagram properties of NGC5548 spectra—FWHM(Hβ) vs. R_{Fe}, in order to investigate the problem of the physical properties of AGN variability along the QSO "main sequence". Modeling of emission lines, and the contribution of the continua of an AGN and host galaxy was obtained as described in Bon et al. (2016), while Fe II pseudo

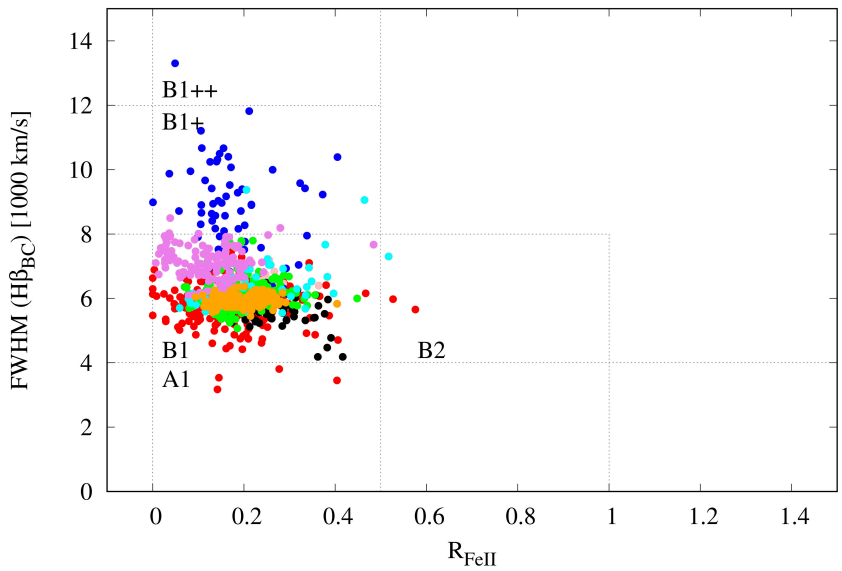

FIGURE 2 | The EV1 diagram of NGC 5548 spectral properties during 43 years of monitoring campaigns. Colors correspond to those in the **Figure 1**.

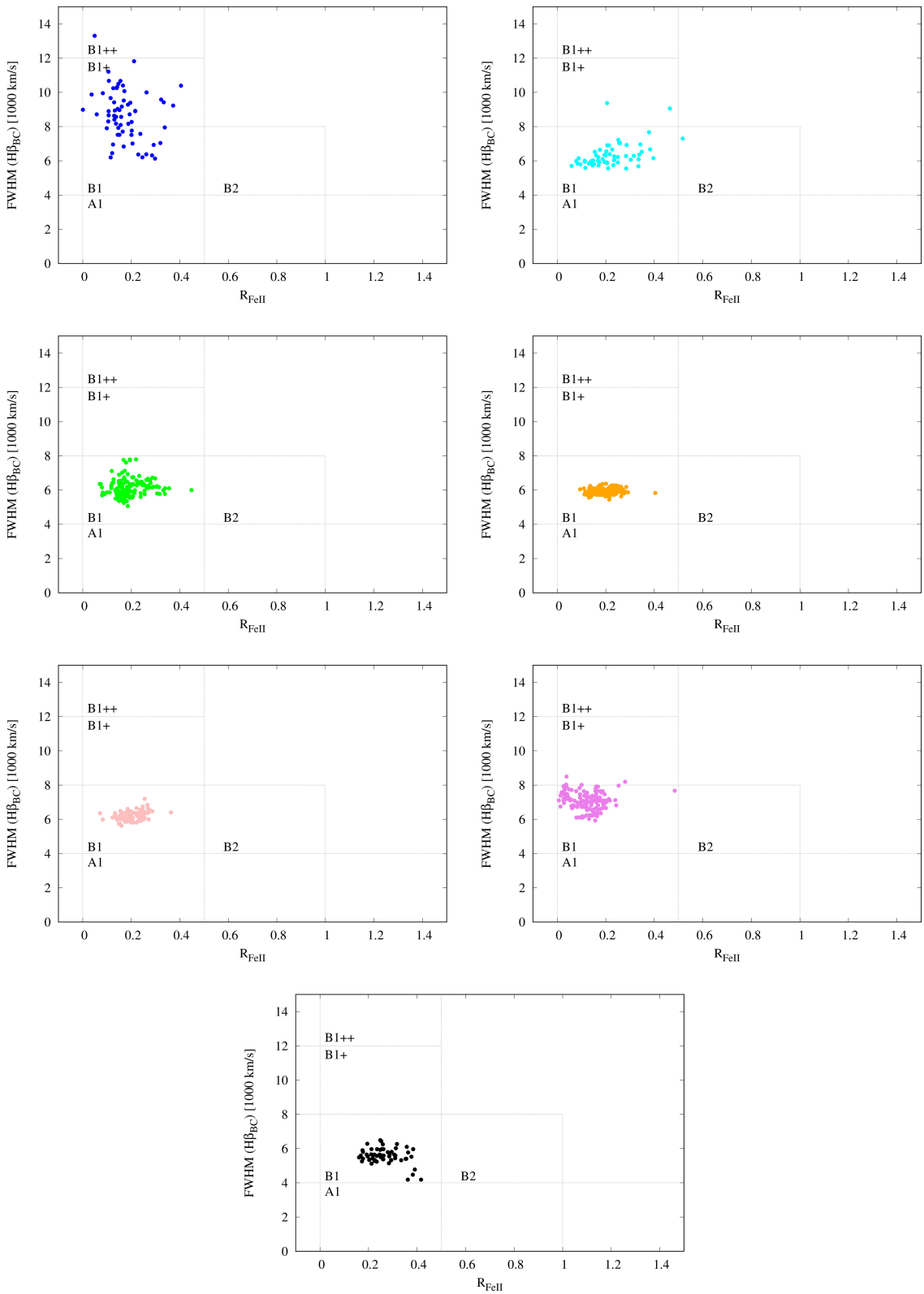

FIGURE 3 | The EV1 diagram of NGC 5548 spectral properties for different time intervals. Colors correspond to those in the **Figure 1**.

continuum was modeled with the template described in Marziani et al. (2009).

Figure 1 shows (a) the light curve in the continuum measured at 5100 Å, (b) the FWHM of Hβ variations during the time, as well as (3) the variability of the R_{FeII} with the time. We also analyzed some fast changing flux variations with flare-like behavior. We selected different time intervals (shorter and longer, in high state and low state of activity as well) in order to analyze their EV1 properties. We presented these intervals with different types of variations in different colors, where each color in all plots correspond to the same time interval, in order to present measured parameters on the EV1 diagram in the **Figure 2** in colors that correspond to those in the **Figure 1**. One can notice that NGC 5548 spectra in an extreme low state of activity (transition from Type 1 to Type 1.8), changes from Pop B1 to Pop B1+ (and in same cases even to Pop B1++), while in a high state object changes toward Pop B1 (and in few cases even to Pop A1). It means that NGC 5548 changes, but mainly stays Pop B. The data of the paper are meant to cover a time lapse that is several time the dynamical time scale. **Figure 2** shows the variability of a single AGN through a large time interval which fills the area of a whole population of AGN with similar observational characteristics (in this case Pop B). At the same time, we are not expecting to find the same relation that are found in reverberation mapping campaign (RM (Peterson et al., 2002), and references therein) on shorter time scales and with frequent sampling. In the **Figure 3** we analyzed short and long term variations separately on EV 1 diagrams. As one can see

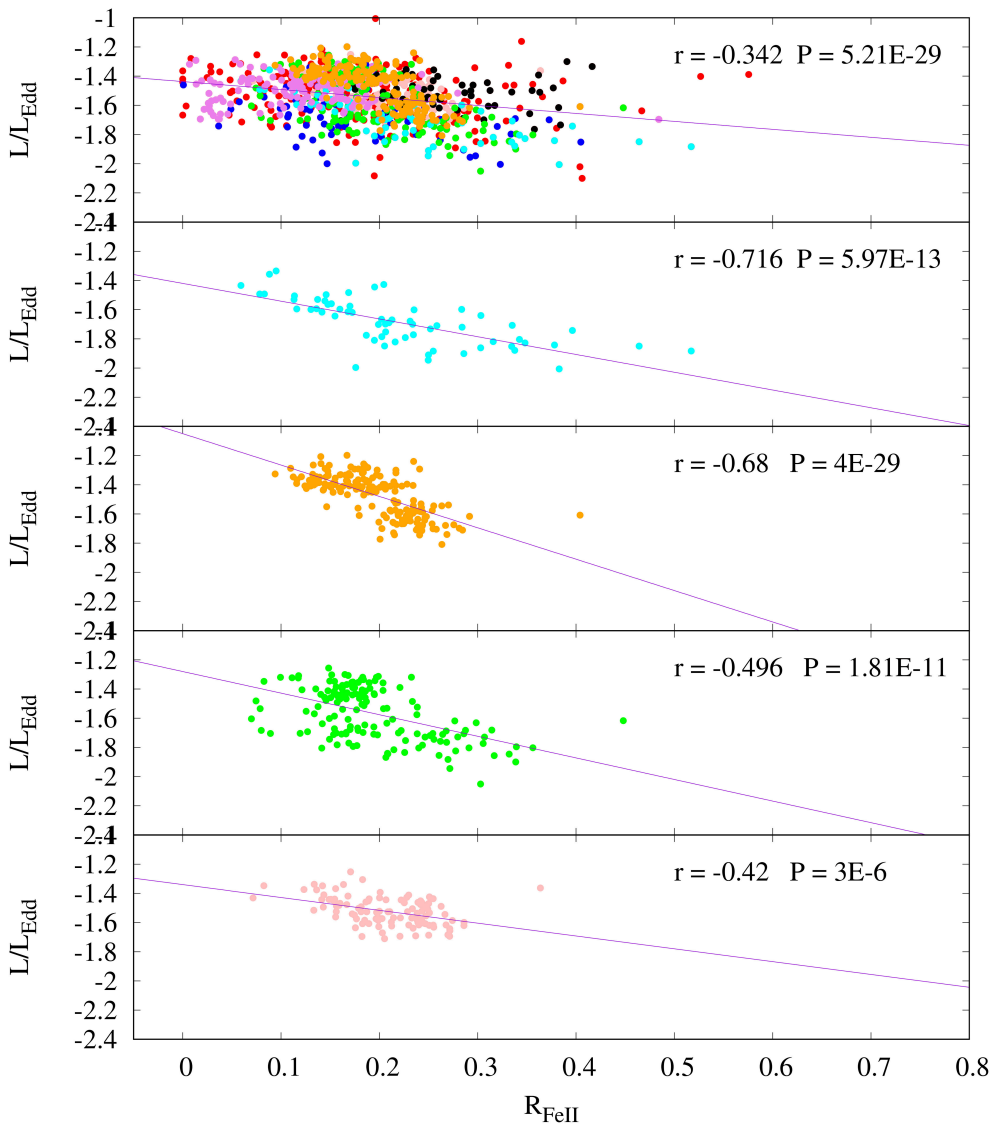

FIGURE 4 | The negative trend: L/L_{Edd} decrease with the increase of R_{FeII} with the time. The strongest anti-correlation was found for well defined time intervals presented on the middle and bottom panel. Colors correspond to those in **Figure 1**, **2**.

the behavior for each segment on time line is very different. The biggest structural change we noticed in the time interval colored in blue and cyan.

It is expected that both inclination and the black hole mass play a significant role in the physical characterization of the AGN main sequence diagram, but in the case of the inspection of EV1 parameters of a single object through time, we expect inclination and black hole mass to be constant during the whole observational time. Therefore, the main driver of the variability along the EV1 diagram is expected to be associated with variations in accretion rate (since the black hole mass is fixed, accretion rate is proportional to both luminosity [for fixed radiative efficiency] and Eddington ratio). To analyze that, we show variations of L/L_{Edd} against R_{FeII} in **Figure 4**. We notice that decrease of L/L_{Edd} is followed by an increasing R_{FeII}, mainly in intervals when the flux shows large changes in very short time intervals (represented with high Pearson's correlation coefficient), both in the continuum, as well as in the Hβ line, indicating that changes along the EV1 diagram of the single object could be due sudden and fast changes in accretion rate. We find also that accretion rate and FWHM show modest correlation coefficient in complete monitoring interval, while in short time variations it may be quite high (see **Figure 5**). The L/L_{Edd} is obtained from the luminosity and the black hole mass, but since the mass is assumed constant, then the FWHM should not affect the L/L_{Edd}. We calculated L/Ledd using continuum flux measurements at 5100 Å assuming the bolometric correction factor 10 to the specific luminosity measured at 5100 Å (see Sulentic et al., 2006). The mass of the black hole is assumed to be $5.7 \times 10^7\ M\odot$, as in the paper (Bon et al., 2016). Therefore, the

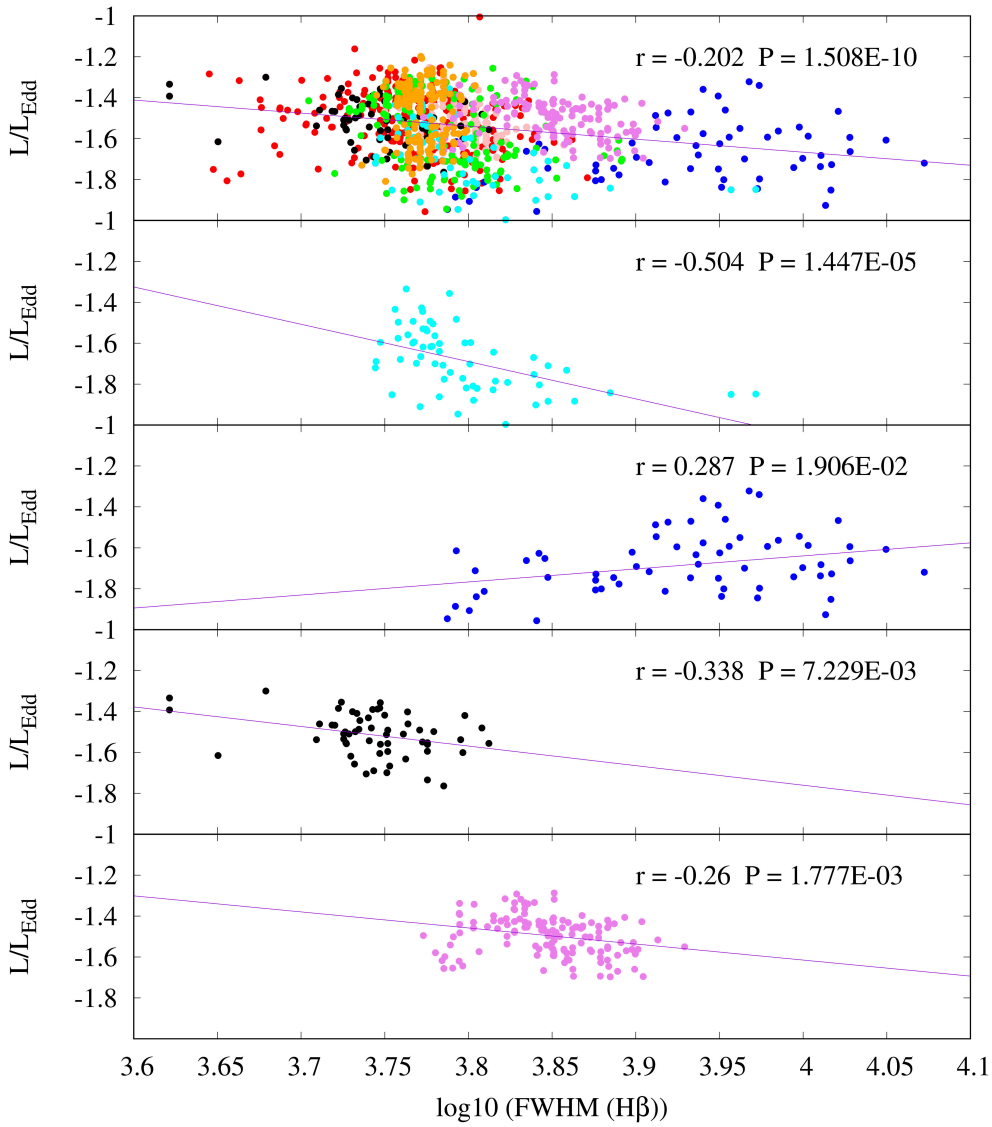

FIGURE 5 | L/L_{Edd} vs. $log_{10}(FWHM)$ trends for long term (**top**) and short term variations (**middle and bottom**). Correlation coefficients are marked on each plot. Colors correspond to those presented in **Figure 1**, **2**.

study of a single object has the advantage that FWHM and L/L_{Edd} measurements are independent. On the converse, in the study of quasar samples, the FWHM is used to compute M_{BH}, and hence L/L_{Edd} and FWHM are not independent parameter.

3. DISCUSSION AND CONCLUSION

Since NGC 5548 has not undergone major structural change over $\sim$ 40 years of observations, if the physical parameter that drive EV 1 is Eddington ratio, then it appears that the source never crossed the boundary for structural changes, indicatively placed at L/LEdd $\sim$ 0.2.

A decrease in FWHM with increasing L/L_{Edd} would be consistent with the expectations of an increasing effect of radiation forces with increasing luminosity. The absence of a strong relation is only in apparent contradiction with the expectation of the model by Netzer and Marziani (2010). We found a very weak anti-correlation between FWHM and L/L_{Edd}, with a slope of ≈ -0.07 [1] (with Pearson correlation coefficient of -0.18, and a significance of 7×10^{-9}). We also found a significant but weak anticorrelation between FWHM of Hβ line and continuum, with a modest slope (see **Figure 6**). For the typical L/L_{Edd} of NGC 5548, radiation forces have a relatively little effect on the dynamics of the line emitting clouds. A FWHM change should be limited to $\lesssim$ 10% (Table 1 of Netzer and Marziani, 2010), as indeed suggested by the trend found from the actual data (with a slope -0.07, a three-fold increase in continuum implies a narrowing by $\approx$ 8%). There is therefore no contradiction between a weak and shallow correlation and a minor role of radiation forces.

In the studies of quasar samples it is showen that FWHM of Hβ increases, because of the increase of the black hole mass For an individual object the story is different. The most reasonable assumption is that the virial product is constant $r \times FWHM^2 =$ constant[2]. If r scales with luminosity as $r \propto L^a$, then $FWHM \propto L^{-a/2}$, which is not far from the trend we detect for the complete monitoring interval (see **Figure 6**). But for short time variability epochs trends are different for each segment that we defined (see **Figure 7** and marked trends on each panel). It is interesting that in the time interval marked with blue, we see the positive trend of luminosity against FWHM of Hβ broad emission line (see **Figure 7**). This time interval corresponds to long term variation of flux slowly increasing for 12 year, starting from deep minimum in the low state and ending up toward the high state. In contrary to it, short term variations (for e.g., cyan and pink) shows negative trends (see panels in **Figure 7**).

In addition, right the recent work of Pei et al. (2017) finds, for two different time lapses T1 and T2, mean continuum fluxes at 5100 Å and line Hβ line widths: T1) mean flux $= 11.31 \pm 0.08$, FWHM (km s^{-1}) $= 9612 \pm 427$ and T2) mean flux $= 12.51 \pm 0.04$, FWHM (km s^{-1}) $= 9380 \pm 158$. The trend between the two time ranges, implies a decrease in the FWHM when the source

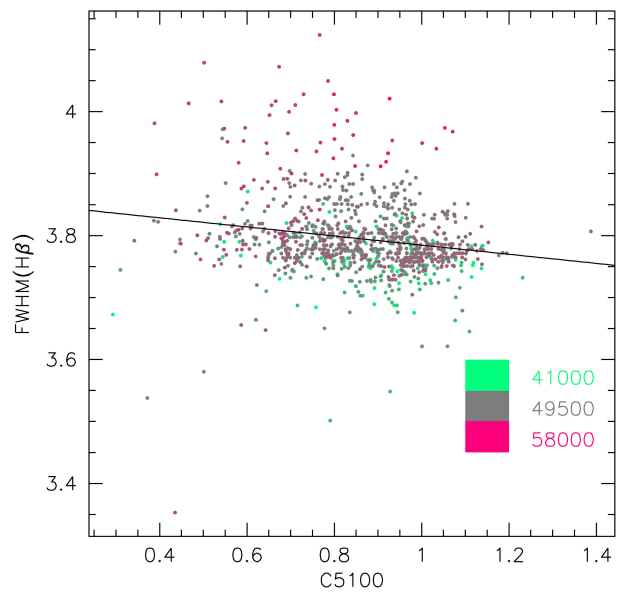

FIGURE 6 | Anti-correlation between FWHM of Hβ and continuum specific flux at 5100 Å. The line shows an unweighted least squares fit. Colors of data points are coded from green to magenta according to Julian date, from 2441000 to 2458000.

is brighter. Without considering the measurement dispersion in FWHM the slope is right -0.25, as predicted by the elementary consideration above in case of $r \propto L^{1/2}$, and therefore $FWHM \propto L^{-1/4}$, since $r \propto FWHM^{-2}$.

The resulting slope for the full sample (-0.07) is the result of mixing together different epochs in which the response of the BLR is different as per the short-term "breathing effect" first described by Netzer and Maoz (1990) and discussed in full by Korista and Goad (2004).

We believe that the weak anticorrelation we found deserves further analysis separately considering different states of continuum level/behavior, as well as changes in the structure factor f_S that, evidently, cannot be assumed as a constant, but we do not think that the shallow trend is inconsistent with existing data of reverberation mapping campaigns.

Flattened, disk like, structure combined with surrounding isotropic region is usually good approximation of the BLR structure, so the line profile of population B sources can be approximated as the sum of a accretion disk profile component describing wings of the broad emission line, + an isotropic component describing the intermediate broad core of the broad line which is blending the double peaked shape of an accretion disk profile, producing the single peaked line profile with very broadened wings, typically seen in the AGN broad emission line profiles (see, e.g., Popović et al., 2004; Bon, 2008; Bon et al., 2009a,b). The optically thick core responding more strongly than continuum changes that the accretion disk component could also produce an anti-correlation between FWHM and continuum intensity. We plan to test this possibility in a forthcoming work.

The trend L/L_{Edd} against R_{FeII} is also difficult to explain. In principle, both Marziani et al. (2001) and Shen and Ho (2014) agree that an increase in L/L_{Edd} should lead to higher R_{FeII}.

[1] $logFWHM \sim (-0.073 \pm 0.0125)(logL) + (3.858 \pm 0.0108)$

[2] Also f, the form factor should not be constant rigorously speaking, but let us assume at the moment it is.

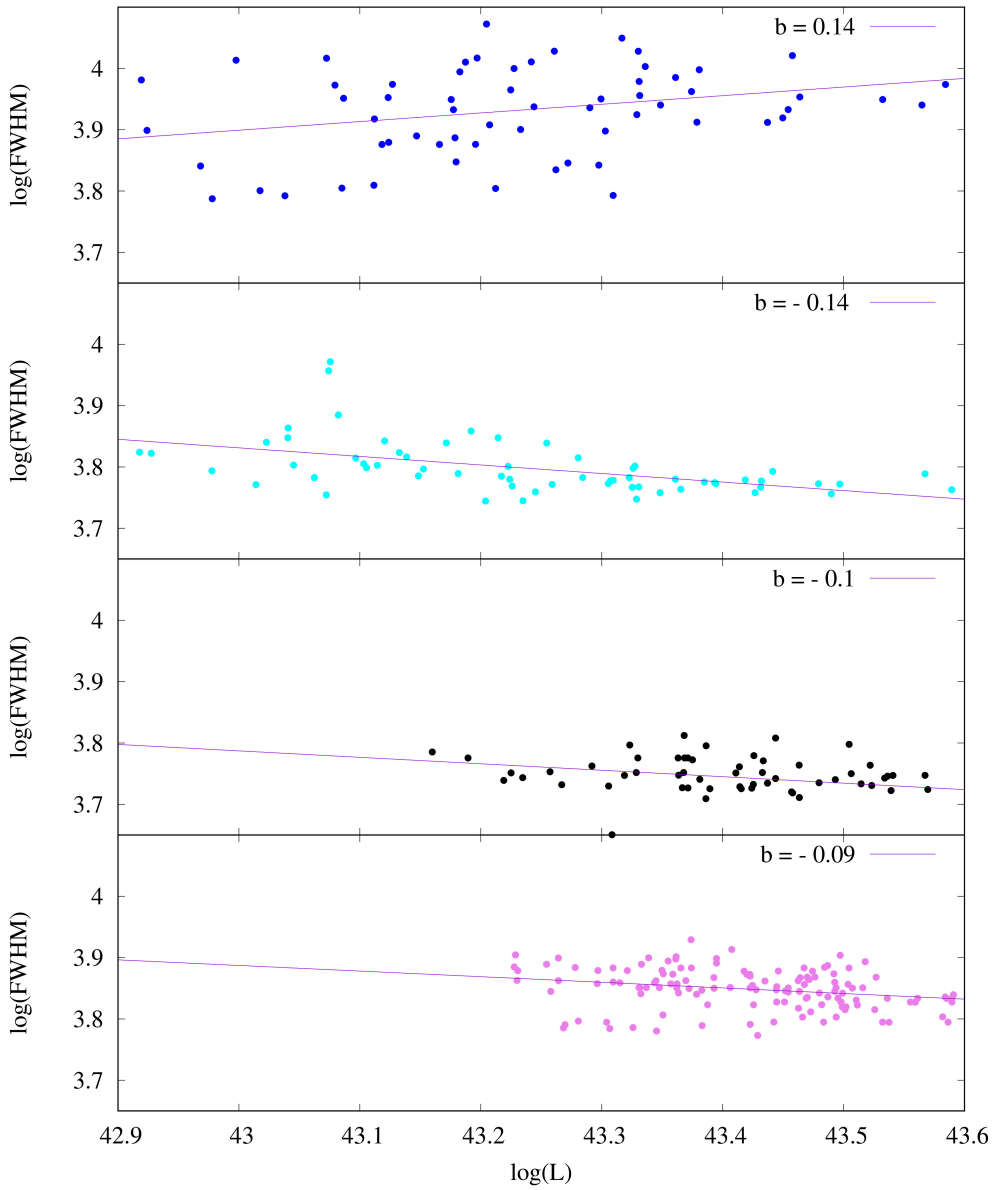

FIGURE 7 | Trends of luminosity against FWHM of Hβ for long term (blue represents last 12 years of observations) and short term variations (cyan, black, and pink are order of months). Lines shows an unweighted least squares fit. Colors of data points correspond to those presented in the **Figure 1**. Values of slope trends are marked on each plot.

This deduction was however reached from the analysis of a large sample of quasars, and not from the behavior of an individual source. Since R_{FeII} is the ratio of two quantities that both vary, it is important to know how the intensity and the EW of Hβ and FeII vary separately. Hβ shows a highly significant anti-correlation between its equivalent width and the continuum, with a lsq best-fit slope of ≈ -0.26 which is highly significant for 980 data points. This anti-correlation (the "Baldwin effect") is significantly steeper for FeII: the slope is ≈ -0.60. These dependencies reflect a different response to continuum changes for Hβ and FeII: while the flux of Hβ is correlated with continuum flux with a slope $\approx$ 0.80, implying a strong response, the response of FeII is much weaker, with I(FeII) $\propto$ 0.40 I(cont). Therefore, the EW of the FeII increases more than the EW of Hβ when continuum is low, in turn increasing R_{FeII}. These considerations suggest that a parallel between the behavior of large samples and the one associated with the variability of an individual object cannot be drawn, and that NGC 5548 does not challenge the notion of a positive relation between R_{FeII} and L/L_{Edd} found in large quasar sample.

The preliminary results summarized in this paper suggest that NGC 5548—a highly variable object that over several decades has seen large-amplitude continuum fluctuations and flaring behavior—remains a source of Pop. B, its variability notwithstanding. The location of NGC 5548 in the optical

plane of E1 remains constrained within spectral type B1. The range in Eddington ratio, even when the source is in a bright state, remains consistent with the value of the lowly—accreting Pop. B, implying that the source has not undergone major structural changes during the 40+ years it was monitored.

AUTHOR CONTRIBUTIONS

EB is responsible for developing the idea, NB for doing the fitting, NB, EB and PM for analysing the results and writing the text of the manuscript and discussing results.

FUNDING

This research is part of projects 176003 "Gravitation and the large scale structure of the Universe" and 176001 "Astrophysical spectroscopy of extragalactic objects" supported by the Ministry of Education and Science of the Republic of Serbia.

ACKNOWLEDGMENTS

We would like to thank to Jack Sulentic and Martin Gaskell for helpful comments.

REFERENCES

Bon, E. (2008). The disk emission in single peaked lines for 12 AGNs. *Serb. Astron. J.* 177, 9–13. doi: 10.2298/SAJ0877009B

Bon, E., Gavrilović, N., La Mura, G., and Popović, L. Č. (2009a). Complex broad emission line profiles of AGN - Geometry of the broad line region. *New Astron. Rev.* 53, 121–127. doi: 10.1016/j.newar.2009.09.007

Bon, E., Popović, L. Č., Gavrilović, N., La Mura, G., and Mediavilla, E. (2009b). Contribution of a disc component to single-peaked broad lines of active galactic nuclei. *Mon. Not. R. Astron. Soc.* 400, 924–936. doi: 10.1111/j.1365-2966.2009.15511.x

Bon, E., Zucker, S., Netzer, H., Marziani, P., Bon, N., Jovanović, P., et al. (2016). Evidence for Periodicity in 43 year-long Monitoring of NGC 5548. *Astrophys. J. Suppl.* 225:29. doi: 10.3847/0067-0049/225/2/29

Bon, N., Popović, L. Č., and Bon, E. (2014). Efficiency tests for estimating the gas and stellar population parameters in Type 2 objects. *Adv. Space Res.* 54, 1389–1400. doi: 10.1016/j.asr.2014.06.040

Boroson, T. A., and Green, R. F. (1992). The emission-line properties of low-redshift quasi-stellar objects. *Astrophys. J. Suppl.* 80, 109–135. doi: 10.1086/191661

Fraix-Burnet, D., Marziani, P., D'Onofrio, M., and Dultzin, D. (2017). The phylogeny of quasars and the ontogeny of their central black holes. *Front. Astron. Space Sci.* 4:1. doi: 10.3389/fspas.2017.00001

Koleva, M., Prugniel, P., Bouchard, A., and Wu, Y. (2009). ULySS: a full spectrum fitting package. *Astron. Astrophys.* 501, 1269–1279. doi: 10.1051/0004-6361/200811467

Korista, K. T., and Goad, M. R. (2004). What the optical recombination lines can tell us about the broad-line regions of active galactic nuclei. *Astrophys. J.* 606, 749–762. doi: 10.1086/383193

Marziani, P., Sulentic, J. W., Stirpe, G. M., Zamfir, S., and Calvani, M. (2009). VLT/ISAAC spectra of the Hβ region in intermediate-redshift quasars. III. Hβ broad-line profile analysis and inferences about BLR structure. *Astron. Astrophys.* 495, 83–112. doi: 10.1051/0004-6361:200810764

Marziani, P., Sulentic, J. W., Zwitter, T., Dultzin-Hacyan, D., and Calvani, M. (2001). Searching for the Physical Drivers of the Eigenvector 1 Correlation Space. *Astrophys. J.* 558, 553–560. doi: 10.1086/322286

Netzer, H., and Maoz, D. (1990). On the emission-line response to continuum variations in the Seyfert galaxy NGC 5548. *Astrophys. J. Lett.* 365, L5–L7. doi: 10.1086/185875

Netzer, H., and Marziani, P. (2010). The effect of radiation pressure on emission-line profiles and black hole mass determination in active galactic nuclei. *Astrophys. J.* 724, 318–328. doi: 10.1088/0004-637X/724/1/318

Pei, L., Fausnaugh, M. M., Barth, A. J., Peterson, B. M., Bentz, M. C., De Rosa, G., et al. (2017). Space telescope and optical reverberation mapping project. V. optical spectroscopic campaign and emission-line analysis for NGC 5548. *Astrophys. J.* 837:131. doi: 10.3847/1538-4357/aa5eb1

Peterson, B. M., Berlind, P., Bertram, R., Bischoff, K., Bochkarev, N. G., Borisov, N., et al. (2002). Steps toward determination of the size and structure of the broad-line region in active galactic nuclei. XVI. A 13 year study of spectral variability in NGC 5548. *Astrophys. J.* 581, 197–204. doi: 10.1086/344197

Popović, L. Č., Mediavilla, E., Bon, E., and Ilić, D. (2004). Contribution of the disk emission to the broad emission lines in AGNs: two-component model. *Astron. Astrophys.* 423, 909–918. doi: 10.1051/0004-6361:20034431

Sergeev, S. G., Doroshenko, V. T., Dzyuba, S. A., Peterson, B. M., Pogge, R. W., and Pronik, V. I. (2007). Thirty years of continuum and emission-line variability in NGC 5548. *Astrophys. J.* 668, 708–720. doi: 10.1086/520697

Shakura, N. I., and Sunyaev, R. A. (1973). Black holes in binary systems. Observational appearance. *Astron. Astrophys.* 24, 337–355.

Shen, Y., and Ho, L. C. (2014). The diversity of quasars unified by accretion and orientation. *Nature* 513, 210–213. doi: 10.1038/nature13712

Sniegowska, M., Czerny, B., You, B., Panda, S., Wang, J.-M., Hryniewicz, K., et al. (2017). The properties of active galaxies at the extreme of eigenvector 1. ArXiv e-prints.

Sulentic, J. W., Marziani, P., Zwitter, T., Dultzin-Hacyan, D., and Calvani, M. (2000). The demise of the classical broad-line region in the luminous quasar PG 1416-129. *Astrophys. J. Lett.* 545, L15–L18. doi: 10.1086/317330

Sulentic, J. W., Repetto, P., Stirpe, G. M., Marziani, P., Dultzin-Hacyan, D., and Calvani, M. (2006). VLT/ISAAC spectra of the Hβ region in intermediate-redshift quasars. II. Black hole mass and Eddington ratio. *Astron. Astrophys.* 456, 929–939. doi: 10.1051/0004-6361:20054153

Zamfir, S., Sulentic, J. W., Marziani, P., and Dultzin, D. (2010). Detailed characterization of Hβ emission line profile in low-z SDSS quasars. *Mon. Not. R. Astron. Soc.* 403, 1759–1786. doi: 10.1111/j.1365-2966.2009

Conflict of Interest Statement: The authors declare that the research was conducted in the absence of any commercial or financial relationships that could be construed as a potential conflict of interest.

The reviewer, MD, declared a shared affiliation, though no other collaboration, with the authors, NB and EB, to the handling Editor.

Copyright © 2018 Bon, Bon and Marziani. This is an open-access article distributed under the terms of the Creative Commons Attribution License (CC BY). The use, distribution or reproduction in other forums is permitted, provided the original author(s) and the copyright owner are credited and that the original publication in this journal is cited, in accordance with accepted academic practice. No use, distribution or reproduction is permitted which does not comply with these terms.

frontiers in Astronomy and Space Sciences

ORIGINAL RESEARCH
published: 22 December 2017
doi: 10.3389/fspas.2017.00064

C IV Broad Absorption Line Variability in QSO Spectra from SDSS Surveys

Demetra De Cicco [1], William N. Brandt [2, 3, 4], Catherine J. Grier [2] and Maurizio Paolillo [1, 5, 6]*

[1] Department of Physics, University of Naples Federico II, Napoli, Italy, [2] 525 Davey Laboratory, Department of Astronomy and Astrophysics, Pennsylvania State University, University Park, PA, United States, [3] Institute for Gravitation and the Cosmos, Pennsylvania State University, University Park, PA, United States, [4] 104 Davey Laboratory, Department of Physics, Pennsylvania State University, University Park, PA, United States, [5] National Institute for Nuclear Physics (INFN) - Sezione di Napoli, Napoli, Italy, [6] Agenzia Spaziale Italiana Science Data Center, Rome, Italy

Broad absorption lines (BALs) in the spectra of quasi-stellar objects (QSOs) are thought to arise from outflowing winds along our line of sight; winds, in turn, are thought to originate from the accretion disk, in the very surroundings of the central supermassive black hole (SMBH), and they likely affect the accretion process onto the SMBH, as well as galaxy evolution. BALs can exhibit variability on timescales typically ranging from months to years. We analyze such variability and, in particular, BAL disappearance, with the aim of investigating QSO physics and structure. We search for disappearing C IV BALs in the spectra of 1,319 QSOs from different programs from the Sloan Digital Sky Survey (SDSS); the analyzed time span covers 0.28–4.9 year (rest frame), and the source redshifts are in the range 1.68–4.27. This is to date the largest sample ever used for such a study. We find 67 sources ($5.1^{+0.7}_{-0.6}$% of the sample) with 73 disappearing BALs in total ($3.9^{+0.5}_{-0.5}$% of the total number of C IV BALs detected; some sources have more than one BAL that disappears). We compare the sample of disappearing BALs to the whole sample of BALs, and investigate the correlation in the variability of multiple troughs in the same spectrum. We also derive estimates of the average lifetime of a BAL trough and of the BAL phase along our line of sight.

Keywords: broad absorption lines, quasars, QSO, BALQSO, variability, active galaxies

OPEN ACCESS

Edited by:
Paola Marziani, Osservatorio Astronomico di Padova (INAF), Italy

Reviewed by:
Damien Hutsemékers, University of Liège, Belgium
Alenka Negrete, Universidad Nacional Autónoma de México, Mexico

****Correspondence:***
Demetra De Cicco
demetradecicco@gmail.com; demetra.decicco@unina.it

Specialty section:
This article was submitted to Milky Way and Galaxies, a section of the journal Frontiers in Astronomy and Space Sciences

Received: *30 September 2017*
Accepted: *12 December 2017*
Published: *22 December 2017*

Citation:
De Cicco D, Brandt WN, Grier CJ and Paolillo M (2017) C IV Broad Absorption Line Variability in QSO Spectra from SDSS Surveys. Front. Astron. Space Sci. 4:64. doi: 10.3389/fspas.2017.00064

1. INTRODUCTION

The ultraviolet spectra of quasi-stellar objects (QSOs) are characterized by prominent emission features originating from transitions such as C IV, Si IV, N V, and additional lower ionization transitions, like Al III and Mg II (e.g., Weymann et al., 1991; Murray et al., 1995; Vanden Berk et al., 2001). In 10–20% of optically selected QSOs, in addition to the emission lines, absorption lines are detected, and they are typically blueshifted up to 0.1c with respect to the corresponding rest-frame feature.

The presence of such absorption lines is thought to be related to a relevant momentum transfer from the QSO radiation field to the gas which gives rise to the observed lines. Specifically, absorption features are thought to originate from radiatively accelerated outflowing winds along our line of sight. According to the leading models, winds originate from the accretion disk, at distances on the order of 10^{-2}–10^{-1} pc from the central supermassive black hole (SMBH); they affect the observed QSO properties, like UV and X-ray line absorption and high-ionization line emission, and enable the accretion mechanism as they remove from the disk the angular

momentum released by the accreting material. Also, they likely play a leading role into galaxy evolution by evacuating and redistributing gas from the host galaxy, and by preventing new gas inflow into the galaxy, thus significantly affecting star formation processes (e.g., Di Matteo et al., 2005; Capellupo et al., 2012).

Several models have been proposed to describe QSO winds and, according to most of them, the observed absorption features could be the effect of a specific viewing angle, as winds are thought to originate in the equatorial region of a QSO. As an example, Elvis (2000) proposes a funnel-shaped, biconical structure for broad absorption lines (BAL) outflowing winds, where some instability in the accretion disk at distances on the order of 10^{-2} pc from the central SMBH originates a vertical, cylindrical stream; centrifugal forces combined with radiation pressure cause the bending of the stream outwards radially when the vertical velocity equals the radial velocity, and the stream is accelerated to typical BAL velocities. Hence, depending on which direction we look at, we will be able or not able to detect absorption features, and such a structure therefore accounts for the lack of detection of absorption lines in a large fraction of QSO spectra, assuming that, in such instances, we are looking at the funnel from a face-on direction. Alternative hypotheses about QSO absorption lines see them as the signature of a peculiar stage of QSO evolution (e.g., Green et al., 2001). Sometimes a blue asymmetry in the C IV emission line is observed, and this has been associated with outflows (see, e.g., Sulentic et al. 2017).

Any model describing QSO winds must take into account the so-called overionization problem: the X-ray and UV emission from QSOs is expected to overionize the gas it encounters in the inner regions of the QSO, hence spectral lines should not be detected at all. Possible explanations for their existence generally involve the presence of some shielding material between the radiation source and the gas (e.g., Murray et al., 1995), or a density gradient along the line of sight, giving rise to different ionization states of the outflowing gas (Baskin et al., 2014).

Absorption lines are delimited by a maximum and a minimum velocity[1], $\upsilon_{\rm max}$ and $\upsilon_{\rm min}$; it follows that we will also have a central velocity $\upsilon_{\rm c} = (\upsilon_{\rm max} + \upsilon_{\rm min})/2$, which identifies the position of the absorption line, and a line width in terms of velocity, defined as $\Delta\upsilon = |\upsilon_{\rm max} - \upsilon_{\rm min}|$. Such width is generally referred to in classifying absorption lines: $\Delta\upsilon \geq 2{,}000$ km s^{-1} defines BALs, while $\Delta\upsilon < 500$ km s^{-1} defines narrow absorption lines (NALs); features in between are labeled "mini-BALs."

Since the 1980s we have known that the equivalent width (EW) of BAL troughs can vary on rest-frame timescales typically ranging from months to years (but also much shorter, sometimes; see, e.g., Grier et al., 2015, where the variability of a C IV BAL trough on rest-frame timescales of ≈1.20 days is discussed), and several attempts to investigate such variability have been made; past studies generally suffered from restrictions either in the sample size or in the length of the observing baseline. In order to report a few examples of such studies, we mention the work by Barlow (1993), where a sample of 23 QSOs were monitored over a ≈1 year timescale, leading to the detection of BAL variability for 15 sources; the analysis by Lundgren et al. (2007), searching for C IV BAL variability in a sample of 29 QSOs over a <1 year baseline, and the work by Gibson et al. (2008), investigating C IV BAL variability in a sample of 13 QSOs over a 3–6 year baseline (all the mentioned timescales are rest frame). Filiz Ak et al. (2012) present the first statistical analysis of C IV BAL disappearance making use of data from various projects that are part of the Sloan Digital Sky Survey-I/II/III (SDSS-I/II/III; e.g., York et al., 2000). A sample of 582 QSOs is analyzed over a 1.1–3.9 year baseline, and disappearances are detected in the spectra of 19 QSOs.

Here we briefly discuss the results of our analysis of C IV BAL variability and, more specifically, disappearance; our work extends the sample analyzed in Filiz Ak et al. (2012), as more SDSS spectra became available, and is based on a sample of 1,319 sources. This makes our sample the largest available so far for such a study, and its size allowed us to perform a reliable statistical analysis. Our ultimate goal is to gain insight into the physical processes driving BAL variability and the properties of the regions where winds are thought to originate, in order to extend our knowledge of QSO structure and evolution. The full work is described in detail in De Cicco et al. (in preparation).

2. MATERIALS AND METHODS

2.1. Sample Selection

We analyzed C IV BAL disappearance in the spectra of 1,319 optically bright (i band magnitude $<$ 19.3 mag) QSOs selected from a larger catalog of 5,039 objects (Gibson et al., 2009) where BALs were detected. Sources must be in the redshift range $1.68 < z < 4.93$ for C IV BALs to be detectable in SDSS spectra, since their blueshifted velocities can be in the range from −30,000 to 0 km s^{-1} (Gibson et al., 2009); in particular, for our sample we have $1.68 < z < 4.27$. For each source at least two spectra are available: one, more recent, from the SDSS-III Baryon Oscillation Spectroscopic Survey (BOSS; e.g., Dawson et al., 2013), and the other from an SDSS-I/II survey program. The rest-frame timescales between observations in a pair are in the range 0.28–4.9 year. Some of the 1,319 sources show more than one C IV BAL trough (Section 3).

Following other works from the literature (e.g., Filiz Ak et al., 2012), we restrict our analysis to C IV BALs with $-30{,}000 \leq \upsilon_{\rm max} \leq -3{,}000$ km s^{-1} in order to minimize contamination from the C IV emission line on the red end of the line and from the Si IV emission/absorption features on the blue end.

2.2. Data Reduction

Here we briefly outline the data reduction process, which will be described in detail in De Cicco et al. (in preparation).

Essentially, we correct for systematics originating from spectrophotometric calibration errors following Margala et al. (2016), and mask bad pixels on the basis of the header files of our spectra. Galactic extinction is corrected following Cardelli et al. (1989), on the basis of a Milky Way extinction model, with visual extinction coefficients from Schlegel et al. (1998). Redshifts from Hewett and Wild (2010) are used to obtain rest-frame wavelengths.

[1]The minus sign due to blueshift is not taken into account.

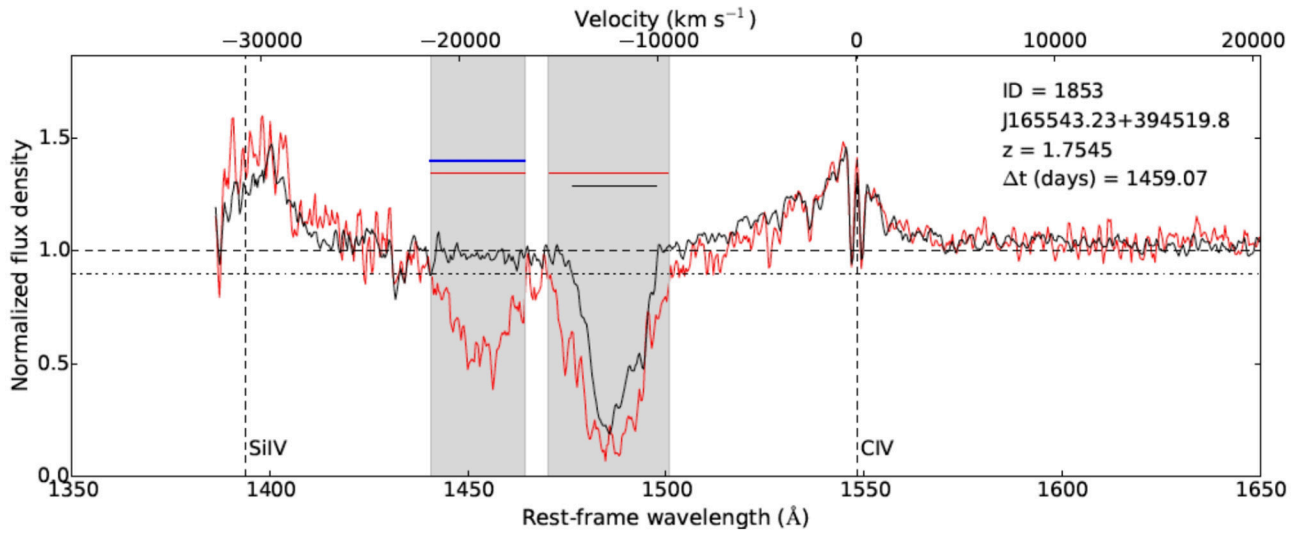

FIGURE 1 | Overplot of a pair of SDSS-I/II (red) and BOSS (black) spectra showing a disappearing BAL trough and an additional non-disappearing BAL trough. We report the source ID in our catalog, the SDSS ID, the redshift, and the rest-frame time difference between the two spectra. Plots are limited to the wavelength window where C IV BAL disappearance can be observed. Horizontal axes: rest-frame wavelength (bottom) and velocity (top); vertical axis: normalized flux. Horizontal dashed line: normalized flux density = 1; dash-dot line: normalized flux density = 0.9. Vertical dashed lines: Si IV (1,394 Å) and C IV (1,549 Å) emission lines (rest-frame wavelengths). Red/black horizontal lines: BAL troughs in the SDSS-I/II/BOSS spectra; blue bars: SDSS-I/II BAL troughs that disappear in BOSS spectra. The regions corresponding to SDSS-I/II BAL troughs are shaded for better visualization.

TABLE 1 | Detailed information about our main sample of sources and the sample of C IV disappearing BAL troughs.

MAIN SAMPLE	
Sources with C IV BAL troughs in their SDSS-I/II spectra	1,319
Total number of C IV BAL troughs detected in SDSS-I/II spectra	1,874
DISAPPEARING BAL SAMPLE	
Sources with a disappearing BAL trough in at least one BOSS spectra	67
Total number of disappearing BAL troughs in BOSS spectra	73
Sources where the disappearing BAL trough is the only BAL trough present	40/67

In some spectra we detect more than one C IV (disappearing) BAL trough.

TABLE 2 | Summary of our main numerical findings.

Fraction of sources with disappearing BAL troughs (f_{QSO})	$5.1^{+0.7}_{-0.6}$% (67/1,319)
Fraction of disappearing BAL troughs (f_{disapp})	$3.9^{+0.5}_{-0.5}$% (73/1,874)
Average BAL-trough lifetime $\bar{t}_{trough}$ (year)	80^{+10}_{-10}
Fraction of BAL QSOs that turn into non-BAL QSOs ($f_{transform}$)	$2.3^{+0.5}_{-0.4}$% (30/1,319)
Average BAL-phase lifetime $\bar{t}_{BAL}$ (year)	136^{+30}_{-24}

In the continuum fit process we follow Grier et al. (2016) and Gibson et al. (2009). We adopt a reddened power law model, making use of the Small Magellanic Cloud-like reddening curve discussed in Pei (1992). We identify a set of regions (labeled "RLF," which stands for "relatively line-free") where emission/absorption features are generally negligible, and use them for the continuum fit. Specifically, our RLF correspond to the following wavelength ranges: 1,280–1,350, 1,425–1,450, 1,700–1,800, 1,950–2,200, 2,650–2,710, 3,010–3,700, 3,950–4,050, 4,140–4,270, 4,400–4,770, and 5,100–6,400 Å. All of them but one (1,425–1,450 Å) where used in Gibson et al. (2009). Here, following Grier et al. (2016), we introduce the mentioned additional RLF, to be used for sources with a redshift $z < 1.85$ in order to obtain a better fitting of the blue end of the spectrum. A non-linear least squares analysis is performed iteratively, with a 3σ threshold allowing us to reject outliers at each iteration in order to minimize the contamination by prominent features happening to fall in our RLF regions. Iterative Monte Carlo simulations, where random Gaussian noise is added to each spectrum to be fitted, define the uncertainties in the continuum, after Peterson et al. (1998) and Grier et al. (2016).

3. RESULTS AND DISCUSSION

After converting wavelengths into velocities, we identify all the C IV BAL troughs in our SDSS-I/II spectra, requiring their flux to extend below 90% of the normalized continuum level, as is common practice. In some cases we detected more than one C IV BAL trough in a spectrum, corresponding to different blueshifted velocities. We then search the corresponding region in the corresponding BOSS spectrum, and assume a BAL disappears if we detect only NALs, or no troughs at all. For some sources we have multiple SDSS-I/II epochs and/or multiple BOSS epochs: if this is the case, we select the most recent SDSS-I/II epoch

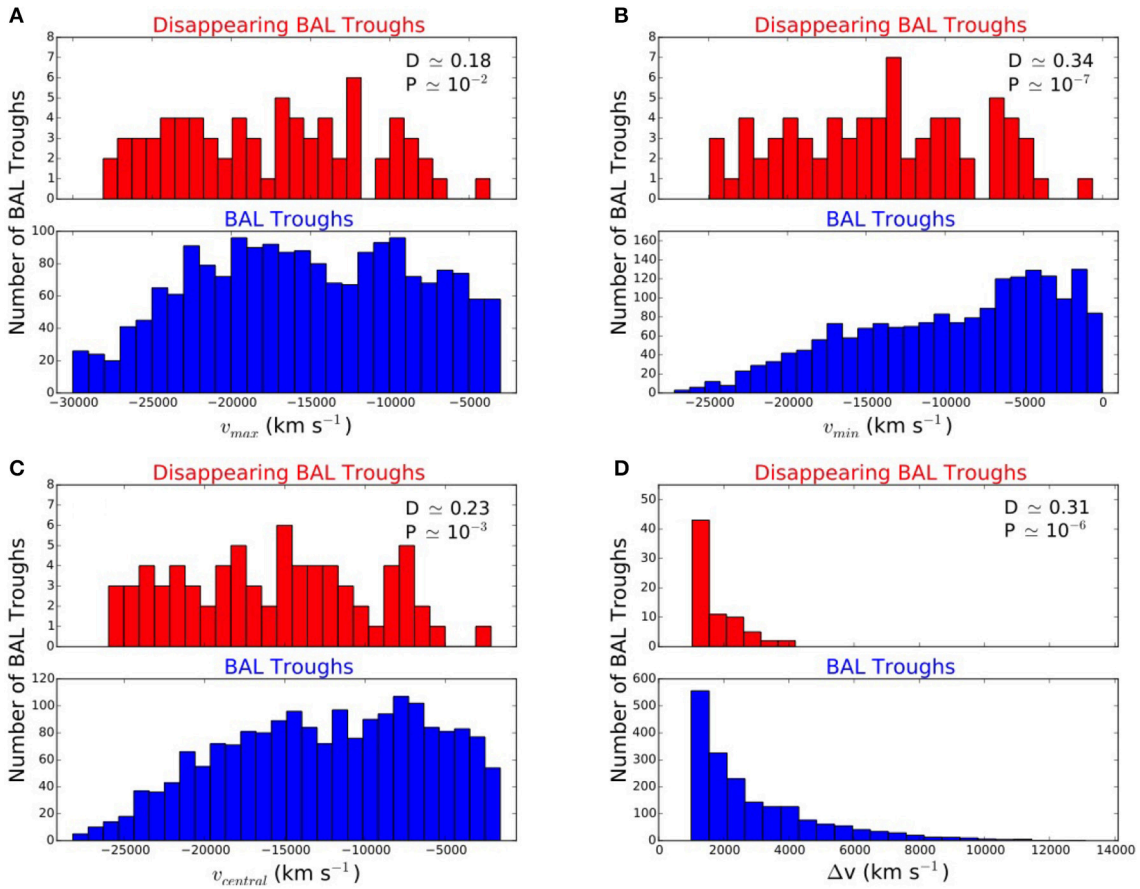

FIGURE 2 | Maximum observed velocity $\upsilon_{\max}$ **(A)**, minimum observed velocity $\upsilon_{\min}$ **(B)**, central velocity υ_C **(C)**, and BAL width $\Delta\upsilon$ **(D)** distributions for the sample of disappearing BAL troughs (upper red histogram in each panel) and for the main sample of BAL troughs (lower blue histogram in each panel). Results of the Kolmogorov-Smirnov test performed on each pair of cumulative distributions are reported in each panel: *D* is the maximum distance between the two cumulative distributions, and *P* is the probability to get a higher *D* value assuming that the two datasets are drawn from the same distribution function.

where we detect a C IV BAL trough, and the less recent BOSS epoch where a BAL disappears, as we aim at probing the shortest accessible timescales and the fastest variability. We find 1,874 BALs (hereafter, main sample) in the SDSS-I/II spectra of our 1,319 BAL QSOs, with the spectra of 427 sources exhibiting more than one C IV BAL trough[2]. In **Figure 1** we show the SDSS-I/II and BOSS spectra of one of our QSOs, where a disappearing BAL, together with a non-disappearing BAL, can be observed.

For each source we perform a two-sample χ^2 test comparing the two sets of points corresponding to normalized flux density values in the SDSS-I/II and BOSS windows where we detect a disappearance (indicated by blue bars in **Figure 1**), and assume that a disappearance is reliable if the χ^2 test probability for the BAL variation to be not random is $P_{\chi^2} \leq 10^{-4}$; this returns a sample of 67 sources with at least one C IV BAL trough that disappears in their spectra. Specifically, this sample includes three objects whose spectra show two C IV BALs that disappear, and two sources where the C IV disappearing BALs are three. This means that, in total, we detect 73 C IV disappearing BALs in the spectra of our sample of 67 sources. This means that in the BOSS spectra of the QSOs in our main sample we detect 1,801 (i.e., 1,874–73) C IV BAL troughs; specifically, if we consider the 67 sources for which we detect a disappearance, there are 40 of them whose BOSS spectra do not show any C IV BALs, and 27 of them where other C IV BAL troughs are still detected. As a consequence, the number of QSOs with C IV BAL troughs in their BOSS spectra is 1,279 (i.e., 1,319–40). We shall deal with the subsample of sources with additional non-disappearing BALs in section 3.3.

The average rest-frame time difference between two spectra where disappearance is observed is Δt is $\simeq$1,123 days, corresponding to a timescale of $\approx$3.1 year. In **Table 1** we gather together all the relevant numbers relative to our sources.

3.1. Lifetime Estimates

The fraction of disappearing BAL troughs is defined as the number of C IV BAL troughs that disappear in the BOSS spectra

[2]Throughout the present work we will refer to BAL QSOs and BAL troughs, and some clarification may be necessary: we define as BAL QSO each QSO whose spectrum exhibits at least one BAL trough, i.e., an absorption line having a width $\Delta\upsilon \geq 2{,}000$ km s^{-1} and extending below 90% of the normalized continuum level. In some cases the BAL troughs detected in a spectrum are more than one. We remind the reader that the present work is focused on C IV BAL troughs.

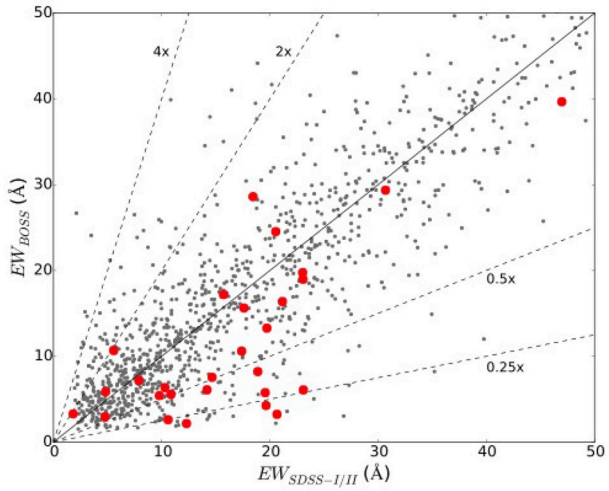

FIGURE 3 | EWs at two different epochs for the sample of additional non-disappearing BALs in the spectra where disappearances are detected (large red dots). For each BAL trough, the two EWs are measured in the same epoch pair where disappearance is detected. Small gray dots in the background represent the EWs at two epochs (one from SDSS-I/II and one from BOSS) for all the sources in the main sample, measured from the most-recent SDSS-I/II epoch and the least-recent BOSS epoch for each source. The solid line indicates where the EWs of the two compared epochs are equal, while the dashed lines indicate where the EW of the BOSS epoch is four times, two times, half of, and a quarter of the EW in the SDSS-I/II epoch.

divided by the number of C IV BAL troughs detected in the SDSS-I/II spectra, i.e., $f_{\rm disapp} = 73/1,874 = 3.9^{+0.5}_{-0.5}$%. The fraction of QSOs with at least one disappearing BAL trough is defined as the number of QSOs where at least one disappearing C IV BAL trough is detected divided by the total number of QSOs where C IV BAL troughs are detected, i.e., $f_{\rm QSO} = 67/1{,}319 = 5.1^{+0.7}_{-0.6}$% (percentage errors are obtained following Gehrels, 1986, where approximated confidence limits are derived based on Poisson and binomial statistics). We can give an estimate of the average lifetime of a BAL trough along our line of sight as the maximum time difference between two epochs for each source divided by the fraction of BAL troughs disappearing over such time; we obtain $\bar{t}_{\rm trough} \approx \langle \Delta t_{\rm max} \rangle / f_{\rm disapp} = 80^{+10}_{-10}$ year, the average value of the maximum time difference being $\langle \Delta t_{\rm max} \rangle \approx 1{,}144$ days.

Our estimate is roughly consistent with the orbital time ($\approx$50 year; e.g., Filiz Ak et al., 2013, and references therein) of the accretion disk at distances where winds are thought to form, typically, i.e., $\approx 10^{-2}$ pc; hence, disk rotation could possibly be the cause of BAL disappearance, and this may mean that BALs moving out of our line of sight will not be observable anymore, though they may still exist physically.

We know from the literature (e.g., Hall et al., 2002; Filiz Ak et al., 2012) that, if all the C IV BAL troughs in a spectrum disappear, there are generally no additional BALs left, meaning that the source is turned into a non-BAL QSO. In our sample there are 30 sources turning into non-BAL QSOs after their C IV BAL troughs disappear; the fraction of BAL QSOs changing into non-BAL QSOs is therefore $f_{\rm transform} = 30/1{,}319 = 2.3^{+0.5}_{-0.4}$%. This allows us to estimate the lifetime of the BAL phase in a QSO, defined approximately as the aforementioned average of the maximum time difference between two epochs divided by the fraction of BAL QSOs that turn into non-BAL QSOs over that time span: $\bar{t}_{\rm BAL} \approx \langle \Delta t_{\rm max} \rangle / f_{\rm transform} \approx 136^{+30}_{-24}$ year. Again, we point out that our lifetime estimates are limited to what we see along our line of sight, but do not necessarily constrain the physical existence of a BAL, as it could simply move out of that direction. Also, we note that a BAL could emerge again in a region where a BAL previously disappeared, making the definition of BAL phase a tricky task.

Table 2 is a summary of the main numerical results of our analysis of C IV BAL trough disappearance.

3.2. Velocity Distributions

BALs show some properties, in terms of their velocities, which can help characterize the BAL population. We compare the $\upsilon_{\rm max}$, $\upsilon_{\rm min}$, $\upsilon_{\rm c}$, and $\Delta\upsilon$ distributions for the disappearing BALs to the corresponding distributions for the whole main sample BALs and, on the basis of a Kolmogorov-Smirnov test comparing each pair (see **Figure 2**), we find that:

- the $\upsilon_{\rm max}$ distributions are not significantly different;
- the disappearing BALs generally have a high $\upsilon_{\rm min}$ and central velocity;
- the disappearing BALs are generally narrow with respect to the whole sample of BALs.

The distributions pairs show that disappearing BAL troughs are generally narrow and characterized by a higher outflow velocity than non-disappearing BALs. This last feature is confirmed by the analysis of the correlation in the variability of multiple BAL troughs in the same spectrum, discussed in next section. We used Kolmogorov-Smirnov test so that our findings can be easily compared to those by Filiz Ak et al. (2012), where part of our sample was analyzed; nevertheless, an Anderson-Darling test would probably be more suitable, as it is more sensitive on the distribution tails. We remind that this work is meant to be a preliminary version of a paper we are about to submit; more detailed results will be presented in the full paper. The results of our Kolmogorov-Smirnov tests are in agreement with the findings by Filiz Ak et al. (2012).

Figure 2 shows the various distribution pairs; in each panel we report the values of the two indicators obtained from the Kolmogorov-Smirnov test comparing each pair of cumulative distributions.

3.3. Correlation in BAL Variability

We already mentioned that sometimes there is more than one C IV BAL trough in a spectrum, and they do not necessarily disappear together. Additional non-disappearing BALs in spectra where we detect disappearing BALs can help us investigating the existence of a correlation in the variability of multiple BAL troughs in the spectra of a given source.

Our sample of 67 sources with disappearing BALs includes 27 objects for which we detect 28 additional non-disappearing BALs. Our investigation is limited to BAL troughs in SDSS-I/II spectra that correspond to BAL troughs in BOSS spectra; BALs turning into mini-BALs, or vice versa, are not taken into account. In all but one case, the disappearing BAL is the one with the higher central velocity. We compute the EW of these BALs from the same two spectra that allowed us to detect a disappearance, and compare them to the whole main sample of BALs, which is used as a reference population, as shown in **Figure 3**. We find that the main sample is characterized by symmetric variations in the EW, meaning they can get stronger as well as weaker, going from the less recent to the more recent epoch; conversely, 79^{+21}_{-17}% (again, percentage errors are computed following Gehrels, 1986) of the additional non-disappearing BALs show a decreasing EW in the more recent spectrum, supporting the idea that some correlation between different BAL troughs in a spectrum exists. This seems to be a persistent phenomenon, concerning even BALs that are very distant from one another (central velocity offset up to ≈20,000 km s^{-1}).

The explanation for such a correlation must be something global; the most accredited hypotheses attribute the observed correlation to variations in the density of the shielding gas, leading to changes in the ionizing flux reaching the absorbing gas and, hence, to variations in the ionization level of the absorbing gas. Nevertheless, recent works (e.g. Baskin et al., 2014) tend to favor models attributing the variations in the ionization level to the radiation pressure compression. However, it is likely that different causes contribute to the BAL variability phenomenon.

4. FUTURE PERSPECTIVES

In the near future we would like to extend our analysis to lower ionization transitions, such as Si IV and Mg II, in order to investigate possible relations between the variability of troughs originating from different transitions; also, a parallel study of BAL emergence would be of interest in the framework of a thorough comprehension of the BAL phenomenon and their physics, structure, and evolution.

AUTHOR CONTRIBUTIONS

All authors contributed to the design of the work, interpretation of data, drafting and revising of the work.

FUNDING

This paper is part of the "Quasars at all Cosmic Epochs" Research Topic and there are no publications fees for all participants to the conference. Publication fees were included in the conference fee and will be covered by the University of Padova.

REFERENCES

Barlow, T. A. (1993). *Time Variability of Broad Absorption-Line QSO's*. Ph.D. Thesis, University of California.

Baskin, A., Laor, A., and Stern, J. (2014). Radiation pressure confinement - IV. Application to broad absorption line outflows. *Mon. Not. Roy. Astron. Soc.* 445, 3025–3038. doi: 10.1093/mnras/stu1732

Capellupo, D. M., Hamann, F., Shields, J. C., Rodríguez Hidalgo, P., and Barlow, T. A. (2012). Variability in quasar broad absorption line outflows - II. Multi-epoch monitoring of Si IV and C IV broad absorption line variability. *Mon. Not. Roy. Astron. Soc.* 422, 3249–3267. doi: 10.1111/j.1365-2966.2012.20846.x

Cardelli, J. A., Clayton, G. C., and Mathis, J. S. (1989). The relationship between infrared, optical, and ultraviolet extinction. *Astrophys. J.* 345, 245–256. doi: 10.1086/167900

Dawson, K. S., Schlegel, D. J., Ahn, C. P., Anderson, S. F., Aubourg, É., Bailey, S., et al. (2013). The Baryon oscillation spectroscopic survey of SDSS-III. *Astron. J.* 145:10. doi: 10.1088/0004-6256/145/1/10

Di Matteo, T., Springel, V., and Hernquist, L. (2005). Energy input from quasars regulates the growth and activity of black holes and their host galaxies. *Nature* 433, 604–607. doi: 10.1038/nature03335

Elvis, M. (2000). A structure for quasars. *Astrophys. J.* 545, 63–76. doi: 10.1086/317778

Filiz Ak, N., Brandt, W. N., Hall, P. B., Schneider, D. P., Anderson, S. F., Gibson, R. R., et al. (2012). Broad absorption line disappearance on multi-year timescales in a large quasar sample. *Astrophys. J.* 757:114. doi: 10.1088/0004-637X/757/2/114

Filiz Ak, N., Brandt, W. N., Hall, P. B., Schneider, D. P., Anderson, S. F., Hamann, F., et al. (2013). Broad absorption line variability on multi-year timescales in a large quasar sample. *Astrophys. J.* 777:168. doi: 10.1088/0004-637X/777/2/168

Gehrels, N. (1986). Confidence limits for small numbers of events in astrophysical data. *Astrophys. J.* 303, 336–346. doi: 10.1086/164079

Gibson, R. R., Brandt, W. N., Schneider, D. P., and Gallagher, S. C. (2008). Quasar broad absorption line variability on multiyear timescales. *Astrophys. J.* 675, 985–1001. doi: 10.1086/527462

Gibson, R. R., Jiang, L., Brandt, W. N., Hall, P. B., Shen, Y., Wu, J., et al. (2009). A catalog of broad absorption line quasars in Sloan Digital Sky Survey data release 5. *Astrophys. J.* 692, 758–777. doi: 10.1088/0004-637X/692/1/758

Green, P. J., Aldcroft, T. L., Mathur, S., Wilkes, B. J., and Elvis, M. (2001). A Chandra survey of broad absorption line quasars. *Astrophys. J.* 558, 109–118. doi: 10.1086/322311

Grier, C. J., Brandt, W. N., Hall, P. B., Trump, J. R., Filiz Ak, N., Anderson, S. F., et al. (2016). C IV broad absorption line acceleration in Sloan Digital Sky Survey Quasars. *Astrophys. J.* 824:130. doi: 10.3847/0004-637X/824/2/130

Grier, C. J., Hall, P. B., Brandt, W. N., Trump, J. R., Shen, Y., Vivek, M., et al. (2015). The Sloan Digital Sky Survey reverberation mapping project: rapid CIV broad absorption line variability. *Astrophys. J.* 806:111. doi: 10.1088/0004-637X/806/1/111

Hall, P. B., Anderson, S. F., Strauss, M. A., York, D. G., Richards, G. T., Fan, X., et al. (2002). Unusual broad absorption line quasars from the Sloan Digital Sky Survey. *Astrophys. J. Suppl.* 141, 267–309. doi: 10.1086/340546

Hewett, P. C., and Wild, V. (2010). Improved redshifts for SDSS quasar spectra. *Mon. Not. Roy. Astron. Soc.* 405, 2302–2316. doi: 10.1111/j.1365-2966.2010.16648.x

Lundgren, B. F., Wilhite, B. C., Brunner, R. J., Hall, P. B., Schneider, D. P., York, D. G., et al. (2007). Broad absorption line variability in repeat quasar observations from the Sloan Digital Sky Survey. *Astrophys. J.* 656, 73–83. doi: 10.1086/510202

Margala, D., Kirkby, D., Dawson, K., Bailey, S., Blanton, M., and Schneider, D. P. (2016). Improved spectrophotometric calibration of the SDSS-III BOSS Quasar sample. *Astrophys. J.* 831:157. doi: 10.3847/0004-637X/831/2/157

Murray, N., Chiang, J., Grossman, S. A., and Voit, G. M. (1995). Accretion disk winds from active galactic nuclei. *Astrophys. J.* 451:498. doi: 10.1086/176238

Pei, Y. C. (1992). Interstellar dust from the milky way to the magellanic clouds. *Astrophys. J.* 395, 130–139. doi: 10.1086/171637

Peterson, B. M., Wanders, I., Bertram, R., Hunley, J. F., Pogge, R. W., and Wagner, R. M. (1998). Optical continuum and emission-line variability of Seyfert 1 galaxies. *Astrophys. J.* 501, 82–93. doi: 10.1086/305813

Schlegel, D. J., Finkbeiner, D. P., and Davis, M. (1998). Maps of dust infrared emission for use in estimation of reddening and cosmic microwave background radiation foregrounds. *Astrophys. J.* 500, 525–553. doi: 10.1086/305772

Sulentic, J. W., del Olmo, A., Marziani, P., Martínez-Carballo, M. A., D'Onofrio, M., Dultzin, D., et al. (2017). What does CIVλ1549 tell us about the physical driver of the eigenvector quasar sequence? *Astron. Astrophys.* 608:A122. doi: 10.1051/0004-6361/201630309

Vanden Berk, D. E., Richards, G. T., Bauer, A., Strauss, M. A., Schneider, D. P., Heckman, T. M., et al. (2001). Composite quasar spectra from the Sloan Digital Sky Survey. *Astron. J.* 122, 549–564. doi: 10.1086/321167

Weymann, R. J., Morris, S. L., Foltz, C. B., and Hewett, P. C. (1991). Comparisons of the emission-line and continuum properties of broad absorption line and normal quasi-stellar objects. *Astrophys. J.* 373, 23–53. doi: 10.1086/170020

York, D. G., Adelman, J., Anderson, J. E. Jr., Anderson, S. F., Annis, J., Bahcall, N. A., et al. (2000). The Sloan Digital Sky Survey: technical summary. *Astron. J.* 120, 1579–1587. doi: 10.1086/301513

Conflict of Interest Statement: The authors declare that the research was conducted in the absence of any commercial or financial relationships that could be construed as a potential conflict of interest.

Copyright © 2017 De Cicco, Brandt, Grier and Paolillo. This is an open-access article distributed under the terms of the Creative Commons Attribution License (CC BY). The use, distribution or reproduction in other forums is permitted, provided the original author(s) or licensor are credited and that the original publication in this journal is cited, in accordance with accepted academic practice. No use, distribution or reproduction is permitted which does not comply with these terms.

frontiers in Astronomy and Space Sciences

ORIGINAL RESEARCH
published: 08 November 2017
doi: 10.3389/fspas.2017.00036

Rapid BAL Variability: Re-Emerging Absorption

Damla Erakuman[1]* *and Nurten Filiz Ak*[1,2]*

[1] *Department of Astronomy and Space Sciences, Faculty of Science, Erciyes University, Kayseri, Turkey,* [2] *Astronomy and Space Sciences Observatory and Research Center, Erciyes University, Kayseri, Turkey*

We study BAL variations of SDSS J141955.28+522741.4 utilizing 32 epochs of spectroscopic observations from SDSS. We identify three individual BAL troughs for C iv and one BAL trough for Si iv. The deepest C iv BAL trough shows significant EW variations in timescales of a few 10 h. The fast component of the deepest C iv BAL presents disappearance and re-emergence preserving its initial velocity range and profile. All identified BAL troughs show coordinated variations supporting that the possible mechanism behind variations are the ionization level changes of the absorbing gas.

Keywords: galaxies, active galaxies, kinematics and dynamics, galaxies, nuclei, quasars, absorption lines

OPEN ACCESS

Edited by:
Mauro D'Onofrio,
Università degli Studi di Padova, Italy

Reviewed by:
Fabio La Franca,
Università degli Studi Roma Tre, Italy
Daniela Bettoni,
Osservatorio Astronomico di Padova (INAF), Italy

***Correspondence:**
Damla Erakuman
damla.erakuman@gmail.com
Nurten Filiz Ak
nfak@erciyes.edu.tr

Specialty section:
This article was submitted to Cosmology, a section of the journal Frontiers in Astronomy and Space Sciences

Received: *23 August 2017*
Accepted: *24 October 2017*
Published: *08 November 2017*

Citation:
Erakuman D and Filiz Ak N (2017) Rapid BAL Variability: Re-Emerging Absorption. Front. Astron. Space Sci. 4:36. doi: 10.3389/fspas.2017.00036

1. INTRODUCTION

Quasar winds are the fastest outflows in the universe and they are observed as blue-shifted Broad Absorption Lines (BALs) in quasar spectra. Quasar winds are substantial part of the nuclear environment; fast outflows play a key role on galaxy feedback by evacuating gas and heat to the host galaxy (Di Matteo et al., 2005; Springel et al., 2005; King, 2010). Therefore, understanding the mechanisms behind these outflows would shed light on dynamics and evolution of super-massive black holes.

BAL troughs observed in quasar spectra present characteristic variations in their equivalent widths (EW), line profiles, and velocities (Barlow et al., 1992; Lundgren et al., 2007; Filiz Ak et al., 2012, 2013, 2014). The timescales of significant variations ranges between a few years to a few tens of hours (Capellupo et al., 2012; Filiz Ak et al., 2012, 2013, 2014; Grier et al., 2015).

In this study, we investigate BAL variations in multi-epoch spectroscopic observations of SDSS J141955.28+522741.4 (hereafter J1419). The Sloan Digital Sky Survey (SDSS) DR 12 Quasar Catalog lists MJD-PLATE-FiberID key parameters for 32 spectroscopic observations of J1419 and the catalog categorizes J1419 as a BAL quasar with $z = 2.14$ (Pâris et al., 2017). Frequent observations allow us to investigate significant rapid BAL variations and correlated variations of multiple BAL troughs.

The main driving mechanisms behind the BAL variations is largely debated in the literature. One scenario involves transverse motion of absorbing gas across the observer's line of sight producing changes in the coverage fraction (e.g., Rogerson et al., 2016). A second scenario considers ionization level changes of the outflowing gas (e.g., Filiz Ak et al., 2013, 2014). Other scenarios (e.g., intrinsic instabilities of an absorbing gas driving BAL variations) are usually found potential but problematic (Capellupo et al., 2012).

2. OBSERVATIONS AND DATA PREPARATION

SDSS BOSS carried out spectroscopic observations of 297301 quasars using a 2.5 m dedicated telescope at Apache Point Observatory (Gunn et al., 2006) between 2009 and 2014 (Eisenstein et al., 2011; Dawson et al., 2013). The main aim of BOSS is to map the spatial distribution of luminous

red galaxies and quasars to detect the characteristic scale imprinted by baryon acoustic oscillations in the early universe. Spectral wavelength coverage of BOSS is between 3,600 and 10,400 Å with a spectral resolution varying between 1,300 and 3,000 (Smee et al., 2013).

SDSS obtained 32 spectroscopic observations of J1419 between MJD 56397 and MJD 56837 with a time spread of 140 days in the quasar rest frame. We follow some simple steps to prepare the spectra: We correct the Galactic extinction using a Milky Way extinction model (Cardelli et al., 1989) for $R_v = 3.1$ and A_V values from Schlafly and Finkbeiner (2011). We fit the continuum with a power-law model that is intrinsically reddened using SMC-like reddening model from Pei (1992). We transform all the available spectra to the quasars rest frame using visually inspected redshift value of $z = 2.14$ (Pâris et al., 2017).

To detect BAL troughs, we follow classical BAL definition that requires absorption lines to have velocity widths $> 2{,}000$ km s^{-1}, and reach at least 10% under the continuum level (Weymann et al., 1991). Considering the variable nature of BAL troughs, we follow Filiz Ak et al. (2013) to determine BAL complexes using multiple-epoch observations.

We identify three individual C IV BAL troughs that are denoted as C_A, C_B, and C_C. Their minimum and maximum velocity limits (v_{min} and v_{max}, respectively) are as follows: $-2{,}000$ and $-7{,}800$ km s^{-1} for C_A, $-8{,}200$ and $-10{,}200$ km s^{-1} for C_B and $-11{,}200$ and $-15{,}600$ km s^{-1} for C_C. We also find a Si IV BAL trough that have v_{min} and v_{max} velocities similar to that of C_A. Multi-epoch observations show that C_A is a BAL trough complex, rather than a single trough with at least two constituent absorption features (see **Figure 1**). Similarly, the detected Si IV BAL trough is likely to be a BAL complex.

Figure 1 shows emission lines and absorption regions for C IV and Si IV transitions in mean spectrum. The mean spectrum is calculated by averaging the 32 spectra for a given wavelength. **Figure 1** shows the identified C IV BAL troughs C_A, C_B, and C_C, and Si IV BAL trough.

3. ANALYSIS AND RESULTS

Traditionally, BAL variability has been assessed considering the time-dependent variations of EWs measured for the identified absorption features. Thus, we measure EW and uncertainties on EW using Equations 1 and 2 of Kaspi et al. (2002). In order to study time dependent variations on EW, we calculate $\Delta EW = EW_2 - EW_1$ where EW_2 is BAL trough EW measured in a latter epoch of the two consecutive spectra. The uncertainties on EW_1 and EW_2 are propagated to calculate uncertainty on ΔEW.

3.1. Rapid BAL Variations

In order to identify significant rapid variations, we require EW to be larger than 5σ for two consecutive observations. The ΔEW measurements fulfill this criterion three times with timescales of 1.3 days (5.1σ), 3.8 days (5.03σ), and 4.1 days (6.5σ). These results show that the most rapid significant variation occurs in timescales as short as ~ 31 h.

Grier et al. (2015) shows that the shortest timescale variation of SDSS J141007.74+541203.3. occurred in $\sim$1.2 rest frame days at 4.67σ. Our finding for J1419 agrees with the results of Grier et al. (2015) indicating that BAL variability on timescales of a few 10 h is likely to be a common behavior.

3.2. Disappearance and Emergence Events

Trough A of C IV is the most significant BAL complex in these spectra and appears to have at least two constituents. The deepest constituent (C_{Aa}) lies in low velocity ranges. The high velocity constituent of C_A (C_{Ab}) presents the strongest variations in multi-epoch observations. We note that C_{Ab} fulfills the traditional BAL criteria only a few times in these available 32 spectra. Definition of a BAL trough complex by Filiz Ak et al. (2012) considers multi-epoch observations rather than a single spectrum. According to this definition, absorption trough is considered as a BAL complex when multiple individual BAL troughs merged in at least one of the available observations (for details, see Filiz Ak et al., 2012). Given that C_{Aa} and C_{Ab} appears merged in more than one available spectra, we consider C_A to be a BAL complex with multiple constituents.

Figure 2 shows spectra for C_A at five different epochs where BAL strength variations, disappearance, and re-emergence events can be seen. The top panel of the figure shows the first spectrum of J1419 obtained by SDSS and thus $t = 0$ days. The spectrum on the second panel is observed at $t \sim 118$ days where C_{Ab} weakens. The third panel shows disappearance event at $t \sim 126$ days. Only ~ 2 days after the disappearance C_{Ab} starts regaining its strength. The bottom panel shows that C_{Ab} is almost fully recovered its strength while conserving initial velocity range and profile. These observations show that re-emergence of C_{Ab} occurred in ~ 4 days.

3.3. Coordinated Variations

We measure EW values for all the identified BAL troughs in 32 epochs of strength spectrum for J1419. **Figure 3** shows time-dependent EW variations for C_A, C_B, C_C, and Si IV BAL troughs. Strengthening and weakening of these four individual BAL troughs appears to be synchronized.

In order to search for possible correlation between EW variations of individual BAL troughs, we use Spearman rank correlation test. BAL trough complexes of C IV (i.e., C_A) and Si IV are both present in the corresponding velocity ranges thus suggesting that both of them are created by the same absorbing material. Therefore, coordinated variations of these BAL complexes is expected (e.g., Filiz Ak et al., 2013). Indeed, we found that these two BAL complexes show 92% correlation ($p = 10^{-14}$) of the time-dependent EW variations.

Trough C_A and C_B have a velocity separation of 4, 300 km s^{-1} from center to center indicating that the absorbing material responsible of these lines is not the same. The time-dependent EW variations of these two BAL have a Spearman rank correlation coefficient of 80% with $p = 10^{-8}$. Similar to that troughs C_A and C_C have a velocity separation of 8,300 km s^{-1} and their EW light curves show 92% correlated with $p = 10^{-14}$.

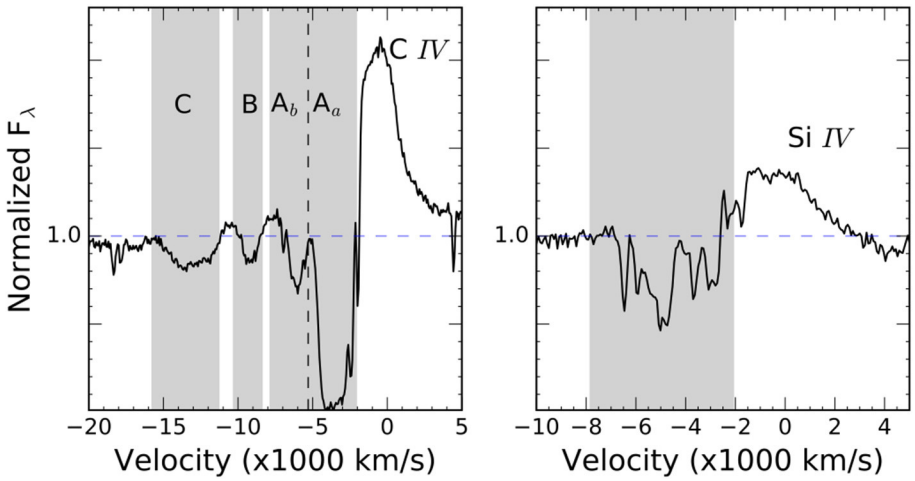

FIGURE 1 | C IV and Si IV emission lines and their BAL regions in the mean spectrum calculated from 32 continuum normalized observations of J1419. The three identified C IV BALs (A, B, and C) and one Si IV BAL are shown in gray areas. The dashed vertical line on C_A separates two main components of the BAL complex. The dashed horizontal line indicates normalized flux density of 1.0.

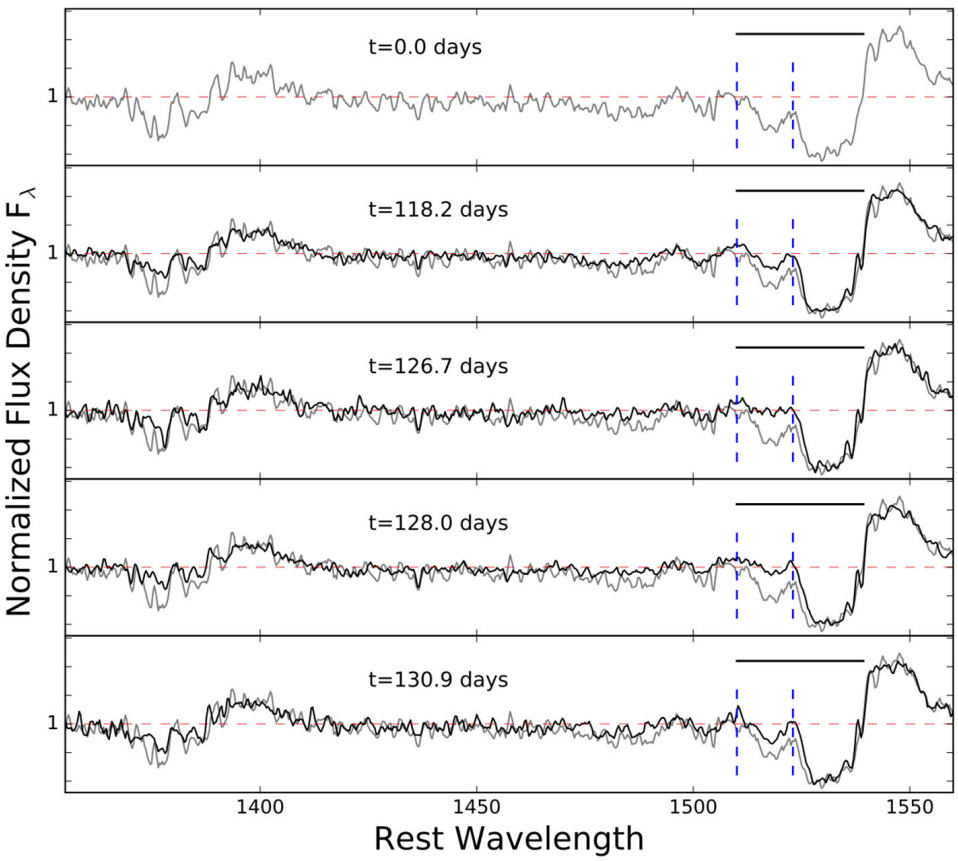

FIGURE 2 | Five epoch observations of J1419 illustrating BAL strength variations. The first epoch spectrum on the top panel is also shown other panels for guidance. The dashed red line indicates the continuum level and the horizontal black line shows C_A BAL region. The high velocity component of the trough (C_{Ab}) is marked with dashed blue lines. Middle panel spectrum at $t = 126.7$ days presents the disappearance event.

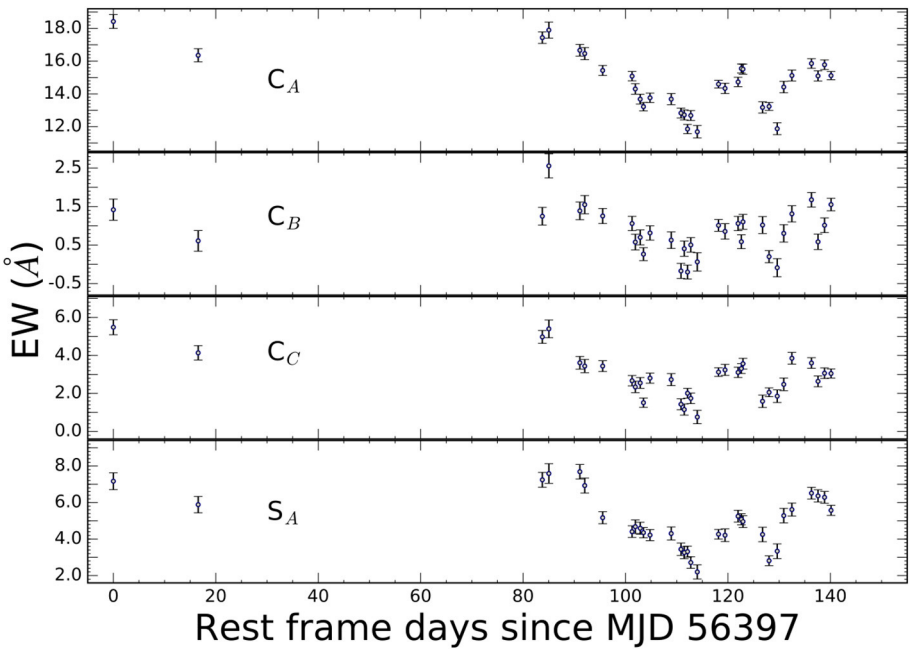

FIGURE 3 | Time dependent EW variations, respectively from top to bottom, for C IV troughs A, B, and C and Si IV trough. BAL EW variations of individual troughs have strong significant correlation.

4. DISCUSSION

We investigate 32 epochs of spectrum for J1419 to assess characteristics of its BAL variations. We identify three individual C IV BAL troughs that one of them appear to have at least two constituent absorption features. In addition, we identify a Si IV BAL trough that lies in similar velocity ranges of the slowest C IV BAL trough. Studying time-dependent EW variations for these BAL troughs, we highlighted three main findings: (1) The strongest BAL trough of J1419 (i.e., C_A) show a rapid significant variation at timescales of ∼31 h where EW variations are as strong as 5.1σ. (2) The faster component of C_A disappears and re-emerges in a short timescale. The BAL component starts weakening compared to the first epoch spectra and disappears at $t = 126.7$ days. Following observations show that the component regains its strength within 4 days. (3) The time-dependent EW variations of four BAL troughs identified in J1419 spectra show strong and significant correlations where Spearman rank correlation coefficients are larger than 80%.

The shortest timescale BAL variation is presented by Grier et al. (2015) showing that a significant (4.67σ) EW variation is detected for C IV BAL trough of SDSS J141007.74+541203.3 at timescales as short as 1.2 days. Given that our findings is consistent with that of Grier et al. (2015), BAL EW variations over timescales of a few 10 h is likely to be a common behavior. In order to assess this suggestion, a larger number of quasars with frequent spectroscopic observations should be investigated.

Time dependent EW variability of BAL troughs is largely investigated at the timescales of years (e.g., Barlow et al., 1992; Lundgren et al., 2007; Capellupo et al., 2012; Filiz Ak et al., 2012, 2013, 2014). So far, however, only a small number of disappearance events are recorded (Filiz Ak et al., 2012; McGraw et al., 2017). The number of quasars presenting BAL re-emergence is only a few (e.g., Lundgren et al., 2007; Filiz Ak et al., 2012; Rogerson et al., 2016). Our findings show that J1419 is the first example of BAL disappearance and re-emergence at timescales as short as ∼4 days.

All the other BAL troughs present in J1419 spectra show weakening and strengthening while C_{Ab} disappears and re-emerges suggesting that the BAL variability is not due to bulk motion of the absorbers. Furthermore, event of re-emergence in less than 14 days support that bulk motion is not the likely scenario to explain BAL variations for J1419.

Coordinated EW variations of BAL troughs that have a large velocity separations in between suggest that cause of BAL variability should effect a large portion of the BAL region for a quasar. Therefore, we conclude that BAL variations is not due to intrinsic instabilities of an absorbing gas. Our finding favor a scenario in which a change in ionization state of the absorbing gas is likely to be dominant mechanism to drive the BAL variability.

For further analysis, we assess emission line variations and photometric variations in coordination with BAL variations. Therefore, physical constraints will be discussed on the light of current models.

AUTHOR CONTRIBUTIONS

All authors listed have made a substantial, direct and intellectual contribution to the work, and approved it for publication.

ACKNOWLEDGMENTS

We would like to thank referees for their comments. Thanks to TUBITAK (115F037) and ERU BAP (FYL 2016-6938) for financial support.

Funding for SDSS-III has been provided by Alfred P. Sloan Foundation, the Participating Institutions, The National Science Foundation, and the U. S. Department of Energy Office of Science. The SDSS-III web site is http://www.sdss3.org/.

SDSS-III is managed by the Astrophysical Research Consortium for the Participating Institutions of the SDSS-III Collaboration including the University of Arizona, the Brazilian Participation Group, Brookhaven National Laboratory, Carnegie Mellon University, University of Florida, the French Participation Group, the German Participation Group, Harvard University, the Instituto de Astrofisica de Canarias, the Michigan State/Notre Dame/JINA Participation Group, Johns Hopkins University, Lawrence Berkeley National Laboratory, Max Planck Institute for Astrophysics, Max Planck Institute for Extraterrestrial Physics, New Mexico State University, New York University, Ohio State University, Pennsylvania University, University of Portsmouth, Princeton University, the Spanish Participation Group, University of Tokyo, University of Utah, Vanderbilt University, University of Virginia, University of Washington, and Yale University.

REFERENCES

Barlow, T. A., Junkkarinen, V. T., and Burbidge, E. M. (1992). "Variable broad absorption-lines in the QSO H 0846+1540," in *American Astronomical Society Meeting Abstracts*, *Vol. 24 of Bulletin of the American Astronomical Society* (Phoenix, AZ; Tempe, AZ), 1135.

Capellupo, D. M., Hamann, F., Shields, J. C., Rodríguez Hidalgo, P., and Barlow, T. A. (2012). Variability in quasar broad absorption line outflows - II. Multi-epoch monitoring of Si IV and C IV broad absorption line variability. *Mon. Not. R. Astron. Soc.* 422, 3249–3267. doi: 10.1111/j.1365-2966.2012.20846.x

Cardelli, J. A., Clayton, G. C., and Mathis, J. S. (1989). The relationship between infrared, optical, and ultraviolet extinction. *Astrophys. J.* 345, 245–256. doi: 10.1086/167900

Dawson, K. S., Schlegel, D. J., Ahn, C. P., Anderson, S. F., Aubourg, É., Bailey, S., et al. (2013). The Baryon Oscillation Spectroscopic Survey of SDSS-III. *Astron. J.* 145:10. doi: 10.1088/0004-6256/145/1/10

Di Matteo, T., Springel, V., and Hernquist, L. (2005). Energy input from quasars regulates the growth and activity of black holes and their host galaxies. *Nature* 433, 604–607. doi: 10.1038/nature03335

Eisenstein, D. J., Weinberg, D. H., Agol, E., Aihara, H., Allende Prieto, C., Anderson, S. F., et al. (2011). SDSS-III: massive spectroscopic surveys of the distant universe, the milky way, and extra-solar planetary systems. *Astron. J.* 142:72. doi: 10.1088/0004-6256/142/3/72

Filiz Ak, N., Brandt, W. N., Hall, P. B., Schneider, D. P., Anderson, S. F., Gibson, R. R., et al. (2012). Broad absorption line disappearance on multi-year timescales in a large quasar sample. *Astrophys. J.* 757:114. doi: 10.1088/0004-637X/757/2/114

Filiz Ak, N., Brandt, W. N., Hall, P. B., Schneider, D. P., Anderson, S. F., Hamann, F., et al. (2013). Broad Absorption Line Variability on Multi-year Timescales in a Large Quasar Sample. *Astrophys. J.* 777:168. doi: 10.1088/0004-637X/777/2/168

Filiz Ak, N., Brandt, W. N., Hall, P. B., Schneider, D. P., Trump, J. R., Anderson, S. F., et al. (2014). The dependence of C IV broad absorption line properties on accompanying Si IV and Al III absorption: relating quasar-wind ionization levels, kinematics, and column densities. *Astrophys. J.* 791:88. doi: 10.1088/0004-637X/791/2/88

Grier, C. J., Hall, P. B., Brandt, W. N., Trump, J. R., Shen, Y., Vivek, M., et al. (2015). The sloan digital sky survey reverberation mapping project: rapid CIV broad absorption line variability. *Astrophys. J.* 806:111. doi: 10.1088/0004-637X/806/1/111

Gunn, J. E., Siegmund, W. A., Mannery, E. J., Owen, R. E., Hull, C. L., Leger, R. F., et al. (2006). The 2.5 m Telescope of the sloan digital sky survey. *Astron. J.* 131, 2332–2359. doi: 10.1086/500975

Kaspi, S., Brandt, W. N., George, I. M., Netzer, H., Crenshaw, D. M., Gabel, J. R., et al. (2002). The ionized gas and nuclear environment in NGC 3783. I. Time-averaged 900 kilosecond chandra grating spectroscopy. *Astrophys. J.* 574, 643–662. doi: 10.1086/341113

King, A. R. (2010). Black hole outflows. *Mon. Not. R. Astron. Soc.* 402, 1516–1522. doi: 10.1111/j.1365-2966.2009.16013.x

Lundgren, B. F., Wilhite, B. C., Brunner, R. J., Hall, P. B., Schneider, D. P., York, D. G., et al. (2007). Broad absorption line variability in repeat quasar observations from the sloan digital sky survey. *Astrophys. J.* 656, 73–83. doi: 10.1086/510202

McGraw, S. M., Brandt, W. N., Grier, C. J., Filiz Ak, N., Hall, P. B., Schneider, D. P., et al. (2017). Broad absorption line disappearance and emergence using multiple-epoch spectroscopy from the Sloan Digital Sky Survey. *Mon. Not. R. Astron. Soc.* 469, 3163–3184. doi: 10.1093/mnras/stx1063

Pâris, I., Petitjean, P., Ross, N. P., Myers, A. D., Aubourg, É., Streblyanska, A., et al. (2017). The sloan digital sky survey quasar catalog: twelfth data release. *Astron. Astrophys.* 597:A79. doi: 10.1051/0004-6361/201527999

Pei, Y. C. (1992). Interstellar dust from the Milky Way to the Magellanic Clouds. *Astrophys. J.* 395, 130–139. doi: 10.1086/171637

Rogerson, J. A., Hall, P. B., Rodríguez Hidalgo, P., Pirkola, P., Brandt, W. N., and Filiz Ak, N. (2016). Multi-epoch observations of extremely high-velocity emergent broad absorption. *Mon. Not. R. Astron. Soc.* 457, 405–420. doi: 10.1093/mnras/stv3010

Schlafly, E. F., and Finkbeiner, D. P. (2011). Measuring reddening with sloan digital sky survey stellar spectra and recalibrating SFD. *Astrophys. J.* 737:103. doi: 10.1088/0004-637X/737/2/103

Smee, S. A., Gunn, J. E., Uomoto, A., Roe, N., Schlegel, D., Rockosi, C. M., et al. (2013). The Multi-object, fiber-fed spectrographs for the sloan digital sky survey and the baryon oscillation spectroscopic survey. *Astron. J.* 146:32. doi: 10.1088/0004-6256/146/2/32

Springel, V., Di Matteo, T., and Hernquist, L. (2005). Modelling feedback from stars and black holes in galaxy mergers. *Mon. Not. R. Astron. Soc.* 361, 776–794. doi: 10.1111/j.1365-2966.2005.09238.x

Weymann, R. J., Morris, S. L., Foltz, C. B., and Hewett, P. C. (1991). Comparisons of the emission-line and continuum properties of broad absorption line and normal quasi-stellar objects. *Astrophys. J.* 373, 23–53. doi: 10.1086/170020

Conflict of Interest Statement: The authors declare that the research was conducted in the absence of any commercial or financial relationships that could be construed as a potential conflict of interest.

Copyright © 2017 Erakuman and Filiz Ak. This is an open-access article distributed under the terms of the Creative Commons Attribution License (CC BY). The use, distribution or reproduction in other forums is permitted, provided the original author(s) or licensor are credited and that the original publication in this journal is cited, in accordance with accepted academic practice. No use, distribution or reproduction is permitted which does not comply with these terms.

frontiers in Astronomy and Space Sciences

ORIGINAL RESEARCH
published: 30 October 2017
doi: 10.3389/fspas.2017.00031

Reverberation Mapping of High-Luminosity Quasars

Shai Kaspi[1], William N. Brandt[2,3,4], Dan Maoz[1], Hagai Netzer[1], Donald P. Schneider[2,3] and Ohad Shemmer[5]*

[1] Raymond and Beverly Sackler Faculty of Exact Sciences, School of Physics and Astronomy, Tel-Aviv University, Tel-Aviv, Israel, [2] Department of Astronomy and Astrophysics, Pennsylvania State University, University Park, PA, United States, [3] Institute for Gravitation and the Cosmos, Pennsylvania State University, University Park, PA, United States, [4] Department of Physics, Pennsylvania State University, University Park, PA, United States, [5] Department of Physics, University of North Texas, Denton, TX, United States

Over the past three decades reverberation mapping (RM) has been applied to about 100 AGNs. Their broad line region (BLR) sizes were measured and yielded mass estimates of the black holes in their center. However, very few attempts were carried out for high-luminosity quasars, at luminosities higher than 10^{46} erg/sec in the optical. Most of these attempts failed since RM of such quasars is difficult due to a number of reasons, mostly due to the long time needed to monitor these objects. During the past two decades we carried out a RM campaign on six high-luminosity quasars. This contribution presents some of the final light curves of that RM campaign in which we measured the BLR size in C IV of three of the objects (S5 0836+71, SBS 1116+603, and SBS 1425+606). We present the C IV BLR size and luminosity relation over eight orders of magnitude in luminosity, pushing the luminosity limit to its highest point so far.

Keywords: quasars, black holes, reverberation mapping, broad line region, AGN

OPEN ACCESS

Edited by:
Mauro D'Onofrio, Università degli Studi di Padova, Italy

Reviewed by:
Milan S. Dimitrijevic, Belgrade Astronomical Observatory, Serbia
Siamak Akhshabi, Golestan University, Iran

****Correspondence:***
Shai Kaspi
shai@wise.tau.ac.il

Specialty section:
This article was submitted to Cosmology, a section of the journal Frontiers in Astronomy and Space Sciences

Received: *31 August 2017*
Accepted: *12 October 2017*
Published: *30 October 2017*

Citation:
Kaspi S, Brandt WN, Maoz D, Netzer H, Schneider DP and Shemmer O (2017) Reverberation Mapping of High-Luminosity Quasars. Front. Astron. Space Sci. 4:31. doi: 10.3389/fspas.2017.00031

1. INTRODUCTION

Reverberation Mapping (RM) is a technique to estimate the size of the Broad Line Region (BLR) in Active Galactic Nuclei (AGNs). The technique relies on using the variability of the central AGN power source and the response of the gas in the BLR to measure a time delay which is used as a measure for the BLR distance from the central source (see e.g., Peterson, 1993; Netzer and Peterson, 1997). Over the past three decades RM has been carried out successfully for almost 100 AGNs (e.g., (Kaspi et al., 2000; Bentz et al., 2006; Bentz and Katz, 2015; Du et al., 2015; Shen et al., 2016); and references therein) and a relation between the BLR size and the luminosity of AGNs was found. Using the assumption that the BLR gas has virialized motions around the central black hole of the AGN and that the velocity of the gas can be inferred from the width of the broad emission lines we can estimate the mass of the central black hole.

The first discussions about the time dependence of emission-line intensities from nebulea that are photoionized by a central source with variable continuum flux was done by Bahcall et al. (1972). Only a decade later Blandford and McKee (1982) put the idea into mathematical formulation and coined the term "Reverberation Mapping." According to this formulation the response of the nebula depends on its geometry and velocity field, and is given by the "transfer function," $\Psi(\nu, \tau)$. The relationship between the continuum light-curve $C(t)$ and the emission-line light-curve $L(\nu, t)$ can be described by

$$L(\nu, t) = \int_{-\infty}^{\infty} \Psi(\nu, \tau) C(t - \tau) d\tau \ , \quad (1)$$

which is known as the "transfer equation." The aim is to use the observables $C(t)$ and $L(\nu, t)$ to solve this integral equation for $\Psi(\nu, \tau)$, and thus infer the geometry and kinematics of the BLR. However, usually the observed light curves do not have the high quality, sampling, and length, that are needed to solve this equation by Fourier methods using the convolution theorem. Thus, the more common use is to solve the *one-dimensional transfer function* (which is the same equations as above but without the dependence in ν) by means of cross correlation of the line light curve with the continuum light curve. The peak of this cross correlation gives the time lag between the two light curves, and this time lag multiplied by the speed of light, c, is considered as a measure for the size of the BLR, R_{BLR}.

Using the assumption that the BLR is in a Keplerian motion around the continuum central source, and equaling the centripetal force of the clouds with the gravity force on them toward the central source, one can find the mass of the central source to be $M = f v^2 R_{BLR}/G$, where G is the Gravitational constant, v is a measure of the BLR velocity, and f is a constant which represent the geometry of the BLR (e.g., Onken et al., 2004). The BLR velocity, v is measured from the line width, either as the Full Width Half Maximum of the line, or the the line dispersion (i.e., the second moment of as defined by Peterson et al., 2004). The choice of method to define the velocity also changes the f factor that is used, as well as the assumed geometry, but overall f is of order of unity.

All objects studied thus far using RM have optical luminosities of up to 10^{46} erg/sec. Only a few attempts of RM for higher luminosity AGNs were carried out thus far and with very limited success (e.g., Welsh et al., 2000; Trevese et al., 2014). Such attempts are difficult to carry out due to several reasons: higher luminosity AGNs have larger BLR distances from the central source and longer variability time scales. Thus, monitoring periods of order a decade are needed for such projects and observations cadence needs to be of order a month. Telescope time allocation committees are usually reluctant to commit telescope time for such long periods. Also, the variability amplitude of high-luminosity AGNs are smaller than low-luminosity AGNs and the BLR size is larger, thus causing the line response to be smeared making line variations harder to detect. Yet another difficulty is that the light curves are stretched by the cosmic time dilation, further extending the monitoring period, thus the response of the BLR gas is harder to detect.

Most of the AGNs which were measured with reverberation mapping thus far were observed using the Hβ emission line and this is the most commonly used line for these studies of low-

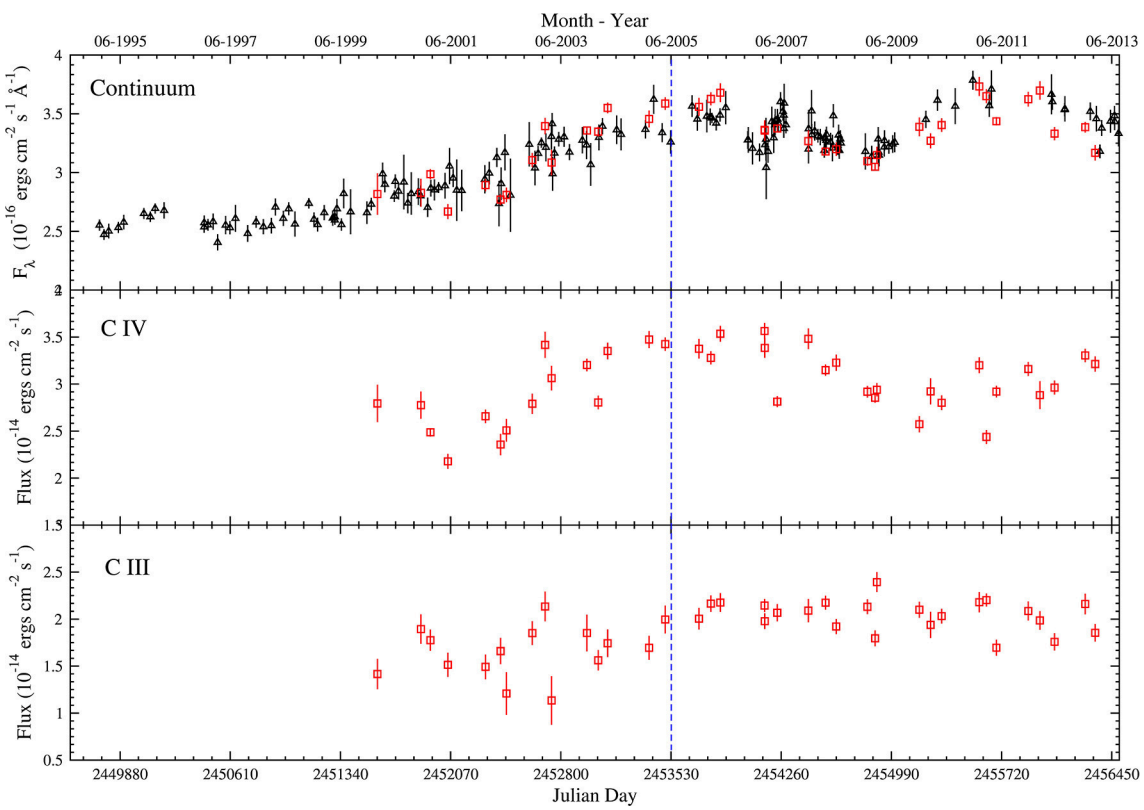

FIGURE 1 | Light curves for SBS 1116+603. Red squares are points measured from the spectroscopic data and black triangles are points measured from the photometric data. The top panel is the continuum light curve (spectroscopic points measured on the red side of the C III] line). The middle panel and lower panel are line light curves for C IV and C III], respectively. Data up to the blue vertical dashed line were published in Kaspi et al. (2007).

redshift, low-luminosity AGNs. High-luminosity AGNs are also generally at high redshift (order of $z \sim 2$–4), thus observations with optical telescopes are monitoring the UV lines (e.g., Lyα, C IV, C III], and Mg II). Since different emission lines are emitted from different parts of the BLR it is hard to compare between objects which were measured in different emission lines and this adds to the difficulties of such studies.

In spite of the above difficulties we initiated two decades ago a reverberation mapping campaign on several high-luminosity quasars. A detailed description of this observing campaign and some initial results from the first 5 years were presented in Kaspi et al. (2007). In this contribution we present some of the final light curves from the campaign and some of the tentative final results. In section 2 we briefly describe the project, how the sample was selected, the observations of the sample, and some final light curves of the sample. In section 3 we present an analysis of the light curve and present the C IV BLR size for three of the objects in our sample (S5 0836+71, SBS 1116+603, and SBS 1425+606) and its relation with the UV luminosity of the AGN.

We note the contribution of Lira et al. to these proceedings which describes another reverberation mapping campaign on high-luminosity quasars and which yields similar results to the results we describe in this contribution.

2. THE PROJECT, SAMPLE SELECTION, AND OBSERVATIONS

In 1995 we started photometric monitoring of 11 quasars at the Wise Observatory, and in 2000 we started spectroscopic monitoring of 6 of them with the Hobby-Eberly Telescope (HET; Ramsey et al., 1998). The objects in our sample are in the optical luminosity range of $10^{46} < \lambda L_\lambda(5100\text{Å}) < 10^{47.5}$ erg/sec, redshift range of $2 \lesssim z \lesssim 3.4$, observed magnitudes of $V \lesssim 18$, and have high declination in order to maximize the monitoring period during the year from northern hemisphere telescopes.

The objects were observed photometrically each month in the B and R filters for about 8 months each year. Spectroscopic observations were obtained ~3 times each year, evenly spaced over a period of about 6 months. In order to achieve quality cross calibration between the individual observations we used a comparison star aligned with the quasar in the spectrograph's slit (e.g., Kaspi et al., 2000).

Light curves for two of the objects, SBS 1116+603 and SBS 1233+594 are shown in **Figures 1**, **2**. All objects in our sample show continuum variations of about 20 to 60% measured relative to the minimum flux of the light curve. Line variations are detected only in some of the lines we monitored. This could be a result of the low amplitude of the line variations that our

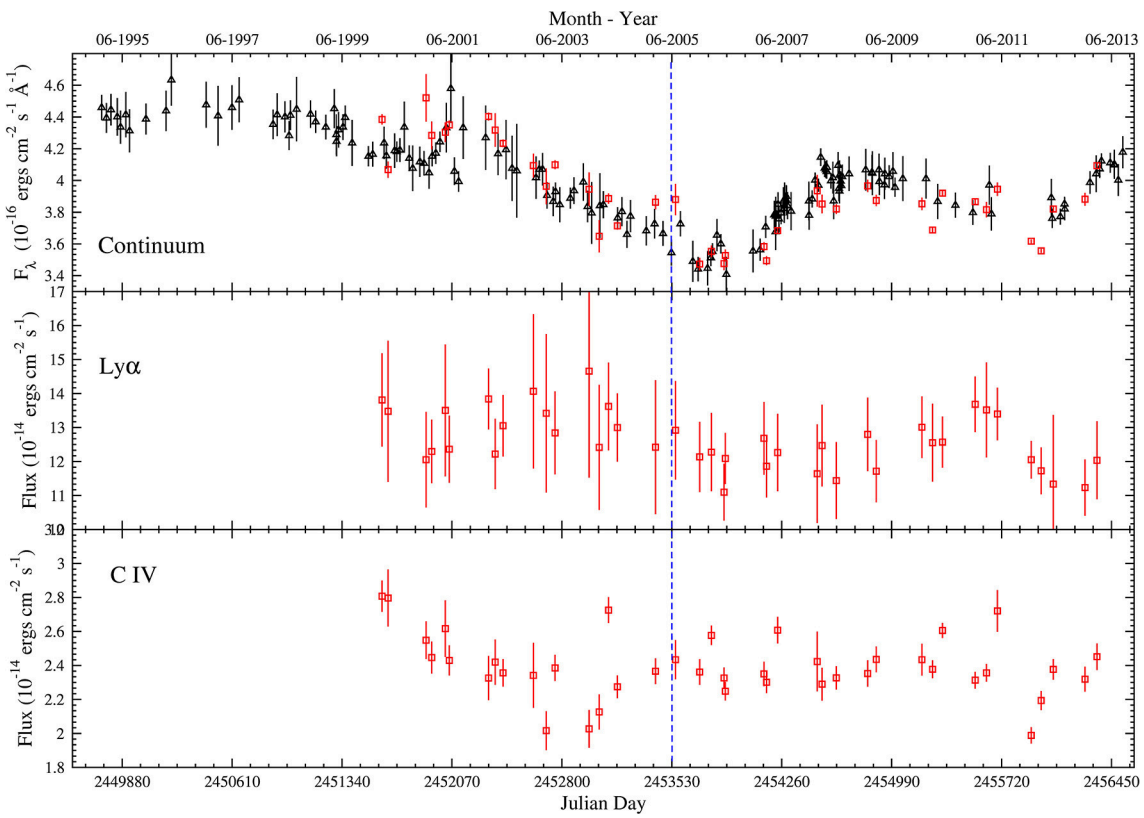

FIGURE 2 | Light curves for SBS 1233+594. Red squares are points measured from the spectroscopic data and black triangles are points measured from the photometric data. The top panel is the continuum light curve (spectroscopic points measured on the red side of the C IV line). The middle panel and lower panel are line light curves for Lyα and C IV, respectively. Data up to the blue vertical dashed line were published in Kaspi et al. (2007).

measurements could not detect, or that the continuum signal processed trough the large BLR is smeared in such a way that there are no variations in the line light curve.

3. ANALYSIS AND RESULTS

In order to estimate the BLR size we use two methods which are commonly used for that purpose. One method is the interpolated cross-correlation function (ICCF: White and Peterson, 1994). In this method one light curve is cross correlated with a linear interpolation of the second light curve, then the second light curve is cross correlated with a linear interpolation of the first light curve, and then the final cross correlation is the average of these two cross correlation functions. The second method is the z-transformed discrete correlation function (ZDCF: Alexander, 1997) which is an improvement of the Discrete Correlation Function (DCF) method suggested by Edelson and Krolik (1988). The ZDCF applies Fisher's z transformation to the correlation coefficients, and uses equal population bins instead of the equal time bins that are used in the DCF. The two methods yield similar results and in the following we use the ICCF method and estimate the uncertainties on the time lags using the model-independent Monte Carlo method called Flux Randomization/Random Subset Selection (FR/RSS) of Peterson (1993). We find significant time lags for C IV in three of our six objects, for the C III] line in one of the objects, and a possible time lag of Lyα in one of the objects. The cross correlation functions (CCFs) for the light curves from **Figures 1**, **2** are shown in **Figure 3**.

As can be seen in **Figure 3C** for the Lyα line of SBS 1233+594, the ICCF gives a peak which is at 165^{+55}_{-451} days in the rest frame. The formal negative 1σ uncertainty includes the possibility that no time lag is detected, i.e., the result is not significant. This is also hinted at from the fact that the ZDCF in **Figure 3C** shows no significant peak. Looking at the light curve of this Lyα line in **Figure 2** it is clear that the peak in the ICCF comes from the two peaks in the line light curve around JDs of 2452900 and 2455700 which follow the peaks in the continuum light curve at JDs 2452300 and 2455100. However, the uncertainties on the line-flux

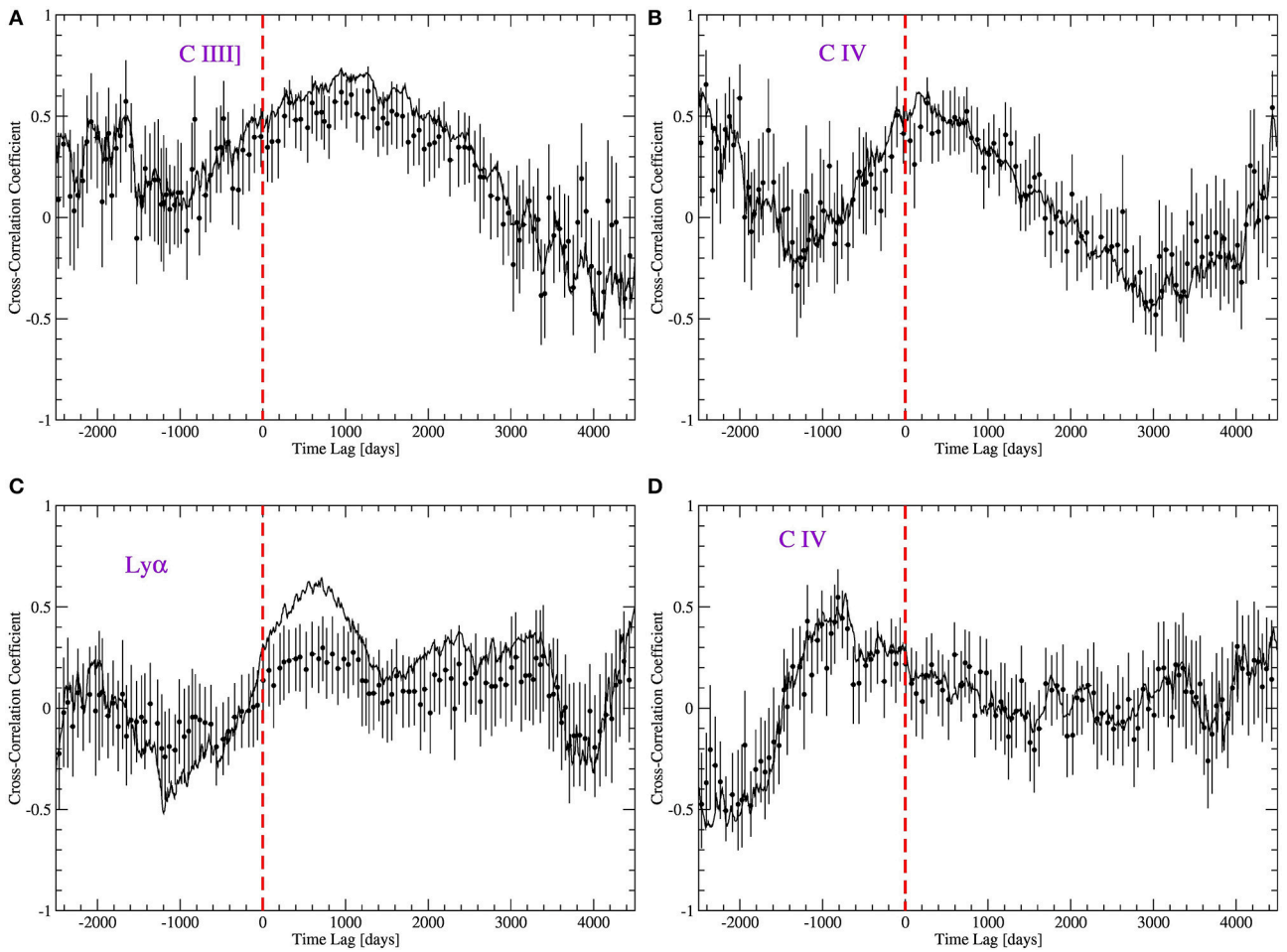

FIGURE 3 | CCFs for the light curves shown in **Figures 1**, **2**. **(A,B)** are the CCFs of Lyα and C IV vs. the continuum of SBS 1233+594. **(C,D)** are the CCFs of Lyα and C IV vs. the continuum of SBS 1233+594. The ICCF method is shown as a solid line and the ZDCF method is shown as filled circles with uncertainties. Time lags are given in the observed frame.

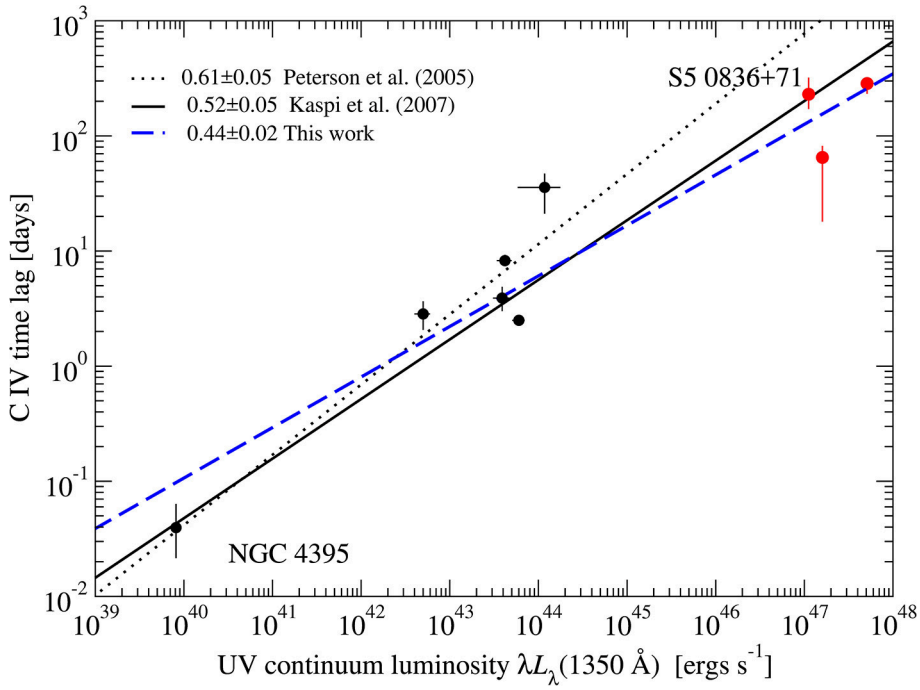

FIGURE 4 | BLR size vs. UV luminosity relation based on the work of Kaspi et al. (2007) together with the three objects reported in this work. See text for details.

measurements are very large and this causes the uncertainty in the time lag determination to be large. The main reason that the uncertainty on the line measurements are large is because in this object the optical spectrum includes only part of the Lyα line, and thus our measurements include only the red half of the line.

Figures 3A,B show the CCFs for the C III] and C IV lines of SBS 1116+603. We find significant time lags of 262^{+72}_{-72} days for the C III] line and 65^{+17}_{-37} days for the C IV line (both measured in the rest frame). The lower ionization line is emitted further away from the central continuum source than the higher ionization line, in accordance with the known stratification of the BLR. For S5 0836+71 and SBS 1425+606 we find a C IV time lags of 230^{+91}_{-59} and 285^{+30}_{-53} days, respectively.

We note that half of the quasars in our sample are radio loud and the light curves and time lags interpretation in these objects may be complicated by the additional jet contribution to the continuum driving the line emission. This may also be the reason why we did not detect a time lag in some of our radio loud objects. However, with respect to the objects presented here, SBS 1233+594 is a radio quiet quasar and we did not find a significant time lag for its lines, while SBS 1116+603 is a radio loud quasar and we find time lags for the two lines measured.

Using the three time lags of C IV lines which we find in this work we can reconstruct the BLR size—UV luminosity relation for that line. In **Figure 4** we show this relation from Kaspi et al. (2007) with the three new points added in red. One point, for S5 0836+71, was reported in Kaspi et al. (2007) as a tentative result and after adding 8 more years of monitoring to the initial reported 5 years the time lag is confirmed. The black points shown in **Figure 4** are from Peterson et al. (2005) as well as the BLR size—UV luminosity relation with a slope of 0.61 ± 0.05. Adding the one point of S5 0836+71 in Kaspi et al. (2007) changed the slope to 0.52 ± 0.05. In this work we updated the result for S5 0836+71 and added two more points. The updated slope, as seen in **Figure 4**, is 0.44 ± 0.02. We note that we did not include in this analysis the few additional time-lag measurements for C IV of high-luminosity quasars that are presented in these proceedings by Lira et al. (submitted). This will be done in a future publication (Kaspi et al., in preparation) and will probably further update the slope of that relation.

In summary, reverberation mapping of high-luminosity, high-redshift quasars is difficult to carry out and requires long monitoring periods of order of at least a decade and probably more. Our reverberation mapping project of a sample of such objects resulted in time lags for the C IV line of order a hundred to a few hundred days in the rest frame for objects with optical luminosity of order 10^{47} erg/sec. The measured black hole masses for these objects are of order $10^9\,M_\odot$ which are the highest black hole masses measured thus far with reverberation mapping.

AUTHOR CONTRIBUTIONS

SK, WB, DM, HN, DS, and OS comply with the requirements for authorship of this article.

REFERENCES

Alexander, T. (1997). "Is AGN variability correlated with other AGN properties? - ZDCF analysis of small samples of aparse light curves," in *Astronomical Time Series*, eds D. Maoz, A. Sternberg, and E. M. Leibowitz (Dordrecht: Kluwer Academic Publishers), 163–166.

Bahcall, J. N., Kozlovsky, B.-Z., and Salpeter, E. E. (1972). On the time dependence of emission-Line strengths from a photoionized nebula. *Astrophys. J.* 171, 467–482. doi: 10.1086/151300

Bentz, M. C., Peterson, B. M., Pogge, R. W., Vestergaard, M., and Onken, C. A. (2006). The radius-luminosity relationship for active galactic nuclei: the effect of host-galaxy starlight on luminosity measurements. *Astrophys. J.* 644, 133–142. doi: 10.1086/503537

Bentz, M. C., and Katz, S. (2015). The AGN black hole mass database. *Publ. Astronom. Soc. Pacific* 127, 67–73. doi: 10.1086/679601

Blandford, R. D., and McKee, C. F. (1982). Reverberation mapping of the emission line regions of Seyfert galaxies and quasars. *Astrophys. J.* 255, 419–439. doi: 10.1086/159843

Du, P., Hu, C., Lu, K.-X., Huang, Y.-K., Cheng, C., Qiu, J. et al. (2015). Supermassive black holes with high accretion rates in active galactic nuclei. IV. Hβ time lags and implications for super-eddington accretion. *Astrophys. J.* 806:22. doi: 10.1088/0004-637X/806/1/22

Edelson, R. A., and Krolik, J. H. (1988). The discrete correlation function - a new method for analyzing unevenly sampled variability data. *Astrophys. J.* 333, 646–659. doi: 10.1086/166773

Kaspi, S., Smith, P. S., Netzer, H., Maoz, D., Jannuzi, B. T., and Giveon, U. (2000). Reverberation measurements for 17 quasars and the size-mass-luminosity relations in active galactic nuclei. *Astrophys. J.* 533, 631–649. doi: 10.1086/308704

Kaspi, S., Brandt, W. N., Maoz, D., Netzer, H., Schneider, D. P., and Shemmer, O. (2007). Reverberation mapping of high-luminosity Quasars: first results. *Astrophys. J.* 659, 997–1007. doi: 10.1086/512094

Netzer, H., and Peterson, B. M. (1997). "Reverberation mapping and the physics of active galactic nuclei," in *Astronomical Time Series*, eds D. Maoz, A. Sternberg, and E. Leibowitz (Dordrecht: Kluwer Academic Publishers), 85–108.

Onken, C. A., Ferrarese, L., Merritt, D., Peterson, B. M., Pogge, R. W., Vestergaard, M. et al. (2004). Supermassive black holes in active galactic nuclei. II. Calibration of the black hole mass-velocity dispersion relationship for active galactic nuclei. *Astrophys. J.* 615, 645–651. doi: 10.1086/424655

Peterson, B. M. (1993). Reverberation mapping of active galactic nuclei. *Publ. Astronom. Soc. Pacific* 105, 247–268. doi: 10.1086/133140

Peterson, B. M., Ferrarese, L., Gilbert, K. M., Kaspi, S., Malkan, M. A., Maoz, D. et al. (2004). Central masses and broad-line region sizes of active galactic nuclei. II. A homogeneous analysis of a large reverberation-mapping database. *Astrophys. J.* 613, 682–699. doi: 10.1086/423269

Peterson, B. M., Bentz, M. C., Desroches, L.-B., Filippenko, A. V., Ho, L. C., Kaspi, S. et al. (2005). Multiwavelength monitoring of the dwarf seyfert 1 galaxy NGC 4395. I. A reverberation-based measurement of the black hole mass. *Astrophys. J.* 632, 799–808. doi: 10.1086/444494; Erratum: 2006, *Astrophys. J.* 641:638. doi: 10.1086/500409

Ramsey, L. W., Adams, M. T., Barnes, T. G., Booth, J. A., Cornell, M. E., Fowler, J. R. et al. (1998). "Early performance and present status of the Hobby-Eberly Telescope," in *Proceedings of the SPIE Advanced Technology Optical/IR Telescopes VI*, ed L. M. Stepp, 34–42.

Shen, Y., Horne, K., Grier, C. J., Peterson, B. M., Denney, K. D., Trump, J. R., et al. (2016). The sloan digital sky survey reverberation mapping project: first broad-line Hβ and Mg ii lags at z $>$ 0.3 from six-month spectroscopy. *Astrophys. J.* 818:30. doi: 10.3847/0004-637X/818/1/30

White, R. J., and Peterson, B. M. (1994). Comments on cross-correlation methodology in variability studies of active galactic nuclei. *Publ. Astronom. Soc. Pacific* 106, 879–889. doi: 10.1086/133456

Trevese, D., Perna, M., Vagnetti, F., Saturni, F. G., and Dadina, M. (2014). C IV and C III] reverberation mapping of the luminous quasar PG 1247+267. *Astrophys. J.* 795:164. doi: 10.1088/0004-637X/795/2/164

Welsh, W., Robinson, E. L., Hill, G., Shields, G., Wills, B., Brandt, N. et al. (2000). The HET echo mapping project. *Bull. Am. Astronom. Soc.* 32:1458.

Conflict of Interest Statement: The authors declare that the research was conducted in the absence of any commercial or financial relationships that could be construed as a potential conflict of interest.

Copyright © 2017 Kaspi, Brandt, Maoz, Netzer, Schneider and Shemmer. This is an open-access article distributed under the terms of the Creative Commons Attribution License (CC BY). The use, distribution or reproduction in other forums is permitted, provided the original author(s) or licensor are credited and that the original publication in this journal is cited, in accordance with accepted academic practice. No use, distribution or reproduction is permitted which does not comply with these terms.

frontiers in Astronomy and Space Sciences

ORIGINAL RESEARCH
published: 09 January 2018
doi: 10.3389/fspas.2017.00071

Reverberation Mapping of High-z, High-Luminosity Quasars

Paulina Lira[1]*, *Ismael Botti*[2], *Shai Kaspi*[3] and *Hagai Netzer*[3,4]

[1] Departamento de Astronomía, Universidad de Chile, Santiago, Chile, [2] School of Department of Physics and Astronomy, University of Nottingham, Nottingham, United Kingdom, [3] School of Physics and Astronomy, Tel Aviv University, Tel Aviv, Israel, [4] Wise Observatory, School of Physics and Astronomy, Tel Aviv University, Tel Aviv, Israel

We present Reverberation Mapping results after monitoring a sample of 17 high-*z*, high-luminosity quasars for more than 10 years using photometric and spectroscopic capabilities. Continuum and line emission flux variability is observed in all quasars. Using cross-correlation analysis we successfully determine lags between the variations in the continuum and broad emission lines for several sources. Here we present a highlight of our results and the determined radius–luminosity relations for Lyα and CIV.

Keywords: quasars, black holes, reverberation mapping, broad line region, AGN

OPEN ACCESS

Edited by:
Paola Marziani, Osservatorio Astronomico di Padova (INAF), Italy

Reviewed by:
Dragana Ilic, University of Belgrade, Serbia
Fausto Vagnetti, Università degli Studi di Roma Tor Vergata, Italy

***Correspondence:**
Paulina Lira
plira@das.uchile.cl

Specialty section:
This article was submitted to Milky Way and Galaxies, a section of the journal Frontiers in Astronomy and Space Sciences

Received: *03 October 2017*
Accepted: *21 December 2017*
Published: *09 January 2018*

Citation:
Lira P, Botti I, Kaspi S and Netzer H (2018) Reverberation Mapping of High-z, High-Luminosity Quasars. Front. Astron. Space Sci. 4:71. doi: 10.3389/fspas.2017.00071

1. INTRODUCTION

Reverberation Mapping (RM) has been an extremely successful technique used to study the innermost regions of Active Galactic Nuclei (AGN). The determination of lags between variations in the continuum emission coming from the accretion disk near the central Black Hole (BH), and the response from the emission lines produced in the Broad Line Region (BLR) have shown that the BLR is an extended, virialized and ionizion-stratified structure. Furthermore, the determination of the radius–luminosity relation between the BLR radius at which Hβ is produced and the luminosity of the central source has open, through cross-calibration to other BLR lines, the possibility to measure BH masses in hundred of thousands of sources. The cross-calibration is, however, subject to many uncertainties due to the extrapolations necessary to apply the radius–luminosity relation to sources of very different luminosities to those actually probed with RM experiments, and to the use of emission lines produced by regions of the BLR that can be far from that producing Hβ. This is the motivation to conduct RM campaigns in high-*z*, high-luminosity quasars for those emission lines available in the observed optical domain.

2. OBSERVATIONAL CAMPAIGN AND RESULTING LIGHT CURVES

Since 2005 we undertook a long observational campaign to monitor a sample of southern, high-redshift ($z \sim 2.5 - 3$, with one source at $z = 1.8$), high-luminosity ($M_B \sim -29$) quasars. Fifty targets were originally selected from the SDSS (Schneider et al., 2005) and Calán-Tololo samples (Maza et al., 1996). We started with a purely R-band imaging (corresponding to rest frame wavelengths $\sim 1,700 - 1,800$Å, depending on the exact redshift of the source) and 2 years later triggered the first spectroscopic observations of those quasars with the largest photometric variations. Over the years the campaign was narrowed down to a final sample of 17 quasars which have good quality R-band and emission line light curves.

Line fluxes were measured using spectral windows tailored to each line and each quasar. We avoided regions where the lines were contaminated by variable absorbing features, but did not attempt to correct for the contribution of other (weaker) emission lines, either narrow or broad. For further details see Lira et al. (submitted).

Over the campaign we found that most quasars showed a substantial degree of variability in the continuum and line emission line fluxes, with typical normalized variability amplitudes $f_{\rm var}$ (Rodríguez-Pascual et al., 1997) of ∼10%. Most quasars also showed the expected behavior, where the emission lines followed the trends seen in the continuum as traced by the R-band light curves. Many sources, unfortunately, did not shown enough structure in their light curves (which in the rest frame only map the continuum and line flux variations during ∼3 years), to allow for statically significant lag determinations.

Two sources showed unexpected Lyα light curves, where the line fluxes depart from the behavior shown by the continuum and the remaining emission lines. One example (J224743) is shown in **Figure 1**, where we also include a source that presents the expected line response to the continuum variations (CT650).

3. TIME SERIES ANALYSIS

Cross-correlation analysis was conducted using the ICCF and ZCCF methods (Gaskell and Sparke, 1986; Alexander, 1997). Errors were determined using Monte Carlo simulations were the light curve fluxes were randomized and bootstrapped to contain about 70% of the original data points (Peterson et al., 2004). We determined statistically significant lags with respect to that of the R-band continuum for 3 Lyα, 5 CIV, 1 SiIV, 1 CIII], and 1 MgII emission line light curves.

In **Figure 2** we reproduce the light curves for two of our sources, CT286 and J221516. The emission line light curves have been shifted according to the calculated lags, while all curves have been taken to a mean of zero and a standard deviation of one. **Figure 2** illustrates that emission line light curves can closely match the observed UV continuum, like in the case of J221516, or can show rather different trends, as seen in CT286, where the line light curves correspond to a heavily smoothed version of the continuum light curve.

Two reasons can be invoked to explain such differences: (1) the response of the BLR to continuum variations differs from object to object, and it can be nonlinear and show variations with time; (2) the observed UV continuum might not be a good representation of the ionizing continuum, which is actually responsible of driving the emission line changes.

The recent monitoring of NGC5548 by the STORM consortium displays several of these traits during the 170 days of monitoring (Goad et al., 2016). Emission line light curves follow closely that of the continuum during the first 1/3 of the campaign, to then disengage from it showing a decorrelated behavior for $\sim 60-70$ days, to finally going back to the original state. Besides, while some emission lines show a smoother light curve than that of the observed continuum during the last segment of the

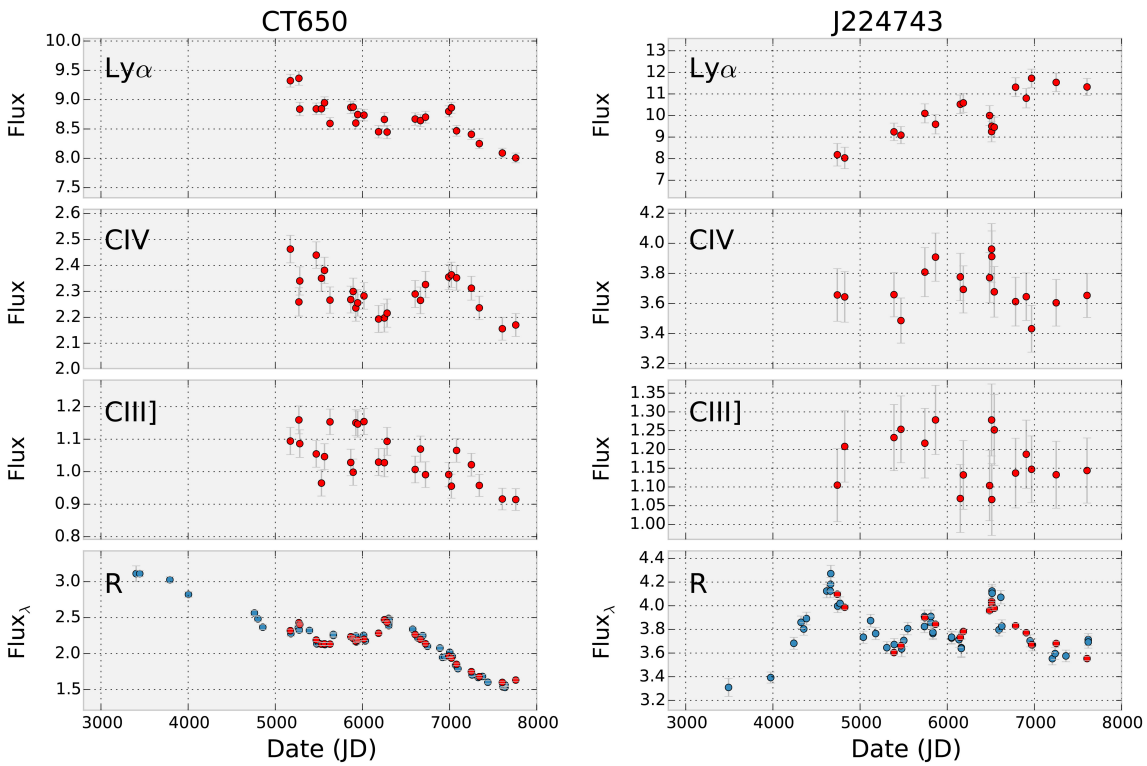

FIGURE 1 | R-band and emission line light curves for a well behaved source, CT650 **(Left)**, and an anomalous quasar, J224743 **(Right)**. The time axis is expressed in Julian Dates - 2,450,000 days. Blue points correspond to photometric observations while red points were obtained from the spectroscopic data. The continuum flux measurements shown in the bottom panel, either photometric or spectroscopic, correspond to the observer-frame R-band, and therefore the corresponding rest-frame spectral coverage changes from quasar to quasar. Taken from Lira et al. (submitted), ©AAS.

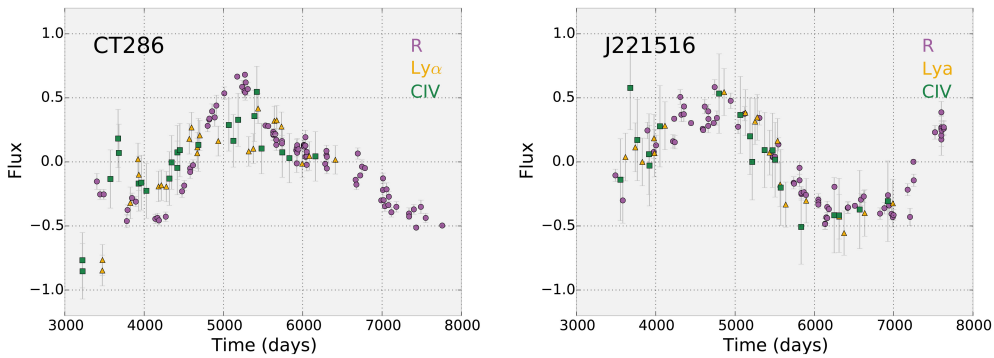

FIGURE 2 | Shifted and normalized continuum and emission line light curves for CT286 **(Left)** and J221516 **(Right)**. The time axis is expressed in Julian Dates - 2,450,000 days. R-band continuum, Lyα, and CIV light curves are presented using circles, triangles, and squares, respectively.

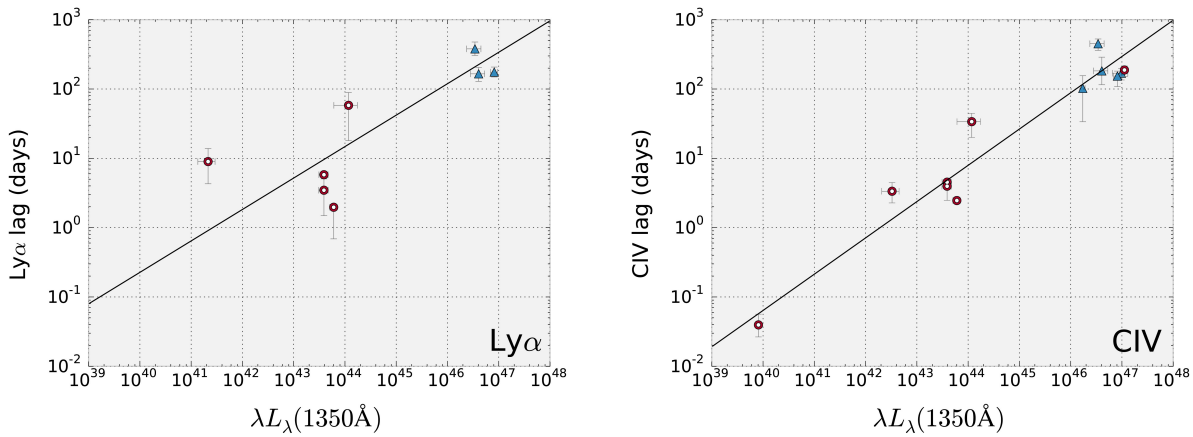

FIGURE 3 | Lyα **(Left)** and CIV **(Right)** radius–luminosity relations. Blue triangles correspond to results from our high-z, high-luminosity sample, while red circles are taken from the literature. These are NGC3783, NGC5548, NGC7469, F9, and 3C390.3 for the Lyα relation, and NGC4395, NGC5548, NGC3783, NGC7469, and 3C390.3 for the CIV relation (Peterson et al., 2005, 2006; De Rosa et al., 2015; Lira et al., submitted). Taken from Lira et al. (submitted), ©AAS.

monitoring, SiIV stands out for showing larger amplitude in its peaks and troughs than that of the continuum.

4. RADIUS–LUMINOSITY RELATIONS

As well as providing extremely valuable information about the innerworks of the BLR (see next section), reverberation mapping has provided a huge scientific legacy with the determination of the so called radius–luminosity relations. This tight correlations between the distance at which one particular emission line is produced and the continuum luminosity of the central engine allows for the determination of BH masses by applying these calibrations to a virialized BLR (i.e., $M_{\rm BH} \propto R\upsilon^2$, where R comes from the radius–luminosity relation and υ is measured from the width of the broad emission lines).

So far, RM of the Hβ line for nearby ($z < 0.3$) AGN has produced a solid radius–luminosity relation for this line (Wandel et al., 1999; Kaspi et al., 2000, 2005; Bentz et al., 2006, 2009, 2013). Cross–calibration of the correlation to other lines has been a significant enterprise which has allowed to determine BH masses of high-z quasars whose Balmer lines are redshifted into the infrared realm. In particular, MgII has proven to be a safe line to be used as BH mass estimator (McLure and Dunlop, 2004; Trakhtenbrot and Netzer, 2012), while it has been extensively shown that CIV yields unreliable results (Baskin and Laor, 2005; Netzer et al., 2007; Shen et al., 2008; Shen and Liu, 2012; Mejía-Restrepo et al., 2016).

Our monitoring effort has provided a sizeable number of Lyα and CIV lags at the high-luminosity end of the quasar distribution. This, together with other measurements found in the literature for lower luminosity AGN allows us now to determine radius–luminosity relations for these lines. These are presented in **Figure 3**, while the analytical expressions are as follows:

$$\frac{R_{\rm Ly\alpha}}{10\ {\rm lt-days}} = (0.52 \pm 0.59)\left[\frac{\lambda L_\lambda(1345\text{Å})}{10^{43}\ {\rm ergs/s}}\right]^{(0.45\ \pm\ 0.22)} \quad (1)$$

$$\frac{R_{\rm CIV}}{10\ {\rm lt-days}} = (0.24 \pm 0.08)\left[\frac{\lambda L_\lambda(1345\text{Å})}{10^{43}\ {\rm ergs/s}}\right]^{(0.52\ \pm\ 0.06)} \quad (2)$$

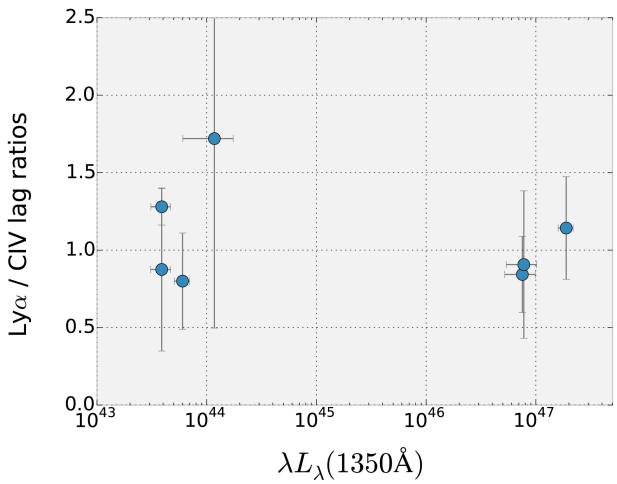

FIGURE 4 | Lyα to CIV lag ratios as a function of the λL_λ (1345Å) luminosity continuum.

where $R_{\rm line}$ is the measured lag and $\lambda L_\lambda(1345Å)$ corresponds to the product $\lambda \times L_\lambda$ as measured at 1,345 Å from each spectra. As can be seen from Equation (1), the zero point and slope of the Lyα radius–luminosity correlation are poorly constrained. The reason is clear after an inspection of **Figure 3** which reveals that Seyfert type sources show a large dispersion around the best fitted correlation, in contrast with the situation for CIV. In fact, the new CIV radius–luminosity relation is very close to that reported by Kaspi et al. (2007), who found a zero point of 0.24 ± 0.06 and a slope of 0.55 ± 0.04. Notice that the Lyα and CIV relations are consistent within the errors.

5. BLR STRATIFICATION

One crucial result that emerged early during the reverberation campaigns of nearby AGN was that the BLR was compact, dense and stratified (Peterson, 1994), in contrast with previous photoionization results that attempted to explain all emission lines as produced by one set of physical parameters (or one single *cloud*). RM results made clear that different regions, with different properties, and located at different distances from the central engine, were producing the observed set of emission lines. To build a consistent picture of the BLR, therefore, it is important to determine where different lines are produced.

Our results allows to put constraints on the distance at which Lyα and CIV are produced by obtaining $R_{\rm Ly\alpha}/R_{\rm CIV}$ for all source for which both lags have been measured. This is presented in **Figure 4**, where three sources at high-luminosities come from our lag determinations. **Figure 4** clearly supports that $R_{\rm Ly\alpha}/R_{\rm CIV} \sim 1$ and that this ratio is independent of luminosity.

6. SUMMARY AND CONCLUSIONS

We have presented selected results from the RM campaign of 17 high-z, high-luminosity quasars, which lasted more than 10 years. For several sources lags between the continuum and BLR line emission were determined, allowing us to extend radius-luminosity relationships up to $\lambda L_\lambda(1345Å) \sim 10^{47}$ ergs/s. Continuum and line light curves for all sources can be found in Lira et al. (submitted).

AUTHOR CONTRIBUTIONS

All authors listed, have made substantial, direct and intellectual contribution to the work, and approved it for publication.

ACKNOWLEDGMENTS

PL greatly acknowledges the support of the Chilean National TAC (CNTAC) which during more than 10 years allocated telescope time to conduct our reverberation campaign and to the funding by Fondecyt along all these years, and in particular to Project #1161184.

REFERENCES

Alexander, T. (1997). "Is AGN variability correlated with other AGN properties? ZDCF analysis of small samples of sparse light curves," in *Astronomical Time Series, Vol. 218, Astrophysics and Space Science Library*, eds D. Maoz, A. Sternberg, and E. M. Leibowitz (Dordrecht: Springer), 163–166.

Baskin, A., and Laor, A. (2005). What controls the CIV line profile in active galactic nuclei? *Month. Not. R. Astron. Soc.* 356, 1029–1044. doi: 10.1111/j.1365-2966.2004.08525.x

Bentz, M. C., Denney, K. D., Grier, C. J., Barth, A. J., Peterson, B. M., Vestergaard, M., et al. (2013). The low-luminosity end of the radius-luminosity relationship for active galactic nuclei. *Astrophys. J.* 767:149. doi: 10.1088/0004-637X/767/2/149

Bentz, M. C., Peterson, B. M., Netzer, H., Pogge, R. W., and Vestergaard, M. (2009). The radius-luminosity relationship for active galactic nuclei: the effect of host-galaxy starlight on luminosity measurements. II. The full sample of reverberation-mapped AGNs. *Astrophys. J.* 697, 160–181. doi: 10.1088/0004-637X/697/1/160

Bentz, M. C., Peterson, B. M., Pogge, R. W., Vestergaard, M., and Onken, C. A. (2006). The radius-luminosity relationship for active galactic nuclei: the effect of host-galaxy starlight on luminosity measurements. *Astrophys. J.* 644, 133–142. doi: 10.1086/503537

De Rosa, G., Peterson, B. M., Ely, J., Kriss, G. A., Crenshaw, D. M., Horne, K., et al. (2015). Space telescope and optical reverberation mapping project. I. Ultraviolet observations of the Seyfert 1 galaxy NGC 5548 with the cosmic origins spectrograph on Hubble space telescope. *Astrophys. J.* 806:128. doi: 10.1088/0004-637X/806/1/128

Gaskell, C. M., and Sparke, L. S. (1986). Line variations in quasars and Seyfert galaxies. *Astrophys. J.* 305, 175–186. doi: 10.1086/164238

Goad, M. R., Korista, K. T., De Rosa, G., Kriss, G. A., Edelson, R., Barth, A. J., et al. (2016). Space telescope and optical reverberation mapping project. IV. Anomalous behavior of the broad ultraviolet emission lines in NGC 5548. *Astrophys. J.* 824:11. doi: 10.3847/0004-637X/824/1/11

Kaspi, S., Brandt, W. N., Maoz, D., Netzer, H., Schneider, D. P., and Shemmer, O. (2007). Reverberation mapping of high-luminosity quasars: first results. *Astrophys. J.* 659, 997–1007. doi: 10.1086/512094

Kaspi, S., Maoz, D., Netzer, H., Peterson, B. M., Vestergaard, M., and Jannuzi, B. T. (2005). The relationship between luminosity and broad-line region size in active galactic nuclei. *Astrophys. J.* 629, 61–71. doi: 10.1086/431275

Kaspi, S., Smith, P. S., Netzer, H., Maoz, D., Jannuzi, B. T., and Giveon, U. (2000). Reverberation measurements for 17 quasars and the size-mass-luminosity relations in active galactic nuclei. *Astrophys. J.* 533, 631–649. doi: 10.1086/308704

Maza, J., Wischnjewsky, M., and Antezana, R. (1996). Calán-Tololo survey. VIII. One hundred southern quasars. *Rev. Mex. Astron. Astrofis.* 32, 35–45.

McLure, R. J., and Dunlop, J. S. (2004). The cosmological evolution of quasar black hole masses. *Month. Not. R. Astron. Soc.* 352, 1390–1404. doi: 10.1111/j.1365-2966.2004.08034.x

Mejía-Restrepo, J. E., Trakhtenbrot, B., Lira, P., Netzer, H., and Capellupo, D. M. (2016). Active galactic nuclei at z $\sim$ 1.5 - II. Black hole mass estimation by means of broad emission lines. *Month. Not. R. Astron. Soc.* 460, 187–211. doi: 10.1093/mnras/stw568

Netzer, H., Lira, P., Trakhtenbrot, B., Shemmer, O., and Cury, I. (2007). Black hole mass and growth rate at high redshift. *Astrophys. J.* 671, 1256–1263. doi: 10.1086/523035

Peterson, B. M. (1994). "Overview of reverberation mapping: progress and problems," in *Reverberation Mapping of the Broad-Line Region in Active Galactic Nuclei, Vol. 69 Astronomical Society of the Pacific Conference Series*, eds P. M. Gondhalekar, K. Horne, and B. M., Peterson (San Francisco: Astronomical Society of the Pacific), 1.

Peterson, B. M., Bentz, M. C., Desroches, L.-B., Filippenko, A. V., Ho, L. C., Kaspi, S., et al. (2005). Multiwavelength monitoring of the dwarf Seyfert 1 galaxy NGC 4395. I. A reverberation-based measurement of the black hole mass. *Astrophys. J.* 632, 799–808. doi: 10.1086/444494

Peterson, B. M., Bentz, M. C., Desroches, L.-B., Filippenko, A. V., Ho, L. C., Kaspi, S., et al. (2006). Erratum: "Multiwavelength monitoring of the dwarf Seyfert 1 galaxy NGC 4395. I. A reverberation-based measurement of the black hole mass" (ApJ,632,799[2005]). *Astrophys. J.* 641, 638–639. doi: 10.1086/500409

Peterson, B. M., Ferrarese, L., Gilbert, K. M., Kaspi, S., Malkan, M. A., Maoz, D., et al. (2004). Central masses and broad-line region sizes of active galactic nuclei. II. A homogeneous analysis of a large reverberation-mapping database. *Astrophys. J.* 613, 682–699. doi: 10.1086/423269

Rodríguez-Pascual, P. M., Alloin, D., Clavel, J., Crenshaw, D. M., Horne, K., Kriss, G. A., et al. (1997). Steps toward determination of the size and structure of the broad-Line region in active galactic nuclei. IX. Ultraviolet observations of fairall 9. *Astrophys. J. Suppl. Ser.* 110, 9–20. doi: 10.1086/312996

Schneider, D. P., Hall, P. B., Richards, G. T., Vanden Berk, D. E., Anderson, S. F., Fan, X., et al. (2005). The sloan digital sky survey quasar catalog. III. Third data release. *Astron. J.* 130, 367–380. doi: 10.1086/431156

Shen, Y., Greene, J. E., Strauss, M. A., Richards, G. T., and Schneider, D. P. (2008). Biases in virial black hole masses: an SDSS perspective. *Astrophys. J.* 680, 169–190. doi: 10.1086/587475

Shen, Y., and Liu, X. (2012). Comparing single-epoch virial black hole mass estimators for luminous quasars. *Astrophys. J.* 753:125. doi: 10.1088/0004-637X/753/2/125

Trakhtenbrot, B., and Netzer, H. (2012). Black hole growth to z = 2 - I. Improved virial methods for measuring M_{BH} and L/L_{Edd}. *Month. Not. R. Astron. Soc.* 427, 3081–3102. doi: 10.1111/j.1365-2966.2012.22056.x

Wandel, A., Peterson, B. M., and Malkan, M. A. (1999). Central masses and broad-line region sizes of active galactic nuclei. I. Comparing the photoionization and reverberation techniques. doi: 10.1086/308017 *Astrophys. J.* 526, 579–591.

Conflict of Interest Statement: The authors declare that the research was conducted in the absence of any commercial or financial relationships that could be construed as a potential conflict of interest.

Copyright © 2018 Lira, Botti, Kaspi and Netzer. This is an open-access article distributed under the terms of the Creative Commons Attribution License (CC BY). The use, distribution or reproduction in other forums is permitted, provided the original author(s) or licensor are credited and that the original publication in this journal is cited, in accordance with accepted academic practice. No use, distribution or reproduction is permitted which does not comply with these terms.

frontiers in Astronomy and Space Sciences

ORIGINAL RESEARCH
published: 05 December 2017
doi: 10.3389/fspas.2017.00055

Continuum Reverberation Mapping of AGN Accretion Disks

Michael M. Fausnaugh[1,2], Bradley M. Peterson[1,3,4], David A. Starkey[5,6], Keith Horne[5] and the AGN STORM Collaboration*

[1] Department of Astronomy, Ohio State University, Columbus, OH, United States, [2] MIT Kavli Institute for Astrophysics and Space Research, Cambridge, MA, United States, [3] Center for Cosmology and AstroParticle Physics, Ohio State University, Columbus, OH, United States, [4] Space Telescope Science Institute, Baltimore, MD, United States, [5] SUPA Physics and Astronomy, University of St. Andrews, Scotland, United Kingdom, [6] Department of Astronomy, University of Illinois at Urbana-Champaign, Urbana, IL, United States

We show recent detections of inter-band continuum lags in three AGN (NGC 5548, NGC 2617, and MCG+08-11-011), which provide new constraints on the temperature profiles and absolute sizes of the accretion disks. We find lags larger than would be predicted for standard geometrically thin, optically thick accretion disks by factors of 2.3–3.3. For NGC 5548, the data span UV through optical/near-IR wavelengths, and we are able to discern a steeper temperature profile than the $T \sim R^{-3/4}$ expected for a standard thin disk. Using a physical model, we are also able to estimate the inclinations of the disks for two objects. These results are similar to those found from gravitational microlensing of strongly lensed quasars, and provide a complementary approach for investigating the accretion disk structure in local, low luminosity AGN.

Keywords: AGN continuum, galaxies: active, individual: NGC5548, NGC2617, MCG+08-11-011

OPEN ACCESS

Edited by:
Mauro D'Onofrio, Universitá degli Studi di Padova, Italy

Reviewed by:
Dragana Ilic, University of Belgrade, Serbia
Giovanna Maria Stirpe, Osservatorio Astronomico di Bologna (INAF), Italy

****Correspondence:***
Michael M. Fausnaugh
faus@mit.edu

Specialty section:
This article was submitted to Milky Way and Galaxies, a section of the journal Frontiers in Astronomy and Space Sciences

Received: *01 October 2017*
Accepted: *20 November 2017*
Published: *05 December 2017*

Citation:
Fausnaugh MM, Peterson BM, Starkey DA, Horne K and the AGN STORM Collaboration (2017) Continuum Reverberation Mapping of AGN Accretion Disks. Front. Astron. Space Sci. 4:55. doi: 10.3389/fspas.2017.00055

1. INTRODUCTION

Active galactic nuclei (AGN) are the markers of rapidly accreting super-massive black holes (SMBHs). The current picture of the sub-parsec scale structure of an AGN includes three main components: an accretion disk around the SMBH, a region of high-velocity gas (the "broad line region," BLR), and a hot, X-ray emitting "corona." Although this simple model can explain the observed features of AGN spectra, the detailed geometry and dynamics of the accretion disk, BLR, and corona are largely unknown. The sub-parsec scale structures are unresolved in even the closest AGN, so additional information must be obtained by indirect means.

Reverberation mapping (Blandford and McKee, 1982; Peterson, 1993, 2014) has emerged as a powerful way to probe these compact structures in the central parts of AGN. The principle of reverberation mapping is to search for time-variable flux signals and their light echoes, which encode information about these unresolved structures. For example, gas in the BLR reprocesses variations in the ionizing continuum flux from the accretion disk as variable emission line flux after a time delay that scales with the light-crossing time of the BLR. Measuring this time delay therefore provides a straightforward estimate of the BLR's spatial extent.

More recently, reverberation mapping techniques have been used to examine the structure of AGN accretion disks. A standard geometrically thin, optically thick accretion disk has a temperature profile of $T \sim R^{-3/4}$ (Shakura and Sunyaev, 1973), so that the hot, inner parts of the accretion disk emit UV photons (∼10–3,000 Å), while the cooler, outer annuli emit in the optical and near IR (∼3,000–10,000 Å). If variations at shorter wavelengths (from the

X-ray emitting corona or the inner edge of the disk) irradiate the outer annuli and drive longer wavelength variations, we expect a time delay between the UV and optical continuum variations that is proportional to the size of the accretion disk (Krolik et al., 1991).

Most attempts to measure continuum lags have not been able to detect time delays at $>3\sigma$ (e.g., Sergeev et al., 2005; Arévalo et al., 2008; Breedt et al., 2010; Lira et al., 2015; Gliozzi et al., 2016; Troyer et al., 2016; Buisson et al., 2017; Jiang et al., 2017). The primary limitation is obtaining continuous, well-sampled (of order 1 day or less) light curves on time scales of weeks to months. However, Shappee et al. (2014) were able to detect continuum lags at high significance in NGC 2617 using rapid cadence *Swift* and ground-based light curves from observations spanning several weeks. Here, we report on recent detections of inter-band continuum lags in two other objects, NGC 5548 and MCG+08-11-011, as well as results from continued monitoring of NGC 2617.

2. AGN STORM

The AGN Space Telescope and Optical Reverberation Mapping project (STORM, De Rosa et al., 2015) is the most ambitious reverberation mapping experiment to date. We monitored the Seyfert 1 galaxy NGC 5548 for 6 months in 2014 with an unprecedented combination of cadence and wavelength coverage. The project was anchored by 171 observations with the Cosmic Origins Spectrograph onboard *HST*, and additional data were supplied by *Chandra* (Mathur et al., 2017) and *Swift* (Edelson et al., 2015), as well as a global compliment of ground-based observatories (Fausnaugh et al., 2016). We obtained light curves with approximately daily cadence over the six month baseline, at wavelengths in the far UV (1,100–1,700 Å with *HST*), near UV (1,900–2,600 Å with *Swift*), and optical/near IR (Johnson/Cousins *UBVRI* and SDSS *ugriz*).

Lags between the continuum emission at different wavelengths (and their uncertainties) were estimated in two ways: traditional cross-correlation techniques (the interpolated cross-correlation function and flux redistribution/random subset sampling; Gaskell and Peterson, 1987; White and Peterson, 1994) and a Bayesian model that infers the response function for an input driving light curve and its light echoes (JAVELIN; Zu et al., 2011). In both cases, the estimated lags agree and are detected at high significance. We measure the continuum lags relative to the light curve for emission at 1,367 Å, and the results are shown in **Figure 1**.

Assuming a disk reprocessing model, we can translate the observed lag-wavelength relation in **Figure 1** to a wavelength dependent emissivity profile, which in turn depends on the temperature profile of the disk. For a given temperature profile $T \sim R^{\beta}$, we expect that $R \sim \lambda^{-1/\beta}$, and we take the lag τ as a measurement of the light crossing time across the disk R/c. The best fit yields $\beta = 1.01 \pm 0.14$ (dashed magenta line in **Figure 1**), and is statistically consistent ($\sim 2\sigma$) with the prediction for a standard thin disk ($\beta = -3/4$, solid magenta line in **Figure 1**). For comparison, the prediction for an $T \sim R^{-3/4}$ thin disk is shown by the dashed magenta lines in **Figure 1**.

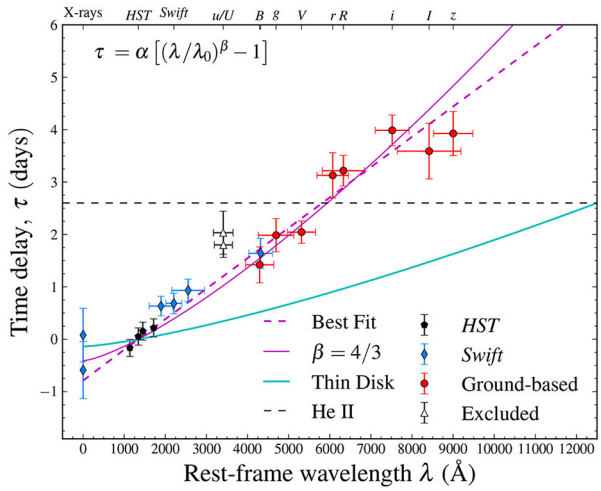

FIGURE 1 | Time delays between inter-band continuum light curves as a function of rest-frame effective wavelength, adapted from Fausnaugh et al. (2016). The time delays are interpreted as reverberations across the accretion disk, with short-wavelength variations driving longer wavelengths. The time delays are measured relative to variations at 1,367 Å and the equation in the upper left corner describes the generic form of the lag-wavelength relation in a geometrically thin accretion disk, normalized to $\lambda_0 = 1{,}367$ Å. The best fit to this relation (with α and β as free parameters) is shown with the dashed magenta line. The excluded points (from the u/U-band light curves) are noticeable outliers, likely because of contamination by Balmer continuum emission originating in the broad line region, and are excluded from the fit (see Fausnaugh et al., 2016 for details). The normalization parameter α can be predicted from the SMBH mass and mass accretion rate—based on values for NGC 5548 (see section 2), we show this prediction with the cyan line. The best-fit value is a factor of 3 larger than this prediction. A standard thin disk also has a temperature profile $T \propto R^{-3/4}$, which predicts $\beta = 4/3$. We show a fit with β fixed to 4/3 by the solid magenta line. Although the best fit is consistent with $\beta = 4/3$ at the 2σ level, physical modeling shows that the data strongly prefer a steeper temperature profile of $T \sim R^{-1}$ (Starkey et al., 2017). Finally, the horizontal dashed black line shows the lag of the high-ionization state lines He II λ1640 and λ4686 relative to the 1,367 Å light curve—the lag is 2.45 days, slightly larger than the lag of the V-band light curve.

In addition, the magnitude of the lags provides information about the absolute size of the disk. In the standard thin accretion disk model, gravitational potential energy is converted into heat and radiation, and the product $M_{\rm BH}\dot{M}$ determines the temperature at the inner edge of the disk. Combined with the temperature profile, this information sets the disk's radial scale—for a fixed black hole mass, a higher accretion rate disk will appear larger at a given wavelength. We adopt a black hole mass of 5.2×10^7 $M_{\odot}$, determined from reverberation mapping of the Hβ emission line (Grier et al., 2012), and we assume an accretion rate of 10% of the Eddington rate, typical of Type 1 Seyfert galaxies (this value is similar to what would be inferred from the optical luminosity at 5,100 Å, see Netzer, 2013; Fausnaugh et al., 2016). For these parameters, the model prediction is shown by the cyan line in **Figure 1**, which underestimates the observed lag-wavelength relation by a factor of 3. In fact, the continuum lags are large enough ($\sim$2 light days from the 1,367 Å emission to the V-band) that they are comparable to the lags of the high-ionization state emission lines (such as HeII, which has a

lag relative to the 1,367 Å emission of 2.45 days, shown by the black dashed horizontal line in **Figure 1**). This suggests that at least part of the BLR and continuum emitting source are of a similar physical size, if they are not identical or contiguous.

This result is fairly insensitive to other parameters in the thin disk reprocessing model, such as the fraction of heating due to X-rays and the assumed radiative efficiency of matter falling onto the black hole (Fausnaugh et al., 2016). We have also taken into account the contribution of emission from a range of disk radii at a given wavelength by estimating R with the flux-weighted mean radius across the entire disk. However, we ignored the inner edge of the disk in this calculation, instead anchoring the physical radius for emission at 1,367 Å (which has zero lag by definition) by extrapolating the fit to zero wavelength. In practice, the inner edge of the disk already makes significant contributions to emission at 1,367 Å and the relation is expected to turn over at shorter wavelengths, although this difference is small compared to the radii at which the disk emits in the optical (~ 2 light days).

More recently, Starkey et al. (2016) developed a physical model for inferring accretion disk properties from continuum reverberation mapping data (the Continuum REprocessing AGN MCMC code, CREAM). CREAM uses Bayesian methods to infer the input driving light curve required to produce the observed light curves as reverberation signals, as well as the detailed transfer functions in a thin disk reprocessing model. The parameters of the model are the temperature normalization at a fiducial radius (which is related to the product $M_{\rm BH}\dot{M}$), the power-law index of the disk's temperature profile, and the inclination of the disk. The model also takes into account changes in the disk's spectrum due to instantaneous perturbations in the local disk temperature from variable irradiation.

For NGC 5548, results from CREAM are detailed by Starkey et al. (2017), who find a temperature profile power-law index consistent with the fit to the lags described above (0.99 ± 0.03), but with a much smaller uncertainty that rules out $T \sim R^{-3/4}$. CREAM also finds an inclination of 36 ± 10 degrees, and the temperature at the inner edge of the disk is consistent with the mass accretion rate required to explain the large continuum lags. However, this accretion rate is well above the Eddington limit and inconsistent with the observed optical luminosity. Finally, there is a poor match between the inferred driving light curve and the X-ray light curves from *Swift* XRT, as shown in **Figure 2**. The X-ray variations are usually taken to drive the reprocessed variations at longer wavelengths because they are energetically dominant over the UV/optical variations (though this is not always the case, see for example Breedt et al., 2010), and the corona is believed to be compact and centrally located near the SMBH. However, the poor correlation shown in **Figure 2** suggests that the X-rays do not directly drive the UV/optical variations, which is problematic for standard disk reprocessing models.

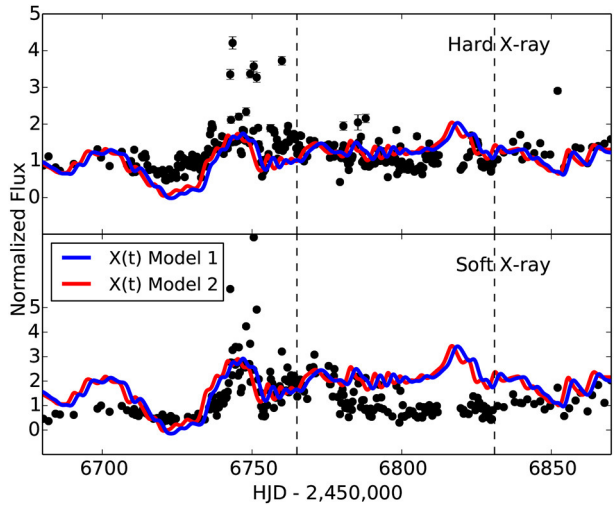

FIGURE 2 | Comparison of the observed X-ray light curve from *Swift* (black points) and the inferred driving continuum light curve from CREAM (solid lines), reproduced from Starkey et al. (2017). The top panel is the hard X-ray (0.8–10 keV) light curve, the bottom panel is the soft X-ray light curve (0.3–0.8 keV). The blue line is for a model with the temperature profile of the disk fixed to $T \sim R^{-3/4}$, the red line is for a model with the temperature profile left as a free parameter (the best fit is $T \sim R^{-0.99 \pm 0.03}$). The poor correlation shows that the observed X-ray light curve does not directly drive the variations in the UV/optical, which may be problematic for disk reprocessing models.

3. AGN 2014 REVERBERATION MAPPING CAMPAIGN

In 2014, we monitored 10 other AGN besides NGC 5548. Space-based resources were not available for these targets—our main goal was to use spectroscopic observations to derive SMBH masses from continuum-Hβ lags. These results are presented by Fausnaugh et al. (2017). However, a unique addition to this campaign was the acquisition of high-quality multi-band imagining on approximately daily cadence, which allowed us to search for optical continuum reverberation signals.

We chose to measure lags relative to the g-band, as this is our bluest light curve that is relatively free of BLR emission (Balmer continuum emission is likely present in the u-band for these objects, see Fausnaugh et al., 2016). For two of our targets, we detected inter-band continuum lags at a statistically significant level: MCG+08-11-011 and NGC 2617 (Fausnaugh et al., submitted). Lags measured from the JAVELIN analysis are shown in **Figure 3**. As expected for the disk-reprocessing model, we generally find larger lags at longer wavelengths, though both objects show outliers and the lag-wavelength relation for NGC 2617 is consistent with a flat relation if the g/V-band lags are outliers. We also compared these results to the theoretical predictions described in section 2, based on the measured black hole masses from Fausnaugh et al. (2017), and accretion rate estimates from the observed optical luminosity at 5,100 Å (Netzer, 2013). Because of the shorter wavelength range of these data (*ugriz* and Johnson V-band), we fixed the lag-wavelength relation to $\tau \sim \lambda^{4/3}$ when fitting for the absolute size of the disk.

We find similar results as in NGC 5548, with larger observed disk sizes compared to theoretical expectations: a factor of 3.3 in MCG+08-11-011 (a 7.2σ result) and a factor of 2.3 in NGC 2617 (a 2.3σ result, which probably also captures the possibility of a flat lag-wavelength relation/unresolved lags). For comparison, we

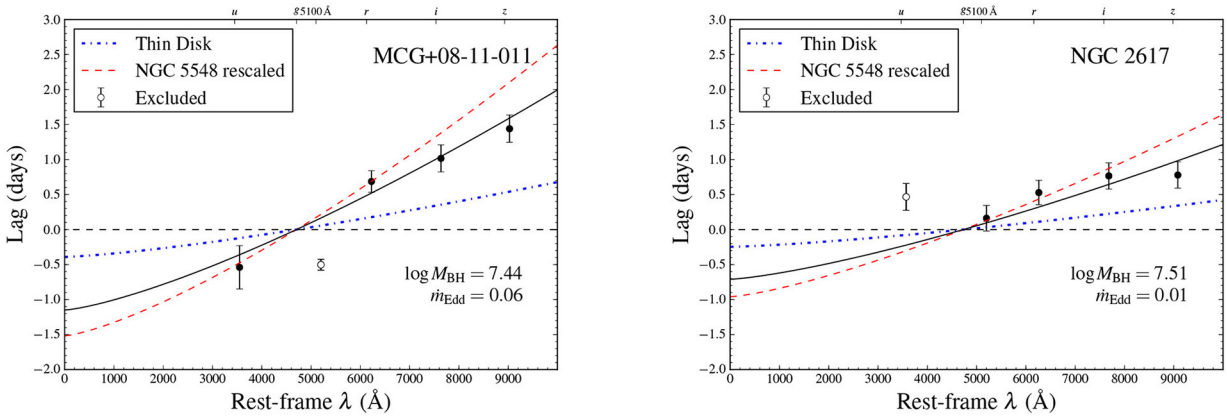

FIGURE 3 | Continuum reverberation mapping results for two objects from the 2014 AGN monitoring campaign, adapted from Fausnaugh et al. (submitted). Only optical data were available for this campaign, and inter-band lags were therefore measured relative to the g-band light curve. The solid black line shows the best fit lag-wavelength relation for a disk with temperature profile fixed to $T \sim R^{-3/4}$ ($\beta = 4/3$). The dot-dashed blue lines show the predicted normalization, based on the black hole masses and Eddington ratios given in the lower right hand corner of each panel (as measured by Fausnaugh et al. 2017). The dashed red lines show the fit to NGC 5548 from the STORM campaign rescaled to the parameters of these systems assuming standard thin-disk theory. The similarity of the solid black and dashed red lines suggests that, after extrapolating to UV wavelengths, the disks are larger than standard predictions by a similar amount as in NGC 5548. The excluded points were identified as outliers (again likely due to contamination by broad line region emission) and are discussed in detail by Fausnaugh et al. (submitted).

rescaled the observed NGC 5548 lag-wavelength relation from the STORM campaign, using the same theoretical dependence on black hole mass and mass accretion rate—these relations are shown by the red lines in **Figure 3**, and are generally consistent with the best fit.

We also analyzed these data using the CREAM physical model. We again fixed the temperature profile power-law index to $-3/4$, and we found temperatures at the inner edge of the disk hotter than would be implied by the SMBH masses and mass accretion rates derived from the optical luminosity. As described in section 2, this is consistent with large disk sizes inferred from the continuum lags. For MCG+08-11-011, we were unable to constrain the disk's inclination, and therefore fixed this parameter to 0 degrees for the final fit. For NGC 2617, we found an inclination of 43 $\pm$ 20 degrees. Given uncertainties in the black hole mass, bolometric corrections, and radiative efficiency, as well as systematic uncertainties such as internal extinction and possible kinematic luminosity in outflows, there are large uncertainties on the predictions for the temperature at the inner edge of the disk. It seems that the disk in NGC 2617 may be consistent with a standard thin disk model, while the total discrepancy in MCG+08-11-011 is difficult to explain with these uncertainties.

NGC 2617 provides a special test case for disk models, since Shappee et al. (2014) also measured the disk size from multi-wavelength monitoring data taken in 2013. The lags we measure here are consistent with those from Shappee et al. (2014) to within $\sim 3\sigma$, but are systematically smaller. This could be caused by two effects. First is a physical change in the disk. The dynamical time at $\sim$1 light day from the black hole in NGC 2617 is $\sim$1 month, so a bulk change in the accretion flow between 2013 and 2014 cannot be ruled out. The size of the disk is also expected to scale with luminosity, and NGC 2617 was a factor of 1.8 less luminous in 2014 than in 2013. However, this scaling of disk size with luminosity is based on a variable accretion rate, and the structure of the disk would then be predicted to respond on the viscous time scale (several decades to centuries for AGN accretion disks; see LaMassa et al., 2015).

An alternative interpretation is systematic effects in the reverberation mapping measurement. The observed time delay is not independent of the auto-correlation of the driving light curve, and the observed continuum variations are very different in the 2014 monitoring campaign compared to the data from 2013. In 2014, the variations are much more rapid and have a smaller amplitude, which will generally result in smaller lags and therefore a smaller inferred disk size (Goad and Korista, 2014).

4. CONCLUSIONS

We have reviewed recent detections of inter-band continuum lags in three AGN, NGC 5548, MCG+08-11-011, and NGC 2617. Our results suggest either larger accretion disks compared to theoretical expectations, or higher mass accretion rates than would be inferred from the optical luminosity. For the highest quality data and best wavelength coverage (AGN STORM observations of NGC 5548), there is also evidence of a departure from a standard temperature profile, with physical modeling preferring $T \sim R^{-1}$.

These results corroborate those from gravitational microlensing of strongly lensed quasars, which also find larger disks sizes than expected and a range of temperature profiles (Blackburne et al., 2011; Mosquera et al., 2013; Jiménez-Vicente et al., 2014). Continuum reverberation mapping therefore promises to be a crucial avenue for further research into the structure of AGN accretion disks, especially for local and low-luminosity sources that are not accessible through microlensing. Several successful *Swift* proposals and ground-based observing campaigns are currently monitoring

many more AGN in order to increase the sample of disk measurements (NGC 4151, Edelson et al., 2017, Mrk 509, PI: Edelson; NGC 4395, PI: McHardy, the LCO AGN Key project, PI: Horne).

AUTHOR CONTRIBUTIONS

MF: wrote the manuscript and performed the photometric and time-series analysis; DS: developed and ran the CREAM models; BP and KH: advised this work; The AGN STORM collaboration consists of over 100 astronomers from around the world, with observers, theoreticians, and observatory directors/PIs, providing support, comments, and telescope time.

FUNDING

This work was supported by a Presidential Fellowship awarded to MF buy the Ohio State University. NSF grant AST-1008882 and STScI Grant GO-13330 supported MF and BP. KH acknowledges support from STFC grant ST/M001296/1.

ACKNOWLEDGMENTS

Based on observations made with the NASA/ESA *Hubble Space Telescope*. This research has made use of the XRT Data Analysis Software (XRTDAS) developed under the responsibility of the ASI Science Data Center (ASDC), Italy. This work is based on observations obtained at the MDM Observatory, operated by Dartmouth College, Columbia University, Ohio State University, Ohio University, and the University of Michigan. This paper is partly based on observations collected at the Wise Observatory with the C18 telescope. The C18 telescope and most of its equipment were acquired with a grant from the Israel Space Agency (ISA) to operate a Near-Earth Asteroid Knowledge Center at Tel Aviv University. The Fountainwood Observatory would like to thank the HHMI for its support of science research for undergraduate students at Southwestern University. This research has made use of NASA's Astrophysics Data System, as well as the NASA/IPAC Extragalactic Database (NED) which is operated by the Jet Propulsion Laboratory, California Institute of Technology, under contract with the National Aeronautics and Space Administration.

REFERENCES

Arévalo, P., Uttley, P., Kaspi, S., Breedt, E., Lira, P., and McHardy, I. M. (2008). Correlated X-ray/optical variability in the quasar. *Mon. Not. R. Astron. Soc.* 389, 1479–1488. doi: 10.1111/j.1365-2966.2008.13719.x

Blackburne, J. A., Pooley, D., Rappaport, S., and Schechter, P. L. (2011). Sizes and temperature profiles of quasar accretion disks from chromatic microlensing. *Astrophys. J.* 729:34. doi: 10.1088/0004-637X/729/1/34

Blandford, R. D., and McKee, C. F. (1982). Reverberation mapping of the emission line regions of Seyfert galaxies and quasars. *Astrophys. J.* 255, 419–439.

Breedt, E., McHardy, I. M., Arévalo, P., Uttley, P., Sergeev, S. G., Minezaki, T., et al. (2010). Twelve years of X-ray and optical variability in the Seyfert galaxy NGC 4051. *Mon. Not. R. Astron. Soc.* 403, 605–619. doi: 10.1111/j.1365-2966.2009.16146.x

Buisson, D. J. K., Lohfink, A. M., Alston, W. N., and Fabian, A. C. (2017). Ultraviolet and X-ray variability of active galactic nuclei with Swift. *Mon. Not. R. Astron. Soc.* 464, 3194–3218. doi: 10.1093/mnras/stw2486

De Rosa, G., Peterson, B. M., Ely, J., Kriss, G. A., Crenshaw, D. M., Horne, K., et al. (2015). Space telescope and optical reverberation mapping project. I. Ultraviolet observations of the seyfert 1 galaxy NGC 5548 with the cosmic origins spectrograph on hubble space telescope. *Astrophys. J.* 806:128. doi: 10.1088/0004-637X/806/1/128

Edelson, R., Gelbord, J. M., Horne, K., McHardy, I. M., Peterson, B. M., Arevalo, P., et al. (2015). Space telescope and optical reverberation mapping project. II. SWIFT and HST reverberation mapping of the accretion disk oF NGC 5548. *Astrophys. J.* 806:129. doi: 10.1088/0004-637X/806/1/129

Edelson, R., Gelbord, J. M., Cackett, E., Connolly, S., Done, C., Fausnaugh, M., et al. (2017). Swift monitoring of NGC 4151: evidence for a second X-ray/UV reprocessing. *Astrophys. J.* 840:41. doi: 10.3847/1538-4357/aa6890

Fausnaugh, M. M., Denney, K. D., Barth, A. J., Bentz, M. C., Bottorff, M. C., Carini, M. T., et al. (2016). Space telescope and optical reverberation mapping project. III. optical continuum emission and broadband time delays in NGC 5548. *Astrophys. J.* 821:56. doi: 10.3847/0004-637X/821/1/56

Fausnaugh, M. M., Grier, C. J., Bentz, M. C., Denney, K. D., De Rosa, G., Peterson, B. M., et al. (2017). Reverberation mapping of optical emission lines in five active galaxies. *Astrophys. J.* 840:97. doi: 10.3847/1538-4357/aa6d52

Gaskell, C. M., and Peterson, B. M. (1987). The accuracy of cross-correlation estimates of quasar emission-line region sizes. *Astrophys. J.* 65, 1–11. doi: 10.1086/191216

Gliozzi, M., Papadakis, I. E., Grupe, D., Brinkmann, W. P., and Raeth, C. (2016). Long-term monitoring of Ark 120 with Swift. *Mon. Not. R. Astron. Soc.* 464, 3955–3964. doi: 10.1093/mnras/stw2636

Goad, M. R., and Korista, K. T. (2014). Interpreting broad emission-line variations - I. Factors influencing the emission-line response. *Mon. Not. R. Astron. Soc.* 444, 43–61. doi: 10.1093/mnras/stu1456

Grier, C. J., Peterson, B. M., Pogge, R. W., Denney, K. D., Bentz, M. C., Paul Martini, et al. (2012). Reverberation mapping results for five Seyfert 1 galaxies. *Astrophys. J.* 755:60. doi: 10.1088/0004-637X/755/1/60

Jiang, Y.-F., Green, P. J., Green, J. E., Morganson, E., Shen, Y., Pancoast, A., et al. (2017). Detection of time lags between Quasar Continuum Emission Bands based on Pan-STARRS Light Curves. *Astrophys. J.* 836:186. doi: 10.3847/1538-4357/aa5b91

Jiménez-Vicente, J., Mediavilla, E., Kochanek, C. S., Muñoz, J. A., Motta, V., Falco, E., et al. (2014). The average size and temperature profile of quasar accretion disks. *Astrophys. J.* 783:47. doi: 10.1088/0004-637X/783/1/47

Krolik, J. H., Horne, K., Kallman, T. R., Malkan, M. A., Edelson, R. A., and Kriss, G. A. (1991). Ultraviolet variability of NGC 5548: dynamics of the continuum production region and geometry of the broad-line region. *Astrophys. J.* 371, 541.

Lira, P., Arévalo, P., Uttley, P., McHardy, I. M. M., and Videla, L. (2015). Long-term monitoring of the archetype Seyfert galaxy MCG-6-30-15: X-ray, optical and near-IR variability of the corona, disc and torus. *Mon. Not. R. Astron. Soc.* 454, 368–379. doi: 10.1093/mnras/stv1945

LaMassa, S. M., Cales, S., Moran, E. C., Myers, A. D., Richards, G. T., Eracleous, M., et al. (2015). The discovery of the first "changing look" quasar: new insights into the physics and phenomenology of active galactic nuclei. *Astrophys. J.* 800:144. doi: 10.1088/0004-637X/800/2/144

Mathur, S., Gupta, A., Page, K., Pogge, R. W., Krongold, Y., Goad, M. R., et al. (2017). Space telescope and optical reverberation mapping project. VII. Understanding the ultraviolet anomaly in NGC 5548 with X-Ray spectroscopy. *Astrophys. J.* 846, 55. doi: 10.3847/1538-4357/aa832b

Mosquera, A. M., Kochanek, C. S., Chen, B., Dai, X., Blackburne, J. A., and Chartas, G. (2013). The structure of the X-ray and optical emitting regions of the lensed Quasar Q 2237+0305. *Astrophys. J.* 769:53. doi: 10.1088/0004-637X/769/1/53

Netzer, H. (2013). *The Physics and Evolution of Active Galactic Nuclei.* Cambridge, UK: Cambridge University Press.

Peterson, B. M. (1993). Reverberation mapping of active galactic nuclei. *PASP* 105, 247–268. doi: 10.1086/133140

Peterson, B. M. (2014). Measuring the masses of supermassive black hole. *Space Sci. Rev.* 183, 253–275. doi: 10.1007/s11214-013-9987-4

Sergeev, S. G., Doroshenko, V. T., Golubinskiy, Y. V., Merkulova, N. I., and Sergeeva, E. A. (2005). Lag-luminosity relationship for interband lags between variations in *B*, *V*, *R*, and *I* bands in active galactic nuclei. *Astrophys. J.* 622, 129–135. doi: 10.1086/427820

Shakura, N. I., and Sunyaev, R. A. (1973). Black holes in binary systems. Observational appearance. *Astron. Astrophys.* 24, 337–355.

Shappee, B. J., Prieto, J. L., Grupe, D., Kochanek, C. S., Stanek, K. Z., De Rosa, G., et al. (2014). The man behind the curtain: X-rays drive the UV through NIR variability in the 2013 active galactic nucleus outburst in NGC 2617. *Astrophys. J.* 788:48. doi: 10.1088/0004-637X/788/1/48

Starkey, D. A., Horne, K., and Villforth, C. (2016). Accretion disc time lag distributions: applying CREAM to simulated AGN light curves. *Mon. Not. R. Astron. Soc.* 456, 1960–1973. doi: 10.1093/mnras/stv2744

Starkey, D., Horne, K., Fausnaugh, M. M., Peterson, B. M., Bentz, M. C., Kochanek, C. S., et al. (2017). Space telescope and optical reverberation mapping project. VI. Reverberating disk models foR NGC 5548. *Astrophys. J.* 835:65. doi: 10.3847/1538-4357/835/1/65

Troyer, J., Starkey, D., Cackett, E. M., Bentz, M. C., Goad, M. R., Horne, K., et al. (2016). Correlated X-ray/ultraviolet/optical variability in NGC 6814. *Mon. Not. R. Astron. Soc.* 456, 4040–4050. doi: 10.1093/mnras/stv2862

White, R. J., and Peterson, B. M. (1994). Comments on cross-correlation methodology in variability studies of active galactic nuclei. *PASP* 106, 879–889. doi: 10.1086/133456

Zu, Y., Kochanek, C. S., and Peterson, B. M. (2011). An alternative approach to measuring reverberation lags in active galactic nuclei. *Astrophys. J.* 735:80. doi: 10.1088/0004-637X/735/2/80

Conflict of Interest Statement: The authors declare that the research was conducted in the absence of any commercial or financial relationships that could be construed as a potential conflict of interest.

Copyright © 2017 Fausnaugh, Peterson, Starkey, Horne and the AGN STORM Collaboration. This is an open-access article distributed under the terms of the Creative Commons Attribution License (CC BY). The use, distribution or reproduction in other forums is permitted, provided the original author(s) or licensor are credited and that the original publication in this journal is cited, in accordance with accepted academic practice. No use, distribution or reproduction is permitted which does not comply with these terms.

frontiers in Astronomy and Space Sciences

ORIGINAL RESEARCH
published: 22 June 2017
doi: 10.3389/fspas.2017.00005

Self-Consistent Dynamical Model of the Broad Line Region

Bozena Czerny[1], Yan-Rong Li[2], Justyna Sredzinska[3], Krzysztof Hryniewicz[3], Swayam Panda[1,3], Conor Wildy[1] and Vladimir Karas[4]*

[1] Center for Theoretical Physics, Polish Academy of Sciences, Warsaw, Poland, [2] Key Laboratory for Particle Astrophysics, Institute of High Energy Physics, Chinese Academy of Sciences, Beijing, China, [3] Copernicus Astronomical Center, Polish Academy of Sciences, Warsaw, Poland, [4] Astronomical Institute, Czech Academy of Sciences, Prague, Czechia

We develop a self-consistent description of the Broad Line Region based on the concept of a failed wind powered by radiation pressure acting on a dusty accretion disk atmosphere in Keplerian motion. The material raised high above the disk is illuminated, dust evaporates, and the matter falls back toward the disk. This material is the source of emission lines. The model predicts the inner and outer radius of the region, the cloud dynamics under the dust radiation pressure and, subsequently, the gravitational field of the central black hole, which results in asymmetry between the rise and fall. Knowledge of the dynamics allows us to predict the shapes of the emission lines as functions of the basic parameters of an active nucleus: black hole mass, accretion rate, black hole spin (or accretion efficiency) and the viewing angle with respect to the symmetry axis. Here we show preliminary results based on analytical approximations to the cloud motion.

Keywords: emission lines, active galactic nuclei, Broad Line Region, accretion disk, black hole

OPEN ACCESS

Edited by:
Paola Marziani, National Institute for Astrophysics (INAF), Italy

Reviewed by:
Giovanna Maria Stirpe, Osservatorio Astronomico di Bologna (INAF), Italy
Edi Bon, Belgrade Astronomical Observatory, Serbia

****Correspondence:***
Bozena Czerny
bcz@cft.edu.pl

Specialty section:
This article was submitted to Cosmology, a section of the journal Frontiers in Astronomy and Space Sciences

Received: *26 April 2017*
Accepted: *08 June 2017*
Published: *22 June 2017*

Citation:
Czerny B, Li Y-R, Sredzinska J, Hryniewicz K, Panda S, Wildy C and Karas V (2017) Self-Consistent Dynamical Model of the Broad Line Region. Front. Astron. Space Sci. 4:5. doi: 10.3389/fspas.2017.00005

1. INTRODUCTION

The Broad Emission Line Region (BLR) is the key ingredient of most active nuclei, and its true nature remains illusive. Huge observational progress allowed the accumulation of a lot of constraints/requirements for the material which is the source of emission lines. This (clumpy ?) wind emission is mostly powered by the emission from the most central parts, with (possibly) some contribution from mechanical heating. The distribution of the emitting material is rather flat since BLR clouds are rarely seen in absorption despite covering a relatively large fraction of the sky as seen from the nucleus, which is required by the total line luminosity. The study of emission line variability allows measurement of the distance to the BLR, and shows that in general the region is extended, with High Ionization Lines (HIL) forming closer in, and Low Ionization Lines (LIL) forming further down (Collin-Souffrin et al., 1986; Gaskell, 2009). The motion is predominantly Keplerian, which opened a way to use the BLR for black hole mass measurements (Wandel et al., 1999). The wavelength-resolved reverberation mapping now allows for a few well-studied sources to provide an insight into the velocity field, confirming predominantly Keplerian motion but with traces of inflow as well as outflow (Grier et al., 2013).

The outflow suggests that the emitting material is connected with the cold accretion disk present in the nucleus, and a disk wind. There are also observational arguments for the co-existence of the cold disk and BLR.

Several mechanisms are known to drive winds (radiation pressure driven winds; e.g., Elvis, 2012; magnetically driven winds, e.g., Fukumura et al., 2015; pressure driven winds, e.g., Fukue, 2004, and the references therein), and a combination of all effects is likely to contribute although

various mechanisms could dominate at various distances from the black hole, as the local densities and ionizing flux changes with the disk radius. Inflow might seem less expected, but the winds in some parameter space are actually failed winds, not escaping to infinity, and reversing to inflow. Also the thermal instability in the circumnuclear material may lead to selective inflow of the denser phase (e.g.,Elvis, 2017).

This tremendously complicated region, however, produces a strikingly good correlation between the BLR size and the source monochromatic luminosity. More specifically, this is the relation between the delay of the β line with respect to the 5,100 Å continuum, which in addition is not the continuum driving this line. This relation is now observationally studied in a broad luminosity range as well as in redshift (Peterson et al., 2004; Bentz et al., 2013; Shen et al., 2016).

Failed Radiatively Accelerated Dusty Outflow (FRADO) model (Czerny and Hryniewicz, 2011; Czerny et al., 2015) offers a natural way to understand this relation. Other BLR models, like the one developed by Netzer and Marziani (2010) are parametric, they do not uniquely predict the radial extension of the BLR without referring to an observational scaling while FRADO gives the location of the LIL part, at the basis of the dust microscopic properties. Below we briefly outline the model itself, the dynamics of the clouds and the exemplary line profiles. The model parameters are just the global parameters of the stationary accretion flow in the nucleus: the black hole mass, the accretion rate, the spin (or accretion efficiency) and the viewing angle toward the nucleus.

2. FRADO MODEL

The model is based on the known observational fact that stellar winds are much more prominent in cooler stars with dusty atmospheres than in the hotter stars. Since the accretion disk in a given source has a broad temperature range, there exists a distance from the black hole where the effective temperature of the disk drops below the dust sublimation temperature. There the material is risen efficiently above the disk by the local radiation pressure. However, with increasing disk height the dusty material is exposed to the irradiation by the central regions, the plasma temperature rises above the sublimation temperature, the dust evaporates, and the radiation pressure vanishes, so the clouds move by following ballistic motion, first up and then down toward the disk surface. We neglect here the other sources of the radiation pressure, like line-driven outflow. In the present work we aim at catching the most characteristic properties of the model in a broad parameter range, so we introduce some simplifications which allow us to describe the cloud dynamics analytically. The basic model parameters are simply the global parameters of an active nucleus, i.e., the black hole mass, accretion rate, black hole spin (or accretion efficiency) and the viewing angle with respect to the symmetry axis. Other parameters, like the dust sublimation temperature and the dust opacity should result, at least in principle, from the basic physics. The scenario is outlined in **Figure 1**.

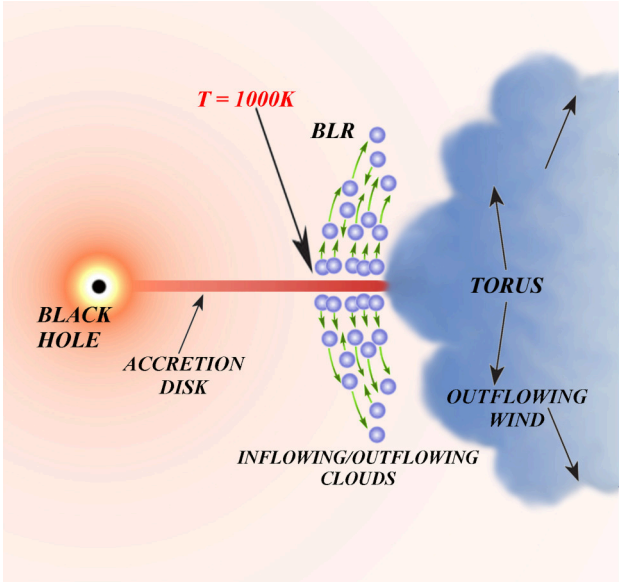

FIGURE 1 | Concept of the FRADO model for the BLR.

3. CLOUD DYNAMICS

We assume that the dust opacity can be described in gray approximation as a wavelength-independent value, and we neglect its dependence on the temperature as well, as long as the temperature is lower than the dust sublimation temperature. In the presence of the dust within the cloud, the cloud motion can be approximated as

$$\frac{dv}{dt} = -\frac{GM_{BH}\zeta}{r^3} + \frac{GM_{BH}}{r^3} H_{disk}\left(\frac{\kappa_P}{\kappa_R} - 1\right). \quad (1)$$

where $\zeta = z - H_{disk}$ is the distance measured from the disk surface. Here H_{disk} is the disk thickness, M_{BH} is the black hole mass, and r is the current disk radius. If the disk is dominated by the radiation pressure, H_{disk} is constant and its value is given by accretion rate $\dot{M}$ as $H_{disk} = \frac{3\kappa_R \dot{M}}{8\pi c}$. The clouds also perform circular motion with the local Keplerian velocity. If both the Planck mean κ_P and the Rosseland mean κ_R are constant and the dust does not evaporate, this equation can be easily integrated analytically to get

$$\zeta = H_{disk}\left(\frac{\kappa_P}{\kappa_R} - 1\right)\left[1 - \cos \Omega_K t\right], \quad (2)$$

where Ω_K is the local Keplerian angular velocity. The cloud does perform an oscillatory motion from $\zeta = 0$ to $\zeta_{max} = 2H_{disk}(\kappa_P/\kappa_R - 1)$. The maximum cloud velocity in the vertical direction is a constant fraction of the local Keplerian velocity so it depends on the radius. The cloud maximum height in this approximation is independent of the radius, so the nearest clouds intercept most of the central radiation. Both the velocity and the height scale with the accretion rate, $\dot{M}$, in physical units, i.e., scales both with the black hole mass and accretion rate in

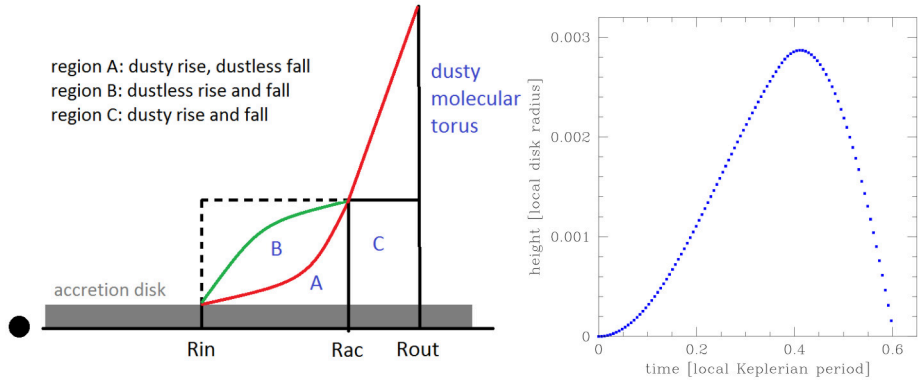

FIGURE 2 | Schematic drawing of the BLR region **(left)** and an example of a single cloud motion in the A/B region showing clear asymmetry in the rise and fall motion due to the dust evaporation **(right)**.

Eddington units. Such a description is only valid when the dust within the cloud survives. However, close to the inner radius of the BLR evaporation is important, and the condition for dust evaporation can be formulated as

$$\zeta_{evap} = \frac{\sigma_B T_{dust}^4 4\pi r^3}{\eta \dot{M} c^2} - \frac{3}{2}\frac{1}{\eta} r_g, \tag{3}$$

where $r_g = GM/c^2$ is the gravitational radius and η is the accretion efficiency which connects the accretion rate to the bolometric luminosity. If $\zeta > \zeta_{evap}$ the pressure term in the equation of motion disappears. The further motion of the cloud up and down can still be calculated analytically but the formulae become more complicated due to asymmetry between part of the rise supported by the dust and the second part of the rise and subsequent fall of the cloud. The schematic structure of the BLR parts is shown in **Figure 2**, left panel, and the asymmetry in motion is illustrated in **Figure 2**, right panel.

The inner radius of the BLR is set by the condition of $\zeta_{max} = 0$, and the outer radius of the BLR is given by $\zeta_{evap} = r$, i.e., by the condition that the dust survives the irradiation even high above the disk mid-plane. This region in general consists of two parts: the inner part where both dusty and dustless clouds are present and the outer region where ζ_{max} is smaller than ζ_{evap} and only dusty clouds exist. The transition between the A/B and C zones is set by the condition $\zeta_{max} = \zeta_{evap}$. This structure is shown schematically in **Figure 2**. The extension of the zones depend on the mass, accretion rate and the accretion efficiency.

The position of the transition radius, r_{AC}, can be used to evaluate the basic expected trends of the model. The ratio of r_{AC} to the inner radius increases with $\dot{M}^{1/3}/M^{1/3}$, i.e., the dimensionless accretion rate, thus the emission comes from a broader range of radii and the double-peak character of the line profile is less expected with the rise of the Eddington ratio.

4. LINE PROFILES

We now assume that the line is emitted as a monochromatic line, later broadened by the vertical and rotational motion. The line emissivity is assumed to be directly proportional to the incident flux, i.e., the efficiency of radiation reprocessing characteristic for a specific emission line is neglected in the current model. Thus, the local emissivity at a given radius is simply assumed to be proportional to the local disk surface element, $drd\phi/r^2$, where dr and $d\phi$ are the elements of the radial and azimuthal grid. The cloud distribution is sampled in all three dimensions, the distribution in the z direction is consistent with the cloud motion, and the Moon-type effect in the cloud emission is taken into account. The computations of the line profile neglect the Doppler boosting and gravitational reddening but the profiles are computed for an arbitrary viewing angle of an observer. The final line shape is then calculated numerically.

In the final computations we adopted at present the following values of the constants: $T_{dust} = 1{,}500$ K, $\kappa_P = 8.0\ \mathrm{cm^{-2}g^{-1}}$, $\kappa_R = 4.0\ \mathrm{cm^{-2}g^{-1}}$, and the accretion efficiency $\eta = 0.1$, corresponding to a moderate black hole spin.

Figure 3 (left) shows the dependence of the predicted line profiles on the accretion rate, for a fixed black hole mass $M = 10^8 M_\odot$ and accretion efficiency of 0.1 but for three values of the accretion rate corresponding to the Eddington ratio of 0.01, 0.1, and 1, for a viewing angle of 30°. The line always shows a two peak structure but this disk-like component is much stronger in the case of a low Eddington ratio than in the case of a high Eddington ratio. This change reflects two trends: (i) with the rise of the accretion rate the BLR moves outwards so the line in general becomes narrower (ii) the ratio of the maximum vertical to the local azimuthal velocity also rises with the accretion rate so that the contribution of the vertical motion to the line profile is more important. This trend well reproduces the fact that the lines in Narrow Line Seyfert galaxies do not show the double peak structure, while this double peak structure is clearly visible in low Eddington ratio sources, particularly in the variable part of the spectrum. In **Figure 3** (right) we show a sequence of the solutions for a different black hole mass and the Eddington ratio 1.0. We see that the line shape still shows some double-peak structure, but it is much smaller in high Eddington ratio sources than in the low Eddington ratio sources. The trend depends also on the black hole mass itself (see **Figure 3**, right panel), with larger black hole

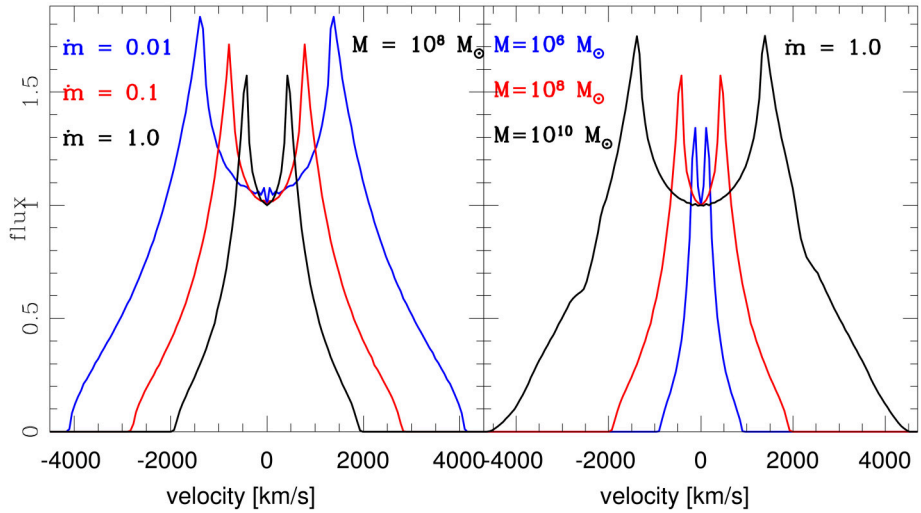

FIGURE 3 | An example of the dependence of the line profile on the accretion rate, for a black hole mass of $10^8 M_\odot$ **(left)**, and on the black hole mass for the Eddington accretion rate **(right)**. The viewing angle is fixed at 30 deg. The inner and outer BLR radii calculated for the model are: 1.98×10^{16} cm and 1.87×10^{17} cm, 4.26×10^{16} cm and 5.91×10^{17} cm, 9.18×10^{16} cm and 1.87×10^{18} cm in the left panel, and 4.26×10^{15} cm and 1.87×10^{17} cm, 9.18×10^{16} cm and 1.87×10^{18} cm, 1.98×10^{18} cm and 1.87×10^{19} cm in the right panel. Line flux is normalized to 1 at zero velocity.

mass showing more double-peak behavior. It is consistent with the division of the Seyfert 1 galaxies into two classes at FWHM of 2,000 km s^{-1} (Seyfert 1 and Narrow Line Seyfert 1 objects) and similar division into class A and B in quasars at much higher FWHM of 4,000 km s^{-1} (type A and type B quasars).

5. DISCUSSION

The results above show the first very simplified attempt to use the FRADO model for explaining the structure of the BLR. It has a number of properties consistent with the observed trends, like narrower lines for higher Eddington rate sources and smaller black hole mass. However, the model is not yet ready for a detailed comparison with the AGN spectra, as the Baldwin effect is not expected from the current version of the model. First of all, the exact values of the physical constants describing the dust properites should be included in the model. The mean time delay suggesting dust values $\sim$ 900K is most likely incorrect since the measured delay does not simply translate to the BLR inner radius. Spectroscopic studies indicate larger hot dust temperatures, which will give broader line profiles. At a later step cloud shielding should be included, combined with a better description of the radial weight of the line contribution due to geometrical setup. The disk thickness should include the transition from the radiation-pressure supported inner part to the gas-supported outer part which makes the disk shape more complex than the constant disk thickness used in the current work. Finally, the real cloud emissivity should be included, and the radiation pressure should be described much more carefully, taking into account the wavelength-dependence of the radiation pressure acting on dust, dust composition and the radiation pressure due to the absorption in lines. Those last aspects are particularly complicated, although some progress have been already done in this direction (Gallagher et al., 2015; Chan and Krolik, 2016; Hönig and Kishimoto, 2017; Waters et al., 2017).

The picture outlined in this paper is basically stationary. In order to include the time-dependent behavior we would have to introduce the time-dependent emission from the inner disk. Thermal and/or magnetic field fluctuations are required to model the usual red noise variability of an AGN continuum, and they would lead to delayed line response but most likely without strong change in the line shape. Observed longer systematic trends in the line shapes (e.g., Bon et al., 2016; Li et al., 2016; Średzińska et al., 2017) require additional factors perturbing the disk symmetry like a secondary black hole, accretion disk precession or spiral waves present in the disk due to self-gravity effects.

AUTHOR CONTRIBUTIONS

BC was responsible for the idea that resulted in the paper and most of the text. KH contributed to the concept and the text. JS derived the basic formulae for dusty clouds, later modified by VK, SP, and CW for the dust evaporation effect. YL contributed to the line profile computations.

FUNDING

Part of this work was supported by Polish grant Nr. 2015/17/B/ST9/03436/.

ACKNOWLEDGMENTS

We are grateful to Jian-Min Wang for many helpful discussions of the project during the stay of BC in Beijing.

REFERENCES

Bentz, M. C., Denney, K. D., Grier, C. J., Barth, A. J., Peterson, B. M., Vestergaard, M., et al. (2013). The Low-luminosity End of the Radius-Luminosity Relationship for Active Galactic Nuclei. *Astrophys. J.* 767:149. doi: 10.1088/0004-637X/767/2/149

Bon, E., Zucker, S., Netzer, H., Marziani, P., Bon, N., Jovanović, P., et al. (2016). Evidence for Periodicity in 43 year-long Monitoring of NGC 5548. *Astrophys. J. Suppl.* 225:29. doi: 10.3847/0067-0049/225/2/29

Chan, C.-H., and Krolik, J. H. (2016). Radiation-driven Outflows from and Radiative Support in Dusty Tori of Active Galactic Nuclei. *Astrophys. J.* 825:67. doi: 10.3847/0004-637X/825/1/67

Collin-Souffrin, S., Joly, M., Pequignot, D., and Dumont, S. (1986). The emission spectrum of active galactic nuclei. II - High column density photoionization models and low ionization lines. *Astron. Astrophys.* 166, 27–35.

Czerny, B., and Hryniewicz, K. (2011). The origin of the broad line region in active galactic nuclei. *Astron. Astrophys.* 525:L8. doi: 10.1051/0004-6361/201016025

Czerny, B., Modzelewska, J., Petrogalli, F., Pych, W., Adhikari, T. P., Życki, P. T., et al. (2015). The dust origin of the Broad Line Region and the model consequences for AGN unification scheme. *Adv. Space Res.* 55, 1806–1815. doi: 10.1016/j.asr.2015.01.004

Elvis, M. (2012). "Quasar structure emerges from the three forms of radiation pressure," in *AGN Winds in Charleston, Vol. 460 of Astronomical Society of the Pacific Conference Series* (Charleston, SC).

Elvis, M. (2017). Quasar Rain: The Broad Emission Line Region as Condensations in the Warm Accretion Disk Wind. *ArXiv e-prints*. arXiv:1703.02956

Fukue, J. (2004). Radiato-magneto-thermal winds from an accretion disk. *Publ. Astronom. Soc. Japan* 56, 181–192. doi: 10.1093/pasj/56.1.181

Fukumura, K., Tombesi, F., Kazanas, D., Shrader, C., Behar, E., and Contopoulos, I. (2015). Magnetically driven accretion disk winds and ultra-fast outflows in PG 1211+143. *Astrophys. J.* 805:17. doi: 10.1088/0004-637X/805/1/17

Gallagher, S. C., Everett, J. E., Abado, M. M., and Keating, S. K. (2015). Investigating the structure of the windy torus in quasars. *Monthly Notices R. Astron. Soc.* 451, 2991–3000. doi: 10.1093/mnras/stv1126

Gaskell, C. M. (2009). What broad emission lines tell us about how active galactic nuclei work. *New Astronom. Rev.* 53, 140–148. doi: 10.1016/j.newar.2009.09.006

Grier, C. J., Peterson, B. M., Horne, K., Bentz, M. C., Pogge, R. W., Denney, K. D., et al. (2013). The Structure of the Broad-line Region in Active Galactic Nuclei. I. Reconstructed Velocity-delay Maps. *Astrophys. J.* 764:47. doi: 10.1088/0004-637X/764/1/47

Hönig, S. F., and Kishimoto, M. (2017). Dusty winds in active galactic nuclei: reconciling observations with models. *Astrophys. J. Lett.* 838:L20. doi: 10.3847/2041-8213/aa6838

Li, Y.-R., Wang, J.-M., Ho, L. C., Lu, K.-X., Qiu, J., Du, P., et al. (2016). Spectroscopic indication of a centi-parsec supermassive black hole binary in the galactic center of NGC 5548. *arXiv* 822:4. doi: 10.3847/0004-637X/822/1/4

Netzer, H., and Marziani, P. (2010). The effect of radiation pressure on emission-line profiles and black hole mass determination in active galactic nuclei. *Astrophys. J.* 724, 318–328. doi: 10.1088/0004-637X/724/1/318

Peterson, B. M., Ferrarese, L., Gilbert, K. M., Kaspi, S., Malkan, M. A., Maoz, D., et al. (2004). Central masses and broad-line region sizes of active galactic nuclei. II. A homogeneous analysis of a large reverberation-mapping database. *Astrophys. J.* 613, 682–699. doi: 10.1086/423269

Shen, Y., Horne, K., Grier, C. J., Peterson, B. M., Denney, K. D., Trump, J. R., et al. (2016). The Sloan Digital Sky Survey Reverberation Mapping Project: First Broad-line Hβ and Mg ii Lags at z > 0.3 from Six-month Spectroscopy. *Astrophys. J.* 818:30. doi: 10.3847/0004-637X/818/1/30

Średzińska, J., Czerny, B., Hryniewicz, K., Krupa, M., Kurcz, A., Marziani, P., et al. (2017). SALT long-slit spectroscopy of quasar HE 0435-4312: fast displacement of the Mg II emission line. *Astron. Astrophys.* 601:A32. doi: 10.1051/0004-6361/201628257

Wandel, A., Peterson, B. M., and Malkan, M. A. (1999). Central masses and broad-line region sizes of active galactic Nuclei. I. Comparing the photoionization and reverberation techniques. *Astrophys. J.* 526, 579–591. doi: 10.1086/308017

Waters, T., Proga, D., Dannen, R., and Kallman, T. R. (2017). Synthetic absorption lines for a clumpy medium: a spectral signature for cloud acceleration in AGN? *Monthly Notices R. Astron. Soc.* 467, 3160–3171. doi: 10.1093/mnras/stx238

Conflict of Interest Statement: The authors declare that the research was conducted in the absence of any commercial or financial relationships that could be construed as a potential conflict of interest.

Copyright © 2017 Czerny, Li, Sredzinska, Hryniewicz, Panda, Wildy and Karas. This is an open-access article distributed under the terms of the Creative Commons Attribution License (CC BY). The use, distribution or reproduction in other forums is permitted, provided the original author(s) or licensor are credited and that the original publication in this journal is cited, in accordance with accepted academic practice. No use, distribution or reproduction is permitted which does not comply with these terms.

frontiers in Astronomy and Space Sciences

ORIGINAL RESEARCH
published: 07 November 2017
doi: 10.3389/fspas.2017.00033

The Physical Driver of the Optical Eigenvector 1 in Quasar Main Sequence

Swayamtrupta Panda[1,2]*, *Bożena Czerny*[1,2] *and Conor Wildy*[1]

[1] *Center for Theoretical Physics, Polish Academy of Sciences, Warsaw, Poland,* [2] *Nicolaus Copernicus Astronomical Center, Polish Academy of Sciences, Warsaw, Poland*

Quasars are complex sources, characterized by broad band spectra from radio through optical to X-ray band, with numerous emission and absorption features. This complexity leads to rich diagnostics. However, Boroson and Green (1992) used Principal Component Analysis (PCA), and with this analysis they were able to show significant correlations between the measured parameters. The leading component, related to Eigenvector 1 (EV1) was dominated by the anticorrelation between the FeII optical emission and [OIII] line and EV1 alone contained 30% of the total variance. It opened a way in defining a quasar main sequence, in close analogy to the stellar main sequence on the Hertzsprung-Russel (HR) diagram (Sulentic et al., 2001). The question still remains which of the basic theoretically motivated parameters of an active nucleus (Eddington ratio, black hole mass, accretion rate, spin, and viewing angle) is the main driver behind the EV1. Here we limit ourselves to the optical waveband, and concentrate on theoretical modeling the FeII to Hβ ratio, and we test the hypothesis that the physical driver of EV1 is the maximum of the accretion disk temperature, reflected in the shape of the spectral energy distribution (SED). We performed computations of the Hβ and optical FeII for a broad range of SED peak position using CLOUDY photoionisation code. We assumed that both Hβ and FeII emission come from the Broad Line Region represented as a constant density cloud in a plane-parallel geometry. We expected that a hotter disk continuum will lead to more efficient production of FeII but our computations show that the FeII to Hβ ratio actually drops with the rise of the disk temperature. Thus either hypothesis is incorrect, or approximations used in our paper for the description of the line emissivity is inadequate.

Keywords: quasars, broad line region, Eigenvector 1, FeII strength, accretion disk temperature, constant density, photoionisation, CLOUDY

OPEN ACCESS

Edited by:
Paola Marziani,
Osservatorio Astronomico di Padova (INAF), Italy

Reviewed by:
Alenka Negrete,
Universidad Nacional Autónoma de México, Mexico
Milan S. Dimitrijevic,
Astronomical Observatory, Serbia
Tomaz Zwitter,
University of Ljubljana, Slovenia

***Correspondence:**
Swayamtrupta Panda
panda@cft.edu.pl

Specialty section:
This article was submitted to Milky Way and Galaxies, a section of the journal Frontiers in Astronomy and Space Sciences

Received: *25 August 2017*
Accepted: *20 October 2017*
Published: *07 November 2017*

Citation:
Panda S, Czerny B and Wildy C (2017) The Physical Driver of the Optical Eigenvector 1 in Quasar Main Sequence. Front. Astron. Space Sci. 4:33. doi: 10.3389/fspas.2017.00033

1. INTRODUCTION

Quasars are rapidly accreting supermassive black holes at the centers of massive galaxies. In type 1 AGN, we see the nucleus directly, the continuum emission dominating the energy output in the optical/UV band comes from an accretion disk surrounding a supermassive black hole (e.g., Czerny and Elvis, 1987; Capellupo et al., 2015), and the optical/UV emission broad emission lines,

FeII pseudo-continuum and Balmer Component are usually considered to be coming from the Broad Line Region (BLR) clouds. Broad band spectral properties and line emissivity are highly correlated (Boroson and Green, 1992; Sulentic et al., 2000, 2002, 2007b; Yip et al., 2004; Shen and Ho, 2014; Sun and Shen, 2015), and the Principal Component Analysis (PCA) analysis is a powerful tool herein. As suggested by Sulentic et al. (2001), those correlations allow the identification of the quasar main sequence, analogous to the stellar main sequence on the HR diagram where the classification was also based purely on spectral properties of the stellar atmospheres. The stellar main sequence found the dependence of the spectra on the effective temperature of stars. Quasar main sequence was suggested to be driven mostly by the Eddington ratio (Boroson and Green, 1992; Sulentic et al., 2000; Shen and Ho, 2014) but also on the additional effect of the black hole mass, viewing angle and the intrinsic absorption (Sulentic et al., 2000; Kuraszkiewicz et al., 2009; Shen and Ho, 2014).

We postulate that the true driver behind the R_{FeII} is the maximum of the temperature in a multicolor accretion disk which is also the basic parameter determining the broad band shape of the quasar continuum emission. The hypothesis seems natural because the spectral shape determines both broad band spectral indices as well as emission line ratios, and has already been suggested by Bonning et al. (2007). We expect an increase in the maximum of the disk temperature as the R_{FeII} increases. According to Figure 1 from Shen and Ho (2014), increase in R_{FeII} implies increase in the Eddington ratio or decrease in the mass of the black hole. We expect that this maximum temperature depends not only on the Eddington ratio (Collin et al., 2006) but on the ratio of the Eddington ratio to the black hole mass (or, equivalently, on the ratio of the accretion rate to square of the black hole mass).

2. THEORY

Most of the quasar radiation comes from the accretion disk and forms the Big Blue Bump (BBB) in the optical-UV (Czerny and Elvis, 1987; Richards et al., 2006), and this thermal emission is accompanied by an X-ray emission coming from a hot optically thin mostly compact plasma, frequently refered to as a corona (Czerny and Elvis, 1987; Haardt and Maraschi, 1991; Fabian et al., 2015). The ionizing continuum emission thus consists of two physically different spectral components. We parameterize this emission in the following way. For convenience, the BBB component is parameterized by the maximum temperature of an accretion disk. In the standard accretion disk model this temperature is related to the black hole mass and accretion rate

$$T_{BBB} = \left[\frac{3GM\dot{M}}{8\pi\sigma r^3}\left(1-\sqrt{\frac{R_{in}}{r}}\right)\right]^{0.25} = 1.732\times10^{19}\left(\frac{\dot{M}}{M^2}\right)^{0.25} \quad (1)$$

where T_{BBB}, maximum temperature corresponding to the Big Blue Bump; G, gravitational constant; M, black hole mass; $\dot{M}$, black hole accretion rate; r, radial distance from the center; R_{in}, radius corresponding to the innermost stable circular orbit. M and $\dot{M}$ are in cgs units. Similar formalism has been used by Bonning et al. (2007) although the coefficient differs by a factor of 2.6 from Equation 1. This maximum is achieved not at the innermost stable orbit around a non-rotating black hole ($3R_{Schw}$) but at $4.08\bar{3}\ R_{Schw}$. The spectral energy distribution (SED) component peaks at the frequency

$$\nu_{max} \sim \left[\frac{\frac{L}{L_{Edd}}}{M}\right]^{0.25}. \quad (2)$$

where ν_{max}, frequency corresponding to T_{BBB}; L, accretion luminosity $(=\eta\dot{M}c^2)$; L_{Edd}, Eddington limit $\left(=\frac{4\pi GMm_pc}{\sigma_T}\right.$, where m_p, mass of a proton, σ_T, Thompson cross section). The exact value of the proportionality coefficient has to be calculated numerically, and for a standard Shakura-Sunyaev disk $h\nu_{max}/kT_{BBB} = 2.092$. We expect that the thin-disk formalism applies to all the Type 1 AGN radiating above $0.01L_{Edd}$ and below $0.3L_{Edd}$. Instead of a full numerical model of an accretion disk spectrum, we simply use a power law with the fixed slope, α_{uv}, and the value of T_{BBB} to determine an exponential cut-off. The X-ray coronal component shape is defined by the slope (α_x) and has an X-ray cut-off. The relative contribution is determined by fixing the broad band spectral index α_{ox}, and finally the absolute normalization of the incident spectrum is set assuming the source bolometric luminosity. We fix most of the parameters, and T_{BBB} is the the basic parameter of our model.

Some of this radiation is reprocessed in the BLR which produces the emission lines. In order to calculate the emissivity, we need to assume the mean hydrogen density (n_H) of the cloud, and a limiting column density (N_H) to define the outer edge of the cloud. Ionization state of the clouds depends also on the distance of the BLR from the nucleus. We fix it using the observational relation by Bentz et al. (2013)

$$\left(\frac{R_{BLR}}{1\ \text{lt-day}}\right) = 10^{\left[1.555+0.542\log\left(\frac{\lambda L_\lambda}{10^{44}\ \text{erg s}^{-1}}\right)\right]} \quad (3)$$

The values for the constants considered in Equation 3 are taken from the Clean Hβ $R_{BLR} - L$ model from Bentz et al. (2013) where $\lambda = 5100$ Å.

3. RESULTS AND DISCUSSIONS

As a first test we check the dependence of the change in the R_{FeII} as a function of the accretion disk maximum temperature, T_{BBB} at constant values of L_{bol}, α_{uv}, α_{ox}, n_H, and N_H. We fix the bolometric luminosity at the AGN, $L_{bol} = 10^{45}$ erg s^{-1} with accretion efficiency $\epsilon = 1/12$, since we consider a non-rotating black hole in Newtonian approximation (see Equation 1). This determines the accretion rate, $\dot{M}$. The BBB's exponential cutoff value is determined by the maximum temperature of the disk. Our branch of solutions covers the disk temperature range between 1.06×10^4 K and 1.53×10^5 K. The corresponding range of the black hole mass range obtained from Equation (1) is [$2.35\times10^7\ M_\odot$, $4.90\times10^9\ M_\odot$], and it implies the range

of Eddington ratio (L/L_{Edd}) [0.002, 0.33] calculated from the mentioned range of maximum disk temperatures. Large disk temperature corresponds to low black hole mass, since we fix the bolometric luminosity. Finally, we use a two-power law SED with optical-UV slope , $\alpha_{uv} = -0.36$, and X-ray slope, $\alpha_x = -0.91$ (Różańska et al., 2014). The exponential cutoff for the X-ray component is fixed at 100 keV (Frank et al., 2002 and references therein). By setting a value for the spectral index, $\alpha_{ox} = -1.6$, we specify the optical-UV and X-ray luminosities. An example of SED is shown in upper panel of **Figure 1**.

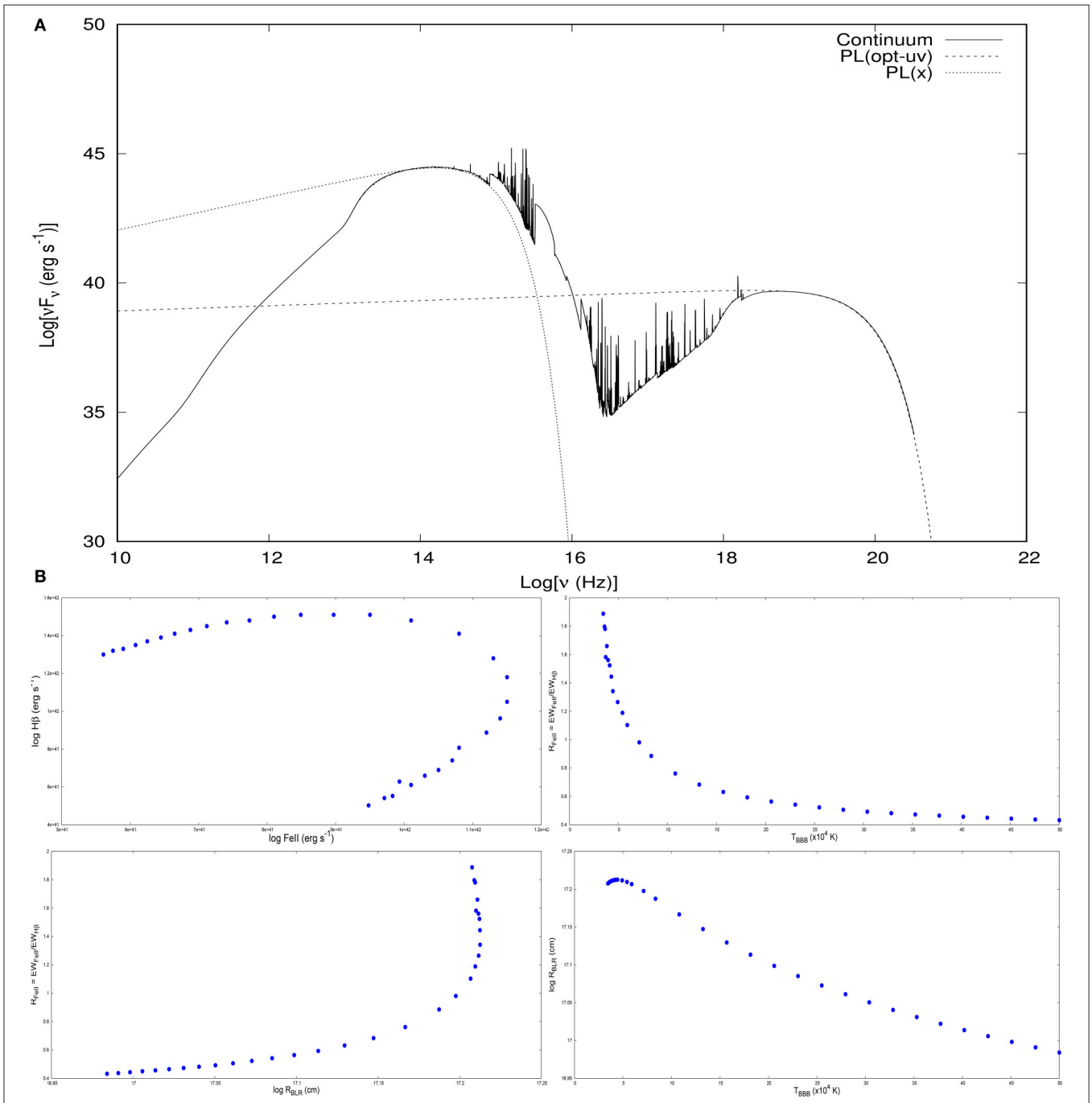

FIGURE 1 | (A) An example of the spectral energy distribution of the AGN transmitted continuum and line emission produced by CLOUDY: $T_{BBB} = 3.45 \times 10^4$ K, $\alpha_{ox} = -1.6$, $\alpha_{uv} = -0.36$, $\alpha_x = -0.9$, $n_H = 10^{11}$ cm^{-3}, $N_H = 10^{24}$ cm^{-2} and log (R_{BLR}) = 17.208. The two-component power law serves as the incident radiation. **(B)** The family of solutions is parameterized by maximum accretion disk temperature: (i) composite Fe_{II} line luminosity [erg s^{-1}] − Hβ line luminosity [erg s^{-1}]; (ii) $T_{BBB} - R_{FeII}$; (iii) log $R_{BLR} - R_{FeII}$; (iv) T_{BBB} − log R_{BLR} . Trends plotted for the following values of the parameters: $L_{bol} = 10^{45}$ erg s^{-1}, $n_H = 10^{11}$ cm^{-3} and $N_H = 10^{24}$ cm^{-2}.

We now use this one-dimensional family of SED to calculate the line emission. We have dropped the X-ray power-law component in the subsequent analyses which we plan to re-introduce once we start to see the expected trend in the $R_{FeII} - T_{BBB}$. As a start, we use the values of parameters from Bruhweiler and Verner (2008) i.e., $\log[n_H/(cm^{-3})] = 11$, $\log[N_H/(cm^{-2})] = 24$, without including microturbulence (the motion that occurs within a cloud's line-forming region to whose variation the line formation and the emission spectrum is sensitive). The distance of the cloud from the source depends on adopted disk temperature. From the incident continuum, we estimate the $L_{5,100\ \text{Å}}$ that in turn is used to calculate the inner radius of the BLR cloud using Equation (3).

Knowing the irradiation, we produce the intensities of the broad FeII emission lines from the corresponding levels of transitions present in CLOUDY 13.04 (Ferland et al., 2013). We calculate the FeII strength ($R_{FeII} = EW_{FeII}$ / $EW_{H\beta}$), which is the ratio of FeII EW within 4,434–4,684 Å to broad Hβ EW. This prescription is taken from Shen and Ho (2014).

The results are shown in lower panel of **Figure 1**. The rise of the disk temperature initially leads to weak change of the cloud distance from the source, since the SED maximum is close to 5,100 Å for such massive black holes, and later with increasing distance from the source it decreases. The FeII intensity changes monotonically with T_{BBB} but it is a decreasing, not an increasing trend. This is not what we have expected—high temperatures should correspond to low mass high accretion rate sources (Shakura and Sunyaev, 1973), Narrow Line Seyfert 1 galaxies, which show strong FeII component. This monotonic trend appears despite non-monotonic change with the disk temperature both in Hβ and FeII itself.

We thus extend our study for a broader parameter range, allowing for $\log(n_H)$ in the range 10–12, and $\log(N_H)$ from the range 22.0–24.0. The range of values obtained for R_{FeII} went up from [0.005, 0.4] to [0.4, 1.95] with increasing N_H. The change in the local density is also important. For a constant $\log(N_H) = 24$, changing $\log(n_H) = 10$–12 shifts the maximum of R_{FeII} from 1.93 [for $\log(n_H) = 10$] down to 0.095 [for $\log(n_H) = 12$], thus, there is a declining trend in the maximum of R_{FeII} with an increase in n_H at constant N_H. We see a definite change in the trend going from lower mean density to higher in the character of $T_{BBB} - R_{FeII}$ dependence. In the case of the lower n_H case, we see the turnover peak close to $\log[T_{BBB}(K)] = 4.2$ which couldn't be reproduced by the models generated using higher values of n_H and N_H owing to non-convergence of the CLOUDY code at lower values of T_{BBB}. But on the higher end of T_{BBB} we still get the same declining behavior of R_{FeII}. The two extreme cases of changing both parameters are in **Figure 2**. We thus find that the obtained values of R_{FeII} are heavily affected by the change in the maximum temperature of the BBB-component. The range of the R_{FeII} is well covered, in comparison with the plots of Shen and Ho (2014): higher density solutions reproduce large values and lower values are obtained by lowering the local density and column density. But, in general, there is a decay in the FeII strength with the rise of the disk temperature while it was expected to follow a rising curve.

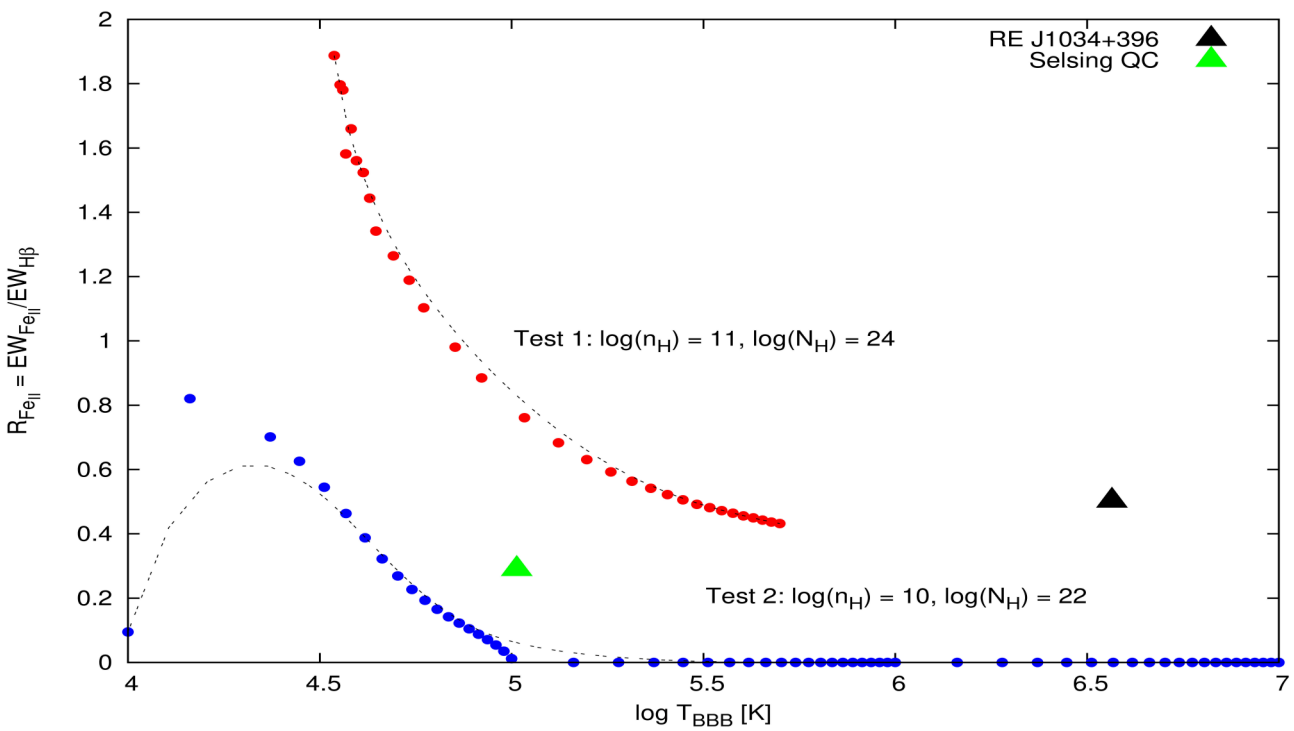

FIGURE 2 | Comparison between R_{FeII}–T_{BBB} for two different constant-density single cloud models. Observational data RE J1034+396 (Czerny et al., 2016) and Selsing quasar composite (Selsing et al., 2016) plotted on the simulated trends.

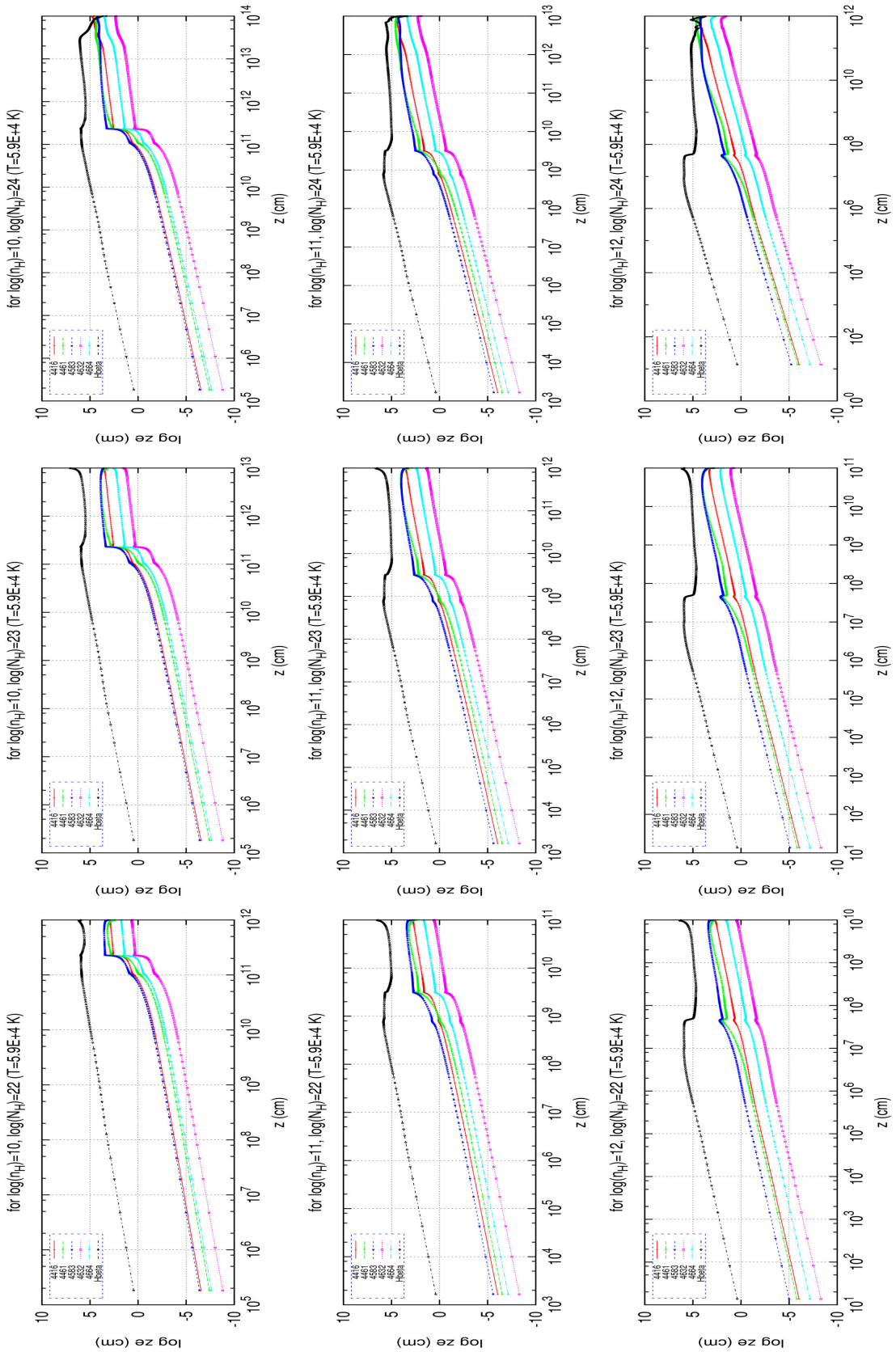

FIGURE 3 | Emissivity profiles of Hβ and FeII for different local densities and column densities: $T_{BBB} = 5.9 \times 10^4$ K. X-axis label, geometrical depth (in cm); Y-axis label, geometrical depth (z) × emissivity (e).

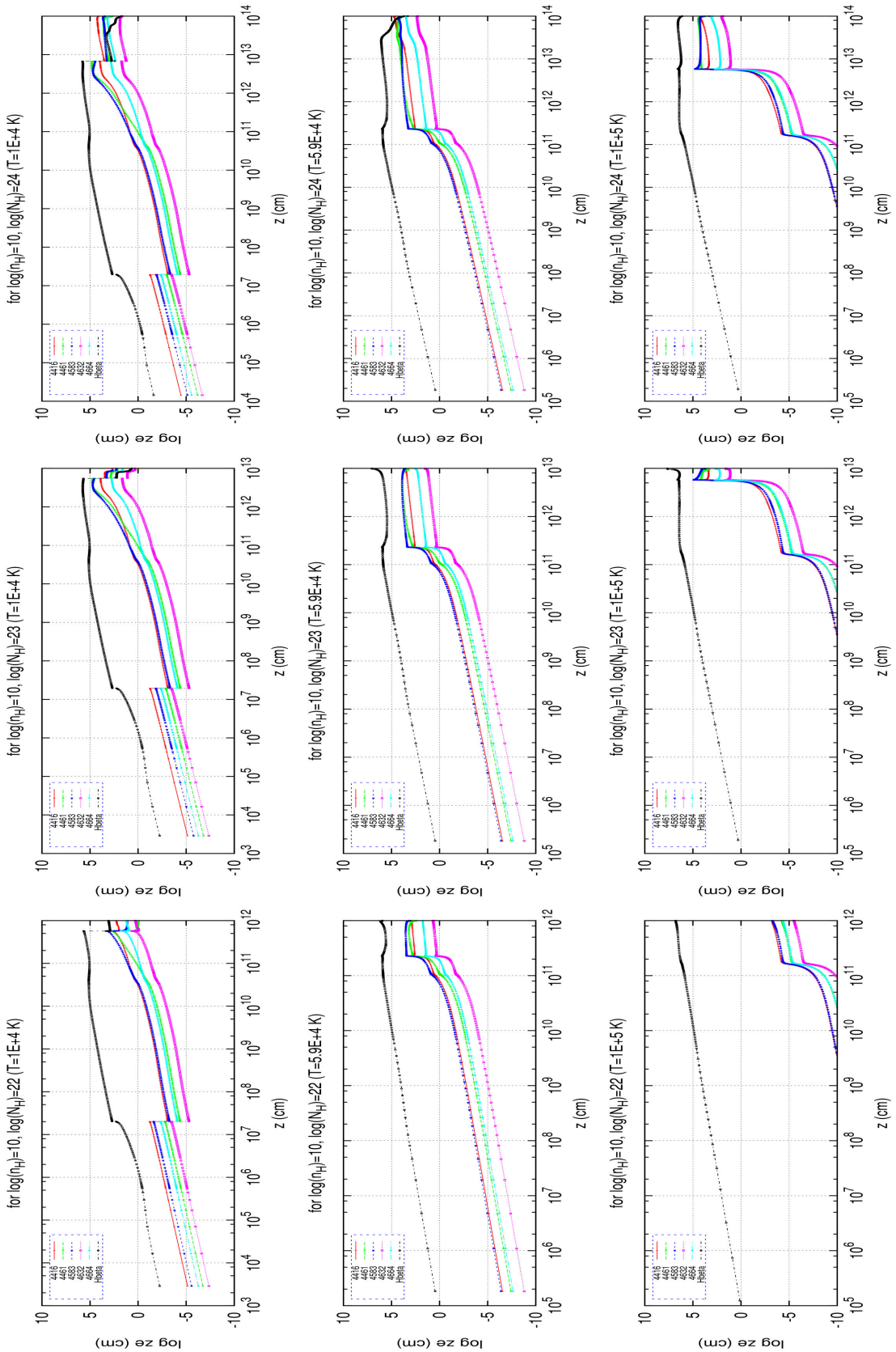

FIGURE 4 | Emissivity profiles of Hβ and FeII: comparison at three different T_{BBB} values and column densities. X-axis label, geometrical depth (in cm); Y-axis label, geometrical depth (z) × emissivity (e).

To understand the nature of this trend in our CLOUDY computations we plot Hβ and FeII emissivity profiles (**Figures 3**, **4**) where we consider only the first five FeII transitions in the 4,434–4,684 Å range. We compute these profiles by varying n_H [$\log(n_H) = (10, 12)$], N_H [$\log(N_H) = (22, 24)$] and testing the dependence of T_{BBB} for three different temperature cases. The Hβ nearly always dominates over the selected FeII emissions. But close to the outer surface of the cloud i.e., as $\log(N_H) \rightarrow 24$, the Hβ emission starts to drop while the FeII increases with increasing N_H, and there is some overlap region (see **Figure 3**, **4**). In **Figure 3**, we find that with increasing n_H, the peak of the Hβ formation shifts closer to the inner surface of the cloud, so the relative contribution of FeII rises. However, with increasing T_{BBB} the emissivity zones move deeper, and the relative role of Hβ (see the extreme right panel of **Figure 4**) goes down.

In general, the emissivity profile is much more shallow for Hβ while FeII emission is more concentrated toward the back of the cloud. Thus, an increase in N_H brings the R_{FeII} ratio up, but increasing irradiation pushes the Hβ and FeII emitting regions deeper into the cloud and R_{FeII} drops (see **Figures 3**, **4**). Our sequence of solutions for fixed bolometric luminosity and rising accretion disk temperature creates an increasing irradiation, and apparently the change of the SED shape cannot reverse the trend.

Therefore, the question is whether our hypothesis of the dominant role is incorrect or the set of computations is not satisfactory. To answer it we used two objects with well measured SED as well as R_{FeII}: RE J1034+396 (Czerny et al., 2016) and an X-Shooter quasar composite from Selsing et al. (2016). In order to determine the parameter T_{BBB} for those sources we created a set of full-GR disk models following the Novikov-Thorne prescription, we simulate an array of SED curves with L_{Edd} parametrization where we consider simultaneous dependence on spin ($0 \leq a \leq 0.998$) and accretion rate ($0.01 \leq \dot{m} \leq 10$; where $\dot{m} = \dot{M}/\dot{M}_{Edd}$, $\dot{M} = 1.678 \times 10^{18} \frac{M}{M_{\odot}}$). The value of the black hole mass has been taken from Capellupo et al. (2016). The two values represent the extreme tails of the possible trend, with X-Shooter composite having the SED peak in UV and RE J1034+396 peaikng in soft X-rays. The corresponding points are shown in **Figure 2**. Observations show a rise in the value of R_{FeII} with increase in T_{BBB} which the simulations have been unable to reproduce so far. However, the rise in R_{FeII} is not very large, from 0.3 to 0.5, despite huge change in the disk temperature difference implied by the observed SED in the two objects.

4. FUTURE

The reason for starting the project from purely theoretical modeling of the line ratios is the fact that determinations of the black hole mass, accretion rate and the observational parameter R_{FeII} available in the literature are not accurate enough to be used to test our hypothesis about the nature of the EVI (Sniegowska et al., 2017). The subsquent tasks will be to check the R_{FeII} dependence on other parameters (see Sulentic et al., 2000; Mao et al., 2009; Marziani et al., 2015) which are used (L_{bol}, α_{uv}, α_{ox}, n_H, N_H, $\cos(i)$, a and others). We intend to incorporate the microturbulence as suggested in Bruhweiler and Verner (2008). Better, more physical description of the SED may be needed, i.e model of a disk + corona with full GR and more complex geometry of the BLR using Czerny et al. (2011), Czerny and Hryniewicz (2011), and Czerny et al. (2015). We intend to implement the constant density LOC (Locally Optimized Cloud) model and subsequently the constant pressure model to repeat the tests and check for discrepancies with respect to the current model. Next stage to consider is the possibility of shielding of some BLR regions by the puffed inner disk (e.g., Wang et al., 2014), or to consider independent production regions of Hβ and FeII. Different studies have proposed that FeII is mainly produced in BLR (Bruhweiler and Verner, 2008; Shields et al., 2010) while many others have suggested that these emissions are mostly produced in the accretion disk (Martínez-Aldama et al., 2015 and references therein). Finally, we have to test our theory observationally for more sources with known SED peak position. To have an overview of the EV1, it is necessary to study it in other ranges of frequencies, including X-ray, radio, UV, and IR spectral ranges. Considerable progress along these line have been made by Sulentic et al. (2007a) and Sulentic et al. (2017) (UV range), Dultzin-Hacyan et al. (1999) (**Figure 4**), and Martínez-Aldama et al. (2015) (IR range).

AUTHOR CONTRIBUTIONS

SP has tested the basic model and carried out the photoionisation simulations based on the idea and formalism proposed by BC. CW has provided computational assistance and helped solve the T_{BBB} issue.

FUNDING

Part of this work was supported by Polish grant No. 2015/17/B/ST9/03436/.

ACKNOWLEDGMENTS

The authors would like to acknoweledge the referees for their comments and suggestions to bring the paper to its current state. SP would like to acknowledge the organizing committee and the participants of the Quasars at all Cosmic Epochs conference held during 2nd Apr–7th Apr 2017 in Padova, Italy and, subsequently for providing the opportunity to present a talk on his research after being adjudged with the Best Poster award. SP would also like to extend his gratitude to the Center for Theoretical Physics and Nicolaus Copernicus Astronomical Center, Warsaw, the National Science Center (NSC) OPUS 9 grant for financing the project and Dr. Gary Ferland and Co. for the photoionisation code CLOUDY. SP would like to acknowledge the unending academic and personal support from Mr. Tek Prasad Adhikari. SP is also obliged to the Strong Gravity group at CAMK, Warsaw for engaging discussions resulting in this work.

REFERENCES

Bentz, M. C., Denney, K. D., Grier, C. J., Barth, A. J., Peterson, B. M., Vestergaard, M., et al. (2013). The low-luminosity end of the radius-luminosity relationship for active galactic nuclei. *Astrophys. J.* 767:149. doi: 10.1088/0004-637X/767/2/149

Bonning, E. W., Cheng, L., Shields, G. A., Salviander, S., and Gebhardt, K. (2007). Accretion disk temperatures and continuum colors in QSOs. *Astrophys. J.* 659, 211–217. doi: 10.1086/510712

Boroson, T. A., and Green, R. F. (1992). The emission-line properties of low-redshift quasi-stellar objects. *Astrophys. J. Suppl. Ser.* 80, 109–135. doi: 10.1086/191661

Bruhweiler, F., and Verner, E. (2008). Modeling fe II emission and revised Fe II (UV) empirical templates for the seyfert 1 galaxy I Zw 1. *Astrophys. J.* 675, 83–95. doi: 10.1086/525557

Capellupo, D. M., Netzer, H., Lira, P., Trakhtenbrot, B., and Mejía-Restrepo, J. (2015). Active galactic nuclei at z 1.5 - I. Spectral energy distribution and accretion discs. *Mon. Not. R. Astron. Soc.* 446, 3427–3446. doi: 10.1093/mnras/stu2266

Capellupo, D. M., Netzer, H., Lira, P., Trakhtenbrot, B., and Mejía-Restrepo, J. (2016). Active galactic nuclei at z 1.5 - III. Accretion discs and black hole spin. *Mon. Not. R. Astron. Soc.* 460, 212–226. doi: 10.1093/mnras/stw937

Collin, S., Kawaguchi, T., Peterson, B. M., and Vestergaard, M. (2006). Systematic effects in measurement of black hole masses by emission-line reverberation of active galactic nuclei: eddington ratio and inclination. *Astron. Astrophys.* 456, 75–90. doi: 10.1051/0004-6361:20064878

Czerny, B., and Elvis, M. (1987). Constraints on quasar accretion disks from the optical/ultraviolet/soft X-ray big bump. *Astrophys. J.* 321, 305–320. doi: 10.1086/165630

Czerny, B., and Hryniewicz, K. (2011). The origin of the broad line region in active galactic nuclei. *Astron. Astrophys.* 525:L8. doi: 10.1051/0004-6361/201016025

Czerny, B., Hryniewicz, K., Nikołajuk, M., and Sądowski, A. (2011). Constraints on the black hole spin in the quasar SDSS J094533.99+100950.1. *Mon. Not. R. Astron. Soc.* 415, 2942–2952. doi: 10.1111/j.1365-2966.2011.18912.x

Czerny, B., Modzelewska, J., Petrogalli, F., Pych, W., Adhikari, T. P., Życki, P. T., et al. (2015). The dust origin of the broad Line region and the model consequences for AGN unification scheme. *Adv. Space Res.* 55, 1806–1815. doi: 10.1016/j.asr.2015.01.004

Czerny, B., You, B., Kurcz, A., Średzińska, J., Hryniewicz, K., Nikołajuk, M., et al. (2016). The mass of the black hole in RE J1034+396. *Astron. Astrophys.* 594:A102. doi: 10.1051/0004-6361/201628103

Dultzin-Hacyan, D., Taniguchi, Y., and Uranga, L. (1999). "Where is the Ca II Triplet Emitting Region in AGN?" in *Structure and Kinematics of Quasar Broad Line Regions*, Vol. 175, eds C. M. Gaskell, W. N. Brandt, M. Dietrich, D. Dultzin-Hacyan, and M.Eracleous (Astronomical Society of the Pacific Conference Series), 303.

Fabian, A. C., Lohfink, A., Kara, E., Parker, M. L., Vasudevan, R., and Reynolds, C. S. (2015). Properties of AGN coronae in the NuSTAR era. *Mon. Not. R. Astron. Soc.* 451, 4375–4383. doi: 10.1093/mnras/stv1218

Ferland, G. J., Porter, R. L., van Hoof, P. A. M., Williams, R. J. R., Abel, N. P., Lykins, M. L., et al. (2013). The 2013 Release of Cloudy. *Rev. Mex. Astron. Astrofis.* 49, 137–163. Available online at: http://adsabs.harvard.edu/abs/2013RMxAA..49..137F

Frank, J., King, A., and Raine, D. J. (2002). *Accretion Power in Astrophysics, 3rd Edn.* Cambridge: Cambridge University Press

Haardt, F., and Maraschi, L. (1991). A two-phase model for the X-ray emission from Seyfert galaxies. *Astrophys. J.* 380, L51–L54. doi: 10.1086/186171

Kuraszkiewicz, J., Wilkes, B. J., Schmidt, G., Smith, P. S., Cutri, R., and Czerny, B. (2009). Principal component analysis of the spectral energy distribution and emission Line properties of Red 2MASS active galactic nuclei. *Astrophys. J.* 692, 1180–1189. doi: 10.1088/0004-637X/692/2/1180

Mao, Y.-F., Wang, J., and Wei, J.-Y. (2009). Extending the Eigenvector 1 space to the optical variability of quasars. *Res. Astron. Astrophys.* 9, 529–537. doi: 10.1088/1674-4527/9/5/004

Martínez-Aldama, M. L., Marziani, P., Dultzin, D., Sulentic, J. W., Bressan, A., Chen, Y., et al. (2015). Observations of the Ca ii IR triplet in high luminosity quasars: exploring the sample. *J. Astrophys. Astron.* 36, 457–465. doi: 10.1007/s12036-015-9354-9

Marziani, P., Sulentic, J. W., Negrete, C. A., Dultzin, D., Del Olmo, A., Martínez Carballo, M. A., et al. (2015). UV spectral diagnostics for low redshift quasars: estimating physical conditions and radius of the broad line region. *Astrophys. Space Sci.* 356, 339–346. doi: 10.1007/s10509-014-2136-z

Richards, G. T., Lacy, M., Storrie-Lombardi, L. J., Hall, P. B., Gallagher, S. C., Hines, D. C., et al. (2006). Spectral energy distributions and multiwavelength selection of Type 1 Quasars. *Astrophys. J. Suppl. Ser.* 166, 470–497. doi: 10.1086/506525

Różańska, A., Nikołajuk, M., Czerny, B., Dobrzycki, A., Hryniewicz, K., Bechtold, J., et al. (2014). Absorption features in the quasar HS 1603 + 3820 II. Distance to the absorber obtained from photoionisation modelling. *New Astron.* 28, 70–78. doi: 10.1016/j.newast.2013.08.009

Selsing, J., Fynbo, J. P. U., Christensen, L., and Krogager, J.-K. (2016). An X-Shooter composite of bright $1 < z < 2$ quasars from UV to infrared. *Astron. Astrophys.* 585:A87. doi: 10.1051/0004-6361/201527096

Shakura, N. I., and Sunyaev, R. A. (1973). Black holes in binary systems. Observational appearance. *Astron. Astrophys.* 24, 337–355. doi: 10.1007/978-94-010-2585-0_13

Shen, Y., and Ho, L. C. (2014). The diversity of quasars unified by accretion and orientation. *Nature* 513, 210–213. doi: 10.1038/nature13712

Shields, G. A., Ludwig, R. R., and Salviander, S. (2010). Fe II emission in active galactic nuclei: the role of total and gas-phase iron abundance. *Astrophys. J.* 721, 1835–1842. doi: 10.1088/0004-637X/721/2/1835

Sniegowska, M., Czerny, B., You, B., Panda, S., Wang, J.-M., Hryniewicz, K., et al. (2017). The properties of active galaxies at the extreme of Eigenvector 1. ArXiv e-prints 1701.03694. Available online at: http://adsabs.harvard.edu/abs/2017arXiv170103694S

Sulentic, J. W., Bachev, R., Marziani, P., Negrete, C. A., and Dultzin, D. (2007a). C IV λ1549 as an Eigenvector 1 parameter for active galactic nuclei. *Astrophys. J.* 666, 757–777. doi: 10.1086/519916

Sulentic, J. W., Calvani, M., and Marziani, P. (2001). Eigenvector 1: an H-R diagram for AGN? *Messenger* 104, 25–28. Available online at: http://adsabs.harvard.edu/abs/2001Msngr.104...25S

Sulentic, J. W., del Olmo, A., Marziani, P., Martínez-Carballo, M. A., D'Onofrio, M., Dultzin, D., et al. (2017). What does C IV λ1549 tell us about the physical driver of the eigenvector quasar sequence? *ArXiv e-prints 1708.03187*. Available online at: http://adsabs.harvard.edu/abs/2017arXiv170803187S

Sulentic, J. W., Dultzin-Hacyan, D., and Marziani, P. (2007b). "Eigenvector 1: Towards AGN Spectroscopic Unification," in *Revista Mexicana de Astronomia y Astrofisica Conference Series*, Vol. 28, *Revista Mexicana de Astronomia y Astrofisica*, Vol. 27, ed S. Kurtz (Mexico City), 83–88.

Sulentic, J. W., Marziani, P., Zamanov, R., Bachev, R., Calvani, M., and Dultzin-Hacyan, D. (2002). Average Quasar Spectra in the Context of Eigenvector 1. *Astrophys. J. Lett.* 566, L71–L75. doi: 10.1086/339594

Sulentic, J. W., Zwitter, T., Marziani, P., and Dultzin-Hacyan, D. (2000). Eigenvector 1: an optimal correlation space for active galactic nuclei. *Astrophys. J. Lett.* 536, L5–L9. doi: 10.1086/312717

Sun, J., and Shen, Y. (2015). Dissecting the quasar main sequence: insight from host galaxy properties. *Astrophys. J. Lett.* 804:L15. doi: 10.1088/2041-8205/804/1/L15

Wang, J.-M., Qiu, J., Du, P., and Ho, L. C. (2014). Self-shadowing effects of slim accretion disks in active galactic nuclei: the diverse appearance of the broad-line region. *Astrophys. J.* 797:65. doi: 10.1088/0004-637X/797/1/65

Yip, C. W., Connolly, A. J., Vanden Berk, D. E., Ma, Z., Frieman, J. A., SubbaRao, M., et al. (2004). Spectral classification of quasars in the sloan digital sky survey: eigenspectra, redshift, and luminosity effects. *Astron. J.* 128, 2603–2630. doi: 10.1086/425626

Conflict of Interest Statement: The authors declare that the research was conducted in the absence of any commercial or financial relationships that could be construed as a potential conflict of interest.

Copyright © 2017 Panda, Czerny and Wildy. This is an open-access article distributed under the terms of the Creative Commons Attribution License (CC BY). The use, distribution or reproduction in other forums is permitted, provided the original author(s) or licensor are credited and that the original publication in this journal is cited, in accordance with accepted academic practice. No use, distribution or reproduction is permitted which does not comply with these terms.

frontiers in Astronomy and Space Sciences

ORIGINAL RESEARCH
published: 08 January 2018
doi: 10.3389/fspas.2017.00066

The Physical Relation between Disc and Coronal Emission in Quasars

Elisabeta Lusso[1]* *and Guido Risaliti*[2,3]

[1] Centre for Extragalactic Astronomy, Durham University, Durham, United Kingdom, [2] Dipartimento di Fisica e Astronomia, Università di Firenze, Firenze, Italy, [3] Osservatorio Astrofisico di Arcetri (INAF), Florence, Italy

We propose a modified version of the observed non-linear relation between the X-ray (2 keV) and the ultraviolet (2,500 Å) emission in quasars (i.e., $L_X \propto L_{UV}^{\gamma}$) which involves the full width at half-maximum, *FWHM*, of the broad emission line, i.e., $L_X \propto L_{UV}^{\hat{\gamma}}\ FWHM^{\hat{\beta}}$. By analyzing a sample of 550 optically selected non-jetted quasars in the redshift range of 0.36–2.23 from the Sloan Digital Sky Survey cross matched with the XMM-Newton catalog 3XMM-DR6, we found that the additional dependence of the observed $L_X - L_{UV}$ correlation on the *FWHM* of the MgII broad emission line is statistically significant. Our statistical analysis leads to a much tighter relation with respect to the one neglecting *FWHM*, and it does not evolve with redshift. We interpret this new relation within an accretion disc corona scenario where reconnection and magnetic loops above the accretion disc can account for the production of the primary X-ray radiation. For a broad line region size depending on the disc luminosity as $R_{blr} \propto L_{disc}^{0.5}$, we find that $L_X \propto L_{UV}^{4/7}\ FWHM^{4/7}$, which is in very good agreement with the observed correlation.

Keywords: active galactic nuclei, quasar, supermassive black holes, accretion disc, X-ray

OPEN ACCESS

Edited by:
Paola Marziani, Osservatorio Astronomico di Padova (INAF), Italy

Reviewed by:
Vahram Chavushyan, National Institute of Astrophysics, Optics and Electronics, Mexico
Luka C. Popovic, Astronomical Observatory Belgrade, Serbia
Alberto Rodriguez-Ardila, Laboratório Nacional de Astrofísica, Brazil

***Correspondence:**
Elisabeta Lusso
elisabeta.lusso@durham.ac.uk

Specialty section:
This article was submitted to Milky Way and Galaxies, a section of the journal Frontiers in Astronomy and Space Sciences

Received: *13 November 2017*
Accepted: *18 December 2017*
Published: *08 January 2018*

Citation:
Lusso E and Risaliti G (2018) The Physical Relation between Disc and Coronal Emission in Quasars. Front. Astron. Space Sci. 4:66. doi: 10.3389/fspas.2017.00066

1. INTRODUCTION

One of the observational evidences for the link between the accretion disc and the X-ray corona in active galactic nuclei (AGN) is given by the observed non-linear correlation between the monochromatic ultraviolet luminosity at 2,500 Å (L_{UV}) and the one in the X–rays at 2 keV (L_X). Such relationship (parameterized as $\log L_X = \gamma \log L_{UV} + \beta$) exhibits a slope, γ, around 0.6, implying that optically bright AGN emit relatively less X-rays than optically faint AGN (Tananbaum et al., 1979). The value of the slope in this relation does not depend on the sample selection, the correlation is also very tight (~ 0.24 dex, Lusso and Risaliti, 2016), and independent on redshift (Vignali et al., 2003; Strateva et al., 2005; Steffen et al., 2006; Just et al., 2007; Green et al., 2009; Lusso et al., 2010; Young et al., 2010; Jin et al., 2012; Marchese et al., 2012). Recently, the $L_X - L_{UV}$ relationship (or, more precisely, its version with fluxes) has also been employed as a distance indicator to estimate cosmological parameters such as Ω_M and Ω_Λ by building a Hubble diagram in a similar way as for Type Ia supernovae (Suzuki et al., 2012; Betoule et al., 2014, and references therein), but extending it up to $z \sim 6$ (Risaliti and Lusso, 2015, 2017). Yet, the challenge in interpreting such relation on physical grounds is that the origin of the X–ray emission in quasars is still a matter of debate.

Some attempts at explaining the quasar X-ray spectra were based upon the reprocessing of radiation from a non-thermal electron-positron pair cascade (e.g., Svensson, 1982, 1984; Zdziarski et al., 1990). Another possibility rests on a two-phase accretion disc model, where a fraction f of gravitational power is dissipated via buoyancy and reconnection of magnetic fields in a uniform,

hot ($T_{\rm cor} \sim 100$ keV $\sim 10^9$ K) plasma close to the cold opaque disc (Haardt and Maraschi, 1991, 1993; Svensson and Zdziarski, 1994; Di Matteo, 1998; Różańska and Czerny, 2000). The scenario for this model is the following. Phase 1 is the optically thick "cold" (tens of eV) disc, whilst phase 2 is a hot optically thin plasma located above (and below) the disc. The seed disc photons illuminate the hot tenuous plasma, and a fraction of them is up-scattered to hard X-rays via inverse Compton scattering, providing the main source of cooling of the plasma. About half of these hard X-ray photons is irradiated back to the disc, contributing to its energy balance, whilst the rest escape and are observed. A stable disc-corona system is then in place only if there is a strong coupling between ultraviolet and X-ray photons. This model retrieves the photon index slope of the coronal X-ray spectrum (i.e., $\Gamma_{\rm X} \simeq 2$), in close agreement with real data. Nonetheless, it also predicts a nearly equal amount of ultraviolet and X-ray radiation (i.e., $\gamma = 1$), which is not in agreement with the observed correlation. If the corona is not uniform, but a rather patchy medium, and only a fraction (f) of the accretion power is released in the hot phase, the resulting γ value is < 1, but one needs to consider a rather arbitrary number of active blobs (Haardt et al., 1994). Magnetic field turbulence has been recognized not only as an additional heating mechanism in the formation of the corona (e.g., Galeev et al., 1979; Liu et al., 2002; Merloni and Fabian, 2002), but also as an efficient means for the transport of the disc angular momentum (e.g., Balbus, 2003). Yet, the value of the fraction f of gravitational power dissipated in the hot corona (needed for keeping the plasma at high temperatures), and how the coronal physical state depends on the black hole mass and disc accretion rate still remain a matter of debate.

In Lusso and Risaliti (2017) we outlined a simple but physically motivated, *ad hoc* model to interpret the observed correlation between the ultraviolet and the X-ray emission in terms of physical parameters such as the black hole mass ($M_{\rm BH}$, here we considered the normalized value $m = M_{\rm BH}/M_{\odot}$), the accretion rate ($\dot{m} = \dot{M}/\dot{M}_{\rm Edd}$, where $\dot{M}_{\rm Edd}$ is the accretion rate at Eddington), and the distance to the black hole ($r = R/R_{\rm S}$, where $R_{\rm S} = 2GM_{\rm BH}/c^2$ is the Schwarzschild radius). Our main aim was to link such relations with observable quantities (i.e., the observed ultraviolet and X-ray luminosities), thus obtaining a relation that can be then compared with the data.

Here, we further analyse the $L_{\rm X} - L_{\rm UV} - FWHM$ relation with the goal of understanding its physical origin in the context of black hole accretion physics.

2. THE OBSERVED $L_{\rm X} - L_{\rm UV} - FWHM$ PLANE

The quasar sample considered by Lusso and Risaliti (2017) is obtained by cross-matching the quasar SDSS catalog published by Shen et al. (2011) with the serendipitous X-ray source catalog 3XMM–DR6 (Rosen et al., 2016). Filters are also applied in order to select a clean quasar sample where biases and contaminants are minimized, namely: (i) jetted, broad absorption line quasars and sources with high levels of absorption in the optical ($E(B-V) > 0.1$) are removed from the sample; (ii) we selected those quasars with a full-width half-maximum, $FWHM$, for the MgII λ 2,800 Å higher than 2,000 km s^{-1}; (iii) only sources with good X-ray data (i.e., S/N>5 in the 0.2–12 keV EPIC band) and low levels of X-ray absorption (i.e., with an X-ray photon index $\Gamma_{\rm X} > 1.6$) are considered; and finally (iii) the *Eddington bias* (see also Risaliti and Lusso, 2015; Lusso and Risaliti, 2016 for further details) is minimized by including only quasars whose minimum detectable X-ray flux is lower than the expected one in each observation. The FWHM values for the MgII emission line as well as the ultraviolet 2,500Å luminosities are taken from the Shen et al. (2011) catalog, which have been measured from the continuum/emission line fitting of the SDSS spectra (see their section 3 for further details). The final clean sample is composed of 550 quasars and it is only ∼25% of the initial sample (∼2,100 quasars with both soft 0.5–2 keV and hard 2–12 keV fluxes), resulting from the stringent filters mentioned above. In the future we will refine the treatment of the systematics by considering additional instrumental systematics, and developing large mock simulations to better understand the impact of the Eddington bias on the results. The main aim is to reduce the rejection fraction, thus maximizing the statistics of the final sample.

Figure 1 shows an edge-on view of the $L_{\rm X} - L_{\rm UV} - FWHM$ plane. The best-fit regression relation for this quasar sample is:

$$(\log L_{\rm X} - 25) = (0.538 \pm 0.022)(\log L_{\rm UV} - 25) + (0.480 \pm 0.078)[\log FWHM - (3 + \log 2)] + (-1.550 \pm 0.122), \quad (1)$$

with an observed dispersion of 0.22 dex, which is a very tight relation. To fit the data, we adopted *emcee* (Foreman-Mackey et al., 2013), which is a pure-Python implementation of Goodman and Weare's affine invariant Markov chain Monte Carlo ensemble sampler.

We then divided the quasar sample into equally spaced narrow redshift intervals in $\log z$ with a $\Delta \log z < 0.1$ to minimize the scatter due to the different luminosity distances within each interval. We split the sample into 10 intervals with $\Delta \log z = 0.08$ and, for each redshift interval, we performed a fit of the $F_{\rm X} - F_{\rm UV} - FWHM$ relation, $\log F_{\rm X} = \hat{\gamma}_z \log F_{\rm UV} + \hat{\beta}_z FWHM + \hat{K}$, with free $\hat{\gamma}_z$ and $\hat{\beta}_z$. The results for the best-fit slopes $\hat{\gamma}_z$ and $\hat{\beta}_z$ as a function redshift are shown in **Figure 1**. Despite the large scatter, both $\hat{\gamma}_z$ and $\hat{\beta}_z$ slopes do not show any significant evolution with time and they are consistent with a constant value in the redshift interval 0.3–2.

3. THE TOY MODEL

Previous works in the literature suggest that the amount of gravitational energy from the accretion disc released in the hot plasma surrounding the disc itself, likely depends on the black hole mass $M_{\rm BH}$, the mass accretion rate $\dot{M}$, and the spin of the black hole. In Lusso and Risaliti (2017), the $L_{\rm X} - L_{\rm UV}$ correlation was reproduced if the energy transfer from an optically thick, geometrically thin accretion disc to the corona is confined to the gas-pressure dominated region of the disc. In such simple model, the monochromatic ultraviolet and X–ray luminosities show an extra dependence on the $FWHM$, thus on the black hole mass and accretion rate as $L_{\rm UV} \propto M_{\rm BH}^{4/3}(\dot{M}/\dot{M}_{\rm Edd})^{2/3}$ and

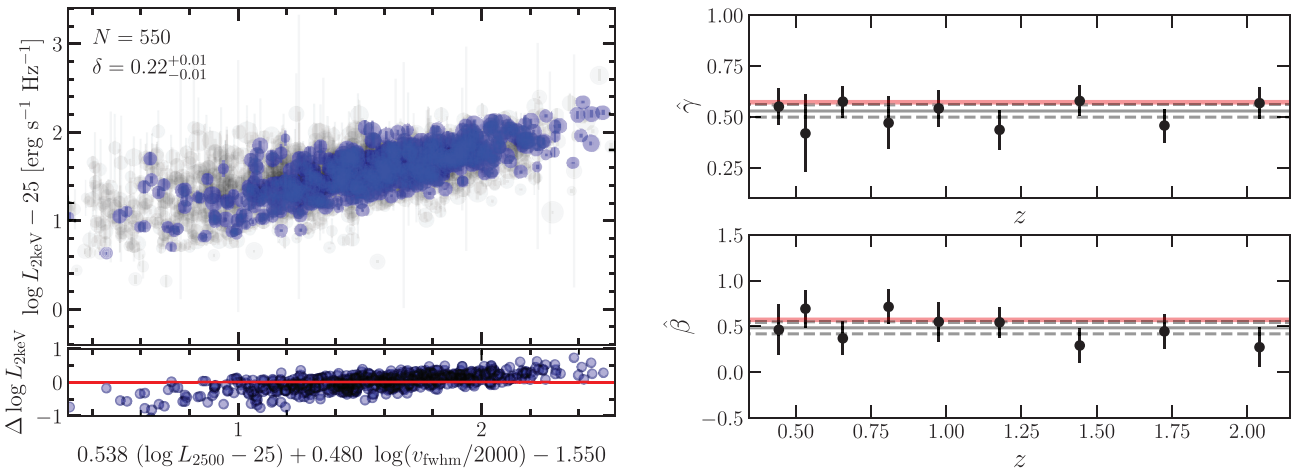

FIGURE 1 | Left: The tight $L_X - L_{UV} - FWHM$ plane (seen edge-on) for the $z < 2.3$ SDSS-3XMM-DR6 quasar sample in Lusso and Risaliti (2017). The full-width half maximum (*FWHM*) is computed from the MgII emission line. The size of the points has been rescaled to the *FWHM* value, the smaller size corresponds to *FWHM* = 2000 km/s. The slopes of this correlation are in very good agreement (within the uncertainties) with the ones predicted by our simple (but physically motivated) model, $L_X \propto L_{UV}^{\hat{\gamma}} FWHM^{\hat{\beta}}$, where $\hat{\gamma} = \hat{\beta} = 4/7$ ($4/7 \sim 0.571$). The quasar sample before applying our filters is also plotted with light gray points. **Right:** Slopes of the $L_X - L_{UV} - FWHM$ plane as a function of redshift. The red solid line represents the predicted value of 4/7. The observed $L_X - L_{UV} - FWHM$ plane does not evolve with redshift up to $z \sim 2.3$, which is an essential requirement in order to utilize this relation to measure cosmological parameters. The gray solid and dashed lines represent the weighted means and uncertainties of the black points, respectively. Figure based on data derived from Lusso and Risaliti (2017).

$L_X \propto M_{BH}^{19/21} (\dot{M}/\dot{M}_{Edd})^{5/21}$, respectively. Assuming a broad line region size function of the disc luminosity as $R_{blr} \propto L_{disc}^{0.5}$ we have that:

$$L_X \simeq 6 \times 10^4\ L_{UV}^{4/7}\ FWHM^{4/7}\ \alpha^{-2/21} \kappa^{2/7} \times (1-f)^{-6/7}\ J(r)^{-16/21}\ \text{erg s}^{-1}\text{Hz}^{-1}, \quad (2)$$

where α is the standard disc viscosity parameter, κ is a calibration constant in the broad line region radius-luminosity relation (i.e., $R_{blr} = kL_{bol}^{0.5}$ Trippe, 2015), and $J(r) = (1 - \sqrt{3/r})$.

In this model the bulk of the radiation budget of the X-ray corona is measured at the transition radius (r_{tr}) where the gas pressure (P_{gas}) in the accretion disc equates the radiation pressure (P_{rad}), and it is defined as:

$$r_{tr} \simeq 120\ (\alpha m)^{2/21}\ \dot{m}^{16/21} (1-f)^{6/7} J(r)^{16/21}, \quad (3)$$

In units of R_S, where $m = \frac{M_{BH}}{M_\odot}$, and $\dot{m} = \frac{\dot{M}}{\dot{M}_{Edd}}$. The transition radius can vary from a few gravitational radii (r_g) to several hundreds r_g for a black hole mass $m = 10^{8-9}$, with an accretion rate in the range $\dot{m} = 0.1 - 0.3$, and $\alpha = 0.4$. This parameter also depends on the value of f (i.e., the higher is f, the smaller is r_{tr}). Yet, the effective location of the corona may also be placed at small radii of less than tens of r_g. From a qualitative perspective, the torque (caused by the disc rotation) of magnetic field lines (originated at $r \geq r_{tr}$) that connects two opposite sides of the accretion disc (e.g., *magnetic reconnection*, a schematic representation of our model is provided in **Figure 2**) could cause particle acceleration at the magnetic reconnection site, located closer to the black hole (at $r < r_{tr}$), where particles lose their energy radiatively via the inverse Compton process.

4. CONSTRAINING THE FRACTION OF ACCRETION POWER RELEASED IN THE CORONA

Our simple (but physically motivated) model also provides constraints on the fraction of accretion power released in the hot plasma in the vicinity of the accretion disc, f, as a function the broad line region size, from the observed normalization of $L_X - L_{UV} - FWHM$ plane.

Figure 3 shows how the normalization of Equation (2) changes as a function of α, κ, and f. We fixed the κ factor to 1.3×10^{-6}, which corresponds to a broad line region size of about 1.3×10^{17} cm ($\sim$ 50 light days) and a bolometric luminosity of 10^{46} erg s^{-1}, typical of quasars (e.g., Kaspi et al., 2005). The viscosity parameter varies from 0.1 to 0.4 (King et al., 2007), whilst f ranges in the interval 0–0.99. Although the normalization of the relation displays a large scatter, which can be a factor of ~ 2 in logarithm (i.e., orders of magnitude), the data suggest a value of f in the range 0.9–0.95.

In the future, by studying larger sample of quasars with M_{BH} and accretion rate values (which are all related to f), we will compare our results on f with the expectations from numerical simulations (e.g., Jiang et al., 2014) and other theoretical models (e.g., Merloni and Fabian, 2002; Cao, 2009; Liu et al., 2016), especially those concerning the physical state and extent of the broad line region (e.g., Failed Radiatively Accelerated Dusty Outflows, FRADO, Czerny et al., 2017).

5. CONCLUSIONS

Our modified $L_X - L_{UV}$ relationship in quasars, which takes into account the full-width half-maximum of the quasar emission line

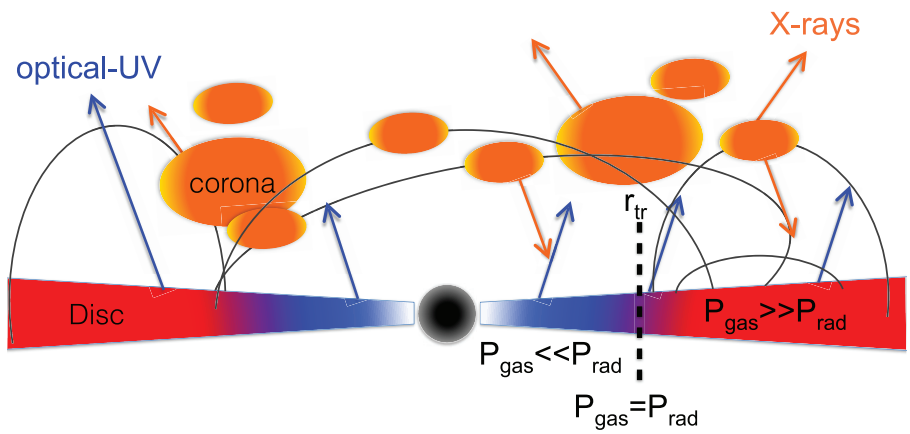

FIGURE 2 | A schematic representation of the toy model discussed in §3. The optically thick, geometrically thin accretion disc emits the seeds photons that illuminate the hot tenuous (possibly clumpy) plasma. A fraction of them is up-scattered to hard X-rays via inverse Compton scattering. Part of these hard X-ray photons is irradiated back to the disc, contributing to its energy balance, whilst the rest escape and are observed. Stable magnetic loop can be formed only in the radiation pressure dominated part of the disc.

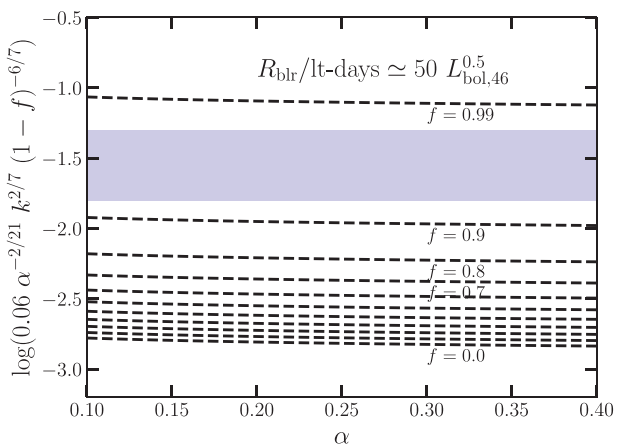

FIGURE 3 | The logarithm of the normalization of Equation (2) as a function of the accretion disc viscosity, α. The factor κ is fixed to 1.3×10^{-6}, which corresponds to a broad line region size of about 1.3×10^{17} cm ($\sim$ 50 light days) and $L_{\rm bol} = 10^{46}$ erg s^{-1}. The dashed black lines represent different values of f in the range from 0 to 0.99. The blue shaded area indicates the observed range of the normalization of the $L_{\rm X} - L_{\rm UV} - FWHM$ plane in a sample of $\sim$ 500 quasars. Figure based on data derived from Lusso and Risaliti (2017).

(i.e., $L_{\rm X} \propto L_{\rm UV}^{\hat{\gamma}} FWHM^{\hat{\beta}}$), has an observed dispersion of $\sim$0.2 dex over $\sim$3 orders of magnitude in luminosity and indicates that there is a good "coupling" between the disc, emitting the primary radiation, and the hot-electron *corona*, emitting X–rays.

We interpreted such relation through a simple (but physically motivated) model based on the ones presented by Svensson and Zdziarski (1994) and Merloni and Fabian (2002), where a geometrically thin, optically thick accretion disc is coupled with a uniform hot plasma. We assumed that the bulk of the corona emission is mainly powered by the accretion disc and it is located at the transition radius ($r_{\rm tr}$) where the gas pressure equates the radiation pressure in the disc. Assuming a broad line region size function of the bolometric luminosity as $R_{\rm blr} \propto L_{\rm bol}^{0.5}$ we have that $M_{\rm BH} \propto \dot{M}/\dot{M}_{\rm Edd} FWHM^4$, which leads to the final relation $L_{\rm X} \propto L_{\rm UV}^{4/7} FWHM^{4/7}$. Such a relation is remarkably consistent with the fit obtained from a sample of 550 optically selected quasars from SDSS DR7 cross matched with the XMM–*Newton* catalog 3XMM-DR6. The toy model we presented, although simplistic, is capable of making robust predictions on the X–ray luminosities (at a given ultraviolet emission and *FWHM*) of unobscured/blue quasars, and puts observational constraints on the fraction of accretion power released in the hot plasma in the vicinity of the accretion disc, f, as a function the broad line region size, from the observed normalization of $L_{\rm X} - L_{\rm UV} - FWHM$ plane. The latter result will provide a new vantage point for the next generation of semi-analytical and magneto-hydrodinamical simulations investigating on the physical link between the accretion disc and the X-ray corona.

The proposed relation $L_{\rm X} \propto L_{\rm UV}^{4/7} FWHM^{4/7}$ does not show significant evolution with time in the redshift range covered by our data, $z = 0.3 - 2.2$, and thus it can be employed as a cosmological indicator to estimate cosmological parameters (e.g., $\Omega_{\rm M}$, Ω_Λ).

AUTHOR CONTRIBUTIONS

All the authors contributed to the work and approved it for publication.

FUNDING

EL is supported by a European Union COFUND/Durham Junior Research Fellowship (under EU grant agreement no. 609412). This work has been supported by the grants PRIN-INAF 2012 and ASI INAF NuSTAR I/037/12/0.

ACKNOWLEDGMENTS

For all catalog correlations we have used the Virtual Observatory software TOPCAT (Taylor, 2005) available online (http://www.star.bris.ac.uk/~mbt/topcat/). This research has made use of data obtained from the 3XMM XMM–Newton serendipitous source catalog compiled by the 10 institutes of the XMM–Newton Survey Science Centre selected by ESA. This research made use of matplotlib, a Python library for publication quality graphics (Hunter, 2007).

REFERENCES

Balbus, S. A. (2003). Enhanced angular momentum transport in accretion disks. *Annu. Rev. Astron. Astrophys.* 41, 555–597. doi: 10.1146/annurev.astro.41.081401.155207

Betoule, M., Kessler, R., Guy, J., Mosher, J., Hardin, D., Biswas, R., et al. (2014). Improved cosmological constraints from a joint analysis of the SDSS-II and SNLS supernova samples. *Astron. Astrophys.* 568:A22. doi: 10.1051/0004-6361/201423413

Cao, X. (2009). An accretion disc-corona model for X-ray spectra of active galactic nuclei. *Monthly Notices R. Astron. Soc.* 394, 207–213. doi: 10.1111/j.1365-2966.2008.14347.x

Czerny, B., Li, Y.-R., Hryniewicz, K., Panda, S., Wildy, C., Sniegowska, M., et al. (2017). Failed radiatively accelerated dusty outflow model of the broad line region in active galactic nuclei. I. Analytical solution. *Astrophys. J.* 846:154. doi: 10.3847/1538-4357/aa8810

Di Matteo, T. (1998). Magnetic reconnection: flares and coronal heating in active galactic nuclei. *Monthly Notices R. Astron. Soc.* 299, L15–Ll20. doi: 10.1046/j.1365-8711.1998.01950.x

Foreman-Mackey, D., Hogg, D. W., Lang, D., and Goodman, J. (2013). emcee: the MCMC Hammer. *Publ. Astron. Soc. Pac.* 125, 306–312. doi: 10.1086/670067

Galeev, A. A., Rosner, R., and Vaiana, G. S. (1979). Structured coronae of accretion disks. *Astrophys. J.* 229, 318–326. doi: 10.1086/156957

Green, P. J., Aldcroft, T. L., Richards, G. T., Barkhouse, W. A., Constantin, A., Haggard, D., et al. (2009). A full year's Chandra exposure on sloan digital sky survey quasars from the Chandra multiwavelength project. *Astrophys. J.* 690, 644–669. doi: 10.1088/0004-637X/690/1/644

Haardt, F., and Maraschi, L. (1991). A two-phase model for the X-ray emission from Seyfert galaxies. *Astrophys. J. Part 2 Lett.* 380, L51–L54. doi: 10.1086/186171

Haardt, F., and Maraschi, L. (1993). X-ray spectra from two-phase accretion disks. *Astrophys. J.* 413, 507–517. doi: 10.1086/173020

Haardt, F., Maraschi, L., and Ghisellini, G. (1994). A model for the X-ray and ultraviolet emission from Seyfert galaxies and galactic black holes. *Astrophys. J. Part 2 Lett.* 432, L95–L99. doi: 10.1086/187520

Hunter, J. D. (2007). Matplotlib: a 2D graphics environment. *Comput. Sci. Eng.* 9, 90–95. doi: 10.1109/MCSE.2007.55

Jiang, Y.-F., Stone, J. M., and Davis, S. W. (2014). A global three-dimensional radiation magneto-hydrodynamic simulation of super-eddington accretion disks. *Astrophys. J.* 796:106. doi: 10.1088/0004-637X/796/2/106

Jin, C., Ward, M., and Done, C. (2012). A combined optical and X-ray study of unobscured type 1 active galactic nuclei - II. Relation between X-ray emission and optical spectra. *Monthly Notices R. Astron. Soc.* 422, 3268–3284. doi: 10.1111/j.1365-2966.2012.20847.x

Just, D. W., Brandt, W. N., Shemmer, O., Steffen, A. T., Schneider, D. P., Chartas, G., et al. (2007). The X-ray properties of the most luminous quasars from the sloan digital sky survey. *Astrophys. J.* 665, 1004–1022. doi: 10.1086/519990

Kaspi, S., Maoz, D., Netzer, H., Peterson, B. M., Vestergaard, M., and Jannuzi, B. T. (2005). The relationship between luminosity and broad-line region size in active galactic nuclei. *Astrophys. J.* 629, 61–71. doi: 10.1086/431275

King, A. R., Pringle, J. E., and Livio, M. (2007). Accretion disc viscosity: how big is alpha? *Monthly Notices R. Astron. Soc.* 376, 1740–1746. doi: 10.1111/j.1365-2966.2007.11556.x

Liu, B. F., Mineshige, S., and Shibata, K. (2002). A simple model for a magnetic reconnection-heated corona. *Astrophys. J. Part 2 Lett.* 572, L173–L176. doi: 10.1086/341877

Liu, J. Y., Qiao, E. L., and Liu, B. F. (2016). Revisiting the structure and spectrum of the magnetic-reconnection-heated corona in luminous AGNs. *Astrophys. J.* 833:35. doi: 10.3847/1538-4357/833/1/35

Lusso, E., Comastri, A., Vignali, C., Zamorani, G., Brusa, M., Gilli, R., et al. (2010). The X-ray to optical-UV luminosity ratio of X-ray selected type 1 AGN in XMM-COSMOS. *Astron. Astrophys.* 512:A34. doi: 10.1051/0004-6361/200913298

Lusso, E., and Risaliti, G. (2016). The tight relation between X-ray and ultraviolet luminosity of quasars. *Astrophys. J.* 819:154. doi: 10.3847/0004-637X/819/2/154

Lusso, E., and Risaliti, G. (2017). Quasars as standard candles. I. The physical relation between disc and coronal emission. *Astron. Astrophys.* 602:A79. doi: 10.1051/0004-6361/201630079

Marchese, E., Della Ceca, R., Caccianiga, A., Severgnini, P., Corral, A., and Fanali, R. (2012). The optical-UV spectral energy distribution of the unabsorbed AGN population in the XMM-Newton Bright Serendipitous Survey. *Astron. Astrophys.* 539:A48. doi: 10.1051/0004-6361/201117562

Merloni, A., and Fabian, A. C. (2002). Coronal outflow dominated accretion discs: a new possibility for low-luminosity black holes? *Monthly Notices R. Astron. Soc.* 332, 165–175. doi: 10.1046/j.1365-8711.2002.05288.x

Risaliti, G., and Lusso, E. (2015). A hubble diagram for quasars. *Astrophys. J.* 815:33. doi: 10.1088/0004-637X/815/1/33

Risaliti, G., and Lusso, E. (2017). Cosmology with AGN: can we use quasars as standard candles? *Astron. Nachrichten* 338, 329–333. doi: 10.1002/asna.201713351

Rosen, S. R., Webb, N. A., Watson, M. G., Ballet, J., Barret, D., Braito, V., et al. (2016). The XMM-Newton serendipitous survey. VII. The third XMM-Newton serendipitous source catalogue. *Astron. Astrophys.* 590:A1. doi: 10.1051/0004-6361/201526416

Różańska, A., and Czerny, B. (2000). Vertical structure of the accreting two-temperature corona and the transition to an ADAF. *Astron. Astrophys.* 360, 1170–1186.

Shen, Y., Richards, G. T., Strauss, M. A., Hall, P. B., Schneider, D. P., Snedden, S., et al. (2011). A catalog of quasar properties from sloan digital sky survey data release 7. *Astrophys. J. Suppl. Series* 194:45. doi: 10.1088/0067-0049/194/2/45

Steffen, A. T., Strateva, I., Brandt, W. N., Alexander, D. M., Koekemoer, A. M., Lehmer, B. D., et al. (2006). The X-ray-to-optical properties of optically selected active galaxies over wide luminosity and redshift ranges. *Astron. J.* 131, 2826–2842. doi: 10.1086/503627

Strateva, I. V., Brandt, W. N., Schneider, D. P., Vanden Berk, D. G., and Vignali, C. (2005). Soft X-ray and ultraviolet emission relations in optically selected AGN samples. *Astron. J.* 130, 387–405. doi: 10.1086/431247

Suzuki, N., Rubin, D., Lidman, C., Aldering, G., Amanullah, R., Barbary, K., et al. (2012). The hubble space telescope cluster supernova survey. V. Improving the dark-energy constraints above z > 1 and building an early-type-hosted supernova sample. *Astrophys. J.* 746:85. doi: 10.1088/0004-637X/746/1/85

Svensson, R. (1982). The pair annihilation process in relativistic plasmas. *Astrophys. J.* 258, 321–334. doi: 10.1086/160081

Svensson, R. (1984). Steady mildly relativistic thermal plasmas - processes and properties. *Monthly Notices R. Astron. Soc.* 209, 175–208. doi: 10.1093/mnras/209.2.175

Svensson, R., and Zdziarski, A. A. (1994). Black hole accretion disks with coronae. *Astrophys. J.* 436, 599–606. doi: 10.1086/174934

Tananbaum, H., Avni, Y., Branduardi, G., Elvis, M., Fabbiano, G., Feigelson, E., et al. (1979). X-ray studies of quasars with the Einstein observatory. *Astrophys. J. Part 2 Lett.* 234, L9–L13. doi: 10.1086/183100

Taylor, M. B. (2005). "TOPCAT & STIL: Starlink Table/VOTable Processing Software," in *Astronomical Data Analysis Software and Systems XIV*, Astronomical Society of the Pacific Conference Series, Vol. 347, eds P. Shopbell, M. Britton, and R. Ebert (SAO/NASA Astrophysics Data System). Available online at: http://adsabs.harvard.edu/abs/2005ASPC..347...29T

Trippe, S. (2015). AGN broad line regions scale with bolometric luminosity. *J. Korean Astron. Soc.* 48, 203–206. doi: 10.5303/JKAS.2015.48.3.203

Vignali, C., Brandt, W. N., and Schneider, D. P. (2003). X-Ray emission from radio-quiet quasars in the sloan digital sky survey early data release: the α_ox dependence upon ultraviolet luminosity. *Astron. J.* 125, 433–443. doi: 10.1086/345973

Young, M., Elvis, M., and Risaliti, G. (2010). The X-ray energy dependence of the relation between Optical and X-ray emission in quasars. *Astrophys. J.* 708, 1388–1397. doi: 10.1088/0004-637X/708/2/1388

Zdziarski, A. A., Ghisellini, G., George, I. M., Fabian, A. C., Svensson, R., and Done, C. (1990). Electron-positron pairs, Compton reflection, and the X-ray spectra of active galactic nuclei. *Astrophys. J. Part 2 Lett.* 363, L1–L4. doi: 10.1086/185851

Conflict of Interest Statement: The handling Editor declared a shared affiliation, though no other collaboration, with one of the authors GR.

The other author declares that the research was conducted in the absence of any commercial or financial relationships that could be construed as a potential conflict of interest.

Copyright © 2018 Lusso and Risaliti. This is an open-access article distributed under the terms of the Creative Commons Attribution License (CC BY). The use, distribution or reproduction in other forums is permitted, provided the original author(s) or licensor are credited and that the original publication in this journal is cited, in accordance with accepted academic practice. No use, distribution or reproduction is permitted which does not comply with these terms.

frontiers in Astronomy and Space Sciences

MINI REVIEW
published: 28 November 2017
doi: 10.3389/fspas.2017.00053

Jet Physics of Accreting Super-Massive Black Holes in the Era of the *Fermi Gamma-ray Space Telescope*

Filippo D'Ammando [1, 2]* ***on behalf of the Fermi Large Area Telescope Collaboration***

[1] *Dipartimento di Fisica e Astronomia, Universitá di Bologna, Bologna, Italy,* [2] *Istituto di Radioastronomia (INAF), Bologna, Italy*

The *Fermi Gamma-ray Space Telescope* with its main instrument on-board, the Large Area Telescope (LAT), opened a new era in the study of high-energy emission from Active Galactic Nuclei (AGN). When combined with contemporaneous ground- and space-based observations, *Fermi*-LAT achieves its full capability to characterize the jet structure and the emission mechanisms at work in radio-loud AGN with different black hole mass and accretion rate, from flat spectrum radio quasars to narrow-line Seyfert 1 (NLSy1) galaxies. Here, I discuss important findings regarding the blazar population included in the third LAT catalog of AGN and the γ-ray emitting NLSy1. Moreover, the detection of blazars at redshift beyond three in γ rays allows us to constrain the growth and evolution of heavy black holes over cosmic time, suggesting that the radio-loud phase may be important for a fast black hole growth in the early Universe. Finally, results on extragalactic objects from the third catalog of hard LAT sources are presented.

Keywords: active galactic nuclei, γ-ray emission, super-massive black hole, narrow-line Seyfert 1 galaxy, blazar, relativistic jet, accretion process, cosmological evolution

OPEN ACCESS

Edited by:
Mauro D'Onofrio,
Università degli Studi di Padova, Italy

Reviewed by:
Maria Dainotti,
Jagiellonian University, Poland
Milan S. Dimitrijevic,
Astronomical Observatory, Serbia

****Correspondence:***
Filippo D'Ammando
dammando@ira.inaf.it

Specialty section:
This article was submitted to Milky Way and Galaxies, a section of the journal Frontiers in Astronomy and Space Sciences

Received: *31 August 2017*
Accepted: *13 November 2017*
Published: *28 November 2017*

Citation:
D'Ammando F (2017) Jet Physics of Accreting Super-Massive Black Holes in the Era of the Fermi Gamma-ray Space Telescope. Front. Astron. Space Sci. 4:53. doi: 10.3389/fspas.2017.00053

1. INTRODUCTION

Relativistic jets are one of the most powerful manifestations of the release of energy related to the super-massive black hole (SMBH) at the center of active galactic nuclei (AGN). In about 10% of AGN, termed radio-loud AGN, the accretion disc is at the base of a bipolar outflow of relativistic plasma, which may extend well beyond the host galaxy, forming the spectacular lobes of plasma visible in the radio band. The jet emission is observed across the entire electromagnetic spectrum, from radio to γ rays. When the jet axis is closely aligned with our line of sight, the rest-frame radiation is strongly amplified due to the Doppler boosting with a large fraction of the output observed at higher energies, and giving rise to the blazar phenomenon. Blazars are traditionally divided into flat spectrum radio quasars (FSRQ) and BL Lac objects, based on the presence or not, respectively, of broad emission lines (i.e., Equivalent Width > 5 Å) in their optical and UV spectrum (e.g., Stickel et al., 1991). Recently, a new classification based on the luminosity of the broad line region (BLR) in Eddington luminosity was proposed by Ghisellini et al. (2011): sources with L_{BLR}/L_{Edd} higher or lower than 5×10^{-4} being classified as FSRQ or BL Lacs, respectively, in agreement with a transition of the accretion regime from efficient to inefficient between these classes. The spectral energy distribution (SED) of blazars are characterized by two bumps with the lower energy peak occurring in the IR/optical band in the FSRQ and at UV/X-rays in the BL Lacs. This first peak is univocally interpreted as synchrotron radiation from highly relativistic electrons

in a jet. The SED higher energy peak, observed at MeV–GeV energies in the FSRQ and at GeV–TeV energies in the BL Lacs, is commonly interpreted as inverse Compton scattering of seed photons, internal or external to the jet, by the same relativistic electrons (e.g., Ulrich et al., 1997). However, other models involving hadronic processes have been proposed (e.g., Böttcher et al., 2013). Fossati et al. (1998) proposed that the SEDs of blazars form a spectral sequence, with the position of the two peaks governed by the observed bolometric luminosity: blazars with lower luminosities have the peaks at higher energies. This was theoretically interpreted by Ghisellini et al. (1998) in terms of different radiative cooling suffered by the electrons emitting at the two peaks.

Radio galaxies are viewed at larger angles than blazars, with less severe boosting effects and classified as Fanaroff-Riley type I (FR I) and type II (FR II) based on their radio power and morphology (Fanaroff and Riley, 1974). Following the Unified model of AGN proposed by Urry and Padovani (1995), FR I and FR II radio galaxies are the non-aligned (to the observer viewing angle) parent populations of BL Lac and FSRQ, respectively. The discovery by *Fermi*-LAT of variable γ-ray emission from a few radio-loud narrow-line Seyfert 1 galaxies (NLSy1) suggested this as the third class of AGN with a relativistic jet (Abdo et al., 2009).

The *Fermi Gamma-ray Space Telescope* with its main instrument on-board, the Large Area Telescope (LAT), opened a new era in the study of high-energy emission from AGN. The γ-ray sky observed by *Fermi*-LAT is dominated by AGN that are ∼60% of the sources included in the Third *Fermi* LAT source catalog (3FGL; Acero et al., 2015). Apart from a handful of starburst galaxies, for which the γ-ray emission originates from the interaction of cosmic rays with gas and interstellar radiation fields (Ackermann et al., 2012), almost all the extragalactic sources are associated with radio-loud AGN.

Important findings regarding the blazar population included in the 3FGL and the NLSy1 are discussed in section 2 and 3, respectively. The high-redshift blazars detected in γ rays are discussed in section 4, while the third catalog of hard LAT sources is presented in section 5. Concluding remarks are reported in section 6.

2. THE THIRD LAT AGN CATALOG

Several γ-ray source catalogs, both general and for specific class of objects (i.e., AGN, pulsars, supernova remnants, pulsar wind nebulae, gamma-ray bursts) have already been produced by the LAT Collaboration. The 3FGL was used as a starting point for producing a catalog of AGN only: the Third LAT AGN catalog (3LAC; Ackermann et al., 2015). The 3FGL includes 3033 sources detected after four years of operation with a Test Statistic[1] greater than 25, corresponding to a significance $> 4\sigma$; 2,192 sources are detected at Galactic latitude $|b| > 10°$. 1,563 sources (71% of the 3FGL objects at $|b| > 10°$) are associated at high-confidence with 1,591 AGN (28 objects have two possible associations), which constitute, together with the low-latitude AGN, the 3LAC sample. Most of the high-latitude objects (98%) are blazars. The 3LAC includes radio-loud AGN of different types: 467 FSRQ, 632 BL Lacs, 460 BCU (Blazar with Uncertain Classification) and 32 non-blazar AGN. Among the non-blazar AGN there are 12 FR I, 3 FR II, 8 steep spectrum radio sources and 5 NLSy1.

Associations for 182 low-latitude ($|b| < 10°$) AGN are reported in the 3LAC: 24 FSRQ, 30 BL Lacs, 125 BCU and 3 non-blazar AGN. Extrapolating the number of high-latitude sources to low-latitude and assuming the same sensitivity, ∼340 sources would have been expected. The discrepancy between expected and associated source numbers is likely due to a higher Galactic diffuse emission background and a higher incompleteness of the catalogs of counterparts at low-latitude.

On average, sources with high γ-ray luminosity (mostly FSRQ) are found to have softer spectra than sources with low γ-ray luminosity (mostly BL Lacs), in agreement with the "blazar sequence" (Ghisellini et al., 1998) and the "blazar divide" (Ghisellini et al., 2009), with the exception of a few outliers (high-synchrotron-peaked-FSRQ and high-luminosity high-synchrotron-peaked BL Lacs). A strong anti-correlation between the synchrotron peak position (ν_{peak}) and the spectral index (Γ_γ) is observed for FSRQ and BL Lacs. A similar trend is noticed for BCU supporting the idea that BCU with low ν_{peak} and high Γ_γ are likely FSRQ, while BCU with high ν_{peak} and low Γ_γ are likely BL Lacs. Based on the 3LAC results, the blazar sequence was recently revised by Ghisellini et al. (2017): FSRQ display approximately the same SED as the luminosity increases, following a sequence only in Compton dominance (i.e., the ratio of the Compton to synchrotron peak luminosities) and in the X-ray slope, while BL Lacs become "redder" (i.e., the peak frequencies becomes smaller) when more luminous. Moreover, a correlation between the jet power and the accretion power has been found in blazars, with the jet power dominating over the accretion disc luminosity by a factor of 10 and somewhat larger than the entire gravitational power (Ghisellini et al., 2014).

At the time of writing, 70 AGN have been detected at TeV energies and listed in the TeVCat[2] All these sources are present in the 3LAC except for HESS J1943+213. A large fraction (> 75%) of blazars detected by *Swift*-BAT in hard X-rays have also been detected by *Fermi*-LAT.

The blazars detected by *Fermi*-LAT in γ rays after 4 years of operation represent a sizeable fraction of the entire population of known blazars as listed in the BZCAT (Massaro et al., 2009). The overall LAT-detected fraction is 24% (409/1,707) for FSRQ, 44% (543/1,221) for BL Lacs and 27% (59/221) for BCU. No strong differences in the radio, optical and X-ray flux distributions are observed between γ-ray detected and non-detected blazars in the BZCAT, suggesting that all blazars could eventually shine in γ rays at LAT-detection level. More BL Lacs than FSRQ have been detected by *Fermi*-LAT so far. This may be related to a longer duty cycle of FSRQ with respect to BL Lacs in γ rays.

[1]The Test Statistic is defined as TS = $2\times(\log L_1 - \log L_0)$, where L is the likelihood of the data given the model with (L_1) or without (L_0) a point source at the position of the target (e.g., Mattox et al., 1996).

[2]http://tevcat.uchicago.edu/.

3. NARROW-LINE SEYFERT 1 GALAXIES

The discovery of variable γ-ray emission from a few NLSy1 confirmed the presence of relativistic jets in these objects. In addition to the 5 objects reported in the 3LAC, *Fermi*-LAT has recently detected γ rays from other 3 new NLSy1: FBQS J1644+2619 (D'Ammando et al., 2015), B3 1441+476 and NVSS J124634+476 (D'Ammando et al., 2016). Luminosity, variability, and spectral properties of these NLSy1 in γ rays indicate a blazar-like behavior (e.g., D'Ammando et al., 2016). Apparent superluminal jet components were detected in SBS 0846+513 (D'Ammando et al., 2012), PMN J0948+0022, and 1H 0323+342 (Lister et al., 2016), supporting the presence of relativistic jets in this class of objects.

The detection of relativistic jets in a class of AGN thought to be hosted in spiral galaxies with a BH mass typically of 10^6-10^7 $M_\odot$ (e.g., Deo et al., 2006), challenges the theoretical scenarios of jet formation (e.g., Böttcher and Dermer, 2002), suggesting two possible interpretations: either relativistic jets in NLSy1 are produced by a different mechanism or the BH mass in NLSy1 is largely underestimated.

In the last years it has been claimed that the BH mass of NLSy1 maybe underestimated due either to the effect of radiation pressure from ionizing photons on BLR (Marconi et al., 2008) or to projection effects (Baldi et al., 2016). By considering these effects, NLSy1 have BH masses of 10^8–10^9 $M_\odot$, in agreement with the values estimated by modeling the optical-UV part of their spectra with a Shakura and Sunyaev disc spectrum (e.g., Calderone et al., 2013). This may solve the problem of the minimum BH mass predicted in different theoretical scenarios of relativistic jet formation, but leaves open the host galaxy issue.

Spiral galaxies are usually formed by minor mergers, with BH masses typically ranging between 10^6–10^7 $M_\odot$ (e.g., Woo and Urry, 2002), so it would not be clear how powerful relativistic jets could form in these galaxies. It is worth mentioning that the morphological classification has been done mainly for radio-quiet nearby NLSy1. Among the NLSy1 detected by *Fermi*-LAT up to now, the morphology of the host galaxy has been investigated only for 1H 0323+342, PKS 2004−447, and FBQS J1644+2619. Observations of 1H 0323+342 with the Hubble Space Telescope and the Nordic Optical Telescope revealed a structure that may be interpreted either as a one-armed spiral galaxy (Zhou et al., 2007) or as a circumnuclear ring produced by a recent merger (Anton et al., 2008; Leon Tavares et al., 2014). A pseudo-bulge morphology of the host galaxy of the NLSy1 PKS 2004−447 and FBQS J1644+2619 have been claimed by Kotilainen et al. (2016) and Olguin-Iglesias et al. (2017), respectively, but no conclusive results have been obtained so far. Hence, it is crucial to determine the type of galaxy hosting γ-ray emitting NLSy1 and their BH mass.

For this reason near-infrared observations in *J* band of FBQS J1644+2619 were performed using the Canarias Infrared Camera Experiment (CIRCE) at the Gran Telescopio Canaries. The 2D surface brightness profile of the source is modeled up to 5 arcsec by the combination of a nuclear component, associated with the AGN contribution, and a bulge component with a Sérsic index n = 3.7, indicative of an elliptical galaxy. The structural parameters of the host are consistent with the correlations of effective radius and surface brightness against absolute magnitude measured for elliptical galaxies. From the infrared bulge luminosity, a BH mass of $(2.1 \pm 0.2) \times 10^8$ $M_\odot$ was estimated (D'Ammando et al., 2017). All these pieces of evidence strongly indicate that the relativistic jet in the NLSy1 FBQS J1644+2619 is produced by a massive BH in an elliptical galaxy, as expected for radio-loud AGN.

4. HIGH-REDSHIFT BLAZARS

High-redshift blazars are the most powerful radio-loud AGN in the Universe and are bright targets in hard X-rays, representing a significant fraction of the extragalactic hard X-ray sky. However, they are not commonly detected in γ rays. In fact, high-redshift ($z > 2$) blazars represent <10% of the AGN population observed by *Fermi*-LAT so far. Flaring activity in the γ-ray energy range from these sources is even more uncommon, with only fourteen FSRQ at $z > 2$ detected during a γ-ray flare.

In the 3LAC there are 64 objects at $z > 2$ (∼3.7 per cent of the γ-ray sources associated with AGN) at $z > 2$, and only 2 at $z > 3$: PKS 0537−286 (z = 3.104) and TXS 0800+618 (z = 3.033). On the other hand, 13 blazars at $z > 3$ have been detected in hard X-rays by *Swift*-BAT, *INTEGRAL*-IBIS, and *NuSTAR* so far. Hard X-ray observations are more suitable for detecting blazars at $z > 3$, and this is mainly due to a spectral bias. In fact, the inverse Compton peak of high-redshift blazars is shifted toward lower energies as the bolometric luminosity increases. Only 10 sources at $z > 2$ are in both the 3LAC and the *Swift*-BAT 70-month catalog (Baumgartner et al., 2013). All high-redshift blazars listed in both 3LAC and *Swift*-BAT Catalogs have an average γ-ray luminosity $L_\gamma > 2\times10^{48}$ erg s^{-1}, indicating that only the most luminous blazars have been detected by both instruments. Furthermore, only blazars with an X-ray photon index $\Gamma_X < 1.6$ have been detected in γ rays, while no dependence on the X-ray spectral luminosity seems to be present (D'Ammando and Orienti, 2015).

As said above, high-redshift blazars at $z > 3.1$ are missing in the *Fermi* catalogs. These objects typically have large bolometric luminosities ($L_{bol} > 10^{48}$ erg s^{-1}) and harbor extremely massive BH ($M_{BH} \sim 10^9$ $M_\odot$). The new Pass 8 data set, with an improved event-level analysis, substantially enhances the sensitivity of the LAT, in particular at lower energies, increasing the capability of the LAT to detect sources with soft spectra like the high-redshift blazars. By analysing 92 months of Pass 8 data between 60 MeV and 300 GeV of a large sample of radio-loud quasars, 5 new γ-ray emitting blazars at $z > 3.1$ have been detected with high significance. Among them, NVSS J151002+570243 (z = 4.31) is now the most distant γ-ray emitting blazar so far. All the blazars discovered show steep γ-ray spectra ($\Gamma_\gamma > 2.5$), indicating an IC peak at MeV energies. These five sources lie in the region of high γ-ray luminosities ($L_\gamma > 10^{47}$ erg s^{-1}) and soft photon indices (**Figure 1**) typical of powerful blazars (Ackermann et al., 2017). Among the 5 new high-redshift blazars there are (at least) two with redshift between 3 and 4 with a $M_{BH} > 10^9$ $M_\odot$, implying the presence of $2\times2\Gamma^2$ (i.e., 675, adopting Γ = 13) similar objects but with a misaligned jet in the same range of redshift. This changes the estimate of the space density of very massive BH

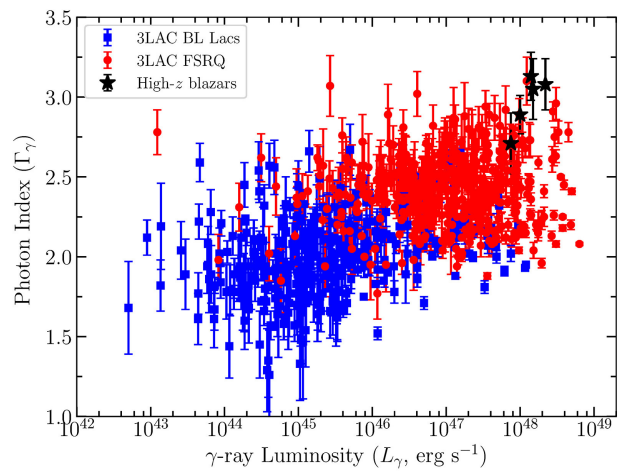

FIGURE 1 | Photon index vs. γ-ray luminosity plane for 3LAC and high-redshift blazars at $z > 3.1$ detected in γ rays. Adapted from Ackermann et al. (2017).

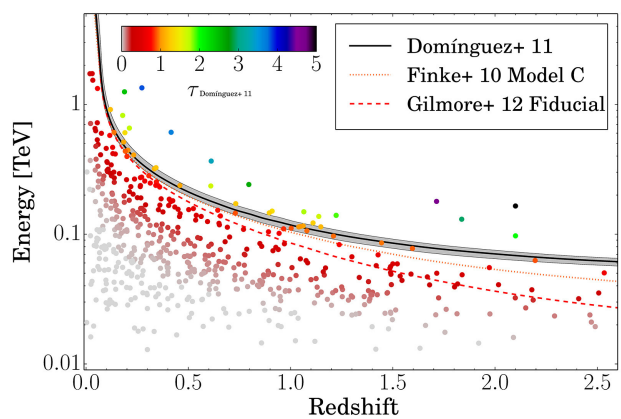

FIGURE 2 | The highest-energy photons vs. redshift for 3FHL blazars, color coded by the optical depth calculated from the model presented by Dominguez et al. (2011). The cosmic γ-ray horizon based on different EBL models is shown. Adapted from Ajello et al. (2017).

hosted in jetted sources to 68^{+36}_{-24} Gpc^{-3}. As a consequence at $z \sim 4$ we should have a similar number of SMBH hosted in radio-loud and radio-quiet sources and, given their strong evolution, above that redshift most massive BH might be hosted in radio-loud AGN. This suggests that the radio-loud phase can be a key ingredient for a rapid BH growth in the early Universe.

5. THE THIRD CATALOG OF HARD FERMI-LAT SOURCES

In addition to the *Fermi*-LAT catalogs with the standard low-energy threshold of 100 MeV, three hard source catalogs have been released: the First *Fermi*-LAT Catalog of Sources above 10 GeV (1FHL; Ackermann et al., 2013), based on the first three years of data analyzed in the 10–500 GeV energy range, the Second Catalog of Hard *Fermi*-LAT Sources (2FHL; Ackermann et al., 2016), based on 80 months of data analyzed in the 50 GeV–2 TeV energy range, and the Third Catalog of Hard *Fermi*-LAT Sources (3FHL; Ajello et al., 2017), based on 7 years of data in the 10 GeV–2 TeV energy range. The 3FHL contains 1556 objects and takes advantage of the improvement provided by Pass 8 by using the PSF-type event classification. The 3FHL includes 214 new γ-ray sources never appeared in previous *Fermi* catalogs. Three of these 214 have been detected with the Imaging Atmospheric Cherenkov Telescopes (IACT). The vast majority of detected sources (79%) are associated with extragalactic counterparts at other wavelengths, including 16 sources located at high-redshift ($z > 2$): 11 FSRQ, 3 BL Lac, and 2 BCU. BL Lacs are the most numerous extragalactic population (61%) followed by BCU (23%) and FSRQ (14%). Only 72 of the 3FHL extragalactic sources have been already detected by current IACT. In this context, the 3FHL is a resource for planning observations of the current (MAGIC, VERITAS, H.E.S.S.) and future (Cherenkov Telescope Array) IACT observatories. Interestingly, a few highest-energy photons from distant blazars included in the 3FHL Catalog are in the region around and beyond the cosmic γ-ray horizon [i.e., the energy at which the cosmic optical depth $\tau = 1$, see e.g., Dominguez et al. (2013)] as shown in **Figure 2**. These photons provide important constraints on extragalactic background light models as they may also help in the understanding of γ-ray propagation over cosmological distances.

6. CONCLUDING REMARKS

Fermi-LAT has been performing the first all-sky survey in γ rays, gathering well-sampled, continuous light curves for hundreds of AGN and compiling source catalogs for different energy ranges and time periods. These observations constitute important resources to the astronomical community for a better understanding of the jet physics, cosmological evolution, and accretion processes of SMBH. In fact, the *Fermi*-LAT observations, in conjunction with the multi-frequency data collected from radio to VHE, are key to revealing the nature of jet physics in different classes of AGN, including particle acceleration, environmental effects, and interaction processes. In addition, Pass 8 LAT data have increased the sensitivity for hard-spectrum sources, which are important targets for ground-based VHE telescopes including the planned Cherenkov Telescope Array. Moreover, the extended energy range reached by the Pass 8 data opens new opportunities for the study of blazars at high redshifts. Over the next years the *Fermi* satellite will provide a fundamental contribution in time domain astronomy and multi-messenger/multi-wavelength studies.

AUTHOR CONTRIBUTIONS

The author confirms being the sole contributor of this work and approved it for publication.

ACKNOWLEDGMENTS

The *Fermi*-LAT Collaboration acknowledges support for LAT development, operation and data analysis from NASA and DOE (United States), CEA/Irfu and IN2P3/CNRS (France), ASI and INFN (Italy), MEXT, KEK, and JAXA (Japan), and the K.A. Wallenberg Foundation, the Swedish Research Council and the National Space Board (Sweden). Science analysis support in the operations phase from INAF (Italy) and CNES (France) is also gratefully acknowledged. This work performed in part under DOE Contract DE-AC02-76SF 00515.

REFERENCES

Abdo, A. A., Ackermann, M., Ajello, M., Baldini, L., Ballet, J., Barbiellini, G., et al. (2009). Radio-loud narrow-line seyfert 1 as a new class of gamma-ray active galactic nuclei. *Astrophys. J.* 707, L142–L147. doi: 10.1088/0004-637X/707/2/L142

Acero, F., Ackermann, M., Ajello, M., Albert, A., Atwood, W. B., Axelsson, M., et al. (2015). Fermi large area telescope third source catalog. *Astrophys. J. Suppl.* 218, 23–63. doi: 10.1088/0067-0049/218/2/23

Ackermann, M., Ajello, M., Allafort, A., Baldini, L., Ballet, J., Bastieri, D., et al. (2012). GeV observations of star-forming galaxies with the Fermi large area telescope. *Astrophys. J.* 755, 164–186. doi: 10.1088/0004-637X/755/2/164

Ackermann, M., Ajello, M., Allafort, A., Atwood, W. B., Baldini, L., Ballet, J., et al. (2013). The first Fermi-LAT catalog of sources above 10 GeV. *Astrophys. J. Suppl.* 209, 34–67. doi: 10.1088/0067-0049/209/2/34

Ackermann, M., Ajello, M., Atwood, W. B., Baldini, L., Ballet, J., Barbiellini, G., et al. (2015). The third catalog of active galactic nuclei detected by the Fermi large area telescope. *Astrophys. J.* 810, 14–47. doi: 10.1088/0004-637X/810/1/14

Ackermann, M., Ajello, M., Atwood, W. B., Baldini, L., Ballet, J., Barbiellini, G., et al. (2016). 2FHL: The second catalog of hard Fermi-LAT sources. *Astrophys. J. Suppl.* 222, 5–23. doi: 10.3847/0067-0049/222/1/5

Ackermann, M., Ajello, M., Baldini, L., Ballet, J., Barbiellini, G., Bastieri, D., et al. (2017). Gamma-ray blazars within the first 2 billion years. *Astrophys. J.* 837, L5–L12. doi: 10.3847/2041-8213/aa5fff

Ajello, M., Atwood, W. B., Baldini, L., Ballet, J., Barbiellini. G., Bastieri, D., et al. (2017). 3FHL: the third catalog of hard Fermi-LAT sources. *Astrophys. J. Suppl.* 232, 18–40. doi: 10.3847/1538-4365/aa8221

Anton, S., Browne, I. W. A., and Marcha, M. J. (2008). The colour of the narrow line Sy1-blazar 0324+3410. *Astron. Astrophys.* 490, 583–587. doi: 10.1051/0004-6361:20078926

Baldi, R., Capetti, A., Robinson, A., Laor, A. and Behar, E. (2016). Radio-loud narrow line seyfert 1 under a different perspective: a revised black hole mass estimate from optical spectropolarimetry. *Month. Notices R. Astron. Soc.* 458, L69–L73. doi: 10.1093/mnrasl/slw019

Baumgartner, W. H., Tueller, J., Markwardt, C. B., Skinner, G. K., Barthelmy, S., Mushotzky, R. F., et al. (2013). The 70 month Swift-BAT all-sky hard X-ray survey. *Astrophys. J. Suppl.* 207, 19–30. doi: 10.1088/0067-0049/207/2/19

Böttcher, M., and Dermer, C. D. (2002). An evolutionary scenario for blazar unification. *Astrophys. J.* 564, 86–91. doi: 10.1086/324134

Böttcher, M., Reimer, A., Sweeney, K., and Prakash, A. (2013). Leptonic and hadronic modeling of Fermi-detected blazars. *Astrophys. J.* 768, 54–67. doi: 10.1088/0004-637X/768/1/54

Calderone, G., Ghisellini, G., Colpi, M., and Dotti, M. (2013). Black hole mass estimate for a sample of radio-loud narrow-line Seyfert 1 galaxies. *Month. Notices R. Astron. Soc.* 431, 210–239. doi: 10.1093/mnras/stt157

D'Ammando, F., Orienti, M., Finke, J., Raiteri, C. M., Angelakis, E., Fuhrmann, L., et al. (2012). SBS 0846+513: a new gamma-ray emitting Narrow-Line Seyfert 1 galaxy. *Month. Notices R. Astron. Soc.* 426, 317–329. doi: 10.1111/j.1365-2966.2012.21707.x

D'Ammando, F., Orienti, M., Larsson, J., and Giroletti, M., (2015). The first γ-ray detection of the narrow-line Seyfert 1 FBQS J1644+2619. *Month. Notices R. Astron. Soc.* 452, 520–524. doi: 10.1093/mnras/stv1278

D'Ammando, F., and Orienti, M. (2015). High-energy properties of the high-redshift flat spectrum radio quasar PKS 2149-306. *Month. Notices R. Astron. Soc.* 455, 1881–1891. doi: 10.1093/mnras/stv2452

D'Ammando, F., Orienti, M., Finke, J., Larsson, J., Giroletti, M., and Raiteri, C. (2016). A panchromatic view of relativistic jets in narrow-line seyfert 1 galaxies. *Galaxies* 4, 11–17. doi: 10.3390/galaxies4030011

D'Ammando, F., Acosta-Pulido, J. A., Capetti, A., Raiteri, C. M., Baldi, R. D., Orienti, M., and Ramos Almeida, C. (2017). Uncovering the host galaxy of the γ-ray-emitting narrow-line Seyfert 1 galaxy FBQS J1644+2619. *Month. Notices R. Astron. Soc.* 469, L11–L15. doi: 10.1093/mnrasl/slx042

Deo, R. P., Crenshow, D. M., and Kraemer, S. B. (2006). The host galaxies of narrow-line seyfert 1 galaxies: nuclear dust morphology and starburst rings. *Astron. J.* 132, 321–346. doi: 10.1086/504894

Dominguez, A., Primack, J. R., Rosario, D. J., Prada, F., Gilmore, R. C., Faber, S. M., et al. (2011). Extragalactic background light inferred from AEGIS galaxy-SED-type fractions. *Month. Notices R. Astron. Soc.* 410, 2556–2578. doi: 10.1111/j.1365-2966.2010.17631.x

Dominguez, A., Finke, J. D., Prada, F., Primack, J. R., Kitaura, F. S., Siana, B., et al. (2013). Detection of the cosmic γ-Ray horizon from multiwavelength observations of blazars. *Astrophys. J.* 70, 77–91. doi: 10.1088/0004-637X/770/1/77

Fanaroff, B. L., and Riley, J. M. (1974). The morphology of extragalactic radio sources of high and low luminosity. *Month. Notices R. Astron. Soc.* 167, 31P–36P. doi: 10.1093/mnras/167.1.31P

Fossati, G., Maraschi, L., Celotti, A., Comastri, A., and Ghisellini, G. (1998). A unifying view of the spectral energy distributions of blazars. *Month. Notices R. Astron. Soc.* 299, 433–448. doi: 10.1046/j.1365-8711.1998.01828.x

Ghisellini, G., Celotti, A., Fossati, G., Maraschi, L., and Comastri, A. (1998). A theoretical unifying scheme for gamma-ray bright blazars. *Month. Notices R. Astron. Soc.* 301, 451–468. doi: 10.1046/j.1365-8711.1998.02032.x

Ghisellini, G., Maraschi, L., and Tavecchio, F. (2009). The Fermi blazars' divide. *Month. Notices R. Astron. Soc.* 396, L105–L109. doi: 10.1111/j.1745-3933.2009.00673.x

Ghisellini, G., Tavecchio, F., Foschini, L., and Ghirlanda, G. (2011). The transition between BL Lac objects and flat spectrum radio quasars. *Month. Notices R. Astron. Soc.* 414, 2674–2689. doi: 10.1111/j.1365-2966.2011.18578.x

Ghisellini, G., Tavecchio, F., Maraschi, L., Celotti, A., and Sbarrato, T. (2014). The power of relativistic jets is larger than the luminosity of their accretion disks. *Nature* 515, 376–378. doi: 10.1038/nature13856

Ghisellini, G., Righi, C., Costamante, L., and Tavecchio, F. (2017). The Fermi blazar sequence. *Month. Notices R. Astron. Soc.* 469, 255–266. doi: 10.1093/mnras/stx806

Kotilainen, J. K., Leon Tavares, J., Olguin-Iglesias, A., Baes, M., Anorve, C., Chavushyan, V., et al. (2016). Discovery of a pseudobulge galaxy launching powerful relativistic jets. *Astrophys. J.* 832, 157–164. doi: 10.3847/0004-637X/832/2/157

Leon Tavares, J., Kotilainen, J., Chavushyan, V., Anorve, C., Puerari, I., Cruz-Gonzalez, I., et al. (2014). The host galaxy of the gamma-ray narrow-line Seyfert 1 galaxy 1H 0323+342. *Astrophys. J.* 795, 58–70. doi: 10.1088/0004-637X/795/1/58

Lister, M. L., Aller, M. F., Aller, H. D., Homan, D. C., Kellermann, K. I., Kovalev, Y. Y., et al. (2016). MOJAVE: XIII. Parsec-scale AGN jet kinematics analysis based on 19 years of VLBA observations at 15 GHz. *Astron. J.* 152, 12–27. doi: 10.3847/0004-6256/152/1/12

Marconi, A., Axon, D. J., Maiolino, R., Nagao, T., Pastorini, G., Pietrini, P., et al. (2008). The effect of radiation pressure on virial black hole mass estimates and the case of narrow-line seyfert 1 galaxies. *Astrophys. J.* 678, 693–700. doi: 10.1086/529360

Massaro, E., Giommi, P., Leto, C., Marchegiani, P., Maselli, A., Perri, M., et al. (2009). Roma-BZCAT: a multifrequency Catalog of blazars. *Astron. Astrophys.* 495, 691–696. doi: 10.1051/0004-6361:200810161

Mattox, J. R., Bertsch, D. L., Chiang, J., Dingus, B. L., Digel, S. W., Esposito, J. A., et al. (1996). The likelihood analysis of EGRET data *Astrophys. J.* 461, 396–407. doi: 10.1086/177068

Olguin-Iglesias, A., Kotilainen, J. K., Leon Tavares, J., Chavushyan, V., and Anorve, C. (2017). Evidence of bar-driven secular evolution in the gamma-ray narrow-line Seyfert 1 galaxy FBQS J164442.5+261913. *Month. Notices R. Astron. Soc.* 467, 3712–3722. doi: 10.1093/mnras/stx022

Stickel, M., Padovani, P., Urry, C. M., Fried, J. W., and Kuehr, H. (1991). The complete sample of 1 Jansky BL Lacertae objects. I - Summary properties. *Astrophys. J.* 374, 431–439. doi: 10.1086/170133

Ulrich, M.-H., Maraschi, L., and Urry, C. M. (1997). Variability of active galactic nuclei. *Annu. Rev. Astron. Astrophys.* 35, 445–502. doi: 10.1146/annurev.astro.35.1.445

Urry, M., and Padovani, P. (1995). Unified schemes for radio-loud active galactic nuclei. *Publ. Astron. Soc. Pac.* 107, 803–845. doi: 10.1086/133630

Woo, J.-H., and Urry, C. M. (2002). Active galactic nucleus black hole masses and bolometric luminosities. *Astrophys. J.* 579, 530–544. doi: 10.1086/342878

Zhou, H., Wang, T., Yuan, W., Shan, H., Komossa, S., Lu, H., et al. (2007). A narrow-line seyfert 1-blazar composite nucleus in 2MASX J0324+3410. *Astrophys. J.* 658, L13–L16. doi: 10.1086/513604

Conflict of Interest Statement: The author declares that the research was conducted in the absence of any commercial or financial relationships that could be construed as a potential conflict of interest.

Copyright © 2017 D'Ammando. This is an open-access article distributed under the terms of the Creative Commons Attribution License (CC BY). The use, distribution or reproduction in other forums is permitted, provided the original author(s) or licensor are credited and that the original publication in this journal is cited, in accordance with accepted academic practice. No use, distribution or reproduction is permitted which does not comply with these terms.

frontiers in Astronomy and Space Sciences

HYPOTHESIS AND THEORY
published: 22 December 2017
doi: 10.3389/fspas.2017.00063

The Correlation between the Total Magnetic Flux and the Total Jet Power

*Elena E. Nokhrina**

Relativistic Astrophysics Laboratory: Basic and Applied Studies of Space Objects, School of Fundamental and Applied Physics, Moscow Institute of Physics and Technology, Dolgoprudny, Russia

Magnetic field threading a black hole ergosphere is believed to play the key role in both driving the powerful relativistic jets observed in active galactic nuclei and extracting the rotational energy from a black hole via Blandford-Znajek process. The magnitude of magnetic field and the magnetic flux in the vicinity of a central black hole is predicted by theoretical models. On the other hand, the magnetic field in a jet can be estimated through measurements of either the core shift effect or the brightness temperature. In both cases the obtained magnetic field is in the radiating domain, so its direct application to the calculation of the magnetic flux needs some theoretical assumptions. In this paper we address the issue of estimating the magnetic flux contained in a jet using the measurements of a core shift effect and of a brightness temperature for the jets, directed almost at the observer. The accurate account for the jet transversal structure allow us to express the magnetic flux through the observed values and an unknown rotation rate of magnetic surfaces. If we assume the sources are in a magnetically arrested disk state, the lower limit for the rotation rate can be obtained. On the other hand, the flux estimate may be tested against the total jet power predicted by the electromagnetic energy extraction model. The resultant expression for power depends logarithmically weakly on an unknown rotation rate. We show that the total jet power estimated through the magnetic flux is in good agreement with the observed power. We also obtain the extremely slow rotation rates, which may be an indication that the majority of the sources considered are not in the magnetically arrested disk state.

Keywords: active galaxies, jets, BL Lacertae objects, non-thermal radiation, magnetic flux

OPEN ACCESS

Edited by:
Mauro D'Onofrio,
Università degli Studi di Padova, Italy

Reviewed by:
Maria Dainotti,
Jagiellonian University, Poland
Alberto Martin Gago,
Pontifical Catholic University of Peru, Peru

***Correspondence:**
Elena E. Nokhrina
nokhrina@phystech.edu

Specialty section:
This article was submitted to Milky Way and Galaxies, a section of the journal Frontiers in Astronomy and Space Sciences

Received: *31 August 2017*
Accepted: *06 December 2017*
Published: *22 December 2017*

Citation:
Nokhrina EE (2017) The Correlation between the Total Magnetic Flux and the Total Jet Power. Front. Astron. Space Sci. 4:63. doi: 10.3389/fspas.2017.00063

1. INTRODUCTION

One of the key issues of theoretical modeling of relativistic jets is determining the magnetic field magnitude. There are several theoretical ways to estimate the latter. The Eddington magnetic field (Beskin, 2010) sets up an upper limit on the magnetic field magnitude in the vicinity of a black hole, since it is set by equipartition of magnetic field density and the total energy density in the accreting plasma that is needed to support the Eddington luminosity. The state of magnetically arrested disk (MAD) (Narayan et al., 2003; Tchekhovskoy et al., 2011; McKinney et al., 2012) sets up the limiting magnetic field that can be accreted onto a black hole basing on an assumption that in such a state the pressure of previously accreted magnetic field can affect the dynamical process of accretion itself.

There are observational means to evaluate the magnetic field in a jet. Blazar spectrum is successfully modeled by the synchrotron self-Compton model. The lower part of the spectrum is dominated by synchrotron radiation of relativistic plasma in a jet magnetic field. Thus, the high-resolution radio interferometry observations provide us with data for unveiling the physical conditions at the very jet origin—in so called radio core. The way to estimate the magnetic field amplitude through the observations is measurements of core shift effect together with several theoretical assumptions on the radiating volume properties (Lobanov, 1998). However, the measurement of radio flux itself, or, equally, the brightness temperature, can provide us with the instrument to probe the magnetic field magnitude (Zdziarski et al., 2015; Nokhrina, 2017).

The magnetic field estimates is an important parameter that allows to test the theoretical models against observations. Zamaninasab et al. (2014) used the magnetic field measurements to calculate the flux and to show that the total flux is in accordance with the magnetically arrested state of the sources. In this paper we make use of the brightness temperature and core shift measurements coupled with the transversal jet model to express the magnetic field magnitude and the magnetic flux contained in a blazar jet through the rotation rate of magnetic surfaces. Our aim is to compare the magnetic flux in a jet against theoretically limited flux by MAD state and to estimate the rotation rate. We also test the obtained magnetic flux against the observed jet power. If the jet power P_Ψ is fully determined by the electromagnetic energy extraction mechanism, so we denote it with the subscript Ψ, than it can be expressed as Beskin (2010)

$$P_\Psi = \left(\frac{\Psi a}{\pi r_g}\right)^2 c, \tag{1}$$

where Ψ is the total magnetic flux, r_g is a gravitational radius, c is a speed of light, and the rotation rate $a = r_g/R_L$ is a ratio of a gravitational radius to the light cylinder radius R_L.

Although there are estimates for magnetic field amplitude (Lobanov, 1998; Hirotani, 2005; OŚullivan and Gabuzda, 2009; Nokhrina et al., 2015; Zdziarski et al., 2015; Nokhrina, 2017), it cannot be explicitly used for flux calculation. Indeed, the magneto hydrodynamical theoretical and numerical modeling (see e.g., Lyubarsky, 2009; Nokhrina et al., 2015; Bromberg and Tchekhovskoy, 2016) show that the toroidal magnetic field is greater than the poloidal one outside the light cylinder radius. Thus, measurements provide us with the magnitude of the toroidal magnetic field, while the poloidal one is needed to estimate the total magnetic flux (Zamaninasab et al., 2014).

2. MAGNETIC FLUX IN A JET

The observed flux, or observed brightness temperature, can be used to estimate the magnetic field in the radiating domain, and, thus, the magnetic flux. The blazar spectrum in radio band is accurately modeled within the self-absorbed synchrotron model (see e.g., Abdo et al., 2011). The simplest model for the source is a uniform sphere with chaotic magnetic field B and relativistic electrons with the power-law energy distribution described by the amplitude particle number density k_e and spectral index p:

$$dn(\gamma) = k_e \gamma^{-p} d\gamma, \tag{2}$$

$\gamma \in [\gamma_{\min}, \gamma_{\max}]$ (Gould, 1979), where γ is a Lorentz factor of relativistic plasma. The observed spectral flux S_ν at the frequency ν for the optically thick uniform self-absorbed source of radius R at the distance d can be written using the spectral photon emission rate ρ_ν and effective absorption coefficient $æ_\nu$ as:

$$S_\nu = \pi \hbar \nu \frac{\rho_\nu}{æ_\nu} \frac{R^2}{d^2} u(2R æ_\nu), \tag{3}$$

and the function of the optical depth $u(2Ræ_\nu)$ is defined by Gould (1979). The emission and absorption coefficients for the self-absorbed synchrotron model ρ_ν and $æ_\nu$ are the functions of the magnetic field B and of particle number density amplitude k_e. These coefficients, written in a jet frame, i.e., in a frame where the electric field vanishes, are:

$$\rho_\nu = 4\pi \left(\frac{3}{2}\right)^{(p-1)/2} a(p) \alpha k_e \left(\frac{\nu_B}{\nu}\right)^{(p+1)/2}, \tag{4}$$

$$æ_\nu = c(p) r_0^2 k_e \left(\frac{\nu_0}{\nu}\right) \left(\frac{\nu_B}{\nu}\right)^{(p+2)/2}. \tag{5}$$

Here $\nu_B = eB/mc$ is a gyrofrequency in the jet frame, $\hbar$ is the Planck constant, $\alpha = e^2/\hbar c$ is the fine structure constant, and the functions $a(p)$ and $c(p)$ of the electron distribution spectral index p are defined in Gould (1979). The spectral flux depends on the magnetic field amplitude, while the particle number density amplitude defines the maximum of a function u and, thus, the position of the observed radio core—the domain where the optical depth τ is equal to unity. So, the spectral flux measurement provide us with an instrument to evaluate the magnetic field in a source. The spectral flux may be expressed through the brightness temperature T_b as

$$S_\nu = \frac{2\pi \nu^2 \theta^2}{c^2} k_B T_b, \tag{6}$$

where θ is the angular size of a radiating domain. Thus one can express the magnetic field amplitude in a source having measured brightness temperature. The method was first applied by Zdziarski et al. (2015) to check the magnetic field amplitude in AGN radio cores independently of the equipartition assumption. Equating the right-hand sides of Equations (3) and (6), and expressing the jet frame values through the nucleus frame values, we obtain for $p = 2$ the magnetic field (Zdziarski et al., 2015, see also details in Nokhrina, 2017)

$$\left(\frac{B_{\rm uni}}{\rm G}\right) = 7.4 \cdot 10^{-4} \frac{\Gamma \delta}{1+z} \left(\frac{\nu_{\rm obs}}{\rm GHz}\right) \left(\frac{T_{\rm b,\,obs}}{10^{12}\rm K}\right)^{-2}. \tag{7}$$

Here Γ is a flow bulk Lorentz factor, z is a source redshift, and δ is a Doppler factor.

On the other hand, the measurements of core shift effect (Lobanov, 1998; Hirotani, 2005; OŚullivan and Gabuzda, 2009;

Zamaninasab et al., 2014) provides the following expression for the magnetic field amplitude B_{cs} at 1 pc distance from the central source:

$$\left(\frac{B_{cs}}{\mathrm{G}}\right) = 0.17\left(\frac{\eta_{cs}}{\mathrm{mas\ GHz}}\right)^{0.75}\left(\frac{D_L}{\mathrm{Gpc}}\right)^{0.75}\frac{\Gamma}{\chi^{0.25}(1+z)^{0.75}\sin^{0.5}\varphi\delta^{0.5}}, \tag{8}$$

here η_{cs} is a coefficient determining the slope of the apparent core position dependence on the inverse observation frequency:

$$\left(\frac{\Delta r}{\mathrm{mas}}\right) = \left(\frac{\eta_{cs}}{\mathrm{mas\ GHz}}\right)\left(\frac{\nu_{obs}}{\mathrm{GHz}}\right)^{-1}. \tag{9}$$

χ is the jet opening angle that may obtained having the measured in Pushkarev et al. (2009) apparent opening angle χ_{app} as $\chi = \chi_{app}\sin\varphi/2$, D_L is a luminosity distance, the bulk plasma motion Lorentz factor is Γ, δ is the Doppler factor, and the observation angle $\varphi = \Gamma^{-1}$ (Cohen et al., 2007). The Expression (Equation 8) has been obtained under the same assumption of synchrotron self-absorbed source, but the method utilizes the core shift effect—the shift of the observed radio core on different frequencies. This shift is due to the fact that the surface of optical depth $\tau = 1$ is situated at different distance from the central source for each frequency. We must stress that the relation (Equation 7) uses only the synchrotron self-absorbed source model, but the position of the radio core in the model is not known. If we use the core shift effect, we may also obtain the core position (Nokhrina, 2017):

$$\left(\frac{r_{core}}{\mathrm{pc}}\right) = \frac{4.85}{\sin\varphi(1+z)^2}\left(\frac{\nu_{obs}}{\mathrm{GHz}}\right)^{-1}\left(\frac{\eta_{cs}}{\mathrm{mas\ GHz}}\right)\left(\frac{D_L}{\mathrm{Gpc}}\right). \tag{10}$$

The relation for B_{cs} (Equation 8) has been obtained with more assumptions: equipartition between magnetic field energy and plasma energy assumption, and the Blanford-Königl model (Blanford and Königl, 1979) $B(r) = B_1(r_1/r)$, $n(r) = n_1(r_1/r)^2$, where n_1 and B_1 are particle number density and magnetic field magnitude at distance r along the jet equal to $r_1 = 1$ pc. Relation (Equation 8) provides the magnetic field amplitude together with its position along the jet.

Both Expressions (Equation 7) and (Equation 8) are based on the model of uniform radiating sphere (Gould, 1979). In particular, such a model does not allow us to estimate the total magnetic flux, contained in a jet—one of the important values, defining the total jet power, and the value that could be restricted by the magnetically arrested disk model. Indeed, as the toroidal magnetic field B_φ dominates the major part of a jet, it is the toroidal component of a field we imply by the spectral flux measurement. However, it is the poloidal component B_P that carries the magnetic flux. However, the transversal modeling of field profiles allow us in a simple case of blazar jets, i.e., jets pointing almost directly at us, to calculate the flux from non-homogeneous cylindrical self-absorbed synchrotron source, and to correlate the measured magnetic field amplitude with the poloidal field in a jet that defines the total flux. Indeed, it has been shown by Lyubarsky (2009), that the relation

$$B_P = B_\varphi\frac{R_L}{r_\perp} \tag{11}$$

holds outside the light cylinder $R_L = c/\Omega_F$. Further we model the transversal magnetic field and particle number density profiles as follows. Inside the light cylinder the poloidal magnetic field remains almost constant (Beskin and Nokhrina, 2009), while $B_\varphi = B_0 r_\perp/R_L$. Both numerical and semi-analytical modeling (Nokhrina et al., 2015; Bromberg and Tchekhovskoy, 2016) show, that outside the light cylinder the power-law is a good approximation for magnetic field and particle number density profiles across the jet for small opening angles. We set

$$B_P = \begin{cases} B_0,\ r_\perp \le R_L, \\ B_0\left(\frac{R_L}{r_\perp}\right)^2,\ R_L < r_\perp \le R_j, \end{cases} \tag{12}$$

$$B_\varphi = \begin{cases} B_0\frac{r_\perp}{R_L},\ r_\perp \le R_L, \\ B_0\left(\frac{R_L}{r_\perp}\right),\ R_L < r_\perp \le R_j. \end{cases} \tag{13}$$

$$n = \begin{cases} n_0,\ r_\perp \le R_L, \\ n_0\left(\frac{R_L}{r_\perp}\right)^2,\ R_L < r_\perp \le R_j, \end{cases} \tag{14}$$

where B_0 and n_0 are the magnetic field and particle number density amplitudes, i.e., magnitudes at the light cylinder R_L.

For the simplest case of a jet pointing almost at us, when the radiation domain may be treated as a stratified cylinder with the profiles (Equations 12–14), we calculate the spectral flux S_ν (see details in Nokhrina, 2017). Equating the obtained S_ν to the expression (Equation 6), we obtain the following relation for the amplitude magnetic field B_0:

$$\left(\frac{B_0}{\mathrm{G}}\right) = 6.4\times10^{-4}\frac{R_j}{R_L}\frac{\Gamma\delta}{1+z}\left(\frac{\nu_{obs}}{\mathrm{GHz}}\right)\left(\frac{T_{b,obs}}{10^{12}\ \mathrm{K}}\right)^{-2}. \tag{15}$$

Here the fast rotation $\Gamma R_L \ll R_j$ is assumed. While R_j can be estimated through observations, the light cylinder radius is usually unknown. However, its value can be somewhat restricted by theoretical models predicting that Blandford-Znajek process works effectively for R_L of the order of $2r_g$ (Blanford and Znajek, 1977; Tchekhovskoy et al., 2012). Still, the value B_0 cannot be readily extracted from the observations.

The total flux Ψ in a jet with given cross-section magnetic filed profile is defined as

$$\Psi = 2\pi\int_0^{R_j} B_P r_\perp dr_\perp. \tag{16}$$

Using the magnetic field profile (Equation 12) we obtain

$$\Psi = \pi B_0 R_L^2 \left(1 + 2\ln\frac{R_j}{R_L}\right). \quad (17)$$

Substituting explicitly $B_0 R_L$ into Equation (17) and using the correlation $B_0 R_L = 0.86 B_{uni} R_j$ following from Equations (7) and (15), we obtain the relation for the magnetic flux:

$$\Psi = 2.7 B_{uni,\,cs} R_j \frac{r_g}{a}\left[1 + 2\ln\frac{R_j\, a}{r_g}\right] = \frac{\Psi_a}{a}. \quad (18)$$

Here one may use B_{cs} or B_{uni}, since both values are obtained under the same assumptions on the geometry and structure of radiating domain. The amplitude magnetic flux $\Psi_a = a\Psi$. The Equation (18) coincides with the expression for the magnetic flux in Zamaninasab et al. (2014). The expression (Equation 18) for the flux depends inversely on a rotation rate a, because the dependence on the physical values in square brackets is logarithmically weak and can be neglected. Taking the fiducial value for $R_j/r_g \sim 10^3$, we take the expression in square brackets being of the order of a few to ten.

3. THE JET POWER AND THE ROTATION RATE

We apply the obtained expression for the flux (Equation 18) to test it against the following theoretical predictions. If we assume that most of the sources are in MAD state, we can compare the amplitude flux Ψ_a and Ψ_{MAD} and obtain the rotation parameter $a = \Psi_a/\Psi_{MAD}$. However, we must bear in mind that the energy losses mechanism Blanford and Znajek (1977) works effectively for relatively high rotation rates $a > 0.5$. Thus, with the difference in Ψ_{MAD} and Ψ_a is greater, we might think that the source is not in the MAD state.

We also use the obtained flux (Equation 18) to calculate the total jet power given by the Equation (1). As the Expression (Equation 1) depends on the product $\Psi a = \Psi_a$ (Equation 18) that depends on a logarithmically weakly only through the term $1 + 2\ln(R_j a/r_g)$, so does the total power. So this result is independent on the assumption of the particular value for a. That is why such a test may be important for the flux determination. We do it for the magnetic field estimated by two methods: the brightness temperature measurements and the core shift measurements in order to compare the two methods.

We have found 48 sources meeting the following conditions: (i) the observational angle of a jet must be small enough for the model of head-on jet for B_{uni} can be applied; (ii) the source has a measured core shift, central black hole mass, and the apparent opening angle. We use the following samples: we take the brightness temperature measured by Kovalev et al. (2005) and the core shifts by Pushkarev et al. (2012). The apparent velocity β_{app} we take from Lister et al. (2009). We also use the black hole masses M_{BH} and the accretion luminosities L_{acc} collected by Zamaninasab et al. (2014). For the unknown Lorentz factor we use $\Gamma = \sigma_M$, and the Michel's magnetization parameter σ_M has been evaluated by Nokhrina et al. (2015), We use for the observed opening angle the results from Pushkarev et al. (2009). This is in contrast with Zamaninasab et al. (2014), where the causal connectivity across the jet $\Gamma\chi \sim 1$ is assumed. We obtain the magnetic field magnitudes using the above values and Equations (7) and (8). On average, the values of B_{uni} is less and more scattered than values of B_{cs}, which is in agreement with results obtained in Zdziarski et al. (2015). To calculate the flux using B_{cs} we employ $R_j = \chi \times 1$ pc. For B_{uni} we use Equation (10), so we define $R_j = r_{core}\chi$.

One of the possible upper limits on the magnetic field amplitude in relativistic jets may be imposed by MAD model. Magnetically arrested disk is a disk in a state of equilibrium of the accretion rate and the pressure of magnetic field frozen in previously accreted matter (Narayan et al., 2003; Tchekhovskoy et al., 2011; McKinney et al., 2012). There is observational support of AGNs staying in MAD state (Zamaninasab et al., 2014). Equation (18) relate the total magnetic flux in a jet with the observable jet radius, magnetic field, gravitational radius (through the black hole mass estimates), and unknown rotation rate a. Setting Ψ_{MAD} as the upper limit on a magnetic flux, one can obtain the lower limit for the rotational rate of a central black hole. Here we compare the magnetic flux Ψ calculated with expression (Equation 18) for B_{uni}, obtained by the brightness temperature measurements, or B_{cs} obtained by core shift measurements, and the magnetic flux Ψ_{MAD} set by MAD model. In order to obtain the magnetic flux predicted by MAD Ψ_{MAD}, we use the equation (Zamaninasab et al., 2014)

$$\Psi_{MAD} \approx 50\sqrt{\dot{M} r_g^2 c}, \quad (19)$$

where we use relation between disk luminosity $L_{acc} = \eta \dot{M} c^2$.

The results for Ψ calculated for $a = 0.5$ and Ψ_{MAD} are presented in **Table 1**. We present in the table the values for Ψ_{MAD} (Zamaninasab et al., 2014), the total magnetic flux obtained using brightness temperature measurements Ψ_{br} and core shift measurements Ψ_{cs}. We see the reasonable agreement between Ψ_{br} and Ψ_{cs}, although the former is more scattered. We see that $a\Psi \ll \Psi_{MAD}$ for almost all the sources for magnetic filed estimates by both methods. If we assume that all the sources are in MAD state, the rotational rate of a black hole must be in a range (0.0001; 0.1) for 36 sources. Only 12 have the rotational rate between 0.1 and 1. Thus, assumption of the sources being in the MAD state leads us to a conclusion that the rotation must be much less than the critical one.

Otherwise, we may assume that 36 sources have rotation parameters close to critical $a \in [0.5;\ 1]$, but not in a MAD state. We must stress that the expressions for the magnetic field estimate through the core shift measurement are different here from the one used in Zamaninasab et al. (2014). In this paper the Equation (8) uses the assumtions from Nokhrina et al. (2015) of the total outflow magnetization equal to the unity. This condition means that the total Poynting flux in a core region is equal to the total bulk particle kinetic energy flux, with about 1% (Sironi et al., 2013) of radiating particles having the relativistic energy distribution (Equation 2). This assumption has been used to estimate maximal possible Lorentz

TABLE 1 | Jet important observed and derived parameters.

Source (1)	z (2)	Ψ_{MAD} G cm^2 (3)	Ψ_{br} G cm^2 (4)	Ψ_{cs} G cm^2 (5)	P_Ψ [erg s^{-1}] (6)	P_{jet} [erg s^{-1}] (7)
0133+476	0.859	5.51×10^{33}	1.17×10^{31}	5.34×10^{32}	1.92×10^{46}	2.54×10^{45}
0212+735	2.367	5.77×10^{35}	5.97×10^{32}	8.93×10^{32}	8.10×10^{43}	5.17×10^{45}
0234+285	1.206	5.71×10^{34}	1.24×10^{34}	5.31×10^{32}	8.65×10^{44}	3.52×10^{45}
0333+321	1.259	9.36×10^{34}	6.00×10^{32}	3.81×10^{32}	3.88×10^{44}	6.72×10^{45}
0336−019	0.852	1.55×10^{34}	1.45×10^{32}	2.12×10^{33}	6.31×10^{46}	3.26×10^{45}
0403−132	0.571	3.00×10^{34}	4.34×10^{33}	1.09×10^{33}	6.89×10^{45}	4.45×10^{45}
0528+134	2.070	6.05×10^{34}	1.61×10^{30}	3.24×10^{32}	7.75×10^{44}	5.85×10^{45}
0605−085	0.870	1.68×10^{34}	9.94×10^{33}	1.70×10^{33}	4.45×10^{46}	2.39×10^{45}
0736+017	0.189	6.94×10^{32}	3.86×10^{30}	1.29×10^{33}	2.68×10^{48}	4.20×10^{44}
0738+313	0.631	1.48×10^{35}	3.22×10^{33}	2.71×10^{33}	4.51×10^{45}	1.48×10^{45}
0748+126	0.889	4.33×10^{34}	1.39×10^{32}	1.90×10^{33}	2.31×10^{46}	2.65×10^{45}
0827+243	0.943	1.81×10^{34}	1.72×10^{32}	6.87×10^{32}	6.62×10^{45}	1.80×10^{45}
0836+710	2.218	1.78×10^{35}	7.19×10^{31}	8.30×10^{32}	1.11×10^{45}	1.78×10^{46}
0906+015	1.026	9.81×10^{33}	5.66×10^{32}	3.90×10^{32}	1.02×10^{46}	3.05×10^{45}
0917+624	1.453	2.25×10^{34}	3.93×10^{33}	5.62×10^{32}	3.68×10^{45}	4.07×10^{45}
0945+408	1.249	2.27×10^{34}	1.29×10^{32}	2.32×10^{33}	4.75×10^{46}	6.30×10^{45}
1,038+064	1.265	4.33×10^{34}	1.16×10^{32}	8.49×10^{32}	3.51×10^{45}	4.32×10^{45}
1,127−127	1.184	7.44×10^{34}	2.10×10^{32}	3.45×10^{33}	2.53×10^{46}	8.94×10^{45}
1,156+295	0.725	6.33×10^{33}	3.48×10^{31}	8.91×10^{32}	5.58×10^{46}	3.89×10^{45}
1,219+285	0.103	2.83×10^{32}	4.34×10^{33}	2.29×10^{33}	1.85×10^{47}	1.90×10^{44}
1,222+216	0.434	1.50×10^{34}	6.71×10^{33}	2.28×10^{33}	8.01×10^{46}	1.90×10^{45}
1,253−055	0.536	2.76×10^{33}	3.93×10^{30}	5.84×10^{33}	7.93×10^{48}	6.31×10^{45}
1,308+326	0.997	1.11×10^{34}	4.89×10^{32}	8.28×10^{32}	2.10×10^{46}	2.79×10^{45}
1,334−127	0.539	1.28×10^{33}	1.01×10^{29}	1.27×10^{32}	1.49×10^{46}	1.71×10^{45}
1,458+718	0.904	5.84×10^{34}	2.83×10^{31}	3.03×10^{33}	2.70×10^{46}	1.33×10^{46}
1,502+106	1.839	2.17×10^{34}	3.48×10^{31}	1.43×10^{33}	5.70×10^{46}	4.92×10^{45}
1,510−089	0.360	2.30×10^{33}	1.01×10^{31}	1.42×10^{33}	6.79×10^{47}	1.22×10^{45}
1,546+027	0.414	5.84×10^{33}	1.11×10^{30}	8.20×10^{33}	6.53×10^{48}	6.10×10^{44}
1,606+106	1.232	2.44×10^{34}	1.86×10^{33}	3.95×10^{33}	1.51×10^{47}	5.30×10^{45}
1,611+343	1.400	5.21×10^{34}	6.59×10^{32}	8.55×10^{33}	2.57×10^{47}	8.44×10^{45}
1,633+382	1.813	4.53×10^{34}	1.20×10^{32}	1.53×10^{33}	1.14×10^{46}	8.48×10^{45}
1,637+574	0.751	5.51×10^{34}	7.76×10^{32}	1.89×10^{33}	1.09×10^{46}	1.88×10^{45}
1,641+399	0.593	5.64×10^{34}	9.82×10^{31}	2.86×10^{33}	1.99×10^{46}	5.13×10^{45}
1,655+077	0.621	1.65×10^{32}	1.77×10^{32}	1.21×10^{32}	3.39×10^{47}	2.33×10^{45}
1,749+096	0.322	7.70×10^{33}	3.28×10^{29}	3.62×10^{33}	3.19×10^{47}	6.10×10^{44}
1,803+784	0.680	1.11×10^{33}	1.04×10^{31}	9.88×10^{32}	1.19×10^{48}	2.23×10^{45}
1,823+568	0.664	7.61×10^{32}	7.49×10^{31}	1.32×10^{33}	1.93×10^{48}	2.52×10^{45}
1,828+487	0.692	5.21×10^{33}	5.52×10^{31}	1.26×10^{33}	2.04×10^{47}	1.56×10^{46}
1,849+670	0.657	1.14×10^{34}	6.34×10^{31}	9.40×10^{33}	1.79×10^{48}	1.22×10^{45}
1,928+738	0.302	5.27×10^{33}	2.58×10^{31}	6.78×10^{32}	7.75×10^{46}	1.40×10^{45}
2,121+053	1.941	3.10×10^{34}	4.34×10^{30}	1.77×10^{32}	7.27×10^{44}	3.99×10^{45}
2,155−152	0.672	3.64×10^{32}	1.94×10^{32}	2.44×10^{31}	3.32×10^{45}	2.43×10^{45}
2,200+420	0.069	9.05×10^{32}	3.27×10^{30}	1.54×10^{34}	6.95×10^{49}	1.20×10^{44}
2,201+315	0.295	2.61×10^{34}	2.54×10^{31}	5.06×10^{32}	2.85×10^{45}	8.80×10^{44}
2,230+114	1.037	2.27×10^{34}	2.64×10^{30}	2.82×10^{32}	9.27×10^{44}	9.25×10^{45}
2,251+158	0.859	1.81×10^{34}	4.89×10^{32}	1.05×10^{33}	3.85×10^{46}	9.39×10^{45}
2,345−167	0.576	3.36×10^{33}	1.32×10^{32}	4.36×10^{32}	1.84×10^{46}	2.21×10^{45}
2,351+456	1.986	5.84×10^{34}	3.36×10^{33}	6.56×10^{32}	9.56×10^{44}	8.54×10^{45}

Columns are as follows: (1) source name (B1950); (2) redshift z as collected by Lister et al. (2013); (3) the MAD magnetic flux obtained using Equation (19); (4) derived total magnetic flux using the brightness temperature measurements; (5) derived total magnetic flux using the core shift measurements; (6) The jet power estimate using the magnetic field B_{cs}; (7) the total jet power estimated using the correlation between the jet power and radio flux (Cavagnolo et al., 2010), collected from Nokhrina et al. (2015).

factor of the flow (Nokhrina et al., 2015), which correlates very good with the Lorentz factor estimates basing the observed super-luminal velocities (Lister et al., 2009). In this point our approach differs from the one used by Zamaninasab et al. (2014).

In order to check our flux estimates, we test it against the total jet power (Equation 1). This result is robust under the model assumptions, since it the total power depends on a very weakly. The calculation of the total jet power for the obtained flux is in **Table 1**. We compare the total power P_Ψ, calculated substituting Equation (18) into Equation (1), with the jet power, estimated basing on the correlation of $P_{\rm jet}$ with the luminosities of jet radio band Cavagnolo et al. (2010):

$$\left(\frac{P_{\rm jet}}{10^{43}\ {\rm erg\ s^{-1}}}\right) = 3.5\left(\frac{P_{200-400}}{10^{40}\ {\rm erg\ s^{-1}}}\right)^{0.64}. \qquad (20)$$

We plot P_Ψ against the obtained with Equation (20) power $P_{\rm jet}$ in **Figure 1**. We observe the reasonable correlation of P_Ψ and $P_{\rm jet}$. The histogram of the ratio of $P_\Psi/P_{\rm jet}$ is presented in **Figure 2**. We see that the ratio has a well determined peak around a few. Although it gives the systematic excess of P_Ψ over $P_{\rm jet}$, we state that P_Ψ is in accordance with $P_{\rm jet}$ bearing in mind uncertainties in the determination of all the values including $P_{\rm tot}$. The systematic excess may be attributed to the probable overestimating the magnetic field $B_{\rm cs}$, the hints of which we see in discrepancy between $B_{\rm cs}$ and $B_{\rm br}$, the latter being lower.

We have also tested the jet power obtained with the flux determined by $B_{\rm uni}$ (see **Figure 1**). The second method provides systematically lower powers and more scattering. This is in agreement with the result by Zdziarski et al. (2015) who have found the scattering in magnetic field amplitude calculated with no equipartition assumption while still have the majority of sources having the equipartition magnetic field.

4. SUMMARY

We have discussed estimates for the magnetic flux using the jet core magnetic field obtained through the brightness temperature measurements and by the core shift effect. Usually, any estimates of the magnetic field in a radiating domain of relativistic jet cannot be readily put into the expression for the magnetic flux. This is because theoretical modeling show, that the toroidal magnetic field dominates the poloidal magnetic field outside the light cylinder. Thus, the field we measure using synchrotron self-Compton model of radiation, must be toroidal, while the magnetic flux is determined by the poloidal one. Consideration of transversal field configuration is needed to estimate accurately the magnetic flux in a jet using the available evaluation of magnetic field magnitude through observations—either using the core-shift effect, or spectral flux measurements. In this work has been considered the simplest case—the transversal structure of jets observed with very small viewing angle.

We test the method of estimating the flux against the limiting flux determined by the magnetically arrested disk model. For 36 of 48 sources the obtained flux is much less than the MAD flux. This suggest either the extremely slow rotation rate $a \in (0.0001;\ 0.1)$ or that the sources are not in MAD state. For 12 sources both fluxes coincide for $a \in (0.1;\ 1)$—the fast rotation that is needed for the efficient energy extraction from a black hole.

We also test the flux estimate against the total jet power determined by the electromagnetic mechanism of energy

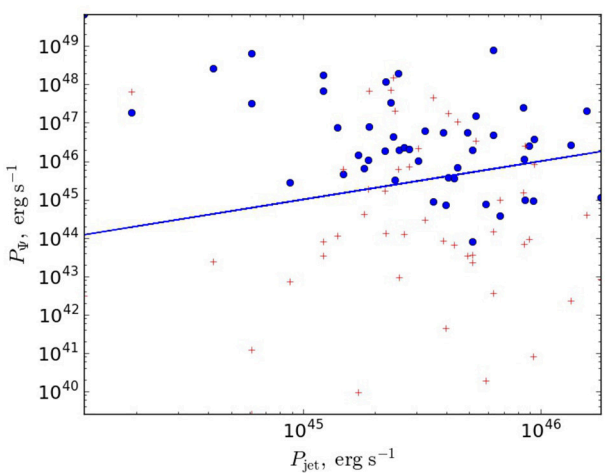

FIGURE 1 | The jet power P_Ψ, calculated using magnetic flux, against the total kinetic jet power. The straight line is a theoretical prediction. The blue circle stand for the total flux obtained using the core shift effect, the red crosses are for the total flux obtained using the brightness temperature. The sources with the flux approximately equal to the MAD flux are in the upper left corner.

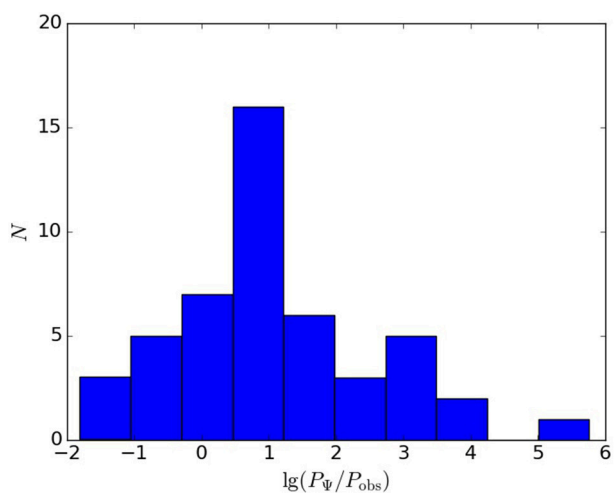

FIGURE 2 | The histogram showing the number of sources with the ration of calculated power P_Ψ to the total jet power $P_{\rm jet}$, the ratio is in the log-scale. We see the systematic excess of power estimated through the flux against the jet power by a factor of few.

extraction. This result does not depend on the particular value for a, as the Expression (Equation 1) depends on the product of Ψ and $a\ \Psi_a$ that can be estimated directly. In this case we see a good agreement between the total power determined by the flux and the total power obtained from the observations, with the distribution of powers ration being well peaked around a few.

AUTHOR CONTRIBUTIONS

The results presented in the paper has been obtained by EN.

FUNDING

This work was supported by Russian Science Foundation, grant 16-12-10051.

ACKNOWLEDGMENTS

The author thanks the referees for the suggestions which helped to improve the paper. This research has made use of data from the MOJAVE database that is maintained by the MOJAVE team (Lister et al., 2009).

REFERENCES

Abdo, A., Ackermann, M., Ajello, M., Baldini, L., Ballet, J., Barbiellini, G., et al. (2011). Fermi large area telescope observations of markarian 421: the missing piece of its spectral energy distribution. *Astrophys. J.* 736:131. doi: 10.1088/0004-637X/736/2/131

Beskin, V. (2010). Magnetohydrodynamic models of astrophysical jets. *Phys. Uspekhi* 53, 1199–1233. doi: 10.3367/UFNe.0180.201012b.1241

Beskin, V., and Nokhrina, E. (2009). On the central core in MHD winds and jets. *Month. Notices R. Astron. Soc.* 397, 1486–1497. doi: 10.1111/j.1365-2966.2009.14964.x

Blanford, R., and Königl, A. (1979). Relativistic jets as compact radio sources. *Astrophys. J.* 232, 34–48. doi: 10.1086/157262

Blanford, R., and Znajek, R. (1977). Electromagnetic extraction of energy from kerr black holes. *Month. Notices R. Astron. Soc.* 179, 433–456. doi: 10.1093/mnras/179.3.433

Bromberg, O., and Tchekhovskoy, A. (2016). Relativistic mhd simulations of core-collapse GRB jets: 3d instabilities and magnetic dissipation. *Month. Notices R. Astron. Soc.* 456, 1739–1760. doi: 10.1093/mnras/stv2591

Cavagnolo, K., McNamara, B., Nulsen, P., Carilli, C., Jones, C., and Brzan, L. (2010). A relationship between agn jet power and radio power. *Astrophys. J.* 720, 1066–1072. doi: 10.1088/0004-637X/720/2/1066

Cohen, M., Lister, M., Homan, D., Kadler, M., Kellermann, K., Kovalev, Y., et al. (2007). Relativistic beaming and the intrinsic properties of extragalactic radio jets. *Astrophys. J.* 658, 232–244. doi: 10.1086/511063

Gould, R. (1979). Compton and synchrotron processes in spherically-symmetric non-thermal sources. *Astron. Astrophys.* 76, 306–311.

Hirotani, K. (2005). Kinetic luminosity and composition of active galactic nuclei jets. *Astrophys. J.* 619, 73–85. doi: 10.1086/426497

Kovalev, Y., Kellermann, K., Lister, M., Homan, D., Vermeulen, R., Cohen, M., et al. (2005). Sub-milliarcsecond imaging of quasars and active galactic nuclei. IV. Fine-scale structure. *Astron. J.* 130, 2473–2505. doi: 10.1086/497430

Lister, M., Aller, H., Aller, M., Cohen, M., Homan, D., Kadler, M., et al. (2009). MOJAVE: monitoring of jets in active galactic nuclei with VLBA experiments. V. Multi-epoch VLBA images. *Astron. J.* 137, 3718–3729. doi: 10.1088/0004-6256/137/3/3718

Lister, M., Aller, M., Aller, H., Homan, D., Kellermann, K., Kovalev, Y., et al. (2013). MOJAVE. X. Parsec-scale jet orientation variations and superluminal motion in active galactic nuclei. *Astron. J.* 146, 120–142. doi: 10.1088/0004-6256/146/5/120

Lobanov, A. (1998). Ultracompact jets in active galactic nuclei. *Astron. Astrophys.* 330, 79–89.

Lyubarsky, Y. (2009). Asymptotic structure of poynting-dominated jets. *Astrophys. J.* 698, 1570–1589. doi: 10.1088/0004-637X/698/2/1570

McKinney, J., Tchekhovskoy, A., and Blandford, R. (2012). General relativistic magnetohydrodynamic simulations of magnetically choked accretion flows around black holes. *Month. Notices R. Astron. Soc.* 423, 3083–3117. doi: 10.1111/j.1365-2966.2012.21074.x

Narayan, R., Igumenshchev, I., and Abramowicz, M. (2003). Magnetically arrested disk: an energetically efficient accretion flow. *Publ. Astron. Soc. Jpn.* 55, L69–L72. doi: 10.1093/pasj/55.6.L69

Nokhrina, E. (2017). Brightness temperature - obtaining the physical properties of a non-equipartition plasma. *Month. Notices R. Astron. Soc.* 468, 2372–2381. doi: 10.1093/mnras/stx521

Nokhrina, E., Beskin, V., Kovalev, Y., and Zheltoukhov, A. (2015). Intrinsic physical conditions and structure of relativistic jets in active galactic nuclei. *Month. Notices R. Astron. Soc.* 447, 2726–2737. doi: 10.1093/mnras/stu2587

OŚullivan, S., and Gabuzda, D. (2009). Magnetic field strength and spectral distribution of six parsec-scale active galactic nuclei jets. *Month. Notices R. Astron. Soc.* 400, 26–42. doi: 10.1111/j.1365-2966.2009.15428.x

Pushkarev, A., Hovatta, T., Kovalev, Y., Lister, M., Lobanov, A., Savolainen, T., et al. (2012). MOJAVE: monitoring of jets in active galactic nuclei with VLBA experiments. IX. Nuclear opacity. *Astron. Astrophys.* 545:A113. doi: 10.1051/0004-6361/201219173

Pushkarev, A., Kovalev, Y., Lister, M., and Savolainen, T. (2009). Jet opening angles and gamma-ray brightness of AGN. *Astron. Astrophys.* 507, L33–L36. doi: 10.1051/0004-6361/200913422

Sironi, L., Spitkovsky, A., and Arons, J. (2013). The maximum energy of accelerated particles in relativistic collisionless shocks. *Astrophys. J.* 771:54. doi: 10.1088/0004-637X/771/1/54

Tchekhovskoy, A., McKinney, J. C., and Narayan, R. (2012). General relativistic modeling of magnetized jets from accreting black holes. *J. Phys.* 372:012040. doi: 10.1088/1742-6596/372/1/012040

Tchekhovskoy, A., Narayan, R., and McKinney, J. (2011). Efficient generation of jets from magnetically arrested accretion on a rapidly spinning black hole. *Month. Notices R. Astron. Soc.* 418, L79–L83. doi: 10.1111/j.1745-3933.2011.01147.x

Zamaninasab, M., Clausen-Brown, E., Savolainen, T., and Tchekhovskoy, A. (2014). Dynamically important magnetic fields near accreting supermassive black holes. *Nature* 510, 126–128. doi: 10.1038/nature13399

Zdziarski, A., Sikora, M., Pjanka, P., and Tchekhovskoy, A. (2015). Core shifts, magnetic fields and magnetization of extragalactic jets. *Month. Notices R. Astron. Soc.* 451, 927–935. doi: 10.1093/mnras/stv986

Conflict of Interest Statement: The author declares that the research was conducted in the absence of any commercial or financial relationships that could be construed as a potential conflict of interest.

Copyright © 2017 Nokhrina. This is an open-access article distributed under the terms of the Creative Commons Attribution License (CC BY). The use, distribution or reproduction in other forums is permitted, provided the original author(s) or licensor are credited and that the original publication in this journal is cited, in accordance with accepted academic practice. No use, distribution or reproduction is permitted which does not comply with these terms.

frontiers in Astronomy and Space Sciences

ORIGINAL RESEARCH
published: 12 October 2017
doi: 10.3389/fspas.2017.00022

Confrontation of the Magnetically Arrested Disc Scenario with Observations of FR II Sources

Katarzyna Rusinek and Marek Sikora*

Nicolaus Copernicus Astronomical Center, Polish Academy of Sciences, Warsaw, Poland

The main aim of our work was to check whether powers of jets in FR II radio galaxies (RGs) and quasars (QSOs) can be reproduced by the Magnetically Arrested Disc (MAD) scenario. Assuming that established in the recent numerical simulations of the MAD scenario the $(H/R)^2$ dependence of the jet production efficiency is correct, we demonstrate that in order to reproduce the observed jet powers in FR II sources: (i) accretion discs must be geometrically much thicker than the standard ones; (ii) and/or that the jet production is strongly modulated.

Keywords: active galactic nuclei (AGN), quasars, relativistic jets, accretion discs, magnetically arrested disc (MAD)

OPEN ACCESS

Edited by:
Paola Marziani, Osservatorio Astronomico di Padova (INAF), Italy

Reviewed by:
Milan S. Dimitrijevic, Belgrade Astronomical Observatory, Serbia
Brian Punsly, International Center for Relativistic Astrophysics, Italy

****Correspondence:***
Katarzyna Rusinek
krusinek@camk.edu.pl

Specialty section:
This article was submitted to Cosmology, a section of the journal Frontiers in Astronomy and Space Sciences

Received: *29 August 2017*
Accepted: *27 September 2017*
Published: *12 October 2017*

Citation:
Rusinek K and Sikora M (2017) Confrontation of the Magnetically Arrested Disc Scenario with Observations of FR II Sources. Front. Astron. Space Sci. 4:22. doi: 10.3389/fspas.2017.00022

1. INTRODUCTION

The primary division of Active Galactic Nuclei (AGNs) is based on their radio loudness which is defined as the ratio of radio luminosity (typically 5 GHz) to the optical luminosity (typically in B band). Minority of AGNs are known to be radio-loud (10% in case of QSOs, Kellermann et al., 1989) and their radio loudness is sometimes even up to 3–4 orders of magnitude higher than that of radio-quiet AGNs. Moreover, which was found in last years (Rawlings and Saunders, 1991; Punsly, 2007; Fernandes et al., 2011; Sikora et al., 2013), jet powers P_j of many radio galaxies reach values comparable to the accretion powers $\dot{M}c^2$, where $\dot{M}$ is the mass accretion rate. In order to produce jets with such high efficiencies, $\eta_j \equiv P_j/(\dot{M}c^2) \simeq 1$, by the Blandford and Znajek (1977) mechanism, the amount of the magnetic flux required to be accumulated on the black hole (BH) is so large that it can only be maintained if it is confined by the ram pressure of the accreting plasma (Sikora and Begelman, 2013). This affects the accretion flow in such a way that the innermost portion of the accretion flow is dynamically dominated by the poloidal magnetic field causing that accretion proceeds via interchange instabilities. This scenario is called Magnetically Arrested Disc (MAD, Narayan et al., 2003; Igumenshchev, 2008; Punsly et al., 2009; Tchekhovskoy et al., 2011; McKinney et al., 2012).

Even though the MAD scenario appears to be an attractive and plausible way to explain the existence of the most powerful jets in radio-loud FR II AGNs (which as described by Fanaroff and Riley, 1974, are characterized by edge-brightened radio structures in contrast to centre-brightened RGs of class I), there are still some open problems. One of them is to establish which parameters truly decide on the MAD occurrence. Assuming that the jet production efficiency depends mostly on the BH spin, van Velzen and Falcke (2013) showed that in fact it is not a dominant parameter for powering jets. Furthermore, since the observed mean efficiency of their FR II quasars sample is much lower than maximal predicted by the MAD model, they concluded that this mechanism does not occur in these sources. On the other hand, in their recent studies, Avara et al. (2016) performed numerical simulations of thin MADs in order to investigate its efficiencies. They found

that not only BH spin a but also a geometrical thickness H/R (where H is the disc height and R is the distance from the black hole) contributes to the jet power efficiency as $\eta_j \sim a^2(H/R)^2$. Their results confirm that the MAD scenario can be responsible for explaining powerful jet systems but also point out that at moderate accretion rates discs must be geometrically thicker than the standard theory predicts.

Given the above we checked whether jet powers in FR II radio galaxies and quasars can be reproduced by the MAD scenario. Our studies were thoroughly described in Rusinek et al. (2017). In this paper we briefly outline samples we used and discuss the origins of results we obtained, especially focusing on the importance of geometrical thickness of accretion discs and modulation of jet production.

2. SAMPLES AND ANALYSIS

In order to adequately assess the distribution of radio galaxies and quasars in the P_j/L_d – $\lambda_{\rm Edd}$ plane (where L_d is the bolometric disc luminosity and $\lambda_{\rm Edd}$ is the Eddington ratio) we have combined four different samples of these sources. We used radio and optical data to calculate necessary values. Including both low- as well as high-redshift objects allowed us to check if cosmological evolution of jet production may have an impact on our final results.

2.1. Samples

1. FR II Narrow-Line Radio Galaxies (NLRGs) were extracted from the sample of $z < 0.4$ radio galaxies with extended radio structure selected by Sikora et al. (2013). The objects are taken from Cambridge catalogues and matched with the SDSS (Sloan Digital Sky Survey), FIRST (Faint Images of the Radio Sky at 20 cm) and NVSS (National Radio Astronomy Observatory (NRAO) Very Large Array (VLA) Sky Survey) catalogues. Due to the available optical data, this sample contains 152 sources;
2. FR II quasar sample was obtained by van Velzen et al. (2015) on the selection of double-lobed radio sources from the FIRST survey catalog, and cross-matching with SDSS quasars. The BH masses and Eddington ratios, when available, were taken from Shen et al. (2011) thereby reducing the sample from 458 to 414 objects;
3. FR II NLRGs selected in $0.9 < z < 1.1$ were taken from Fernandes et al. (2011, 2015). The main reason of adding these sources was to verify how much the incompleteness of very massive BHs in the local Universe affects the jet production efficiency FR II NLRGs (the first sample). This sample contains 27 objects;
4. Low-redshift Broad-Line Radio Galaxies (BLRGs) and radio-loud quasars (RLQs) were used by Sikora et al. (2007) to study radio loudness of these objects. We decided to add this sample (86 sources) to check if the incompleteness of SDSS quasars at moderate accretion rates (the second sample) can significantly influence the average value of P_j/L_d of the FR II quasar sample.

2.2. Jet Production Efficiency

For each of mentioned in the previous paragraph samples we calculated the following properties:

– The jet power P_j was obtained from the different radio luminosities (from the range of 151 MHz to 5 GHz) according to the formula based on calorimetry of radio lobes which was proposed by Willott et al. (1999) as

$$P_j[\mathrm{erg\,s^{-1}}] = 5.0 \times 10^{22}(f/10)^{3/2}(L_{1.4}[\mathrm{W\,Hz^{-1}}])^{6/7}, \quad (1)$$

where f is the parameter accounting for errors in the model assumptions. Its value (typically between 10 and 20, Blundell and Rawlings, 2000) is established based on comparing jet powers of luminous FR II sources calculated from the model of hotspots Godfrey and Shabala (2013) and the one provided by Willott et al. (1999), and is adpoted as $f = 10$;

– The bolometric disc luminosity L_d which is related to the line or optical/IR luminosities via respective bolometric corrections. It is used as a proxy of the accretion power $\dot{M}c^2 = L_d/\epsilon_d$ where ϵ_d is the disc radiation efficiency depending on BH spin. In standard disc theory it is assumed to be $\epsilon_d = 0.1$;

– The Eddington luminosity $L_{\rm Edd}$ which is necessary to establish the Eddington ratio $\lambda_{\rm Edd} \equiv L_d/L_{\rm Edd}$ describing the accretion rate, $L_{\rm Edd} \propto M_{\rm BH}$ where $M_{\rm BH}$ is the BH mass.

We have adopted the Λ cold dark matter (ΛCDM) cosmology with $H_0 = 70\mathrm{km\,s^{-1}}$, $\Omega_m = 0.3$ and $\Omega_\Lambda = 0.7$. Uncertainties of P_j/L_d and $\lambda_{\rm Edd}$, calculated as standard deviations of ratios of two independently determined quantities, are not bigger than 0.4 dex for each of the samples. All details about samples and methods used to estimate our calculations are described in Rusinek et al. (2017).

2.3. Results

The dependence of P_j/L_d on the $\lambda_{\rm Edd}$ for all four samples is presented in **Figure 1**. The distribution of all objects confirms the trend of the increase of P_j/L_d with decreasing Eddington ratio (Sikora et al., 2007). All samples are pretty consistent with each other: $z < 0.4$ FR II NLRGs and $0.9 < z < 1.1$ NLRGs samples have similar median of P_j/L_d at moderate accretion rates (which corresponds to $\lambda_{\rm Edd} > 0.003$); FR II quasars and BLRGs+RLQs samples overlap each other.

The horizontal dashed line marks the upper limits for P_j/L_d predicted by the MAD model for the maximal BH spin and adopting $\epsilon_d = 0.1$. The inclined dashed line results from the dependence of the jet production efficiency on H/R given as

$$\eta_j \simeq 4a^2\left(1 + \frac{0.3a}{1 + 2(H/R)^4}\right)^2 (H/R)^2 \quad (2)$$

(Avara et al., 2016). For $0.03 < \lambda_{\rm Edd} < 1.0$ discs have $H/R \geq 1$ and then such a dependence disappears. The existence of objects in the shaded area, which represents a significant fraction of all studied sources, contradicts with the above predictions and challenges current jet production theories.

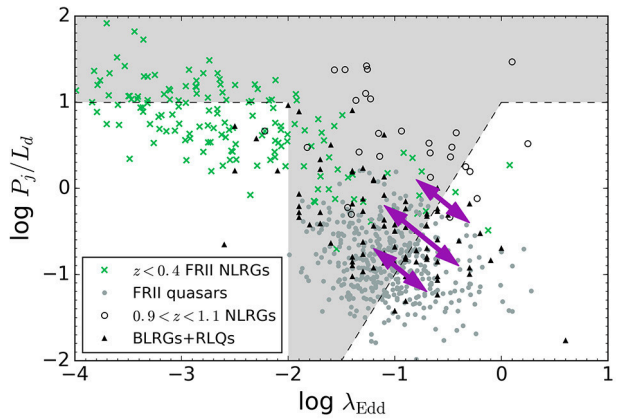

FIGURE 1 | The dependence of P_j/L_d on the $\lambda_{\rm Edd}$ for all samples: $z < 0.4$ FR II NLRGs as green crosses; FR II quasars as grey dots; $0.9 < z < 1.1$ NLRGs as empty circles; BLRGs+RLQs as black triangles. The horizontal dashed line corresponds to $P_j = (\epsilon_d/0.1)\dot{M}c^2$. The inclined dashed line is derived from the Equation (2) for $a = 0.5$ and assuming a correct normalization. The presence of objects in the shaded region of the plot calls into question our underlying assumptions. Purple arrows show how the modulation of jet production affects the $P_j/L_d - \lambda_{\rm Edd}$ distribution.

3. DISCUSSION

Depending on the Eddington ratio few different explanations for obtained by us jet powers can be proposed. The transition from Radiatively Inefficient, optically thin Accretion Flows (RIAF) to the standard, optically thick accretion discs occurs at $\lambda_{\rm Edd} \simeq 0.01$ (Best and Heckman, 2012). At lower Eddington ratios the disc radiative efficiency ϵ_d is expected to be much lower than usually assumed 0.1 and this can explain the presence of objects with $P_j/L_d > 10$ in this area. At higher Eddington ratios there are still some sources with $P_j/L_d > 10$. All of them belong to the $0.9 < z < 1.1$ NLRGs sample for which the bolometric disc luminosity was calculated from the mid-IR data. As it was pointed out by Ogle et al. (2006) this method is not very accurate and therefore discs luminosities of sources taken from Fernandes et al. (2011) may be overestimated.

The presence of objects in the shaded area corresponding to moderate accretion ratios and above the sloping dashed line may indicate that the accretion discs are thicker than the standard ones or/and that the jet production is modulated. However it should be noted here that the extension of the shaded area towards $P_j/L_d \ll 1$ on the **Figure 1** may be inappropriate by noting that the dependence of the jet production efficiency on geometrical thickness of the disk given by Equation (2) can be overestimated resulting from the very approximate treatment of the radiative transfer in Avara et al. (2016) simulations and by not including contribution to the vertical pressure in the MAD zone from toroidal magnetic fields.

3.1. Thicker Accretion Discs

Assuming maximally rotating black hole with $a = 1$ and producing radiation at a rate $\lambda_{\rm Edd} \sim 0.01$, the standard accretion disc model (Novikov and Thorne, 1973; Laor and Netzer, 1989) predicts that the maximal value of geometrical thickness of the disc is $H/R \sim 0.4$ which gives the jet production efficiency equal to 0.01 (from the Equation 2). This value is much lower than the median value of FR II quasars sample as well as its upper bound in the $P_j/L_d - \lambda_{\rm Edd}$ plot. This discrepancy can be explained if instead of optically thick, geometrically thin standard disc the thicker ones will be considered. These kind of discs have been proposed to avoid gravitational and thermal instabilities in gas and radiation pressure supported discs and they can be formed in presence of strong toroidal magnetic fields (e.g., Begelman and Pringle, 2007; Sądowski, 2016).

Different approach assumes the existence of moderately hot, optically thick and massive layer on top of the relatively colder, accretion disc which stays geometrically thin and optically thick as it was originally developed by Shakura and Sunyaev (1973). Różańska et al. (2015), and Begelman et al. (2015) proved that the model of heavly, viscously driven corona is real if the disc/corona system is stabilized by either strong magnetic fields or vertical outflows. The massive, dense coronas can also arise during the transition from Shakura and Sunyaev (1973) discs to Advection-Dominated Acretion Flows (ADAFs, Abramowicz et al., 1995; Narayan and Yi, 1995) which the transition coincides with the Luminous Hot Accretion Flow (LHAF, Yuan, 2003; Yuan and Narayan, 2014).

3.2. Modulation of Jet Production

Another worth considering idea which may explain the visible $P_j/L_d - \lambda_{\rm Edd}$ distribution is taking into account the variability of accretion rate. The method we used to establish jet powers is based on the total energy content of the radio lobes. Their lifetime is long (even up to 10^8 years, Komissarov and Gubanov, 1994) so the only possibility of observing variations of jet powers is connected with the hotspot luminosity which may vary on much shorter time-scales. Hotspots however make a small contribution to the total radio luminosity (Mullin et al., 2008) as a result of which jet powers from integrated lobe luminosities are not significantly affected by the variability of the accretion rate. This property may be noticed in the disc luminosity though, which is a direct measure of instantaneous accretion rate. Taken together these findings implicate a modulation of both, the "apparent" jet production efficiency as well as the Eddington ratio in such a way that with decreasing $\lambda_{\rm Edd}$ the P_j/L_d increases. This causes the stretching with the slope -1 on the plot which is presented as the set of arrows on the **Figure 1**. just as the sources are distributed. Variability of accretion rate may be naturally caused by the viscous instabilities in accretion discs (Janiuk et al., 2002; Janiuk and Czerny, 2011).

4. SUMMARY

In this proceeding we argue that jets in FR II radio galaxies and quasars accreting at moderate accretion rates are not only powered by MAD scenario but they are also much more powerful than this mechanism predicts. We highlight two possible reasons for this discrepancy. The first one indicates that the geometrical thickness of accretion flows can have much bigger impact on jets formation and evolution than it was originally considered. Here we point out that the future work should concentrate on

the existence of thicker than the standard accretion discs as well as on systems with massive, hot coronas. The second solution focuses on the variability of accretion rate which can significantly influence observed $P_j/L_d - \lambda_{\rm Edd}$ distribution. Since estimated by us jet powers are based on the calorimetry on the radio lobes and thereby they are averaged over the lifetime of the source, an important issue to resolve for future studies is to check if using different methods for calculating jet powers such as X-ray cavities (Cavagnolo et al., 2010; Nemmen and Tchekhovskoy, 2015) or model of hotspots (Godfrey and Shabala, 2013) such a trend of decreasing $\lambda_{\rm Edd}$ with increasing P_j/L_d will be still visible.

AUTHOR CONTRIBUTIONS

Both authors made substantial, direct and intellectual contribution to the work. KR collected and analyzed presented data. MS formulated the original problem, provided direction and guidance. Both authors contributed to the discussion of the obtained results.

FUNDING

The research leading to these results has received funding from the Polish National Science Centre grant 2016/21/B/ST9/01620.

ACKNOWLEDGMENTS

We are particularly grateful to Dorota Kozieł-Wierzbowska and Leith Godfrey for their significant contribution in the analysis of the results and a crucial discussion on their possible explanations. We also thank Greg Madejski for helpful comments.

REFERENCES

Abramowicz, M. A., Chen, X., Kato, S., Lasota, J.-P., and Regev, O. (1995). Thermal equilibria of accretion disks. *Astrophys. J.* 438, L37–L39. doi: 10.1086/187709

Avara, M. J., McKinney, J. C., and Reynolds, C. S. (2016). Efficiency of thin magnetically arrested discs around black holes. *Mon. Not. R. Astron. Soc.* 462:636. doi:10.1093/mnras/stw1643

Begelman, M. C., and Pringle, J. E. (2007). Accretion discs with strong toroidal magnetic fields. *Mon. Not. R. Astron. Soc.* 375, 1070–1076. doi: 10.1111/j.1365-2966.2006.11372.x

Begelman, M. C., Armitage, P. J., and Reynolds, C. S. (2015). Accretion disk dynamo as the trigger for X-ray binary state transitions. *Astrophys. J.* 809:118. doi: 10.1088/0004-637X/809/2/118

Best, P. N., and Heckman, T. M. (2012). On the fundamental dichotomy in the local radio-AGN population: accretion, evolution and host galaxy properties. *Mon. Not. R. Astron. Soc.* 421, 1569–1582. doi: 10.1111/j.1365-2966.2012.20414.x

Blandford, R. D., and Znajek, R. L. (1977). Electromagnetic extraction of energy from Kerr black holes. *Mon. Not. R. Astron. Soc.* 179, 433–456. doi: 10.1093/mnras/179.3.433

Blundell, K. M., and Rawlings, S. (2000). The spectra and energies of classical double radio lobes. *Astron. J.* 119, 1111–1122. doi: 10.1086/301254

Cavagnolo, K. W., McNamara, B. R., Nulsen, P. E. J., Carilli, C. L., Jones, C., and Birzan, L. (2010). A relationship between AGN jet power and radio power. *Astrophys. J.* 720, 1066–1072. doi: 10.1088/0004-637X/720/2/1066

Fanaroff, B. L., and Riley, J. M. (1974). The morphology of extragalactic radio sources of high and low luminosity. *Mon. Not. R. Astron. Soc.* 167:31P. doi: 10.1093/mnras/167.1.31P

Fernandes, C. A. C., Jarvis, M. J., Rawlings, S., Martinez-Sansigre, A., Hatziminaoglou, E., Lacy, M., et al. (2011). Evidence for a maximum jet efficiency for the most powerful radio galaxies. *Mon. Not. R. Astron. Soc.* 411, 1909–1916. doi: 10.1111/j.1365-2966.2010.17820.x

Fernandes, C. A. C., Jarvis, M. J., Martínez-Sansigre, A., Rawlings, S., Afonso, J., Hardcastle, M. J., et al. (2015). Black hole masses, accretion rates and hot- and cold-mode accretion in radio galaxies at z $\sim$ 1. *Mon. Not. R. Astron. Soc.* 447, 1184–1203. doi:10.1093/mnras/stu2517

Godfrey, L. E. H., and Shabala, S. S. (2013). AGN jet kinetic power and the energy budget of radio galaxy lobes. *Astrophys. J.* 767:12. doi: 10.1088/0004-637X/767/1/12

Igumenshchev, I. V. (2008). Magnetically arrested disks and the origin of poynting jets: a numerical study. *Astrophys. J.* 677, 317–326. doi: 10.1086/529025

Janiuk, A., and Czerny, B. (2011). On different types of instabilities in black hole accretion discs: implications for X-ray binaries and active galactic nuclei. *Mon. Not. R. Astron. Soc.* 414, 2186–2194. doi: 10.1111/j.1365-2966.2011.18544.x

Janiuk, A., Czerny, B., and Siemiginowska, A. (2002). Radiation pressure instability driven variability in the accreting black holes. *Astrophys. J.* 576, 908–922. doi:10.1086/341804

Kellermann, K. I., Sramek, R., Schmidt, M., Shaffer, D. B., and Green, R. (1989). VLA observations of objects in the Palomar Bright Quasar Survey. *Astron. J.* 98, 1195–1207. doi: 10.1086/115207

Komissarov, S. S., and Gubanov, A. G. (1994). Relic radio galaxies: evolution of synchrotron spectrum. *Astron. Astrophys.* 285, 27–43

Laor, A., and Netzer, H. (1989). Massive thin accretion discs. I - Calculated spectra. *Mon. Not. R. Astron. Soc.* 238, 897–916. doi: 10.1093/mnras/238.3.897

McKinney, J. C., Tchekhovskoy, A., and Blandford, R. D. (2012). General relativistic magnetohydrodynamic simulations of magnetically choked accretion flows around black holes. *Mon. Not. R. Astron. Soc.* 423, 3083–3117. doi: 10.1111/j.1365-2966.2012.21074.x

Mullin, L. M., Riley, J. M., and Hardcastle, M. J. (2008). Observed properties of FRII quasars and radio galaxies at z < 1.0. *Mon. Not. R. Astron. Soc.* 390, 595–621. doi: 10.1111/j.1365-2966.2008.13534.x

Narayan, R., and Yi, I. (1995). Advection-dominated accretion: self-similarity and bipolar outflows. *Astrophys. J.* 444, 231–243. doi: 10.1086/175599

Narayan, R., Igumenshchev, I. V., and Abramowicz, M. A. (2003). Magnetically arrested disk: an energetically efficient accretion flow. *Publ. Astron. Soc. Japan* 55, L69–L72. doi: 10.1093/pasj/55.6.L69

Nemmen, R. S., and Tchekhovskoy, A. (2015). On the efficiency of jet production in radio galaxies. *Mon. Not. R. Astron. Soc.* 449, 316–327. doi: 10.1093/mnras/stv260

Novikov, I. D., and Thorne, K. S. (1973). "Astrophysics of black holes," in *Black Holes (Les Astres Occlus)*, eds C. Dewitt and B. S. Dewitt (New York, NY: Gordon and Breach Science Publishers), 343–450.

Ogle, P., Whysong, D., and Antonucci, R. (2006). Spitzer reveals hidden quasar nuclei in some powerful FR II radio galaxies. *Astrophys. J.* 647:161. doi: 10.1086/505337

Punsly, B. (2007). Kinetically dominated FRII radio sources. *Mon. Not. R. Astron. Soc.* 374, L10–L14. doi: 10.1111/j.1745-3933.2006.00254.x

Punsly, B., Igumenshchev, I. V., and Hirose, S. (2009). Three-dimensional simulations of vertical magnetic flux in the immediate vicinity of black holes. *Astrophys. J.* 704, 1065–1085. doi: 10.1088/0004-637X/704/2/1065

Rawlings, S., and Saunders, R. (1991). Evidence for a common central-engine mechanism in all extragalactic radio sources. *Nature* 349, 138–140. doi: 10.1038/349138a0

Różańska, A., Malzac, J., Belmont, R., Czerny, B., and Petrucci, P.-O. (2015). Warm and optically thick dissipative coronae above accretion disks. *Astron. Astrophys.* 580:A77. doi: 10.1051/0004-6361/201526288

Rusinek, K., Sikora, M., Kozieł-Wierzbowska, D., and Godfrey, L. (2017). On the efficiency of jet production in FR II radio galaxies and quasars. *Mon. Not. R. Astron. Soc.* 466, 2294–2301. doi: 10.1093/mnras/stw3330

Sądowski, A. (2016). Thin accretion discs are stabilized by a strong magnetic field. *Mon. Not. R. Astron. Soc.* 459, 4397–4407. doi: 10.1093/mnras/stw913

Shakura, N. I., and Sunyaev, R. A. (1973). Black holes in binary systems. Observational appearance. *Astron. Astrophys.* 24, 337–355

Shen, Y., Richards, G. T., Strauss, M. A., Hall, P. B., Schneider, D. P., Snedden, S., et al. (2011). A catalog of quasar properties from sloan digital sky survey data release 7. *Astrophys. J.* 194:45. doi: 10.1088/0067-0049/194/2/45

Sikora, M., and Begelman, M. C. (2013). Magnetic flux paradigm for radio loudness of active galactic nuclei. *Astrophys. J.* 764:L24. doi: 10.1088/2041-8205/764/2/L24

Sikora, M., Stawarz, Ł., and Lasota, J.-P. (2007). Radio loudness of active galactic nuclei: observational facts and theoretical implications. *Astrophys. J.* 658, 815–828. doi: 10.1086/511972

Sikora, M., Stasińska, G., Kozieł-Wierzbowska, D., Madejski, G. M., and Asari, N. V. (2013). Constraining jet production scenarios by studies of narrow-line radio galaxies. *Astrophys. J.* 765:62. doi: 10.1088/0004-637X/765/1/62

Tchekhovskoy, A., Narayan, R., and McKinney, J. C. (2011). Efficient generation of jets from magnetically arrested accretion on a rapidly spinning black hole. *Mon. Not. R. Astron. Soc.* 418, L79–L83. doi: 10.1111/j.1745-3933.2011.01147.x

Yuan, F. (2003). Luminous hot accretion flows: thermal equilibrium curve and thermal stability. *Astrophys. J.* 594, L99–L102. doi: 10.1086/378666

Yuan, F., and Narayan, R. (2014). Hot accretion flows around black holes. *Annu. Rev. Astron. Astrophys.* 52, 529–588. doi: 10.1146/annurev-astro-082812-141003

van Velzen, S., and Falcke, H. (2013). The contribution of spin to jet-disk coupling in black holes. *Astron. Astrophys.* 557:L7. doi: 10.1051/0004-6361/201322127

van Velzen, S., Falcke, H., and Körding, E. (2015). Nature and evolution of powerful radio galaxies at z $\sim$ 1 and their link with the quasar luminosity function. *Mon. Not. R. Astron. Soc.* 446, 2985–3001. doi: 10.1093/mnras/stu2213

Willott, C. J., Rawlings, S., Blundell, K. M., and Lacy, M. (1999). The emission line-radio correlation for radio sources using the 7C Redshift Survey. *Mon. Not. R. Astron. Soc.* 309, 1017–1033. doi: 10.1046/j.1365-8711.1999.02907.x

Conflict of Interest Statement: The authors declare that the research was conducted in the absence of any commercial or financial relationships that could be construed as a potential conflict of interest.

Copyright © 2017 Rusinek and Sikora. This is an open-access article distributed under the terms of the Creative Commons Attribution License (CC BY). The use, distribution or reproduction in other forums is permitted, provided the original author(s) or licensor are credited and that the original publication in this journal is cited, in accordance with accepted academic practice. No use, distribution or reproduction is permitted which does not comply with these terms.

frontiers in Astronomy and Space Sciences

ORIGINAL RESEARCH
published: 12 December 2017
doi: 10.3389/fspas.2017.00060

Dynamics and Formation of Obscuring Tori in AGNs

Elena Yu. Bannikova [1, 2*] *and Alexey V. Sergeyev* [1, 2]

[1] *Institute of Radio Astronomy, National Academy of Science of Ukraine, Kharkiv, Ukraine,* [2] *Institute of Astronomy, V. N. Karazin Kharkiv National University, Kharkiv, Ukraine*

We considered the evolution of a self-gravitating clumpy torus in the gravitational field of the central mass of an active galactic nucleus (AGN) in the framework of the N-body problem. The initial conditions take into account winds with different opening angles. Results of our N-body simulations show that the clouds moving on orbits with a spread in inclinations and eccentricities form a toroidal region. The velocity of the clouds at the inner boundary of the torus is lower than in a disk model that can explain the observed rotation curves. We discuss the scenario of torus formation related with the beginning of the AGN stage.

Keywords: active galactic nuclei (AGN), quasars, Seyfert galaxies, N-body problems, gravitation

OPEN ACCESS

Edited by:
Mauro D'Onofrio, Università degli Studi di Padova, Italy

Reviewed by:
Omaira Gonzàlez Martín, Instituto de Radioastronomía y Astrofísica, Mexico
Alessandro Ballone, Osservatorio Astronomico di Padova (INAF), Italy

Correspondence:
Elena Yu. Bannikova
bannikova@astron.kharkov.ua

Specialty section:
This article was submitted to Milky Way and Galaxies, a section of the journal Frontiers in Astronomy and Space Sciences

Received: *30 August 2017*
Accepted: *28 November 2017*
Published: *12 December 2017*

Citation:
Bannikova EY and Sergeyev AV (2017) Dynamics and Formation of Obscuring Tori in AGNs. Front. Astron. Space Sci. 4:60. doi: 10.3389/fspas.2017.00060

1. INTRODUCTION

A dusty torus is an important structural element of an active galactic nucleus (AGN). In the framework of the unified scheme, the observational properties of AGNs (of type 1 and 2) are explained by the different orientation of the torus relative to an observer. This scheme was applied to Sy-galaxies (Antonucci, 1993) and generalized to other classes of AGNs (Urry and Padovani, 1995). Direct observations of obscuring tori exist only for a the nearby Sy-galaxies NGC 1068 (Jaffe et al., 2004; Raban et al., 2009), Circinus (Tristram et al., 2007, 2014).

The observed spectral energy distributions (SEDs) in the IR correspond to the model of a clumpy thick torus with a Gaussian distribution of clouds in its cross-section (Toroidal Obscuration Region) (Nenkova et al., 2008a,b). The radiative transfer model of a clumpy torus with 3D cloud distributions was considered in (Hönig and Kishimoto, 2010; Stalevski et al., 2012). In the other radiative transfer models the IR emission is explained by two components: disk and wind (Hönig and Kishimoto, 2017 and references therein). ALMA observations allowed to estimate the mass of the torus in NGC 1068: $M_{torus} = 10^5 M_{\odot}$ (García-Burillo et al., 2016). It means that self-gravity of the torus can influence the motion of the clouds in it. In fact, the dynamics of the matter in the torus shows non-circular motions which can be related to its self-gravitating properties.

One of the main problem concerns the explanation of the geometrical thickness of the torus. In such a torus the vertical velocity component of the clouds must be of the same order of magnitude as the orbital velocity. Several mechanisms were offered for the solution of this problem. The geometrical thickness of the torus can be explained by IR radiation pressure (Krolik, 2007; Dorodnitsyn et al., 2016; Chan and Krolik, 2017), by turbulent motions (Schartmann et al., 2010), or by starburst processes (Wada, 2012; Wada et al., 2016). Other models propose clumpy or dusty winds as an obscuring region (for example, Elitzur and Shlosman, 2006). Indeed, many AGNs show the presence of outflows (winds) which can appear due to influence of the radiation pressure or of a magnetic field (Proga and Kallman, 2004; Netzer, 2013, and references therein).

Our main idea is that the geometrical thickness of torus can be achieved by the motion of clouds in inclined orbits (Bannikova et al., 2012). This assumption is quite natural because there is the

external accretion of matter which replenishes the central region of AGN. On the other hand, since we consider a discrete medium in the torus, the orbital plane of each cloud must pass through the central mass. In this case, the toroidal structure may form due to the motion of the clouds in inclined orbits.

In our previous papers (Bannikova et al., 2012), we used special initial conditions (Keplerian torus) for the investigation of the torus evolution (see also Bannikova, 2015). In a Keplerian torus, the distribution of particles by eccentricities and inclinations obeys some law and all major semi-axes equal a major radius of the torus. Here we continue to investigate the properties and stability of a self-gravitating clumpy torus in the framework of N-body problem for more general initial conditions, taking into account the wind cones with different opening angles. In section 2 we discuss the initial conditions and present the result of N-body simulation. Sections 3 and 4 are devoted to the main results on the cloud dynamics in the torus and to the conditions of obscuration (section 5). A discussion of possible scenario of torus formation is provided in section 6.

2. N-BODY SIMULATION OF A TORUS: INITIAL CONDITIONS

We consider, as initial conditions, the random distribution of clouds over all orbital elements: eccentricity, inclination, major semi-axis, and three angles. Such an initial distribution is more general than in Bannikova et al. (2012). To form a toroidal structure, an anisotropy in the distribution of the clouds associated with winds in AGNs is needed. In these wind cones, the clouds acquire additional momentum due to radiation pressure and may overcome the gravitational forces of the central mass (and torus), leaving the system. This fact is accounted here by a simple assumption: the clouds from two opposite polar opening angles are excluded. In this case, the half-opening angle of the wind is a parameter influencing the resulting equilibrium cross-section of the torus and the obscuration condition. Three projections of the initial distribution of the clouds for the half-opening angle of the winds, $\theta_{wind} = 30^\circ$, are shown in **Figure 1**, (top panels). We will use in the following a value of the half-opening angle of the torus, $\theta_0 = \pi/2 - \theta_{wind}$, and show the results of simulations for different values of θ_0 in section 5.

N-body problem is reduced to the numerical integration of the equations of motion taking account the gravitational field of the central mass and $(N-1)$ clouds of constant mass, $M_{cl} = M_{torus}/(N-1)$:

$$\mathbf{a}_i = -\frac{G}{R^2}\left(M_{BH}\frac{\mathbf{r}_i}{r_i^3} + M_{cl}\sum_{j=1,j\neq i}^{N-1}\frac{\mathbf{r}_i - \mathbf{r}_j}{\left(\left|\mathbf{r}_i - \mathbf{r}_j\right|^2 + \epsilon^2\right)^{3/2}}\right), \quad (1)$$

where $\mathbf{r}_\mathrm{i} = (\mathrm{x,y,z})$ is the vector of a cloud from the central mass normalized to the major radius of the torus (R); $\mathbf{a}_\mathrm{i}$ is the vector of the acceleration of the i-th cloud acquired from all of the clouds of the torus M_{torus} and from the central mass M_{BH}. A softening length ϵ in the N-body problem allows us to avoid unlimited increasing of the gravitational forces by collisions of particles and can be interpreted as the radius of the cloud $R_{cl} = \epsilon R$. We choose the physical parameters corresponding to the case of NGC1068: $M_{BH} = 10^7 M_\odot$ and $M_{torus} = 10^5 M_\odot = 0.01 M_{BH}$. Since the method of parallel calculations is used, the number of particle in N-body problem must be $N = 2^n$. In presented simulations we adopt $n = 14$ (or $n = 13$), thus the number of clouds comes $N_{cl} = N - 1 = 16,383$ (or $N_{cl} = 8,191$).

N-body simulations were carried out using a technology of parallel calculations with GPU (CUDA). We used the Euler method with a step 0.001 to solve equation (1). In this case the total energy of the system E is a constant with a good accuracy, $|E - E_0| = 5 \cdot 10^{-6}$, where E_0 is the initial value of the total energy. We use the unity system: $M_{BH} = G = R = 1$.

The result of the simulation shows that the torus cross-section is changed and achieves its equilibrium state after a few hundred orbital periods. The distribution of clouds after 1,000 orbital periods are shown in the bottom panels of **Figure 1**. (One orbital period corresponds $T = 30,000$ years for $M_{BH} = 10^7 M_\odot$ and $R = 1\,pc$.) It is seen that the clouds are spread along z-axis as compared to the initial state, and that the cloud density increases towards the center of the torus cross-section. Indeed, the torus potential in the N-body problem might be divided into two summands (Bannikova et al., 2012): a regular part which is related with a smooth potential of the torus, and an irregular one which is due to the gravitational interactions of the clouds. The regular potential leads to an increase of the cloud density towards the center of the torus cross-section, but the irregular forces between clouds tend to stretch it. As the result, the self-gravitating torus is geometrically thick, which is needed for the obscuration condition (see section 5).

We can suggest that the behaviour of the system for a larger number of clouds N will not essentially differ from the obtained results. For example, if two toroidal systems have the same mass but different numbers of clouds (N_1, N_2), the same velocity dispersion of the clouds in the torus will be reached for the second system in the time interval $\Delta t_2 = \Delta t_1 N_2/N_1$, where Δt_1 is the time interval for the first system (Bannikova et al., 2012).

3. DISTRIBUTION OF THE CLOUDS IN A TORUS

At equilibrium, the clouds are distributed in such a way that they form the toroidal structure: the number of clouds is exponentially decreasing along the z-axis (**Figure 1**, bottom panels), and the distribution of the clouds in the torus cross-section is Gaussian. This distribution is similar to that obtained by (Nenkova et al., 2008a,b) from the analysis of the spectral energy distribution (SED) in the IR and was also used in 3D radiative transfer model of a clumpy torus (Hönig and Kishimoto, 2010). In our simulation, such a distribution is produced by the gravitational interaction between all the clouds and the central black hole.

Knowing from N-body simulations the coordinates and velocity components, we can calculate the orbital elements of each cloud. **Figure 2** shows a comparison of the cloud distribution in the initial state (*red curves*) and after 1,000 average orbital periods for two values of the softening length $\epsilon = 0.01$

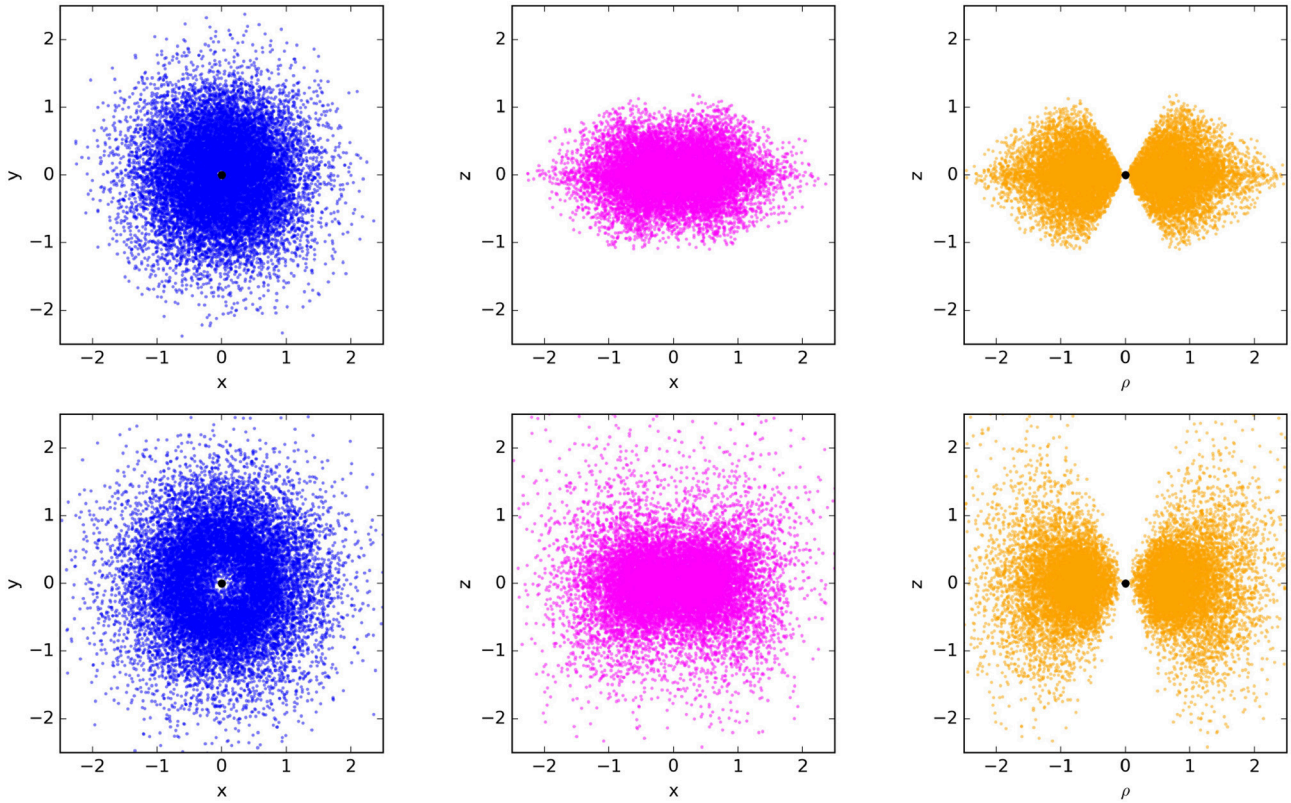

FIGURE 1 | Distribution of the clouds in the torus for the initial state **(top panels)** and after 1,000 average orbital periods **(bottom panels)**: projections on the equatorial plane **(left)**, on the meridional plane **(center)**, and with all the clouds gathered in one meridional plane $\rho = \pm\sqrt{x^2 + y^2}$ **(right)**. Initial conditions: $M_{torus} = 0.01 M_{BH}$, $N = 16,384$, $\epsilon = 0.01$, $\theta_0 = 60°$.

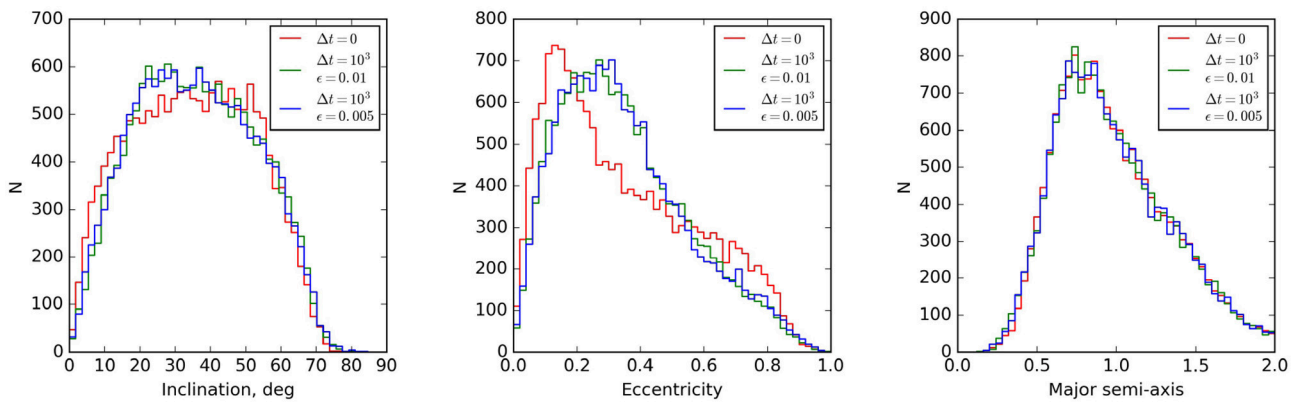

FIGURE 2 | Histograms of the orbital elements for the initial condition *(red)* and after 1,000 average orbital periods for inclination **(left)**, eccentricity **(center)**, and major semi-axis **(right)**, for $\epsilon = 0.01$; 0.005 *(green, blue)*. All other parameters correspond to **Figure 1**.

(*green curves*) and $\epsilon = 0.005$ (*blue curves*). It can be seen that the resulting distributions for the inclination and the major semi-axis (**Figure 2**, left, right) do not essentially differ from the initial ones, while there is a little difference in the distribution for eccentricity (**Figure 2**, center). This result shows that the initial state is near to the equilibrium one, and therefore, these distributions are statistically similar. Note that this torus evolution differs from the result presented in Bannikova et al. (2012), where the initial condition (Keplerian torus) was far from equilibrium and the distribution of clouds was noticeably modified by the evolution of the system. It is seen that the softening length does not influence the resulting distribution of the clouds because the equilibrium state, achieved due to self-gravity, depends on the mass (or the volume density) of the torus.

4. DYNAMICS OF THE CLOUDS IN DUSTY TORUS

Rotation curves allow us to understand the dynamics of clouds in a dusty torus from observations of the megamaser emission. Indeed, the conditions for the formation of water maser emission ($\lambda = 1.35\,cm$) appear at the inner region of the torus. Rotation curves were obtained only for a few nearby Sy-galaxies, including NGC1068 (Gallimore et al., 1996, 2001, 2004; Greenhill et al., 1996), and demonstrated that the matter in the torus is in sub-keplerian motion. Some models were proposed to explain such a motion and the rotation curve in NGC1068, considering the torus in the approximation of a self-gravitating disk with the mass comparable to the central mass (Huré, 2002; Lodato and Bertin, 2003). This does not agree with the mass of the torus obtained from ALMA observations, $M_{torus} = 10^5 M_\odot$ (García-Burillo et al., 2016), which corresponds to $0.01 M_{BH}$.

It is seen from **Figure 3** (left) that the motion at the inner boundary of the torus (*black and blue points* at **Figure 3**, left) is sub-keplerian. Indeed, the inner boundary of the torus is formed by the clouds that move in orbits with different eccentricities and inclinations (**Figure 3**, right). These clouds can pass through the apocenter or occupy some arbitrary (temporary) position on these orbits. A spread of the cloud velocities at the inner boundary of the torus can explain the observational data usually assigned to a turbulent motion. The clouds have high values of the velocity in the equatorial plane near the supermassive black hole (*orange points* at **Figure 3**, left). These clouds move on orbits with large values of the eccentricity passing exactly through the pericenter; they could ultimately feed the accretion disk.

5. CONDITION OF OBSCURATION

Here we will determine the probability of obscuration of the central source by clouds of spherical shape with the radius $R_{cl} = \epsilon \cdot R$, where the major radius of the torus is $R = 1$. It is convenient to use spherical coordinates, (r, θ, ϕ), and consider a sphere of unit radius $r = R$. We divide the sphere by the coordinate θ into n uniform parts (bins) whose length on the unit sphere of visibility is $h = \pi/n$. The ring length on the sphere for each angle θ_i is determined by the expression: $l(\theta) = 2\pi \cdot cos\,\theta$. Thus, an area of a ring on the sphere can be written as:

$$S_{bin}(\theta) = l(\theta) \cdot h. \tag{2}$$

Using the results of N-body simulations, we construct a histogram of the cloud distribution with respect to the angle θ between the equatorial plane and the line-of-sight with a cell size equal to h. The area of the projection of the cloud on the sphere is $S_i^{cl} = \pi(\epsilon/r_i)^2$. Let us suppose that the obscuration area equals the sum of all the cloud areas in the bin:

$$S_{bin}^{cl}(\theta) = \sum_i S_i^{cl}. \tag{3}$$

Then we determine an obscuration coefficient as the ratio of these areas:

$$k_{obsc} = \frac{S_{bin}^{cl}(\theta)}{S_{bin}(\theta)}. \tag{4}$$

It is seen from **Figure 4** that the obscuration coefficient depends on the inclination angle of the torus θ which is well fitted by the Gaussian function:

$$k_{obsc}(\theta) = A(N, \epsilon) \cdot \exp\left(-\frac{\theta^2}{\sigma^2(\theta_0)}\right), \tag{5}$$

where $\sigma(\theta_0)$ is the width of the torus half-opening angle, and the amplitude A characterizes the number of the clouds in the equatorial line-of-sight for the certain value of ϵ. **Figure 4** shows that the amplitude A has a linear dependence on the cloud number N and a square dependence of the size ϵ (see also Bannikova et al., 2012). The amplitude values for $N = 16,384$ is $A = 1.26$, while for $N = 8,192$ is $A = 0.68$. So, we can predict that for $N = 10^5$ the number of clouds in the equatorial line-of-sight is about 7.7 (for $\epsilon = 0.01$), which is consistent with the estimations of radiative transfer models (Nenkova et al., 2008a,b; Hönig and Kishimoto, 2010).

The width of the Gaussian function, σ, depends on the initial half-opening angle of the torus. The right panel of **Figure 4** shows the dependence of the obscuration coefficient on the angle between the line-of-sight and the equatorial plane. The fitting of function, $k_{obs}(\theta)$, gives the values of $\sigma(45°) = 24.5°$, $\sigma(60°) = 32.4°$, $\sigma(75°) = 41.9°$, and the amplitude A takes the values 1.35, 1.26, and 1.16.

6. DISCUSSION

N-body simulations show that a torus like the one observed in NGC1068 can stay thick, if its clouds initially have a random distribution of the orbital elements and anisotropy in two polar directions. The clouds in such a toroidal structure move in inclined orbits with a spread in eccentricity, and the equilibrium state of the torus corresponds to Gaussian density distribution, which satisfies the obscuration conditions and the observed SED in the IR.

The considered initial distribution of the clouds may be a consequence of the evolutionary processes in AGNs. It may suggest that, at the first stage, the supermassive black hole and the accretion disk are embedded in a quasi spherical distribution of dust (Liu and Zhang, 2011). An example could be the system IRAS16399-0937, a galaxy whose core is immersed in quasi spherically distributed optically thick clouds (Sales et al., 2015). The beginning of the active stage may lead to an increase of the wind energy and to the anisotropy in the cloud distribution. Within the wind cones, the clouds acquire additional impulse against the gravitational forces due to radiation pressure. The dusty clouds located outside of the wind cones are unaffected by the wind and continue to move in inclined and eccentric orbits. These clouds can form the thick toroidal distribution (**Figure 1**, bottom) which plays the role of an obscuring structure in AGNs.

These simulations do not take into account the effects of dissipation, which will influence the distribution of the clouds and the stability of the torus. The dissipation can be related to the collisions of the clouds and their heating. More frequent collisions will occur near the center of torus cross-section, where

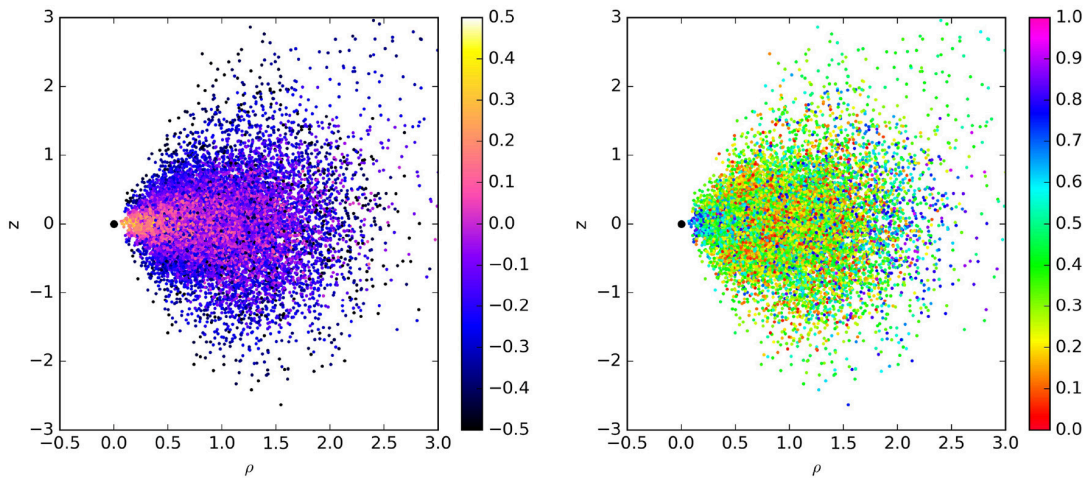

FIGURE 3 | Distribution of clouds in the torus. All particles are gathered in the meridional plane (ρ, z), where $\rho = \sqrt{x^2 + y^2}$. **Left panel**: colors mark the deviations of the cloud velocity in the torus (V) from a keplerian velocity for the case of a disk (V_k): $(V/V_k - 1)$. **Right panel**: colors mark the values of the eccentricity of the cloud orbits.

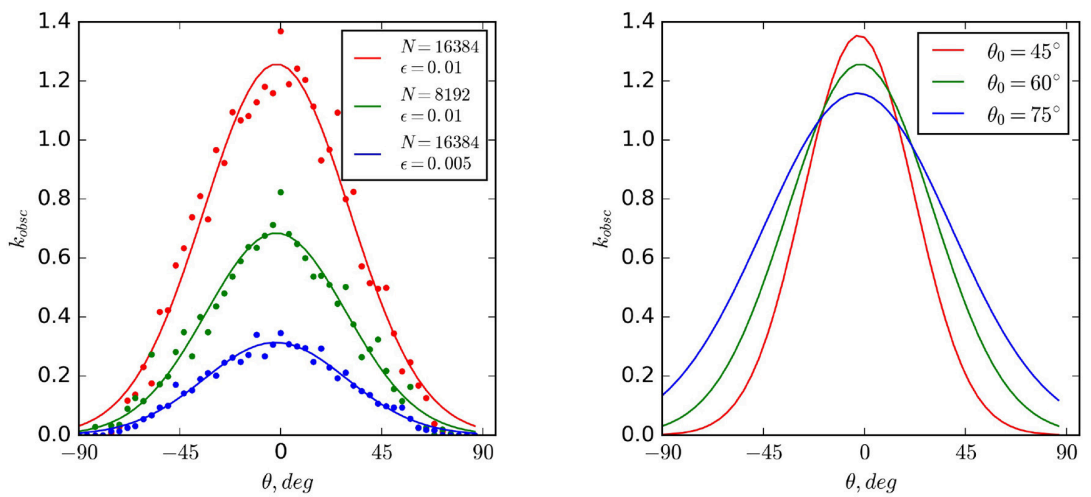

FIGURE 4 | Dependence of the obscuration coefficient on the angle between the line-of-sight and the equatorial plane. **Left panel**: values and the corresponding best-fitting curves are obtained from simulations for $\theta_0 = 45°$, $N = 16,384$ and $\epsilon = 0.01, 0.005$; $N = 8,192$ and $\epsilon = 0.01$. **Right panel**: each curve corresponds to the different initial half-opening angle of the torus: $\theta_0 = 45°, 60°, 75°$.

density is higher. The heating of the clouds in this region can boost the radiation pressure which may be an additional factor compensating the dissipation effects. The clouds near the supermassive black hole will move to the center due to dissipation and eventually feed the accretion disk. The clouds moving in the inner (and outer) boundary of the torus will rarely collide because their number decreases exponentially. Thus, it can be assumed that the toroidal structure can be conserved for certain values of the dissipation coefficient. Note, that the main mechanisms which were proposed to explain the geometrical thickness of the torus may work in such a dynamical clumpy model.

AUTHOR CONTRIBUTIONS

All authors listed have made a substantial, direct and intellectual contribution to the work, and approved it for publication.

ACKNOWLEDGMENTS

We thank Massimo Capaccioli for the useful discussions, and the referees for helpful comments that improved the manuscript. One of us (EB) likes to thank the Organizing Committee of the conference "Quasars at all cosmic epochs" for financial support to present this work.

REFERENCES

Antonucci, R. (1993). Unified models for active galactic nuclei and quasars. *Annu. Rev. Astron. Astrophys.* 31, 473–521. doi: 10.1146/annurev.aa.31.090193.002353

Bannikova, E. Y. (2015). Clouds distribution in obscuring tori of active galactic nuclei. *Radio Phys. Radio Astron.* 20, 191–204. doi: 10.15407/rpra20.03.191

Bannikova, E. Y., Vakulik, V. G., and Sergeev, A. V. (2012). N-body simulation of a clumpy torus: application to active galactic nuclei. *Month. Notices R. Astron. Soc.* 424, 820–829. doi: 10.1111/j.1365-2966.2012.21186.x

Chan, C.-H., and Krolik, J. H. (2017). Geometrically thick obscuration by radiation-driven outflow from magnetized tori of active galactic nuclei. *Astrophys. J.* 843:58. doi: 10.3847/1538-4357/aa76e4

Dorodnitsyn, A., Kallman, T., and Proga, D. (2016). Parsec-scale accretion and winds irradiated by a quasar. *Astrophys. J.* 819:115. doi: 10.3847/0004-637X/819/2/115

Elitzur, M., and Shlosman, I. (2006). The AGN-obscuring torus: The end of the "Doughnut" paradigm? *Astrophys. J. Lett.* 648, L101–L104. doi: 10.1086/508158

Gallimore, J. F., Baum, S. A., and O'Dea, C. P. (2004). The parsec-scale radio structure of NGC 1068 and the nature of the nuclear radio source. *Astrophys. J.* 613, 794–810. doi: 10.1086/423167

Gallimore, J. F., Baum, S. A., O'Dea, C. P., Brinks, E., and Pedlar, A. (1996). H 2O and OH masers as probes of the obscuring torus in NGC 1068. *Astrophys. J.* 462:740. doi: 10.1086/177187

Gallimore, J. F., Henkel, C., Baum, S. A., Glass, I. S., Claussen, M. J., Prieto, M. A., et al. (2001). The nature of the nuclear H_2O masers of NGC 1068: reverberation and evidence for a rotating disk geometry. *Astrophys. J.* 556, 694–715. doi: 10.1086/321616

García-Burillo, S., Combes, F., Ramos Almeida, C., Usero, A., Krips, M., Alonso-Herrero, A., et al. (2016). ALMA resolves the torus of NGC 1068: Continuum and molecular line emission. *Astrophys. J. Lett.* 823:L12. doi: 10.3847/2041-8205/823/1/L12

Greenhill, L. J., Gwinn, C. R., Antonucci, R., and Barvainis, R. (1996). VLBI imaging of water maser emission from the nuclear torus of NGC 1068. *Astrophys. J. Lett.* 472:L21. doi: 10.1086/310346

Hönig, S. F., and Kishimoto, M. (2010). The dusty heart of nearby active galaxies. II. From clumpy torus models to physical properties of dust around AGN. *Astron. Astrophys.* 523:A27. doi: 10.1051/0004-6361/200912676

Hönig, S. F., and Kishimoto, M. (2017). Dusty winds in active galactic nuclei: reconciling observations with models. *Astrophys. J. Lett.* 838:L20. doi: 10.3847/2041-8213/aa6838

Huré, J.-M. (2002). Origin of non-keplerian motions of masers in NGC 1068. *Astron. Astrophys.* 395, L21–L24. doi: 10.1051/0004-6361:20021445

Jaffe, W., Meisenheimer, K., Röttgering, H. J. A., Leinert, C., Richichi, A., Chesneau, O., et al. (2004). The central dusty torus in the active nucleus of NGC 1068. *Nature* 429, 47–49. doi: 10.1038/nature02531

Krolik, J. H. (2007). AGN obscuring tori supported by infrared radiation pressure. *Astrophys. J.* 661, 52–59. doi: 10.1086/515432

Liu, Y., and Zhang, S. N. (2011). Dusty torus formation by anisotropic radiative pressure feedback of active galactic nuclei. *Astrophys. J. Lett.* 728:L44. doi: 10.1088/2041-8205/728/2/L44

Lodato, G., and Bertin, G. (2003). Non-keplerian rotation in the nucleus of NGC1068: evidence for a massive accretion disk? *Astron. Astrophys.* 398, 517–524. doi: 10.1051/0004-6361:20021672

Nenkova, M., Sirocky, M. M., Ivezić, Ž., and Elitzur, M. (2008a). AGN dusty tori. I. Handling of clumpy media. *Astrophys. J.* 685, 147–159. doi: 10.1086/590482

Nenkova, M., Sirocky, M. M., Nikutta, R., Ivezić, Ž., and Elitzur, M. (2008b). AGN Dusty Tori. II. Observational implications of clumpiness. *Astrophys. J.* 685, 160–180. doi: 10.1086/590483

Netzer, H. (2013). *The Physics and Evolution of Active Galactic Nuclei.* Cambridge, UK: Cambridge University Press.

Proga, D., and Kallman, T. R. (2004). Dynamics of line-driven disk winds in active galactic nuclei. II. effects of disk radiation. *Astrophys. J.* 616, 688–695. doi: 10.1086/425117

Raban, D., Jaffe, W., Röttgering, H., Meisenheimer, K., and Tristram, K. R. W. (2009). Resolving the obscuring torus in NGC 1068 with the power of infrared interferometry: revealing the inner funnel of dust. *Month. Notices R. Astron. Soc.* 394, 1325–1337. doi: 10.1111/j.1365-2966.2009.14439.x

Sales, D. A., Robinson, A., Axon, D. J., Gallimore, J., Kharb, P., Curran, R. L., et al. (2015). An embedded active nucleus in the OH megamaser galaxy IRAS16399-0937. *Astrophys. J.* 799:25. doi: 10.1088/0004-637X/799/1/25

Schartmann, M., Burkert, A., Krause, M., Camenzind, M., Meisenheimer, K., and Davies, R. I. (2010). Gas dynamics of the central few parsec region of NGC 1068 fuelled by the evolving nuclear star cluster. *Month. Notices R. Astron. Soc.* 403, 1801–1811. doi: 10.1111/j.1365-2966.2010.16250.x

Stalevski, M., Fritz, J., Baes, M., Nakos, T., and Popović, L. Č. (2012). 3D radiative transfer modelling of the dusty tori around active galactic nuclei as a clumpy two-phase medium. *Month. Notices R. Astron. Soc.* 420, 2756–2772. doi: 10.1111/j.1365-2966.2011.19775.x

Tristram, K. R. W., Burtscher, L., Jaffe, W., Meisenheimer, K., Hönig, S. F., Kishimoto, M., et al. (2014). The dusty torus in the Circinus galaxy: a dense disk and the torus funnel. *Astron. Astrophys.* 563:A82. doi: 10.1051/0004-6361/201322698

Tristram, K. R. W., Meisenheimer, K., Jaffe, W., Schartmann, M., Rix, H.-W., Leinert, C., et al. (2007). Resolving the complex structure of the dust torus in the active nucleus of the Circinus galaxy. *Astron. Astrophys.* 474, 837–850. doi: 10.1051/0004-6361:20078369

Urry, C. M., and Padovani, P. (1995). Unified schemes for radio-loud active galactic nuclei. *Publ. Astron. Soc. Pac.* 107:803. doi: 10.1086/133630

Wada, K. (2012). Radiation-driven fountain and origin of torus around active galactic nuclei. *Astrophys. J.* 758:66. doi: 10.1088/0004-637X/758/1/66

Wada, K., Schartmann, M., and Meijerink, R. (2016). Multi-phase nature of a radiation-driven fountain with nuclear starburst in a low-mass active galactic nucleus. *Astrophys. J. Lett.* 828:L19. doi: 10.3847/2041-8205/828/2/L19

Conflict of Interest Statement: The authors declare that the research was conducted in the absence of any commercial or financial relationships that could be construed as a potential conflict of interest.

Copyright © 2017 Bannikova and Sergeyev. This is an open-access article distributed under the terms of the Creative Commons Attribution License (CC BY). The use, distribution or reproduction in other forums is permitted, provided the original author(s) or licensor are credited and that the original publication in this journal is cited, in accordance with accepted academic practice. No use, distribution or reproduction is permitted which does not comply with these terms.

frontiers in Astronomy and Space Sciences

ORIGINAL RESEARCH
published: 08 December 2017
doi: 10.3389/fspas.2017.00056

Modeling the Broad-Band Emission from the Gamma-Ray Emitting Narrow-Line Seyfert-1 Galaxies 1H 0323+342 and B2 0954+25A

Maialen Arrieta-Lobo, Catherine Boisson and Andreas Zech*

Laboratoire Univers et Theories, Observatoire de Paris, CNRS, Université Paris-Diderot, PSL Research University, Meudon, France

Prior to the Fermi-LAT era, only two classes of Active Galactic Nuclei (AGN) were thought to harbor relativistic jets that radiate up to gamma-ray energies: blazars and radio galaxies. The detection of variable gamma-ray emission from Narrow Line Seyfert 1 (NLSy1) galaxies has put them on the spotlight as a new class of gamma-ray emitting AGN. In this respect, gamma-ray emitting NLSy1s seem to be situated between blazars (dominated by non-thermal emission) and Seyferts (accretion disc dominated). In this work, we model the Spectral Energy Distribution (SED) of two gamma-loud NLSy1s, 1H 0323+342 and B2 0954+25A, during quiescent and flaring episodes via a multi-component radiative model that features a relativistic jet and external photon fields from the torus, disc, corona and Broad Line Region (BLR). We find that the interpretation of the high-energy emission of jetted NLSy1s requires taking into account Inverse Compton emission from particles in the relativistic jet that interact with external photon fields. Minimal changes are applied to the model parameters to transition from average to flaring states. In this scenario, the observed variability is explained mainly by means of changes in the jet density and Doppler factor.

Keywords: AGN, quasar, NLSy1, blazar, gamma-ray, modeling, 1H 0323+342, B2 0954+25A

OPEN ACCESS

Edited by:
Deborah Dultzin, Universidad Nacional Autónoma de México, Mexico

Reviewed by:
Omaira González Martín, Instituto de Radioastronomía y Astrofísica, Mexico
Alenka Negrete, Universidad Nacional Autónoma de México, Mexico

****Correspondence:***
Maialen Arrieta-Lobo
maialen.arrieta@obspm.fr

Specialty section:
This article was submitted to Milky Way and Galaxies, a section of the journal Frontiers in Astronomy and Space Sciences

Received: *22 August 2017*
Accepted: *24 November 2017*
Published: *08 December 2017*

Citation:
Arrieta-Lobo M, Boisson C and Zech A (2017) Modeling the Broad-Band Emission from the Gamma-Ray Emitting Narrow-Line Seyfert-1 Galaxies 1H 0323+342 and B2 0954+25A. Front. Astron. Space Sci. 4:56. doi: 10.3389/fspas.2017.00056

1. INTRODUCTION

Blazars are AGN whose relativistic jet is pointing closely toward the Earth, which results in strong relativistic beaming of the observed radiation (a.k.a. Doppler boosting). This type of AGN can be further classified into Flat Spectrum Radio Quasars (FSRQs) and BL Lac objects, the main difference being the presence of features in the optical spectra of the former, and lack thereof in the case of the latter. The SED of both blazar subtypes spans a frequency range over 20 orders of magnitude in frequency, from radio frequencies up to gamma-rays. However, while the BL Lac subclass presents a SED with two clearly defined bumps, namely the synchrotron and the Inverse Compton (IC) bumps that can be accurately described by a simple one-zone leptonic Synchrotron Self-Compton (SSC) emission model, the FSRQ subtype features a more complex emission spectrum that requires radiation from external photon fields such as the accretion disc or the dusty torus to be accounted for (see e.g., Ghisellini and Tavecchio, 2009). The unexpected detection of gamma-ray emission from a particular type of Seyfert 1 galaxies, NLSy1s, who were not expected to harbor relativistic jets that could create such high-energy emission, has originated a new gamma-loud class of AGN. So far, 10 gamma-ray emitting NLSy1 galaxies have been detected with the Large Area Telescope onboard the Fermi satellite (see for instance, the 3FGL catalog Acero et al., 2015).

The fact that this new type of gamma-loud AGN features both blazar- and Seyfert-like characteristics could bring us closer to a better understanding of AGN unification theories. In fact, their broad-band SED resembles the one of FSRQs, since emission from features other than the relativistic jet are observed. Here, we consider two different states, based on the variability of the gamma-ray flux, for two of the NLSy1s detected with Fermi, 1H 0323+342 and B2 0954+25A, and apply a multi-component radiative model that considers both the emission from the relativistic jet and the external photon fields (torus, disc, corona, and BLR). Further details and references are given in section 2. The main difference between our model and previous models (e.g., Calderone et al., 2012; Paliya et al., 2014) is that we consider several emission lines from the BLR (Cerruti et al., 2013b) and we describe different states of the same source by applying minimal changes to the jet parameters of the model. In the following sections, we present the multi-component model (section 2), along with the application to two datasets of each selected source (section 3) to conclude with a brief discussion and outlook (section 4). Throughout this work, a ΛCDM cosmology is assumed with $H_0 = 70$ km s^{-1} Mpc^{-1}, $\Omega_m = 0.3$ and $\Omega_\Lambda = 0.7$.

2. THE MULTI-COMPONENT CODE

In the pure one-zone SSC model, radiation is produced in a single zone of the jet approximated as a sphere of radius R_{src} (a.k.a. the blob) with a tangled magnetic field B which moves through the jet with bulk Lorentz factor Γ oriented at a small viewing angle θ (see Katarzyński et al., 2001 for further details). This description implies that the photons up to X-ray energies forming the first broad bump observed in the SED of BL Lac type blazars are produced by a population of relativistic electrons via synchrotron radiation. These synchrotron photons are then IC scattered by the same population of electrons up to gamma-ray energies, creating the second broad bump featured in the SED.

Although this simple SSC model approximation quite accurately describes the SED of BL Lac type objects, it is not sufficient to account for the radiation observed in other gamma-loud AGN classes, e.g., FSRQs or certain NLSy1 galaxies. Thus, in addition to the synchrotron and Inverse Compton radiation from the blob-in-jet scenario, it is necessary to add external photon-field contributions. Our multi-component code is based on a stationary homogeneous one-zone SSC model with additional external photon fields from the dusty torus, the accretion disc, the X-ray corona and the Broad-Line Region (BLR) as illustrated in **Figure 1**, and based on Cerruti et al. (2013b), Dermer and Menon (2009), Donea and Protheroe (2003), Finke et al. (2008), Finke and Dermer (2010), and Finke (2016).

The accretion disc is described as a multi-temperature black body (Dermer and Menon, 2009), while the torus is a simple black body (Dermer and Menon, 2009). The X-ray corona is treated as a simple power law function with an exponential cut-off at around 150 keV (Ghisellini et al., 2009). Accretion disc and corona photons will ionize the BLR, which is considered as a spherical shell of width ΔR expanding between an inner and an outer radius ($\Delta R \ll R_{in}, R_{out}$). The density of the BLR has a power law shape within ΔR, with an index ξ fixed to $\xi = -2$ that implies that most of the ionization takes place close to the inner edge of the BLR (see Dermer and Menon, 2009; Finke and Dermer, 2010 for a detailed explanation). Thus, the BLR will emit a spectrum of monochromatic emission lines (see Cerruti et al., 2013b for more details). The torus, the corona and the BLR are scaled to the disc luminosity through the covering factors τ_{IR}, τ_X and τ_{BLR} respectively that are considered as free parameters (see **Figure 1**). The external photon fields are comptonized when they encounter the relativistic electrons from the blob (Dermer and Menon, 2009). The luminosity of the EIC components is strongly dependent on the distance between the black hole and the blob within the jet. Note that the radius of the torus and the radius of the BLR scale with the disc luminosity, which depends on the black hole mass M_{BH} and the radiative efficiency (see for instance Ghisellini and Tavecchio, 2009), reducing the number of free parameters of the model.

3. APPLICATION

In the following section, we present some of the main characteristics of the gamma-loud NLSy1s to which we applied our multi-component model, namely 1H0323+342 and B2 0954+25A. For the modeling, two different datasets are considered for each source: a quiescent/average dataset and a flaring state dataset w.r.t. gamma-ray emission seen by Fermi. The parameter sets that best describe the data along with a brief discussion on the model interpretation are then provided.

3.1. 1H 0323+342

1H 0323+342 is the closest gamma-loud NLSy1 known, located at $z = 0.063$. One of its most interesting features is its frequent variability both in X-rays and gamma-rays which, although often uncorrelated, sometimes presents hints of correlation (Paliya et al., 2014). The black hole mass is $M_{BH} = 2 \times 10^7\, M_\odot$ (Landt et al., 2017), and the viewing angle was estimated to be $\theta \sim 4^\circ - 13^\circ$ in Fuhrmann et al. (2016). For our models, we arbitrarily fixed $\theta = 5^\circ$.

3.1.1. Data Sample and Analysis

Average Swift XRT and UVOT data from observations taken in September 2013 and December 2014 with NuSTAR data from March 2014 (see Landt et al., 2017 for further details) and Fermi data from the low state in Paliya et al. (2014) are considered as the quiescent state of the source, depicted in light green in **Figure 2**. Simultaneous Fermi-LAT from August 27th 2013 to August 31st 2013 and Swift UVOT and XRT data from Paliya et al. (2014) are taken into account for the flaring state (orange data points and bow-tie in **Figure 2**).

3.1.2. Modeling the SED

Top and bottom panels in **Figure 2** present the quiescent state and high state model results for 1H 0323+342 respectively. The corresponding model parameters are shown in **Table 1**. We are trying to model the two states with a minimum of parameter changes, assuming that only the compact jet component varies.

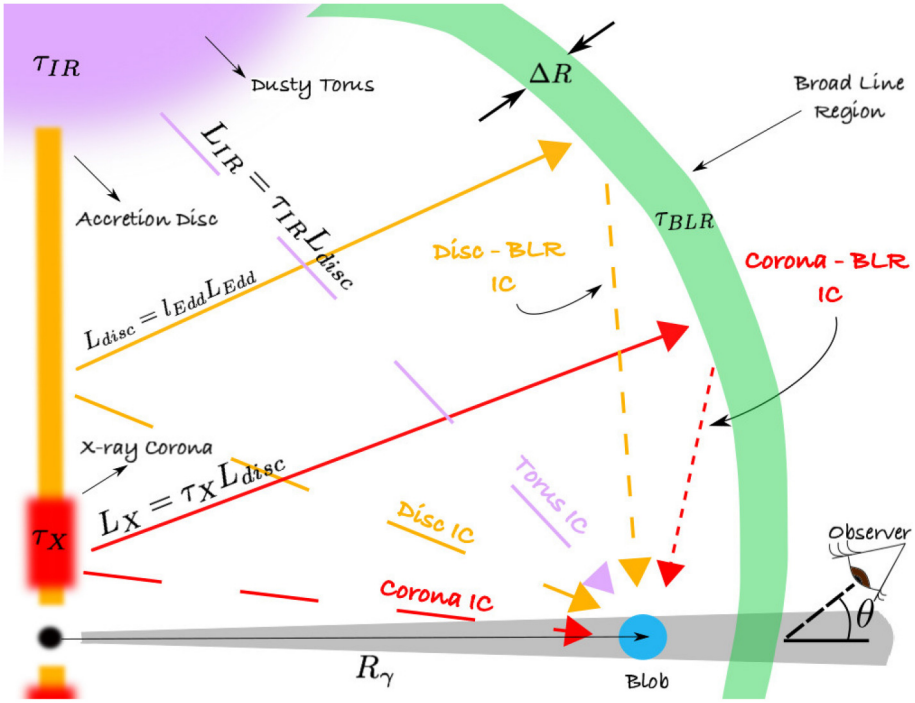

FIGURE 1 | Sketch showing the different external photon fields featured in our multi-component model. The direct radiation from the components are scaled by the black hole accretion rate, and they are also dependent on the characteristics of corresponding photon field, under the form of the scaling factors τ_{IR} for the dusty torus and τ_X for the X-ray corona. As for the IC components, they also depend on the opacities of the different photon fields, $\tau_{X,BLR}$ and τ_{BLR} for the accretion disc photons IC scattered in the BLR and for the X-ray corona photons IC scattered in the BLR respectively. Note that for our model we consider a BLR of width $\Delta R = R^{in}_{BLR} - R^{out}_{BLR}$.

At sub-millimeter and infrared frequencies, the relativistic jet is necessary to account for the radiation from the source both in the quiescent and high states. The presence of the accretion disc is a major contribution in this source at UV/optical wavelengths. During flaring states the larger contribution from the jet in combination with direct emission from the torus and disc gives a good description of the observed radiation. The dip at optical frequencies in the quiescent state model is due to the steep slope of the Fermi-LAT data that forces the index of the particle distribution after the energy break to be steep too. However, we need to remark that these are not simultaneous data.

As for X-rays, in the quiescent state the hard emission is well explained by the X-ray corona component, while a larger contribution from the jet SSC radiation by means of a larger Doppler factor ($\delta = 11$ vs. $\delta = 9$ for the quiescent state) is necessary to reach the observed hard X-ray flux levels in the flaring state. At gamma-ray frequencies, the EIC emission from the jet explains the observed emission in both the quiescent and the high state: gamma-rays are attributed to the BLR emission lines comptonized by the electrons within the relativistic blob, with a disc EIC component bridging the X-ray and gamma-ray radiation in both states. The change in the slope of the gamma-ray Fermi-LAT spectrum between both states requires a harder electron distribution slope n_2 after the break energy γ_b value in the flare state, a hint of a "harder when brighter" trend. The difference in gamma-ray flux levels between both states is accounted for by the larger Doppler factor of the flare and higher particle density.

The flaring state features a larger particle density w.r.t. the quiescent state. The magnetic field also remains the same between the two states. In this scenario, flaring states seem to occur when a newly expelled blob with a larger Doppler factor goes through a stationary shock within the jet.

Note that to reduce the number of free parameters from our model, we assume that neither the torus, nor the accretion disc not the BLR change during different states of the source. Both quiescent and flaring state models are relatively close to equipartition between the electron distribution kinematic energy density u_e and the magnetic field energy density u_b.

The fact that lowest-energy radio data are not well described by our model is caused by the synchrotron self-absorption of the electron population. Radio data are usually attributed to an extended jet component (Katarzyński et al., 2008; Lenain et al., 2008). Such a component is not considered in our model, but could be added.

3.2. B2 0954+25A

With a redshift of $z = 0.7$, B2 0954+25A is a more distant source than 1H0323+342. Calderone et al. (2012) give a black hole mass of $M_{BH} = 1.5 \times 10^8\ M_\odot$, and consider a viewing angle of $\theta = 3^\circ$. As documented in the same paper, only a single flare is observed in gamma-ray frequencies during the first half

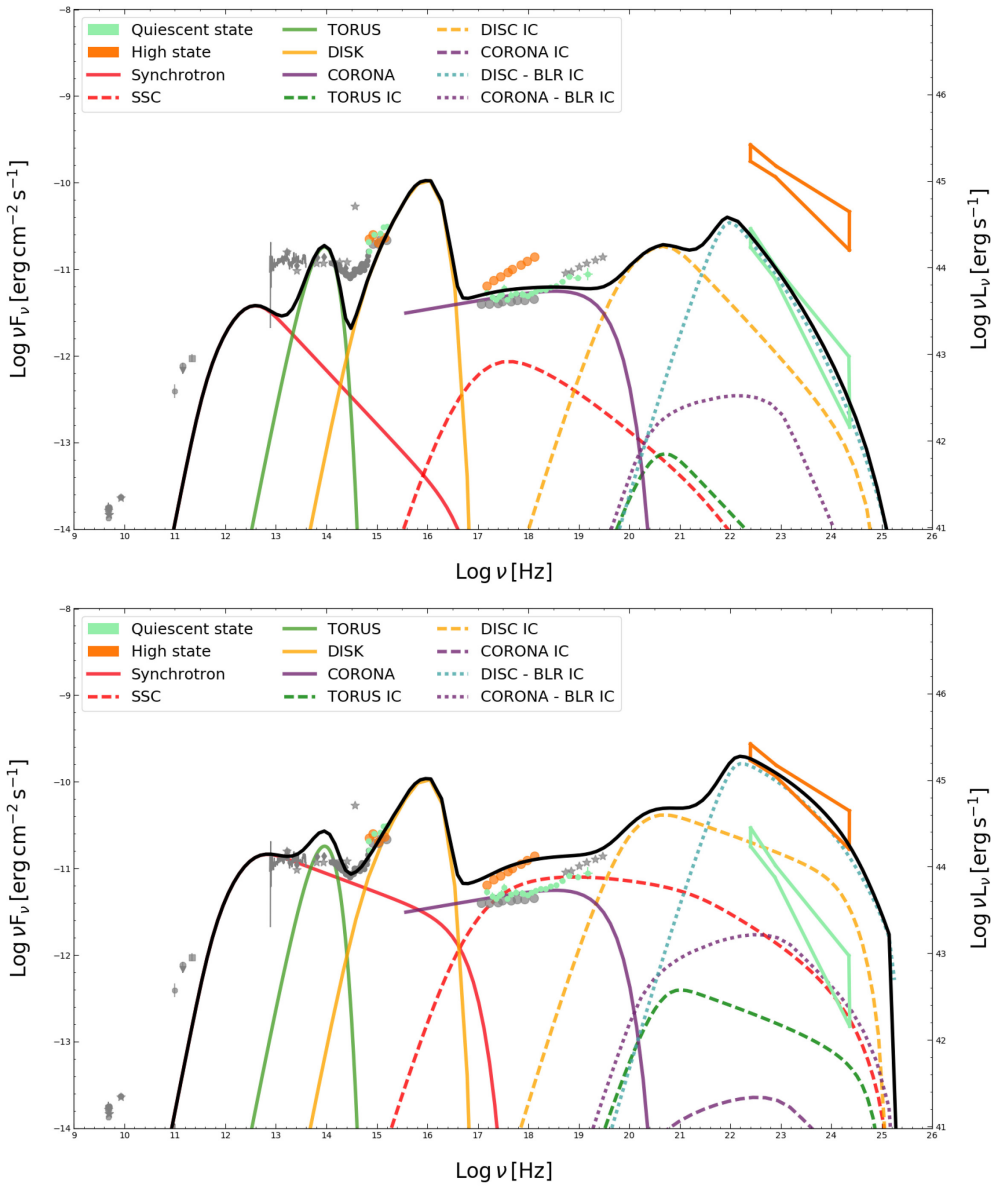

FIGURE 2 | Multi-component model for the quiescent state **(Top)** and the flaring state **(Bottom)** of 1H 0323+342. The quiescent state is depicted in light green, and the flaring state in orange. The bow-ties in the 10^{22}–10^{25} Hz range represent Fermi/LAT spectrum and corresponding uncertainties. Archival data are represented in gray. Synchrotron and SSC emission from the jet are shown by solid and dashed red lines respectively. Direct emission from the torus, the accretion disc and the X-ray corona is shown in green, yellow and purple solid lines respectively. Torus, accretion disc and corona IC emission follow the same color code and are represented by dashed lines. BLR reprocessed disc and corona components are shown in dotted blue and purple, although their contribution is negligible in both cases. The total model is depicted with a black solid line.

of 2010, while the source is quite variable in X-rays. Another interesting fact is that Calderone et al. (2012) propose this source to be a transition object between FSRQs and gamma-loud NLSy1s.

3.2.1. Data Sample and Analysis

To construct the average state, we consider archival Chandra data from 2009 from Calderone et al. (2012) along with long-term averaged (3FGL, 48 months of observations) Fermi-LAT data (Acero et al., 2015). For the flaring state, we analyzed Fermi-LAT data from the flaring period of the source, i.e., Jan 2010–Jul 2010, and considered them along with Swift XRT and UVOT data from the X-ray flaring period in June 2007. Although there was a contemporary Swift observation taken on June 15, 2010, the statistics are poor due to short exposure time and no good-quality spectrum can be extracted. Given that the count rates between both observations are compatible, we consider the observation from June 2007 for modeling purposes,

TABLE 1 | Model parameters for 1H 0323+342 and B2 0954+25A.

	1H 0323+342		B2 0954+25A	
	Quiescent	**Flare**	**Average**	**Flare**
δ	9	11	13	15
K [1/cm^3]	6.5×10^6	8×10^6	8×10^6	1.3×10^7
R_{src} [cm]	1.15×10^{15}	1.15×10^{15}	4.97×10^{15}	4.97×10^{15}
B [G]	2.6	2.6	2.0	2.0
$n1$	2.2	2.2	2.6	2.7
$n2$	4.2	3.4	3.4	3.4
R_γ [R_G]	3×10^3	3×10^3	3×10^3	3×10^3
l_{Edd}	~ 0.76		~ 0.66	
$\dot{m}$ [$M_\odot$ yr^{-1}]	~ 0.43		~ 2.19	
L_{Disc} [erg s^{-1}]	2×10^{45}		1.13×10^{46}	
u_e/u_b	5.66	9.63	2.7	2.04
n_e [1/cm^3]	1.85×10^6	3.16×10^6	2.87×10^6	2.54×10^6

All the quantities are input parameters to the model except for the last four quantities i.e., $\dot{m}$, L_{Disc}, u_e/u_B and n_e which are derived from the input parameters.

since it is the only Swift observation for which the source was significantly detected. As for 1H0323+342, the average state is depicted in light green, whereas the flare is plotted in orange.

3.2.2. Modeling the SED

Figure 3 shows the multi-component model results for B2 0954+25A in the average and flaring state (top and bottom panels respectively). We follow the same approach as for 1H 0323+342.

In the case of this source, the non-simultaneous infrared and sub-mm emission are underestimated by the synchrotron radiation from the relativistic jet in the average state. Similar to 1H 0323+342, radio data of B2 0954+25A are not well described by our model due to the synchrotron self-absorption of the electron population.

Although less prominent than for 1H0323+342, the presence of the accretion disc is also important in this source at optical/UV frequencies. Unlike for 1H0323+342, the hard X-ray emission is well explained simply by the SSC contribution from the jet both for the average and flaring state. The presence of a X-ray corona is not necessary in this scenario. The jet is necessary to explain gamma-ray emission in both states via inverse comptonization of external photons. In this respect, in both states the gamma emission is attributed to a combination of disc and BLR IC components. No change of the gamma-ray slope is observed between the two states, so the indexes of the electron energy distribution remain unchanged in the case of B2 0954+25A.

Similar to 1H 0323+342, the Doppler factor is higher during the flaring state, while the blob remains at the same position. The blob density remains approximately the same between both states, but there is a small change in the electron spectrum though. No increase of the magnetic field is required from the quiescent to the flaring state, since the only major change is the luminosity of the IC component, which can be well described by the increase in the electron distribution normalization K and Doppler factor. These variations provide the larger contribution of inverse comptonized external photon fields that is necessary to model the higher fluxes during the flare. Finally, both average state and flaring state solutions are close to equipartition.

4. DISCUSSION AND OUTLOOK

Our multi-component radiative model describes the SED of the two NLSy1s presented here, both in the flaring and quiescent/average states. For both 1H 0323+342 and B2 0954+25A, the gamma-ray radiation is explained by a combination of EIC emission from jet electrons on the photon field from the accretion disc and (dominantly) the BLR. The fact that we model these sources with the same model that is usually applied to FSRQs underlines the similarities between both types of objects.

For each source, the characteristics of the external photon fields are kept constant between different states, to reduce the number of free parameters of the model. All variations are explained by changes in the electron population in the compact relativistic jet.

The transition from quiescent/average to flaring states in both sources is accounted for by a more relativistic flare, i.e., larger Doppler factors, and higher particle densities for 1H 0323+342 while the density is approximately constant for B2 0954+25A. The indexes of the particle energy distribution also vary due to a hardening/flattening of the gamma-ray spectrum. Infrared and sub-mm data are underestimated in the case of B2 0954+25A. This is also the case for the quiescent state of 1H 0323+342, and somewhat less for its flaring state. This might be a hint of the presence of an extended jet in these objects, although data are not simultaneous.

Comparing the present work to previous existing models for the two sources presented here, the scenario in which we model the sources is similar as far as the origin of the external Compton dominance is concerned: in their respective models for 2 states of 1H 0323+342 and one state of B2 0954+25A, Paliya et al. (2014) and Calderone et al. (2012) also describe the high energy emission from the source via the re-emission of disc and BLR photons. The disc luminosities they feature are similar to ours. However, in our scenario the SSC emission is necessary to account for X-ray emission except for the quiescent state of 1H 0323+342.

Due to the large number of free parameters of the model, this type of model is necessarily degenerate. For the simpler SSC model scenario, there are methods to explore the parameter space (Cerruti et al., 2013a), but for more complex EC models like the one we present, this is not the case yet. Our approach is a test for the hypothesis that this type of source can be modeled by this scenario. This is a standard practice for blazar-type source modeling.

Finally, we want to remark that, although solutions dominated by disc and BLR radiation at high energies are presented in this proceeding, models in which the inverse Compton component at high energies is explained mostly by comptonized dusty

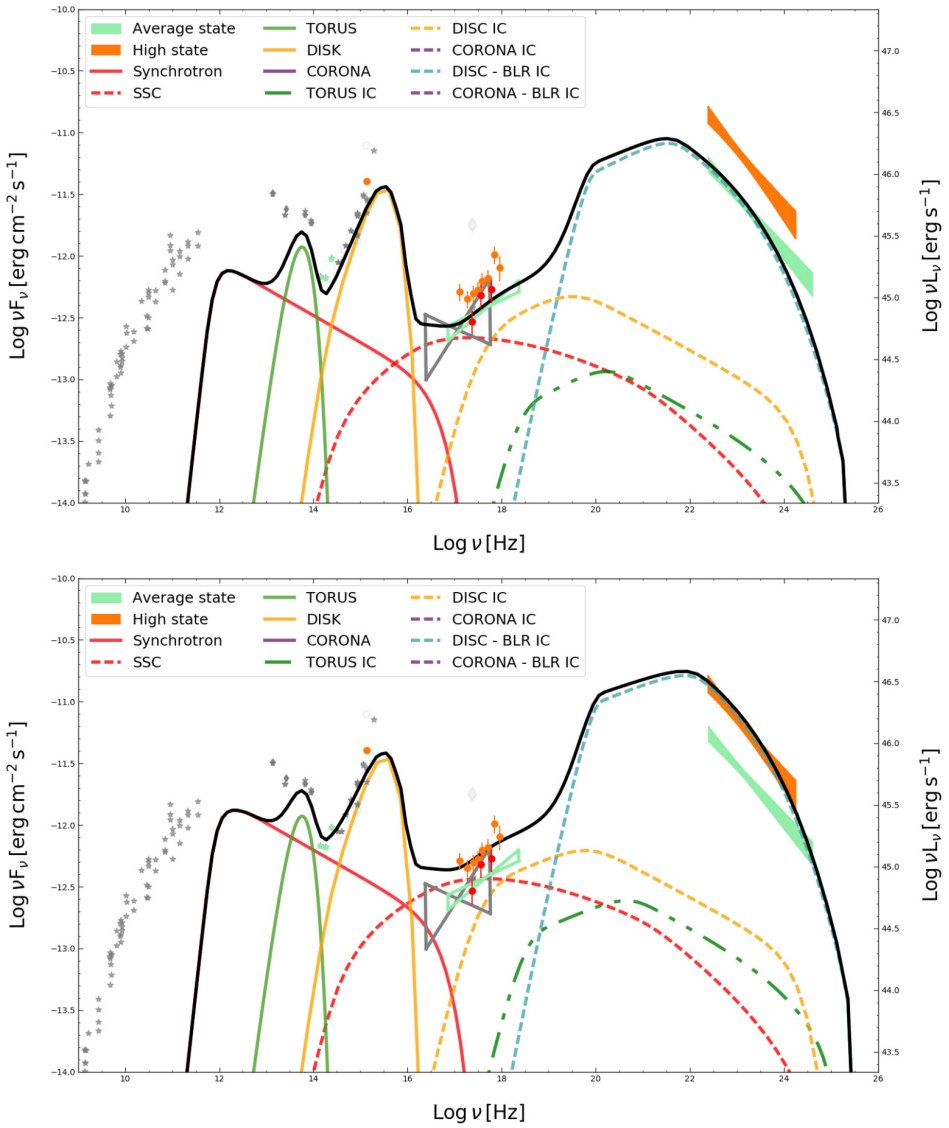

FIGURE 3 | Multi-component model for the average state **(Top)** and the high state **(Bottom)** of B2 0954+25A. The quiescent state is depicted in light green, and the flaring state in orange. The bow-ties in the 10^{22}–10^{25} Hz range represent Fermi/LAT spectrum and corresponding uncertainties. Archival data are represented in gray. Synchrotron and SSC emission from the jet are shown by solid and dashed red lines respectively. Direct emission from the torus and the accretion disc is shown in green and yellow solid lines respectively. Torus and accretion disc IC emission follow the same color code and are represented by dashed lines. The BLR reprocessed disc photon component is shown in dotted blue. Note that there is no presence of the X-ray corona in this scenario. The total model is depicted with a black solid line.

torus radiation can account for NLSy1 SEDs. One of the main differences w.r.t. the disc-dominated scenario is the position of the gamma-ray emitting region: while for the solutions presented here the blob is located well below the BLR, for dust-dominated scenarios the blob is at the outer edge of the BLR where the ionization by the disc photons is at its minimum. Thus, the contribution from the disc and BLR components is minor w.r.t. that of the torus. Furthermore, the dust-dominated scenario requires much larger electron distribution break energies, which means a larger contribution from low-energy electrons that yields solutions that are less absorbed at synchrotron frequencies, such that the synchrotron emission from the blob might account for radio data.

AUTHOR CONTRIBUTIONS

All authors listed, have made substantial, direct and intellectual contribution to the work, and approved it for publication.

FUNDING

MA-L's work is supported by a PSL Research University Ph.D. fellowship.

ACKNOWLEDGMENTS

We want to thank our colleagues from Durham for data on 1H 0323+342 and for useful discussions throughout this work.

REFERENCES

Acero, F., Ackermann, M., Ajello, M., Albert, A., Atwood, W. B., Axelsson, M., et al. (2015). Fermi large area telescope third source catalog. *Astrophys. J. Suppl.* 218:23. doi: 10.1088/0067-0049/218/2/23

Calderone, G., Ghisellini, G., Colpi, M., and Dotti, M. (2012). B2 0954+25A: a typical Fermi blazar or a γ-ray loud Narrow Line Seyfert 1. *Month. Notices R. Astron. Soc.* 424, 3081–3093. doi: 10.1111/j.1365-2966.2012.21456.x

Cerruti, M., Boisson, C., and Zech, A. (2013a). Constraining the parameter space of the one-zone synchrotron-self-Compton model for GeV-TeV detected BL Lacertae objects. *Astron. Astrophys.* 558:A47. doi: 10.1051/0004-6361/201220963

Cerruti, M., Dermer, C. D., Lott, B., Boisson, C., and Zech, A. (2013b). Gamma-ray blazars near equipartition and the origin of the gev spectral break in 3c 454.3. *Astrophys. J. Lett.* 771:L4. doi: 10.1088/2041-8205/771/1/L4

Dermer, C. D., and Menon, G. (2009). *High Energy Radiation from Black Holes: Gamma Rays, Cosmic Rays, and Neutrinos*. Princeton, NJ: Princeton University Press.

Donea, A.-C., and Protheroe, R. J. (2003). Radiation fields of disk, BLR and torus in quasars and blazars: implications for /γ-ray absorption. *Astropart. Phys.* 18, 377–393. doi: 10.1016/S0927-6505(02)00155-X

Finke, J. D. (2016). External compton scattering in blazar jets and the location of the gamma-ray emitting region. *Astrophys. J.* 830:94. doi: 10.3847/0004-637X/830/2/94

Finke, J. D., and Dermer, C. D. (2010). On the break in the fermi-large area telescope spectrum of 3C 454.3. *Astrophys. J. Lett.* 714, L303–L307. doi: 10.1088/2041-8205/714/2/L303

Finke, J. D., Dermer, C. D., and Böttcher, M. (2008). Synchrotron self-compton analysis of TeV X-ray-selected BL lacertae objects. *Astrophys. J.* 686, 181–194. doi: 10.1086/590900

Fuhrmann, L., Karamanavis, V., Komossa, S., Angelakis, E., Krichbaum, T. P., Schulz, R., et al. (2016). Inner jet kinematics and the viewing angle towards the γ-ray narrow-line Seyfert 1 galaxy 1H 0323+342. *Res. Astron. Astrophys.* 16:176. doi: 10.1088/1674-4527/16/11/176

Ghisellini, G., and Tavecchio, F. (2009). Canonical high-power blazars. *Month. Notices R. Astron. Soc.* 397, 985–1002. doi: 10.1111/j.1365-2966.2009.15007.x

Ghisellini, G., Tavecchio, F., and Ghirlanda, G. (2009). Jet and accretion power in the most powerful Fermi blazars. *Month. Notices R. Astron. Soc.* 399, 2041–2054. doi: 10.1111/j.1365-2966.2009.15397.x

Katarzyński, K., Lenain, J.-P., Zech, A., Boisson, C., and Sol, H. (2008). Modelling rapid TeV variability of PKS2155-304. *Month. Notices R. Astron. Soc.* 390, 371–376. doi: 10.1111/j.1365-2966.2008.13753.x

Katarzyński, K., Sol, H., and Kus, A. (2001). The multifrequency emission of Mrk 501. From radio to TeV gamma-rays. *Astron. Astrophys.* 367, 809–825. doi: 10.1051/0004-6361:20000538

Landt, H., Ward, M. J., Baloković, M., Kynoch, D., Storchi-Bergmann, T., Boisson, C., et al. (2017). On the black hole mass of the γ-ray emitting narrow-line Seyfert 1 galaxy 1H 0323+342. *Month. Notices R. Astron. Soc.* 464, 2565–2576. doi: 10.1093/mnras/stw2447

Lenain, J.-P., Boisson, C., Sol, H., and Katarzyński, K. (2008). A synchrotron self-Compton scenario for the very high energy γ-ray emission of the radiogalaxy M 87. Unifying the TeV emission of blazars and other AGNs? *Astron. Astrophys.* 478, 111–120. doi: 10.1051/0004-6361:20077995

Paliya, V. S., Sahayanathan, S., Parker, M. L., Fabian, A. C., Stalin, C. S., Anjum, A., et al. (2014). The peculiar radio-loud narrow line seyfert 1 galaxy 1H 0323+342. *Astrophys. J.* 789:143. doi: 10.1088/0004-637X/789/2/143

Conflict of Interest Statement: The authors declare that the research was conducted in the absence of any commercial or financial relationships that could be construed as a potential conflict of interest.

The reviewer AN and handling Editor declared their shared affiliation.

Copyright © 2017 Arrieta-Lobo, Boisson and Zech. This is an open-access article distributed under the terms of the Creative Commons Attribution License (CC BY). The use, distribution or reproduction in other forums is permitted, provided the original author(s) or licensor are credited and that the original publication in this journal is cited, in accordance with accepted academic practice. No use, distribution or reproduction is permitted which does not comply with these terms.

frontiers in Astronomy and Space Sciences

REVIEW
published: 01 March 2018
doi: 10.3389/fspas.2018.00006

A Main Sequence for Quasars

Paola Marziani[1], Deborah Dultzin[2], Jack W. Sulentic[3], Ascensión Del Olmo[3], C. A. Negrete[2], Mary L. Martínez-Aldama[3], Mauro D'Onofrio[4], Edi Bon[5], Natasa Bon[5] and Giovanna M. Stirpe[6]*

[1] INAF, Osservatorio Astronomico di Padova, Padua, Italy, [2] Instituto de Astronomía, Universidad Nacional Autonoma de Mexico, Mexico City, Mexico, [3] Instituto de Astrofísica de Andalucía (CSIC), Granada, Spain, [4] Dipartimento di Fisica e Astronomia "Galileo Galilei", Università di Padova, Padova, Italy, [5] Belgrade Astronomical Observatory, Belgrade, Serbia, [6] INAF, Osservatorio di Astrofisica e Scienza dello Spazio di Bologna, Bologna, Italy

The last 25 years saw a major step forward in the analysis of optical and UV spectroscopic data of large quasar samples. Multivariate statistical approaches have led to the definition of systematic trends in observational properties that are the basis of physical and dynamical modeling of quasar structure. We discuss the empirical correlates of the so-called "main sequence" associated with the quasar Eigenvector 1, its governing physical parameters and several implications on our view of the quasar structure, as well as some luminosity effects associated with the virialized component of the line emitting regions. We also briefly discuss quasars in a segment of the main sequence that includes the strongest FeII emitters. These sources show a small dispersion around a well-defined Eddington ratio value, a property which makes them potential Eddington standard candles.

Keywords: galaxy evolution, quasars, eigenvector 1, outflows, emission lines, supermassive black holes, black hole physics

OPEN ACCESS

Edited by:
Sandor Mihaly Molnar, National Taiwan University, Taiwan

Reviewed by:
Shai Kaspi, Tel Aviv University, Israel
Gordon Richards, Drexel University, United States

****Correspondence:***
Paola Marziani
paola.marziani@oapd.inaf.it

Specialty section:
This article was submitted to Milky Way and Galaxies, a section of the journal Frontiers in Astronomy and Space Sciences

Received: *17 October 2017*
Accepted: *07 February 2018*
Published: *01 March 2018*

Citation:
Marziani P, Dultzin D, Sulentic JW, Del Olmo A, Negrete CA, Martínez-Aldama ML, D'Onofrio M, Bon E, Bon N and Stirpe GM (2018) A Main Sequence for Quasars. Front. Astron. Space Sci. 5:6. doi: 10.3389/fspas.2018.00006

1. INTRODUCTION

A defining property of type-1 quasars is the presence of broad and narrow optical and UV lines emitted by ionic species over a wide range of ionization potentials (IPs, Vanden Berk et al., 2001) which can be conveniently grouped in high-ionization lines (HILs) involving IP $\gtrsim$ 50 eV, and low-ionization lines from ionic species with IP $\lesssim$ 20 eV (**Table 1**). Optical and UV lines do not all show the same profiles, and quasar redshifts measured on different lines often show significant differences. Internal line shifts (i.e., differences in redshift from different emission lines measured for the same object) involve both broad and narrow emission lines and have offered a powerful diagnostic tool of the quasar innermost structure and of the emitting region dynamics since a few years after the discovery of quasars (Burbidge and Burbidge, 1967). This is true even if the assumption that unobscured type-1 quasars have very similar properties has remained widespread until very recent times. This assumption has been, in our opinion, one of the most damaging prejudices in the development of quasar research. At a meeting in 1999 in Mexico City Deborah Dultzin half-jokingly suggested that "a thousand spectra are worth more than one average spectrum" as an extension of the aphorism "a spectrum is worth a thousand pictures" (Dultzin-Hacyan et al., 2000). The developments in the last 15+ years have proved that this is indeed the case, although the value of single-epoch observations may have gone under appreciated with respect to other lines of evidence. We will therefore focus the scope of this review mainly to the organization of single-epoch spectra of large samples of quasars, following the "bottom-up" approach developed by Jack Sulentic and by his collaborators.

TABLE 1 | Identification of high- and low-ionization lines.

	Broad	Narrow	low-*z*	high-*z*
HILs (IP $\gtrsim$ 50 eV)	CIVλ1549, HeIIλ1640	[OIII]λλ4959,5007, HeIIλ1640,	Space	Visual
	NVλ1240	[Ne III]λ3869		
LILs (IP $\lesssim$ 20 eV)	HI Balmer (Hβ), FeII,	Balmer, [OII]λ3727, [OI]λ6300	Visual	IR
	MgIIλ2800, Ca IR Triplet	[SII]λλ6716,6731		

Over the years, the UV resonance line CIVλ1549 was considered as representative of broad HILs, and [OIII]λ4959,5007 were employed as strong and easily accessible narrow HILs. Typical broad LILs include Balmer lines, FeII emission as well as MgIIλ2800. Their analysis requires an accurate measurement of the quasar redshift. Narrow LILs (Hβ and [OII]λ3727) have been found to be the best estimator of the quasar systemic redshift which defines the quasar "rest-frame" (e.g., Eracleous and Halpern, 2003; Hu et al., 2008; Bon et al., in preparation). The representative narrow and broad HILs [OIII]λλ4959,5007 and CIVλ1549 show systematic blueshifts with respect to LILs in a large fraction of type-1 AGN (see e.g., Gaskell 1982; Tytler and Fan 1992; Corbin and Boroson 1996; Marziani et al. 1996; Richards et al. 2002; Zamanov et al. 2002; Zhang et al. 2011; Marziani et al. 2016b, and Shen et al. 2016 for broad and narrow lines, respectively). Broad LILs could be used as a last resort especially in high-redshift quasars where the UV rest-frame is accessible from optical observations and no narrow lines are observable (Negrete et al., 2014). Even if broad LILs can show significant shifts with respect to rest frame, these are infrequent, and rarely as large as those found among HILs.

The interpretation of inter-line shifts in quasar spectra is mainly based on the Doppler effect due to gas motion with respect to the observer, along with selective obscuration. This explanation is almost universally accepted. For [OIII]λ4959,5007 blueshifts, it is consistent with a moderately dense outflow ($\log n \sim 2-5$ [cm^{-3}]) of optically thin gas. For CIVλ1549, the explanation is not fully consistent if line emission occurs from optically thick clouds distributed, for example, symmetrically in a bicone whose axis is aligned with the spin of the black hole (e.g., Zheng et al., 1990). Such optically thick outflows might more easily give rise to a net redshift, if the receding part of the outflow remains visible. While it is no longer under discussion that large CIV blueshifts (amplitude $\gtrsim$ 1,000 km/s) involve radial motion + obscuration, Gaskell and Goosmann (2013) suggested an alternative explanation involving infall and "reflection." The observer does not see photons from the line emitting gas, but photons backscattered toward herself from a sea of hot electrons over the accretion disk. If the photons were originally emitted from infalling gas (i.e., approaching the disk), the observer should see a net blueshift. This explanation has some appeal for CIVλ1549, but sounds very unlikely for [OIII]λ4959,5007 because [OIII]λλ4959,5007 is emitted on spatial scales ranging from a few pc to thousands of pc, where a suitable "mirror" as the one potentially offered by hot electrons surrounding the accretion disk may not exist. In view of source commonality in terms of CIVλ1549 and [OIII]λ4959,5007 blueshifts (Marziani et al., 2016a,b), we will follow the most widely accepted interpretation that blueshifts involve outflow and obscuration for both CIVλ1549 and [OIII]λ4959,5007. The interpretation of LIL blue- and redshifts will follow the same assumption (with some caveats, section 8.1).

This review will be focused on the way internal line shifts and other quasar properties can be efficiently organized. A major step was an application to quasar spectra of the Principal Component Analysis (PCA) carried out in the early 1990s (Boroson and Green, 1992; Francis et al., 1992). Boroson and Green (1992) measured the most prominent emission features in the Hβ spectral region, and found the first hint of the quasar "main sequence" (MS; their Figure 9). The PCA and other statistical techniques require measurable parameters for a set of sources. The starting point is therefore the definition of a set of parameters (section 2) that may be conductive to the identification of fundamental correlations (the Eigenvectors) as well as to physics. The PCA of type-1 quasars (we remark in section 3 that we are dealing exclusively with type-1, unobscured quasars) yields a first eigenvector from which the MS is defined (section 4). After reviewing the MS correlates (section 5), we show how the "empirical" eigenvector 1 can be connected to the main physical parameters of quasars seen as accreting systems (sections 6 and 7). The most intriguing results point toward two different accretion structures in type-1 quasars (section 8), which are however largely self-similar over a wide range in luminosity. As an example of the power of the MS to identify sources that are physically similar, we consider quasars located at the extreme tip of the MS which are potential distance indicators (section 9).

2. DIAGNOSTICS FROM SINGLE-EPOCH SPECTRA: INTERNAL LINE SHIFTS AND INTENSITY RATIOS

Single-epoch spectroscopy of large quasar samples yields data defined by limits in multiplexing (i.e., by the ability to obtain a record of signals in different wavebands with the same observations): synoptical observations of the UV, visual, NIR rest frame have been challenging until a few years ago (and, in part, they are still challenging to-date). Given the limit in multiplexing, observations of low- and high-*z* quasars provide different information since different rest-frame wavelength ranges are covered: visual spectrometers provide the rest-frame Hβ range at low *z* but the rest-frame UV at $z \gtrsim 1.5$. To cover the rest-frame UV at low-*z*, space-based observations are needed. To cover Hβ at high *z*, NIR spectroscopy is needed. These limitations are being overcome by new generation instruments mounted at the focus of 8m-class telescopes which provide simultaneous coverage of visual and NIR, but these facilities were not available at the time most of the work reviewed in this paper was done. Synoptic observations of visual and UV at low-*z* still require coordinated ground and space-based observations which are especially hard to come by.

Table 1 provides an overview of the lines covered in the different domains. When we speak of intermediate to high-z objects (a population of behemoth quasars that is now extinguished), we are speaking of sources that are not anymore observed at $z \lesssim 1$ (mainly for the "downsizing" of nuclear activity, see e.g. Springel et al., 2005; Sijacki et al., 2015; Fraix-Burnet et al., 2017, and references therein). On the other hand, at high-z, only relatively few quasars with luminosities comparable to those of low-z quasars are known since their apparent magnitude would be too faint. They aren't yet efficiently sampled by the major optical source of quasar discovery, the Sloan Digital Sky Survey (SDSS, Blanton et al. 2017, and references therein).

2.1. Analysis

A prerequisite for a meaningful analysis of internal line shifts and intensity is a spectral resolution $R = \lambda/\delta\lambda \gtrsim 1,000$ and S/N $\gtrsim 20$. In addition, the quasar rest frame must be known with good precision. As mentioned in the Introduction, accurate redshifts can be obtained by limiting the measurements to narrow LILs (Hβ) and [OII]λ3727, the latter with some caveats (Bon et al., in preparation). Narrow HILs (e.g., [OIII]$\lambda\lambda$4959,5007) show systematic blueshifts (Zamanov et al., 2002; Eracleous and Halpern, 2003; Rodríguez-Ardila et al., 2006; Hu et al., 2008) whose amplitude is a strong function of their location along the quasar main sequence (section 5).

Once the rest frame is known, quantitative measurements of emission line profiles centroids, line widths at different fractional heights become possible. Centroids are defined by: $c(\frac{i}{4}) = (\mathrm{FW}(\frac{i}{4}) - 2 \cdot \lambda_0)/2$, $\forall i = 1, \ldots, 4$, where the full width is $\mathrm{FW}(\frac{i}{4}) = \lambda_R(\frac{i}{4}) - \lambda_B(\frac{i}{4})$.

In more recent times, we have applied a heuristic multicomponent decomposition whose rationale will be given in section 6.2, that is in part equivalent to a inter-percentile profile analysis (Shang et al., 2007; Marziani et al., 2010). This more model-dependent approach has been used along with centroids and width measurements on the full profile. Intensity ratios are computed separately for each profile component. The multicomponent fits have the advantage of isolating regions that are partly resolved in the radial velocity dimension and in different physical conditions (section 6.3).

An important element in the analysis of optical and UV lines is the measurement of the FeII emission contribution. As shown in Figure 1 of Marziani et al. (2006), FeII multiplets are strong in the optical and UV and even create a pseudo continuum in the range 2,100–3,000 Å. Contamination in the Hβ spectral range is also strong. Within the limits of the past analysis, it has proven appropriate to assume that the FeII multiplet ratios are always the same, even if the FeII features change equivalent width and FWHM from object to object (Boroson and Green, 1992). The trend shown in **Figure 1** motivates this assumption. In practice, it has been possible to model the FeII emission using a scaled and broadened template obtained from the Narrow Line Seyfert 1 (NLSy1) galaxy I Zw 1, a strong FeII emitter with narrow broad lines. More sophisticated approaches varying multiplet ratios (e.g., Kovačević et al., 2010) are needed in the rare cases where FeII emission appears peculiar.

Given the quantitative measurements on line profile and line profile components, much of the past work has been inspired by the Baconian approach (Bacon, 1902), deriving inferences by induction from observations without (much) prior benefit of theory. In practice this translated into (1) classifying data in a systematic way, to avoid a mixup of sources which are empirically different; (2) applying a quantitative but phenomenological description of the data, (3) performing uni- and multivariate statistics with a quantitative treatment of errors (including, for example, also the analysis of censored data). Model inferences have been deduced from the data separating aspects that were strongly constrained (for example, physical conditions derived from nebular physics), from those that required more speculative assumptions.

3. UNIFICATION MODELS AND TYPE-1 QUASARS

Unification schemes have provided a powerful conceptual framework suitable for organizing the analysis of AGN. The precursor distinction between type 1 and 2 Seyfert (Khachikian and Weedman, 1974) gained a convincing interpretation when Antonucci and Miller (1985) reported the discovery of a broad line component visible in the polarized spectrum of Seyfert 2 nuclei but invisible in natural light: the broad line region is hidden from view and only photons scattered by hot electrons toward our line of sight are received by the observer. This explanation remains alive and widely accepted today (e.g., Eun et al., 2017), even if we now know that is only a part of the story: type-2 AGN differ for environmental properties (Dultzin-Hacyan et al., 1999; Koulouridis et al., 2006; Villarroel and Korn, 2014), may intrinsically lack a BLR (Laor, 2000) at very low accretion rates, or may even be unobscured normal type-1 under special conditions (Marinucci et al., 2012). The point here is that unification models of RQ AGN separate two types of quasars on the basis of the viewing angle between the line of sight and the symmetry axis of the system (i.e., the spin axis of the black hole or the angular momentum vector of the inner accretion disk) but make no prediction on unobscured type 1 AGN. Orientation effects are expected also for unobscured type-1s, as we should observe them in the range of viewing angles, $0 \lesssim \theta \lesssim 45 - 60$. There is little doubt that broad line width is affected by orientation, especially for RL sources (e.g., Wills and Browne, 1986; Rokaki et al., 2003; Sulentic et al., 2003; Jarvis and McLure, 2006; Runnoe et al., 2014): a comparison between RL sources that are core-dominated (believed to be oriented with the jet axis close to the line-of-sight) and lobe-dominated (misaligned) shows that the Hβ FWHM is larger in the latter class. This result strongly suggests a flattened, axisymmetric structure for the BLR. For RQ objects, the evidence is not obvious and an estimate of θ remains an unsolved problem at the time of writing. However, orientation effects are certainly not enough to explain the diversity of quasar spectral properties.

4. THE QUASAR MAIN SEQUENCE

At the time the Boroson and Green (1992) paper appeared, studies based on moderately sized samples (20-30 objects) were

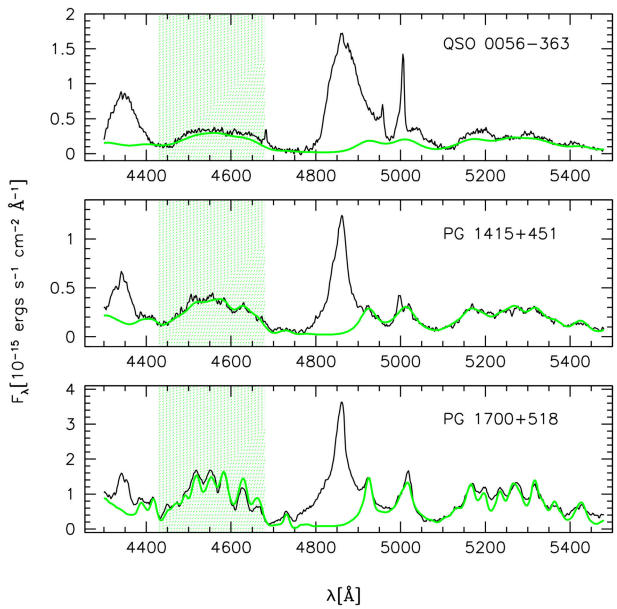

FIGURE 1 | Three type-1 quasars. The green line represents the FeII emission template, scaled and broadened to fit the observed FeII emission. The shaded area between 4,340 and 4,680 Å covers the wavelength range used to compute the total intensity of the blended emission at 4,570 Å to estimate the relative intensity between FeII λ 4,570 and Hβ i.e., the $R_{\rm FeII}$ parameter (Boroson and Green 1992, section 4). The three spectra show different $R_{\rm FeII}$: as the intensity ratio $R_{\rm FeII}$ decreases (from bottom to top), the Hβ line width increases. Also notable is the change in profile shape of Hβ. The spectra of the three quasars are exemplary of general trends involving LILs observed along the quasar main sequence.

common and often reached confusing results from correlation analysis. The best example is the Baldwin effect (an anti-correlation between equivalent width of HILs and luminosity) which was found in some and then not found in similar samples without apparent explanation.[1] In this respect the sheer size of the Boroson and Green (1992) sample was a key improvement. A novel aspect was also the application of the PCA which considers each parameter as a dimension of a parameter space, and searches for a new parameter space with fewer dimensions (defined by linear combinations of the original parameters) as needed to explain most of the data variance (Murtagh and Heck, 1987; Marziani et al., 2006). The application of the PCA was not unprecedented in extragalactic astronomy (e.g., Diaz et al., 1989) but was well suited to quasar data that appeared weakly correlated among themselves without providing a clear insight of which correlations were the most relevant ones.

The quasar Eigenvector 1 was originally defined by a PCA of ≈ 80 Palomar-Green (PG) quasars and associated with an anti-correlation between strength of FeIIλ4570, $R_{\rm FeII}$ (or [OIII] 5007 peak intensity) and FWHM of Hβ (Boroson and Green, 1992). The parameter $R_{\rm FeII}$ is defined as the ratio between the integrated flux of FeIIλ4570 blend of multiplets, and that of the Hβ broad component:[2] $R_{\rm FeII}$ = I(FeIIλ4570)/I(Hβ). Since 1992, various aspects of the Eigenvector 1 (E1) of quasars involving widely different datasets as well multi-frequency parameters have been discussed in more than 400 papers, as found on NASA ADS in August 2017 (Boroson and Green, 1992; Dultzin-Hacyan et al., 1997; Sulentic et al., 2000a,b, 2007; Shang et al., 2003; Grupe, 2004; Kuraszkiewicz et al., 2009; Mao et al., 2009; Tang et al., 2012). Earlier analyses have been more recently confirmed by the exploitation of SDSS-based samples (Yip et al., 2004; Wang et al., 2006; Zamfir et al., 2008; Kruczek et al., 2011; Richards et al., 2011; Marziani et al., 2013b; Shen and Ho, 2014; Brotherton et al., 2015; Sun and Shen, 2015).

The second eigenvector – Eigenvector 2 – was found to be proportional to luminosity, and eventually associated with the HIL Baldwin effect(s) that are the most-widely discussed luminosity effects in quasar samples (Baldwin et al., 1978; Dietrich et al., 2002; Bian et al., 2012). The smaller fraction of variance carried by the Eigenvector 2 indicates that luminosity is not the major driver of quasar diversity, especially if samples are restricted to low-z. We will not further consider HIL luminosity effects[3] but only discuss the influence of luminosity on the LIL FWHM (section 8.2).

The distribution of data points in the optical plane of the Eigenvector 1 FWHM(Hβ) vs. $R_{\rm FeII}$ traces the quasar main sequence (MS, **Figure 2**), defined for quasars of luminosity $\log L \lesssim 47$ [erg s^{-1}], and $z < 0.7$. The MS shape allows for the definition of a sequence of spectral types (**Figure 2**), and motivates subdividing the 4DE1 optical plane into a grid of bins of FWHM(Hβ) and FeII emission strength. Bins A1, A2, A3, A4 are defined in terms of increasing $R_{\rm FeII}$ with bin size $\Delta R_{\rm FeII} = 0.5$, while bins B1, B1+, B1++, etc. are defined in terms of increasing FWHM(Hβ) with Δ FWHM = 4,000 km s^{-1}. Sources belonging to the same spectral type show similar spectroscopic measurements (e.g., line profiles and line flux ratios). Spectral types are assumed to isolate sources with similar broad line physics and geometry. Systematic changes are reduced within each spectral type. If so, an additional advantage is that an individual quasar can be taken as a bona fide representative of all sources within a spectral type. The binning adopted (see **Figure 2**) has been derived for low-z (< 0.7) quasars. Systematic changes may not be eliminated in full, if an interpretation scheme such as the one of Marziani et al. (2001) applies, who posited a continuous effect of Eddington ratio and viewing angle (at a fixed $M_{\rm BH}$) as the origin of the MS shape (section 7.5 provides further explanations).

Developments in the analysis before late 1999 of low-z quasar spectral properties are reviewed in Sulentic et al. (2000a). Data

[1]The Baldwin effect was originally described by Baldwin et al. (1978) and later detected in several samples (Laor et al., 1995; Wills et al., 1999); negative results were concurrently obtained (Wu et al., 1983; Wilkes et al., 1999). Sulentic et al. (2000a) discuss early works, and the main reason of this apparent contradiction.

[2]The term broad component without the suffix BC is used here to identify the full broad profile excluding the Hβ narrow component. In more recent times, we have distinguished between two components, the broad component $H\beta_{\rm BC}$ and the very broad component $H\beta_{\rm VBC}$. The $H\beta_{\rm BC}$ is associated with the core of the Hβ broad line, and the $H\beta_{\rm VBC}$ with its broader base (see section 6.2).

[3]HIL luminosity effects are subject to strong biases. It is as yet unclear whether such biases can entirely account for the weak luminosity effects observed in large samples.

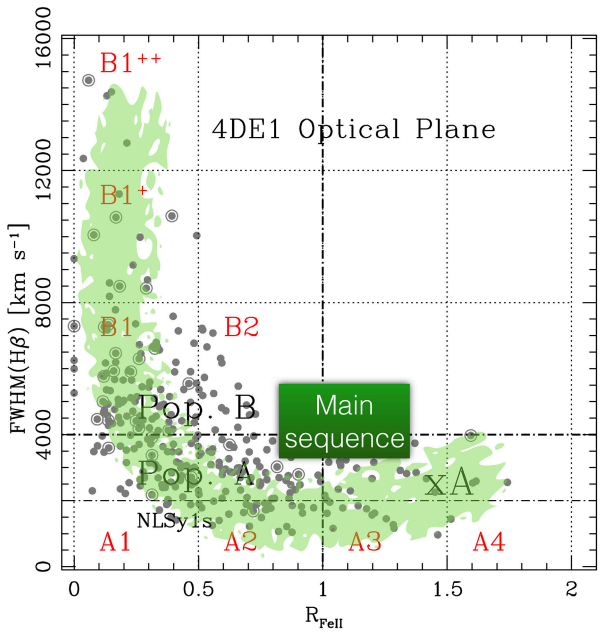

FIGURE 2 | The optical plane of the Eigenvector 1, FWHM(Hβ) vs. $R_{\rm FeII}$. The green shaded area indicatively traces the distribution of a quasar sample from Zamfir et al. (2010), defining the quasar MS. The thick horizontal dot-dashed line separates populations A and B; the thin identifies the limit of NLSy1s. The vertical dot-dashed line marks the limit for extreme Population A (xA) sources with $R_{\rm FeII} \gtrsim 1$. Dotted lines separate spectral types, identified as explained in section 4.

and ideas were in place as early as in year 2000 to introduce the idea of two quasar populations, A and B: Population A with FWHM(Hβ) $\leq$ 4,000 km s^{-1}; Population B (broader) with FWHM(Hβ) $>$ 4,000 km s^{-1} (Sulentic et al., 2000a,b). Later developments have confirmed that the two populations are two distinct quasar classes. Population A may be seen as the class that includes local NLSy1s as well as high accretors (Marziani and Sulentic, 2014), and Population B as a class capable of high-power radio-loudness (Zamfir et al., 2008, see section 5). It now seems unlikely that the two populations are just the opposite extremes of a single quasar "main sequence" defined in the plane FWHM(Hβ) vs. $R_{\rm FeII}$ (Sulentic et al., 2011, section 5), although the subdivision at FWHM(Hβ) = 4,000 km s^{-1} is not widely considered in literature. It is therefore worth analyzing the issue in some more detail after considering the main correlates along the MS.

5. A BIRD'S EYE VIEW OF THE MS CORRELATES

Several correlates have been proved as especially relevant in the definition of the MS multifrequency properties.

- Balmer emission line profile shape – Several past works found a clear distinction between Pop. A and B in terms of Balmer line profile shapes (Sulentic et al., 2002; Marziani et al., 2003b): Pop. A sources show Lorentzian Balmer line profiles, symmetric and unshifted; Pop. B, Double Gaussian (broad + very broad component, H$\beta_{\rm BC}$ + H$\beta_{\rm VBC}$, section 6.2), most often redward asymmetric. While several authors described the Balmer line profiles of NLSy1s as Lorentzian (e.g., Véron-Cetty et al., 2001; Cracco et al., 2016), the transition between the profile types is apparently occurring at 4,000 km s^{-1} and not at 2,000 km s^{-1}, the canonical limit of NLSy1. This early result (Sulentic et al., 2002) has been confirmed by several later analyses (e.g., Zamfir et al., 2010; Marziani et al., 2013b; Negrete et al., 2017). **Figure 3** shows composite spectra in the FWHM range 2,000–4,000 and 0–2,000 km s^{-1}: the profile shape remains the same as the line gets broader (Negrete et al., 2017). Mirroring Paolo Padovani's prescription as enunciated at the Padova meeting (Padovani 2017: no more RL, only jetted!), we would recommend to speak of Population A and B... and no more NLSy1s! In both cases, it is not just a matter of nomenclature: inter-sample comparison will be biased if the subdivision is inappropriate.
- UV diagnostic ratios – Major trends involve strong UV emission lines. Schematically, moving from spectral type B1++ to A4 we find: NVλ1240/Lyα: $\nearrow$; AlIIIλ1860/SiIII]λ1892: $\nearrow$ CIII]λ1909/SiIII]λ1892 $\searrow$ W(NIII]1750) $\nearrow$ W(CIVλ1549) $\searrow$. These trends can be interpreted as an increase in density and metallicity and decrease in ionization parameter of the LIL-emitting part of the BLR toward the strongest FeII emitters at the tip of the MS (Baldwin et al., 1996; Wills et al., 1999; Bachev et al., 2004; Nagao et al., 2006; Negrete et al., 2012, 2013).
- CIVλ1549 centroid shifts – The CIV1549 centroid blueshifts are a strong function of a source location along the E1 MS, reaching maximum values in correspondence of the extreme Pop. A (xA, spectral types A3 and A4). They can be accounted for by a scaled, almost symmetric and unshifted profile (such as the one of Hβ) plus an excess of blueshifted emission, corresponding to a "virialized" emitting region plus an outflow/wind component, respectively (Marziani et al., 2010). The relative prominence of the two components is a function of the location on the MS: the outflow component can dominate in xA sources, and be undetectable in sources at the other end of the MS (B1++) where the broader profiles are found. If we measure the centroid shift at half maximum $c(\frac{1}{2})$, large blueshifts are found only in Pop. A (Sulentic et al., 2007). The blueshifted excess is at the origin of a correlation between centroid shifts of CIVλ1549 and FWHM CIV (Coatman et al., 2016; Sulentic et al., 2017). This has important implications for $M_{\rm BH}$ estimates.
- [OIII] blueshifts – The [OIII]$\lambda\lambda$4959,5007 doublet mimics the blueshift observed for CIVλ1549 with respect to the rest frame. The average blueshift amplitude increases toward the high $R_{\rm FeII}$ end of the MS (Zamanov et al., 2002; Marziani et al., 2003a; Zhang et al., 2013; Cracco et al., 2016). This is emphasized by the distribution in the OP of the [OIII]$\lambda\lambda$4959,5007 "blue outliers" (BOs) which show blueshift at peak of amplitude $\gtrsim$ 250 km s^{-1}. Large [OIII] shifts such as those of the BOs are found for FWHM(Hβ)$<$ 4,000 km/s.

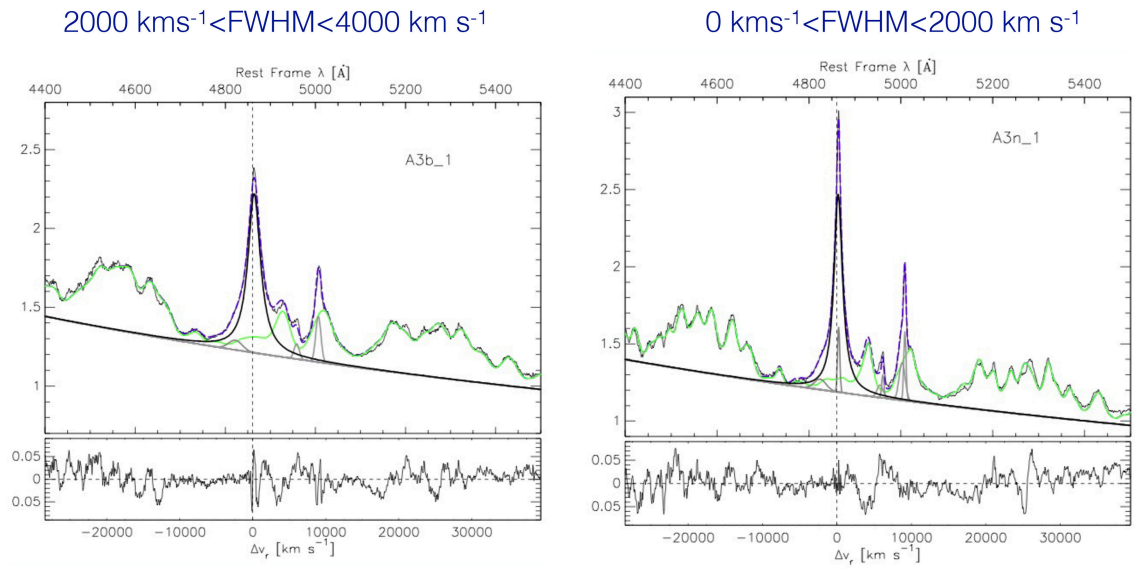

FIGURE 3 | Fits of the A3 spectral type composites, obtained for the broader (A3b_1) and narrow (A3n_1) half of the spectral bin. The original spectrum (thin black line) is shown with FeII emission (pale green) superimposed to the continuum and the Hβ line with a Lorentzian profiles (thick black lines). Thin gray lines trace H$\beta_{\rm NC}$ and [OIII]$\lambda\lambda$4959,5007 emission and, on the blue side of Hβ, a faint excess emission that is not accounted for by the symmetric shape of Hβ.

- LIL blueshifts – The profile of the resonance LIL MgIIλ2800 also suggests evidence of outflow (somewhat unexpectedly, Marziani et al. 2013b,a): low ionization outflows are detected in the xA spectral types, but lower radial velocities are involved in MgII λ2800 than in CIVλ 1549 ($\sim$ 100 vs. $\sim$ 1,000 km/s).
- Radio loudness – The probability of being RL is much larger among Pop. B sources: 25%, among Pop. A $\approx$ 3 – 4% (Zamfir et al., 2008). Core-dominated RL sources are displaced toward Pop. A in the optical plane of the E1 because of orientation effects. Zamfir et al. (2008) suggest that RL sources should be considered as such only if very powerful with $\log P_\nu$ > 31.6 [erg s^{-1} Hz^{-1}] at 20 cm, and Kellerman's $\log R_{\rm K}$ > 1.8 (Kellermann et al., 1989), in line with the distinction of jetted and non-jetted suggested by Padovani (2016) which considers as jetted only sources for which there is evidence of powerful, relativistic ejections. On a broader perspective, radio-loudness may not be restricted to low Eddington ratio, once the basic prescriptions for explaining jet formation that involve extraction of the rotational energy of the black hole or of the accretion disk in the presence of a large-scale, well-ordered, and powerful magnetic field are satisfied (Blandford and Znajek, 1977; Blandford and Payne, 1982). Compact-steep spectrum (CSS) RL sources show high radio power (O'Dea, 1998) and properties that are of Pop. A, with relatively high $L/L_{\rm Edd}$ (Wu, 2009). Formation of jetted sources may occur also at high Eddington ratio, although the physical mechanism leading to jet production and collimation is presently unclear (for a review, see Czerny and You, 2016), and the jet properties may also be different (Gu, 2017, and references therein). If relatively low power is considered ($\log P_\nu$ $\sim$ 31 [erg s^{-1} Hz^{-1}]), the RL Pop. A sources include RL NSLy1s (Komossa et al., 2006). The γ-ray detection for some of them (Abdo et al., 2009; Foschini et al., 2010) may confirm their "jetted" nature. It has been suggested that RL NLSy1s have CSSs as a mis-aligned parent population (Berton et al., 2016). Therefore, the absence of luminous RL sources among Pop. A sources may be related to the absence of highly-accreting very massive black holes $M_{\rm BH}(\gtrsim 10^9 M_\odot)$ at relatively low-z (e.g., Cavaliere and Vittorini, 2000; Fraix-Burnet et al., 2017, and references therein).
- Soft X-ray slope – The steepness of the soft X-ray continuum measured by the photon index $\Gamma_{\rm soft}$ is also dependent on the location along the MS. $\Gamma_{\rm soft}$ is the measure of the soft-X excess (0.2–2 KeV) above a canonical power law with Γ $\approx$ 2. Values of $\Gamma_{\rm soft}$ > 2 are mainly found for FWHM(Hβ) < 4,000 km/s (i.e., in Pop. A, Boller et al., 1996; Wang et al., 1996; Sulentic et al., 2000a; Grupe, 2004; Shen and Ho, 2014; Bensch et al., 2015).

Tables reporting main-sequence correlates are provided in several recent review and research papers (e.g., Sulentic et al., 2011; Fraix-Burnet et al., 2017), and in Chapter 3 and 6 of D'Onofrio et al. (2012). To restrict the attention of a subset of especially significant parameters, Sulentic et al. (2000a) introduced a 4DE1 parameter space. In addition to FWHM(Hβ) and $R_{\rm FeII}$, two more observationally "orthogonal" parameters, $\Gamma_{\rm soft}$ and $c(\frac{1}{2})$ CIVλ1549 are meant to help establish a connection between observations and physical properties. The 4DE1 parameters clearly support the separation of Population A (FWHM

Hβ<4,000 km s^{-1}) and Population B(broader) sources,[4] although the non-optical parameters are not always useful since they are MS correlates and often unavailable. The immediate interpretation of the 4DE1 parameters is summarized in **Table 2**. In the simplest term, the FWHM Hβ is related to the velocity dispersion in the LIL emitting part of the BLR. On the converse, $c(\frac{1}{2})$ CIV yields a measurement affected by the high-ionization outflow detected in the HIL profile. The largest $c(\frac{1}{2})$ values indicate a decoupling between the strongest HIL and LIL features, with the latter remaining symmetric and unshifted (Marziani et al., 1996). The parameter $R_{\rm FeII}$ is of more complex interpretation. $R_{\rm FeII}$ is affected by the metallicity (obviously, if [Fe/H]$= -10$, $R_{\rm FeII}\approx 0$) but metallicity is most likely not all of the story (Joly et al., 2008), since FeII strength tends to saturate for high metallicity values. The main dependence is probably on ionization conditions, density and column density (section 7.5). A $\Gamma_{\rm soft} > 2$ is usually ascribed to Compton thick soft X-ray emission from a hot corona above the disk, but may also be the high-energy tail of the spectral energy distribution of the disk itself, in case the inner disk is very hot (e.g., Done et al., 2012; Wang et al., 2014a).

5.1. Pop. A and B: Really a Dichotomy?

Supporting evidence in favor of a dichotomy between Pop. A and B includes the change in the Hβ profile shape from Lorentzian-like to double Gaussian, with a redward asymmetry that is not detected in the narrower sources of Pop. A, not even in spectral type A1 where FeII emission is weak. Large CIVλ1549 centroid blueshifts are not observed in Pop. B unless sources of very high-luminosity are considered (Bischetti et al., 2017; Bisogni et al., 2017; Sulentic et al., 2017). Therefore, a dichotomy at $\approx$4,000 km s^{-1} for $z \lesssim 1$ and $\log L \lesssim 47$ [erg s^{-1}] is empirically supported by a sudden change in observations parameters. On the other hand, if $R_{\rm FeII}$ is mainly affected by $L/L_{\rm Edd}$ and the Hβ FWHM by the viewing angle, it is hard to justify a dichotomy (Shen and Ho, 2014). The analysis of Marziani et al. (2001) indicates that spectral type A1 may include sources which are intrinsically of Pop. B and observed almost pole on. However, the FWHM Hβ is also dependent on Eddington ratio (Nicastro, 2000, Figure 3 of Marziani et al. 2001). Most sources in bin A1 ($R_{\rm FeII} \leq 0.5$) are true Pop. A with Lorentzian Hβ profiles. The Eddington ratio corresponding to the change in Hβ and CIVλ1549 properties has been estimated to be $\approx 0.2 \pm 0.1$ in low-z, low-to-moderate L samples (Sulentic et al., 2000b; Marziani et al., 2003b). This is also the limit for the presence of a fully thin accretion disk (section 8.1; Abramowicz et al., 1988, 1997; Szuszkiewicz et al., 1996). At any rate, one should be aware that a fixed FWHM value only approximately corresponds to a well-defined Eddington ratio. The minimum FWHM for virialized systems (reached at maximum $L/L_{\rm Edd}$) is luminosity-dependent (section 8.2), and so is the FWHM corresponding to any fixed $L/L_{\rm Edd}$ even if the luminosity dependence is weak up lo $\log L \approx 47$ [erg s^{-1}] (Marziani et al., 2009).

[4]The 4,000 km s^{-1} limit is appropriate at low redshift and moderate luminosity $\log L \lesssim 47$ [erg s^{-1}]; see the discussion in section 8.2.

TABLE 2 | Interpretation of the 4FE1 parameter space.

Parameter	Immediate interpretation	Relation to accretion parameters and orientation at low-to-moderate L ($\lesssim 10^{47}$ erg/s)
FWHM Hβ	LIL-BLR velocity field	$L/L_{\rm Edd}$, θ, $M_{\rm BH}$
c(1/2) CIV	HIL-BLR velocity field (outflow)	$L/L_{\rm Edd}$, θ
$R_{\rm FeII}$	LIL ionization and density, $Z/Z_\odot$	$L/L_{\rm Edd}$, possibly θ
$\Gamma_{\rm soft}$	Compton-thick X-ray emission, accretion disk emission	$L/L_{\rm Edd}$

6. FROM EMPIRICISM TO PHYSICS

6.1. Synergy Between Reverberation Mapping and Single-Epoch Spectroscopy of Quasars

Reverberation mapping derived from the response of the emitting regions with respect to continuum changes resolves the radial stratification of the line emitting regions and helps assess their velocity field (e.g., Peterson, 1998; Peterson and Horne, 2006). The synergy with reverberation mapping helps to partially remove the spatial degeneracy of single-epoch spectra. The strongest evidence in support of virial motion for the line emitting gas comes from two lines of reverberation mapping investigation: (1) the anticorrelation between line broadening and the time lag of different lines in response to continuum variation (Peterson and Wandel, 1999; Peterson et al., 2004). This relation has been found for some nearby Seyfert-1 nuclei with a slope close to the one expected from the virial relation. (2) Velocity-resolved reverberation mapping (e.g., Gaskell, 1988; Koratkar and Gaskell, 1991; Grier et al., 2013) rules out outflow as the main broadening mechanism for LILs. A general assumption adopted in the interpretation of single-epoch spectra is that virial motion is indicated by almost symmetric and unshifted line profiles (within $\approx$100 km s^{-1} from rest frame, the typical rest frame uncertainty for moderate dispersion spectra).

6.2. Multi-Component Interpretation of Emission Lines

The broad profile of both LILs and HILs in each quasar spectrum can be modeled by changing the relative intensity of three main components, as shown schematically in **Figure 4**.

- The broad component (BC), which has been referred to by various authors as the broad component, the intermediate component, or the central broad component (e.g., Brotherton et al., 1994a; Popović et al., 2002; Kovačević-Dojčinović and Popović, 2015; Adhikari et al., 2016). As mentioned, the BC is represented by a symmetric and unshifted profile (Lorentzian for Pop. A or Gaussian for Pop. B) and is therefore assumed to be associated with a virialized BLR subsystem. The virialized BLR could be defined as the subregion that is in the condition to produce FeII emission.
- The blue shifted component (BLUE). A strong blue excess in Pop. A CIV profiles is not in doubt. In some CIV profiles

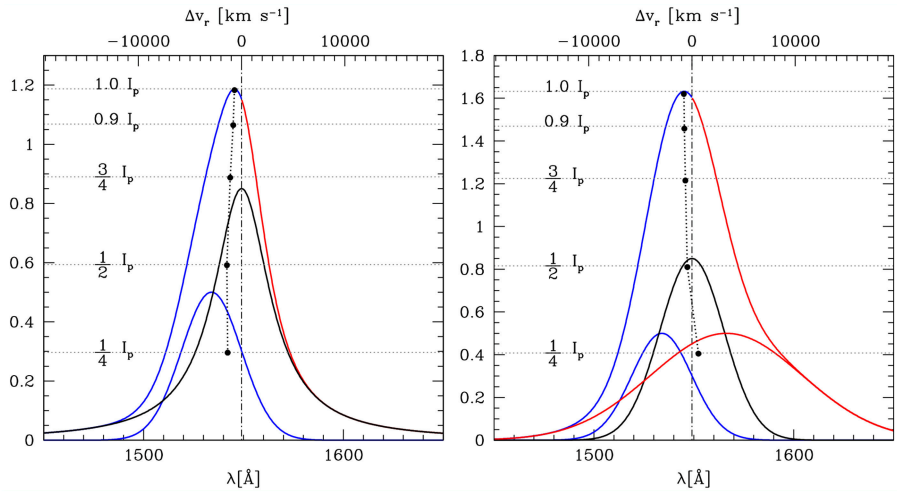

FIGURE 4 | Interpretation of line profiles, for Pop A, and Pop. B (right). Fractional intensity levels where line centroids are measured are identified. Mock profiles are shown to represent the bare broad profile of any of the strongest emission lines of quasars. The left one is built on 2 components, as appropriate for Pop. A, which are the BC and a blue shifted excess BLUE. The blue shifted component is strong in HILs and weak in LILs. Pop. B profiles are accounted for by three components: in addition to the BC and BLUE, a redshifted VBC is needed to account for the prominent redward line profile asymmetry.

like the extreme Population A prototype I Zw1 the blue excess is by far the dominant contributor to the total emission line flux (Marziani et al., 1996; Leighly and Moore, 2004). BLUE is modeled by one or more skew-normal distributions (Azzalini and Regoli, 2012). The "asymmetric Gaussian" use is, at present, motivated empirically by the often irregular appearance of the blueshifted excess in CIV and MgIIλ2800.

- The very broad component (VBC). The VBC was postulated because of typical Hβ profile of Pop. B sources, that can be (empirically) modeled with amazing fidelity (i.e., with no significant residuals above noise in the fit composite spectra), using the sum of two Gaussians, one narrower and almost unshifted (the BC) and one broader showing a significant redshift $\sim$ 2,000 km/s (Wills et al., 1993; Brotherton et al., 1994b; Zamfir et al., 2010). We expect a prominent CIV VBC associated with high ionization gas in the innermost BLR (Snedden and Gaskell, 2007; Marziani et al., 2010; Wang and Li, 2011; Goad and Korista, 2014). Past works indeed provided evidence of a VBC in CIV and Balmer lines (e.g., Marziani et al., 1996, 2010; Sulentic et al., 2000c; Punsly, 2010). Mirroring the definition of BLR, a VBLR may be defined as the region that is not able to emit significant FeII. Imposing significant FeII VBC emission in the multicomponent maximum likelihood fits of Population B Hβ produces unrealistic emission patterns in the FeII blend. Agreement is restored only when VBC emission is assumed negligible. At high L, BLUE can dominate in Pop. B CIVλ1549 profile, too, but the VBC remains well-visible, especially in Hβ.

6.3. LIL- and HIL-Emitting Regions

The symmetric BC and the BLUE are consistent with a two-region model proposed since the late 1980s (Collin-Souffrin et al., 1988), where the BC is emitted in a flattened distribution of gas while BLUE is associated with an high ionization outflow. A two region model such as a disk + radiation dominated wind is also qualitatively consistent with the data (Elvis, 2000).

Considering intensity ratios using the full line profiles can be misleading and may yield to problematic inferences. For example, the explanation of the Lyα/Hβ ratio has been one of the most challenging problems in the interpretation of line formation within the BLR (Netzer et al., 1995). It is easier to account for the observed ratios if BLUE and BC are kept separated. In the BLUE case, the ratio Lyα/Hβ is very high, consistent with relatively low density and high ionization ($\approx$ 30 close to the case A in the low-density limit, Osterbrock and Ferland 2006), while in the BC case Lyα/Hβ is low ($\approx 5-10$) which requires high density and low-ionization, following CLOUDY simulations (Marziani et al., 2010). It has proven possible to reproduce the profiles of the strongest broad emission lines along the MS changing the relative proportion of the three components, BLUE, BC, and VBC, but assuming consistent component shift, width and shape parameter for all lines. As a second example, it is interesting to consider the case of the CIVλ1549 profile in broad Pop. B RL and RQ sources. The centroid shifts to the blue are modest for both RQ and RL; however, redshifted $c(\frac{1}{2})$ are not unfrequent among RL but very rare among RQ (Sulentic et al., 2007; Richards et al., 2011). Comparing the CIV profile to Hβ offers a clue: Hβ can be accounted for by two Gaussians, one of them redshifted by $\sim$ 1,000–2,000 km/s. With respect to the Hβ profile, the CIV lines shows a blueshifted excess (the BLUE component) that, even if not as strong as in Pop. A, has nonetheless the effect to symmetrize their profile. In some RL it may be completely absent, so that centroid measurements of CIV and Hβ agree (Marziani et al., 1996). This analysis allows us to infer two interesting facts: whenever BLUE is present we have CIV/H$\beta \gg 1$ (if BLUE is not detected in Hβ, a lower limit to CIV/Hβ is measured from the

noise); BLUE is apparently more prominent in Pop. B RQ than in RL, an effect that may be associated with the effect of the jet lateral expansion on the accretion disk wind (Sulentic et al., 2015).

The relative prominence of the three components can be accounted for in terms of balance of radiation and gravitation forces, at least in RQ quasars. If line emitting gas is optically thick to the Lyman continuum then the radiation will exert an outward acceleration that is inversely proportional to the column density N_c and directly proportional to the ionizing luminosity. The ratio between the radiative and gravitational acceleration for gas optically thick to the Lyman continuum is: $r_a = a_{rad}/a_{grav} \approx 0.176\kappa L_{44} M_{BH,8}^{-1} N_{c,23}^{-1}$ where M_{BH} is in units of 10^8 solar masses, and L_{44} the bolometric luminosity in units of 10^{44} erg/s, κ the fraction of the bolometric continuum that is ionizing HI ($\lambda < 912$Å), $\alpha \approx 0.5$ (Marziani et al., 2010). The equation can take the form $r_a \approx 7.2\, L/L_{Edd} N_{c,23}^{-1}$, and shows that the net outward acceleration is proportional to L/L_{Edd}, and inversely proportional to column density N_c. If $r_a \gg 1$, radiative acceleration dominates, as it is apparently the case of the high ionization gas emitting the blueshifted excess (i.e., BLUE). If $r_a \ll 1$, the emitting gas may be infalling toward the central black hole, yielding the observed redshifted VBC. This interpretation is compatible with large N_c values for the VBLR and would naturally explain why the VBC is observed in objects with low Eddington ratio, $L/L_{Edd} \lesssim 0.1$. Similar considerations have been made to explain the origin of an FeII redshift with respect to the broad FeII emission (Ferland et al., 2009; Hu et al., 2012). While the reality of FeII emission shifts is debatable (Sulentic et al., 2012), an infall scenario may well apply to inner BLR yielding a redshifted VBC, provided that column density is high enough to withstand radiation forces.

7. CONNECTION TO ACCRETION PARAMETERS

Several physical parameters (black hole mass M_{BH}, Eddington ratio, spin, and the aspect angle θ) are expected to affect the parameters of the E1 MS, even if in an indirect way as in the case of the spin. Establishing a connection between a physical and an observational set of parameters is precisely the aim of the 4DE1 parameter space. **Table 2** lists the main physical parameters on which the empirical 4DE1 parameters are expected to be dependent. We still have a very incomplete view of the physics along the Eigenvector 1 sequence because we are able to make only coarse estimates of physical parameters. However, Eddington ratio and viewing angle θ are likely to be the main culprits affecting the location of a quasar along the MS, as discussed in the next sections.

7.1. Black Hole Mass

The virial black hole mass can be written as $M_{BH} = f r_{BLR} \delta v^2/G$, where f is the emitting region structure or form factor, δv is a VBE (typically the line FWHM or its dispersion), and r_{BLR} is a characteristic distance from the black hole of the line emitting gas (i.e., in practice the distance derived from reverberation mapping or from the photoionization method). There are two fundamental aspects to consider: evaluating M_{BH} requires consistent estimates of r_{BLR} and δv, for different lines; in addition, the parameters entering the virial expression of M_{BH} $(f, r_{BLR}, \delta v)$ *all depend on the location of the E1 sequence.* It is an unfortunate circumstance that, to-date, this fact has not been taken into account in an exhaustive way. In the following we just mention how the applications of the E1 trends on the computation of M_{BH} can improve the accuracy of its estimates.

7.1.1. The Virial Broadening Estimator (VBE)

There is a growing consensus that the line width of the strongest LILs (Hβ and Mgλ2800) provide a reliable VBE, up to the highest luminosities (e.g., Trakhtenbrot and Netzer, 2012; Mejía-Restrepo et al., 2016; Sulentic et al., 2017). UV intermediate emission lines – have been found suitable as well, at least for low-z quasars (Negrete et al., 2013), The HIL CIV has been considered as a sort of taboo, as it offers a highly biased VBE (Baskin and Laor, 2005; Netzer et al., 2007; Sulentic et al., 2007). The broadening of CIVλ1549 is affected by shear velocity in an outflow, and its FWHM is not immediately offering a reliable VBE (as recently discussed in the review of Marziani et al., 2017a). Figure 1 of Marziani et al. (2017a) shows the bias introduced into CIV M_{BH} computations along the MS by using uncorrected FWHM CIV values. Actually, in Pop. A errors on M_{BH} as large as factor of 100 are possible if the CIV FWHM is measured on the full CIV profile. Even if corrections can be derived, whether the CIV width may be a reliable VBE remains controversial (Denney et al., 2013; Coatman et al., 2017; Marziani et al., 2017a, and references therein). It is possible to identify corrections that would reduce the scatter between Hβ and CIV-based M_{BH} estimates to ≈ 0.33 (Coatman et al., 2017; Marziani et al., 2017a). In other words, applying corrections to the CIV FWHM, the Hβ and CIV FWHM lines would become equivalent VBEs. While important conceptually, these corrections may be cumbersome to apply in practice: since they are based on measures of the CIV line shift [the nonparametric measure of Coatman et al. 2017 is equivalent to $c(\frac{1}{2})$], they still require the knowledge of the quasar rest frame which is not always straightforward to estimate (as pointed out in section 1; see also Hewett and Wild 2010 for a discussion of z-dependent biases). In addition, corrections are different for Pop. A and B, and considering the Eddington ratio bias implicit in flux limited samples (Sulentic et al., 2015), they may remain sample-dependent.

We are now able to analyze systematic trends for the virial broadening of low-ionization lines along the E1 MS leaving aside random orientation effects that are expected to influence δv estimates. We can define a parameter ξ yielding a correction to the observed profile: $\xi = \mathrm{FWHM_{VBE}}/\mathrm{FWHM_{obs}} \approx \mathrm{FWHM_{BC}}/\mathrm{FWHM_{obs}}$, where the VBE FWHM can be considered best estimated by the FWHM of the broad component of any line, $\mathrm{FWHM_{BC}}$. The non-virial broadening affecting the integrated profiles of LILs along the E1 sequence is due to different mechanisms (as mentioned in section 5): the A3/A4 spectral types are affected by outflow, while the Hβ redward asymmetry may suggest an infall of the VBC emitting gas. However, the correction factor is modest ($0.75 \leq \xi \leq 1.0$) for both Hβ and MgIIλ2800, with $\xi \approx 1.0$ in spectral types A1 and A2. In

other words, a simple correction is sufficient to extract a VBE from the observed FWHM. The correction can be evaluated for each spectral type or by applying individual source corrections as described in Marziani et al. (2017a).

7.1.2. Estimates of $r_{\rm BLR}$

We can distinguish primary and secondary estimates of the radius of the BLR $r_{\rm BLR}$. Primary determinations come from reverberation mapping monitoring (Horne et al., 2004; Peterson, 2014, and references therein) and are measured from the time lag τ yielded by the peak or centroid of the cross-correlation function between continuum and line light curves. Primary estimates can be also obtained from rest-frame, single-epoch UV spectra using the so-called photoionization method, as summarized below. Secondary determinations are computed using the correlation between $r_{\rm BLR}$ and luminosity that has been derived from reverberation-mapped sources (e.g., Kaspi et al., 2000, 2007; Bentz et al., 2009; Du et al., 2016): $r_{\rm BLR} \propto L^a$, a≈0.5 – 0.65 (Kaspi et al., 2000; Bentz et al., 2006).

There are several caveats underlying the RM measure of $r_{\rm BLR}$ and its scaling law with luminosity (Marziani and Sulentic, 2012). This correlation has a considerable scatter (Marziani and Sulentic, 2012) that is propagating itself on the mass scaling laws written in the form $M_{\rm BH} = M_{\rm BH}(L, FWHM) = kL^a FWHM^b$ (e.g., Vestergaard and Peterson, 2006; Shen and Liu, 2012; Trakhtenbrot and Netzer, 2012). In addition, the $r_{\rm BLR}$ – L scaling relation depends on dimensionless accretion rate (Du et al., 2016). Therefore the scaling laws should be redefined for at least Pop. A, extreme Pop. A (as actually done by Du et al. 2016) and Pop. B along the E1 sequence.

The ionization parameter U can be written as $U = Q(H)/4\pi r_{\rm BLR}^2 n_{\rm H} c \propto L/r^2 n$ (Netzer, 2013), where $Q(H)$ is the number of hydrogen ionizing photons. The radius of the BLR then can be recovered as $r_{\rm BLR} = \frac{1}{h^{1/2}c}(n_{\rm H}U)^{-1/2}\left(\int_0^{\lambda_{Ly}} f_\lambda \lambda d\lambda\right)^{1/2} d_{\rm C}$, where $d_{\rm C}$ is the comoving distance to the source (Hogg and Fruchter, 1999), and the integration is carried out to the Lyman limit $\lambda_{\rm Ly} = 912$ Å. Clearly, the ionizing photon flux $Un_{\rm H}$ is a measurement of the exposure of the BLR to ionizing photons and hence has an intrinsic, strong dependence on $r_{\rm BLR}$. The first explorative estimates of $M_{\rm BH}$ using the photoionization method were based on the rough similarity of AGN spectra, and on the consequent assumption of constant U or of constant product $Un_{\rm H}$ (Padovani and Rafanelli, 1988; Wandel et al., 1999). The consideration of UV line ratios which can be used as diagnostics constraining ionizing photon flux, and, in some cases, $n_{\rm H}$ (Verner et al., 2004; Negrete et al., 2013, 2014) yielded a major improvement. It is remarkable that the $r_{\rm BLR}$ estimates from the $Un_{\rm H}$ product and the Hβ $r_{\rm BLR} = c\tau$ from reverberation mapping are in very good agreement, at least for 12 low-L AGNs. In both cases (photoionization and reverberation) we are trying to give *one* number that should be representative of a very complex region, probably stratified, perhaps chaotic. Evidently, the 1,900 blend lines of AlIIIλ1860 and SiIII]λ1892 (but not CIIIλ1909!) trace the physical conditions of the Hβ emitting gas with maximum responsivity, which is not surprising since AlIIIλ1860 and SiIIλ1816 are lines emitted by ionic species with low-to-intermediate ionization potential, $\approx 15 - 20$ eV (Negrete et al., 2012).

A second remarkable aspect emerges from the analysis of the 1,900 blend. Negrete et al. (2013) showed that the solutions yielding the $Un_{\rm H}$ product differ significantly if the CIIIλ1909 is involved with other high ionization lines, or if CIVλ1549, AlIIIλ1860, SiIII]λ1892, SiIVλ1397,1402, SiIIλ1816 are considered. Their Figure 2 clearly shows that CIIIλ1909 involves a solution of lower density and higher ionization. This can be interpreted as evidence of stratification within the BLR. If extreme Population A sources are considered, CIIIλ1909 is weak in their spectra and only the low-ionization solution remains. The CIIIλ1909/SiIII]λ1892 ratio may be further lowered because of the relatively soft spectral energy distribution of xA sources (Casebeer et al., 2006). Apparently, the xA sources have their LIL/IIL emission dominated by dense, low-ionization gas (as lower density and column density gas is being pushed away from the BLR in a high ionization outflow with CIVλ1549/CIIIλ1909≫1).

The application of the photoionization method has been extended to high-L quasars where it remains basically untested: apart from the absence of systematic effects with scaling laws prediction, the precision and accuracy of individual photoionization estimates have nothing they can be compared with. Negrete et al. (2013) suggested a tentative correction on the basis of the equivalent width ratio between AlIII and CIII] (an E1 correlate) but the correction is highly uncertain. More objects are needed to better understand the behavior of the photoionization-derived $r_{\rm BLR}$ along the E1 sequence. In principle, however, the photoionization method has the potential to reduce the intrinsic scatter in $M_{\rm BH}$ determination, if it is really able to produce $r_{\rm BLR}$ estimates in close agreement with the RM $c\tau$.

7.2. Orientation Effects

There is no doubt that orientation effects influence the FWHM of Hβ in radio loud type-1 quasars (as mentioned in section 3): the line is systematically broader in FRII than in CD sources (e.g., Wills and Browne, 1986; Rokaki et al., 2003; Sulentic et al., 2003). It is reasonable to assume that similar amplitude effects are present also in RQ sources (Marziani et al., 2001) although defining a reliable orientation indicator has proved elusive. Recent results suggest that orientation is affecting the shifts of [OIII] (as well as the EW, Risaliti et al. 2011) and of FeII: face-on sources should show no FeII shifts and high amplitude blueshifts; more inclined sources should show FeII redshifts (associated with an equatorial inflow) and no net [OIII] blueshifts (Hu et al., 2008; Boroson, 2011). While [OIII] shifts and EWs are most likely affected by orientation, orientation does not appear to be the main parameter, if [OIII] emission is considered in different parts of the E1 sequence. Highly blueshifted sources (such as the BOs) are apparently associated exclusively with high Eddington ratio, more than those with a face-on orientation (Marziani et al., 2003b; Xu et al., 2012). The distribution of [OIII] blueshift amplitudes along the E1 sequence is qualitatively not consistent with orientation-only

effects. As already mentioned, the reality of FeII high-amplitude redshifts that would serve as indicators has been questioned recently (Sulentic et al., 2012). Even if we have not yet identified an orientation indicator, orientation effects most likely account for a large part of the scatter in $M_{\rm BH}$ determinations. The observed velocity can be parameterized as $v^2_{\rm obs} = v^2_{\rm iso}/3 + v^2_{\rm Kepl}\sin^2\theta$, and if $v_{\rm iso}/v_{\rm Kepl} \approx 0.1$, where $v_{\rm iso}$ is an isotropic velocity component, and $v_{\rm Kepl}$ the Keplerian velocity. For a geometrically thin disk, it implies $v_{\rm obs} \approx v_{\rm Kepl}/\sin\theta$ (if the FWHM is taken as the $v_{\rm obs}$, and $v_{\rm Kepl} = 0$ i.e., in the case of isotropic velocity dispersion, $f = \frac{3}{4}$). If the VBE estimates are not corrected beforehand for orientation, the structure (or form) factor is $f \propto 1/\sin^2\theta$ (Jarvis and McLure, 2006). The structure factor is also expected to depend on physical parameters (Eddington ratio, metallicity, disk temperature etc.) apart from aspect effects.

7.3. The Structure Factor

The velocity resolved RM yields an amazing variety of velocity fields for different objects (e.g., Grier et al., 2013; Peterson, 2017). The evidence favoring a rotational component has been steadily growing, in part due to deep, single-epoch spectropolarimetric observations (e.g., Smith et al., 2005; Afanasiev et al., 2015) that revealed the polarization vector changes expected from the Keplerian velocity field as seen from an equatorial scatter. Systematic outflows have been made evident by the ubiquitous blueshifts of the CIVλ1549 emission line. A hint to the BLR structure is provided by the FWHM/σ ratio, where σ is the velocity dispersion of the profile. For Pop. A, the ratio is low, while it is close to the value expected for a Gaussian in Pop. B (Collin et al., 2006; Kollatschny and Zetzl, 2011). The implication drawn from this result by Kollatschny and Zetzl (2011) is that broader lines imply faster rotation, which is consistent with the inferences based on the 4DE1 context (section 8.1). The structures underlying the typical Pop. A and B broad profiles (section 8.1) are however still unclear.

In Pop. A the Lorentzian profiles are consistent with an extended accretion disk seen at moderate inclinations (Dumont and Collin-Souffrin, 1990), but in the context of AGN, several velocity fields can produce Lorentzian-like profiles (e.g., Mathews, 1993; Netzer and Marziani, 2010; Czerny et al., 2017). Recent works suggest a disk-core with wings produced in a region of enhanced vertical velocity dispersion with respect to the disk (Goad et al., 2012).

On the other hand the quasi-symmetric profiles of the Pop. B LILs imply virial/Keplerian motion with stratified physical properties (e.g., Fausnaugh et al., 2017). An intriguing possibility is that the VBC may be emitted by the inner accretion disk (Bon et al., 2009; Storchi-Bergmann et al., 2017), with the BC masking the double-peaked accretion disk profile expected if the disk external radius is not extremely large, $\gtrsim 10^3 R_{\rm g}$.

Collin et al. (2006) derived different values for $f_{\rm S}$ for Pop. A and B, 2.1 and 0.5 respectively, with a substantial scatter. The distinction between Pop. A and B therefore appears to be the minimal criterion to reduce scatter in $M_{\rm BH}$ estimates, also because comparison of the same line width measure is not easy to understand if profile shapes are different. A more refined approach may consider individual spectral types along the quasar MS.

7.4. $L/L_{\rm Edd}$

The $M_{\rm BH}$ scaling laws provide a simple recipe usable with single-epoch spectra of large samples of quasars. Estimates of the Eddington ratio are derived by applying a constant bolometric correction to the observed luminosity, typically a factor 10–13 from the flux at 5100 Å and 3.5–5 from the measured at 1450 Å (Elvis et al., 1994; Richards et al., 2006; Krawczyk et al., 2013). Bolometric corrections most likely depend on the source location along the MS: the anti correlation between UV luminosity and optical-to-X spectral index (between 2500 Å and 2 KeV) may go in the sense of softer continua in Pop. A (Laor et al., 1997; Steffen et al., 2006). In addition, bolometric corrections are most likely luminosity as well as orientation dependent (Runnoe et al., 2013). However, our group did not carry out a systematic study as yet, and applied almost always constant corrections.

7.5. Why Does Ionization Level Decrease With Increasing $L/L_{\rm Edd}$?

As early as in the 2000s, a puzzling but remarkable aspect appeared to be the decrease in ionization degree at high Eddington ratio: Pop. A spectra show strong FeII, low [OIII] and CIVλ1549, while Pop. B sources with $L/L_{\rm Edd} \lesssim 0.2$ show prominent (high EW) HILs.

The ionization parameter U can be rewritten in terms of $L/M_{\rm BH}$ and $M_{\rm BH}$, under several assumptions. The number of ionizing photons is $Q(H) \approx \kappa L/ < h\nu >$. A typical AGN continuum as parameterized by Mathews and Ferland (1987) yields $< \nu > \approx 1 \times 10^{16}$ Hz and $\kappa \approx 0.5$. The velocity field for the LIL-emitting gas is mainly virial, so that we can write: FWHM $\propto M^{1/2} r^{-1/2}$. We can consider that the ratio I(AlIIIλ1860)/I(SiIII]λ1892) is a density-dependent diagnostics (almost independent of the ionization parameter)[5], and that I(Al III)/I(Si III]λ1892) and I(Si III]λ1892)/I(C III]) are inversely correlated with FWHM. Using the trend found by Wills et al. (1999), $n \propto {\rm FWHM}^{-4/3}$. At this point it is possible to write $R_{\rm FeII}$ as a function of $L/L_{\rm Edd}$ and $M_{\rm BH}$ using two approaches (Marziani et al., 2001).

- Considering that $L/M_{\rm BH} \propto {\rm FWHM}^{-2}$, with $M_{\rm BH}$ estimated from X-ray variability, not from the virial relation, to avoid circularity. The expression for $U \propto \frac{L}{r^2 n} \propto (L/M_{\rm BH})^{-5/3} M^{-1}$ follows from $n \propto {\rm FWHM}^{-4/3}$ and $r \propto M/{\rm FWHM}^2$.
- Adopting the $r \propto L^a$ scaling law, and considering again that $n \propto {\rm FWHM}^{-4/3}$ and FWHM $\propto M^{1/2}_{\rm BH} r^{-1/2}$, $U \propto \frac{L}{r^2 n} \propto \frac{L^{1-2a}}{n} \propto (L/M_{\rm BH})^{1-\frac{8}{3}a} M_{\rm BH}^{\frac{5-8a}{3}}$. With $a = 1$, the first expression

[5] While the ratio I(SiIII]λ1892)/I(CIIIλ1909) may depend on the spectral energy distribution (Casebeer et al., 2006), the ratio I(AlIIIλ1860)/I(SiIII]λ1892) is unlikely to show a strong dependence because the involved ionic species have similar ionization potential, and the transition upper levels are close in energy above ground level.

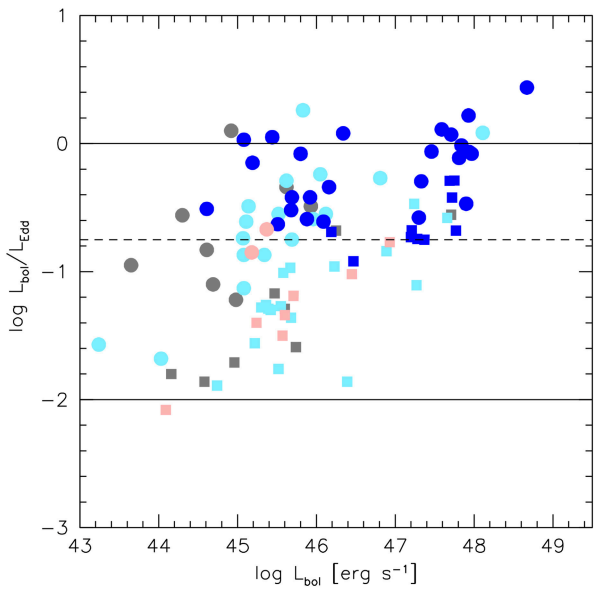

FIGURE 5 | Behavior of CIV shifts in the plane Eddington ratio versus bolometric luminosity. Circles indicate Pop. A, squares Pop. B. Color coding is as follows: blue, $c(\frac{1}{2}) \leq -1,000$ km s^{-1}; pale blue: $-1,000 < c(\frac{1}{2}) \leq -300$ km s^{-1}; gray $-300 < c(\frac{1}{2}) \leq 300$ km s^{-1}; pale red: $300 < c(\frac{1}{2}) \leq 1,000$ km s^{-1}; red $c(\frac{1}{2}) > 1,000$ km s^{-1}. The sample sources correspond to the Hamburg-ESO sample (all above $L \gtrsim 10^{47}$ erg s^{-1}) and FOS-based control sample of Sulentic et al. (2017).

is recovered. For $a = 0.5$ there is a weaker dependence on $(L/M_{\rm BH})$ to the power of $-\frac{1}{3}$.[6]

The grid shown in Marziani et al. (2001) obtained using the first approach does not make it possible to derive orientation angle θ and $L/L_{\rm Edd}$ for individual quasars, as it was computed for a fixed $M_{\rm BH}$. These considerations provide a first account of why sources at the high-$L/M_{\rm BH}$ tip are associated with a lower ionization degree. Other explanations are possible as well: the line emitting gas is shielded from the most intense UV radiation, for example by an optically and geometrically thick slim disk (Wang et al., 2014b) or by an inner, over-ionized failed wind (Leighly, 2004) but the intensity ratios of I(Al III)/I(Si III]λ1892) and I(Si III]λ1892)/I(C III]) point toward an increase of the emissivity-weighted density values of the line emitting gas. This alone yields a decrease in U at high $L/L_{\rm Edd}$, all other parameters left unchanged.

8. SELF-SIMILARITY OF THE ACCRETION PROCESS

The accretion process is apparently largely self-similar over several order of magnitudes in black hole mass and luminosity. The general fundamental plane of accreting black holes emphasizes the invariance of the accretion disk-jet scaling phenomena (Merloni et al., 2003). The Eigenvector 1 scheme is also emphasizing a scale invariance, albeit more oriented toward the radiatively-efficient domain and, in the quasar context, limited to unobscured type-1 quasars. As far as the radiatively efficient accretion mode is concerned, the invariance may hold over a factor of almost $\sim 10^{10}$ in solar mass (Zamanov and Marziani, 2002). Restricting the attention to RQ quasars, very large blueshifts are observed over at least four orders of magnitude in luminosity. The distribution of data points in **Figure 5** is clearly affected by selection effects; however, it shows that large CIV $c(\frac{1}{2}) \lesssim -1,000$ km s^{-1} do occur also at relatively low luminosity. Outflow velocities are apparently more related to Eddington ratio than to L or $M_{\rm BH}$: large $c(\frac{1}{2})$ blueshifts may occur only above a threshold at about $L/L_{\rm Edd} \approx 0.2 - 0.3$ which may in turn correspond to a change in accretion disk structure (Abramowicz and Straub, 2014, and references therein). Intriguingly, the threshold matches the FWHM(Hβ)$\approx 4,000$ km s^{-1} limit separating Population A from Population B (if $L \lesssim 10^{47}$ erg s^{-1}). At this limiting FWHM we observe also a change in Hβ profile shape, from Lorentzian-like to double Gaussian (Sulentic et al., 2002; Zamfir et al., 2010).

8.1. Pop. A and B: A Different Accretion Structure

We propose the two panels with the sketches shown in **Figure 6** as a pictorial view of quasars accreting at high (left) and low rate respectively (c.f. Marinucci et al., 2012; Marziani et al., 2014; Luo et al., 2015). The main theoretical prediction is that we expect an inner accretion disk region assimilable to a slim disk (Abramowicz et al., 1988; Szuszkiewicz et al., 1996; Frank et al., 2002). Apart from this, the structure of the BLR and its relation to the accretion disk structure remains unclear.

In Pop. A sources, as mentioned before (section 7.5), it is tempting to speculate that LILs may be favored with respect to HILs by the shielding of the hottest continuum due to the slim disk geometry. However, the question remains whether the ionized outflow we see in CIVλ1549 is associated with the central cone defined by the walls of the slim disk (which may be much steeper than the ones deducted in the cartoon, Sądowski et al. 2014). In Pop. A, the CIV shifts are largest but the CIV EW is lowest (Pop. A includes weak lined quasars, Diamond-Stanic et al. 2009; Shemmer et al. 2010), which may imply that the gas is over-ionized or, alternatively, that the FUV continuum is absorbed/weakened, as in the case of emission from the shielded part of the disk between the slim structure and the torus (Luo et al., 2015). Against the latter interpretation goes the higher ratio of radiation-to-gravitation forces of Pop. A which yields a higher terminal velocity and hence systematically large blueshifts in the HILs: continuum seen by the gas should at least roughly correspond to the continuum seen by us.

In the case of a flat-disk (Pop. B right-panel), the problem of disk wind over-ionization may be solved by the failed wind scenario (Murray et al., 1995): inner gas may offer an effective screen and only shielded gas is efficiently accelerated (Leighly,

[6]Note that, in this case, it is not necessary that $a = 0.5$ to recover spectral similarity. Different spectral types are likely to be associated with different scaling with luminosity.

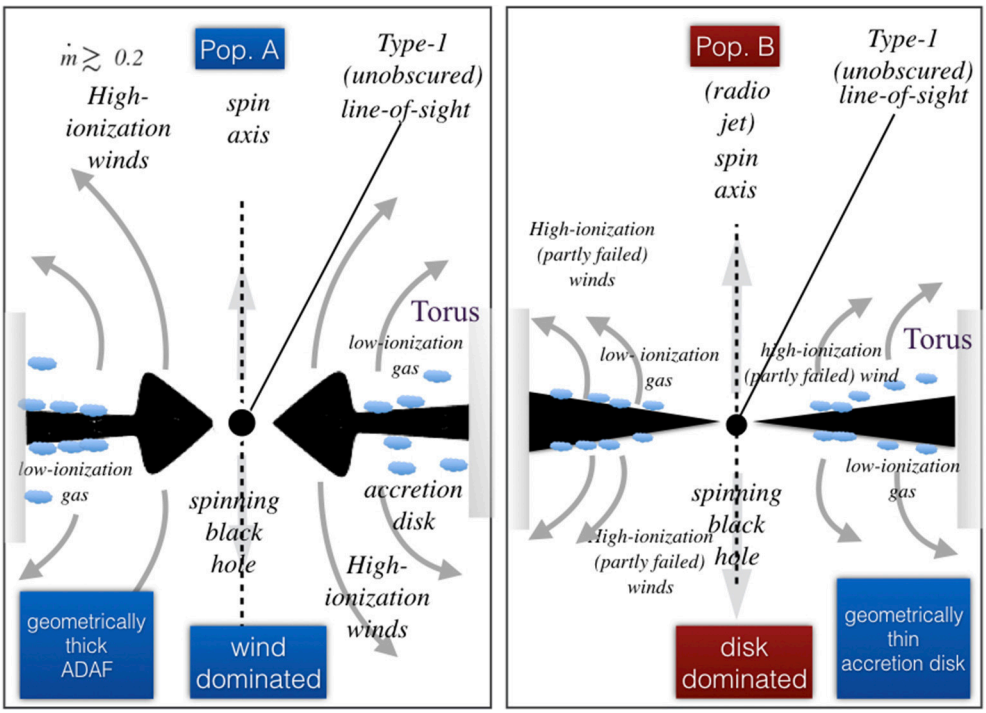

FIGURE 6 | Different structure for Pop. A (left) and B (right), with a slim and a flat disk respectively. The sketch is not drawn to scale and the relation between line emitting regions (shown here as clouds) and accretion disk structure is still debated. See section 8.1 for a more detailed explanation.

2004). Models of disk-wind systems are successful in reproducing the profiles of Balmer lines (Flohic et al., 2012). To explain the redward asymmetries often observed in Pop. B, either Balmer lines are emitted in an infall scenario (which require large column density to withstand radiation forces) or the accretion disk itself could be emitter. In the latter case the redward asymmetry could be ascribed in full to transverse and gravitational redshift (Bon et al., 2009, 2015).

Apart from these considerations, the sketch of **Figure 6** raises more questions than it provides answers. For example, can the inner part of the torus contribute to the velocity dispersion and yield a Lorentzian profile (Goad et al., 2012)? This question raises a conflict with the virial assumption for Pop. A sources, whereas the line wings are expected to be emitted closer to the black hole. Electron scattering may also produce extended line wings in the Balmer lines (Laor, 2006). Roles of magnetic fields and of black hole spin are not considered although presumably important, black hole spin because of its effect on the inner accretion disk temperature, and magnetic fields because they may provide an acceleration mechanism for disk wind (Emmering et al., 1992).

8.2. The Quasar Main Sequence at High Luminosity

We still lack a comprehensive view of the MS at high L (we consider high-luminosity sources the quasars with bolometric $\log L \gtrsim 47$ [erg/s]), not last because the Hβ spectral range is accessible only with IR spectrometers, and high-luminosity quasars are exceedingly rare at $z \lesssim 1$. The main effect that we expect in the optical plane of the 4DE1 space is related to their systematic increase in mass: if the motion in the LIL-BLR is predominantly virial ($M_{\rm BH} \propto r\delta FWHM^2$) and the BLR radius follows a scaling power-law with luminosity ($r \propto L^{\rm a}$), then FWHM $\propto (L/M_{\rm BH})^{-1} L^{\frac{1-a}{2}}$. Assuming that $L/L_{\rm Edd}$ saturates toward values $\mathcal{O}(1)$ (Mineshige et al., 2000), the *minimum* FWHM should show a clear trend with luminosity. This prediction has been confirmed by joining samples covering more than 4dex in $\log L$, from 44 to 48 (Marziani et al., 2009). At each L there is a large spread of value that reflect the dependence of FWHM by Eddington ratio and mass.

At high L, the MS becomes displaced toward higher FWHM values in the OP of the E1, as schematically represented in the diagram of **Figure 7**. At present, we cannot say whether there is also a luminosity effect on FeII prominence: relatively few sources are available to map the broad distribution of $R_{\rm FeII}$. Reports of an FeII Baldwin effect appear unconvincing and contradicted by the best available observations of the Hβ range at high luminosity. In addition, observations of high-L quasars from flux-limited surveys are subject to a strong Eddington ratio bias (Sulentic et al., 2014) which may instead suggest an anti-Baldwin effect in FeII (Kovačević et al., 2010). The Eddington ratio bias involves the preferential selection of higher $L/L_{\rm Edd}$ sources at higher z. Since $R_{\rm FeII}$ strongly depends on $L/L_{\rm Edd}$ (section 7.5), low $R_{\rm FeII}$ might be preferentially lost at high-z.

The comparison between low- and high-ionization lines has provided insightful constraints on the BLR at low-z (Marziani et al., 1996). The comparison of Hβ and CIVλ1549 is yielding

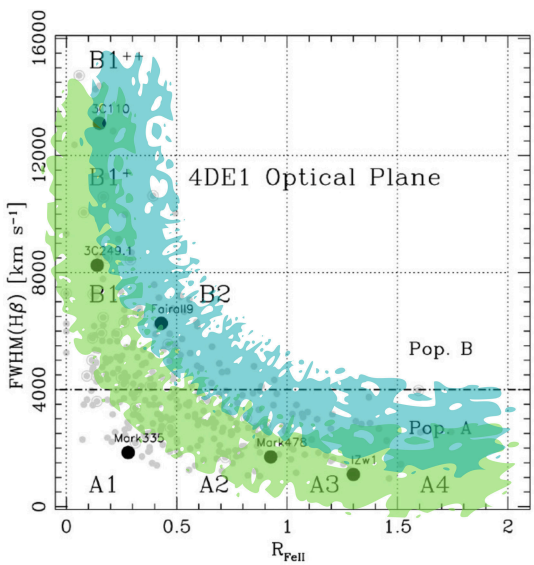

FIGURE 7 | Schematic representation of the E1 MS displacement in high luminosity samples. The dark green shaded area represents a high luminosity $\log L \gtrsim 47$ sample. In that case, NLSy1s are not anymore possible, if the virial assumption holds up to the Eddington limit.

interesting clues also at high L (Shen, 2016; Bisogni et al., 2017; Sulentic et al., 2017). Perhaps the most remarkable fact is that a LIL-BLR appears to remain basically virialized (Marziani et al., 2009; Sulentic et al., 2017). The CIVλ1549 blueshift depends on luminosity (the median $c(\frac{1}{2})$ is $\approx$ 2,600 km s^{-1} and 1,800 km s^{-1} for Pop. A and B RQ at high-L against $<$ 1,000 km s^{-1}at low-L), but the dependence is not strong, and can be accounted for in the framework of a radiation driven winds. Assuming $L/L_{\rm Edd}\approx$ const. (as is the case if a strong Eddington bias yields to a narrow range of $L/L_{\rm Edd}$ as in high-z, present-day flux-limited samples), a luminosity dependence for $c(\frac{1}{2})$ arises in the form $\propto L^{1/4}$. If L is restricted to a narrow range, the $L/L_{\rm Edd}$ dependence dominates. If $L/L_{\rm Edd}$ and L both span significant ranges, a multivariate analysis confirms the concomitant dependence on both parameters (Sulentic et al., 2017).

9. EXTREME POPULATION A SOURCES: EXTREME RADIATORS AND POTENTIAL DISTANCE INDICATORS

Sources belonging to spectral types A3 and A4 (i.e., satisfying the criterion $R_{\rm FeII} > 1$) are found to be radiating at the highest Eddington ratio. They show a relatively small dispersion along a well-defined, extreme value of order (1)[7] (Marziani and Sulentic, 2014). The xA selection criterion is consistent with the parameter $\propto$ FWHM/σ+$R_{\rm FeII}$ used to identify super-massive extremely accreting BHs (SEAMBHs Wang et al., 2013; Du et al., 2016). Since xA sources show Lorentzian profiles, the criterion based on $R_{\rm FeII}$ should be sufficient unless relatively broad profiles with FWHM$\gtrsim$4,000 km s^{-1} are considered, a case still under scrutiny.

If $L/M_{\rm BH} \approx$ *const.*, then the luminosity can be retrieved once the mass is known. xA sources show very similar spectra over a broad range of luminosity. The self-similarity in terms of diagnostic line ratios justifies the use of the scaling law $r_{\rm BLR} \propto L^{0.5}$ that implies spectral invariance. The luminosity can then be written as $L \propto (\delta v)^4$, where δv is a suitable VBE. It is interesting to note that this relation is in the same form of the Faber-Jackson law as originally defined (Faber and Jackson, 1976). Assuming that spheroidal galaxies are virialized systems, radiating at a constant $L/M_{\rm BH}$ ratio implies that their luminosity is $L \propto \sigma^4/\mu_B$, where μ_B is the surface brightness within the effective radius. Later developments yielded a different exponent for the dependence on σ (e.g., D'Onofrio et al., 2017, and references theerin), as the assumption of a constant surface brightness proved untenable. There should be no similar difficulties for quasars, although statistical and systematic sources of error should be carefully assessed (Marziani and Sulentic, 2014). The distance modulus computed from the virial equation, $\mu = 2.5[\log L(\delta v) - BC] - 2.5\log(f_\lambda\lambda) - const. + 5\cdot\log(1+z)$, where $f_\lambda\lambda$ is the flux at 5100 Å, and BC the bolometric correction, is in agreement with the expectation of the concordance ΛCDM cosmology, providing a proof of the conceptual validity of the virial luminosity $L \propto (\delta v)^4$ estimates (a plot of μ for several quasar samples is provided by Marziani et al., 2017b, and by Negrete et al. 2017).

10. CONCLUSION

The quasar MS provides a tool to systematically organize quasar multifrequency properties. It allows the identification of spectral types with fairly well-defined spectral properties. In this paper, we have described a simple parameterization that is able to describe the quasar emission line profiles, as well as a heuristic technique motivated by the internal line shifts yielding the separation of components in different physical conditions.

We then considered the MS defined in the so-called optical plane of the 4D eigenvector 1 parameter space, and analyzed several correlates involving the profile of Hβ and MgIIλ2800 (the representative LILs), of the CIVλ1549 (the representative HIL), broad-line UV diagnostic ratios that provide trends in density and ionization level, [OIII]λλ4959,5007 shifts, the prevalence of radio-loudness, and the soft X-ray spectral slope.

The trends defined in this paper offer a consistent, empirical systematization of quasar properties for $z \lesssim 1$, low-to moderate luminosity quasars. The difference between Pop. A and B is evident at the extremes: spectral type A4 sources typically show very strong FeII ($R_{\rm FeII} \gtrsim 1.5$), blueward asymmetry in Hβ, large CIVλ1549 blueshift, weak and blue shifted [OIII]λλ4959,5007 (Negrete et al., 2017). Extreme Pop. B show undetectable FeII, very broad red-ward asymmetric Hβ profiles, small-amplitude CIVλ1549 shifts, prominent [OIII]λλ4959,5007. There is evidence that the two populations represent structurally different objects. The blue shifted excess (BLUE) is interpreted as due to outflowing gas dominating HIL emission only in Pop. A (unless sources at very high L are considered). A redshifted VBC

[7]The exact values depend on the normalization assumed for $M_{\rm BH}$ estimates and for the bolometric correction.

is present only in Pop. B, for values of FWHM Hβ above 4,000 km s^{-1}, and has been interpreted as due to gas close to the central continuum source. The relative balance between gravitational and radiation forces (i.e., $L/L_{\rm Edd}$) appears as a major factor influencing *both* the dynamics and the physical conditions of the line emitting gas (Sect. 8.2), and an accretion mode change may be associated with a critical $L/L_{\rm Edd} \sim 0.2 \pm 0.1$, leading to the two quasar populations: A (wind-dominated, following Richards et al. 2011), and B (virial or disk-dominated).

Luminosity trends are weak as they become significant only over a wide luminosity range $\sim 10^{43} - 10^{48}$ erg/s. They involve an overall increase in virial line broadening (LILs) and an increase of blueshift frequency and amplitude consistent with the dominance of radiation forces (HILs).

The presence of a virialized subregion identified along the MS at low-L as well as at high-L has important consequences. xA quasars at the high $R_{\rm FeII}$ end (spectral type A3 and A4) may be suitable as Eddington standard candles since their Eddington ratio scatters around a well-defined value (e.g., Negrete et al., 2017).

The contextualization offered by the MS is instrumental to the development of better-focused physical models along the quasar main sequence. As examples of the advantages offered by the E1 MS, we just mention the possibility of contextualizing orientation effects in RQ quasars, and of performing a meaningful comparison between RL and RQ samples with similar optical properties. An aspect still to clarify is the connection between disk structure and the dynamics of the line emitting gas.

AUTHOR CONTRIBUTIONS

PM wrote the paper; DD, MD, GS, EB, and NB contributed with a critical reading and suggestions; AD, CN, MM-A, and JS contributed with a critical reading.

FUNDING

AD and MM-A acknowledge financial support from the Spanish Ministry for Economy and Competitiveness through grants AYA2013-42227-P and AYA2016-76682-C3-1-P. DD and CN acknowledge support from grants PAPIIT108716, UNAM, and CONACyT221398. EB and NB acknowledge grants 176003 Gravitation and the large scale structure of the Universe and 176001 Astrophysical spectroscopy of extragalactic objects supported by the Ministry of Education and Science of the Republic of Serbia.

ACKNOWLEDGMENTS

It is a pleasure to thank the SOC of the meeting Quasar at all cosmic epoch for inviting a talk on the quasar main sequence.

REFERENCES

Abdo, A. A., Ackermann, M., Ajello, M., Axelsson, M., Baldini, L., Ballet, J., et al. (2009). Fermi/large area telescope discovery of gamma-ray emission from a relativistic jet in the narrow-line quasar PMN J0948+0022. *Astrophys.J* 699, 976–984. doi: 10.1088/0004-637X/699/2/976

Abramowicz, M. A., Czerny, B., Lasota, J. P., and Szuszkiewicz, E. (1988). Slim accretion disks. *Astrophys.J* 332, 646–658. doi: 10.1086/166683

Abramowicz, M. A., Lanza, A., and Percival, M. J. (1997). Accretion disks around kerr black holes: vertical equilibrium revisited. *Astrophys. J* 479:179. doi: 10.1086/303869

Abramowicz, M. A., and Straub, O. (2014). Accretion discs. *Scholarpedia* 9:2408. doi: 10.4249/scholarpedia.2408

Adhikari, T. P., Różańska, A., Czerny, B., Hryniewicz, K., and Ferland, G. J. (2016). The Intermediate-line region in active galactic nuclei. *Astrophys. J* 831:68. doi: 10.3847/0004-637X/831/1/68

Afanasiev, V. L., Shapovalova, A. I., Popović, L. Č., and Borisov, N. V. (2015). Spectropolarimetric monitoring of active galaxy 3C 390.3 with 6-m telescope SAO RAS in the period 2009-2014. *Mon. Not. R. Astron. Soc.* 448, 2879–2889. doi: 10.1093/mnras/stv210

Antonucci, R. R. J., and Miller, J. S. (1985). Spectropolarimetry and the nature of NGC 1068. *Astrophys. J* 297, 621–632. doi: 10.1086/163559

Azzalini, A., and Regoli, G. (2012). Some properties of skew-symmetric distributions. *Ann. Inst. Statist. Math.* 64, 857–879. doi: 10.1007/s10463-011-0338-5

Bachev, R., Marziani, P., Sulentic, J. W., Zamanov, R., Calvani, M., and Dultzin-Hacyan, D. (2004). Average ultraviolet quasar spectra in the context of eigenvector 1: a baldwin effect governed by the eddington ratio? *Astrophys.J* 617, 171–183. doi: 10.1086/425210

Bacon, F. (1902). *Novum Organum* (New York, NY: P. F. Collier & Son)

Baldwin, J. A., Burke, W. L., Gaskell, C. M., and Wampler, E. J. (1978). Relative quasar luminosities determined from emission line strengths. *Nature* 273, 431–435. doi: 10.1038/273431a0

Baldwin, J. A., Ferland, G. J., Korista, K. T., Carswell, R. F., Hamann, F., Phillips, M. M., et al. (1996). Very high density clumps and outflowing winds in QSO broad-line regions. *Astrophys. J* 461, 664–682. doi: 10.1086/177093

Baskin, A., and Laor, A. (2005). What controls the CIV line profile in active galactic nuclei? *Mon. Not. Roy. Astron. Soc.* 356, 1029–1044. doi: 10.1111/j.1365-2966.2004.08525.x

Bensch, K., del Olmo, A., Sulentic, J., Perea, J., and Marziani, P. (2015). Measures of the Soft X-ray excess as an eigenvector 1 parameter for active galactic nuclei. *J. Astrophys. Astron.* 36, 467–474. doi: 10.1007/s12036-015-9355-8

Bentz, M. C., Peterson, B. M., Pogge, R. W., and Vestergaard, M. (2009). The black hole mass-bulge luminosity relationship for active galactic nuclei from reverberation mapping and hubble space telescope imaging. *Astrophys. J. Lett.* 694, L166–L170. doi: 10.1088/0004-637X/694/2/L166

Bentz, M. C., Peterson, B. M., Pogge, R. W., Vestergaard, M., and Onken, C. A. (2006). The radius-luminosity relationship for active galactic nuclei: the effect of host-galaxy starlight on luminosity measurements. *Astrophys. J.* 644, 133–142. doi: 10.1086/503537

Berton, M., Caccianiga, A., Foschini, L., Peterson, B. M., Mathur, S., Terreran, G., et al. (2016). Compact steep-spectrum sources as the parent population of flat-spectrum radio-loud narrow-line Seyfert 1 galaxies. *Astron. Astrophys.* 591:A98. doi: 10.1051/0004-6361/201628171

Bian, W.-H., Fang, L.-L., Huang, K.-L., and Wang, J.-M. (2012). The C IV baldwin effect in quasi-stellar objects from seventh data release of the sloan digital sky survey. *Month. Notices R. Astron. Soc.* 427, 2881–2888. doi: 10.1111/j.1365-2966.2012.22123.x

Bischetti, M., Piconcelli, E., Vietri, G., Bongiorno, A., Fiore, F., Sani, E., et al. (2017). The WISSH quasars project. I. Powerful ionised outflows in hyper-luminous quasars. *Astron. Astrophys.* 598:A122. doi: 10.1051/0004-6361/201629301

Bisogni, S., di Serego Alighieri, S., Goldoni, P., Ho, L. C., Marconi, A., Ponti, G., et al. (2017). Simultaneous detection and analysis of optical and ultraviolet broad emission lines in quasars at z $\sim$ 2.2. *Astron. Astrophys.* 603:A1. doi: 10.1051/0004-6361/201630143

Blandford, R. D., and Payne, D. G. (1982). Hydromagnetic flows from accretion discs and the production of radio jets. *Month. Notices R. Astron. Soc.* 199, 883–903. doi: 10.1093/mnras/199.4.883

Blandford, R. D., and Znajek, R. L. (1977). Electromagnetic extraction of energy from Kerr black holes. *Month. Notices R. Astron. Soc.* 179, 433–456.

Blanton, M. R., Bershady, M. A., Abolfathi, B., Albareti, F. D., Allende Prieto, C., Almeida, A., et al. (2017). Sloan digital sky survey IV: mapping the milky way, nearby galaxies, and the distant universe. *Astron. J.* 154:28. doi: 10.3847/1538-3881/aa7567

Boller, T., Brandt, W. N., and Fink, H. (1996). Soft X-ray properties of narrow-line Seyfert 1 galaxies. *Astron. Astrophys.* 305:53.

Bon, E., Popović, L. Č., Gavrilović, N., Mura, G. L., and Mediavilla, E. (2009). Contribution of a disc component to single-peaked broad lines of active galactic nuclei. *Month. Notices R. Astron. Soc.* 400, 924–936. doi: 10.1111/j.1365-2966.2009.15511.x

Bon, N., Bon, E., Marziani, P., and Jovanović, P. (2015). Gravitational redshift of emission lines in the AGN spectra. *Astrophys. Space Sci.* 360:7. doi: 10.1007/s10509-015-2555-5

Boroson, T. A. (2011). A new orientation indicator for radio-quiet quasars. *Astrophys. J. Lett.* 735:L14+. doi: 10.1088/2041-8205/735/1/L14

Boroson, T. A., and Green, R. F. (1992). The emission-line properties of low-redshift quasi-stellar objects. *Astrophys. J. Suppl.* 80, 109–135. doi: 10.1086/191661

Brotherton, M. S., Runnoe, J. C., Shang, Z., and DiPompeo, M. A. (2015). Bias in C IV-based quasar black hole mass scaling relationships from reverberation mapped samples. *Month. Notices R. Astron. Soc.* 451, 1290–1298. doi: 10.1093/mnras/stv767

Brotherton, M. S., Wills, B. J., Francis, P. J., and Steidel, C. C. (1994a). The intermediate line region of QSOs. *Astrophys. J.* 430, 495–504. doi: 10.1086/174425

Brotherton, M. S., Wills, B. J., Steidel, C. C., and Sargent, W. L. W. (1994b). Statistics of QSO broad emission-line profiles. 2: the C IV wavelength 1549, C III) wavelength 1909, and MG II wavelength 2798 lines. *Astrophys. J.* 423, 131–142. doi: 10.1086/1737194

Burbidge, G. R., and Burbidge, E. M. (1967). *Quasi-Stellar Objects* (San Francisco, CA:Freeman).

Casebeer, D. A., Leighly, K. M., and Baron, E. (2006). FUSE observation of the narrow-Line seyfert 1 galaxy RE 1034+39: dependence of broad emission line strengths on the shape of the photoionizing spectrum. *Astrophys. J.* 637, 157–182. doi: 10.1086/498125

Cavaliere, A., and Vittorini, V. (2000). The fall of the quasar population. *Astrophys. J.* 543, 599–610. doi: 10.1086/317155

Coatman, L., Hewett, P. C., Banerji, M., and Richards, G. T. (2016). C iv emission-line properties and systematic trends in quasar black hole mass estimates. *Month. Notices R. Astron. Soc.* 461, 647–665. doi: 10.1093/mnras/stw1360

Coatman, L., Hewett, P. C., Banerji, M., Richards, G. T., Hennawi, J. F., and Prochaska, J. X. (2017). Correcting C IV-based virial black hole masses. *Month. Notices R. Astron. Soc.* 465, 2120–2142. doi: 10.1093/mnras/stw2797

Collin, S., Kawaguchi, T., Peterson, B. M., and Vestergaard, M. (2006). Systematic effects in measurement of black hole masses by emission-line reverberation of active galactic nuclei: eddington ratio and inclination. *Astron. Astrophys.* 456, 75–90. doi: 10.1051/0004-6361:20064878

Collin-Souffrin, S., Dyson, J. E., McDowell, J. C., and Perry, J. J. (1988). The environment of active galactic nuclei. I - A two-component broad emission line model. *Month. Notices R. Astron. Soc.* 232, 539–550.

Corbin, M. R., and Boroson, T. A. (1996). Combined ultraviolet and optical spectra of 48 low-redshift QSOs and the relation of the continuum and emission-line properties. *Astrophys. J. Suppl.* 107:69. doi: 10.1086/192355

Cracco, V., Ciroi, S., Berton, M., Di Mille, F., Foschini, L., La Mura, G., et al. (2016). A spectroscopic analysis of a sample of narrow-line Seyfert 1 galaxies selected from the Sloan Digital Sky Survey. *Month. Notices R. Astron. Soc.* 462, 1256–1280. doi: 10.1093/mnras/stw1689

Czerny, B., Li, Y.-R., Sredzinska, J., Hryniewicz, K., Panda, S., Wildy, C., et al. (2017). Self-consistent dynamical model of the broad line region. *Front. Astron. Space Sci.* 4:5 doi: 10.3389/fspas.2017.00005

Czerny, B., and You, B. (2016). Accretion in active galactic nuclei and disk-jet coupling. *Astron. Nachr.* 337:73. doi: 10.1002/asna.201512268

Denney, K. D., Pogge, R. W., Assef, R. J., Kochanek, C. S., Peterson, B. M., and Vestergaard, M. (2013). C IV line-width anomalies: the perils of low signal-to-noise spectra. *Astrophys. J.* 775:60. doi: 10.1088/0004-637X/775/1/60

Diamond-Stanic, A. M., Fan, X., Brandt, W. N., Shemmer, O., Strauss, M. A., Anderson, S. F., et al. (2009). High-redshift SDSS Quasars with weak emission lines. *Astrophys. J.* 699, 782–799. doi: 10.1088/0004-637X/699/1/782

Diaz, A. I., Terlevich, E., and Terlevich, R. (1989). Near-IR features in late type stars - Their relation with stellar atmosphere parameters. *Month. Notices R. Astron. Soc.* 239, 325–345. doi: 10.1093/mnras/239.2.325

Dietrich, M., Hamann, F., Shields, J. C., Constantin, A., Vestergaard, M., Chaffee, F., et al. (2002). Continuum and emission-Line strength relations For a large active galactic nuclei sample. *Astrophys. J.* 581, 912–924. doi: 10.1086/344410

Done, C., Davis, S. W., Jin, C., Blaes, O., and Ward, M. (2012). Intrinsic disc emission and the soft X-ray excess in active galactic nuclei. *Month. Notices R. Astron. Soc.* 420, 1848–1860. doi: 10.1111/j.1365-2966.2011.19779.x

D'Onofrio, M., Cariddi, S., Chiosi, C., Chiosi, E., and Marziani, P. (2017). On the origin of the fundamental plane and faber-jackson relations: implications for the star formation problem. *Astrophys. J.* 838:163. doi: 10.3847/1538-4357/aa6540

D'Onofrio, M., Marziani, P., and Sulentic, J. W. (eds.) (2012). *Fifty Years of Quasars From Early Observations and Ideas to Future Research, Vol. 386, Astrophysics and Space Science Library.* Berlin; Heidelberg: Springer Verlag.

Du, P., Lu, K.-X., Hu, C., Qiu, J., Li, Y.-R., Huang, Y.-K., et al. (2016). Supermassive black holes with high accretion rates in active galactic nuclei. VI. velocity-resolved reverberation mapping of the Hβ line. *Astrophys. J.* 820:27. doi: 10.3847/0004-637X/820/1/27

Dultzin-Hacyan, D., Krongold, Y., Fuentes-Guridi, I., and Marziani, P. (1999). The close environment of seyfert galaxies and its implication for unification models. *Astrophys. J.* 513, L111–L114. doi: 10.1086/311925

Dultzin-Hacyan, D., Marziani, P., and Sulentic, J. W. (2000). "The Broad Line Region in Active Galactic Nuclei," in *Revista Mexicana de Astronomia y Astrofisica Conference Series*, Vol. 9, eds S. J. Arthur, N. S. Brickhouse, and J. Franco (Mexico City), 308–315.

Dultzin-Hacyan, D., Sulentic, J., Marziani, P., Calvani, M., and Moles, M. (1997). "A Correlation Analysis for Emission Lines in 52 AGN," in *IAU Colloq. 159: Emission Lines in Active Galaxies: New Methods and Techniques*, *Vol 113, Astronomical Society of the Pacific Conference Series*, eds B. M. Peterson, F.-Z. Cheng, and A. S. Wilson (San Francisco, CA), 262.

Dumont, A. M. and Collin-Souffrin, S. (1990). Line and continuum emission from the outer regions of accretion discs in Active Galactic Nuclei. V - Detailed computational results. *Astron. Astrophys.* 83, 71–89.

Elvis, M. (2000). A structure for quasars. *Astrophys. J.* 545, 63–76. doi: 10.1086/317778

Elvis, M., Wilkes, B. J., McDowell, J. C., Green, R. F., Bechtold, J., Willner, S. P., et al. (1994). Atlas of quasar energy distributions. *Astroph. J. Supp* 95, 1–68. doi: 10.1086/192093

Emmering, R. T., Blandford, R. D., and Shlosman, I. (1992). Magnetic acceleration of broad emission-line clouds in active galactic nuclei. *Astrophys. J.* 385, 460–477. doi: 10.1086/170955

Eracleous, M., and Halpern, J. P. (2003). Completion of a survey and detailed study of double-peaked emission lines in radio-loud active galactic nuclei. *Astrophys. J.* 599, 886–908. doi: 10.1086/379540

Eun, D.-I., Woo, J.-H., and Bae, H.-J. (2017). A systematic Search for hidden type 1 AGNs: gas kinematics and scaling relations. *Astrophys. J.* 842:5. doi: 10.3847/1538-4357/aa6daf

Faber, S. M., and Jackson, R. E. (1976). Velocity dispersions and mass-to-light ratios for elliptical galaxies. *Astrophys. J.* 204, 668–683. doi: 10.1086/154215

Fausnaugh, M. M., Grier, C. J., Bentz, M. C., Denney, K. D., De Rosa, G., Peterson, B. M., et al. (2017). Reverberation mapping of optical emission lines in five active galaxies. *Astrophys. J.* 840:97. doi: 10.3847/1538-4357/aa6d52

Ferland, G. J., Hu, C., Wang, J., Baldwin, J. A., Porter, R. L., van Hoof, P. A. M., et al. (2009). Implications of infalling fe II-emitting clouds in active galactic nuclei: anisotropic properties. *Astrophys. J. Lett.* 707, L82–L86. doi: 10.1088/0004-637X/707/1/L82

Flohic, H. M. L. G., Eracleous, M., and Bogdanović, T. (2012). Effects of an accretion disk wind on the profile Of the balmer emission lines from active galactic nucle . *Astrophys. J.* 753:133. doi: 10.1088/0004-637X/753/2/133

Foschini, L., Fermi/Lat Collaboration, Ghisellini, G., Maraschi, L., Tavecchio, F., and Angelakis, E. (2010). "Fermi/lAT discovery of gamma-ray emission from a relativistic jet in the narrow-line seyfert 1 quasar PMN J0948+0022," in *Accretion and Ejection in AGN: a Global View*, *Vol. 427, Astronomical Society of the Pacific Conference Series,* eds L. Maraschi, G. Ghisellini, R. Della Ceca, and F. Tavecchio (San Francisco, CA), 243–248.

Fraix-Burnet, D., Marziani, P., D'Onofrio, M., and Dultzin, D. (2017). The phylogeny of quasars and the ontogeny of their central black holes. *Front. Astron. Space Sci.* 4:1. doi: 10.3389/fspas.2017.00001

Francis, P. J., Hewett, P. C., Foltz, C. B., and Chaffee, F. H. (1992). An objective classification scheme for QSO spectra. *Astrophys. J.* 398, 476–490. doi: 10.1086/171870

Frank, J., King, A., and Raine, D. J. (2002). *Accretion Power in Astrophysics: 3rd Edn.* Cambridge: Cambridge University Press.

Gaskell, C. M. (1982). A redshift difference between high and low ionization emission-line regions in QSOs - evidence for radial motions. *Strophys. J.* 263, 79–86. doi: 10.1086/160481

Gaskell, C. M. (1988). Direct evidence for gravitational domination of the motion of gas within one light-week of the central object in NGC 4151 and the determination of the mass of the probable black hole. *Astrophys. J.* 325, 114–118. doi: 10.1086/165986

Gaskell, C. M., and Goosmann, R. W. (2013). Line Shifts, Broad-line Region Inflow, and the Feeding of Active Galactic Nuclei. *Astrophys. J.* 769:30. doi: 10.1088/0004-637X/769/1/30

Goad, M. R., and Korista, K. T. (2014). Interpreting broad emission-line variations-I. Factors influencing the emission-line response. *Month. Notices R. Astron. Soc.* 444, 43–61. doi: 10.1093/mnras/stu1456

Goad, M. R., Korista, K. T., and Ruff, A. J. (2012). The broad emission-line region: the confluence of the outer accretion disc with the inner edge of the dusty torus. *Month. Notices R. Astron. Soc.* 426, 3086–3111. doi: 10.1111/j.1365-2966.2012.21808.x

Grier, C. J., Peterson, B. M., Horne, K., Bentz, M. C., Pogge, R. W., Denney, K. D., et al. (2013). The structure of the broad-line region in active galactic nuclei. I. reconstructed velocity-delay maps. *Astrophys. J.* 764:47. doi: 10.1088/0004-637X/764/1/47

Grupe, D. (2004). A complete sample of soft X-ray-selected AGNs. II. statistical analysis. *Astron. J.* 127, 1799–1810. doi: 10.1086/382516

Gu, M. (2017). "The jet detection in radio-loud narrow-line Seyfert 1 galaxies," in *New Frontiers in Black Hole Astrophysics*, *Vol. 324*, *IAU Symposium,* ed A. Gomboc (Cambridge), 188–191. doi: 10.1017/S1743921317001740

Hewett, P. C., and Wild, V. (2010). Improved redshifts for SDSS quasar spectra. *Month. Notices R. Astron. Soc.* 405, 2302–2316. doi: 10.1111/j.1365-2966.2010.16648.x

Hogg, D. W., and Fruchter, A. S. (1999). The faint-galaxy hosts of gamma-ray bursts. *Astrophys. J.* 520, 54–58. doi: 10.1086/307457

Horne, K., Peterson, B. M., Collier, S. J., and Netzer, H. (2004). Observational requirements for high-fidelity reverberation mapping. *Publicat. Astron. Soc. Pac.* 116, 465–476. doi: 10.1086/420755

Hu, C., Wang, J.-M., Ho, L. C., Chen, Y.-M., Bian, W.-H., and Xue, S.-J. (2008). Hβ profiles in quasars: evidence for an intermediate-line region. *Astrophys. J. Lett.* 683, L115–L118. doi: 10.1086/591848

Hu, C., Wang, J.-M., Ho, L. C., Ferland, G. J., Baldwin, J. A., and Wang, Y. (2012). Two-component structure of the Hβ broad-line region in quasars. I. evidence from spectral principal component analysis. *Astrophys. J.* 760:126. doi: 10.1088/0004-637X/760/2/126

Jarvis, M. J., and McLure, R. J. (2006). Orientation dependency of broad-line widths in quasars and consequences for black hole mass estimation. *Month. Notices R. Astron. Soc.* 369, 182–188. doi: 10.1111/j.1365-2966.2006.10295.x

Joly, M., Véron-Cetty, M., and Véron, P. (2008). "Fe II emission in AGN," in *Revista Mexicana de Astronomia y Astrofisica Conference Series*, Vol. 32 (Mexico City), 59–61.

Kaspi, S., Brandt, W. N., Maoz, D., Netzer, H., Schneider, D. P., and Shemmer, O. (2007). Reverberation mapping of high-luminosity quasars: first results. *Astrophys. J.* 659, 997–1007. doi: 10.1086/512094

Kaspi, S., Smith, P. S., Netzer, H., Maoz, D., Jannuzi, B. T., and Giveon, U. (2000). Reverberation measurements for 17 quasars and the size-mass-luminosity relations in active galactic nuclei. *Astrophys. J.* 533, 631–649. doi: 10.1086/308704

Kellermann, K. I., Sramek, R., Schmidt, M., Shaffer, D. B., and Green, R. (1989). VLA observations of objects in the palomar bright quasar survey. *Astron. J.* 98, 1195–1207. doi: 10.1086/115207

Khachikian, E. Y., and Weedman, D. W. (1974). An atlas of Seyfert galaxies. *Astrophys. J.* 192, 581–589. doi: 10.1086/153093

Kollatschny, W., and Zetzl, M. (2011). Broad-line active galactic nuclei rotate faster than narrow-line ones. *Nature* 470, 366–368. doi: 10.1038/nature09761

Komossa, S., Voges, W., Xu, D., Mathur, S., Adorf, H.-M., Lemson, G., et al. (2006). Radio-loud narrow-line type 1 quasars. *Astron. J.* 132, 531–545. doi: 10.1086/505043

Koratkar, A. P., and Gaskell, C. M. (1991). Structure and kinematics of the broad-line regions in active galaxies from IUE variability data. *Astrophys. J. Suppl.* 75, 719–750. doi: 10.1086/191547

Koulouridis, E., Plionis, M., Chavushyan, V., Dultzin-Hacyan, D., Krongold, Y., and Goudis, C. (2006). Local and large-scale environment of seyfert galaxies. *Astrophys. J.* 639, 37–45. doi: 10.1086/498421

Kovačević, J., Popović, L. Č., and Dimitrijević, M. S. (2010). Analysis of optical Fe II emission in a sample of active galactic nucleus spectra. *Astrophys. J. Suppl.* 189, 15–36. doi: 10.1088/0067-0049/189/1/15

Kovačević-Dojčinović, J. and Popović, L. Č. (2015). The connections between the UV and optical Fe II emission lines in type 1 AGNs. *Astrophys. J. Suppl.* 221:35. doi: 10.1088/0067-0049/221/2/35

Krawczyk, C. M., Richards, G. T., Mehta, S. S., Vogeley, M. S., Gallagher, S. C., Leighly, K. M., et al. (2013). Mean spectral energy distributions and bolometric corrections for luminous quasars. *Astrophys. J. Suppl.* 206:4. doi: 10.1088/0067-0049/206/1/4

Kruczek, N. E., Richards, G. T., Gallagher, S. C., Deo, R. P., Hall, P. B., Hewett, P. C., et al. (2011). C IV emission and the ultraviolet through X-Ray spectral energy distribution of radio-quiet quasars. *Astron. J.* 142:130. doi: 10.1088/0004-6256/142/4/130

Kuraszkiewicz, J., Wilkes, B. J., Schmidt, G., Smith, P. S., Cutri, R., and Czerny, B. (2009). Principal component analysis of the spectral energy distribution and emission line properties of red 2MASS active galactic nuclei. *Astrophys. J.* 692, 1180–1189. doi: 10.1088/0004-637X/692/2/1180

Laor, A. (2000). On black hole masses and radio loudness in active galactic nuclei. *Astrophys. J. Lett.* 543, L111–L114. doi: 10.1086/317280

Laor, A. (2006). Evidence for line broadening by electron scattering in the broad-line region of NGC 4395. *Astrophys. J.* 643, 112–119. doi: 10.1086/502798

Laor, A., Bahcall, J. N., Jannuzi, B. T., Schneider, D. P., and Green, R. F. (1995). The Ultraviolet Emission properties of 13 quasars. *Astrophys. J. Suppl.* 99:1. doi: 10.1086/192177

Laor, A., Fiore, F., Elvis, M., Wilkes, B. J., and McDowell, J. C. (1997). The soft X-ray properties of a complete sample of optically selected quasars. II. final results. *Astrophys. J.* 477:93. doi: 10.1086/303696

Leighly, K. M. (2004). Hubble space telescope STIS ultraviolet spectral evidence of outflow in extreme narrow-line seyfert 1 galaxies. II. Modeling and interpretation. *Astrophys. J.* 611:125. doi: 10.1086/422089

Leighly, K. M. and Moore, J. R. (2004). Hubble space telescope stis ultraviolet spectral evidence of outflow in extreme narrow-line seyfert 1 galaxies. I. Data and analysis. *Astrophys. J.* 611, 107–124. doi: 10.1086/422088

Luo, B., Brandt, W. N., Hall, P. B., Wu, J., Anderson, S. F., Garmire, G. P., et al. (2015). X-ray Insights into the Nature of PHL 1811 analogs and weak emission-line quasars: unification with a geometrically thick accretion disk? *Astrophys. J.* 805:122. doi: 10.1088/0004-637X/805/2/122

Mao, Y.-F., Wang, J., and Wei, J.-Y. (2009). Extending the Eigenvector 1 space to the optical variability of quasars. *Res. Astron. Astrophys.* 9, 529–537. doi: 10.1088/1674-4527/9/5/004

Marinucci, A., Bianchi, S., Nicastro, F., Matt, G., and Goulding, A. D. (2012). The link between the hidden broad line region and the accretion rate in seyfert 2 galaxies. *Astrophys. J.* 748:130. doi: 10.1088/0004-637X/748/2/130

Marziani, P., Bon, E., Bon, N., Dultzin, D., Del Olmo, A., et al. (2017a). Quasar black hole mass estimates from high-ionization lines: breaking a taboo? *Atoms* 5:33. doi: 10.3390/atoms5030033

Marziani, P., Dultzin-Hacyan, D., D'Onofrio, M., and Sulentic, J. W. (2003a). Arp 194: evidence of tidal stripping of gas and cross-fueling. *Astron. J.* 125, 1897–1907. doi: 10.1086/368142

Marziani, P., Dultzin-Hacyan, D., and Sulentic, J. W. (2006). "Accretion onto supermassive black holes in quasars: learning from optical/UV observations," in *New Developments in Black Hole Research*, ed P. V. Kreitler (New York, NY: Nova Press). 123.

Marziani, P., Martínez Carballo, M. A., Sulentic, J. W., Del Olmo, A., Stirpe, G. M., and Dultzin, D. (2016a). The most powerful quasar outflows as revealed by the Civ λ1549 resonance line. *Astrophys. Space Sci.* 361:29. doi: 10.1007/s10509-015-2611-1

Marziani, P., Negrete, C. A., Dultzin, D., Martinez-Aldama, M. L., Del Olmo, A., Esparza, D., et al. (2017b). "Highly accreting quasars: a tool for cosmology?," in *IAU Symposium*. Vol. 324, 245–246.

Marziani, P. and Sulentic, J. W. (2012). Estimating black hole masses in quasars using broad optical and UV emission lines. *New Astron. Rev.* 56, 49–63. doi: 10.1016/j.newar.2011.09.001

Marziani, P. and Sulentic, J. W. (2014). Highly accreting quasars: sample definition and possible cosmological implications. *Month. Notices R. Astron. Soc.* 442, 1211–1229. doi: 10.1093/mnras/stu951

Marziani, P., Sulentic, J. W., Dultzin-Hacyan, D., Calvani, M., and Moles, M. (1996). Comparative analysis of the high- and low-ionization lines in the broad-line region of active galactic nuclei. *Astrophys. J. Suppl.* 104:37. doi: 10.1086/192291

Marziani, P., Sulentic, J. W., Negrete, C. A., Dultzin, D., D'Onofrio, M., Del Olmo, A., et al. (2014). Low- and high-z highly accreting quasars in the 4D Eigenvector 1 context. *Astron. Rev.* 9, 1–20. doi: 10.1080/21672857.2014.11519739

Marziani, P., Sulentic, J. W., Negrete, C. A., Dultzin, D., Zamfir, S., and Bachev, R. (2010). Broad-line region physical conditions along the quasar eigenvector 1 sequence. *Month. Notices R. Astron. Soc.* 409, 1033–1048. doi: 10.1111/j.1365-2966.2010.17357.x

Marziani, P., Sulentic, J. W., Plauchu-Frayn, I., and del Olmo, A. (2013a). Is Mg II 2800 a reliable virial broadening estimator for quasars? *Astron. Astrophys.* 555:16. doi: 10.1051/0004-6361/201321374

Marziani, P., Sulentic, J. W., Plauchu-Frayn, I., and del Olmo, A. (2013b). Low-Ionization Outflows in High Eddington Ratio Quasars. *Astrophys. J.* 764:150. doi: 10.1088/0004-637X/764/2/150

Marziani, P., Sulentic, J. W., Stirpe, G. M., Dultzin, D., Del Olmo, A., and Martínez-Carballo, M. A. (2016b). Blue outliers among intermediate redshift quasars. *Astrophys. Space Sci.* 361:3. doi: 10.1007/s10509-015-2590-2

Marziani, P., Sulentic, J. W., Stirpe, G. M., Zamfir, S., and Calvani, M. (2009). VLT/ISAAC spectra of the Hβ region in intermediate-redshift quasars. III. Hβ broad-line profile analysis and inferences about BLR structure. *Astron. Astrophys.* 495, 83–112. doi: 10.1051/0004-6361:200810764

Marziani, P., Sulentic, J. W., Zwitter, T., Dultzin-Hacyan, D., and Calvani, M. (2001). Searching for the physical drivers of the eigenvector 1 correlation space. *Astrophys. J.* 558, 553–560. doi: 10.1086/322286

Marziani, P., Zamanov, R. K., Sulentic, J. W., and Calvani, M. (2003b). Searching for the physical drivers of eigenvector 1: influence of black hole mass and Eddington ratio. *Month. Notices R. Astron. Soc.* 345, 1133–1144. doi: 10.1046/j.1365-2966.2003.07033.x

Mathews, W. G. (1993). Bouncing clouds-A model for the quasar broad-line region. *Astrophys. J. Lett.* 412, L17–L20. doi: 10.1086/186929

Mathews, W. G. and Ferland, G. J. (1987). What heats the hot phase in active nuclei? *Astrophys. J.* 323, 456–467. doi: 10.1086/165843

Mejía-Restrepo, J. E., Trakhtenbrot, B., Lira, P., Netzer, H., and Capellupo, D. M. (2016). Active galactic nuclei at z˜1.5: II. Black hole mass estimation by means of broad emission lines. *Month. Notices R. Astron. Soc.* 460, 187–211.

Merloni, A., Heinz, S., and di Matteo, T. (2003). A fundamental plane of black hole activity. *Month. Notices R. Astron. Soc.* 345, 1057–1076. doi: 10.1046/j.1365-2966.2003.07017.x

Mineshige, S., Kawaguchi, T., Takeuchi, M., and Hayashida, K. (2000). Slim-disk model for soft X-Ray excess and variability of narrow-line seyfert 1 galaxies. *Public. Astron. Soc. Jpn* 52, 499–508. doi: 10.1093/pasj/52.3.499

Murray, N., Chiang, J., Grossman, S. A., and Voit, G. M. (1995). Accretion disk winds from active galactic nuclei. *Astrophys. J.* 451:498. doi: 10.1086/176238

Murtagh, F., and Heck, A. (eds.) (1987). *Multivariate Data Analysis, Vol. 131, Astrophysics and Space Science Library*. Berlin: Springer.

Nagao, T., Marconi, A., and Maiolino, R. (2006). The evolution of the broad-line region among SDSS quasars. *Astron. Astrophys.* 447, 157–172. doi: 10.1051/0004-6361:20054024

Negrete, A., Dultzin, D., Marziani, P., and Sulentic, J. (2012). BLR physical conditions in extreme population a quasars: a method to estimate central black hole mass at high redshift. *Astrophys. J.* 757:62. doi: 10.1088/0004-637X/757/1/62

Negrete, C. A., Dultzin, D., Marziani, P., and Sulentic, J. W. (2013). Reverberation and photoionization estimates of the broad-line region radius in low-z quasars. *Astrophys. J.* 771:31. doi: 10.1088/0004-637X/771/1/31

Negrete, C. A., Dultzin, D., Marziani, P., and Sulentic, J. W. (2014). A new method to obtain the broad line region size of high redshift quasars. *Astrophys. J.* 794:95. doi: 10.1088/0004-637X/794/1/95

Negrete, C. A., Dultzin, D., Marziani, P., Sulentic, J. W., Esparza-Arredondo, D., Martínez-Aldama, M. L., et al. (2017). Quasars as cosmological standard candles. *Front. Astron. Space Sci.* 4:59. doi: 10.3389/fspas.2017.00059

Netzer, H. (2013). *The Physics and Evolution of Active Galactic Nuclei* (Cambridge: Cambridge University Press).

Netzer, H., Brotherton, M. S., Wills, B. J., Han, M., Wills, D., Baldwin, J. A., et al. (1995). The hubble space telescope sample of radio-loud quasars: the LY alpha /H beta ratio. *Astrophys. J.* 448:27. doi: 10.1086/175939

Netzer, H., Lira, P., Trakhtenbrot, B., Shemmer, O., and Cury, I. (2007). Black hole mass and growth rate at high redshift. *Astrophys. J.* 671, 1256–1263. doi: 10.1086/523035

Netzer, H. and Marziani, P. (2010). The effect of radiation pressure on emission-line profiles and black hole mass determination in active galactic nuclei. *Astrophys. J.* 724, 318–328. doi: 10.1088/0004-637X/724/1/318

Nicastro, F. (2000). Broad emission line regions in active galactic nuclei: the link with the accretion power. *Astrophys. J. Lett.* 530, L65–L68. doi: 10.1086/312491

O'Dea, C. P. (1998). The compact steep-spectrum and gigahertz peaked-spectrum radio sources. *Public. Astron. Soc. Pac.* 110, 493–532. doi: 10.1086/316162

Osterbrock, D. E. and Ferland, G. J. (2006). *Astrophysics of Gaseous Nebulae and Active Galactic Nuclei* (Mill Valley, CA: University Science Books).

Padovani, P. (2016). The faint radio sky: radio astronomy becomes mainstream. *Astron. Astrophys. Rev.* 24:13. doi: 10.1007/s00159-016-0098-6

Padovani, P. (2017). Active galactic nuclei at all wavelengths and from all angles. *Front. Space Sci.* 4:35. doi: 10.3389/fspas.2017.00035

Padovani, P. and Rafanelli, P. (1988). Mass-luminosity relationships and accretion rates for Seyfert 1 galaxies and quasars. *Astron. Astrophys.* 205, 53–70.

Peterson, B. M. (1998). Reverberation mapping of active nuclei. *Adv. Space Res.* 21, 57–66. doi: 10.1016/S0273-1177(97)00614-5

Peterson, B. M. (2014). Measuring the masses of supermassive black holes. *Space Sci. Rev.* 183, 253–275. doi: 10.1007/s11214-013-9987-4

Peterson, B. M. (2017). "Space telescope and Optical reverberation mapping project: a leap forward in reverberation mapping," in *IAU Symposium. Vol. 324, IAU Symposium* (Cambridge), 215–218.

Peterson, B. M., Ferrarese, L., Gilbert, K. M., Kaspi, S., Malkan, M. A., Maoz, D., et al. (2004). Central masses and broad-line region sizes of active galactic nuclei. II. A homogeneous analysis of a large reverberation-mapping database. *Astrophys. J.* 613, 682–699. doi: 10.1086/423269

Peterson, B. M., and Horne, K. (2006). "Reverberation mapping of active galactic nuclei," in *Planets to Cosmology: Essential Science in the Final Years of the Hubble Space Telescope*, ed M. Livio & S. Casertano (Cambridge, UK: Cambridge University Press). 89.

Peterson, B. M. and Wandel, A. (1999). Keplerian motion of broad-line region gas as evidence for supermassive black holes in active galactic nuclei. *Astrophys. J. Lett.* 521, L95–L98. doi: 10.1086/312190

Popović, L. Č., Mediavilla, E. G., Kubičela, A., and Jovanović, P. (2002). Balmer lines emission region in NGC 3516: Kinematical and physical properties. *Astron. Astrophys.* 390, 473–480. doi: 10.1051/0004-6361:20020724

Punsly, B. (2010). The redshifted excess in quasar C IV broad emission lines. *Astrophys. J.* 713, 232–238. doi: 10.1088/0004-637X/713/1/232

Richards, G. T., Kruczek, N. E., Gallagher, S. C., Hall, P. B., Hewett, P. C., Leighly, K. M., et al. (2011). Unification of luminous type 1 quasars through C IV emission. *Astron. J.* 141:167. doi: 10.1088/0004-6256/141/5/167

Richards, G. T., Lacy, M., Storrie-Lombardi, L. J., Hall, P. B., Gallagher, S. C., Hines, D. C., et al. (2006). Spectral energy distributions and multiwavelength selection of type 1 quasars. *Astrophys. J. Suppl.* 166:162. doi: 10.1086/506525

Richards, G. T., Vanden Berk, D. E., Reichard, T. A., Hall, P. B., Schneider, D. P., SubbaRao, M., et al. (2002). Broad emission-line shifts in quasars: an orientation measure for radio-quiet quasars? *Astron. J.* 124, 1–17. doi: 10.1086/341167

Risaliti, G., Salvati, M., and Marconi, A. (2011). [O III] equivalent width and orientation effects in quasars. *Month. Notices R. Astron. Soc.* 411, 2223–2229. doi: 10.1111/j.1365-2966.2010.17843.x

Rodríguez-Ardila, A., Prieto, M. A., Viegas, S., and Gruenwald, R. (2006). Outflows of very ionized gas in the centers of seyfert galaxies: kinematics and physical conditions. *Astrophys. J.* 653, 1098–1114. doi: 10.1086/508864

Rokaki, E., Lawrence, A., Economou, F., and Mastichiadis, A. (2003). Is there a disc in the superluminal quasars? *Month. Notices R. Astron. Soc.* 340, 1298–1308. doi: 10.1046/j.1365-8711.2003.06414.x

Runnoe, J. C., Brotherton, M. S., DiPompeo, M. A., and Shang, Z. (2014). The behaviour of quasar C IV emission-line properties with orientation. *Month. Notices R. Astron. Soc.* 438, 3263–3274. doi: 10.1093/mnras/stt2429

Runnoe, J. C., Shang, Z., and Brotherton, M. S. (2013). The orientation dependence of quasar spectral energy distributions. *Month. Notices R. Astron. Soc.* 435, 3251–3261. doi: 10.1093/mnras/stt1528

Sądowski, A., Narayan, R., McKinney, J. C., and Tchekhovskoy, A. (2014). Numerical simulations of super-critical black hole accretion flows in general relativity. *Month. Notices R. Astron. Soc.* 439, 503–520. doi: 10.1093/mnras/stt2479

Shang, Z., Wills, B. J., Robinson, E. L., Wills, D., Laor, A., Xie, B., et al. (2003). The baldwin effect and black hole accretion: a spectral principal component analysis of a complete quasar sample. *Astrophys. J.* 586, 52–71. doi: 10.1086/367638

Shang, Z., Wills, B. J., Wills, D., and Brotherton, M. S. (2007). Spectral Properties from Lyα to Hα for an Essentially Complete sample of quasars. I. Data. *Astron. J.* 134, 294–393. doi: 10.1086/518505

Shemmer, O., Trakhtenbrot, B., Anderson, S. F., Brandt, W. N., Diamond-Stanic, A. M., Fan, X., et al. (2010). Weak line quasars at high redshift: extremely high accretion rates or anemic broad-line regions? *Astrophys. J. Lett.* 722, L152–L156. doi: 10.1088/2041-8205/722/2/L152

Shen, Y. (2016). Rest-frame optical properties of luminous $1.5 < z < 3.5$ quasars: the Hβ-[O iii] region. *Astrophys. J.* 817:55. doi: 10.3847/0004-637X/817/1/55

Shen, Y., Brandt, W. N., Richards, G. T., Denney, K. D., Greene, J. E., Grier, C. J., et al. (2016). The sloan digital sky survey reverberation mapping project: velocity shifts of quasar emission lines. *Astrophys. J.* 831:7. doi: 10.3847/0004-637X/831/1/7

Shen, Y., and Ho, L. C. (2014). The diversity of quasars unified by accretion and orientation. *Nature* 513, 210–213. doi: 10.1038/nature13712

Shen, Y., and Liu, X. (2012). Comparing single-epoch virial black hole mass estimators for luminous quasars. *Astrophys. J.* 753:125. doi: 10.1088/0004-637X/753/2/125

Sijacki, D., Vogelsberger, M., Genel, S., Springel, V., Torrey, P., Snyder, G. F., et al. (2015). The Illustris simulation: the evolving population of black holes across cosmic time. *Month. Notices R. Astron. Soc.* 452, 575–596. doi: 10.1093/mnras/stv1340

Smith, J. E., Robinson, A., Young, S., Axon, D. J., and Corbett, E. A. (2005). Equatorial scattering and the structure of the broad-line region in Seyfert nuclei: evidence for a rotating disc. *Month. Notices R. Astron. Soc.* 359, 846–864. doi: 10.1111/j.1365-2966.2005.08895.x

Snedden, S. A., and Gaskell, C. M. (2007). The case for optically thick high-velocity broad-line region gas in active galactic nuclei. *Astrophys. J.* 669, 126–134. doi: 10.1086/521290

Springel, V., Di Matteo, T., and Hernquist, L. (2005). Modelling feedback from stars and black holes in galaxy mergers. *Month. Notices R. Astron. Soc.* 361, 776–794. doi: 10.1111/j.1365-2966.2005.09238.x

Steffen, A. T., Strateva, I., Brandt, W. N., Alexander, D. M., Koekemoer, A. M., Lehmer, B. D., et al. (2006). The X-ray-to-optical properties of optically selected active galaxies over wide luminosity and redshift ranges. *Astron. J.* 131, 2826–2842. doi: 10.1086/503627

Storchi-Bergmann, T., Schimoia, J. S., Peterson, B. M., Elvis, M., Denney, K. D., Eracleous, M., et al. (2017). Double-peaked profiles: ubiquitous signatures of disks in the broad emission lines of active galactic nuclei. *Astrophys. J.* 835:236. doi: 10.3847/1538-4357/835/2/236

Sulentic, J., Marziani, P., and Zamfir, S. (2011). The case for two quasar populations. *Baltic Astron.* 20, 427–434.

Sulentic, J. W., Bachev, R., Marziani, P., Negrete, C. A., and Dultzin, D. (2007). C IV λ1549 as an eigenvector 1 parameter for active galactic nuclei. *Astrophys. J.* 666, 757–777. doi: 10.1086/519916

Sulentic, J. W., del Olmo, A., Marziani, P., Martínez-Carballo, M. A., D'Onofrio, M., Dultzin, D., et al. (2017). What does Civλ1549 tell us about the physical driver of the eigenvector quasar sequence? *Astron. Astroph.* 608:A122. doi: 10.1051/0004-6361/201630309

Sulentic, J. W., Martínez-Carballo, M. A., Marziani, P., del Olmo, A., Stirpe, G. M., Zamfir, S., et al. (2015). 3C 57 as an atypical radio-loud quasar: implications for the radio-loud/radio-quiet dichotomy. *ArXiv e-prints.* doi: 10.1093/mnras/stv710

Sulentic, J. W., Marziani, P., del Olmo, A., Dultzin, D., Perea, J., and Alenka Negrete, C. (2014). GTC spectra of $z \approx 2.3$ quasars: comparison with local luminosity analogs. *Astron. Astrophys.* 570:A96. doi: 10.1051/0004-6361/201423975

Sulentic, J. W., Marziani, P., and Dultzin-Hacyan, D. (2000a). Phenomenology of broad emission lines in active galactic nuclei. *Ann. Rev. Astron. Astrophys.* 38, 521–571. doi: 10.1146/annurev.astro.38.1.521

Sulentic, J. W., Marziani, P., Zamanov, R., Bachev, R., Calvani, M., and Dultzin-Hacyan, D. (2002). Average quasar spectra in the context of eigenvector 1. *Astrophys. J. Lett.* 566, L71–L75. doi: 10.1086/339594

Sulentic, J. W., Marziani, P., Zamfir, S., and Meadows, Z. A. (2012). No evidence for a systematic Fe II emission line redshift in type 1 active galactic nuclei. *Astrophys. J. Lett.* 752:L7. doi: 10.1088/2041-8205/752/1/L7

Sulentic, J. W., Marziani, P., Zwitter, T., Dultzin-Hacyan, D., and Calvani, M. (2000b). The demise of the classical broad-line region in the luminous quasar PG 1416-129. *Astrophys. J. Lett.* 545, L15–L18. doi: 10.1086/317330

Sulentic, J. W., Zamfir, S., Marziani, P., Bachev, R., Calvani, M., and Dultzin-Hacyan, D. (2003). Radio-loud active galactic nuclei in the context of the eigenvector 1 parameter space. *Astrophys. J. Lett.* 597, L17–L20. doi: 10.1086/379754

Sulentic, J. W., Zwitter, T., Marziani, P., and Dultzin-Hacyan, D. (2000c). Eigenvector 1: an optimal correlation space for active galactic nuclei. *Astrophys. J. Lett.* 536, L5–L9. doi: 10.1086/312717

Sun, J., and Shen, Y. (2015). Dissecting the quasar main sequence: insight from host galaxy properties. *Astrophys. J. Lett.* 804:L15. doi: 10.1088/2041-8205/804/1/L15

Szuszkiewicz, E., Malkan, M. A., and Abramowicz, M. A. (1996). The observational appearance of slim accretion disks. *Astrophys. J.* 458:474. doi: 10.1086/176830

Tang, B., Shang, Z., Gu, Q., Brotherton, M. S., and Runnoe, J. C. (2012). The optical and ultraviolet emission-line properties of bright quasars with detailed spectral energy distributions. *Astrophys. J. Suppl.* 201:38. doi: 10.1088/0067-0049/201/2/38

Trakhtenbrot, B., and Netzer, H. (2012). Black hole growth to z = 2 - I. Improved virial methods for measuring M_{BH} and L/L_{Edd}. *Month. Notices R. Astron. Soc.* 427, 3081–3102. doi: 10.1111/j.1365-2966.2012.22056.x

Tytler, D., and Fan, X.-M. (1992). Systematic QSO emission-line velocity shifts and new unbiased redshifts. *Astrophys. J. Suppl.* 79, 1–36. doi: 10.1086/191642

Vanden Berk, D. E., Richards, G. T., Bauer, A., Strauss, M. A., Schneider, D. P., Heckman, T. M., et al. (2001). Composite quasar spectra from the sloan digital sky survey. *Astron. J.* 122, 549–564. doi: 10.1086/321167

Verner, E., Bruhweiler, F., Verner, D., Johansson, S., Kallman, T., and Gull, T. (2004). Fe II diagnostic tools for quasars. *Astrophys. J.* 611, 780–785. doi: 10.1086/422303

Véron-Cetty, M.-P., Véron, P., and Gonçalves, A. C. (2001). A spectrophotometric atlas of narrow-line seyfert 1 galaxies. *Astron. Astrophys.* 372, 730–754. doi: 10.1051/0004-6361:20010489

Vestergaard, M., and Peterson, B. M. (2006). Determining central black hole masses in distant active galaxies and quasars. II. Improved optical and UV scaling relationships. *Astrophys. J.* 641, 689–709. doi: 10.1086/500572

Villarroel, B., and Korn, A. J. (2014). The different neighbours around Type-1 and Type-2 active galactic nuclei. *Nat. Phys.* 10, 417–420. doi: 10.1038/nphys2951

Wandel, A., Peterson, B. M., and Malkan, M. A. (1999). Central masses and broad-line region sizes of active galactic nuclei. I. Comparing the photoionization and reverberation techniques. *Astrophys. J.* 526, 579–591. doi: 10.1086/308017

Wang, J., and Li, Y. (2011). Strong response of the very broad Hβ emission line in the luminous radio-quiet quasar PG 1416-129. *Astrophys. J. Lett.* 742:L12. doi: 10.1088/2041-8205/742/1/L12

Wang, J., Wei, J. Y., and He, X. T. (2006). A sample of IRAS infrared-selected seyfert 1.5 galaxies: infrared color α(60, 25)-dominated eigenvector 1. *Astrophys. J.* 638, 106–119. doi: 10.1086/498667

Wang, J.-M., Du, P., Li, Y.-R., Ho, L. C., Hu, C., and Bai, J.-M. (2014a). A new approach to constrain black hole spins in active galaxies using optical reverberation mapping. *Astrophys. J. Lett.* 792:L13. doi: 10.1088/2041-8205/792/1/L13

Wang, J.-M., Du, P., Valls-Gabaud, D., Hu, C., and Netzer, H. (2013). Super-eddington accreting massive black holes as long-lived cosmological standards. *Phys. Rev. Lett.* 110:081301. doi: 10.1103/PhysRevLett.110.081301

Wang, J.-M., Qiu, J., Du, P., and Ho, L. C. (2014b). Self-shadowing effects of slim accretion disks in active galactic nuclei: the diverse appearance of the broad-line region. *Astrophys. J.* 797:65. doi: 10.1088/0004-637X/797/1/65

Wang, T., Brinkmann, W., and Bergeron, J. (1996). X-ray properties of active galactic nuclei with optical FeII emission. *Astron. Astrophys.* 309, 81–96.

Wilkes, B. J., Kuraszkiewicz, J., Green, P. J., Mathur, S., and McDowell, J. C. (1999). Investigation of the relation between the spectral energy distributions and the emission lines in low-redshift quasars. *Astrophys. J.* 513, 76–107. doi: 10.1086/306828

Wills, B. J., Brotherton, M. S., Fang, D., Steidel, C. C., and Sargent, W. L. W. (1993). Statistics of QSO broad emission-line profiles. I. The C IV lambda 1549 line and the lambda 1400 feature. *Astrophys. J.* 415:563–+. doi: 10.1086/173186

Wills, B. J., and Browne, I. W. A. (1986). Relativistic beaming and quasar emission lines. *Astrophys. J.* 302, 56–63. doi: 10.1086/163973

Wills, B. J., Laor, A., Brotherton, M. S., Wills, D., Wilkes, B. J., Ferland, G. J., et al. (1999). The PG X-ray QSO sample: links between the ultraviolet-x-ray continuum and emission lines. *Astrophys. J. Lett.* 515, L53–L56. doi: 10.1086/311980

Wu, C.-C., Boggess, A., and Gull, T. R. (1983). Prominent ultraviolet emission lines from Type 1 seyfert galaxies. *Astrophys. J.* 266, 28–40. doi: 10.1086/160756

Wu, Q. (2009). The black hole mass, Eddington ratio and M_{BH}-$\sigma_{[OIII]}$ relation in young radio galaxies. *Month. Notices R. Astron. Soc.* 398, 1905–1914. doi: 10.1111/j.1365-2966.2009.15127.x

Xu, D., Komossa, S., Zhou, H., Lu, H., Li, C., Grupe, D., et al. (2012). Correlation analysis of a large sample of narrow-line seyfert 1 galaxies: linking central engine and host properties. *Astron. J.* 143:83. doi: 10.1088/0004-6256/143/4/83

Yip, C. W., Connolly, A. J., Vanden Berk, D. E., Ma, Z., Frieman, J. A., SubbaRao, M., et al. (2004). Spectral classification of quasars in the sloan digital sky survey: eigenspectra, redshift, and luminosity effects. *Astron. J.* 128, 2603–2630. doi: 10.1086/425626

Zamanov, R. and Marziani, P. (2002). Searching for the physical drivers of eigenvector 1: from quasars to nanoquasars. *Astrophys. J.* 571, L77–L80. doi: 10.1086/341367

Zamanov, R., Marziani, P., Sulentic, J. W., Calvani, M., Dultzin-Hacyan, D., and Bachev, R. (2002). Kinematic linkage between the broad- and narrow-line-emitting gas in active galactic nuclei. *Astrophys. J. Lett.* 576, L9–L13. doi: 10.1086/342783

Zamfir, S., Sulentic, J. W., and Marziani, P. (2008). New insights on the QSO radio-loud/radio-quiet dichotomy: SDSS spectra in the context of the 4D eigenvector1 parameter space. *Month. Notices R. Astron. Soc.* 387, 856–870. doi: 10.1111/j.1365-2966.2008.13290.x

Zamfir, S., Sulentic, J. W., Marziani, P., and Dultzin, D. (2010). Detailed characterization of Hβ emission line profile in low-z SDSS quasars. *Month. Notices R. Astron. Soc.* 403:1759. doi: 10.1111/j.1365-2966.2009.16236.x

Zhang, K., Dong, X.-B., Wang, T.-G., and Gaskell, C. M. (2011). The blueshifting and baldwin effects for the [O III] λ5007 emission line in Type 1 active galactic nuclei. *Astrophys. J.* 737:71. doi: 10.1088/0004-637X/737/2/71

Zhang, K., Wang, T.-G., Gaskell, C. M., and Dong, X.-B. (2013). The baldwin effect in the narrow emission lines of active galactic nuclei. *Astrophys. J.* 762:51. doi: 10.1088/0004-637X/762/1/51

Zheng, W., Sulentic, J. W., and Binette, L. (1990). A double-stream model for line profiles. *Astrophys. J.* 365, 115–118. doi: 10.1086/169462

Conflict of Interest Statement: The authors declare that the research was conducted in the absence of any commercial or financial relationships that could be construed as a potential conflict of interest.

Copyright © 2018 Marziani, Dultzin, Sulentic, Del Olmo, Negrete, Martínez-Aldama, D'Onofrio, Bon, Bon and Stirpe. This is an open-access article distributed under the terms of the Creative Commons Attribution License (CC BY). The use, distribution or reproduction in other forums is permitted, provided the original author(s) and the copyright owner are credited and that the original publication in this journal is cited, in accordance with accepted academic practice. No use, distribution or reproduction is permitted which does not comply with these terms.

frontiers in Astronomy and Space Sciences

MINI REVIEW
published: 31 January 2018
doi: 10.3389/fspas.2017.00070

The Virial Factor and Biases in Single Epoch Black Hole Mass Determinations

Julián E. Mejía-Restrepo[1], Paulina Lira[1], Hagai Netzer[2], Benny Trakhtenbrot[3] and Daniel Capellupo[4]*

[1] Departamento de Astronomía, Universidad de Chile, Santiago, Chile, [2] School of Physics and Astronomy, Tel Aviv University, Tel Aviv, Israel, [3] Department of Physics, Institute for Astronomy, ETH Zurich, Zurich, Switzerland, [4] Department of Physics, McGill University, Montreal, QC, Canada

Accurately determining the masses of supermassive black holes is crucial to understand their evolution and the establishment of their relationship with their host galaxy properties. Beyond the local universe, the single epoch mass estimation method provides a simple procedure to estimate black hole masses in large spectroscopic samples of type-1 active galactic nuclei. The method assumes virialized motion of gas in the close vicinity to the active black holes, traced through broad emission lines. However, because of the assumption of a universal virial factor, this procedure has uncertainties associated with the unknown distribution of the gas clouds. Here, using a sample of 39 quasars observed with the VLT/X-shooter spectrograph, we compare alternative estimations of black hole masses determined from the properties of the accretion disk emission around the black hole with the single epoch virial mass estimations. We find that the virial factor is inversely proportional to the observed width of the broad emission lines. This result implies that current virial masses can be miss-estimated by up to a factor of 6. Our analysis indicates that either the effect of line-of-sight inclination in a planar distribution of the broad line emitting gas or the radiation pressure perturbations to the distribution of gas can reproduce our findings.

Keywords: active galactic nuclei, supermassive black holes, broad line region, accretion discs, virial coefficient

OPEN ACCESS

Edited by:
Deborah Dultzin, Universidad Nacional Autónoma de México, Mexico

Reviewed by:
Milan S. Dimitrijevic, Astronomical Observatory, Serbia
Omar López-Cruz, National Institute of Astrophysics, Optics and Electronics, Mexico
Alenka Negrete, Universidad Nacional Autónoma de México, Mexico

****Correspondence:***
Julián E. Mejía-Restrepo
jemejia@ug.uchile.cl

Specialty section:
This article was submitted to Milky Way and Galaxies, a section of the journal Frontiers in Astronomy and Space Sciences

Received: *31 August 2017*
Accepted: *20 December 2017*
Published: *31 January 2018*

Citation:
Mejía-Restrepo JE, Lira P, Netzer H, Trakhtenbrot B and Capellupo D (2018) The Virial Factor and Biases in Single Epoch Black Hole Mass Determinations. Front. Astron. Space Sci. 4:70. doi: 10.3389/fspas.2017.00070

1. INTRODUCTION

Active supermassive black holes (SMBHs) are powered by accretion flows, probably in the form of accretion disks (ADs) that convert gravitational energy into radiation (Shakura and Sunyaev, 1973). Gas in the Broad Line Region (BLR), located in the vicinity of the SMBH and moving at Keplerian velocities of thousands of kilometers per second, is photo-ionized by the AD producing broad emission lines. Under virial equilibrium, their observed full width at half maximum ($\mathrm{FWHM_{obs}}$) can be used as a proxy for the virial velocity (V_{BLR}) to estimate M_{BH} (e.g., Shen, 2013):

$$M_{\mathrm{BH}} = G^{-1} R_{\mathrm{BLR}}\, V_{\mathrm{BLR}}^2 = f\, G^{-1} R_{\mathrm{BLR}}\, \mathrm{FWHM}_{\mathrm{obs}}^2 \quad (1)$$

here, G is the gravitational constant, R_{BLR} is the mean BLR distance to the SMBH and f is the virial factor that accounts for the differences between the unknown V_{BLR} and $\mathrm{FWHM_{obs}}$ due to the unknown geometrical gas distribution. Since even in the closest active galaxies the BLR cannot be

resolved with current capabilities, $R_{\rm BLR}$ is derived from reverberation mapping (RM) experiments that show a strong correlation between this distance and the continuum luminosity known as the $R_{\rm BLR} - L$ relation (Kaspi et al., 2000; Bentz et al., 2013). f is assumed to be constant for all systems and is usually determined by requiring RM-based masses (from Equation 1) to agree, on average, with masses estimated from the relation between $M_{\rm BH}$ and the stellar velocity dispersion found in local galaxies (Onken et al., 2004; Graham, 2015; Woo et al., 2015). This indirect technique to determine $M_{\rm BH}$ is known as the single epoch (SE) virial method ($M_{\rm BH}^{\rm SE}$) and is commonly used for large samples of growing SMBHs (Trakhtenbrot and Netzer, 2012; Shen, 2013).

Unfortunately, the virial method is subject to biases and uncertainties associated with our ignorance of the dependence of f on additional physical properties. These could include radiation pressure perturbations (Marconi et al., 2008; Netzer and Marziani, 2010), non virial velocity components (Denney et al., 2009, 2010), the relative thickness ($H/R_{\rm BLR}$, where H is the BLR thickness) of the Keplerian BLR orbital plane (Gaskell, 2009), and the line-of-sight (LOS) inclination angle (i) of this plane (Wills and Browne, 1986; Runnoe et al., 2014; Shen and Ho, 2014). An analytical expression for f in the case of a planar BLR of thickness $H/R_{\rm BLR}$ is given by:

$$f = \left[4\left(\sin^2 i + (H/R_{\rm BLR})^2\right)\right]^{-1} \quad (2)$$

Decarli et al. (2008) where $\sin^2 i$ accounts for the line-of-sight projection of the Keplerian velocity of the BLR orbital plane. The nature of the velocity component responsible for the thickness of the BLR is unclear. However, ideas such as non-coplanar orbits, accretion disk pressure, induced turbulence and outflowing disk winds have been suggested in the literature as plausible mechanisms to puff up the BLR (Collin et al., 2006; Czerny et al., 2016). Given all these, the assumption of an universal f introduces an uncertainty in the single epoch method which is estimated to be at least a factor of 2–3.

In Capellupo et al. (2015, 2016, hereafter papers I and III) we introduced an alternative method to estimate $M_{\rm BH}$ ($M_{\rm BH}^{\rm AD}$) based on a Bayesian spectral energy distribution (SED) fitting of the accretion disk. We modeled the accretion disk using the standard Shakura and Sunyaev (1973) geometrically thin optically thick model with general relativistic and disc atmosphere corrections (Slone and Netzer, 2012). Each model is defined by its black hole mass ($M_{\rm BH}^{\rm AD}$), accretion ratio ($\dot{M}$), black hole spin (a_*) and the intrinsic reddening in the host galaxy ($A_{\rm V}$). Using this model we successfully reproduced the SED emission in 37 out of 39 objects of our X-Shooter sample described below.

The purpose of this work is to compare $M_{\rm BH}^{\rm AD}$ (from paper III) and $M_{\rm BH}^{\rm SE}$ (FWHM, L_λ) estimations (from Mejía-Restrepo et al., 2016, hereafter paper II) of the X-Shooter sample in terms of the observational properties of the BLR and the SMBH properties. This analysis will allow us to determine possible biases in $M_{\rm BH}^{\rm SE}$ (FWHM, L_λ) estimations and look for possible corrections in terms of the BLR properties. The full presentation of this study was recently published in *Nature Astronomy* (Mejía-Restrepo et al., 2017, MR17) and here we only provide a brief summary of the sample, the different black hole mass determinations, and our main results. The interested reader is encouraged to refer to MR17 for any additional detail.

This document is structured as follows, in section 2 we introduce the X-Shooter sample. In section 3 we describe in detail both the SE and SED fitting methods to estimate $M_{\rm BH}$. In section 4 we quantify the virial factor from the comparison of both black hole mass approaches and discuss the most relevant results. Finally, in section 5 we present our main conclusions.

2. SAMPLE DESCRIPTION

The main sample that we use in this paper consist of 39 type-I AGN selected to be within a narrow redshift range around $z \simeq 1.55$. For this sample we obtained high signal to noise (S/N) single epoch spectroscopic observations using the VLT/X-Shooter spectrograph as described in papers I, II and III. At the selected narrow redshift range, the X-Shooter spectrograph covers the range of ∼1,200Å to ∼9,200Å in the rest-frame. The sample was selected to homogeneously map the parameter space of $M_{\rm BH}$ and $L/L_{\rm Edd}$. The initial values of these quantities were obtained from the SE calibrations of Trakhtenbrot and Netzer (2012) using their fitting technique of the Mg II broad emission line and its adjacent continuum.

3. ESTIMATING $M_{\rm BH}$

In papers I, II, and III we describe two alternative procedures to estimate $M_{\rm BH}$, one based on the standard SE $M_{\rm BH}$ determination (paper II) and the other on the SED fitting of the accretion disc spectrum (papers I and III). In this section we briefly describe both approaches and comment on the sources of uncertainties of each method.

3.1. Single Epoch $M_{\rm BH}$ Estimates

In paper II we present new calibrations of the SE black hole mass estimators using the broad $H\alpha$, $H\beta$, MgII and CIV emission lines. The underlying assumptions is that Eqn. 1 holds for all broad emission lines and $V_{\rm BLR}$ can be estimated from the FWHM of the line in question (FWHM (line)). In this case:

$$M_{\rm BH}^{\rm SE}\,({\rm FWHM}, L_\lambda) = f_{\rm FWHM} G^{-1} R_{\rm BLR} {\rm FWHM}^2 \quad (3)$$

(e.g., Shen, 2013) where $f_{\rm FWHM}$ is the virial factor associated with the line FWHM and $R_{\rm BLR}$ is obtained from various RM studies (see e.g., Kaspi et al., 2000, 2005; Bentz et al., 2009, 2013, and references therein) and can be written as:

$$R_{\rm BLR} \propto (L_\lambda)^{\alpha_{\rm line}} \quad (4)$$

here L_λ stands for $\lambda L(\lambda)$ at various wavelengths: 6,200Å for the Hα line, 5,100Å for the Hβ line, 3,000Å for the Mg II λ2798 line and 1,450Å for the C IV λ1549line.

It is important to note that $M_{\rm BH}$ estimates derived from high ionization lines such as C IV have a bias due the presence of an associated outflow blue shifted component. For objects with high Eddington ratios, the blue shifted component in C IV

predominates over the component from the virialized region Sulentic, 2017.

3.2. Black Hole Mass Estimates from SED Fitting

In papers I and III we implemented an alternative method to estimate the black hole mass in type1-AGN based on fitting the SED of the accretion disk. We used the geometrically thin, optically thick accretion disc model from Slone and Netzer (2012) which are based on Shakura and Sunyaev (1973). Using this model we obtained successful fits in 37 out 39 objects in our sample. The model is fully determined by $M_{\rm BH}^{\rm AD}$, a_*, $\dot{M}$, the inclination ($i_{\rm LOS}$) with respect to the line-of-sight (LOS) and $A_{\rm V}$. The procedure consisted of a Bayesian minimization over a grid of models covering a range in values for these parameters following the procedure described in paper III. Particularly, we assumed Gaussian priors centered around the observational estimations of $M_{\rm BH}^{\rm SE}$ (Hα, L_{6200}) and $\dot{M}$. $M_{\rm BH}^{\rm SE}$ (Hα, L_{6200}) and $\dot{M}$ are calculated assuming a virial factor $f_{\rm FWHM} = 1$. We also assume scatters in both quantities of 0.3 and 0.2 dex respectively. The minimization process uses 6 continuum windows and the posterior probability of the models is unaffected by the broad emission lines. The role of the priors is to penalize models which deviate significantly from the observational estimation of $M_{\rm BH}$ (Hα) and $\dot{M}_{\rm SE}$. In spite of this, the code can freely move in the parameter space either side of $M_{\rm BH}$ (Hα) and $\dot{M}_{\rm SE}$.

A major goal of the present paper is to set limits on $M_{\rm BH}$ under the assumption that thin accretion disks provide an accurate explanation for the observed continuum in AGNs. We therefore try to test the reliability of the results of our Bayesian procedures using different central values for our priors as well as different scatters around them ($\sigma_{M_{\rm BH}}$). In practice, this is done by considering a large range of virial factors ($f_{\rm FWHM} = \{0.25, 0.4, 1, 2.5, 4\}$) to compute $M_{\rm BH}^{\rm SE}$ (Hα, L_{6200}) and $\dot{M}_{\rm SE}$ and a range of $\sigma_{M_{\rm BH}}$ for each. Each combination of $f_{\rm FWHM}$ and $\sigma_{M_{\rm BH}}$ is used to find the best fit SED and calculate a range of posteriors exactly as done in papers I and III. We find that when the scatter around the central values is small ($<$0.4 dex), the posterior probability distributions of $M_{\rm BH}^{\rm AD}$ and $\dot{M}$ depends on the chosen value of $f_{\rm FWHM}$. However, when the scatter is large ($>$0.8 dex), we find that the posterior probability distributions of $M_{\rm BH}^{\rm AD}$ and $\dot{M}$ are insensitive to the assumed $f_{\rm FWHM}$ and they all tend to converge to the posterior probability distributions of $M_{\rm BH}^{\rm AD}$ and $\dot{M}$ when $f_{\rm FWHM} \sim 1$ and the scatter is $\sim$0.3 dex. This would indicate that $f_{\rm FWHM} \sim 1$ is a close representation of the median virial factor of the AGN population within the $M_{\rm BH}$ range that our sample is covering ($7.5 \lesssim M_{\rm BH} \lesssim 10$).

A major drawback of the above approach is the assumption that the simplified accretion disks SEDs used here, that neglect the effect of disk-winds, complex transfer in the disk atmosphere and other simplifications, provide an accurate description of the geometry and physics close to the central BH. In this approach, there is a degeneracy between the accretion rate and the inclination angle of the disk. For a given flux, larger inclinations will return larger intrinsic luminosities which in turn will return larger accretion rates. Fortunately, the derived black hole mass does not strongly depend on either inclination or accretion rate. As a consequence, the derived inclination does not bias the estimation of the black hole mass as it does in the virial SE method. From all the test described here, we can conclude AD mass estimations are reliable and of comparable accuracy to SE masses.

4. RESULTS AND DISCUSSION

$M_{\rm BH}$ determinations from the SE and the AD methods are compared in the left panel of **Figure 1**. The approaches yield masses in very good agreement with each other, albeit with significant scatter of a factor of about 2. We looked for possible drivers for this scatter and found a strong gradient in FWHM$_{\rm obs}$ across the relation, as can be seen by the color gradient of the data points in **Figure 1**.

The ratio between $M_{\rm BH}^{\rm AD}$ and $M_{\rm BH}^{\rm SE}/f = G^{-1}R_{\rm BLR}{\rm FWHM}_{\rm obs}^2$ allows us to determine a proxy for the virial factor f which we define as $f_{\rm AD}\left({\rm line}\right) \equiv M_{\rm BH}^{\rm AD} \,/\, \left(G^{-1}R_{\rm BLR}\,\left({\rm FWHM}_{\rm obs}\left({\rm line}\right)\right)^2\right)$. In the right panel of **Figure 1** we show $f_{\rm AD}\left({\rm line}\right)$ as a function of the FWHM$_{\rm obs}$ for the Hα, Hβ, Mg II and C IV broad emission lines. Strong anti-correlations between $f_{\rm AD}$ and FWHM$_{\rm obs}$ are present for all lines. As can be seen in **Table 1**, these correlations are found to be significantly stronger than the expected correlations between $f_{\rm AD}$ and $G^{-1}R_{\rm BLR}{\rm FWHM}_{\rm obs}^2$. We can thus conclude that the FWHM$_{\rm obs}$ of the broad lines drives the discrepancies between $M_{\rm BH}^{\rm AD}$ and $M_{\rm BH}^{\rm SE}$.

We also determined how $M_{\rm BH}^{\rm AD}$ depends on the FWHM$_{\rm obs}$ of the lines and the associated L_λ used in single epoch mass determinations methods. To this end, we used the following expression:

$$\log M_{\rm BH}^{\rm AD}\,({\rm FWHM}, L_\lambda) \equiv \alpha_{\rm AD}\log(L_\lambda) + E\log{\rm FWHM}\left({\rm line}\right) + F \quad (5)$$

and implemented an ordinary bi-variate least square linear regression to determine the coefficients in the equation. We summarize the results in the Table S1, where we also show $\alpha_{\rm line}$, which represents the slope of the power-law coefficient of L_λ in Equation (4). We also list the scatter between $M_{\rm BH}^{\rm AD}$ and $M_{\rm BH}^{\rm SE}$ (FWHM, L_λ) as well as the scatter between $M_{\rm BH}^{\rm AD}$ and the *corrected* $M_{\rm BH}^{\rm SE}$ (FWHM, L_λ) ($M_{\rm BH}^{\rm SE}({\rm corr}) \equiv {\rm M}_{\rm BH}^{\rm AD}\,({\rm FWHM}, {\rm L}_\lambda)$) after the dependency of $f_{\rm AD}$ on FWHM$_{\rm obs}$ is taken into account. In the case of the Balmer lines, the scatter is reduced by about a factor 2. Thus, correcting for the correlation between $\log f_{\rm AD}$ and the FWHM$_{\rm obs}$ of the Balmer lines provides an important improvement in our $M_{\rm BH}$ estimations.

The results of the linear regressions presented in Table S1 highlight two important findings. First, $\alpha_{\rm AD}$ and $\alpha_{\rm line}$ are basically indistinguishable from each other. This indicates that L_λ has no impact on the scatter between $M_{\rm BH}^{\rm SE}$ and $M_{\rm BH}^{\rm AD}$ and that $f_{\rm AD}$ can be expressed as a single function of the FWHM$_{\rm obs}$ of the broad emission lines. In **Table 1** we show the explicit expressions relating $f_{\rm AD}$ in terms of FWHM$_{\rm obs}$ for the Hα, Hβ, Mg II and the C IV lines. It can be observed that our measurements are consistent within uncertainties with $f_{\rm AD} \propto {\rm FWHM}_{\rm obs}{}^{-1}$ for all lines.

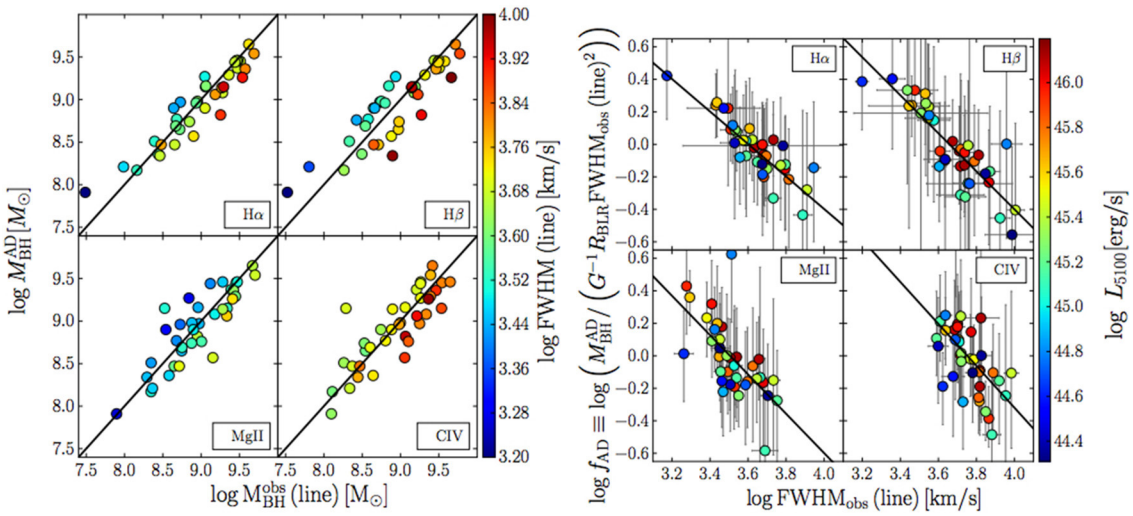

FIGURE 1 | Comparison of black hole mass estimations from the single epoch virial method and the accretion disk modeling Left: log M_{BH}^{AD} vs. log M_{BH}^{SE} (FWHM, L_λ). The color of the points in each panel represent the FWHMs of the labeled emission lines in each panel as indicated in the color bar. The black solid line represents the 1:1 relation. Right: log f_{AD} (lines) vs. log FWHM (line). The color of the points in each panel represents the monochromatic luminosity L_{5100} as indicated in the color bar. The black solid line represents the best linear fit the observed relations.

TABLE 1 | The virial factor as a function of FWHM$_{obs}$ for the broad emission lines.

Broad line	FWHM$^0_{obs}$ [km s^{-1}]	β	FWHM$_{obs}$(†)		G^{-1}R$_{BLR}$ FWHM$^2_{obs}$(‡)	
			r_s	P_s	r_s	P_s
Hα	4,000 ± 700	−1.00±0.10	−0.85	4×10^{-11}	−0.44	5×10^{-3}
Hβ	4,550 ± 1,000	−1.17±0.11	−0.84	8×10^{-11}	−0.48	2×10^{-3}
Mg II λ2798	3,200 ± 800	−1.21±0.24	−0.75	9×10^{-8}	−0.23	2×10^{-1}
C IV λ1549	5,650 ± 3,000	−1.29±0.35	−0.61	6×10^{-5}	−0.25	1×10^{-1}

FWHM$^0_{obs}$ and β are best fit parameters found for $f_{AD} = \left(FWHM_{obs}\,(line)\,/FWHM^0_{obs}\right)^\beta$. r_s and P_s are the Spearman correlation coefficient and associated null-hypothesis probability for the f_{AD} vs. FWHM$_{obs}$ (†) and f_{AD} vs. G^{-1}R$_{BLR}$FWHM$^2_{obs}$ (‡) correlations.

4.1. Inclination as the Source of the f−FWHM$_{obs}$ Correlation

In this section we present different tests that we carried out to determine whether inclination is driving the correlation between f and FWHM$_{obs}$.

Hereafter when referring to logf_{AD}, M_{BH}^{SE} (FWHM, L_λ) and FWHM$_{obs}$ we are meaning logf_{AD} (Hα), M_{BH}^{SE} (FWHM$_{obs}$ (Hα)) and the observed value of FWHM$_{obs}$(Hα), unless otherwise specified. The reason to select the Hα line instead of the Hβ line for the following analysis is the better S/N and hence more accurate measurements of FWHM$_{obs}$(Hα) in our sample. As shown in earlier works, FWHM$_{obs}$ in both Balmer lines are the same within uncertainties (Greene and Ho, 2005; Mejía-Restrepo et al., 2016).

The anti-correlation between logf_{AD} and FWHM$_{obs}$ could be explained by the inclination of the axis of symmetry of a planar BLR with respect to the LOS. If we consider the median LOS inclination, i_{median}, at which Type-1 AGN are typically observed, we can also define a median virial factor f_{median} at which the SE M_{BH} calibration represents an accurate black hole mass for objects observed at i_{median}. Objects with narrower than usual broad emission lines are more likely observed at $i < i_{median}$ (face-on orientations) and objects with broader than usual emission are more likely observed at $i > i_{median}$ (edge-on orientations). This will produce too large (too small) SE mass estimates for objects with very broad (very narrow) emission lines, and would translate into a virial factor that anti-correlates with the line FWHMs.

For a planar BLR with a thickness ratio H/R and inclination i with respect to the line-of-sight we will have FWHM$_{obs}$ = FWHM$_{int}$ × $\sqrt{\sin^2(i) + (H/R)^2}$. Thus, for an ensemble of randomly orientated BLRs the final distribution of FWHM$_{obs}$ will depend on (1) the intrinsic FWHM$_{int}$ distribution and (2) the range of possible random orientations at which the BLR can be observed, both of which are, a priori, not known.

To check the inclination hypothesis we first need to determine the distribution of FWHM$_{int}$ that is consistent with the probability density distribution (PDF) of the observed FWHM$_{obs}$. We then need to test whether it is possible to recover the anti-correlation of f with FWHM$_{obs}$. In other words, we need to test whether a population of randomly generated inclinations

and $\mathrm{FWHM_{int}}$ that satisfy the PDF of $\mathrm{FWHM_{obs}}$, can also account for the bidimensional distribution of the parameter space given by f and $\mathrm{FWHM_{obs}}$.

We first assumed a thin BLR by taking $H/R = 0$. We computed the PDF as the product of two independent random variables (Glen et al., 2004) and applied it to the special case where $\mathrm{FWHM_{obs}} = \mathrm{FWHM_{int}} \times \sin(i)$ (Lopez and Jenkins, 2012). For the $\mathrm{FWHM_{int}}$ distribution, we assumed an underlying truncated normal distribution with certain mean ($\mathrm{FWHM_{mean}}$) and dispersion ($\mathrm{FWHM_{std}}$). Our normal distribution was truncated to allow $\mathrm{FWHM_{int}}$ to vary between 1,000 and 30,000 $\mathrm{km\,s^{-1}}$. We also assumed that our sample is limited to objects with line-of-sight inclination angles between $i_{\min} = 0^\circ$ and $i_{\max} = 70^\circ$, with $i_{\max}$ determined by the torus opening angle. For an optimal exploration of the parameter space we ran a Monte Carlo Markov Chain simulation using the python code EMCEE (Foreman-Mackey et al., 2013). For the simulation we used 20 independent walkers and 5,000 iterations that mapped a total of 10^5 models.

In the Figure S1 we compare the observed cumulative PDF (FWHM_{obs}) and its uncertainty (magenta thin line and shadowed region, respectively) with the predicted cumulative PDF from the model with the highest posterior probability (orange line). The parameters of this model are: $i_{\min} = 19^\circ$, $i_{\max} = 45^\circ$, $\mathrm{FWHM_{mean}}$ =8,500, $\mathrm{FWHM_{std}}$ =2,150, $\mathrm{FWHM_{min}}$ = 4,200 and $\mathrm{FWHM_{max}}$ =30,000. Our model successfully reproduces the observed cumulative PDF. However, a simple normal distribution (turquoise line) is also consistent with the data and cannot be rejected. We also determined the best fit model for a distribution with $\mathrm{FWHM_{std}} = 0$, i.e., effectively a single velocity. This model (dashed blue-line) is able to reproduce the distribution at low values of $\mathrm{FWHM_{obs}}$, but it is unable to account for the distribution at large velocity widths.

First, we tested whether our thin BLR model is successful in reproducing the $f-\mathrm{FWHM_{obs}}$ distribution seen in the data. In the right panel of **Figure 1** we show the predicted bi-dimensional probability density distribution of the virial factor and the observed $\mathrm{FWHM_{obs}}(\mathrm{H}\alpha)$ as predicted by the thin BLR model. The Figure includes contours showing 25, 50, 75, and 99% confidence limits contours (black-thin lines) centred around the maximum probability point. We also superposed the data from the right panel of **Figure 2** (open-blue circles). The magenta line represents the derived relation $f = \left(\mathrm{FWHM_{obs}}\,(\mathrm{H}\alpha)\,/4{,}000\ \mathrm{km\,s^{-1}}\right)$. The thick yellow line is the median of the $f-\mathrm{FWHM_{obs}}$ distributions derived using a quantile non-parametric spline regression (COBS, Ng and Maechler, 2007). Analogously, the blue-dashed lines represent the 25, 50, and 75% quantiles of the observational

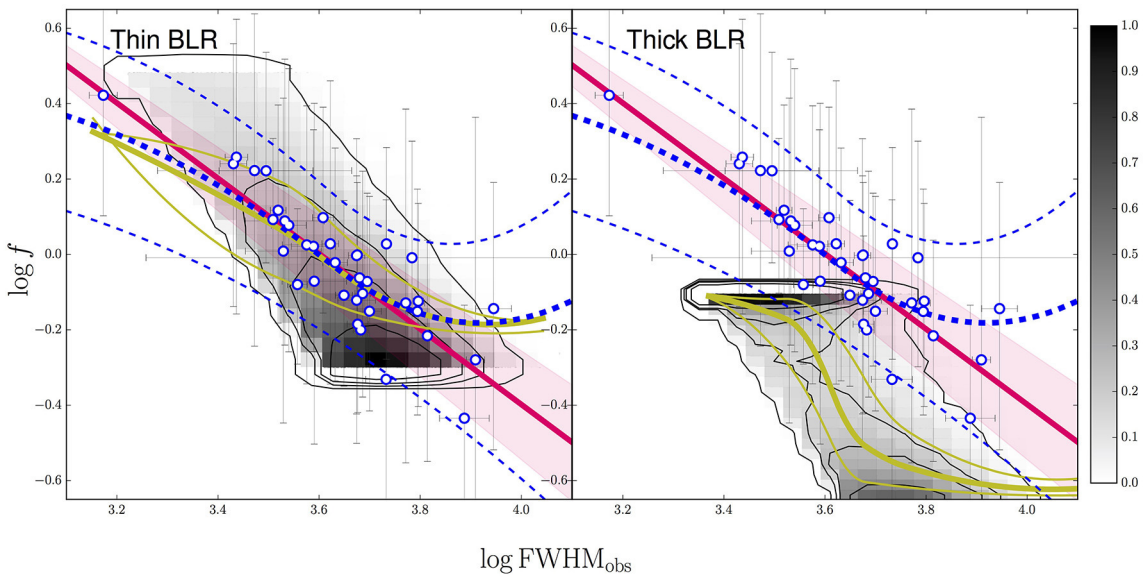

FIGURE 2 | Virial factor–$\mathrm{FWHM_{obs}}$ bi–dimensional distributions for a thin and thick BLR. Predicted bi-dimensional probability distribution functions of the virial factor and $\mathrm{FWHM_{obs}}$ for a thin BLR **(left)** and a thick BLR **(right)**, as predicted by the best-fit models, are shown in gray. The darkest regions represent the most probable combinations of these quantities as quantified in the color-bar. The thin black lines are the 25, 50, and 75% and 99% confidence limit contours centered around the maximum probability point. The thick yellow lines are the median of the $f-\mathrm{FWHM_{obs}}$ distributions derived from a quantile non-parametric spline regression (COBS). The open-blue circles are data from the right panel of **Figure 1** for the Hα line. The magenta lines are the derived relation $f = \left(\mathrm{FWHM_{obs}}\,(\mathrm{H}\alpha)\,/4{,}000\ \mathrm{km\,s^{-1}}\right)$ and the shadowed regions the associated uncertainties. The thin blue-dashed lines are the 25, 50, and 75% quantiles of the observational distribution after accounting for the measurement errors in f_{AD} and $\mathrm{FWHM_{obs}}(\mathrm{H}\alpha)$. We see that for the thin BLR the 50%-quantile (median) of the theoretical and observational distributions are in very good agreement with each other. Additionally, the distribution of the data points shows good agreement with the predicted bi-dimensional distribution confidence limits. Explicitly, we find that 21% of the points fall inside the central 25% confidence level region, 51% fall inside the 50% confidence level region, 78% fall inside the 75% confidence level region, and 87% fall inside the 99% confidence region level. On the other hand, the thick BLR model cannot reproduce the bi-dimensional $f-\mathrm{FWHM_{obs}}$ distribution.

distribution. To obtained these quantiles, for each observed data we randomly generated 1,000 points following the error distributions in $f_{\rm AD}$ and $\rm FWHM_{obs}(H\alpha)$ and then applied the COBS method to characterize the resulting distribution. We can notice that the median (50%-quantile) of the theoretical and observational distributions are in very good agreement. The scattered open-blue circles also show excellent agreement with the the bi-dimensional probability density function from the best model. Explicitly, we find that from our 37 objects, 21% fall inside the central 25% confidence level region, 51% fall inside the 50% confidence level region, 74% fall inside the 75% confidence level region, and 85% fall inside the 99% confidence level region.

In order to test the effects introduced by a thick BLR ($0 < H/R < 1$), we assumed a single H/R for all objects and followed the same steps outlined for the case of a thin BLR. We found that a wide range in BLR thickness ratios ($H/R < 0.5$) is able to reproduce the cumulative $\rm FWHM_{obs}$ PDF. However, objects with large thickness ratios clearly fail to reproduce the bi-dimensional distributions of $f-\rm FWHM_{obs}$ as can be seen in the right panel of **Figure 2**. We generally find that only relatively thin BLRs, i.e., those with $H/R < 0.1$, are able to reproduce both the bi-dimensional distributions and the cumulative $\rm FWHM_{obs}(H\alpha)$ PDF. In particular, for a BLR with $H/R \rightarrow 0$, we find that the derived $f_{\rm AD}$ values constrain the range of inclinations at which the BLR is observed in our sample to $15^\circ \lesssim i \lesssim 50^\circ$. This upper limit is consistent with typical expectations of a central torus hiding the BLR. We also find that the median virial factor in our sample, $f = 0.95$, corresponds to a median orientation of $i_{\rm median} = 31^\circ$.

In summary, our results show that a population of randomly orientated, thin BLRs can successfully reproduce our observations. We can thus conclude that inclination is very likely the main reason for the observed $f-\rm FWHM_{obs}$ correlations.

4.2. Radiation Pressure Effects

We finally considered the possibility that radiation pressure perturbations to the BLR motions might cause the observed $f_{\rm AD}$-$\rm FWHM_{obs}$ dependency. A recent model considers the effects of radiation pressure in a BLR composed of pressure confined clouds, hence allowing the gas density of individual clouds to decrease with distance to the central black hole (Netzer and Marziani, 2010). In this model the system is still bound by gravity and $\rm FWHM_{obs}$ becomes smaller with increasing $\lambda_{\rm Edd}$. The reason for this trend is that as $\lambda_{\rm Edd}$ increases, the clouds spend more time at large distances from the black hole, therefore increasing the median $R_{\rm BLR}$ and decreasing the median BLR Keplerian velocities. To account for this effect, the authors of this model proposed a modified expression for $R_{\rm BLR}$:

$$R_{\rm BLR} = R^0_{\rm BLR}\left[a_1 L_\lambda^{\alpha_{\rm line}} + a_2\,(L_\lambda/M_{\rm BH})\right] \quad (6)$$

where a_1 and a_2 are constants. The first term accounts for the observational relation described in Equation (4) and the second term represents a radiation pressure perturbation quantified by $L_\lambda/M_{\rm BH} \propto \lambda_{\rm Edd}$. When replaced into the virial mass equation (Equation 1) this relation leads to a simple quadratic equation on $M_{\rm BH}$ with solution:

$$M^{\rm rad}_{\rm BH} = \frac{a_{10}}{2} L^{\alpha_{\rm line}} {\rm FWHM_{obs}}^2 \left[1 + \sqrt{1 + \frac{4\,a_{20} L_\lambda^{1-2\alpha_{\rm line}}}{a_{10}^2\,{\rm FWHM}^2_{\rm obs}}}\right] \quad (7)$$

or equivalently:

$$f_{\rm rad} \propto \left[1 + \sqrt{1 + \frac{4\,a_{20} L_\lambda^{1-2\alpha_{\rm line}}}{a_{10}^2\,{\rm FWHM}^2_{\rm obs}}}\right] \quad (8)$$

where ${M_{\rm BH}}^{\rm rad}$ and $f_{\rm rad}$ are the black hole mass and virial factor for a radiation pressure dominated BLR. $a_{10} = a_1 f_0\, R^0_{\rm BLR} G^{-1}$, $a_{20} = a_2 f_0\, R^0_{\rm BLR} G^{-1}$, and f_0 is a normalization constant. In the case when $4\,a_{20} L_\lambda^{1-2\alpha_{\rm line}}/a_{10}^2\,{\rm FWHM}^2_{\rm obs} \gg 1$ this would result in a close agreement with the inverse proportionality between $f_{\rm AD}$ and $\rm FWHM_{obs}$ found in our data. Given that $\alpha_{\rm line}$ is found to be $\sim$0.6 for all lines (see Table S1), this would translate into an explicit dependency of f on L_λ. We would then expect that the scatter in the $f_{\rm AD}-\rm FWHM_{obs}$ relation should be driven by L_λ. In the right panel of **Figure 1** larger (smaller) values of L_{5100} are represented by redder (bluer) colors. We can see that there is no clear suggestion that the scatter in driven by L_{5100} in any of the lines. Note however that the relatively narrow range in L_{5100} covered by our sample (from $L_{5100} = 2.0 \times 10^{44}$ to $L_{5100} = 1.6 \times 10^{46}$ ergs/s, corresponding to a factor of 80), together with the uncertainties in our estimations of f, do not allow us to rule out this mechanism.

Testing this model further, we found the combination of parameters a_1, a_2, and f_0 that best reproduce our $M^{\rm AD}_{\rm BH}$ measurements and the observed relation between f and $\rm FWHM_{obs}$ for the Hα line. To obtain dimensionless values for a_1 and a_2 we expressed $M_{\rm BH}$, L_λ and FWHM in units of $10^8 M_\odot$, $10^{44}{\rm erg\,s^{-1}}$ and 1,000 $\rm km\,s^{-1}$, respectively. Taking $\alpha_{\rm line} = 0.63$, as suggested by the observations (see Table S1), we carried out a Monte-Carlo Markov Chain exploration of the parameter space of the model and found that $a_1 = 0.88$, $a_2 = 0.36$ and $f_o = 0.51$ are able to reproduce our $M^{\rm AD}_{\rm BH}$ measurements with a scatter of 0.12 dex, preserving the experimental dependence of $R_{\rm BLR}$ on L_λ as expressed in Equation 4 with a scatter of 0.05 dex. At the same time the results are able to reproduce the observed $f-\rm FWHM_{obs}$ relation with a scatter of 0.11 dex [see **Figure 3**, which presents our observations (black squares with error bars) together with the prescribed values for f as given by Equation 8 (colored circles without error bars)]. However, we also found that the residuals between the predicted values and the best fit to the correlation are heavily correlated with L_{5100} ($\rm r_s > 0.63$, $\rm P_s < 2 \times 10^{-5}$), as can be seen by the color gradient of our simulated points in the direction perpendicular to the correlation best fit in **Figure 3**. This bias is introduced by the explicit dependence of $f_{\rm rad}$ on L_λ which is not observed in our sample, although notice that the error bars of our derived f values are of the order of, if not larger, than the expected dependence (see **Figure 3**). Finally, the dependency on L_{5100} vanishes when $\alpha_{\rm line} = 0.5$. For this case, however, we were unable to reproduce any the observables. Extending our sample towards lower luminosities will allow us to determine

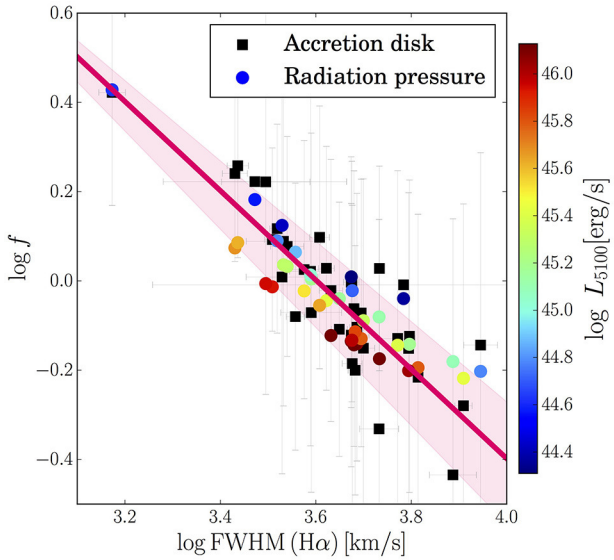

FIGURE 3 | Radiation pressure in a gravitationally bound BLR. The observed virial factor vs. $\mathrm{FWHM_{obs}}$ for the Hα line is shown (black squares). The magenta line is the derived relation $f = \left(\mathrm{FWHM_{obs}}\,(\mathrm{H}\alpha)\,/4{,}000\ \mathrm{km\,s^{-1}}\right)$ and the width of the shadowed region accounts for the uncertainties in that relation. The filled points represent the modeled f_{rad} from the best fit model for radiation pressure in a gravitationally bound BLR. The color of the points scales with the measured monochromatic luminosity at 5,100Å (L_{5100}) for each object, as indicated by the color bar. Redder (bluer) points correspond to larger (smaller) values of L_{5100}. As can be observed, the model predicts that the scatter in f_{rad} (colored points) is driven by L_{5100} (see Equation 8). This dependence is not seen in our data (black squares) as shown in the right panel of **Figure 1**. Nevertheless, the relatively large errors in f_{AD} and the weak dependence of f_{rad} in L_{5100} may probably hide the expected dependence from this radiation pressure model.

a possible dependence of f_{rad} on L_λ. This should yield the final test to be able to confidently conclude whether this model can be the driving mechanism for the observed $f-\mathrm{FWHM_{obs}}$ correlation.

5. SUMMARY AND CONCLUSIONS

In this paper we compared Single Epoch black hole masses ($M_{\mathrm{BH}}^{\mathrm{SE}}$ (FWHM, L_λ)), obtained from the spectral properties of the BLR, with the black hole masses ($M_{\mathrm{BH}}^{\mathrm{AD}}$) that we derived through SED fitting of the accretion disk emission by assuming a standard geometrically thin and optically thick disk model. Because of the independence of $M_{\mathrm{BH}}^{\mathrm{AD}}$ masses on BLR properties, the comparison of these quantities allowed us to quantify the discrepancies between both black hole mass approaches expressing them in terms of the virial factor f_{AD}.

Our results suggest a strong anti-correlation between $\mathrm{FWHM_{obs}}(\mathrm{H}\alpha)$ and f_{AD} which indicates that $M_{\mathrm{BH}}^{\mathrm{SE}}$ (FWHM, L_λ) estimations are presumably biased. In particular we found that our results are consistent, within uncertainties, with $f_{\mathrm{AD}} \propto 1/\mathrm{FWHM_{obs}}$ for the case of the Hα, Hβ, Mg II and C IV lines.

Our analysis suggests that LOS inclination in a planar BLR and/or radiation pressure perturbations to the BLR distribution can reproduce our findings. Regardless of its physical origin, the dependence of f with $\mathrm{FWHM_{obs}}(\mathrm{H}\alpha)$ implies that M_{BH} has been, on average, systematically overestimated for systems with large $\mathrm{FWHM_{obs}}(\mathrm{H}\alpha)$ ($\gtrsim$ 4,000 km s^{-1}) and underestimated for systems with small $\mathrm{FWHM_{obs}}(\mathrm{H}\alpha)$ ($\lesssim$ 4,000 km s^{-1}). The range of f_{AD} values presented in the right panel of **Figure 1**, which are associated with $\mathrm{FWHM_{obs}}(\mathrm{H}\alpha) = 1{,}600$–$8{,}000$ km s^{-1}, imply a range in f, and hence M_{BH}, of factor ~6. However, this range should not be taken as representative of the entire population of AGN since our sample is too small (37 objects) and was not defined to be complete in terms of BLR properties.

AUTHOR CONTRIBUTIONS

JM-R and PL co-developed the idea and wrote the manuscript; JM-R, PL, and DC wrote the codes needed for the different measurements and fittings procedures, JM-R obtained the measurements and performed the analysis. HN, DC, and BT contributed to the accretion disc calculations, the error estimates of the black hole mass and the interpretation of the results and improvements to the manuscript.

ACKNOWLEDGMENTS

Support for the work of JM-R was provided by "CONICYT-PCHA/doctorado Nacional para extranjeros/2013-63130316". PL acknowledges support by Fondecyt Project #1161184. HN acknowledges support by the Israel Science Foundation grant 234/13. BT is a Zwicky Fellow at the ETH Zurich.

SUPPLEMENTARY MATERIAL

The Supplementary Material for this article can be found online at: https://www.frontiersin.org/articles/10.3389/fspas.2017.00070/full#supplementary-material

REFERENCES

Bentz, M. C., Denney, K. D., Grier, C. J., Barth, A. J., Peterson, B. M., Vestergaard, M., et al. (2013). The low-luminosity end of the radius-luminosity relationship for active galactic nuclei. *Astrophys. J.* 767:149. doi: 10.1088/0004-637X/767/2/149

Bentz, M. C., Peterson, B. M., Netzer, H., Pogge, R. W., and Vestergaard, M. (2009). The radius-luminosity relationship for active galactic nuclei: the effect of host-galaxy starlight on luminosity measurements. II. The full sample of reverberation-mapped AGNs. *Astrophys. J.* 697, 160–181. doi: 10.1088/0004-637X/697/1/160

Capellupo, D. M., Netzer, H., Lira, P., Trakhtenbrot, B., and Mejía-Restrepo, J. (2015). Active galactic nuclei at z~1.5 - I. Spectral energy distribution and accretion discs. *Monthly Not. R. Astron. Soc.* 446, 3427–3446. doi: 10.1093/mnras/stu2266

Capellupo, D. M., Netzer, H., Lira, P., Trakhtenbrot, B., and Mejía-Restrepo, J. (2016). Active galactic nuclei at z~1.5 - III. Accretion discs and black hole spin. *Monthly Not. R. Astron. Soc.* 460, 212–226. doi: 10.1093/mnras/stw937

Collin, S., Kawaguchi, T., Peterson, B. M., and Vestergaard, M. (2006). Systematic effects in measurement of black hole masses by emission-line reverberation of active galactic nuclei: eddington ratio and inclination. *Astron. Astrophys.* 456, 75–90. doi: 10.1051/0004-6361:20064878

Czerny, B., Du, P., Wang, J.-M., and Karas, V. (2016). A test of the formation mechanism of the broad line region in active galactic nuclei. *Astrophys. J.* 832:15. doi: 10.3847/0004-637X/832/1/15

Decarli, R., Dotti, M., Fontana, M., and Haardt, F. (2008). Are the black hole masses in narrow-line Seyfert 1 galaxies actually small? *Monthly Not. R. Astron. Soc.* 386, L15–L19. doi: 10.1111/j.1745-3933.2008.00451.x

Denney, K. D., Peterson, B. M., Pogge, R. W., Adair, A., Atlee, D. W., Au-Yong, K., et al. (2009). Diverse kinematic signatures from reverberation mapping of the broad-line region in AGNs. *Astrophys. J.* 704, L80–L84. doi: 10.1088/0004-637X/704/2/L80

Denney, K. D., Peterson, B. M., Pogge, R. W., Adair, A., Atlee, D. W., Au-Yong, K., et al. (2010). Reverberation mapping measurements of black hole masses in six local seyfert galaxies. *Astrophys. J.* 721, 715–737. doi: 10.1088/0004-637X/721/1/715

Foreman-Mackey, D., Hogg, D. W., Lang, D., and Goodman, J. (2013). emcee: the MCMC hammer. *Publ. Astrono. Soc. Pac.* 125, 306–312. doi: 10.1086/670067

Gaskell, C. M. (2009). What broad emission lines tell us about how active galactic nuclei work. *New Astron. Rev.* 53, 140–148. doi: 10.1016/j.newar.2009.09.006

Glen, A. G., Leemis, L. M., and Drew, J. H. (2004). Computing the distribution of the product of two continuous random variables. *Comput. Stat. Data Anal.* 44, 451–464. doi: 10.1016/S0167-9473(02)00234-7

Graham, A. W. (2015). Galaxy bulges and their massive black holes: a review. *ArXiv*. doi: 10.1007/978-3-319-19378-6_11

Greene, J. E., and Ho, L. C. (2005). Estimating black hole masses in active galaxies using the Hα emission line. *Astrophys. J.* 630, 122–129. doi: 10.1086/431897

Kaspi, S., Maoz, D., Netzer, H., Peterson, B. M., Vestergaard, M., and Jannuzi, B. T. (2005). The relationship between luminosity and broad-line region size in active galactic nuclei. *Astrophys. J.* 629, 61–71. doi: 10.1086/431275

Kaspi, S., Smith, P. S., Netzer, H., Maoz, D., Jannuzi, B. T., and Giveon, U. (2000). Reverberation measurements for 17 quasars and the size-mass-luminosity relations in active galactic nuclei. *Astrophys. J.* 533, 631–649. doi: 10.1086/308704

Lopez, S., and Jenkins, J. S. (2012). The effects of viewing angle on the mass distribution of exoplanets. *Astrophys. J.* 756:177. doi: 10.1088/0004-637X/756/2/177

Marconi, A., Axon, D. J., Maiolino, R., Nagao, T., Pastorini, G., Pietrini, P., et al. (2008). The effect of radiation pressure on virial black hole mass estimates and the case of narrow-line seyfert 1 galaxies. *Astrophys. J.* 678, 693–700. doi: 10.1086/529360

Mejía-Restrepo, J. E., Lira, P., Netzer, H., Trakhtenbrot, B., and Capellupo, D. M. (2017). The effect of nuclear gas distribution on the mass determination of supermassive black holes. *Nat. Astron.* 2, 63–68. doi: 10.1038/s41550-017-0305-z

Mejía-Restrepo, J. E., Trakhtenbrot, B., Lira, P., Netzer, H., and Capellupo, D. M. (2016). Active galactic nuclei at z∼1.5 - II. Black hole mass estimation by means of broad emission lines. *Monthly Not. R. Astron. Soc.* 460, 187–211. doi: 10.1093/mnras/stw568

Netzer, H., and Marziani, P. (2010). The effect of radiation pressure on emission-line profiles and black hole mass determination in active galactic nuclei. *Astrophys. J.* 724, 318–328. doi: 10.1088/0004-637X/724/1/318

Ng, P., and Maechler, M. (2007). A fast and efficient implementation of qualitatively constrained quantile smoothing splines. *Stat. Model.* 7, 315–328. doi: 10.1177/1471082X0700700403

Onken, C. A., Ferrarese, L., Merritt, D., Peterson, B. M., Pogge, R. W., Vestergaard, M., et al. (2004). Supermassive black holes in active galactic nuclei. II. Calibration of the black hole mass-velocity dispersion relationship for active galactic nuclei. *Astrophys. J.* 615, 645–651. doi: 10.1086/424655

Runnoe, J. C., Brotherton, M. S., DiPompeo, M. A., and Shang, Z. (2014). The behaviour of quasar C IV emission-line properties with orientation. *Monthly Not. R. Astron. Soc.* 438, 3263–3274. doi: 10.1093/mnras/stt2429

Shakura, N. I., and Sunyaev, R. A. (1973). Black holes in binary systems. Observational appearance. *Astron. Astrophys.* 24, 337–355. doi: 10.1007/978-94-010-2585-0_13

Shen, Y. (2013). The mass of quasars. *Bull. Astron. Soc. India* 41, 61–115.

Shen, Y., and Ho, L. C. (2014). The diversity of quasars unified by accretion and orientation. *Nature* 513, 210–213. doi: 10.1038/nature13712

Slone, O., and Netzer, H. (2012). The effects of disc winds on the spectrum and black hole growth rate of active galactic nuclei. *Monthly Not. R. Astron. Soc.* 426, 656–664. doi: 10.1111/j.1365-2966.2012.21699.x

Trakhtenbrot, B., and Netzer, H. (2012). Black hole growth to z = 2 - I. Improved virial methods for measuring M_{BH} and L/L_{Edd}. *Monthly Not. R. Astron. Soc.* 427, 3081–3102. doi: 10.1111/j.1365-2966.2012.22056.x

Wills, B. J., and Browne, I. W. A. (1986). Relativistic beaming and quasar emission lines. *Astrophys. J.* 302, 56–63. doi: 10.1086/163973

Woo, J.-H., Yoon, Y., Park, S., Park, D., and Kim, S. C. (2015). The black hole mass-stellar velocity dispersion relation of narrow-line seyfert 1 galaxies. *Astrophys. J.* 801:38. doi: 10.1088/0004-637X/801/1/38

Conflict of Interest Statement: The authors declare that the research was conducted in the absence of any commercial or financial relationships that could be construed as a potential conflict of interest.

The reviewer, AN, and handling Editor declared their shared affiliation.

Copyright © 2018 Mejía-Restrepo, Lira, Netzer, Trakhtenbrot and Capellupo. This is an open-access article distributed under the terms of the Creative Commons Attribution License (CC BY). The use, distribution or reproduction in other forums is permitted, provided the original author(s) and the copyright owner are credited and that the original publication in this journal is cited, in accordance with accepted academic practice. No use, distribution or reproduction is permitted which does not comply with these terms.

frontiers in Astronomy and Space Sciences

MINI REVIEW
published: 24 July 2017
doi: 10.3389/fspas.2017.00007

Black Hole Mass Estimation in Type 1 AGN: Hβ vs. Mg II Lines and the Role of Balmer Continuum

Jelena Kovačević-Dojčinović [1], Sladjana Marčeta-Mandić [1,2] and Luka Č. Popović [1,2]**

[1] Astronomical Observatory, Belgrade, Serbia, [2] Department of Astronomy, Faculty of Mathematics, University of Belgrade, Belgrade, Serbia

Here we investigate the Hβ and Mg II spectral line parameters used for the black hole mass (M_{BH}) estimation for a sample of Type 1 Active Galactic Nuclei (AGN) spectra selected from the Sloan Digital Sky Survey (SDSS) database. We have analyzed and compared the virialization of the Hβ and Mg II emission lines, and found that the Hβ line is more confident virial estimator than Mg II. We have investigated the influence of the Balmer continuum emission to the M_{BH} estimation from the UV parameters, and found that the Balmer continuum emission can contribute to the overestimation of the M_{BH} on average for ∼5% (up to 10%).

Keywords: galaxies:active, galaxies:nuclei, quasars:supermassive black holes, techniques:spectroscopic, quasars:emission lines, line:profiles

OPEN ACCESS

Edited by:
Paola Marziani, National Institute for Astrophysics (INAF), Italy

Reviewed by:
Luigi Foschini, Brera Astronomical Observatory, Italy
Erika Maria Benitez, National Autonomous University of Mexico, Mexico

****Correspondence:***
Sladjana Marčeta-Mandić
sladjana@aob.rs
Luka Č. Popović
lpopovic@aob.bg.ac.rs

Specialty section:
This article was submitted to Milky Way and Galaxies, a section of the journal Frontiers in Astronomy and Space Sciences

Received: *10 May 2017*
Accepted: *29 June 2017*
Published: *24 July 2017*

Citation:
Kovačević-Dojčinović J, Marčeta-Mandić S and Popović LČ (2017) Black Hole Mass Estimation in Type 1 AGN: Hβ vs. Mg II Lines and the Role of Balmer Continuum. Front. Astron. Space Sci. 4:7. doi: 10.3389/fspas.2017.00007

1. INTRODUCTION

Several methods are used to estimate central black hole (BH) mass M_{BH} in galaxies (for review see e.g., Marziani and Sulentic, 2012; Shen, 2013; Ilić and Popović, 2014; Peterson, 2014). For Type 1 AGN, the most appropriate methods for the M_{BH} estimation are those using the strong broad emission lines (BELs), as the most prominent features in their spectra. The virial methods (see Peterson et al., 2004; Vestergaard and Peterson, 2006) are based on the assumption that the Broad Line Region (BLR) gas is bounded to the central BH (see Gaskell, 2009) and the main broadening mechanism of the BELs is the Keplerian motion around the supermassive BH, so the full width at half maximum (FWHM) of BELs indicates the velocity of the emitting gas. We should note that in principle the line dispersion much better represents this motion (Peterson et al., 2004; Collin et al., 2006), however in order to find the line dispersion one should assume some type of line profile (that may be very complex), therefore the FWHM is often used instead of the line dispersion.

One of these methods is based on the R–L relationship (see e.g., Bentz et al., 2006), the outcome of the reverberation mapping (see Blandford and McKee, 1982; Peterson et al., 2004, etc.), which enables the estimation of the photometric radius from only one epoch spectrum (see e.g., Vestergaard and Peterson, 2006). An alternative method for M_{BH} estimation using the BEL parameters is based on the gravitational redshift in the broad line profiles (see Zheng and Sulentic, 1990; Popović et al., 1995; Bon et al., 2015; Jonić et al., 2016; Liu et al., 2017). The advantage of this method is that it does not depend on the BLR inclination, unlike the virial methods.

There are many unresolved questions relevant for the application of these methods. For example, since the BLR geometry could be complex (see e.g., Sulentic et al., 2000; Popović et al., 2004; Gaskell, 2009, etc.), it is essential to confirm if the virial assumption is correct for all BELs which are used in the methods for the M_{BH} estimation and if the gravitational redshift could be measured from the BELs complex shapes, or if it may be suppressed by some other effects.

The most frequently used BELs as the virial estimators are the broad Hβ (in the optical) and Mg II (in the UV) lines (see Marziani and Sulentic, 2012). Both, Hβ and Mg II lines have complex profiles, which should be considered if these lines are used for the M_{BH} estimation. Extracting refined Hβ and Mg II profiles is a difficult task and it is essential for an accurate M_{BH} estimation. Especially since the broad Hβ overlaps with a numerous optical Fe II lines, the [O III] doublet and the Hβ narrow line component, while the Mg II line overlaps with a numerous UV Fe II lines. Finally, the presence of the Balmer continuum for $\lambda < 3{,}646$Å, is contributing to the uncertainty of the M_{BH} estimation from the UV parameters and it has to be subtracted for obtaining the pure power law luminosity in the UV band.

In this paper we first present the models of the optical Fe II, UV Fe II emission and Balmer continuum, that could give more precise measurements of the optical and UV parameters [Hβ and Mg II broad line profiles, power law luminosity at $\lambda = 3{,}000$Å, as $L_\lambda(3{,}000\text{Å})$] used for the M_{BH} estimation. Then, we analyze the virialization assumption for the Hβ and Mg II broad lines, and the influence of the Balmer continuum to the M_{BH} estimation from the UV parameters.

2. THE SAMPLE AND ANALYSIS

The used sample consists of the 287 spectra of Type 1 AGN, obtained from the SDSS Data Release 7 (DR7). The sample is the same as in Kovačević-Dojčinović and Popović (2015) where the detailed description of the sample selection criteria is given. For the investigation of the virialization of the emission regions, we exclude all spectra with the blue asymmetry, which resulted with the sample of 123 objects used in this research of the Hβ and Mg II profiles (see Jonić et al., 2016). In the future work we plan to investigate in more details radio properties for this sample, and to search for the connection between the radio-loudness and M_{BH}.

2.1. Model of the Optical Emission Lines in 4,000–5,500Å: Extracting the Pure Broad Hβ Profile

To obtain a pure broad Hβ component, the narrow Hβ and [O III] lines have to be carefully subtracted, as well as the optical Fe II lines. After correcting the spectra for the Galactic reddening and the cosmological redshift, and subtracting the underlying continuum, we applied the multi-Gaussian fitting procedure in 4,000–5,500Å range, described in details in Kovačević et al. (2010) and Kovačević-Dojčinović and Popović (2015). In the fitting procedure, the number of free parameters was reduced assuming that the lines or the line components which originate from the same emission region, have the same widths and shifts. Therefore all narrow Balmer lines (Hδ, Hγ, and Hβ) have the same widths and shifts as [O III] lines, since we assume that they all originate from the Narrow Line Region (NLR). The broad part of the Balmer lines was modeled with two Gaussian functions representing the emission from the Intermediate Line Region (ILR) and from the Very Broad Line Region (VBLR) (see Popović et al., 2004; Bon et al., 2006, 2009; Hu et al., 2008).

We have made a Fe II template as a sum of the most prominent Fe II lines, described with Gaussian functions, with the same widths and shifts, since we assumed that all optical Fe II lines were originating from the same emission region. The number of free parameters was reduced by calculating the relative intensities for the Fe II lines with the same lower term of transition (see Kovačević et al., 2010). Finally, the Fe II template was described with five parameters of intensity, width, shift, and temperature, which was included in the calculation of the relative intensities. For more details about the optical Fe II template see Kovačević et al. (2010) and Shapovalova et al. (2012), and this Fe II template is also available on line (http://servo.aob.rs/FeII_AGN). The example of the spectral decomposition in 4,000–5,500Å range is shown in the optical part in **Figure 1**.

2.2. The Balmer Continuum Model

The UV pseudo-continuum consists of the power law, which represents the emission from the accretion disc and the bump at 3,000Å, which represents the sum of the blended, high-order broad Balmer lines, and the Balmer continuum ($\lambda < 3{,}646$Å). In order to measure the flux or luminosity of the power law at UV spectral range (e.g., 3,000Å), one needs to subtract the Balmer continuum emission first (see **Figure 1**). The model of the Balmer continuum first given in Kovačević et al. (2014), is based on the function for the Balmer continuum given in Grandi (1982) for the case of a partially optically thick cloud, with one degree of freedom decreased, as the intensity of the Balmer continuum was calculated, obtaining in that way lower uncertainty. The intensity of the Balmer continuum was estimated at the Balmer edge ($\lambda = 3{,}646$Å), as a sum of the intensities of all high-order Balmer lines at the same wavelength. All broad Balmer lines were represented with one Gaussian function only, with the same width and shift of a prominent Balmer line, and their relative intensities were taken from the literature or were calculated (see Kovačević et al., 2014). Therefore, if only one prominent Balmer line was fitted (e.g., Hβ), and the shift, width, and intensity were obtained from that fit, than the fluxes of all other Balmer lines would be known, and the Balmer continuum at the Balmer edge could be calculated. Finally, with this model, the UV pseudo-continuum was fitted with four free parameters: the width, shift, and intensity of the one prominent Balmer line, and the exponent of the power law. An example of the Balmer continuum fit is shown below in **Figure 1**.

2.3. Model of the UV Emission Lines in 2,650–3,050Å: Extracting the Pure Mg II Profile

We performed the spectral decomposition in 2,650–3,050Å range in order to estimate the pure Mg II profile, which overlaps with the UV Fe II lines (**Figure 1**). The Mg II line was fitted with two Gaussian functions, the one that represents the line core and the other that fits the line wings (see Kovačević-Dojčinović

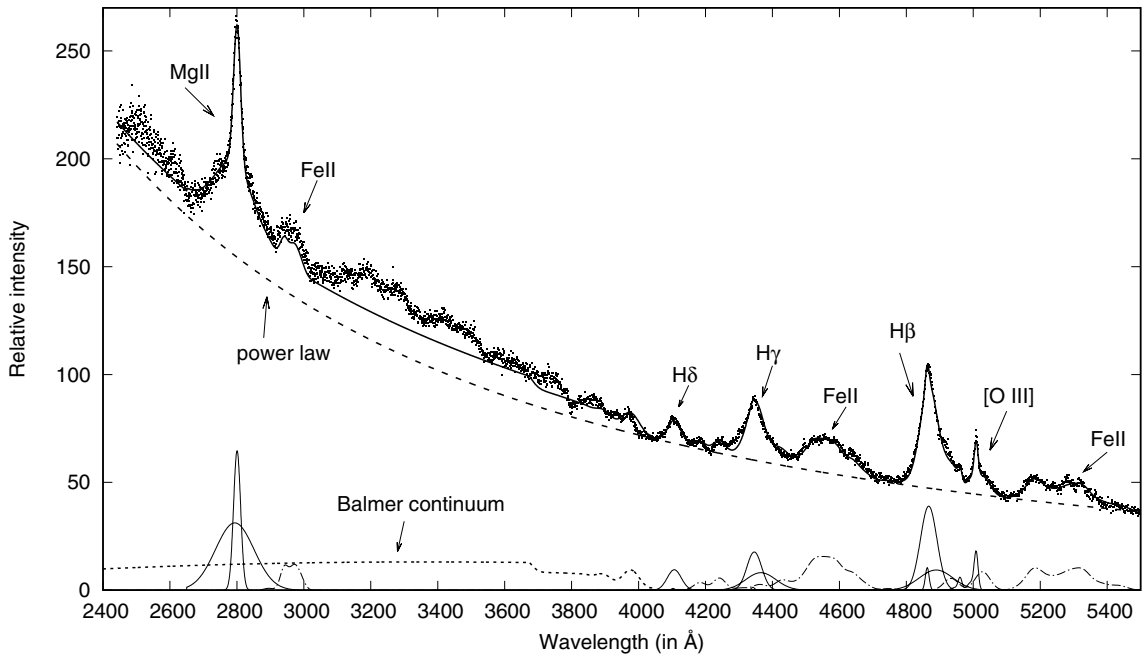

FIGURE 1 | The example of the decomposition of the UV-optical pseudo-continuum (power law + Balmer continuum) and emission lines in ranges 2,650–3,050Å and 4,000–5,500Å for object SDSS J014942.50+001501.7. The observations are denoted with dots, the sum of pseudo-continuum and emission line model with solid line, and the power law continuum with dashed line. Bellow, the Balmer continuum is given with dotted line, and UV/optical Fe II templates with dotted-dashed line and all emission lines with solid line.

and Popović, 2015), and a sum of those two components represents the broad Mg II line. The narrow Mg II line was not detected in analyzed spectra. The numerous Fe II lines in the range 2,650–3,050Å were all fitted with the Fe II template presented in Popović et al. (2003) and Kovačević-Dojčinović and Popović (2015). The Fe II lines in the 2,650–3,050Å range were divided into four multiplets, and relative intensities of the lines within each multiplet were taken from literature. Finally, the Fe II template was described with six parameters: four parameters for the intensity, line width, and shift. The example of the spectral decomposition in the 2,650–3,050Å range with UV pseudo-continuum fit is shown in the UV part in **Figure 1**.

2.4. Measuring the Spectral Parameters

From the pure broad profiles of the Hβ and Mg II lines, we measured the FWHM of these lines, as well as Full Width at 10% of the Maximum (FW10%M). The asymmetries of these lines (intrinsic shifts) were measured at different levels of the line maximal intensity (at 50%, z_{50} and at 10%, z_{10}), as the centroid shift with respect to the broad line peak (see Jonić et al., 2016, their Figure 2). The luminosity of the continuum was calculated using the formula given in Peebles (1993) with adopted cosmological parameters of $\Omega_M = 0.3$, $\Omega_\Lambda = 0.7$, $\Omega_k = 0$, and Hubble constant $H_o = 70$ km s^{-1} Mpc^{-1}. The virial M_{BH} for the UV parameters [FWHM Mg II, $L_\lambda(3,000\text{Å})$] was calculated using the formula given in Wang et al. (2009) [their Equation (9), for $\gamma = 2$].

3. RESULTS

3.1. Testing the Virialization of the Broad Hβ and Mg II Lines

If the emission gas in the BLR is virialized, one can expect to observe correlations between the widths and the gravitational redshifts of the BELs, which comes from the equations for the M_{BH} estimation by the virial method using the line width (see Zheng and Sulentic, 1990; Peterson et al., 2004). The expected relation is: $z_G \sim \text{FWHM}^2$, i.e., $\log(z_G) \sim \log(\text{FWHM})$ (see Jonić et al., 2016). This correlation is expected since at the same distance from a BH the line is broadened by the gravitational rotational effect which depends from the distance as $\sim \sqrt{\frac{M}{r}}$, and by the gravitational shift (red-shifting of photons) that also depends from the distance as $\sim \frac{M}{r}$ (see Popović et al., 1995).

We investigated correlation between the intrinsic shifts, as indicators of the gravitational redshifts, and the widths of the Hβ or the Mg II lines, at different levels (50 and 10%) of their maximal intensity, for the sample of 123 Type 1 AGNs with the red asymmetry in BELs. We have found that the width of the Hβ line is well correlated with the line's intrinsic shift measured at the 50% and at the 10% of the maximal intensity. However, in the case of the Mg II line, the correlation between the Mg II width and intrinsic shift is detected only at the 50% of the line maximal intensity, whereas at the 10% of the line maximal intensity an anti-correlation is seen (for more detail see Jonić et al., 2016).

Note here that the literature in the field presents comparisons on the use of the optical and the UV lines, like Hβ and Mg II, as virial estimators of the M_{BH} in AGN, pointing out that in some cases Mg II is more reliable as M_{BH} estimator then Hβ (e.g., Marziani et al., 2013, and references therein). However, it has been shown that the Mg II wings are emitted from the weakly gravitationally bounded gas (see Kovačević-Dojčinović and Popović, 2015; Jonić et al., 2016), i.e., the assumption of virialization may be problem in using Mg II line as the BH mass estimator.

3.2. Influence of the Blamer Continuum to the M_{BH} Estimation Using the UV Spectral Parameters

We calculated the luminosity at 3,000Å before [$L_\lambda(3{,}000\text{Å})_{tot}$] and after the Balmer continuum [$L_\lambda(3{,}000\text{Å})_{pow}$] contribution was subtracted. In the sample of 287 Type 1 AGN spectra, the Balmer continuum contributes to the continuum $L_\lambda(3{,}000\text{Å})$ on average for ∼10%, with the maximal value of 18%. The ratios of the $L_\lambda(3{,}000\text{Å})$, with and without the Balmer continuum contribution, are shown on the histogram (**Figure 2A**). The majority of the equations for the M_{BH} estimation using the UV parameters neglect the contribution of the Balmer continuum (see e.g., McLure and Jarvis, 2002; Vestergaard and Osmer, 2009). Wang et al. (2009) give the relation for the assessment of M_{BH} using the FWHM Mg II and $L_\lambda(3{,}000\text{Å})$, assuming that after subtraction of the Balmer continuum, the $L_\lambda(3{,}000\text{Å})$ is the pure power law continuum, therefore we then compared M_{BH} calculated with and without consideration of the Balmer continuum contribution. We got that the Balmer continuum increased M_{BH} on average for ∼5% (0.02 dex), with the maximal value of the M_{BH} overestimation up to 10% (0.04 dex). The ratio of the M_{BH} estimates before and after the Balmer continuum subtraction is shown in **Figure 2B**. The comparison of M_{BH} values before (index "tot") and after the Balmer continuum subtractions (index "pow") are also given in **Figure 3**, where the correlation coefficients ρ (ρ_{tot} = 0.783 and ρ_{pow} = 0.786), *P*-values (P_{tot} = 0 and P_{pow} = 0) and linear best-fit (y = a*x+b) coefficients are given: slope a, (a_{tot} = 0.85 and a_{pow} = 0.84) and y-intercept b, (b_{tot} = 1.36 and b_{pow} = 1.43). It can be seen that the influence of the Balmer continuum to the M_{BH} estimation is so small that it barely changes the correlation coefficient (ρ) or the coefficients of the linear best-fit (a, b) between the M_{BH} estimated with the optical and the one estimated with the UV parameters. Also, it seams that removing the Balmer continuum does not affect the outliers in this relationship.

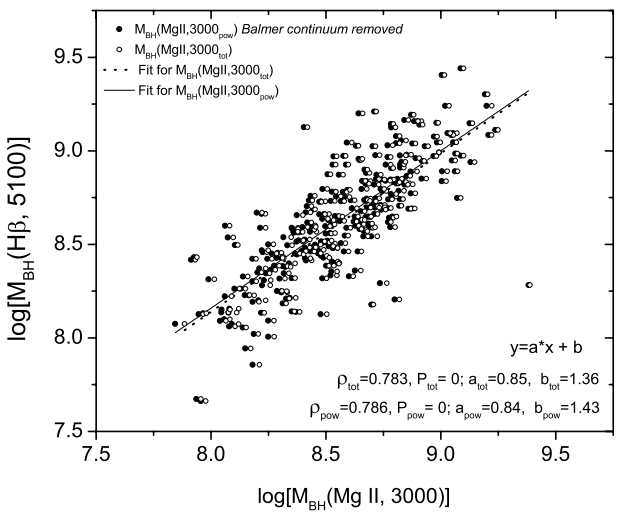

FIGURE 3 | The relation of the M_{BH}[Hβ, L_λ(5,100Å)] vs. M_{BH}[MgII, L_λ(3,000Å)] before (index "tot," open circles) and after the Balmer continuum subtraction (index "pow," full circles). The corresponding correlation coefficients, *P*-values, and coefficients of the liner best-fit are also given.

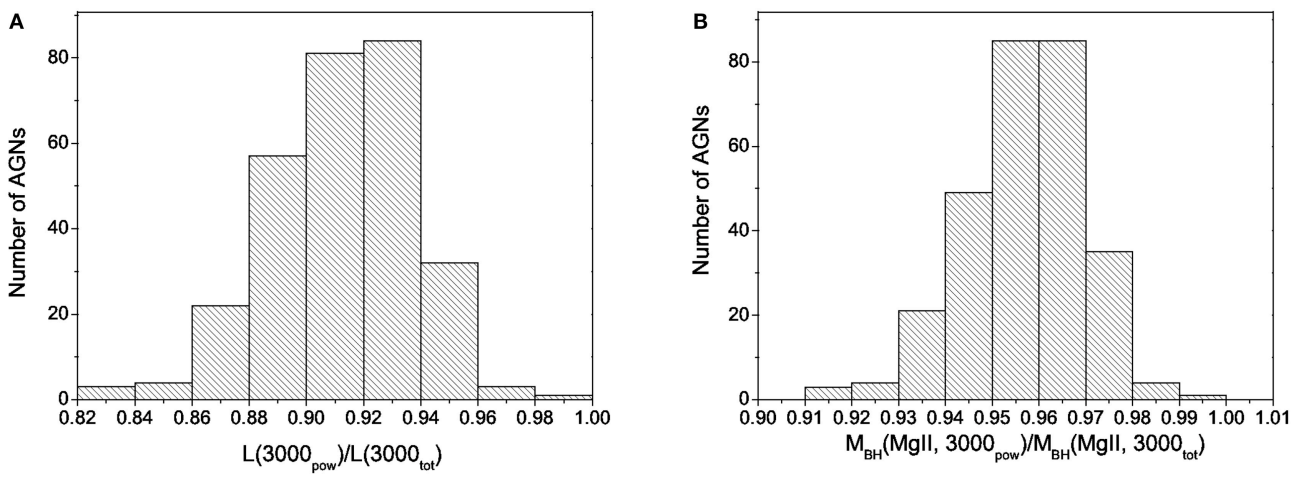

FIGURE 2 | (A) The ratio of the continuum L_λ(3,000Å) before [L(3,000$_{tot}$)] and after [L(3,000$_{pow}$)] the Balmer continuum subtraction. **(B)** The ratio of the M_{BH} estimate before [M_{BH} (L_{tot})] and after [M_{BH} (L_{pow})] the Balmer continuum subtraction.

4. CONCLUSIONS

Here we have used the sample of the SDSS Type 1 AGN spectra to compare the most frequently used emission lines for the M_{BH} estimation, Hβ (in the optical band) and Mg II (in the UV band), in order to assess which line is better virial estimator and thus more convenient for that purpose. We investigated how the Balmer continuum affect the BH mass estimation using the UV parameters.

From our investigation we can outline the following conclusions:

I) The Hβ line is a more reliable virial estimator than the Mg II line, since the expected linear relationship between logarithms of the widths (influenced by the Keplerian motion) and red asymmetries (caused by the gravitational redshift) was evidenced for both lines when measured at the 50% of the line maximal intensities, but when measured in the line wings (at the 10% of the line maximal intensities) the expected relationship was present only for Hβ (see Jonić et al., 2016).

II) The disregard of the Balmer continuum emission, in the case of the M_{BH} estimation using the UV parameters [Mg II, L_λ(3,000Å)], causes the overestimation of the M_{BH} on average for ∼5% (0.02 dex) and up to 10% (0.04 dex).

At the end, let us note that similar investigation should be performed on the sample where more reliable methods for mass measurements (as e.g., reverberation) should be applied to explore the influence of the Balmer continuum and this we postpone for our future work. Moreover, some additional effects (as e.g., relativistic jets) can significantly affect line profiles, i.e., the radio loudness which can indicate the presence of relativistic jets, therefore in the future work radio properties of the sample should also be explored.

AUTHOR CONTRIBUTIONS

JK, SM, and LP: Developing concept of the work; the acquisition, analysis and interpretation of data for the work; drafting the work and revising it critically for important intellectual content; final approval of the version to be published; being accountable for all aspects of the work in ensuring that questions related to the accuracy or integrity of any part of the work are appropriately investigated and resolved.

ACKNOWLEDGMENTS

The work is a part of the project 176001 financed by the Ministry of Education, Science, Technology and Development, Republic of Serbia.

REFERENCES

Bentz, M. C., Peterson, B. M., Pogge, R. W., Vestergaard, M., and Onken, C. A. (2006). The radius-luminosity relationship for active galactic nuclei: the effect of host-galaxy starlight on luminosity measurements.. *Astrophys. J.* 644, 133–142. doi: 10.1086/503537

Blandford, R. D., and McKee, C. F. (1982). Reverberation mapping of the emission line regions of seyfert galaxies and quasars.. *Astrophys. J.* 255, 419–439.

Bon, E., Popović, L. Č., Gavrilović, N., La Mura, G., and Mediavilla, E. (2009). Contribution of a disc component to single-peaked broad lines of active galactic nuclei. *Mon. Not. R. Astron. Soc.* 400, 924–936. doi: 10.1111/j.1365-2966.2009.15511.x

Bon, E., Popović, L. Č., Ilić, D., and Mediavilla, E. (2006). Stratification in the broad line region of AGN: the two-component model. *New Astron. Rev.* 50, 716–719. doi: 10.1016/j.newar.2006.06.015

Bon, N., Bon, E., Marziani, P., and Jovanović, P. (2015). Gravitational redshift of emission lines in the AGN spectra. *Astrophys. Space Sci.* 360:7. doi: 10.1007/s10509-015-2555-5

Collin, S., Kawaguchi, T., Peterson, B. M., and Vestergaard, M. (2006). Systematic effects in measurement of black hole masses by emission-line reverberation of active galactic nuclei: eddington ratio and inclination. *Astron. Astrophys.* 456, 75–90. doi: 10.1051/0004-6361:20064878

Gaskell, C. M. (2009). What broad emission lines tell us about how active galactic nuclei work. *New Astron. Rev.* 53, 140–148. doi: 10.1016/j.newar.2009.09.006

Grandi, S. A. (1982). The 3000 Å bump in quasars. *Astrophys. J.* 255, 25–38.

Hu, C., Wang, J. M., Ho, L. C., Chen, Y.-M., Bian, W.-H., and Xue, S.-J. (2008). Hβ profiles in quasars: evidence for an intermediate-line region. *Astrophys. J.* 683:L115. doi: 10.1086/591848

Ilić, D., and Popović, L. Č. (2014). Supermassive black holes and spectral emission lines. *J. Phys. Conf. Ser.* 548:012002. doi: 10.1088/1742-6596/548/1/012002

Jonić, S., Kovačević-Dojčinović, J., Ilić, D., and Popović, L. Č. (2016). irilization of the broad line region in active galactic nuclei: connection between sshifts and widths of broad emission lines. *Astrophys. Space Sci.* 361:101. doi: 10.1007/s10509-016-2680-9

Kovačević, J., Popović, L. Č., and Dimitrijević, M. S. (2010). Analysis of optical Fe II emission in a sample of active galactic nucleus spectra. *Astrophys. J. Suppl.* 189, 15–36. doi: 10.1088/0067-0049/189/1/15

Kovačević, J., Popović, L. Č., and Kollatschny, W. (2014). A model for the balmer pseudocontinuum in spectra of type 1 AGNs. *Adv. Space Res.* 54, 1347–1354. doi: 10.1016/j.asr.2013.11.035

Kovačević-Dojčinović, J., and Popović, L. Č. (2015). The connections between the UV and optical Fe ii emission lines in type 1 AGNs. *Astrophys. J. Suppl.* 221:35. doi: 10.1088/0067-0049/221/2/35

Liu, H. T., Feng, H. C., and Bai, J. M. (2017). A new method to measure the virial factors in the reverberation mapping of active galactic nuclei. *Mon. Not. R. Astron. Soc.* 466, 3323–3330. doi: 10.1093/mnras/stw3261

Marziani, P., Sulenti, J. W., Plauchu-Frayn, I., and del Olmo, A. (2013). Is MgIIλ2800 a reliable virial broadening estimator for quasars? *Astron. Astrophys.* 555:16. doi: 10.1051/0004-6361/201321374

Marziani, P., and Sulentic, J. W. (2012). Estimating black hole masses in quasars using broad optical and UV emission lines. *New Astron. Rev.* 56, 49–63. doi: 10.1016/j.newar.2011.09.001

McLure, R. J., and Jarvis, M. J. (2002). Measuring the black hole masses of high-redshift quasars. *Mon. Not. R. Astron. Soc.* 337, 109–116. doi: 10.1046/j.1365-8711.2002.05871.x

Peebles, P. J. E. (1993). *Principles of Physical Cosmology*. Princeton, NJ: Princeton University Press.

Peterson, B. M. (2014). Measuring the masses of supermassive black holes. *Space Sci. Rev.* 183, 253–275. doi: 10.1007/s11214-013-9987-4

Peterson, B. M., Ferrarese, L., Gilbert, K. M., Kaspi, S., Malkan, M. A., Maoz, D., et al. (2004). Central masses and broad-line region sizes of active galactic nuclei. II. A homogeneous analysis of a large reverberation-mapping database. *Astrophys. J.* 613, 682–699. doi: 10.1086/423269

Popović, L. Č., Mediavilla, E., Bon, E., and Ilić, D. (2004). Contribution of the disk emission to the broad emission lines in AGNs: two-component model. *Astron. Astrophys.* 423, 909–918. doi: 10.1051/0004-6361:20034431

Popović, L. Č., Mediavilla, E. G., Bon, E., Stanić, N., and Kubičela, A. (2003). The line emission region in III Zw 2: kinematics and variability. *Astrophys. J.* 599, 185–192. doi: 10.1086/379277

Popović, L. Č., Vince, I., Atanacković-Vukmanović, O., and Kubičela, A. (1995). Contribution of gravitational redshift to spectral line profiles of seyfert galaxies and quasars. *Astron. Astrophys.* 293, 309–314.

Shapovalova, A. I., Popović, L. Č., Burenkov, A. N., Chavushyan, V. H., Ilić, D., Kovačević, A., et al. (2012). Spectral optical monitoring of the narrow-line seyfert 1 Galaxy Ark 564. *Astrophys. J. Suppl.* 202:10. doi: 10.1088/0067-0049/202/1/10

Shen, Y. (2013). The mass of quasars. *Bull. Astron. Soc. India* 41, 61–115.

Sulentic, J. W., Marziani, P., and Dultzin-Hacyan, D. (2000). Phenomenology of broad emission lines in active galactic nuclei. *Annu. Rev. Astron. Astrophys.* 38, 521–571. doi: 10.1146/annurev.astro.38.1.521

Vestergaard, M., and Osmer, P. S. (2009). Mass functions of the active black holes in distant quasars from the large bright quasar survey, the bright quasar survey, and the color-selected Sample of the SDSS fall equatorial stripe. *Astrophys. J.* 699, 800–816. doi: 10.1088/0004-637X/699/1/800

Vestergaard, M., and Peterson, B. M. (2006). Determining central black hole masses in distant active galaxies and quasars. II. Improved optical and UV scaling relationships. *Astrophys. J.* 641, 689–709. doi: 10.1086/500572

Wang, J.-G., Dong, X.-B., Wang, T.-G., Ho, L. C., Yuan, W., Wang, H., et al. (2009). Estimating black hole masses in active galactic nuclei using the Mg II λ2800 emission line. *Astrophys. J.* 707, 1334–1346. doi: 10.1088/0004-637X/707/2/1334

Zheng, W., and Sulentic, J. W. (1990). Internal redshift difference and central mass in QSOs. *Astrophys. J.* 350, 512–517.

Conflict of Interest Statement: The authors declare that the research was conducted in the absence of any commercial or financial relationships that could be construed as a potential conflict of interest.

Copyright © 2017 Kovačević-Dojčinović, Marčeta-Mandić and Popović. This is an open-access article distributed under the terms of the Creative Commons Attribution License (CC BY). The use, distribution or reproduction in other forums is permitted, provided the original author(s) or licensor are credited and that the original publication in this journal is cited, in accordance with accepted academic practice. No use, distribution or reproduction is permitted which does not comply with these terms.

frontiers in Astronomy and Space Sciences

ORIGINAL RESEARCH
published: 02 November 2017
doi: 10.3389/fspas.2017.00032

Ultraviolet/Optical Emission of the Ionized Gas in AGN: Diagnostics of the Ionizing Source and Gas Properties

Anna Feltre[1,2], Stephane Charlot[2], Marco Mignoli[3], Angela Bongiorno[4], Francesco Calura[3], Jacopo Chevallard[5], Emma Curtis-Lake[2], Roberto Gilli[3] and Adele Plat[2]*

[1] Univ Lyon, Univ Lyon1, Ens de Lyon, Centre National de la Recherche Scientifique, Centre de Recherche Astrophysique de Lyon UMR5574, Saint-Genis-Laval, France, [2] Sorbonne Universités, UPMC-Centre National de la Recherche Scientifique, UMR7095, Institut d'Astrophysique de Paris, Paris, France, [3] INAF-Osservatorio Astronomico di Bologna, Bologna, Italy, [4] INAF-Osservatorio Astronomico di Roma, Monteporzio Catone, Italy, [5] Scientific Support Office, Directorate of Science and Robotic Exploration, European Space Research and Technology Centre (ESTEC), European Space Agency (ESA), Noordwijk, Netherlands

Spectroscopic studies of active galactic nuclei (AGN) are powerful means of probing the physical properties of the ionized gas within them. In particular, near future observational facilities, such as the *James Webb Space Telescope* (JWST), will allow detailed statistical studies of rest-frame ultraviolet and optical spectral features of the very distant AGN with unprecedented accuracy. In this proceedings, we discuss the various ways of exploiting new dedicated photoionization models of the narrow-line emitting regions (NLR) of AGN for the interpretation of forthcoming revolutionary datasets.

Keywords: active galaxies, emission lines, ultraviolet, spectral models, spectroscopy

OPEN ACCESS

Edited by:
Paola Marziani, Osservatorio Astronomico di Padova (INAF), Italy

Reviewed by:
José María Solanes, University of Barcelona, Spain
Milan S. Dimitrijevic, Astronomical Observatory, Serbia

***Correspondence:**
Anna Feltre
anna.feltre@univ-lyon1.fr

Specialty section:
This article was submitted to Milky Way and Galaxies, a section of the journal Frontiers in Astronomy and Space Sciences

Received: *30 August 2017*
Accepted: *19 October 2017*
Published: *02 November 2017*

Citation:
Feltre A, Charlot S, Mignoli M, Bongiorno A, Calura F, Chevallard J, Curtis-Lake E, Gilli R and Plat A (2017) Ultraviolet/Optical Emission of the Ionized Gas in AGN: Diagnostics of the Ionizing Source and Gas Properties. Front. Astron. Space Sci. 4:32. doi: 10.3389/fspas.2017.00032

1. INTRODUCTION

Nebular emission lines observed in galaxy spectra contain valuable information about the nature of the ionizing source and physical conditions of the ionized gas within these same galaxies. Current (e.g., VLT-KMOS/MUSE, Keck-MOSFIRE) and future (e.g., the Near Infrared Spectrograph, NIRSpec, on-board JWST) near infrared spectrographs will provide ultraviolet, in addition to optical, rest-frame spectra of galaxies out to the epoch of Reionization. In this context, it is extremely important to develop physically motivated spectral models, along with analysis tools based on advanced statistical techniques, for the interpretation of the rest-frame optical/ultraviolet spectra of both active and inactive galaxies at all cosmic epochs. In section 2 we describe photoionization models of the AGN NLR. In the following Sections we show how (i) new ultraviolet, in addition to standard optical, spectral diagnostic diagrams allow one to distinguish between nuclear activity and star formation, (ii) these new models can be best used to understand the physical properties of the gas in the AGN NLR and (iii) the implementation of these AGN photoionization calculations in an innovative bayesian fitting code can help us best interpret current, and future, spectro-photometric data on active galaxies.

2. SPECTRAL MODELS

The nebular emission of the AGN NLR is computed combining the AGN ionizing spectrum, described as a series of broken power laws (Equation 5 of Feltre et al., 2016), with the photoionization code CLOUDY (version c13.03, latest described in Ferland et al., 2013). The

gas in the NLR is modeled with clouds of single type using the approach described in Feltre et al. (2016)[1]. The models are parametrized in terms of (i) the ultraviolet spectral index, α, of the incident radiation field, (ii) the ionization parameter, (iii) the hydrogen gas density of the clouds, (iv) the gas metallicity, and (v) the dust-to-heavy element mass ratio. A more detailed explanation of the physical parameters is provided in Feltre et al. (2016). Note that we have improved the original model grid by adding two new adjustable parameters, namely the inner radius of the NLR and the internal microturbulence velocity of the gas cloud. The addition of these two parameters have been found to be critical for reproducing high ionization emission-lines, such as N V λ1240 and C IV λ1550 (Mignoli et al., in prep., Feltre et al., in prep.). We also consider new generation photoionization calculations of the nebular emission from stars (Gutkin et al., 2016), parametrized in analogous way to the AGN NLR models. We remind the reader to the papers of Charlot and Longhetti (2001), Gutkin et al. (2016) for a detailed description of these spectral models.

3. DIAGNOSTIC DIAGRAMS IN THE ULTRAVIOLET

Standard diagnostic diagrams, based on ratios of optical emission-lines (such as [O III]λ5007, [N II]λ6584, [S II]λ6724, Hα and Hβ) are commonly used to distinguish between stellar and nuclear activity (e.g., Baldwin et al., 1981; Veilleux and Osterbrock, 1987). In addition to optical, we explored new diagnostics at ultraviolet wavelengths for three reasons: (i) future facilities will provide high quality rest-ultraviolet spectra of the most distant sources, (ii) models are usually calibrated on optical observations of the local Universe and this might not always be appropriated to study the emission from star-formation and interstellar gas at high redshift, and (iii) standard optical diagnostic diagrams might fail to distinguish between stellar and AGN activity at higher redshift (e.g., in the case of low metallicity Groves et al., 2006; Coil et al., 2015; Feltre et al., 2016; Hirschmann et al., 2017). Diagrams involving combinations of a collisionally excited metal line or line multiplet, such as C IV λλ1548, 1551, O III]λλ1661, 1666, N III]λ1750, [Si III]λ1883+Si III]λ1892 and [C III]λ1907+C III]λ1909, with the He II λ1640 recombination line have been found to allow a good distinction of the nature of the ionizing source as well as valuable constraints on interstellar gas parameters and the shape of the ionizing radiation (Feltre et al., 2016). **Figure 1** shows the predictions from photoionization models of both AGN and star-forming galaxies, for different values of metallicity and ionization parameter in two diagnostic diagrams, namely C III]λ1909/He II λ1640 vs. C IV λ1550/He II λ1640 (left panel) and C IV λ1550/C III]λ1909 vs. C IV λ1550/He II λ1640 (right panel). Note that model predictions agree well with data measurements of AGN (Dors et al., 2014) and star-forming galaxies (Stark et al., 2014) currently available in the literature.

[1]Predictions of the intensities of the main optical and ultraviolet emission-lines are available through http://www.iap.fr/neogal/models.html

4. GAS METALLICITY IN THE NLR OF Z∼2 TYPE 2 AGN

As case study, to illustrate a potential application of photoionization models described above (section 2), we compare the model predictions with the emission line measurements of a sample of C IV λ1550-selected Type 2 AGN (see section 4.1). The ionized gas in the NLR of AGN surrounds the black hole at the galaxy centre and it is likely connected to the nuclear star formation. By measuring the metal abundance of the ionized gas in the AGN NLR, we can obtain indirect information about the star formation history of the host galaxy.

4.1. Sample Description

To pursue our goals we appeal to VIMOS observations from the z-COSMOS Deep Survey (Lilly et al., 2007). We limited our study to the redshift range $1.45 < z < 3.05$ to assure that the C IV λ1550 emission line is well covered by the observed spectral range. The presence of this feature in a galaxy spectrum is indicative of nuclear activity. We identified 192 C IV λ1550-selected objects, i.e., sources with a C IV λ1550 line intensity 5 times larger than the significance level. Out of these 192, we classified 90 sources as Type 2, i.e., narrow line, AGN (i.e., full width half maximum, FWHM, of the C IV λ1550 line lower than 2,000 km/s). From the rest-frame ultraviolet spectra of our sample of Type 2 AGN we measured fluxes, velocity dispersions and equivalent widths of the emission lines. Note that the AGN-selection effectiveness has been also confirmed by the ultraviolet diagnostic diagrams. The spectral observations, sample selection and data measurements will be presented in further details in Mignoli et al., in prep.

4.2. Gas Metallicity from Ultraviolet Emission-Lines

The C IV λ1550selected Type 2 AGN sample, described in section 4.1, is ideal to estimate the metal content of the ionized gas in the AGN NLR thanks to the simultaneous presence of two or more emission lines of Oxygen, Nitrogen and/or Carbon ions in the same spectra, along with the plethora of the other ultraviolet emission lines. In particular, we consider ratios of any possibile combination of the N V λ1240, N IV]λ1485, C IV λ1550, He II λ1640, C III]λ1909, C II]λ2326 and [Ne IV]λ2424 emission lines. We perform a spectral fitting by applying a simple least square minimization[2] to infer the total Oxygen (both gas and dust phase) abundance, expressed as $12 + \log(O/H)$[3]. Note that, further improvements will include the exploitation of a new generation fitting tool, BEAGLE (Chevallard and Charlot, 2016, Chevallard et al., in prep.), based on sophisticated bayesian statistic techniques (see section 5).

[2]Note that we consider a galactic attenuation curve (Cardelli et al., 1989), for consistency with the fitting procedure used to derive the host galaxy stellar masses.
[3]For a direct translation between metallicity, Z, and Oxygen abundance we remind to Table 2 of Gutkin et al. (2016), where solar metallicity $Z_{\odot} = 0.01524$ correspond to $12 + \log(O/H) = 8.83$

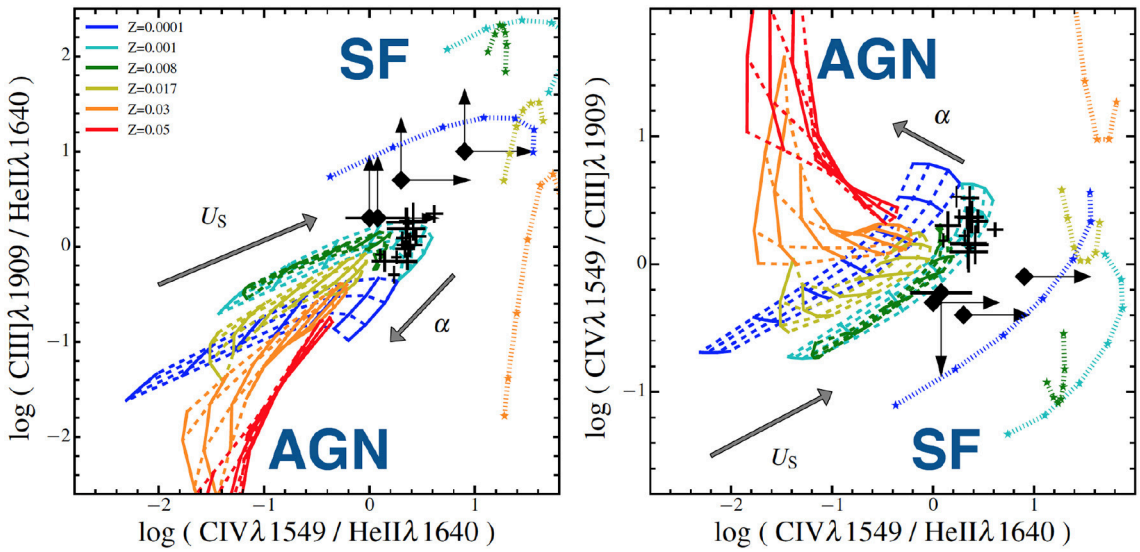

FIGURE 1 | Predictions of the AGN NLR and star-forming galaxy models described in section 2 in the diagnostic diagrams C IV λ1550/He II λ1640 vs. C III]λ1909/He II λ1640 and C IV λ1550/C III]λ1909 (**left** and **right**, respectively). Dashed and continuous lines are AGN models corresponding to wide ranges in power-law index, α, and ionization parameter, $-4.0 < \log(U) < -1.0$. Stars connected by dotted lines are star-forming galaxy models. All the models are shown for different metallicity Z (color coded as indicated on the left panel). Also shown in each panel are the observations of AGN (crosses with error bars) and star-forming galaxies (large diamonds with upper and lower limits) described in section 3.

We also compute the stellar masses of the host galaxy by appealing to a multi-band spectral energy distribution (SED) fitting technique (Bongiorno et al., 2012). A combination of AGN and host-galaxy templates is used to fit the large set of optical and near-infrared photometry from the Cosmic Evolution Survey (COSMOS; Scoville et al., 2007) available for our sources. The left panel of **Figure 2** shows the NLR gas metallicity, 12+log(O/H), vs. the stellar mass. The first thing to note is that the fit favors models with solar (black dashed lines) or slightly subsolar metal content. This is in contrast with previous findings, where the N V λ1240/He II λ1640 ratio has been often found to be stronger than model predictions. Among the solutions, proposed in the literature, to explain this high N V λ1240/He II λ1640 ratio, there are very high metallicities (up to 5–10 time solar metallicity) and "selectively" enhanced Nitrogen (e.g., Hamann and Ferland, 1992, 1993; Shemmer and Netzer, 2002; Nagao et al., 2006). Solving this problem was one of the main reason for the update of the AGN NRL models of Feltre et al. (2016) with additional physical parameters (i.e., NLR inner radius and internally microturbulent clouds). We also do not observed any correlation between the metallicity and the stellar mass of the host galaxy. One can interpret this as a missing link between the gas in the NLR and the interstellar gas in the galaxy. Nevertheless, our analysis is based on a restricted range of stellar masses and the stellar mass host estimates depends both on the templates and fitting technique used for the analysis. To have a more comprehensive analysis, we plan to derive both metallicity and stellar masses from the same fitting technique, based on advanced statistical methods (see section 5).

The right panel of **Figure 2** suggests a decrease of metallicity with increasing redshift. Despite previous findings in the literature, where no evidence for a redshift evolution of the metallicity in AGN was found (Nagao et al., 2006), a lower metal content moving in more distant sources is what one would expect from models of cosmic chemical evolution. Note also, that the observed trend in **Figure 2** is opposite to the trend, commonly observed in the literature, introduced by the presence of the N V λ1240 line which was favoring very high metallicities, as discussed above.

5. SED FITTING TOOL

Future plans include the implementation of the AGN NLR models in a fitting tool based on sophisticated fitting technique, i.e., BEAGLE (Chevallard and Charlot, 2016, Chevallard et al., in prep.). Briefly, BEAGLE combines in a coherent way emission from different components (stars, gas, dust, AGN), adopts Bayesian approach to obtain posterior probability distribution functions of every model parameter and includes predictions from galaxy formation models. BEAGLE allows to chose between different options based on the user's aims: (i) to fit spectro-photometric data at ultaviolet to infrared wavelengths, (ii) to create synthetic catalogs of galaxy SEDs and (iii) to the study retrievability of galaxy physical parameters for different type of observations. BEAGLE can handle data from broad-band photometry and/or spectroscopic information (e.g., full spectra, emission line intensities or equivalent widths). With the implementation of the AGN NRL photoionization models, BEAGLE will be an ideal tool to (i) fit ultraviolet/optical spectra of obscured AGN at any redshift, (ii) study the effects of the presence of AGN with

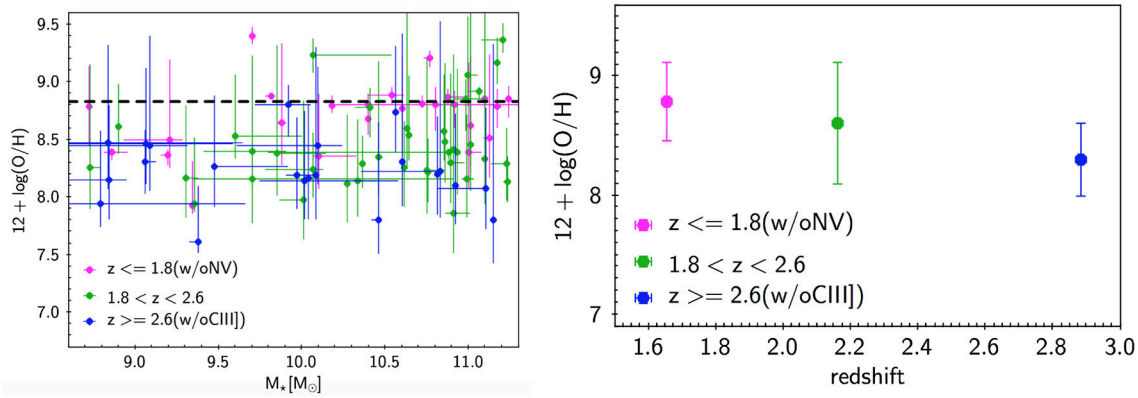

FIGURE 2 | Left: AGN NLR gas metallicity, in terms of Oxygen abundance 12 + log(O/H), for the C IV λ1550-selected Type 2 AGN described in section 4.1 vs. stellar masses of the host galaxies The measurements are color coded for different redshift bins as shown in the legend. The black dashed line indicates the value of the solar metallicity, $Z_{\odot} = 0.01524$, used in the models described in section 2. **Right:** Oxygen abundance, 12 + log(O/H), of the AGN NLR averaged for three redshift bins as labeled in the legend.

different accretion luminosities on the ultraviolet/optical spectral features of a galaxy spectrum and (iii) to produce mock catalogs of ultraviolet/optical spectra of Type 2 AGN.

6. CONCLUSIONS

In the previous Sections we have described new photoinization calculations for the NLR of AGN. We showed how ratios of emission-lines at ultraviolet wavelengths are good diagnostics of the ionizing source (nuclear vs. stellar activity). Moreover, photoionization models are useful tools for the study of the physical properties of the ionized gas (e.g., metallicity, density) of AGN and they can be easily implemented in fitting tools to interpret current spectroscopic observations of high redshift sources. The exploitation of these spectral models and analysis tools will be particularly useful to interpret observations of high-redshift galaxies with future facilities, such as the James Webb Space Telescope and extremely large ground-based telescopes, which will push previous studies up to the epoch of reionization (z>7).

AUTHOR CONTRIBUTIONS

AF and SC developed the spectral models and the diagnostic diagrams. MM assembled the sample, performed the spectral measurements and coordinated the analysis, in collaboration with AF, AB, FC, and RG. AF, AP, EC, JC, and SC all contributed at the implementation of the AGN module within the fitting code BEAGLE.

ACKNOWLEDGMENTS

AF, AP, EC, and SC acknowledge support from the ERC via an Advanced Grant under grant agreement no. 321323-NEOGAL. AF acknowledges support from the ERC via an Advanced Grant under grant agreement no. 339659-MUSICOS. Part of this study is based on observations made with ESO Telescopes at the La Silla or Paranal Observatories under programme ID 175.A-0839 (zCOSMOS redshits survey). Part of the analysis presented in this work was done with TOPCAT (http://www.star.bris.ac.uk/~mbt/topcat/), developed by M. Taylor.

REFERENCES

Baldwin, J. A., Phillips, M. M., and Terlevich, R. (1981). Classification parameters for the emission-line spectra of extragalactic objects. *Publ. Astron. Soc. Pac.* 93, 5–19. doi: 10.1086/130766

Bongiorno, A., Merloni, A., Brusa, M., Magnelli, B., Salvato, M., Mignoli, M., et al. (2012). Accreting supermassive black holes in the COSMOS field and the connection to their host galaxies. *Mon. Not. R. Astron. Soc.* 427, 3103–3133. doi: 10.1111/j.1365-2966.2012.22089.x

Cardelli, J. A., Clayton, G. C., and Mathis, J. S. (1989). The relationship between infrared, optical, and ultraviolet extinction. *Astrophys. J.* 345, 245–256. doi: 10.1086/167900

Charlot, S., and Longhetti, M. (2001). Nebular emission from star-forming galaxies. *Mon. Not. R. Astron. Soc.*, 323, 887–903. doi: 10.1046/j.1365-8711.2001.04260.x

Chevallard, J., and Charlot, S. (2016). Modelling and interpreting spectral energy distributions of galaxies with BEAGLE. *Mon. Not. R. Astron. Soc.* 462, 1415–1443. doi: 10.1093/mnras/stw1756

Coil, A. L., Aird, J., Reddy, N., Shapley, A. E., Kriek, M., Siana, B., et al. (2015). The MOSDEF Survey: optical Active Galactic Nucleus Diagnostics at z∼2.3. *Astrophys. J.* 801:35. doi: 10.1088/0004-637X/801/1/35

Dors, O. L., Cardaci, M. V., Hägele, G. F., and Krabbe, Â. C. (2014). Metallicity evolution of AGNs from UV emission lines based on a new index. *Mon. Not. R. Astron. Soc.* 443, 1291–1300. doi: 10.1093/mnras/stu1218

Feltre, A., Charlot, S., and Gutkin, J. (2016). Nuclear activity versus star formation: emission-line diagnostics at ultraviolet and optical wavelengths. *Mon. Not. R. Astron. Soc.* 456, 3354–3374. doi: 10.1093/mnras/stv2794

Ferland, G. J., Porter, R. L., van Hoof, P. A. M., Williams, R. J. R., Abel, N. P., Lykins, M. L., et al. (2013). The 2013 release of cloudy. *Rev. Mex. Astron. Astrofis* 49, 137–163.

Groves, B. A., Heckman, T. M., and Kauffmann, G. (2006). Emission-line diagnostics of low-metallicity active galactic nuclei. *Mon. Not. R. Astron. Soc.* 371, 1559–1569. doi: 10.1111/j.1365-2966.2006.10812.x.

Gutkin, J., Charlot, S., and Bruzual, G. (2016). Modelling the nebular emission from primeval to present-day star-forming galaxies. *Mon. Not. R. Astron. Soc.* 462, 1757–1774. doi: 10.1093/mnras/stw1716

Hamann, F. and Ferland, G. (1992). The age and chemical evolution of high-redshift QSOs. *Astrophys. J.* 391, L53–L57.

Hamann, F., and Ferland, G. (1993). The chemical evolution of QSOs and the implications for cosmology and galaxy formation. *Astrophys. J.* 418:11.

Hirschmann, M., Charlot, S., Feltre, A., Naab, T., Choi, E., Ostriker, J. P., et al. (2017). Synthetic nebular emission from massive galaxies I: origin of the cosmic evolution of optical emission-line ratios. *ArXiv e-prints*. doi: 10.1093/mnras/stx2180

Lilly, S. J., Le Fèvre, O., Renzini, A., Zamorani, G., Scodeggio, M., Contini, T., et al. (2007). zCOSMOS: a large VLT/VIMOS redshift survey covering $0 < z < 3$ in the COSMOS field. *Astrophys. J.* 172, 70–85. doi: 10.1086/516589

Nagao, T., Maiolino, R., and Marconi, A. (2006). Gas metallicity diagnostics in star-forming galaxies. *Astron. Astrophys.* 459, 85–101. doi: 10.1051/0004-6361:20065216

Scoville, N., Aussel, H., Brusa, M., Capak, P., Carollo, C. M., Elvis, M., et al. (2007). The cosmic evolution survey (COSMOS): overview. *Astrophys. J. Suppl. Ser.* 172, 1–8. doi: 10.1086/516585

Shemmer, O., and Netzer, H. (2002). Is there a metallicity-luminosity relationship in active galactic nuclei? The case of narrow-line seyfert 1 galaxies. *Astrophys. J.* 567, L19–L22. doi: 10.1086/339797

Stark, D. P., Richard, J., Siana, B., Charlot, S., Freeman, W. R., Gutkin, J., et al. (2014). Ultraviolet emission lines in young low-mass galaxies at $z \simeq 2$: physical properties and implications for studies at $z > 7$. *Mon. Not. R. Astron. Soc.* 445, 3200–3220. doi: 10.1093/mnras/stu1618

Veilleux, S., and Osterbrock, D. E. (1987). Spectral classification of emission-line galaxies. *Astrophys. J. Suppl. Ser.* 63, 295–310. doi: 10.1086/191166

Conflict of Interest Statement: The handling Editor declared a shared affiliation, though no other collaboration, with one of the authors, AB.

The authors declare that the research was conducted in the absence of any commercial or financial relationships that could be construed as a potential conflict of interest.

Copyright © 2017 Feltre, Charlot, Mignoli, Bongiorno, Calura, Chevallard, Curtis-Lake, Gilli and Plat. This is an open-access article distributed under the terms of the Creative Commons Attribution License (CC BY). The use, distribution or reproduction in other forums is permitted, provided the original author(s) or licensor are credited and that the original publication in this journal is cited, in accordance with accepted academic practice. No use, distribution or reproduction is permitted which does not comply with these terms.

frontiers in Astronomy and Space Sciences

ORIGINAL RESEARCH
published: 14 November 2017
doi: 10.3389/fspas.2017.00043

The Relationship between Mg II Broad Emission and Quasar Inclination Angle

Conor Wildy and Bozena Czerny*

Center for Theoretical Physics, Polish Academy of Sciences, Warsaw, Poland

Several observed spectral properties of quasars are believed to be influenced by quasar orientation. In this investigation we examine the effect of orientation on the Mg II line located at 2,798 Å in a sample of 36 radio-loud quasars, with orientation angles having been obtained in a previous study using radio observations. We find no significant relationship between orientation angle and either Mg II line full-width at half-maximum or equivalent width. The lack of correlation with inclination angle contradicts previous studies which also use radio data as a proxy for inclination angle and suggests the Mg II emission region does not occupy a disk-like geometry. The lack of correlation with Mg II equivalent width, however, is reported in at least one previous study. Although the significance is not very strong (86%), there is a possible negative relationship between inclination angle and Fe II strength which, if true, could explain the Fe II anti-correlation with [O III] strength associated with Eigenvector 1. Interestingly, there are objects having almost edge-on inclinations while still exhibiting broad lines. This could be explained by a torus which is either clumpy (allowing sight lines to the central engine) or mis-aligned with the accretion disk.

Keywords: active galaxies, accretion, broad line region, Mg II, spectroscopy

OPEN ACCESS

Edited by:
Mauro D'Onofrio,
Universita degli Studi di Padova, Italy

Reviewed by:
Giovanna Maria Stirpe,
Osservatorio astronomico di Bologna (INAF), Italy
Milan S. Dimitrijevic,
Belgrade Astronomical Observatory, Serbia

****Correspondence:***
Conor Wildy
wildy@cft.edu.pl

Specialty section:
This article was submitted to Milky Way and Galaxies, a section of the journal Frontiers in Astronomy and Space Sciences

Received: *31 August 2017*
Accepted: *30 October 2017*
Published: *14 November 2017*

Citation:
Wildy C and Czerny B (2017) The Relationship between Mg II Broad Emission and Quasar Inclination Angle Front. Astron. Space Sci. 4:43. doi: 10.3389/fspas.2017.00043

1. INTRODUCTION

Active Galactic Nuclei (AGN) are luminous sources powered by accretion onto supermassive black holes at the centres of galaxies. Orientation angles are known to affect the observed properties of AGN. For example it is thought that Type 1 objects, which show broad lines in their unpolarized spectra, have a low inclination angle with respect to the accretion disk axis and therefore enable an unobscured view of the central engine, while Type 2 objects, which only exhibit narrow lines, are thought to be viewed at high inclination and therefore obscured by a dusty torus oriented such that it is co-planar with the accretion disk (Urry and Padovani, 1995). This is supported by the detection of broad lines in polarized light from Type 2 objects (Miller and Goodrich, 1990) and higher column density x-ray absorbers in Type 2 objects compared with Type 1 (Turner and Pounds, 1989). It is plausible that the inclination angle can influence the broad line morphology within the group of Type 1 objects. Studies have already indicated this for Hβ in multi-quasar samples, where the width of the broad emission line is dependent on the inclination angle such that at higher inclinations the line tends to be broader (Wills and Browne, 1986; Runnoe et al., 2013). Such a phenomenon is easily explained by assuming that the bulk of the broad line region (BLR) is located in a flattened disk-like structure, with the observed velocity of an individual BLR cloud (v_{obs}) being related to its intrinsic velocity (v_{int}) by $\mathrm{v_{obs}} = \mathrm{v_{int}}\sin\theta_\mathrm{i}$, where θ_i is the inclination angle.

Quasars are a luminous sub-category of AGN mostly exhibiting Type 1 features. Many thousands have their observed optical spectra catalogued within the Sloan Digital Sky Survey (SDSS) (Adelman-McCarthy et al., 2008), enabling statistical analysis of large samples of these objects. One such example relevant to quasar inclination angles was that of Shen and Ho (2014) which examined the so-called Eigenvector 1 correlations originally described by Boroson and Green (1992). This correlation is mainly due to the inverse relationship between the strengths of Fe II and the optical narrow lines of [O III], and also shows an inverse relationship between the width of Hβ and its strength. The paper of Shen and Ho (2014) showed that, in a sample of approximately 20,000 objects, [O III] strength is roughly constant at a given Fe II strength, while the full-width at half-maximum (FWHM) of Hβ varies significantly between objects. That paper concluded that this variation in FWHM was due to orientation, while the strength anti-correlation of Fe II with [O III] was not. It was described in Risaliti et al. (2011) that, since the emission of [O III] is probably isotropic and scales with the quasar bolometric luminosity, then it is plausible that [O III] EW tracks the quasar inclination angle, with higher EW indicating higher inclination angle. This was further supported in that paper by examination of the shape of the distribution of EW values. A recent study by Bisogni et al. (2017), revealed that the Mg II equivalent width (EW) was not dependent on [O III] EW, suggesting that the emission of Mg II, unlike the case of [O III],

TABLE 1 | List of quasars used for Mg II analysis.

SDSS name	Redshift	Inclination angle (°)	Mg II EW (Å)	Mg II FWHM (km s^{-1})	Fe II EW (Å)
SDSS J005115.11−090208.5	1.259	55	53.0 ± 6.6	8,920 ± 463	175 ± 8
SDSS J021008.48+011839.6	0.870	63	41.1 ± 4.7	4,840 ± 265	120 ± 8
SDSS J075448.86+303355.1	0.796	87	54.1 ± 5.4	5,340 ± 391	131 ± 8
SDSS J080906.22+291235.4	1.481	28	33.5 ± 3.5	5,240 ± 465	77.5 ± 3.6
SDSS J081240.08+303109.4	1.313	71	43.8 ± 19.2	2,790 ± 220	192 ± 59
SDSS J081409.22+323731.9	0.843	72	87.8 ± 5.3	3,390 ± 234	196 ± 13
SDSS J090207.20+570737.8	1.592	79	32.2 ± 4.2	5,610 ± 1,130	117 ± 8
SDSS J090429.62+281932.7	1.122	45	23.8 ± 4.0	3,420 ± 244	77.4 ± 3.6
SDSS J090649.98+083255.8	1.616	86	36.4 ± 11.4	5,300 ± 757	115 ± 10
SDSS J091858.15+232555.4	0.690	81	65.4 ± 6.2	6,670 ± 688	81.7 ± 5.9
SDSS J092425.02+354712.6	1.344	84	48.1 ± 8.7	4,980 ± 1,340	127 ± 7
SDSS J094418.85+233119.9	0.989	83	63.2 ± 7.4	5,600 ± 381	107 ± 6
SDSS J095206.38+235245.2	0.971	89	34.1 ± 9.9	3,900 ± 203	62.2 ± 4.0
SDSS J095934.49+121631.5	1.091	73	40.1 ± 5.5	5,550 ± 389	186 ± 13
SDSS J100507.07+501929.8	2.016	76	26.3 ± 21.6	4,390 ± 201	159 ± 37
SDSS J100607.70+323626.1	1.026	80	85.2 ± 7.5	3,340 ± 259	142 ± 13
SDSS J102026.87+044752.0	1.134	61	48.3 ± 10.9	6,560 ± 314	153 ± 19
SDSS J102041.14+395811.2	0.830	58	77.3 ± 29.5	9,440 ± 1,390	247 ± 16
SDSS J105636.25+410041.2	1.781	87	42.0 ± 12.5	5,510 ± 534	189 ± 29
SDSS J111023.84+032136.1	0.966	85	46.6 ± 11.2	3,090 ± 329	90.8 ± 14.6
SDSS J111858.62+382852.2	0.747	55	36.4 ± 2.9	4,920 ± 467	53.3 ± 8.4
SDSS J111903.28+385852.5	0.735	64	42.4 ± 28.5	8,790 ± 191	49.7 ± 8.3
SDSS J115139.68+335541.4	0.851	32	43.6 ± 5.7	7,200 ± 612	79.9 ± 5.1
SDSS J121701.37+101952.9	1.884	87	47.2 ± 2.4	4,110 ± 330	103 ± 7
SDSS J122925.53+355532.1	0.828	57	33.3 ± 6.7	4,080 ± 191	149 ± 14
SDSS J123604.51+103449.2	0.667	63	34.7 ± 6.0	4,890 ± 791	39.2 ± 8.0
SDSS J125607.67+100853.6	0.824	69	89.2 ± 25.6	3,030 ± 151	140 ± 20
SDSS J132106.65+374153.4	1.135	79	28.1 ± 19.9	11,600 ± 837	85.4 ± 9.4
SDSS J133411.70+550124.9	1.247	89	49.7 ± 15.7	13,100 ± 292	54.7 ± 7.0
SDSS J134034.70+423232.1	1.345	89	87.0 ± 16.5	6,630 ± 687	243 ± 20
SDSS J135817.60+575204.5	1.372	85	27.2 ± 1.9	4,760 ± 276	109 ± 4
SDSS J155002.00+365216.7	2.071	64	47.3 ± 34.8	5,920 ± 346	192 ± 18
SDSS J155729.93+330446.9	0.944	89	49.3 ± 6.2	5,640 ± 204	147 ± 9
SDSS J162229.93+353125.3	1.471	82	43.3 ± 11.4	4,550 ± 621	133 ± 10
SDSS J162336.45+341946.3	1.994	13	43.8 ± 7.7	7,360 ± 485	0.103 ± 11.548
SDSS J223458.73−022419.0	0.550	83	41.0 ± 7.6	5,300 ± 629	41.0 ± 4.7

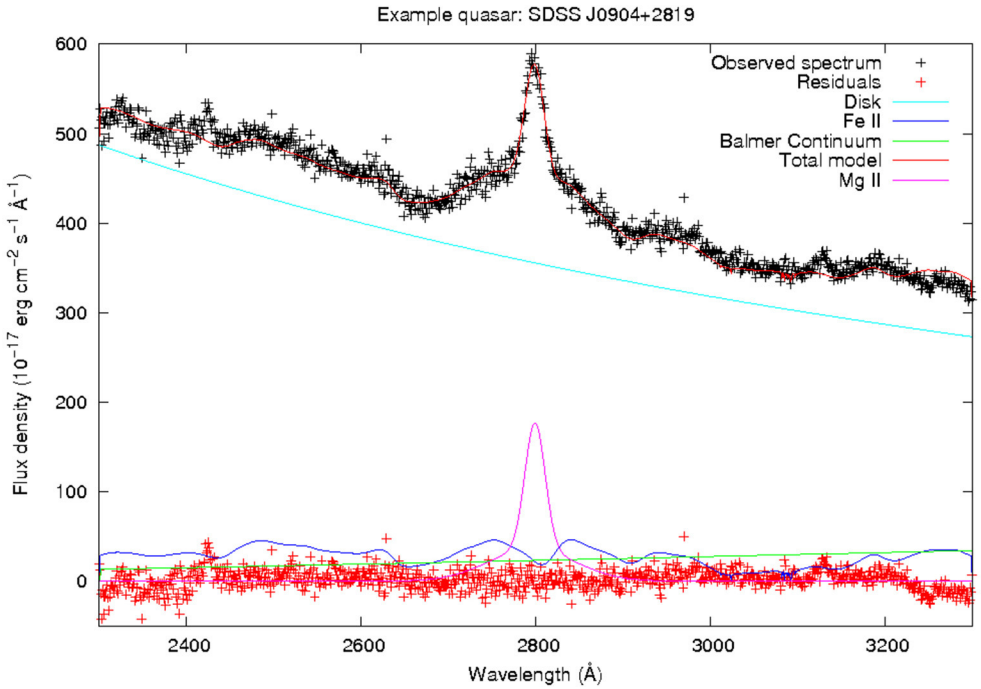

FIGURE 1 | Final fit to the spectrum of quasar SDSS J090429.62+281932.7 (black crosses) showing all four spectral components and the total model. Residuals are the difference between the total model and the observed datapoints.

was anisotropic. This is consistent with the postulate that BLR emission is located in a disk-like structure.

In this investigation we test the dependence of Mg II width and strength on inclination angle. To do so we selected objects from those listed in Kuźmicz and Jamrozy (2012), which have direct measurements of quasar orientation obtained from radio data and whose spectra are archived in the SDSS. We improve on the multi-component fit of the underlying continuum in that paper by including the Balmer continuum emission as well as the power-law continuum and broadened Fe II templates, allowing us to obtain more accurate Mg II EW measurements and profile shapes.

2. OBJECTS USED IN THE QUASAR SAMPLE

There are 91 quasars in the Kuźmicz and Jamrozy (2012) paper with optical and radio observations obtained from previous catalogs (see references therein), for which inclination angle measurements were obtainable. Inclination angles were calculated in that study using the follow equation:

$$\theta_i = \mathrm{acos}\left(\frac{1}{\beta_\mathrm{j}}\frac{(\mathrm{s}-1)}{(\mathrm{s}+1)}\right), \quad (1)$$

where $s = (S_j/S_{cj})^{\frac{1}{(2-\alpha)}}$, S_j and S_{cj} are the peak flux density of the lobes appearing closer to and further from the core respectively and α is the spectral index which is assumed to be $\alpha = -0.6$ from Wardle and Aaron (1997). The constant β_j is the jet velocity which, in agreement with Wardle and Aaron (1997) and Arshakian and Longair (2004), was fixed at 0.6c.

Of the 91 quasars are included 43 objects which are categorized as *Giant Radio Quasars* (GRQs), defined as objects having a radio structure >0.72 Mpc after applying the cosmological parameters of Spergel et al. (2003). As that study was designed to reveal any differences between GRQs and the rest of the radio-loud quasar population, they also selected a comparison sample made up of 48 objects having a smaller radio structure. As their study found on average no statistically significant differences in quasar optical spectra between the two populations, we made no distinction between the two categories and treated all objects as one sample. Only objects having SDSS spectral coverage spanning the entire range 2,300–3,300 Å in the quasar rest frame were subject to analysis, as this allows an adequate span to fit the underlying emission made up of the power-law continuum from the accretion disk, broadened Fe II emission and Balmer continuum emission from the BLR. Finally, only 36 objects from the sample underwent scientific analysis due to: (i) five objects having no SDSS spectra; (ii) 30 objects not meeting the 2,300–3,300 Å criterion; (iii) one object having heavily absorbed Mg II emission; and (iv) 19 objects being unable to be fitted satisfactorily. These 36 objects and their spectral parameters measured in this study are listed in **Table 1**. All EW values are calculated with respect to the disk power-law continuum.

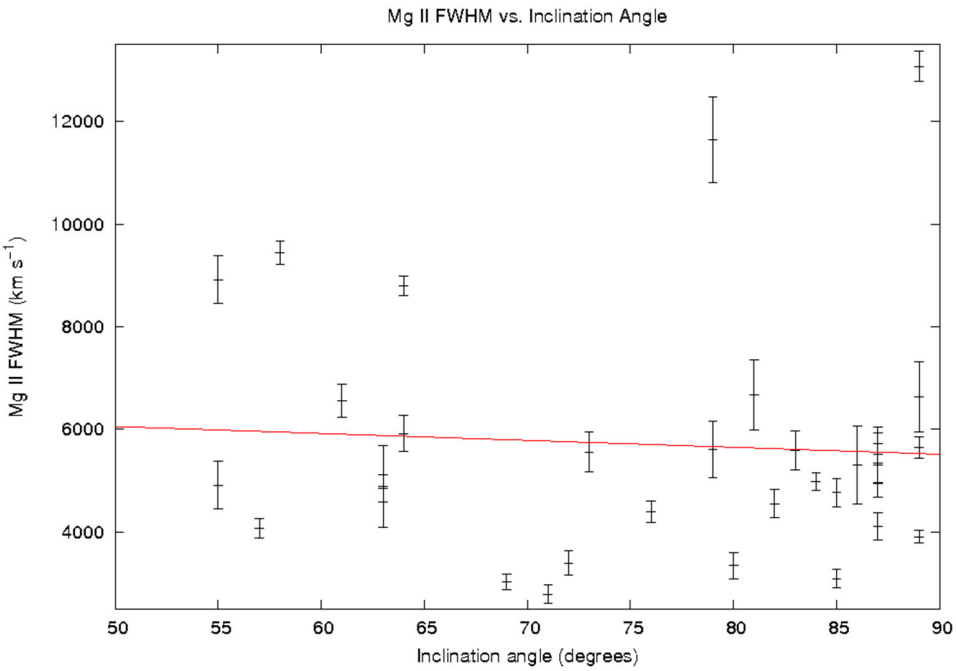

FIGURE 2 | Quasar Mg II FWHM plotted against inclination angle, with vertical bars at each point indicating FWHM 1σ error range for each object. A best-fitting trend line (red) shows a small negative gradient, however a Pearson test indicates no correlation.

3. EMISSION COMPONENTS IN THE SPECTRAL REGION OF MG II

The Mg II line exists in a complex spectral region of the UV known as the "small blue bump" (SBB), whose underlying emission must be accurately reconstructed in order to correctly measure the Mg II strength and width. The SBB consists of a BLR Balmer continuum and Fe II emission made up of many overlapping broadened lines which, as they are blended, give the appearance of continuous emission. The SBB adds to the underlying power-law continuum to give the total continuous emission spanning the wavelengths occupied by the Mg II line. This line itself is modelled using 1 or 2 Gaussian profiles, in the two profile case no significance is assigned to the properties of the individual components, they are used simply to generate the total profile from their sum. The modelled Fe II emission is based on the template of Tsuzuki et al. (2006). The calculation of the Balmer continuum was not performed in the fitting procedure of Kuźmicz and Jamrozy (2012), hence our fitting method represents an important improvement over their technique. The Balmer continuum was calculated using the following equation obtained from Grandi (1982):

$$F_\nu^{\mathrm{BC}} = F_\nu^{\mathrm{BE}} e^{(-h-\nu_{\mathrm{BE}})/(kT_e)}, \tag{2}$$

where F_ν^{BC} is the BC flux at frequency ν, F_ν^{BE} is the flux of the BC at the Balmer edge (3,646 Å), T_e is the electron temperature, k is the Boltzmann constant and h is the Planck constant. The fitting of all three SBB components was performed in a four-step manner for each quasar. First, the power-law continuum was fitted to relatively line-free regions outside the approximate extent of the SBB (less than 2,300 Å and greater than 3,700 Å) using the *specfit* software within the Image Reduction and Analysis Facility (IRAF). Second, the Fe II template and Balmer continuum were fitted to spectral regions spanning 2,300–2,600 Å and 3,000–3,300 Å using chi-square minimization, after subtraction of the power-law continuum. These wavelength ranges were used as they are neighbouring bands on either side of the Mg II line. The electron temperature of the plasma generating the Balmer continuum was treated as a free parameter and allowed to vary between 4,000 and 20,000 K in steps of 1,000 K, as was the Balmer edge flux which varied in steps of 0.01% of the continuum subtracted quasar flux. For the Fe II template, the free parameters were Gaussian broadening of between 0 and 3,000 km s^{-1} in steps of 1,000 km s^{-1} and the normalization, which varied in steps of 0.01% of the continuum subtracted quasar flux. Third, the Mg II model was fitted to each quasar spectrum with the power-law and SBB continuum subtracted, using *specfit*. Fourth, all four components were simultaneously re-fitted to the region 2,300–3,300 Å using *specfit*, with only normalizations allowed to vary. An image of an example resultant fit is shown in **Figure 1**.

4. ANALYSIS

4.1. Relationship between Mg II Width and Quasar Inclination Angle

A Pearson test for correlation between the Mg II FWHM and the quasar inclination angle for the 36 objects was

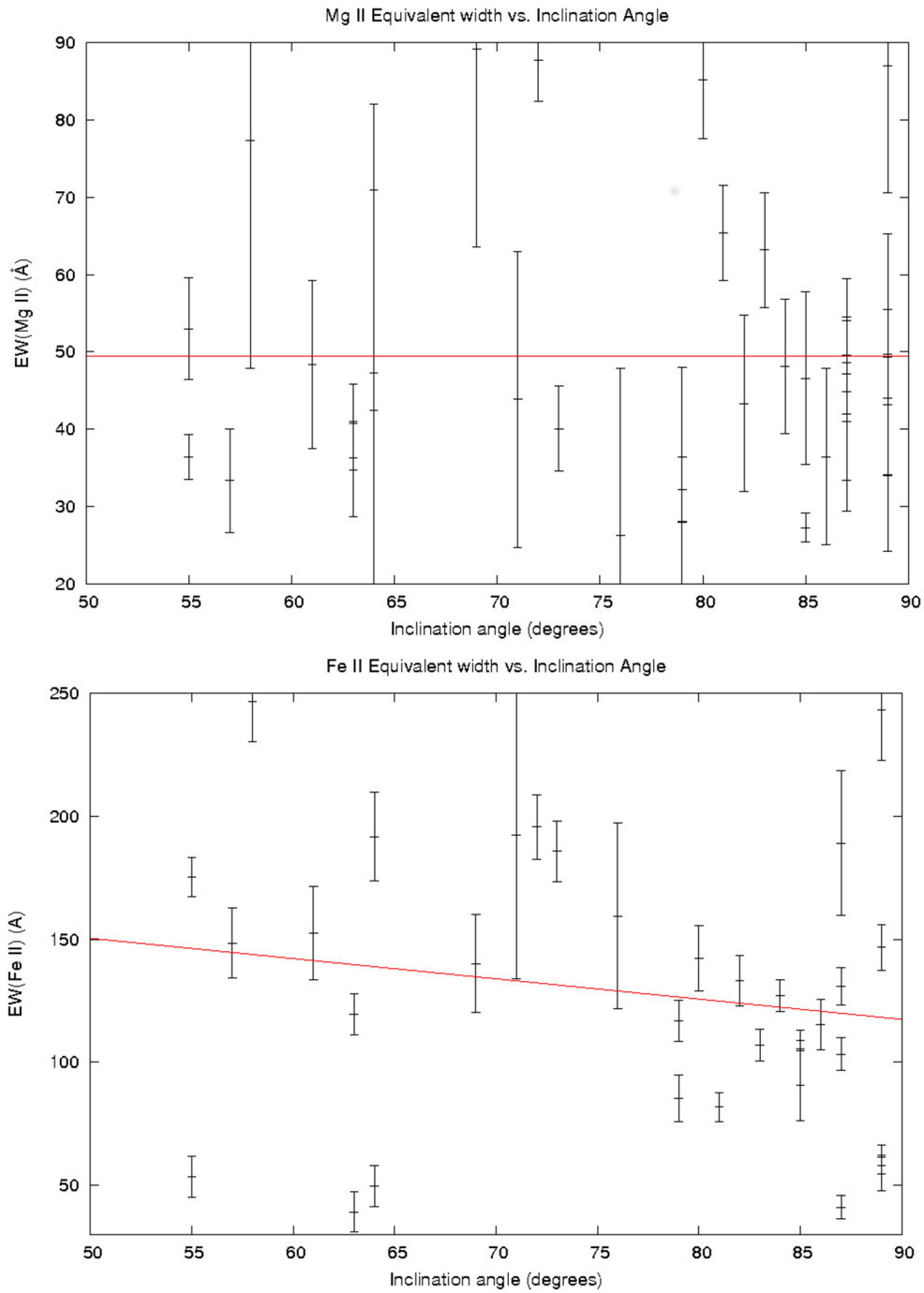

FIGURE 3 | Quasar Mg II EW (top panel) and Fe II EW (bottom panel) plotted against inclination angle along with the respective best-fitting trend lines (red). Vertical bars at each point indicate EW 1σ error range for each object. For Fe II the correlation likelihood is higher (86%) when compared to that of Mg II (38%).

performed. This found a probability of 38% that there is an actual correlation between the two variables, indicating that the data is consistent with the null hypothesis (no correlation). Each quasar's FWHM and inclination angle, along with the best-fitting linear trend-line, is illustrated in **Figure 2**.

4.2. Relationship between Equivalent Width and Inclination Angle

Similar to the procedure for Mg II FWHM, the EW of the line was tested across all 36 quasars using a Pearson test for correlation. This provided a value of 38% likelihood of correlation. Again, this is consistent with the null hypothesis of no correlation. The

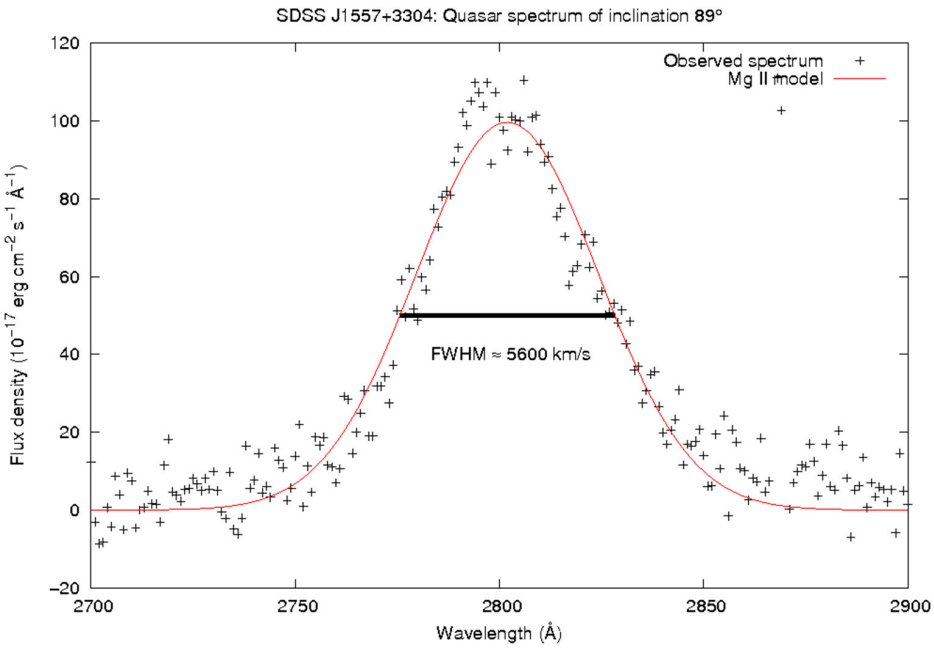

FIGURE 4 | Mg II broad line emission as it appears in the quasar SDSS J155729.93+330446.9. The black crosses indicate the quasar flux after the disk power-law and the SBB emission were subtracted. The red line indicates the model Mg II emission which, at 5,600 km s^{-1}, easily meets the definition of a broad line.

Fe II EW was also measured over the same wavelength span as the Mg II line, revealing that there may be a hint of a correlation between the Fe II EW and inclination angle since the Pearson test indicates an 86% likelihood of correlation, much higher than for the other cases mentioned so far. If such a correlation does in fact exist, it is likely to be a negative relationship given that the correlation coefficient is negative. The relationship of both Mg II and Fe II EW as a function of inclination angle is illustrated in **Figure 3**.

4.3. Broad Line Detection at Large Inclination Angles

One of the most interesting findings from the sample is the detection of broad emission lines at almost edge-on inclinations. This is somewhat surprising as it could be expected that at high inclinations the dusty torus obscures the view to the central source of the quasar. There are several examples of such objects in our sample, one of which is shown in **Figure 4**.

5. DISCUSSION

The fact that we do not detect a correlation between the Mg II broad line width in our sample and the inclination angle is a somewhat surprising result which contradicts reports in other studies. For example, Aars et al. (2005) found a correlation between the radio-derived inclination angle and the Mg II FWHM, which is in accordance with what would be expected if the broad line region, including the Mg II emitting gas, were located in a flattened-disk geometry. A flattened BLR is further supported by the study of Kimball et al. (2011) which found no correlation between the Mg II EW and the ratio of radio core flux to lobe flux, the latter being an inclination indicator. If instead a dependence between these two values was to have been found, this would imply that the broad line emission is substantially more isotropic than that of the accretion disk and therefore that the BLR cannot have a disk geometry. In the case of [O III] the line emission is isotropic and therefore its EW could potentially track the inclination angle (Risaliti et al., 2011).

Like Kimball et al. (2011) our findings also indicate a lack of correlation between Mg II EW and inclination angle. Considering the lack of correlation of either line width or EW with inclination in our study, it is possible that the BLR exists in an intermediate geometry between an isotropically emitting sphere and an anisotropically emitting thin-disk. Possibilities for such geometries include a thick disk, a distorted disk, or some combination of both. This could result in only a weak relationship between inclination and line width, rendering it undetectable in our sample size, while still presenting no strong evidence of isotropic emission from the relationship between inclination angle and line EW. This could explain the correlation between [O III] EW and broad line width seen in Risaliti et al. (2011), as their sample size is much larger than ours, consisting of approximately 6,000 SDSS quasars.

There is no strong indication of a correlation between Fe II EW and inclination (such a conclusion would require a confidence >95%), however it is stronger than the others, at 86%. This correlation, if it exists, is negative. If the [O III] emission is an accurate indicator of inclination, then this would support the findings of Bisogni et al. (2017) and may be a contributor to the anti-correlation between [O III] and Fe II strength found from the Eigenvector 1 relationship (Boroson and Green, 1992). A possible physical explanation for this, if the anti-correlation is

true, is the Fe II emission being located in a disk which is even thinner than the accretion disk (Bisogni et al., 2017), however this is speculative. It is not possible to accurately measure the Fe II line widths using our method as there are only three values of broadening used and in many cases more than one value gives an acceptable fit to the spectrum.

The fact that broad lines are visible at high inclinations requires an explanation, since, in the common unification explanation for different AGN types, Type 1 Seyferts/quasars should have an inclination angle lower than approximately 45°. Broad lines are only visible in Type 2 objects in polarized light (Antonucci and Miller, 1985). In fact, most of the objects studied here have inclination angles greater than 45°. If the torus is not smooth but is instead a clumpy structure, then this may allow a line-of-sight toward the central engine in the objects observed. In such a case the probability of detecting a broad line doesn't reach zero even if the inclination angle tends toward 90°. Gas inflow models have given support to a clumpy nature of the dusty torus (Netzer, 2015), providing evidence that this structure is possible. A further possibility is that of the torus being misaligned with the accretion disk in these cases. It should be noted in any case that the Kuźmicz and Jamrozy (2012) selection process necessarily found quasars at high inclination angle, since the selection criteria required objects to have both a large angular size and to be lobe-dominated. Quasars of this kind are very rare in the general quasar population (de Vries et al., 2006) and so our sample objects may have unusual properties compared to those in previous quasar samples compiled to determine the effects of inclination angle on spectral morphology.

AUTHOR CONTRIBUTIONS

CW was responsible for obtaining and analyzing the data from the SDSS, as well as interpreting the results. BC devised and supervised the project.

FUNDING

This project was supported by the Polish Funding Agency National Science Centre, project 2015/17/B/ST9/03436/ (OPUS 9).

ACKNOWLEDGMENTS

This work is based on spectroscopic observations made by the Sloan Digital Sky Survey. Funding for the Sloan Digital Sky Survey IV has been provided by the Alfred P. Sloan Foundation, the U.S. Department of Energy Office of Science, and the Participating Institutions.

REFERENCES

Aars, C. E., Hough, D. H., Vermeulen, R. C., Readhead, A. C. S., Yu, L. H., Linick, J.P., et al. (2005). Optical spectrophotometry of a complete sample of 3CR lobe-dominated quasars. *Astron. J.* 130, 23–46. doi: 10.1086/430530

Adelman-McCarthy, J. K., Agüeros, M. A., Allam, S. S., Prieto, C. A., Anderson, K. S. J., Anderson, S. F., et al. (2008). The sixth data release of the sloan digital sky survey. *Astrophys. J. Suppl.* 175, 297–313. doi: 10.1086/524984

Antonucci, R. R. J., and Miller, J. S. (1985). Spectropolarimetry and the nature of NGC 1068. *Astrophys. J.* 297, 621–632. doi: 10.1086/163559

Arshakian, T. G., and Longair, M. S. (2004). On the jet speeds of classical double radio sources. *Month. Notices R. Astron. Soc.* 351, 727–732. doi: 10.1111/j.1365-2966.2004.07823.x

Bisogni, S., Marconi, A., and Risaliti, G. (2017). Orientation effects on spectral emission features of quasars. *Month. Notices R. Astron. Soc.* 464, 385–397. doi: 10.1093/mnras/stw2324

Boroson, T. A., and Green, R. F. (1992). The emission-line properties of low-redshift quasi-stellar objects. *Astrophys. J. Suppl.* 80, 109–135. doi: 10.1086/191661

de Vries, W. H., Becker, R. H., and White, R. L. (2006). Double-lobed radio quasars from the sloan digital sky survey. *Astron. J.* 131, 666–679. doi: 10.1086/499303

Grandi, S. A. (1982). The 3000 A bump in quasars. *Astrophys. J.* 255, 25–38. doi: 10.1086/159799

Kimball, A. E., Ivezić, Ž., Wiita, P. J., and Schneider, D. P. (2011). Correlations of quasar optical spectra with radio morphology. *Astron. J.* 141, 182. doi: 10.1088/0004-6256/141/6/182

Kuźmicz, A., and Jamrozy, M. (2012). Optical and radio properties of giant radio quasars: central black hole characteristics. *Month. Notices R. Astron. Soc.* 426, 851–867. doi: 10.1111/j.1365-2966.2012.21576.x

Miller, J. S., and Goodrich, R. W. (1990). Spectropolarimetry of high-polarization Seyfert 2 galaxies and unified Seyfert theories. *Astrophys. J.* 355, 456–467. doi: 10.1086/168780

Netzer, H. (2015). Revisiting the unified model of active galactic nuclei. *Annu. Rev. Astron. Astrophys.* 53, 365–408. doi: 10.1146/annurev-astro-082214-122302

Risaliti, G., Salvati, M., and Marconi, A. (2011). [O III] equivalent width and orientation effects in quasars. *Month. Notices R. Astron. Soc.* 411, 2223–2229. doi: 10.1111/j.1365-2966.2010.17843.x

Runnoe, J. C., Brotherton, M. S., Shang, Z., Wills, B. J., and DiPompeo, M. A. (2013). The orientation dependence of quasar single-epoch black hole mass scaling relationships. *Month. Notices R. Astron. Soc.* 429, 135–149. doi: 10.1093/mnras/sts322

Shen, Y., and Ho, L. C. (2014). The diversity of quasars unified by accretion and orientation. *Nature* 513, 210–213. doi: 10.1038/nature13712

Spergel, D. N., Verde, L., Peiris, H. V., Komatsu, E., Nolta, M. R., Bennett, C. l., et al. (2003). First-Year Wilkinson Microwave Anisotropy Probe (WMAP) Observations: Determination of Cosmological Parameters. *Astrophys. J. Suppl.* 148, 175–194. doi: 10.1086/377226

Tsuzuki, Y., Kawara, K., Yoshii, Y., Oyabu, S., Tanabe, T., and Matsuoka, Y. (2006). Fe II Emission in 14 Low-Redshift Quasars. I. Observations. *Astrophys. J.* 650, 57–79. doi: 10.1086/506376

Turner, T. J., and Pounds, K. A. (1989). The EXOSAT spectral survey of AGN. *Month. Notices R. Astron. Soc.* 240, 833–880. doi: 10.1093/mnras/240.4.833

Urry, C. M., and Padovani, P. (1995). Unified schemes for radio-loud active galactic nuclei. *PASP* 107, 803. doi: 10.1086/133630

Wardle, J. F. C., and Aaron, S. E. (1997). How fast are the large-scale jets in quasars? Constraints on both Doppler beaming and intrinsic asymmetries. *Month. Notices R. Astron. Soc.* 286, 425–435. doi: 10.1093/mnras/286.2.425

Wills, B. J., and Browne, I. W. A. (1986). Relativistic beaming and quasar emission lines. *Astrophys. J.* 302, 56–63. doi: 10.1086/163973

Conflict of Interest Statement: The authors declare that the research was conducted in the absence of any commercial or financial relationships that could be construed as a potential conflict of interest.

Copyright © 2017 Wildy and Czerny. This is an open-access article distributed under the terms of the Creative Commons Attribution License (CC BY). The use, distribution or reproduction in other forums is permitted, provided the original author(s) or licensor are credited and that the original publication in this journal is cited, in accordance with accepted academic practice. No use, distribution or reproduction is permitted which does not comply with these terms.

frontiers in Astronomy and Space Sciences

ORIGINAL RESEARCH
published: 29 September 2017
doi: 10.3389/fspas.2017.00019

On the Intermediate Line Region in AGNs

Tek P. Adhikari[1], Agata Różańska[1], Krzysztof Hryniewicz[1], Bozena Czerny[1,2] and Gary J. Ferland[3]*

[1] Nicolaus Copernicus Astronomical Center, Polish Academy of Sciences, Warsaw, Poland, [2] Center for Theoretical Physics, Polish Academy of Sciences, Warsaw, Poland, [3] Department of Physics and Astronomy, The University of Kentucky, Lexington, KY, United States

In this paper we explore the intermediate line region (ILR) by using the photoionisation simulations of the gas clouds present at different radial distances from the center, corresponding to the locations from BLR out to NLR in four types of AGNs. We let for the presence of dust whenever conditions allow for dust existence. All spectral shapes are taken from the recent multi-wavelength campaigns. The cloud density decreases with distance as a power law. We found that the slope of the power law density profile does not affect the line emissivity radial profiles of major emission lines: Hβ, He II, Mg II, C III, and O III. When the density of the cloud at the sublimation radius is as high as $10^{11.5}$ cm^{-3}, the ILR should clearly be seen in the observations independently of the shape of the illuminating radiation. Moreover, our result is valid for low ionization nuclear emission regions of active galaxies.

Keywords: active galaxies, emission lines, photoionisation, radiative transfer, accrection disk

OPEN ACCESS

Edited by:
Paola Marziani, Osservatorio Astronomico di Padova (INAF), Italy

Reviewed by:
Marco Berton, Università degli Studi di Padova, Italy
Milan S. Dimitrijevic, Astronomical Observatory, Serbia

****Correspondence:***
Tek P. Adhikari
tek@camk.edu.pl

Specialty section:
This article was submitted to Milky Way and Galaxies, a section of the journal Frontiers in Astronomy and Space Sciences

Received: *25 August 2017*
Accepted: *21 September 2017*
Published: *29 September 2017*

Citation:
Adhikari TP, Różańska A, Hryniewicz K, Czerny B and Ferland GJ (2017) On the Intermediate Line Region in AGNs. Front. Astron. Space Sci. 4:19. doi: 10.3389/fspas.2017.00019

1. INTRODUCTION

The emission lines in active galactic nuclei (AGNs) provide a unique opportunity to study the properties of the materials located in the environment of the supermassive black hole (SMBH). From the measurement of full width at half maxima (FWHM) of lines in the observed AGN spectra, it is well understood that there exist two separate regions of the line emission. Lines with FWHM $\geq$ 3,000 km s^{-1} are emitted by materials with densities $\sim 10^{10}$ cm^{-3} in the broad line region (BLR) located closer to the AGN central engine. Whereas, the narrow line region (NLR) with gas densities $\sim 10^{5}$ cm^{-3}, located much farther from the AGN center, emits the narrow lines with FWHM $\sim$500 km s^{-1}. A clear spatial separation in between BLR and NLR is present where the emission of lines with intermediate FWHM is not seen in the observations.

Theoretically, the lack of emission from the intermediate line region (ILR) was explained by Netzer and Laor (1993, hereafter NL93) as an effect of dust extinction, both in absorption and scattering of line photons and continuum. The authors considered radially distributed clouds of different density and ionization level. Broad and narrow line regions were separated due to the dust content which cannot be present in BLR since the gas temperatures are so high that the dust grains cannot survive there. Nevertheless, further out from the nucleus there is a boundary radius named sublimation radius, $R_{\rm d}$, where temperature drops substantially, and dust can sustain up to the distances where NLR is located. NL93 presented that, for assumed gas parameters, the strong drop of line emission appears at distances where potential ILR is expected. Therefore natural separation between BLR and NLR occurs when the dust is taken into account in photoionisation calculations of cloud's emission. This natural separation disclaims the existence of the ILR. In

the ILR, the ionization parameter is higher than in further located NLR clouds and hence the relative effect of the dust absorption is stronger. The dust suppressed emission in ILR reappears on transition to the NLR when dust absorption becomes negligible due to the low gas temperature. However, in the recent observations of some AGNs, additional intermediate line component of FWHM ∼700–1,200 km s^{-1} is clearly required to fit the lines in their emission spectra (Brotherton et al., 1994; Mason et al., 1996; Crenshaw and Kraemer, 2007; Hu et al., 2008a,b; Zhu et al., 2009; Li et al., 2015). The open questions are: does the ILR exist physically separated from BLR and NLR? What are the mechanisms that give rise to ILR in some sources but not in others?

Recently, Adhikari et al., (2016 hereafter AD16) have shown, using the framework put forward by NL93, that when the density of illuminated clouds is high enough, the dust does not suppress the gap between BLR and NLR and intermediate line emission is clearly visible. The authors performed photoionisation simulations of radially distributed clouds subject to the radiation of four different spectral energy distributions (SEDs), most common types of AGN. The dust content was introduced at the sublimation radius of assumed value: $R_d = 0.1$ pc. In NL93, the authors assumed a power law with slope −1.5 and normalization $10^{9.4}$ cm^{-3} at R_d to describe the variation of the density of gas clouds with distance from the nucleus. These clouds were then illuminated by the mean AGN spectrum. Resulting emissivity profiles contained the suppression of line emission between BLR and NLR as it is commonly observed. AD16 made one step forward, showing that if the density at the sublimation radius is high, of the order of $10^{11.5}$ cm^{-3}, the ILR is clearly visible. Such result appeared to be independent on SED of illuminated radiation taken into account. Additionally, the authors argued that the low ionization nuclear emission regions (LINERs) should also exhibit the ILR.

In this paper, we expand the work of AD16 and investigate the variation of density profile of radially distributed clouds. All photoionisation simulations are done with the most recent version of the CLOUDY code (Ferland et al., 2017). To accommodate broad types of ionizing SEDs in our calculations, we considered four distinct AGN types: Sy1.5 galaxy Mrk 509 (Kaastra et al., 2011), Sy1 galaxy NGC 5548 (Mehdipour et al., 2015), NLSy1 galaxy PMN J0948+0022 (D'Ammando et al., 2015), and LINER NGC 1097 (Nemmen et al., 2014), each of them obtained from currently available simultaneous multi-wavelength observations. As a result of our simulations, we derived the line emissivity radial profiles for major emission lines:[Hβ λ4861.36 Å, He II λ1640.00 Å, Mg II λ2798.0 Å, C III] λ1909.00 Å and [O III] λ5006.84 Å.

Adopting the density normalization to be $10^{11.5}$ cm^{-3} at $R_d = 0.1$ pc, all the power law density distribution yield continuous line emissivity profiles with prominent intermediate line emission component in permitted lines Hβ, He II, and Mg II, independent of the density slopes and the spectral radiation shapes adopted. Below we briefly outline the photoionisation model itself, and discuss the resulting line emissivity profiles focusing mainly on the visibility of ILR in different AGN.

2. PHOTOIONISATION MODEL

The simulation of the photoionisation process is done with the publicly available numerical code CLOUDY version c17 (Ferland et al., 2017), which takes into account all the relevant radiative processes when a gas cloud is subjected to an incident radiation field. A simplistic geometrical set up of gas distributed from BLR further out to NLR is arranged by assuming spherical clouds with varying gas density, n_H ,and the total column density N_H, at each radial distances, r, from the SMBH:

$$n_H(r) = 10^{11.5}\,(r/R_d)^{-\beta}, \qquad N_H(r) = 10^{23.4}\,(r/R_d)^{-1} \quad (1)$$

where β is the power law density slope, and R_d is arbitrarily chosen to be equal 0.1 pc (following NL93 and AD16). The total column density of a cloud located at the sublimation radius is assumed after NL93: N_H (at R_d) $= 10^{23.4}$ cm^{-2}, and the gas hydrogen density after AD16 : n_H (at R_d) $= 10^{11.5}$ cm^{-3}. Here, we stress that the density normalizations lower than the value adopted in this paper, do not reproduce the intermediate line emission as shown by AD16.

Besides three previously considered types of AGN incident radiation shapes: Sy1.5 galaxy Mrk 509 (Kaastra et al., 2011), Sy1 galaxy NGC 5548 (Mehdipour et al., 2015), NLSy1 PMN J0948+0022 (D'Ammando et al., 2015), in this paper we also used the shape appropriate for LINER NGC 1097 (Nemmen et al., 2014). This choice of SED covers the general shapes of the radiation emanating from the AGN central engine. Adopted SEDs are the incident spectra used in the photoionisation simulation, where clouds distributed along the range of radii are exposed to the same type of radiation. All the SEDs are normalized to the bolometric luminosity 10^{45} erg s^{-1} which is an input to the CLOUDY code. This allows to compute the ionizing flux i.e., ionization parameter at each cloud radius.

We adopted the CLOUDY default chemical abundances, which are mostly the Solar values derived by Grevesse and Sauval (1998) for the gas clouds at $r \leq R_d$, whereas the interstellar medium (ISM) composition[1] with dust grains is used for the clouds at $r > R_d$. This assumption is consistent with the observational suggestions that the BLR is devoid of dust whereas the lower temperature in NLR allows its existence. On moving further out from BLR to NLR, the increase in radial distance is accompanied by the decrease in ionization degree and a cloud thickness.

The aim of this paper is to search how the appearance of intermediate line emission is sensitive on the value of density power law slope. Below we present line luminosity radial profiles for six values of β = 0.5, 1.0, 1.5, 2.0, 2.5, 3.0. We are aware that the power law density distribution of clouds does not reflect realistic situation in AGN, but it is sufficient for the purpose of this paper. In the forthcoming paper (Adhikari et al., in preparation), we plan to use realistic density profile, which is expected where clouds form from outflowing gas above the accretion disk atmosphere. Furthermore, we plan to consider measured values of bolometric luminosities, which give the realistic position of sublimation radius for each type of AGN due to the formula by Nenkova et al. (2008).

[1] for details see the Hazy1 CLOUDY documentation.

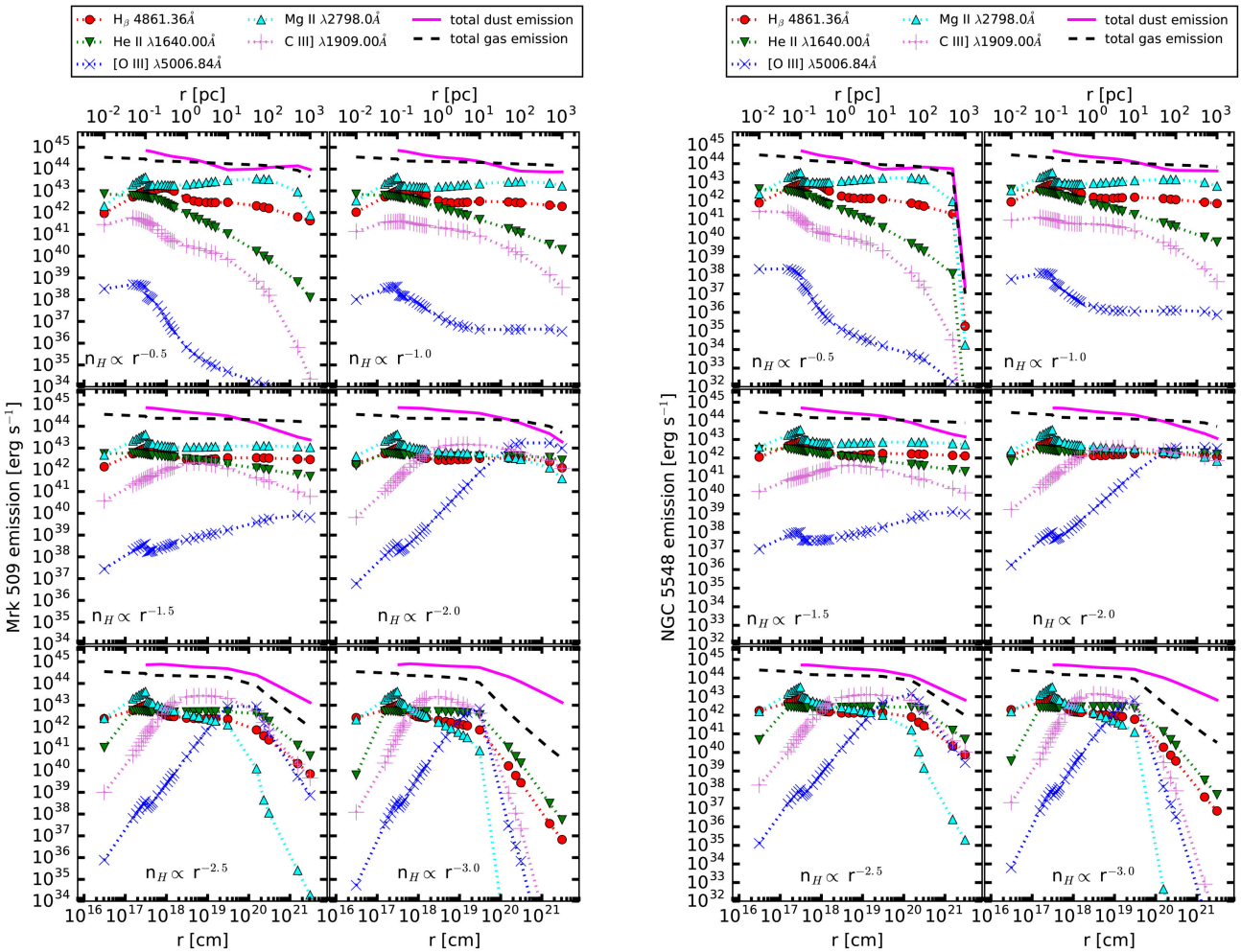

FIGURE 1 | Left: Line emission vs. radius for Mrk 509 SED. Different subplots are for various density slopes given in the left corners. Major emission lines: Hβ (red circles), He II (green triangles down), [O III] (blue crosses), Mg II (cyan triangles up) and [C III] (magenta pluses) are shown for each density profile cases. For clarity total dust emission (magenta continuous line) and total gas emission (black dashed line) are also shown. **Right**: The same as in **left** but with the spectral radiation shape of NGC 5548.

3. LINE EMISSIVITIES

As the results of photoionisation simulations, we compute line luminosities emitted from clouds located at the each radii. Therefore, by presenting line luminosity dependence on the distance from SMBH, i.e., line luminosity radial profile, we can check if the emission from ILR is comparable to the BLR and NLR or substantially lower. This is our basic test for the existence of ILR in all considered types of AGN.

We derived the line luminosity radial profiles for the major emission lines : [Hβ λ4861.36 Å, He II λ1640.00 Å, Mg II λ2798.0 Å, C III] λ1909.00 Å, and [O III] λ5006.84 Å. The resulting line emissivity profiles for the four cases of SED are presented in the **Figures 1**, **2**. In all cases of density power law slopes, we recovered a continuous line emission, with a small enhancement of the permitted lines Hβ and He II at the radial distance around 0.1 pc corresponding to the intermediate region, independent of the shape of the SEDs in consideration. There is a small reduction of Mg II line at 0.1 pc though not very significant as compared to the suppression presented by NL93. The semi forbidden line C III contribution to the intermediate emission component becomes the most prominent for the density profile with $\beta = 1.5$. These results corroborate with the conclusion of AD16 that when the density of the emitting gas is high enough, the extinction effect of dust grains on line production is negligible.

The most noticeable effects of different density profiles on line emissivities occur in the NLR range, i.e., for $r > 50$ pc. This behavior is quite obvious since for those radii, differences in densities between profiles are the biggest. For $\beta = 0.5$ and 1.0, density falls slowly and remains moderately high across the radii causing the strong suppression of forbidden line [O III]. [O III] is effectively produced in low density environment and becomes prominent when the density around the radius 10 pc becomes low enough, the cases for the profiles with $\beta \geq 2.0$. Narrow

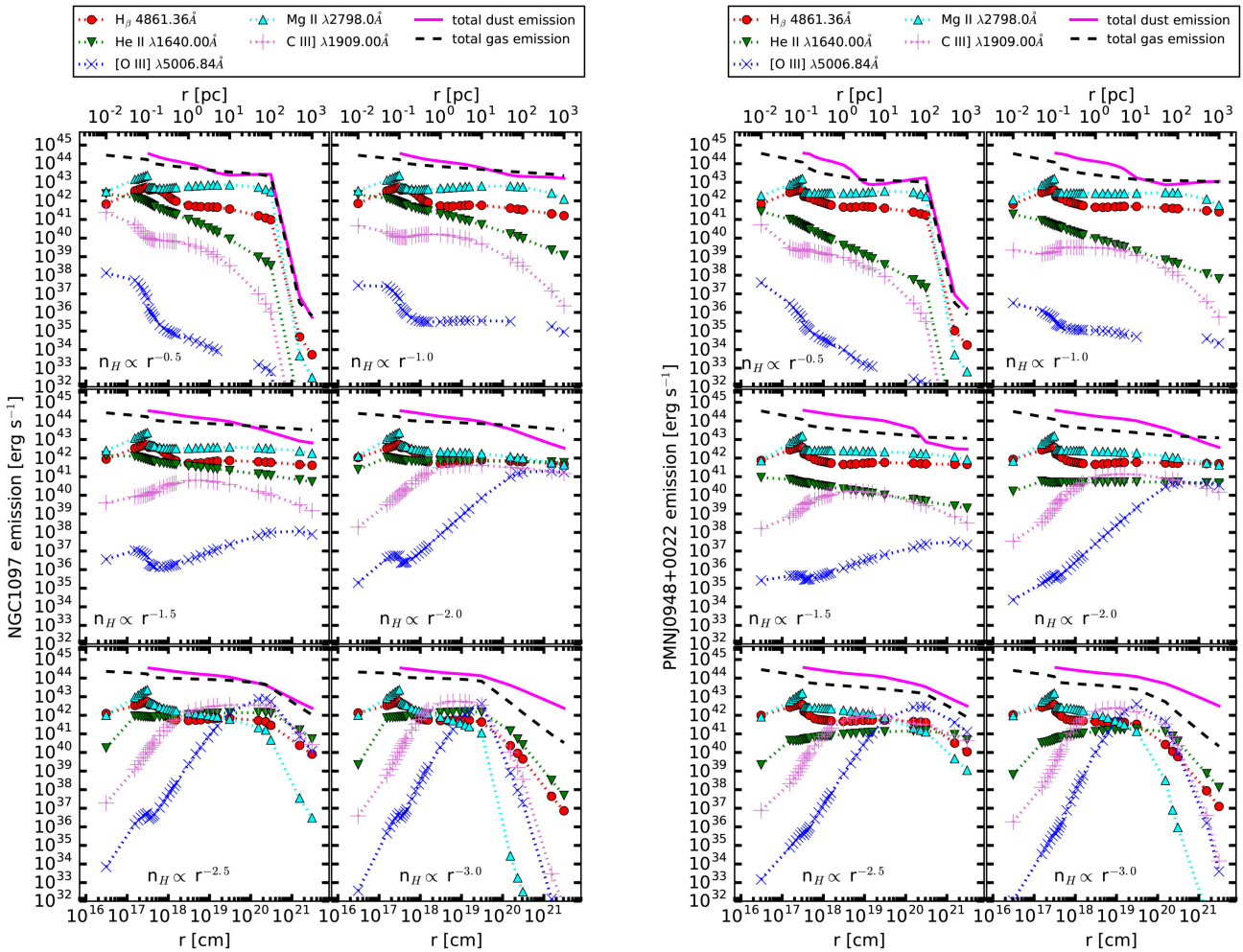

FIGURE 2 | The same as in **Figure 1** but for the SED of NGC 1097 **(left)** and PMN J0948+0022 **(right)**.

line emission is dominated by the [C III] components when the density distribution is given by the profiles with $\beta \geq 2.0$. We found that the derived line emissivities for all cases of power law density slopes, particularly in the region of intermediate line emission, do not strongly depend on the shapes of the SED used. There are subtle differences in emissivities corresponding to the BLR and NLR due to the different amount of UV and soft X-ray photons among the SEDs. This result is in agreement with the conclusion of AD16, that the presence of ILR emission is not determined by the shape of the incident radiation.

4. DISCUSSION

The results above confirm the conclusion of AD16, that the dust extinction of the emission lines in AGN introduced by NL93 is important only when the gas density is low. In AD16, the authors adopted only a density power law of slope $\beta = 1.5$ whereas this work demonstrates that the different slopes of the density distribution do not matter significantly as long as the gas density at the sublimation radius is high, in this case being $10^{11.5}$ cm^{-3}. In all cases of considered density profiles, we obtained an intermediate line emission around 0.1–1 pc, mostly manifested in permitted lines Hβ, He II, and Mg II, and weakly present in the semi forbidden line [C III]. This indicates that the high density and the low ionization environment favors the intermediate line emission rather than the high ionization environment where the forbidden line [O III] is produced. So, in the AGNs where the ILR is seen in observations, the emitting region is composed of the dense and less ionized gas.

The physical reason for the disappearance of the effect of dust is connected with the size of H- ionized front in the gas. At very high value of ionization parameter, i.e., for the low density case, the volume of the H-ionized region is very large, if not the full cloud volume. When the density of cloud increases, the ionization decreases, and a cloud consists of two regions: H-ionized region and H-neutral region. The line emission comes from the H-ionized region, and only the dust in this region competes with the gas for the photons. In other words, the dense clouds have much smaller geometrical thickness of H -ionized layer, smaller dust column density in the region with abundant

photons, and therefore the dust absorption is negligible. Our simulations are not yet aimed to make a quantitative statements about the studied objects. For that, we would need to do more extensive study, representing the bolometric luminosity and the position of the inner radius of the dust distribution appropriate for a given object. However, the grid of results shows a clear trend.

In the recent years, there has been promising claims that, broad line emission clouds in AGN are connected with the wind from the upper part of an accretion disk atmosphere (Gaskell, 2009; Czerny and Hryniewicz, 2011). As shown in the Fig. 6 of AD16, the density profiles computed in the upper part of the standard disk atmosphere can be quite dense with values up to $\sim 10^{15}$ cm^{-3} at the assumed position of sublimation radius. Those density values depend on the mass of the black hole and the disk accretion rate. Because of the high gas density, photoionisation simulations outcome with continuous line luminosity radial profile for the reason discussed in the previous paragraph. As the consequence, ILR should be observed together with BLR and NLR. The use of realistic density profiles expected from the accretion disk atmosphere is very important in the aim to understand the nature and origin of the ILR observed in some AGNs. This work is in progress and will be presented by Adhikari et al. (in preparation).

AUTHOR CONTRIBUTIONS

TPA, AR, and KH were responsible for developing the idea, doing the simulations, analyzing the results and writing the text for the manuscript, BC provided the concept and GF discussed the results.

FUNDING

This research was supported by Polish National Science Center grants No. 2016/21/N/ST9/03311, 2015/17/B/ST9/03422, 2015/18/M/ST9/00541, 2015/17/B/ST9/03436, and by Ministry of Science and Higher Education grant W30/7.PR/2013. It received funding from the European Union Seventh Framework Program (FP7/2007-2013) under the grant agreement No. 312789. TPA received funding from NCAC PAS grant for young researchers.

REFERENCES

Adhikari, T. P., Różańska, A., Czerny, B., Hryniewicz, K., and Ferland, G. J. (2016). The intermediate-line region in active galactic nuclei. *Astrophys. J.* 831:68. doi: 10.3847/0004-637X/831/1/68

Brotherton, M. S., Wills, B. J., Francis, P. J., and Steidel, C. C. (1994). The intermediate line region of QSOs. *Astrophys. J.* 430, 495–504. doi: 10.1086/174425

Crenshaw, D. M., and Kraemer, S. B. (2007). Mass Outflow from the nucleus of the seyfert 1 galaxy NGC 4151. *Astrophys. J.* 659, 250–256. doi: 10.1086/511970

Czerny, B., and Hryniewicz, K. (2011). The origin of the broad line region in active galactic nuclei. *Astron. Astrophys.* 525:L8. doi: 10.1051/0004-6361/201016025

D'Ammando, F., Orienti, M., Finke, J., Raiteri, C. M., Hovatta, T., Larsson, J., et al. (2015). The most powerful flaring activity from the NLSy1 PMN J0948+0022. *Mon. Not. R. Astron. Soc.* 446, 2456–2467. doi: 10.1093/mnras/stu2251

Ferland, G. J., Chatzikos, M., Guzmán, F., Lykins, M. L., van Hoof, P. A. M., Williams, R. J. R., et al. (2017). The 2017 Release of cloudy. *ArXiv E-Prints*.

Gaskell, C. M. (2009). What broad emission lines tell us about how active galactic nuclei work. *New Astron. Rev.* 53, 140–148. doi: 10.1016/j.newar.2009.09.006

Grevesse, N., and Sauval, A. J. (1998). Standard solar composition. *Space Sci. Rev.* 85, 161–174. doi: 10.1023/A:1005161325181

Hu, C., Wang, J.-M., Ho, L. C., Chen, Y.-M., Bian, W.-H., and Xue, S.-J. (2008a). Hβ profiles in quasars: evidence for an intermediate-line region. *Astrophys. J. Lett.* 683:L115. doi: 10.1086/591848

Hu, C., Wang, J.-M., Ho, L. C., Chen, Y.-M., Zhang, H.-T., Bian, W.-H., et al. (2008b). A systematic analysis of Fe II emission in quasars: evidence for inflow to the central black hole. *Astrophys. J.* 687:78–96. doi: 10.1086/591838

Kaastra, J. S., Petrucci, P.-O., Cappi, M., Arav, N., Behar, E., Bianchi, S., et al. (2011). Multiwavelength campaign on Mrk 509. I. Variability and spectral energy distribution. *Astron. Astrophys.* 534:A36. doi: 10.1051/0004-6361/201116869

Li, Z., Zhou, H., Hao, L., Wang, H., Ji, T., Shi, X., et al. (2015). Detection of the intermediate-width emission line region in quasar OI 287 with the broad emission line region obscured by the dusty torus. *Astrophys. J.* 812:99. doi: 10.1088/0004-637X/812/2/99

Mason, K. O., Puchnarewicz, E. M., and Jones, L. R. (1996). The origin of the optical emission lines in the narrow-line Seyfert 1 galaxy RE J1034+396. *Mon. Not. R. Astron. Soc.* 283, L26–L29. doi: 10.1093/mnras/283.1.L26

Mehdipour, M., Kaastra, J. S., Kriss, G. A., Cappi, M., Petrucci, P.-O., Steenbrugge, K. C., et al. (2015). Anatomy of the AGN in NGC 5548. I. A global model for the broadband spectral energy distribution. *Astron. Astrophys.* 575:A22. doi: 10.1051/0004-6361/201425373

Nemmen, R. S., Storchi-Bergmann, T., and Eracleous, M. (2014). Spectral models for low-luminosity active galactic nuclei in LINERs: the role of advection-dominated accretion and jets. *Mon. Not. R. Astron. Soc* 438, 2804–2827. doi: 10.1093/mnras/stt2388

Nenkova, M., Sirocky, M. M., Ivezić, Ž., and Elitzur, M. (2008). AGN dusty tori. I. handling of clumpy media. *Astrophys. J.* 685, 147–159. doi: 10.1086/590482

Netzer, H., and Laor, A. (1993). Dust in the narrow-line region of active galactic nuclei. *Astrophys. J. Lett.* 404, L51–L54. doi: 10.1086/186741

Zhu, L., Zhang, S. N., and Tang, S. (2009). Evidence for an intermediate line region in active galactic nuclei's inner torus region and its evolution from narrow to broad line seyfert I galaxies. *Astrophys. J.* 700, 1173–1189. doi: 10.1088/0004-637X/700/2/1173

Conflict of Interest Statement: The authors declare that the research was conducted in the absence of any commercial or financial relationships that could be construed as a potential conflict of interest.

Copyright © 2017 Adhikari, Różańska, Hryniewicz, Czerny and Ferland. This is an open-access article distributed under the terms of the Creative Commons Attribution License (CC BY). The use, distribution or reproduction in other forums is permitted, provided the original author(s) or licensor are credited and that the original publication in this journal is cited, in accordance with accepted academic practice. No use, distribution or reproduction is permitted which does not comply with these terms.

frontiers in Astronomy and Space Sciences

ORIGINAL RESEARCH
published: 21 November 2017
doi: 10.3389/fspas.2017.00048

EW[OIII] as an Orientation Indicator for Quasars: Implications for the Torus

Susanna Bisogni[1,2]*, *Alessandro Marconi*[2,3], *Guido Risaliti*[2,3] *and Elisabeta Lusso*[4]

[1] Harvard-Smithsonian Center for Astrophysics, Cambridge, MA, United States, [2] Osservatorio Astrofisico di Arcetri, INAF, Florence, Italy, [3] Dipartimento di Fisica e Astronomia, Università degli Studi di Firenze, Florence, Italy, [4] Centre for Extragalactic Astronomy, Department of Physics, Durham University, Durham, United Kingdom

We present an analysis of the average spectral properties of 12,000 SDSS quasars as a function of accretion disc inclination, as measured from the equivalent width of the [OIII] 5007Å line. The use of this indicator on a large sample of quasars from the SDSS DR7 has proven the presence of orientation effects on the features of UV/optical spectra, confirming the presence of outflows in the NLR gas and that the geometry of the BLR is disc-like. Relying on the goodness of this indicator, we are now using it to investigate other bands/components of AGN. Specifically, the study of the UV/optical/IR SED of the same sample provides information on the obscuring "torus." The SED shows a decrease of the IR fraction moving from face-on to edge-on sources, in agreement with models where the torus is co-axial with the accretion disc. Moreover, the fact we are able to observe the broad emission lines also in sources in an edge-on position, suggests that the torus is rather clumpy than smooth as in the Unified Model. The behavior of the SED as a function of EW[OIII] is in agreement with the predictions of the clumpy torus models as well.

Keywords: galaxies: active, galaxies: nuclei, galaxies: Seyfert, quasars: emission lines, quasars: general

OPEN ACCESS

Edited by:
Paola Marziani, Osservatorio Astronomico di Padova (INAF), Italy

Reviewed by:
Víctor Manuel Patiño Álvarez, National Institute of Astrophysics, Optics and Electronics, Mexico
Luka C. Popovic, Belgrade Astronomical Observatory, Serbia

***Correspondence:**
Susanna Bisogni
susanna.bisogni@cfa.harvard.edu

Specialty section:
This article was submitted to Milky Way and Galaxies, a section of the journal Frontiers in Astronomy and Space Sciences

Received: *25 September 2017*
Accepted: *06 November 2017*
Published: *21 November 2017*

Citation:
Bisogni S, Marconi A, Risaliti G and Lusso E (2017) EW[OIII] as an Orientation Indicator for Quasars: Implications for the Torus. Front. Astron. Space Sci. 4:48. doi: 10.3389/fspas.2017.00048

1. INTRODUCTION

The fact we are not able to spatially resolve the inner regions of Active Galactic Nuclei (AGN), combined with their axisymmetric geometry (Antonucci and Miller, 1985; Antonucci, 1993), can make it difficult to interpret their emissions. The Unified Model predicts the orientation to be one of the main drivers of the diversification in quasars spectra. For this reason, an indicator of the inclination of the source with respect the line of sight of the observer is essential to get further in studying these objects.

Despite several quasars properties have been found to provide information on the inclination of the inner nucleus (Wills and Browne, 1986; Wills and Brotherton, 1995; Boroson, 2011; Decarli et al., 2011; Van Gorkom et al., 2015), we still lack an univocal measurement of this quantity. This problem is even harder when dealing with not-jetted objects, the most among quasars (>90%, Padovani, 2011), for which we can not rely on the presence of the strongly collimated radio-jets, directed perpendicularly to the accretion disc.

In order to give a more accurate description of the components surrounding the central engine and to understand where are the boundaries between one and another, we need to know which components are being intercepted by our line of sight.

Assuming that some of these inner components are characterized by a spherical geometry can often simplify the scenario, while at the same time misleading us. We use the emission lines coming from the Broad Line Region (BLR) to give an estimate of the mass of the central Super Massive Black Hole (SMBH), but in doing that we do not take properly into consideration the geometry of the BLR, i.e., we use an average *virial factor f* to account for the uknown in the geometry and kinematics of the emitting region and we overlook the effects of orientation on the emission lines (Jarvis and McLure, 2006; Shen, 2013). These measurements can then be used in turn to examine the relations between the SMBH and their host galaxies—one of the few tools available to understand the connection between structures on such different spatial scales—their uncertainties affecting these studies (e.g., Shen and Kelly, 2010). If the BLR is characterized by a non-spherical geometry we are sistematically underestimating the BH masses in all the sources in which the velocity we intercept, i.e., the line width we measure, is only a fraction of the intrinsic velocity of the emitting gas orbiting around the SMBH. The inclination of the source with respect to the line of sight is therefore crucial to both the understanding of how the nuclei work and how they affect the formation and evolution of galaxies in the Universe. In this proceeding we show recent results on the optical spectra and we present a preliminary result on the Spectral Energy Distribution of quasars, that we obtained using the EW[OIII] as an orientation indicator.

2. ORIENTATION EFFECTS ON EMISSION FEATURES

2.1. Optical Spectra

Based on the properties of the [OIII] 5007Å line—negligibly contaminated by non-AGN processes and coming from the Narrow Line Region (NLR), whose dimensions ensure the isotropy of the emissions (Mulchaey et al., 1994; Heckman et al., 2004)—and on the strong anisotropy of the continuum emitted by the optically-thick/geometrically-thin accretion disc (Shakura and Sunyaev, 1973), we proposed the equivalent width (EW) of the [OIII] line, the ratio between the two luminosities, as an indicator of quasars orientation (Risaliti et al., 2011; Bisogni et al., 2017).

In Risaliti et al. (2011) we examined the distribution of the observed EW[OIII] in a large sample of quasars from the SDSS DR5 ($\sim 6,000$) and verified the presence of an orientation effect: the distribution shows a power law tail at the high EW[OIII] values that can not be ascribable to the intrinsic differences in the NLR among different objects, i.e., the intrinsic EW[OIII] distribution, the one we would observe if all the sources were seen in a face-on position. The observed EW[OIII] distribution is a convolution of the intrinsic properties of the NLR emissions in the different objects, such as the ionising continuum and the covering factor of the clouds, and the effects due to their inclination angle.

In Bisogni et al. (2017) we selected a larger sample of objects from the SDSS DR7 ($\sim$12,000), this time with the aim of looking for evidences of orientation effects in the optical spectra. We split our sample in six bins of EW[OIII], each one corresponding to an inclination angle range. Within each bin, the spectra were stacked in order to produce a master spectrum. We then analysed both the broad and the narrow emission lines as a function of EW[OIII], i.e., of the inclination angle, finding orientation effects on both of them. **Figure 1** shows the presence of orientation effects on the broad component of Hβ: the width of the broad line, either represented by the line dispersion σ, the Full Width Half Maximum (FWHM) or the Inter-Percentile Velocity width (IPV), increases steadily when we move from low to high EW[OIII]. We found the same result for the other broad lines examined (Hα and MgII, see Bisogni et al., 2017 for more details). This behavior is what is expected if the BLR geometry is disc-like and we are moving from sources in a face-on position to sources in an edge-on position.

As for the narrow emission lines, we examined the [OIII] λ5007Å, the most prominent among them in the optical spectrum. This line is known to be contaminated by emissions coming from non-virialized gas, i.e., not orbiting around the central SMBH, but outflowing perpendicularly to the accretion disc (Heckman et al., 1984; Boroson, 2005). If the EW[OIII] is a good indicator of the inclination of the source, we should see the blue component of the line, emitted by outflowing gas, decreasing both in intensity and in velocity shift with respect to the nominal wavelength of the emission moving to high EW[OIII] values. Going from face-on to edge-on position in fact we are not intercepting anymore the outflow perpendicular to the accretion disc. This behavior is found in the [OIII] line profile (**Figure 2**).

We want to stress that within each EW[OIII] bin, therefore within each inclination angle range, the population of quasars is characterized by different SMBH masses, luminosities and accretion rates. These properties are considered among the main drivers of the variance in quasars spectra (Zamanov and Marziani, 2002; Marziani et al., 2003; Shen and Ho, 2014). In our study however, as it is designed, even if the effects produced by these properties are present, they are diluited in the stacked representative spectra. As a confirmation that the orientation, even if not the only driver, plays a major role in the variance of quasars spectra, we found a clear trend of the Eigenvector 1, i.e., the anticorrelation between the FeII and [OIII] emissions intensity that Boroson and Green (1992) identify as the main responsible for quasars spectral variance, with the EW[OIII]. Specifically, when we move from low to high EW[OIII], i.e., from low to high inclination angles, we see the [OIII] intensity increasing, while FeII emission becomes less and less intense. This can be explained in terms of orientation: the BLR shares the same anisotropy of the accretion disc and therefore the intensity of its emissions, in this case FeII, is decreased by a factor $\cos\theta$, i.e., decreases when moving to edge-on sources. On the other hand the [OIII] line appears as more evident in edge on positions because the luminosity of the continuum emitted by the accretion disc is decreased by the factor $\cos\theta$.

2.2. Infrared Emissions

The observed EW[OIII] distribution has implications for the obscuring component as well.

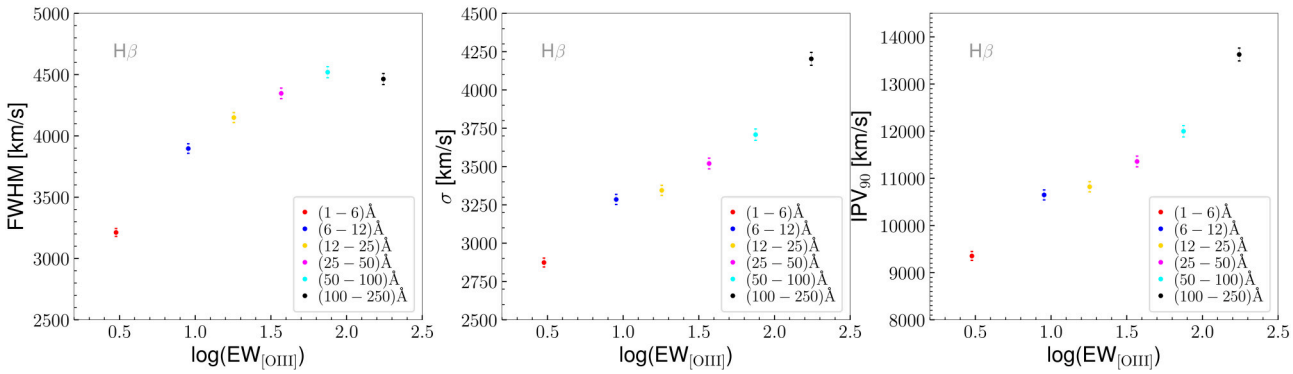

FIGURE 1 | Full Width Half Maximum, Inter-Percentile Velocity width and dispersion σ as a function of the EW[OIII] for the Hβ line. All these quantities, describing the rotational velocity of the gas orbiting around the central SMBH, increase moving from low to high EW[OIII] as expected if the BLR is disc-shaped and we are moving from face-on to edge-on positions.

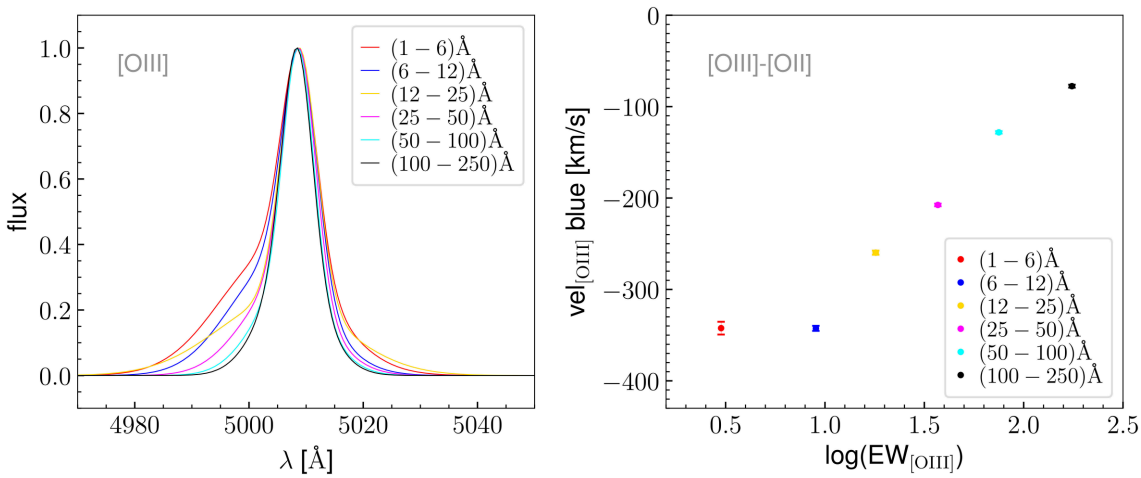

FIGURE 2 | Left: [OIII] 5007Å line profile as a function of EW[OIII]. The blue component of the line decreases moving from low to high EW[OIII]. **Right:** velocity shift of the blue component of the [OIII] line with respect to the velocity of the [OII] λ3727 line, accounting for the systemic velocity of the host galaxy. The shift is decreasing (in modulus) when moving from low to high EW[OIII]. Both the trends are expected if we are moving from face-on to edge-on positions, where the outflow velocity component of the gas is not intercepted anymore by the line of sight.

The torus is depicted in the Unified Model as a smooth and toroidal structure that can reach ∼1–10 pc in size (Burtscher et al., 2013). If this is true then, there is a maximum inclination angle beyond which we are not able anymore to intercept the emissions coming from the very inner components, such as the continuum emitted by the accretion disc and the broad lines emitted by the BLR. In this case, however, the observed EW[OIII] distribution would drop when the line of sight is starting to intercept the torus. This is not what we observe: the power law keeps going very steadily to the highest EW[OIII] values. Moreover, we are intercepting broad emission lines in positions corresponding to high inclination angles. Both these facts are not compatible with the torus being a smooth structure and rather suggest a clumpy structure.

To test the indicator and exploit its potential, we are now interested in investigating the infrared emissions.

We then collect photometric data for the same sample in the UV, optical and IR band to study the Spectral Energy Distributions (SED) of the sources.

3. SAMPLE AND DATA ANALYSIS

For the sample of ∼12,000 objects we selected from the SDSS DR7 the following photometric data are available:

- Far Ultra Violet and Near Ultra Violet bands from *Galaxy Evolution Explorer* (*GALEX*) DR5 (Bianchi et al., 2011).
- *ugriz* SDSS photometric data from Shen et al. (2011).
- The J, H, and K bands from the *Two Micron All-Sky Survey* (2MASS) (Skrutskie et al., 2006).
- The 3.4, 4.6, 12, and 22 μm photometric data from the *Wide-field Infrared urvey Explorer* (*WISE*) (Wright et al., 2010).

We first correct all the magnitudes for Galactic extinction using the maps from the Schlegel et al. (1998). Then, for each EW[OIII] bin, we use the same approach as for the optical spectroscopic data: we rest-frame the data according to the sources redshift and then we perform a stacking of the interpolated SED in order to produce a master SED, on which we can examine the effects produced by the orientation. Before stacking them, we normalize each SED by dividing for the value of νL_ν at $\lambda = 15\,\mu$m, a reference wavelength in the mid-infrared spectral range, the band in which the torus emits. In doing that, we are normalizing the individual SED for the intrinsic differences of the torus and of other components in the different objects, such as the size and covering factor of the obscuring region, its distance from the central engine and the properties of the ionising continuum, whose emission is being reprocessed by the torus. This makes us able to compare the average behavior of the obscuring structure at different inclinations with respect to the line of sight of the observer. The final SED are shown in **Figure 3**.

4. RESULTS AND DISCUSSION: IMPLICATIONS FOR THE OBSCURING TORUS

In the optical stacks corresponding to the highest inclination angles (high EW[OIII]) we are able to detect emissions from the BLR. This evidence implies three possible scenarios: the absence of the torus, a torus that is mis-aligned with respect the plane of the accretion disc (and of the BLR) and a clumpy torus. The first scenario is ruled out by the fact that the IR emission is clearly visible in the SED of the sample (**Figure 3**). As for the second one, we see the IR emission in the stacked SED decreasing progressively as a function of the indicator, defined through the anisotropic properties of the emission coming from the accretion disc itself. If torus and accretion disc were not co-axial, we would not see such an orderly behavior.

The only scenario we are left with is therefore a clumpy torus, leading to a differention between type 1 and type 2 AGN due only to the photon escaping probability (Elitzur, 2008). Due to the selection we performed (i.e., we selected blue objects, and verified that the continuum in our stacked optical spectra was not experiencing any reddening, see Bisogni et al., 2017), when we are looking at sources with a high EW[OIII], i.e., with a high inclination angle, we are dealing with type 1 sources in which the BLR is intercepted through the dusty clouds of the torus.

We can compare our results with the clumpy models in literature (Nenkova et al., 2008a,b) that examine the infrared emission of the torus as a function of the inclination angle with respect to the observer. If the torus is a clumpy structure, what we expect is that the IR emission at shorter wavelengths decreases progressively more than the ones at longer wavelengths when we are reaching edge-on position, due to the combination of an increasing number of clouds intercepted by the line of sight and of a higher absorption at the shorter than at the longer wavelengths (Nenkova et al., 2008b).

The behavior of the stacked SED as a function of EW[OIII] confirms this scenario. At low EW[OIII] (low inclination angle) we are able to intercept the IR emissions coming from the inner clouds of the torus, that are directly illuminated by the ionizing continuum, while at high EW[OIII] (high inclination angle) the IR emission coming from the inner clouds is shielded and we can detect it only after it is absorbed by the clouds in the outskirts of the torus. This produces the decrease in the flux at the shorter wavelengths, that becomes progressively more important for stacks corresponding to higher inclinations.

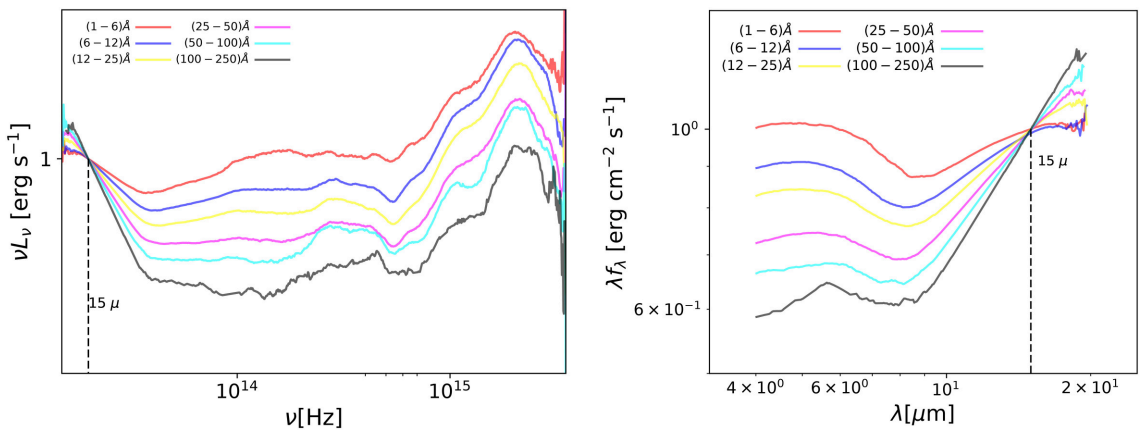

FIGURE 3 | Left: Spectral Energy Distributions for the six EW[OIII] bins, corresponding to different inclination angle ranges. The master SED for a EW[OIII] bin was realized as follows: the photometric data for each source from the *GALEX*, SDSS, 2MASS and *WISE* surveys were corrected for Galactic reddening, rest-framed, interpolated on a common grid and normalized to the νL_ν value corresponding to the reference wavelength (15μm); for every channel in the grid we then selected the median value. **Right:** Total flux for the six EW[OIII] bins in the spectral range in which the emission coming from the torus is predominant. SED corresponding to low EW[OIII] values are characterized by a shallower decrease in the emission at the shorter IR wavelengths with respect to the longer ones, while in the case of high EW[OIII] the decrease is steeper. This behavior is in agreement with the clumpy torus models (see text for details).

As a final verification that our results are not biased by any characteristics of the sample, we made the following checks:

(1) Since our sample contains non-jetted as well as jetted quasars, the most extreme among them (blazars) could contaminate the part of the SED pertaining to the torus emission. We verified that the sub-sample composed by non-jetted quasars only gives the same result as the complete sample.
(2) Approximately 50% of the objects in our sample has a redshift $z > 0.47$. This is the critical value beyond which the normalization flux at 15 μm is retrieved through an extrapolation rather than an interpolation of the SED. We verified that the analysis on the $z > 0.47$ and $z > 0.47$ sub-samples does not give different results. The only differences in the $z > 0.47$ ($z > 0.47$) sub-sample we recognize with respect to the complete sample SED are: a lower (higher) luminosity in Big Blue Bump (accretion disc), due to the fact that our sample is on average more luminous at higher redshifts, and a higher (lower) emission in the optical/NIR band, due to a higher contribution from the host galaxy for sources at lower redshift. We conclude that the extrapolation of the 15 μm flux in $z > 0.47$ sources does not affect our results.

5. CONCLUSIONS

In this proceeding we summarize the results of the analysis on the optical spectra and we present the preliminary results of the analysis on the infrared emission of 12,000 sources of the SDSS DR7 as a function of the EW[OIII], a new orientation indicator. We find that:

- the BLR shares the same geometry of the accretion disc; we are intercepting the intrinsic velocity of the orbiting gas only when we are looking at sources in edge-on positions. If not properly taken into account, the orientation effects affecting the broad emissions lead to an underestimation of the SMBH virial masses in every position but the edge-on ones.
- the presence of outflowing gas in the NLR is clearly seen in the profile of the [OIII] λ5007Å as a function of the inclination angle. The blue component decreases both in intensity and in the shift with respect to the reference wavelength moving from face-on to edge-on positions.
- the preliminary analysis of the SED reveals a stronger decrease in the IR emission corresponding to the shorter wavelengths with respect to the longer ones when moving from low to high EW[OIII] values, as expected in the theoretical models for clumpy tori when moving from low to high inclination angles.

Further analysis is needed in order to investigate properly the emission coming from the torus. Starting from these first results, we are in the process of performing a SED fitting for each source in the sample with *AGNfitter* (Calistro Rivera et al., 2016). We will then be able to repeat the analysis on the representative SED, this time having also information on the single components contributing to the total emission.

We will also investigate the sources in our sample for which multiple observations are available (e.g., Stripe82, new BOSS spectra) in order to look for evidences of *changing look* behaviors as a function of the EW[OIII]. If our interpretation of the data implying a clumpy structure for the torus is correct, we expect to see some of the sources that were included in our sample as Type 1 AGN changing to Type 2 objects at a different epoch. This behavior is expected more frequently for sources with a high EW[OIII], where the orientation effect is dominant, but it is not excluded even for sources with low EW[OIII] values.

AUTHOR CONTRIBUTIONS

All the authors contributed to the work and approved it for publication.

FUNDING

Support for this work was provided by the National Aeronautics and Space Administration through Chandra Award Number AR7-18013 X issued by the Chandra X-ray Observatory Center, which is operated by the Smithsonian Astrophysical Observatory for and on behalf of the National Aeronautics Space Administration under contract NAS8-03060 (10.13039/100000104). EL is supported by a European Union COFUND/Durham Junior Research Fellowship (under EU grant agreement no. 609412).

REFERENCES

Antonucci, R. (1993). Unified models for active galactic nuclei and quasars. *Annu. Rev. Astron. Astrophys.* 31, 473–521. doi: 10.1146/annurev.aa.31.090193.002353

Antonucci, R. R. J., and Miller, J. S. (1985). Spectropolarimetry and the nature of NGC 1068. *Astrophys. J.* 297, 621–632. doi: 10.1086/163559

Bianchi, L., Efremova, B., Herald, J., Girardi, L., Zabot, A., Marigo, P., et al. (2011). VizieR online data catalog: hot white dwarfs in GALEX-DR5 (Bianchi+, 2011). *VizieR Online Data Catalog* 335, 161–169. doi: 10.1007/s10509-010-0581-x

Bisogni, S., Marconi, A., and Risaliti, G. (2017). Orientation effects on spectral emission features of quasars. *Month. Notices R. Astron. Soc.* 464, 385–397. doi: 10.1093/mnras/stw2324

Boroson, T. (2005). Blueshifted [OIII] emission: indications of a dynamic narrow-line region. *Astron. J.* 130, 381–386. doi: 10.1086/431722

Boroson, T. A. (2011). A new orientation indicator for radio-quiet quasars. *Astrophys. J. Lett.* 735:L14. doi: 10.1088/2041-8205/735/1/L14

Boroson, T. A., and Green, R. F. (1992). The emission-line properties of low-redshift quasi-stellar objects. *Astrophys. J. Suppl.* 80, 109–135. doi: 10.1086/191661

Burtscher, L., Meisenheimer, K., Tristram, K. R. W., Jaffe, W., Hönig, S. F., Davies, R. I., et al. (2013). A diversity of dusty AGN tori. Data release for the VLTI/MIDI AGN Large Program and first results for 23 galaxies. *Astron. Astrophys.* 558:A149. doi: 10.1051/0004-6361/201321890

Calistro Rivera, G., Lusso, E., Hennawi, J. F., and Hogg, D. W. (2016). AGNfitter: a bayesian MCMC approach to fitting spectral energy distributions of AGNs. *Astrophys. J.* 833:98. doi: 10.3847/1538-4357/833/1/98

Decarli, R., Dotti, M., and Treves, A. (2011). Geometry and inclination of the broad-line region in blazars. *Month. Notices R. Astron. Soc.* 413, 39–46. doi: 10.1111/j.1365-2966.2010.18102.x

Elitzur, M. (2008). The toroidal obscuration of active galactic nuclei. *Astrophysics* 52, 274–288. doi: 10.1016/j.newar.2008.06.010

Heckman, T. M., Kauffmann, G., Brinchmann, J., Charlot, S., Tremonti, C., and White, S. D. M. (2004). Present-Day Growth of Black Holes and Bulges: The Sloan Digital Sky Survey Perspective. *Astrophys. J.* 613, 109–118. doi: 10.1086/422872

Heckman, T. M., Miley, G. K., and Green, R. F. (1984). The kinematics of the narrow-line region in active galaxies and quasars. III - Correlations with the broad-line region and radio emission. *Astrophys. J.* 281, 525–534. doi: 10.1086/162125

Jarvis, M. J., and McLure, R. J. (2006). Orientation dependency of broad-line widths in quasars and consequences for black hole mass estimation. *Month. Notices R. Astron. Soc.* 369, 182–188. doi: 10.1111/j.1365-2966.2006.10295.x

Marziani, P., Zamanov, R. K., Sulentic, J. W., and Calvani, M. (2003). Searching for the physical drivers of eigenvector 1: influence of black hole mass and Eddington ratio. *Month. Notices R. Astron. Soc.* 345, 1133–1144. doi: 10.1046/j.1365-2966.2003.07033.x

Mulchaey, J. S., Koratkar, A., Ward, M. J., Wilson, A. S., Whittle, M., Antonucci, R. R. J., et al. (1994). Multiwavelength tests of the dusty torus model for Seyfert galaxies. *Astrophys. J.* 436, 586–598. doi: 10.1086/174933

Nenkova, M., Sirocky, M. M., Ivezić, Ž., and Elitzur, M. (2008a). AGN Dusty Tori. I. Handling of Clumpy Media. *Astrophys. J.* 685, 147–159. doi: 10.1086/590482

Nenkova, M., Sirocky, M. M., Nikutta, R., Ivezić, Ž., and Elitzur, M. (2008b). AGN dusty tori. II. Observational implications of clumpiness. *Astrophys. J.* 685, 160–180. doi: 10.1086/590483

Padovani, P. (2011). The microjansky and nanojansky radio sky: source population and multiwavelength properties. *Month. Notices R. Astron. Soc.* 411, 1547–1561. doi: 10.1111/j.1365-2966.2010.17789.x

Risaliti, G., Salvati, M., and Marconi, A. (2011). [OIII] equivalent width and orientation effects in quasars. *Month. Notices R. Astron. Soc.* 411, 2223–2229. doi: 10.1111/j.1365-2966.2010.17843.x

Schlegel, D. J., Finkbeiner, D. P., and Davis, M. (1998). Maps of dust infrared emission for use in estimation of reddening and cosmic microwave background radiation foregrounds. *Astrophys. J.* 500, 525–553. doi: 10.1086/305772

Shakura, N. I., and Sunyaev, R. A. (1973). Black holes in binary systems. Observational appearance. *Astron. Astrophys.* 24, 337–355.

Shen, Y. (2013). The mass of quasars. *Bull. Astron. Soc. India* 41, 61–115. Available online at: http://cdsads.u-strasbg.fr/abs/2013BASI...41...61S

Shen, Y., and Ho, L. C. (2014). The diversity of quasars unified by accretion and orientation. *Nature*, 513, 210–213. doi: 10.1038/nature13712

Shen, Y., and Kelly, B. C. (2010). The impact of the uncertainty in single-epoch virial black hole mass estimates on the observed evolution of the black hole-bulge scaling relations. *Astrophys. J.* 713, 41–45. doi: 10.1088/0004-637X/713/1/41

Shen, Y., Richards, G. T., Strauss, M. A., Hall, P. B., Schneider, D. P., Snedden, S., et al. (2011). A catalog of quasar properties from sloan digital sky survey data release 7. *Astrophys. J. Suppl.* 194:45. doi: 10.1088/0067-0049/194/2/45

Skrutskie, M. F., Cutri, R. M., Stiening, R., Weinberg, M. D., Schneider, S., Carpenter, J. M., et al. (2006). The two micron all sky survey (2MASS). *Astron. J.* 131, 1163–1183. doi: 10.1086/498708

Van Gorkom, K. J., Wardle, J. F. C., Rauch, A. P., and Gobeille, D. B. (2015). Comparing different indicators of quasar orientation. *Month. Notices R. Astron. Soc.* 450, 4240–4247. doi: 10.1093/mnras/stv912

Wills, B. J., and Brotherton, M. S. (1995). An improved measure of quasar orientation. *Astrophys. J. Lett.* 448:L81. doi: 10.1086/309614

Wills, B. J., and Browne, I. W. A. (1986). Relativistic beaming and quasar emission lines. *Astrophys. J.* 302, 56–63. doi: 10.1086/163973

Wright, E. L., Eisenhardt, P. R. M., Mainzer, A. K., Ressler, M. E., Cutri, R. M., Jarrett, T., et al. (2010). The wide-field infrared survey explorer (WISE): mission description and initial on-orbit performance. *Astron. J.* 140, 1868–1881. doi: 10.1088/0004-6256/140/6/1868

Zamanov, R., and Marziani, P. (2002). Searching for the physical drivers of eigenvector 1: From quasars to nanoquasars. *Astrophys. J. Lett.* 571, L77–L80. doi: 10.1086/341367

Conflict of Interest Statement: The authors declare that the research was conducted in the absence of any commercial or financial relationships that could be construed as a potential conflict of interest.

Copyright © 2017 Bisogni, Marconi, Risaliti and Lusso. This is an open-access article distributed under the terms of the Creative Commons Attribution License (CC BY). The use, distribution or reproduction in other forums is permitted, provided the original author(s) or licensor are credited and that the original publication in this journal is cited, in accordance with accepted academic practice. No use, distribution or reproduction is permitted which does not comply with these terms.

frontiers in Astronomy and Space Sciences

PERSPECTIVE
published: 29 September 2017
doi: 10.3389/fspas.2017.00018

New Constraints on Quasar Broad Absorption and Emission Line Regions from Gravitational Microlensing

Damien Hutsemékers[1], Lorraine Braibant[1], Dominique Sluse[1], Timo Anguita[2] and René Goosmann[3]*

[1] Institut d'Astrophysique et de Géophysique, Université de Liège, Liège, Belgium, [2] Departamento de Ciencias Fisicas, Universidad Andres Bello, Santiago, Chile, [3] Observatoire Astronomique de Strasbourg, Université de Strasbourg, Strasbourg, France

Gravitational microlensing is a powerful tool allowing one to probe the structure of quasars on sub-parsec scale. We report recent results, focusing on the broad absorption and emission line regions. In particular microlensing reveals the intrinsic absorption hidden in the P Cygni-type line profiles observed in the broad absorption line quasar H1413+117, as well as the existence of an extended continuum source. In addition, polarization microlensing provides constraints on the scattering region. In the quasar Q2237+030, microlensing differently distorts the Hα and CIV broad emission line profiles, indicating that the low- and high-ionization broad emission lines must originate from regions with distinct kinematical properties. We also present simulations of the effect of microlensing on line profiles considering simple but representative models of the broad emission line region. Comparison of observations to simulations allows us to conclude that the Hα emitting region in Q2237+030 is best represented by a Keplerian disk.

Keywords: quasars, broad emission lines, broad absorption lines, gravitational microlensing, polarization

OPEN ACCESS

Edited by:
Mauro D'Onofrio, Università degli Studi di Padova, Italy

Reviewed by:
Giovanna Maria Stirpe, Osservatorio Astronomico di Bologna (INAF), Italy
Milan S. Dimitrijevic, Astronomical Observatory, Serbia

****Correspondence:***
Damien Hutsemékers
hutsemekers@astro.ulg.ac.be

Specialty section:
This article was submitted to Milky Way and Galaxies, a section of the journal Frontiers in Astronomy and Space Sciences

Received: *23 August 2017*
Accepted: *19 September 2017*
Published: *29 September 2017*

Citation:
Hutsemékers D, Braibant L, Sluse D, Anguita T and Goosmann R (2017) New Constraints on Quasar Broad Absorption and Emission Line Regions from Gravitational Microlensing. Front. Astron. Space Sci. 4:18. doi: 10.3389/fspas.2017.00018

1. INTRODUCTION

When the light from a distant quasar passes through the gravitational field of a galaxy, it is deflected and multiple magnified images of the source are observed. In addition, stars in the lensing galaxy can act as microlenses and produce an extra magnification of some images. The collective effect of these stars generates a complex magnification pattern in the source plane that takes the form of a caustic network. Microlensing magnification varies in time due to the relative motions of the source, lens and observer, on timescales of weeks to years. High magnification events occur when caustics are close to the line of sight (e.g., Schmidt and Wambsganss, 2010, for a review).

Gravitational lensing magnification strongly depends on the Einstein radius of the system, in the sense that only sources smaller than this radius can be significantly magnified. For a typical lensed system with a lensing galaxy at redshift $z \sim 0.5$ and a source quasar at $z \sim 2$, the projected Einstein radius of an average 0.3 $M_\odot$ star in the lensing galaxy is of the order of 10^{-3} pc, which is comparable to the size of the quasar continuum-emitting accretion disk. Microlensing thus mainly magnifies the continuum source. The more extended broad emission line region is either unaffected or only partly magnified. The much larger narrow line region is totally unaffected.

Therefore, microlensing differently magnifies the various components of the quasar spectrum. By comparing the spectra of two images of a lensed quasar, one affected by microlensing and the other not, one can separate the part of the spectrum which is microlensed, that is the part coming from the most compact source, from the part of the spectrum which is not affected by microlensing and originates from a more extended region. Information on the geometry and kinematics of the quasar inner regions can thus be obtained. This is illustrated in the following sections, focusing on the broad absorption and emission line regions (respectively, BALR and BELR).

2. MICROLENSING IN THE BROAD ABSORPTION LINE QUASAR H1413+117

H1413+117, the cloverleaf, is a quadruply lensed broad absorption line (BAL) quasar in which a slowly varying microlensing effect lasting for ∼20 years magnifies the continuum of image D, leaving the emission lines essentially unchanged (Angonin et al., 1990; Hutsemékers, 1993; Anguita et al., 2008; Hutsemékers et al., 2010; O'Dowd et al., 2015; Sluse et al., 2015). Image A is not or weakly affected by microlensing, thus providing a reference spectrum. We can then separate the part of the line profiles that is microlensed from the part that is not microlensed using the macro-micro decomposition (MmD) method presented in Sluse et al. (2007) and Hutsemékers et al. (2010).

Figure 1 illustrates the decomposition of the CIV λ1549Å P Cygni-type line profile into its microlensed ($F_{M\mu}$) and non-microlensed (F_M) components (see Hutsemékers et al., 2010; Sluse et al., 2015, for more details). $F_{M\mu}$ comes from a compact region that essentially produces the absorbed continuum, while F_M comes from a more extended region too large to be microlensed. From this spectral decomposition, it results that (1) the BAL profile consists of a completely black absorption (seen in $F_{M\mu}$) partially filled in by the broad emission line (seen in F_M); (2) this absorption does not start at zero-velocity but at an onset velocity of ∼2,000 km/s; (3) the broad emission line itself is re-absorbed (see F_M) over a wavelength range narrower than the full absorption profile, revealing the existence of an additional, more extended BALR; (4) a part of the continuum (seen in F_M) is not microlensed thus originating from a region larger than the source of the continuum seen in $F_{M\mu}$. These observations suggest a two-component outflow: one component is co-spatial with the BELR, while the other one, more distant, partially re-absorbs the emission from the BELR (Borguet and Hutsemékers, 2010). O'Dowd et al. (2015) found in addition an ionization dependence of the BAL onset velocity that they interpreted in the framework of a disk-wind model.

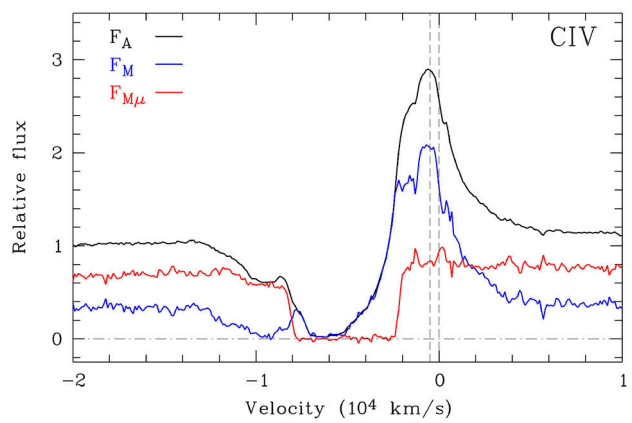

FIGURE 1 | Microlensing in the CIV line of the BAL quasar H1413+117. F_A is the observed spectrum of image A which is not affected by microlensing. The line profile can be decomposed in a part affected by microlensing, $F_{M\mu}$, and another part not affected by microlensing, F_M, with $F_A = F_M + F_{M\mu}$.

The light from H1413+117 is linearly polarized and Chae et al. (2001) found evidence for polarization microlensing. Hutsemékers et al. (2015) obtained spectropolarimetric observations of the different images that suggest that the continuum is scattered off two regions generating roughly orthogonal polarizations: a compact region located in the equatorial plane close to the accretion disk, which is microlensed, and an extended region located along the polar axis, which is not microlensed. This indicates that the non-microlensed extended continuum seen in F_M (**Figure 1**) could originate from scattering.

3. MICROLENSING OF THE BROAD EMISSION LINE REGION IN Q2237+030

3.1. Observed Line Profile Distortions

Though larger than the source of continuum, the BELR can be partly magnified by microlensing, which results in line profile deformations. Such microlensing-induced line profile deformations have been observed in several lensed quasar spectra, exhibiting various symmetric and asymmetric distortions in both low- and high-ionization lines (Richards et al., 2004; Wayth et al., 2005; Sluse et al., 2007, 2011, 2012; O'Dowd et al., 2011; Guerras et al., 2013; Braibant et al., 2014, 2016; Goicoechea and Shalyapin, 2016; Motta et al., 2017). By selectively magnifying different subregions of the broad line region, gravitational microlensing can thus provide information on the size, geometry and kinematics of the BELR in quasars (Nemiroff, 1988; Schneider and Wambsganss, 1990). In particular, the size of the BELR has been estimated in a few objects and found compatible with reverberation mapping measurements (Wayth et al., 2005; Sluse et al., 2011; Guerras et al., 2013).

Making use of the MmD line profile disentangling technique, Braibant et al. (2014, 2016) have extracted the part of the emission line profiles that is affected by microlensing in two lensed quasars for which high quality data were available. **Figure 2** illustrates the $F_{M\mu}$ / F_M decomposition of the CIV λ1549Å and Hα broad emission line profiles for the quadruply lensed quasar Q2237+030, the Einstein Cross, at an epoch when microlensing was prominent in image A and negligible in image D. A clear difference in the distortions suffered by the CIV and Hα emission

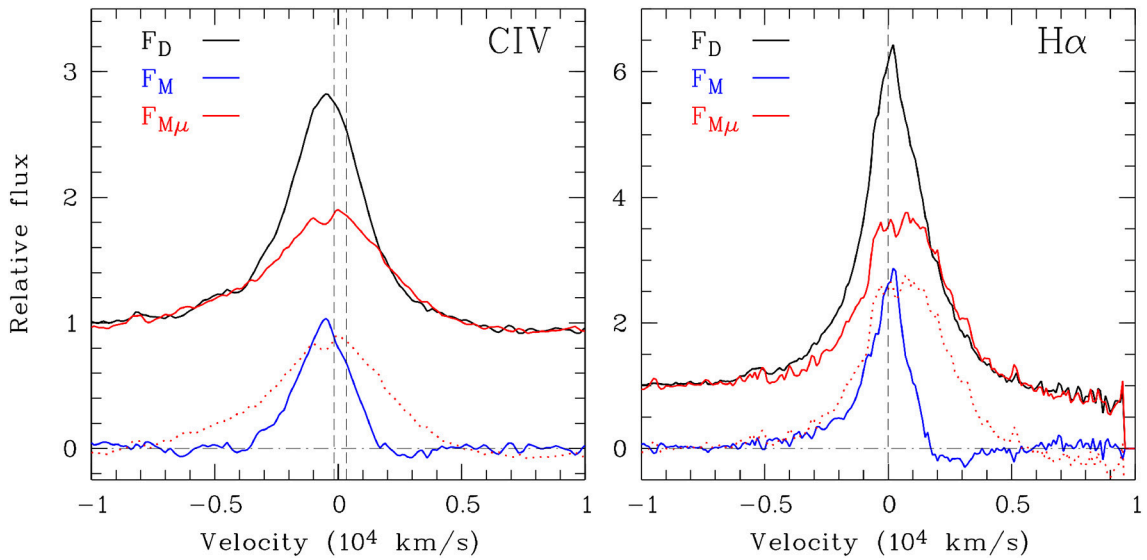

FIGURE 2 | Microlensing in the CIV and Hα lines of the quasar Q2237+030. F_D is the observed spectrum of image D which is not affected by microlensing. The line profile can be decomposed in a part affected by microlensing, $F_{M\mu}$, and another part not affected by microlensing, F_M, with $F_D = F_M + F_{M\mu}$. The dotted line profile represents the continuum-subtracted $F_{M\mu}$.

lines can be noticed. In CIV the effect is essentially symmetric, the wings of the line being more magnified than the core, while in Hα the effect is asymmetric, the red wing being more magnified than the blue wing. Since these observations were obtained at the same epoch, both the CIV and Hα emitting regions are magnified by the same caustic pattern. This indicates that the high- and low-ionization emission lines must originate from regions with distinct kinematical properties.

As illustrated in **Figure 3**, the detection of a red/blue differential microlensing effect in the Hα line profile suggests that the low-ionization BELR is likely a Keplerian disk, while the wings/core distortion observed in the CIV line can be interpreted assuming a polar outflow model. However, the mapping between a wavelength range in the line profile and subregions of the BELR seen in projection is usually not unique and a confrontation of the observations to detailed modeling appeared necessary.

3.2. Simulations of Line Profile Distortions

Possible effects of microlensing on broad emission lines have been theoretically investigated by several authors (Nemiroff, 1988; Schneider and Wambsganss, 1990; Hutsemékers et al., 1994; Popović et al., 2001; Abajas et al., 2002, 2007; Lewis and Ibata, 2004; O'Dowd et al., 2011; Simić and Popović, 2014) considering various BELR models and magnification patterns.

In Braibant et al. (2017), we extend those works focusing on wings/core and red/blue line profile distortions in order to constrain the BELR models. The effects of gravitational microlensing on the quasar broad emission line profiles and their underlying continuum have been simultaneously computed, considering simple, representative BELR, accretion disk, and magnifying caustic models. Keplerian disks as well as polar and equatorial outflow models of various sizes have been considered. The effect of microlensing has been quantified using four observables: μ^{BLR}, the total magnification of the broad emission line, μ^{cont}, the magnification of the underlying continuum, as well as red/blue, *RBI*, and wings/core, *WCI*, indices that characterize the line profile distortions. Those quantities were designed to not depend on the exact profile of the broad emission lines, so that they can be directly compared to observations.

The simulations show that asymmetric distortions of broad line profiles like those reported in Braibant et al. (2014, 2016) can be reproduced, and attributed to the differential effect of microlensing on spatially and kinematically separated regions of the BELR. In particular, red/blue asymmetric distortions constitute a good discriminant between the polar outflow and other models. We then built diagrams that can serve as diagnostic tools to discriminate between the different BELR models making use of quantitative measurements of the four observables μ^{cont}, μ^{BLR}, *RBI*, *WCI*. It appeared from the simulations that only strong microlensing effects can produce distinctive line profile distortions for a limited number of caustic configurations, i.e., distortions that allow us to put serious constraints on the various BELR models.

The four indices μ^{cont}, μ^{BLR}, *RBI*, *WCI* were then measured for both the CIV and Hα emission lines observed in the lensed quasar Q2237+030, and compared to the values generated by the simulations (Braibant et al., in preparation). In the simulations, we assumed that the CIV and Hα BELRs, and the continuum-emitting accretion disk share the same inclination with respect to the line of sight and the same location on the caustic network. From this comparison it results that the Hα low-ionization BELR is best represented by a Keplerian disk while the CIV high-ionization BELR can be either a Keplerian disk

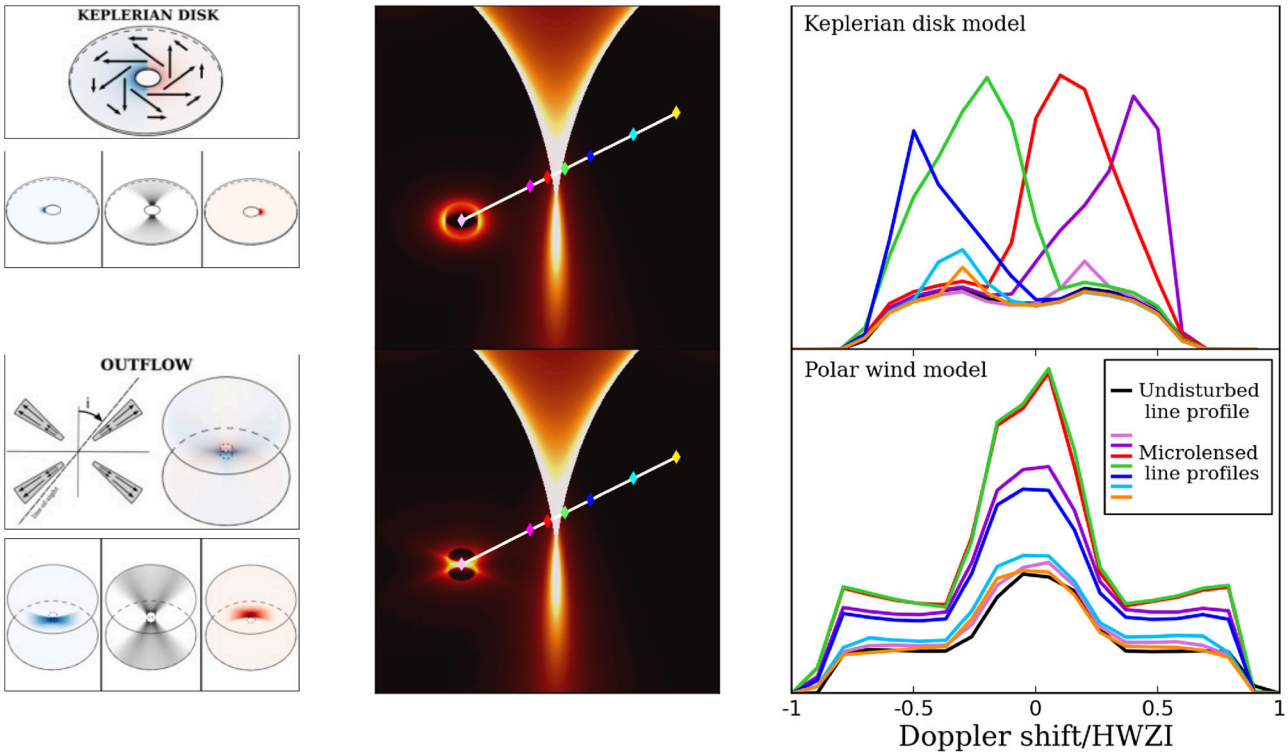

FIGURE 3 | Microlensing of different BELR structures and the resulting line profile distortions. The left panel sketches two models: a rotating Keplerian disk and a biconical outflow, both seen at intermediate inclination. The location of the approaching and receding gas is indicated in blue and red, respectively. The middle panel shows the BELR superimposed on a typical caustic. At the different positions indicated by colored losanges, different subregions of the BELR are magnified by the caustic. The right panel illustrates the line profiles corresponding to the different positions of the BELR onto the caustic pattern. Microlensing of the Keplerian disk is characterized by asymmetric red/blue line profile distortions while microlensing of the biconical outflow is characterized by symmetric wings/core distortions.

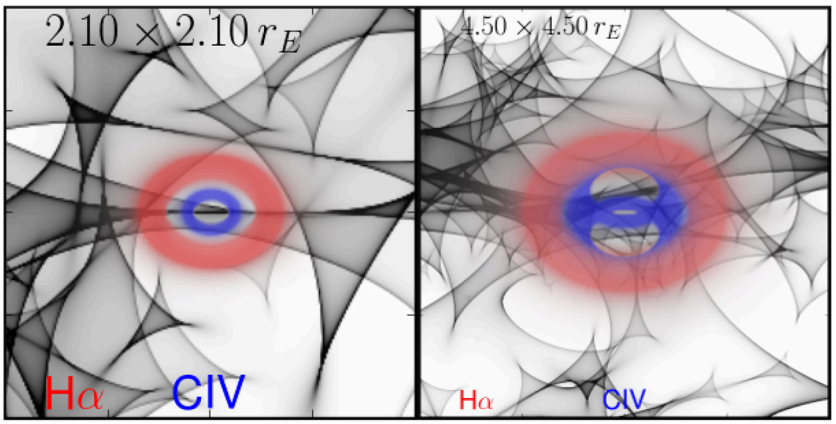

FIGURE 4 | Examples of models of the CIV and Hα BELRs and their location on the caustic network that simultaneously fit the microlensing observables μ^{cont}, μ^{BLR}, *RBI*, *WCI* measured for both the CIV and Hα lines in the lensed quasar Q2237+030. **Left**: Keplerian disks for both Hα and CIV BELRs. **Right**: Keplerian disk for Hα and polar wind for CIV. All models are seen under intermediate inclination, $i = 44°$. The CIV emitting region (in blue) is more compact than the Hα emitting region (in red).

or a polar wind. Examples of fitting models are illustrated in **Figure 4**. In all cases the Hα BELR is roughly a factor 2 larger than the CIV BELR. Recent results from velocity-resolved reverberation mapping also suggest that the low-ionization BELR can be a Keplerian disk (Grier et al., 2017, and references therein).

4. CONCLUSIONS

These results demonstrate the potential of microlensing to probe the geometry and kinematics of the broad line regions and outflows in quasars. Constraints on the location of the scattering regions at the origin of the polarization can also be obtained. Simulations of line profile distortions show that only strong microlensing effects can produce line profile distortions allowing us to discriminate between various BELR models using single epoch data. To benefit from weaker microlensing effects, statistical analyses of larger data sets would be needed. In particular, a long-term spectrophotometric monitoring of the different images of lensed quasars would provide a real scan of their line emitting regions, with the possibility to constrain more complex models than those considered here. Microlensing can thus be a powerful and alternative approach to reverberation mapping, especially since it can be applied to high redshift quasars, with little dependence on their luminosity, and to the study of both the low- and high-ionization BLRs.

AUTHOR CONTRIBUTIONS

DH and DS initiated the project. LB, DH, DS, and TA contributed to the observations, data reduction and analysis. LB, DH, DS, and RG contributed to the BELR microlensing modeling. All authors contributed to the discussions. DH wrote the paper with contributions from DS. LB made the artwork in **Figure 3**.

ACKNOWLEDGMENTS

DH and LB acknowledge support of Belgian F.R.S.-FNRS. Support for TA is provided by project FONDECYT 11130630 and the Ministry of Economy, Development, and Tourism's Millennium Science Initiative through grant IC120009, awarded to The Millennium Institute of Astrophysics, MAS.

REFERENCES

Abajas, C., Mediavilla, E., Muñoz, J. A., Gómez-Álvarez, P., and Gil-Merino, R. (2007). Microlensing of a biconical broad-line region. *Astrophys. J.* 658, 748–762. doi: 10.1086/511023

Abajas, C., Mediavilla, E., Muñoz, J. A., Popović, L. Č., and Oscoz, A. (2002). The influence of gravitational microlensing on the broad emission lines of quasars. *Astrophys. J.* 576, 640–652. doi: 10.1086/341793

Angonin, M.-C., Vanderriest, C., Remy, M., and Surdej, J. (1990). First spectroscopic evidence of microlensing on a BAL quasar? The case of H 1413+117. *Astron. Astrophys.* 233, L5–L8.

Anguita, T., Schmidt, R. W., Turner, E. L., Wambsganss, J., Webster, R. L., Loomis, K. A., et al. (2008). The multiple quasar Q2237+0305 under a microlensing caustic. *Astron. Astrophys.* 480, 327–334. doi: 10.1051/0004-6361:20078221

Borguet, B., and Hutsemékers, D. (2010). A polar+equatorial wind model for broad absorption line quasars. I. Fitting the C IV BAL profiles. *Astron. Astrophys.* 515:A22. doi: 10.1051/0004-6361/200913255

Braibant, L., Hutsemékers, D., Sluse, D., and Anguita, T. (2016). The different origins of high- and low-ionization broad emission lines revealed by gravitational microlensing in the Einstein cross. *Astron. Astrophys.* 592:A23. doi: 10.1051/0004-6361/201628594

Braibant, L., Hutsemékers, D., Sluse, D., Anguita, T., and García-Vergara, C. J. (2014). Microlensing of the broad-line region in the quadruply imaged quasar HE0435-1223. *Astron. Astrophys.* 565:L11. doi: 10.1051/0004-6361/201423633

Braibant, L., Hutsemékers, D., Sluse, D., and Goosmann, R. (2017). Constraining the geometry and kinematics of the quasar broad emission line region using gravitational microlensing. I. Models and simulations. arXiv:1707.09159.

Chae, K.-H., Turnshek, D. A., Schulte-Ladbeck, R. E., Rao, S. M., and Lupie, O. L. (2001). Hubble space telescope observations of the gravitationally lensed cloverleaf broad absorption line QSO H1413+1143: imaging polarimetry and evidence for microlensing of a scattering region. *Astrophys. J.* 561, 653–659. doi: 10.1086/323318

Goicoechea, L. J., and Shalyapin, V. N. (2016). Gravitational lens system SDSS J1339+1310: microlensing factory and time delay. *Astron. Astrophys.* 596:A77. doi: 10.1051/0004-6361/201628790

Grier, C. J., Pancoast, A., Barth, A. J., Fausnaugh, M. M., Brewer, B. J., Treu, T., et al. (2017). The structure of the broad-line region in active galactic nuclei. II. Dynamical modeling of data from the AGN10 reverberation mapping campaign. arXiv:1705.02346.

Guerras, E., Mediavilla, E., Jimenez-Vicente, J., Kochanek, C. S., Muñoz, J. A., Falco, E., and Motta, V. (2013). Microlensing of quasar broad emission lines: constraints on broad line region size. *Astrophys. J.* 764:160. doi: 10.1088/0004-637X/764/2/160

Hutsemékers, D. (1993). Selective gravitational microlensing and line profile variations in the BAL quasar H 1413+117. *Astron. Astrophys.* 280, 435–442.

Hutsemékers, D., Borguet, B., Sluse, D., Riaud, P., and Anguita, T. (2010). Microlensing in H1413+117: disentangling line profile emission and absorption in a broad absorption line quasar. *Astron. Astrophys.* 519:A103. doi: 10.1051/0004-6361/200913247

Hutsemékers, D., Sluse, D., Braibant, L., and Anguita, T. (2015). Polarization microlensing in the quadruply imaged broad absorption line quasar H1413+117. *Astron. Astrophys.* 584:A61. doi: 10.1051/0004-6361/201527243

Hutsemékers, D., Surdej, J., and van Drom, E. (1994). The use of gravitational microlensing to scan the structure of BAL QSOs. *Astrophys. Space Sci.* 216, 361–365. doi: 10.1007/BF00982519

Lewis, G. F., and Ibata, R. A. (2004). Gravitational microlensing of quasar broad-line regions at large optical depths. *Month. Notices R. Astron. Soc.* 348, 24–33. doi: 10.1111/j.1365-2966.2004.07349.x

Motta, V., Mediavilla, E., Rojas, K., Falco, E. E., Jiménez-Vicente, J., and Muñoz, J. A. (2017). Probing the Broad-line Region and the Accretion Disk in the Lensed Quasars HE 0435-1223, WFI 2033-4723, and HE 2149-2745 Using Gravitational Microlensing. *Astrophys. J.* 835:132. doi: 10.3847/1538-4357/835/2/132

Nemiroff, R. J. (1988). AGN broad emission line amplification from gravitational microlensing. *Astrophys. J.* 335, 593–605. doi: 10.1086/166951

O'Dowd, M., Bate, N. F., Webster, R. L., Wayth, R., and Labrie, K. (2011). Differential microlensing measurements of quasar broad-line kinematics in Q2237+0305. *Month. Notices R. Astron. Soc.* 415, 1985–1998. doi: 10.1111/j.1365-2966.2010.18119.x

O'Dowd, M. J., Bate, N. F., Webster, R. L., Labrie, K., and Rogers, J. (2015). Microlensing constraints on broad absorption and emission line flows in the Quasar H1413+117. *Astrophys. J.* 813:62. doi: 10.1088/0004-637X/813/1/62

Popović, L. Č., Mediavilla, E. G., and Muñoz, J. A. (2001). The influence of microlensing on spectral line shapes generated by a relativistic accretion disc. *Astron. Astrophys.* 378, 295–301. doi: 10.1051/0004-6361:20011169

Richards, G. T., Keeton, C. R., Pindor, B., Hennawi, J. F., Hall, P. B., Turner, E. L., et al. (2004). Microlensing of the Broad Emission Line Region in the Quadruple Lens SDSS J1004+4112. *Astrophys. J.* 610, 679–685. doi: 10.1086/421868

Schmidt, R. W., and Wambsganss, J. (2010). Quasar microlensing. *General Relat. Gravit.* 42, 2127–2150. doi: 10.1007/s10714-010-0956-x

Schneider, P., and Wambsganss, J. (1990). Are the broad emission lines of quasars affected by gravitational microlensing? *Astron. Astrophys.* 237, 42–53.

Simić, S., and Popović, L. Č. (2014). Broad spectral line and continuum variabilities in QSO spectra induced by microlensing of diffusive massive substructure. *Adv. Space Res.* 54, 1439–1447. doi: 10.1016/j.asr.2013.11.016

Sluse, D., Claeskens, J.-F., Hutsemékers, D., and Surdej, J. (2007). Multi-wavelength study of the gravitational lens system RXS J1131-1231. III. Long slit spectroscopy: micro-lensing probes the QSO structure. *Astron. Astrophys.* 468, 885–901. doi: 10.1051/0004-6361:20066821

Sluse, D., Hutsemékers, D., Anguita, T., Braibant, L., and Riaud, P. (2015). Evidence for two spatially separated UV continuum emitting regions in the Cloverleaf broad absorption line quasar. *Astron. Astrophys.* 582:A109. doi: 10.1051/0004-6361/201526832

Sluse, D., Hutsemékers, D., Courbin, F., Meylan, G., and Wambsganss, J. (2012). Microlensing of the broad line region in 17 lensed quasars. *Astron. Astrophys.* 544:A62. doi: 10.1051/0004-6361/201219125

Sluse, D., Schmidt, R., Courbin, F., Hutsemékers, D., Meylan, G., Eigenbrod, A., et al. (2011). Zooming into the broad line region of the gravitationally lensed quasar QSO 2237+0305 ≡ the Einstein Cross. III. Determination of the size and structure of the C iv and C iii] emitting regions using microlensing. *Astron. Astrophys.* 528:A100. doi: 10.1051/0004-6361/201016110

Wayth, R. B., O'Dowd, M., and Webster, R. L. (2005). A microlensing measurement of the size of the broad emission-line region in the lensed quasar QSO 2237+0305. *Month. Notices R. Astron. Soc.* 359, 561–566. doi: 10.1111/j.1365-2966.2005.08919.x

Conflict of Interest Statement: The authors declare that the research was conducted in the absence of any commercial or financial relationships that could be construed as a potential conflict of interest.

Copyright © 2017 Hutsemékers, Braibant, Sluse, Anguita and Goosmann. This is an open-access article distributed under the terms of the Creative Commons Attribution License (CC BY). The use, distribution or reproduction in other forums is permitted, provided the original author(s) or licensor are credited and that the original publication in this journal is cited, in accordance with accepted academic practice. No use, distribution or reproduction is permitted which does not comply with these terms.

frontiers in Astronomy and Space Sciences

ORIGINAL RESEARCH
published: 31 October 2017
doi: 10.3389/fspas.2017.00030

Disentangling Accretion Disk and Dust Emissions in the Infrared Spectrum of Type 1 AGN

Antonio Hernán-Caballero[1,2]*, *Evanthia Hatziminaoglou*[2], *Almudena Alonso-Herrero*[3] *and Silvia Mateos*[4]

[1] Departamento de Astrofísica y CC. de la Atmósfera, Facultad de CC. Físicas, Universidad Complutense de Madrid, Madrid, Spain, [2] European Southern Observatory, Garching bei München, Germany, [3] Centro de Astrobiología (CSIC-INTA), Madrid, Spain, [4] Instituto de Física de Cantabria (CSIC-UC), Santander, Spain

We use a semi-empirical model to reproduce the 0.1–10 μm spectral energy distribution (SED) of a sample of 85 luminous quasars. In the model, the continuum emission from the accretion disk as well as the nebular lines are represented by a single empirical template (disk), where differences in the optical spectral index are reproduced by varying the amount of extinction. The near- and mid-infrared emission of the AGN-heated dust is modeled as the combination of two black-bodies (dust). The model fitting shows that the disk and dust components are remarkably uniform among individual quasars, with differences in the observed SED largely accounted for by varying levels of obscuration in the disk as well as differences in the relative luminosity of the disk and dust components. By combining the disk-subtracted SEDs of the 85 quasars, we generate a template for the 1–10 μm emission of the AGN-heated dust. Additionally, we use a sample of local Seyfert 1 galaxies with full spectroscopic coverage in the 0.37–39 μm range to demonstrate a method for stitching together spectral segments obtained with different PSF and extraction apertures. We show that the disk and dust templates obtained from luminous quasars also reproduce the optical-to-mid-infrared spectra of local Seyfert 1s when the contribution from the host galaxy is properly subtracted.

Keywords: galaxies:active, galaxies:Seyfert, quasars:general, infrared:galaxies, methods:data analysis, techniques:spectroscopic

OPEN ACCESS

Edited by:
Ascensión Del Olmo, Consejo Superior de Investigaciones Científicas (CSIC), Spain

Reviewed by:
Isabel Marquez Perez, Instituto de Astrofísica de Andalucía (CSIC), Spain
Øyvind Geelmuyden Grøn, Oslo and Akershus University College, Norway

***Correspondence:**
Antonio Hernán-Caballero
a.hernan@ucm.es

Specialty section:
This article was submitted to Cosmology, a section of the journal Frontiers in Astronomy and Space Sciences

Received: *23 August 2017*
Accepted: *11 October 2017*
Published: *31 October 2017*

Citation:
Hernán-Caballero A, Hatziminaoglou E, Alonso-Herrero A and Mateos S (2017) Disentangling Accretion Disk and Dust Emissions in the Infrared Spectrum of Type 1 AGN. Front. Astron. Space Sci. 4:30. doi: 10.3389/fspas.2017.00030

1. OBTAINING ACCRETION DISK AND DUST TEMPLATES FROM LUMINOUS QUASARS

We use a sample of 85 luminous quasars ($\nu L_\nu[3\,\mu\mathrm{m}]>10^{45.5}$ erg s^{-1}) selected for their spectroscopic coverage (AKARI and/or Spitzer/IRS) in the rest-frame 2.5–10 μm range. In addition to the AKARI and Spitzer spectroscopy we obtain optical photometry from the Sloan Digital Sky Survey (SDSS) Data Release 12, near-infrared (NIR) photometry from the Two Micron All Sky Survey (2MASS), the VISTA Hemisphere Survey (VHS), and the UKIRT Infrared Deep Sky Survey (UKIDSS), and mid-infrared photometry in 4 bands from WISE (see Hernán-Caballero et al., 2016, for details).

In such luminous quasars the optical emission of the AGN easily outshines that of the host galaxy. The emission from dust is expected to be negligible at $\lambda \lesssim 0.85\,\mu$m because the maximum temperature of dust grains is limited by sublimation to ∼1,500 K (Granato and Danese, 1994). As a

consequence, only the accretion disk and the emission lines from the broad line region (BLR) and narrow line region (NLR) contribute significantly to the rest-frame 0.1–0.85 μm spectrum.

In Hernán-Caballero et al. (2016) we showed that a single empirical quasar template like that of Shen (2016) suffices to model the rest-frame UV-optical (0.1–0.85 μm) SED of luminous quasars if we allow for an adjustable extinction to reproduce the diversity in optical spectral indices among individual quasars. To extend the template into the NIR and MIR ranges, we assumed that the disk emission follows a power-law with the theoretical slope $\alpha = 1/3$ predicted for a locally heated optically thick disk (e.g., Shakura and Sunyaev, 1973; Hubeny et al., 2001) and confirmed through polarized light observations (Kishimoto et al., 2008). We also added to the new template the NIR nebular lines extracted from the quasar template of Glikman et al. (2006).

We fit the rest-frame 0.1–10 μm SED of the 85 quasars with a two component disk+dust model. The disk component (plus nebular lines) is represented by the template described above, modified by an adjustable level of extinction with a wavelength dependency following the Small Magellanic Cloud Bar extinction law (Gordon et al., 2003). This law is often used to de-redden quasars (e.g., Hopkins et al., 2004; Glikman et al., 2012) since it lacks the 2,175 Å absorption feature. The AGN-heated dust component is represented by the linear combination of two black-bodies (hot and warm) at adjustable temperatures within the intervals 850–2,000 K and 150–900 K, respectively.

Figure 1 shows examples of the best-fitting disk+dust decomposition model for a representative sub-sample of the 85 quasars. The residuals of the fit around ∼10% are consistent with the photometric uncertainties. We find a systematic excess emission in the 1.0–1.5 μm range relative to the model. The median, mean, and standard deviation of the excess at restframe 1.2 μm is 32, 40, and 33%, respectively. This is comparable to the values found in Hernán-Caballero et al. (2016) in spite of the stronger NIR continuum and inclusion of NIR nebular lines in the new disk template, supporting our previous claim that the excess originates in the dust component.

The distributions of A_V for the extinction of the accretion disk and the relative luminosity of the dust and disk components (represented by the luminosity ratio between $\lambda = 3.0$ μm and $\lambda = 0.5$ μm) are shown in **Figure 2**. Negative values of A_V are needed to model the disk of the bluest ∼25% of quasars because the disk template is an average of observed spectra that have not been de-reddened. Therefore the extinction values obtained in the fit are relative to the (unknown) average extinction of the sample in Shen (2016). Moderate values of A_V (between −0.2 and 0.2 mag) fit all but the reddest 15% of quasars. The $\nu L_\nu(3\mu m)/\nu L_\nu(0.5\mu m)$ ratio peaks at ∼1, indicating that the peak luminosities of the disk and dust components are typically similar, albeit the full range of variation being a whole order of magnitude.

Figure 3 shows the infrared SEDs of the individual quasars, normalized at rest-frame 3 μm, after subtraction of the disk component. The SEDs show little dispersion (<0.3 dex) between ∼1.5 and ∼6 μm, suggesting a largely invariable spectrum for the hot dust, that is consistent with black-body emission at a temperature close to the grain sublimation limit. The dispersion increases at longer wavelengths at least in part due to the

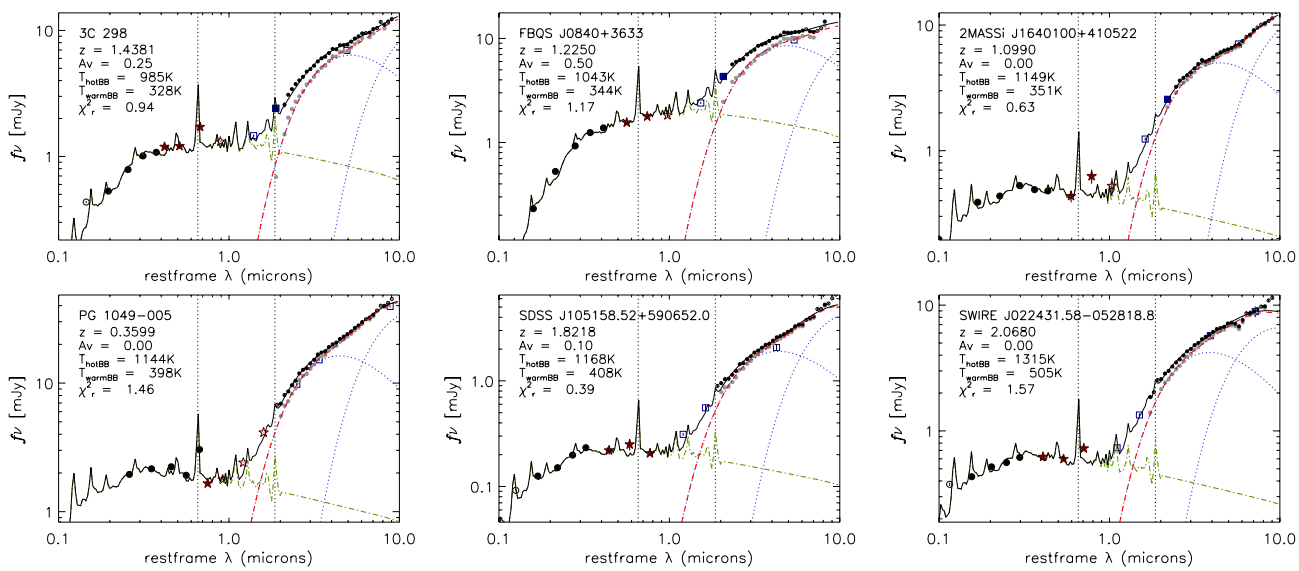

FIGURE 1 | Spectral energy distributions and their best fitting disk+dust models for a representative subsample of the luminous quasar sample showing a range of A_V and dust-to-disk luminosity ratios. Circles, stars, and squares represent, respectively, broadband photometry in the observed-frame optical (from SDSS), NIR (2MASS/UKIDSS/VHS), and MIR (WISE). Open symbols indicate bands outside the wavelength range used to fit the disk or dust components. The disk model is shown as a green dot-dashed line. The (AKARI+)IRS spectrum resampled at $\Delta\lambda/\lambda = 0.05$ is shown with small black dots. Gray dots below the (AKARI+)IRS spectrum represent the dust spectrum obtained after subtraction of the disk component. The model for the AGN-heated dust emission (red dashed line) is the linear combination of two black-bodies at adjustable temperatures (blue dotted lines). The combined disk+dust model is represented by the solid black line. The vertical dotted lines indicate the rest-frame wavelength of the recombination lines Hα and Paα.

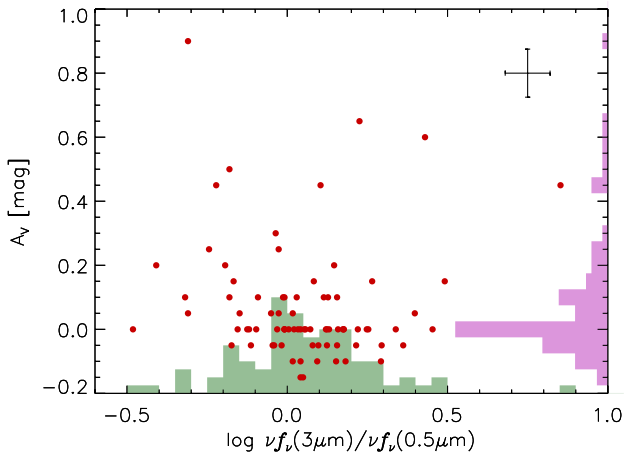

FIGURE 2 | Distribution of the extinction level applied to the disk component in the best fitting model and the dust-to-disk luminosity ratio for the whole sample of luminous quasars. Error bars in the top right corner indicate the typical uncertainties.

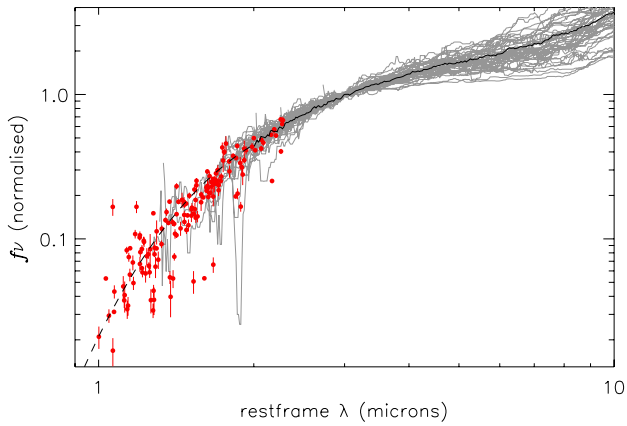

FIGURE 3 | Infrared SEDs of the individual quasars in the sample after subtraction of the disk component. The gray lines represent the (AKARI+)IRS spectrum, while the red dots represent the broadband data points at wavelengths with no spectroscopic coverage. All the individual SEDs are normalized at rest-frame 3 μm. The solid black line is the composite AKARI+IRS spectrum obtained for the same sample in Hernán-Caballero et al. (2016). The dashed black line is an extrapolation of this composite using a T = 1,400 K black-body spectrum.

onset of the broad silicate feature (which may be in emission or absorption). On the other hand, the larger dispersion at $\lambda \lesssim 1.5\,\mu$m is a consequence of the uncertainty introduced by the subtraction of a disk component that is increasingly dominant at shorter wavelengths.

We obtain a template for the AGN-heated dust by averaging the AKARI+IRS spectra of the individual quasars. At $\lambda < 2\,\mu$m only a few quasars have spectroscopic coverage, therefore we rely on the disk-subtracted broadband photometry to extend the template to $\lambda < 2\,\mu$m. We find that a 1,400 K black-body is consistent with most of the broadband data-points.

2. APPLICATION TO LOCAL SEYFERT 1 GALAXIES

To test whether the templates for disk and dust emission obtained for luminous quasars are also representative of the nuclear emission in less luminous type 1 AGN, we have performed spectral decomposition of a sample of 13 local ($z < 0.07$) Seyferts and quasars with rest-frame 3μm luminosities in the range $10^{42.8-44.4}$ erg s^{-1}. The sample is a subset of the 23 broad-emission line AGN observed by Landt et al. (2008). We chose this sample because they obtained nearly simultaneous spectra in the optical (0.37–0.75 μm) and NIR (0.8–2.4 μm) with the FAST and SpeX spectrographs on the Tillinghast 1.5 m telescope and the NASA Infrared Telescope Facility, respectively. Out of their 23 sources, we select only the 13 that also have AKARI 2.5–5.0 μm spectra from (Kim et al., 2015) and Spitzer/IRS 5.2–39 μm spectra in the CASSIS (Lebouteiller et al., 2011, 2015) or ATLAS-IRS (Hernán-Caballero and Hatziminaoglou, 2011) databases. Therefore we have continuous spectroscopic coverage from ∼0.35 to ∼35 μm in the restframe. However, since our templates are not defined beyond 10 μm, we perform the spectral decomposition only in the ∼0.35–10 μm range.

Spectral decomposition on local type 1 AGN is more challenging compared to luminous quasars because the emission from the host galaxy is no longer negligible. The contribution from the stars to the total flux is important only at optical and NIR wavelengths, while the emission of the interstellar medium (ISM), in particular dust grains and aromatic hydrocarbons, is significant only in the mid-infrared. Since the integrated spectrum of the stars in a galaxy peaks at 1.6 μm and its NIR shape does not vary substantially among the different spectral types, we can use a single template to represent the stellar emission of the host galaxy in all the sources. We choose the S0 galaxy template from Polletta et al. (2007). In the optical, the actual spectra of the host galaxies may diverge from the template at shorter wavelengths depending on the age and extinction of the stellar population, but the difference only becomes important at $\lambda \lesssim 0.4\,\mu$m.

Another difficulty in decomposing local galaxies is that while the AGN emission is always spatially unresolved, the host galaxy is extended and its contribution to the observed spectrum depends on the spatial resolution of the observations and the size of the extraction aperture (see Hernán-Caballero et al., 2015 for a discussion). The extraction aperture of the slit-less AKARI observations (60″ × 7.5″) is wider than the IRS slit (3.6″ for SL1 and SL2 modules), and both are larger than those of the FAST (3″) and SpeX (0.8″) observations. To compensate for this, we compute the best-fitting disk+dust+stellar model for the local AGN as follows: for each of the four spectral segments (FAST, SpeX, AKARI, IRS) we obtain the values of the parameters that minimize the residuals while fitting by least squares the model:

$$F(\lambda) = af_{disk}(\lambda)e^{-A_V\tau(\lambda)} + bf_{dust}(\lambda) + cf_{star}(\lambda) \qquad (1)$$

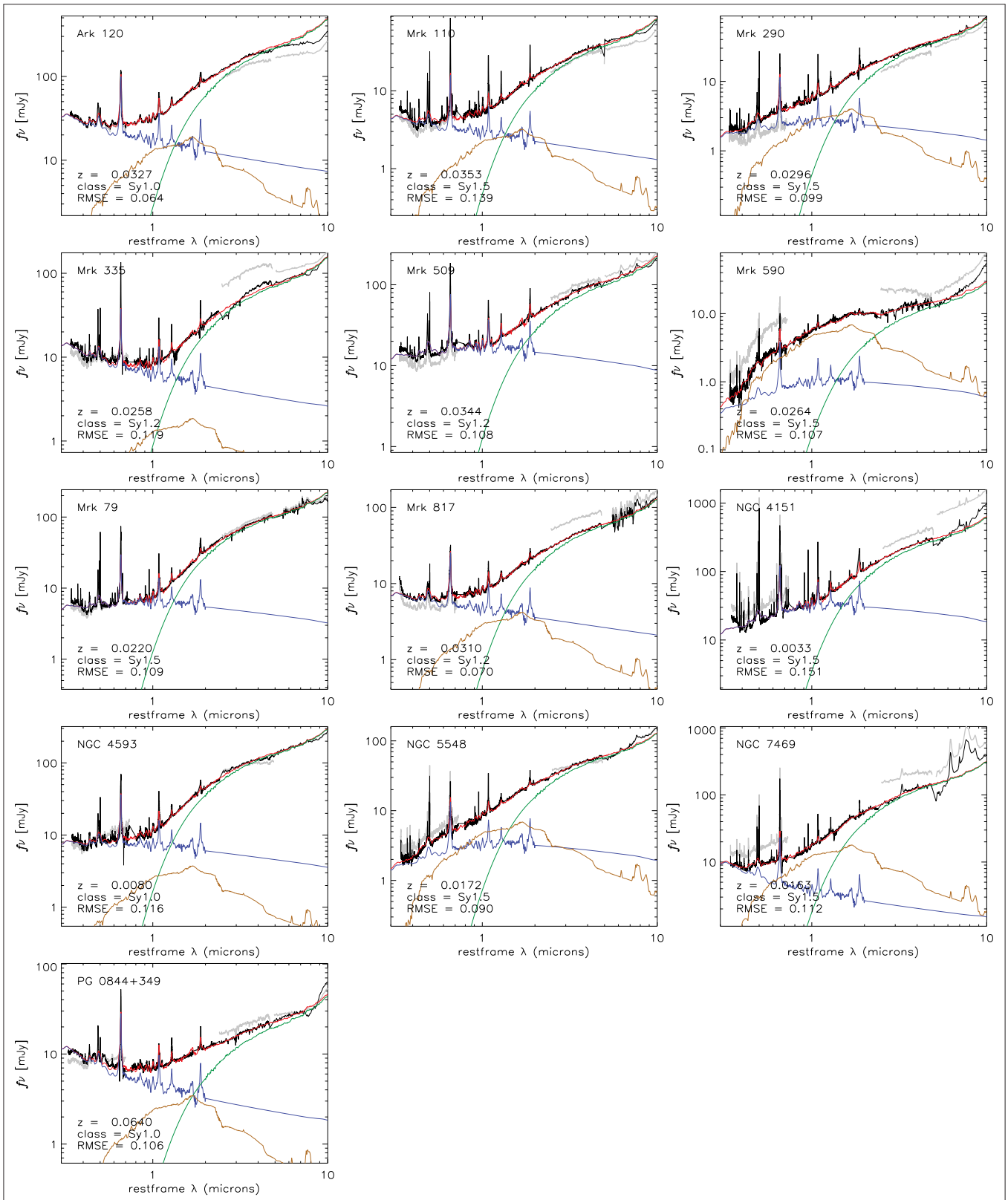

FIGURE 4 | Spectral decompositions of local type 1 AGN. The gray thick lines represent spectral segments from observations with FAST, SpeX, AKARI, and IRS. The black line is the stitched spectrum. The red line is the best fitting disk+dust+stellar model for the stitched spectrum, while the blue, green, and yellow lines represent the individual disk, dust, and host galaxy components.

where $f_{disk}(\lambda)$, $f_{dust}(\lambda)$, and $f_{star}(\lambda)$ are the templates and $e^{-A_V\tau(\lambda)}$ is the extinction correction for the disk template. The coefficients a, b, and A_V must be the same for all four spectral segments, but coefficient c may take different values in each segment to compensate for the different amounts of host galaxy light in each aperture. We also apply a scaling factor between 0.7 and 1.3 to the fluxes in the FAST, AKARI and IRS segments to correct for any potential biases in the absolute flux calibration of up to ∼30% relative to the SpeX spectrum. The values of these scaling factors are treated as free parameters in the fitting algorithm and they are computed independently for each source.

We use the coefficients in the best fitting model to obtain a stitched spectrum that merges the FAST, SpeX, AKARI, and IRS segments. For this we first multiply each segment (except the SpeX one, which is taken as reference) by its corresponding scaling factor, and then subtract the excess stellar component given by:

$$\Delta F^i_{star}(\lambda) = (c^i - c^{SpeX}) f_{star}(\lambda) \quad (2)$$

where the superscript i indicates the spectral segment. The resulting stitched spectrum corresponds to our prediction of the spectrum that would be observed if all the segments had the same PSF, were extracted in the same aperture, and had perfectly consistent absolute calibrations.

We evaluate the quality of the fits using the normalized root mean square error (RMSE), defined as:

$$RMSE = \sqrt{\frac{1}{N}\sum_i^N \frac{(f_i - F(\lambda_i))^2}{f_i^2}} \quad (3)$$

where f_i and $F(\lambda_i)$ are the flux densities at wavelength λ_i in the stitched spectrum and the model, respectively. This statistic represents the typical relative residual between the stitched spectrum and the model, and is more informative than χ^2 in situations where residuals are not dominated by noise but differences between the model and the intrinsic spectrum of the source (Hernán Caballero, 2012; Hernán-Caballero et al., 2015).

Figure 4 shows the original and stitched spectra for the 13 sources in the sample, as well as the best fitting decomposition into disk, dust, and stellar components. The contribution from the stellar component to the total emission varies from negligible (e.g., Mrk 79, Mrk 509, and Mrk 335) to dominant (e.g., Mrk 590), while the interstellar emission is negligible in all but NGC 7469. There is no obvious correlation between the spectral class (Seyfert types 1.0, 1.2, and 1.5) and model parameters such as A_V of the disk or the relative luminosities of the components, albeit the sample size is too small to draw any strong conclusions. The fits are remarkably good for most sources (typical RMSE ∼10%), with significant discrepancies arising only at very short ($\lambda < 0.4\,\mu$m) and long ($\lambda > 7$–$8\,\mu$m) wavelengths. This suggests that the optical and NIR spectrum of the disk and dust emissions are relatively uniform among type 1 AGN regardless of luminosity. The discrepancies at short wavelength may be caused by uncertainty in the extinction affecting the disk component due to lack of restframe-UV observations, as well as increasing discrepancy between the assumed template for the stellar population and the actual spectrum of the host at short wavelengths. Discrepancies at $\lambda > 7$–$8\,\mu$m are caused by source-to-source variation in the strength of the mid-infrared aromatic features relative to the stellar continuum, and in some cases like Mrk 590, NGC 4151, and PG 0844+349, an unusually strong silicate emission feature at ∼10 μm. Hatziminaoglou et al. (2015) showed that accurate modeling of the mid-infrared spectrum of Seyfert 1 s requires a different approach, splitting the stellar and ISM emissions into separate spectral components and using multiple dust templates with different spectral indices and silicate strengths.

AUTHOR CONTRIBUTIONS

AH selected the sample, performed most of the data analysis, and wrote the manuscript. EH compiled the broadband observations, contributed to the data analysis and corrected the manuscript. AA and SM contributed to the discussion of the analysis and results and provided further corrections to the manuscript.

FUNDING

This work was funded through the Spanish Ministry of Economy and Competitiveness (MINECO) grants AYA2015-70815-ERC, AYA2015-63650-P, and AYA2015-64346-C2-1-P.

ACKNOWLEDGMENTS

AH acknowledges support from the ESO Scientific Visitor Programme. This work is based on observations made with the *Spitzer Space Telescope*, which is operated by the Jet Propulsion Laboratory, Caltech under NASA contract 1407. The Cornell Atlas of *Spitzer*/IRS Sources (CASSIS) is a product of the Infrared Science Center at Cornell University, supported by NASA and JPL. This publication makes use of data products from the Two Micron All Sky Survey, which is a joint project of the University of Massachusetts and the Infrared Processing and Analysis Center/California Institute of Technology, funded by the National Aeronautics and Space Administration and the National Science Foundation. This research has made use of the NASA/IPAC Infrared Science Archive, which is operated by the Jet Propulsion Laboratory, California Institute of Technology, under contract with the National Aeronautics and Space Administration.

REFERENCES

Glikman, E., Helfand, D. J., and White, R. L. (2006). A near-infrared spectral template for quasars. *Astrophys. J.* 640, 579–591. doi: 10.1086/500098

Glikman, E., Urrutia, T., Lacy, M., Djorgovski, S. G., Mahabal, A., Myers, A. D., et al. (2012). FIRST-2MASS red quasars: transitional objects emerging from the dust. *Astrophys. J.* 757:51. doi: 10.1088/0004-637X/757/1/51

Gordon, K. D., Clayton, G. C., Misselt, K. A., Landolt, A. U., and Wolff, M. J. (2003). A quantitative comparison of the small magellanic cloud, large magellanic cloud, and milky way ultraviolet to near-infrared extinction curves. *Astrophys. J.* 594, 279–293. doi: 10.1086/376774

Granato, G. L., and Danese, L. (1994). Thick tori around active galactic nuclei - a comparison of model predictions with observations of the infrared continuum and silicate features. *Month. Notices R. Astron. Soc.* 268:235.

Hatziminaoglou, E., Hernán-Caballero, A., Feltre, A., and Piñol Ferrer, N. (2015). A complete census of silicate features in the mid-infrared spectra of active galaxies. *Astrophys. J.* 803:110. doi: 10.1088/0004-637X/803/2/110

Hernán Caballero, A. (2012). Automated measurement of redshifts from mid-infrared low-resolution spectroscopy. *Month. Notices R. Astron. Soc.* 427, 816–827. doi: 10.1111/j.1365-2966.2012.22047.x

Hernán-Caballero, A., Alonso-Herrero, A., Hatziminaoglou, E., Spoon, H. W. W., Ramos Almeida, C., Díaz Santos, T., et al. (2015). Resolving the AGN and host emission in the mid-infrared using a model-independent spectral decomposition. *Astrophys. J.* 803:109. doi: 10.1088/0004-637X/803/2/109

Hernán-Caballero, A., and Hatziminaoglou, E. (2011). An atlas of mid-infrared spectra of star-forming and active galaxies. *Month. Notices R. Astron. Soc.* 414, 500–511. doi: 10.1111/j.1365-2966.2011.18413.x

Hernán-Caballero, A., Hatziminaoglou, E., Alonso-Herrero, A., and Mateos, S. (2016). The near-to-mid infrared spectrum of quasars. *Month. Notices R. Astron. Soc.* 463, 2064–2078. doi: 10.1093/mnras/stw2107

Hopkins, P. F., Strauss, M. A., Hall, P. B., Richards, G. T., Cooper, A. S., Schneider, D. P., et al. (2004). Dust reddening in sloan digital sky survey quasars. *Astron. J.* 128, 1112–1123. doi: 10.1086/423291

Hubeny, I., Blaes, O., Krolik, J. H., and Agol, E. (2001). Non-LTE models and theoretical spectra of accretion disks in active galactic nuclei. IV. Effects of compton scattering and metal opacities. *Astrophys. J.* 559, 680–702. doi: 10.1086/322344

Kim, D., Im, M., Kim, J. H., Jun, H. D., Woo, J.-H., Lee, H. M., et al. (2015). The AKARI 2.5-5.0 μm spectral atlas of type-1 active galactic nuclei: black hole mass estimator, line ratio, and hot dust temperature. *Astrophys. J. Suppl.* 216:17. doi: 10.1088/0067-0049/216/1/17

Kishimoto, M., Antonucci, R., Blaes, O., Lawrence, A., Boisson, C., Albrecht, M., et al. (2008). The characteristic blue spectra of accretion disks in quasars as uncovered in the infrared. *Nature* 454, 492–494. doi: 10.1038/nature07114

Landt, H., Bentz, M. C., Ward, M. J., Elvis, M., Peterson, B. M., Korista, K. T., et al. (2008). The near-infrared broad emission line region of active galactic nuclei. I. The observations. *Astrophys. J. Suppl.* 174, 282–312. doi: 10.1086/522373

Lebouteiller, V., Barry, D. J., Goes, C., Sloan, G. C., Spoon, H. W. W., Weedman, D. W., et al. (2015). CASSIS: the cornell atlas of *spitzer/infrared* spectrograph sources. II. High-resolution observations. *Astrophys. J. Suppl.* 218:21. doi: 10.1088/0067-0049/218/2/21

Lebouteiller, V., Barry, D. J., Spoon, H. W. W., Bernard-Salas, J., Sloan, G. C., Houck, J. R., et al. (2011). CASSIS: the cornell atlas of *spitzer/infrared* spectrograph sources. *Astrophys. J. Suppl.* 196:8. doi: 10.1088/0067-0049/196/1/8

Polletta, M., Tajer, M., Maraschi, L., Trinchieri, G., Lonsdale, C. J., Chiappetti, L., et al. (2007). Spectral energy distributions of hard X-ray selected active galactic nuclei in the XMM-newton medium deep survey. *Astrophys. J.* 663, 81–102. doi: 10.1086/518113

Shakura, N. I., and Sunyaev, R. A. (1973). Black holes in binary systems. Observational appearance. *Astron. Astrophys.* 24, 337–355. doi: 10.1007/978-94-010-2585-0_13

Shen, Y. (2016). Rest-frame optical properties of luminous $1.5 < Z < 3.5$ quasars: the Hβ-[O III] region. *Astrophys. J.* 817:55. doi: 10.3847/0004-637X/817/1/55

Conflict of Interest Statement: The authors declare that the research was conducted in the absence of any commercial or financial relationships that could be construed as a potential conflict of interest.

Copyright © 2017 Hernán-Caballero, Hatziminaoglou, Alonso-Herrero and Mateos. This is an open-access article distributed under the terms of the Creative Commons Attribution License (CC BY). The use, distribution or reproduction in other forums is permitted, provided the original author(s) or licensor are credited and that the original publication in this journal is cited, in accordance with accepted academic practice. No use, distribution or reproduction is permitted which does not comply with these terms.

frontiers in Astronomy and Space Sciences

ORIGINAL RESEARCH
published: 06 February 2018
doi: 10.3389/fspas.2018.00002

NGC 1275: An Outlier of the Black Hole-Host Scaling Relations

Eleonora Sani[1], Federica Ricci[1,2], Fabio La Franca[2], Stefano Bianchi[2], Angela Bongiorno[3], Marcella Brusa[4,5], Alessandro Marconi[6,7], Francesca Onori[8], Francesco Shankar[9] and Cristian Vignali[4,5]*

[1] European Southern Observatory, Santiago de Chile, Chile, [2] Dipartimento di Matematica e Fisica, Università degli Studi Roma Tre, Rome, Italy, [3] Istituto Nazionale di Astrofisica Osservatorio Astronomico di Roma, Rome, Italy, [4] Dipartimento di Fisica e Astronomia, Università di Bologna, Bologna, Italy, [5] Istituto Nazionale di Astrofisica Osservatorio Astronomico di Bologna, Bologna, Italy, [6] Dipartimento di Fisica e Astronomia, Università degli Studi di Firenze, Firenze, Italy, [7] Istituto Nazionale di Astrofisica Osservatorio Astrofisico di Arcetri, Firenze, Italy, [8] SRON Netherlands Institute for Space Research, Utrecht, Netherlands, [9] Department of Physics and Astronomy, University of Southampton, Southampton, United Kingdom

The active galaxy NGC 1275 lies at the center of the Perseus cluster of galaxies, being an archetypal BH-galaxy system that is supposed to fit well with the M_{BH}-host scaling relations obtained for quiescent galaxies. Since it harbors an obscured AGN, only recently our group has been able to estimate its black hole mass. Here our aim is to pinpoint NGC 1275 on the less dispersed scaling relations, namely the M_{BH}-$\sigma_\star$ and $M_{BH} - L_{bul}$ planes. Starting from our previous work (Ricci et al., 2017a), we estimate that NGC 1275 falls well outside the intrinsic dispersion of the M_{BH}-$\sigma_\star$ plane being 1.2 dex (in black hole mass) displaced with respect to the scaling relations. We then perform a 2D morphological decomposition analysis on Spitzer/IRAC images at 3.6 μm and find that, beyond the bright compact nucleus that dominates the central emission, NGC 1275 follows a de Vaucouleurs profile with no sign of significant star formation nor clear merger remnants. Nonetheless, its displacement on the $M_{BH} - L_{3.6,bul}$ plane with respect to the scaling relation is as high as observed in the M_{BH}-$\sigma_\star$. We explore various scenarios to interpret such behaviors, of which the most realistic one is the evolutionary pattern followed by NGC 1275 to approach the scaling relation. We indeed speculate that NGC 1275 might be a specimen for those galaxies in which the black holes adjusted to its host.

Keywords: AGN1, AGN2, black hole mass, scaling realtions, infrared, NGC 1275

OPEN ACCESS

Edited by:
Paola Marziani, Osservatorio Astronomico di Padova (INAF), Italy

Reviewed by:
Brian Punsly, International Center for Relativistic Astrophysics, Italy
Edi Bon, Astronomical Observatory, Serbia

****Correspondence:***
Eleonora Sani
esani@eso.org

Specialty section:
This article was submitted to Milky Way and Galaxies, a section of the journal Frontiers in Astronomy and Space Sciences

Received: *15 November 2017*
Accepted: *11 January 2018*
Published: *06 February 2018*

Citation:
Sani E, Ricci F, La Franca F, Bianchi S, Bongiorno A, Brusa M, Marconi A, Onori F, Shankar F and Vignali C (2018) NGC 1275: An Outlier of the Black Hole-Host Scaling Relations. Front. Astron. Space Sci. 5:2. doi: 10.3389/fspas.2018.00002

1. OVERVIEW

Although active galactic nuclei (AGN) are divided in many flavors, the Unified Model (Antonucci, 1993) explains these observational properties with a line-of-sight-dependent scenario, in which a dusty torus makes the emission anisotropic. Nowadays however there is growing observational evidence that type 1 AGN (AGN1) and type 2 (AGN2) are actually characterized by intrinsically different physical properties [e.g., different luminosity functions (La Franca et al., 2005; Ueda et al., 2015); accretion rates (Winter et al., 2010); intrinsic X-ray luminosity and black hole (BH) masses (Tueller et al., 2008)]. Thanks to our new virial relation based on unbiased physical quantities, i.e., hard X-ray luminosity and Paβ emission line FWHM, we have been able to measure, for the first time, with virial methods the supermassive black hole mass (M_{BH}) of AGN2 (La Franca et al., 2015, 2016; Onori et al., 2017b), whose values have been up today estimated using scaling relations.

These relations are calibrated on AGN1 and are unlikely to hold also for all AGN2 (Graham, 2008). With direct virial masses for AGN2, we can investigate the relation between the M_{BH} and the bulge properties, thus putting a missing piece to the AGN/galaxy coevolution puzzle. By selecting unbiased samples of type 1 and type 2 AGN, we have found (Onori et al., 2017b) that in the luminosity range $42.5 < \log(L_X/erg\ s^{-1}) < 44.5$, where the two distributions of main AGN types overlap, AGN2 show, on average, significantly smaller Paβ and HeI FWHM than AGN1 (1,970 km/s instead of 3,400 km/s). As expected from the analysis of the FWHM distributions, it results that in this luminosity range, the average M_{BH} of the AGN2 sample $[\log(M_{BH}/M_\odot) = 7.08 \pm 0.10]$ is ~0.5 dex smaller than measured in the AGN1 sample $[\log(M_{BH}/M_\odot) = 7.61 \pm 0.01]$. In Ricci et al. (2017a) we have investigated the M_{BH}-$\sigma_\star$ relation and seen how AGN2 harbor less massive BHs than AGN1 at a given velocity dispersion, with BH masses of AGN2 $\sim$ 0.9 dex smaller than AGN1 at $\sigma_\star \sim 185$ km/s. Equivalently, AGN2 host galaxies have stellar velocity dispersions $\sim$ 0.2 dex higher than AGN1 hosts at $M_{BH} \sim 10^7$ $M_\odot$. Moreover, such feature is not related to the morphological type but could rather be intrinsic.

To further test this scenario, and to verify whether such a discrepancy holds also for other scaling relations still related to fundamental physical quantities, we are going to investigate the M_{BH} vs. bulge luminosity relation and we present here the case study of NGC 1275.

Throughout this paper we assume the standard cosmology with $H_0 = 70$ km/s/Mpc, $\Omega_M = 0.3$, $\Omega_\Lambda = 0.7$.

2. NGC 1275: PROPERTIES, AND BH MASS ESTIMATE

NGC 1275 is the brightest and most massive galaxy in the Perseus Cluster (Abell 426), it is a mildly star-forming early-type cD galaxy with a stellar mass of $M_\star = 2.43 \times 10^{11}$ $M_\odot$(Mathews et al., 2006), i.e., the archetypal BH-galaxy system that is supposed to fit well with the M_{BH}-host scaling relations obtained for quiescent galaxies. By adopting such stellar mass and the M_{BH}-$M_\star$ relation of Sani et al. (2011) (see their Equation 8), one would expect a BH mass of 2.9×10^8 $M_\odot$. Here we want to verify whether such estimate is consistent with direct measurements and investigate the locus of NGC 1275 over the M_{BH}-$\sigma_\star$ and M_{BH}-$L_{3.6,bul}$ scaling relations. Since it also harbor a partially obscured/faint AGN, it represents an excellent laboratory to examine the intrinsic differences between AGN1, AGN2, and quiescent BH.

A direct M_{BH} measurement by means of molecular gas kinematics is discussed by Wilman et al. (2005) and more recently by Scharwächter et al. (2013), the latter having the advance of a spatial resolution twice higher than the former. According to Scharwächter et al. (2013) then, the inner (R$\sim$ 50 pc) molecular H_2 gas kinematics is consistent with a circumnuclear disk and the authors estimate a black hole mass of 8×10^8 $M_\odot$, which would be slightly overmassive of a factor of 2 with respect to the M_{BH}-$M_\star$ plane taking into account the rms scatter of the M_{BH}-$M_\star$ in Kormendy and Ho (2013). Moreover, such estimate is highly uncertain and considered by Scharwächter et al. (2013) as an upper limit for M_{BH} in NGC 1275. Several sources of uncertainties can be identified and are also partly discussed in Scharwächter et al. (2013). (I) The spatial resolution should be such to allow a resolution at least 2.5 times the sphere of influence of the BH (Hicks et al., 2010), while that on IFU data for NGC 1275 can barely relove it. Even though improved by adaptive optics corrections, the resolution of IFU data in Scharwächter et al. (2013) does not allow to resolve well enough the BH sphere of influence. (II) The molecular gas mass in the inner region is non negligible and, just considering it, the BH mass is halved. (III) Since the disk inclination i highly degenerate with M_{BH}, it cannot be a free paramer of the kinematical modeling. Unfortunately it can be measured in very few cases: when the disk itself is spatially resolved, e.g., with water maser observations, or when very high S/N IFU data permit to take into account the residual projected velocity on cos i (see Appendix B in Marconi et al., 2003). This is not the case for Wilman et al. (2005) and Scharwächter et al. (2013) and they need to assume the inclination of the circumnuclear disk, whose rotational axis is supposed to be oriented as the axis of the radio jet. This is a strong assumption, as radio jets may not necessarily be aligned perpendicular to the disk. Pastorini et al. (2007) showed how the broad range of allowed inclinations leads to M_{BH} upper limits rather than reliable measurements. Finally, (IV) the H_2 disk kinematics can be significantly affected by bulk motions and non-gravitational forces like gas streams, which are likely to be falling into the core of NGC 1275 (Scharwächter et al., 2013).

As a valid alternative to direct dynamical measurements, we can use single epoch (SE) scaling relations to estimate M_{BH} in AGN, a method that is widely accepted and not expensive in terms of telescope time (Peterson, 2008; Shen, 2013). SE relations are most commonly calibrated by means of either the continuum or broad emission line luminosity and the FWHM of optical emission line (for a review of these calibrations see Shen, 2013). Recently Koss et al. (2017) gave estimates based on broad Hβ FWHM and 5,100 Å continuum luminosity, and on broad Hα FWHM and integrated luminosity, the latter is considered by the authors as more reliable and leads to $M_{BH} \sim 1.4 \times 10^7 M_\odot$. While such optical SE prescriptions are ideal for type 1 AGN, they can be anyhow problematic for a galaxy such as NGC 1275 which is optically classified as Seyfert 1.5 by Ho et al. (1997), and dimmed optical features produce a high uncertainty in the BH mass estimate. For intermediate type 1 Seyfert, the continuum luminosity and the H_β complex can be polluted by the FeII emission which is difficult to disentangle, and attenuated by gas extinction; extinction also dims significantly the Hβ emission and partially the Hα so that the second estimate is expected to give a higher mass than the first one and a more reliable value. We note that absorption is consistently detected also in X-rays, having NGC 1275 a gas column density of $\log N_H \sim 21.2$ (Tueller et al., 2008).

Rather than on the Balmer serie emission lines, we can resort to infrared features to pierce the absorbing gas and have a direct view of the broad line region. Combined with hard X-ray luminosity, IR features have been used by Ricci et al. (2017b) to

calibrate new and accurate single epoch viral relations that can be used for obscured or faint AGN.

With a hard X-ray luminosity of $L_{14-195} = 5.13 \times 10^{43}$ erg/s and a broad Paβ with FWHM=2824 km/s (Onori et al., 2017a), we recently estimated a BH mass of $(2.9 \pm 0.4) \times 10^7$ $M_\odot$ for NGC 1275 (Onori et al., 2017b).

Inclination can be a factor of uncertainty also for M_{BH} estimates based on SE scaling relations. The relations depend indeed on the viar factor factor f that account for our ignorance of the morphology, geometry, and kinematics of the BLR. There are evidences for example that more inclined AGN have a larger FWHM of the broad H_beta (Bisogni et al., 2017), while the f factor decreases with inclination (Risaliti et al., 2011; Pancoast et al., 2014). Considered together these results point out a possible disc-like structure of the BLR. Anyhow, the only way to match the single-epoch based M_{BH} with molecular gas kinematic measurements is to increase f of about an order of magnitude, which can happen only under extreme conditions like an Eddington ratio $\lambda_Edd < 0.01$ and inclination $i < 20$ deg (see plot 19 and 20 in Pancoast et al., 2014).

Our measure is consistent with Koss et al. (2017) results. Since the two methods are completely independent, we consider SE estimates reliable, while direct kinematical modeling of molecular gas can provide only upper limits of M_{BH} in NGC 1275. The following analysis is therefore based on our value of $M_{BH} \sim 3 \times 10^7$ $M_\odot$. Such low value, an order of magnitude lower than what expected for quiescent galaxies and AGN1, is intriguing and deserve further discussion.

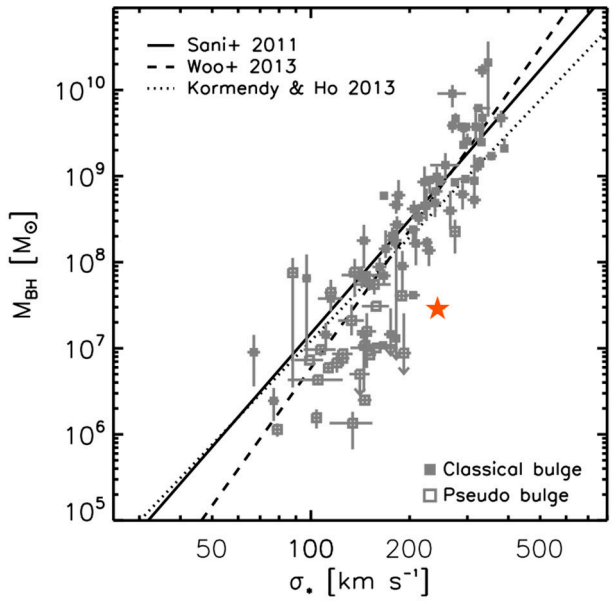

FIGURE 1 | The M_{BH}-$\sigma_\star$ plane for a local sample of BHs with dynamically measured M_{BH} from Sani et al. (2011) and Kormendy and Ho (2013), scaling relations computed in this two works are also shown. Since our M_{BH} are based on a virial factor $f = 4.31$, we also shown the scaling relation by Woo et al. (2013) that adopts the same f factor. The position of NGC 1275 is marked with an orange star. Classical and pseudo-bulges are marked with filled and open squares, respectively.

3. NGC 1275: AN OUTLIER OF M_{BH}-$\sigma_\star$ PLANE

In Ricci et al. (2017a) we have located type 2 AGN having virial BH mass estimates on the M_{BH}-$\sigma_\star$ scaling relation for unobscured and quiescent galaxies.

For a median stellar velocity of $\sigma_\star \sim 185$ km/s this analysis shows that AGN2 harbor black holes with a mass $\sim$ 0.9 dex smaller than in AGN1 or, equivalently, that host galaxies for type 2 AGN have a hotter kinematics than for type 1, being $\sigma_\star$ 0.2 dex higher at $M_{BH} \sim 10^7$ $M_\odot$. Such result does not depend on the host galaxy morphology (i.e., early vs. late type).

In such framework, NGC 1275 represents the most extreme case as shown in **Figure 1**. For seek of comparison, we show only dynamically measured M_{BH}. The new sample has been obtained merging the selection of Sani et al. (2011) with those done in Kormendy and Ho (2013), and the velocity dispersion for NGC 1275 has been measured following Ricci et al. (2017a). With a stellar velocity dispersion of ∼240 km/s, NGC 1275 falls well outside the intrinsic dispersion of the M_{BH}-$\sigma_\star$ plane in **Figure 1** and is indeed 1.2 dex displaced with respect to the (Sani et al., 2011; Kormendy and Ho, 2013) relations (and 1.35 dex from Woo et al., 2013), i.e., $\gtrsim$30% more with respect to the average displacement observed for type 2 AGN in Ricci et al. (2017a). Several checks against possible biases in the measurements of M_{BH} of AGN2 have been discussed in Onori et al. (2017b) and no correlation was found between the BLR detectability and infrared flux, nor Xray flux and luminosity, EW, FWHM, S/N of the spectral features, and not even host orientation or column density as measured in the X-rays. The displacement of NGC 1275 with respect to the M_{BH}-$\sigma_\star$ plane could be due to an overestimate of the stellar velocity dispersion. This is indeed a system composed by the central Perseus galaxy in a late merger state with a smaller spiral galaxy, quite challenging to be interpreted. While indeed an emission-line high velocity component (HVC) is moving toward the dominant system, it lies 57 kpc from the dominant body and cannot affect significantly its bulge kinematics (Gillmon et al., 2004), on the other hand galaxy merger (independent of the HV system) is still invoked, as an alternative to cooling flow, to explain the present formation of massive and short-lived stars (Conselice et al., 2001).

Alternatively, the displacement could be explained by an underestimate of SE M_{BH}. We note that to match our single-epoch based M_{BH} with those from 2D gas kinematics so that NGC 1275 lies on the M_{BH}-$\sigma_\star$ of qiescent galaxies, the virial f factor should increase of an order of magnitude. Moreover, the agreement of our results with Koss et al. (2017), hints at an actual undermassive BH in NGC 1275 (see Discussion in Section 2 for details).

To further investigate whether NGC 1275 is an extreme object in terms of BH and host galaxy scaling relations and to verify whether galaxy merging can play a significant role in such puzzle, we dissect mid-infrared images with the goal to measure the bulge luminosity and verify the stellar component morphology.

4. NGC 1275: AN OUTLIER OF THE $M_{BH} - L_{3.6,BUL}$ PLANE

As we aim at performing a detailed photometric bulge decomposition, we choose to analyse mid-infrared images as these wavelengths are tracing both young and old stellar populations. In fact, as demonstrated in Sani et al. (2011), the mass-to-light ratio at 3.6 μm doesn't require a color correction to estimate the bulge stellar mass, therefore confirming that the 3.6 μm luminosity is the best tracer of stellar mass yet studied. In the following we describe the image analysis of Spitzer data and discuss the location of NGC 1275 with respect to the $M_{BH} - L_{3.6,bul}$ plane.

4.1. Spitzer/IRAC Data Analysis

We downloaded post-BCD data[1] from the Spitzer Heritage Archive[2] (SHA) the deepest and most recent available 3.6 μm IRAC Astronomical Observation Request (AOR) of NGC 1275, to allow a reliable 2D decomposition in bulge/disc components using the software GALFIT (Peng et al., 2002, 2007). Besides the standard inputs [e.g., data, point spread function (PSF) images, etc.], GALFIT requires a standard deviation image (which can be directly retrieved from the SHA), used to give relative weights to the pixels during the fit, and a bad pixel mask. Following the work by Sani et al. (2011), we construct a bad pixel frame masking out foreground stars, background galaxies and possible irregularly shaped regions such as dust lanes across the galaxy. The frames were corrected for geometrical distortion and projected on to a north-east coordinate system with pixel sizes of 1.20 arcsec, equivalent to the original pixels.

We fix the background in the fit, estimating it as the mean surface brightness (with the relative standard deviation) over an annular region surrounding the galaxy between two and three times the optical radius. Foreground sources such as stars or galaxies are not considered in the background calculation by means of a 2.5σ rejection criterion. We then fitted the image with a bulge+psf model, where the bulge is represented with a Sersic profile and the PSF takes into account the nuclear AGN emission. As the uncertainties associated to the best-fit parameters are only statistical in GALFIT (Häussler et al., 2007), and hence underestimate the true uncertainties and degeneracies due to 2D fitting, we run a grid of four fits, varying the Sersic index by ±0.5 with respect to the best fit value, and by adding/subtracting to the sky flux its standard deviation. In these four grid fits, all the parameters are fixed to the best-fit values obtained in the previous step of fitting, with the exception of the magnitude and the effective radius of the Sersic. We then took the maximal magnitude variation among the 4 fits as the absolute error. With this choice, we overestimate the statistical fit errors, but carefully constrain the effects due to an uncertain estimate of the background. The resulting best fit parameters[3] are: $m_{3.6,bul} = 9.42 \pm 0.21$, $R_e = 42 \pm 15$ kpc, $n_{sers} = 4 \pm 0.5$ and $m_{3.6,psf} = 12.12$.

Figure 2 shows the two-dimensional analysis of NGC 1275.

4.2. NGC 1275 and the M_{BH}-$L_{3.6,bul}$ Plane

In **Figure 3** we show the position of NGC 1275 with respect to the M_{BH}-$L_{3.6,bul}$ where the data have been taken from Sani et al. (2011) who also computed the BH-luminosity scaling relation and measured its intrinsic scatter of 0.35 dex.

The BH hosted in NGC 1275 is significantly under-massive also with respect to the mass-luminosity plane, as the bulge luminosity measured in the previous section of $L_{3.6,bul} = 2.2 \times 10^{11}$ $L_\odot$ would imply a BH mass ∼ 12 times more massive than what measured with single-epoch virial methods. Equivalently, given the BH mass of 2.9×10^7 $M_\odot$ the bulge luminosity would be ∼1.12 dex lower than what actually measured with our 2D decomposition.

The galaxy morphology may play an important role to explain this discrepancy. We already mentioned above that NGC 1275 is presumably in a post-merger state, nonetheless the merging process is most probably not altering the bulk of the stellar mass and its distribution. Even though it is classified as an early type galaxy (with morphological type $t = -2$ according to the Hyperleda database, Paturel et al., 2003), it is significantly bluer than usual elliptical galaxies. On the other hand, the stellar surface brightness follows a de Vaucouleurs profile at optical wavelengths (Mathews et al., 2006) as well as in the mid-IR. This supports the idea that NGC 1275 is dominated by an old stellar population, as in normal elliptical galaxies, mixed with an additional population of young, luminous stars that does not contribute significantly to the total mass.

Our 2D analysis confirms the picture: beyond the bright compact nucleus that dominates the central emission in **Figure 2**, star forming regions and dust lanes typical of merging systems are not detected. Nor are detected the mid-IR counterpart of the filaments detected in H_α (Conselice et al., 2001) and X-ray (Fabian et al., 2003) meaning that such filaments are mainly gaseous, and poor in dust content. Additional asymmetric components, as relics of a past merging with a smaller galaxy, might be present and visible in the residuals of the 2D fitting (right panel in **Figure 2**) toward the west/north-west (but the reader should keep in mind the strong stretch of the plot).

We note that the displacement from the BH-host planes is consistent with NGC 1275 Seyfert classification. Indeed local black holes for which a reliable dynamic measumerement of M_{BH} is possible tend to bias the BH-host scaling relations toward the most massive objects given the requirement to spatially resolve the BH sphere of influence, and AGN that don't suffer such a bias are actually located below the scaling relations (see Figure 3 in Shankar et al., 2016) According to our analysis therefore, it is not possible to address the displacement of NGC 1275 from the scaling relations to its morphology.

The alternative explanation consists in invoking an evolutionary origin. Since their discovery, scaling relations

[1]The individual data frames that emerge, calibrated, from the Spitzer pipeline are Level 1, or Basic Calibrated Data, or BCDs. The products that come from combining these individual data frames (such as mosaics of individual pointings) are Level 2, or post-BCD, or PBCD data.

[2]http://irsa.ipac.caltech.edu/applications/Spitzer/SHA/.

[3]To compute the magnitudes at 3.6 μm, we adopt a zero-point of 17.25 in Vega magnitudes, according to the IRAC photometric system (Reach et al., 2005).

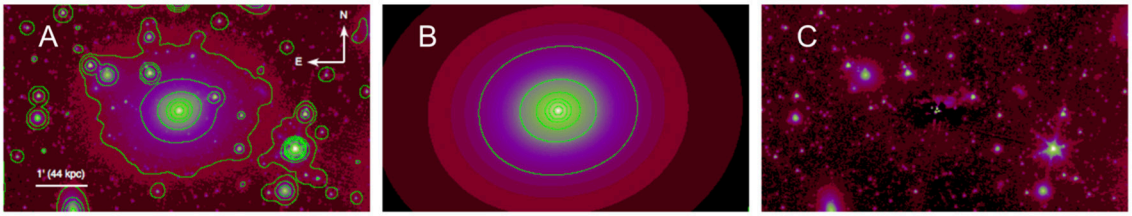

FIGURE 2 | Two-dimensional decomposition of Spitzer/IRAC 3.6*mu*m data of NGC1275 performed with GALFIT.The image **(A)**, best-fit model **(B)**, and residuals **(C)** are shown in logarithmic scale. The residuals are stretched (±0.25dex) to highlight the finest details.

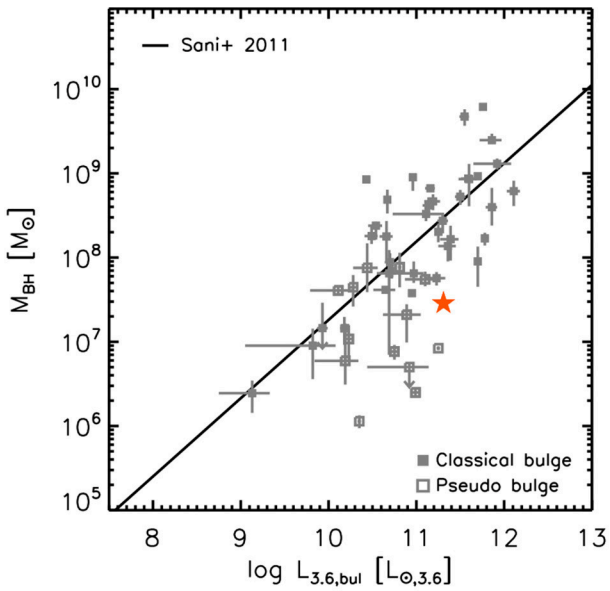

FIGURE 3 | The M_{BH}-$L_{3.6,bul}$ plane for local sample of galaxies with a dynamic or maser measurements of M_{BH}, the position of NGC 1275 is marked with an orange star. The scaling relation of Sani et al. (2011) is also shown for seek of comparison.

point to a joint galaxy and black hole cosmic evolution. To establish such correlation, one can envisage three possibilities (Volonteri, 2012). "(i) Massive black holes may have grown in symbiosis with their hosts (ii), the BH may have dominated the process, with the galaxy catching up later; (iii), the galaxy grew first, and the black hole adjusted to its host."

It is intriguing to note the position of NGC 1275 in the M_{BH}-$L_{bul,3.6}$ plane: it lies below the scaling relation at the edge between massive BHs in classical bulges and in pseudobulges. When it is possible to populate the M_{BH}-L plane with pseudobulges in fact, we can note an interesting behavior: while those with a significant BH mass lie on the scaling relations within the observed scatter, those with small mass (lower than few 10^7 $M_\odot$) are significantly displaced (Sani et al., 2011; Kormendy and Ho, 2013).

We are tempted to interpret the displacement of NGC 1275 from the scaling relation as due to an evolutionary pattern. Even though there is no trace of a pseudobulge from the 2D image analysis, it hosts a relatively small AGN2, and could represent a kind of observational link between secular evolution (thought to be the main mechanism producing pseudobulges) and merger (the builder of massive elliptical galaxies) where the common denominator is the small mass of the black hole, which is obliged by distinct evolutionary processes to adjust to the galaxy.

5. SUMMARY AND CONCLUSIONS

In this work we have investigated the behaviors of NGC 1275, the dominant galaxy of the Perseus cluster, in the framework of the M_{BH}-host scaling relations.

Starting from our previous work (Ricci et al., 2017a), we have seen how, given the stellar velocity dispersion of ∼240 km/s, NGC 1275 falls well outside the intrinsic dispersion of the M_{BH}-$\sigma_\star$ plane being 1.2 dex displaced with respect to the scaling relations, i.e. 30% more with respect to the average displacement observed for type 2 AGN in Ricci et al. (2017a).

By means of a 2D morphological decomposition of Spiter/IRAC images at 3.6 μm, we have found that:

- the AGN dust heated emission dominates the nucleus with a magnitude of $m_{3.6,psf} = 12.12$.
- NGC 1275 follows a de Vaucouleurs law extended at large spatial scales with no sign of merger remanence nor of significant star formation activity.
- Given a bulge luminosity of $L_{bul,3.6} = 2.17 \times 10^{11}$ $L_\odot$, NGC 1275 harbors a black holes 15 times under-massive than what expected for quiescent galaxies that lie within the intrinsic scatter of the $M_{BH} - L_{3.6,bul}$ scaling relation.

We speculate that the displacement of NGC 1275 with respect to the BH-host scaling relations might depend on its evolutionary path where the galaxy grew first, and the black hole is adjusting to its host. We stress that to draw firmer conclusions, it is mandatory to pinpoint on the BH-host planes a statistically significant sample of both type 1 and 2 AGN (Ricci et al., in preparation).

AUTHOR CONTRIBUTIONS

All authors contributed to the interpretation of the observations and the writing of the paper. ES led the analysis, interpretation, and wrote the paper. ES, FL, FR defined the strategy. FR performed the 2D modeling. Discussion on the black hole mass measurement has been provided by AM and on scaling relation biases by FS.

ACKNOWLEDGMENTS

This work has been possible thanks to DGDF ESO funding. FR is grateful for the hospitality at by ESO-Chile. ES thanks Dr. Vardha Bennert for fruitful discussion on the AGN scaling relations. We acknowledge the usage of the Hyper-Leda database (http://leda.univ-lyon1.fr). This research has made use of the NASA/IPAC extragalactic database (NED).

REFERENCES

Antonucci, R. (1993). Unified models for active galactic nuclei and quasars. *Annu. Rev. Astron. Astrophys.* 31, 473–521.

Bisogni, S., Marconi, A., and Risaliti, G. (2017). Orientation effects on spectral emission features of quasars. *Mon. Not. Roy. Astron. Soc.* 464, 385–397. doi: 10.1093/mnras/stw2324

Conselice, C. J., Gallagher, J. S. III, and Wyse, R. F. G. (2001). On the nature of the NGC 1275 system. *Astrophys. J.* 122, 2281–2300. doi: 10.1086/323534

Fabian, A. C., Sanders, J. S., Allen, S. W., Crawford, C. S., Iwasawa, K., Johnstone, R. M., et al. (2003). A deep Chandra observation of the Perseus cluster: shocks and ripples. *Mon. Not. Roy. Astron. Soc.* 344, L43–L47. doi: 10.1046/j.1365-8711.2003.06902.x

Gillmon, K., Sanders, J. S., and Fabian, A. C. (2004). An X-ray absorption analysis of the high-velocity system in NGC 1275. *Mon. Not. Roy. Astron. Soc.*, 348, 159–164. doi: 10.1111/j.1365-2966.2004.07336.x

Graham, A. W. (2008). Fundamental planes and the barless M_{BH}-σ relation for supermassive black holes. *Astrophys. J.* 680, 143–153. doi: 10.1086/587473

Häussler, B., McIntosh, D. H., Barden, M., Bell, E. F., Rix, H.-W., Borch, A., et al. (2007). GEMS: galaxy fitting catalogs and testing parametric galaxy fitting codes: GALFIT and GIM2D. *Astrophys. J. Suppl.* 172, 615–633. doi: 10.1086/518836

Hicks, E. K. S., Davies, R. I., Malkan, M. A., Genzel, R., and Tacconi, L. J. (2010). "A survey of seyfert AGN: nuclear gas disks and direct black hole mass estimates," in *Co-Evolution of Central Black Holes and Galaxies, Vol. 267 of IAU Symposium*, eds B. M. Peterson, R. S. Somerville, and T. Storchi-Bergmann (Rio de Janeiro: International Astronomical Union), 177–182.

Ho, L. C., Filippenko, A. V., Sargent, W. L. W., and Peng, C. Y. (1997). A search for "Dwarf" seyfert nuclei. IV. Nuclei with broad Hα emission. *Astrophys. J. Suppl.* 112, 391–414. doi: 10.1086/313042

Kormendy, J., and Ho, L. C. (2013). Coevolution (or not) of supermassive black holes and host galaxies. *Annu. Rev. Astron. Astrophys.* 51, 511–653. doi: 10.1146/annurev-astro-082708-101811

Koss, M., Trakhtenbrot, B., Ricci, C., Lamperti, I., Oh, K., Berney, S., et al. (2017). BAT AGN spectroscopic survey. I. Spectral measurements, derived quantities, and AGN demographics. *Astrophys. J.* 850:74. doi: 10.3847/1538-4357/aa8ec9

La Franca, F., Fiore, F., Comastri, A., Perola, G. C., Sacchi, N., Brusa, M., et al. (2005). The HELLAS2XMM survey. VII. The hard x-ray luminosity function of AGNs up to z = 4: more absorbed AGNs at low luminosities and high redshifts. *Astrophys. J.* 635, 864–879. doi: 10.1086/497586

La Franca, F., Onori, F., Ricci, F., Bianchi, S., Marconi, A., Sani, E., et al. (2016). Detection of faint BLR components in the starburst/Seyfert galaxy NGC 6221 and measure of the central BH mass. *Front. Astron. Space Sci.* 3:12. doi: 10.3389/fspas.2016.00012

La Franca, F., Onori, F., Ricci, F., Sani, E., Brusa, M., Maiolino, R., et al. (2015). Extending virial black hole mass estimates to low-luminosity or obscured AGN: the cases of NGC 4395 and MCG -01-24-012. *Mon. Not. Roy. Astron. Soc.* 449, 1526–1535. doi: 10.1093/mnras/stv368

Marconi, A., Axon, D. J., Capetti, A., Maciejewski, W., Atkinson, J., Batcheldor, D., et al. (2003). Is there really a black hole at the center of NGC 4041? Constraints from gas kinematics. *Astrophys. J.* 586, 868–890. doi: 10.1086/367764

Mathews, W. G., Faltenbacher, A., and Brighenti, F. (2006). Heating cooling flows with weak shock waves. *Astrophys. J.* 638, 659–667. doi: 10.1086/499119

Onori, F., La Franca, F., Ricci, F., Brusa, M., Sani, E., Maiolino, R., et al. (2017a). Detection of faint broad emission lines in type 2 AGN - I. Near-infrared observations and spectral fitting. *Mon. Not. Roy. Astron. Soc.* 464, 1783–1832. doi: 10.1093/mnras/stw2368

Onori, F., Ricci, F., La Franca, F., Bianchi, S., Bongiorno, A., Brusa, M., et al. (2017b). Detection of faint broad emission lines in type 2 AGN - II. On the measurement of the black hole mass of type 2 AGN and the unified model. *Mon. Not. Roy. Astron. Soc.* 468, L97–L102. doi: 10.1093/mnrasl/slx032

Pancoast, A., Brewer, B. J., Treu, T., Park, D., Barth, A. J., Bentz, M. C., et al. (2014). Modelling reverberation mapping data - II. Dynamical modelling of the Lick AGN Monitoring Project 2008 data set. *Mon. Not. Roy. Astron. Soc.* 445, 3073–3091. doi: 10.1093/mnras/stu1419

Pastorini, G., Marconi, A., Capetti, A., Axon, D. J., Alonso-Herrero, A., Atkinson, J., et al. (2007). Supermassive black holes in the Sbc spiral galaxies NGC 3310, NGC 4303 and NGC 4258. *Astron. Astrophys.* 469, 405–423. doi: 10.1051/0004-6361:20066784

Paturel, G., Petit, C., Prugniel, P., Theureau, G., Rousseau, J., Brouty, M., et al. (2003). HYPERLEDA. I. Identification and designation of galaxies. *Astron. Astrophys.* 412, 45–55. doi: 10.1051/0004-6361:20031411

Peng, C. Y., Ho, L. C., Impey, C. D., and Rix, H.-W. (2002). Detailed structural decomposition of galaxy images. *Astron. J.* 124, 266–293. doi: 10.1086/340952

Peng, C. Y., Ho, L. C., Impey, C. D., and Rix, H. W. (2007). "Detailed decomposition of galaxy images II: fitting spiral arms, bars, and non-axisymmetric structures in GALFIT 3.0," in *American Astronomical Society Meeting Abstracts, Vol. 39 of Bulletin of the American Astronomical Society* (Austin, TX), 804.

Peterson, B. M. (2008). The central black hole and relationships with the host galaxy. *New Astron. Rev.* 52, 240–252. doi: 10.1016/j.newar.2008.06.005

Reach, W. T., Megeath, S. T., Cohen, M., Hora, J., Carey, S., Surace, J., et al. (2005). Absolute calibration of the infrared array camera on the spitzer space telescope. *Publ. Astron. Soc. Pac.* 117, 978–990. doi: 10.1086/432670

Ricci, F., La Franca, F., Marconi, A., Onori, F., Shankar, F., Schneider, R., et al. (2017a). Detection of faint broad emission lines in type 2 AGN: III. On the $M_BH - \sigma_\star$ relation of type 2 AGN. *ArXiv e-prints*.

Ricci, F., La Franca, F., Onori, F., and Bianchi, S. (2017b). Novel calibrations of virial black hole mass estimators in active galaxies based on X-ray luminosity and optical/near-infrared emission lines. *Astron. Astrophys.* 598:A51. doi: 10.1051/0004-6361/201629380

Risaliti, G., Salvati, M., and Marconi, A. (2011). [O III] equivalent width and orientation effects in quasars. *Mon. Not. Roy. Astron. Soc.* 411, 2223–2229. doi: 10.1111/j.1365-2966.2010.17843.x

Sani, E., Marconi, A., Hunt, L. K., and Risaliti, G. (2011). The Spitzer/IRAC view of black hole-bulge scaling relations. *Mon. Not. Roy. Astron. Soc.* 413, 1479–1494. doi: 10.1111/j.1365-2966.2011.18229.x

Scharwächter, J., McGregor, P. J., Dopita, M. A., and Beck, T. L. (2013). Kinematics and excitation of the molecular hydrogen accretion disc in NGC 1275. *Mon. Not. Roy. Astron. Soc.* 429, 2315–2332. doi: 10.1093/mnras/sts502

Shankar, F., Bernardi, M., Sheth, R. K., Ferrarese, L., Graham, A. W., Savorgnan, G., et al. (2016). Selection bias in dynamically measured supermassive black hole samples: its consequences and the quest for the most fundamental relation. *Mon. Not. Roy. Astron. Soc.* 460, 3119–3142. doi: 10.1093/mnras/stw678

Shen, Y. (2013). The mass of quasars. *Bull. Astron. Soc. Ind.* 41, 61–115.

Tueller, J., Mushotzky, R. F., Barthelmy, S., Cannizzo, J. K., Gehrels, N., Markwardt, C. B., et al. (2008). Swift BAT survey of AGNs. *Astrophys. J.* 681, 113–127. doi: 10.1086/588458

Ueda, Y., Hashimoto, Y., Ichikawa, K., Ishino, Y., Kniazev, A. Y., Väisänen, P., et al. (2015). [O iii] λ5007 and x-ray properties of a complete sample of hard x-ray selected AGNs in the local universe. *Astrophys. J.* 815:1. doi: 10.1088/0004-637X/815/1/1

Volonteri, M. (2012). The formation and evolution of massive black holes. *Science* 337:544. doi: 10.1126/science.1220843

Wilman, R. J., Edge, A. C., and Johnstone, R. M. (2005). The nature of the molecular gas system in the core of NGC 1275. *Mon. Not. Roy. Astron. Soc.* 359, 755–764. doi: 10.1111/j.1365-2966.2005.08956.x

Winter, L. M., Lewis, K. T., Koss, M., Veilleux, S., Keeney, B., and Mushotzky, R. F. (2010). Optical spectral properties of swift burst alert telescope hard x-ray-selected active galactic nuclei sources. *Astrophys. J.* 710, 503–539. doi: 10.1088/0004-637X/710/1/503

Woo, J.-H., Schulze, A., Park, D., Kang, W.-R., Kim, S. C., and Riechers, D. A. (2013). Do quiescent and active galaxies have different M_{BH}-σ_* relations? *Astrophys. J.* 772:49. doi: 10.1088/0004-637X/772/1/49

Conflict of Interest Statement: The authors declare that the research was conducted in the absence of any commercial or financial relationships that could be construed as a potential conflict of interest.

Copyright © 2018 Sani, Ricci, La Franca, Bianchi, Bongiorno, Brusa, Marconi, Onori, Shankar and Vignali. This is an open-access article distributed under the terms of the Creative Commons Attribution License (CC BY). The use, distribution or reproduction in other forums is permitted, provided the original author(s) and the copyright owner are credited and that the original publication in this journal is cited, in accordance with accepted academic practice. No use, distribution or reproduction is permitted which does not comply with these terms.

frontiers in Astronomy and Space Sciences

HYPOTHESIS AND THEORY
published: 21 September 2017
doi: 10.3389/fspas.2017.00015

Theoretical Re-evaluations of Scaling Relations between SMBHs and Their Host Galaxies—1. Effect of Seed BH Mass

Hikari Shirakata[1], Toshihiro Kawaguchi[2], Takashi Okamoto[1], Ryu Makiya[3,4], Tomoaki Ishiyama[5], Yoshiki Matsuoka[6], Masahiro Nagashima[7], Motohiro Enoki[8], Taira Oogi[3] and Masakazu A. R. Kobayashi[9]*

[1] Department of Cosmosciences, Graduate School of Science, Hokkaido University, Sapporo, Japan, [2] Department of Economics, Management and Information Science, Onomichi City University, Onomichi, Japan, [3] Kavli Institute for the Physics and Mathematics of the Universe, Todai Institutes for Advanced Study, University of Tokyo, Kashiwa, Japan, [4] Max-Planck-Institut fur Astrophysik, Garching, Germany, [5] Institute of Management and Information Technologies, Chiba University, Chiba, Japan, [6] Research Center for Space and Cosmic Evolution, Ehime University, Matsuyama, Japan, [7] Faculty of Education, Bunkyo University, Koshigaya, Japan, [8] Faculty of Business Administration, Tokyo Keizai University, Kokubunji, Japan, [9] Faculty of Natural Sciences, National Institute of Technology, Kure College, Kure, Japan

OPEN ACCESS

Edited by:
Mauro D'Onofrio,
University of Padua, Italy

Reviewed by:
Jaime Perea,
Instituto de Astrofísica de Andalucía (CSIC), Spain
Vyacheslav Ivanovich Dokuchaev,
Institute for Nuclear Research (RAS), Russia

***Correspondence:**
Hikari Shirakata
shirakata@astro1.sci.hokudai.ac.jp

Specialty section:
This article was submitted to Milky Way and Galaxies, a section of the journal Frontiers in Astronomy and Space Sciences

Received: 10 July 2017
Accepted: 08 September 2017
Published: 21 September 2017

Citation:
Shirakata H, Kawaguchi T, Okamoto T, Makiya R, Ishiyama T, Matsuoka Y, Nagashima M, Enoki M, Oogi T and Kobayashi MAR (2017) Theoretical Re-evaluations of Scaling Relations between SMBHs and Their Host Galaxies—1. Effect of Seed BH Mass. Front. Astron. Space Sci. 4:15. doi: 10.3389/fspas.2017.00015

We use a semi-analytic model of galaxy formation and investigate how the mass of a seed black hole affect the scaling relation between black hole mass and bulge mass at $z \sim 0$. When the mass of the seed is set at $10^5 M_\odot$, we find that the model results become inconsistent with recent observational results of the scaling relation for dwarf galaxies. On the other hand, when we set seed black hole mass as $10^3 M_\odot$ or as randomly chosen value within a $10^{3-5} M_\odot$ range, we find the results are consistent with observational results including the dispersion. We also find that black hole mass—bulge mass relations for less massive bulges at $z \sim 0$ put stronger constraints on the seed BH mass than the relations at higher redshifts.

Keywords: galaxies, active galactic nuclei, bulge, galaxy formation, statistics

1. INTRODUCTION

Many observations (e.g., Kormendy and Richstone, 1995; Magorrian et al., 1998; Häring and Rix, 2004; McConnell and Ma, 2013) have suggested that the mass of supermassive black holes ($M_{\rm BH}$) correlates with the properties of their host galaxies such as stellar mass of bulges ($M_{\rm bulge}$) at $z \sim 0$. This $M_{\rm BH}$ – $M_{\rm bulge}$ relation might suggest that supermassive black holes (SMBHs) would have co-evolved with their host galaxies.

SMBHs grow to the current mass ($\gtrsim 10^6 M_\odot$) from their initial mass. The initial mass and its distribution have been debating. Although, there are many theoretical suggestions of formation mechanism and mass of seed BHs (e.g., Begelman et al., 2006), we cannot obtain what is the dominant mechanism by comparing theoretical models with observations since seed BHs are not observable directly.

Here, we focus on the $M_{\rm BH}$ – $M_{\rm bulge}$ relation for galaxies with bulge mass is less than $10^{10} M_\odot$ to get the constraints on mass of seed BHs. This paper is a summary of Shirakata et al. (2016) in which we investigate the effect of the seed BHs' mass on model predictions of $M_{\rm BH}$ – $M_{\rm bulge}$ relation at $M_{\rm bulge} \lesssim 10^{10} M_\odot$ by using an semi-analytic model of galaxy formation (hereafter SA model). In section 2 we briefly review the SA model we used. Section 3 includes the main results. Finally, in section 4, we summarize this review and briefly mention future prospects.

2. MODELS

We use a revised version of an SA model, "*New Numerical Galaxy Catalogue*" (ν^2GC ; Makiya et al., 2016, hereafter M16), where the models related to the SMBH and AGNs are described in Enoki et al. (2003), Enoki et al. (2014), and Shirakata et al. (2015). We consider star formation in galactic disk and bulge, mergers of galaxies, atomic gas cooling, gas heating by UV feedback and feedbacks via supernovae and AGNs, and the growth of SMBHs by coalescence and gas accretion from their host galaxies.

Merging histories of dark matter halos are calculated from state-of-the-art cosmological N-body simulations (Ishiyama et al., 2015). The cosmological simulations have a high mass resolution and large volume compared to previous simulations (e.g., mass resolution is roughly four times better than those of Millennium simulations, Springel et al., 2005). Here we employ a simulation with $L = 70.0$ [h^{-1} Mpc] of box size and 512^3 particles, which corresponds to $M_{\rm min} = 2.20 \times 10^8 [h^{-1} M_\odot]$ of minimum halo mass.

We assume a ΛCDM universe which have the following parameters: $\Omega_0 = 0.31$, $\lambda_0 = 0.69$, $\Omega_{\rm b} = 0.048$, $\sigma_8 = 0.83$, $n_{\rm s} = 0.96$, and a Hubble constant of $H_0 = 100\,h$ km s^{-1} Mpc^{-1}, where $h = 0.68$ (Planck Collaboration et al., 2014).

2.1. Setting of Seed Black Holes

We place a seed BH soon after the time of a galaxy formation. We present results with $M_{\rm BH,seed} = 10^3 M_\odot$ (hereafter "light seed model") where $M_{\rm BH,seed}$ is the seed BH mass, and $10^5 M_\odot$ ("massive seed model"). In addition, we employ the model in which $M_{\rm BH,seed}$ takes uniformly random values in the logarithmic scale in the range of $3 \leq \log(M_{\rm BH,seed}/M_\odot) \leq 5$ (hereafter "random seed model").

2.2. Summary of Bulge and SMBH Growth Model

We assume that the bulge grows via starbursts and the migration of disk stars. Starbursts are triggered by mergers of galaxies (major and minor) or disk instability. The model of merger driven bulge formation in ν^2GC is based on Hopkins et al. (2009). We consider that mergers of galaxies occur both by dynamical friction (central-satellite merger) and random collision (satellite-sattelite merger). We also introduce the spheroid formation by disk instability following Mo et al. (1998) and Cole et al. (2000). In both cases, the gas supplyed from galactic disk to the bulge is completely exhausted by a starburst and fueling onto their central SMBHs.

SMBHs in ν^2GC are mainly grown by gas accretion from their host galaxy. When a starburst occurs in a bulge, a part of cold gas gets accreted by the SMBH :

$$M_{\rm acc} = f_{\rm BH} \ \ \Delta M_{*,\rm burst}, \tag{1}$$

where $M_{\rm acc}$ is the cold gas mass accreted onto the SMBH, which is assumed to be proportional to the stellar mass formed by a current starburst, $\Delta M_{*,\rm burst}$. Here we set $f_{\rm BH} = 0.01$. SMBHs also grow via coalescence of BHs which occurs with mergers of host galaxies. For simplicity, we assume BHs merge instantaneously when their host galaxies merge.

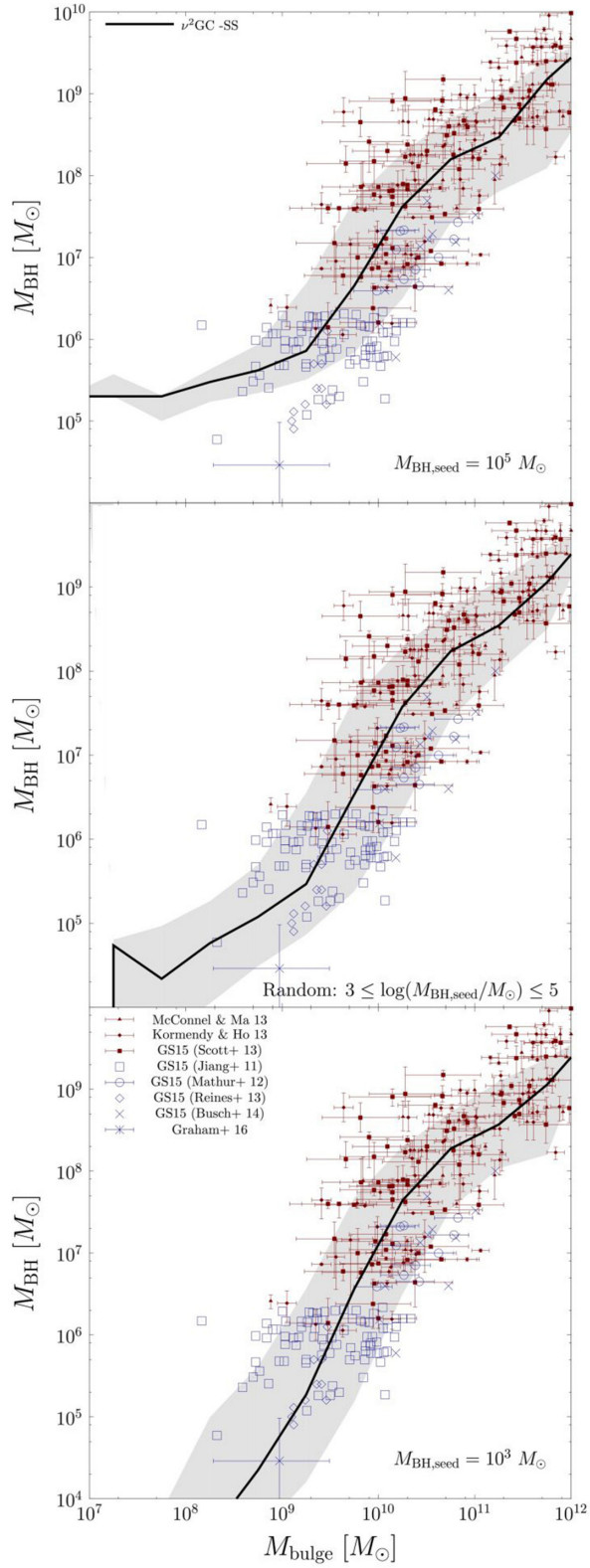

FIGURE 1 | $M_{\rm BH} - M_{\rm bulge}$ relations at $z \sim 0$ for different $M_{\rm BH,seed}$; the massive **(top)**, random **(middle)**, and light **(bottom)** seed models. Black solid

(Continued)

FIGURE 1 | Continued
lines track the median, and shaded regions indicate 10–90 percentile of the models of the model result. Red filled symbols indicate observational results obtained from McConnell and Ma (2013), Kormendy and Ho (2013), and GS15[3](triangles, diamonds, and squares, respectively). Blue open symbols are AGN sample obtained from GS15, (see the text for more details). Blue asterisks correspond LEDA 87300 (Baldassare et al., 2015; Graham et al., 2016).

3. RESULTS

Figure 1 shows the main result which depicts the $M_{\rm BH}$ – $M_{\rm bulge}$ relation at $z \sim 0$ obtained from the model and observations. Each panels correspond to the results of massive seed model (top), random seed model (middle), and light seed model (bottom), respectively. Red solid lines represents the model result, blue and green points represents the observational data.

We find all of the models reproduce the relation at $M_{\rm bulge} \gtrsim 10^{10} M_\odot$, while the massive seed model has an inconsistency in the observational results for less massive galaxies ($M_{\rm bulge} \lesssim 10^{10} M_\odot$). Random and light seed models, on the other hand, provide the consistent results in the range of $M_{\rm BH} \gtrsim 10^{5.5} M_\odot$, with observational estimates. We thus conclude that to explain recent observational data of the $M_{\rm BH}$ – $M_{\rm bulge}$ relation at $z \sim 0$, seed BH mass should dominate with $\sim 10^3 M_\odot$.

We note that since the number of samples of galaxies with $M_{\rm BH} \lesssim 10^{5.5} M_\odot$ (corresponds to $M_{\rm bulge} \lesssim 10^{10} M_\odot$) are not sufficient. Observational data with the mass range are thus necessary to investigate the detailed mass distribution of the seed BHs. It is however difficult to estimate BH and bulge mass of less massive galaxies. We thus investigate whether the $M_{\rm BH}$ – $M_{\rm bulge}$ relation at higher redshifts could be useful for getting further constraints on the mass of seed BHs. **Figure 2** displays the ratio of the average BH masses in the light seed model ($\equiv \langle M_{\rm BH} \rangle_3$) and those in the massive seed model ($\equiv \langle M_{\rm BH} \rangle_5$), as a function of bulge masses. The difference in the seed mass significantly appears in galaxies with bulge mass below $3 \times 10^9 M_\odot$ at $z \sim 0, 1$, and 2. We also find that the difference becomes smaller at higher redshift for a given $M_{\rm bulge}$. Observations of less massive bulges at $z \sim 0$ would thus be more important than at higher redshifts for investigating the mass distribution of seed BHs.

4. SUMMARY AND FUTURE PROSPECTS

We investigate how the mass of the seed BHs affects model predictions of the local $M_{\rm BH}$ – $M_{\rm bulge}$ relation by using an SA model. The results suggest that seed BHs with as massive as $10^5 M_\odot$ should not be dominant for reproducing the observed $M_{\rm BH}$ – $M_{\rm bulge}$ relation at $z \sim 0$ over a wide range of bulge masses down to $M_{\rm bulge} \lesssim 10^{10} M_\odot$. Obtaining stronger constraints of the detailed mass distribution of seed BHs observations of $M_{\rm BH} \lesssim 10^{5.5} M_\odot$ would be required.

[3]Originally obtained from Scott et al. (2013).

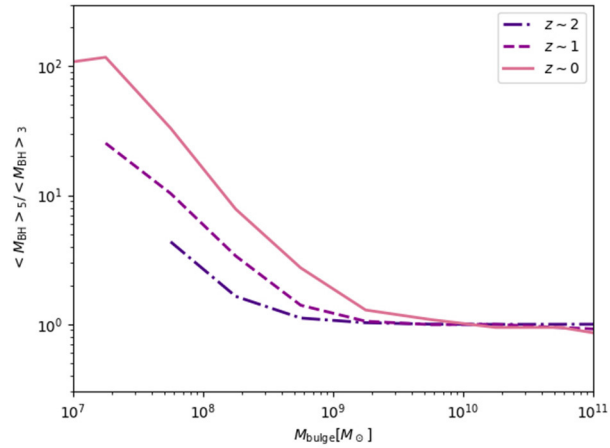

FIGURE 2 | The difference of averaged SMBH mass due to the seed BH mass at $z \sim 2$ (dash-doted line in blue), $z \sim 1$ (dashed line in purple), and $z \sim 0$ (solid line in pink) as a function of their bulge stellar mass with the ν^2GC -H2 simulation. The difference becomes smaller at higher redshift.

We have shown results of the local $M_{\rm BH}$ – $M_{\rm bulge}$ relations varying the mass of seed BHs. According to Shankar et al. (2016), $M_{\rm bulge}$ obtained from observations could be biased in favor of larger stellar masses. If so, we might have to use $M_{\rm BH}$ – velocity dispersion relation instead of the local $M_{\rm BH}$ – $M_{\rm bulge}$. We leave it for future studies.

The spheroids formed through disk instability might be classified as so-called "pseudo bulges". There are some debates whether pseudo bulges and classical bulges follow the same $M_{\rm BH}$ – $M_{\rm bulge}$ relation (e.g., Kormendy and Ho, 2013). We might need the model of the properties of pseudo bulges in the near future.

AUTHOR CONTRIBUTIONS

HS, RM, MN, ME, and MK have developed ν^2GC . In addition, HS analyze the output data obtained from ν^2GC . TK, TakO, and TaiO gave comments for the analysis. TI provides merger trees obtained from cosmological N-body simulations for ν^2GC . YM gave fruitful comments from a standpoint of AGN observations.

FUNDING

TK was supported in part by an University Research Support Grant from the NAOJ and JSPS KAKENHI (17K05389). TakO was supported by JSPS Grant-in-Aid for Young Scientists (16H01085). RM was supported in part by MEXT KAKENHI (15H05896). TI was supported by MEXT HPCI STRATEGIC PROGRAM and MEXT/JSPS KAKENHI (15K12031) and by Yamada Science Foundation. MN was supported by the Grant-in-Aid (25287041 and 17H02867) from the MEXT of Japan.

REFERENCES

Baldassare, V. F., Reines, A. E., Gallo, E., and Greene, J. E. (2015). A $\sim$ 50,000 $M_{\odot}$ solar mass black hole in the nucleus of RGG 118. *Astrophys. J. Lett.* 809:L14. doi: 10.1088/2041-8205/809/1/L14

Begelman, M. C., Volonteri, M., and Rees, M. J. (2006). Formation of supermassive black holes by direct collapse in pre-galactic haloes. *Mon. Not. R. Astron. Soc.* 370, 289–298. doi: 10.1111/j.1365-2966.2006.10467.x

Cole, S., Lacey, C. G., Baugh, C. M., and Frenk, C. S. (2000). Hierarchical galaxy formation. *Mon. Not. R. Astron. Soc.* 319, 168–204. doi: 10.1046/j.1365-8711.2000.03879.x

Enoki, M., Ishiyama, T., Kobayashi, M. A. R., and Nagashima, M. (2014). Anti-hierarchical evolution of the active galactic nucleus space density in a hierarchical universe. *Astrophys. J.* 794:69. doi: 10.1088/0004-637X/794/1/69

Enoki, M., Nagashima, M., and Gouda, N. (2003). Relations between galaxy formation and the environments of quasars. *Publ. Astron. Soc. Jpn.* 55, 133–142. doi: 10.1093/pasj/55.1.133

Graham, A. W., Ciambur, B. C., and Soria, R. (2016). Does the intermediate-mass black hole in LEDA 87300 (RGG 118) follow the near-quadratic $M_{\rm BH}$–$M_{\rm Spheroid}$ relation? *Astrophys. J.* 818:172. doi: 10.3847/0004-637X/818/2/172

Graham, A. W., and Scott, N. (2015). The (black hole)-bulge mass scaling relation at low masses. *Astrophys. J.* 798:54. doi: 10.1088/0004-637X/798/1/54

Häring, N., and Rix, H.-W. (2004). On the black hole mass-bulge mass relation. *Astrophys. J. Lett.* 604, L89–L92. doi: 10.1086/383567

Hopkins, P. F., Cox, T. J., Younger, J. D., and Hernquist, L. (2009). How do disks survive mergers? *Astrophys. J.* 691, 1168–1201. doi: 10.1088/0004-637X/691/2/1168

Ishiyama, T., Enoki, M., Kobayashi, M. A. R., Makiya, R., Nagashima, M., and Oogi, T. (2015). The ν^2GC simulations: quantifying the dark side of the universe in the Planck cosmology. *Publ. Astron. Soc. Jpn.* 67:61. doi: 10.1093/pasj/psv021

Kormendy, J., and Ho, L. C. (2013). Coevolution (or not) of supermassive black holes and host galaxies. *Annu. Rev. Astron. Astrophys.* 51, 511–653. doi: 10.1146/annurev-astro-082708-101811

Kormendy, J., and Richstone, D. (1995). Inward bound—the search for supermassive black holes in galactic nuclei. *Annu. Rev. Astron. Astrophys.* 33:581.

Magorrian, J., Tremaine, S., Richstone, D., Bender, R., Bower, G., Dressler, A., et al. (1998). The demography of massive dark objects in galaxy centers. *Astron. J.* 115, 2285–2305.

Makiya, R., Enoki, M., Ishiyama, T., Kobayashi, M. A. R., Nagashima, M., Okamoto, T., et al. (2016). The new numerical galaxy catalog (ν^2GC): an updated semi-analytic model of galaxy and active galactic nucleus formation with large cosmological N-body simulations. *Publ. Astron. Soc. Jpn.* 68:25. doi: 10.1093/pasj/psw005

McConnell, N. J., and Ma, C.-P. (2013). Revisiting the scaling relations of black hole masses and host galaxy properties. *Astrophys. J.* 764:184. doi: 10.1088/0004-637X/764/2/184

Mo, H. J., Mao, S., and White, S. D. M. (1998). The formation of galactic discs. *Mon. Not. R. Astron. Soc.* 295, 319–336. doi: 10.1046/j.1365-8711.1998.01227.x

Planck Collaboration, Ade, P. A. R., Aghanim, N., Alves, M. I. R., Armitage-Caplan, C., Arnaud, M., et al. (2014). Planck 2013 results. I. Overview of products and scientific results. *Astron. Astrophys.* 571:A1. doi: 10.1051/0004-6361/201321529

Scott, N., Graham, A. W., and Schombert, J. (2013). The supermassive black hole mass-spheroid stellar mass relation for sérsic and core-Sérsic galaxies. *Astrophys. J.* 768:76. doi: 10.1088/0004-637X/768/1/76

Shankar, F., Bernardi, M., Sheth, R. K., Ferrarese, L., Graham, A. W., Savorgnan, G., et al. (2016). Selection bias in dynamically-measured super-massive black holes: its consequences and the quest for the most fundamental relation. *Mon. Not. R. Astron. Soc. arXiv:1603.01276*.

Shirakata, H., Kawaguchi, T., Okamoto, T., Makiya, R., Ishiyama, T., Matsuoka, Y., et al. (2016). Theoretical re-evaluations of the black hole mass-bulge mass relation - I. Effect of seed black hole mass. *Mon. Not. R. Astron. Soc.* 461, 4389–4394. doi: 10.1093/mnras/stw1798

Shirakata, H., Okamoto, T., Enoki, M., Nagashima, M., Kobayashi, M. A. R., Ishiyama, T., et al. (2015). The impact of dust in host galaxies on quasar luminosity functions. *Mon. Not. R. Astron. Soc.* 450, L6–L10. doi: 10.1093/mnrasl/slv035

Springel, V., White, S. D. M., Jenkins, A., Frenk, C. S., Yoshida, N., Gao, L., et al. (2005). Simulations of the formation, evolution and clustering of galaxies and quasars. *Nature* 435, 629–636. doi: 10.1038/nature03597

Conflict of Interest Statement: The authors declare that the research was conducted in the absence of any commercial or financial relationships that could be construed as a potential conflict of interest.

Copyright © 2017 Shirakata, Kawaguchi, Okamoto, Makiya, Ishiyama, Matsuoka, Nagashima, Enoki, Oogi and Kobayashi. This is an open-access article distributed under the terms of the Creative Commons Attribution License (CC BY). The use, distribution or reproduction in other forums is permitted, provided the original author(s) or licensor are credited and that the original publication in this journal is cited, in accordance with accepted academic practice. No use, distribution or reproduction is permitted which does not comply with these terms.

frontiers in Astronomy and Space Sciences

ORIGINAL RESEARCH
published: 17 October 2017
doi: 10.3389/fspas.2017.00023

Statistical Detection of the He II Transverse Proximity Effect: Evidence for Sustained Quasar Activity for >25 Million Years

Tobias M. Schmidt[1,2], Gabor Worseck[2], Joseph F. Hennawi[1,2], J. Xavier Prochaska[3], Neil H. M. Crighton[4], Zarija Lukić[5] and Jose Oñorbe[2]*

[1] Department of Physics, University of California, Santa Barbara, Santa Barbara, CA, United States, [2] Max-Planck-Institut für Astronomie, Heidelberg, Germany, [3] Department of Astronomy and Astrophysics, UCO/Lick Observatory, University of California, Santa Cruz, Santa Cruz, CA, United States, [4] Centre for Astrophysics and Supercomputing, Swinburne University of Technology, Melbourne, VIC, Australia, [5] Lawrence Berkeley National Laboratory, Berkeley, CA, United States

The reionization of helium at $z \sim 3$ is the final phase transition of the intergalactic medium and supposed to be driven purely by quasars. The He II transverse proximity effect—enhanced He II transmission in a background sightline caused by the ionizing radiation of a foreground quasar—therefore offers a unique opportunity to probe the morphology of He II reionization and to investigate the emission properties of quasars, e.g., ionizing emissivity, lifetime and beaming geometry. We use the most-recent *HST*/COS far-UV dataset of 22 He II absorption spectra and conduct our own dedicated optical spectroscopic survey to find foreground quasars around these He II sightlines. Based on a set of 66 foreground quasars, we perform the first statistical analysis of the He II transverse proximity effect. Despite a large object-to-object variance, our stacking analysis reveals an excess in the average He II transmission near the foreground quasars at 3σ significance. This statistical evidence for the transverse proximity effect is corroborated by a clear dependence of the signal strength on the inferred He II ionization rate at the background sightline. Our detection places, based on the transverse light crossing time, a geometrical limit on the quasar lifetime of $t_Q > 25$ Myr. This evidence for sustained activity of luminous quasars is relevant for the morphology of H I and He II reionization and helps to constrain AGN triggering mechanisms, accretion physics and models of black hole mass assembly. We show how future modeling of the transverse proximity effect can additionally constrain quasar emission geometries and e.g., clarify if the large observed object-to-object variance can be explained by current models of quasar obscuration.

Keywords: dark ages, reionization, first stars – intergalactic medium, – quasars: general, – quasars: lifetime, – quasars: obscuration

OPEN ACCESS

Edited by:
Mauro D'Onofrio,
Università degli Studi di Padova, Italy

Reviewed by:
José María Solanes,
University of Barcelona, Spain
Milan S. Dimitrijevic,
Astronomical Observatory, Serbia

****Correspondence:***
Tobias M. Schmidt
tschmidt@mpia.de

Specialty section:
This article was submitted to Milky Way and Galaxies, a section of the journal Frontiers in Astronomy and Space Sciences

Received: *01 September 2017*
Accepted: *29 September 2017*
Published: *17 October 2017*

Citation:
Schmidt TM, Worseck G, Hennawi JF, Prochaska JX, Crighton NHM, Lukić Z and Oñorbe J (2017) Statistical Detection of the He II Transverse Proximity Effect: Evidence for Sustained Quasar Activity for >25 Million Years. Front. Astron. Space Sci. 4:23. doi: 10.3389/fspas.2017.00023

1. INTRODUCTION

The double ionization of helium, known as He II reionization, marks the final phase transition of the intergalactic medium (IGM) and is closely related to the emission properties of the quasar population that is supposed to drive He II reionization. Hydrogen, according to the currently accepted picture (Haardt and Madau, 2012; Planck Collaboration et al., 2016), was reionized

at redshifts $z \sim 8$ primarily by the UV photons from stars. However, stellar spectra are not hard enough to supply sufficient numbers of photons with energies >4 Ry, required to doubly ionize helium. He II reionization therefore took place much later, when quasars became sufficiently abundant, culminating in the completion of helium reionization at $z \approx 2.7$ (Madau and Meiksin, 1994; Reimers et al., 1997; Miralda-Escudé et al., 2000; Faucher-Giguère et al., 2009; McQuinn, 2009; Worseck et al., 2011; Haardt and Madau, 2012; Compostella et al., 2013, 2014; Worseck et al., 2016). In the general picture of He II reionization, quasars create photoionized bubbles in the IGM which expand with time and eventually overlap, leading to the present day situation that the IGM is kept in photoionization equilibrium and highly ionized by a homogeneous and uniform UV background (Bolton et al., 2006; Furlanetto and Oh, 2008; McQuinn, 2009; Furlanetto and Dixon, 2010; Furlanetto and Lidz, 2011; Haardt and Madau, 2012; Meiksin and Tittley, 2012; Compostella et al., 2013, 2014; Davies et al., 2017). Since quasars are rare but bright sources, the reionization process is rather patchy and inhomogeneous. Its morphology therefore contains extensive information about the emission properties of the quasars.

At redshift $z \sim 3$, the $\lambda_{\rm rest} = 304$ Å He II Lyα transition is redshifted sufficiently into the far-UV (FUV) to be observable with space based telescopes, in particular the Hubble Space Telescope (*HST*). The usual technique is to take FUV spectra of background quasars and infer the helium ionization characteristics along the sightline from the absorption properties of the He II Lyα forest. The presence of a foreground quasar close to such a He II sightline allows to explore the effect of the foreground quasars ionizing radiation on the helium ionization state along the background sightline.

Figure 1 illustrates the prototype sightline of such a constellation. The bottom panel shows a Space Telescope Imaging Spectrograph (*HST*/STIS) FUV spectra (Heap et al., 2000) along the sightline toward the background quasars Q 0303−003. It shows over large regions Gunn-Peterson troughs (Gunn and Peterson, 1965) of saturated He II Lyα absorption, very similar to hydrogen Lyα spectra of high-redshift $z > 6$ quasars. Substantial He II transmission is only observed close to the background quasar, the so called line of sight proximity region. Here, the ionizing radiation from the background quasar has already sufficiently ionized helium to allow high He II transmission. In addition, the spectrum shows a striking transmission spike at $z = 3.05$. At the same redshift and with a separation of $\Delta\theta = 6'$ from the background sightline Jakobsen et al. (2003) found a foreground quasar and established the picture on the He II transverse proximity effect. In this picture, the foreground quasar photoionizes its surrounding and the background sightline intersects this ionization bubble, leading to strong He II transmission at the position of the foreground quasar.

Observing a strong transverse proximity effect in such a constellation allows to infer a geometric limit on the age of the quasar. Since one observed the quasar and the enhanced He II transmission at the same redshift and therefore same lookback time, the quasar has to already shine for at least the transverse light crossing time to give the photons enough time to reach the background sightline. This constellation might also give

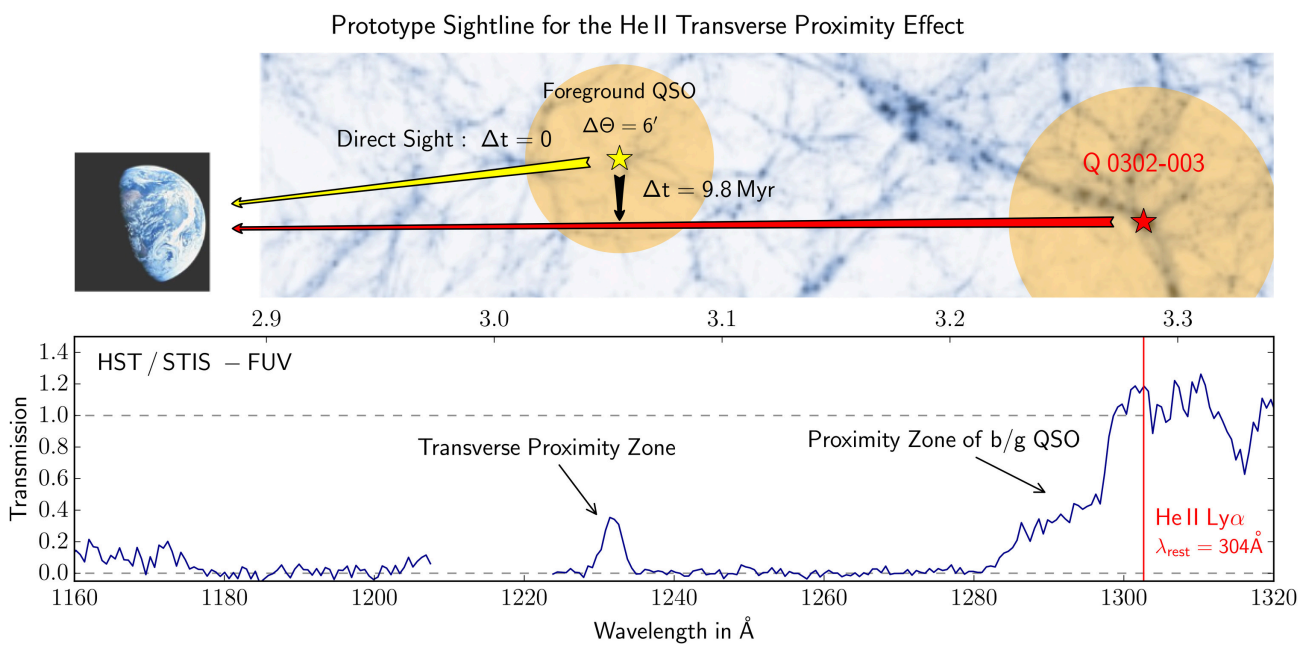

FIGURE 1 | This illustration shows the basic concept of the He II transverse proximity effect using the example of the Q 0302−003 prototype sightline. The bottom panel shows the *HST*/STIS FUV spectra from Heap et al. (2000), exhibiting an extended line of sight proximity effect close to the background sightline and a strong transmission peak at $z = 3.05$, caused by the proximity region of a close-by foreground quasar (Jakobsen et al., 2003). This constellation allows to derive a geometrical constraint on the age of the foreground quasar, based on the transverse light crossing time.

insights into the quasar emission geometry. The foreground quasar appears as unobscured Type I from Earth but its effect on the background sightline crucially depends on the obscuration properties toward the background sightline.

This illustrates the unique abilities to infer quasar properties offered by the He II transverse proximity effect. However, up to now, the Q 0302−003 sightline represents the only strong detection of a He II transverse proximity effect. Our aim is therefore to expand the sample, find additional foreground quasars close to He II sightlines and conduct a systematic investigation of the He II transverse proximity effect.

2. DEDICATED HELIUM REIONIZATION SURVEY

To increase the data sample and facilitate a statistical analysis of helium reionization, we are performing a comprehensive helium reionization survey. This includes the discovery and observation of new He II sightlines and a homogeneous and extremely careful reduction of all existing *HST* observations presented in Worseck et al. (2016). In addition, we conducted a dedicated optical foreground quasar survey around the 22 available He II sightlines which is described in Schmidt et al. (2017) and shall be summarized in the following.

The foreground quasar survey consists of a deep narrow survey conducted on 8 m class telescopes covering the immediate vicinity of the He II sightline and a wider survey targeting individual quasars on 4 m telescopes. The deep survey covers separations from the He II sightline up to $\Delta\theta \leq 10'$ and reaches a limiting magnitude of $r \leq 23.5$ mag. Quasar candidates were selected using deep multi-color imaging, primarily obtained with the Large Binocular Cameras at the Large Binocular Telescope (LBT/LBC, Giallongo et al., 2008; Speziali et al., 2008). The main concern here was to reach a U-band limiting magnitude of ≈ 26 mag. For spectroscopic confirmation the VIsible MultiObject Spectrograph (VIMOS, Le Fèvre et al., 2003) at the Very Large Telescope (VLT) was used. To find foreground quasars with larger separations from the background sightline, which are in particular important to probe long quasar lifetimes, we conducted a wide but shallower survey on 4 m class telescopes. We selected candidates from public quasar catalogs (DiPompeo et al., 2015; Richards et al., 2015) which are based on optical imaging (SDSS) and mid-infrared photometry from the *Wide-field Infrared Survey Explorer* (*WISE*, Wright et al., 2010). Using the *WISE* 3.6 and 4.5 μm bands allow very efficient quasar selection (Stern et al., 2012; Assef et al., 2013). Spectroscopic confirmation was done with the European Southern Observatory 3.5 m New Technology Telescope Faint Object Spectrograph and Camera (NTT/EFOSC2, Buzzoni et al., 1984) and the Calar Alto Observatory (CAHA) 3.5 m telescope TWIN spectrograph within 37 nights between November 2014 and August 2015. The wide survey reaches down to $r \leq 21.5$ mag and extends out to $\Delta\theta \approx 90'$ in case the quasar candidates were bright enough to expect a measurable effect on the background sightline.

In total, our surveys discovered 121 new quasars. We complement this sample by selecting quasars from the literature and in particular the spectroscopic catalogs of the Sloan Digital Sky Survey (SDSS, York et al., 2000) and the Baryon Oscillation Spectroscopic Surveys (BOSS, Eisenstein et al., 2011;

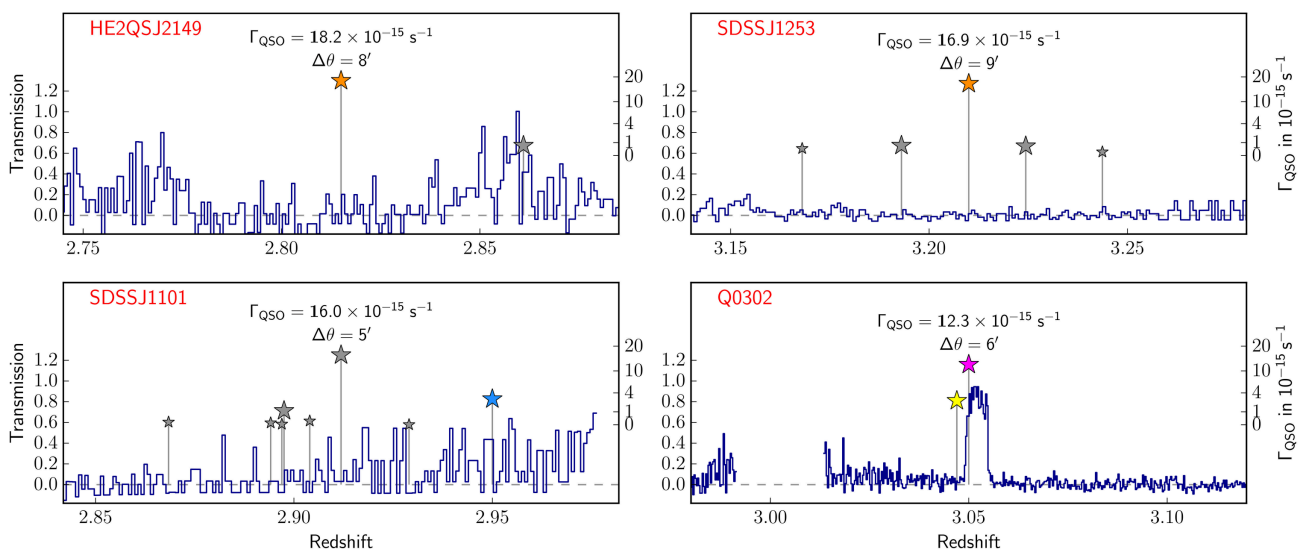

FIGURE 2 | He II spectra in the vicinity of the four foreground quasars with the highest estimated He II ionization rate Γ_{QSO}^{HeII} from Schmidt et al. (2017). Colors indicate the origin of the objects. (yellow: VLT/VIMOS; orange: CAHA/TWIN; blue: ESO NTT/EFOSC2; gray: SDSS/BOSS; pink: Literature). Size and vertical displacement of star symbols represent He II ionization rate. Only the previously known quasar along the Q 0302−003 sightline (Jakobsen et al., 2003) is associated with a strong He II transmission peak. The other three objects show, despite their up to 50% higher He II ionization rate and comparable other properties, extremely low He II transmission along the background sightline. One could speculate that these objects might be either very young or highly obscured toward the background sightline. ©: AAS. Figure reproduced from Schmidt et al. (2017).

Dawson et al., 2013) twelfth data release (Alam et al., 2015; Pâris et al., 2016). For all objects we calculate the estimated He II photoionization rate at the background sightline $\Gamma_{\rm QSO}^{\rm HeII}$ assuming isotropic emission, infinite quasar lifetime and no IGM absorption. For details see Schmidt et al. (2017). Our sample contains 66 foreground quasars for which we have full spectral coverage along the background sightline and which exceed $\Gamma_{\rm QSO}^{\rm HeII} > 0.5 \times 10^{-15}\,{\rm s}^{-1}$. For comparison, the He II UV background at $z \sim 3$ should be approximately $\Gamma_{\rm UVB}^{\rm HeII} \approx 1 \times 10^{-15}\,{\rm s}^{-1}$(Faucher-Giguère et al., 2009; Haardt and Madau, 2012; Khrykin et al., 2016).

3. THE TRANSVERSE PROXIMITY EFFECT OF INDIVIDUAL QUASARS

For the prototype object at $z = 3.05$ along the Q 0302−003 sightline we calculate an expected ionization rate of $\Gamma_{\rm UVB}^{\rm HeII} \approx 12 \times 10^{-15}\,{\rm s}^{-1}$. Thus, this object should exceed the He II UV background by approximately one order of magnitude. Observing a strong transverse proximity effect is therefore not surprising. Within our study we find three other foreground quasars that should cause up to 50% higher He II ionization rates at the background sightlines. The He II spectra associated with all four of these objects are shown in **Figure 2**. Surprisingly, the three new objects show no evidence for strong transverse proximity effect. On the contrary, we find completely ordinary and in several cases even fully saturated He II absorption. The three new foreground quasars are in terms of luminosity, separation from the background sightline and redshift comparable to the prototype quasar. It is therefore rather unexpected to find not even the slightest indication of a transverse proximity effect for any of them.

Possible explanations are that these quasars might be too young and therefore the ionizing radiation had not enough time to reach the background sightline. Given the transverse separations, this would point toward quasar ages below 8–15 Myr. Another possible explanation would be quasar obscuration. According to the common quasar unification models (e.g., Antonucci, 1993; Elvis, 2000), the dichotomy between Type I and Type II quasars is purely an orientation effect. Each quasar should emit only toward some part of the sky, approximately 50% according to (e.g., Brusa et al., 2010; Lusso et al., 2013; Marchesi et al., 2016), and be obscured toward the other directions. However, it seems quite unlikely that three out of four quasars are oriented in a way that no ionizing radiation at all reaches the background sightline. Without further investigation it therefore remains purely speculative why we find no strong transverse proximity effect for the three strongest foreground quasars.

4. STATISTICAL DETECTION OF THE TRANSVERSE PROXIMITY EFFECT

Apart form the non-detection of the proximity effect for individual quasars, we search for statistical evidence in the average He II transmission profile around foreground quasars. We therefore select foreground quasars with $\Gamma_{\rm QSO}^{\rm HeII} > 2 \times 10^{-15}\,{\rm s}^{-1}$ and stack the He II spectra on the positions of these foreground quasars. The result is shown in **Figure 3**, top panel. Despite the large scatter, we find a clear enhancement in the average He II transmission right at the location of the foreground quasars. We conduct a Monte Carlo analysis by stacking the He II spectra on random positions and find a significance of $3.1\,\sigma$ for the measured transmission enhancement. In addition, we show in Schmidt et al. (2017) that the strength of this transmission enhancement roughly scales with the ionization rate of the foreground quasars and vanishes for $\Gamma_{\rm QSO}^{\rm HeII} < 2 \times 10^{-15}\,{\rm s}^{-1}$ which is roughly comparable to the He II UV background (Faucher-Giguère et al., 2009; Haardt and Madau, 2012). We are therefore confident that the observed effect is actually caused by the ionizing radiation of the foreground quasars.

Based on this statistical detection of the He II transverse proximity effect we can investigate the quasar lifetime. Therefore,

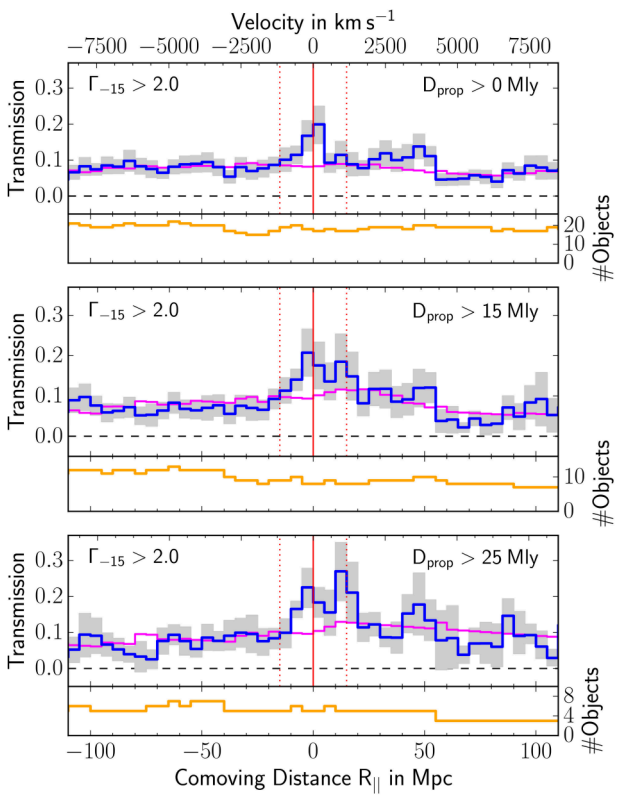

FIGURE 3 | Statistical detection of the He II transverse proximity effect from Schmidt et al. (2017). We compute an average He II transmission profile in the vicinity of the foreground quasars (blue) by stacking the He II spectra on the positions of known foreground quasars. Bootstrap errors are given in gray, the number of contributing objects in yellow. The purple line shows a simple model for the average He II transmission in the IGM. The top plot includes all quasars with $\Gamma_{\rm QSO}^{\rm HeII} > 2 \times 10^{-15}\,{\rm s}^{-1}$ and shows a clear transmission enhancement at the position of the foreground quasars (red). The other two plots include only a subset of foreground quasars with a minimum separation from the background sightline larger than 15 and 25 Mlyr. The transmission enhancement persists in these stacks, setting a clear constraint on the age of the foreground quasars. ©: AAS. Figure reproduced from Schmidt et al. (2017).

we include only foreground quasars in the stack that have a given minimum separation from the background sightline. As shown in **Figure 3**, the transverse proximity effect persists in the average transmission profile even for quasars with separations > 25 Mlyr. The significance of the He II transverse proximity effect in the >15 and >25 Mlyr stacks was determined to be 3.2 σ and 2.6 σ. Based on the transverse light crossing time we conclude that the quasars have to shine for at least 25 Myr.

5. SUMMARY AND OUTLOOK ON FUTURE MODELING ATTEMPTS

In Schmidt et al. (2017) we have described our dedicated foreground quasar survey around 22 He II sightlines and the discovery of 121 new quasars. With the addition of quasars from SDSS/BOSS we have composed a relatively large foreground quasar sample that allows for the first time a statistical analysis of the He II transverse proximity effect. By the means of a stacking analysis, we were able to find statistical evidence for the presence of a He II transverse proximity effect in the average transmission profile around 20 foreground quasars and by cutting on the transverse separation we could place a clear constraint on the quasar lifetime of >25 Myr. What remains however, is the surprising and to some degree contradictory result that our stacking analysis shows evidence for a long quasar lifetime while among the four strongest foreground quasars which all should exceed the He II UV background by an order of magnitude and are at most 15 Mlyr away from the background sightline only the previously known quasar is associated with a strong He II transmission spike.

We would like to apply our method to an even larger dataset. However, given the capabilities of the current UV space telescopes (*GALEX*, *HST*), the discovery of many new He II sightlines is unlikely and a good fraction of the known sightlines has now been searched for foreground quasars. In the near future, new insight into the He II transverse proximity effect will therefore probably come from dedicated modeling. A first attempt for this is shown in **Figure 4**. We take outputs of a cosmological hydrodynamical simulation computed with the

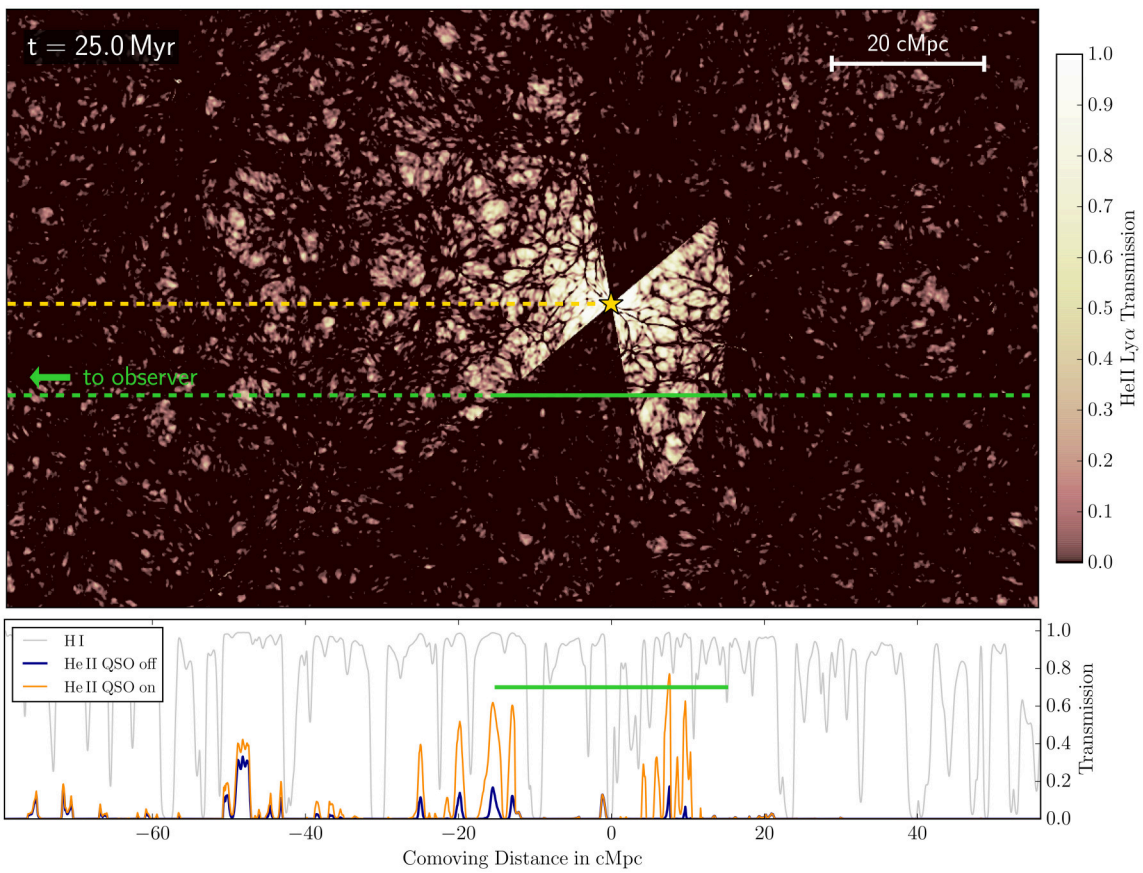

FIGURE 4 | Illustration of our photoionization model we use to investigate the effect of obscuration and finite quasar age. The top panel displays the He II transmission in a slice through the simulation box. It clearly shows the bi-conical emission of the quasar and the parabolic shaped region that can be reached by the quasar emission within the given time. The bottom panel shows the computed hydrogen and helium transmission spectra along a background sightline (green). A strong He II transmission enhancements is visible in regions that are illuminated by the quasar. The solid green bar marks the ±15 cMpc wide region we use to measure the transmission enhancement (Schmidt et al., 2017).

Eulerian grid code Nyx (Almgren et al., 2013; Lukić et al., 2015) and post-process these with a photo-ionization model that simulates a single bright foreground quasar. In this model we can explicitly vary quasar age and emission geometry. The case shown in **Figure 4** is matched in quasar luminosity and sightline geometry to the Q 0302−003 $z = 3.05$ foreground quasar. We chose a classical bi-conical emission geometry with a half-opening angle of $\alpha = 60^\circ$, therefore illuminating 50% of the sky. The quasar is inclined by 20° and assumed to be 25 Myr old. For an observer on Earth, the low redshift parts of the background sightline appears to be illuminated first while the quasar radiation arrive at successively later times at higher redshifts. For a given quasar age, the illuminated region has a parabolic shape, open toward the observer and with the quasar at the focus. The finite quasar age limits the extend of the illuminated region toward high redshifts (larger comoving distance, right side). This is well visible in the top panel of **Figure 4** which shows the simulated He II transmission in a thin slice through the simulation. The bottom panel clearly shows the He II transverse proximity effect along the background sightline and the substantially enhanced transmission compared to the the effect of the $\Gamma_{\rm UVB}^{\rm HeII} \approx 1 \times 10^{-15}\,{\rm s}^{-1}$ UV background alone, but also the effect of obscuration and finite quasar age.

With these models, we intent to investigate the combined effect of quasar obscuration and finite quasar age on the expected He II transmission, compare them to the observed He II spectra associated with the strongest foreground quasars and infer their age and obscuration properties. It is obvious that due to the random quasar orientation any constraints will only be of probabilistic nature and our endeavor will probably require a large Monte Carlo analysis and sophisticated statistical methods. However, given the high expected photoionization rate of the foreground quasars, it should still be possible to rule out certain parts of the parameter space and give insights if a reference model with e.g., 50% obscuration and 25 Myr lifetime is actually consistent with our observations and the non-detection of strong transmission peaks for the strongest foreground quasars.

AUTHOR CONTRIBUTIONS

This work is part of the Ph.D. project of TS under supervision of JH and GW. GW is responsible for the He II FUV spectra. JP and NC provided optical observational data and data reduction tools. Cosmological hydrodynamical simulations were provided by ZL and JO.

FUNDING

GW has been supported by the Deutsches Zentrum für Luft- und Raumfahrt (DLR) under contracts 50 OR 1317 and 50 OR 1512.

ACKNOWLEDGMENTS

We thank Robert Simcoe for kindly supplying Magellan/Megacam imaging for the SDSS J1237+0126 field. We would like to thank the members of the ENIGMA[1] group at the Max Planck Institute for Astronomy (MPIA) for useful discussions and support.

Based on observations made with the NASA/ESA Hubble Space Telescope, obtained at the Space Telescope Science Institute, which is operated by the Association of Universities for Research in Astronomy, Inc., under NASA contract NAS 5-26555. These observations are associated with programs 11528, 11742, 12033, 12178, 12249, 13013.

The LBT is an international collaboration among institutions in the United States, Italy, and Germany. LBT Corporation partners are: The University of Arizona on behalf of the Arizona Board of Regents; Istituto Nazionale di Astrofisica, Italy; LBT Beteiligungsgesellschaft, Germany, representing the Max-Planck Society, The Leibniz Institute for Astrophysics Potsdam, and Heidelberg University; The Ohio State University, and The Research Corporation, on behalf of The University of Notre Dame, University of Minnesota and University of Virginia.

This paper includes data gathered with the 6.5 m Magellan Telescopes located at Las Campanas Observatory, Chile.

Based in part on observations at Cerro Tololo Inter-American Observatory and Kitt Peak National Observatory, National Optical Astronomy Observatory, which are operated by the Association of Universities for Research in Astronomy (AURA) under a cooperative agreement with the National Science Foundation. The authors are honored to be permitted to conduct astronomical research on Iolkam Du'ag (Kitt Peak), a mountain with particular significance to the Tohono O'odham. Based on observations collected at the European Organization for Astronomical Research in the Southern Hemisphere under ESO programmes 088.A-0835(B), 090.A-0664(B), 094.A-0500(A), 094.A-0782(A).

Based on observations collected at the Centro Astronómico Hispano Alemán (CAHA) at Calar Alto, operated jointly by the Max-Planck Institut für Astronomie and the Instituto de Astrofísica de Andalucía (CSIC).

Some of the data presented herein were obtained at the W. M. Keck Observatory, which is operated as a scientific partnership among the California Institute of Technology, the University of California and the National Aeronautics and Space Administration. The Observatory was made possible by the generous financial support of the W. M. Keck Foundation. The authors wish to recognize and acknowledge the very significant cultural role and reverence that the summit of Mauna Kea has always had within the indigenous Hawaiian community. We are most fortunate to have the opportunity to conduct observations from this mountain.

Funding for SDSS-III has been provided by the Alfred P. Sloan Foundation, the Participating Institutions, the National Science Foundation, and the U.S. Department of Energy Office of Science. The SDSS-III web site is http://www.sdss3.org/. SDSS-III is managed by the Astrophysical Research Consortium for the Participating Institutions of the SDSS-III Collaboration including the University of Arizona, the Brazilian Participation Group, Brookhaven National Laboratory, Carnegie Mellon

[1] http://enigma.physics.ucsb.edu/

University, University of Florida, the French Participation Group, the German Participation Group, Harvard University, the Instituto de Astrofisica de Canarias, the Michigan State/Notre Dame/JINA Participation Group, Johns Hopkins University, Lawrence Berkeley National Laboratory, Max Planck Institute for Astrophysics, Max Planck Institute for Extraterrestrial Physics, New Mexico State University, New York University, Ohio State University, Pennsylvania State University, University of Portsmouth, Princeton University, the Spanish Participation Group, University of Tokyo, University of Utah, Vanderbilt University, University of Virginia, University of Washington, and Yale University.

REFERENCES

Alam, S., Albareti, F. D., Allende Prieto, C., Anders, F., Anderson, S. F., Anderton, T., et al. (2015). The eleventh and twelfth data releases of the sloan digital sky survey: final data from SDSS-III. *Astrophys. J. Suppl.* 219:12. doi: 10.1088/0067-0049/219/1/12

Almgren, A. S., Bell, J. B., Lijewski, M. J., Lukić, Z., and Van Andel, E. (2013). Nyx: a massively parallel AMR code for computational cosmology. *Astrophys. J.* 765:39. doi: 10.1088/0004-637X/765/1/39

Antonucci, R. (1993). Unified models for active galactic nuclei and quasars. *Ann. Rev. Astron. Astrophys.* 31, 473–521. doi: 10.1146/annurev.aa.31.090193.002353

Assef, R. J., Stern, D., Kochanek, C. S., Blain, A. W., Brodwin, M., Brown, M. J. I., et al. (2013). Mid-infrared selection of active galactic nuclei with the wide-field infrared survey explorer. II. Properties of WISE-selected active galactic nuclei in the NDWFS Boötes field. *Astrophys. J.* 772:26. doi: 10.1088/0004-637X/772/1/26

Bolton, J. S., Haehnelt, M. G., Viel, M., and Carswell, R. F. (2006). Spatial fluctuations in the spectral shape of the ultraviolet background at $2 < z < 3$ and the reionization of helium. *Month. Notices RAS* 366, 1378–1390. doi: 10.1111/j.1365-2966.2006.09927.x

Brusa, M., Civano, F., Comastri, A., Miyaji, T., Salvato, M., Zamorani, G., et al. (2010). The XMM-Newton wide-field survey in the cosmos field (XMM-COSMOS): demography and multiwavelength properties of obscured and unobscured luminous active galactic nuclei. *Astrophys. J.* 716, 348–369. doi: 10.1088/0004-637X/716/1/348

Buzzoni, B., Delabre, B., Dekker, H., Dodorico, S., Enard, D., Focardi, P., et al. (1984). The ESO faint object spectrograph and camera (EFOSC). *Messenger* 38, 9–13.

Compostella, M., Cantalupo, S., and Porciani, C. (2013). The imprint of inhomogeneous He II reionization on the H I and He II Lyα forest. *Month. Notices RAS* 435, 3169–3190. doi: 10.1093/mnras/stt1510

Compostella, M., Cantalupo, S., and Porciani, C. (2014). AGN-driven helium reionization and the incidence of extended He III regions at redshift $z > 3$. *Month. Notices RAS* 445, 4186–4196. doi: 10.1093/mnras/stu2035

Davies, F. B., Furlanetto, S. R., and Dixon, K. L. (2017). A self-consistent 3D model of fluctuations in the helium-ionizing background. *Month. Notices RAS* 465, 2886–2894. doi: 10.1093/mnras/stw2868

Dawson, K. S., Schlegel, D. J., Ahn, C. P., Anderson, S. F., Aubourg, É., Bailey, S., et al. (2013). The Baryon oscillation spectroscopic survey of SDSS-III. *Astron. J.* 145:10. doi: 10.1088/0004-6256/145/1/10

DiPompeo, M. A., Bovy, J., Myers, A. D., and Lang, D. (2015). Quasar probabilities and redshifts from WISE mid-IR through GALEX UV photometry. *Month. Notices RAS* 452, 3124–3138. doi: 10.1093/mnras/stv1562

Eisenstein, D. J., Weinberg, D. H., Agol, E., Aihara, H., Allende Prieto, C., Anderson, S. F., et al. (2011). SDSS-III: massive spectroscopic surveys of the distant universe, the milky way, and extra-solar planetary systems. *Astron. J.* 142:72. doi: 10.1088/0004-6256/142/3/72

Elvis, M. (2000). A structure for quasars. *Astrophys. J.* 545, 63–76. doi: 10.1086/317778

Faucher-Giguère, C.-A., Lidz, A., Zaldarriaga, M., and Hernquist, L. (2009). A new calculation of the ionizing background spectrum and the effects of He II reionization. *Astrophys. J.* 703, 1416–1443. doi: 10.1088/0004-637X/703/2/1416

Furlanetto, S. R., and Dixon, K. L. (2010). Large-scale fluctuations in the He II Lyα forest and He II reionization. *Astrophys. J.* 714, 355–366. doi: 10.1088/0004-637X/714/1/355

Furlanetto, S. R., and Lidz, A. (2011). Constraints on quasar lifetimes and beaming from the He II Lyα forest. *Astrophys. J.* 735:117. doi: 10.1088/0004-637X/735/2/117

Furlanetto, S. R., and Oh, S. P. (2008). The history and morphology of helium reionization. *Astrophys. J.* 681, 1–17. doi: 10.1086/588546

Giallongo, E., Ragazzoni, R., Grazian, A., Baruffolo, A., Beccari, G., de Santis, C., et al. (2008). The performance of the blue prime focus large binocular camera at the large binocular telescope. *Astron. Astrophys.* 482, 349–357. doi: 10.1051/0004-6361:20078402

Gunn, J. E., and Peterson, B. A. (1965). On the density of neutral hydrogen in intergalactic space. *Astrophys. J.* 142, 1633–1641. doi: 10.1086/148444

Haardt, F., and Madau, P. (2012). Radiative transfer in a clumpy universe. IV. New synthesis models of the cosmic UV/X-ray background. *Astrophys. J.* 746:125. doi: 10.1088/0004-637X/746/2/125

Heap, S. R., Williger, G. M., Smette, A., Hubeny, I., Sahu, M. S., Jenkins, E. B., et al. (2000). STIS observations of HE II Gunn-Peterson absorption toward Q0302-003. *Astrophys. J.* 534, 69–89. doi: 10.1086/308719

Jakobsen, P., Jansen, R. A., Wagner, S., and Reimers, D. (2003). Caught in the act: a helium-reionizing quasar near the line of sight to Q0302-003. *Astron. Astrophys.* 397, 891–898. doi: 10.1051/0004-6361:20021579

Khrykin, I. S., Hennawi, J. F., McQuinn, M., and Worseck, G. (2016). The He II proximity effect and the lifetime of quasars. *Astrophys. J.* 824:133. doi: 10.3847/0004-637X/824/2/133

Le Fèvre, O., Saisse, M., Mancini, D., Brau-Nogue, S., Caputi, O., Castinel, L., et al. (2003). "Commissioning and performances of the VLT-VIMOS instrument," in *Instrument Design and Performance for Optical/Infrared Ground-based Telescopes, Volume 4841 of Proceedings of SPIE*, eds M. Iye and A. F. M. Moorwood, 1670–1681. Available online at: http://adsabs.harvard.edu/abs/2003SPIE.4841.1670L

Lukić, Z., Stark, C. W., Nugent, P., White, M., Meiksin, A. A., and Almgren, A. (2015). The Lyman α forest in optically thin hydrodynamical simulations. *Month. Notices RAS* 446, 3697–3724. doi: 10.1093/mnras/stu2377

Lusso, E., Hennawi, J. F., Comastri, A., Zamorani, G., Richards, G. T., Vignali, C., et al. (2013). The obscured fraction of active galactic nuclei in the XMM-COSMOS survey: a spectral energy distribution perspective. *Astrophys. J.* 777:86. doi: 10.1088/0004-637X/777/2/86

Madau, P., and Meiksin, A. (1994). The He II Lyman-alpha opacity of the universe. *Astrophys. J. Lett.* 433, L53–L56. doi: 10.1086/187546

Marchesi, S., Lanzuisi, G., Civano, F., Iwasawa, K., Suh, H., Comastri, A., et al. (2016). The chandra COSMOS-legacy survey: source X-ray spectral properties. *Astrophys. J.* 830:100. doi: 10.3847/0004-637X/830/2/100

McQuinn, M. (2009). The implications of Gunn-Peterson troughs in the He II Lyα forest. *Astrophys. J. Lett.* 704, L89–L92. doi: 10.1088/0004-637X/704/2/L89

Meiksin, A., and Tittley, E. R. (2012). The impact of helium reionization on the structure of the intergalactic medium. *Month. Notices RAS* 423, 7–25. doi: 10.1111/j.1365-2966.2011.20380.x

Miralda-Escudé, J., Haehnelt, M., and Rees, M. J. (2000). Reionization of the inhomogeneous universe. *Astrophys. J.* 530, 1–16. doi: 10.1086/308330

Pâris, I., Petitjean, P., Ross, N. P., Myers, A. D., Aubourg, É., Streblyanska, A., et al. (2016). The sloan digital sky survey quasar catalog: twelfth data release. ArXiv e-prints.

Planck Collaboration, Adam, R., Aghanim, N., Ashdown, M., Aumont, J., Baccigalupi, C., et al. (2016). Planck intermediate results. XLVII. Planck constraints on reionization history. *Astron. Astrophys.* 596:A108. doi: 10.1051/0004-6361/201628897

Reimers, D., Kohler, S., Wisotzki, L., Groote, D., Rodriguez-Pascual, P., and Wamsteker, W. (1997). Patchy intergalactic He II absorption in HE 2347-4342. II. The possible discovery of the epoch of He-reionization. *Astron. Astrophys.* 327, 890–900.

Richards, G. T., Myers, A. D., Peters, C. M., Krawczyk, C. M., Chase, G., Ross, N. P., et al. (2015). Bayesian high-redshift quasar classification from optical and Mid-IR photometry. *Astrophys. J. Suppl.* 219:39. doi: 10.1088/0067-0049/219/2/39

Schmidt, T. M., Worseck, G., Hennawi, J. F., Prochaska, J. X., and Crighton, N. H. M. (2017). Statistical detection of the HeII transverse proximity effect: evidence for sustained quasar activity for >25 million years. *Astrophys. J.* 847:81. doi: 10.3847/1538-4357/aa83ac

Speziali, R., Di Paola, A., Giallongo, E., Pedichini, F., Ragazzoni, R., Testa, V., et al. (2008). "The Large Binocular Camera: description and performances of the first binocular imager," in *Ground-based and Airborne Instrumentation for Astronomy II, Volume 7014 of Proceedings of the SPIE*, eds I. S. McLean and M. M. Casali. Available online at: http://adsabs.harvard.edu/abs/2008SPIE.7014E..4TS

Stern, D., Assef, R. J., Benford, D. J., Blain, A., Cutri, R., Dey, A., et al. (2012). Mid-infrared selection of active galactic nuclei with the wide-field infrared survey explorer. I. Characterizing WISE-selected active galactic nuclei in COSMOS. *Astrophys. J.* 753:30. doi: 10.1088/0004-637X/753/1/30

Worseck, G., Prochaska, J. X., Hennawi, J. F., and McQuinn, M. (2016). Early and extended helium reionization over more than 600 million years of cosmic time. *Astrophys. J.* 825:144. doi: 10.3847/0004-637X/825/2/144

Worseck, G., Prochaska, J. X., McQuinn, M., Dall'Aglio, A., Fechner, C., Hennawi, J. F., et al. (2011). The end of helium reionization at z ˜= 2.7 inferred from cosmic variance in HST/COS He II Lyα absorption spectra. *Astrophys. J. Lett.* 733:L24. doi: 10.1088/2041-8205/733/2/L24

Wright, E. L., Eisenhardt, P. R. M., Mainzer, A. K., Ressler, M. E., Cutri, R. M., Jarrett, T., et al. (2010). The wide-field infrared survey explorer (WISE): mission description and initial on-orbit performance. *Astron. J.* 140, 1868–1881. doi: 10.1088/0004-6256/140/6/1868

York, D. G., Adelman, J., Anderson, J. E. Jr., Anderson, S. F., Annis, J., Bahcall, N. A., et al. (2000). The sloan digital sky survey: technical summary. *Astron. J.* 120, 1579–1587. doi: 10.1086/301513

Conflict of Interest Statement: The authors declare that the research was conducted in the absence of any commercial or financial relationships that could be construed as a potential conflict of interest.

Copyright © 2017 Schmidt, Worseck, Hennawi, Prochaska, Crighton, Lukić and Oñorbe. This is an open-access article distributed under the terms of the Creative Commons Attribution License (CC BY). The use, distribution or reproduction in other forums is permitted, provided the original author(s) or licensor are credited and that the original publication in this journal is cited, in accordance with accepted academic practice. No use, distribution or reproduction is permitted which does not comply with these terms.

frontiers in Astronomy and Space Sciences

REVIEW
published: 29 November 2017
doi: 10.3389/fspas.2017.00042

The Many Routes to AGN Feedback

Raffaella Morganti [1, 2]*

[1] ASTRON, Netherlands Institute for Radio Astronomy, Dwingeloo, Netherlands, [2] Kapteyn Astronomical Institute, University of Groningen, Groningen, Netherlands

The energy released by Active Galactic Nuclei (AGN) in the form of radiation, winds, or radio plasma jets, is known to impact on the surrounding interstellar medium. The result of these processes, known as AGN (negative) feedback, is suggested to prevent gas, in and around galaxies, from cooling, and to remove, or at least redistribute, gas by driving massive and fast outflows, hence playing a key role in galaxy evolution. Given its importance, a large effort is devoted by the astronomical community to trace the effects of AGN on the surrounding gaseous medium and to quantify their impact for different types of AGN. This review briefly summarizes some of the recent observational results obtained in different wavebands, tracing different phases of the gas. I also summarize the new insights they have brought, and the constraints they provide to numerical simulations of galaxy formation and evolution. The recent addition of deep observations of cold gas and, in particular, of cold molecular gas, has brought some interesting surprises and has expanded our understanding of AGN and AGN feedback.

Keywords: active galactic nuclei, interstellar medium, outflows, extragalactic radio jets, spectroscopy

OPEN ACCESS

Edited by:
Paola Marziani, Osservatorio Astronomico di Padova (INAF), Italy

Reviewed by:
Vyacheslav Ivanovich Dokuchaev, Institute for Nuclear Research (RAS), Russia
Anna Lia Longinotti, National Institute of Astrophysics, Optics and Electronics, Mexico

***Correspondence:**
Raffaella Morganti
morganti@astron.nl

Specialty section:
This article was submitted to Milky Way and Galaxies, a section of the journal Frontiers in Astronomy and Space Sciences

Received: *09 September 2017*
Accepted: *30 October 2017*
Published: *29 November 2017*

Citation:
Morganti R (2017) The Many Routes to AGN Feedback. Front. Astron. Space Sci. 4:42. doi: 10.3389/fspas.2017.00042

INTRODUCTION: AGN AND FEEDBACK

AGN are fascinating objects. Since more than 50 years, astronomers have studied the effects of the extreme processes and the conditions that they cause. The huge amounts of energy released by the active super massive black hole (SMBH) can have an impact on the life and evolution of their entire host galaxy. This has made AGN relevant for an even broader community of astronomers. What is now commonly called *AGN feedback* has become a key ingredient in simulations of galaxy evolution. AGN feedback is the (self-regulating) process which links the energy released by the AGN to the surrounding gaseous medium and in this way, impacting on the evolution of the host galaxy. The energy injected by the AGN can provide the mechanism, either by preventing the cooling of gas or by expelling gas from the galaxy, to quench star formation (thus limiting the number of massive galaxies) and to limit the growth of the SMBH. Thus, it helps explaining key observations in these areas obtained in the recent years (e.g., Silk and Rees, 1998; Gebhardt et al., 2000). In addition, the energy dumped in the environment of the AGN affects the fuelling of the nuclear activity itself, thereby regulating its duty-cycle.

AGN feedback is now included in many theoretical, numerical, and semi-analytic models (e.g., Kauffmann and Haehnelt, 2000; Di Matteo et al., 2005; Schaye et al., 2015; Sijacki et al., 2015). The goal of the observations is to provide constraints to help a realistic implementation of feedback effects in these simulations. This is still a challenging task. As described below, the results from the increasingly accurate and deep observations have shown how complex these processes are.

Interestingly, the study of AGN in the context of their feedback effects has brought a number of unexpected discoveries (some of them described in this review) about the physical conditions of the gas in the surroundings of an active nucleus. Given its complexity, the treatment of feedback in numerical simulations is still extremely difficult. However, the implementation is becoming more sophisticated and reaching the stage where observables can be extracted from the simulations and compared with observations.

This review will concentrate on recent results from observations at low redshift and will focus on *negative feedback*. The energy released by the AGN and the related feedback effect can operate on very different distances from the central, active SMBH and can be traced by different phases of the gas. Particular emphasis will be given to the new information provided by the cold molecular gas. The review starts by summarizing some of the results on the impact of the radio plasma on the hot and cold gas distributed on large (many tens to hundred of kpc) scales. A more extended part of the review is dedicated to outflows occurring in the inner regions (kpc-scale). The mechanisms that may drive these outflows and their effects on the ISM are discussed. Finally, two examples of the diversity of mechanisms obtained thanks to multi-wavelengths observations will be presented.

It is impossible in this short paper to do justice to all exciting results. However, several other reviews have extensively covered various aspects and results of AGN feedback (see e.g., Cattaneo et al., 2009; Alexander and Hickox, 2012; Fabian, 2012; Harrison, 2017) and the reader can refer to them for further information.

Before entering the description of the results from observations, it is important to note that, to first order, there are two modes in which AGN feedback can operate and they depend mostly on the type of nuclear activity (see Alexander and Hickox, 2012; Fabian, 2012; Harrison, 2017 for reviews). Examples of manifestations of these modes are described in section Feedback on Large (tens of kpc) Scales: Radio Lobes and X-ray Cavities and Effects of AGN on kpc Scales: Multi-Phase Gas Outflows.

The *quasar (or radiative) mode* is mostly associated with high luminosity AGN, i.e., those emitting close to the Eddington limit, where most of the energy is released by radiation (or a wind) from the accretion disk but where also radio jets can play a role. The release of energy drives gas outflows expelling gas from the galaxy. The *jet (or kinetic) mode* is, instead, considered to be dominant in low-power AGN where the radio plasma provides the main source of energy, preventing the gaseous atmosphere from cooling back into the galaxy. While in the most extreme cases—high luminosity AGN and cool-core clusters—the separation between the two modes can be clear-cut, in other more intermediate situations, and for the most common types of AGN, the separation may not be always so sharp. Multi-wavelengths observations are often needed to recognize and disentangle different modes of feedback. Furthermore, the luminosity (or radio power) of the AGN is not the only parameter defining the impact. The coupling between the energy released and the medium is important (Tadhunter, 2008; Alexander and Hickox, 2012) as well as the duty-cycle of the activity (Fabian, 2012; Morganti, 2017).

FEEDBACK ON LARGE (TENS OF KPC) SCALES: RADIO LOBES AND X-RAY CAVITIES

The most clear observational evidence of the impact of the nuclear activity on the surrounding medium comes from X-ray and radio observations, in particular in gas rich cool-core clusters (McNamara and Nulsen, 2007, 2012 for reviews). X-ray images have revealed giant cavities and shock fronts in the hot gas, often filled with radio plasma lobes. The spatial coincidence between these cavities and the emission from radio lobes, suggests that the hot gas has been displaced by the expanding radio bubbles inflated by radio jets emitted by the central active SMBH. These studies have shown that the power associated to the radio jet provides the mechanism to offset radiative losses and to suppress gas cooling. They have provided a direct and relatively reliable mean of measuring the energy injected by the AGN (see McNamara and Nulsen, 2007, 2012 for reviews). Given that the radiative cooling time at the centers of hot atmospheres in groups, clusters and elliptical galaxies can be short (ranging from < 1 Gyr to below 0.1 Gyr for the latter group), without this energy input, the gas would cool from the surrounding atmosphere. This will produce a large amount of molecular gas and star formation that instead is not observed in e.g., central cluster galaxies or any massive galaxy (Ciotti et al., 2017).

X-ray cavities are detected in about 50% of galaxy clusters, groups and individual galaxies. Their scales range from a few kpc to 200 kpc and the associated cavity power typically balances (or exceed) the X-ray cooling in galaxy clusters and also in some isolated elliptical galaxies (see **Figure 1,** left). Furthermore, from the combined X-ray and radio studies, we have learned about the energetics involved**.** The mechanical power of radio jets largely exceeds their synchrotron power, suggesting that even weak radio sources—both in clusters and in elliptical galaxies—are mechanically powerful enough (Cavagnolo et al., 2010). Thus, this phenomenon appears to be important even in AGN of moderate radio luminosity. This is important because these AGN are much more common compared to the high power radio sources. Finally, it is worth to underline that the effect of the radio plasma can be relevant also in sources outside large clusters, as demonstrated by the work on isolated galaxies (e.g., Nulsen et al., 2007; Cavagnolo et al., 2010).

A small fraction (few %) of the most rapidly cooling gas in clusters is known to cool to low temperatures. This gas can provide the observed cold molecular gas reservoirs and feed the star formation in the central galaxy (Edge, 2001; Salomé and Combes, 2003). These initial findings are now, especially thanks to ALMA, expanded for more objects and they show a possible coupling between radio bubbles and cold gas. **Figure 1** (right) shows the case of the Phoenix cluster (Russell et al., 2017) where the extended filaments are draped around the expanding radio bubbles suggesting that the molecular gas flow is shaped by the radio-jet activity and possibly lifted by the radio bubbles. In the case of this cluster, the smooth velocity gradient observed in the filaments suggests an ordered flow with the gas velocities too low for the bulk of the cold gas to escape the galaxy. This gas will eventually fall back toward the galaxy center: this further support the (short) duty cycle of activity observed especially for cluster radio sources (Hogan et al., 2015). An increasing number of ALMA observations of molecular gas at the centers of clusters have now shown this synergy, with cold gas filaments extending along the radio bubbles (McNamara et al., 2014; Russell et al., 2014, 2017; Tremblay et al., 2016).

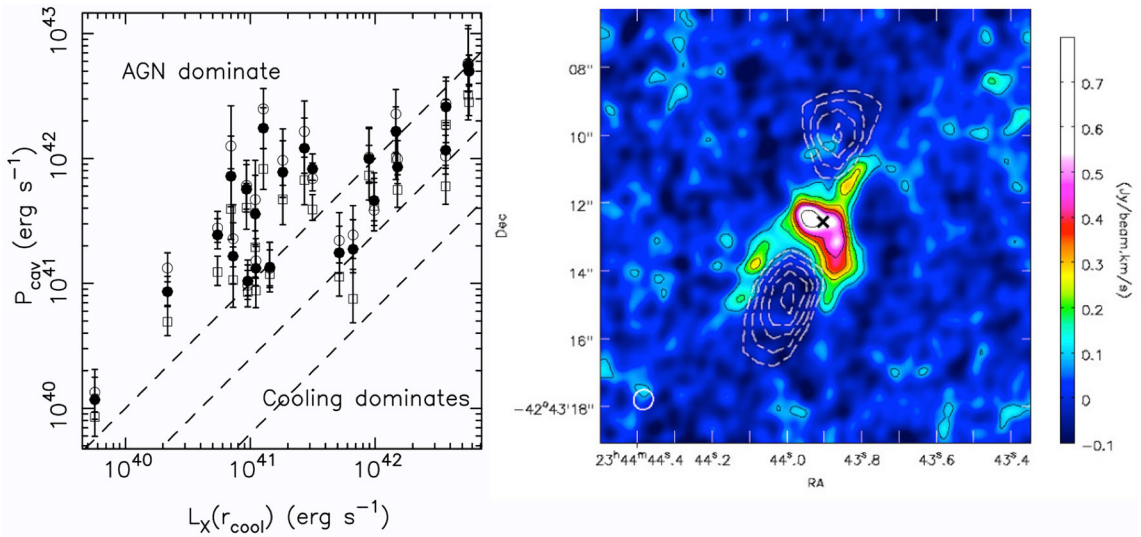

FIGURE 1 | Left: Cavity heating power (estimated as pV/t_a, i.e., pressure, volume, and age, see Nulsen et al., 2009) plotted against the cooling power for objects ranging from luminous clusters, through groups, to nearby elliptical galaxies. The dashed lines represent the pV, 4 and 16 pV, from top to bottom reproduced from Nulsen et al. (2009), with the permission of AIP Publishing). **Right:** CO(3-2) integrated intensity map for velocities 0 to +480 km s^{-1} in the Phoenix Cluster. The X-ray cavities are shown by the dashed white contours. Image taken from Russell et al. (2017), ©AAS. Reproduced with permission.

This close coupling is essential to explain the self-regulation of feedback.

EFFECTS OF AGN ON KPC SCALES: MULTI-PHASE GAS OUTFLOWS

Quenching star formation and stopping gas accretion onto the SMBH can also be achieved by massive outflows that can expel the gas from the central regions of galaxies. AGN-driven outflows, observed from pc to kpc scales, are known since a long time. The recent observations confirm that they are a relatively common phenomenon. Historically, they have been traced using mostly the ionized gas, observed in optical, UV and X-ray emission, and absorption lines (see Veilleux et al., 2005; Bland-Hawthorn et al., 2007; Tadhunter, 2008; King and Pounds, 2015 for reviews).

However, the most recent view that emerges from the continuously improving observations and by new or upgraded facilities—in particular radio and millimeter telescopes—is that the gas *outflows are truly complex and multi-phase*. The discovery of massive and fast outflows of cold gas (HI and cold molecular, Morganti et al., 2005; Feruglio et al., 2010) has taken everybody by surprise. Thus, different phases of the gas take part in the outflows and, in order to get the full picture of their physical properties, multi-wavelengths observations are needed. An overview of what found in term of mass outflow rate and kinetic comparison for the various components of the outflows, is presented in Tadhunter (2008). This shows how important is to trace and measure all these components.

Furthermore, to fully gauge the impact of the outflows, both detailed single objects studies (see section The Variety of Outflows through Two Case Studies) as well as observations of large samples are required. Below we start with a summary of some of the main results obtained using the different gas tracers.

Ultra-Fast Outflows (UFO)

X-ray and UV observations have had, from the beginning, an important role in tracing outflows using absorption lines from ionized gas (Crenshaw et al., 2003; Costantini, 2010; Crenshaw and Kraemer, 2012; King and Pounds, 2015). About half of local Seyfert galaxies host a photoionized warm absorber (WA), which produces features detectable in soft X–ray (∼0.3–2 keV) spectra and in the UV band. The latter absorption lines are usually blueshifted several 100 km s^{-1} with respect of the systemic velocity, which indicates a global outflow of the absorbing gas with mass outflow rates in the range 0.01–0.06 $M_\odot$ year^{-1}. These values are often comparable to the mass accretion rate but they provide only a small fraction of the bolometric luminosity, i.e., $L_{kin} < 0.1\% L_{bol}$ (Costantini, 2010). Likely of higher impact are the highly ionized outflows with mildly relativistic velocities (i.e., $v \sim 0.1$–$0.25c$, where c is the speed of light) traced by highly blue-shifted X-ray absorption lines in the iron K band (Pounds et al., 2003; Reeves et al., 2009; Tombesi et al., 2011, 2012). These ultrafast outflows are also known as UFO (Tombesi et al., 2011). A blind search carried out in archival spectra of the XMM-Newton archive has shown that they are present in about 35% of Seyfert galaxies. They differ from classical WA because of the higher outflow velocity and of the higher ionization. Indirect arguments indicate that their location is at sub-pc scales, i.e., ∼0.0003–0.03 pc (see Reeves et al., 2009; Tombesi et al., 2011, 2012 and ref. therein).

Thus, these highly ionized flows are originated in the inner regions of the AGN outflows, and are likely driven by wide-angle winds launched from the accretion disks, accelerated by radiation pressure (e.g., Elvis, 2000; King and Pounds, 2003; Proga and Kallman, 2004). Their mass outflow rate is in the range ∼0.01–1 $M_\odot$ year^{-1} and the mechanical power is between ∼10^{42} and 10^{45} erg s^{-1}. These values typically correspond to >0.5% L_{bol} (Tombesi et al., 2012; King and Pounds, 2015). Important is the connection with the large scale outflows: the UFO likely represent the inner wind, which would then drive the massive molecular outflow (see below) on larger distances (see e.g., Feruglio et al., 2015; Tombesi et al., 2015; Veilleux et al., 2017), making them very relevant for feedback (see also section The Variety of Outflows through Two Case Studies).

Outflows of Warm Ionised Gas on Kpc Scales

Outflows of warm (T ∼ 10^4 K) ionized gas have been observed in optical/IR lines and mostly traced, in low-redshifts objects, by the strong forbidden emission lines, e.g., [O III]λ5007 (see also discussion in Zakamska and Greene, 2014). Outflows have been detected in ∼30% of Seyfert galaxies (e.g., Crenshaw et al., 2003, 2012; Crenshaw and Kraemer, 2007), but they are common also in AGN of different luminosity selected from spectroscopic surveys (Mullaney et al., 2013; e.g., Zakamska and Greene, 2014).

Radiative winds are considered often at the origin of these outflows (see below). However, other mechanisms are also observed. For example, radio plasma jets are known since early studies to affect the kinematics of the gas (e.g., Whittle, 1985; Holt et al., 2008; Nesvadba et al., 2008 for some examples). Interestingly, a connection between the radio luminosity and the presence of outflows has been seen also in samples not selected based on radio properties and including radio weak ($L_{1.4GHz}$ = 10^{23}–10^{25} W Hz^{-1}, Mullaney et al., 2013) or even radio-quiet (<10^{23} W Hz^{-1}, Zakamska and Greene, 2014) objects. **Figure 2** shows the trend found by Mullaney et al. (2013). In such weak radio sources, the radio emission is typically small or confined to faint radio jets. In the case of the faintest objects, the radio may even be a by-product of the shocks associated to the outflows, as suggested by Zakamska and Greene (2014).

The mass outflow rates associated with the outflows of warm ionized gas are usually found to be modest (at most a few $M_\odot$ year^{-1}). However, these values are affected by uncertainties, in particular on the density of the outflowing gas (Holt et al., 2011) and on the spatial extent of the outflows (Husemann et al., 2013). The latter is still a matter of debate. The outflows of warm ionized gas are seen to extent up to ∼10 kpc in the sample studied by Sun et al. (2017). On the other hand, for a sample of low-redshift QSOs, Husemann et al. (2013) found signatures of outflowing (>400 km s^{-1}) ionized gas on kpc scales only in three objects where a radio jet is most likely driving the outflow. These differences imply a wide range of energy efficiency for the outflows (e.g., $\eta = \dot{E}/L_{bol}$ = 0.01−30% estimated by Sun et al., 2017). It is also interesting to note the suggestion that outflows are driven by AGN episodes with ∼10^8-year durations and shorter flickers 10^6 year (Sun et al., 2017).

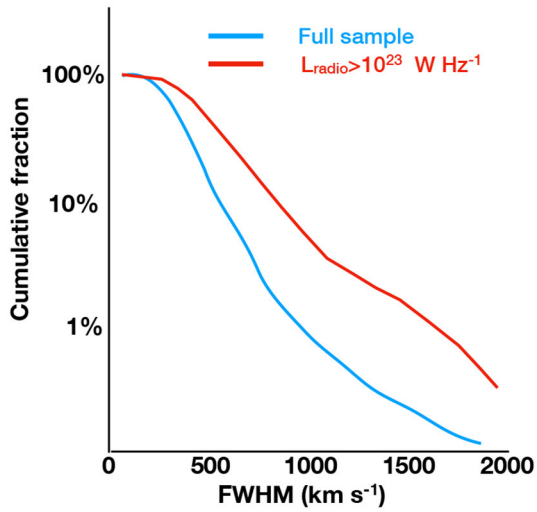

FIGURE 2 | Trend of the fraction FWHM of the [O III]λ5007 lines for the AGN in Mullaney et al. (2013). The cyan line represents the entire sample while the red line illustrates that objects with FWHM > 1,000 km s^{-1} are ≈5 times more prevalent among AGNs with L >1,023 W Hz^{-1} compared to the overall AGN population. The figure is based on data from Mullaney et al. (2013) and that no permission is required as the figure is original.

Finally, although outflows are common, it is worth notice that detailed work both with long slit and, more recently, with integral field units (IFU) shows that a complex interplay exists between outflows and infalling gas (e.g., Riffel et al., 2015), complicating in many objects the interpretation of the data.

The Surprising Presence of Massive Outflows of Cold Gas (HI and Molecular)

The new "*entry*" in the study of AGN-driven outflows has been the discovery that a cold component of gas, i.e., in the neutral atomic (HI) and molecular (CO, OH) phases, can be associated even with fast outflows (with velocities ≥ 1,000 km/s). This discovery has challenged our ideas on how the energy released by an AGN affects its surroundings. This component is particularly interesting for two main reasons: its uncertain origin (see section Driving Mechanisms and Energetics of the Outflows)—perhaps the result of a very efficient cooling of the gas—and its impact. Surprisingly, this component (and in particular the cold molecular component) has been found to represent the most massive component of the outflow.

An extensive literature is available on the properties of these outflows: for the atomic gas by e.g., Morganti et al., 2005, 2013a, 2016; Lehnert et al., 2011; Rupke and Veilleux, 2011, 2013; for the warm and cold molecular gas by e.g., Feruglio et al., 2010; Alatalo et al., 2011; Dasyra and Combes, 2011, 2012; Guillard et al., 2012; Cicone et al., 2014; García-Burillo et al., 2014; Tadhunter et al., 2014; Morganti et al., 2015a; and for OH by e.g., Fischer, 2010; Sturm et al., 2011; Veilleux et al., 2013.

Figure 3 shows the intriguing similarities between the CO and HI profiles for three objects suggesting similar kinematics for

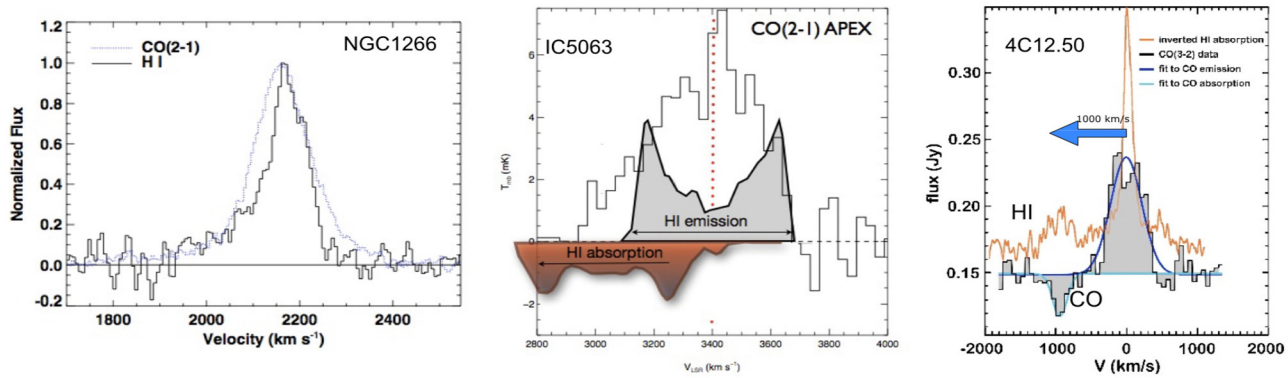

FIGURE 3 | Three examples of HI and CO integrated line profiles suggesting similar kinematical properties of the two phases of the gas, From left to right: NGC1266 (figure taken from Alatalo et al., 2011, ©AAS. Reproduced with permission), IC5063 (figure taken from Morganti et al., 2013b, reproduced with permission ©ESO) and 4C12.50 (Figure taken from Dasyra and Combes, 2012, reproduced with permission ©ESO).

these components. It is not yet clear how far this synergy extends, given the limited number of objects with HI and CO observations available.

Using data from literature, Cicone et al. (2014) and Fiore et al. (2017) have shown correlations between the AGN-driven molecular and ionized-wind mass outflow rates and the AGN bolometric luminosity. The mass outflow rates of the molecular gas are systematically the highest, except for the most luminous AGN where the two rates appear to converge (Fiore et al., 2017). A correlation is also found between the momentum carried in the outflow ($v\mathrm{d}M/\mathrm{d}t$, where v is the outflow velocity) with the photon momentum output of the AGN, L_{AGN}/c but with a "momentum boosting" of about a factor 20, suggesting an energy-driven nature of the outflows (see e.g., Cicone et al., 2014).

Fast HI outflows are observed using HI absorption. The planned upcoming surveys (Morganti et al., 2015b) make this method quite powerful for investigating the presence of these outflows in large samples. A proof-of-concept survey is presented in Geréb et al. (2015) and Maccagni et al. (2017). Of the galaxies detected in HI, at least 15% show fast outflows (Geréb et al., 2015) with mass outflow rates between a few and $\sim$30 $M_{\odot}$ year^{-1}. The radio jets drive at least some of these outflows. In particular, young radio sources are those where the plasma jet has the strongest impact on the surrounding medium and where most of the HI outflows are occurring (Geréb et al., 2015). A possible correlation has been observed between the amplitude (in velocity) of the outflow and the radio power (Maccagni et al., 2017). Finally, the presence of clumpy gas medium in the regions surrounding the radio sources may enhance the impact of the jet (as suggested by some simulations, see section Driving Mechanisms and Energetics of the Outflows). The presence of such a clumpy medium (embedded in a diffuse component) is confirmed by the results of deep, high-resolution (VLBI) observations tracing HI clouds with tens of pc sizes (with cloud masses up to $\sim 10^4$ $M_{\odot}$, Morganti et al., 2013a; Schulz et al., in preparation). Molecular clouds are also traced by high resolution ALMA observations (Maccagni et al., 2017).

DRIVING MECHANISMS AND ENERGETICS OF THE OUTFLOWS

Different mechanisms have been proposed to drive the outflowing gas (see e.g., Veilleux et al., 2005; King and Pounds, 2015). Wide-angle winds can be launched from the accretion disk and driven by the coupling of the radiation to the ambient medium through radiation pressure on dust. It is also possible to have a hot thermal wind (e.g., Compton-heated) colliding with and accelerating the ISM. Parsec-scale jets can produce over-pressured cavities from which the wide-angled outflow can be launched. Alternatively, outflows can be driven by the mechanical action of the radio plasma emanating from the AGN (Wagner et al., 2012; Mukherjee et al., 2016).

For powerful AGN, the scenario that has been suggested to better match the observations—in particular the presence of cold, molecular gas—is the one where winds launched from the accretion disk interact and shock the surrounding medium. This interaction can create an (energy-conserving) adiabatically expanding hot bubble. The adiabatically expanding wind sweeps up gas and drives an outer shock into the host ISM (Faucher-Giguère and Quataert, 2012; Zubovas and King, 2012, 2014). The outflowing gas is able to cool radiatively into clumps of cold molecular material. This would explain the presence of fast outflows ($\sim$1,300 km s^{-1}) of neutral-atomic (HI, NaI D) and molecular gas (Costa et al., 2017; Richings and Faucher-Giguere, 2017). An alternative scenario to explain the fast outflows of molecular gas assumes that pre-existing molecular clouds from the host ISM are entrained in the adiabatically expanding shocked wind and they can be accelerated to the observed velocities without being destroyed (see e.g., Scannapieco, 2017).

The role of radio jets is also relevant. In this case, the structure of the medium is playing an important role in defining the impact that the radio plasma jets can have (e.g., Wagner et al., 2012). Following the results of recent simulations, a jet entering a clumpy medium can have a larger impact than previously proposed. Numerical simulations of a newly created radio jet

entering a two-phase clumpy medium (dense molecular clouds, i.e., a few 100 cm^{-3}, embedded in a lower-density medium) show that the jet expands following a path of less resistance but still colliding with the gas clouds. This originates a cocoon of disturbed and outflowing gas around the jet, affecting a *large* region of the galaxy (see simulations by Wagner et al., 2012 and Mukherjee et al., 2016).

The requirements from the simulations in order to explain the observations are such that the kinetic power in the wind has to be a substantial fraction of the available accretion power ($\dot{E}/L_{edd}$ ~0.05–0.1, Di Matteo et al., 2005). Although uncertainties still affect some key parameters of the outflows (like e.g., mass, mass outflow rate etc.), the results so far suggest that these requirements are not always met. Alternatively, the coupling between the energy released and the surrounding medium has to be particularly efficient, i.e., as a consequence of the conditions of the medium. For example, and as mentioned above for the case of radio jets, an important factor for the coupling of photons or plasma with the multiphase galactic gas is the presence of a clumpy medium with dense clouds (Wagner et al., 2012; Bieri et al., 2017). This is important both for radiation-driven as for the jet-driven outflows (Wagner et al., 2012, 2013). Furthermore, a "two stage" model has been proposed by Hopkins and Elvis (2010) in which the outflow passing over a cold cloud, will be able to affect the cloud material and expand it in the direction perpendicular to the outflow direction. This shredding/expansion will amplify the effect of the interaction and substantially reduce (i.e., up to an order of magnitude) the required energy budget for feedback to affect a host galaxy.

Finally, connecting outflows observed on different scales, i.e., connecting the inner wind with large-scale molecular outflows, is important for obtaining a global view of outflows. This has been possible so far only for a limited number of objects. These cases suggest that most of the nuclear wind kinetic energy produced on the pc scale is transferred to mechanical energy on the kpc scale outflow. At least in some cases, the outflow is undergoing an energy conserving expansion (Cicone et al., 2014; Tombesi et al., 2015; Stern et al., 2016) although more detailed data are needed to confirm this scenario (see e.g., Veilleux et al., 2017).

THE VARIETY OF OUTFLOWS THROUGH TWO CASE STUDIES

Despite these exciting results, the number of objects where extensive multi-wavelengths data are available to characterize the different phases of the outflow is still limited. This is mainly because of the time and effort needed to collect data from a variety of (often highly oversubscribed) telescopes. Expanding this limited statistics and connecting the different scales and phases of the outflowing gas is the goal of many on-going projects. Below, I summarize the results for two of the best-studied objects. They represent cases where, thanks to detailed observations, two different mechanisms for driving the outflows have been suggested.

The Wind-Driven Outflow in Mrk 231

Mrk 231 represents one of the best examples of wind-driven outflow and the first case where fast outflowing molecular gas was observed (Feruglio et al., 2010; Fischer, 2010). Being the nearest quasar, it allows a detailed exploration of the physical conditions of the gas in the outflow. A nuclear UFO has been observed in X-ray with velocity 20,000 km s^{-1} and mass outflow rate in the range 0.3–1.6 $M_\odot$ $year^{-1}$ (Feruglio et al., 2015). On the sub-kpc scale, an HI outflow of ~1,300 km s^{-1} has been detected (Morganti et al., 2016) while the molecular outflow extend to kpc scale with a mass outflow rate in the range 500–1,000 $M_\odot$ $year^{-1}$ and associated kinetic energy of $E_{kin,mol}$ = [7–10] − 10^{43} erg s^{-1} (Feruglio et al. 2015). The NaI outflow is the most extended, reaching 3 kpc and mass outflow rate of 179 $M_\odot$ $year^{-1}$ (Rupke and Veilleux, 2011, 2013). This complex outflow is explained as driven by a wide angle, wind (see Figure 17 in Feruglio et al., 2015). Although Mrk 231 contains a radio plasma jet and radio lobes, the deep and detailed observations available show that the jet power does not seem large enough to drive and sustain the outflow. Mrk 231 is one of the few objects where the parameters of the outflow on different scales have been connected. Interestingly $E_{kin,UFO} \sim E_{kin,mol}$ as expected for outflows undergoing an energy conserving expansion. Thus, this confirms that most of the UFO kinetic energy is transferred to mechanical energy of the kpc-scale outflow (Feruglio et al., 2015).

The Jet-Driven Outflow in the Seyfert 2 IC 5063

IC 5063 represents one of the most radio-loud Seyfert galaxies (albeit still a relatively weak radio AGN in a general sense; $P_{1.4GHz}$ = 3 $\times 10^{23}$ W Hz^{-1}) and it was the first object where a fast AGN-driven HI outflow was discovered (Morganti et al., 1998; Oosterloo et al., 2000). The outflow is multi-phase (including HI, ionized, warm and cold molecular gas, see Morganti et al., 2015a for a summary). Although the radio power is actually lower than the one of Mrk 231, the location of the outflow suggests that in IC5063 the radio jet is the dominant driving mechanism of the outflow (Tadhunter et al., 2014; Morganti et al., 2015a). ALMA observations of the molecular gas show that disturbed kinematics of the gas occur across the entire extension of the radio source (~1 kpc, see **Figure 4,** left). Furthermore, not only the kinematics is affected by the jet but also the excitation of the gas, with the outflowing gas having high excitation (with T_{ex} 30–50 K) and optically thin conditions compared to the gas in the quiescent disk (Oosterloo et al., 2017; see **Figure 4,** right; Dasyra et al., 2016). The mass of the cold molecular outflow ~1.2 × 10^6 $M_\odot$ is much higher than the one associated to warm H_2 and to ionized gas. This suggests that most of the cold molecular outflow is due to fast cooling after the passage of a shock. The mass outflow rate of the cold molecular gas is ~4 $M_\odot year^{-1}$ (while for the ionized gas is ~0.08 $M_\odot year^{-1}$). In this object, the kinetic power of the outflow appears to be a relative high fraction of the nuclear bolometric luminosity. However, the global impact is modest and only a small fraction of the outflowing gas may leave the galaxy. The main effect of the outflow is to increase the turbulence of the medium and redistribute the gas (see e.g., Guillard et al., 2012, 2015).

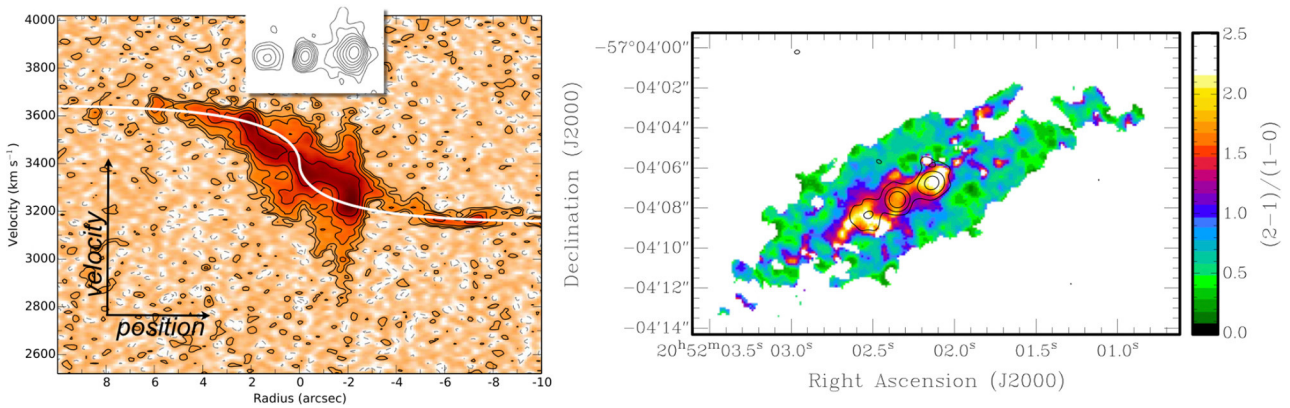

FIGURE 4 | ALMA observations of IC 5063. **Left:** integrated position-velocity map of the CO(2-1) along the radio axis of IC 5063. The white line indicates the expected kinematics of gas following regular rotation (figure modified from Morganti et al., 2015a, reproduced with permission ©ESO). **Right:** Ratio CO(2-1)/CO(1-0) integrated brightness temperatures I (in K kms^{-1}), courtesy of T. Oosterloo. Overplotted are the contours of the 346 GHz continuum emission of IC 5063 (see also Oosterloo et al., 2017).

SUMMARY AND CONCLUSIONS

As described in this review, there are a variety of ways in which the energy released by the AGN affects the surrounding medium.

On large scales, radio plasma lobes excavate cavities in the hot gas depositing enough energy to prevent this large reservoir of gas from cooling. The X-ray cavities are detected in ∼50% of galaxy clusters, groups, and individual galaxies. Some of the gas manages to cool and can be followed to trace its interaction with the radio plasma. New exciting possibilities to explore this phenomenon are open up by ALMA. The velocities of the cold molecular gas observed so far are not high enough for the gas to escape. The gas would fall back, further supporting the (short) duty cycle of activity observed especially for radio sources in cool-core clusters (Hogan et al., 2015).

Closer to the nucleus, outflows are found in a large fraction of AGN while, at the same time, infall is also required to maintain the AGN active (Kurosawa et al., 2009): a complex interplay—still to be fully disentangled—is occurring in these central regions. The gas participating to the outflows is multi-phase and includes also a cold (HI and cold molecular) component. Thus, different tracers can be used to study the physical properties of the outflows and the driving mechanisms. Surprisingly, the component of cold molecular gas is often the most massive and, therefore, represents an important component for feedback. The mechanism(s) that can produce fast outflows of cold (molecular) gas are still uncertain. This gas could be the result of fast cooling after the passage of a shock: the cold molecular gas would be the end product of the cooling. However, alternative scenarios have been suggested and need to be verified with more data. The kinetic energy of the outflows is not always matching the requirements from numerical simulations but more sophisticated models of the coupling between the energy and the medium is needed to fully assess the impact. The effect of radio jets can be important, also for low power radio sources. Interestingly, the initial phase of a radio jet (i.e., in young or restarted radio source) appears to have the largest impact on the surrounding gas. Also in the case of the outflows, the gas does not always escape the galaxy: the main effect of the AGN appears to be to inject turbulence and relocate the gas.

This review has focused on AGN at low redshift. However, the results presented here can provide an important reference point for the studies at high-z where the effects of AGN feedback are expected to be larger. Interesting results for high redshift objects are now starting to appear (e.g., Carniani et al., 2017). Finally, this review has focused on *negative* feedback but *positive* feedback is also expected to occur (see e.g., Maiolino et al., 2017). At low redshift this effect, albeit observed, seems to be limited (Santoro et al., 2016 and ref. therein, see also Combes, 2017, these Proceedings) but more dedicated observations are needed to quantify its importance.

In summary, the field is expanding extremely rapidly and, thanks to the many upcoming new observing facilities, our view of AGN will become increasingly detailed. An even tighter collaboration between observers and theorists will be necessary to interpret this wealth of data for understanding the complex phenomenon of AGN feedback.

ACKNOWLEDGMENTS

RM would like to thank the organizers for the interesting and pleasant conference and for giving the chance to the participants to visit unique places in Padova, taking advantage of the 250th anniversary of the Astronomical Observatory (la Specola). RM gratefully acknowledges support from the European Research Council under the European Union's Seventh Framework Programme (FP/2007–2013)/ERC Advanced Grant RADIOLIFE-320745.

REFERENCES

Alatalo, K., Blitz, L., Young, L. M., Davis, T. A., Bureau, M., Lopez, L. A., et al. (2011). Discovery of an active galactic nucleus driven molecular outflow in the local early-type galaxy NGC 1266. *Astrophys. J.* 735, 88–100. doi: 10.1088/0004-637X/735/2/88

Alexander, D. M., and Hickox, R. C. (2012). What drives the growth of black holes? *New Astron. Rev.* 56, 93–121. doi: 10.1016/j.newar.2011.11.003

Bieri, R., Dubois, Y., Rosdahl, J., Wagner, A., Silk, J., and Mamon, G.A. (2017). Outflows driven by quasars in high-redshift galaxies with radiation hydrodynamics. *Mon. Not. R. Astron. Soc.* 464, 1854–1873. doi: 10.1093/mnras/stw2380

Bland-Hawthorn, J., Veilleux, S., and Cecil, G. (2007). Galactic winds: a short review. *Astrophys. Space Sci.* 311, 87–98. doi: 10.1007/s10509-007-9567-8

Carniani, S., Marconi, A., Maiolino, R., Feruglio, C., Brusa, M., Cresci, G., et al., (2017). AGN feedback on molecular gas reservoirs in quasars at z 2.4. *Astron. Astrophys.* 605, 105–119. doi: 10.1051/0004-6361/201730672

Cattaneo, A., Faber, S. M., Binney, J., Dekel, A., Kormendy, J., Mushotzky, R., et al. (2009). The role of black holes in galaxy formation and evolution. *Nature* 460, 213–219. doi: 10.1038/nature08135

Cavagnolo, K. W., McNamara, B. R., Nulsen, P. E. J., Carilli, C. L., Jones, C., and Bîrzan, L. (2010). A relationship between AGN jet power and radio power. *Astrophys. J.* 720, 1066–1072. doi: 10.1088/0004-637X/720/2/1066

Cicone, C., Maiolino, R., Sturm, E., Graciá-Carpio, J., Feruglio, C., Neri, R., et al. (2014). Massive molecular outflows and evidence for AGN feedback from CO observations. *Astron. Astrophys.* 562, 21–46. doi: 10.1051/0004-6361/201322464

Ciotti, L., Pellegrini, S., Negri, A., and Ostriker, J. P. (2017). The effect of the AGN feedback on the interstellar medium of early-type galaxies:2D hydrodynamical simulations of the low-rotation case. *Astrophys. J.* 835, 15–37. doi: 10.3847/1538-4357/835/1/15

Combes, F. (2017). AGN feedback and its quenching efficiency. *Front. Astron. Space Sci.* 4:10. doi: 10.3389/fspas.2017.00010

Costa, T., Rosdahl, J., Sijacki, D., and Haehnelt, M. G. (2017). Quenching star formation with quasar outflows launched by trapped IR radiation. *ArXiv e-prints* arXiv:1709.08638.

Costantini, E. (2010). The ultraviolet-X-ray connection in AGN outflows. *Space Sci. Rev.* 157, 265–277. doi: 10.1007/s11214-010-9706-3

Crenshaw, D. M., and Kraemer, S. B. (2012). Feedback from mass outflows in nearby active galactic nuclei. I. Ultraviolet and X-ray absorbers. *Astrophys. J.* 753, 75–86. doi: 10.1088/0004-637X/753/1/75

Crenshaw, D. M., and Kraemer, S. B. (2007). "Mass outflows from seyfert galaxies as seen in emission and absorption," in *The Central Engine of Active Galactic Nuclei, ASP Conference Series*, Vol. 373, eds L. C. Ho and J.-M. Wang (Xi'an), 319–328.

Crenshaw, D. M., Fischer, T. C., Kraemer, S. B., Schmitt, H. R., and Turner, T. J. (2012). "Measuring feedback in nearby AGN," in *AGN Winds in Charleston, Astronomical Society of the Pacific Conference Series*, Vol. 460 (San Francisco, CA: Astronomical Society of the Pacific), 261–265.

Crenshaw, D. M., Kraemer, S. B., and George, I. M. (2003). Mass loss from the nuclei of active galaxies. *Annu. Rev. Astron. Astrophys.* 41, 117–167. doi: 10.1146/annurev.astro.41.082801.100328

Dasyra, K. M., and Combes, F. (2011). Turbulent and fast motions of H2 gas in active galactic nuclei. *Astron. Astrophys.* 533, L10–L14. doi: 10.1051/0004-6361/201117730

Dasyra, K. M., and Combes, F. (2012). Cold and warm molecular gas in the outflow of 4C 12.50. *Astron. Astrophys.* 541, L7–L11. doi: 10.1051/0004-6361/201219229

Dasyra, K. M., Combes, F., Oosterloo, T., Oonk, J. B. R., Morganti, R., Salomé, P., et al. (2016). ALMA reveals optically thin, highly excited CO gas in the jet-driven winds of the galaxy IC 5063. *Astron. Astrophys.* 595, L7–L11. doi: 10.1051/0004-6361/201629689

Di Matteo, T., Springel, V., and Hernquist, L. (2005). Energy input from quasars regulates the growth and activity of black holes and their host galaxies. *Nature* 433, 604–607. doi: 10.1038/nature03335

Edge, A. C. (2001). The detection of molecular gas in the central galaxies of cooling flow clusters. *Mon. Not. R. Astron. Soc.* 328, 762–782. doi: 10.1046/j.1365-8711.2001.04802.x

Elvis, M. (2000). A structure for quasars. *Astrophys. J.* 545, 63–76. doi: 10.1086/317778

Fabian, A. C. (2012). Observational evidence of active galactic nuclei feedback. *Annu. Rev. Astron. Astrophys.* 50, 455–489. doi: 10.1146/annurev-astro-081811-125521

Faucher-Giguère, C.-A., and Quataert, E. (2012). The physics of galactic winds driven by active galactic nuclei. *Mon. Not. R. Astron. Soc.* 425, 605–622. doi: 10.1111/j.1365-2966.2012.21512.x

Feruglio, C., Maiolino, R., Piconcelli, E., Menci, N., Aussel, H., Lamastra, A., et al. (2010). Quasar feedback revealed by giant molecular outflows. *Astron. Astrophys.* 518, L155–L159. doi: 10.1051/0004-6361/201015164

Feruglio, C., Fiore, F., Carniani, S., Piconcelli, E., Zappacosta, L., Bongiorno, A., et al. (2015). The multi-phase winds of Markarian 231: from the hot, nuclear, ultra-fast wind to the galaxy-scale, molecular outflow. *Astron. Astrophys.* 583, 99–115. doi: 10.1051/0004-6361/201526020

Fiore, F., Feruglio, C., Shankar, F., Bischetti, M., Bongiorno, A., Brusa, M., et al. (2017). AGN wind scaling relations and the co-evolution of black holes and galaxies. *Astron. Astrophys.* 601, 143–164. doi: 10.1051/0004-6361/201629478

Fischer, J., Sturm, E., González-Alfonso, E., Graciá-Carpio, J., Hailey-Dunsheath, S., and Poglitsch, A., (2010). Herschel-PACS spectroscopic diagnostics of local ULIRGs: conditions and kinematics in Markarian 231. *Astron. Astrophys.* 518, L41–45. doi: 10.1051/0004-6361/201014676

García-Burillo, S., Combes, F., Usero, A., Aalto, S., Krips, M., Viti, S., et al. (2014). Molecular line emission in NGC 1068 imaged with ALMA. I. An AGN-driven outflow in the dense molecular gas. *Astron. Astrophys.* 567, 125–149. doi: 10.1051/0004-6361/201423843

Gebhardt, K., Bender, R., Bower, G., Dressler, A., Faber, S. M., Filippenko, A. V., et al. (2000). A relationship between nuclear black hole mass and galaxy velocity dispersion. *Astrophys. J.* 539, L13–L16. doi: 10.1086/312840

Geréb, K., Maccagni, F. M., Morganti, R., and Oosterloo, T. A. (2015). The HI absorption "Zoo". *Astron. Astrophys.* 575, 44–61. doi: 10.1051/0004-6361/201424655

Guillard, P., Boulanger, F., Lehnert, M. D., Pineau des Forêts, G., Combes, F., Falgarone, E., et al. (2015). Exceptional AGN-driven turbulence inhibits star formation in the 3C 326N radio galaxy. *Astron. Astrophys.* 574, 32–47. doi: 10.1051/0004-6361/201423612

Guillard, P., Ogle, P. M., Emonts, B. H. C., Appleton, P. N., Morganti, R., Tadhunter, C., et al. (2012). Strong molecular hydrogen emission and kinematics of the multiphase gas in radio galaxies with fast jet-driven outflows. *Astrophys. J.* 747, 95–120. doi: 10.1088/0004-637X/747/2/95

Harrison, C. M. (2017). Impact of supermassive black hole growth on star formation. *Nature Astron.* 1:0165. doi: 10.1038/s41550-017-0165

Hogan, M. T., Edge, A. C., Geach, J. E., Grainge, K. J. B., Hlavacek-Larrondo, J., Hovatta, T., et al. (2015). High radio-frequency properties and variability of brightest cluster galaxies. *Mon. Not. R. Astron. Soc.* 453, 1223–1240. doi: 10.1093/mnras/stv1518

Holt, J., Tadhunter, C. N., and Morganti, R. (2008). Fast outflows in compact radio sources: evidence for AGN-induced feedback in the early stages of radio source evolution. *Mon. Not. R. Astron. Soc.* 387, 639–659. doi: 10.1111/j.1365-2966.2008.13089.x

Holt, J., Tadhunter, C. N., Morganti, R., and Emonts, B. H. C. (2011). The impact of the warm outflow in the young (GPS) radio source and ULIRG PKS 1345+12 (4C 12.50). *Mon. Not. R. Astron. Soc.* 410, 1527–1536. doi: 10.1111/j.1365-2966.2010.17535.x

Hopkins, P. F., and Elvis, M. (2010). Quasar feedback: more bang for your buck. *Mon. Not. R. Astron. Soc.* 401, 7–14. doi: 10.1111/j.1365-2966.2009.15643.x

Husemann, B., Wisotzki, L., Sánchez, S. F., and Jahnke, K. (2013). The properties of the extended warm ionised gas around low-redshift QSOs and the lack of extended high-velocity outflows. *Astron. Astrophys.* 549, 43–76. doi: 10.1051/0004-6361/201220076

Kauffmann, G., and Haehnelt, M. (2000). A unified model for the evolution of galaxies and quasars. *Mon. Not. R. Astron. Soc.* 311, 576–588. doi: 10.1046/j.1365-8711.2000.03077.x

King, A., and Pounds, K. (2015). Powerful outflows and feedback from active galactic nuclei. *Annu. Rev. Astron. Astrophys.* 53, 115–154. doi: 10.1146/annurev-astro-082214-122316

King, A. R., and Pounds, K. A. (2003). Black hole winds. *Mon. Not. R. Astron. Soc.* 345, 657–659. doi: 10.1046/j.1365-8711.2003.06980.x

Kurosawa, R., Proga, D., and Nagamine, K. (2009). On the feedback efficiency of active galactic nuclei. *Astrophys. J.* 707:823. doi: 10.1088/0004-637X/707/1/823

Lehnert, M. D., Tasse, C., Nesvadba, N. P. H., Best, P. N., and van Driel, W. (2011). The Na D profiles of nearby low-power radio sources: jets powering outflows. *Astron. Astrophys.* 532, L3–L8. doi: 10.1051/0004-6361/201117323

Maccagni, F.M., Morganti, R., Oosterloo, T.A., Geréb, K., and Maddox, N. (2017). Kinematics and physical conditions of HI in nearby radio sources. The last survey of the old westerbork synthesis radio Telescope. *Astron. Astrophys.* 604, 43–65. doi: 10.1051/0004-6361/201730563

Maiolino, R., Russell, H. R., Fabian, A. C., Carniani, S., Gallagher, R., Cazzoli, S., et al. (2017). Star formation inside a galactic outflow. *Nature* 544, 202–206. doi: 10.1038/nature21677

McNamara, B. R., and Nulsen, P. E. J. (2007). Heating hot atmospheres with active galactic nuclei. *Annu. Rev. Astron. Astrophys.* 45, 117–175. doi: 10.1146/annurev.astro.45.051806.110625

McNamara, B. R., and Nulsen, P. E. J. (2012). Mechanical feedback from active galactic nuclei in galaxies, groups and clusters. *New J. Phys.* 14:055023. doi: 10.1088/1367-2630/14/5/055023

McNamara, B. R., Russell, H. R., Nulsen, P. E. J., Edge, A. C., Murray, N. W., Main, R. A., et al. (2014). A 1010 solar mass flow of molecular gas in the A1835 brightest cluster galaxy. *Astrophys. J.* 785:44. doi: 10.1088/0004-637X/785/1/44

Morganti, R. (2017). Archaeology of active galaxies across the electromagnetic spectrum. *Nat. Astron.* 1, 596–605. doi: 10.1038/s41550-017-0223-0

Morganti, R., Fogasy, J., Paragi, Z., Oosterloo, T., and Orienti, M. (2013a). Radio jets clearing the way through a galaxy: watching feedback in action. *Science* 341, 1082–1085. doi: 10.1126/science.1240436

Morganti, R., Frieswijk, W., Oonk, R. J. B., Oosterloo, T., and Tadhunter, C. (2013b). Tracing the extreme interplay between radio jets and the ISM in IC 5063. *Astron. Astrophys.* 552, L4–L9. doi: 10.1051/0004-6361/201220734

Morganti, R., Oosterloo, T., and Tsvetanov, Z. (1998). A radio study of the seyfert galaxy ic 5063: evidence for fast gas outflow. *Astron. J.* 115, 915–927. doi: 10.1086/300236

Morganti, R., Oosterloo, T., Oonk, J. B. R., Frieswijk, W., and Tadhunter, C. (2015a). The fast molecular outflow in the Seyfert galaxy IC 5063 as seen by ALMA. *Astron. Astrophys.* 580, 1–12. doi: 10.1051/0004-6361/201525860

Morganti, R., Sadler, E. M., and Curran, S. (2015b). *Cool Outflows and HI Absorbers with SKA. Advancing Astrophysics with the Square Kilometre Array (AASKA14) 134*. Avaliable online at: http://pos.sissa.it/cgi-bin/reader/conf.cgi?confid=215, id.134

Morganti, R., Tadhunter, C. N., and Oosterloo, T. A. (2005). Fast neutral outflows in powerful radio galaxies: a major source of feedback in massive galaxies. *Astron. Astrophys.* 444, L9–L13. doi: 10.1051/0004-6361:200500197

Morganti, R., Veilleux, S., Oosterloo, T., Teng, S. H., and Rupke, D. (2016). Another piece of the puzzle: the fast H I outflow in Mrk 231. *Astron. Astrophys.* 593, 30–41. doi: 10.1051/0004-6361/201628978

Mukherjee, D., Bicknell, G.V., Sutherland, R., and Wagner, A. (2016). Relativistic jet feedback in high-redshift galaxies - I. Dynamics. *Mon. Not. R. Astron. Soc.* 461, 967–983. doi: 10.1093/mnras/stw1368

Mullaney, J. R., Alexander, D. M., Fine, S., Goulding, A. D., Harrison, C. M., and Hickox, R. C. (2013). Narrow-line region gas kinematics of 24 264 optically selected AGN: the radio connection. *Mon. Not. R. Astron. Soc.* 433, 622–638. doi: 10.1093/mnras/stt751

Nesvadba, N. P. H., Lehnert, M. D., De Breuck, C., and Gilbert, A. M., van Breugel, W. (2008). Evidence for powerful AGN winds at high redshift: dynamics of galactic outflows in radio galaxies during the "Quasar Era". *Astron. Astrophys.* 491, 407–424. doi: 10.1051/0004-6361:200810346

Nulsen, P., Jones, C., Forman, W., Churazov, E., McNamara, B., David, L., et al. (2009). "Radio mode outbursts in giant elliptical galaxies," in *American Institute of Physics Conference Series,* Vol. 1201, 198–201. doi: 10.1063/1.3293033

Nulsen, P. E. J., Jones, C., Forman, W. R., David, L. P., McNamara, B. R., Rafferty, D. A., et al. (2007). "AGN heating through cavities and shocks," in *Heating versus Cooling in Galaxies and Clusters of Galaxies*, eds P. Schuecker, H. Böhringer, A. Finoguenov, and G. W. Pratt (Berlin; Heidelberg: Springer-Verlag), 210–215.

Oosterloo, T., Oonk, J. B. R., Morganti, R., Combes, F., Dasyra, K., Salomé, P., et al. (2017). Properties of the molecular gas in the fast outflow in the Seyfert Galaxy IC. 5063. arXiv:1710.01570.

Oosterloo, T. A., Morganti, R., Tzioumis, A., Reynolds, J., King, E., McCulloch, P., et al. (2000). A strong jet-cloud interaction in the seyfert galaxy IC 5063: VLBI observations. *Astron. J.* 119, 2085–2091. doi: 10.1086/301358

Pounds, K. A., Reeves, J. N., King, A. R., Page, K. L., O'Brien, P. T., and Turner, M. J. L. (2003). A high-velocity ionized outflow and XUV photosphere in the narrow emission line quasar PG1211+143. *Mon. Not. R. Astron. Soc.* 345, 705–713. doi: 10.1046/j.1365-8711.2003.07006.x

Proga, D., and Kallman, T. R. (2004). Dynamics of line-driven disk winds in active galactic nuclei. II. Effects of disk radiation. *Astrophys. J.* 616, 688–695. doi: 10.1086/425117

Reeves, J. N., O'Brien, P. T., Braito, V., Behar, E., Miller, L., Turner, T. J., et al. (2009). A compton-thick wind in the High-luminosity Quasar, PDS 456. *Astrophys. J.* 701, 493–507. doi: 10.1088/0004-637X/701/1/493

Richings, A. J., and Faucher-Giguere, C.-A. (2017). Radiative cooling of swept up gas in AGN-driven galactic winds and its implications for molecular outflows. *ArXiv e-prints* arXiv1710.09433.

Riffel, R. A., Storchi-Bergmann, T., and Riffel, R. (2015). Feeding versus feedback in active galactic nuclei from near-infrared integral field spectroscopy - X. NGC 5929. *Mon. Not. R. Astron. Soc.* 451, 3587–3605. doi: 10.1093/mnras/stv1129

Rupke, D. S. N., and Veilleux, S. (2011). Integral field spectroscopy of massive, kiloparsec-scale outflows in the Infrared-luminous QSO Mrk 231. *Astrophys. J.* 729, L27. doi: 10.1088/2041-8205/729/2/L27

Rupke, D. S. N., and Veilleux, S. (2013). The multiphase structure and power sources of galactic winds in major mergers. *Astrophys. J.* 768:75. doi: 10.1088/0004-637X/768/1/75

Russell, H. R., McDonald, M., McNamara, B. R., Fabian, A. C., Nulsen, P. E. J., Bayliss, M. B., et al. (2017). Alma observations of massive molecular gas filaments encasing radio bubbles in the phoenix cluster. *Astrophys. J.* 836:130. doi: 10.3847/1538-4357/836/1/130

Russell, H. R., McNamara, B. R., Edge, A. C., Nulsen, P. E. J., Main, R. A., Vantyghem, A. N., et al. (2014). Massive molecular gas flows in the A1664 brightest cluster galaxy. *Astrophys. J.* 784:78. doi: 10.1088/0004-637X/784/1/78

Salomé, P., and Combes, F. (2003). Cold molecular gas in cooling flow clusters of galaxies. *Astron. Astrophys.* 412, 657–667. doi: 10.1051/0004-6361:20031438

Santoro, F., Oonk, J. B. R., Morganti, R., Oosterloo, T. A., and Tadhunter, C. (2016). Embedded star formation in the extended narrow line region of Centaurus A: extreme mixing observed by MUSE. *Astron. Astrophys.* 590, 37–44. doi: 10.1051/0004-6361/201628353

Scannapieco, E. (2017). The production of cold gas within galaxy outflows. *Astrophys. J.* 837, 28–45. doi: 10.3847/1538-4357/aa5d0d

Schaye, J., Crain, R. A., Bower, R. G., Furlong, M., Schaller, M., Theuns, T., et al. (2015). The EAGLE project: simulating the evolution and assembly of galaxies and their environments. *Mon. Not. R. Astron. Soc.* 446, 521–554. doi: 10.1093/mnras/stu2058

Sijacki, D., Vogelsberger, M., Genel, S., Springel, V., Torrey, P., Snyder, G. F., et al. (2015). The Illustris simulation: the evolving population of black holes across cosmic time. *Mon. Not. R. Astron. Soc.* 452, 575–596. doi: 10.1093/mnras/stv1340

Silk, J., and Rees, M. J. (1998). Quasars and galaxy formation. *Astron. Astrophys.* 331, L1–L4.

Stern, J., Faucher-Giguère, C.-A., Zakamska, N. L., and Hennawi, J. F. (2016). Constraining the dynamical importance of hot gas and radiation pressure in quasar outflows using emission line ratios. *Astrophys. J.* 819, 130–150. doi: 10.3847/0004-637X/819/2/130

Sturm, E., González-Alfonso, E., Veilleux, S., Fischer, J., Graciá-Carpio, J., Hailey-Dunsheath, S., et al. (2011). Massive molecular outflows and negative feedback in ULIRGs observed by Herschel-PACS. *Astrophys. J.* 733, L16–L21. doi: 10.1088/2041-8205/733/1/L16

Sun, A.-L., Greene, J. E., and Zakamska, N. L. (2017). Sizes and kinematics of extended narrow-line regions in luminous obscured AGN selected by broadband images. *Astrophys. J.* 835, 222–248. doi: 10.3847/1538-4357/835/2/222

Tadhunter, C. (2008). The importance of sub-relativistic outflows in AGN host galaxies. *Mem. della Soc. Astron. Italiana* 79:1205.

Tadhunter, C., Morganti, R., Rose, M., Oonk, J. B., and Oosterloo, T. (2014). Jet acceleration of the fast molecular outflows in the Seyfert galaxy IC 5063. *Nature* 511, 440–443. doi: 10.1038/nature13520

Tombesi, F., Cappi, M., Reeves, J. N., and Braito, V. (2012).Evidence for ultrafast outflows in radio-quiet AGNs - III. Location and energetics. *Mon. Not. R. Astron. Soc.* 422, L1–L5. doi: 10.1111/j.1745-3933.2012.01221.x

Tombesi, F., Cappi, M., Reeves, J. N., Palumbo, G. G. C., Braito, V., and Dadina, M. (2011). Evidence for ultra-fast outflows in radio-quiet active galactic nuclei. II. detailed photoionization modeling of Fe K-shell absorption lines. *Astrophys. J.* 742:44. doi: 10.1088/0004-637X/742/1/44

Tombesi, F., Meléndez, M., Veilleux, S., Reeves, J. N., González-Alfonso, E., and Reynolds, C. S. (2015). Wind from the black-hole accretion disk driving a molecular outflow in an active galaxy. *Nature* 519, 436–438. doi: 10.1038/nature14261

Tremblay, G. R., Oonk, J. B., Combes, F., Salomé, P., O'Dea, C., Baum, S. A., et al. (2016). Cold, clumpy accretion onto an active supermassive black hole. *Nature* 534, 218–221. doi: 10.1038/nature17969

Veilleux, S., Bolatto, A., Tombesi, F., Meléndez, M., Sturm, E., González-Alfonso, E., et al. (2017). Quasar feedback in the ultraluminous infrared galaxy F11119+3257: connecting the accretion disk wind with the large-scale molecular outflow. *Astrophys. J.* 843, 18–29. doi: 10.3847/1538-4357/aa767d

Veilleux, S., Cecil, G., and Bland-Hawthorn, J. (2005). Galactic winds. *Annu. Rev. Astron. Astrophys.* 43, 769–826. doi: 10.1146/annurev.astro.43.072103.150610

Veilleux, S., Meléndez, M., Sturm, E., Gracia-Carpio, J., Fischer, J., González-Alfonso, E., et al. (2013). Fast molecular outflows in luminous galaxy mergers: evidence for quasar feedback from Herschel. *Astrophys. J.* 776, 27–48. doi: 10.1088/0004-637X/776/1/27

Wagner, A. Y., Bicknell, G. V., Umemura, M. (2012). Driving outflows with relativistic jets and the dependence of active galactic nucleus feedback efficiency on interstellar medium inhomogeneity. *Astrophys. J.* 757:136. doi: 10.1088/0004-637X/757/2/136

Wagner, A. Y., Umemura, M., and Bicknell, G. V. (2013). Ultrafast outflows: galaxy-scale active galactic nucleus feedback. *Astrophys. J.* 763:L18. doi: 10.1088/2041-8205/763/1/L18

Whittle, M. (1985). The narrow line region of active galaxies. I - nuclear forbidden line profiles. II - relations between forbidden line profile shape and other properties. *Mon. Not. R. Astron. Soc.* 213, 1–31. doi: 10.1093/mnras/213.1.1

Zakamska, N. L., and Greene, J. E. (2014). Quasar feedback and the origin of radio emission in radio-quiet quasars. *Mon. Not. R. Astron. Soc.* 442, 784–804. doi: 10.1093/mnras/stu842

Zubovas, K., and King, A. (2012). Clearing out a galaxy. *Astrophys. J.* 745:L34. doi: 10.1088/2041-8205/745/2/L34

Zubovas, K., and King, A. R. (2014). Galaxy-wide outflows: cold gas and star formation at high speeds. *Mon. Not. R. Astron. Soc.* 439, 400–406. doi: 10.1093/mnras/stt2472

Conflict of Interest Statement: The author declares that the research was conducted in the absence of any commercial or financial relationships that could be construed as a potential conflict of interest.

Copyright © 2017 Morganti. This is an open-access article distributed under the terms of the Creative Commons Attribution License (CC BY). The use, distribution or reproduction in other forums is permitted, provided the original author(s) or licensor are credited and that the original publication in this journal is cited, in accordance with accepted academic practice. No use, distribution or reproduction is permitted which does not comply with these terms.

frontiers in Astronomy and Space Sciences

MINI REVIEW
published: 21 September 2017
doi: 10.3389/fspas.2017.00010

AGN Feedback and Its Quenching Efficiency

*Francoise Combes**

Observatoire de Paris, LERMA, Centre National de la Recherche Scientifique, College de France, PSL, Sorbonne University UPMC, Paris, France

In the last decade, observations have accumulated on gas outflows in galaxies, and in particular massive molecular ones. The mass outflow rate is estimated between 1 and 5 times the star formation rate. For the highest maximal velocities, they are driven by AGN; these outflows are therefore a clear way to moderate or suppress star formation. Some of the most convincing examples at low redshift come from the radio mode, when the radio jets are inclined toward the galaxy plane, or expand in the hot intra-cluster medium, in cool core clusters. However, AGN feedback can also be positive in many occasions, and the net effect is difficult to evaluate. The quenching efficiency is discussed in view of recent observations.

Keywords: galaxies, active galaxy nuclei, black holes, outflows, molecules

OPEN ACCESS

Edited by:
Mauro D'Onofrio, University of Padua, Italy

Reviewed by:
Paola Severgnini, INAF-Osservatorio Astronomico di Brera, Italy
Anna Lia Longinotti, National Institute of Astrophysics, Optics and Electronics, Mexico

***Correspondence:**
Francoise Combes
francoise.combes@obspm.fr

Specialty section:
This article was submitted to Milky Way and Galaxies, a section of the journal Frontiers in Astronomy and Space Sciences

Received: *30 July 2017*
Accepted: *16 August 2017*
Published: *21 September 2017*

Citation:
Combes F (2017) AGN Feedback and Its Quenching Efficiency. Front. Astron. Space Sci. 4:10. doi: 10.3389/fspas.2017.00010

1. TYPES OF FEEDBACK

Cosmological simulations in the CDM scenario predict too many galaxies at both ends of the mass function. If it is possible to suppress star formation through supernovae feedback in dwarf galaxies, we have to rely on AGN feedback to quench star formation in massive galaxies. There are two main modes of AGN feedback: first, the quasar mode, called also radiative mode or wind mode. This occurs when the AGN luminosity is high, close to Eddington, mainly for young QSO at high redshift. Due to radiation pressure on the ionized gas, the nucleus reaches its gas accretion limit, and begins to eject some gas in a wind. Since the Eddington luminosity L_{Edd} is proportional to M_{BH}/σ_T, where M_{BH} is the supermassive black hole mass and σ_T the Thomson cross section, the Eddington limitation in BH growth might explain the M-σ relation, i.e., $M_{BH} \propto f\sigma_T\sigma^4$, where f is the gas fraction, and σ the central velocity dispersion. The same consideration can be made, when a central starburst reaches its Eddington luminosity, with radiation pressure on dust. Now the cross section is σ_d, which is 1,000 times higher than σ_T. This could lead to a limitation of the bulge mass to 1,000 M_{BH}, quite close to the observed M_{bulge}/M_{BH} ratio (Fabian, 2012).

The second feedback scenario is the radio mode, or kinetic mode, due to radio jets. This takes place in very low luminosity AGN, when L $< 0.01\ L_{Edd}$, mainly at low redshift. It is frequent in relatively massive galaxies, like the radio-loud ellipticals, powered by a radiatively inefficient flow (ADAF). A particular example of this feedback mode is the moderation of cooling flows in clusters, through radio-jets from the brightest central galaxy (BCG). It is observed also in low-luminosity AGN, like Seyfert galaxies (Combes et al., 2013; Dasyra et al., 2016).

Frequently, star formation and nuclear activity are associated, and it is difficult to disentangle the supernovae and AGN feedback. Galactic winds coming from a starburst (like the prototypical M82) are in general less violent, with smaller maximum velocity, and un-collimated. An example of both is provided by the galaxy merger NGC 3256, an ultra-luminous starburst at $z = 0.01$. ALMA

observations of the molecular gas (through the CO(3-2) line) have revealed high-velocity wings in both nuclei, the face-on N3256N and almost edge-on N3256S (Sakamoto et al., 2014). For the latter, the outflow is highly collimated, and likely due to an AGN (cf. **Figure 1**). The derived maximum velocity is ∼2,000 km/s out to 300 pc, and corresponds to 50 $M_{\odot}$/yr. For the northern galaxy, the maximum velocity is ∼750 km/s, and the outflow rate of 60 $M_{\odot}$/yr. In both cases, these rates are comparable to the star formation rate, showing that the implied quenching is significant. The time-scale to develop these outflows is ∼1 Myr (Sakamoto et al., 2014).

Numerical simulations have begun to study the radiative mode, depending however on small-scale recipes, which are calibrated on observations. Recipes are required to take into account the black hole growth and its associated feedback, all being sub-grid physics. Different groups do not converge to the same conclusions. While Springel et al. (2005) and Hopkins et al. (2006) found a good coupling between the AGN and the galaxy, Gabor and Bournaud (2014) conclude that the quasar mode has no quenching effect. Observations are therefore key to solve the issue of the AGN quenching efficiency.

2. COOL-CORE CLUSTERS

One example where AGN feedback is clearly demonstrated is found in the center of cool-core clusters. It has been known for a long time that the cooling time-scale of the hot ICM gas becomes smaller than the Hubble time in the center, and cooling flows are expected. However, only 10% of the expected cooling rate is observed, and this is now understood to be due to the radio jets of the central AGN reheating the gas. The jets carve cavities in the ICM, and uplift some hot gas. The denser regions around cavities cool in filaments, which infall after losing their pressure support, and are conspicuous in Hα (shocks) and molecular gas (Salomé et al., 2006, 2008).

Although most Hα is excited by shocks, there are some clumps of star formation (Canning et al., 2014). The observed scenario is far from the simple model of cooling flows, where most of the cooling occurred in the center. In real clusters, gas cools in the border of cavities, which can occur 20–50 kpc from the center. When the central galaxies is not at rest but oscillating in the cluster potential well, a cooling wake extends over ∼50 kpc (Salomé P and Combes, 2004; Russell et al., in press). In this

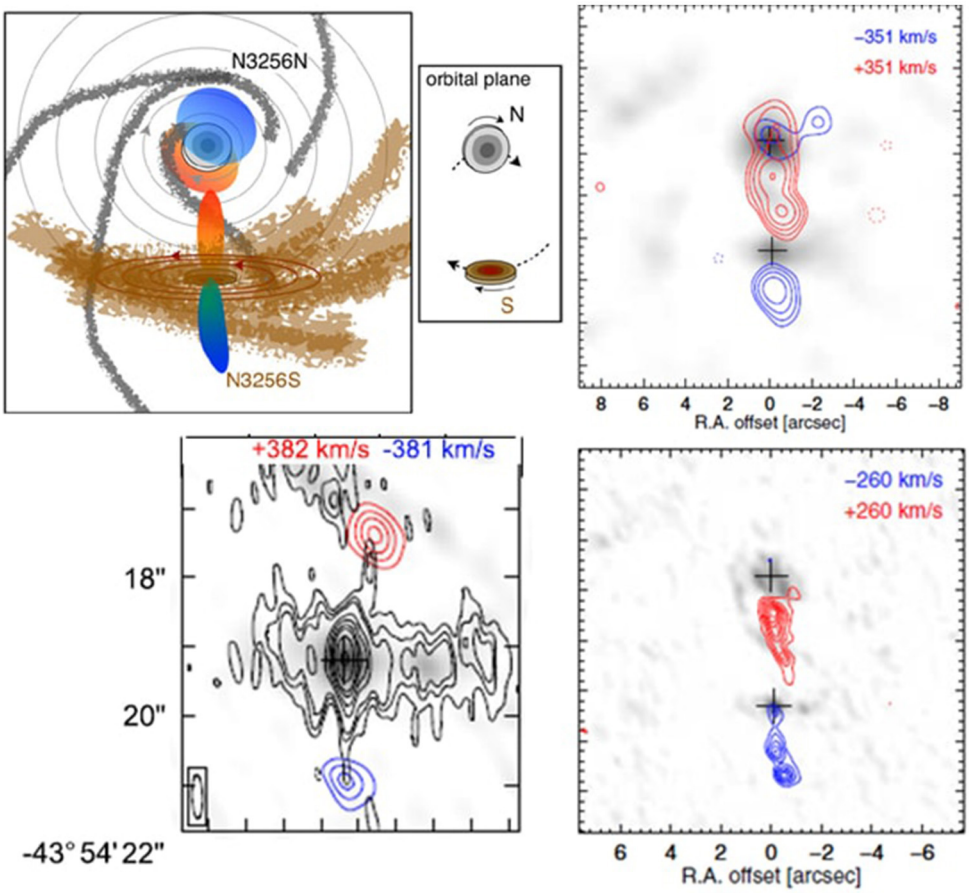

FIGURE 1 | ALMA observations of two molecular outflows in the merging galaxies NGC3256 (sketched at top left), adapted from Sakamoto et al. (2014), figure reproduced with permission. The northern object, almost face-on, reveals an outflow toward the observer, while the southern galaxy, nearly edge-on, shows a collimated outflow in the plane of the sky. The latter appears to coincide with a small radio jet, according to the VLA 3.6 cm radio map at the bottom left. The two CO maps at the right (top at low resolution, and bottom at high resolution) show that the northern outflow is resolved out. It must be a wide-angle outflow, uncollimated.

complex picture, gas inflow and outflow coexist; the molecular gas coming from previous cooling is dragged out by the AGN feedback, and can explain the large metallicity, necessary to detect the CO lines. The uplifted bubbles of hot gas create inhomogeneities and further cooling, and the cooled gas fuels the AGN, to close the loop. Through ram-pressure forces, the cold gas velocity is much lower than free-fall (Salomé et al., 2008).

3. MOLECULAR OUTFLOWS

Molecular outflows are now frequently observed in nearby galaxies, and statistics have been made with respect to their starburst or AGN origin (Cicone et al., 2014). For AGN-host galaxies, the outflow rate correlates with the AGN power, and also the L_{AGN}/L_{bol} luminosity ratio (L_{bol} being the total luminosity of the galaxy, including the AGN). The correlation does not exist for starbursts. What is also highly interesting is the good correlation between the momentum carried in the outflow (vdM/dt, where v is the outflow velocity)with the photon momentum output of the AGN L_{AGN}/c. The average value is vdM/dt $\sim$20 L_{AGN}/c, which is only possible with energy-driven outflows (Zubovas and King, 2012), i.e., when the energy injected by the inner wind is fully conserved throughout the outflow, unless the outflowing shell is optically thick to the infrared radiation, implying high momentum flux (Ishibashi and Fabian, 2015).

For the radio mode to be efficient in quenching star formation, there must be a strong coupling with galaxy disks. This is the case when the radio jet is not perpendicular to the galaxy plane, but is inclined so that the jet can sweep out some significant region in the disk. For example, the radio jet starts its way in the plane of the Seyfert 2 galaxy NGC1068: a molecular outflow of 63 $M_{\odot}$/yr, about 10 times the SFR has been observed by ALMA in the circum nuclear disk region (Garcia-Burillo et al., 2014). In the extreme case of IC5063, the jet is entirely in the plane, and creates secondary outflow features, at each collision with in-plane clouds (Morganti et al., 2015; Dasyra et al., 2016). Some of the gas might be optically thin in theses flows.

Feedback is also observed in low-luminosity AGN. One of the smallest outflow detected up to now is that of the Seyfert 2 NGC1433, with a maximum outflow of 100 km/s, along the minor axis (Combes et al., 2013). The case of the lenticular NGC1377 is very puzzling (Aalto et al., 2016). There is no radio AGN emission, although a very collimated molecular outflow is detected, with even a precession, visible since the outflow is almost in the plane of the sky (see **Figure 2**).

4. JET-INDUCED STAR FORMATION

The AGN feedback is frequently negative, but can be also positive, and trigger star formation. One of the most convincing examples of jet-induced star formation has been found in the Minkowski object (NGC541, distance of 82 Mpc), where conspicuous HII regions are observed at the extremity of the radio jet, outside of the optical galaxy (Croft et al., 2006). Molecular gas has been found in NGC541, but only an upper limit in the HII region with IRAM (Salomé et al., 2015), suggesting a high efficiency of star formation. Recently, CO emission was detected with ALMA (Lacy et al., 2017), compatible with the IRAM upper limit. However, when taken into account the low metallicity of the gas, which increases the CO-to-H_2 conversion ratio and thus the gas mass, and the excitation by shocks (reducing the SFR, for a given Hα flux), the star formation efficiency is now much lower in the triggered region.

A more nearby example of jet-induced star formation has been studied in Centaurus A, at a distance of 3.4 Mpc. Atomic gas has been mapped in shells around the galaxy by Schiminovich et al. (1994), and molecular gas has been found in those shells on the path of the radio jet by Charmandaris et al. (2000). Near the

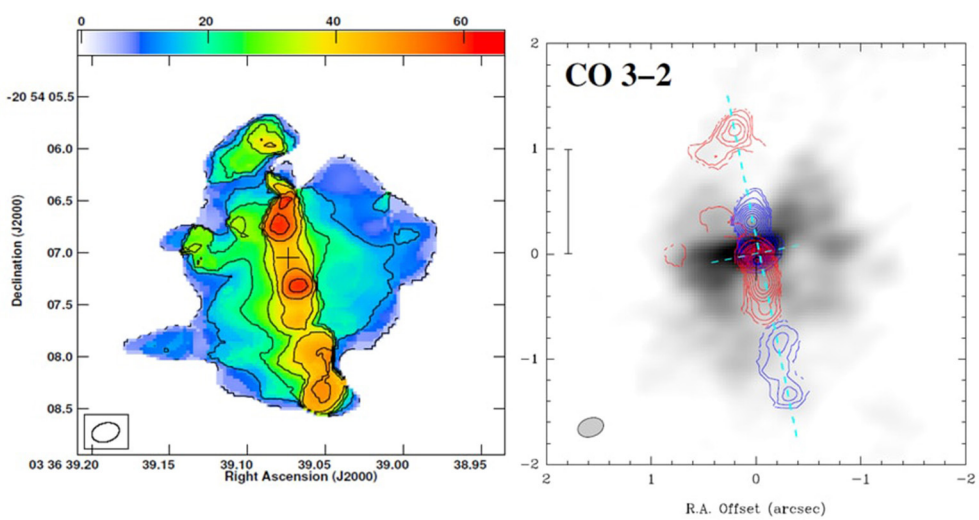

FIGURE 2 | The highly collimated molecular outflow in NGC1377, from Aalto et al. (2016), figure reproduced with permission. The left map is the velocity dispersion, and the right shows the blue and red-shifted CO emission. Note that the velocity of the flow changes sign at mid-way, symmetrically in the North and South.

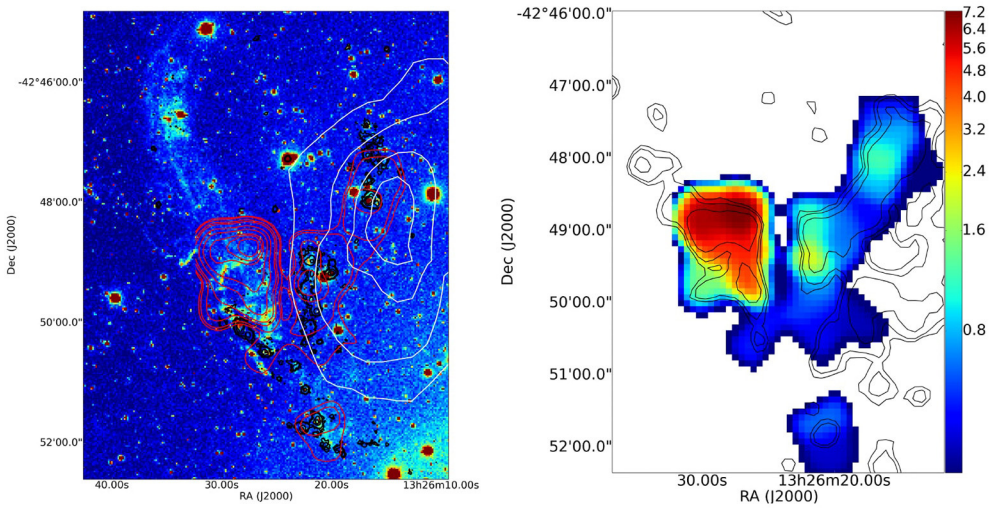

FIGURE 3 | Multi-phase filament in the radio jet of Centaurus A, from Salomé et al. (2016b), figure reproduced with permission. **(Left)** Superposed on the Hα map, the red contours correspond to CO emission, the white to HI, and the black to FUV from GALEX. **(Right)** The black HI contours are superposed on the CO emission map, showing that most of the molecular gas is outside the HI region.

northern shell, there is a conspicuous filament of star formation, aligned along the jet, mapped in Hα, FUV-GALEX, and dust emission with Herschel. Molecular gas has been mapped with APEX and ALMA, and surprisingly, there is even more CO detected outside the HI shell that inside (Salomé et al., 2016b). The molecular gas is concentrated at the region where the jet encounters the HI shell, and the atomic gas is then transformed in the molecular phase under the impact of the jet pressure (see **Figure 3**). Ionized gas excitation was determined with MUSE spectral observations, with the help of the BPT diagnostics (Salomé et al., 2016a), and is mainly due to shocks, with some contribution of star formation.

There is clearly star formation triggering from the radio jet, however, the star formation efficiency is lower than in galaxy disks. This is a situation comparable to what is found in the outer parts of galaxies, where gas layers are flaring (e.g., Dessauges-Zavadsky et al., 2014). The reason might be a lack of pressure, due to low or absent restoring force from a stellar disk. The importance of pressure, and of the surface density of stars for the star formation efficiency has been emphasized by Blitz and Rosolowsky (2006) and Shi et al. (2011).

5. CONCLUSIONS

AGN feedback is required to quench star formation in massive galaxies, to reproduce the observed galaxy mass function, and avoid the over-production of very massive galaxies in cosmological simulations. One can consider two types of AGN feedback: the quasar mode more frequent at high redshift, and the radio mode, more easy to observe in nearby galaxies.

One environment where the AGN feedback efficiency is clear is represented by cool core clusters, where the radio jets of the central bright galaxy carve bubbles and cavities in the hot intra-cluster gas, and moderate the gas cooling. Nearby galaxies frequently reveal significant molecular outflows, with a loading factor, the ratio between the outflow rate and the star formation rate, between 1 and 10. Given the high momentum rate, the outflows appear to be energy conserving.

AGN feedback can also be positive. Some evidence of jet-induced star formation has been observed. In particular, the high jet pressure can trigger the phase transformation from atomic to molecular gas, favoring star formation. This triggered star formation is however less efficient than in normal galaxy disks.

AUTHOR CONTRIBUTIONS

The author confirms being the sole contributor of this work and approved it for publication.

ACKNOWLEDGMENTS

All appropriate permissions have been obtained from the copyright holders of the figures reproduced in the manuscript. Many thanks to Mauro d'Onofrio and the organizing committee for this exciting conference on Quasars in Padova, on April 2017.

REFERENCES

Aalto, S., Costagliola, F., Muller, S., Sakamoto, K., Gallagher, J. S., Dasyra, K., et al. (2016). A precessing molecular jet signaling an obscured, growing supermassive black hole in NGC 1377? *Astron. Astrophys.* 590:12. doi: 10.1051/0004-6361/201527664

Blitz, L., and Rosolowsky, E. (2006). The role of pressure in GMC formation II: the H2-pressure relation. *Astrophys. J.* 650, 933–944. doi: 10.1086/505417

Canning, R. E. A., Ryon, J. E., Gallagher, J. S., Kotulla, R., O'Connell, R. W., Fabian, A. C., et al. (2014). Filamentary star formation in NGC 1275. *Month. Notices R. Astron.* 444, 336–349. doi: 10.1093/mnras/stu1191

Charmandaris, V., Combes, F., and van der Hulst, J. M. (2000). First detection of molecular gas in the shells of CenA. *Astron. Astrophys.* 356, L1–L4.

Cicone, C., Maiolino, R., Sturm, E., Graci-Carpio, J., Feruglio, C., Neriet, R., et al. (2014). Massive molecular outflows and evidence for AGN feedback from CO observations. *Astron. Astrophys.* 562:25. doi: 10.1051/0004-6361/201322464

Combes, F., Garcia-Burillo, S., Casasola, V., Hunt, L. K., Krips, M., Baker, A. J., et al. (2013). ALMA observations of feeding and feedback in nearby Seyfert galaxies: an AGN-driven outflow in NGC 1433. *Astron. Astrophys.* 558:11. doi: 10.1051/0004-6361/201322288

Croft, S., van Breugel, W., de Vries, W., Dopita, M., Martin, C., Morganti, R., et al. (2006). Minkowski's object: a starburst triggered by a radio jet. *Astrophys. J.* 647, 1040–1055. doi: 10.1086/505526

Dasyra, K. M., Combes, F., Oosterloo, T., Oonk, J. B. R., Morganti, R., Salomé, P., et al. (2016). ALMA reveals optically thin, highly excited CO gas in the jet-driven winds of the galaxy IC 5063. *Astron. Astrophys.* 595:4. doi: 10.1051/0004-6361/201629689

Dessauges-Zavadsky, M., Verdugo, C., Combes, F., and Pfenniger, D. (2014). CO map and steep Kennicutt-Schmidt relation in the extended UV disk of M 63. *Astron. Astrophys.* 566:12. doi: 10.1051/0004-6361/201323330

Fabian, A. C. (2012). Observational evidence of active galactic nuclei feedback. *Ann. Rev. Astron. Astrophys.* 50, 455–489. doi: 10.1146/annurev-astro-v081811-125521

Gabor, J. M., and Bournaud, F. (2014). Active galactic nuclei-driven outflows without immediate quenching in simulations of high-redshift disc galaxies. *Month. Notices R. Astron.* 441, 1615–1627. doi: 10.1093/mnras/stu677

Garcia-Burillo, S., Combes, F., and Usero, A. (2014). Molecular line emission in NGC 1068 imaged with ALMA. I. An AGN-driven outflow in the dense molecular gas. *Astron. Astrophys.* 567:24. doi: 10.1051/0004-6361/201423843

Hopkins, P., Hernquist, L., Cox, T. J., Di Matteo, T., Robertson, B., Springel, V., et al. (2006). A Unified, merger-driven model of the origin of starbursts, quasars, the cosmic X-ray background, supermassive black holes, and galaxy spheroids. *Astrophys. J. Suppl.* 163, 1–49. doi: 10.1086/499298

Ishibashi, W., and Fabian, A. C. (2015). AGN feedback: galactic-scale outflows driven by radiation pressure on dust. *Month. Notices R. Astron.* 451, 93–102. doi: 10.1093/mnras/stv944

Lacy, M., Croft, S., Fragile, C., Wood, S., and Nyland, K. (2017). ALMA observations of the interaction of a radio jet with molecular gas in Minkowski's object. *Astrophys. J.* 838:9. doi: 10.3847/1538-4357/aa65d7

Morganti, R., Oosterloo, T., Oonk, J. B. R., Frieswijk, W., and Tadhunter, C. (2015). The fast molecular outflow in the Seyfert galaxy IC 5063 as seen by ALMA. *Astron. Astrophys.* 580:11. doi: 10.1051/0004-6361/201525860

Russell, H. R., McNamara, B. R., Fabian, A. C., Nulsen, P. E. J., Combes, F., Edge, A. C., et al. (in press). Close entrainment of massive molecular gas flows by radio bubbles in the central galaxy of Abell 1795. *Month. Notices R. Astron.*

Sakamoto, K., Aalto, S., Combes, F., Evans, A., and Peck, A. (2014). An infrared-luminous merger with two bipolar molecular outflows: ALMA and SMA observations of NGC 3256. *Astrophys. J.* 797:28.

Salomé P., and Combes F. (2004). Mapping the cold molecular gas in a cooling flow cluster: Abell 1795. *Astron. Astrophys.* 415, L1–L5.

Salomé, P., Combes, F., Edge, A. C., Crawford, C., Erlund, A., Fabian, A. C., et al. (2006). Cold molecular gas in the Perseus cluster core. Association with X-ray cavity, H? filaments and cooling flow. *Astron. Astrophys.* 454, 437–445. doi: 10.1051/0004-6361:20054745

Salomé, P., Combes, F., Revaz, Y., Edge, A. C., Hatch, N. A., Fabian, A. C., et al. (2008). Cold gas in the Perseus cluster core: excitation of molecular gas in filaments. *Astron. Astrophys.* 484, 317–325. doi: 10.1051/0004-6361:200809493

Salomé, Q., Salomé, P., and Combes, F. (2015). Jet-induced star formation in 3C 285 and Minkowski's Object. *Astron. Astrophys.* 574:9. doi: 10.1051/0004-6361/201424932

Salomé, Q., Salomé, P., Combes, F., Hamer, S., and Heywood, I. (2016a). Star formation efficiency along the radio jet in Centaurus A. *Astron. Astrophys.* 593:13. doi: 10.1051/0004-6361/201526409

Salomé, Q., Salomé, P., Combes, F., and Hamer, S. (2016b). Atomic-to-molecular gas phase transition triggered by the radio jet in Centaurus A. *Astron. Astrophys.* 595:14. doi: 10.1051/0004-6361/201628970

Schiminovich, D., van Gorkom, J., van der Hulst, T., and Kasow, S. (1994). Discovery of neutral hydrogen associated with the diffuse shells of NGC 5128 (centaurus A). *Astrophys. J.* 423, L101–L104. doi: 10.1086/187246

Shi, Y., Helou, G., Yan, L., Armus, L., Wu, Y., Papovich, S., et al. (2011). Extended schmidt law: role of existing stars in current star formation. *Astrophys. J.* 733:15.

Springel, V., Di Matteo, T., and Hernquist, L. (2005). Modelling feedback from stars and black holes in galaxy merger. *Month. Notices R. Astron.* 361, 776–794.

Zubovas, K., and King, A. (2012). Clearing out a galaxy. *Astrophys. J.* 745:5. doi: 10.1111/j.1365-2966.2005.09238.x

Conflict of Interest Statement: The author declares that the research was conducted in the absence of any commercial or financial relationships that could be construed as a potential conflict of interest.

Copyright © 2017 Combes. This is an open-access article distributed under the terms of the Creative Commons Attribution License (CC BY). The use, distribution or reproduction in other forums is permitted, provided the original author(s) or licensor are credited and that the original publication in this journal is cited, in accordance with accepted academic practice. No use, distribution or reproduction is permitted which does not comply with these terms.

frontiers in Astronomy and Space Sciences

PERSPECTIVE
published: 12 December 2017
doi: 10.3389/fspas.2017.00058

Probing the Gas Fueling and Outflows in Nearby AGN with ALMA

Anelise Audibert[1], Françoise Combes[1,2], Santiago García-Burillo[3] and Philippe Salomé[1]*

[1] Observatoire de Paris, LERMA, Centre National de la Recherche Scientifique, PSL University, Sorbonne University, UPMC, Paris, France, [2] College de France, Paris, France, [3] Observatorio Astronómico Nacional, Observatorio de Madrid, Madrid, Spain

Feeding and feedback in AGN play a very important role to gain a proper understanding of galaxy formation and evolution. The interaction between activity mechanisms in the nucleus and its influence in the host galaxy are related to the physical processes involved in feedback and the gas fueling of the black hole. The discovery of many massive molecular outflows in the last few years have been promoting the idea that winds may be major actors in sweeping the gas out of galaxies. Also, the widely observed winds from the central regions of AGN are promising candidates to explain the scaling relations (e.g., the black hole-bulge mass relation, BH accretion rate tracking the star formation history) under the AGN feedback scenario. Out goal is to probe these phenomena through the kinematic and morphology of the gas inside the central kpc in nearby AGN. This has recently been possible due to the unprecedented ALMA spatial resolution and sensitivity. We present results on NGC7213 and NGC1808, the latter is part of a new ALMA follow-up of the NuGa project, a previous high-resolution (0.5–1″) CO survey of low luminosity AGN performed with the IRAM PdBI.

Keywords: active galactic nuclei, extragalactic astronomy, evolution of galaxies, galaxies, spectroscopy

OPEN ACCESS

Edited by:
Mauro D'Onofrio, Università degli Studi di Padova, Italy

Reviewed by:
Daniela Bettoni, Osservatorio Astronomico di Padova (INAF), Italy
Anna Lia Longinotti, National Institute of Astrophysics, Optics and Electronics, Mexico

****Correspondence:***
Anelise Audibert
anelise.audibert@obspm.fr

Specialty section:
This article was submitted to Milky Way and Galaxies, a section of the journal Frontiers in Astronomy and Space Sciences

Received: *30 September 2017*
Accepted: *27 November 2017*
Published: *12 December 2017*

Citation:
Audibert A, Combes F, García-Burillo S and Salomé P (2017) Probing the Gas Fueling and Outflows in Nearby AGN with ALMA. Front. Astron. Space Sci. 4:58. doi: 10.3389/fspas.2017.00058

1. INTRODUCTION

The fueling of SMBH at the center of galaxies and the subsequent feedback from its active nuclei, are among the key processes to understand the concerted growth of galaxies and BH. AGN feedback is invoked to explain the formation of massive galaxies when we compare the luminosity function of galaxies to theoretical simulations based on the cold dark matter models (Silk and Mamon, 2012). Winds and outflows produced by the AGN can eject or heat the gas, terminate the star formation and through the lack of fuel for accretion, quench the black hole activity. Recent discovery of many massive molecular outflows (e.g., Feruglio et al., 2010; Fischer et al., 2010; Alatalo et al., 2011; Sturm et al., 2011; Dasyra and Combes, 2012; Veilleux et al., 2013; Cicone et al., 2014; Dasyra et al., 2014; García-Burillo et al., 2014) have been promoting the idea that winds may be major actors in sweeping the gas out of galaxies, in agreement with theoretical predictions of AGN driven winds models (Faucher-Giguère and Quataert, 2012; Zubovas and King, 2012, 2014). However, it is still difficult to distinguish the origin of the outflows, whether they are AGN-driven or starburst-driven.

On the other hand, AGN are fueled by accretion of material onto the BH and the gas component can form stars on its way to the BH (García-Burillo and Combes, 2012; Combes et al., 2014). It is important to study the efficiency of angular momentum transport in galaxy disks in order to understand how the star formation and nuclear activity are fueled and what are the timescales involved, since both feeding process rely on a common cold gas supply, but in very different periods of time ($\sim 10^5$ year for BH growth and $\sim 10^{7-9}$ year for star formation; García-Burillo, 2016). In

addition to this scenario, one of the outstanding problems is to identify the mechanism that drives gas from the disk toward the nucleus, removing its large angular momentum and forming large non-axisymmetric perturbations, such as bars or spirals.

This work aims to better understand the galaxies chemical and thermal evolution by studying in detail the physical processes acting on the nucleus of a sample of nearby AGN. Probing AGN feeding and feedback phenomena through the kinematic and morphology of the gas inside the central kpc have recently been possible due to the unprecedented Atacama Millimeter/Submillimeter Array (ALMA) spatial resolution ($\lesssim 0.5''$) and sensitivity. Since there are only a few AGN observed with high spatial resolution, we investigate the nuclear molecular emission in a sample of nearby AGN making use of spectroscopic techniques.

2. METHODOLOGY

By applying the velocity channel maps on the dense molecular gas tracers, e.g., HCN, HCO^+, CS, and mid transition of CO, we can access the gas kinematics. To detect possible inflows or outflows, we can compare the CO rotation curve with a rotational velocity model based on the Hα kinematics and then subtract the model to analyse the velocity residuals in order to search for blue and redshifted patterns. Another possibility is to explore the current models for the rotation curve, when previous Hα or H I are not available in the literature. One of this model is described by Bertola et al. (1991), assuming the gas is on circular orbits in a plane, $\upsilon_c = Ar/(r^2 + c^2)^{p/2}$, where for $p = 1$ the velocity curve is asymptotically flat and $p = 3/2$ the system has a finite total mass, therefore we expect $1 \leq p \leq 3/2$. The observed radial velocity at a position (R, Ψ) on the plane of the sky can be described as:

$$\upsilon_{mod}(R, \Psi) = \upsilon_{sys} + \frac{ARcos(\Psi - \Psi_0)sin(\theta)cos^p(\theta)}{\left\{R^2\left[sin^2(\Psi - \Psi_0) + cos^2(\theta)cos^2(\Psi - \Psi_0)\right] + c^2cos^2(\theta)\right\}^{p/2}} \quad (1)$$

where θ is the inclination of the disk (with $\theta = 0$ for a face-on disk), Ψ_0 is the position angle of the line of nodes, v_{sys} is the systemic velocity and R is the radius and A, c, and p are parameters of the model. In the cases of NGC 7213 and NGC 1808, we have used the Bertola et al. (1991) model to search for non-circular motions in their observed velocity field.

3. RESULTS

3.1. NGC 7213

We report ALMA Cycle 1 observations of CO(2-1) at 229.2 GHz of NGC 7213, an early-type SA(s)a galaxy harboring a Seyfert 1/LINER. Previous neutral and ionized gas observations suggest the presence of a warped gaseous disk that could be the result of a merger. It presents a giant Hα filament and two HI tidal tails, confirming to be a highly disturbed interaction system (Hameed et al., 2001). Stellar kinematics is dominated by non-circular motions, along two spiral arms (Schnorr-Müller et al., 2014). In the central ~3 kpc, the CO map reveals a a widely distributed multiple-arm spiral structure, tracing the dusty spiral arms, as can be seen in the HST image (**Figure 1**). There is an offset peak located at 200 pc north from the center, meaning that the peak of the CO emission is not concentrated in the very center.

In general, the velocity field in the left panel of **Figure 2** is well-described by rotation, presenting some slightly perturbations along the minor axis (at $10''$) probably due to streaming motions from the spiral arms. By applying the Bertola et al. (1991) model to generate a 2-D velocity model that minimizes the residuals, we find that the position angle is $-18°$ and the systemic velocity should be corrected in 30 km/s. The residuals do not indicate hints of a significant blue and/or red-shifted components and this result indicates that probably there is no molecular outflow in NGC 7213.

3.2. NGC 1808

The "hot spot" galaxy NGC 1808 is remarkable for its very dusty appearance and especially for its well-known system of dark radial filaments. NGC 1808 is a Starburst/Seyfert 2 galaxy located at 9.1 Mpc and it is classified as a SAB(s)a. Accordingly to Reif et al. (1982), it has an inclination of 57°. Atomic gas traced with H I is concentrated in the galactic bar, disk, and a warped outer ring, indicating a tidal interaction in the past with the neighbor galaxy NGC 1792 (Koribalski et al., 1996). It presents prominent polar dust lanes and gas outflow emerging from the nucleus, as revealed in optical studies that indicate an outflow of dust and neutral and ionized gas (as seen in Hα, [N II], Na I D, and H I by Koribalski et al., 1993; Phillips, 1993). In particular, Na I D is seen blueshifted in absorption and redshifted in emission and *B-R* images show that the dust plumes associated with the outflow reach ~3 kpc above the plane. Near-infrared integral-field spectroscopy with SINFONI by Busch et al. (2017) showed a large gas reservoir and a disturbed gas velocity field that shows signs of inflowing streaming motion in the central ~100 pc.

We report ALMA Cycle 3 observations of CO(3-2), CS(7-6), HCN(4-3), and HCO^+(4-3) in band 7 with a resolution of $0.27''$. **Figure 3** shows that the CO emission follows the star-forming central 500 pc ring and the very center has a spiral trailing structure, that is also observed in CS, HCN, and HCO^+.

From the velocity map in **Figure 4**, the dominant velocity feature appears to be due to circular rotation in the disk. After subtracting a model for the velocity field by Bertola et al. (1991), we do not find significant patterns in the residuals and if there is a presence of an molecular outflow in the galaxy, it will be difficult to disentangle from the dominant circular motion in the 1st moment distribution. We need to explore in details the position-velocity diagrams along the dust lanes observed in the HST images. Additionally, Salak et al. (2016) presented evidence of a molecular gas outflow seen in CO(1-0) from the nuclear starburst region ($r \lesssim 250$ pc) that could be only detected in the position-velocity diagram. The outflow has a maximum velocity of υ_{out} ~180 km/s and mass outflow rate between 1 and 10 $M_\odot$/year, comparable to the total star formation rate in the starburst 500 pc region, that corresponds to SFR ~ $5M_\odot$/year in the "hot spots." The kinematics of our CO(3-2) observations

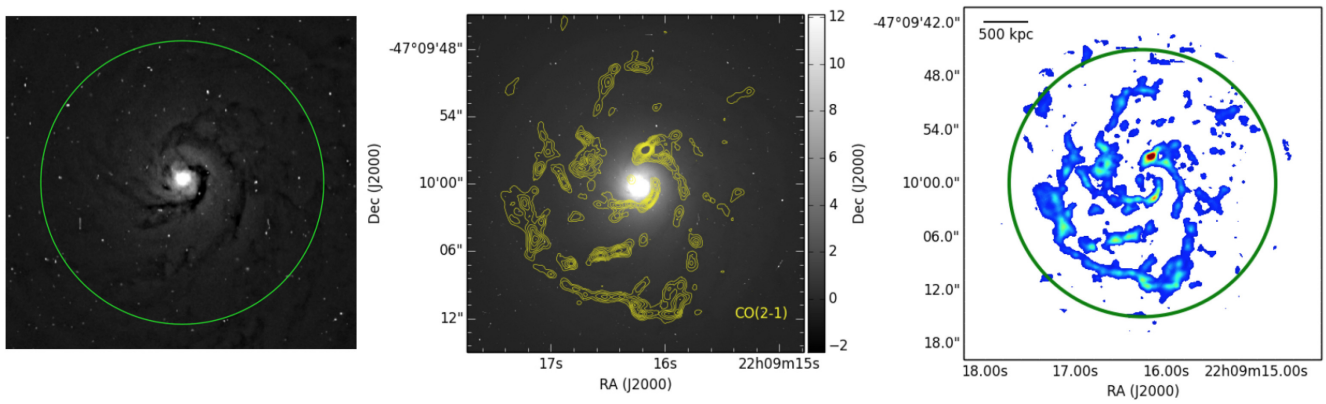

FIGURE 1 | In the left and middle panels we show an unsharp-masked F606W HST image and the original image with CO(2-1) contours overlaid, respectively. Right: CO(2-1) intensity map of NGC 7213 clipped at $>5\sigma$. The green circle represents a 30″ diameter.

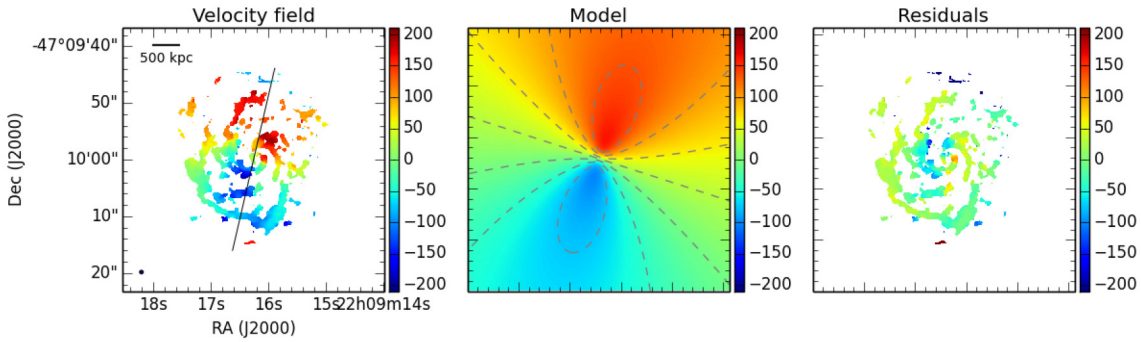

FIGURE 2 | Left: Velocity map of NGC 7213 clipped at $>5\sigma$. In the middle panel the best fit model using the Bertola et al. (1991) function and the residuals, after subtracting the model from the data, are shown on the right.

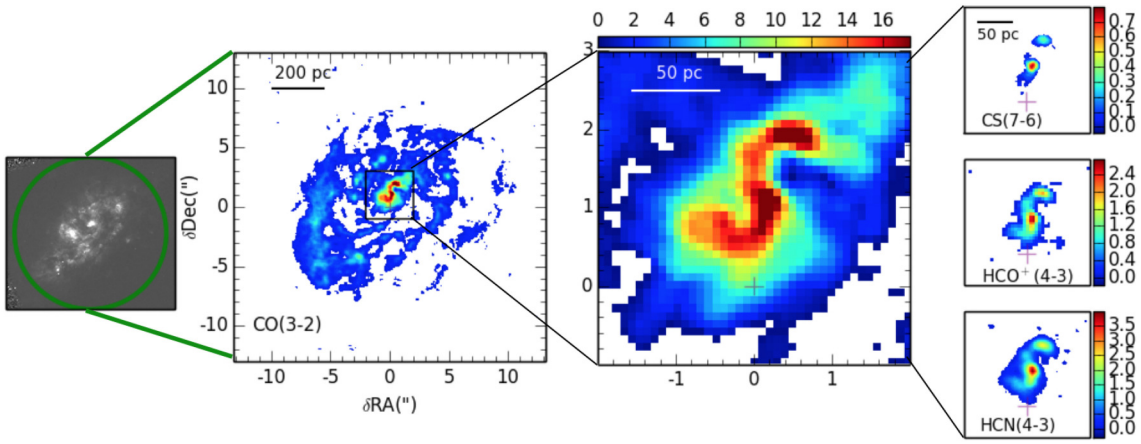

FIGURE 3 | From the left to the right panels: a WFC/F658N HST image followed by the 26″ diameter imaged area of CO(3-2) observations with ALMA. The next panels shows a zoom of the spiral trailing structure observed, and the subsequent plots show the same detection as seen in CS(7-6), HCO^{+}(4-3), and HCN(4-3). All the intensity maps were clipped at $>5\sigma$.

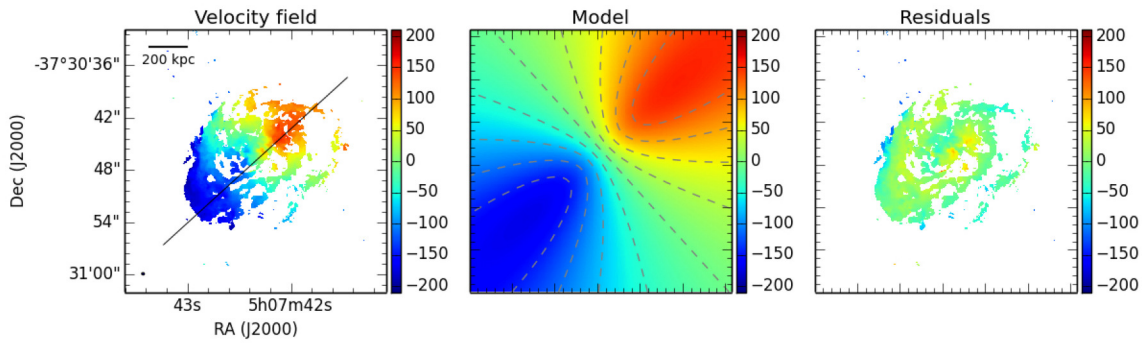

FIGURE 4 | Left: Velocity map of NGC 1808 clipped at $>5\sigma$. In the middle panel the best fit model using the Bertola et al. (1991) function and the residuals, after subtracting the model from the data, are shown on the right.

do not show strong outflows at this scale. Certainly, the outflow is more significant at larger scales. A further analysis of the molecular gas and the outflow in NGC 1808 will be present in a forthcoming paper (Audibert et al., in preparation).

4. PERSPECTIVES

We are going to apply the same methodology to search for outflows and inflows in a modest sample of nearby Seyfert/LINERs galaxies that are part of a new ALMA follow-up of the—NUclei of GAlaxies (NuGa) project, a previous CO survey of low luminosity AGN performed with the IRAM PdBI. The new ALMA observations have the remarkable spatial resolution of $\sim$0.06–0.09″.

AUTHOR CONTRIBUTIONS

AA has written the article; AA and FC have contributed to reduce the data; FC and SG-B have written the proposal; and all four authors have contributed to interpret the data and comment the paper.

ACKNOWLEDGMENTS

AA thanks the organizers of the "Quasars at All Cosmic Epochs" conference for support and the referees for useful comments. AA would like to acknowledge the financial support from the Brazilian scholarship program Science Without Borders—CNPq (scholarship reference 234043/2014-8). This paper makes use of the following ALMA data: ADS/JAO.ALMA# 2012.1.00474.S (PI: N. Nagar) and ADS/JAO.ALMA# 2015.1.00404.S (PI: FC). ALMA is a partnership of ESO (representing its member states), NSF (USA), and NINS (Japan), together with NRC (Canada), NSC and ASIAA (Taiwan), and KASI (Republic of Korea), in cooperation with the Republic of Chile. The Joint ALMA Observatory is operated by ESO, AUI/NRAO, and NAOJ. We used observations made with the NASA/ESA Hubble Space Telescope, and obtained from the Hubble Legacy Archive, which is a collaboration between the Space Telescope Science Institute (STScI/NASA), the Space Telescope European Coordinating Facility (ST-ECF/ESA), and the Canadian Astronomy Data Center (CADC/NRC/CSA). This research has made use of the NASA/IPAC Extragalactic Database (NED) and of the HyperLeda database.

REFERENCES

Alatalo, K., Blitz, L., Young, L. M., Davis, T. A., Bureau, M., Lopez, L. A., et al. (2011). Discovery of an active galactic nucleus driven molecular outflow in the local early-type Galaxy NGC 1266. *Astrophys. J.* 735:88. doi: 10.1088/0004-637X/735/2/88

Bertola, F., Bettoni, D., Danziger, J., Sadler, E., Sparke, L., and de Zeeuw, T. (1991). Testing the gravitational field in elliptical galaxies - NGC 5077. *Astrophys. J.* 373, 369–390.

Busch, G., Eckart, A., Valencia,-S. M., Fazeli, N., Scharwächter, J., Combes, F., et al. (2017). Star formation and gas flows in the centre of the NUGA galaxy NGC 1808 observed with SINFONI. *Astron. Astrophys.* 598:A55. doi: 10.1051/0004-6361/201629440

Cicone, C., Maiolino, R., Sturm, E., Graciá-Carpio, J., Feruglio, C., Neri, R., et al. (2014). Massive molecular outflows and evidence for AGN feedback from CO observations. *Astron. Astrophys.* 562:A21. doi: 10.1051/0004-6361/201322464

Combes, F., García-Burillo, S., Casasola, V., Hunt, L. K., Krips, M., Baker, A. J., et al. (2014). ALMA reveals the feeding of the Seyfert 1 nucleus in NGC 1566. *Astron. Astrophys.* 565:A97. doi: 10.1051/0004-6361/201423433

Dasyra, K. M., and Combes, F. (2012). Cold and warm molecular gas in the outflow of 4C 12.50. *Astron. Astrophys.* 541:L7. doi: 10.1051/0004-6361/201219229

Dasyra, K. M., Combes, F., Novak, G. S., Bremer, M., Spinoglio, L., Pereira Santaella, M., et al. (2014). Heating of the molecular gas in the massive outflow of the local ultraluminous-infrared and radio-loud galaxy 4C12.50. *Astron. Astrophys.* 565:A46. doi: 10.1051/0004-6361/201323070

Faucher-Giguère, C.-A., and Quataert, E. (2012). The physics of galactic winds driven by active galactic nuclei. *Mon. Not. R. Astron. Soc.* 425, 605–622. doi: 10.1111/j.1365-2966.2012.21512.x

Feruglio, C., Maiolino, R., Piconcelli, E., Menci, N., Aussel, H., Lamastra, A., et al. (2010). Quasar feedback revealed by giant molecular outflows. *Astron. Astrophys.* 518:L155. doi: 10.1051/0004-6361/201015164

Fischer, J., Sturm, E., González-Alfonso, E., Graciá-Carpio, J., Hailey-Dunsheath, S., Poglitsch, A., et al. (2010). Herschel-PACS spectroscopic diagnostics of local ULIRGs: conditions and kinematics in Markarian 231. *Astron. Astrophys.* 518:L41. doi: 10.1051/0004-6361/201014676

García-Burillo, S. (2016). Gas flows in galactic nuclei: observational constraints on BH-galaxy coevolution. *Proc. Int. Astron. Union* 11, 207–214. doi: 10.1017/S1743921316007511

García-Burillo, S., and Combes, F. (2012). The feeding of activity in galaxies: a molecular line perspective. *J. Phys. Conf. Ser.* 372:012050. doi: 10.1088/1742-6596/372/1/012050

García-Burillo, S., Combes, F., Usero, A., Aalto, S., Krips, M., Viti, S., et al. (2014). Molecular line emission in NGC 1068 imaged with ALMA. I. An AGN-driven outflow in the dense molecular gas. *Astron. Astrophys.* 567:A125. doi: 10.1051/0004-6361/201423843

Hameed, S., Blank, D. L., Young, L. M., and Devereux, N. (2001). The discovery of a giant Hα filament in NGC 7213. *Astrophys. J. Lett.* 546, L97–L100. doi: 10.1086/318865

Koribalski, B., Dahlem, M., Mebold, U., and Brinks, E. (1993). A comprehensive study of the peculiar spiral galaxy NGC 1808. II - VLA H I line observations. *Astron. Astrophys.* 268, 14–24.

Koribalski, B., Dettmar, R.-J., Mebold, U., and Wielebinski, R. (1996). Gas streaming along the bar in NGC 1808. A combination of high-resolution Hα and HI data. *Astron. Astrophys.* 315, 71–76.

Phillips, A. C. (1993). Nuclear and large-scale outflow in NGC 1808. *Astron. J.* 105, 486–498.

Reif, K., Mebold, U., Goss, W. M., van Woerden, H., and Siegman, B. (1982). An HI survey of southern galaxies. *Astron. Astrophys. Suppl. Ser.* 50, 451–479.

Salak, D., Nakai, N., Hatakeyama, T., and Miyamoto, Y. (2016). Gas dynamics and outflow in the barred starburst galaxy NGC 1808 revealed with ALMA. *Astrophys. J.* 823:68. doi: 10.3847/0004-637X/823/1/68

Schnorr-Müller, A., Storchi-Bergmann, T., Nagar, N. M., and Ferrari, F. (2014). Gas inflows towards the nucleus of the active galaxy NGC 7213. *Mon. Not. R. Astron. Soc.* 438, 3322–3331. doi: 10.1093/mnras/stt2440

Silk, J., and Mamon, G. A. (2012). The current status of galaxy formation. *Res. Astron. Astrophys.* 12, 917–946. doi: 10.1088/1674-4527/12/8/004

Sturm, E., González-Alfonso, E., Veilleux, S., Fischer, J., Graciá-Carpio, J., Hailey-Dunsheath, S., et al. (2011). Massive molecular outflows and negative feedback in ULIRGs observed by herschel-PACS. *Astrophys. J. Lett.* 733:L16. doi: 10.1088/2041-8205/733/1/L16

Veilleux, S., Meléndez, M., Sturm, E., Gracia-Carpio, J., Fischer, J., González-Alfonso, E., et al. (2013). Fast molecular outflows in luminous galaxy mergers: evidence for quasar feedback from herschel. *Astrophys. J.* 776:27. doi: 10.1088/0004-637X/776/1/27

Zubovas, K., and King, A. (2012). Clearing out a galaxy. *Astrophys. J. Lett.* 745:L34. doi: 10.1088/2041-8205/745/2/L34

Zubovas, K., and King, A. R. (2014). Galaxy-wide outflows: cold gas and star formation at high speeds. *Mon. Not. R. Astron. Soc.* 439, 400–406. doi: 10.1093/mnras/stt2472

Conflict of Interest Statement: The authors declare that the research was conducted in the absence of any commercial or financial relationships that could be construed as a potential conflict of interest.

Copyright © 2017 Audibert, Combes, García-Burillo and Salomé. This is an open-access article distributed under the terms of the Creative Commons Attribution License (CC BY). The use, distribution or reproduction in other forums is permitted, provided the original author(s) or licensor are credited and that the original publication in this journal is cited, in accordance with accepted academic practice. No use, distribution or reproduction is permitted which does not comply with these terms.

frontiers in Astronomy and Space Sciences

ORIGINAL RESEARCH
published: 15 December 2017
doi: 10.3389/fspas.2017.00062

Negative and Positive Outflow-Feedback in Nearby (U)LIRGs

*Sara Cazzoli**

Instituto de Astrofisica de Andalucia (CSIC), Granada, Spain

The starburst-AGN coexistence in local (U)LIRGs makes these galaxies excellent laboratories for the study of stellar and AGN outflows and feedback. Outflows regulate star formation and AGN activity, redistributing gas, dust and metals over large scales in the interstellar and intergalactic media (negative feedback) being also considered to be able to undergo vigorous star formation (positive feedback). In this contribution, I will summarize the results from a search for outflows in a sample of nearby 38 local (U)LIRG systems observed with VIMOS/VLT integral field unit. For two galaxies of the sample I will detail the outflow properties and discuss the observational evidence for negative and positive outflow-feedback. The assessment of both negative and positive feedback effects represent a novel approach toward a comprehensive understanding of the impact of outflow feedback in the galaxy evolution.

Keywords: galaxies: starburst, evolution, feedback, ISM: jets and outflows, ISM: kinematics and dynamics, techniques: spectroscopic

OPEN ACCESS

Edited by:
Mauro D'Onofrio,
Università degli Studi di Padova, Italy

Reviewed by:
José María Solanes,
University of Barcelona, Spain
Omaira Gonzàlez Martín,
Instituto de Radioastronomía y Astrofísica, Mexico

***Correspondence:**
Sara Cazzoli
sara@iaa.es

Specialty section:
This article was submitted to Milky Way and Galaxies, a section of the journal Frontiers in Astronomy and Space Sciences

Received: *29 August 2017*
Accepted: *04 December 2017*
Published: *15 December 2017*

Citation:
Cazzoli S (2017) Negative and Positive Outflow-Feedback in Nearby (U)LIRGs. Front. Astron. Space Sci. 4:62. doi: 10.3389/fspas.2017.00062

1. INTRODUCTION

In the last decade, our understanding of the formation and evolution of galaxies over cosmic time has been significantly enhanced by large scale galaxy surveys. These surveys have drawn a detailed picture of the global properties of the galaxies, establishing the galaxy stellar mass function and scaling relations (e.g., mass-metallicity, Tremonti et al., 2004; Brooks et al., 2006). Galaxy evolution models attempt to reproduce the properties of the galaxies and those of the surrounding Inter Galactic Medium (IGM) invoking the need of feedback mechanisms from starbursts or Active Galactic Nuclei (AGN). In fact, models of galaxy evolution without a strong (stellar or AGN) feedback, lead galaxies to have much higher Star Forming Rates (SFR) and larger stellar masses than observed (e.g., Hopkins et al., 2006). Outflows regulate Star Formation (SF) and AGN activity (negative feedback), and they are also considered the primary mechanism by which dust and metals are redistributed over large scales in the Inter Stellar Medium (ISM), or even expelled outside the galaxy into the IGM (e.g., Aguirre et al., 2001). In addition, it has been recently proposed that outflows can undergo vigorous SF (positive feedback, Ishibashi and Fabian, 2012; Zubovas et al., 2013). In this context, the study of the of feedback mechanisms is of critical importance to trace the build-up of stellar mass and evolution of galaxies in the Universe. Multiphase outflows are ubiquitous at any redshift. Although the bulk of the black hole growth, SF, and galaxy mergers are believed to occur at $z \sim 1$–3, studies of outflows in nearby galaxies offer detailed insights into feedback phenomena as one of the primary drivers of galaxy evolution.

In this context, local Luminous and Ultra-Luminous Infrared Galaxies [(U)LIRGs] are particularly interesting populations. On the one hand these objects show the most conspicuous

cases for outflows in the local Universe (e.g., Heckman et al., 2000; Rupke et al., 2002). On the other hand, local (U)LIRGs have a SF-activity similar to that found for "main-sequence" high-z star-forming galaxies, and share with distant galaxies some structural and kinematical properties (e.g., Elbaz et al., 2011; Arribas et al., 2012; Bellocchi et al., 2013). Therefore, local (U)LIRGs allow us to study the outflow phenomenon at environments similar to those observed at high-z, but with a much higher signal-to-noise and spatial resolution.

The large majority of previous outflow studies are based on long slit observations giving only a partial description of the outflow phenomenon (e.g., Rupke et al., 2005). However, Integral Field Spectroscopy (IFS) is well suited for search for and characterize outflows as it allows the spectroscopic measurement of large areas of e.g., interstellar (outflowing) gas and therefore allows to study the 2D structure of outflows.

Outflows are made up of a number of gas phases with a wide range of physical conditions, as the ISM surrounding the starburst and the AGN (see Veilleux et al., 2005 for a review). Of particular interest are the cold phases as cold gas represents the fuel of SF. In the optical range, the cold neutral gas entrained in outflows is detected through the sodium doublet absorption: NaD$\lambda\lambda$5890, 5896.

We search for outflows in a sample of 38 local (U)LIRG systems (51 individual galaxies) with $z < 0.09$ observed with the VIMOS/VLT integral field unit. This allows us to extend the census of the 2D mapping of neutral outflows in local (U)LIRGs, covering the less studied LIRG luminosity range. In fact, previous IFS studies are limited to a small number of extreme objects, mainly major-mergers (e.g., Rupke and Veilleux, 2013). We exploit these optical IFS-observations to make a significant step forwards in understanding the outflow properties such as their geometry and their connection/feedback with those of the host galaxy. Two galaxies in the sample have been considered as a pilot studies for negative and positive feedback. These were analyzed thoroughly with a multi wavelength approach.

2. SPATIALLY RESOLVED KINEMATICS, GALACTIC WIND, AND QUENCHING OF SF IN THE LIRG IRAS F11506-3851

We choose the nearby LIRG IRAS F11506-3851 as a pilot study, since the availability of both optical and near-IR IFS-data that allows to simultaneously trace different galaxy components (ISM and stars). We have accomplished such a multiwavelength study with VIMOS/VLT and SINFONI/VLT data (Cazzoli et al., 2014). The morphology and the 2D kinematics of the gaseous (neutral and ionized) and stellar components have been mapped in the central regions (<3 kpc) using the NaD absorption doublet, the H$\alpha\lambda$6563 emission line, and the near-IR CO(2-0)λ2.293 μm and CO(3-1)λ2.322 μm absorption bands.

The NaD and the Hα-[NII] emission-line complex profiles were modeled with two kinematic components (i.e., a couple Gaussians per line) on spaxel-by-spaxel basis. The output of the fitting (line flux, central wavelength and intrinsic width) were used to generate spectral maps (**Figure 1**). To obtain the stellar kinematic, we first binned SINFONI/VLT data using the Voronoi 2D-binning method (Cappellari and Emsellem, 2004) and then we used the Penalized PiXel-Fitting method (pPXF; Cappellari and Emsellem, 2004), to fit a library of stellar templates (Winge et al., 2009) to individual spectra to create the spectral maps (**Figure 1**).

The kinematics of the ionized gas and the stars are dominated by rotation, with large observed velocity amplitudes and centrally peaked dispersion maps. In contrast, we have found that the ISM-NaD absorption shows a complex kinematic structure dominated by two main components. On the one hand, we observe an irregular slowly rotating thick disk which lags significantly compared to the ionized gas and stars. On the other hand, we find a kpc-scale outflow perpendicular to the disk, which is ejecting a significant amount of gas (3×10^8 M$_\odot$) from the central regions at a rate of 1.4 times larger than the ongoing SF. The relatively strong emission by SNe in the central regions as traced by the [Fe II]λ1.64 μm emission, indicates a recent ($\sim$7 Myr ago) episode of SF. All these results strongly suggest that we are witnessing (nuclear) quenching due to SF feedback in IRAS F11506-3851 (negative feedback, section 1). However, the relatively large mass of molecular gas detected in the nuclear region via the H_2(1-0)S(1)λ2.12 μm line suggests that further episodes of SF may take place again. In addition, there is evidence of the presence of an ionized outflow that partially overlaps with the neutral one.

Thanks to recent ALMA observations (Pereira-Santaella et al., 2016) we have confirmed the presence of the outflow in molecular gas [via CO(1-0) emission line] with an excellent consistency with that of neutral gas presented in Cazzoli et al. (2014).

3. NEUTRAL GAS OUTFLOW IN NEARBY (U)LIRGS VIA OPTICAL NAD FEATURE

We have performed a systematic study of the properties of the neutral gas in the whole sample of (U)LIRGs, on the basis of spatially integrated, as well as the spatially resolved IFS-spectra of the NaD feature obtained with VIMOS/VLT (Cazzoli et al., 2016).

We have found that neutral outflows are frequent (71 and 55 % detection rate for the integrated and spatially resolved analyses, respectively). Outflow (integrated) velocities, V, are in the range: 65–260 km/s and these scale with the SFR as $V \propto SFR^{0.15}$ (excluding AGNs), in rather good agreement with previous results (Martin, 2005). The spatially resolved analysis could be performed for 40 galaxies. In a minor but significant fraction (11 targets) we found disk-rotation signatures, whereas for more than half of the cases (22 targets) the neutral gas velocity fields are dominated by non-circular motions with signatures of cone-like outflows.

Based on a simple model, we have found that the outflow mass ranges from 0.4 to 7.5×10^8 M$_\odot$, reaching up to $\sim$3% of the dynamical mass of the host. The mass rates are typically only $\sim$0.2-0.4 times the corresponding SFR indicating that, in general, the mass-loss is small for slowing down significantly the SF. In the majority of the cases, the velocity of the outflowing gas is not enough to escape the host potential well and, therefore, most of it will rain-back into the galaxy disk (fountain scenario).

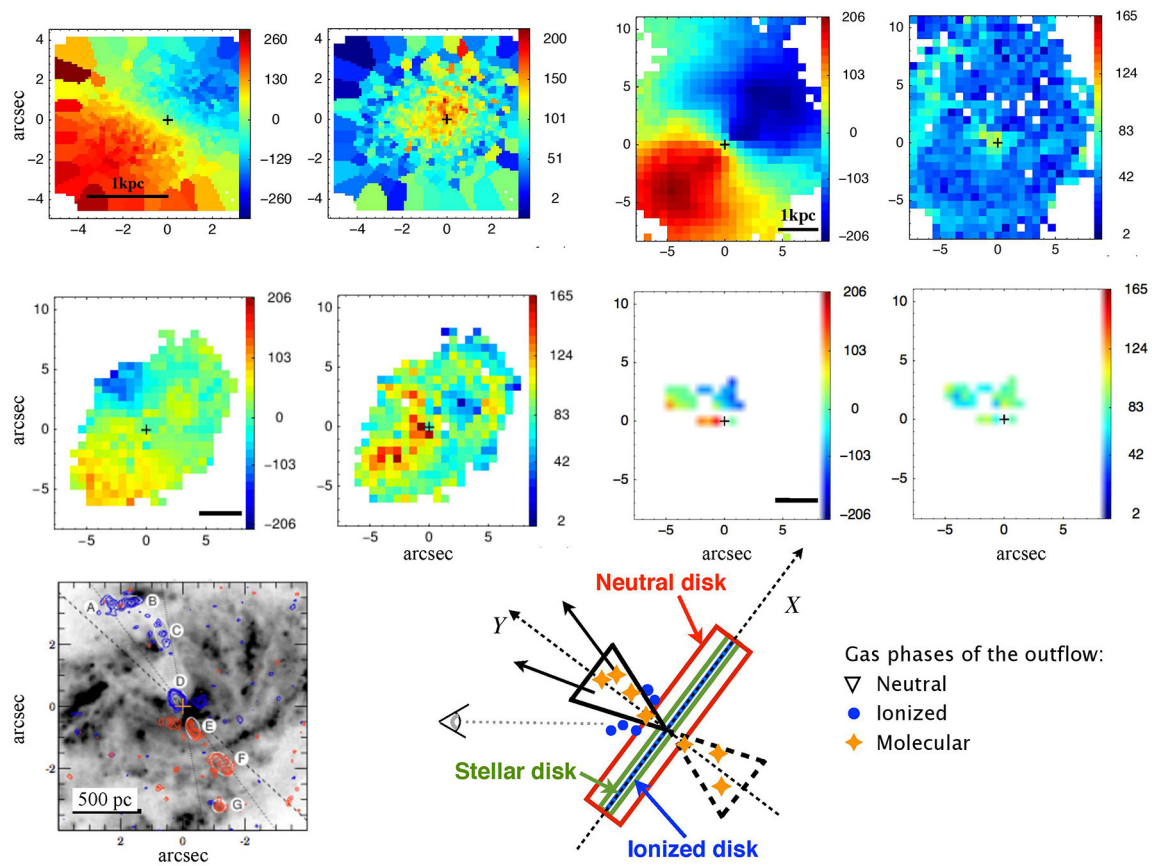

FIGURE 1 | Spectral maps and HST image of IRAS F 11506-3851. **Top-left:** SINFONI/VLT velocity and velocity dispersion maps of stars (CO absorption bands). **Top-right:** the same maps but for the ionized gas (Hα narrow component) obtained using VIMOS/VLT cubes. **Middle:** velocity and velocity dispersion maps of neutral gas (left) and ionized gas (right) obtained analyzing the NaD absorption and the Hα broad component in VIMOS/VLT data. All these maps, from Cazzoli et al. (2014), are in km/s units. The cross marks the galaxy nucleus. **Bottom-left:** A zoomed-in view of the optical morphology (ACS/HST F814W-image) in gray scale with red and blue contours indicating the redshifted and blueshifted, respectively, molecular outflowing clumps detected by ALMA. The dashed lines indicate the minor axis and dotted lines the opening angle. The figure is adapted from Pereira-Santaella et al. (2016). **Bottom-right:** toy model of the outflows and disks summarizing our results, adapted from Cazzoli et al. (2014). Credit: Cazzoli, A&A, 569, A14, 2014, and PereiraSantaella2016, A&A, 594, A81, 2016, reproduced with permission © ESO.

The comparison between the outflow power and the kinetic power of the starburst associated to SNe (**Figure 2**) indicates that only the starburst could drive the outflow in nearly all the (U)LIRGs galaxies, as the outflow power is generally lower than the 20% of the kinetic power supplied by the starburst. Only in two cases the contribution of the AGN is, in principle, significant.

4. STAR FORMATION INSIDE THE OUTFLOW OF IRAS F23128-5919

The nearby ULIRG IRAS F23128-5919 is a system of two interacting galaxies. The southern galaxy is characterized by a prominent outflow studied by various authors through emission and absorption lines (Piqueras López et al., 2012; Bellocchi et al., 2013; Arribas et al., 2014; Cazzoli et al., 2016). In order to investigate if the multiphase outflow is able to undergo vigorous SF as expected in case of positive feedback (section 1) we have combined archival optical MUSE/VLT data with new X-shooter/VLT observations (Maiolino et al., 2017).

Our strategy enabled the detection of spectral diagnostics over the spectral range from 0.35 to 2.5 μm. The optical nebular emission lines are clearly characterized by two kinematic components: a narrow component tracing the disks of the two merging galaxies and a broad blueshifted component, with velocities up to 600 km/s and width up to 1,000 km/s, tracing the prominent outflow extending for several kpc toward the East. The receding component of the outflow is also seen as broad and redshifted component toward the West, though fainter due dust obscuration in the galaxy disk. The multi-component decomposition of the set of near-IR emission lines we consider: Pa$\alpha\lambda$1.88 μm, Pa$\beta\lambda$1.28 μm, Br$\gamma\lambda$2.16 μm, $H_2$1-0 S(1), [P II]λ1.18 μm, [Fe II]λ1.25,1.64 μm, follows that of optical lines.

By studying multiple diagnostics we obtain independent pieces of evidence that stars are forming in the outflow of IRAS 2312-59. On the basis of optical and near-IR diagnostic

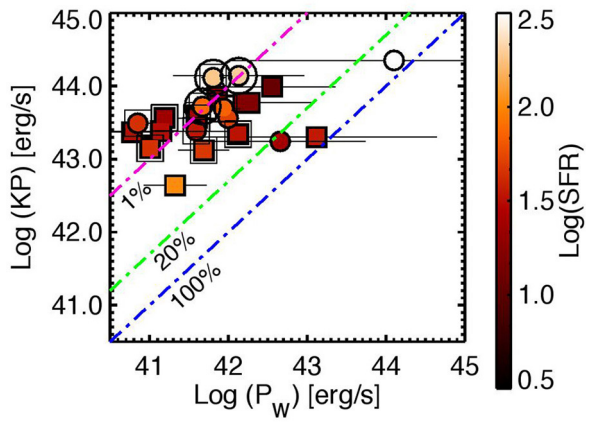

FIGURE 2 | Logarithm of kinetic power of the starburst associated to SNe (KP) as a function of the outflow power (Pw), color coded by their SFR. We identify pure starbursts and AGN-hosts with squares and circles, respectively, while very strong-AGN are marked with an additional circle. Those galaxies for which we were unable to infer in detail the outflow morphology are marked with an additional square. The pink, green and blue lines represent respectively the positions for which the power of the outflow is equal to the 1, 20, and 100% of the kinetic power supplied by the starburst. Credit: Cazzoli, A&A, 590, A125, 2016, reproduced with permission © ESO.

diagrams (also called BPTs) we discriminate the dominant source of ionization of the kinematic components used to model emission lines (Baldwin et al., 1981; Riffel et al., 2013; Colina et al., 2015). In all the five diagnostic diagrams (**Figure 2** in Maiolino et al., 2017) we have found that the line ratios for the broad outflowing component are typical of HII star-forming regions. Furthermore, on the one hand coronal lines associated with AGN excitation (e.g., S IXλ1.252 and Al IXλ2.045μm) are absent in the near IR spectra. On the other hand, we have found signature of a young stellar population (age a few tens Myr) formed at high velocity in the inner region of the outflowing gas and then decelerated by the gravitational potential of the galaxy (reacting only to gravity and not to radiation pressure as the outflowing gas). This implies that the young stars are formed in situ, i.e., within the outflow, as also indicated by the values of the gas ionization parameter (no photoionization by the UV radiation field of the galaxy disk).

Finally, we translate the luminosity of the broad component of Hα into a SFR of 15 $M_{\odot}$/yr that is a substantial fraction, i.e., 13 % (up to 25 % if we consider the outflow is biconical) of the total SFR of 115 $M_{\odot}$/yr of the ULIRG system.

5. SUMMARY

Outflows have been proposed as an effective way to quench and enhance star formation and AGN activities. In (U)LIRGs starburst-AGN coexist and this galaxies represent a transitional phase from star-forming to quiescent galaxies offering a unique insight for the understanding of how feedback mechanisms regulate the gas reservoir. The aim of the works presented in this contribution is to study how negative and positive feedback phenomena, as consequence of starburst and AGN activities, are able to shape the gas life-cycle and observed properties via multiphase outflows. This represent a novel approach toward a comprehensive understanding of the impact of outflow feedback in the galaxy evolution.

The main conclusions of this contribution can be summarized as follows:

- Neutral gas massive SNe-powered outflows are observed frequently in our sample of (U)LIRGs, with velocities V = 65–260 km/s, and loading factors ranging from 0.2 to 0.4 $M_{\odot}$/yr (Cazzoli et al., 2016). Most of the cold outflowing material is likely falling back to the disk (fountain scenario). We studied in detail the neutral, ionized and molecular phases of the outflow in the LIRG IRAS F11506-3851 (Cazzoli et al., 2014; Pereira-Santaella et al., 2016). The outflow (a galactic fountain) is ejecting a significant amount of gas from the central regions at a rate of 1.4 times larger than the ongoing SF.
  For some of the LIRGs in the sample, we will study the IGM enrichment caused by large scale outflows on the basis of the detection and kinematic of the NaD absorption in background galaxies.
- By studying multiple diagnostics we obtain independent pieces of evidence that stars are forming in the outflow of the nearby ULIRG IRAS 2312-59 (Maiolino et al., 2017). More specifically, these evidence include diagnostic ratios typical of those of star-forming HII regions (as indicated by optical and near-IR diagnostic diagrams) and the detection of young $\sim$10 Myr stars in the outflow which move ballistically. We excluded that the outflowing gas is photoionized by the UV radiation field of the galaxy disk on the basis of ionization parameter arguments. Therefore, for the first time we have unambiguously identifying a case of outflow positive feedback as star formation occurring within the outflow.

Star formation may also be occurring in other outflows. Future works by our group include the increment the census of the cases of positive feedback and the investigation of the properties of the star-forming outflowing-gas.

Finally, we remark that the type of studies presented in this contribution set the ground for future studies. More insights on the outflows feedback will come in the next decade thanks to upcoming ground based telescopes or space missions, as the European Extremely Large Telescope and James Webb Space Telescope.

AUTHOR CONTRIBUTIONS

The analysis of optical VIMOS IFS data come from the PhD thesis by SC (Cazzoli, 2016) and referred papers (Cazzoli et al., 2014, 2016). SC contributed also the analysis and interpretation of SINFONI and X-shooter observations (Cazzoli et al., 2014 and Maiolino et al., 2017, respectively). SC contributed also to interpretation of ALMA data (Pereira-Santaella et al., 2016).

FUNDING

SC acknowledges financial support by the Spanish grant AYA2013-42227-P, as well as, that of organisers through a grant for the accommodation. The work was also funded

by the Marie Curie Initial Training Network ELIXIR of the European Commission under contract PITN-GA-2008-214227 and the Spanish grants AYA2010-21161-C02-01 and AYA2012-32295.

ACKNOWLEDGMENTS

SC is especially grateful to S. Arribas, R. Maiolino, and L. Colina. SC thanks I. Marquez, J. Masegosa and A. del Olmo for their support. SC acknowledges all the collaborators in the different papers produced and that are summarized in this contribution.

This manuscript is partially based on the PhD thesis of SC (available online at http://hdl.handle.net/10486/676308, in line with Universidad Autonoma de Madrid policies). This thesis is the only medium that all the work done by SC during her Ph.D. has appeared in. The publication of manuscripts based on SC thesis work is in line with the Universidad Autonoma de Madrid policies.

REFERENCES

Aguirre, A., Hernquist, L., Schaye, J., Katz, N., Weinberg, D. H., and Gardner, J. (2001). Metal enrichment of the intergalactic medium in cosmological simulations. *Astrophys. J.* 561, 521–549. doi: 10.1086/323370

Arribas, S., Colina, L., Alonso-Herrero, A., Rosales-Ortega, F. F., Monreal-Ibero, A., García-Marín, M., et al. (2012). Integral field spectroscopy based Hα sizes of local luminous and ultraluminous infrared galaxies. A direct comparison with high-z massive star-forming galaxies. *Astron. Astrophys.* 541:A20. doi: 10.1051/0004-6361/201118007

Arribas, S., Colina, L., Bellocchi, E., Maiolino, R., and Villar-Martín, M. (2014). Ionized gas outflows and global kinematics of low-z luminous star-forming galaxies. *Astron. Astrophys.* 568:A14. doi: 10.1051/0004-6361/201323324

Baldwin, J. A., Phillips, M. M., and Terlevich, R. (1981). Classification parameters for the emission-line spectra of extragalactic objects. *Publ. Astron. Soc. Pacific* 93, 5–19. doi: 10.1086/130766

Bellocchi, E., Arribas, S., Colina, L., and Miralles-Caballero, D. (2013). VLT/VIMOS integral field spectroscopy of luminous and ultraluminous infrared galaxies: 2D kinematic properties. *Astron. Astrophys.* 557:A59. doi: 10.1051/0004-6361/201221019

Brooks, A., Governato, F., Booth, C. M., Willman, B., Gardner, J. P., Wadsley, J., et al. (2006). "The origin and evolution of the mass-metallicity relationship for galaxies: results from cosmological N-body simulations," in *Bulletin of the American Astronomical Society, Vol. 38, American Astronomical Society Meeting Abstracts,* 925.

Cappellari, M., and Emsellem, E. (2004). Parametric recovery of line-of-sight velocity distributions from absorption-line spectra of galaxies via penalized likelihood. *Publ. Astron. Soc. Pacific* 116, 138–147. doi: 10.1086/381875

Cazzoli, S. (2016). *A Search For Neutral Gas Outflows In Nearby Luminous Star-Forming Galaxies.* Ph.D. thesis, Universidad Autonóma de Madrid, UAM.

Cazzoli, S., Arribas, S., Colina, L., Piqueras-López, J., Bellocchi, E., Emonts, B., et al. (2014). Spatially resolved kinematics, galactic wind, and quenching of star formation in the luminous infrared galaxy IRAS F11506-3851. *Astron. Astrophys.* 569:A14. doi: 10.1051/0004-6361/201323296

Cazzoli, S., Arribas, S., Maiolino, R., and Colina, L. (2016). Neutral gas outflows in nearby [U]LIRGs via optical NaD feature. *Astron. Astrophys.* 590:A125. doi: 10.1051/0004-6361/201526788

Colina, L., Piqueras López, J., Arribas, S., Riffel, R., Riffel, R. A., Rodriguez-Ardila, A., et al. (2015). Understanding the two-dimensional ionization structure in luminous infrared galaxies. A near-IR integral field spectroscopy perspective. *Astron. Astrophys.* 578:A48. doi: 10.1051/0004-6361/201425567

Elbaz, D., Dickinson, M., Hwang, H. S., Díaz-Santos, T., Magdis, G., Magnelli, B., et al. (2011). GOODS-Herschel: an infrared main sequence for star-forming galaxies. *Astron. Astrophys.* 533:A119. doi: 10.1051/0004-6361/201117239

Heckman, T. M., Lehnert, M. D., Strickland, D. K., and Armus, L. (2000). Absorption-line probes of gas and dust in galactic superwinds. *Astrophys. J. Suppl.* 129, 493–516. doi: 10.1086/313421

Hopkins, P. F., Hernquist, L., Cox, T. J., Di Matteo, T., Robertson, B., and Springel, V. (2006). A unified, merger-driven model of the origin of starbursts, quasars, the cosmic X-ray background, supermassive black holes, and galaxy spheroids. *Astrophys. J. Suppl.* 163, 1–49. doi: 10.1086/499298

Ishibashi, W., and Fabian, A. C. (2012). Active galactic nucleus feedback and triggering of star formation in galaxies. *Month. Notices R. Astron. Soc.* 427, 2998–3005. doi: 10.1111/j.1365-2966.2012.22074.x

Maiolino, R., Russell, H. R., Fabian, A. C., Carniani, S., Gallagher, R., Cazzoli, S., et al. (2017). Star formation inside a galactic outflow. *Nature* 544, 202–206. doi: 10.1038/nature21677

Martin, C. L. (2005). Mapping large-scale gaseous outflows in ultraluminous galaxies with keck II ESI spectra: variations in outflow velocity with galactic mass. *Astrophys. J.* 621, 227–245. doi: 10.1086/427277

Pereira-Santaella, M., Colina, L., García-Burillo, S., Alonso-Herrero, A., Arribas, S., Cazzoli, S., et al. (2016). High-velocity extended molecular outflow in the star-formation dominated luminous infrared galaxy ESO 320-G030. *Astron. Astrophys.* 594:A81. doi: 10.1051/0004-6361/201628875

Piqueras López, J., Colina, L., Arribas, S., Alonso-Herrero, A., and Bedregal, A. G. (2012). VLT-SINFONI integral field spectroscopy of low-z luminous and ultraluminous infrared galaxies. I. Atlas of the 2D gas structure. *Astron. Astrophys.* 546:A64. doi: 10.1051/0004-6361/201219372

Riffel, R., Rodríguez-Ardila, A., Aleman, I., Brotherton, M. S., Pastoriza, M. G., Bonatto, C., et al. (2013). Molecular hydrogen and [Fe II] in active galactic nuclei - III. Low-ionization nuclear emission-line region and star-forming galaxies. *Month. Notices R. Astron. Soc.* 430, 2002–2017. doi: 10.1093/mnras/stt026

Rupke, D. S., Veilleux, S., and Sanders, D. B. (2002). Keck absorption-line spectroscopy of galactic winds in ultraluminous infrared galaxies. *Astrophys. J.* 570, 588–609. doi: 10.1086/339789

Rupke, D. S., Veilleux, S., and Sanders, D. B. (2005). Outflows in active galactic nucleus/starburst-composite ultraluminous infrared galaxies1. *Astrophys. J.* 632, 751–780. doi: 10.1086/444451

Rupke, D. S. N., and Veilleux, S. (2013). The multiphase structure and power sources of galactic winds in major mergers. *Astrophys. J.* 768:75. doi: 10.1088/0004-637X/768/1/75

Tremonti, C. A., Heckman, T. M., Kauffmann, G., Brinchmann, J., Charlot, S., White, S. D. M., et al. (2004). The origin of the mass-metallicity relation: insights from 53,000 star-forming galaxies in the sloan digital sky survey. *Astrophys. J.* 613, 898–913. doi: 10.1086/423264

Veilleux, S., Cecil, G., and Bland-Hawthorn, J. (2005). Galactic winds. *Annu. Rev. Astron. Astrophys.* 43, 769–826. doi: 10.1146/annurev.astro.43.072103.150610

Winge, C., Riffel, R. A., and Storchi-Bergmann, T. (2009). The gemini spectral library of near-IR late-type stellar templates and its application for velocity dispersion measurements. *Astrophys. J. Suppl.* 185, 186–197. doi: 10.1088/0067-0049/185/1/186

Zubovas, K., Nayakshin, S., Sazonov, S., and Sunyaev, R. (2013). Outflows of stars due to quasar feedback. *Month. Notices R. Astron. Soc.* 431, 793–798. doi: 10.1093/mnras/stt214

Conflict of Interest Statement: The author declares that the research was conducted in the absence of any commercial or financial relationships that could be construed as a potential conflict of interest.

Copyright © 2017 Cazzoli. This is an open-access article distributed under the terms of the Creative Commons Attribution License (CC BY). The use, distribution or reproduction in other forums is permitted, provided the original author(s) or licensor are credited and that the original publication in this journal is cited, in accordance with accepted academic practice. No use, distribution or reproduction is permitted which does not comply with these terms.

frontiers in Astronomy and Space Sciences

ORIGINAL RESEARCH
published: 24 November 2017
doi: 10.3389/fspas.2017.00046

Ionized Gas Outflows from the MAGNUM Survey: NGC 1365 and NGC 4945

Giacomo Venturi[1,2], Alessandro Marconi[1,2], Matilde Mingozzi[2,3], Stefano Carniani[4,5], Giovanni Cresci[2], Guido Risaliti[1,2] and Filippo Mannucci[2]*

[1] Dipartimento di Fisica e Astronomia, Università degli Studi di Firenze, Sesto Fiorentino, Italy, [2] Osservatorio Astrofisico di Arcetri (INAF), Firenze, Italy, [3] Dipartimento di Fisica e Astronomia, Università di Bologna, Bologna, Italy, [4] Cavendish Laboratory, Department of Physics, University of Cambridge, Cambridge, United Kingdom, [5] Kavli Institute for Cosmology, University of Cambridge, Cambridge, United Kingdom

AGN feedback, acting through strong outflows accelerated in the nuclear region of AGN hosts, is invoked as a key ingredient for galaxy evolution by many models to explain the observed BH-galaxy scaling relations. Recently, some direct observational evidence of radiative mode feedback in action has been finally found in quasars at $z > 1.5$. However, it is not possible to study outflows in quasars at those redshifts on small scales ($\lesssim$100 pc), as spatial information is limited by angular resolution. This is instead feasible in nearby active galaxies, which are ideal laboratories to explore outflow structure and properties, as well as the effects of AGN on their host galaxies. In this proceeding we present preliminary results from the MAGNUM survey, which comprises nearby Seyfert galaxies observed with the integral field spectrograph VLT/MUSE. We focus on two sources, NGC 1365 and NGC 4945, that exhibit double conical outflows extending on distances >1 kpc. We disentangle the dominant contributions to ionization of the various gas components observed in the central ∼5.3 kpc of NGC 1365. An attempt to infer outflow 3D structure in NGC 4945 is made via simple kinematic modeling, suggesting a hollow cone geometry.

Keywords: active galactic nuclei, galaxies, outflows, NGC 1365, NGC 4945, imaging spectroscopy

OPEN ACCESS

Edited by:
Paola Marziani, Osservatorio Astronomico di Padova (INAF), Italy

Reviewed by:
Giovanna Maria Stirpe, Osservatorio astronomico di Bologna (INAF), Italy
Begoña Garcia-Lorenzo, Instituto de Astrofísica de Canarias, Spain

****Correspondence:***
Giacomo Venturi
gventuri@arcetri.astro.it

Specialty section:
This article was submitted to Milky Way and Galaxies, a section of the journal Frontiers in Astronomy and Space Sciences

Received: *16 September 2017*
Accepted: *02 November 2017*
Published: *24 November 2017*

Citation:
Venturi G, Marconi A, Mingozzi M, Carniani S, Cresci G, Risaliti G and Mannucci F (2017) Ionized Gas Outflows from the MAGNUM Survey: NGC 1365 and NGC 4945. Front. Astron. Space Sci. 4:46. doi: 10.3389/fspas.2017.00046

1. INTRODUCTION

AGN are believed to have a strong influence on their host galaxies, accelerating fast outflows able to quench star formation (negative feedback). Many models invoke AGN feedback as a key ingredient for galaxy evolution (e.g., Springel et al., 2005; Hopkins et al., 2006; Ciotti et al., 2010; Scannapieco et al., 2012), shaping galaxy properties and giving rise to the observed black hole-host galaxy relations ($M_{\rm BH} - \sigma_{\rm bulge}$, $M_{\rm BH} - L_{\rm bulge}$, $M_{\rm BH} - M_{\rm bulge}$; e.g., Ferrarese and Merritt, 2000; Gebhardt et al., 2000; Marconi and Hunt, 2003; Kormendy and Ho, 2013; McConnell and Ma, 2013). According to radiative (or wind) mode feedback models, AGN at the Eddington limit can sweep away surrounding gas by radiation pressure, driving fast outflows which overcome the gravitational potential of the galaxy. Momentum balance in radiative mode gives a $M_{\rm BH} - \sigma_{\rm bulge}$ relation which is in agreement with the observed one (e.g., Fabian, 1999; King, 2003, 2005; Murray et al., 2005).

Luminous AGN are the best candidates to detect ongoing star formation being quenched by AGN feedback, as indeed found in recent works (e.g., Cano-Díaz et al., 2012; Brusa et al., 2015; Cresci et al., 2015a; Carniani et al., 2016, 2017). However, it is not possible to study high-z quasar

outflows on small spatial scales ($\lesssim$100 pc), due to their large distances (e.g., even with adaptive optics Williams et al., 2017 achieve a spatial resolution of ∼1 kpc at $z = 2.4$). On the contrary, nearby active galaxies are ideal laboratories to explore in detail outflow properties, their formation and acceleration mechanisms, as well as the effects of AGN activity on host galaxies (e.g., García-Burillo et al., 2014; Cresci et al., 2015b; Storchi-Bergmann, 2015; Davies et al., 2016). Here we present preliminary results from our MAGNUM survey (Measuring Active Galactic Nuclei Under MUSE Microscope), which aims at investigating the properties of outflows in nearby AGN, the physical conditions of the ionized gas and the interplay between nuclear activity and star formation in the host galaxy, thanks to the unprecedented combination of spatial and spectral coverage provided by the integral field spectrograph MUSE at VLT ($1'\times1'$ FOV with $0.2''$ per spaxel and 4750–9300 Å spectral coverage; Bacon et al., 2010). The first result from the MAGNUM survey is presented in Cresci et al. (2015b), where tentative evidence of star formation induced by the AGN outflow (positive feedback; e.g., Silk, 2013) is found in the nearby Seyfert galaxy NGC 5643. Here two young ($\sim10^7$ yr) isolated star-forming clumps are observed in the direction of the AGN-ionized outflow, where this impacts the dense material at the edge of the dust lane, suggesting a case of occurring positive feedback.

2. MAGNUM SURVEY: OVERVIEW

2.1. Sample Selection

MAGNUM galaxies have been picked out from the optically-selected samples of Maiolino and Rieke (1995) and Risaliti et al. (1999) (MR95 and R99, respectively, from now on) and from Swift-BAT 70-month Hard X-ray Survey (Baumgartner et al., 2013; hereafter SB-70m). The latter includes optically-obscured AGN which are excluded by the constraints given in MR95 and R99. On the other hand, a hard-X ray selection, as it is SB-70m, misses Compton-thick AGN, embraced instead by a selection based on optical emission lines (like MR95 and R99), which are spatially extended and not confined to the nuclear spot as the hard X-ray emission. We chose only those sources which are observable from Paranal Observatory ($-70^\circ < \delta < 20^\circ$) and have a distance <50 Mpc, ending up with a total of 73 objects.

So far, we have analyzed MUSE data of 10 galaxies belonging to the MAGNUM sample, comprising Centaurus A, Circinus, IC 5063, NGC 1068, NGC 1365, NGC 1386, NGC 2992, NGC 4945, NGC 5643, and NGC 6810.

2.2. Data Analysis

We have fitted and subtracted the stellar continuum, after having Voronoi-binned (Cappellari and Copin, 2003) the data cube so as to get an average signal-to-noise ratio per wavelength channel (1.25 Å/channel) on the stellar continuum of at least 50 in each bin. We made use of a linear combination of Vazdekis et al. (2010) synthetic spectral energy distributions (SEDs) for single-age, single-metallicity stellar populations (SSPs), employing pPXF code (Penalized Pixel-Fitting; Cappellari and Emsellem, 2004) to convolve the linearly combined stellar templates with a Gaussian profile so as to reproduce the systemic velocity and the velocity dispersion of the stellar absorption lines. The resulting star-subtracted cube has then been spatially smoothed with a 1σ-px Gaussian kernel. All the main emission lines have been fitted, spaxel-by-spaxel, with 1, 2, or 3 Gaussian components to best reproduce the total line profiles. The number of components in the best fits is set by the value of the reduced χ^2 with the aim of providing the best fit with the minimum number of free parameters. The same number of components is used for all emission lines imposing the same velocity and width to each component.

All the details about the MAGNUM sample selection and the data analysis will be given in Venturi et al. (2018, in preparation).

3. MUSE MAPS

Ionized outflows are observed in all the galaxies of our sample, with a more or less defined conical shape and a complex kinematics. In the following, we present the representative cases of NGC 1365 and NGC 4945. The former was observed with MUSE on October 12, 2014, for a total exposure time of ∼4000 s, the latter on January 17, 2015, for a total of ∼2000 s. NGC 1365 was studied in the ionized gas in many articles, e.g., Storchi-Bergmann and Bonatto (1991); Veilleux et al. (2003); Sharp and Bland-Hawthorn (2010). Lindblad (1999) gives a comprehensive review about the early work on this galaxy. An analysis of the ionized gas in NGC 4945 is reported (e.g., in Marconi et al., 2000; Rossa and Dettmar, 2003).

3.1. NGC 1365

NGC 1365 is a barred spiral Seyfert galaxy at $z = 0.00546$, extending for $11.2'\times6.2'$, so that the $\sim1'\times1'$ FOV of MUSE covers the central $\sim5.3\times5.3$ kpc^2 of the galaxy. In **Figures 1A–C** we show the stellar velocity field, the average velocity of the [OIII] λ5007 line ([OIII] hereafter) subtracted, spaxel-by-spaxel, by the stellar velocity and the map of [OIII] line width W70 (i.e., the difference between the velocities at the 85th and at the 15th percentile of the total fitted profile; see Harrison et al., 2014), respectively. The first one exhibits the rotational motion of the stars (approaching to the NE, receding to the SW), which has a twisted shape probably associated with the presence of the bar. We subtract the average [OIII] velocity by the stellar one so as to isolate gas motions deviating from stellar rotation. The two kinematic maps of [OIII] reveal a double conical outflow with a clumpy morphology, oriented in the direction SE-NW, where [OIII] velocity deviates most from stellar one (by over 150 km/s) and total line profile is broader compared to the rest of the FOV, giving rise to W70 values greater than 500 km/s. The broadening is due to the fact that in each spaxel all the kinematic components in the line of sight, the one from the outflow and the one from the disk, sum up giving a complex line profile. Double-peaked line profiles are indeed ubiquitous in the regions having higher W70. As shown by the velocity map the SE cone is approaching to the observer, while the NW one is receding.

The outflow is part of the [OIII]-emitting cone, which can be seen in **Figure 1D** in green, where Hα, tracing star formation in the disk, is instead reported in red. Both represent

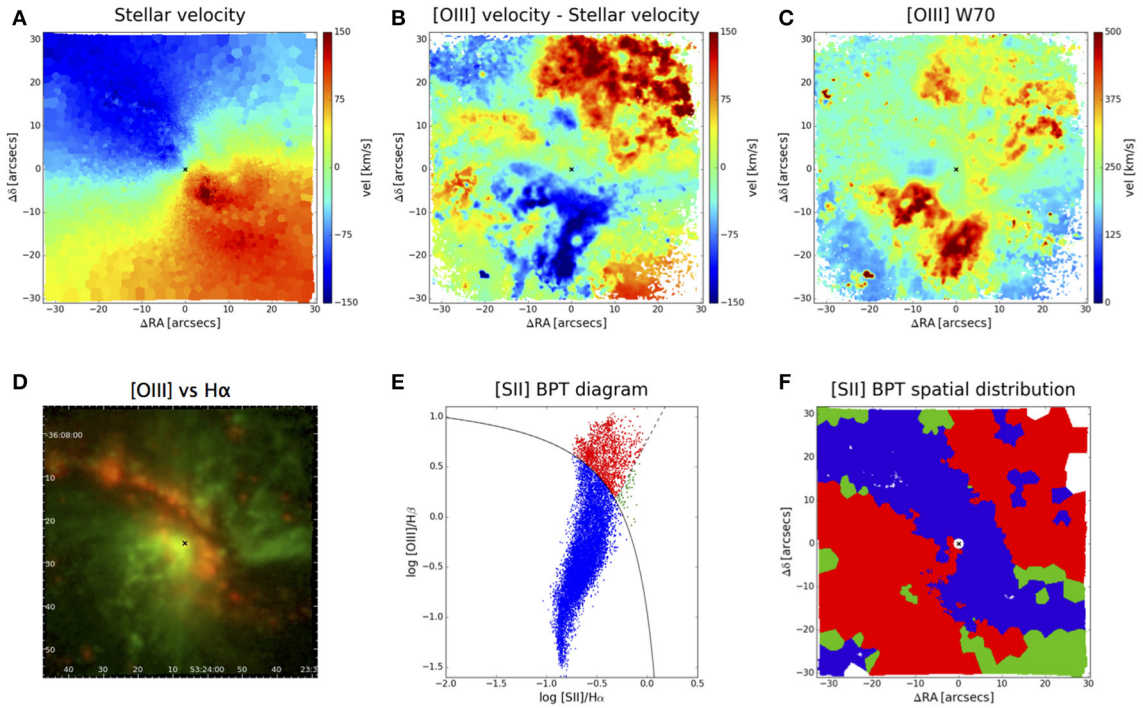

FIGURE 1 | Maps from our analysis of MUSE observations of NGC 1365. North is up. The cross marks the active nucleus. [OIII] kinematic maps in **(B,C)** are 1px-σ spatially re-smoothed to get a better visual output. **(A)** Stellar velocity map, w.r.t. the systemic velocity of 1630 km/s adopted. The map has been obtained from the spectral shift of the stellar absorption lines resulting from the fit of the stellar emission carried out on the Voronoi-binned data cube, for which an average signal-to-noise ratio per wavelength channel of 50 has been requested in each bin. **(B)** Difference between the [OIII] velocity and the stellar velocity, in order to isolate the proper motions of the gas w.r.t. the stars. The [OIII] velocity is the first-order moment of the total fitted line profile. **(C)** [OIII] W70 map, i.e., the difference between the velocities at the 85th and at the 15th percentile of the total fitted line profile. **(D)** Two-color image of [OIII] (green) and Hα (red) integrated emission of the total fitted line profile. **(E)** [SII] $\lambda\lambda$6716,6731/Hα vs. [OIII] λ5007/Hβ spatially resolved BPT diagram, obtained from the fit of the star-subtracted Voronoi-binned cube (so as to have an average signal-to-noise ratio per wavelength channel around Hβ of at least 4 in each bin). Each point in the diagram then corresponds to a bin in the FOV. The solid curve marks (Kewley et al., 2001) theoretical upper bound for pure star formation, while the dashed line separates Seyferts from LI(N)ERs (Kewley et al., 2006). Blue points are then star-formation dominated bins, red ones are AGN-dominated ones, while green one have LI(N)ER-like ratios. **(F)** Spatial distribution of the bins, color-coded according to the spatially resolved BPT diagram in **(E)**.

the integrated flux of the total fitted line profile. The spatial distribution of the two emission lines is clearly different, with the Hα being dominant in the direction NE-SW (along the galactic bar), almost perpendicular to the [OIII] double cone. BPT diagnostic diagrams (Baldwin et al., 1981; Veilleux and Osterbrock, 1987) give a quantitative assessment regarding the dominant ionizing source. In **Figure 1E** we report the spatially resolved [SII] $\lambda\lambda$6716,6731/Hα BPT diagram of NGC 1365, generated, differently from the other maps, from the fit of another data cube, produced by performing a Voronoi binning on the star-subtracted one, so as to get an average signal-to-noise ratio per wavelength channel around Hβ of at least 4 in each bin. This allows to get more reliable line ratios for the diagnostic diagram. Each point in the BPT corresponds to a single bin in the FOV and they are color-coded in the following way: blue points mark star-forming dominated bins, standing below (Kewley et al., 2001) upper limit for pure star formation (solid curve), while red ones indicate AGN-dominated bins, separated by Kewley et al. (2006) dashed line from the green ones having LI(N)ER-like line ratios. The spatial distribution of the bins in the FOV is presented in **Figure 1F**, using the same color coding adopted in the diagram. The diagonal lane in the direction NE-SW is dominated by ionization from OB stars in star-forming regions, while the almost perpendicular [OIII]-emitting cone is AGN-dominated, indicating that the ionized outflow is AGN-driven. Besides the diagonal lane, some isolated bins far from the center, emerging from the cone, have star-forming ratios as well and correspond to the strong red Hα blobs standing out against the green [OIII] in **Figure 1C**. A circular area surrounding the nucleus has been masked due to the presence of BLR lines disturbing the fit and giving highly deviant values of the line ratios.

The maps in **Figure 1** then suggest that the SE lobe of the AGN-ionized cones is the nearest to the observer and stands above the disk while the NW one is the furthest and resides behind the disk, as the former shows approaching velocities and the strongest flux between the two, especially going closer to the center, while the latter recedes and is fainter and overcome by the dusty star-forming regions near the center.

3.2. NGC 4945

A double conical outflow is observed in another source belonging to our MAGNUM survey, i.e., NGC 4945, an almost perfectly edge-on galaxy at $z = 0.00188$. [NII] total integrated flux, average velocity (spaxel-by-spaxel subtracted by the stellar velocity) and W70 maps of this galaxy obtained from the star-subtracted spatially-smoothed data cube are presented in **Figures 2A–C**, respectively. The side of the FOV corresponds to ∼3.5 kpc. The presence of the outflow is clear in W70 map, where a NW lobe and a SE one can be observed, the former being more extended than the latter, reaching a distance of ∼1.8 kpc from the center. In the flux map too the NW lobe is much stronger and more extended than the SE one. The galaxy is nearly edge on and dusty, in fact, and so it is plausible that the galactic plane resides behind the NW lobe w.r.t. the observer, while the SE one stands behind the disk and is obscured by dust close to the center but emerges from it at a certain point. The velocity map of [NII] shows the kinematic structure of the two cones, the NW one having approaching velocities at its edges and receding ones around its axis, the SE lobe having an opposite behavior, i.e., receding velocities at its edges and approaching ones around its axis. As in the case of NGC 1365, double-peaked and complicated line profiles are ubiquitous along the outflow.

The aspect of the velocity map of the NW cone could be explained thinking to a hollow cone which has an axis inclination w.r.t. the l.o.s. $<90^\circ$ and a sufficient aperture such that the far part of the cone intercepts the plane of the sky (the same holds for the SE lobe, but with opposite geometry). Another feature supporting this scenario is the flux enhancement at the edges of [NII] cone in **Figure 2A**, compatible with an effect of limb brightening in a hollow cone. To test this hypothesis a simple kinematic model has been realized. The model features a hollow cone having inclination w.r.t. line of sight of 75°, inner and outer half opening angle of 25° and 35°, respectively, and constant velocity field. The resulting maps of flux, velocity and velocity dispersion are reported in **Figures 2D–F**, respectively. The velocity map of the model resembles the observed one, with approaching velocities at the edges of the cone and receding ones in the middle, and also the velocity dispersion spatial distribution seems to reproduce well the observed one. Although this simple model does not take into account the clumpiness of the ionized gas, it seems to be a fairly good representation of the observed maps, and thus a hollow cone intercepting the plane of the sky appears to be a promising way to explain the complex kinematics that we observe in NGC 4945. We are developing a more detailed and sophisticated kinematic model to actually reconstruct outflow 3D shape and intrinsic properties.

4. CONCLUSIONS

We presented a study of ionized outflows in nearby AGN in the field of our MAGNUM survey, which takes advantage of the

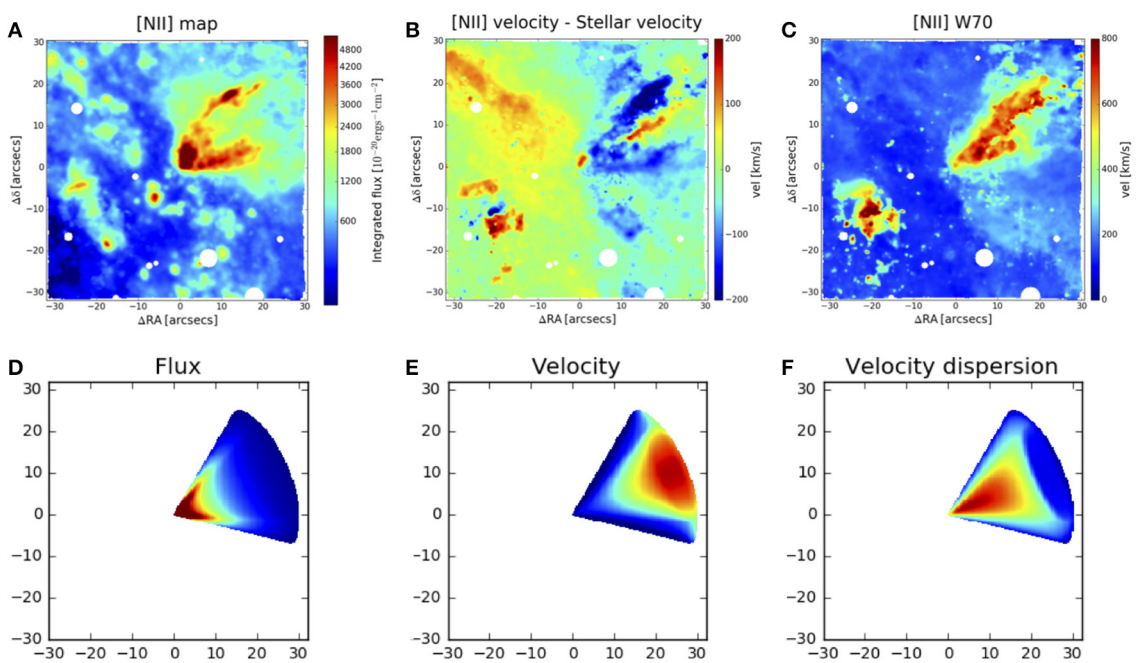

FIGURE 2 | Maps from our analysis of MUSE data of NGC 4945 (top) and from kinematic model (bottom). North is up. [NII] maps on top are 1px-σ spatially re-smoothed, so as to get a better visual output. White circles indicate masked regions coinciding with foreground stars. **(A)** [NII] flux map. **(B)** [NII] velocity spaxel-by-spaxel subtracted by the stellar velocity, in order to isolate proper motions of the gas w.r.t. stars. The [NII] velocity is the first-order moment of the total fitted line profile. **(C)** [NII] W70 map, i.e., difference between the 85th-percentile velocity and the 15th-percentile one calculated on the fitted line profile. **(D)** Flux map from simple model of hollow cone having inclination of 75° w.r.t. line of sight, inner and outer half opening angle of 25° and 35°, respectively (thus intercepting the plane of the sky), and constant velocity field. **(E)** Velocity map from model in **(D)**. **(F)** Velocity dispersion map from model in **(D)**. Data maps in **(A–C)** and model maps in **(D–F)** have matching color scales.

unprecedented capabilities of MUSE at VLT to study in detail outflows, photoionization and the interplay between AGN and host galaxies. We first gave a brief overview of the MAGNUM survey, describing the sample selection and the standard data analysis carried out on the 10 targets we studied up to now. We then presented preliminary maps and results obtained for two targets of the MAGNUM survey, NGC 1365 and NGC 4945.

MUSE observations of NGC 1365 reveal a clumpy double conical outflow, propagating from the center in the SE-NW direction, the brighter SE lobe approaching, the fainter NW one receding. The outflow is almost perpendicular to the stellar rotational field and is part of the [OIII]-emitting double cone, whose ionization is dominated by the AGN continuum, as established by [SII] $\lambda\lambda$6716,6731/Hα vs. [OIII] λ5007/Hβ spatially resolved BPT diagram. The BPT also shows that the diagonal elongated area of the galaxy following the bar direction, nearly perpendicular to the AGN-ionized double cone, is instead dominated by ionization in star-forming regions. The fact that the SE cone is approaching and is brighter w.r.t. the NW receding one, in particular near the center where the star formation is dominant, suggests that the NW cone is partially hidden behind the galaxy disk, especially near the central dusty region, while the SE one points toward the observer above the disk.

NGC 4945 shows a double conical outflow as well, the NW lobe being much brighter than the SE one, which appears only at $\sim$15″ from the center, likely being completely dust-obscured at smaller radius, as the galaxy is almost edge-on. The kinematic structure of the NW cone reveals approaching velocities at the edges of the cone and receding ones along its axis. A simple kinematic model of a hollow cone pointing toward the observer's side but intercepting the plane of the sky accounts for this observed field. Consistently, the SE lobe shows an opposite behavior, with receding velocities at the edges of the cone and approaching ones along its axis.

AUTHOR CONTRIBUTIONS

GV wrote the article and performed the data reduction using both the ESO pipeline. Python scripts written by SC and AM wrote the first version of the python scripts for data analysis. GV and MM tested and implemented the scripts and performed the analysis of the sources, finally producing the maps. All the co-authors provided a critical review to the article.

FUNDING

SC acknowledges financial support from the Science and Technology Facilities Council (STFC).

REFERENCES

Bacon, R., Accardo, M., Adjali, L., Anwand, H., Bauer, S., Biswas, I., et al. (2010). "The MUSE second-generation VLT instrument," in *Society of Photo-Optical Instrumentation Engineers (SPIE) Conference Series, Vol. 7735, Society of Photo-Optical Instrumentation Engineers (SPIE) Conference Series* (San Diego, CA), 773508.

Baldwin, J. A., Phillips, M. M., and Terlevich, R. (1981). Classification parameters for the emission-line spectra of extragalactic objects. *Publ. ASP* 93, 5–19. doi: 10.1086/130766

Baumgartner, W. H., Tueller, J., Markwardt, C. B., Skinner, G. K., Barthelmy, S., Mushotzky, R. F., et al. (2013). The 70 month swift-BAT all-sky hard X-ray survey. *Astrophys. J. Suppl.* 207:19. doi: 10.1088/0067-0049/207/2/19

Brusa, M., Feruglio, C., Cresci, G., Mainieri, V., Sargent, M. T., Perna, M., et al. (2015). Evidence for feedback in action from the molecular gas content in the z $\sim$ 1.6 outflowing QSO XID2028. *Astron. Astrophys.* 578:A11. doi: 10.1051/0004-6361/201425491

Cano-Díaz, M., Maiolino, R., Marconi, A., Netzer, H., Shemmer, O., and Cresci, G. (2012). Observational evidence of quasar feedback quenching star formation at high redshift. *Astron. Astrophys.* 537:L8. doi: 10.1051/0004-6361/201118358

Cappellari, M., and Copin, Y. (2003). Adaptive spatial binning of integral-field spectroscopic data using Voronoi tessellations. *Month. Notices RAS* 342, 345–354. doi: 10.1046/j.1365-8711.2003.06541.x

Cappellari, M., and Emsellem, E. (2004). Parametric recovery of line-of-sight velocity distributions from absorption-line spectra of galaxies via penalized likelihood. *Publ. ASP* 116, 138–147. doi: 10.1086/381875

Carniani, S., Marconi, A., Maiolino, R., Balmaverde, B., Brusa, M., Cano-Díaz, M., et al. (2016). Fast outflows and star formation quenching in quasar host galaxies. *Astron. Astrophys.* 591:A28. doi: 10.1051/0004-6361/201528037

Carniani, S., Marconi, A., Maiolino, R., Feruglio, C., Brusa, M., Cresci, G., et al. (2017). AGN feedback on molecular gas reservoirs in quasars at $z \sim$2.4. *ArXiv e-prints*.

Ciotti, L., Ostriker, J. P., and Proga, D. (2010). Feedback from central black holes in elliptical galaxies. III. models with both radiative and mechanical feedback. *Astrophys. J.* 717, 708–723. doi: 10.1088/0004-637X/717/2/708

Cresci, G., Mainieri, V., Brusa, M., Marconi, A., Perna, M., Mannucci, F., et al. (2015a). Blowin' in the wind: both "negative" and "positive" feedback in an obscured high-z quasar. *Astrophys. J.* 799:82. doi: 10.1088/0004-637X/799/1/82

Cresci, G., Marconi, A., Zibetti, S., Risaliti, G., Carniani, S., Mannucci, F., et al. (2015b). The MAGNUM survey: positive feedback in the nuclear region of NGC 5643 suggested by MUSE. *Astron. Astrophys.* 582:A63. doi: 10.1051/0004-6361/201526581

Davies, R. L., Dopita, M. A., Kewley, L., Groves, B., Sutherland, R., Hampton, E. J., et al. (2016). The role of radiation pressure in the narrow line regions of Seyfert host galaxies. *Astrophys. J.* 824:50. doi: 10.3847/0004-637X/824/1/50

Fabian, A. C. (1999). The obscured growth of massive black holes. *Month. Notices RAS* 308, L39–L43.

Ferrarese, L., and Merritt, D. (2000). A fundamental relation between supermassive black holes and their host galaxies. *Astrophys. J. Lett.* 539, L9–L12. doi: 10.1086/312838

García-Burillo, S., Combes, F., Usero, A., Aalto, S., Krips, M., Viti, S., et al. (2014). Molecular line emission in NGC 1068 imaged with ALMA. I. An AGN-driven outflow in the dense molecular gas. *Astron. Astrophys.* 567:A125. doi: 10.1051/0004-6361/201423843

Gebhardt, K., Bender, R., Bower, G., Dressler, A., Faber, S. M., Filippenko, A. V., et al. (2000). A relationship between nuclear black hole mass and galaxy velocity dispersion. *Astrophys. J. Lett.* 539, L13–L16. doi: 10.1086/312840

Harrison, C. M., Alexander, D. M., Mullaney, J. R., and Swinbank, A. M. (2014). Kiloparsec-scale outflows are prevalent among luminous AGN: outflows and feedback in the context of the overall AGN population. *Month. Notices RAS* 441, 3306–3347. doi: 10.1093/mnras/stu515

Hopkins, P. F., Hernquist, L., Cox, T. J., Di Matteo, T., Robertson, B., and Springel, V. (2006). A unified, merger-driven model of the origin of starbursts, quasars, the cosmic X-ray background, supermassive black holes, and galaxy spheroids. *Astrophys. J. Suppl.* 163, 1–49. doi: 10.1086/499298

Kewley, L. J., Dopita, M. A., Sutherland, R. S., Heisler, C. A., and Trevena, J. (2001). Theoretical modeling of starburst galaxies. *Astrophys. J.* 556, 121–140. doi: 10.1086/321545

Kewley, L. J., Groves, B., Kauffmann, G., and Heckman, T. (2006). The host galaxies and classification of active galactic nuclei. *Month. Notices RAS* 372, 961–976. doi: 10.1111/j.1365-2966.2006.10859.x

King, A. (2003). Black holes, galaxy formation, and the $M_{\rm BH}$-σ relation. *Astrophys. J. Lett.* 596, L27–L29. doi: 10.1086/379143

King, A. (2005). The AGN-starburst connection, galactic superwinds, and M_{BH}-σ. *Astrophys. J. Lett.* 635, L121–L123. doi: 10.1086/499430

Kormendy, J., and Ho, L. C. (2013). Coevolution (or not) of supermassive black holes and host galaxies. *Annual Rev. Astron. Astrophys.* 51, 511–653. doi: 10.1146/annurev-astro-082708-101811

Lindblad, P. O. (1999). NGC 1365. *Astron. Astrophys. Rev.* 9, 221–271. doi: 10.1007/s001590050018

Maiolino, R., and Rieke, G. H. (1995). Low-luminosity and obscured seyfert nuclei in nearby galaxies. *Astrophys. J.* 454:95. doi: 10.1086/176468

Marconi, A., and Hunt, L. K. (2003). The relation between black hole mass, bulge mass, and near-infrared luminosity. *Astrophys. J. Lett.* 589, L21–L24. doi: 10.1086/375804

Marconi, A., Oliva, E., van der Werf, P. P., Maiolino, R., Schreier, E. J., Macchetto, F., et al. (2000). The elusive active nucleus of NGC 4945. *Astron. Astrophys.* 357, 24–36. Available online at: http://aa.springer.de/bibs/0357001/2300024/small.htm

McConnell, N. J., and Ma, C.-P. (2013). Revisiting the scaling relations of black hole masses and host galaxy properties. *Astrophys. J.* 764:184. doi: 10.1088/0004-637X/764/2/184

Murray, N., Quataert, E., and Thompson, T. A. (2005). On the maximum luminosity of galaxies and their central black holes: feedback from momentum-driven winds. *Astrophys. J.* 618, 569–585. doi: 10.1086/426067

Risaliti, G., Maiolino, R., and Salvati, M. (1999). The distribution of absorbing column densities among Seyfert 2 galaxies. *Astrophys. J.* 522, 157–164. doi: 10.1086/307623

Rossa, J., and Dettmar, R.-J. (2003). An Hα survey aiming at the detection of extraplanar diffuse ionized gas in halos of edge-on spiral galaxies. II. The Hα survey atlas and catalog. *Astron. Astrophys.* 406, 505–525. doi: 10.1051/0004-6361:20030698

Scannapieco, C., Wadepuhl, M., Parry, O. H., Navarro, J. F., Jenkins, A., Springel, V., et al. (2012). The Aquila comparison project: the effects of feedback and numerical methods on simulations of galaxy formation. *Month. Notices RAS* 423, 1726–1749. doi: 10.1111/j.1365-2966.2012.20993.x

Sharp, R. G., and Bland-Hawthorn, J. (2010). Three-dimensional integral field observations of 10 galactic winds. I. Extended phase (gsim10 Myr) of mass/energy injection before the wind blows. *Astrophys. J.* 711, 818–852. doi: 10.1088/0004-637X/711/2/818

Silk, J. (2013). Unleashing positive feedback: linking the rates of star formation, supermassive black hole accretion, and outflows in distant galaxies. *Astrophys. J.* 772:112. doi: 10.1088/0004-637X/772/2/112

Springel, V., Di Matteo, T., and Hernquist, L. (2005). Modelling feedback from stars and black holes in galaxy mergers. *Month. Notices RAS* 361, 776–794. doi: 10.1111/j.1365-2966.2005.09238.x

Storchi-Bergmann, T. (2015). "The Narrow Line Region in 3D: mapping AGN feeding and feedback," in *Galaxies in 3D Across the Universe, Vol. 309, IAU Symposium*, eds B. L. Ziegler, F. Combes, H. Dannerbauer, and M. Verdugo (Vienna), 190–195.

Storchi-Bergmann, T., and Bonatto, C. J. (1991). Detection of a forbidden O III 5007-a radiation cone in the nuclei of NGC 1365 and 7582. *Month. Notices RAS* 250, 138–143. doi: 10.1093/mnras/250.1.138

Vazdekis, A., Sánchez-Blázquez, P., Falcón-Barroso, J., Cenarro, A. J., Beasley, M. A., Cardiel, N., et al. (2010). Evolutionary stellar population synthesis with MILES - I. The base models and a new line index system. *Month. Notices RAS* 404, 1639–1671. doi: 10.1111/j.1365-2966.2010.16407.x

Veilleux, S., and Osterbrock, D. E. (1987). Spectral classification of emission-line galaxies. *Astrophys. J. Suppl.* 63, 295–310. doi: 10.1086/191166

Veilleux, S., Shopbell, P. L., Rupke, D. S., Bland-Hawthorn, J., and Cecil, G. (2003). A Search for very extended ionized gas in nearby starburst and active galaxies. *Astron. J.* 126, 2185–2208. doi: 10.1086/379000

Williams, R. J., Maiolino, R., Krongold, Y., Carniani, S., Cresci, G., Mannucci, F., and Marconi, A. (2017). An ultra-dense fast outflow in a quasar at z = 2.4. *Month. Notices RAS* 467, 3399–3412. doi: 10.1093/mnras/stx311

Conflict of Interest Statement: The authors declare that the research was conducted in the absence of any commercial or financial relationships that could be construed as a potential conflict of interest.

Copyright © 2017 Venturi, Marconi, Mingozzi, Carniani, Cresci, Risaliti and Mannucci. This is an open-access article distributed under the terms of the Creative Commons Attribution License (CC BY). The use, distribution or reproduction in other forums is permitted, provided the original author(s) or licensor are credited and that the original publication in this journal is cited, in accordance with accepted academic practice. No use, distribution or reproduction is permitted which does not comply with these terms.

frontiers in Astronomy and Space Sciences

MINI REVIEW
published: 27 September 2017
doi: 10.3389/fspas.2017.00016

Quasar Massive Ionized Outflows Traced by CIV λ1549 and [OIII]λλ4959,5007

Paola Marziani[1], C. Alenka Negrete[2], Deborah Dultzin[2], Mary L. Martínez-Aldama[3], Ascensión Del Olmo[3], Mauro D'Onofrio[4] and Giovanna M. Stirpe[5]*

[1] National Institute for Astrophysics, Osservatorio Astronomico di Padova, Rome, Italy, [2] Instituto de Astronomía, Universidad Nacional Autonoma de Mexico, Mexico City, Mexico, [3] Instituto de Astrofísica de Andalucía (CSIC), Granada, Spain, [4] Dipartimento di Fisica e Astronomia, Università di Padova, Padova, Italy, [5] Osservatorio Astronomico di Bologna (INAF), Bologna, Italy

The most luminous quasars (with bolometric luminosities are $\gtrsim 10^{47}$ erg/s) show a high prevalence of CIV λ1549 and [OIII]λλ4959,5007 emission line profiles with strong blueshifts. Blueshifts are interpreted as due to Doppler effect and selective obscuration, and indicate outflows occurring over a wide range of spatial scales. We found evidence in favor of the nuclear origin of the outflows diagnosed by [OIII]λλ4959,5007. The ionized gas mass, kinetic power, and mechanical thrust are extremely high, and suggest widespread feedback effects on the host galaxies of very luminous quasars, at cosmic epochs between 2 and 6 Gyr from the Big Bang. In this mini-review we summarize results obtained by our group and reported in several major papers in the last few years with an eye on challenging aspects of quantifying feedback effects in large samples of quasars.

Keywords: galaxy evolution, quasars, feedback, outflows, quasars: emission lines, quasars: supermassive black holes

OPEN ACCESS

Edited by:
Jirong Mao, Yunnan Observatories, National Astronomical Observatories (CAS), China

Reviewed by:
Milan S. Dimitrijevic, Astronomical Observatory, Serbia
Anna Lia Longinotti, National Institute of Astrophysics, Optics and Electronics, Mexico

****Correspondence:***
Paola Marziani
paola.marziani@oapd.inaf.it

Specialty section:
This article was submitted to Milky Way and Galaxies, a section of the journal Frontiers in Astronomy and Space Sciences

Received: *10 July 2017*
Accepted: *13 September 2017*
Published: *27 September 2017*

Citation:
Marziani P, Negrete CA, Dultzin D, Martínez-Aldama ML, Del Olmo A, D'Onofrio M and Stirpe GM (2017) Quasar Massive Ionized Outflows Traced by CIV λ1549 and [OIII]λλ4959,5007. Front. Astron. Space Sci. 4:16. doi: 10.3389/fspas.2017.00016

1. INTRODUCTION

The broad and narrow high-ionization emission lines (HILs) in the optical and UV spectra of quasars frequently show significant blueshifts with respect to the quasar rest frame (e.g., Gaskell, 1982; Tytler and Fan, 1992; Corbin and Boroson, 1996; Marziani et al., 1996; Zamanov et al., 2002, for some early papers). The interpretation involves the Doppler shift of line radiation due to the emitting gas motion toward the observer, with the part of line emitted by receding gas suppressed by obscuration. In the following we will adhere with this interpretation (for a dissenting view see however, Gaskell and Goosmann, 2013 who posit that we see light originally emitted by gas falling toward the black hole and backscattered toward us), and consider [OIII]λ4959,5007 as representative of narrow high-ionization lines (HILs), and CIVλ1549 as a prototypical broad HIL.

2. THE QUASAR MAIN SEQUENCE: CONTEXTUALIZING OUTFLOWS AT LOW-TO-MODERATE *L*

The diversity of quasar spectroscopic properties as found in single epoch observations of large samples has been organized along a quasar main sequence (Sulentic et al., 2000a,b; Marziani et al., 2001; Shen and Ho, 2014). Boroson and Green (1992) identified a first eigenvector in their sample of ≈80 Palomar-Green quasars which is associated with an anticorrelation between FWHM (Hβ) and a parameter measuring the prominence of FeII emission (the intensity ratio between the FeII

blend at λ4570 and Hβ). Along the main sequence defined by this anti-correlation, Sulentic et al. (2000a) suggested a change in properties in correspondence of FWHM H$\beta \approx$ 4,000 km/s, and distinguished two populations: Population A (FWHM $\lesssim$ 4,000 km/s) and B (where the B stands for broader than 4,000 km/s; e.g., Marziani et al., 2014; Fraix-Burnet et al., 2017, for reviews; Table 1 of Fraix-Burnet et al., 2017 summarized parameter systematic differences between the two populations). Population A and B have been associated with high and low accretion, respectively.

The CIVλ1549 large blueshifts (above 1,000 km/s) are a Population A phenomenon, likely associated with a disk wind (see Figure 7 of Sulentic and Marziani, 2015). Population A sources, at low z ($\lesssim$ 1), encompass relatively low black hole mass quasars ($\sim 10^7 - 10^8 M_\odot$) radiating at a relatively high Eddington ratio ($\gtrsim 0.1 - 0.2$). In many ways Pop. A sources can be considered as an extension of Narrow Line Seyfert 1 (NLSy1) with moderate or strong FeII emission: the limit FWHM $\approx$ 4,000 km/s (valid at bolometric luminosity $\log L \lesssim 47$ [erg s^{-1}]) allows one to include sources with the same Balmer line profiles and intensity ratios as observed in NLSy1s. This is not to imply that Pop. B sources (with FWHM H$\beta \gtrsim$ 4,000 km/s) do not show evidence of outflows. Evidence of outflow is, for example, overwhelming in the prototypical Pop. B source NGC 5548 (Kaastra et al., 2014). The latest developments suggest that outflows are ubiquitous, also in forms that may not provide striking optical/UV spectral phenomenologies (e.g., Harrison et al., 2014; Tombesi et al., 2015). Only, outflows are more difficult to trace in Population B single-epoch spectra, as the CIV integrated line profiles are relatively symmetric. In both Pop. A and B, the CIVλ1549 line profile can be represented as a scaled Hβ profile plus an excess of blueshifted emission: the two components are assumed to be representative of a "virialized" low-ionization broad line region (producing a fairly symmetric and unshifted line) plus an outflow/wind component with different physical conditions. In Pop. B, CIVλ1549 shows only a small blueshifted excess if compared to Hβ.

Similarly, large blueshifts of [OIII]λλ4959,5007 above 250 km/s are rare in z samples (they are real statistical outliers, called "blue outliers" [BOs] by Zamanov et al., 2002) and have been preferentially found among Population A sources (e.g., Zamanov et al., 2002; Xu et al., 2012; Zhang et al., 2013; Cracco et al., 2016). Sulentic and Marziani (2015) show the distribution of [OIII]λλ4959,5007 peak shifts for the spectral types defined along the Eigenvector 1 sequence: the prevalence of [OIII]λλ4959,5007 large blueshifts increases in Pop. A and reaches a maximum in extreme sources with FeIIλ4570/H$\beta \gtrsim 1$ (Figure 5 of Sulentic and Marziani, 2015; Negrete et al., in preparation). Blueshifts of [OIII]λλ4959,5007 trace larger scale outflows than CIVλ1549, outside of the broad line region (BLR).

3. THE SCENARIO AT HIGH *L*, AND INTERMEDIATE-*Z*

A recent result is that the prevalence of large blueshifts in both CIVλ1549 and [OIII]λ4959,5007 quasars is much higher at high L in intermediate-z samples ($1 \lesssim z \lesssim 2.5$, Coatman et al., 2016; Marziani et al., 2016a,b; Zakamska et al., 2016; Bischetti et al., 2017; Vietri, 2017). Blueshifts of CIVλ1549 reach several thousands km/s in Pop. A. BOs become much more frequent in the high z and L samples. The [OIII] shift and FWHM distributions at high-L are remarkably different from those of low-z, low L samples. **Figure 1** shows an example of a luminous Pop. A source in the sample of Sulentic et al. (2017): the left panel shows, overlaid to the continuum-subtracted spectrum, a decomposition of the CIVλ1549 profile into an unshifted and symmetric component (thick black line) and a blue shifted component (blue line). Without involving any profile decomposition (the caveats of the technique are discussed in Negrete et al., 2014), it is easy to see that about 80% of the line flux is emitted short-wards of the rest wavelength. At the same time, the Hβ remains symmetric. **Figure 1** (rightmost panel) shows an enlargement of the [OIII]λ4959,5007 profile: the FWHM $\approx$ 3,600 km/s is extremely broad by [OIII]λ5007 standards (at low-z, [OIII]λ5007 FWHM is $\lesssim 1,000$ km/s). The profile appears boxy, and fully displaced to the blue.

Figure 1 represents the diagnostic provided by single epoch observations for quasars at intermediate-to-high z (1–5), with CIVλ1549 covered by optical spectrometers and [OIII]λλ4959,5007 requiring near-IR spectroscopic observations. The latter have become possible for relatively faint quasars only in recent times, with the advent of second generation IR spectrometers mounted at the foci of large aperture telescopes; two major examples are XSHOOTER at VLT and LUCI at LBT. Near IR observations provide a reliable estimate of the quasar systemic redshift if the narrow component of Hβ or the [OII]λ3727 can be effectively measured. If these lines are detected above noise, then a good precision in the rest frame can be achieved, and the uncertainty is typically $\delta z \lesssim 3 \cdot 10^{-4}$. An accurate knowledge of the rest frame is not an end in itself, since an important physical parameter such as the outflow kinetic power depends on the third power of the outflow velocity υ_o. The availability of such observations should increase dramatically in the next few years, providing useful data (even with lack of real spatial resolution) for a better understanding of the outflow prevalence and power as a function of luminosity and cosmic epoch. At low-z, partial spatial resolution of the [OIII]λλ4959,5007 emitting regions is currently obtained (and will be more frequently obtained in the coming years) with the use of integral-field unit spectrographs with adaptive optics (e.g., Cresci et al., 2015). Observations of CIVλ1549 are and will remain challenging for sources at $z \lesssim 1.2$ i.e., for all the low-z quasar population.

3.1. The Nuclear Nature of the Outflow

CIVλ1549 emission is expected to originate within a few hundred gravitational radii from the central black hole even in luminous quasars (Kaspi et al., 2007). Reverberation mapping studies indicate that the CIV emitting region scaling law with luminosity is a power-law with exponent 0.5–0.7 (results by Shai Kaspi in this research topic). The nuclear nature of the CIVλ1549 outflow is not in question.

The [OIII]λλ4959,5007 prominence is affected by the "Baldwin effect" (Zhang et al., 2011), which is perhaps the main

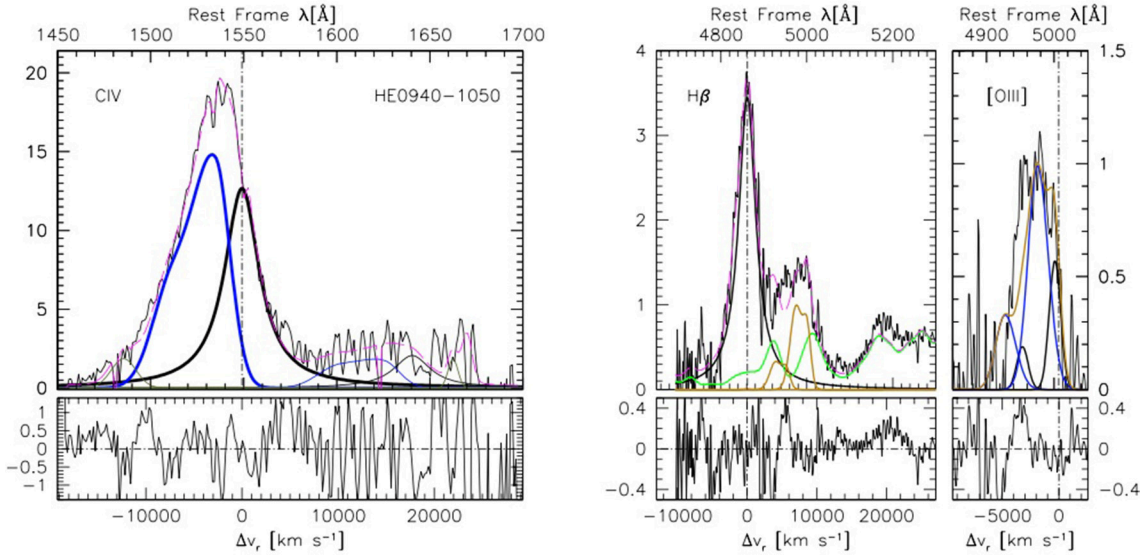

FIGURE 1 | (Left panel) CIVλ1549 emission after continuum subtraction. A scaled Hβ profile is superimposed (adapted from Sulentic et al., 2017). **(Right panel)** Hβ spectral range. The green line shows the adopted FeII template. The full profiles of [OIII]λλ4959,5007 are shown in orange. The thick black lines identify a symmetric unshifted emission that is dominating Hβ and still contributing to CIVλ1549. The thick blue lines trace the excess emission once the symmetric component is subtracted. The thin lines in the CIV panel show the interpretation of the HeII λ 1640 profile assuming a symmetric and a blue shifted component, as for CIV. The rightmost panel provides an enlargement on the [OIII]λλ4959,5007, semi-broad, boxy and blue-shifted profile (not a unique case at high *L*: e.g., Cano-Díaz et al., 2012). The [OIII] profile is modeled as the sum of a moderately blueshifted core component (black line) and of a semi-broad component, blue-shifted by $\approx -2,500$ km/s (blue line). The vertical scale is 10^{-15} erg s^{-1} cm^{-2} Å^{-1} in the rest frame, as applied by Sulentic et al. (2017).

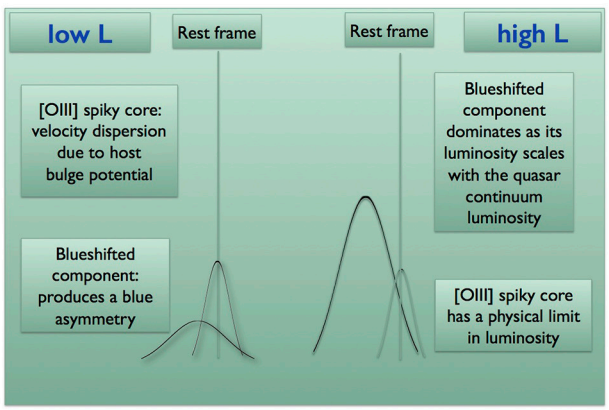

FIGURE 2 | The high prevalence of large [OIII]λλ4959,5007 blueshift at high *L* explained as a luminosity effect. The luminosity of the blue shifted component grows with the nuclear continuum luminosity, dominating the total [OIII] emission in very luminous quasars. Figure 6 of Marziani et al. (2016b) shows the same same effect in terms of EW: the EW of the core component is lower in very luminous sources because of the strong nuclear continuum, while the EW of the blue shifted component remains constant.

luminosity effect affecting all HILs (Dietrich et al., 2002). The observations of samples covering a wide range in luminosity ($43 \lesssim \log L \lesssim 48.5$ [erg/s]) confirm the [OIII] Baldwin effect: $W \propto L_{5100}^{-0.26 \pm 0.03}$ (Marziani et al., 2016b), steeper than the "classical" CIV Baldwin effect. However, a most intriguing result is that sources with large [OIII] blueshifts (the "blue outliers" of Zamanov et al., 2002) do not follow any Baldwin effect: $W \propto L_{5100}^{0.050 \pm 0.066}$, as shown in Figure 4 of Marziani et al. (2016b). In other words, for sources with large blueshifts, the line luminosity is proportional to the continuum luminosity. The simplest explanation is that [OIII]λλ4959,5007 emission is due to photoionization by the nuclear continuum.

Figure 2 shows a sketch explaining this result. At low-*L*, emission of [OIII]λ4959,5007 shows a spiky core and a prominent blueward asymmetry, especially in Pop. B sources. If the line profile is interpreted as made of a core component and a blue shifted semi broad component, then the latter component is not dominating at low-*z* and low-*L* unless we are considering a system radiating at high- Eddington ratio: these sources show *only* the semi broad component. At high-*L* the semi-broad component becomes so luminous to overwhelm the core component whose luminosity is expected to be upper-bound by the physical size and gas content of the host galaxy (Netzer et al., 2004).

4. ESTIMATES OF OUTFLOW DYNAMICAL PARAMETERS AND CONSIDERATIONS ON THEIR RELIABILITY

Computing the kinetic power and the thrust from single-epoch spectra is possible under several caveats and assumptions. Here we briefly recall a simplified way to estimate the mass of ionized gas, the mass outflow rate, the thrust, and the kinetic power of the outflow for collisional excited lines in photoionized gases

(Cano-Díaz et al., 2012). The formulation of these authors allows to write the outflow parameters in a form independent from the covering and filling factor, provided that all emitting gas has the same density. The simplified approach is well-suited to elucidate the role of the most relevant outflow parameters in the computation of the thrust and kinetic power. We will then consider the specific assumptions needed to apply the following relations to [OIII] and CIV measurements from single epoch spectra.

The luminosity of any collisionally-excited line[1] is given by $L(\mathrm{line}) = \int_V j_{\mathrm{line}}\, f_{\mathrm{f}}\, dV$, where j_{line} is the line emissivity per unit volume, and can be written as: $j_{\mathrm{line}} = h\nu q_{\mathrm{lu}} n_{\mathrm{e}} n_{\mathrm{l}}$, where n_{e} the electron density, and n_{l} the number density of ions at the lower level of the transition. The collisional excitation rate at electron temperature T is $q_{\mathrm{lu}} = \frac{\beta}{\sqrt{T}} \frac{\Upsilon_{\mathrm{lu}}}{g_l} \exp\left(-\frac{\epsilon_{\mathrm{lu}}}{kT}\right)$, where g_{l} is the statistical weight of the lower level, and Υ_{lu} is the effective collision strength. The line luminosity can be connected to the mass of ionized gas since $M_{\mathrm{out}}^{\mathrm{ion}} \propto L_{\mathrm{line}} \left(\frac{Z}{Z_\odot}\right)^{-1} n^{-1}$. Up to this point the main assumptions are: (1) constant density; (2) all emitting gas being in the ionization stage that is producing the line; (3) well defined chemical abundances.

The mass outflow rate at a distance r can be written as, if the flow is confined to a solid angle of Ω of volume $\frac{4}{3}\pi r^3 \frac{\Omega}{4\pi}$: $\dot{M}_{\mathrm{o}}^{\mathrm{ion}} = \rho\, \Omega r^2 \upsilon_{\mathrm{o}} = \frac{M_{\mathrm{o}}^{\mathrm{ion}}}{V} \Omega r^2 \upsilon_{\mathrm{o}} \propto L \upsilon_{\mathrm{o}} r^{-1}$. This requires the knowledge of (4) a typical emitting region radius, and (5) the outflow velocity υ_{o}. Assuming a single r value is already a strong simplification, especially for [OIII]. If the line emitting gas is still being accelerated (as in the CIV case), and the terminal velocity is $\upsilon_{\mathrm{term}} = k\upsilon_{\mathrm{o}}$, then the thrust should be $\propto \dot{M} k \upsilon_{\mathrm{o}}$ and the kinetic power of the outflow $\dot{\epsilon} \sim \frac{1}{2}\dot{M}^{\mathrm{ion}} k^2 \upsilon_{\mathrm{o}}^2 \propto L_{\mathrm{line}} k^2 \upsilon_{\mathrm{o}}^3 r^{-1}$. A value of k=1 can be assumed for [OIII] (as explained in section 4.2). The parameters of **Table 1** can be all written in the form $\propto L_{\mathrm{line}} r^{-1} n^{-1} (Z/Z_\odot)^{-1} \upsilon_{\mathrm{o}}^{\mathrm{n}}$, with $0 \leq n \leq 3$. The BLR gas exhibits highly super-solar chemical composition (Nagao et al., 2006; Shin et al., 2013), so that assuming $Z = 5Z_\odot$ is a reasonable choice for both [OIII] and CIV outflow, if the [OIII] emission is ascribed to a nuclear outflow. Finally, to be consistent with the idea of a *bipolar* outflow, all the quantities in **Table 1** have been multiplied by a factor 2.

It is interesting to make some considerations on the most likely values of the outflow parameters in very luminous quasars, and somehow constrain their upper limits. The considerations below are focused on very luminous quasars such as the ones studied by the WISSH project and by Sulentic et al. (2017) and Marziani et al. (2016b). We will consider here the 14 Pop. A objects of the "HE" sample of Marziani et al. (2016a,b) with $47.5 \lesssim \log L \lesssim 48.5$ erg s^{-1}. The relations of **Table 1** are scaled to values typical of the HE sample. In the redshift range $1 \lesssim z \lesssim 2.5$ where the population of most luminous quasars peaks, the angular distance is not increasing anymore with redshift (Hogg, 1999), implying a fairly constant scale around 8 Kpc/arcsec. For standard ground based observations, with a slit width of 0.5–1 arcs, all emission from CIV is collected (obviously) and most or at least a significant fraction of [OIII] should be collected as well, although not necessarily all of it: [OIII] emission may extend to the outer boundaries of optical galaxies and even beyond (see for instance, the impressive case of NGC 5252, Tadhunter and Tsvetanov, 1989).

4.1. CIV

Estimating L_{line} associated with unbound gas is not trivial, since the CIV emitting gas is probably still being accelerated by strong radiation forces within the BLR. As a lower limit, one can consider the fraction of the line that is already above a projected escape velocity. A more proper approach may be to consider that the gas is outflowing (i.e., the blue shifted component of **Figure 1**), and use a model in which gas cloud motions are accelerated under the effects of gravitation and radiation forces (for example Netzer and Marziani, 2010). In this case the v entering the equations of the thrust and the kinetic power should be the terminal velocity υ_{term}, larger than the outflow velocity v at r_{CIV}. The CIV emitting region radius can be computed from the radius-luminosity relation derived for CIV, $r_{\mathrm{CIV}} \propto L^b$, with $b \approx 0.5 - 0.7$ (Kaspi et al., 2007, see also contribution in the same research topic). While the density of the low-ionization part of the BLR is fairly well constrained (Negrete et al., 2012; Martínez-Aldama et al., 2015), the density of the outflowing component is not, although we can assume $8 \leq \log n \leq 10$ [cm^{-3}], $0.2 \leq L_{\mathrm{line}}/L_{\mathrm{line,tot}} \leq 1$. The thrust and the kinetic power may be larger than the values reported in **Table 1** by a factor 10 and 100, respectively, if radiative acceleration drives a wind with $k \approx 10$ which may be the case for high Eddington ratio ($\gtrsim 0.7$, following Netzer and Marziani, 2010).

4.2. [OIII]

For reasonable values of r, almost all of the blue shifted [OIII] emission should have escaped from the BH gravitational pull ($k = 1$). The full value of L_{line} could be taken as a first guess of the outflowing gas luminosity. It is also reasonable to

[1]While the ionic stages of C^{3+} and O^{2+} are due to photoionization, the CIV and [OIII] lines are produced via collisional excitation which is dominant over recombination, as shown in detail for [OIII] in Pradhan and Nahar (2015), section 12.4.

TABLE 1 | Outflow physical parameters derived for CIV and [OIII]: mass of ionized gas, mass outflow rate, thrust and kinetic power.

Parameter	Units	CIV	[OIII]
M^{ion}	$M_\odot$	$1.9 \cdot 10^3\, L_{45} \left(\frac{Z}{5Z_\odot}\right)^{-1} n_9^{-1}$	$1 \cdot 10^7\, L_{44} \left(\frac{Z}{5Z_\odot}\right)^{-1} n_3^{-1}$
$\dot{M}^{\mathrm{ion}}$	$M_\odot$ yr^{-1}	$30 L_{45} \upsilon_{\mathrm{o},5000} r_{1\mathrm{pc}}^{-1} \left(\frac{Z}{5Z_\odot}\right)^{-1} n_9^{-1}$	$30 L_{44} \upsilon_{\mathrm{o},1000} r_{1\mathrm{kpc}}^{-1} \left(\frac{Z}{5Z_\odot}\right)^{-1} n_3^{-1}$
$\dot{M}^{\mathrm{ion}} k \upsilon_{\mathrm{o}}$	g cm s^{-2}	$1 \cdot 10^{36} L_{45} k \upsilon_{\mathrm{o},5000}^2 r_{1\mathrm{pc}}^{-1} \left(\frac{Z}{5Z_\odot}\right)^{-1} n_9^{-1}$	$1.9 \cdot 10^{35} L_{44} k \upsilon_{\mathrm{o},1000}^2 r_{1\mathrm{kpc}}^{-1} \left(\frac{Z}{5Z_\odot}\right)^{-1} n_3^{-1}$
$\dot{\epsilon}$	erg s^{-1}	$2.4 \cdot 10^{44} L_{45} k^2 \upsilon_{\mathrm{o},5000}^3 r_{1\mathrm{pc}}^{-1} \left(\frac{Z}{5Z_\odot}\right)^{-1} n_9^{-1}$	$9.6 \cdot 10^{42} L_{44} k^2 \upsilon_{\mathrm{o},1000}^3 r_{1\mathrm{kpc}}^{-1} \left(\frac{Z}{5Z_\odot}\right)^{-1} n_3^{-1}$

assume that the gas density is between the [OIII] critical density $\log n \sim 5.5$ [cm^{-3}] and the typical density of outer narrow line regions, $\log n \sim 3$ [cm^{-3}]. The distance r remains a critical parameter in the absence of spatially resolved information. The ISAAC observations of the HE sample (Marziani et al., 2016b) were carried out with a slit width of 0.6 arcs centered on the quasar: this implies that emission within ≈ 2.4 kpc was collected. Imposing mass conservation ($\dot{M}_{[\mathrm{OIII}]} \approx \dot{M}_{\mathrm{CIV}}$, and [OIII] emission at critical density implies $r_{[\mathrm{OIII}]} \sim [5 \cdot 10^9/10^5]^{\frac{1}{2}} \sim 10^{2.35} \sim 2 \cdot 10^2$ pc, if $\upsilon_{[\mathrm{OIII}]}/\upsilon_{\mathrm{CIV}} \approx 5$, and $r_{\mathrm{CIV}} \approx 1$ pc. An alternative assumption is motivated by previous results on the low-z blue outliers: it was possible to model both CIV and [OIII] with the same velocity field, assuming that the two lines were emitted with a velocity a constant factor 1.5 the local virial velocity i.e., slightly above the local escape velocity (Zamanov et al., 2002, cf. Komossa et al., 2008). Then $\upsilon_{[\mathrm{OIII}]}/\upsilon_{\mathrm{CIV}} = \sqrt{r_{\mathrm{CIV}}/r_{[\mathrm{OIII}]}}$, if the factor remains the same for the two lines. We derive $r_{[\mathrm{OIII}]} \approx 25$ pc. This line of reasoning clearly emphasizes the necessity of obtaining spatially-resolved [OIII] data with density diagnostics, and of tracking the velocity field as close as possible to the nucleus in prototypical cases that could help constrain observations lacking spatial resolution.

4.3. Relation to Luminosity and Radiation Thrust

The average luminosity of the Population A HE sample sources is $\approx 10^{47.8}$ erg/s. The average peak velocity shift of the Pop. A CIV blueshifted component is $\approx -3,000$ km/s. Typical r_{CIV} are around 1pc, and the typical CIV luminosity is 10^{45} erg/s. Even assuming $k = 10$, $\upsilon_{\mathrm{o}} \approx 3,000$ km/s, the $\dot{\epsilon}$ value is several orders of magnitude below the bolometric luminosity: $\log \dot{\epsilon} \approx \log L - 2.4$, a factor ten lower than the value of 5% efficiency needed for a structural and dynamical effect on the host galaxy (e.g., King and Pounds, 2015). This limit might however be reached if the gas density is a factor ≈ 10 lower than assumed. Similar considerations apply to [OIII]: if the outflow is more compact than assumed in **Table 1**, then an increase by a factor 10–50 is possible. However, with the values of **Table 1** the estimates for $\log \dot{\epsilon}$ for [OIII] are three-four orders of magnitude below $0.05L$.

The mechanical thrust values $\dot{M}\upsilon_{\mathrm{o}}$ are also lower than the radiation trust $L/c \sim 10^{37.3}$ g cm s^{-2}. Again, $\dot{M}\upsilon_{\mathrm{o}}$ may reach values of the same order or in excess by a factor of 20 of the radiation thrust (Zubovas and King, 2012) if n is lower in the case of CIV and r for [OIII] is $\ll$1 Kpc. A similar scenario involving $\dot{M}\upsilon_{\mathrm{o}}$ and $\dot{\epsilon}$ too low at face values to explain the black hole—bulge mass relation was depicted by Carniani et al. (2015). Accepted at face values, these estimates suggest that, even in these very luminous quasars, the mechanical feedback estimated from mildly ionized gas may not be sufficient to reach the effect necessary for an evolutionary feedback on the host galaxy, unless the outflow parameter are stretched to the limit of plausible values. Even if the required conditions are met, the observations do not exclude an important role of the active nucleus radiation force in driving the outflow. In addition, the estimates sample only one component of the nuclear outflow: the mildly ionized one which is, especially for the BLR, associated to a relatively small amount of matter. High ionization plasma, atomic and molecular gases are not considered, although even in the local Universe we have a spectacular example of massive molecular outflow, Mark 231 (e.g., Feruglio et al., 2015).

5. CONCLUSION

Evidence of HIL blueshifts are ubiquitous, and at high luminosity they become impressive involving very large shifts in broad and narrow HILs. The mass outflow rates indicated by both [OIII] and CIV are extremely high, only somewhat lower than the accretion mass influx needed to sustain the observed luminosity for modest radiative efficiency ($\sim$100 M$_\odot$ yr^{-1} at efficiency 0.1). Even in the most luminous quasars, it is not obvious whether powerful outflows can have the ability to disrupt the host galaxy gas. However, it is likely that [OIII] and CIV trace only a part of the mass outflow. Accounting for multiphase outflows will be one of the major challenges of present and future observational and theoretical studies.

AUTHOR CONTRIBUTIONS

PM wrote the review. AD contributed to some of the papers reviewed in the present contribution. Other authors contributed with suggestions and critical reading.

FUNDING

AD and MM acknowledge financial support from the Spanish Ministry for Economy and Competitiveness through grants AYA2013-42227-P and AYA2016-76682-C3-1-P. DD and CN acknowledge support from grants PAPIIT108716, UNAM, and CONACyT221398.

REFERENCES

Bischetti, M., Piconcelli, E., Vietri, G., Bongiorno, A., Fiore, F., Sani, E., et al. (2017). The WISSH quasars project. I. Powerful ionised outflows in hyper-luminous quasars. *Astron. Astrophys.* 598:A122. doi: 10.1051/0004-6361/201629301

Boroson, T. A., and Green, R. F. (1992). The emission-line properties of low-redshift quasi-stellar objects. *Astroph. J. Suppl. Ser.* 80, 109–135. doi: 10.1086/191661

Cano-Díaz, M., Maiolino, R., Marconi, A., Netzer, H., Shemmer, O., and Cresci, G. (2012). Observational evidence of quasar feedback quenching star formation at high redshift. *Astron. Astrophys.* 537:L8. doi: 10.1051/0004-6361/201118358

Carniani, S., Marconi, A., Maiolino, R., Balmaverde, B., Brusa, M., Cano-Díaz, M., et al. (2015). Ionised outflows in z ˜ 2.4 quasar host galaxies. *Astron. Astrophys.* 580:A102. doi: 10.1051/0004-6361/201526557

Coatman, L., Hewett, P. C., Banerji, M., and Richards, G. T. (2016). C iv emission-line properties and systematic trends in quasar black hole mass estimates. *Mon. Not. R. Astron. Soc.* 461, 647–665. doi: 10.1093/mnras/stw1360

Corbin, M. R., and Boroson, T. A. (1996). Combined ultraviolet and optical spectra of 48 low-redshift QSOs and the relation of the continuum and emission-line properties. *Astroph. J. Suppl. Ser.* 107:69. doi: 10.1086/192355

Cracco, V., Ciroi, S., Berton, M., Di Mille, F., Foschini, L., La Mura, G., et al. (2016). A spectroscopic analysis of a sample of narrow-line Seyfert 1 galaxies selected from the Sloan Digital Sky Survey. *Mon. Not. R. Astron. Soc.* 462, 1256–1280. doi: 10.1093/mnras/stw1689

Cresci, G., Marconi, A., Zibetti, S., Risaliti, G., Carniani, S., Mannucci, F., et al. (2015). The MAGNUM survey: positive feedback in the nuclear region of NGC 5643 suggested by MUSE. *Astron. Astrophys.* 582:A63. doi: 10.1051/0004-6361/201526581

Dietrich, M., Hamann, F., Shields, J. C., Constantin, A., Vestergaard, M., Chaffee, F., et al. (2002). Continuum and emission-line strength relations for a large active galactic nuclei sample. *Astrophys. J.* 581, 912–924. doi: 10.1086/344410

Feruglio, C., Fiore, F., Carniani, S., Piconcelli, E., Zappacosta, L., Bongiorno, A., et al. (2015). The multi-phase winds of Markarian 231: from the hot, nuclear, ultra-fast wind to the galaxy-scale, molecular outflow. *Astron. Astrophys.* 583:A99. doi: 10.1051/0004-6361/201526020

Fraix-Burnet, D., Marziani, P., D'Onofrio, M., and Dultzin, D. (2017). The phylogeny of quasars and the ontogeny of their central black holes. *Front. Astron. Space Sci.* 4:1. doi: 10.3389/fspas.2017.00001

Gaskell, C. M. (1982). A redshift difference between high and low ionization emission-line regions in QSOs - Evidence for radial motions. *Astrophys. J.* 263, 79–86. doi: 10.1086/160481

Gaskell, C. M., and Goosmann, R. W. (2013). Line shifts, broad-line region inflow, and the feeding of active galactic nuclei. *Astrophys. J.* 769:30. doi: 10.1088/0004-637X/769/1/30

Harrison, C. M., Alexander, D. M., Mullaney, J. R., and Swinbank, A. M. (2014). Kiloparsec-scale outflows are prevalent among luminous AGN: outflows and feedback in the context of the overall AGN population. *Mon. Not. R. Astron. Soc.* 441, 3306–3347. doi: 10.1093/mnras/stu515

Hogg, D. W. (1999). Distance measures in cosmology. *Astrophysics*. arXiv:astro-ph/9905116.

Kaastra, J. S., Kriss, G. A., Cappi, M., Mehdipour, M., Petrucci, P.-O., Steenbrugge, K. C., et al. (2014). A fast and long-lived outflow from the supermassive black hole in NGC 5548. *Science* 345, 64–68. doi: 10.1126/science.1253787

Kaspi, S., Brandt, W. N., Maoz, D., Netzer, H., Schneider, D. P., and Shemmer, O. (2007). Reverberation mapping of high-luminosity quasars: first results. *Astrophys. J.* 659, 997–1007. doi: 10.1086/512094

King, A., and Pounds, K. (2015). Powerful outflows and feedback from active galactic nuclei. *Ann. Rev. Astron. Astrophys.* 53, 115–154. doi: 10.1146/annurev-astro-082214-122316

Komossa, S., Xu, D., Zhou, H., Storchi-Bergmann, T., and Binette, L. (2008). On the nature of seyfert galaxies with high [O III] λ5007 blueshifts. *Astrophys. J.* 680, 926–938. doi: 10.1086/587932

Martínez-Aldama, M. L., Dultzin, D., Marziani, P., Sulentic, J. W., Bressan, A., Chen, Y., et al. (2015). O I and Ca II observations in intermediate redshift quasars. *Astroph. J. Suppl. Ser.* 217:3. doi: 10.1088/0067-0049/217/1/3

Marziani, P., Martínez Carballo, M. A., Sulentic, J. W., Del Olmo, A., Stirpe, G. M., and Dultzin, D. (2016a). The most powerful quasar outflows as revealed by the Civ λ1549 resonance line. *Astrophys. Space Sci.* 361:29. doi: 10.1007/s10509-015-2611-1

Marziani, P., Sulentic, J. W., Dultzin-Hacyan, D., Calvani, M., and Moles, M. (1996). Comparative analysis of the high- and low-ionization lines in the broad-line region of active galactic nuclei. *Astroph. J. Suppl. Ser.* 104:37. doi: 10.1086/192291

Marziani, P., Sulentic, J. W., Negrete, C. A., Dultzin, D., D'Onofrio, M., Del Olmo, A., et al. (2014). Low- and high-z highly accreting quasars in the 4D Eigenvector 1 context. *Astronom. Rev.* 9, 6–25. doi: 10.1080/21672857.2014.11519739

Marziani, P., Sulentic, J. W., Stirpe, G. M., Dultzin, D., Del Olmo, A., and Martínez-Carballo, M. A. (2016b). Blue outliers among intermediate redshift quasars. *Astrophys. Space Sci.* 361:3. doi: 10.1007/s10509-015-2590-2

Marziani, P., Sulentic, J. W., Zwitter, T., Dultzin-Hacyan, D., and Calvani, M. (2001). Searching for the physical drivers of the eigenvector 1 correlation space. *Astrophys. J.* 558, 553–560. doi: 10.1086/322286

Nagao, T., Marconi, A., and Maiolino, R. (2006). The evolution of the broad-line region among SDSS quasars. *Astron. Astrophys.* 447, 157–172. doi: 10.1051/0004-6361:20054024

Negrete, A., Dultzin, D., Marziani, P., and Sulentic, J. (2012). BLR physical conditions in extreme population a quasars: a method to estimate central black hole mass at high redshift. *Astrophys. J.* 757:62. doi: 10.1088/0004-637X/757/1/62

Negrete, C. A., Dultzin, D., Marziani, P., and Sulentic, J. W. (2014). A new method to obtain the broad line region size of high redshift quasars. *Astrophys. J.* 794:95. doi: 10.1088/0004-637X/794/1/95

Netzer, H., and Marziani, P. (2010). The effect of radiation pressure on emission-line profiles and black hole mass determination in active galactic nuclei. *Astrophys. J.* 724, 318–328. doi: 10.1088/0004-637X/724/1/318

Netzer, H., Shemmer, O., Maiolino, R., Oliva, E., Croom, S., Corbett, E., et al. (2004). Near-infrared spectroscopy of high-redshift active galactic nuclei. II. Disappearing narrow-line regions and the role of accretion. *Astrophys. J.* 614, 558–567. doi: 10.1086/423608

Pradhan, A. K., and Nahar, S. N. (2015). *Atomic Astrophysics and Spectroscopy*. Cambridge: Cambridge University Press.

Shen, Y., and Ho, L. C. (2014). The diversity of quasars unified by accretion and orientation. *Nature* 513, 210–213. doi: 10.1038/nature13712

Shin, J., Woo, J.-H., Nagao, T., and Kim, S. C. (2013). The chemical properties of low-redshift QSOs. *Astrophys. J.* 763:58. doi: 10.1088/0004-637X/763/1/58

Sulentic, J., and Marziani, P. (2015). Quasars in the 4D eigenvector 1 context: a stroll down memory lane. *Front. Astron. Space Sci.* 2:6. doi: 10.3389/fspas.2015.00006

Sulentic, J. W., del Olmo, A., Marziani, P., Martínez-Carballo, M. A., D'Onofrio, M., Dultzin, D., et al. (2017). What does Civλ1549 tell us about the physical driver of the Eigenvector Quasar Sequence? *arXiv*:1708.03187. doi: 10.1051/0004-6361/201630309

Sulentic, J. W., Marziani, P., and Dultzin-Hacyan, D. (2000a). Phenomenology of broad emission lines in active galactic nuclei. *Annu. Rev. Astron. Astrophys.* 38, 521–571. doi: 10.1146/annurev.astro.38.1.521

Sulentic, J. W., Marziani, P., Zwitter, T., Dultzin-Hacyan, D., and Calvani, M. (2000b). The demise of the classical broad-Line region in the luminous quasar PG 1416-129. *Astrophys. J. Lett.* 545, L15–L18. doi: 10.1086/317330

Tadhunter, C., and Tsvetanov, Z. (1989). Anisotropic ionizing radiation in NGC5252. *Nature* 341, 422–424. doi: 10.1038/341422a0

Tombesi, F., Meléndez, M., Veilleux, S., Reeves, J. N., González-Alfonso, E., and Reynolds, C. S. (2015). Wind from the black-hole accretion disk driving a molecular outflow in an active galaxy. *Nature* 519, 436–438. doi: 10.1038/nature14261

Tytler, D., and Fan, X.-M. (1992). Systematic QSO emission-line velocity shifts and new unbiased redshifts. *Astron. Astrophys.* 79, 1–36. doi: 10.1086/191642

Vietri, G. (2017). "The LBT/WISSH quasar survey: revealing powerful winds in the most luminous AGN," in *American Astronomical Society Meeting Abstracts*. vol. 229 of *American Astronomical Society Meeting Abstracts*, 302.06

Xu, D., Komossa, S., Zhou, H., Lu, H., Li, C., Grupe, D., et al. (2012). Correlation analysis of a large sample of narrow-line seyfert 1 galaxies: linking central engine and host properties. *Astron. J.* 143:83. doi: 10.1088/0004-6256/143/4/83

Zakamska, N. L., Hamann, F., Pâris, I., Brandt, W. N., Greene, J. E., Strauss, M. A., et al. (2016). Discovery of extreme [O III] λ5007 Å outflows in high-redshift red quasars. *Mon. Not. R. Astron. Soc.* 459, 3144–3160. doi: 10.1093/mnras/stw718

Zamanov, R., Marziani, P., Sulentic, J. W., Calvani, M., Dultzin-Hacyan, D., and Bachev, R. (2002). Kinematic linkage between the broad- and narrow-line-emitting gas in active galactic nuclei. *Astrophys. J. Lett.* 576, L9–L13. doi: 10.1086/342783

Zhang, K., Dong, X.-B., Wang, T.-G., and Gaskell, C. M. (2011). The blueshifting and Baldwin effects for the [O III] λ5007 emission line in type 1 active galactic nuclei. *Astrophys. J.* 737:71. doi: 10.1088/0004-637X/737/2/71

Zhang, K., Wang, T.-G., Gaskell, C. M., and Dong, X.-B. (2013). The Baldwin effect in the narrow emission lines of active galactic nuclei. *Astrophys. J.* 762:51. doi: 10.1088/0004-637X/762/1/51

Zubovas, K., and King, A. (2012). Clearing out a galaxy. *Astrophys. J. Lett.* 745:L34. doi: 10.1088/2041-8205/745/2/L34

Conflict of Interest Statement: The authors declare that the research was conducted in the absence of any commercial or financial relationships that could be construed as a potential conflict of interest.

Copyright © 2017 Marziani, Negrete, Dultzin, Martínez-Aldama, Del Olmo, D'Onofrio and Stirpe. This is an open-access article distributed under the terms of the Creative Commons Attribution License (CC BY). The use, distribution or reproduction in other forums is permitted, provided the original author(s) or licensor are credited and that the original publication in this journal is cited, in accordance with accepted academic practice. No use, distribution or reproduction is permitted which does not comply with these terms.

frontiers in Astronomy and Space Sciences

MINI REVIEW
published: 16 October 2017
doi: 10.3389/fspas.2017.00024

Star Formation Quenching in Quasar Host Galaxies

Stefano Carniani [1, 2*]

[1] *Cavendish Laboratory, University of Cambridge, Cambridge, United Kingdom,* [2] *Kavli Institute for Cosmology, University of Cambridge, Cambridge, United Kingdom*

Galaxy evolution is likely to be shaped by negative feedback from active galactic nuclei (AGN). In the whole range of redshifts and luminosities studied so far, galaxies hosting an AGN frequently show fast and extended outflows consisting in both ionized and molecular gas. Such outflows could potentially quench the start formation within the host galaxy, but a clear evidence of negative feedback in action is still missing. Hereby I will analyse integral-field spectroscopic data for six quasars at $z \sim 2.4$ obtained with SINFONI in the H- and K-band. All the quasars show [OIII]λ5007 line detection of fast, extended outflows. Also, the high signal-to-noise SINFONI observations allow the identification of faint narrow Hα emission (FWHM < 500 km/s), which is spatially extended and associated with star formation in the host galaxy. On paper fast outflows are spatially anti-correlated with star-formation powered emission, i.e., star formation is suppressed in the area affected by the outflow. Nonetheless as narrow, spatially-extended Hα emission, indicating star formation rates of at least 50–100 $M_{\odot}$ yr^{-1}, has been detected, either AGN feedback is not affecting the whole host galaxy, or star formation is completely quenched only by several feedback episodes. On the other hand, a positive feedback scenario, supported by narrow emission in Hα extending along the edges of the outflow cone, suggests that galaxy-wide outflows could also have a twofold role in the evolution of the host galaxy. Finally, I will present CO(3-2) ALMA data for three out of the six QSOs observed with SINFONI. Flux maps obtained for the CO(3-2) transition suggest that molecular gas within the host galaxy is swept away by fast winds. A negative-feedback scenario is supported by the inferred molecular gas mass in all three objects, which is significantly below what observed in non-active main-sequence galaxies at high-*z*.

Keywords: QSO, high-redshifts galaxies, galaxy evolution, AGN negative-feedback, AGN positive-feedback, ALMA, molecular gas, emission lines

OPEN ACCESS

Edited by:
Ascensión Del Olmo, Consejo Superior de Investigaciones Científicas (CSIC), Spain

Reviewed by:
Daniela Bettoni, Osservatorio Astronomico di Padova (INAF), Italy
Viviana Casasola, Arcetri Astrophysical Observatory, Italy

***Correspondence:**
Stefano Carniani
sc888@mrao.cam.ac.uk

Specialty section:
This article was submitted to Milky Way and Galaxies, a section of the journal Frontiers in Astronomy and Space Sciences

Received: *23 August 2017*
Accepted: *02 October 2017*
Published: *16 October 2017*

Citation:
Carniani S (2017) Star Formation Quenching in Quasar Host Galaxies. Front. Astron. Space Sci. 4:24. doi: 10.3389/fspas.2017.00024

1. INTRODUCTION

Negative feedback from accreting black holes (BH) is considered a fundamental physical process in galaxy evolution: it is believed to inhibit the excessive growth of massive galaxies and to explain the steep stellar mass function at its high end, to explain the existence of the "red and dead" elliptical galaxies, and to provide a connection between the supermassive BH growth and host galaxy evolution (e.g., Hopkins et al., 2006). Feedback from accreting BH, i.e., from an AGN, takes the form of a fast outflow accelerated by the AGN radiation pressure which pushes gas away from the host galaxy, suppressing both star formation activity and BH accretion (e.g., Fabian, 2012). The recent discoveries of massive, powerful molecular outflows on galactic scales have partially

confirmed the AGN feedback scenario by showing that the observed outflow rates are larger than the star formation rates and that they can expel the gas from the host galaxy on very short time scales (Cicone et al., 2014, and references therein). Recent ALMA CO observations have also revealed massive molecular outflows in nearby Seyfert 2 galaxies with a outflow rate of an order of magnitude higher than the SFR (Combes et al., 2013; García-Burillo et al., 2014). However, although AGN-driven outflows have been detected in several AGN, we are still missing the "smoking gun" evidence that they are effectively quenching star formation: what we are seeking is a proof that star formation is indeed inhibited in the galaxy regions swept by the outflows.

Here, I report the results obtained by Carniani et al. (2015, 2016, 2017): the characterization of AGN-driven ionized outflows in a sample of quasars at $z \sim 2.4$ and their interaction with the host galaxies.

2. AGN-DRIVEN OUTFLOWS AT $Z \sim 2.4$

2.1. Sample Selection and Observations

Most of following results are based on seeing limited ($\sim$0.6″) integral field observations of six luminous ($L_{AGN} \sim 10^{47}$ erg/s) quasars (QSOs) at $z \sim 2.4$ with SINFONI at VLT, aimed at mapping the kinematics of the AGN ionized gas by using the [OIII]λ5007 emission line (Carniani et al., 2015). The six QSOs have been drawn from the samples of Netzer et al. (2004), Shemmer et al. (2004), and Marziani et al. (2009). The selected sample is characterized by large [OIII]λ5007 equivalent width (>10Å) and H-band magnitude <16.5 mag. The redshift of the sample has been selected to increase the chances of detecting QSO-feedback, since QSOs activity is expected to reach its peak a $z \sim 2-3$. The QSOs are listed in **Table 1**.

TABLE 1 | Properties of our quasar sample.

Target name (a)	α(J200) (b)	δ(J2000) (c)	Redshift (d)	L_{AGN} [10^{47} erg/s] (e)
LBQS 0109 + 0213	01:12:16.9	02:29:48	2.35 ± 0.08	3.0 ± 0.5
2QZ J0028 − 2830	−00:28:30.4	−28:17:06	2.40 ± 0.09	1.9 ± 0.4
HB89 0504 + 030	03:31:06.3	−38:24:05	2.48 ± 0.09	1.7 ± 0.4
HE 0109 − 3518	01:11:43.5	−35:03:01	2.407 ± 0.007	4.4 ± 0.9
HB89 0329 − 385	05:07:36.4	03:07:52	2.44 ± 0.03	3.0 ± 1.2
HE 0251 − 5550	02:52:40.1	−55:38:32	2.35 ± 0.05	4.1 ± 0.8

(a), ID of the target; (b) and (c), coordinates; (d), redshift inferred from the [Oiii]λ5007 line; (e), AGN bolometric luminosity that has been estimated using the relation $L_{AGN} \sim 6\lambda L(\lambda 5100Å)$ (Marconi et al., 2004).

2.2. Ionized Outflow Properties

The [OIII]λ5007 line profiles in the integrated spectra extracted from the QSO nuclei show prominent blueshifted wings (FWHM ∼1,000–1,500 km/s) that suggests the presence of fast gas approaching along the line-of-sight. A kinematical analysis also reveals that the optical line is spatially resolved in five sources and its emission is extended up to ∼2 kpc. The morphology of the [OIII]λ5007 velocity maps are characterized by conical blue-shifted region that is completely different from the typical "spider" diagram of a simple rotating disc. The shape of the [OIII]λ5007 velocity maps and the asymmetric line profiles support the presence of ionized outflowing gas with velocities >300 km/s in our QSOs. Given the observed velocities, the outflows can only be ascribed to the AGN.

The spatially resolved observations enable to infer the mass (M_o), radius (v_o) and velocity (R_o) of the outflowing material and, then, to calculate the outflow mass rate ($\dot{M}_o$) as follow

$$\dot{M}_o = \frac{M_o v_o}{R_o}. \quad (1)$$

The broad wings of the [OIII]λ5007 line yield to a ionized mass outflow rate of ∼10–700 $M_\odot$ yr^{-1}. **Figure 1** shows the outflow velocity and outflow mass rate as a function of the AGN luminosity. Comparing this results with those obtained from previous studies in literature (Greene et al., 2012; Cicone et al., 2014; Harrison et al., 2014; Sun et al., 2014; Brusa et al., 2015; Cresci et al., 2015; Feruglio et al., 2015), we clearly observe a relation between outflow properties and AGN luminosities (L_{AGN}). The velocity and mass rate of the fast gas increase with the L_{AGN} supporting the scenario that these outflows are AGN-driven and their properties depend on the AGN activity.

The molecular and ionized outflow seems to follow two different $\dot{M}_o$–L_{AGN} relations: mass rate estimated in molecular outflows is ∼50 higher than that estimated in ionized outflows. This discrepancy may indicate that most of the gas in the outflow is in molecular gas phase, while the ionized gas content is <10% of the total fast gas. Similar results have recently confirmed also in the work by Fiore et al. (2017).

2.3. Star Formation in the QSO Host Galaxies

In three QSOs of the selected sample (2QZ J0028–2830, HB89 0329−385 and LBQS 0109 + 0213) we have also detected narrow (FWHM < 500 km/s) and spatially diffuse emission in [OIII]λ5007 and Hα. The non-detection of the corresponding narrow [NII] component exclude excitation by the AGN radiation, since the optical line ratio is well consistent with gas excited in HII region. The detection of the narrow Hα component indicates ongoing star-formation in the AGN host galaxies with SFR ∼50–100 $M_\odot$ yr^{-1} (assuming the $Log(SFR/M_\odot\ yr^{-1}) = Log(L_{H\alpha}/erg\ s^{-1}) - 41.27$ relation by Kennicutt and Evans 2012).

More intriguingly, the presence of the ionized outflows appears to be spatially anti-correlated with the emission of the narrow components indicating that the star formation is suppressed and/or prevented in the outflow region (**Figure 2**). A similar scenario has also been observed by Cresci et al. (2015) in a radio-quiet QSO at $z = 1.7$. Even in this case, the star-formation activity is absent in the AGN-driven outflow, while star-formation regions are clearly visible at the edges of the outflow cone.

All these observations may be interpreted as evidences for AGN negative feedback in action, since star formation is quenched in the regions where the fast outflows interact with the

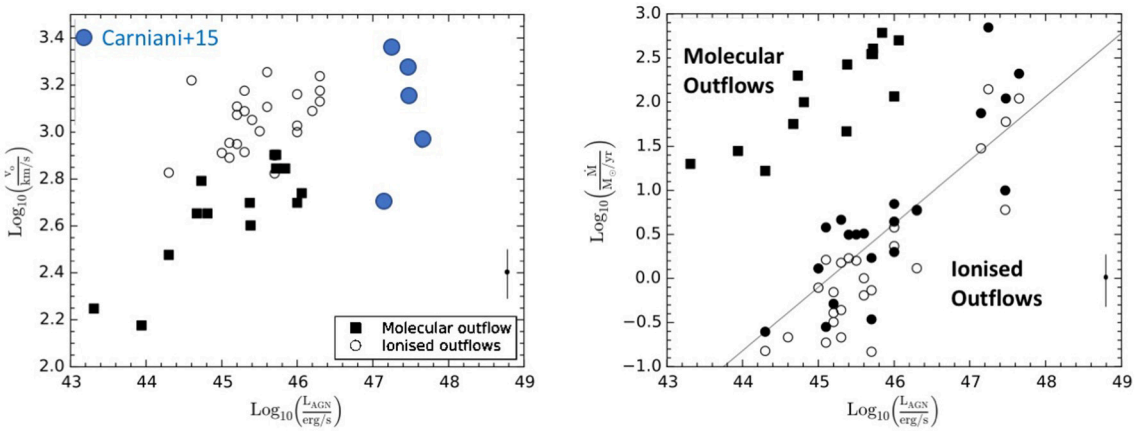

FIGURE 1 | Outflow velocity **(left)** and mass rate **(right)** vs. AGN luminosity (Figure is an adaption from Carniani et al., 2015). Open circles represent the estimates of ionized outflows obtained from [OIII]λ5007 line, while the filled marks are based on Hβ. A representative error bar is shown at right in each plot and it corresponds to an average error of ±0.2 dex for the outflow velocity and ±0.3 dex for the outflow mass rate. The errors take also in account for uncertainties due to projection effects. The best-fit $\dot{M}_O - L_{AGN}$ relation for the ionized outflows is indicated in the panel with a black line. Square points indicate velocities and outflow rate inferred from molecular outflows. Carniani, A&A, 580, A102, 2015, reproduced with permission © ESO.

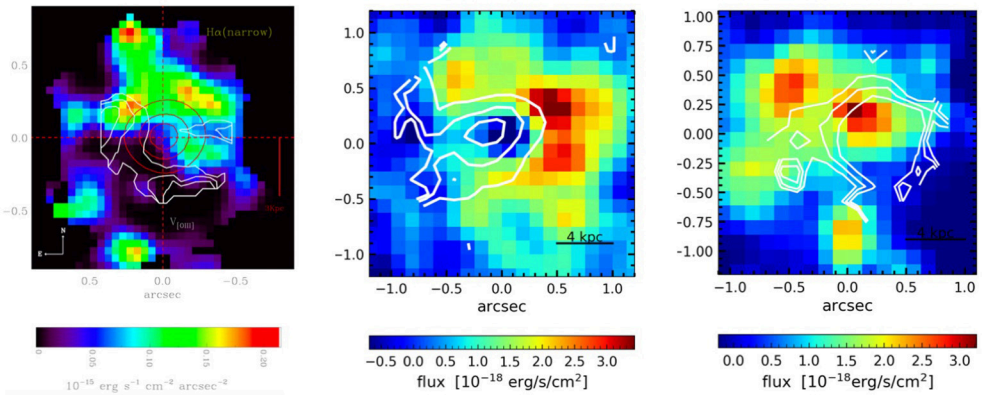

FIGURE 2 | Intensity map of narrow Hα **(left and middle)** emission and [OIII]λ5007 **(right)** emission for the three quasars showing ionized outflow anti-correlated with the star formation: 2QZ J0028–2830 from Cano-Díaz et al. (2012), HB89 0329−385 and LBQS 0109 + 0213 from Carniani et al. (2015, 2016). The stamps are 1″×1″, 1.2″×1.2″, and 1.2″×1.2″, respectively for the three sources. The white contours in both maps trace the blue shifted [OIII]λ5007 velocities of the broad component tracing the ionized outflow. The contours represent the velocities −390, −360, and 330 km/s for 2QZ J0028–2830, −150, 100, −50 km/s for HB89 0329 − 38, and 300, 275, and 250 km/s for LBQS 0109 + 0213. Credit: Cano-Díaz, A&A, 537, L8, 2012, reproduced with permission© ESO; Carniani, A&A, 591, 28C, 2016, reproduced with permission© ESO.

host galaxy. However, optical emission lines, such as [OIII]λ5007 and Hα, can be affected by differential extinction effects and current SINFONI observations are not sufficient to rule out the possibility that the lack of star formation emission in the outflow region is caused by dust obscuration. In this regards, these QSOs were proposed as targets of two ALMA programs in Cycle 2 and 3 with the goal to observe the CO(3-2) line and map the distribution of the cold molecular gas in the host galaxies. Indeed, since the CO emission line is a good tracer of the cold molecular gas, which is the main fuel of star formation activity, and it is not affected by dust obscuration, the spatially distribution of molecular gas may support (or confute) negative feedback scenario in the QSOs.

2.4. Molecular Gas

The three QSOs, showing star formation spatially anti-correlated to ionized outflows, have been observed with ALMA in the band at ∼3 mm, where CO(3-2) is redshifted. Although the targets have similar properties and the continuum emission at ∼3 mm (∼0.9 mm rest frame) is visible in all of them, CO(3-2) transition at the systemic velocity of the sources is detectable only in one out of three QSOs (LBQS 0109 + 0213).

Both redshift and line width of the molecular line are consistent, within the errors, with those of the narrow [OIII]λ5007 and Hα component observed with SINFONI and discussed in the previous section. As expected, the CO(3-2) surface brightness appears to be asymmetrically distributed

around the nucleus, similarly to the flux map of the narrow optical lines, indicating that the emission from molecular gas is absent or faint in the outflow region (**Figure 3**). Since the CO line is not affected by dust attenuation, ALMA observations support the scenario in which AGN-driven fast winds clear out ionized and molecular gas from the host galaxy, and quench star formation at least in the outflow region.

Assuming a $L'_{CO(3\text{-}2)}/L'_{CO(1\text{-}0)}$ ratio of 1 (Carilli and Walter, 2013; Carniani et al., 2017) infer a molecular gas mass for LBQS 0109 + 0213 of $M_{gas} = 0.8\text{–}4 \times 10^{10}$ $M_\odot$ depending on the assumed conversion factor between CO(1-0) luminosity and gas mass ($\alpha_{CO} = 0.8\text{–}4$ $M_\odot$/K km/s pc^2; Bolatto et al. 2013). For the other two QSOs, non-detections yield to an upper limit on the molecular mass of $M_{gas} < 0.2 - 1.2 \times 10^{10}$ for 2QZ J0028–2830 and $M_{gas} < 0.2 - 1.0 \times 10^{10}$ for HB89 0329–385. The inferred molecular masses (or upper limits) are clearly below what observed in main-sequence galaxies with similar redshift and SFR, while they are comparable to molecular masses observed in active galaxies (**Figure 4**). Indeed, the depletion timescale, which is the time required for the outflow to remove the gas from the galaxy ($\tau_{dep} = M_{gas}$/SFR), estimated for each QSOs of our sample ($\tau_{dep} < 800$ Myr) is consistent to those observed in high—z submillimetre galaxies (SMGs) and obscured QSOs at $z = 1.5 - 2.5$ (Banerji et al., 2017; Kakkad et al., 2017).

The low depletion timescale may yield to the conclusion that the three QSOs host galaxies are still in a starburst phase and the AGN-driven outflows do not influence the star formation activity. However, the CO, [OIII]λ5007 and Hα maps clearly exhibits a cavity in the outflow region leading to the conclusion that a fraction of molecular gas has been removed from the galaxy by the outflow (*negative feedback*), but, at the same time, we have star-formation on-going in the rest of the galaxy. This star-formation could be also enhanced by the outflow pressure itself (*positive feedback*), as expected by recent simulation (e.g., Zubovas and Bourne, 2017). Unfortunately, the sensitivity of current ALMA observations is not sufficient to reveal the presence outflowing molecular gas in LBQS 0109 + 0213 and we cannot evaluate the fraction of the gas that has been already removed due the AGN-driven outflow.

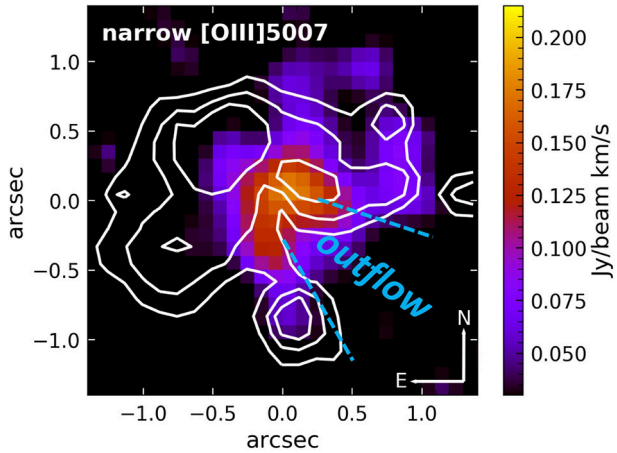

FIGURE 3 | The color background image CO(3-2) flux map of LBQS0109, while white contours indicate the narrow [OIII]λ5007 emission tracing star-formation emission in the host galaxy. Contours are in steps of $1\sigma = 0.4 \times 10^{-18}$ erg/s/cm^2, starting at 2σ. The blue dashed line indicates the direction of the AGN-driven outflow inferred from the velocity map of the broad components. Star-formation and molecular gas emission is faint/absent in the outflow region. The figure is an adaptation from Carniani et al. (2017). Credit: Carniani, A&A, 605, A105, 2017, reproduced with permission © ESO.

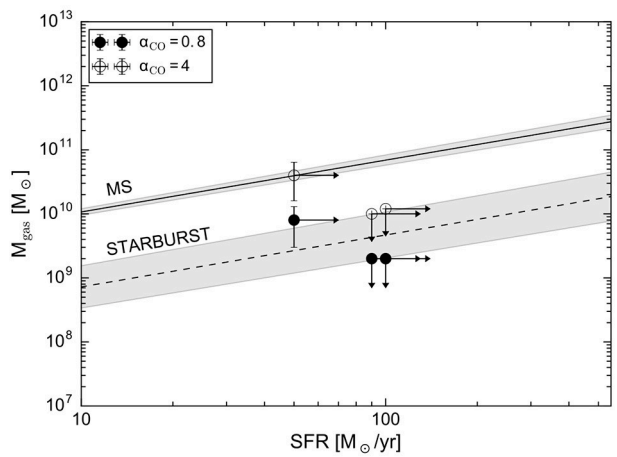

FIGURE 4 | M_{gas}-SFR plane from Carniani et al. (2017). The solid black line is the best-fit relation for main sequence galaxies and the dashed indicate the relation for the starburst galaxies (Sargent et al., 2014). Filled black circles corresponds to the three QSOs assuming a $\alpha_{CO} = 0.8$ $M_\odot$/K km/s pc^2 and open circles are derived supposing a $\alpha_{CO} = 4$ $M_\odot$/K km/s pc^2. Credit: Carniani, A&A, 605, A105, 2017, reproduced with permission © ESO.

3. SUMMARY AND CONCLUSIONS

Carniani et al. (2015, 2016, 2017) carried out seeing-limited, near-IR integral-field spectroscopic observations with SINFONI in H- and K-band of six high-luminosity ($L_{bol} > 10^{47}$ erg/s) QSOs at $z \sim 2.4$.

- Five objects show a broad [OIII]λ5007 line revealing spatially extended ionized fast gas with velocities >500 km/s and outflow mass rates of $\sim 10 - 700$ $M_\odot$ yr^{-1}.
- Velocity, mass rate, kinetic energy, momentum mass rate of the ionized outflows seem to correlate with the observed AGN luminosities, indicating the these outflows are AGN-driven.
- The comparison between the relation mass outflow rate and AGN luminosity obtained from molecular and ionized outflow suggests that outflow masses are mainly dominated by molecular gas.
- In three QSOs, we detect narrow [OIII]λ5007 and Hα emission tracing quiescent gas in the host galaxy and excited by star formation activity. The emission of these narrow components is absent and/or faint in the outflow regions supporting a clear evidence of negative-feedback in action. However, the high SFR (>50 $M_\odot$ yr^{-1}) inferred from the narrow Hα line indicates the star formation is halted only in the outflow regions.

- ALMA observations have revealed CO(3-2) emission at the systemic velocity of the host galaxy only in one QSO and the flux map of the molecular line is similar to those obtained from the narrow optical lines. The lack of CO(3-2) emission in the outflow region indicates that both ionized and molecular gas have been removed by AGN-driven outflow

SINFONI and ALMA observations hint that AGN feedback is not able to prevent completely star formation in QSO host galaxies. On the other hand, theses results suggest that several explosive events are necessary to accomplish the suppression. This research would benefit from a larger sample with similar AGN luminosities and redshift in order to reach more reliable results. In addition, new deeper ALMA observations may reveal the presence of molecular outflow in these QSOs and evaluate what fraction of the total molecular gas content has been swiped out from the host galaxy.

AUTHOR CONTRIBUTIONS

The author confirms being the sole contributor of this work and approved it for publication.

ACKNOWLEDGMENTS

I thank A. Marconi, R. Maiolino, C. Cicone, G. Cresci, C. Feruglio, M. Brusa, M. Cano-Díaz, V. Mainieri, B. Balmaverde, R. Schneider, F. Fiore, A. Ferrara, F. La Franca, S. Gallerani, F. Mannucci, T. Nagao, H. Netzer, E. Piconcelli, A. Comastri, E. Sani, L. Testi, G. Risaliti, and O. Shemmer for the useful comments and discussions. SC acknowledges financial support from the Science and Technology Facilities Council (STFC). We thank the reviewers for a very quick and thoughtful report.

REFERENCES

Banerji, M., Carilli, C. L., Jones, G., Wagg, J., McMahon, R. G., Hewett, P. C., et al. (2017). The discovery of gas-rich, dusty starbursts in luminous reddened quasars at $z \sim 2.5$ with ALMA. *Month. Notices R. Astron. Soc.* 465, 4390–4405. doi: 10.1093/mnras/stw3019

Bolatto, A. D., Wolfire, M., and Leroy, A. K. (2013). The CO-to-H_2 conversion factor. *Annu. Rev. Astron. Astrophys.* 51, 207–268. doi: 10.1146/annurev-astro-082812-140944

Brusa, M., Bongiorno, A., Cresci, G., Perna, M., Marconi, A., Mainieri, V., et al. (2015). X-shooter reveals powerful outflows in z$\tilde{1}$.5 X-ray selected obscured quasi-stellar objects. *Month. Notices R. Astron. Soc.* 446, 2394–2417. doi: 10.1093/mnras/stu2117

Cano-Díaz, M., Maiolino, R., Marconi, A., Netzer, H., Shemmer, O., and Cresci, G. (2012). Observational evidence of quasar feedback quenching star formation at high redshift. *Astron. Astrophys.* 537:L8. doi: 10.1051/0004-6361/201118358

Carilli, C. L., and Walter, F. (2013). Cool Gas in High-Redshift Galaxies. *Annu. Rev. Astron. Astrophys.* 51, 105–161. doi: 10.1146/annurev-astro-082812-140953

Carniani, S., Marconi, A., Maiolino, R., Balmaverde, B., Brusa, M., Cano-Díaz, M., et al. (2015). Ionised outflows in z $\sim$ 2.4 quasar host galaxies. *Astron. Astrophys.* 580:A102. doi: 10.1051/0004-6361/201526557

Carniani, S., Marconi, A., Maiolino, R., Balmaverde, B., Brusa, M., Cano-Díaz, M., et al. (2016). Fast outflows and star formation quenching in quasar host galaxies. *Astron. Astrophys.* 591:A28. doi: 10.1051/0004-6361/201528037

Carniani, S., Marconi, A., Maiolino, R., Feruglio, C., Brusa, M., Cresci, G., et al. (2017). AGN feedback on molecular gas reservoirs in quasars at $z \sim 2.4$. *Astron. Astrophys.* 605:A105. doi: 10.1051/0004-6361/201730672

Cicone, C., Maiolino, R., Sturm, E., Graciá-Carpio, J., Feruglio, C., Neri, R., et al. (2014). Massive molecular outflows and evidence for AGN feedback from CO observations. *Astron. Astrophys.* 562:A21. doi: 10.1051/0004-6361/201322464

Combes, F., García-Burillo, S., Casasola, V., Hunt, L., Krips, M., Baker, A. J., et al. (2013). ALMA observations of feeding and feedback in nearby Seyfert galaxies: an AGN-driven outflow in NGC 1433. *Astron. Astrophys.* 558:A124. doi: 10.1051/0004-6361/201322288

Cresci, G., Mainieri, V., Brusa, M., Marconi, A., Perna, M., Mannucci, F., et al. (2015). Blowin' in the Wind: Both "Negative" and "Positive" Feedback in an Obscured High-z Quasar. *Astrophys. J.* 799:82. doi: 10.1088/0004-637X/799/1/82

Fabian, A. C. (2012). Observational evidence of active galactic nuclei feedback. *Annu. Rev. Astron. Astrophys.* 50, 455–489. doi: 10.1146/annurev-astro-081811-125521

Feruglio, C., Fiore, F., Carniani, S., Piconcelli, E., Zappacosta, L., Bongiorno, A., et al. (2015). The multi-phase winds of Markarian 231: from the hot, nuclear, ultra-fast wind to the galaxy-scale, molecular outflow. *Astron. Astrophys.* 583:A99. doi: 10.1051/0004-6361/201526020

Fiore, F., Feruglio, C., Shankar, F., Bischetti, M., Bongiorno, A., Brusa, M., et al. (2017). AGN wind scaling relations and the co-evolution of black holes and galaxies. *Astron. Astrophys.* 601:A143. doi: 10.1051/0004-6361/201629478

García-Burillo, S., Combes, F., Usero, A., Aalto, S., Krips, M., Viti, S., et al. (2014). Molecular line emission in NGC 1068 imaged with ALMA. I. An AGN-driven outflow in the dense molecular gas. *Astron. Astrophys.* 567:A125. doi: 10.1051/0004-6361/201423843

Greene, J. E., Zakamska, N. L., and Smith, P. S. (2012). A spectacular outflow in an obscured quasar. *Astrophys. J.* 746:86. doi: 10.1088/0004-637X/746/1/86

Harrison, C. M., Alexander, D. M., Mullaney, J. R., and Swinbank, A. M. (2014). Kiloparsec-scale outflows are prevalent among luminous AGN: outflows and feedback in the context of the overall AGN population. *MNRAS* 441, 3306–3347. doi: 10.1093/mnras/stu515

Hopkins, P. F., Somerville, R. S., Hernquist, L., Cox, T. J., Robertson, B., and Li, Y. (2006). The relation between quasar and merging galaxy luminosity functions and the merger-driven star formation history of the universe. *Astrophys. J.* 652, 864–888. doi: 10.1086/508503

Kakkad, D., Mainieri, V., Brusa, M., Padovani, P., Carniani, S., Feruglio, C., et al. (2017). ALMA observations of cold molecular gas in AGN hosts at z = 1.5 - evidence of AGN feedback? *Month. Notices R. Astron. Soc.* 468, 4205–4215. doi: 10.1093/mnras/stx726

Kennicutt, R. C., and Evans, N. J. (2012). Star formation in the milky way and nearby galaxies. *Annu. Rev. Astron. Astrophys.* 50, 531–608. doi: 10.1146/annurev-astro-081811-125610

Marconi, A., Risaliti, G., Gilli, R., Hunt, L. K., Maiolino, R., and Salvati, M. (2004). Local supermassive black holes, relics of active galactic nuclei and the X-ray background. *Month. Notices R. Astron. Soc.* 351, 169–185. doi: 10.1111/j.1365-2966.2004.07765.x

Marziani, P., Sulentic, J. W., Stirpe, G. M., Zamfir, S., and Calvani, M. (2009). VLT/ISAAC spectra of the Hβ region in intermediate-redshift quasars. III. Hβ broad-line profile analysis and inferences about BLR structure. *Astron. Astrophys.* 495, 83–112. doi: 10.1051/0004-6361:200810764

Netzer, H., Shemmer, O., Maiolino, R., Oliva, E., Croom, S., Corbett, E., et al. (2004). Near-infrared spectroscopy of high-redshift active galactic nuclei. II. Disappearing narrow-line regions and the role of accretion. *Astrophys. J.* 614, 558–567. doi: 10.1086/423608

Sargent, M. T., Daddi, E., Béthermin, M., Aussel, H., Magdis, G., Hwang, H. S., et al. (2014). Regularity underlying complexity: a redshift-independent description of the continuous variation of galaxy-scale molecular gas properties in the mass-star formation rate plane. *Astrophys. J.* 793:19. doi: 10.1088/0004-637X/793/1/19

Shemmer, O., Netzer, H., Maiolino, R., Oliva, E., Croom, S., Corbett, E., et al. (2004). Near-infrared spectroscopy of high-redshift active galactic nuclei. I. A metallicity-accretion rate relationship. *Astrophys. J.* 614, 547–557. doi: 10.1086/423607

Sun, A.-L., Greene, J. E., Zakamska, N. L., and Nesvadba, N. P. H. (2014). ALMA observations of a candidate molecular outflow in an obscured quasar. *Astrophys. J.* 790:160. doi: 10.1088/0004-637X/790/2/160

Zubovas, K., and Bourne, M. A. (2017). Do AGN outflows quench or enhance star formation? *Month. Notices R. Astron. Soc.* 468, 4956–4967. doi: 10.1093/mnras/stx787e

Conflict of Interest Statement: The author declares that the research was conducted in the absence of any commercial or financial relationships that could be construed as a potential conflict of interest.

Copyright © 2017 Carniani. This is an open-access article distributed under the terms of the Creative Commons Attribution License (CC BY). The use, distribution or reproduction in other forums is permitted, provided the original author(s) or licensor are credited and that the original publication in this journal is cited, in accordance with accepted academic practice. No use, distribution or reproduction is permitted which does not comply with these terms.

frontiers in Astronomy and Space Sciences

ORIGINAL RESEARCH
published: 12 January 2018
doi: 10.3389/fspas.2017.00067

Luminous and Obscured Quasars and Their Host Galaxies

Agnese Del Moro[1], David M. Alexander[2], Franz E. Bauer[3,4,5,6], Emanuele Daddi[7], Dale D. Kocevski[8], Flora Stanley[9] and Daniel H. McIntosh[10]*

[1] Max-Planck-Institut für Extraterrestrische Physik, Garching, Germany, [2] Department of Physics, Centre for Extragalactic Astronomy, Durham University, Durham, United Kingdom, [3] Facultad de Física, Instituto de Astrofísica, Pontificia Universidad Católica de Chile, Santiago, Chile, [4] Millennium Institute of Astrophysics (MAS), Santiago, Chile, [5] EMBIGGEN Anillo, Concepción, Chile, [6] Space Science Institute, Boulder, CO, United States, [7] CEA, IRFU, DAp, AIM, Université Paris-Saclay, Université Paris Diderot, Sorbonne Paris Cité, CNRS, Gif-sur-Yvette, France, [8] Department of Physics and Astronomy, University of Kentucky, Lexington, KY, United States, [9] Department of Space Earth and Environment, Chalmers University of Technology, Onsala Space Observatory, Onsala, Sweden, [10] Department of Physics and Astronomy, University of Missouri-Kansas City, Kansas City, MO, United States

The most heavily-obscured, luminous quasars might represent a specific phase of the evolution of the actively accreting supermassive black holes and their host galaxies, possibly related to mergers. We investigated a sample of the most luminous quasars at $z \approx 1-3$ in the GOODS fields, selected in the mid-infrared band through detailed spectral energy distribution (SED) decomposition. The vast majority of these quasars (∼80%) are obscured in the X-ray band and ∼30% of them to such an extent, that they are undetected in some of the deepest (2 and 4 Ms) *Chandra* X-ray data. Although no clear relation is found between the star-formation rate of the host galaxies and the X-ray obscuration, we find a higher incidence of heavily-obscured quasars in disturbed/merging galaxies compared to the unobscured ones, thus possibly representing an earlier stage of evolution, after which the system is relaxing and becoming unobscured.

Keywords: galaxies: active, quasars: general, quasars: supermassive black holes, X-rays: galaxies, infrared: galaxies, galaxies: star formation

OPEN ACCESS

Edited by:
Ascensión Del Olmo, Instituto de Astrofísica de Andalucía (CSIC), Spain

Reviewed by:
Lorena Hernandez-Garcia, University of Valparaíso, Chile
Begoña Garcia-Lorenzo, Instituto de Astrofísica de Canarias, Spain

****Correspondence:***
Agnese Del Moro
adelmoro@mpe.mpg.de

Specialty section:
This article was submitted to Cosmology, a section of the journal Frontiers in Astronomy and Space Sciences

Received: *30 October 2017*
Accepted: *18 December 2017*
Published: *12 January 2018*

Citation:
Del Moro A, Alexander DM, Bauer FE, Daddi E, Kocevski DD, Stanley F and McIntosh DH (2018) Luminous and Obscured Quasars and Their Host Galaxies. Front. Astron. Space Sci. 4:67. doi: 10.3389/fspas.2017.00067

1. INTRODUCTION

The similarity between the accretion history of galaxies and supermassive black holes (SMBHs), peaking at redshift $z \approx 1-2$ (e.g., Madau et al., 1996; Hopkins et al., 2006; Brandt and Alexander, 2015), suggests that there is a connection between the evolution of a galaxy and the black hole in their center. Such connection has also been hinted by the observed correlations between the BH mass and the velocity dispersion of the stars in the bulge ($M_{\rm BH} - \sigma$ relation; Ferrarese and Merritt, 2000; Gebhardt et al., 2000) or with the bulge mass ($M_{\rm BH} - M_{bulge}$; Kormendy and Richstone, 1995; Magorrian et al., 1998). Whether this parallel evolution is simply due to a larger gas supply at high redshift, feeding both the SMBH and star formation (SF), or whether there are other processes self-regulating the SMBH and galaxy growth (e.g., AGN feedback) is still uncertain (e.g., Alexander and Hickox, 2012; Kormendy and Ho, 2013).

Studying active galactic nuclei (AGN) at all cosmic epochs is crucial to fully understand the accretion history of the SMBHs and their role in galaxy evolution. However, most of the accretion onto SMBHs is expected to be heavily obscured by dust and gas, making the identification of the most obscured AGN population very challenging, even in the deepest X-ray surveys. According to the unified model (e.g., Antonucci, 1993), AGN appear obscured due to orientation effects,

when our line-of-sight crosses high column densities ($N_{\rm H}$) of circumnuclear material, the so called "torus". However, it has been suggested that the most heavily-obscured, Compton-thick (CT; where $N_{\rm H} > 1.5 \times 10^{24}$ cm^{-2}) AGN, especially the (intrinsically) most luminous ones, could represent a particular phase of galaxy evolution, associated to a major merger, when a lot of gas and dust are funneled into the center of the galaxy, deeply hiding the active nucleus within it (Di Matteo et al., 2005; Hopkins et al., 2006; see also Alexander and Hickox, 2012, for a review). Yet, the emission reprocessed by the obscuring dust is re-emitted in the mid-infrared (MIR) band, which can therefore be used to find even the most obscured and elusive quasars.

2. SAMPLE SELECTION

The sample was selected from a large catalog of 24 μm-detected sources within the GOODS-*Herschel* North and South fields. We performed detailed SED decomposition using *Spitzer* 8, 16, and 24 μm and *Herschel* 100, 160, and 250 μm data, to separate the AGN from SF emission. We adopted the AGN and star-forming galaxy (SFG) templates described in Mullaney et al. (2011) and Del Moro et al. (2013); details of the SED fitting are described in Del Moro et al. (2016). Amongst these sources we selected the most luminous quasars in the MIR band, with rest-frame 6 μm luminosity of $\nu L_{\rm AGN,6\,\mu m} > 6 \times 10^{44}$ erg s^{-1}, corrected for the galaxy contribution, at redshift $z = 1 - 3$. This selection results in a sample of 33 sources.

3. ANALYSES AND RESULTS

3.1. AGN: Heavily Obscured Population at $z \approx 2$

To characterize the quasars in our sample, we used the deep X-ray *Chandra* data available in the *Chandra* Deep Field North (CDF-N; 2 Ms; Alexander et al., 2003) and *Chandra* Deep Field South (CDF-S 4 Ms; Xue et al., 2011). For details on the data reduction we refer to Alexander et al. (2003), Luo et al. (2008), and Xue et al. (2011). Of our 33 quasars, 24 (∼73%) are detected in the X-ray band, while 9 (∼27%) remain undetected, despite being intrinsically very luminous in the MIR band. These sources are candidates to be the most heavily obscured, CT AGN.

For the sources that are detected in the X-rays, we extracted the spectra using *ACIS Extract* (AE; Broos et al., 2010, 2012) and analyzed them using a simple absorbed power-law model (including Galactic and intrinsic absorption) to constrain the amount of $N_{\rm H}$. In **Figure 1** we show the $N_{\rm H}$ distribution of the sample. We find that the majority of these quasars (16/24; ∼67%) are obscured by columns of $N_{\rm H} > 10^{22}$ cm^{-2}, of which more than half (9/16) are heavily obscured ($N_{\rm H} > 2 \times 10^{23}$ cm^{-2}). Amongst these heavily-obscured sources, we identified six of them as CT quasars from the X-ray spectral analysis, using spectral models appropriate for heavily-obscured sources, such as, PLCABS (Yaqoob, 1997) and TORUS (Brightman and Nandra, 2011). The fraction of obscured quasars in our sample reaches ∼76%, and 54% of heavily-obscured quasars, if we include

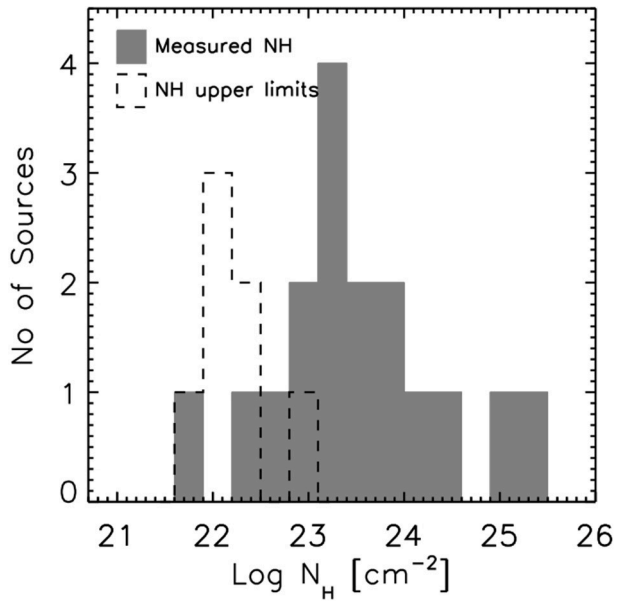

FIGURE 1 | Distribution of the X-ray column density ($N_{\rm H}$) for the X-ray-detected MIR quasars (∼70% of the sample). The dashed histogram represents the $N_{\rm H}$ upper limits (calculated at a 90% confidence level).

the X-ray-undetected sources, assuming these are the most heavily CT ones. Indeed, the comparison between the intrinsic luminosity at 6 μm and the X-ray luminosity upper limit of these sources suggests that the X-ray emission is heavily suppressed compared to the intrinsic $L_{\rm X} - L_{6\,\mu m}$ relation found for AGN (e.g., Lutz et al., 2004; Fiore et al., 2009; Gandhi et al., 2009), making them very good candidates to be heavily CT quasars.

We note that amongst the X-ray undetected quasars in the sample, there is one source, #28 (see Table 1 from Del Moro et al., 2016), that is now detected in the 7 Ms CDF-S catalog (XID 28; Luo et al., 2017). This source has a very flat effective photon index of $\Gamma < 0.93$ (compared to the typical $\Gamma \approx 1.8$ for unabsorbed AGN) and an extremely low rest-frame X-ray luminosity ($L_{0.5-7\,\rm keV} \approx 1.5 \times 10^{41}$ erg s^{-1}, uncorrected for absorption) compared to its intrinsic luminosity measured in the MIR band (log $\nu\, L_{6\,\mu m} = 45.97$ erg s^{-1}), consistent with the upper limit reported in our analysis (Del Moro et al., 2016)[1], supporting our assumption that the source might be a heavily obscured, CT quasar.

These results suggest that there is a large population of heavily-obscured, intrinsically luminous quasars at high redshift, which are very elusive even for deep X-ray surveys. These sources might constitute a special phase of the BH-galaxy evolution, where the actively growing BH is embedded in large amounts of gas and dust, possibly as a result of a recent merger.

[1]We note however, that the photometric redshift assumed in our analysis of this source ($z = 2.55$) differs from that reported in the Luo et al. (2017) catalog ($z = 1.81$).

3.2. AGN Host Galaxies: Star-Formation Rates and Merger Fraction

To study the characteristics of the host galaxies of these MIR-luminous quasars, we investigated their star-formation rates (SFRs) and their morphologies, in particular the disturbance or distortion of their morphology, as an indication of galaxy mergers and interactions. We derived the SFR of each galaxy from its far-infrared (FIR) luminosity (or upper limit) resulting from the SED decomposition in the IR band (see section 2 and Del Moro et al., 2016), assuming a Salpeter initial mass function (Salpeter, 1955) and the relation from Kennicutt (1998). We also calculated the average SFR separately for the unobscured/moderately obscured quasars ($N_{\rm H} < 2 \times 10^{23}$ cm^{-2}) and for the heavily-obscured quasars ($N_{\rm H} > 2 \times 10^{23}$ cm^{-2}) in three different redshift bins (see **Figure 2**). To estimate the average SFRs accounting for the upper limits, we used the Kaplan-Meier (KM) product limit estimator (Kaplan and Meier, 1958), a non-parametric maximum-likelihood estimator of the distribution function (see Stanley et al., 2015, for details on the method).

We find that the average SFR increases with redshift, in general agreement with the SFR main sequence of galaxies (**Figure 2**). Moreover, although the heavily-obscured sources seem to have a slightly enhanced SFR compared to the unobscured/moderately obscured ones (especially at $z \approx 2$), these differences are not statistically significant, and therefore we find no clear dependence of the amount of SF in the galaxy with the X-ray obscuration of the quasar. This suggests that the obscuration in the X-ray band is likely confined in the nuclear regions and not related to the presence of gas on larger scales (e.g., Rosario et al., 2012; Rovilos et al., 2012).

Using the high-resolution optical HST images available in the GOODS-N and GOODS-S fields, as part of the GOODS and CANDELS projects (Giavalisco et al., 2004; Grogin et al., 2011), we visually inspected the morphology of these galaxies to identify signs of distortions or disturbances, which would indicate a recent galaxy merger/interaction event. We adopted a similar classification scheme to that used by Kocevski et al. (2012); see Del Moro et al. (2016, for details), separating the sources into "disturbed" and "undisturbed". In **Figure 3** we show the fraction of sources having disturbed and undisturbed morphologies over the total, dividing them again into unobscured/moderately obscured (blue squares) and heavily obscured (magenta circles), as in **Figure 2**. We find that a relatively high fraction of our sources shows signs of distortions/interactions (≈40%), higher than those typically found at low redshift (∼15–20% at $z < 1$; e.g., Cisternas et al., 2011). This is in agreement with the trend of increasing major-merger fraction with redshift seen in previous works (e.g., Conselice et al., 2003; Treister and Urry, 2006; Kartaltepe et al., 2007). We find that, on average, the most-heavily obscured quasars tend to have more disturbed morphologies than the unobscured/moderately obscured ones (≈53 vs. ≈20%, respectively); although the errors on these fractions are large due to the small number of sources in our sample, the difference between the two quasar populations is

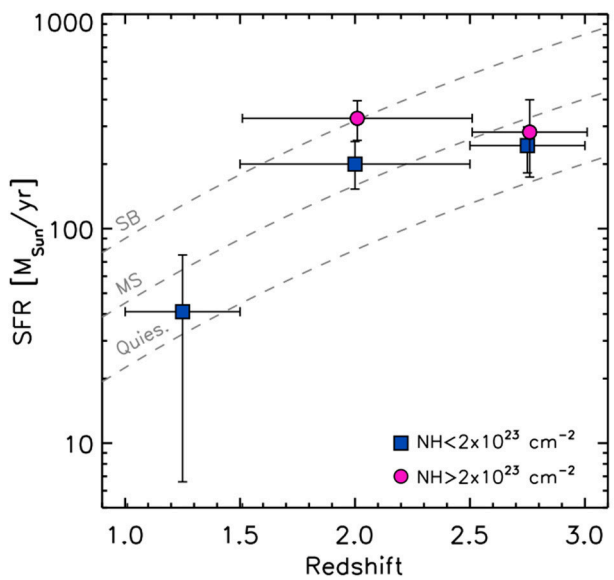

FIGURE 2 | Average star-formation rate (SFR) for the unobscured/moderately-obscured quasars ($N_{\rm H} < 2 \times 10^{23}$ cm^{-2}; blue squares) and the heavily-obscured quasars ($N_{\rm H} > 2 \times 10^{23}$ cm^{-2}; magenta circles) in our sample, divided in three redshift bins. None of heavily-obscured quasars are detected in the lowest redshift bin. The gray dashed lines represent the SFR track for main-sequence (MS), starburst (SB; SFR$_{MS} \times 2$) and quiescent (Quies.; SFR$_{MS}$/2) galaxies with a typical mass of $M_* = 9 \times 10^{10}$ M$_\odot$ (e.g., Elbaz et al., 2011).

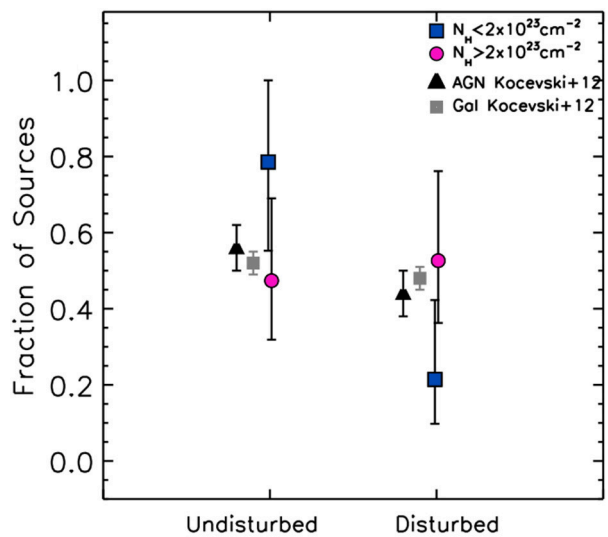

FIGURE 3 | Fraction of MIR quasar hosts showing disturbed and undisturbed galaxy morphologies, classified using HST images. The fractions and 1σ uncertainties for the unobscured/moderately-obscured quasar hosts ($N_{\rm H} < 2 \times 10^{23}$ cm^{-2}) are plotted as blue squares and for the heavily-obscured quasars ($N_{\rm H} \geq 2 \times 10^{23}$ cm^{-2}) as magenta circles. For comparison we also show the fractions for $z \approx 2$ AGN and non-AGN samples from Kocevski et al. (2012): filled black triangles and gray squares, respectively. The unobscured/moderately-obscured quasars reside preferentially in undisturbed systems, while the heavily-obscured quasars are equally found in disturbed and undisturbed systems.

significant at the 90% confidence level (Fisher exact probability test: $P = 0.087$). This trend is seen also in other studies (e.g., Kocevski et al., 2015; Ricci et al., 2017). We note, however, that these studies investigated samples in different redshift and/or luminosity ranges compared to ours, and therefore the actual fractions of sources with disturbed morphologies are not directly comparable. The smaller fraction of disturbed systems we found for the unobscured/moderately-obscured quasars could be interpreted within the SMBH-galaxy evolutionary models, as the unobscured quasars would represent a later stage of the evolution compared to the heavily-obscured sources and the distortion features due to mergers or interactions might have faded by the time these quasars are observed as unobscured, given the relaxation time of a galaxy is typically $\sim$ 200–400 Myr (e.g., Lotz et al., 2010). On the other hand, for the most heavily-obscured quasars, which might represent a younger stage of evolution after a merger in this scenario, the signatures of the recent interactions are still evident in their hosts.

4. CONCLUSIONS

We have investigated the AGN and host galaxy properties of a sample of 33 quasars at $z = 1 - 3$ within the GOODS-*Herschel* fields, selected in the MIR band through detailed SED analysis to have an intrinsic AGN luminosity of $\nu L_{6\,\mu m} > 6 \times 10^{44}$ erg s^{-1}. Despite being intrinsically the most luminous quasars within these fields, $\sim$26% of them are not detected in the deep 2 and 4 Ms *Chandra* X-ray data covering these sky areas.

We performed X-ray spectral analysis of the 24 X-ray-detected sources to investigate the AGN properties, and we found that the vast majority ($\sim$67%; 16/24 sources) are obscured by $N_H > 10^{22}$ cm^{-2}, with more than half of them (9/16) being heavily obscured ($N_H > 2 \times 10^{23}$ cm^{-2}). Including the X-ray undetected sources, which are likely to be the most heavily CT AGN, these fractions reach $\sim$76% ($\sim$54% are heavily obscured). This means that there is a very large population of heavily obscured, intrinsically luminous quasars at redshift $z \approx 2$, which can be revealed in the IR band, but remains (in part) undetected in the X-ray band.

We investigated the host galaxy properties of these quasars through their SFR, measured in the FIR band from SED fitting using *Spitzer* and *Herschel* data, and did not find any strong link between the amount of SF and the X-ray obscuration, possibly suggesting that the X-ray obscuration is mostly concentrated in the nuclear regions and does not depend on the presence of gas on larger scales.

We also visually classified the morphology of these quasars as disturbed or undisturbed using high-resolution HST data to identify signs of distortions/asymmetries in the galaxies. We find that a significant fraction ($\sim$40%) have disturbed morphologies, suggesting they have experienced a recent merger or interaction event. We find a larger fraction of sources with disturbed morphologies amongst the heavily-obscured quasars ($\sim$53%) rather than the unobscured/moderately-obscured ones ($\sim$20%). Our results possibly support the SMBH-galaxy evolutionary scenario where the heavily-obscured quasars represent an earlier stage of evolution after the merger, while the unobscured quasars represent a later stage of the evolution, when the system has relaxed, the signs of interaction have already faded, and the nucleus becomes unobscured.

AUTHOR CONTRIBUTIONS

AD developed the concept, performed all the analyses and wrote the manuscript. DA initiated and helped developing the concept. FB provided the X-ray spectra. ED compiled the multiwavelength catalog, which was used for the SED analysis. DK and DM provided the optical HST images, used to classify the galaxy morphology. FS calculated the mean star-formation rates.

FUNDING

This research was supported by the UK Science and Technology Facilities Council (STFC, ST/L00075X/1); CONICYT-Chile (Basal-CATA PFB-06/2007, "EMBIGGEN" Anillo ACT1101, FONDECYT Regular 1141218); the Ministry of Economy, Development, and Tourism's Millennium Science Initiative through grant IC120009, awarded to The Millennium Institute of Astrophysics (MAS).

REFERENCES

Alexander, D. M., Bauer, F. E., Brandt, W. N., Schneider, D. P., Hornschemeier, A. E., Vignali, C., et al. (2003). The chandra deep field north survey. XIII. 2 Ms point-source catalogs. *Astron. J.* 126, 539–574. doi: 10.1086/376473

Alexander, D. M., and Hickox, R. C. (2012). What drives the growth of black holes? *New A Rev.* 56, 93–121. doi: 10.1016/j.newar.2011.11.003

Antonucci, R. (1993). Unified models for active galactic nuclei and quasars. *Annu. Rev. Astron. Astrophys.* 31, 473–521. doi: 10.1146/annurev.aa.31.090193.002353

Brandt, W. N., and Alexander, D. M. (2015). Cosmic X-ray surveys of distant active galaxies. The demographics, physics, and ecology of growing supermassive black holes. *Astron. Astrophys. Rev.* 23:1. doi: 10.1007/s00159-014-0081-z

Brightman, M., and Nandra, K. (2011). An XMM-Newton spectral survey of 12 μm selected galaxies - I. X-ray data. *Month. Notices R. Astron. Soc.* 413, 1206–1235. doi: 10.1111/j.1365-2966.2011.18207.x

Broos, P., Townsley, L., Getman, K., and Bauer, F. (2012). *AE: ACIS Extract*. Astrophysics Source Code Library.

Broos, P. S., Townsley, L. K., Feigelson, E. D., Getman, K. V., Bauer, F. E., and Garmire, G. P. (2010). Innovations in the analysis of chandra-ACIS observations. *Astrophys. J.* 714, 1582–1605. doi: 10.1088/0004-637X/714/2/1582

Cisternas, M., Jahnke, K., Inskip, K. J., Kartaltepe, J., Koekemoer, A. M., Lisker, T., et al. (2011). The bulk of the black hole growth since $z \sim 1$ occurs in a secular universe: no major merger-AGN connection. *Astrophys. J.* 726:57. doi: 10.1088/0004-637X/726/2/57

Conselice, C. J., Bershady, M. A., Dickinson, M., and Papovich, C. (2003). A direct measurement of major galaxy mergers at $z \lesssim 3$. *Astron. J.* 126, 1183–1207. doi: 10.1086/377318

Del Moro, A., Alexander, D. M., Bauer, F. E., Daddi, E., Kocevski, D. D., McIntosh, D. H., et al. (2016). Mid-infrared luminous quasars in the GOODS-Herschel fields: a large population of heavily obscured, Compton-thick quasars at z ≈ 2. *Month. Notices R. Astron. Soc.* 456, 2105–2125. doi: 10.1093/mnras/stv2748

Del Moro, A., Alexander, D. M., Mullaney, J. R., Daddi, E., Pannella, M., Bauer, F. E., et al. (2013). GOODS-Herschel: radio-excess signature of hidden

AGN activity in distant star-forming galaxies. *Astron. Astrophys.* 549:A59. doi: 10.1051/0004-6361/201219880

Di Matteo, T., Springel, V., and Hernquist, L. (2005). Energy input from quasars regulates the growth and activity of black holes and their host galaxies. *Nature* 433, 604–607. doi: 10.1038/nature03335

Elbaz, D., Dickinson, M., Hwang, H. S., Díaz-Santos, T., Magdis, G., Magnelli, B., et al. (2011). GOODS-Herschel: an infrared main sequence for star-forming galaxies. *Astron. Astrophys.* 533:A119. doi: 10.1051/0004-6361/201117239

Ferrarese, L., and Merritt, D. (2000). A fundamental relation between supermassive black holes and their host galaxies. *Astrophys. J. Lett.* 539, L9–L12. doi: 10.1086/312838

Fiore, F., Puccetti, S., Brusa, M., Salvato, M., Zamorani, G., Aldcroft, T., et al. (2009). Chasing highly obscured QSOs in the COSMOS field. *Astrophys. J.* 693, 447–462. doi: 10.1088/0004-637X/693/1/447

Gandhi, P., Horst, H., Smette, A., Hönig, S., Comastri, A., Gilli, R., et al. (2009). Resolving the mid-infrared cores of local Seyferts. *Astron. Astrophys.* 502, 457–472. doi: 10.1051/0004-6361/200811368

Gebhardt, K., Bender, R., Bower, G., Dressler, A., Faber, S. M., Filippenko, A. V., et al. (2000). A relationship between nuclear black hole mass and galaxy velocity dispersion. *Astrophys. J. Lett.* 539, L13–L16. doi: 10.1086/312840

Giavalisco, M., Ferguson, H. C., Koekemoer, A. M., Dickinson, M., Alexander, D. M., Bauer, F. E., et al. (2004). The great observatories origins deep survey: initial results from optical and near-infrared imaging. *Astrophys. J. Lett.* 600, L93–L98. doi: 10.1086/379232

Grogin, N. A., Kocevski, D. D., Faber, S. M., Ferguson, H. C., Koekemoer, A. M., Riess, A. G., et al. (2011). CANDELS: the cosmic assembly near-infrared deep extragalactic legacy survey. *Astrophys. J. Suppl.* 197:35. doi: 10.1088/0067-0049/197/2/35

Hopkins, P. F., Hernquist, L., Cox, T. J., Di Matteo, T., Robertson, B., and Springel, V. (2006). A unified, merger-driven model of the origin of starbursts, quasars, the cosmic X-ray background, supermassive black holes, and galaxy spheroids. *Astrophys. J. Suppl.* 163, 1–49. doi: 10.1086/499298

Kaplan, E. L., and Meier, P. (1958). Nonparametric estimation from incomplete observations. *J. Am. Stat. Assoc.* 53, 457–481. doi: 10.1080/01621459.1958.10501452

Kartaltepe, J. S., Sanders, D. B., Scoville, N. Z., Calzetti, D., Capak, P., Koekemoer, A., et al. (2007). Evolution of the frequency of luminous ($>=L^*_V$) close galaxy pairs at $z < 1.2$ in the COSMOS field. *Astrophys. J. Suppl.* 172, 320–328. doi: 10.1086/519953

Kennicutt, R. C. Jr. (1998). Star formation in galaxies along the hubble sequence. *Annu. Rev. Astron. Astrophys.* 36, 189–232. doi: 10.1146/annurev.astro.36.1.189

Kocevski, D. D., Brightman, M., Nandra, K., Koekemoer, A. M., Salvato, M., Aird, J., et al. (2015). Are compton-thick AGNs the missing link between mergers and black hole growth? *Astrophys. J.* 814:104. doi: 10.1088/0004-637X/814/2/104

Kocevski, D. D., Faber, S. M., Mozena, M., Koekemoer, A. M., Nandra, K., Rangel, C., et al. (2012). CANDELS: constraining the AGN-Merger connection with host morphologies at $z \sim 2$. *Astrophys. J.* 744:148. doi: 10.1088/0004-637X/744/2/148

Kormendy, J., and Ho, L. C. (2013). Coevolution (or not) of supermassive black holes and host galaxies. *Annu. Rev. Astron. Astrophys.* 51, 511–653. doi: 10.1146/annurev-astro-082708-101811

Kormendy, J., and Richstone, D. (1995). Inward bound—the search for supermassive black holes in galactic nuclei. *Annu. Rev. Astron. Astrophys.* 33:581.

Lotz, J. M., Jonsson, P., Cox, T. J., and Primack, J. R. (2010). The effect of mass ratio on the morphology and time-scales of disc galaxy mergers. *Month. Notices R. Astron. Soc.* 404, 575–589. doi: 10.1111/j.1365-2966.2010.16268.x

Luo, B., Bauer, F. E., Brandt, W. N., Alexander, D. M., Lehmer, B. D., Schneider, D. P., et al. (2008). The chandra deep field-south survey: 2 ms source catalogs. *Astrophys. J. Suppl.* 179, 19–36. doi: 10.1086/591248

Luo, B., Brandt, W. N., Xue, Y. Q., Lehmer, B., Alexander, D. M., Bauer, F. E., et al. (2017). The chandra deep field-south survey: 7 ms source catalogs. *Astrophys. J. Suppl.* 228:2. doi: 10.3847/1538-4365/228/1/2

Lutz, D., Maiolino, R., Spoon, H. W. W., and Moorwood, A. F. M. (2004). The relation between AGN hard X-ray emission and mid-infrared continuum from ISO spectra: scatter and unification aspects. *Astron. Astrophys.* 418, 465–473. doi: 10.1051/0004-6361:20035838

Madau, P., Ferguson, H. C., Dickinson, M. E., Giavalisco, M., Steidel, C. C., and Fruchter, A. (1996). High-redshift galaxies in the Hubble Deep Field: colour selection and star formation history to z˜4. *Month. Notices R. Astron. Soc.* 283, 1388–1404. doi: 10.1093/mnras/283.4.1388

Magorrian, J., Tremaine, S., Richstone, D., Bender, R., Bower, G., Dressler, A., et al. (1998). The demography of massive dark objects in galaxy centers. *Astron. J.* 115, 2285–2305. doi: 10.1086/300353

Mullaney, J. R., Alexander, D. M., Goulding, A. D., and Hickox, R. C. (2011). Defining the intrinsic AGN infrared spectral energy distribution and measuring its contribution to the infrared output of composite galaxies. *Month. Notices R. Astron. Soc.* 414, 1082–1110. doi: 10.1111/j.1365-2966.2011.18448.x

Ricci, C., Bauer, F. E., Treister, E., Schawinski, K., Privon, G. C., Blecha, L., et al. (2017). Growing supermassive black holes in the late stages of galaxy mergers are heavily obscured. *Month. Notices R. Astron. Soc.* 468, 1273–1299. doi: 10.1093/mnras/stx173

Rosario, D. J., Santini, P., Lutz, D., Shao, L., Maiolino, R., Alexander, D. M., et al. (2012). The mean star formation rate of X-ray selected active galaxies and its evolution from $z \sim 2.5$: results from PEP-Herschel. *Astron. Astrophys.* 545:A45. doi: 10.1051/0004-6361/201219258

Rovilos, E., Comastri, A., Gilli, R., Georgantopoulos, I., Ranalli, P., Vignali, C., et al. (2012). GOODS-Herschel: ultra-deep XMM-Newton observations reveal AGN/star-formation connection. *Astron. Astrophys.* 546:A58. doi: 10.1051/0004-6361/201218952

Salpeter, E. E. (1955). The luminosity function and stellar evolution. *Astrophys. J.* 121:161.

Stanley, F., Harrison, C. M., Alexander, D. M., Swinbank, A. M., Aird, J. A., Del Moro, A., et al. (2015). A remarkably flat relationship between the average star formation rate and AGN luminosity for distant X-ray AGN. *Month. Notices R. Astron. Soc.* 453, 591–604. doi: 10.1093/mnras/stv1678

Treister, E., and Urry, C. M. (2006). The evolution of obscuration in active galactic nuclei. *Astrophys. J. Lett.* 652, L79–L82. doi: 10.1086/510237

Xue, Y. Q., Luo, B., Brandt, W. N., Bauer, F. E., Lehmer, B. D., Broos, P. S., et al. (2011). The chandra deep field-south survey: 4 ms source catalogs. *Astrophys. J. Suppl.* 195:10. doi: 10.1088/0067-0049/195/1/10

Yaqoob, T. (1997). X-ray transmission in cold matter: nonrelativistic corrections for compton scattering. *Astrophys. J.* 479, 184–189. doi: 10.1086/303843

Conflict of Interest Statement: The authors declare that the research was conducted in the absence of any commercial or financial relationships that could be construed as a potential conflict of interest.

Copyright © 2018 Del Moro, Alexander, Bauer, Daddi, Kocevski, Stanley and McIntosh. This is an open-access article distributed under the terms of the Creative Commons Attribution License (CC BY). The use, distribution or reproduction in other forums is permitted, provided the original author(s) or licensor are credited and that the original publication in this journal is cited, in accordance with accepted academic practice. No use, distribution or reproduction is permitted which does not comply with these terms.

frontiers in Astronomy and Space Sciences

PERSPECTIVE
published: 24 October 2017
doi: 10.3389/fspas.2017.00027

Extended Narrow-Line Region in Seyfert Galaxies

Enrico Congiu[1,2], Marcella Contini[3], Stefano Ciroi[1], Valentina Cracco[1], Francesco Di Mille[4], Marco Berton[1,2], Michele Frezzato[1], Giovanni La Mura[1] and Piero Rafanelli[1]*

[1] Dipartimento di Fisica e Astronomia "G. Galilei", Università di Padova, Padova, Italy, [2] Astronomical Observatory of Brera, National Institute for Astrophysics, Milan, Italy, [3] School of Physics and Astronomy, Tel Aviv University, Tel Aviv, Israel, [4] Las Campanas Observatory, La Serena, Chile

We present our recent results about the extended narrow-line region (ENLR) of two nearby Seyfert 2 galaxies (IC 5063 and NGC 7212) obtained by modeling the observed line profiles and spectra with composite models (photoionization+shocks) in the different regions surrounding the AGN. Then, we compare the Seyfert 2 ENLRs with the very extended one recently discovered in the narrow-line Seyfert 1 (NLS1) galaxy Mrk 783. We have found several evidences of interaction between the ISM of the galaxies and their radio jets, such as (a) the contribution of shocks in ionizing the high velocity gas, (b) the complex kinematics showed by the profile of the emission lines, (c) the high fragmentation of matter, etc. The results suggest that the ENLR of IC 5063 have a hollow bi-conical shape, with one edge aligned to the galaxy disk, which may cause some kind of dependence on velocity of the ionization parameter. Regarding the Mrk 783 properties, it is found that the extension of the optical emission is almost twice the size of the radio one and it seems due to the AGN activity, although there is contamination by star formation around 12 arcsec from the nucleus. Diagnostic diagrams excluded the contribution of star formation in IC 5063 and NGC 7212, while the shock contribution was used to explain the spectra emitted by their high velocity gas.

Keywords: active galactic nuclei, Seyfert galaxies, emission lines, extended narrow-line region, IC 5063, NGC 7212, Mrk 783

OPEN ACCESS

Edited by:
Deborah Dultzin, National Autonomous University of Mexico, Mexico

Reviewed by:
Alenka Negrete, National Autonomous University of Mexico, Mexico
Mirjana Povic, Ethiopian Space Science and Technology Institute (ESSTI), Ethiopia

****Correspondence:***
Enrico Congiu
enrico.congiu@phd.unipd.it

Specialty section:
This article was submitted to Milky Way and Galaxies, a section of the journal Frontiers in Astronomy and Space Sciences

Received: *28 July 2017*
Accepted: *02 October 2017*
Published: *24 October 2017*

Citation:
Congiu E, Contini M, Ciroi S, Cracco V, Di Mille F, Berton M, Frezzato M, La Mura G and Rafanelli P (2017) Extended Narrow-Line Region in Seyfert Galaxies. Front. Astron. Space Sci. 4:27. doi: 10.3389/fspas.2017.00027

1. INTRODUCTION

The extended narrow-line region (ENLR) is one of the most intriguing structures which characterize active galactic nuclei (AGN). Predicted by the unified model (Antonucci and Miller, 1985; Antonucci, 1993), the ENLR is a region of highly ionized gas which is probably produced by the ionizing radiation escaping the AGN along the axis of the dusty torus. It is characterized by strong and narrow optical emission lines, both permitted and forbidden, similar to those emitted from the narrow-line region (NLR)[1], which usually can be traced up to few kiloparsecs from the nucleus. However, in some cases, the strongest lines (e.g., [O III]λ5007) can be traced up to ∼20 kpc or more (Mulchaey et al., 1994; Schmitt et al., 2003a).

[1] We consider the ENLR the natural extension of the NLR over ∼1 kpc.

The ENLR is often characterized by a conical or bi-conical shape whose apexes are pointing toward the active nucleus. In these cases it can be referred to as *ionization cones*. They are usually observed in nearby Seyfert 2 galaxies, but only a few tens of them are known and well studied (∼50 at $z < 0.05$, Netzer, 2015). ENLRs are also observed in Seyfert 1 galaxies, but because of the origin of the ionizing radiation, they are expected to be smaller and halo-like (not conical) (Evans et al., 1993; Schmitt et al., 2003a,b). Although this is true for most Seyfert 1, some exceptions, such as NGC 4151, show a conical ENLR (Pogge, 1989). Mulchaey et al. (1996), showed that the ENLR shape is not only determined by the orientation of the AGN, but it strongly depends on the gas distribution throughout the galaxy. The ENLR gas is usually considered as the host galaxy gas ionized by the AGN, but in some objects, e.g., NGC 4388 (Ciroi et al., 2003), Mrk 315 (Ciroi et al., 2005), NGC 7212 (Cracco et al., 2011), merging with small gas rich galaxies could provide a new gas supply. The fast outflows observed in several galaxies (e.g., Baldwin et al., 1987; Dasyra et al., 2015; Morganti et al., 2015) could also be an important source of gas.

A peculiar characteristic of the ENLR consists in its complex kinematics. Emission lines with multiple peaks and asymmetries are observed in several objects (e.g., Dietrich and Wagner, 1998; Morganti et al., 2007; Ozaki, 2009; Cracco et al., 2011; Congiu et al., 2017b) and high resolution images (Schmitt et al., 2003a) indicate that the gas is concentrated in filaments and cloud substructures. Mergers and outflows could be responsible for this kind of kinematics, likewise the interaction between the galaxy interstellar medium (ISM) and the AGN radio jet. The ionization cone axis is often aligned with that of the galaxy radio emission (Wilson and Tsvetanov, 1994; Nagar et al., 1999; Schmitt et al., 2003a,b) and strong outflows in all the gas phases are observed near radio hotspots (Morganti et al., 1998, 2007, 2015).

To have a better insight of the ENLR gas properties, we have studied high resolution spectra of two nearby Seyfert 2 galaxies with ENLR: IC 5063 and NGC 7212 (Congiu et al., 2017b). In sections 2 and 3 we summarize the main results of that work, while in section 4 we compare them with the ENLR in Mrk 783, a narrow-line Seyfert 1 (NLS1) galaxy with a recently discovered extended radio emission (Congiu et al., 2017a).

2. SAMPLE AND OBSERVATIONS

IC 5063 and NGC 7212 , two Seyfert 2 galaxies with well known ENLR were the targets of our observations. IC 5063 is a lenticular galaxy ($z = 0.01135$) characterized by a complex system of dust lanes, aligned with the major axis of the galaxy and by a very bright radio source (Morganti et al., 1998). The galaxy shows fast outflows in all the gas phases, from cold molecular gas to warm ISM (Morganti et al., 1998, 2007; Tadhunter et al., 2014; Dasyra et al., 2015; Morganti et al., 2015). Its ENLR was first discovered by Colina et al. (1991). NGC 7212 is a spiral galaxy ($z = 0.02663$) interacting with other two galaxies of its group (e.g., Wasilewski, 1981). The ENLR was first discovered in polarized light by Tran (1995) then Falcke et al. (1998) found an extended NLR also in non-polarized light. Cracco et al. (2011) confirmed the presence of ionization cones on both sides of the galaxy. The targets were observed with the MagE (Magellan echellette) spectrograph of the Magellan telescopes of Las Campanas Observatory. The instrument covers the whole optical spectrum (3,100–10,000 Å) with a resolution R ∼8,000 (Marshall et al., 2008). All the data needed for reduction and calibration process were also acquired. The data reduction process is described in details in Congiu et al. (2017b).

3. GAS PROPERTIES AS A FUNCTION OF VELOCITY

We analyzed the high resolution spectra of the ENLR because they allow to understand the complex profiles of the emission lines. Moreover, (see Ozaki, 2009) it is possible to study the properties of the gas clouds as a function of velocity. Ozaki (2009) divided the profile of few important emission lines in velocity bins, according to the peculiarities of the profile, and he analyzed the gas properties in these bins by means of line ratios and photo-ionization simulations. We applied his method to our spectra of IC 5063 and NGC 7212 increasing the number of studied lines, uniforming the width of the velocity bins to 100 km s^{-1} and reproducing the observed spectra with composite models[2] calculated by the code SUMA (Contini et al., 2002). We divided the two-dimensional spectra in several regions, to study the behavior of the gas properties as a function of the distance from the nucleus. The complete data analysis is shown in Congiu et al. (2017b). With this method we were able to produce diagnostic diagrams and several plots of the principal gas properties as a function of velocity for each examined region.

The analysis of the emission line profiles confirmed that the kinematics of the analyzed gas is complex and that the emission lines are often composed by several components which strongly vary from region to region while the profiles observed in the same region are mostly constant. The variations in some cases occur because the physical conditions and the ion fractional abundances change moving from region to region. To study the ionization mechanism of the gas we compared the result of four different diagnostic diagrams. Three of them are the classical BPT diagrams from Baldwin et al. (1981) and Veilleux and Osterbrock (1987) (log([O III]/Hβ vs. log([N II]/Hα), log([S II]/Hα), log([O I]/Hα)) while the last one is a combination of the previous ratios with [O II]λ3727/[O III]λ5007, which is able to discern between photo-ionization by a power-law, star formation or ionization by shocks (ΔE diagram, Baldwin et al., 1981). All the diagnostic diagrams show that the main ionization mechanism of the gas is photo-ionization by the AGN. There is no substantial contamination by star formation in any of our spectra. However, the high velocity gas often show low log([OIII]/Hβ) and high ratios of low ionization lines to Hα, shifting their points toward the LINER region of the BPT diagrams and the shock region of the ΔE diagram (Figure 6, Congiu et al., 2017b). This should be interpreted as a strong contribution of shocks to the ionization of high velocity gas.

[2]SUMA models consider both photo-ionization and shocks at the same time to reproduce the line ratios of the analyzed spectrum.

Shocks are most likely created by the interaction of the AGN jets with the galaxy ISM. The results of composite models confirm this hypothesis. The ratios of the low ionization lines to Hβ in the high velocity bins can be reproduced accurately only adopting shocks with velocities comparable with the velocity of the gas, while the spectra of the low velocity bins can be reproduced using radiation dominated models.

The models also show that a wide range of cloud geometrical thicknesses is needed to reproduce the spectra. This is the result of cloud fragmentation in the turbulent regime created by the shocks which originate from the interaction of the jet with the ISM. According to Roche et al. (2016), this kind of interaction should increase the temperature of the gas. Indeed, this is observed in the nuclear regions of NGC 7212, the only regions of this object in which we were able to measure this quantity. Using the total flux of the lines, the galaxy show slightly higher temperatures than expected (∼15,000 K with respect to the expected 10,000 K; Osterbrock and Ferland, 2006). Adopting composite models, the temperature is maintained at 10,000–20,000 K by diffuse secondary radiation (e.g., Figure 10, Contini et al., 2012) in a large region within the clouds. The temperatures evaluated in IC 5063 are closer to 10,000 K.

Another interesting result is the behavior of the ionization parameter U as a function of velocity in IC 5063 (Figure 8, Congiu et al., 2017b). U (defined as the number of ionizing photons reaching the cloud per number of electrons in the gas) is usually used to estimate the ionization degree of the gas. We measured U for each velocity bin using the Penston et al. (1990) relation, which links U to the [O II]λ3727/[O III]λ5007 ratio. U is not expected to depend on the velocity of the gas, in fact for NGC 7212 it can be considered almost constant in all the velocity bins of the same region. However, for IC 5063 a clear dependence is noticed, similar to what observed by Ozaki (2009) in NGC 1068. Following his model, a possible explanation could be the orientation of the ionization cones with respect to the line of sight. This suggests that the ENLR has a hollow bi-conical shape with one edge lying on the galactic disk. This part of the cones is ionized by a partly absorbed flux leading to a lower ionization degree of the gas with respect to the side of the cone reached by the unabsorbed continuum.

Finally, by the detailed modeling of the spectra we obtained the metallicity of the gas. Previous results (e.g., Contini, 2017) show that most AGN and HII regions can be reproduced with solar metallicities. However, we tried to reproduce the spectra with several values of metallicity. The best results for all the regions and all the bins of the ionization cones could be obtained using abundances close to the Grevesse and Sauval (1998) solar ones in agreement with the results previously mentioned. Comparing our results with those obtained by modeling spectra observed outside the ionization cone, could be a way to study the origin of the gas. If a difference in metallicity is detected, the origin of the ENLR gas might be different from that of the galaxy.

4. COMPARISON WITH NLS1: MRK 783

The ENLR is often associated with extended radio emission, both in Seyfert 1 and Seyfert 2 galaxies. An extended radio emission with very steep in band spectral index was discovered in the NLS1 Mrk 783 (Congiu et al., 2017a). The optical follow-up of the source (Congiu et al., in preparation) shows an extended optical emission aligned to the radio axis. The observed spectrum has a spatial resolution of 0.189 arcsec px^{-1} and a dispersion of ∼2 Å px^{-1}. **Figure 1** shows the radio map of the object and the Hβ region of the acquired spectrum.

The [O III] and Hβ lines were tracked up to ∼27 arcsec from the nucleus of the galaxy (**Figure 1B**), which corresponds to a projected dimension of ∼35 kpc. This makes this ENLR one of the most extended discovered so far. Also Hα can be traced up to the same distance, while none of the other low ionization lines (e.g., [N II]$\lambda\lambda$6548, 6584, [S II]$\lambda\lambda$6717, 6731) can be detected in the most extended emission region (**Figure 2**, left panel). Due to the sharp end of the emission at the edge of the slit, it seems that the ENLR can extend even further. For comparison, the MagE spectra of IC 5063 and NGC 7212 do not cover the whole extension of the ionization cones, however Morganti et al. (2007) measured a maximum extension of ∼3.8 kpc in IC 5063 and Cracco et al. (2011) measured ∼4 kpc in NGC 7212. An ENLR with a similar size is observed in NGC 5252, which has a maximum extension of ∼33 kpc (Tadhunter and Tsvetanov, 1989).

It is also worth noting that the optical emission is far more extended with respect to the radio one and that it is observed only on the south-east side of the nucleus, while in our other sources the ionization cones are observed on both sides of the nucleus. This is probably the consequence of a strong extinction or of a lack of gas in the north-west side of the nucleus. There is also a region between the nucleus and the most extended emission, from ∼12 to ∼ 22 arcsec (∼ 16–28 kpc), where we cannot trace any emission line. However, we exclude that the extended emission could belong to another object, because its redshift is compatible with the rotation curve of the galaxy derived from the central region of the spectrum. Moreover, both optical and radio images do not show any close object bright enough to produce such an emission. The apparent separation is probably due to the lack of gas in that region of the galaxy. Such kind of structure is not observed neither in NGC 7212 nor in IC 5063. Deep images with narrow-band filters are needed to understand the complete morphology of the emission.

An exam of the Hβ region of the spectrum extracted at 27 arcsec from the nucleus (**Figure 1C**), seems to indicate that the [O III]/Hβ ratio is higher with respect to what expected for star forming regions. Therefore, a preliminary diagnostic diagram (Baldwin et al., 1981; Veilleux and Osterbrock, 1987) was assembled (**Figure 2**, right panel) using only the narrow component of the broad lines (Hα and Hβ) and binning the spectrum in 3 px bins in the spatial direction to increase the signal-to-noise ratio (SNR). In some cases we could not measure some of the emission lines needed to the plot (typically Hβ and [N II]), so we estimated an upper limit for their flux using the rms of the continuum and the FWHM of the [O III] line. We used Kewley et al. (2006) relation to discern the ionization mechanism of the gas. The diagram in **Figure 2** (right panel) shows that most of the extended emission is photo-ionized by the AGN, particularly the most extended part, while closer to the nucleus there might be contamination by star formation.

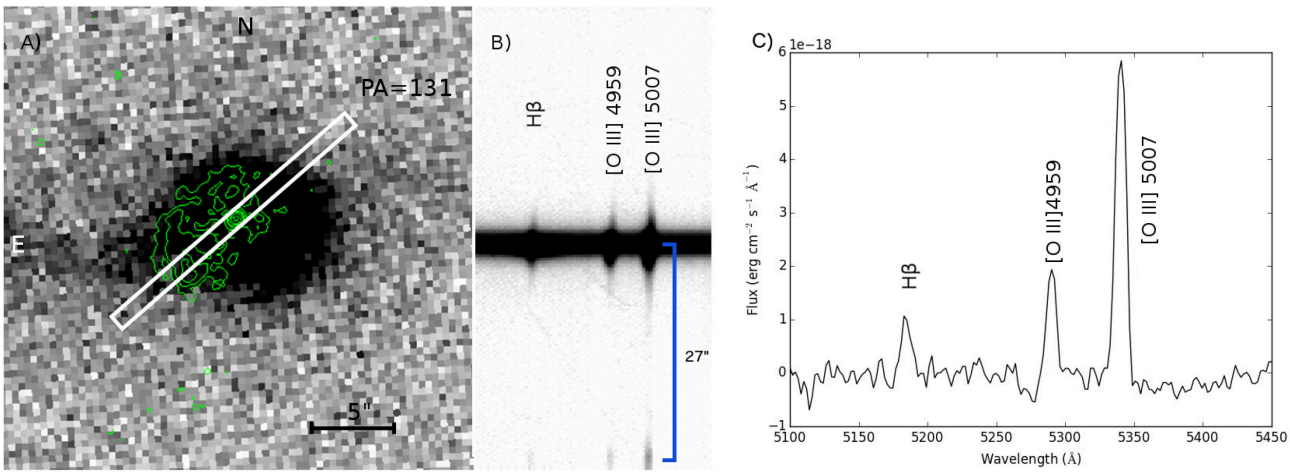

FIGURE 1 | From left to right: **(A)** SDSS g-band image of Mrk 783 with the contours of the emission at 5 GHz. The contours are 3, 6, 12, 24, 48, 96, and 192 × σ ($\sigma = 11\,\mu$Jy beam^{-1}). The beam size is 0.45 × 0.40 arcsec and the scale is 1.3 kpc arcsec^{-1}. The position of the slit used for the observations with the Magellan telescope is shown. The galaxy is characterized by a radio emission with a maximum extension of ∼5 arcsec on the south-east side of the nucleus (Congiu et al., 2017a). **(B)** A small region of the LDSS3 spectra of Mrk 783 containing three emission lines: Hβ, [O III]λ4959 and [O III]λ5007. The data were acquired with a total exposure time of 1 h, with a seeing of 0.8 arcsec and the slit oriented as in **(A)**. The spatial resolution is 0.189 arcsec px^{-1} and the dispersion is ∼ 2 Å px^{-1} . **(C)** Plot of the spectrum in **(B)** at 27 arcsec from the galactic nucleus.

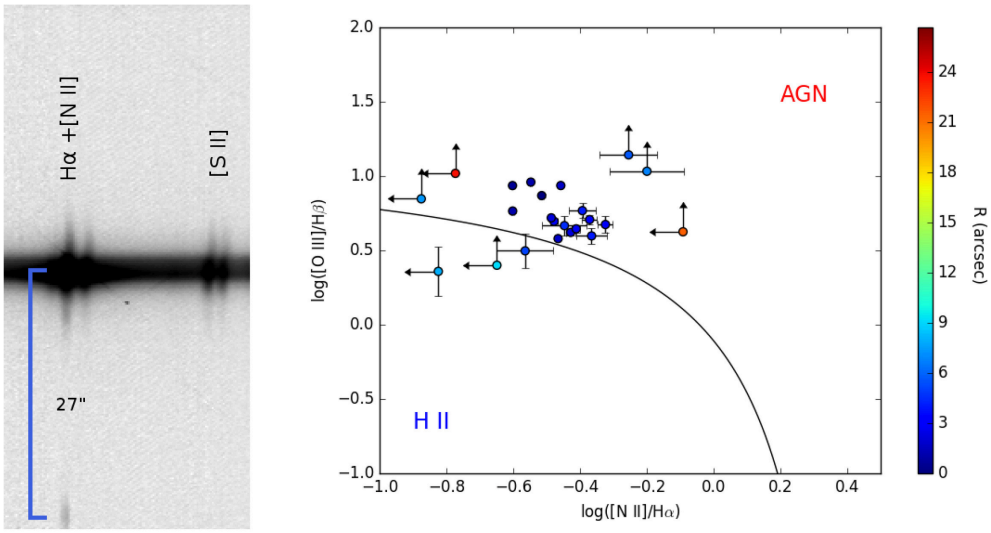

FIGURE 2 | Left: Hα region of the same spectrum in **Figure 1B**. **Right:** Preliminary diagnostic diagram of the ENLR of Mrk 783. The colorbar show the distance of the bin from the nucleus. The black line dividing the plot in two regions is the relation from Kewley et al. (2006) for extreme starburst. The arrows show the limit derived where we could not measure all the emission line.

Interestingly, star contamination is excluded in both the other galaxies presented in this paper. Additional higher quality observations are needed to study the ENLR in NLS1 in general and Mrk 783 in details.

5. SUMMARY

We report the main results of our recent work on the ENLR of nearby AGN. We used high resolution spectra of two nearby Seyfert 2 galaxies, together with combined models of photo-ionization and shocks to study the properties of the gas, in general, and as function of velocity in the different galaxy regions, in particular. We found several evidences of interaction between the ISM of the galaxies and their radio jets, such as (a) the contribution of shocks in ionizing the high velocity gas, (b) the complex kinematics showed by the profile of the emission lines, (c) the high fragmentation of matter, etc. The results show that the ENLR of IC 5063 most likely has a hollow bi-conical shape,

with one edge aligned with the galaxy disk. This may explain the velocity dependence of the ionization parameter observed in this galaxy.

We then compared the ENLR of our two galaxies with the preliminary results of the analysis of a newly discovered ENLR in a NLS1 galaxy: Mrk 783. The object shows an extended optical emission aligned with the radio emission first observed by Congiu et al. (2017a). The extension of the optical emission is almost twice the size of the radio emission which seems mainly due to the AGN activity, even though there is contamination by star formation around 12 arcsec from the nucleus. While star contamination was excluded by the diagnostic diagrams both in IC 5963 and NGC 7212 and shock contribution was used to explain the spectra of high velocity gas, it seems that in Mrk 783 there might be a significant contribution of star formation to the extended optical emission.

Further detailed observations of ENLRs will be crucial to investigate the still poorly understood feedback between AGN and host galaxy, and to understand the effects of relativistic jets on their surrounding environment.

AUTHOR CONTRIBUTIONS

EC was responsible for most of the data reduction, data analysis and the text. MC produced all the simulations and contributed to part of the text. SC and VC contributed to the main idea of the paper and the data analysis. FD observed all the target with the Magellan telescopes and with the review of the final text. MB, MF, GL, and PR contributed with the data reduction and analysis and with the review of the final text.

ACKNOWLEDGMENTS

This research has made use of the NASA/IPAC Extragalactic Database (NED) which is operated by the Jet Propulsion Laboratory, California Institute of Technology, under contract with the National Aeronautics and Space Administration. This paper includes data gathered with the 6.5-m Magellan Telescopes located at Las Campanas Observatory, Chile. This paper is based on observations collected with the 1.22 m Galileo telescope of the Asiago Astrophysical Observatory, operated by the Department of Physics and Astronomy "G. Galilei" of the University of Padova. Funding for the Sloan Digital Sky Survey has been provided by the Alfred P. Sloan Foundation, and the U.S. Department of Energy Office of Science. The SDSS web site is http://www.sdss.org. SDSS-III is managed by the Astrophysical Research Consortium for the Participating Institutions of the SDSS-III Collaboration including the University of Arizona, the Brazilian Participation Group, Brookhaven National Laboratory, Carnegie Mellon University, University of Florida, the French Participation Group, the German Participation Group, Harvard University, the Instituto de Astrofisica de Canarias, the Michigan State/Notre Dame/JINA Participation Group, Johns Hopkins University, Lawrence Berkeley National Laboratory, Max Planck Institute for Astrophysics, Max Planck Institute for Extraterrestrial Physics, New Mexico State University, University of Portsmouth, Princeton University, the Spanish Participation Group, University of Tokyo, University of Utah, Vanderbilt University, University of Virginia, University of Washington, and Yale University.

REFERENCES

Antonucci, R. (1993). Unified models for active galactic nuclei and quasars. *Ann. Rev. Astron. Astrophys.* 31, 473–521. doi: 10.1146/annurev.aa.31.090193.002353

Antonucci, R. R. J., and Miller, J. S. (1985). Spectropolarimetry and the nature of NGC 1068. *Astrophys. J.* 297, 621–632. doi: 10.1086/163559

Baldwin, J. A., Phillips, M. M., and Terlevich, R. (1981). Classification parameters for the emission-line spectra of extragalactic objects. *Publ. ASP* 93, 5–19. doi: 10.1086/130766

Baldwin, J. A., Wilson, A. S., and Whittle, M. (1987). Kinematics and ionization of extended gas in active galaxies. III—The extranuclear properties of NGC 1068. *Astrophys. J.* 319, 84–104. doi: 10.1086/165435

Ciroi, S., Afanasiev, V. L., Moiseev, A. V., Botte, V., Di Mille, F., Dodonov, S. N., et al. (2005). New photometric and spectroscopic observations of the Seyfert galaxy Mrk 315. *Month. Notices RAS* 360, 253–271. doi: 10.1111/j.1365-2966.2005.09031.x

Ciroi, S., Contini, M., Rafanelli, P., and Richter, G. M. (2003). 2-D spectroscopy and modeling of the biconical ionized gas in NGC 4388. *Astron. Astrophys.* 400, 859–870. doi: 10.1051/0004-6361:20030008

Colina, L., Sparks, W. B., and Macchetto, F. (1991). IC 5063—A merger remnant with a hidden luminous active nucleus. *Astrophys. J.* 370, 102–117. doi: 10.1086/169795

Congiu, E., Berton, M., Giroletti, M., Antonucci, R., Caccianiga, A., Kharb, P., et al. (2017a). Kiloparsec-scale emission in the narrow-line Seyfert 1 galaxy Mrk 783. *Astron. Astrophys.* 603:A32. doi: 10.1051/0004-6361/201730616

Congiu, E., Contini, M., Ciroi, S., Cracco, V., Berton, M., Di Mille, F., et al. (2017b). High resolution spectroscopy of the extended narrow-line region of IC 5063 and NGC 7212. ArXiv e-prints.

Contini, M. (2017). N/O abundance ratios in gamma-ray burst and supernova host galaxies at z<4. Comparison with AGN, starburst and HII regions. ArXiv e-prints.

Contini, M., Cracco, V., Ciroi, S., and La Mura, G. (2012). Distribution of the heavy elements throughout the extended narrow-line region of the Seyfert galaxy NGC 7212. *Astron. Astrophys.* 545:A72. doi: 10.1051/0004-6361/201219184

Contini, M., Viegas, S. M., and Prieto, M. A. (2002). The signature of high-velocity gas in the spectra of NGC 4151. *Astron. Astrophys.* 386, 399–414. doi: 10.1051/0004-6361:20020245

Cracco, V., Ciroi, S., di Mille, F., Vaona, L., Frassati, A., Smirnova, A. A., et al. (2011). The origin of gas in extended narrow-line regions of nearby Seyfert galaxies—I. NGC 7212. *Month. Notices RAS* 418, 2630–2641. doi: 10.1111/j.1365-2966.2011.19654.x

Dasyra, K. M., Bostrom, A. C., Combes, F., and Vlahakis, N. (2015). A radio jet drives a molecular and atomic gas outflow in multiple regions within one square kiloparsec of the nucleus of the nearby galaxy IC5063. *Astrophys. J.* 815:34. doi: 10.1088/0004-637X/815/1/34

Dietrich, M., and Wagner, S. J. (1998). Kinematics of the narrow-line region of NGC 1068. *Astron. Astrophys.* 338, 405–412.

Evans, I. N., Tsvetanov, Z., Kriss, G. A., Ford, H. C., Caganoff, S., and Koratkar, A. P. (1993). Hubble space telescope imaging of the narrow-line region of NGC 4151. *Astrophys. J.* 417:82. doi: 10.1086/173292

Falcke, H., Wilson, A. S., and Simpson, C. (1998). Hubble space telescope and VLA observations of seyfert 2 galaxies: the relationship between radio ejecta and the narrow-line region. *Astrophys. J.* 502, 199–217. doi: 10.1086/305886

Grevesse, N., and Sauval, A. J. (1998). Standard solar composition. *Space Sci. Rev.* 85, 161–174. doi: 10.1023/A:1005161325181

Kewley, L. J., Groves, B., Kauffmann, G., and Heckman, T. (2006). The host galaxies and classification of active galactic nuclei. *Month. Notices RAS* 372, 961–976. doi: 10.1111/j.1365-2966.2006.10859.x

Marshall, J. L., Burles, S., Thompson, I. B., Shectman, S. A., and Bigelow, B. C., Burley, G. et al. (2008). "The MagE spectrograph," in *Ground-based and Airborne Instrumentation for Astronomy II, SPIE conference Proc. 7014*, (Marseille).

Morganti, R., Holt, J., Saripalli, L., Oosterloo, T. A., and Tadhunter, C. N. (2007). IC 5063: AGN driven outflow of warm and cold gas. *Astron. Astrophys.* 476, 735–743. doi: 10.1051/0004-6361:20077888

Morganti, R., Oosterloo, T., Oonk, J. B. R., Frieswijk, W., and Tadhunter, C. (2015). The fast molecular outflow in the Seyfert galaxy IC 5063 as seen by ALMA. *Astron. Astrophys.* 580:A1. doi: 10.1051/0004-6361/201525860

Morganti, R., Oosterloo, T., and Tsvetanov, Z. (1998). A radio study of the seyfert galaxy IC 5063: evidence for fast gas outflow. *Astron. J.* 115, 915–927. doi: 10.1086/300236

Mulchaey, J. S., Wilson, A. S., Bower, G. A., Heckman, T. M., Krolik, J. H., and Miley, G. K. (1994). Hubble space telescope imaging of the Seyfert 2 galaxy NGC 2110. *Astrophys. J.* 433, 625–630. doi: 10.1086/174671

Mulchaey, J. S., Wilson, A. S., and Tsvetanov, Z. (1996). An emission-line imaging survey of early-type seyfert galaxies. II. Implications for unified schemes. *Astrophys. J.* 467:197. doi: 10.1086/177595

Nagar, N. M., Wilson, A. S., Mulchaey, J. S., and Gallimore, J. F. (1999). Radio structures of seyfert galaxies. VIII. A distance- and magnitude-limited sample of early-type galaxies. *Astrophys. J. Suppl.* 120, 209–245. doi: 10.1086/313183

Netzer, H. (2015). Revisiting the unified model of active galactic nuclei. *Ann. Rev. Astron. Astrophys.* 53, 365–408. doi: 10.1146/annurev-astro-082214-122302

Osterbrock, D. E., and Ferland, G. J. (2006). "Astrophysics of gaseous nebulae and active galactic nuclei," in *Astrophysics of Gaseous Nebulae and Active Galactic Nuclei, 2nd Edn.*, eds D. E. Osterbrock and G. J. Ferland. (Sausalito, CA: University Science Books). Available online at: http://adsabs.harvard.edu/abs/2006agna.book.....O

Ozaki, S. (2009). Kinematic and excitation structure of the NGC 1068 narrow-line region. *Publ. ASJ* 61:259. doi: 10.1093/pasj/61.2.259

Penston, M. V., Robinson, A., Alloin, D., Appenzeller, I., Aretxaga, I., Axon, D. J., et al. (1990). The extended narrow line region of NGC 4151. I - Emission line ratios and their implications. *Astron. Astrophys.* 236, 53–62.

Pogge, R. W. (1989). The circumnuclear environment of nearby, noninteracting Seyfert galaxies. *Astrophys. J.* 345, 730–751. doi: 10.1086/167945

Roche, N., Humphrey, A., Lagos, P., Papaderos, P., Silva, M., Cardoso, L. S. M., et al. (2016). MUSE three-dimensional spectroscopy and kinematics of the gigahertz peaked spectrum radio galaxy PKS 1934-63: interaction, recently triggered active galactic nucleus and star formation. *Month. Notices RAS* 459, 4259–4280. doi: 10.1093/mnras/stw765

Schmitt, H. R., Donley, J. L., Antonucci, R. R. J., Hutchings, J. B., and Kinney, A. L. (2003a). A hubble space telescope survey of extended [O III] λ5007 emission in a far-infrared selected sample of seyfert galaxies: observations. *Astrophys. J. Suppl.* 148, 327–352. doi: 10.1086/377440

Schmitt, H. R., Donley, J. L., Antonucci, R. R. J., Hutchings, J. B., Kinney, A. L., and Pringle, J. E. (2003b). A hubble space telescope survey of extended [O III] λ5007 Å emission in a far-infrared-selected sample of seyfert galaxies: results. *Astrophys. J.* 597, 768–779. doi: 10.1086/381224

Tadhunter, C., Morganti, R., Rose, M., Oonk, J. B. R., and Oosterloo, T. (2014). Jet acceleration of the fast molecular outflows in the Seyfert galaxy IC 5063. *Nature* 511, 440–443. doi: 10.1038/nature13520

Tadhunter, C., and Tsvetanov, Z. (1989). Anisotropic ionizing radiation in NGC5252. *Nature* 341, 422–424. doi: 10.1038/341422a0

Tran, H. D. (1995). The nature of seyfert 2 galaxies with obscured broad-line regions. II. Individual objects. *Astrophys. J.* 440:578. doi: 10.1086/175297

Veilleux, S., and Osterbrock, D. E. (1987). Spectral classification of emission-line galaxies. *Astrophys. J. Suppl.* 63, 295–310. doi: 10.1086/191166

Wasilewski, A. J. (1981). A new Seyfert galaxy with asymmetric forbidden-line profiles in an interacting system. *Publ. ASP* 93, 560–563. doi: 10.1086/130887

Wilson, A. S., and Tsvetanov, Z. I. (1994). Ionization cones and radio ejecta in active galaxies. *Astron. J.* 107, 1227–1234. doi: 10.1086/116935

Conflict of Interest Statement: The authors declare that the research was conducted in the absence of any commercial or financial relationships that could be construed as a potential conflict of interest.

The reviewer, AN, and handling Editor declared their shared affiliation.

Copyright © 2017 Congiu, Contini, Ciroi, Cracco, Di Mille, Berton, Frezzato, La Mura and Rafanelli. This is an open-access article distributed under the terms of the Creative Commons Attribution License (CC BY). The use, distribution or reproduction in other forums is permitted, provided the original author(s) or licensor are credited and that the original publication in this journal is cited, in accordance with accepted academic practice. No use, distribution or reproduction is permitted which does not comply with these terms.

frontiers in Astronomy and Space Sciences

PERSPECTIVE
published: 17 October 2017
doi: 10.3389/fspas.2017.00026

How Quasar Feedback May Shape the Co-evolutionary Paths

*Wako Ishibashi**

Physik-Institut, University of Zurich, Zürich, Switzerland

Observations point toward some form of "co-evolutionary sequence," from dust-enshrouded starbursts to luminous unobscured quasars. Active galactic nucleus (AGN) feedback is generally invoked to expel the obscuring dusty gas in a blow-out event, eventually revealing the hidden central quasar. However, the physical mechanism driving AGN feedback, either due to winds or radiation, remains uncertain and is still a source of much debate. We consider quasar feedback, based on radiation pressure on dust, which directly acts on the obscuring dusty gas. We show that AGN radiative feedback is capable of efficiently removing the obscuring cocoon, and driving powerful outflows on galactic scales, consistent with recent observations. I will discuss how such quasar feedback may provide a natural physical interpretation of the observed evolutionary path, and the physical implications in the broader context of black hole-host galaxy co-evolution.

Keywords: active galactic nuclei, quasars, feedback, starbursts, galaxies

OPEN ACCESS

Edited by:
Mauro D'Onofrio,
Università degli Studi di Padova, Italy

Reviewed by:
Francoise Combes,
Observatoire de Paris, France
Giulia Rodighiero,
Università degli Studi di Padova, Italy

Correspondence:
Wako Ishibashi
wako.ishibashi@physik.uzh.ch

Specialty section:
This article was submitted to Milky Way and Galaxies, a section of the journal Frontiers in Astronomy and Space Sciences

Received: *24 August 2017*
Accepted: *02 October 2017*
Published: *17 October 2017*

Citation:
Ishibashi W (2017) How Quasar Feedback May Shape the Co-evolutionary Paths. Front. Astron. Space Sci. 4:26. doi: 10.3389/fspas.2017.00026

1. INTRODUCTION

Active galactic nuclei (AGN) and nuclear starbursts are observed to be intimately coupled, both fueled by the rapid infall of matter, possibly triggered by galaxy mergers (e.g., Alexander and Hickox, 2012, and references therein). A "co-evolutionary sequence," starting from dust-obscured starbursts (e.g., ultraluminous infrared galaxies or ULIRG) leading to unobscured optical quasars, has been widely discussed since Sanders et al. (1988). In most evolutionary scenarios, some form of AGN feedback is required to expel the obscuring gas and dust in a short-lived "blow-out" event.

Numerical simulations try to reproduce such an evolutionary sequence, with AGN feedback usually implemented by coupling a fixed fraction of the accretion luminosity to the surrounding medium (Di Matteo et al., 2005; Hopkins et al., 2005). However, the physical mechanism for AGN feedback is not specified, and in particular no explicit connection is made with the dust component (which is the fundamental parameter determining both the source visibility and the spectral energy distribution). On the observational side, there has been renewed interest in the topic, following the discovery of new populations of dust-reddened quasars at high redshifts (close to the peak epoch of both AGN and starburst activities), likely caught in the short-lived blow-out phase (e.g., Banerji et al., 2012, 2015).

Here we propose a physical mechanism that directly makes use of the dust in order to drive AGN feedback, and we briefly discuss how such AGN radiative feedback may naturally explain the observed co-evolutionary path (Ishibashi and Fabian, 2016b).

2. AGN RADIATIVE FEEDBACK: RADIATION PRESSURE ON DUST

We consider AGN feedback driven by radiation pressure on dust. The ambient dusty gas is swept up into an outflowing shell, with the corresponding equation of motion given by:

$$\frac{d}{dt}[M_{sh}(r)v] = \frac{L}{c}(1 + \tau_{IR} - e^{-\tau_{UV}}) - \frac{GM(r)M_{sh}(r)}{r^2} \quad (1)$$

where L is the central luminosity, $M(r)$ is the total mass distribution, $M_{sh}(r)$ is the shell mass, and $\tau_{IR,UV}(r) = \frac{\kappa_{IR,UV} M_{sh}(r)}{4\pi r^2}$ are the infrared (IR) and ultraviolet (UV) optical depths (Ishibashi and Fabian, 2015; Thompson et al., 2015). We recall that there are 3 distinct physical regimes depending on the optical depth of the medium: optically thick to both IR and UV, optically thick to UV but optically thin to IR (single scattering limit), and optically thin to UV. The associated shell column density is defined as:

$$N_{sh}(r) = \frac{M_{sh}(r)}{4\pi r^2 m_p} \quad (2)$$

where m_p is the proton mass.

By equating the outward force due to radiation pressure to the inward force due to gravity, we can define a critical luminosity, $L_E^{'}$, which may be considered as a generalized form of the effective Eddington luminosity. We recall that the effective Eddington luminosity for dusty gas is distinct from the standard Eddington luminosity relevant for ionized gas (Fabian et al., 2006). The corresponding effective Eddington ratio is then given by:

$$\Gamma = \frac{L}{L_E^{'}} = \frac{Lr^2}{cGM(r)M_{sh}(r)}(1 + \tau_{IR} - e^{-\tau_{UV}}) \quad (3)$$

The effective Eddington ratios in the 3 optical depth regimes are respectively given by:

$$\Gamma_{IR} = \frac{\kappa_{IR} L}{4\pi GcM(r)}\ ;\ \Gamma_{SS} = \frac{L}{4\pi Gcm_p M(r) N_{sh}(r)}\ ;$$
$$\Gamma_{UV} = \frac{\kappa_{UV} L}{4\pi GcM(r)} \quad (4)$$

Figure 1 shows the effective Eddington ratio as a function of radius, and its dependence on the underlying physical parameters. The effective Eddington ratio basically corresponds to the ratio of the radiative force to the gravitational force, and must exceed unity for an outflowing shell (the standard Eddington limit does not apply here). From **Figure 1**, we see that an increase in the shell mass leads to a lower Eddington ratio in the single scattering regime (cyan curve); while in the IR-optically thick and UV-optically thin regimes, Γ_{IR} and Γ_{UV} are independent of the shell mass (cf. Equation 4), hence the cyan and black curves overlap at small and large radii. In contrast, enhanced opacities (e.g., due to a higher dust-to-gas ratio) lead to higher Eddington ratios in the IR-optically thick and UV-optically thin regimes (magenta curve); whereas in the single scattering regime, Γ_{SS} is independent of the opacity (cf. Equation 4), and thus the magenta and black curves overlap at intermediate radii. We note that there are two interesting trends in the IR-optically thick regime:

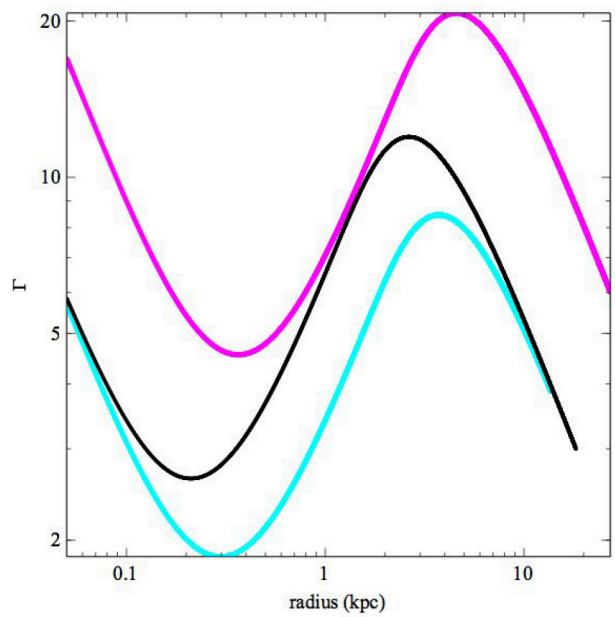

FIGURE 1 | Effective Eddington ratio as a function of radius: $L = 5\times 10^{46}$erg/s, $M_{sh} = 5 \times 10^8 M_\odot$, $f_{dg} = 1/150$ (black, fiducial); $L = 5 \times 10^{46}$erg/s, $M_{sh} = 1 \times 10^9 M_\odot$, $f_{dg} = 1/150$ (cyan); $L = 5 \times 10^{46}$erg/s, $M_{sh} = 5 \times 10^8 M_\odot$, $f_{dg} = 1/50$ (magenta).

1. The effective Eddington ratio is independent of the shell column density (or shell mass).
2. The effective Eddington ratio directly scales with the opacity, and hence dust-to-gas ratio (as $\kappa_{IR} \propto f_{dg}$).

The first point implies that even dense material can potentially be disrupted; while the second point implies that the more dusty gas is more easily ejected (Ishibashi and Fabian, 2016b).

3. DUST OBSCURATION AND BLOW-OUT

In physical terms, dusty gas surrounding the central source absorbs UV radiation and re-emits in the IR band. If the reprocessed IR photons remain trapped in the nuclear regions, the system is effectively in the IR-optically thick regime, where the Eddington ratio is independent of the column density (Equation 4). Such conditions are likely reached in the nuclear regions of ULIRG-like systems, characterized by high densities and high dust-to-gas fractions. This leads to both higher IR optical depth and higher IR-Eddington ratio, which combine to facilitate the blow-out of dusty gas.

In **Figure 2** (left panel) we plot the temporal evolution of the shell column density for different values of the central luminosity. We see that the obscuration falls off with time, with the decline being more rapid for brighter sources. In fact, an increase in the

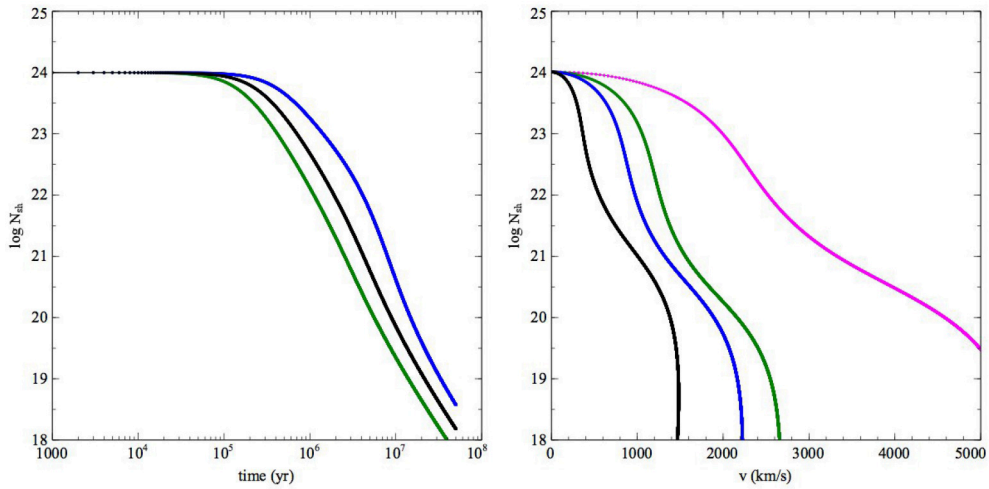

FIGURE 2 | Left: shell column density vs. time for variations in luminosity ($N_{sh,0} = 10^{24}\text{cm}^{-2}$, $f_{dg} = 1/150$): $L = 3 \times 10^{46}$erg/s (blue), $L = 5 \times 10^{46}$erg/s (black), $L = 1 \times 10^{47}$erg/s (green). **Right:** shell column density vs. velocity for variations in the dust-to-gas ratio ($L = 2 \times 10^{46}$erg/s, $N_{sh,0} = 10^{24}\text{cm}^{-2}$): $f_{dg} = 1/150$ (black), $f_{dg} = 1/50$ (blue), $f_{dg} = 1/30$ (green). High-luminosity case: $L = 10^{47}$erg/s, $f_{dg} = 1/50$ (magenta).

luminosity leads to an increase in the effective Eddington ratio in all 3 optical depth regimes, and thus efficient acceleration, and resulting high velocity. The right panel in **Figure 2** shows the shell column density as a function of velocity for different values of the dust-to-gas ratio. We observe that a given column is accelerated to higher velocities for larger dust-to-gas fractions: at a given time, the column density is lower for higher dust-to-gas ratios. Indeed, an increase in the dust-to-gas ratio leads to enhanced IR opacity, which in turn leads to a higher Eddington ratio in the IR-optically thick regime. Thus the more dusty gas (which provides much of the obscuration) is preferentially ejected by radiative feedback, and therefore the central quasar has a natural tendency to remove its own obscuring cocoon and reveal itself. We have previously discussed how such AGN-driven dusty outflows may propagate on larger scales beyond the host galaxy, and contribute to the enrichment of the circum-galactic medium (Ishibashi and Fabian, 2016a).

The model results can be compared with observational samples of the recently uncovered populations of dust-reddened quasars and dust-obscured galaxies (Assef et al., 2015; Banerji et al., 2015; Zakamska et al., 2016). These sources are likely observed close to the point of ejecting their obscuring cocoon, and thus may represent the long-sought "sources in transition" (as discussed in Ishibashi and Fabian, 2016b).

4. THE DUAL ROLE OF DUST: HIDING AND REVEALING THE CENTRAL QUASAR

The large amounts of gas and dust surrounding the nuclear source provide potential fuel for the central black hole, but that same accreting material is also responsible for significant obscuration. Although AGN feedback is generally invoked to clear the obscuring gas and dust in co-evolutionary scenarios, the actual physical mechanism remains uncertain, with no clear connection to the dust component. In our picture, AGN radiative feedback directly acts on the dusty gas, which forms the obscuring medium. Large amounts of dust imply heavy obscuration, but also powerful feedback, suggesting a causal link between dust obscuration and blow-out. In this scenario, dust plays a dual role: it is responsible for both hiding, but eventually revealing the central quasar.

An important requirement in our model is the presence of dust, since the whole AGN feedback process relies on radiation pressure on dust. The large amount of dust required in order to sustain feedback may be provided by supernovae in the starburst phase. In fact, recent observations indicate that significant quantities of dust can be produced in core-collapse supernovae (Owen and Barlow, 2015; Wesson et al., 2015). Continued star formation in the starburst is beneficial, as it helps keeping the ambient medium dusty, and thus supporting the overall AGN feedback process. Stellar feedback likely disrupts the starburst activity, but the nuclear gas reservoir may also be replenished by re-accretion episodes. Furthermore, we previously suggested that star formation (with subsequent supernova explosions and associated dust release) may be triggered within the AGN feedback-driven outflow itself (Ishibashi and Fabian, 2012). Interestingly, the first direct detection of star formation occurring inside a galactic outflow has now been observationally confirmed (Maiolino et al., 2017), nicely supporting our model predictions. In our framework, AGN feedback and starburst phenomena are intrinsically coupled through the production of dust in supernova explosions, leading to a natural interpretation of the co-evolutionary path.

AUTHOR CONTRIBUTIONS

The author confirms being the sole contributor of this work and approved it for publication.

REFERENCES

Alexander, D. M., and Hickox, R. C. (2012). What drives the growth of black holes?. *New Astron. Rev.* 56, 93–121. doi: 10.1016/j.newar.2011.11.003

Assef, R. J., Eisenhardt, P. R. M., Stern, D., Tsai, C.-W., Wu, J., Wylezalek, D., et al. (2015). Half of the most luminous quasars may be obscured: investigating the nature of WISE-selected hot dust-obscured galaxies. *Astrophys. J.* 804:27. doi: 10.1088/0004-637X/804/1/27

Banerji, M., Alaghband-Zadeh, S., Hewett, P. C., and McMahon, R. G. (2015). Heavily reddened type 1 quasars at z > 2 - I. Evidence for significant obscured black hole growth at the highest quasar luminosities. *Mon. Not. R. Astron. Soc.* 447, 3368–3389. doi: 10.1093/mnras/stu2649

Banerji, M., McMahon, R. G., Hewett, P. C., Alaghband-Zadeh, S., Gonzalez-Solares, E., Venemans, B. P., et al. (2012). Heavily reddened quasars at z∼2 in the UKIDSS Large Area Survey: a transitional phase in AGN evolution. *Mon. Not. R. Astron. Soc.* 427, 2275–2291. doi: 10.1111/j.1365-2966.2012.22099.x

Di Matteo, T., Springel, V., and Hernquist, L. (2005). Energy input from quasars regulates the growth and activity of black holes and their host galaxies. *Nature* 433, 604–607. doi: 10.1038/nature03335

Fabian, A. C., Celotti, A., and Erlund, M. C. (2006). Radiative pressure feedback by a quasar in a galactic bulge. *Mon. Not. R. Astron. Soc.* 373, L16–L20. doi: 10.1111/j.1745-3933.2006.00234.x

Hopkins, P. F., Hernquist, L., Cox, T. J., Di Matteo, T., Martini, P., Robertson, B., et al. (2005). Black holes in galaxy mergers: evolution of quasars. *Astrophys. J.* 630, 705–715. doi: 10.1086/432438

Ishibashi, W., and Fabian, A. C. (2012). Active galactic nucleus feedback and triggering of star formation in galaxies. *Mon. Not. R. Astron. Soc.* 427, 2998–3005. doi: 10.1111/j.1365-2966.2012.22074.x

Ishibashi, W., and Fabian, A. C. (2015). AGN feedback: galactic-scale outflows driven by radiation pressure on dust. *Mon. Not. R. Astron. Soc.* 451, 93–102. doi: 10.1093/mnras/stv944

Ishibashi, W., and Fabian, A. C. (2016a). AGN-starburst evolutionary connection: a physical interpretation based on radiative feedback. *Mon. Not. R. Astron. Soc.* 463, 1291–1296. doi: 10.1093/mnras/stw2063

Ishibashi, W., and Fabian, A. C. (2016b). The connection between AGN-driven dusty outflows and the surrounding environment. *Mon. Not. R. Astron. Soc.* 457, 2864–2870. doi: 10.1093/mnras/stw182

Maiolino, R., Russell, H. R., Fabian, A. C., Carniani, S., Gallagher, R., Cazzoli, S., et al. (2017). Star formation inside a galactic outflow. *Nature* 544, 202–206. doi: 10.1038/nature21677

Owen, P. J., and Barlow, M. J. (2015). The dust and gas content of the crab nebula. *Astrophys. J.* 801:141. doi: 10.1088/0004-637X/801/2/141

Sanders, D. B., Soifer, B. T., Elias, J. H., Madore, B. F., Matthews, K., Neugebauer, G., et al. (1988). Ultraluminous infrared galaxies and the origin of quasars. *Astrophys. J.* 325, 74–91. doi: 10.1086/165983

Thompson, T. A., Fabian, A. C., Quataert, E., and Murray, N. (2015). Dynamics of dusty radiation-pressure-driven shells and clouds: fast outflows from galaxies, star clusters, massive stars, and AGN. *Mon. Not. R. Astron. Soc.* 449, 147–161. doi: 10.1093/mnras/stv246

Wesson, R., Barlow, M. J., Matsuura, M., and Ercolano, B. (2015). The timing and location of dust formation in the remnant of SN 1987A. *Mon. Not. R. Astron. Soc.* 446, 2089–2101. doi: 10.1093/mnras/stu2250

Zakamska, N. L., Hamann, F., Pâris, I., Brandt, W. N., Greene, J. E., Strauss, M. A., et al. (2016). Discovery of extreme [O III] λ5007 Å outflows in high-redshift red quasars. *Mon. Not. R. Astron. Soc.* 459, 3144–3160. doi: 10.1093/mnras/stw718

Conflict of Interest Statement: The author declares that the research was conducted in the absence of any commercial or financial relationships that could be construed as a potential conflict of interest.

The reviewer GR and handling Editor declared their shared affiliation.

Copyright © 2017 Ishibashi. This is an open-access article distributed under the terms of the Creative Commons Attribution License (CC BY). The use, distribution or reproduction in other forums is permitted, provided the original author(s) or licensor are credited and that the original publication in this journal is cited, in accordance with accepted academic practice. No use, distribution or reproduction is permitted which does not comply with these terms.

frontiers in Astronomy and Space Sciences

HYPOTHESIS AND THEORY
published: 12 September 2017
doi: 10.3389/fspas.2017.00013

Theoretical Re-evaluations of Scaling Relations between SMBHs and Their Host Galaxies–2. Importance of AGN Feedback Suggested by Stellar Age–Velocity Dispersion Relation

Hikari Shirakata[1]*, *Toshihiro Kawaguchi*[2], *Takashi Okamoto*[1] *and Tomoaki Ishiyama*[3]

[1] Department of Cosmosciences, Graduate School of Science, Hokkaido University, Sapporo, Japan, [2] Department of Economics, Management and Information Science, Onomichi City University, Onomichi, Hiroshima, Japan, [3] Institute of Management and Information Technologies, Chiba University, Chiba, Japan

We present the galactic stellar age—velocity dispersion relation obtained from a semi-analytic model of galaxy formation. We divide galaxies into two populations: galaxies which have over-massive/under-massive black holes (BHs) against the best-fitting BH mass—velocity dispersion relation. We find that galaxies with larger velocity dispersion have older stellar ages. We also find that galaxies with over-massive BHs have older stellar ages. These results are consistent with observational results obtained from Martín-Navarro et al. (2016). We tested the model with weak AGN feedback and find that galaxies with larger velocity dispersion have a younger stellar age.

Keywords: galaxies, active galaxies, nuclei galaxies, formation galaxies, evolution galaxies, statistics

OPEN ACCESS

Edited by:
Mauro D'Onofrio, University of Padua, Italy

Reviewed by:
Elena Bannikova, V. N. Karazin Kharkiv National University, Ukraine
Eija Irene Laurikainen, University of Oulu, Finland

***Correspondence:**
Hikari Shirakata
shirakata@astro1.sci.hokudai.ac.jp

Specialty section:
This article was submitted to Milky Way and Galaxies, a section of the journal Frontiers in Astronomy and Space Sciences

Received: *10 July 2017*
Accepted: *28 August 2017*
Published: *12 September 2017*

Citation:
Shirakata H, Kawaguchi T, Okamoto T and Ishiyama T (2017) Theoretical Re-evaluations of Scaling Relations between SMBHs and Their Host Galaxies–2. Importance of AGN Feedback Suggested by Stellar Age–Velocity Dispersion Relation. Front. Astron. Space Sci. 4:13. doi: 10.3389/fspas.2017.00013

1. INTRODUCTION

There is a lot of work aimed at understanding star formation histories by comparing theoretical models with observational results. Recent theoretical work has revealed that in order to explain observational properties of galaxies, some feedback effects are important, which suppress star formation activities by heating or ejecting cold gas (e.g., Springel et al., 2005; Okamoto et al., 2010; Vogelsberger et al., 2014). Supernovae (SN) feedback is important for less massive (less luminous) galaxies (Benson et al., 2003) with $M_K \gtrsim -22$, where M_K is K-band absolute magnitude of galaxies. On the other hand, SN feedback cannot quench the cooling flow of massive and luminous galaxies because such massive galaxies have deep potential wells and cold gas cannot escape from the galaxies. Some theoretical studies (e.g., Bower et al., 2006; Croton et al., 2006; Okamoto et al., 2014) reveals that feedback processes related to active galactic nuclei (AGNs) are important for such massive galaxies. Observational studies have explored whether AGN feedback really exists. Their results are controversial (see, e.g., McNamara et al., 2016; Nesvadba et al., 2017; Smolčić et al., 2017).

It is necessary to compare theoretical models with "statistical" observational properties of galaxies in order to investigate the existence of AGN feedback because individual AGN has different stages of AGN and star formation activities. Martín-Navarro et al. (2016) present evidence of existing AGN feedback by re-analyzing observational data. They divide galaxy sample obtained from van den Bosch (2016) between "over-/under- massive black hole galaxies" following the $M_{\rm BH} - \sigma$ relation. They then estimate stacked, luminosity weighted age of galaxies with these two populations and find that over massive BH galaxies are older than under massive galaxies.

Over-massive BH galaxies have potential to have experienced energetic AGN phases and to have stronger AGN feedback effects since over massive BHs might have grown in earlier universe in which the amount of the cold gas is larger.

Here we investigate, by using a semi-analytic model of galaxy formation (hereafter SA model), whether the relation proposed by Martín-Navarro et al. (2016) can really be explained with AGN feedback effect. In Section 2 we briefly review the SA model we used. Section 3 includes the main results.

2. METHODS

We employ a revised version of an SA model, "*New Numerical Galaxy Catalog*" (ν^2GC; Makiya et al., 2016). We consider star formation in galactic disk and bulge, mergers of galaxies, atomic gas cooling, gas heating by UV feedback and feedbacks via supernovae and AGNs, and the growth of super massive black holes (SMBHs) by coalescence and gas fueling. We here skipped the detailed model description about SMBH growth via galaxy mergers and disk instability because of the limited numbers of characters for this paper. In our model, we assume the timescale of gas accretion onto a SMBH is proportional to the dynamical timescale of the bulge in the host galaxy. We neglect the mass which might be in the dusty torus surrounding a SMBH since it is uncertain that how the dusty tori form and grow with their host galaxies. In addition, it is not clear whether the tori really exist for all types of AGNs including violent quasars, Seyfert galaxies, and low luminosity AGNs. We leave the treatment of the torus for future work. We have confirmed that the model can explain SMBH mass function at $z \sim 0$ and bright ends of quasar luminosity functions in $0.0 < z < 6.0$. More detailed descriptions are available in Shirakata et al. (2016) and Shirakata et al. in preparation.

We create merging histories of dark matter haloes from N-body simulations. In this paper, we employ ν^2GC-SS simulation, which has $70\mathrm{h}^{-1}$Mpc (comoving) in box size, 512^3 simulated particles, $2.20 \times 10^8 M_\odot$ in particle mass resolution. Minimum halo mass of this simulation is $8.79 \times 10^9 M_\odot$. We employ ν^2GC-S simulation which has $280\mathrm{h}^{-1}$Mpc in box size in order to obtain K-band luminosity functions of galaxies (**Figure 1**). The mass resolution of ν^2GC-S simulation is the same as ν^2GC-SS. The details of the merger trees are given in Ishiyama et al. (2015).

We assume a ΛCDM universe with the following parameters: $\Omega_0 = 0.31$, $\lambda_0 = 0.69$, $\Omega_\mathrm{b} = 0.048$, $\sigma_8 = 0.83$, $n_\mathrm{s} = 0.96$, and a Hubble constant of $H_0 = 100$ h km s^{-1} Mpc^{-1}, where $h = 0.68$ (Planck Collaboration et al., 2014).

2.1. Gas Cooling

Here we describe how we calculate the amount of the cold gas, which gets accreted to a central galaxy. We note that we define a central galaxy as a central galaxy of the most massive progenitor halo.

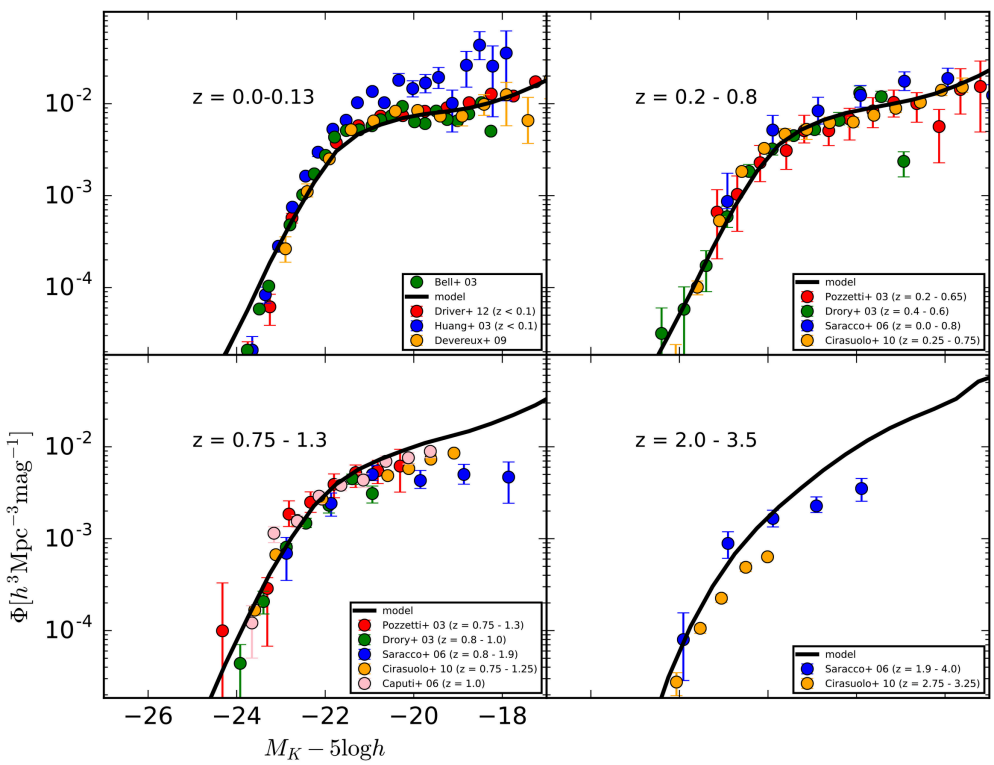

FIGURE 1 | K-band luminosity functions of galaxies from $z = 3.5$ to 0. The model results are shown in black lines. Dots describe observational results obtained from Bell et al. (2003); Driver et al. (2012); Huang et al. (2003); Devereux et al. (2009); Pozzetti et al. (2003); Drory et al. (2003); Saracco et al. (2006); Cirasuolo et al. (2010); Caputi et al. (2006) (see labels in this figure).

We firstly calculate cooling radius $r_{\rm cool}(t)$. Same as Makiya et al. (2016), we assume Navarro-Frenk-White (NFW) density profile (Navarro et al., 1997) for dark matter (DM) haloes and isothermal density profile with a finite core radius, r_c for hot gas haloes;

$$\rho_{\rm NFW}(r) = \frac{\rho_{\rm DM,0}}{(r/r_s)(1+r/r_s)^2}, \quad (1)$$

$$\rho_{\rm hot}(r) = \frac{\rho_{\rm hot,0}}{1+(r/r_c)^2}, \quad (2)$$

where r_s is the specific radius of the DM halo, which is described by using concentration parameter, c, and virial radius, $R_{\rm vir}$, as $R_{\rm vir}/r_s \equiv c$. We assume $r_c = 0.22 r_s$ (Makino et al., 1998). We use the analytical formulae of c obtained from fitting of cosmological N-body simulations (Prada et al., 2012). After the collapse of a DM halo, the hot gas gradually cools via radiative cooling. Then, the cooling time is described with $r_{\rm cool}$ as

$$t_{\rm cool}(r_{\rm cool}) = \frac{3}{2}\frac{\rho_{\rm hot}(r_{\rm cool})}{\mu m_p}\frac{k_B T_{\rm vir}}{n_e^2(r)\Lambda(T_{\rm vir}, Z_{\rm hot})}, \quad (3)$$

where μ, m_p, k_B, and n_e are the mean molecular weight, proton mass, Boltzmann constant, and electron number density, respectively. We employ a cooling function, Λ, provided by Sutherland and Dopita (1993), which is a function of hot gas metallicity, $Z_{\rm hot}$, and virial temperature, $T_{\rm vir}$. Virial temperature is calculated from circular velocity of the host DM halo, $V_{\rm circ}$, as

$$T_{\rm vir} = \frac{1}{2}\frac{\mu m_p}{k_B} V_{\rm circ}^2. \quad (4)$$

$r_{\rm cool}(t)$ is defined at which $t_{\rm cool}$ of Equation (3) is equal to the time elapsed since the halo formation epoch.

We next calculate free fall radius, $r_{\rm ff}(t)$ with $\rho_{\rm NFW}(r)$;

$$t_{\rm ff}(r_{\rm ff}) = \frac{\pi}{2}\sqrt{\frac{r_{\rm ff}^3}{2GM(r<r_{\rm ff})}}, \quad (5)$$

where G is the gravitational constant. Now $t_{\rm ff} = t_{\rm cool}$, in order to compare the size of $r_{\rm cool}$ with $r_{\rm ff}$ at the same time.

We then evaluate the accretion radius, $r_{\rm acc}(t)$, in which gas can actually cool and get accreted to the central galaxy. We set $r_{\rm acc}$ as the minimum value among $r_{\rm cool}, r_{\rm ff}$, and $R_{\rm vir}$, where $R_{\rm vir}$ is the virial radius of the halo. The case with $r_{\rm acc} = r_{\rm cool}$ means the gas cooling is not so efficient and gas can free-fall rapidly. This case occurs only for the massive ($>10^{13}\ M_\odot$) haloes. Since Makiya et al. (2016) assume $r_{\rm acc} = MIN\{r_{\rm cool}, R_{\rm vir}\}$, they would overestimate the amount of cold gas especially at $z < 1.0$ if they employ the same parameter set as that of in this paper. We note that we assume that the existence of a "cooling hole" same as Makiya et al. (2016); the radial profile of hot gas remains unchanged until the DM halo mass doubles.

2.2. Radio Mode AGN Feedback

We introduce the so-called radio-mode AGN feedback process in order to prevent gas in massive haloes from cooling and forming stars. Following Bower et al. (2006), gas cooling in a halo is quenched when the following two conditions are satisfied:

$$t_{\rm ff}(r_{\rm cool}) < \alpha_{\rm cool} t_{\rm cool}, \quad (6)$$

$$\epsilon_{\rm SMBH} L_{\rm Edd} > L_{\rm cool}, \quad (7)$$

where $L_{\rm Edd}$ is the Eddington luminosity, $L_{\rm cool}$ is the cooling luminosity of the gas, $\alpha_{\rm cool}$ and $\epsilon_{\rm SMBH}$ are free parameters which are determined in order to reproduce the luminous end of the luminosity function of galaxies at $z \sim 0$. In this paper, we fiducially set $(\alpha_{\rm cool}, \epsilon_{\rm SMBH}) = (1.00, 0.012)$.

From Equation (6), we can see that the radio-mode AGN feedback is more efficient for more massive galaxies at lower redshifts since $t_{\rm ff}$ and $t_{\rm cool}$ are roughly proportional to $(1+z)^{-3/2}$ and $(1+z)^{-3}$, respectively. Galaxies with radio-mode AGN feedback might correspond to FR-I radio galaxies (Fanaroff and Riley, 1974). It is however uncertain how the FR-I radio galaxies have triggered their activity. We thus cannot define galaxies with radio-mode AGN feedback in our model as mock FR-I radio galaxies. We have not included the model of FR-II radio galaxies, which would have intense cold gas accretion. We leave it for future work.

3. RESULTS AND FUTURE PROSPECTS

3.1. Basic Statistical Properties of Galaxies

The model which employed for this study includes some revisions from Makiya et al. (2016). We skipped the details of the revisions because of the limitation of the numbers of characters for this paper. For more details appear in Shirakata et al. (2016) and Shirakata et al. in preparation. We find that the fiducial model can explain observational galaxy properties well. In **Figure 1**, we compare K-band luminosity functions obtained from the model with observations (see the figure caption). The bright end slope of K-band luminosity function of galaxies at $z \sim 0$ is sensitive to the strength of the radio-mode AGN feedback. If the AGN feedback is weak, we overproduce bright galaxies with $M_K < -22.0$ and the luminosity function has a single-power law. We also find that the fiducial model can explain SMBH mass function, Faber-Jackson relation, Tully-Fisher relation at $z \sim 0$.

3.2. $M_{\rm BH}$, σ, and Luminosity Weighted Age Relations

Figure 2 shows the $M_{\rm BH} - \sigma$ relation at $z \sim 0$ with the fiducial model. We select the galaxies with $M_V < -20$, where M_V is the absolute AB magnitude in V-band. We derive the best fit function with the least square method (black line):

$$\log\left(\frac{M_{\rm BH}}{M_\odot}\right) = 2.35\log\left(\frac{\sigma}{200{\rm km/s}}\right) + 8.24. \quad (8)$$

For comparison, we also depict the best fit function obtained from van den Bosch (2016) (gray line):

$$\log\left(\frac{M_{\rm BH}}{M_\odot}\right) = 5.27\log\left(\frac{\sigma}{200{\rm km/s}}\right) + 8.33. \quad (9)$$

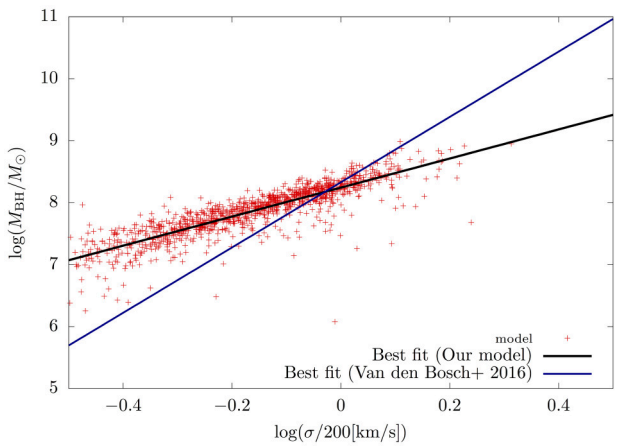

FIGURE 2 | $M_{BH} - \sigma$ relation at $z \sim 0$. Red points are model result, and black thick line describes the fitting function of the model result. Blue line is the fitting function of the data obtained from van den Bosch (2016).

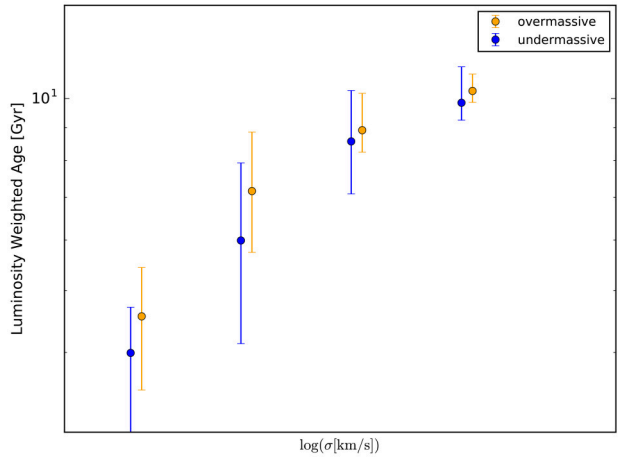

FIGURE 3 | $\sigma -$ age relation with the fiducial model. The age is luminosity weighted. Orange and blue points with errorbars show the median values of over-/under- massive BH galaxies with $1 - \sigma$ error.

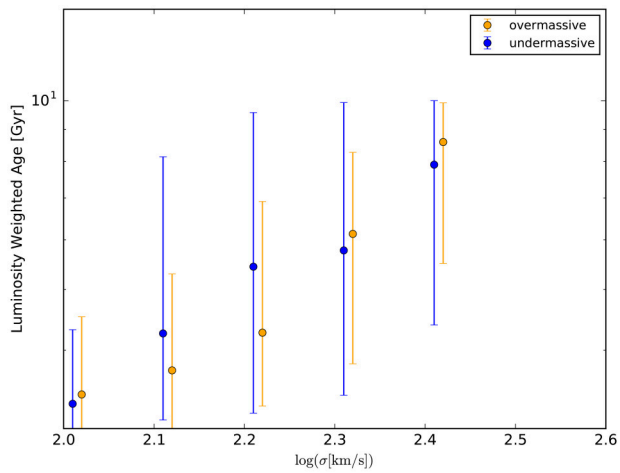

FIGURE 4 | The same figure as **Figure 3** with weak AGN feedback model: the parameter, α_{cool}, is 0.1 times smaller than the fiducial value.

We classify galaxies between over-massive BH galaxies and under-massive BH galaxies following our best fit function of $M_{BH} - \sigma$ relation with 1σ errors. We then depict $M_{BH}-$age relation in **Figure 3**. We find that galaxies with larger σ have older stellar ages and over-massive BH galaxies have older stellar ages. These results are roughly consistent with the result obtained from Martín-Navarro et al. (2016). On the other hand, when we employ the model with weak AGN feedback, in which α_{cool} set 0.1 times smaller than the fiducial value, the model cannot explain the result of Martín-Navarro et al. (2016) (**Figure 4**); all galaxies have younger stellar age than those obtained from Martín-Navarro et al. (2016) and galaxies with under-massive BHs become older. This result would be explained as follows. From Equation (6), more massive (i.e., more luminous) galaxies tend to be quenched their star formation by the AGN feedback. We thus get the steeper slope for the fiducial model compared to the model with the weak AGN feedback (α_{cool} is smaller). In addition, from Equation (7), galaxies with more massive SMBHs should have so much heating luminosity with the AGN activity that compensates the cooling luminosity. Therefore, we can get the same trend as Martín-Navarro et al. (2016), over-massive black hole galaxies have older stellar ages. From these results, we have concluded that radio mode AGN feedback model might play a role for quenching the star formation of massive galaxies.

We find that the difference between galaxies with over-massive BHs and under-massive BHs is smaller than those obtained from the observation (Martín-Navarro et al., 2016). For observations, as noted in Martín-Navarro et al. (2016), their estimation of the galactic ages have large observational errors especially for the galaxies with smaller velocity dispersion. It would thus be important to use a larger amount of observational data.

For the theoretical model, the smaller difference between galaxies with over- and under- massive BHs would be partly because of the radio-mode AGN feedback modeling. Since more massive haloes tend to have more massive SMBHs, under-massive galaxies with larger velocity dispersion (and with larger bulge mass) could be quenched their star formation because of the AGN feedback. The ages of over- and under- massive galaxies with large velocity dispersion in the model thus overlap. We then test the effect of the galaxy selection and find the relation between M_{BH}, σ, and stellar age is sensitive to the sample selection; when we select only brighter galaxies with $M_V < -22.0$, the difference between galaxies with over- and under- massive BHs becomes clear. It might suggest that the efficiency of the radio-mode AGN feedback should more strongly depend on the BH mass.

Another possible way to explain the results of Martín-Navarro et al. (2016) would be to introduce quasar-mode AGN feedback. Since the number density of bright quasars peaks at higher redshift (e.g., Ueda et al., 2014), quasar-mode AGN feedback could be effective at higher redshift while the radio-mode becomes efficient at lower redshift. We will leave it for future work.

AUTHOR CONTRIBUTIONS

HS has developed ν^2GC. In addition, HS analyze the output data obtained from ν^2GC. TK and TO gave comments for the analysis. TI provides merger trees obtained from cosmological *N*-body simulations for ν^2GC.

FUNDING

TK was supported in part by a University Research Support Grant from the NAOJ and JSPS KAKENHI (17K05389). TO was financially supported by JSPS Grant-in-Aid for Young Scientists (16H01085). TI has been supported by MEXT HPCI STRATEGIC PROGRAM and MEXT/JSPS KAKENHI (15K12031) and by Yamada Science Foundation.

ACKNOWLEDGMENTS

We deeply appreciate the detailed review and useful suggestions by the referees, which have drastically improved our paper. We also appreciate the comments about English grammar by A. Pettitt.

REFERENCES

Bell, E. F., McIntosh, D. H., Katz, N., and Weinberg, M. D. (2003). The optical and near-infrared properties of galaxies. I. luminosity and stellar mass functions. *Astrophys. J. Suppl.* 149, 289–312. doi: 10.1086/378847

Benson, A. J., Bower, R. G., Frenk, C. S., Lacey, C. G., Baugh, C. M., and Cole, S. (2003). What shapes the luminosity function of galaxies? *Astrophys. J.* 599, 38–49. doi: 10.1086/379160

Bower, R. G., Benson, A. J., Malbon, R., Helly, J. C., Frenk, C. S., Baugh, C. M., et al. (2006). Breaking the hierarchy of galaxy formation. *Month. Notices R. Astron. Soc.* 370, 645–655. doi: 10.1111/j.1365-2966.2006.10519.x

Caputi, K. I., McLure, R. J., Dunlop, J. S., Cirasuolo, M., and Schael, A. M. (2006). Further constraints on the evolution of K_s-selected galaxies in the GOODS/CDFS field. *Month. Notices R. Astron. Soc.* 366, 609–623. doi: 10.1111/j.1365-2966.2005.09887.x

Cirasuolo, M., McLure, R. J., Dunlop, J. S., Almaini, O., Foucaud, S., and Simpson, C. (2010). A new measurement of the evolving near-infrared galaxy luminosity function out to z∼4: a continuing challenge to theoretical models of galaxy formation. *Month. Notices R. Astron. Soc.* 401, 1166–1176. doi: 10.1111/j.1365-2966.2009.15710.x

Croton, D. J., Springel, V., White, S. D. M., De Lucia, G., Frenk, C. S., Gao, L., et al. (2006). The many lives of active galactic nuclei: cooling flows, black holes and the luminosities and colours of galaxies. *Month. Notices R. Astron. Soc.* 365, 11–28. doi: 10.1111/j.1365-2966.2005.09675.x

Devereux, N., Hriljac, P., Willner, S. P., Ashby, M. L. N., and Willmer, C. N. A. (2009). "The morphological type dependence of K-band luminosity functions," in *Galaxy Evolution: Emerging Insights and Future Challenges*, Vol. 419 of *Astronomical Society of the Pacific Conference Series*, eds S. Jogee, I. Marinova, L. Hao, and G. A. Blanc (San Fransisco, CA), 171.

Driver, S. P., Robotham, A. S. G., Kelvin, L., Alpaslan, M., Baldry, I. K., Bamford, S. P., et al. (2012). Galaxy And Mass Assembly (GAMA): the $0.013 < z < 0.1$ cosmic spectral energy distribution from 0.1 μm to 1 mm. *Month. Notices R. Astron. Soc.* 427, 3244–3264. doi: 10.1111/j.1365-2966.2012.22036.x

Drory, N., Bender, R., Feulner, G., Hopp, U., Maraston, C., Snigula, J., et al. (2003). The munich near-infrared cluster survey. II. The K-Band luminosity function of field galaxies to z∼1.2. *Astrophys. J.* 595, 698–711. doi: 10.1086/377497

Fanaroff, B. L. and Riley, J. M. (1974). The morphology of extragalactic radio sources of high and low 179 luminosity. *MNRAS* 167, 31P–36P. doi: 10.1093/mnras/167.1.31P

Huang, J.-S., Glazebrook, K., Cowie, L. L., and Tinney, C. (2003). The Hawaii+Anglo-Australian Observatory K-Band Galaxy Redshift Survey. I. The Local K-Band Luminosity Function. *Astrophys. J.* 584, 203–209. doi: 10.1086/345619

Ishiyama, T., Enoki, M., Kobayashi, M. A. R., Makiya, R., Nagashima, M., and Oogi, T. (2015). The ν^2GC simulations: quantifying the dark side of the universe in the Planck cosmology. *Publ. Astron. Soc. Jap.* 67:61. doi: 10.1093/pasj/psv021

Makino, N., Sasaki, S., and Suto, Y. (1998). X-Ray Gas Density Profile of Clusters of Galaxies from the Universal Dark Matter Halo. *Astrophys. J.* 497, 555–558. doi: 10.1086/305507

Makiya, R., Enoki, M., Ishiyama, T., Kobayashi, M. A. R., Nagashima, M., Okamoto, T., et al. (2016). The New Numerical Galaxy Catalog (ν^2GC): an updated semi-analytic model of galaxy and active galactic nucleus formation with large cosmological N-body simulations. *Publ. Astron. Soc. Jap.* 68:25. doi: 10.1093/pasj/psw005

Martín-Navarro, I., Brodie, J. P., van den Bosch, R. C. E., Romanowsky, A. J., and Forbes, D. A. (2016). Stellar populations across the Black Hole Mass-Velocity dispersion relation. *Astrophys. J. Lett.* 832:L11. doi: 10.3847/2041-8205/832/1/L11

McNamara, B. R., Russell, H. R., Nulsen, P. E. J., Hogan, M. T., Fabian, A. C., Pulido, F., et al. (2016). A Mechanism for stimulating AGN feedback by lifting gas in massive galaxies. *Astrophys. J.* 830:79. doi: 10.3847/0004-637X/830/2/79

Navarro, J. F., Frenk, C. S., and White, S. D. M. (1997). A Universal density profile from hierarchical clustering. *Astrophys. J.* 490:493. doi: 10.1086/304888

Nesvadba, N. P. H., De Breuck, C, Lehnert, M. D., Best, P. N. and Collet, C. (2017). The SINFONI survey of powerful radio galaxies at z∼2: jet-driven AGN feedback during the Quasar Era. *Astron. Astrophys.* 599:A123. doi: 10.1051/0004-6361/201528040

Okamoto, T., Frenk, C. S., Jenkins, A., and Theuns, T. (2010). The properties of satellite galaxies in simulations of galaxy formation. *Month. Notices R. Astron. Soc.* 406, 208–222. doi: 10.1111/j.1365-2966.2010.16690.x

Okamoto, T., Shimizu, I., and Yoshida, N. (2014). Reproducing cosmic evolution of galaxy population from z = 4 to 0. *Publ. Astron. Soc. Jap.* 66:70. doi: 10.1093/pasj/psu046

Planck Collaboration, Ade, P. A. R., Aghanim, N., Alves, M. I. R., Armitage-Caplan, C., Arnaud, M., et al. (2014). Planck 2013 results. I. Overview of products and scientific results. *Astron. Astrophys.* 571:A1. doi: 10.1051/0004-6361/201321529

Pozzetti, L., Cimatti, A., Zamorani, G., Daddi, E., Menci, N., Fontana, A., et al. (2003). The K20 survey. V. The evolution of the near-IR Luminosity Function. *Astron. Astrophys.* 402, 837–848. doi: 10.1051/0004-6361:20030292

Prada, F., Klypin, A. A., Cuesta, A. J., Betancort-Rijo, J. E., and Primack, J. (2012). Halo concentrations in the standard Λ cold dark matter cosmology. *Month. Notices R. Astron. Soc.* 423, 3018–3030. doi: 10.1111/j.1365-2966.2012.21007.x

Saracco, P., Fiano, A., Chincarini, G., Vanzella, E., Longhetti, M., Cristiani, S., et al. (2006). Probing the evolution of the near-infrared luminosity function of galaxies to z∼3 in the Hubble Deep Field-South. *Month. Notices R. Astron. Soc.* 367, 349–365. doi: 10.1111/j.1365-2966.2006.09967.x

Shirakata, H., Kawaguchi, T., Okamoto, T., Makiya, R., Ishiyama, T., Matsuoka, Y., et al. (2016). Theoretical re-evaluations of the black hole mass-bulge mass relation - I. Effect of seed black hole mass. *Month. Notices R. Astron. Soc.* 461, 4389–4394. doi: 10.1093/mnras/stw1798

Smolčić, V., Novak, M., Delvecchio, I., Ceraj, L., Bondi, M., Delhaize, J. (2017). The VLA-COSMOS 3 GHz Large Project: cosmic evolution of radio AGN and implications for radio-mode feedback since z∼5. *Astron. Astrophys.* 602:A6. doi: 10.1051/0004-6361/201730685

Springel, V., White, S. D. M., Jenkins, A., Frenk, C. S., Yoshida, N., Gao, L., et al. (2005). Simulations of the formation, evolution and clustering of galaxies and quasars. *Nature* 435, 629–636. doi: 10.1038/nature03597

Sutherland, R. S., and Dopita, M. A. (1993). Cooling functions for low-density astrophysical plasmas. *Astrophys. J. Suppl.* 88, 253–327. doi: 10.1086/191823

Ueda, Y., Akiyama, M., Hasinger, G., Miyaji, T., and Watson, M. G. (2014). Toward the Standard Population Synthesis Model of the X-Ray Background:

Evolution of X-Ray Luminosity and Absorption Functions of Active Galactic Nuclei Including Compton-thick Populations. *Astrophys. J.* 786:104. doi: 10.1088/0004-637X/786/2/104

van den Bosch, R. C. E. (2016). Unification of the fundamental plane and Super Massive Black Hole Masses. *Astrophys. J.* 831:134. doi: 10.3847/0004-637X/831/2/134

Vogelsberger, M., Genel, S., Springel, V., Torrey, P., Sijacki, D., Xu, D., et al. (2014). Introducing the Illustris Project: simulating the coevolution of dark and visible matter in the Universe. *Month. Notices R. Astron. Soc.* 444, 1518–1547. doi: 10.1093/mnras/stu1536

Conflict of Interest Statement: The authors declare that the research was conducted in the absence of any commercial or financial relationships that could be construed as a potential conflict of interest.

Copyright © 2017 Shirakata, Kawaguchi, Okamoto and Ishiyama. This is an open-access article distributed under the terms of the Creative Commons Attribution License (CC BY). The use, distribution or reproduction in other forums is permitted, provided the original author(s) or licensor are credited and that the original publication in this journal is cited, in accordance with accepted academic practice. No use, distribution or reproduction is permitted which does not comply with these terms.

frontiers in Astronomy and Space Sciences

ORIGINAL RESEARCH
published: 16 November 2017
doi: 10.3389/fspas.2017.00044

On the Role of the Environments and Star Formation for Quasar Activity

Daniela Bettoni[1], Renato Falomo[1], Jari K. Kotilainen[2,3] and Kalle Karhunen[3]*

[1] INAF - Osservatorio Astronomico di Padova, Padua, Italy, [2] Finnish Centre for Astronomy with ESO (FINCA), University of Turku, Turku, Finland, [3] Tuorla Observatory, Department of Physics and Astronomy, University of Turku, Turku, Finland

We investigate the host galaxy and environment properties of a sample of 400 low z (<0.5) quasars that were imaged in the SDSS Stripe82. We can detect and study the properties of the host galaxy for more than 75% of the data sample. We discover that quasar are mainly hosted in luminous galaxies of absolute magnitude $M^* - 3 < M(R) < M^*$[1] and that in the quasar environments the galaxy number density is comparable to that of inactive galaxies of similar luminosities. For these quasars we undertake also a study in u,g,r,i, and z SDSS bands and again we discover that the mean colors of the quasar host galaxy it is not very different with respect to the values of the sample of inactive galaxies. For a subsample of low z sources the imaging study is complemented by spectroscopy of quasar hosts and of close companion galaxies. This study suggests that the supply and cause of the nuclear activity depends only weakly on the local environment of quasars. Contrary to past suggestions, for low redshift quasar there is a very modest connection between recent star formation and the nuclear activity.

Keywords: galaxies active, galaxies evolution, galaxies nuclei, quasars general, quasars environment

OPEN ACCESS

Edited by:
Deborah Dultzin, Universidad Nacional Autónoma de México, Mexico

Reviewed by:
Paolo Salucci, Scuola Internazionale di Studi Superiori Avanzati (SISSA), Italy
Zurab Silagadze, Budker Institute of Nuclear Physics (RAS), Russia

****Correspondence:***
Daniela Bettoni
daniela.bettoni@oapd.inaf.it

Specialty section:
This article was submitted to Cosmology, a section of the journal Frontiers in Astronomy and Space Sciences

Received: *23 August 2017*
Accepted: *31 October 2017*
Published: *16 November 2017*

Citation:
Bettoni D, Falomo R, Kotilainen JK and Karhunen K (2017) On the Role of the Environments and Star Formation for Quasar Activity. Front. Astron. Space Sci. 4:44. doi: 10.3389/fspas.2017.00044

1. INTRODUCTION

Quasar phenomenon assumes that the nuclear activity can be due to the major merger of two gas-rich galaxies that feed the central engine and enable the growth of a spheroidal stellar component. However, important details on the mechanisms that triggers the gas fueling and how nuclear activity influence the successive evolution of the host galaxies remain poorly understood. The study of correlations among black hole masses, properties of the host galaxies and their environments may provide relevant clues to investigate the fundamental issues on quasar activity and its role on the evolution of galaxies. Simulations (e.g., Hopkins et al., 2013; Menci et al., 2014) suggest that minor and major merging events may have a key role for triggering and fueling the nuclear/quasar activity. These effects strictly depend on the global properties of the galaxy environment (Haehnelt and Kauffmann, 2000; Di Matteo et al., 2005).

The quasars, at low-redshift, follow the large-scale structure traced by galaxy clusters but they eschew the very centre of clusters (Söchting et al., 2002, 2004). On the other hand the quasar environment, on small scales (projected distance < 0.5 Mpc), appear overpopulated by blue disc galaxies having a significant star formation rate (Coldwell and Lambas, 2003, 2006). At higher redshifts, quasars are in some cases associated with richer environments (Hall and Green, 1998; Djorgovski, 1999) but also examples of modest galaxy environments are observed. The comparison of the environments of quasars, at Mpc scales, to those of galaxies has given contradictory results

[1] M^* and L^* are the characteristic absolute magnitude and luminosity of the Schechter luminosity function of galaxies (Schechter, 1976).

partially due to small samples and non homogeneous datasets. Early studies suggested that the galaxy environment of quasars is more strongly clustered than that of inactive galaxies (e.g., Shanks et al., 1988), while later studies based on surveys such as the Two Degree Field (2dF) and the Sloan Digital Sky Survey (SDSS) (Abazajian et al., 2009) found galaxy densities around quasars and inactive galaxies to be comparable to each other (e.g., Smith et al., 2000; Wake et al., 2004).

More recent studies using the SDSS archives such as Serber et al. (2006) and Strand et al. (2008) have taken advantage of the large datasets provided by the survey to study quasars at $z < 0.4$. Both studies found that quasars are on average located in higher local over-density regions than typical L* galaxies, and that within 100 kpc from the quasar the density enhancement is strongest. Serber et al. (2006) also claimed that: "high luminosity quasars have denser small-scale environments than those of lower luminosity." These studies are, however, limited by the deepness of the surveys that do not enable to study the galaxy population much fainter that L*. Meanwhile, a study by Bennert et al. (2008) found that many low-z quasars show signs of recent or on-going interactions with nearby galaxies, suggesting a connection between the environment and the quasar activation. In spite of these imaging studies our knowledge of the physical association of the galaxies around quasars and their dynamical properties remains uncertain.

To overcome these issues we recently carried out a systematic study of the the host galaxy and environment properties of a large ($\sim$ 400) sample of low redshift ($z < 0.5$) quasars based on the deep images available from the SDSS Stripe82 survey. These co-added images are $\sim$2 magnitudes more profound with respect to the standard Sloan data and give the possibility to study both the quasar hosts and the immediate environments. We are able to resolve the host galaxy for $\sim$ 300 targets (Falomo et al., 2014) and to investigate the the large scale galaxy environment of all quasars (Karhunen et al., 2014). For this work we adopt the concordance cosmology with $H_0 = 70$ km s^{-1} Mpc^{-1}, $\Omega_m = 0.3$ and $\Omega_\Lambda = 0.7$.

2. THE SAMPLE AND ANALYSIS

The sample of quasar we used, described in detail in Falomo et al. (2014), is derived from the fifth release of the SDSS Quasar Catalog (Schneider et al., 2010) that is based on the SDSS-DR7 data release (Abazajian et al., 2009). Our analysis is done only in the region of sky covered by the stripe82 data, these images go deeper of about $\sim$2 magnitudes with respect to the usual Sloan data and make possible the study of the quasar hosts, with these images we reach $m_{i(limit)} = 24.1$ (Annis et al., 2014). The final sample is composed by 416 quasars in the range of redshift $0.1 < z < 0.5$. In this sample we are dominated by radio quiet quasars only 24 are radio loud (about 5%). The mean redshift of the sample is $< z > = 0.39 \pm 0.08$ (median 0.41 ± 0.06) and the average absolute magnitude is :$< M_i > = -22.68 \pm 0.61$ (median -22.52 ± 0.35). To perform the analysis of the images we used the tool AIDA (Astronomical Image Decomposition and Analysis) (Uslenghi and Falomo, 2011). The tool is designed to perform 2D model fitting of quasar images including Adaptive Optics data and with detailed modeling of the PSF and its variations. In **Figure 1** we show an example of our analysis and of the AIDA fit.

To perform the analysis of the large scale environment we used SExtractor (Bertin and Arnouts, 1996) to create our own galaxy catalogs for each image, measuring the magnitudes of the galaxies in each of the five filters separately. A comparison of the catalog generated with SExtractor to those of SDSS, and a visual inspection on a number of frames to further to study the validity of our classification is fully described in Karhunen et al. (2014). We found a good match between the SDSS and SExtractor catalogs at apparent magnitudes $m_i < 23$, but at fainter magnitudes the number of objects detected by SExtractor dropped dramatically compared to those in the SDSS catalog. A visual inspection of these faint objects showed that they are mainly background noise which is either undetected by SExtractor or classified as an unknown object. We chose a conservative limit of classification value ≤ 0.20 for our galaxies, to make sure we avoid all the stars and majority of the unknown objects.

3. HOST GALAXIES

For our sample we found that the morphology of the quasars host galaxy ranges from pure ellipticals to complex/composite morphologies that combine disks, spheroids, lens and halo and are dominated by luminous galaxies with absolute magnitude in the range M*-3 < M(R) < M* and the average absolute magnitude of this sample is $< M_i >= -22.68 \pm 0.61$. The galaxy sizes (defined here as the half-light radius) range from very compact (few kpc) up to more extended galaxies (10–15 kpc) and, in our redshift range, not significant trend of change of the galaxy size with z is found. However, note that the sampled redshift range is small thus possibly hiding systematic changes of size with z. It is interesting to note that the distribution of sizes of the quasars hosts is very similar to that of the sample of inactive galaxies of similar luminosity and redshift distribution as shown in **Figure 2**. The black hole mass of the quasar, estimated from the spectral properties of the nuclei, are poorly correlated with the total luminosity of the host galaxies but the relation between M_{BH} and the luminosity of the spheroidal component is consistent with that of local inactive galaxies (Falomo et al., 2014). We can resolve the host galaxy in $\sim$73% of the quasar sample but in u-band only for the 48%.

Only the $(g - i)$ color is slighter bluer (1.06 ± 0.11) than that of inactive galaxies (1.19 ± 0.25) of similar luminosity and redshift (see Bettoni et al., 2015). The average absolute magnitude ($< M_i >_{QSOHOST} = -22.52 < M_i >_{GAL} = -22.26$) are very similar and also $(u - g)$ color of quasar hosts are similar (1.40 ± 0.30) to that of inactive galaxies (1.54 ± 0.62). Quasar and control sample have the same distribution of close (< 50 kpc projected) companion galaxies (Bettoni et al., 2015). This result is in contrast with that obtained by Matsuoka et al. (2014) who find similar (g–i) color for the quasar hosts but claim they are systematically bluer than the ensemble of normal galaxies in SDSS. Because of the different selection of active and non active galaxies of our and Matsuoka et al. (2014) samples it is not clear what is the cause of this discrepancy.

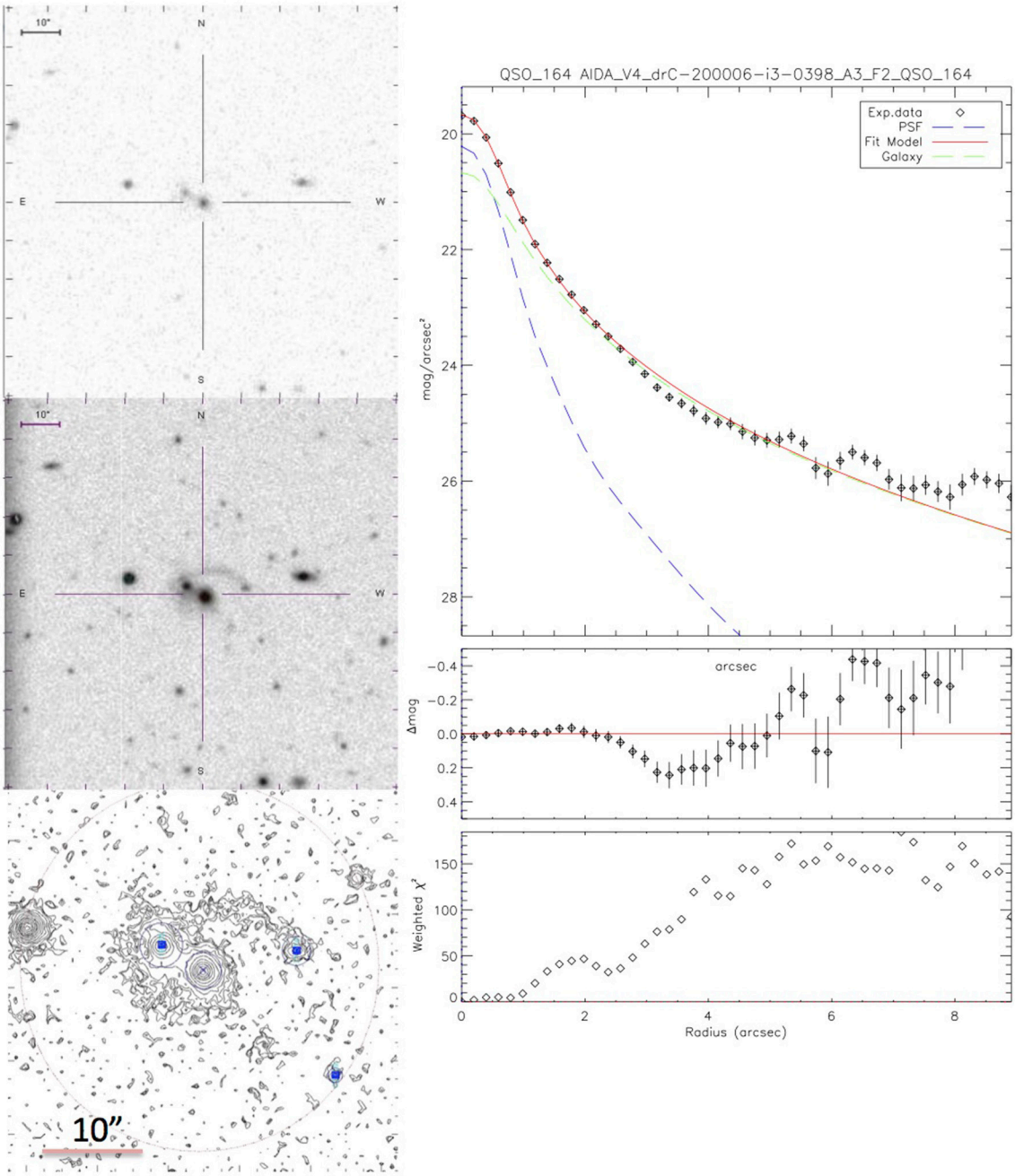

FIGURE 1 | Upper left: SDSS-DR7 i-band image, **middle left:** corresponding data from Stripe 82, **bottom left:** contour plot zoomed on the central object of the Stripe 82 i-band image (north at top, east left). **Upper right:** i-band radial profile together with the AIDA decomposition and fit. **Middle right:** distribution of residual for the best fit. **Lower right:** distribution of χ^2.

4. GALAXY ENVIRONMENT

The large scale galaxy environment (<1 Mpc) of the 302 resolved quasars compared with those of a sample of inactive galaxies at same redshift (Karhunen et al., 2014) shows that the galaxy number density is comparable to that of inactive galaxies with similar luminosities, as seen in **Figure 3**. For distances <400 kpc both quasars and inactive galaxies environments shows a significant excess compared to the background galaxy density. In particular the quasars, on average, have the tendency to be associated with small group of galaxies. No statistically significant difference is found between the over densities of low z quasar around the quasars and the inactive galaxies (Karhunen et al., 2014). No dependence of the over density on redshift, quasar

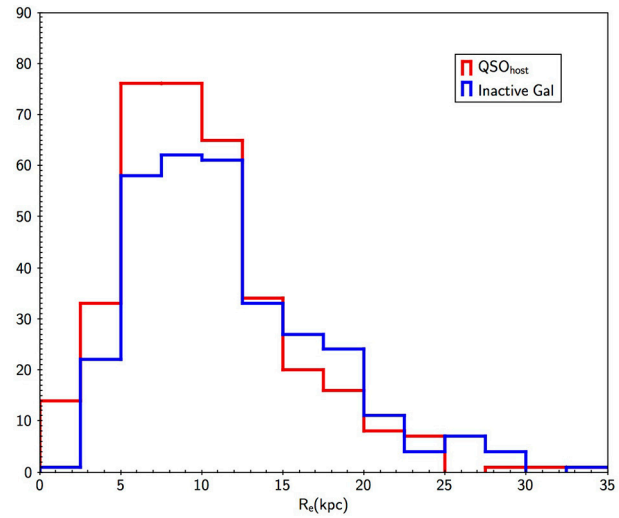

FIGURE 2 | Distribution of effective radius R_e for quasar hosts (red line) and that of a sample of inactive galaxies (blue line) that have similar luminosity and redshift of quasar hosts.

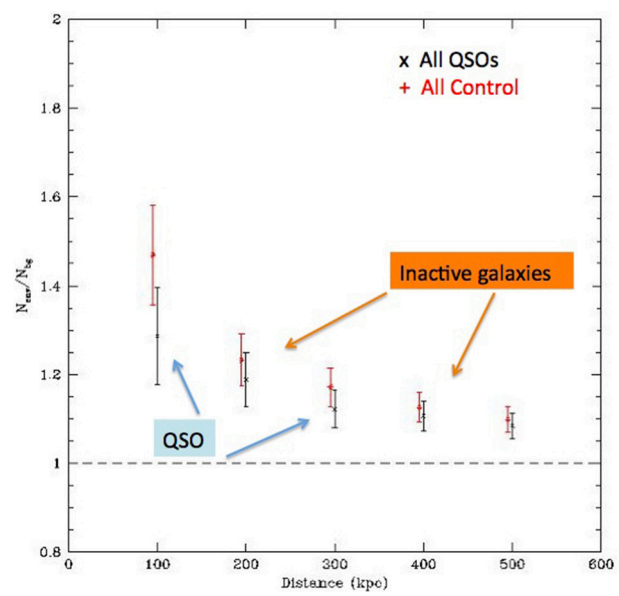

FIGURE 3 | Galaxy over-density in the environment of quasar compared with that of inactive galaxies at same redshift and luminosity.

luminosity, the galaxies at same luminosity of the host galaxy, the radio luminosity or BH mass was found.

The lack of a notable difference between the quasars and non-active galaxies (Karhunen et al., 2014) environments suggests that the connection between the quasar activity and its environment is less important than believed for fueling and activate the quasar. This may also indicate that secular evolution (e.g., disc instabilities, see; Ciotti et al., 2010) may play an important role in triggering the quasar activity, and that mergers are less important than expected.

As a second step in this environment study we used all five SDSS filters to analyze the color properties of the quasar environment (Karhunen et al. in preparation). This was done for a subsample of objects for which the SDSS-Stripe82 u-band image was deep enough to allow the detection of nearby galaxies. This implies that we have to discard ∼20% of our original sample (typically u-band images with exposures <40 min). We find that the colors of the environments of the quasars are slightly bluer than those of inactive galaxies at all distances, with the effect being most noticeable in g–i. The color of the environment depends on the density of the environment, with denser areas being redder. We also find that quasars at higher redshifts have redder environments.

4.1. Close Environments

To better investigate, in all 5 Sloan bands, the very close environment of quasars in our sample, we selected both from the full sample of 416 quasar and from the comparison sample only objects at $z < 0.3$ in fact, beyond this limit, the characterization of the quasar host galaxies becomes difficult at bluer filters due to the reduced contrast between the host galaxy and the nuclear emission. The detailed description of the final sample, composed by 52 quasars, is described in Bettoni et al. (2015). To compare the colors of the host galaxy we need to evaluate the K-correction for each filter, to this purpose we used the KCORRECT package (Blanton and Roweis, 2007). This allow us, using the luminosity+SED fitting, to derive also an estimate of the stellar mass for this subsample of quasar hosts and we used the stellar masses to derive the relation $LogM_*$-LogM_{BH} shown in **Figure 4**. Our data are well fitted by the relation for nearby normal elliptical and S0 galaxies as derived by Reines and Volonteri (2015), confirming our findings that quasars are hosted in luminous early-type galaxies.

The two samples show similar properties in particular, for our sample of resolved objects, we find an average mass of the quasar host galaxy of $< M_* >=4.28 \pm 2.76 \times 10^{10} M_\odot$ and $< M_* >= 5.27 \pm 3.88 \times 10^{10} M_\odot$ for the comparison sample of normal galaxies. The overall mean colors of the quasar host galaxy are indistinguishable from those of inactive galaxies of similar luminosity and redshift. There is a suggestion that the most massive quasar hosts have bluer colors and show a higher star formation rate than those in the sample of inactive galaxies.

4.2. Star Formation

As a last step in our study we obtained with NOT+ALFOSC instrumentation long slit spectra of a subsample of the 52 quasar in Bettoni et al. (2015) and of the close companions (see details in Bettoni et al., 2017). We found that in 8 out of 12 (∼67%) quasar the closest companion galaxy is associated to the quasar (same redshift). However the average level of star formation of companion galaxies that are associated with the quasar appears similar to that of the companion galaxies that are not associated with the quasar. These results suggest a modest role of the quasar emission for the SF in nearby companion galaxies. Finally for 3 targets we observed also the spectrum of the host galaxy which turned out to be typical of an old stellar population.

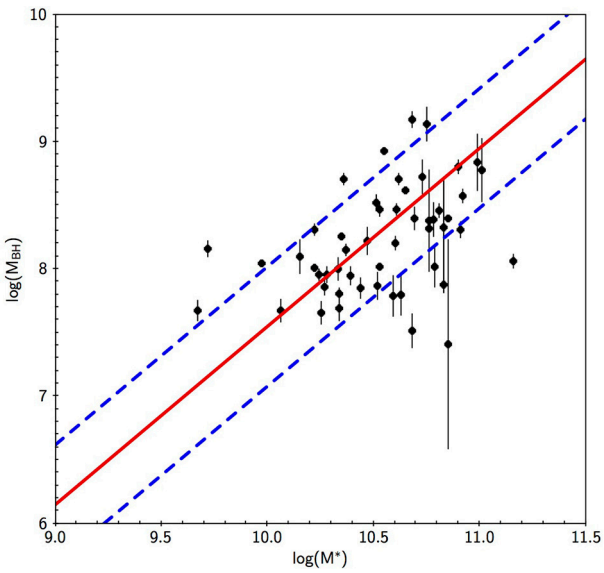

FIGURE 4 | Correlation between quasar virial black hole mass and the total stellar mass of their host galaxies as derived from SED fitting. Despite the large scatter the relation is similar to that obtained by Reines and Volonteri (2015) for inactive galaxies and bulges (red solid line). The 1σ uncertainties are indicated by blue dashed lines.

5. CONCLUSIONS

From our multi-band study of a large sample of nearby quasar we found that:

Quasar host galaxy luminosity is mainly in the range $M^* - 3 < M_R < M^*$.

Galaxy environments of quasar are similar to those of a sample of inactive galaxies at similar redshift and luminosity. The colors of the galaxies in the immediate environments of the quasars are slightly bluer than those of inactive galaxies at all distances; the effect being most noticeable in $(g - i)$ color.

Overall the mean colors ($g - i = 0.82 \pm 0.26$; $r - i = 0.26 \pm 0.16$ and $u - g = 1.32 \pm 0.25$) of the quasar host galaxy are indistinguishable from those of inactive galaxies of similar luminosity and redshift.

In ∼50% of the quasar in the z < 0.3 sample, we found companion galaxies at projected distance <50 kpc that could be associated to the quasar.

Optical spectroscopy of a subsample of 12 quasar shows that these associated companions exhibit [OII] λ 3,727 Å emission lines suggestive of episodes of (recent) star formation possibly induced by past interactions. The rate of star formation is, however, similar to that of companions of inactive galaxies. This may indicate that the presence of the quasar do not change the star formation in the associated close companions. Contrary to past suggestions (e.g., Matsuoka et al., 2014) the role of these associated companion galaxies for triggering and fueling the nuclear activity appears thus marginal as similar conditions are observed in inactive galaxies of mass similar to that of quasar hosts. Contrary to past suggestions. A significant time delay between the phase of nuclear activity and the star formation in the immediate environments could smear the link between them.

AUTHOR CONTRIBUTIONS

DB and RF wrote the paper and analyzed the data JK helped in the selection of the sample and the discussion of the results and KK made the NOT observations. All authors participated in the discussion of the final results.

ACKNOWLEDGMENTS

Funding for the SDSS and SDSS-II has been provided by the Alfred P. Sloan Foundation, the Participating Institutions, the National Science Foundation, the U.S. Department of Energy, the National Aeronautics and Space Administration, the Japanese Monbukagakusho, the Max Planck Society, and the Higher Education Funding Council for England. The SDSS Web Site is http://www.sdss.org/.

The SDSS is managed by the Astrophysical Research Consortium for the Participating Institutions. The Participating Institutions are the American Museum of Natural History, Astrophysical Institute Potsdam, University of Basel, University of Cambridge, Case Western Reserve University, University of Chicago, Drexel University, Fermilab, the Institute for Advanced Study, the Japan Participation Group, Johns Hopkins University, the Joint Institute for Nuclear Astrophysics, the Kavli Institute for Particle Astrophysics and Cosmology, the Korean Scientist Group, the Chinese Academy of Sciences (LAMOST), Los Alamos National Laboratory, the Max-Planck-Institute for Astronomy (MPIA), the Max-Planck-Institute for Astrophysics (MPA), New Mexico State University, Ohio State University, University of Pittsburgh, University of Portsmouth, Princeton University, the United States Naval Observatory, and the University of Washington.

REFERENCES

Abazajian, K. N., Adelman-McCarthy, J. K., Agüeros, M. A., Allam, S. S., Allende Prieto, C., An, D., et al. (2009). The seventh data release of the sloan digital sky survey. *Astrophys. J. Suppl.* 182, 543–558. doi: 10.1088/0067-0049/182/2/543

Annis, J., Soares-Santos, M., Strauss, M. A., Becker, A. C., Dodelson, S., Fan, X., et al. (2014). The sloan digital sky survey coadd: 275 deg^2 of deep sloan digital sky survey imaging on stripe 82. *Astrophys. J.* 794:120. doi: 10.1088/0004-637X/794/2/120

Bennert, N., Canalizo, G., Jungwiert, B., Stockton, A., Schweizer, F., Peng, C. Y., et al. (2008). Evidence for merger remnants in early-type host galaxies of low-redshift QSOs. *Astrophys. J.* 677, 846–857. doi: 10.1086/529068

Bertin, E., and Arnouts, S. (1996). SExtractor: Software for source extraction. *Astron. Astrophys. Suppl.* 117, 393–404. doi: 10.1051/aas:1996164

Bettoni, D., Falomo, R., Kotilainen, J. K., and Karhunen, K. (2017). Low-redshift quasars in the SDSS Stripe 82: associated companion galaxies and signature of star formation. *Month. Notices R. Astron. Soc.* 466, 3600–3611. doi: 10.1093/mnras/stw3284

Bettoni, D., Falomo, R., Kotilainen, J. K., Karhunen, K., and Uslenghi, M. (2015). Low-redshift quasars in the SDSS Stripe 82. Host galaxy colours and close environment. *Month. Notices R. Astron. Soc.* 454, 4103–4113. doi: 10.1093/mnras/stv2233

Blanton, M. R., and Roweis, S. (2007). K-corrections and filter transformations in the ultraviolet, optical, and near-infrared. *Astron. J.* 133, 734–754. doi: 10.1086/510127

Ciotti, L., Ostriker, J. P., and Proga, D. (2010). Feedback from central black holes in elliptical galaxies. III. models with both radiative and mechanical feedback. *Astrophys. J.* 717, 708–723. doi: 10.1088/0004-637X/717/2/708

Coldwell, G. V., and Lambas, D. G. (2003). Star formation in quasar and active galaxy environments. *Month. Notices R. Astron. Soc.* 344, 156–160. doi: 10.1046/j.1365-8711.2003.06804.x

Coldwell, G. V., and Lambas, D. G. (2006). Properties of galaxies in Sloan Digital Sky Survey quasar environments at $z < 0.2$. *Month. Notices R. Astron. Soc.* 371, 786–792. doi: 10.1111/j.1365-2966.2006.10712.x

Di Matteo, T., Springel, V., and Hernquist, L. (2005). Energy input from quasars regulates the growth and activity of black holes and their host galaxies. *Nature* 433, 604–607. doi: 10.1038/nature03335

Djorgovski, G. (1999). "GRB host galaxies," *KITP Conference: Gamma Ray Bursts and their Afterglows* (Santa Barbara, CA).

Falomo, R., Bettoni, D., Karhunen, K., Kotilainen, J. K., and Uslenghi, M. (2014). Low-redshift quasars in the Sloan Digital Sky Survey Stripe 82. The host galaxies. *Month. Notices R. Astron. Soc.* 440, 476–493. doi: 10.1093/mnras/stu283

Haehnelt, M. G., and Kauffmann, G. (2000). The correlation between black hole mass and bulge velocity dispersion in hierarchical galaxy formation models. *Month. Notices R. Astron. Soc.* 318, L35–L38. doi: 10.1046/j.1365-8711.2000.03989.x

Hall, P. B., and Green, R. F. (1998). An optical/near-infrared study of radio-loud quasar environments. II. Imaging results. *Astrophys. J.* 507, 558–584. doi: 10.1086/306349

Hopkins, P. F., Cox, T. J., Hernquist, L., Narayanan, D., Hayward, C. C., and Murray, N. (2013). Star formation in galaxy mergers with realistic models of stellar feedback and the interstellar medium. *Month. Notices R. Astron. Soc.* 430, 1901–1927. doi: 10.1093/mnras/stt017

Karhunen, K., Kotilainen, J. K., Falomo, R., and Bettoni, D. (2014). Low-redshift quasars in the SDSS Stripe 82. The local environments. *Month. Notices R. Astron. Soc.* 441, 1802–1816. doi: 10.1093/mnras/stu688

Matsuoka, Y., Strauss, M. A., Price, III, T. N., and DiDonato, M. S. (2014). Massive star-forming host galaxies of quasars on sloan digital sky survey stripe 82. *Astrophys. J.* 780:162. doi: 10.1088/0004-637X/780/2/162

Menci, N., Gatti, M., Fiore, F., and Lamastra, A. (2014). Triggering active galactic nuclei in hierarchical galaxy formation: disk instability vs. interactions. *Astron. Astrophys.* 569:A37. doi: 10.1051/0004-6361/201424217

Reines, A. E., and Volonteri, M. (2015). Relations between central black hole mass and total galaxy stellar mass in the local universe. *Astrophys. J.* 813:82. doi: 10.1088/0004-637X/813/2/82

Schechter, P. (1976). An analytic expression for the luminosity function for galaxies. *Astrophys. J.* 203, 297–306. doi: 10.1086/154079

Schneider, D. P., Richards, G. T., Hall, P. B., Strauss, M. A., Anderson, S. F., Boroson, T. A., et al. (2010). The sloan digital sky survey quasar catalog. V. seventh data release. *Astron. J.* 139:2360. doi: 10.1088/0004-6256/139/6/2360

Serber, W., Bahcall, N., Ménard, B., and Richards, G. (2006). The small-scale environment of quasars. *Astrophys. J.* 643, 68–74. doi: 10.1086/501443

Shanks, T., Boyle, B. J., and Peterson, B. A. (1988). "The spatial clustering of QSO's," in *Optical Surveys for Quasars*, *Vol. 2* of *Astronomical Society of the Pacific Conference Series* (San Francisco, CA), 244.

Smith, R. J., Boyle, B. J., and Maddox, S. J. (2000). The environments of intermediate-redshift QSOs: $0.3<z<0.7$. *Month. Notices R. Astron. Soc.* 313, 252–262. doi: 10.1046/j.1365-8711.2000.03225.x

Söchting, I. K., Clowes, R. G., and Campusano, L. E. (2002). Quasar environment in the context of large-scale structure at $z\sim0.3$. *Month. Notices R. Astron. Soc.* 331, 569–577. doi: 10.1046/j.1365-8711.2002.05123.x

Söchting, I. K., Clowes, R. G., and Campusano, L. E. (2004). Relation of radio-quiet quasars to galaxy clusters at $z < 0.3$. *Month. Notices R. Astron. Soc.* 347, 1241–1254. doi: 10.1111/j.1365-2966.2004.07306.x

Strand, N. E., Brunner, R. J., and Myers, A. D. (2008). AGN environments in the sloan digital sky survey. I. dependence on type, redshift, and luminosity. *Astrophys. J.* 688, 180–189. doi: 10.1086/592099

Uslenghi, M., and Falomo, R. (2011). AIDA: a software package for 2D model fitting analysis of astronomical images. *Appl. Digital Image Process. XXXIV*, 8135:813524. doi: 10.1117/12.913305

Wake, D. A., Miller, C. J., Di Matteo, T., Nichol, R. C., Pope, A., Szalay, A. S., et al. (2004). The clustering of active galactic nuclei in the sloan digital sky survey. *Astrophys. J. Lett.* 610, L85–L88. doi: 10.1086/423317

Conflict of Interest Statement: The authors declare that the research was conducted in the absence of any commercial or financial relationships that could be construed as a potential conflict of interest.

Copyright © 2017 Bettoni, Falomo, Kotilainen and Karhunen. This is an open-access article distributed under the terms of the Creative Commons Attribution License (CC BY). The use, distribution or reproduction in other forums is permitted, provided the original author(s) or licensor are credited and that the original publication in this journal is cited, in accordance with accepted academic practice. No use, distribution or reproduction is permitted which does not comply with these terms.

frontiers in Astronomy and Space Sciences

PERSPECTIVE
published: 21 November 2017
doi: 10.3389/fspas.2017.00051

The Overdense Environments of *WISE*-Selected, Ultra-Luminous, High-Redshift AGN in the Submillimeter

*Suzy F. Jones**

Department of Space, Earth, and Environment, Chalmers University of Technology, Onsala Space Observatory, Onsala, Sweden

The environments around *WISE*-selected hot dust obscured galaxies (Hot DOGs) and *WISE*/radio-selected active galactic nuclei (AGNs) at average redshifts of $z = 2.7$ and $z = 1.7$, respectively, were found to have overdensities of companion Submillimeter-selected sources. The overdensities were of ∼2–3 and ∼5–6 , respectively, compared with blank field submm surveys. The space densities in both samples were found to be overdense compared to normal star-forming galaxies and Submillimeter galaxies (SMGs). All of the companion sources have consistent mid-IR colors and mid-IR to submm ratios to SMGs. Monte Carlo simulations show no angular correlation, which could indicate protoclusters on scales larger than the SCUBA-2 1.5 arcmin scale maps. *WISE*-selected AGNs appear to be good indicators of overdense areas of active galaxies at high redshift.

Keywords: galaxies: active, galaxies: clusters: general, galaxies: high-redshift, galaxies: quasars: general, infrared: galaxies, submillimeter: galaxies

OPEN ACCESS

Edited by:
Paola Marziani, Osservatorio Astronomico di Padova (INAF), Italy

Reviewed by:
Mauro D'Onofrio, Università degli Studi di Padova, Italy
Daniela Bettoni, Osservatorio Astronomico di Padova (INAF), Italy
Giulia Rodighiero, Dipartimento di Fisica e Astronomia, Università degli Studi di Padova, Italy

***Correspondence:**
Suzy F. Jones
suzy.jones@chalmers.se

Specialty section:
This article was submitted to Milky Way and Galaxies, a section of the journal Frontiers in Astronomy and Space Sciences

Received: *12 July 2017*
Accepted: *07 November 2017*
Published: *21 November 2017*

Citation:
Jones SF (2017) The Overdense Environments of WISE-Selected, Ultra-Luminous, High-Redshift AGN in the Submillimeter. Front. Astron. Space Sci. 4:51. doi: 10.3389/fspas.2017.00051

1. INTRODUCTION

There has been previous evidence of overdense regions around high-redshift luminous galaxies (Blain et al., 2004; Borys et al., 2004; Farrah et al., 2006; Scott et al., 2006; Gilli et al., 2007; Magliocchetti and Brüggen, 2007; Chapman et al., 2009; Hickox et al., 2009; Cooray et al., 2010; Hickox et al., 2012; Donoso et al., 2014; Umehata et al., 2014). The evolution and properties of active galactic nuclei (AGNs) are connected to their host galaxies properties and their environments. The environments around high-redshift radio galaxies (HzRGs) and radio loud AGNs (RLAGNs)[1] have also been found to be overdense in dusty companions (Stevens et al., 2003; De Breuck et al., 2004; Falder et al., 2010; Galametz et al., 2010, 2012; Stevens et al., 2010; Mayo et al., 2012; Wylezalek et al., 2013; Dannerbauer et al., 2014; Hatch et al., 2014; Rigby et al., 2014; Wylezalek et al., 2014). RLAGNs are mostly found in giant, massive, elliptical galaxies and are in very dense environments (Matthews et al., 1964; Best et al., 2005; Donoso et al., 2010; Wylezalek et al., 2013). These could be signposts of high-redshift galaxy clusters (Wylezalek et al., 2013; Hatch et al., 2014).

Overdense environments around AGNs could be evidence for massive dark matter halos and highlight the bias of this distribution as compared with the underlying dark matter distribution. It is important to understand the evolution of the underlying dark matter distribution because the formation of dark matter halos are connected to the formation of galaxies and therefore to the

[1] RLAGNs can be classified by $S_{5GHz} / S_B \geq 10$ (Kellermann et al., 1989; Miller and Goodrich, 1990; Urry and Padovani, 1995) and $L_{500\,MHz} \geq 10^{27.5}$ W Hz^{-1} (Donoso et al., 2010; Hatch et al., 2014).

properties of galaxies in the local Universe (Mo and White, 2002; Wechsler et al., 2006; Bett et al., 2007; Gao et al., 2007; Jing et al., 2007; Wetzel et al., 2007; Fakhouri and Ma, 2009; Fakhouri et al., 2010; Faltenbacher and White, 2010; Wake et al., 2012; Avila et al., 2014). Studying galaxies at higher redshifts can reveal the processes that have formed galaxies around us today.

The question of why AGN lie in dense regions and how they are affected by their environments is still debated. One suggestions is that there is hot halo mode accretion (cooling of the hot viralised atmospheres) in dense environments and cold mode accretion (galaxies accrete gas directly from cold dense intergalactic filaments) in less dense environments (Coil et al., 2009; Fanidakis et al., 2011). Coldwell and Lambas (2006) concluded that the number density of galaxies around AGN is similar to that around normal galaxies. Likewise Miller et al. (2003) found no difference in the local density around field galaxies and AGN. This is in contrast to results from for example, Kauffmann et al. (2004), Ruderman and Ebeling (2005), Serber et al. (2006), and Georgakakis et al. (2007) that indicate higher galaxy density around AGN. Quasars ($M_i \leq -22$, $z \leq 0.4$) have been found to have high density regions around them at radii between 25 kpc and 1 Mpc, with the overdensity being greatest closest to the quasar (Serber et al., 2006). Hatch et al. (2011) also found overdense regions surround Hα emitters at $z \sim 2$ that could be signposts to protocluster environments. They concluded that galaxy growth was accelerated in dense environments in the early Universe. Simulations have shown small-scale excess at scales below $\sim$100 h^{-1} kpc (Degraf et al., 2011), consistent with observational evidence (Hennawi et al., 2006; Myers et al., 2007).

The clustering of galaxies is important because it signposts the environment richness of the galaxies. Galaxies reside in dark matter halos and the mass of the dark matter halos determines the clustering strength and the strength of the biasing (Strauss and Willick, 1995). Clustering can be used to measure dark matter halo mass and how the galaxies populate the dark matter halos (Coil, 2013), and constrain cosmological parameters in galaxy evolution models for example baryon density (Davis et al., 1985; Kauffmann et al., 1993; Navarro et al., 1996; Springel et al., 2005; Coil, 2013).

Studying the environments of Hot DOGs and *WISE*/radio AGNs will help to understand the evolution of galaxies and the link with their host galaxy.

2. SAMPLES

Advances in infrared (IR) telescope technology like the NASA's *Wide-Field Infrared Survey Explorer* (*WISE*; Wright et al., 2010) have enabled observations of luminous AGN that have been difficult to find with previous IR missions. *WISE* is able to find luminous, dusty, high-redshift, active galaxies because the hot dust heated by AGN and/or starburst activity can be traced using the *WISE* 12 μm (W3) and 22 μm (W4) bands. Eisenhardt et al. (2012), Bridge et al. (2013), and Lonsdale et al. (2015) have shown that *WISE* can find different classes of interesting, luminous, high-redshift, dust-obscured AGN.

Submillimeter observations using the James Clerk Maxwell Telescope (JCMT) Submillimeter Common-User Bolometer Array 2 (SCUBA-2) (Holland et al., 2013) of two subsamples of *Wide-Field Infrared Survey Explorer* (*WISE*; Wright et al., 2010) selected galaxies found overdensities of Submillimeter galaxies (SMGs)[2] (Jones et al., 2014, 2015).

The first subsample of *WISE*-selected galaxies were faint or undetectable flux densities in the 3.4 μm (W1) and 4.6 μm (W2) bands, and well detected fluxes in the W3 and/or W4 bands, with a radio blind selection, giving a "W1W2-dropout" selection yielding hot, dust obscured galaxies (Hot DOGs) (Eisenhardt et al., 2012; Wu et al., 2012).

The second subsample were found by Lonsdale et al. (2015), by combining *WISE* and National Radio Astronomy Observatory (NRAO) Very Large Array (VLA) Sky Survey (NVSS) (Condon et al., 1998) and/or Faint Images of the Radio Sky at Twenty-cm (FIRST) (Becker et al., 1995). They were selected in a similar method in the mid-IR, and are a similarly high luminosity, dust-obscured population and in this paper are known as *WISE*/radio AGNs. The strong compact radio emission could be from AGN jets (Lonsdale et al., 2015).

3. OVERDENSITY

JCMT SCUBA-2 observations of all the *WISE*-selected AGN were in the "CV DAISY" mode that produces a uniformly deep coverage 3-arcmin diameter map (Holland et al., 2013). Seventeen companion sources were detected at 3 σ significance or above in 10 JCMT SCUBA-2 fields of Hot DOGs reported by Jones et al. (2014) with an average root mean square (RMS) noise of 1.8 mJy beam^{-1}. Comparing these number counts to "blank field submm" surveys shows them to be overdense, with overdensity factor of 2–3, Jones et al. (2015).

Eighty-one companion sources were detected at 3 σ or greater significance in 30 *WISE*/radio-selected AGN fields reported by Jones et al. (2015) with average RMS noise of 2.1 mJy beam^{-1}. Comparing these number counts to "blank field submm" surveys shows them to be overdense, with overdensity factor of 5–6, Jones et al. (2014). The typical redshift of the 10 observed Hot DOGs is $z = 2.7$ (Jones et al., 2014).

WISE/radio-selected AGN were found to have a higher density of SMGs when compared with Hot DOGs by a factor of 2.4 ± 0.9 (Jones et al., 2015). The *WISE*/radio AGNs have a lower redshift range, fewer of the *WISE*-selected AGNs are submm detected and lower total IR luminosities compared with Hot DOGs (Jones et al., 2014, 2015). The K-correction at wavelengths longer than 500 μm remains approx. constant with increasing redshift. Due to this K-correction effect the SCUBA-2 fraction of SMG detection should be independent of redshift.

[2]Submm galaxies (SMGs) were historically defined by having a submm flux density of $S_{850\,\mu m} > 2$ mJy. SMGs are massive gas-rich, high-redshift galaxies with high IR luminosities, $L_{IR} \geq 10^{12}$ $L_\odot$, believed to be from starburst activity, with star formation rates (SFRs) of several 100–1,000 $M_\odot$ yr^{-1} (Smail et al., 1997; Ivison et al., 1998; Eales et al., 1999; Smail et al., 2000; Blain et al., 2002; Pope et al., 2006; Casey et al., 2014; Swinbank et al., 2014). SMGs are enshrouded by dust and hence are faint in optical and near-IR wavelengths.

The typical redshift of *WISE*/radio AGNs, $z = 1.3$ (Jones et al., 2015).

4. PROPERTIES OF COMPANION SOURCES

The average submm flux density of SMGs around Hot DOGs is $S_{850\,\mu m} = 6.2 \pm 1.8$ mJy, which is comparable to SMGs around *WISE*/radio AGNs, $S_{850\,\mu m} = 7.2 \pm 2.1$ mJy. Submm flux densities provide a reliable measurement of SFR (Alexander et al., 2016). The average SFR is $\simeq$1,240 $M_{\odot} yr^{-1}$ for SMGs around *WISE*/radio AGNs, slightly lower than the SFR $\simeq$1,460 $M_{\odot} yr^{-1}$ for SMGs around Hot DOGs.

The star formation rate density (SFRD) represents the total star formation transpiring per unit time and volume at a given redshift. The SFRDs range for Hot DOGs from $1{,}523 \pm 30 M_{\odot}$ yr^{-1} Mpc^{-3} to $7{,}949 \pm 159$ $M_{\odot}$ yr^{-1} Mpc^{-3}, and average 3,533 $M_{\odot}$ yr^{-1} Mpc^{-3}. These are lower than *WISE*/radio AGNs with a range from $1{,}219 \pm 49$ $M_{\odot}$ yr^{-1} Mpc^{-3} to $18{,}715 \pm 374$ $M_{\odot}$ yr^{-1} Mpc^{-3}, and average 3,929 $M_{\odot}$ yr^{-1} Mpc^{-3}. These values are consistent to four *Herschel* Multitiered Extragalactic Survey (HerMES) clusters of dusty, star-forming galaxies at redshifts between $z = 0.76$ to $z = 2.26$, and other clusters with MIR/FIR measurements from the literature with SFRDs ranging from $\sim$200$M_{\odot}$ yr^{-1} Mpc^{-3} to $\sim$3,000$M_{\odot}$ yr^{-1} Mpc^{-3}.

No counterparts to the companion sources from point sources were found in the third *XMM-Newton* companion Source Catalog, *3XMM*-DR5 (Rosen et al., 2015). None of the companion sources around Hot DOGs or *WISE*/radio AGNs were detected at radio wavelengths in FIRST and/or NVSS, where the typical 1.4 GHz detection limit was 1.0 mJy/beam.

Both sets of companion sources have similar *WISE* colors, Jones et al. (2017). When comparing with the *WISE* color-color diagram of different galaxy populations in Figure 12 in Wright et al. (2010) and Figure 26 in Jarrett et al. (2011), the companion sources lie in both the starburst (star-forming) galaxy zone and AGN zone.

The Hot DOGs and *WISE*/radio AGNs are redder than the companion sources, due to the *WISE*-selected AGN having higher dust obscuration and/or a higher AGN contribution, and higher dust temperatures than that of their companion sources. Hot DOGs and *WISE*/radio AGNs are predominantly powered by AGN (Wu et al., 2012; Jones et al., 2014, 2015; Lonsdale et al., 2015; Tsai et al., 2015). SMGs are predominantly powered by star formation (Alexander et al., 2005), with cooler dust emission (20–50 K) (Hainline et al., 2009).

5. CLUSTERING

The angular two-point correlation function $\omega(\theta)$ is a statistical way to determine the clustering of galaxies in 2D space (Efstathiou et al., 1991; Connolly et al., 1998), using the angular version of the 3D spatial correlation function (Peebles, 1980). It is the excess probability of finding galaxies separated by θ above the probability with a random distribution. The popular estimators described by Landy and Szalay (1993) was used, see **Figure 1**.

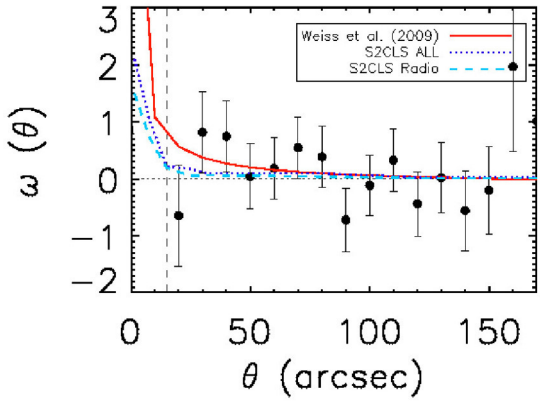

FIGURE 1 | Observed angular two-point correlation function using the Landy and Szalay (1993) equation, from Jones et al. (2017). The red solid curve shows the observed angular two-point correlation function for Weiß et al. (2009). The blue dotted line and cyan dashed line show the observed angular two-point correlation function for all the SMGs and the subset of radio-detected SMGs, respectively, in the S2CLS (Wilkinson et al., 2017). Black points represent the observed angular two-point correlation function for the companion sources detected around *WISE*/radio AGNs. The dashed line represents the JCMT SCUBA-2 850 μm beam size (15 arc s). There were not enough data for reliable and accurate results using the Hot DOGs.

The two-point angular clustering signal provided an upper limit to the strength of angular clustering (Jones et al., 2017), see **Figure 1**. Monte Carlo simulations showed no angular correlation, which could indicate protoclusters on scales larger than the SCUBA-2 1.5 arcmin scale maps.

Muldrew et al. (2015) investigated protoclusters and their environments using the Millennium Simulation. They found that protocluster structures are very extended at redshifts $z = 2$, with 90% of their mass is dispersed across $\sim$30 arcmin ($\sim$35 h^{-1} Mpc comoving). This suggests that many observations of protoclusters and high-redshift clusters are not imaging the full cluster. This could explain why there is an upper limit of angular clustering in the Hot DOGs and *WISE*/radio AGNs fields on $\sim$1.5 arcmin scales. Alternatively, the cluster might be peaked substantially off-center from the *WISE* target. Further and wider observations of companion sources in the fields around *WISE*/radio AGN are needed to determine the clustering of *WISE*-selected AGN.

6. DISCUSSION/CONCLUSION

1. Hot DOGs and *WISE*/radio AGNs have very high total IR luminosities, hot dust temperatures (60–120 K), and SEDs that are not well fitted by many standard AGN templates due to excess mid-IR emission and less submm emission (Jones et al., 2014, 2015).

2. Hot DOGs and *WISE*/radio AGNs appear to be consistent with the same population of very luminous, AGN-dominated galaxies but are different redshifts. They could be a new transient phase of the major merger model (Jones et al., 2014, 2015).

3. *WISE*/radio AGNs are typically at a lower redshift ($z = 1.7$) than Hot DOGs ($z = 2.7$). The lower redshift *WISE*/radio AGNs appear to reside in higher density regions compared with higher redshift Hot DOGs. This could be due to differences in redshift and/or radio emission. However, more observations are needed because only 10 targets in each sample have known redshifts, Jones et al. (2017).

4. The space densities of SMGs around the *WISE*-selected AGNs were found to overdense compared to normal star-forming galaxies and SMGs in the S2CLS, Jones et al. (2017).

5. There is an upper limit to the strength of angular clustering of the companion SMG sources in Hot DOGs and *WISE*/radio AGNs on SCUBA-2 1.5 arcmin scales. The typical separations when compared to Monte Carlo simulations showed no angular clustering. This is an agreement with the cumulative fraction of companion sources in different radii from the *WISE* target. This could be because they are satellite galaxies in the massive halo or that the protocluster is on bigger scales (up to ~ 30 arcmin) and we are not fully probing the protocluster, Jones et al. (2017).

6. The SMGs around *WISE*/radio AGNs $\sim 18\%$ higher SFRs than SMGs around Hot DOGs, Jones et al. (2017).

7. The SFRDs of the *WISE*-selected AGNs are higher than field galaxies, and consistent with values for known clusters of dusty galaxies, Jones et al. (2017).

8. The companion sources detected around Hot DOGs and *WISE*/radio AGNs have *WISE* colors consistent with star-forming galaxies and mid-IR to submm ratios not consistent with AGN dominated sources. This could imply that they are all consistent with SMGs, Jones et al. (2017).

9. All the companion sources have bluer mid-IR positions in the *WISE* color-color plot compared with Hot DOGs and *WISE*/radio AGNs, which implies cooler dust temperatures than 60–120 K, Jones et al. (2017).

10. Hot DOGs and *WISE*/radio AGNs appear to be good indicators of overdense environments of active galaxies in arcmin scales, Jones et al. (2017).

11. Further spectroscopic redshift data of the *WISE*-selected targets and their companion SMG sources are needed.

12. Further submm data of *WISE*-selected targets are needed to increase the sample size of *WISE*-selected targets. Also high-resolution ALMA data are needed to resolve the galaxies to see if there are multiple components for example of *WISE*-selected Hot DOG W2026+0716.

AUTHOR CONTRIBUTIONS

The author confirms being the sole contributor of this work and approved it for publication.

ACKNOWLEDGMENTS

This publication makes use of data products from the *Wide-field Infrared Survey Explorer*, which is a joint project of the University of California, Los Angeles, and the Jet Propulsion Laboratory/California Institute of Technology, funded by the National Aeronautics and Space Administration. The James Clerk Maxwell Telescope has historically been operated by the Joint Astronomy Centre on behalf of the Science and Technology Facilities Council of the United Kingdom, the National Research Council of Canada and the Netherlands Organization for Scientific Research. Additional funds for the construction of SCUBA-2 were provided by the Canada Foundation for Innovation. The program IDs under which the data were obtained were M12AU10, M12BU07, and M13BU02.

REFERENCES

Alexander, D. M., Simpson, J. M., Harrison, C. M., Mullaney, J. R., Smail, I., Geach, J. E., et al. (2016). ALMA observations of a z ≈ 3.1 protocluster: star formation from active galactic nuclei and Lyman-alpha blobs in an overdense environment. *Month. Notices R. Astron. Soc.* 461, 2944–2952. doi: 10.1093/mnras/stw1509

Alexander, D. M., Smail, I., Bauer, F. E., Chapman, S. C., Blain, A. W., Brandt, W. N., et al. (2005). Rapid growth of black holes in massive star-forming galaxies. *Nature* 434, 738–740. doi: 10.1038/nature03473

Avila, S., Knebe, A., Pearce, F. R., Schneider, A., Srisawat, C., Thomas, P. A., et al. (2014). SUSSING MERGER TREES: the influence of the halo finder. *Month. Notices R. Astron. Soc.* 441, 3488–3501. doi: 10.1093/mnras/stu799

Becker, R. H., White, R. L., and Helfand, D. J. (1995). The FIRST survey: Faint images of the radio sky at twenty centimeters. *Astrophys. J.* 450:559. doi: 10.1086/176166

Best, P. N., Kauffmann, G., Heckman, T. M., Brinchmann, J., Charlot, S., Ivezić, Ž., et al. (2005). The host galaxies of radio-loud active galactic nuclei: mass dependences, gas cooling and active galactic nuclei feedback. *Month. Notices R. Astron. Soc.* 362, 25–40. doi: 10.1111/j.1365-2966.2005.09192.x

Bett, P., Eke, V., Frenk, C. S., Jenkins, A., Helly, J., and Navarro, J. (2007). The spin and shape of dark matter haloes in the Millennium simulation of a Λ cold dark matter universe. *Month. Notices R. Astron. Soc.* 376, 215–232. doi: 10.1111/j.1365-2966.2007.11432.x

Blain, A. W., Chapman, S. C., Smail, I., and Ivison, R. (2004). Clustering of Submillimeter-selected Galaxies. *Astrophys. J.* 611, 725–731. doi: 10.1086/422353

Blain, A. W., Smail, I., Ivison, R. J., Kneib, J.-P., and Frayer, D. T. (2002). Submillimeter galaxies. *Phys. Rep.* 369, 111–176. doi: 10.1016/S0370-1573(02)00134-5

Borys, C., Scott, D., Chapman, S., Halpern, M., Nandra, K., and Pope, A. (2004). The hubble deep field north SCUBA super-map - II. Multiwavelength properties. *Month. Notices R. Astron. Soc.* 355, 485–503. doi: 10.1111/j.1365-2966.2004.08335.x

Bridge, C. R., Blain, A., Borys, C. J. K., Petty, S., Benford, D., Eisenhardt, P., et al. (2013). A new population of high-z, dusty Lyα emitters and blobs discovered by WISE: feedback caught in the act? *Astrophys. J.* 769:91. doi: 10.1088/0004-637X/769/2/91

Casey, C. M., Scoville, N. Z., Sanders, D. B., Lee, N., Cooray, A., Finkelstein, S. L., et al. (2014). Are dusty galaxies blue? Insights on UV attenuation from dust-selected galaxies. *Astrophys. J.* 796:95. doi: 10.1088/0004-637X/796/2/95

Chapman, S. C., Blain, A., Ibata, R., Ivison, R. J., Smail, I., and Morrison, G. (2009). Do submillimeter galaxies really trace the most massive dark-matter halos? Discovery of a high-z cluster in a highly active phase of evolution. *Astrophys. J.* 691, 560–568. doi: 10.1088/0004-637X/691/1/560

Coil, A. L. (2013). *The Large-Scale Structure of the Universe*. Dordrecht: Springer Science+Business Media.

Coil, A. L., Georgakakis, A., Newman, J. A., Cooper, M. C., Croton, D., Davis, M., et al. (2009). AEGIS: the clustering of X-ray active galactic

nucleus relative to galaxies at z ∼ 1. *Astrophys. J.* 701, 1484–1499. doi: 10.1088/0004-637X/701/2/1484

Coldwell, G. V., and Lambas, D. G. (2006). Properties of galaxies in Sloan Digital Sky Survey quasar environments at z<0.2. *Month. Notices R. Astron. Soc.* 371, 786–792. doi: 10.1111/j.1365-2966.2006.10712.x

Condon, J. J., Cotton, W. D., Greisen, E. W., Yin, Q. F., Perley, R. A., Taylor, G. B., et al. (1998). The NRAO VLA sky survey. *Astron. J.* 115, 1693–1716. doi: 10.1086/300337

Connolly, A. J., Szalay, A. S., and Brunner, R. J. (1998). Evolution of the angular correlation function. *Astrophys. J. Lett.* 499, L125–L129. doi: 10.1086/311362

Cooray, A., Amblard, A., Wang, L., Arumugam, V., Auld, R., Aussel, H., et al. (2010). HerMES: Halo occupation number and bias properties of dusty galaxies from angular clustering measurements. *Astron. Astrophys.* 518:L22. doi: 10.1051/0004-6361/201014597

Dannerbauer, H., Kurk, J. D., De Breuck, C., Wylezalek, D., Santos, J. S., Koyama, Y., et al. (2014). An excess of dusty starbursts related to the Spiderweb galaxy. *Astron. Astrophys.* 570:A55. doi: 10.1051/0004-6361/201423771

Davis, M., Efstathiou, G., Frenk, C. S., and White, S. D. M. (1985). The evolution of large-scale structure in a universe dominated by cold dark matter. *Astrophys. J.* 292, 371–394. doi: 10.1086/163168

De Breuck, C., Bertoldi, F., Carilli, C., Omont, A., Venemans, B., Röttgering, H., et al. (2004). A multi-wavelength study of the proto-cluster surrounding the z = 4.1 radio galaxy TN J1338-1942. *Astron. Astrophys.* 424, 1–12. doi: 10.1051/0004-6361:20035885

Degraf, C., Di Matteo, T., and Springel, V. (2011). Black hole clustering in cosmological hydrodynamic simulations: evidence for mergers. *Month. Notices R. Astron. Soc.* 413, 1383–1394. doi: 10.1111/j.1365-2966.2011.18221.x

Donoso, E., Li, C., Kauffmann, G., Best, P. N., and Heckman, T. M. (2010). Clustering of radio galaxies and quasars. *Month. Notices R. Astron. Soc.* 407, 1078–1089. doi: 10.1111/j.1365-2966.2010.16907.x

Donoso, E., Yan, L., Stern, D., and Assef, R. J. (2014). The angular clustering of WISE-selected active galactic nuclei: different halos for obscured and unobscured active galactic nuclei. *Astrophys. J.* 789:44. doi: 10.1088/0004-637X/789/1/44

Eales, S., Lilly, S., Gear, W., Dunne, L., Bond, J. R., Hammer, F., et al. (1999). The Canada-UK deep submillimeter survey: first submillimeter images, the source counts, and resolution of the background. *Astrophys. J.* 515, 518–524. doi: 10.1086/307069

Efstathiou, G., Bernstein, G., Tyson, J. A., Katz, N., and Guhathakurta, P. (1991). The clustering of faint galaxies. *Astrophys. J. Lett.* 380, L47–L50. doi: 10.1086/186170

Eisenhardt, P. R. M., Wu, J., Tsai, C.-W., Assef, R., Benford, D., Blain, A., et al. (2012). The first hyper-luminous infrared galaxy discovered by WISE. *Astrophys. J.* 755:173. doi: 10.1088/0004-637X/755/2/173

Fakhouri, O., and Ma, C.-P. (2009). Environmental dependence of dark matter halo growth - I. Halo merger rates. *Month. Notices R. Astron. Soc.* 394, 1825–1840. doi: 10.1111/j.1365-2966.2009.14480.x

Fakhouri, O., Ma, C.-P., and Boylan-Kolchin, M. (2010). The merger rates and mass assembly histories of dark matter haloes in the two Millennium simulations. *Month. Notices R. Astron. Soc.* 406, 2267–2278. doi: 10.1111/j.1365-2966.2010.16859.x

Falder, J. T., Stevens, J. A., Jarvis, M. J., Hardcastle, M. J., Lacy, M., McLure, R. J., et al. (2010). The environments of z ∼ 1 active galactic nuclei at 3.6 μm. *Month. Notices R. Astron. Soc.* 405, 347–358. doi: 10.1111/j.1365-2966.2010.16444.x

Faltenbacher, A., and White, S. D. M. (2010). Assembly bias and the dynamical structure of dark matter halos. *Astrophys. J.* 708, 469–473. doi: 10.1088/0004-637X/708/1/469

Fanidakis, N., Baugh, C. M., Benson, A. J., Bower, R. G., Cole, S., Done, C., et al. (2011). Grand unification of AGN activity in the ΛCDM cosmology. *Month. Notices R. Astron. Soc.* 410, 53–74. doi: 10.1111/j.1365-2966.2010.17427.x

Farrah, D., Lonsdale, C. J., Borys, C., Fang, F., Waddington, I., Oliver, S., et al. (2006). The spatial clustering of ultraluminous infrared galaxies over 1.5 < z < 3. *Astrophys. J. Lett.* 641, L17–L20. doi: 10.1086/503769

Galametz, A., Stern, D., De Breuck, C., Hatch, N., Mayo, J., Miley, G., et al. (2012). The mid-infrared environments of high-redshift radio galaxies. *Astrophys. J.* 749:169. doi: 10.1088/0004-637X/749/2/169

Galametz, A., Vernet, J., De Breuck, C., Hatch, N. A., Miley, G. K., Kodama, T., et al. (2010). Galaxy protocluster candidates at 1.6<z<2. *Astron. Astrophys.* 522:A58. doi: 10.1051/0004-6361/201015035

Gao, L., Yoshida, N., Abel, T., Frenk, C. S., Jenkins, A., and Springel, V. (2007). The first generation of stars in the Λ cold dark matter cosmology. *Month. Notices R. Astron. Soc.* 378, 449–468. doi: 10.1111/j.1365-2966.2007.11814.x

Georgakakis, A., Nandra, K., Laird, E. S., Cooper, M. C., Gerke, B. F., Newman, J. A., et al. (2007). AEGIS: the environment of X-ray sources at z ˜ 1. *Astrophys. J. Lett.* 660, L15–L18. doi: 10.1086/517920

Gilli, R., Comastri, A., and Hasinger, G. (2007). The synthesis of the cosmic X-ray background in the Chandra and XMM-Newton era. *Astron. Astrophys.* 463, 79–96. doi: 10.1051/0004-6361:20066334

Hainline, L. J., Blain, A. W., Smail, I., Frayer, D. T., Chapman, S. C., Ivison, R. J., et al. (2009). A mid-infrared imaging survey of submillimeter-selected galaxies with the spitzer space telescope. *Astrophys. J.* 699, 1610–1632. doi: 10.1088/0004-637X/699/2/1610

Hatch, N. A., De Breuck, C., Galametz, A., Miley, G. K., Overzier, R. A., Röttgering, H. J. A., et al. (2011). Galaxy protocluster candidates around z∼2.4 radio galaxies. *Month. Notices R. Astron. Soc.* 410, 1537–1549. doi: 10.1111/j.1365-2966.2010.17538.x

Hatch, N. A., Wylezalek, D., Kurk, J. D., Stern, D., De Breuck, C., Jarvis, M. J., et al. (2014). Why z>1 radio-loud galaxies are commonly located in protoclusters. *Month. Notices R. Astron. Soc.* 445, 280–289. doi: 10.1093/mnras/stu1725

Hennawi, J. F., Prochaska, J. X., Burles, S., Strauss, M. A., Richards, G. T., Schlegel, D. J., et al. (2006). Quasars probing quasars. I. Optically thick absorbers near luminous quasars. *Astrophys. J.* 651, 61–83. doi: 10.1086/507069

Hickox, R. C., Jones, C., Forman, W. R., Murray, S. S., Kochanek, C. S., Eisenstein, D., et al. (2009). Host galaxies, clustering, eddington ratios, and evolution of radio, X-ray, and infrared-selected AGNs. *Astrophys. J.* 696, 891–919. doi: 10.1088/0004-637X/696/1/891

Hickox, R. C., Wardlow, J. L., Smail, I., Myers, A. D., Alexander, D. M., Swinbank, A. M., et al. (2012). The LABOCA survey of the Extended Chandra Deep Field-South: clustering of submillimetre galaxies. *Month. Notices R. Astron. Soc.* 421, 284–295. doi: 10.1111/j.1365-2966.2011.20303.x

Holland, W. S., Bintley, D., Chapin, E. L., Chrysostomou, A., Davis, G. R., Dempsey, J. T., et al. (2013). SCUBA-2: the 10 000 pixel bolometer camera on the James Clerk Maxwell Telescope. *Month. Notices R. Astron. Soc.* 430, 2513–2533. doi: 10.1093/mnras/sts612

Ivison, R. J., Smail, I., Le Borgne, J.-F., Blain, A. W., Kneib, J.-P., Bezecourt, J., et al. (1998). A hyperluminous galaxy at z=2.8 found in a deep submillimetre survey. *Month. Notices R. Astron. Soc.* 298, 583–593. doi: 10.1046/j.1365-8711.1998.01677.x

Jarrett, T. H., Cohen, M., Masci, F., Wright, E., Stern, D., Benford, D., et al. (2011). The Spitzer-WISE survey of the ecliptic poles. *Astrophys. J.* 735:112. doi: 10.1088/0004-637X/735/2/112

Jing, Y. P., Suto, Y., and Mo, H. J. (2007). The dependence of dark halo clustering on formation epoch and concentration parameter. *Astrophys. J.* 657, 664–668. doi: 10.1086/511130

Jones, S. F., Blain, A. W., Assef, R. J., Eisenhardt, P., Lonsdale, C., Condon, J., et al. (2017). Overdensities of SMGs around WISE-selected, ultraluminous, high-redshift AGNs. *Month. Notices R. Astron. Soc.* 469, 4565–4577. doi: 10.1093/mnras/stx1141

Jones, S. F., Blain, A. W., Lonsdale, C., Condon, J., Farrah, D., Stern, D., et al. (2015). Submillimetre observations of WISE/radio-selected AGN and their environments. *Month. Notices R. Astron. Soc.* 448, 3325–3338. doi: 10.1093/mnras/stv214

Jones, S. F., Blain, A. W., Stern, D., Assef, R. J., Bridge, C. R., Eisenhardt, P., et al. (2014). Submillimetre observations of WISE-selected high-redshift, luminous, dusty galaxies. *Month. Notices R. Astron. Soc.* 443, 146–157. doi: 10.1093/mnras/stu1157

Kauffmann, G., White, S. D. M., and Guiderdoni, B. (1993). The formation and evolution of galaxies within merging dark matter haloes. *Month. Notices R. Astron. Soc.* 264:201. doi: 10.1093/mnras/264.1.201

Kauffmann, G., White, S. D. M., Heckman, T. M., Ménard, B., Brinchmann, J., Charlot, S., et al. (2004). The environmental dependence of the relations between stellar mass, structure, star formation and nuclear activity in galaxies. *Month. Notices R. Astron. Soc.* 353, 713–731. doi: 10.1111/j.1365-2966.2004.08117.x

Kellermann, K. I., Sramek, R., Schmidt, M., Shaffer, D. B., and Green, R. (1989). VLA observations of objects in the Palomar Bright Quasar Survey. *Astron. J.* 98, 1195–1207. doi: 10.1086/115207

Landy, S. D., and Szalay, A. S. (1993). Bias and variance of angular correlation functions. *Astrophys. J.* 412, 64–71. doi: 10.1086/172900

Lonsdale, C. J., Lacy, M., Kimball, A. E., Blain, A., Whittle, M., Wilkes, B., et al. (2015). Radio jet feedback and star formation in heavily obscured, hyperluminous quasars at redshifts ∼0.5–3. I. ALMA observations. *Astrophys. J.* 813:45. doi: 10.1088/0004-637X/813/1/45

Magliocchetti, M., and Brüggen, M. (2007). The interplay between radio galaxies and cluster environment. *Month. Notices R. Astron. Soc.* 379, 260–274. doi: 10.1111/j.1365-2966.2007.11939.x

Matthews, T. A., Morgan, W. W., and Schmidt, M. (1964). A discussion of galaxies indentified with radio sources. *Astrophys. J.* 140:35. doi: 10.1086/147890

Mayo, J. H., Vernet, J., De Breuck, C., Galametz, A., Seymour, N., and Stern, D. (2012). Overdensities of 24 μm sources in the vicinities of high-redshift radio galaxies. *Astron. Astrophys.* 539:A33. doi: 10.1051/0004-6361/201118254

Miller, C. J., Nichol, R. C., Gómez, P. L., Hopkins, A. M., and Bernardi, M. (2003). The environment of active galactic nuclei in the sloan digital sky survey. *Astrophys. J.* 597, 142–156. doi: 10.1086/378383

Miller, J. S., and Goodrich, R. W. (1990). Spectropolarimetry of high-polarization Seyfert 2 galaxies and unified Seyfert theories. *Astrophys. J.* 355, 456–467. doi: 10.1086/168780

Mo, H. J., and White, S. D. M. (2002). The abundance and clustering of dark haloes in the standard ΛCDM cosmogony. *Month. Notices R. Astron. Soc.* 336, 112–118. doi: 10.1046/j.1365-8711.2002.05723.x

Muldrew, S. I., Hatch, N. A., and Cooke, E. A. (2015). What are protoclusters? - Defining high-redshift galaxy clusters and protoclusters. *Month. Notices R. Astron. Soc.* 452, 2528–2539. doi: 10.1093/mnras/stv1449

Myers, A. D., Brunner, R. J., Nichol, R. C., Richards, G. T., Schneider, D. P., and Bahcall, N. A. (2007). Clustering analyses of 300,000 photometrically classified quasars. I. Luminosity and redshift evolution in quasar bias. *Astrophys. J.* 658, 85–98. doi: 10.1086/511519

Navarro, J. F., Frenk, C. S., and White, S. D. M. (1996). The structure of cold dark matter halos. *Astrophys. J.* 462:563. doi: 10.1086/177173

Peebles, P. J. E. (1980). *The Large-Scale Structure of the Universe*. Princeton, NJ: Princeton University Press.

Pope, A., Scott, D., Dickinson, M., Chary, R.-R., Morrison, G., Borys, C., et al. (2006). The hubble deep field-north SCUBA super-map - IV. Characterizing submillimetre galaxies using deep Spitzer imaging. *Month. Notices R. Astron. Soc.* 370, 1185–1207. doi: 10.1111/j.1365-2966.2006.10575.x

Rigby, E. E., Hatch, N. A., Röttgering, H. J. A., Sibthorpe, B., Chiang, Y. K., Overzier, R., et al. (2014). Searching for large-scale structures around high-redshift radio galaxies with Herschel. *Month. Notices R. Astron. Soc.* 437, 1882–1893. doi: 10.1093/mnras/stt2019

Rosen, S., Watson, M., Pye, J., Webb, N., Schwope, A., Freyberg, M., et al. (2015). "The 3XMM-DR4 catalogue," in *Astronomical Data Analysis Software an Systems XXIV (ADASS XXIV), Vol. 495 of Astronomical Society of the Pacific Conference Series*, eds A. R. Taylor and E. Rosolowsky (San Francisco, CA), 319.

Ruderman, J. T., and Ebeling, H. (2005). The origin of the spatial distribution of X-ray-luminous active galactic nuclei in massive galaxy clusters. *Astrophys. J. Lett.* 623, L81–L84. doi: 10.1086/430131

Scott, S. E., Dunlop, J. S., and Serjeant, S. (2006). A combined re-analysis of existing blank-field SCUBA surveys: comparative 850-μm source lists, combined number counts, and evidence for strong clustering of the bright submillimetre galaxy population on arcminute scales. *Month. Notices R. Astron. Soc.* 370, 1057–1105. doi: 10.1111/j.1365-2966.2006.10478.x

Serber, W., Bahcall, N., Ménard, B., and Richards, G. (2006). The small-scale environment of quasars. *Astrophys. J.* 643, 68–74. doi: 10.1086/501443

Smail, I., Ivison, R. J., and Blain, A. W. (1997). A deep sub-millimeter survey of lensing clusters: a new window on galaxy formation and evolution. *Astrophys. J. Lett.* 490:L5. doi: 10.1086/311017

Smail, I., Ivison, R. J., Owen, F. N., Blain, A. W., and Kneib, J.-P. (2000). Radio constraints on the identifications and redshifts of submillimeter galaxies. *Astrophys. J.* 528, 612–616. doi: 10.1086/308226

Springel, V., White, S. D. M., Jenkins, A., Frenk, C. S., Yoshida, N., Gao, L., et al. (2005). Simulations of the formation, evolution and clustering of galaxies and quasars. *Nature* 435, 629–636. doi: 10.1038/nature03597

Stevens, J. A., Ivison, R. J., Dunlop, J. S., Smail, I. R., Percival, W. J., Hughes, D. H., et al. (2003). The formation of cluster elliptical galaxies as revealed by extensive star formation. *Nature* 425, 264–267. doi: 10.1038/nature01976

Stevens, J. A., Jarvis, M. J., Coppin, K. E. K., Page, M. J., Greve, T. R., Carrera, F. J., et al. (2010). An excess of star-forming galaxies in the fields of high-redshift QSOs. *Month. Notices R. Astron. Soc.* 405, 2623–2638. doi: 10.1111/j.1365-2966.2010.16641.x

Strauss, M. A., and Willick, J. A. (1995). The density and peculiar velocity fields of nearby galaxies. *Phys. Rep.* 261, 271–431. doi: 10.1016/0370-1573(95)00013-7

Swinbank, A. M., Simpson, J. M., Smail, I., Harrison, C. M., Hodge, J. A., Karim, A., et al. (2014). An ALMA survey of sub-millimetre Galaxies in the Extended Chandra Deep Field South: the far-infrared properties of SMGs. *Month. Notices R. Astron. Soc.* 438, 1267–1287. doi: 10.1093/mnras/stt2273

Tsai, C.-W., Eisenhardt, P. R. M., Wu, J., Stern, D., Assef, R. J., Blain, A. W., et al. (2015). The most luminous galaxies discovered by WISE. *Astrophys. J.* 805:90. doi: 10.1088/0004-637X/805/2/90

Umehata, H., Tamura, Y., Kohno, K., Hatsukade, B., Scott, K. S., Kubo, M., et al. (2014). AzTEC/ASTE 1.1-mm survey of SSA22: counterpart identification and photometric redshift survey of submillimetre galaxies. *Month. Notices R. Astron. Soc.* 440, 3462–3478. doi: 10.1093/mnras/stu447

Urry, C. M., and Padovani, P. (1995). Unified Schemes for Radio-Loud Active Galactic Nuclei. *Publ. Astron. Soc. Pacific* 107:803. doi: 10.1086/133630

Wake, D. A., Franx, M., and van Dokkum, P. G. (2012). Which galaxy property is the best indicator of its host dark matter halo properties? arXiv:1201.1913.

Wechsler, R. H., Zentner, A. R., Bullock, J. S., Kravtsov, A. V., and Allgood, B. (2006). The dependence of halo clustering on halo formation history, concentration, and occupation. *Astrophys. J.* 652, 71–84. doi: 10.1086/507120

Weiß, A., Kovács, A., Coppin, K., Greve, T. R., Walter, F., Smail, I., et al. (2009). The large apex bolometer camera survey of the extended chandra deep field south. *Astrophys. J.* 707, 1201–1216. doi: 10.1088/0004-637X/707/2/1201

Wetzel, A. R., Cohn, J. D., White, M., Holz, D. E., and Warren, M. S. (2007). The clustering of massive halos. *Astrophys. J.* 656, 139–147. doi: 10.1086/510444

Wilkinson, A., Almaini, O., Chen, C.-C., Smail, I., Arumugam, V., Blain, A., et al. (2017). The SCUBA-2 cosmology legacy survey: the clustering of submillimetre galaxies in the UKIDSS UDS field. *Month. Notices R. Astron. Soc.* 464, 1380–1392. doi: 10.1093/mnras/stw2405

Wright, E. L., Eisenhardt, P. R. M., Mainzer, A. K., Ressler, M. E., Cutri, R. M., Jarrett, T., et al. (2010). The wide-field infrared survey explorer (WISE): mission description and initial on-orbit performance. *Astron. J.* 140, 1868–1881. doi: 10.1088/0004-6256/140/6/1868

Wu, J., Tsai, C.-W., Sayers, J., Benford, D., Bridge, C., Blain, A., et al. (2012). Submillimeter follow-up of WISE-selected hyperluminous galaxies. *Astrophys. J.* 756:96. doi: 10.1088/0004-637X/756/1/96

Wylezalek, D., Galametz, A., Stern, D., Vernet, J., De Breuck, C., Seymour, N., et al. (2013). Galaxy clusters around radio-loud active galactic nuclei at $1.3 < z < 3.2$ as seen by spitzer. *Astrophys. J.* 769:79. doi: 10.1088/0004-637X/769/1/79

Wylezalek, D., Vernet, J., De Breuck, C., Stern, D., Brodwin, M., Galametz, A., et al. (2014). The galaxy cluster mid-infrared luminosity function at $1.3 < z < 3.2$. *Astrophys. J.* 786:17. doi: 10.1088/0004-637X/786/1/17

Conflict of Interest Statement: The author declares that the research was conducted in the absence of any commercial or financial relationships that could be construed as a potential conflict of interest.

The reviewer DB and handling Editor declared their shared affiliation.

Copyright © 2017 Jones. This is an open-access article distributed under the terms of the Creative Commons Attribution License (CC BY). The use, distribution or reproduction in other forums is permitted, provided the original author(s) or licensor are credited and that the original publication in this journal is cited, in accordance with accepted academic practice. No use, distribution or reproduction is permitted which does not comply with these terms.

frontiers in Astronomy and Space Sciences

MINI REVIEW
published: 30 November 2017
doi: 10.3389/fspas.2017.00054

Large-Scale Environment Properties of Narrow-Line Seyfert 1 Galaxies at $z < 0.4$

Emilia Järvelä[1,2]*, *A. Lähteenmäki*[1,2,3] *and H. Lietzen*[3]

[1] Metsähovi Radio Observatory, Aalto University, Espoo, Finland, [2] Department of Electronics and Nanoengineering, Aalto University, Espoo, Finland, [3] Tartu Observatory, Tõravere, Estonia

The large-scale environment is believed to affect the evolution and intrinsic properties of galaxies. It offers a new perspective on narrow-line Seyfert 1 galaxies (NLS1) which have not been extensively studied in this context before. We study a large and diverse sample of 960 NLS1 galaxies using a luminosity-density field constructed using Sloan Digital Sky Survey. We investigate how the large-scale environment is connected to the properties of NLS1 galaxies, especially their radio loudness. Furthermore, we compare the large-scale environment properties of NLS1 galaxies with other active galactic nuclei (AGN) classes, for example, other jetted AGN and broad-line Seyfert 1 (BLS1) galaxies, to shed light on their possible relations. In general NLS1 galaxies reside in less dense large-scale environments than any of our comparison samples, thus supporting their young age. The average luminosity-density and distribution to different luminosity-density regions of NLS1 sources is significantly different compared to BLS1 galaxies. This contradicts the simple orientation-based unification of NLS1 and BLS1 galaxies, and weakens the hypothesis that BLS1 galaxies are the parent population of NLS1 galaxies. The large-scale environment density also has an impact on the intrinsic properties of NLS1 galaxies; the radio loudness increases with the increasing luminosity-density. However, our results suggest that the NLS1 population is indeed heterogeneous, and that a considerable fraction of them are misclassified. We support a suggested description that the traditional classification based on the radio loudness should be replaced with the division to jetted and non-jetted sources.

Keywords: active galactic nuclei, narrow-line Seyfert 1 galaxies, large-scale environment, radio loudness, relativistic jets

OPEN ACCESS

Edited by:
Ascensión Del Olmo, Instituto de Astrofísica de Andalucía (CSIC), Spain

Reviewed by:
Daniela Bettoni, Osservatorio Astronomico di Padova (INAF), Italy
Elias Koulourids, CEA Saclay, France

***Correspondence:**
Emilia Järvelä
emilia.jarvela@aalto.fi

Specialty section:
This article was submitted to Milky Way and Galaxies, a section of the journal Frontiers in Astronomy and Space Sciences

Received: *25 August 2017*
Accepted: *16 November 2017*
Published: *30 November 2017*

Citation:
Järvelä E, Lähteenmäki A and Lietzen H (2017) Large-Scale Environment Properties of Narrow-Line Seyfert 1 Galaxies at z < 0.4. Front. Astron. Space Sci. 4:54. doi: 10.3389/fspas.2017.00054

1. INTRODUCTION

An intriguing class of active galactic nuclei (AGN) are narrow-line Seyfert 1 (NLS1) galaxies. They are characterized by narrow permitted emission lines (Goodrich, 1989), relatively weak [O III] (Osterbrock and Pogge, 1985) and strong Fe II (Osterbrock and Pogge, 1985). They host low or intermediate mass black holes (Peterson et al., 2000) accreting close to the Eddington limit (Boroson and Green, 1992). NLS1 sources are preferably, but not exclusively, hosted by disk-like galaxies. These remarkable properties indicate that they are evolutionarily young, or possibly rejuvenated, AGN (Mathur et al., 2001).

Only ∼7% of these sources are radio-loud (RL) (Komossa et al., 2006). They usually show only a compact radio core, but recent studies suggest that pc- and kpc-scale structures are not that rare

either (e.g., Gliozzi et al., 2010; Doi et al., 2013; Richards and Lister, 2015; Lister et al., 2016). Moreover, *Fermi* detected gamma-ray emission in some NLS1 galaxies (e.g., Abdo et al., 2009), confirming the presence of powerful relativistic jets.

NLS1 population is seemingly heterogeneous including radio- and gamma-loud sources as well as totally radio-silent (RS) sources. This divergence complicates the studies of the whole NLS1 population. An alternative take on this issue is to study the environments of NLS1 galaxies. The environment affects the evolution of galaxies, and consequently their nuclear activity. The environment can be divided into several scales: (1) the host galaxy; (2) the local environment, including the closest galaxies and the group or cluster the galaxy belongs to; and (3) the large-scale environment, tracing the cosmic web of voids, filaments and superclusters.

Here we present the main results of a study of the large-scale environments of NLS1 galaxies. The large-scale environment position of the galaxy affects its properties; the galaxies residing in the densest environments are preferably ellipticals, and the fraction of late-type galaxies increases as the density decreases (Lietzen et al., 2012; Einasto et al., 2014; Chen et al., 2017; Kuutma et al., 2017; Pandey and Sarkar, 2017). Using a diverse and large, statistically significant sample we examine the large-scale environments of NLS1 galaxies. We compare the environment properties of NLS1 galaxies and other types of AGN, as well as study the trends within the NLS1 population. In addition, we investigate whether the large-scale environment is connected to the intrinsic properties of NLS1 galaxies. We assume a cosmology with $H_0 = 73$ km s^{-1} Mpc^{-1}, $\Omega_{\rm matter} = 0.27$ and $\Omega_{\rm vacuum} = 0.73$ (Spergel et al., 2007).

2. SAMPLE AND DATA

Our sample includes 960 sources from Zhou et al. (2006), Komossa et al. (2006), Whalen et al. (2006), Yuan et al. (2008), and Foschini (2011) at a redshift range of $z = 0.0726 - 0.3996$, and with a mean redshift of $z = 0.2340$. The radio-loudness (R, the ratio between the radio flux density, $F_{\rm R}$, and the optical flux density, $F_{\rm O}$) was computed for sources with radio (1.4 GHz) and optical (468.6 nm) data, obtained from ASI Science Data Center (ASDC[1]). The archival data are non-simultaneous.

K-correction was not applied since the variability of NLS1 sources in radio and optical bands affects R significantly more than the K-correction. Even though R is not an ideal way to estimate the radio characteristics of AGN, it is commonly used and enables us to compare our results with earlier studies. Accordingly, 74 of our sources are RL ($10 < R < 100$), 13 are very radio-loud (VRL, $R > 100$) and 73 RQ ($R < 10$). 161 sources are radio-detected (RD), leaving 799 seemingly RS sources. Some RS NLS1 galaxies have been detected at Metsähovi Radio Observatory at 37 GHz (Lähteenmäki et al. in preparation.), indicating that a fraction of them is misclassified. The arbitrary boundary between RL and RQ sources, their variability, and misclassifications might affect the data analysis. Additionally we use a subsample of 15 jetted NLS1 galaxies in which the radio emission is known to be dominated by a relativistic jet (see section 5.3).

We estimated black hole masses ($M_{\rm BH}$) using the $FWHM$(Hβ)—luminosity mass scaling relation (Greene and Ho, 2005)

$$M_{\rm BH} = (4.4 \pm 0.2) \times 10^6 \left(\frac{\lambda L_{5100}}{10^{44}\ {\rm ergs\ s^{-1}}}\right)^{0.64\pm0.02} \left(\frac{FWHM(H\beta)}{10^3\ {\rm km\ s^{-1}}}\right)^2 M_\odot \quad (1)$$

The λL_{5100} and $FWHM$(Hβ) values were from Zhou et al. (2006). We were able to estimate $M_{\rm BH}$ for 937 sources. This method does not take into account possible inclination effects caused by the geometry of the BLR (Decarli et al., 2011), and for jetted sources it overestimates the $M_{\rm BH}$ (Wu et al., 2004). Regardless, this method can be used as an order of magnitude estimate in statistical studies.

3. LARGE-SCALE ENVIRONMENT

3.1. SDSS LRG LDF

SDSS LRG LDF is a three-dimensional low-resolution luminosity-density field (LDF) limited to 225–1,000 h^{-1} Mpc and constructed using a sample of luminous red galaxies (LRG) in SDSS DR7 (Abazajian et al., 2009). The mean luminosity-density around each source is calculated in a volume of 3 h^{-1} Mpc, using a 16 h^{-1} Mpc smoothing. Detailed description is available in Lietzen et al. (2011) and Liivamägi et al. (2012).

We study the large-scale environments of the subsamples and the total NLS1 sample and compare them to AGN samples studied in Lietzen et al. (2011) using the same LDF. **Table 1** lists average luminosity-densities and the distributions into different luminosity-density regions. For the average luminosity-densities the error is the standard error of the mean and for the percentages it is the Poissonian error. Seyfert 1 (Sy1) galaxies from Lietzen et al. (2011) are also listed. They used a cut of [O III]/Hβ > 3 when selecting their Sy1 sample thus it is a pure BLS1 sample. The regions are defined as in Lietzen et al. (2011); in a void the luminosity-density is <1.0, in an intermediate luminosity-density region it is between 1.0 and 3.0, and in a supercluster >3.0. The intermediate luminosity-density regions might correspond to either physical filaments or other areas of intermediate density, e.g., the outer parts of superclusters. It should be kept in mind that whereas superclusters are the densest structures at these scales this study does not probe smaller-scale galaxy clusters which are the densest regions in the Universe.

The large-scale environment properties of NLS1 galaxies are distinct when compared to samples in Lietzen et al. (2011); they have smaller average luminosity-density than any comparison sample, and a different spatial distribution. Of the samples in Lietzen et al. (2011) NLS1 galaxies most resemble BLS1 and Sy2 galaxies; this was expected since Seyfert galaxies in general are young, late-type galaxies, whereas other AGN classes in Lietzen et al. (2011) are evolved, older galaxies, for example, BL Lac objects and Fanaroff-Riley I and II galaxies. Nevertheless, the difference is significant and supported by the divergence in their

[1] www.asdc.asi.it

TABLE 1 | Average density of the total SDSS LRG sample and the NLS1 subsamples, percentage in voids, intermediate density regions, and superclusters, and average black hole masses of different NLS1 subsamples.

	N	Average density	LD<1 (%)	1<LD<3 (%)	LD>3 (%)	log *M*_BH
Total	960	1.50 ± 0.04	44 ± 2	44 ± 2	12 ± 1	6.86 ± 0.01
RS	799	1.48 ± 0.05	45 ± 2	43 ± 2	12 ± 1	6.85 ± 0.01
RD	161	1.61 ± 0.10	40 ± 4	47 ± 4	13 ± 2	6.91 ± 0.03
RQ	73	1.48 ± 0.08	40 ± 5	52 ± 5	8 ± 3	6.91 ± 0.05
RL	74	1.66 ± 0.16	41 ± 5	43 ± 5	16 ± 4	6.91 ± 0.04
VRL	13	2.01 ± 0.36	38 ± 15	38 ± 15	23 ± 15	6.96 ± 0.10
RL and VRL	87	1.71 ± 0.14	40 ± 6	43 ± 6	17 ± 5	6.91 ± 0.04
BLS1 galaxies	1,095	1.73 ± 0.04	34 ± 1	51 ± 2	15 ± 1	

BLS1 galaxies from Lietzen et al. (2011) listed for comparison.

TABLE 2 | Results of the LRG PCA.

-	EV	+
R4570 -0.39	EV1 (30%)	F([O III]) 0.65 F_O 0.57 $FWHM$(Hβ) 0.31 Density 0.07
R4570 -0.60 F_O -0.42 F([O III]) -0.27 density -0.12	EV2 (25%)	$FWHM$(Hβ) 0.62
F_O -0.09 F([O III]) -0.07	EV3 (20%)	Density 0.98 $FWHM$(Hβ) 0.14 R4570 0.05

The coefficients have been grouped together based on their sign.

spatial distributions; compared to BLS1 and Sy2 galaxies a larger fraction of NLS1 galaxies reside in voids and a smaller fraction in intermediate-density regions. In superclusters the percentage is almost the same. Welch's t-test for the average luminosity-densities of the NLS1 and BLS1 samples gives a t-value of 3.96 which corresponds to the p-value of 0.0001, so it is highly unlikely that the averages are different by chance.

Among the NLS1 subsamples the average luminosity-density seems to increase with increasing R. Statistically the differences in the averages are not so significant and suffer from the small sample sizes; for RS and RQ, RS and RL, and RQ and RL samples the p-values according to Welch's t-test are 0.98, 0.11, and 0.23, respectively. Interestingly, the average luminosity-density of RL subsample is similar to the average luminosity-density of BLS1 sources in Lietzen et al. (2011). Increasing R also seems to induce changes in the spatial distribution, but confirming this would require a larger sample.

4. PRINCIPAL COMPONENT ANALYSIS

Principal component analysis (PCA, e.g., Abdi and Williams, 2010) is a useful tool in AGN studies. It can be utilized to find underlying connections and the most dominant variables in a data set, and helps to identify the physical properties connected with the eigenvectors (EV). Previous PCA studies of AGN (Boroson and Green, 1992; Boroson, 2002; Grupe, 2004; Xu et al., 2012; Järvelä et al., 2015) have led to the discovery of the 4DE1 parameter space, defined by $FWHM$(Hβ), F([O III]) λ5007, R4570, and C IV λ1549, explaining a host of differences observed in AGN, and possibly tracing the general AGN evolution (Marziani et al., 2006; Sulentic et al., 2007).

We performed weighted PCA using the `pca`[2] function in MATLAB Statistics and Machine Learning Toolbox. Including a large-scale environment parameter to the PCA allows us to investigate its connection to the AGN correlation space. In PCA we used F_O, $FWHM$(Hβ), R4570, F([O III]), and the luminosity-density. $FWHM$(Hβ), R4570, and F([O III]) were from Zhou et al. (2006). The results are presented in **Table 2**. The coefficients have been grouped together based on their sign, i.e., whether they correlate or anticorrelate with the EV and each other. The sign of the coefficient is insignificant as such and only their respective direction matters.

4.1. Eigenvectors and Their Correlations

4.1.1. EV1

EV1 accounts for 30% of the variance. It is dominated by F_O and F([O III]), which are anticorrelated with R4570. It is not exactly similar to the traditional EV1 driven by the anticorrelation of $FWHM$(Hβ) and F([O III]), and R4570. EV1 correlates with the Eddington ratio[3] to some extent (Spearman rank correlation coefficient $\rho = -0.506$, and probability value $p = 0.000$) and weakly with the M_{BH} ($\rho = 0.291$, $p = 0.000$).

4.1.2. EV2

EV2 25% of the variance is explained by EV2. It is dominated by the anticorrelation of R4570 and F_O, and $FWHM$(Hβ), and is similar to EV1 found in Boroson and Green (1992), Boroson (2002), and Xu et al. (2012). It indeed correlates strongly with the Eddington ratio (ρ = -0.764, $p = 0.000$), and significantly also with M_{BH} ($\rho = 0.394$, $p = 0.000$).

4.1.3. EV3

EV3 explains 20% of the variance. Density has the strongest impact on EV3 and all the other parameters are negligible. EV3 does not correlate strongly with the Eddington ratio (ρ = -0.157, $p = 0.000$) or M_{BH} ($\rho = 0.100$, $p = 0.002$). These results indicate that the large-scale environment density does not directly affect any singular properties, but rather the overall evolution of the galaxies.

5. DISCUSSION

5.1. NLS1s Compared to Other AGN

Earlier studies have found NLS1 galaxies to be morphologically young, late-type sources. In the framework of the density—morphology relation (Hubble and Humason, 1931; Dressler,

[2]https://se.mathworks.com/help/stats/pca.html

[3]L_{bol} / $L_{Edd} = 9\lambda\ L_{5100}$ / $1.3\times10^{38}\ M_{BH}$ / $M_\odot$

1980)—more evolved galaxies are found in denser regions—our results support this and confirm the young nature of the NLS1 population.

There is a clear difference in the average luminosity-densities of the NLS1 and BLS1 sources, contradicting the simple orientation-based unification model in which they can be unified when the geometrical effects are taken into account (Decarli et al., 2008; Rakshit et al., 2017). However, the diversity of BLS1 galaxies was not taken into account in Lietzen et al. (2011) and might affect the results; for example, BLS1 galaxies with pseudobulges might be alike to NLS1 galaxies and possibly part of their parent population. Alternatively, NLS1 and BLS1 galaxies might be unified through evolution; if the narrower broad lines of NLS1 galaxies compared to BLS1 galaxies are due to an undermassive black hole, growing NLS1 galaxies would eventually evolve to have higher mass black holes and broader broad lines, thus, BLS1 galaxies.

Recently, a few higher-inclination NLS1 sources have been found (Doi et al., 2015; Congiu et al., 2017), proving that the narrow lines in these sources are due to the undermassive black hole and indicating that no additional broad-line parent population is necessarily needed. However, the parent population studies are in the early stage and include a variety of scenarios, for example, compact steep-spectrum sources and disk-hosted radio galaxies have been proposed as possible parent populations of jetted NLS1 sources (Berton et al., 2015, 2016, 2017).

PCA supports the idea that NLS1 sources are a part of the AGN continuum; NLS1 EVs 1 and 2 are a manifestation of the 4DE1 AGN correlation space. Shen and Ho (2014) propose that the variations in $FWHM(\mathrm{H}\beta)$, R4570, and [O III], and their correlations can be explained with the Eddington ratio and the orientation; increasing Eddington ratio leads to increasing R4570 and decreasing [O III], and the scatter in $FWHM(\mathrm{H}\beta)$ is mainly a geometrical effect. NLS1 galaxies follow the same trend as broad-line AGN and complete the high R4570, low [O III] extreme of the continuum. We can not confirm or disprove the role of the orientation, but if the $FWHM(\mathrm{H}\beta)$ was orientation-dependent BLS1 sources should form the parent population of NLS1 galaxies, which, based on our large-scale environment results, seems improbable.

5.2. NLS1s as a Class

The incidence of RL sources increases toward the denser regions, indicating that the large-scale environment holds the capacity to alter the radio characteristics of NLS1 sources. The average M_{BH} of the subsamples at fixed redshift are similar, as can be seen in **Table 1**, and R does not correlate with M_{BH}, suggesting that M_{BH} and the radio properties do not have a strong connection. The average M_{BH} within the different luminosity-density regions are similar. For example, RL sources have similar average M_{BH} in voids, intermediate-density regions, and superclusters, as well as do RQ and RS sources. This might indicate that, at least up to this point, the accretion history of these sources has been similar in all density regions.

There is some indication that the spatial distributions of subsamples change with the changing R, which would be a natural consequence of the changing average luminosity-density, but a larger, cafefully classified, sample will be needed to verify this result. Heterogeneous samples are one of the caveats in extensive AGN population studies, and a possible reason why large statistical studies might give complex, or even inconsistent, results. Our study is no exception; some faint radio sources might be incorrectly in the RS subsample, R might be too high for sources with enhanced star formation, and the variability of NLS1 sources causes R to be time-dependent. Indeed, according to the two-sample Kolmogorov-Smirnov test our subsamples are drawn from the same luminosity-density distribution, further indicating that they are, in some degree, mixed.

5.3. Special Case of Jetted NLS1s

Padovani (2016) suggests that the main difference between RQ and RL sources is the presence of a powerful relativistic jet, and that definitions RQ and RL should be replaced with non-jetted and jetted. While this is true for most sources the situation is more complicated, for example, we know that radio-loudness can be induced by enhanced star formation (Caccianiga et al., 2015) and some RS sources do host relativistic jets (Lähteenmäki et al. in preparation.). Instead of using radio-loudness as a proxy for the nuclear activity the real physical properties, specifically the presence of a jet, should be used, but this is often impossible due to the lack of data.

We can begin to address this issue by concentrating on the sources known to have jets. We implement this by selecting a sample of NLS1 galaxies whose radio emission is dominated by the AGN; gamma-detected NLS1 galaxies, NLS1 sources with extended jets, sources detected at Metsähovi (Lähteenmäki et al. (2017) and Lähteenmäki et al. in preparation), and sources in which the radio emission is jet dominated based on the q22 parameter [$\log(F_{22\,\mu\mathrm{m}}/F_{1.4\,\mathrm{GHz}})$, Caccianiga et al., 2015].

After excluding two sources from the Metsähovi sample, initially selected for the observing programme due to their extraordinarily dense environments, we have 15 almost certainly jetted sources. For these sources the average luminosity-density is 1.75 ± 0.31 ($N = 15$). The average luminosity-densities for the mixed and star formation (SF) dominated subsamples (based on q22) are 1.68 ± 0.15 ($N = 82$) and 1.44 ± 0.14 ($N = 57$), respectively.

Despite the rather small subsamples it seems clear that the jetted NLS1 galaxies tend to reside in denser environments. Interestingly, the average luminosity-density of these is almost similar to the traditionally defined RL NLS1 sources (1.71 ± 0.14) and the average luminosity-density of the SF dominated sources is similar to the RS sources.

These results are consistent with the LRG LDF results; the increasing R increases the probability that the radio emission originates from the jet, and in SF dominated sources the contribution of the probably faint AGN to the radio emission is negligible. This does not exclude the possibility that jetted sources could have enhanced SF.

It is noteworthy that the average large-scale environment density of jetted NLS1 galaxies is similar to that of BLS1 galaxies (Lietzen et al., 2011). Jetted AGN samples in Lietzen et al. (2011) include BL Lac objects (2.50 ± 0.20), flat-spectrum radio galaxies (2.60 ± 0.07), FR I radio galaxies (3.01 ± 0.07), and

FR II radio galaxies (3.20 ± 0.04), all with significantly higher average luminosity-densities than the jetted NLS1 galaxies (1.75 ± 0.31). This pronounced difference confirms that jets are not exclusive to evolved galaxies in high density regions, but it is possible to trigger a jet in diverse environments. The large-scale environment affects the incidence of jets, but the triggering mechanism remains unclear.

6. SUMMARY

We examined the large-scale environment of NLS1 galaxies and its effect on their intrinsic properties. The environment provides an interesting new perspective on the AGN phenomena and helps us to understand how changes at the largest cosmic scales affect the smaller-scale properties of AGN and their evolution. Our main conclusions are the following.

1. Our results further establish the young, unevolved nature of NLS1 galaxies, and show that their radio properties are affected by the environment; RL and jetted NLS1 galaxies are more frequent in denser regions compared to RS, RQ and non-jetted sources.
2. As a class NLS1 galaxies are diverse and heterogeneous, and a considerable amount of them are misclassified. Our study supports the proposition to start using definitions non-jetted and jetted instead of RQ and RL (Padovani, 2016), and we further suggest that this division should be based on observed physical properties instead of radio-loudness parameter.
3. Our study suggests that NLS1 and BLS1 galaxies can not be unified only based on orientation. It is improbable that BLS1 galaxies would constitute the parent population of NLS1 galaxies. However, an evolutionarily link might exist.
4. NLS1 sources are part of the AGN 4DE1 continuum, but clearly distinctive in their nature when compared to the other gamma-ray emitting AGN.

The large-scale environment has an impact on the properties and evolution of AGN, amongst them NLS1 galaxies. However, it likely affects at very long time-scales and thus its connection to specific characteristics of variable and intermittent nuclear activity is weak. To effectively exploit this novel perspective the NLS1 environment studies should be extended to concern smaller-scale environment; the group and cluster scales, and host galaxy properties, both of which are likely to induce changes in AGN properties at shorter time-scales. The local environment studies (e.g., Dultzin-Hacyan et al., 1999; Krongold et al., 2001; Koulouridis et al., 2006, 2013; Koulouridis, 2014; Villarroel and Korn, 2014) indicate that Sy1 and Sy2 galaxies differ in their smaller-scale environments and host galaxies, but comprehensive studies including NLS1 galaxies are still needed. Extensive studies at various scales will clarify how the environment affects the AGN evolution, and help us establish the big picture of AGN. In addition, multiwavelength observations will be crucial to correctly classify the various NLS1 sources. This is essential to properly perform population-wide studies and address the heterogeneity issue of the NLS1 class.

AUTHOR CONTRIBUTIONS

All of the authors mentioned below fulfil the criteria for an authorship. EJ: data analysis and interpretation, main writer, final acceptance. AL: original research idea, writing and revision of the draft, final acceptance. HL: construction of the luminosity-density field, revision of the draft, final acceptance.

FUNDING

HL is funded by PUT1627 grant from Estonian Research Council.

ACKNOWLEDGMENTS

This research has made use of the NASA/IPAC Extragalactic Database (NED) which is operated by the Jet Propulsion Laboratory, California Institute of Technology, under contract with the National Aeronautics and Space Administration.

The National Radio Astronomy Observatory is a facility of the National Science Foundation operated under cooperative agreement by Associated Universities, Inc.

Funding for the Sloan Digital Sky Survey (SDSS) has been provided by the Alfred P. Sloan Foundation, the Participating Institutions, the National Aeronautics and Space Administration, the National Science Foundation, the U.S. Department of Energy, the Japanese Monbukagakusho, and the Max Planck Society. The SDSS Web site is http://www.sdss.org/.

The SDSS is managed by the Astrophysical Research Consortium (ARC) for the Participating Institutions. The Participating Institutions are The University of Chicago, Fermilab, the Institute for Advanced Study, the Japan Participation Group, The Johns Hopkins University, the Korean Scientist Group, Los Alamos National Laboratory, the Max-Planck-Institute for Astronomy (MPIA), the Max-Planck-Institute for Astrophysics (MPA), New Mexico State University, University of Pittsburgh, University of Portsmouth, Princeton University, the United States Naval Observatory, and the University of Washington.

REFERENCES

Abazajian, K. N., Adelman-McCarthy, J. K., Agüeros, M. A., Allam, S. S., Allende Prieto, C., An, D., et al. (2009). The seventh data release of the sloan digital sky survey. *Astrophys. J. Suppl.* 182, 543–558. doi: 10.1088/0067-0049/182/2/543

Abdi, H., and Williams, L. J. (2010). Principal component analysis. *Wiley Interdiscip. Rev.* 2, 433–459. doi: 10.1002/wics.101

Abdo, A. A., Ackermann, M., Ajello, M., Axelsson, M., Baldini, L., Ballet, J., et al. (2009). Fermi/large area telescope discovery of gamma-ray emission from a relativistic jet in the narrow-line quasar PMN J0948+0022. *Astrophys. J.* 699, 976–984. doi: 10.1088/0004-637X/699/2/976

Berton, M., Caccianiga, A., Foschini, L., Peterson, B. M., Mathur, S., Terreran, G., et al. (2016). Compact steep-spectrum sources as the parent population of flat-spectrum radio-loud narrow-line Seyfert 1 galaxies. *Astron. Astrophys.* 591:A98. doi: 10.1051/0004-6361/201628171

Berton, M., Foschini, L., Caccianiga, A., Ciroi, S., Congiu, E., Cracco, V., et al. (2017). An orientation-based unification of young jetted active galactic nuclei. ArXiv:1705.07905.

Berton, M., Foschini, L., Ciroi, S., Cracco, V., La Mura, G., Lister, M. L., et al. (2015). Parent population of flat-spectrum radio-loud narrow-line Seyfert 1 galaxies. *Astron. Astrophys.* 578:A28. doi: 10.1051/0004-6361/201525691

Boroson, T. A. (2002). Black hole mass and eddington ratio as drivers for the observable properties of radio-loud and radio-quiet QSOs. *Astrophys. J.* 565, 78–85. doi: 10.1086/324486

Boroson, T. A., and Green, R. F. (1992). The emission-line properties of low-redshift quasi-stellar objects. *Astrophys. J. Suppl.* 80, 109–135. doi: 10.1086/191661

Caccianiga, A., Antón, S., Ballo, L., Foschini, L., Maccacaro, T., Della Ceca, R., et al. (2015). WISE colours and star formation in the host galaxies of radio-loud narrow-line Seyfert 1. *Month. Notices R. Astron. Soc.* 451, 1795–1805. doi: 10.1093/mnras/stv939

Chen, Y.-C., Ho, S., Mandelbaum, R., Bahcall, N. A., Brownstein, J. R., Freeman, P. E., et al. (2017). Detecting effects of filaments on galaxy properties in the Sloan Digital Sky Survey III. *Month. Notices R. Astron. Soc.* 466, 1880–1893. doi: 10.1093/mnras/stw3127

Congiu, E., Berton, M., Giroletti, M., Antonucci, R., Caccianiga, A., Kharb, P., et al. (2017). Kiloparsec-scale emission in the narrow-line Seyfert 1 galaxy Mrk 783. ArXiv:1704.03881.

Decarli, R., Dotti, M., Fontana, M., and Haardt, F. (2008). Are the black hole masses in narrow-line Seyfert 1 galaxies actually small? *Month. Notices R. Astron. Soc.* 386, L15–L19. doi: 10.1111/j.1745-3933.2008.00451.x

Decarli, R., Dotti, M., and Treves, A. (2011). Geometry and inclination of the broad-line region in blazars. *Month. Notices R. Astron. Soc.* 413, 39–46. doi: 10.1111/j.1365-2966.2010.18102.x

Doi, A., Asada, K., Fujisawa, K., Nagai, H., Hagiwara, Y., Wajima, K., et al. (2013). Very long baseline array imaging of parsec-scale radio emissions in nearby radio-quiet narrow-line seyfert 1 galaxies. *Astrophys. J.* 765:69. doi: 10.1088/0004-637X/765/1/69

Doi, A., Wajima, K., Hagiwara, Y., and Inoue, M. (2015). A fanaroff-riley type I candidate in narrow-line seyfert 1 galaxy Mrk 1239. *Astrophys. J. Lett.* 798:L30. doi: 10.1088/2041-8205/798/2/L30

Dressler, A. (1980). Galaxy morphology in rich clusters - implications for the formation and evolution of galaxies. *Astrophys. J.* 236, 351–365. doi: 10.1086/157753

Dultzin-Hacyan, D., Krongold, Y., Fuentes-Guridi, I., and Marziani, P. (1999). The close environment of seyfert galaxies and its implication for unification models. *Astrophys. J. Lett.* 513, L111–L114. doi: 10.1086/311925

Einasto, M., Lietzen, H., Tempel, E., Gramann, M., Liivamägi, L. J., and Einasto, J. (2014). SDSS superclusters: morphology and galaxy content. *Astron. Astrophys.* 562:A87. doi: 10.1051/0004-6361/201323111

Foschini, L. (2011). "Evidence of powerful relativistic jets in narrow-line Seyfert 1 galaxies," in *Narrow-Line Seyfert 1 Galaxies and their Place in the Universe* (Milano).

Gliozzi, M., Papadakis, I. E., Grupe, D., Brinkmann, W. P., Raeth, C., and Kedziora-Chudczer, L. (2010). A panchromatic view of PKS 0558-504: an ideal laboratory to study the disk-jet link. *Astrophys. J.* 717, 1243–1252. doi: 10.1088/0004-637X/717/2/1243

Goodrich, R. W. (1989). Spectropolarimetry of 'narrow-line' Seyfert 1 galaxies. *Astrophys. J.* 342, 224–234. doi: 10.1086/167586

Greene, J. E., and Ho, L. C. (2005). Estimating black hole masses in active galaxies using the Hα emission line. *Astrophys. J.* 630, 122–129. doi: 10.1086/431897

Grupe, D. (2004). A complete sample of soft X-ray-selected AGNs. II. Statistical analysis. *Astron. J.* 127, 1799–1810. doi: 10.1086/382516

Hubble, E., and Humason, M. L. (1931). The velocity-distance relation among extra-galactic nebulae. *Astrophys. J.* 74:43. doi: 10.1086/143323

Järvelä, E., Lähteenmäki, A., and León-Tavares, J. (2015). Statistical multifrequency study of narrow-line Seyfert 1 galaxies. *Astron. Astrophys.* 573:A76.

Komossa, S., Voges, W., Xu, D., Mathur, S., Adorf, H.-M., Lemson, G., et al. (2006). Radio-loud narrow-line type 1 quasars. *Astron. J.* 132, 531–545. doi: 10.1086/505043

Koulouridis, E. (2014). The dichotomy of Seyfert 2 galaxies: intrinsic differences and evolution. *Astron. Astrophys.* 570:A72. doi: 10.1051/0004-6361/201424622

Koulouridis, E., Plionis, M., Chavushyan, V., Dultzin, D., Krongold, Y., Georgantopoulos, I., et al. (2013). Activity of the Seyfert galaxy neighbours. *Astron. Astrophys.* 552:A135. doi: 10.1051/0004-6361/201219606

Koulouridis, E., Plionis, M., Chavushyan, V., Dultzin-Hacyan, D., Krongold, Y., and Goudis, C. (2006). Local and large-scale environment of seyfert galaxies. *Astrophys. J.* 639, 37–45. doi: 10.1086/498421

Krongold, Y., Dultzin-Hacyan, D., and Marziani, P. (2001). Host galaxies and circumgalactic environment of "narrow line" seyfert 1 nuclei. *Astron. J.* 121, 702–709. doi: 10.1086/318768

Kuutma, T., Tamm, A., and Tempel, E. (2017). From voids to filaments: environmental transformations of galaxies in the SDSS. *Astron. Astrophys.* 600:L6. doi: 10.1051/0004-6361/201730526

Lähteenmäki, A., Järvelä, E., Hovatta, T., Tornikoski, M., Harrison, D. L., López-Caniego, M., et al. (2017). 37 GHz observations of narrow-line Seyfert 1 galaxies. ArXiv: 1703.10365.

Lietzen, H., Heinämäki, P., Nurmi, P., Liivamägi, L. J., Saar, E., Tago, E., et al. (2011). Large-scale environments of z < 0.4 active galaxies. *Astron. Astrophys.* 535:A21. doi: 10.1051/0004-6361/201116550

Lietzen, H., Tempel, E., Heinämäki, P., Nurmi, P., Einasto, M., and Saar, E. (2012). Environments of galaxies in groups within the supercluster-void network. *Astron. Astrophys.* 545:A104. doi: 10.1051/0004-6361/201219353

Liivamägi, L. J., Tempel, E., and Saar, E. (2012). SDSS DR7 superclusters. The catalogues. *Astron. Astrophys.* 539:A80. doi: 10.1051/0004-6361/201016288

Lister, M. L., Aller, M. F., Aller, H. D., Homan, D. C., Kellermann, K. I., Kovalev, Y. Y., et al. (2016). MOJAVE: XIII. Parsec-scale AGN jet kinematics analysis based on 19 years of VLBA observations at 15 GHz. *Astron. J.* 152:12. doi: 10.3847/0004-6256/152/1/12

Marziani, P., Dultzin-Hacyan, D., and Sulentic, J. W. (2006). *Accretion onto Supermassive Black Holes in Quasars: Learning from Optical/UV Observations*. New York, NY: Nova Science Publishers. 123.

Mathur, S., Kuraszkiewicz, J., and Czerny, B. (2001). Evolution of active galaxies: black-hole mass-bulge relations for narrow line objects. *NewA* 6, 321–329. doi: 10.1016/S1384-1076(01)00058-6

Osterbrock, D. E., and Pogge, R. W. (1985). The spectra of narrow-line Seyfert 1 galaxies. *Astrophys. J.* 297, 166–176. doi: 10.1086/163513

Padovani, P. (2016). The faint radio sky: radio astronomy becomes mainstream. *Astron. Astrophys. Rev.* 24:13. doi: 10.1007/s00159-016-0098-6

Pandey, B., and Sarkar, S. (2017). How much a galaxy knows about its large-scale environment?: an information theoretic perspective. *Month. Notices R. Astron. Soc.* 467, L6–L10. doi: 10.1093/mnrasl/slw250

Peterson, B. M., McHardy, I. M., Wilkes, B. J., Berlind, P., Bertram, R., Calkins, M., et al. (2000). X-ray and optical variability in NGC 4051 and the nature of narrow-line seyfert 1 galaxies. *Astrophys. J.* 542, 161–174. doi: 10.1086/309518

Rakshit, S., Stalin, C. S., Chand, H., and Zhang, X.-G. (2017). A catalog of narrow line seyfert 1 galaxies from the sloan digital sky survey data release 12. *Astrophys. J. Suppl.* 229:39. doi: 10.3847/1538-4365/aa6971

Richards, J. L., and Lister, M. L. (2015). Kiloparsec-scale jets in three radio-loud narrow-line seyfert 1 galaxies. *Astrophys. J. Lett.* 800:L8. doi: 10.1088/2041-8205/800/1/L8

Shen, Y., and Ho, L.C. (2014). The diversity of quasars unified by accretion and orientation. *Nature* 513, 210–213. doi: 10.1038/nature13712

Spergel, D. N., Bean, R., Doré, O., Nolta, M. R., Bennett, C. L., Dunkley, J., et al. (2007). Three-year Wilkinson microwave anisotropy probe (WMAP) observations: implications for cosmology. *Astrophys. J. Suppl.* 170, 377–408. doi: 10.1086/513700

Sulentic, J. W., Bachev, R., Marziani, P., Negrete, C. A., and Dultzin, D. (2007). C IV λ1549 as an eigenvector 1 parameter for active galactic nuclei. *Astrophys. J.* 666, 757–777. doi: 10.1086/519916

Villarroel, B., and Korn, A. J. (2014). The different neighbours around Type-1 and Type-2 active galactic nuclei. *Nat. Phys.* 10, 417–420. doi: 10.1038/nphys2951

Whalen, D. J., Laurent-Muehleisen, S. A., Moran, E. C., and Becker, R. H. (2006). Optical properties of radio-selected narrow-line seyfert 1 galaxies. *Astron. J.* 131, 1948–1960. doi: 10.1086/500825

Wu, X.-B., Wang, R., Kong, M. Z., Liu, F. K., and Han, J. L. (2004). Black hole mass estimation using a relation between the BLR size and emission line luminosity of AGN. *Astron. Astrophys.* 424, 793–798. doi: 10.1051/0004-6361:20035845

Xu, D., Komossa, S., Zhou, H., Lu, H., Li, C., Grupe, D., et al. (2012). Correlation analysis of a large sample of narrow-line seyfert 1 galaxies: linking central engine and host properties. *Astron. J.* 143:83. doi: 10.1088/0004-6256/143/4/83

Yuan, W., Zhou, H. Y., Komossa, S., Dong, X. B., Wang, T. G., Lu, H. L., et al. (2008). A population of radio-loud narrow-line seyfert 1 galaxies with blazar-like properties? *Astrophys. J.* 685, 801–827. doi: 10.1086/591046

Zhou, H., Wang, T., Yuan, W., Lu, H., Dong, X., Wang, J., et al. (2006). A comprehensive study of 2000 narrow line seyfert 1 galaxies from the sloan digital sky survey. I. The sample. *Astrophys. J. Suppl.* 166, 128–153. doi: 10.1086/504869

Conflict of Interest Statement: The authors declare that the research was conducted in the absence of any commercial or financial relationships that could be construed as a potential conflict of interest.

Copyright © 2017 Järvelä, Lähteenmäki and Lietzen. This is an open-access article distributed under the terms of the Creative Commons Attribution License (CC BY). The use, distribution or reproduction in other forums is permitted, provided the original author(s) or licensor are credited and that the original publication in this journal is cited, in accordance with accepted academic practice. No use, distribution or reproduction is permitted which does not comply with these terms.

frontiers in Astronomy and Space Sciences

PERSPECTIVE
published: 15 January 2018
doi: 10.3389/fspas.2017.00069

Tracing the External Origin of the AGN Gas Fueling Reservoir

*Sandra I. Raimundo**

Dark Cosmology Centre, Niels Bohr Institute, University of Copenhagen, Copenhagen, Denmark

Near-infrared observations of the active galaxy MCG–6-30-15 provide strong evidence that its molecular gas fueling reservoir is of external origin. MCG–6-30-15 has a counter-rotating core of stars within its central 400 pc and a counter-rotating disc of molecular gas that extends as close as ∼50–100 pc from the central black hole. The gas counter-rotation establishes that the gas reservoir in the center of the galaxy originates from a past external accretion event. In this contribution we discuss the gas and stellar properties of MCG–6-30-15, its past history and how the findings on this galaxy can be used to understand AGN fueling in S0 galaxies with counter-rotating structures.

Keywords: Active Galactic Nuclei, black hole, MCG–6-30-15, counter-rotation, fueling, infrared

OPEN ACCESS

Edited by:
Ascensión Del Olmo, Instituto de Astrofísica de Andalucía (CSIC), Spain

Reviewed by:
José María Solanes, University of Barcelona, Spain
Daniela Bettoni, Osservatorio Astronomico di Padova (INAF), Italy

***Correspondence:**
Sandra I. Raimundo
s.raimundo@dark-cosmology.dk

Specialty section:
This article was submitted to Milky Way and Galaxies, a section of the journal Frontiers in Astronomy and Space Sciences

Received: *30 August 2017*
Accepted: *20 December 2017*
Published: *15 January 2018*

Citation:
Raimundo SI (2018) Tracing the External Origin of the AGN Gas Fueling Reservoir. Front. Astron. Space Sci. 4:69. doi: 10.3389/fspas.2017.00069

1. INTRODUCTION

Supermassive black hole accretion, the powering mechanism behind Active Galactic Nuclei (AGN), requires a supply of gas to the central supermassive black hole. To understand the physics of how AGN are powered, or fueled, it is therefore essential to study the environment in the host galaxy and the mechanisms able to drive gas to its central regions. The active S0 galaxy MCG–6-30-15 provides an excellent opportunity to study the origin of the AGN fueling gas. It has recently been discovered that the stellar core in MCG–6-30-15 counter-rotates with respect to the main stellar body of the galaxy (Raimundo et al., 2013). The counter-rotating core has a relatively small size ($r < 1.25'' \sim 200$ pc) and was only discovered as a result of the high spatial resolution achievable with SINFONI on the VLT, using a combination of adaptive optics and infrared integral field spectroscopy.

The formation scenarios for counter-rotating stellar cores require the accretion of stars and/or gas with a distinct angular momentum, into the center of the galaxy. The main mechanisms to form counter-rotating structures are thought to be: (i) major mergers (e.g., Hernquist and Barnes, 1991; Bois et al., 2011; Tsatsi et al., 2015), (ii) non-merger mechanisms that include the infall of gas with misaligned spin through large scale filaments, early in the history of the galaxy (Algorry et al., 2014) or (iii) late accretion of gas (from galaxy neighbors or via a minor merger) followed by in-situ star formation (e.g., McDermid et al., 2006). The late accretion of gas from companions is thought to produce small stellar counter-rotating cores (diameter < 1 kpc). The stellar populations in these cores are younger than the main stellar body of the galaxy, similar to what is observed in MCG–6-30-15 (Raimundo et al., 2013).

In this contribution we present the stellar and molecular gas dynamics in the nucleus of MCG–6-30-15 and use the results on this galaxy to discuss the implications of counter-rotating stellar core formation to AGN fueling.

2. RESULTS

To evaluate the impact on AGN fueling we are interested in identifying mechanisms that can drive molecular gas to the center of galaxies so that it can then be accreted by the supermassive black

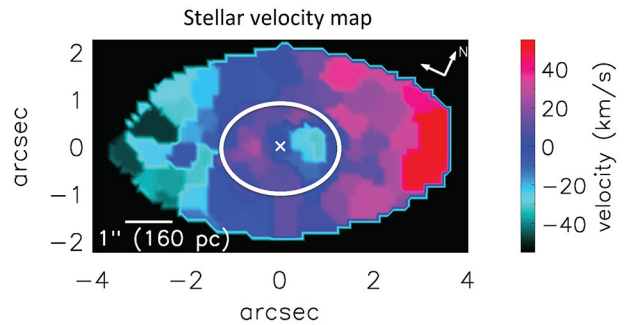

FIGURE 1 | Stellar velocity field for MCG–6-30-15. The region of the counter-rotating core is indicated by the white ellipse. The cross indicates the position of the AGN. Reproduced with permission from Raimundo et al. (2017).

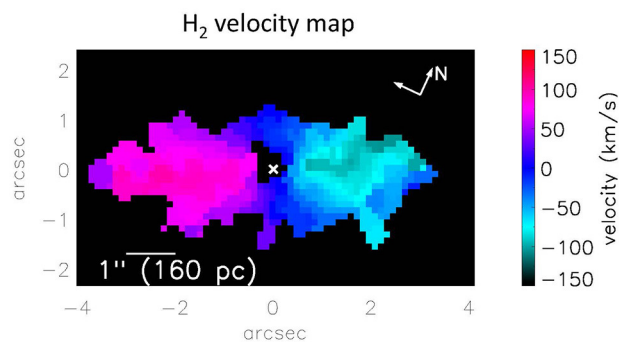

FIGURE 2 | Molecular gas velocity field determined from the H_2 2.12 μm emission line. The cross indicates the position of the AGN. Reproduced with permission from Raimundo et al. (2017).

hole. Counter-rotating stellar nuclear structures may contribute to AGN fueling if their formation is associated with inflow of gas into the center of the galaxy. With new K-band SINFONI data, Raimundo et al. (2017) determined the molecular gas dynamics in MCG–6-30-15 to investigate if the stellar counter-rotating core and molecular gas share similar dynamics. In **Figure 1** we show the stellar velocity field first measured in Raimundo et al. (2013). The stellar core rotates in the opposite direction of the main stellar body of the galaxy. The black ellipse delimits the counter-rotating stellar core. In **Figure 2** we show the dynamics of the molecular gas determined from the H_2 2.12 μm emission line observed in the K-band. It is clear from **Figures 1**, **2** that the molecular gas has the same direction of rotation as the stellar counter-rotating core, i.e. the molecular gas counter-rotates with respect to the main stellar body of the galaxy (Raimundo et al., 2017). From the integrated H_2 2.12 μm line luminosity and using a conversion between line luminosity and molecular gas mass (Mazzalay et al., 2013), the estimated total molecular gas mass is $M_{mol} = 3.4 \times 10^7$ $M_\odot$ within the spatial region of the counter-rotating core and $M_{mol} = 5.8 \times 10^7$ $M_\odot$ in total (i.e. for $r < 3.5''$).

3. DISCUSSION

3.1. Origin of the Counter-Rotating Gas

Molecular gas counter-rotation is a clear signature of its external origin, in particular in S0 galaxies (e.g., Bertola et al., 1992; García-Burillo et al., 1998; Davis and Bureau, 2016). MCG–6-30-15 is part of a small group of galaxies and therefore there are neighbor galaxies that could in theory provide this gas. There is also a dust lane across the plane of the galaxy that indicates the possibility of a past galaxy interaction. The dynamics of the molecular gas indicates that it is associated with the counter-rotating stellar core, as they both counter-rotate in the same direction, 180 degrees from the rotation of the main stellar body of the galaxy. Additionally, there is evidence that the stellar population in the counter-rotating core is somewhat younger than in the main body of the galaxy (Raimundo et al., 2013). The best explanation for the set of observations and properties of MCG–6-30-15 is that this galaxy had an external accretion event in its recent past. The external accretion event could have been the accretion of gas from a neighbor or a minor merger with a small gas-rich satellite galaxy. From this external interaction, gas with a distinct angular momentum was driven to the center of the galaxy, where it settled on a disc that counter-rotates with respect to the galaxy's main body rotation. A younger stellar population formed from the accreted gas and created the stellar counter-rotating core we observe. The external gas formed or replenished the AGN fueling reservoir at hundreds of parsecs scales and the molecular gas observed today is a remnant of the initial gas inflow.

3.2. Impact on AGN Fueling

S0 galaxies have typically low levels of native gas and therefore external gas can be a significant source of fresh fuel. As can be seen from the observations of MCG–6-30-15, the externally accreted gas is able to reach the central $r \sim 50$–100 pc of the galaxy which is the physical scale of the AGN molecular gas fueling reservoir. The presence of counter-rotating molecular gas at these scales means that the external gas creates or replenishes the AGN gas reservoir. The amount of molecular gas is significant, we observe $M_{mol} = 3.4 \times 10^7$ $M_\odot$ in the central 400 pc. This means that the counter-rotating gas is enough to power the AGN for 6.9 Gyr, assuming that the gas is used solely to power the AGN at its current mass accretion rate of $\dot{M} = 5 \times 10^{-3} M_\odot/yr$ (assuming accretion efficiency $\epsilon = 0.1$ and $L_{bol} = 3 \times 10^{43}$ erg s^{-1} from Lira et al., 2015). The reservoir of molecular gas in the central hundreds of parsecs can also be used to form stars which may in turn fuel the AGN (Davies et al., 2007). Our results on MCG–6-30-15 are in line with suggestions that AGN fueling in S0 galaxies is predominantly driven by external gas accretion (Davies et al., 2014).

3.3. General Implications

MCG–6-30-15 is one of the brightest AGN with a counter-rotating core of stars. Most of the other systems with counter-rotating stellar cores are quiescent or show low level of nuclear activity. This does not necessarily mean that there

is lack of AGN with counter-rotating cores. To detect small counter-rotating cores, high spatial resolution observations are needed and integral field spectroscopy has opened up the possibilities in this field. However, AGN are typically selected out of studies with integral field spectroscopy since the frequent goal of these studies is to probe the host galaxy properties. The presence of an AGN hinders this goal due to the characteristic broadband AGN emission that masks the host galaxy spectral features. Therefore it is possible that our current knowledge of counter-rotating systems is biased toward quiescent galaxies and low luminosity AGN. To understand if there is a direct connection between external gas accretion and AGN fueling, future work will have to extend the study of counter-rotating cores to target galaxies with a broad range of AGN activity.

3.4. Conclusions

In this contribution we presented the results on the origin of the AGN molecular gas fueling reservoir in the S0 galaxy MCG–6-30-15, determined from the dynamics of the stars and gas in the central hundreds of parsecs of the galaxy. The work on MCG–6-30-15 shows that counter-rotating stellar cores, when associated with gas, may act as a tracer of external gas inflow into the nuclei of galaxies. In S0 galaxies in particular, the external accretion of gas is likely to create, or make a significant contribution to the existing central gas reservoir for AGN fueling.

AUTHOR CONTRIBUTIONS

The author confirms being the sole contributor of this work and approved it for publication.

REFERENCES

Algorry, D. G., Navarro, J. F., Abadi, M. G., Sales, L. V., Steinmetz, M., and Piontek, F. (2014). Counterrotating stars in simulated galaxy discs. *Monthly Not. R. Astron. Soc.* 437, 3596–3602. doi: 10.1093/mnras/stt2154

Bertola, F., Buson, L. M., and Zeilinger, W. W. (1992). The external origin of the gas in S0 galaxies. *Astrophys. J.* 401, L79–L81. doi: 10.1086/186675

Bois, M., Emsellem, E., Bournaud, F., Alatalo, K., Blitz, L., Bureau, M., et al. (2011). The ATLAS^{3D} project - VI. Simulations of binary galaxy mergers and the link with fast rotators, slow rotators and kinematically distinct cores. *Monthly Not. R. Astron. Soc.* 416, 1654–1679. doi: 10.1111/j.1365-2966.2011.19113.x

Davies, R. I., Maciejewski, W., Hicks, E. K. S., Emsellem, E., Erwin, P., Burtscher, L., et al. (2014). Fueling active galactic nuclei. II. spatially resolved molecular inflows and outflows. *Astrophys. J.* 792:101. doi: 10.1088/0004-637X/792/2/101

Davies, R. I., Müller Sánchez, F., Genzel, R., Tacconi, L. J., Hicks, E. K. S., Friedrich, S., et al. (2007). A close look at star formation around active galactic nuclei. *Astrophys. J.* 671, 1388–1412. doi: 10.1086/523032

Davis, T. A., and Bureau, M. (2016). On the depletion and accretion time-scales of cold gas in local early-type galaxies. *Monthly Not. R. Astron. Soc.* 457, 272–280. doi: 10.1093/mnras/stv2998

García-Burillo, S., Sempere, M. J., and Bettoni, D. (1998). First detection of a counterrotating molecular gas disk in a spiral galaxy: NGC 3626. *Astrophys. J.* 502, 235–244.

Hernquist, L., and Barnes, J. E. (1991). Origin of kinematic subsystems in elliptical galaxies. *Nature* 354, 210–212. doi: 10.1038/354210a0

Lira, P., Arévalo, P., Uttley, P., McHardy, I. M. M., and Videla, L. (2015). Long-term monitoring of the archetype Seyfert galaxy MCG-6-30-15: X-ray, optical and near-IR variability of the corona, disc and torus. *Monthly Not. R. Astron. Soc.* 454, 368–379. doi: 10.1093/mnras/stv1945

Mazzalay, X., Saglia, R. P., Erwin, P., Fabricius, M. H., Rusli, S. P., Thomas, J., et al. (2013). Molecular gas in the centre of nearby galaxies from VLT/SINFONI integral field spectroscopy - I. Morphology and mass inventory. *Monthly Not. R. Astron. Soc.* 428, 2389–2406. doi: 10.1093/mnras/sts204

McDermid, R. M., Emsellem, E., Shapiro, K. L., Bacon, R., Bureau, M., Cappellari, M., et al. (2006). The SAURON project - VIII. OASIS/CFHT integral-field spectroscopy of elliptical and lenticular galaxy centres. *Monthly Not. R. Astron. Soc.* 373, 906–958. doi: 10.1111/j.1365-2966.2006.11065.x

Raimundo, S. I., Davies, R. I., Canning, R. E. A., Celotti, A., Fabian, A. C., and Gandhi, P. (2017). Tracing the origin of the AGN fuelling reservoir in MCG-6-30-15. *Monthly Not. R. Astron. Soc.* 464, 4227–4246. doi: 10.1093/mnras/stw2635

Raimundo, S. I., Davies, R. I., Gandhi, P., Fabian, A. C., Canning, R. E. A., and Ivanov, V. D. (2013). The black hole and central stellar population of MCG-6-30-15. *Monthly Not. R. Astron. Soc.* 431, 2294–2306. doi: 10.1093/mnras/stt327

Tsatsi, A., Macciò, A. V., van de Ven, G., and Moster, B. P. (2015). A new channel for the formation of kinematically decoupled cores in early-type galaxies. *Astrophys. J. Lett.* 802:L3. doi: 10.1088/2041-8205/802/1/L3

Conflict of Interest Statement: The author declares that the research was conducted in the absence of any commercial or financial relationships that could be construed as a potential conflict of interest.

Copyright © 2018 Raimundo. This is an open-access article distributed under the terms of the Creative Commons Attribution License (CC BY). The use, distribution or reproduction in other forums is permitted, provided the original author(s) or licensor are credited and that the original publication in this journal is cited, in accordance with accepted academic practice. No use, distribution or reproduction is permitted which does not comply with these terms.

frontiers in Astronomy and Space Sciences

ORIGINAL RESEARCH
published: 22 November 2017
doi: 10.3389/fspas.2017.00052

Direct HST Dust Lane Detection in Powerful Narrow-Line Radio Galaxies

Edgar A. Ramírez[1]*, *Itziar Aretxaga*[1], *Clive N. Tadhunter*[2], *Enrique Lopez-Rodriguez*[3,4,5] *and Chris Packham*[6,7]

[1] Instituto Nacional de Astrofísica, Óptica y Electrónica, Puebla, Mexico, [2] Department of Physics and Astronomy, University of Sheffield, Sheffield, United Kingdom, [3] NASA Ames Research Center, SOFIA Science Center, SOFIA/USRA, Mountain View, CA, United States, [4] Department of Astronomy, University of Texas at Austin, Austin, TX, United States, [5] McDonald Observatory, University of Texas at Austin, Austin, TX, United States, [6] Department of Physics and Astronomy, University of Texas at San Antonio, San Antonio, TX, United States, [7] National Astronomical Observatory of Japan, Tokyo, Japan

We present the analysis of near-infrared *Hubble Space Telescope* imaging of 10 Fanaroff Riley II powerful radio galaxies at low redshift ($0.03 < z < 0.11$) optically classified as narrow-line radio galaxies. The photometric properties of the host galaxy are measured using GALFIT, and compared with those from the literature. Our high resolution near-infrared observations provide new and direct information on the central kpc-scale dust lanes in our sample that could be connected to the pc-scale torus structure. Moreover, analyzing the infrared spectrograph *Spitzer* spectra of our sample, we suggest properties of the dust size of the torus.

Keywords: active galactic nuclei, infrared imaging, dust grains, narrow-line radio galaxy, 3CRR

OPEN ACCESS

Edited by:
Deborah Dultzin, Universidad Nacional Autónoma de México, Mexico

Reviewed by:
Omaira González Martín, Instituto de Radioastronomía y Astrofísica, Mexico
Daniela Bettoni, Osservatorio Astronomico di Padova (INAF), Italy
Jaime Perea, Instituto de Astrofísica de Andalucía (CSIC), Spain

***Correspondence:**
Edgar A. Ramírez
e.ramirez@inaoep.mx

Specialty section:
This article was submitted to Milky Way and Galaxies, a section of the journal Frontiers in Astronomy and Space Sciences

Received: *23 August 2017*
Accepted: *09 November 2017*
Published: *22 November 2017*

Citation:
Ramírez EA, Aretxaga I, Tadhunter CN, Lopez-Rodriguez E and Packham C (2017) Direct HST Dust Lane Detection in Powerful Narrow-Line Radio Galaxies. Front. Astron. Space Sci. 4:52. doi: 10.3389/fspas.2017.00052

1. INTRODUCTION

Under the context of the unified schemes for active galactic nuclei (AGN, Barthel, 1989; Urry and Padovani, 1995), the pc-scale torus structure is perpendicular to the radio jet axis. Simplifying, measuring the offset in position angle between the torus and the radio axis close to the nuclei would be a direct test of the unified schemes of powerful radio galaxies. Near-infrared (near-IR) observations can give us direct information about the kpc-scale region of the AGN, close to the pc-scale torus, because such wavelengths suffer less extinction than optical wavelengths.

Besides, various studies suggest that AGN have a lower dust-to-gas ratio than the Galactic standard value: $A_V/N_H = 5.3 \times 10^{-22}$ mag cm^{-2} (Bohlin et al., 1978; Maccacaro et al., 1982; Reichert et al., 1985; Maiolino et al., 2001). This result is interpreted as the circumnuclear region of the AGN is composed of large grains, because the small grains, responsible for absorbing the most of the optical radiation, are depleted or become large grains by a coagulation process.

In this work we present the analysis of near-IR images to investigate the connection between the pc-scale torus structure and the kpc-scale dust lane. This can potentially help us to inquire into the unified schemes. Also, we used archived infrared spectrograph (IRS) *Spitzer* data of our sample, to shed light on the extinction imposed by the dust structures and on the dust characteristics of the torus.

2. SAMPLE AND OBSERVATIONS

The sample is composed of all 10 FRII powerful radio galaxies classified as narrow-line radio galaxies at redshift $0.03 < z < 0.11$ from the 3CRR catalog (Laing et al., 1983, see **Table 1**). These objects are ideal sources for a critical analysis of the orientation-based unified model and for investigating the torus properties, because their radio jets are close to the plane of the sky, and, according to the unified scheme, for these sources we have no direct view to the AGN.

TABLE 1 | The analyzed sample.

Source	Redshift	Class
3C 33	0.0597	NLRG/FR II
3C 98	0.0306	NLRG/FR II
3C 192	0.0598	NLRG/FR II
3C 236	0.1005	WLRG/FR II
3C 277.3	0.0850	WLRG/FR I/FR II
3C 285	0.0794	NLRG/FR II
3C 321	0.0961	NLRG/FR II
3C 433	0.1016	NLRG/FR II
3C 452	0.0811	NLRG/FR II
4C 73.08	0.0580	NLRG/FR II

The images were obtained with the *Hubble Space Telescope* (*HST*) Near Infrared Camera and Multi-Object Spectrometer (NICMOS) at 1.025 and 2.05 μm with NICMOS 2 (F110W and POL-L filters, respectively), and at 1.45 and 1.70 μm with NICMOS 1 (F145M and F170M filters, respectively. Program ID: 10410, PI: C. N. Tadhunter). The low redshift of the sample and the high resolution and stability of the near-IR observations obtained with the *HST* allows us to have access to the inner region of the AGN and to trace the dust geometry in the AGN inner region without precedent.

We also made use of *Spitzer* spectroscopic data of our sample taken with the IRS instrument. The *Spitzer* data were obtained from the Spitzer Science Centre's archive. We use the IRS spectra to measure the optical depth of the silicate feature.

3. MODELING THE NEAR-IR HST IMAGES

We fitted the near-IR galaxy profile of our sample with a Sérsic plus a point spread function (PSF) and an Exponential components using GALFIT (Peng et al., 2002). The Sérsic component takes into account the light of the underlying host galaxy, the PSF considers the unresolved quasar, and the Exponential component characterizes a possible disc component. The PSF was included only for those galaxies showing an unresolved source reported in Ramírez et al. (2014). We find preference of the host galaxies to prefer a Sérsic+Exponential components over a single Sérsic component, indicating that the host galaxies tend to be E-like galaxies with a disk component. However, the values of the χ^2 given by the two models (two components and single component) are close each other ($\Delta < 0.25$) to give a conclusive statement. We apply a *F*-test to test the null hypothesis that the two components and the single component models yields the same good quality fit. We find that we cannot reject this null hypothesis at a 35% level of significance.

Figure 1 presents the Sérsic indexes of the model with the lowest reduced χ^2 for each observed wavelength. The spectral index of the host galaxy expands a broad range of values: from 0.5 to 8. Despite this, there is a slightly tendency of the host galaxies to prefer low Sérsic indexes toward short near-IR wavelengths. This indicates that at longer near-IR wavelengths the profile of the host galaxy is cuspy at small radii, while at shorter near-IR wavelengths the the profile of the host galaxy is flat at small radii.

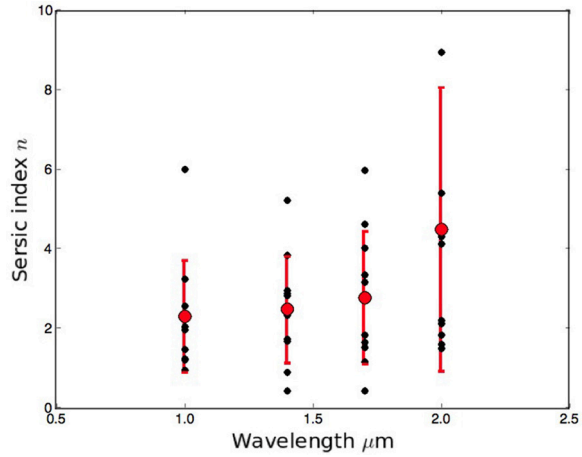

FIGURE 1 | Sérsic indexes (*n*) vs. observed wavelengths. Red symbols indicates the index mean value.

3.1. Residual after Modeling Subtraction

Following subtraction of the best host galaxy model, interesting complex kpc-scale dust features become more evident. Such features are dust lanes and irregular structures. To make sure that such dust features are real and not product of the model subtraction, we applied the alternative approach of "unsharp masking." We found that the residual from both approaches is consistent, therefore concluding that the dusty features are real. The residual dust features at each wavelength is presented in **Figure 2** for the case of 3C 33.

We found dust lanes in 6/10 AGN of our sample (3C 33, 3C 236, 3C 285, 3C 321, 3C 433, and 3C 452). As expected, the dust lanes become clearer at the shorter 1.025 μm wavelength. We measured the position angle (PA) of the dust lanes, and we find that the kpc-scale dust lane of 3/6 galaxies: 3C 236, 3C 433, and 3C 452 is perpendicular to the inner kpc-scale radio jet axis within ±20°.

We have included to our analysis the PA offset between the dust lane and the radio jet axis of the 8 galaxies reported in Madrid et al. (2006) with same redshift and kpc-scale to our sample (i.e., those with $z < 0.1$ and 2.5 kpc-scale dust). There is a tendency of the dust lanes to be perpendicular to the radio axis, as can be seen in the **Figure 3**. The 7/14 of the sample is perpendicular within ±20°. Note, however, that the uncertainties in the offsets (∼ 5°) give a distribution peaking at bin 60 − 70°, which is within the general half-opening angle considered in the torus models (30 − 40°; e.g., Hönig and Kishimoto, 2017).

3.2. IRS Spectra: Silicate Absorption Features

In Ramírez et al. (2014), we measured the optical extinction toward the AGN by different techniques, one of such techniques was by measuring the optical depth of the silicate feature, $\tau_{9.7}$, considering a Gaussian plus a continuum.

It is interesting that two objects: 3C 98 and 3C 192, that have no silicate detections also have no evidence for large scale dust lanes. As silicate absorption requires significant column densities,

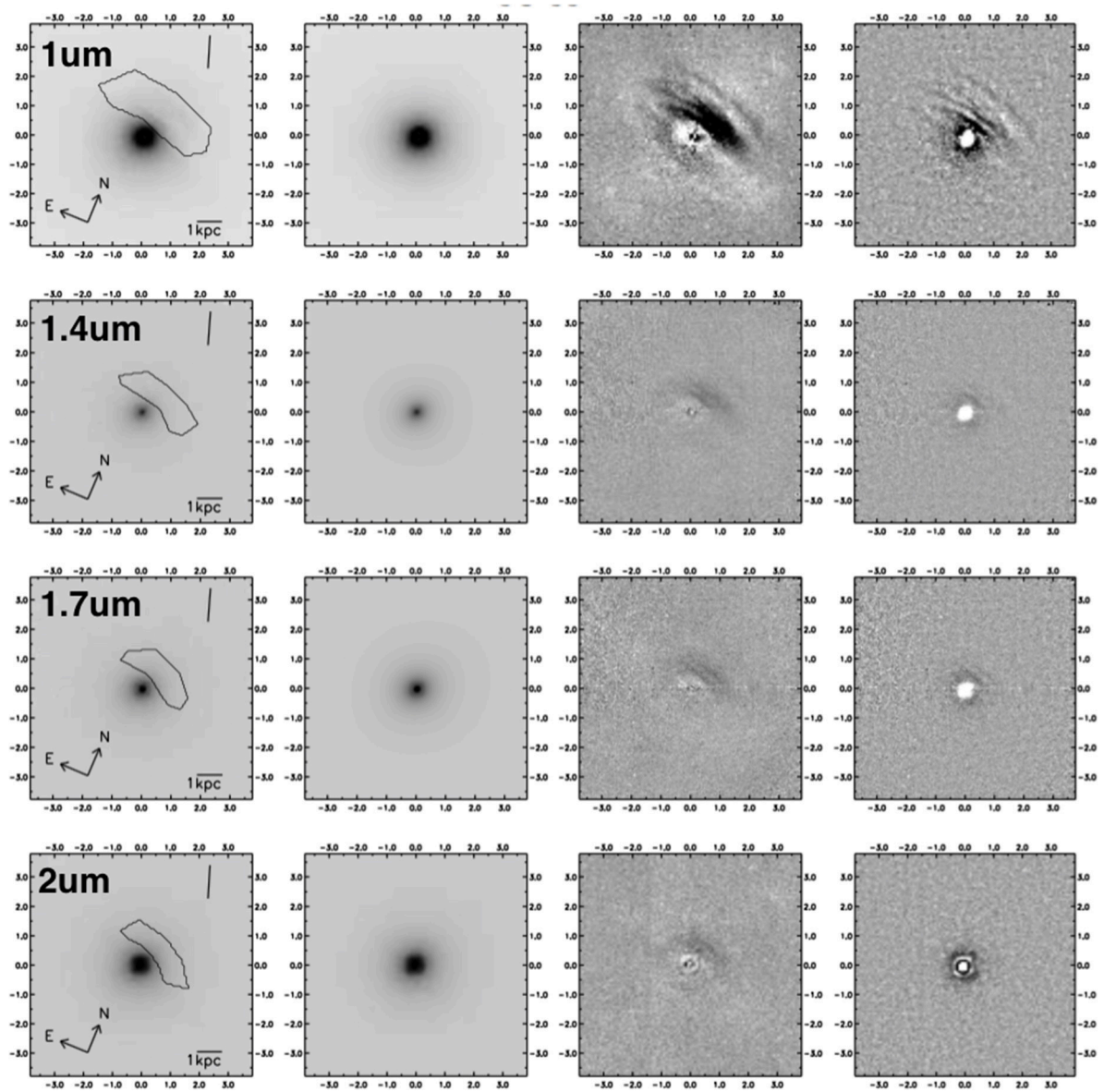

FIGURE 2 | *HST* residuals after galaxy model subtraction: the case 3C 33. From top to bottom row: 1.0, 1.4, 1.7, and 2.0 μm. Field of 7.6 × 7.6 acsec size. The line in the upper-right corner represent the orientation of the inner radio jet. Contours represent a masked region where traces of dust lane are detected—excluded for the fit. The images are shown in gray linear scale.

it is possible that the large scale dust lanes contributes to the silicate extinction where otherwise the strong AGN continuum dominates, resulting in the objects without clear dust lane detections having none or low silicate absorption depths.

However, the optical extinction of 3C 98 and 3C 192 derived from de-reddening their near-IR SED spectral index and from the X-ray luminosity is high ($A_V \sim 30 - 50$ Ramírez et al., 2014). This can be explained by the presence of big grains in the torus. Big grains can extinguish the optical wavelengths and not produce silicate absorption line (Lyu et al., 2014). Unfortunately, the other two sources with no dust lane detection (3C 277.3 and 4C 73.08) have no IRS *Spitzer* data. Mid-IR spectroscopic observations would give essential information to clarify this issue.

Moreover, we have plotted our sample on the diagram of Maiolino et al. (2001, his figure 1), and we find that our sample follows the same trend found by Maiolino et al. (2001): that radio-quiet AGN have lower dust-to-gas ratios than the standard dust-to-gas ratio of the Galaxy. Therefore, the interpretation that Maiolino et al. (2001) gave to their results—that the circumnuclear region of the AGN is composed of large grains—can also be valid for radio-loud AGN sources. Also, it has been found that AGN have ratios $A_V/\tau_{9.7} \sim 5.5$ lower than in the interstellar Galaxy medium (= 18; Shao et al., 2017), suggesting

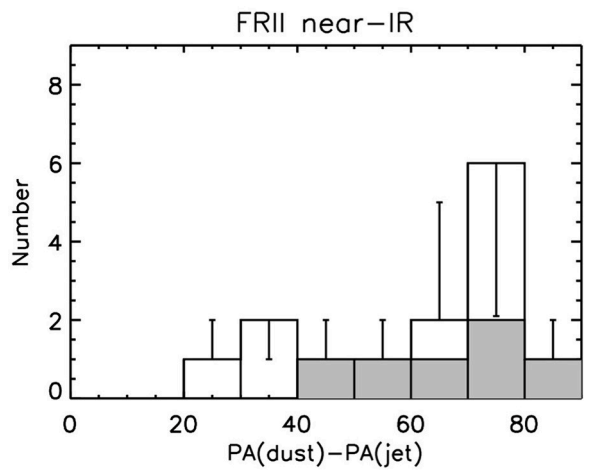

FIGURE 3 | The distribution of the offsets between the radio jet and the ∼ 2 kpc-scale dust features of our sample (filled bars), and from the literature (open bars; Madrid et al., 2006).

that the torus is composed of dust grains bigger than those in the interstellar medium of the Milky Way.

4. CONCLUSIONS

- We measured the Sérsic indexes of the host galaxy of our sample at near-IR wavelengths, and we find a slightly tendency to have lower Sérsic indexes toward shorter near-IR wavelengths.
- We detect kpc-scale dust lanes in 6 out of 10 of the sources, of which 3/6 are perpendicular to the kpc-scale radio axis within ±20° range. After adding 8 galaxies from the literature, 7/14 of the dust lane structures are perpendicular to the kpc-scale radio axis within the same range.

  Assuming that the torus is perpendicular to the radio jet axis, our result suggests a continuity between the dust in the pc-scale torus and the more extended kpc-scale dust lanes. The misalignment of the rest can be explained as a warping disks.
- The near-IR images of 3C 98 and 3C 192 show no traces of a kpc-scale dust lane and their IRS *Spitzer* spectrum shows no silicate absorption line. This suggests that the torus is composed of big grains that extinguish the quasar optical light, but do not extinguishes the silicate line.

AUTHOR CONTRIBUTIONS

ER analyzed the near-infrared HST images, produced the plots and the manuscript. ER and IA performed the galaxy fitting profile. All the co-authors contributed with the analysis and interpretation of the results.

FUNDING

Funding from the Mexican Council of Science and Technology (CONACyT) through a research grant no. 012650001912098767.

ACKNOWLEDGMENTS

ER acknowledges the financial support from the Mexican Council of Science and Technology (CONACyT). We would like to thank the referees for the constructive comments.

REFERENCES

Barthel, P. D. (1989). Is every quasar beamed? *Astrophys. J.* 336, 606–611. doi: 10.1086/167038

Bohlin, R. C., Savage, B. D., and Drake, J. F. (1978). A survey of interstellar H I from L-alpha absorption measurements. II. *Astrophys. J.* 224, 132–142. doi: 10.1086/156357

Hönig, S. F., and Kishimoto, M. (2017). Dusty winds in active galactic nuclei: reconciling observations with models. *Astrophys. J. Lett.* 838:L20. doi: 10.3847/2041-8213/aa6838

Laing, R. A., Riley, J. M., and Longair, M. S. (1983). Bright radio sources at 178 MHz - Flux densities, optical identifications and the cosmological evolution of powerful radio galaxies. *Month. Notices R. Astron. Soc.* 204, 151–187. doi: 10.1093/mnras/204.1.151

Lyu, J., Hao, L., and Li, A. (2014). Dust in active galactic nuclei: anomalous silicate to optical extinction ratios? *Astrophys. J. Lett.* 792:L9. doi: 10.1088/2041-8205/792/1/L9

Maccacaro, T., Perola, G. C., and Elvis, M. (1982). X-ray observations with the Einstein Observatory of emission-line galaxies. *Astrophys. J.* 257, 47–55. doi: 10.1086/159961

Madrid, J. P., Chiaberge, M., Floyd, D., Sparks, W. B., Macchetto, D., Miley, G. K., et al. (2006). Hubble space telescope near-infrared snapshot survey of 3CR radio source counterparts at low redshift. *Astrophys. J. Suppl.* 164, 307–333. doi: 10.1086/504480

Maiolino, R., Marconi, A., Salvati, M., Risaliti, G., Severgnini, P., Oliva, E., et al. (2001). Dust in active nuclei. I. Evidence for "anomalous" properties. *Astron. Astrophys.* 365, 28–36. doi: 10.1051/0004-6361:20000177

Peng, C. Y., Ho, L. C., Impey, C. D., and Rix, H.-W. (2002). Detailed structural decomposition of galaxy images. *Astron. J.* 124, 266–293. doi: 10.1086/340952

Ramírez, E. A., Tadhunter, C. N., Dicken, D., Rose, M., Axon, D., Sparks, W., et al. (2014). Hubble space telescope and spitzer point-source detection and optical extinction in powerful narrow-line radio galaxies. *Month. Notices R. Astron. Soc.* 439, 1270–1285. doi: 10.1093/mnras/stt2444

Reichert, G. A., Mushotzky, R. F., Holt, S. S., and Petre, R. (1985). Soft X-ray spectral observations of low-luminosity active galaxies. *Astrophys. J.* 296, 69–89. doi: 10.1086/163421

Shao, Z., Jiang, B. W., and Li, A. (2017). On the optical-to-silicate extinction ratio as a probe of the dust size in active galactic nuclei. *Astrophys. J.* 840:27. doi: 10.3847/1538-4357/aa6ba4

Urry, C. M., and Padovani, P. (1995). Unified schemes for radio-loud active galactic nuclei. *Publ. ASP* 107:803. doi: 10.1086/133630

Conflict of Interest Statement: The authors declare that the research was conducted in the absence of any commercial or financial relationships that could be construed as a potential conflict of interest.

Copyright © 2017 Ramírez, Aretxaga, Tadhunter, Lopez-Rodriguez and Packham. This is an open-access article distributed under the terms of the Creative Commons Attribution License (CC BY). The use, distribution or reproduction in other forums is permitted, provided the original author(s) or licensor are credited and that the original publication in this journal is cited, in accordance with accepted academic practice. No use, distribution or reproduction is permitted which does not comply with these terms.

frontiers in Astronomy and Space Sciences

ORIGINAL RESEARCH
published: 30 November 2017
doi: 10.3389/fspas.2017.00049

Fast-Growing SMBHs in Fast-Growing Galaxies, at High Redshifts: The Role of Major Mergers As Revealed by ALMA

Benny Trakhtenbrot[1]*, *Paulina Lira*[2], *Hagai Netzer*[3], *Claudia Cicone*[1,4], *Roberto Maiolino*[5,6] and *Ohad Shemmer*[7]

[1] Department of Physics, ETH Zurich, Zurich, Switzerland, [2] Departamento de Astronomia, Universidad de Chile, Santiago, Chile, [3] Raymond and Beverly Sackler Faculty of Exact Sciences, School of Physics and Astronomy and the Wise Observatory, Tel-Aviv University, Tel-Aviv, Israel, [4] INAF-Osservatorio Astronomico di Brera, Milan, Italy, [5] Cavendish Laboratory, University of Cambridge, Cambridge, United Kingdom, [6] Kavli Institute for Cosmology, University of Cambridge, Cambridge, United Kingdom, [7] Department of Physics, University of North Texas, Denton, TX, United States

We present a long-term, multi-wavelength project to understand the epoch of fastest growth of the most massive black holes by using a sample of 40 luminous quasars at $z \simeq 4.8$. These quasars have rather uniform properties, with typical accretion rates and black hole masses of $L/L_{\rm Edd} \simeq 0.7$ and $M_{\rm BH} \simeq 10^9\,M_\odot$. The sample consists of "FIR-bright" sources with a previous *Herschel*/SPIRE detection, suggesting SFR $>1{,}000\,M_\odot\,{\rm yr}^{-1}$, as well as of "FIR-faint" sources for which *Herschel* stacking analysis implies a typical SFR of $\sim 400\,M_\odot\,{\rm yr}^{-1}$. Six of the quasars have been observed by ALMA in [C II] $\lambda 157.74\,\mu$m line emission and adjacent rest-frame 150 μm continuum, to study the dusty cold ISM. ALMA detected companion, spectroscopically confirmed sub-mm galaxies (SMGs) for three sources—one FIR-bright and two FIR-faint. The companions are separated by ∼14–45 kpc from the quasar hosts, and we interpret them as major galaxy interactions. Our ALMA data therefore clearly support the idea that major mergers may be important drivers for rapid, early SMBH growth. However, the fact that not all high-SFR quasar hosts are accompanied by interacting SMGs, and their ordered gas kinematics observed by ALMA, suggest that other processes may be fueling these systems. Our analysis thus demonstrates the diversity of host galaxy properties and gas accretion mechanisms associated with early and rapid SMBH growth.

Keywords: sub-millimeter galaxies, galaxy mergers, quasars: supermassive black holes, Quasars: host galaxies, high-redshift galaxies

OPEN ACCESS

Edited by:
Paola Marziani, Osservatorio Astronomico di Padova (INAF), Italy

Reviewed by:
Francoise Combes, Observatoire de Paris, France
Daniela Bettoni, Osservatorio Astronomico di Padova (INAF), Italy

***Correspondence:**
Benny Trakhtenbrot
benny.trakhtenbrot@phys.ethz.ch

Specialty section:
This article was submitted to Milky Way and Galaxies, a section of the journal Frontiers in Astronomy and Space Sciences

Received: *30 September 2017*
Accepted: *06 November 2017*
Published: *30 November 2017*

Citation:
Trakhtenbrot B, Lira P, Netzer H, Cicone C, Maiolino R and Shemmer O (2017) Fast-Growing SMBHs in Fast-Growing Galaxies, at High Redshifts: The Role of Major Mergers As Revealed by ALMA. Front. Astron. Space Sci. 4:49. doi: 10.3389/fspas.2017.00049

1. INTRODUCTION

The highest-redshift quasars, observed at $z \sim 5$–7 suggest that supermassive black holes (SMBHs) with $M_{\rm BH} \simeq 10^9\,M_\odot$ existed about 1 Gyr after the big bang, which challenges our understanding of BH formation and early growth, and how these processes relate to the galaxies that host the earliest SMBHs.

In order to account for the observed high BH masses of the earliest quasars, many models have promoted the possibility of high-mass BH seed formation, in dense stellar populations in

proto-galaxies and/or through the direct collapse of gaseous halos (see, e.g., Natarajan, 2011; Volonteri, 2012, for reviews). Regardless of the seed mass, the subsequent BH growth must proceed at high accretion rates and high duty cycles. The former is indeed directly observed, as the accretion rate of high-z quasars approaches $L/L_{\rm Edd} \simeq 1$ (e.g., Kurk et al., 2007; Willott et al., 2010; De Rosa et al., 2011; Trakhtenbrot et al., 2011). The latter requirement is found to be somewhat more challenging. One way to efficiently fuel SMBH accretion is through major mergers of gas rich galaxies (Sanders et al., 1988; Hopkins et al., 2006). Such mergers would be more common in dense large-scale environments. Moreover, several simulations have suggested that over-dense large-scale environments would expedite the growth of the most massive early BHs, as large amounts of inter galactic gas could stream onto the SMBHs host galaxies (Dekel et al., 2009; Di Matteo et al., 2012; Dubois et al., 2012; Costa et al., 2014).

Regardless of the exact mechanism driving the nearly continuous SMBH fueling, the low angular momentum gas is expected to trigger intense star formation (SF) throughout the host, and any interacting galaxy. Several observations of high-redshift quasars (including our own; see §2) have indeed identified intense SF, with growth rates exceeding SFR $\sim$1,000 $M_\odot\,{\rm yr}^{-1}$ (e.g., Mor et al., 2012; Netzer et al., 2014, 2016). Although these high SFRs are suggestive of merger activity, the low spatial resolution of the far-IR (FIR) data prohibited any detailed investigation of this possibility. Other dedicated searches for close companions have identified some examples of major mergers (Wagg et al., 2012), but most searches did not yield convincing evidence for merger activity (e.g., Willott et al., 2005). Similarly, wide-field imaging campaigns aimed at determining whether high-z quasars are found in over-dense large-scale environments yielded ambiguous results (Willott et al., 2005; Kim et al., 2009; Husband et al., 2013; Bañados et al., 2013; Simpson et al., 2014).

Here we describe a pilot study with ALMA that aims to identify major galaxy-galaxy interactions among a sample of six fast-growing SMBHs at $z \simeq 4.8$. The full presentation of this study was recently published in *The Astrophysical Journal* (Trakhtenbrot et al., 2017, T17 hereafter), and here we only provide a brief summary of the sample, the ALMA observations, and our main results. The interested reader is encouraged to refer to T17 for any additional details. Throughout this work, we assume a cosmological model with $\Omega_\Lambda = 0.7$, $\Omega_{\rm M} = 0.3$, and $H_0 = 70\,{\rm km\,s^{-1}\,Mpc^{-1}}$.

2. SAMPLE AND ALMA OBSERVATIONS

Our sample of six quasars is drawn from a larger sample of 40 sources at $z \simeq 4.8$, for which reliable estimates of $M_{\rm BH}$, $L/L_{\rm Edd}$, and integrated host SFRs are available through our long-term, multi-wavelength observational effort, conducted using the VLT, Gemini, *Spitzer*, and *Herschel* facilities. The $z \simeq 4.8$ quasars typically have $M_{\rm BH} \simeq 10^9\,M_\odot$ and $L/L_{\rm Edd} \simeq 0.7$, and the sample covers a rather limited range in these two quantities (see Trakhtenbrot et al., 2011, T11 hereafter). The host galaxies, on the other hand, exhibit a wide range in SFRs. While $\sim$75% of the systems have SFR $\sim 400\,M_\odot\,{\rm yr}^{-1}$, as determined from *Herschel* stacking analysis ("FIR-faint" systems), the outstanding 25% are individually detected and have SFR $\sim$1,000–4,000 $M_\odot\,{\rm yr}^{-1}$ ("FIR-bright" systems; see Netzer et al., 2014, 2016). The *Herschel* data available prior to the ALMA campaign is therefore suggestive of a scenario where major mergers may be in play in at least in a fraction of these systems. The six quasars selected for our pilot ALMA study are equally split between "FIR-bright" and "FIR-faint" subsets, in an attempt to address this possibility.

The ALMA band-7 observations were designed to detect and resolve, at kpc scales, the emission from the prominent [C II] λ157.74 μm line and the adjacent continuum. While the continuum emission probes the spatial distribution of cold dusty ISM in the quasar hosts, the [C II] emission line—which is an efficient ISM coolant—probes their kinematics and can be used to spectroscopically confirm the nature of any companion galaxies (e.g., Maiolino et al., 2009; Wagg et al., 2012; Wang et al., 2013; Neri et al., 2014). We used the extended C34-4 configuration of ALMA, providing a resolution of $\sim$0.″3 at 330 GHz. This corresponds to about 2 kpc at $z \simeq 4.8$. The ALMA field of view covers distances of $\sim$6.″8, or almost 50 kpc, from the quasar locations. The chosen spectral setup provided four windows, each covering 1,875 MHz ($\sim$1,650 km s^{-1}), at a resolution of $\sim$30 km s^{-1}. On-source integrations lasted between 11 and 54 min, with longer integrations for the "FIR-faint" sources. The resulting limiting flux densities were $F_\nu \sim (4.2\text{–}9.2)\times10^{-2}$ mJy/beam (rms). At the redshifts of the quasars, and under reasonable assumptions regarding the possible shapes of their FIR SEDs, this corresponds to lower limits of roughly 4–11 $M_\odot\,{\rm yr}^{-1}\,{\rm kpc}^{-2}$ (at the 3σ level).

3. RESULTS

The host galaxies of all six quasars are robustly detected, and (marginally) resolved, in both continuum and [C II] emission. As an example, we show inf **Figure 1** the continuum and [C II] emission maps of one of the "FIR-faint" sources in our sample, SDSS J092303.53+024739.5 ($z_{\rm QSO} = 4.6589$; J0923 hereafter).

In what follows, we highlight our main findings from the analysis of these data. We demonstrate these findings using different diagrams for the aforementioned source J0923. We note that many of the choices we made through the analysis of the ALMA data were motivated by recent sub-mm studies of $z \gtrsim 5$ quasars (Wang et al., 2013; Willott et al., 2015; Venemans et al., 2016). The reader is referred to T17 for a detailed discussion of our analysis and assumptions.

3.1. Quasar Hosts

We measure a wide range in (spatially-integrated) 345 GHz continuum flux densities, between $F_\nu \simeq 1.6\text{–}18.5$ mJy. This wide range in continuum levels is reminiscent of that of the FIR luminosities and SFRs measured from the *Herschel*/SPIRE data (which covered rest-frame wavelengths of $\sim$45–90 μm). Indeed, we find that the new ALMA continuum measurements are generally in very good agreement with the *Herschel* measurements, under reasonable assumptions regarding the

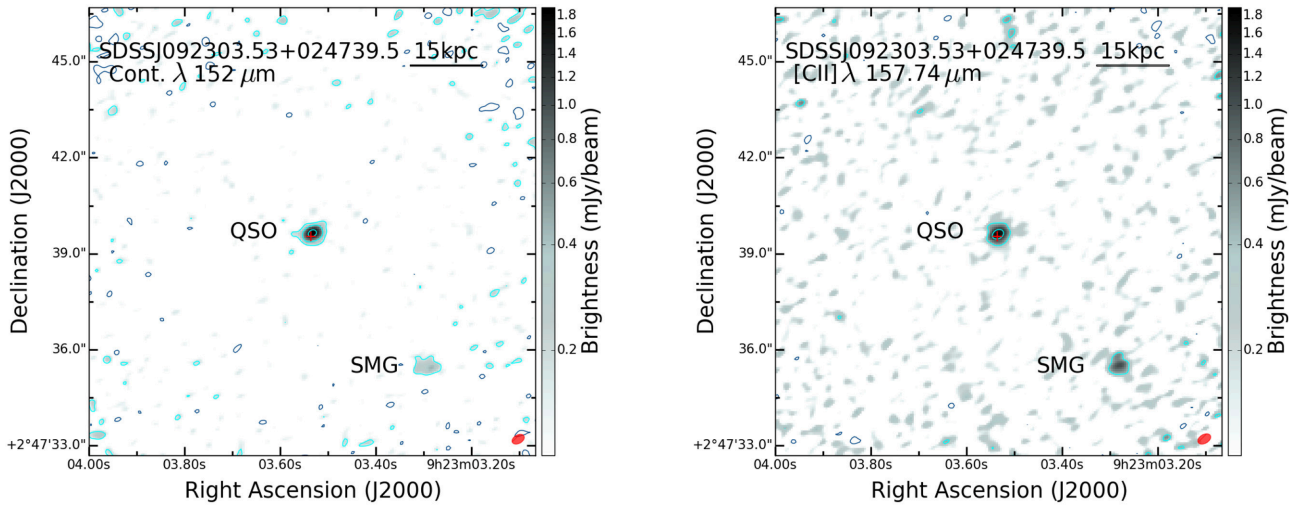

FIGURE 1 | Maps of the dust continuum **(left)** and [C II] λ157.74 μm line **(right)** emission for one of the quasars in our sample, SDSS J092303.53+024739.5 at $z_{\rm QSO} = 4.6589$. Both the quasar host (marked as "QSO") and a sub-mm companion galaxy ("SMG") are robustly detected and marginally resolved (see the synthetized ALMA beam at the bottom right of each panel). The companion galaxy is separated by 36.5 kpc and 246 km s^{-1} from the quasar host.

shape of the FIR SED, namely a gray-body with dust temperature $T_{\rm d} = 47$ K and $\beta = 1.6$. Some sources require somewhat warmer dust temperatures (up to $T_{\rm d} \simeq 60$ K). Moreover, most sources are consistent with the FIR SED templates of Chary and Elbaz (2001). Importantly, we note that the ALMA continuum measurements for the FIR-faint sources, are consistent with the extrapolation of the *stacking* measurements of the *Herschel* data, thus reassuring that our interpretation of the *Herschel* results was robust. **Figure 2** demonstrates these findings for J0923.

By combining the new ALMA continuum measurements and the assumed FIR SEDs, we estimate (spatially integrated) total FIR luminosities of $L(8\text{–}1{,}000\,\mu\text{m}) \simeq (1.9\text{–}35.5) \times 10^{12}\,L_{\odot}$. These luminosities translate to host SFRs in the range SFR $\sim$ 190–3,500 $M_{\odot}$ yr^{-1}. This is, again, consistent with our *Herschel*-based findings, but now robustly resolving the hosts, which is crucial in several cases (see §3.2 below).

The spatially resolved [C II] line emission maps allow us to study the kinematics of the hosts, and estimate their dynamical masses. Most sources (at least four out of six) show [C II] velocity gradients that are consistent with rotation, as shown in the left panel of **Figure 3** for J0923. We therefore assume a simple model of an inclined rotating disk for the [C II]-emitting ISM in the hosts. Following common practices with similar data, we can then deduce *dynamical* host masses, by combining the size of the [C II]-emitting region ($D_{\rm [C\,II]}$) with the typical velocity of the gas (FWHM [C II]), corrected for the inclination of the disk (i):

$$M_{\rm dyn} = 9.8 \times 10^{8} \left(\frac{D_{\rm [C\,II]}}{\rm kpc}\right) \left[\frac{\rm FWHM\,[C\,II]}{100\ {\rm km\,s^{-1}}}\right]^{2} \sin^{-2}(i)\ M_{\odot}\ . \quad (1)$$

The inclination of each system is estimated from the spatial shape (morphology) of the [C II] emitting region, available from our resolved ALMA data (i.e., the major-to-minor axis ratio).

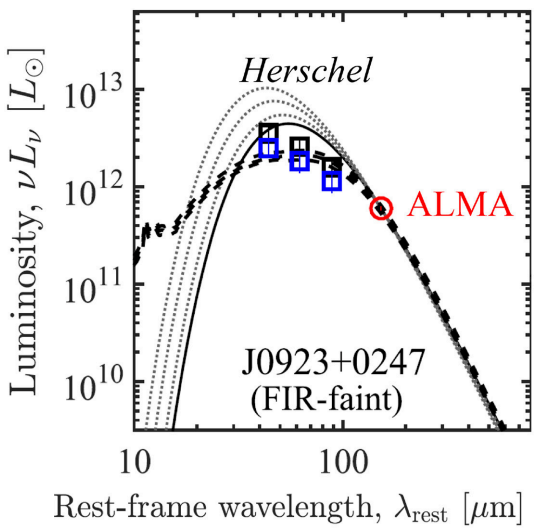

FIGURE 2 | The FIR SED of J0923. The new ALMA continuum measurement (red) is broadly consistent with the previous *Herschel* data (based on stacking analysis; black squares). Blue squares show the *Herschel* data after correcting for the fraction of the flux that comes from the companion galaxy. The solid black line traces a gray-body SED with $T_{\rm d} = 47$ K and $\beta = 1.6$, while the dotted lines trace different temperatures. The dashed lines illustrate several relevant templates from Chary and Elbaz (2001).

The resulting dynamical masses cover a rather limited range, $M_{\rm dyn} \simeq (3.7\text{–}7.4) \times 10^{10}\,M_{\odot}$. By assuming that the dynamical masses are dominated by the stellar components, and considering the wide range in SFRs, this means that the lower-SFR (FIR-faint) hosts are consistent with the so-called "main sequence" of SF galaxies (e.g., Speagle et al., 2014; Steinhardt et al., 2014, and references therein), while the high-SFR (FIR-bright)

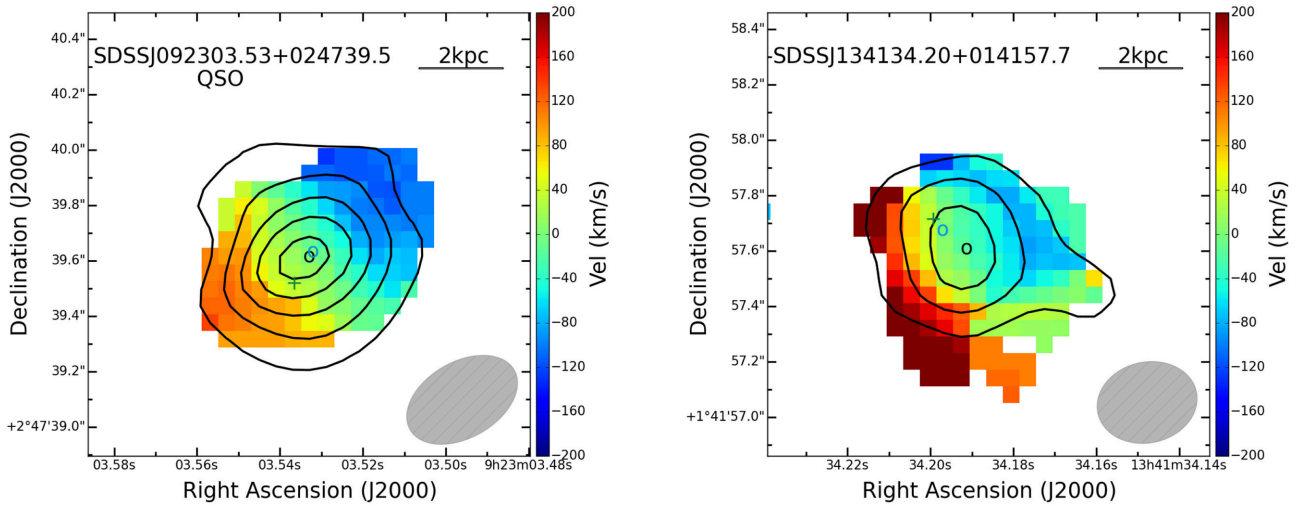

FIGURE 3 | Velocity maps of the [C II] λ157.74 μm emission line for J0923 **(left)** and J1341 **(right)**, with the velocities indicated by color and the [C II] flux contours overlaid (note that the contour levels differ between the two sources). The kinematics of the cold gas in the host galaxies appears to be dominated by rotation.

hosts would lie above it. Moreover, given the narrow range in $M_{\rm BH}$ and $L/L_{\rm Edd}$ of the quasars themselves, it appears that these host properties are not directly linked to the SMBH properties.

3.2. Companion Galaxies

Our most intriguing finding is related to the detection of several gas rich companions, which are likely interacting with the quasar hosts.

We robustly detect companion galaxies for three of the six quasar hosts, in both continuum and [C II] emission. These companions are separated by ∼14–45 kpc and $|\Delta v| < 450\,{\rm km\,s^{-1}}$ from the quasar hosts, thus being truly physically related to the quasars systems. An additional continuum source that lacks [C II] emission is detected ∼25 kpc away from one of the FIR-bright systems, which also has a more distant spectroscopically-confirmed companion. **Figure 4** demonstrates the spectral proximity of the companion of J0923 to the quasar host.

Following the same procedures as those used for the quasar hosts, we find that the companion galaxies have continuum fluxes that translate to SFRs of $\simeq$ 100–200 $M_\odot\,{\rm yr}^{-1}$, and dynamical masses of $M_{\rm dyn} \simeq (2.1\text{–}10.7) \times 10^{10}\,M_\odot$. Compared to the respective quasar host masses, the companions have mass ratios $|q| \lesssim 2{:}1$, suggestive of *major* galaxy interactions. Moreover, the companion galaxies are consistent with being on the main sequence of SF galaxies.

4. DISCUSSION AND CONCLUSION

The most intriguing finding of our ALMA study is the identification of spectroscopically-confirmed companion galaxies for three out of the six quasar hosts in our sample. Considering the small field of view (FoV) of our ALMA data (∼13.5″or ∼100 kpc in diameter), the number of sub-mm bright galaxies we find is much higher than what is found in "blind" surveys. For example, surveys of rest-frame UV selected SF galaxies predict roughly 0.01 galaxies with SFR $\simeq 100\,M_\odot\,{\rm yr}^{-1}$ in a single ALMA FoV (e.g., Bouwens et al., 2015; Stark, 2016). Even more complete surveys of [C II]-emitting galaxies at $z \gtrsim 5$ predict of about 0.05 galaxies per each of our ALMA pointings (e.g., Aravena et al., 2016). We therefore conclude that fast-growing $z \sim 5$ SMBHs reside in over-dense environments in the early universe, and that their fast accumulation of mass may be related to enhanced major-merger activity. Further support for this scenario was recently presented in a large ALMA study of $z \sim 6$ quasars, using identical methods to those we used in our study (Decarli et al., 2017).

The naive expectation from the previously available *Herschel* data would be that the high-SFR (FIR-bright) systems would be associated with major mergers, while the lower-SFR (FIR-faint) systems would show no signs of interaction. Our ALMA data show a very different picture. Two of the three companions are found near FIR-faint systems, and only one is associated with a FIR-bright system. Conversely, two of the three FIR-bright systems in our sample are not associated with companion, interacting galaxies. Although in principle these quasar hosts may be in an advanced merger stage (which would remain unresolved in our data), the signatures of rotationally-dominated gas structures would not support this scenario.. This is exemplified in the system J1341, which has SFR $\simeq$3,000 $M_\odot\,{\rm yr}^{-1}$, and shows signatures of rotation-dominated gas and no companion galaxies (see **Figure 3**, right). The two lower-SFR systems with companion galaxies are expected to experience a later increase in SFR. This means that the low SFRs we deduced for the "FIR-faint" T11 $z \simeq 4.8$ systems cannot be simply due to the onset of "AGN feedback" in the final stages of an episode of SMBH and host growth. However, a larger sample is needed to clarify which of all these processes dominates the growth of the general $z \sim 5$ SMBH population.

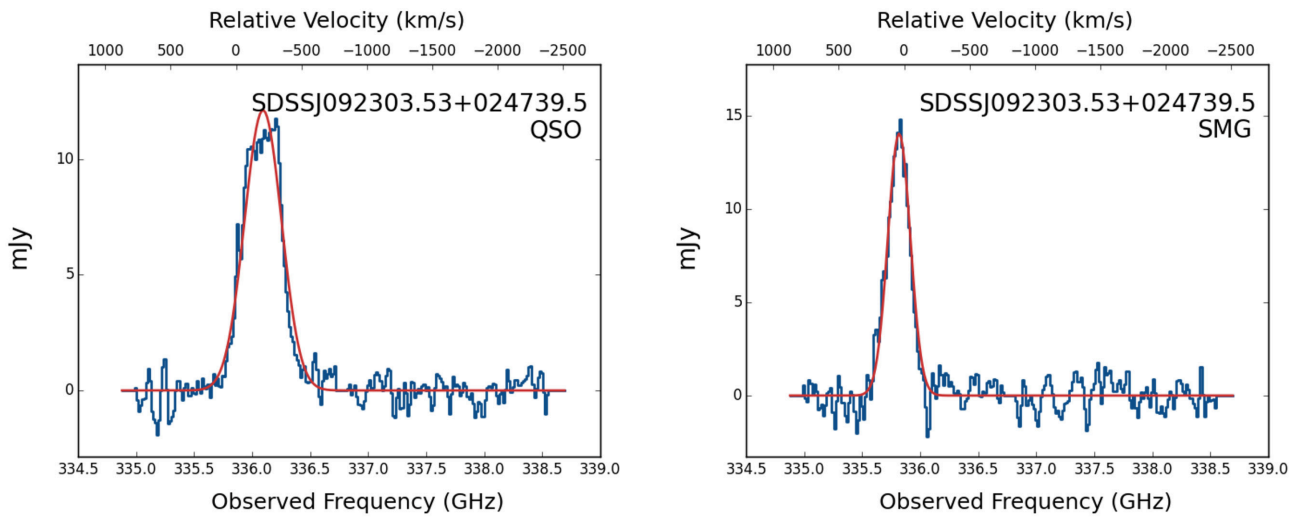

FIGURE 4 | Spatially-integrated spectra of the [C II] emission line in the quasar host **(left)** and the interacting companion **(right)** of J0923. The relative velocities (top *x*-axis) are calculated relative to the rest-frame UV Mg II λ2798 broad emission line of the quasar. These data confirm the physical association of the companion source to the quasar host.

The companion galaxies detected with ALMA were *not* seen in our *Spitzer* data. Given their SFRs and (dynamical) masses, and what is known about the population of rest-frame UV selected SF galaxies at $z \simeq 4.8$ (e.g., Steinhardt et al., 2014; Stark, 2016), we conclude that this is due to significant dust obscuration. This may explain the fact that many previous studies were unable to identify companions and/or over-dense environments for $z \gtrsim 5$ quasars. High resolution, spectroscopic sub-mm observations are therefore crucial for the study of mergers and environments among the highest-redshift quasars.

We are currently leading an ALMA cycle-4 program that would provide similar data for a dozen additional $z \simeq 4.8$ quasars from the T11 sample, bringing the total number of such quasars with resolved host ISM kinematics, and close companion mapping, to 18. Analysis of the ALMA data for the 12 additional sources is ongoing. Moreover, we were recently awarded *HST*/WFC3/IR time to map the *stellar* component in the host galaxies, and in the close companions of the six quasars described here. The *HST* data will also probe the larger-scale environments of the quasars, out to ∼400 kpc, allowing us to detect any additional (unobscured) companions that may be present in this field.

AUTHOR CONTRIBUTIONS

BT led the interpretation of the ALMA data, the preparation of the paper describing our results (T17), and presented the results as a contributed talk in the "Quasars at All Cosmic Epochs" meeting. PL was the PI of the ALMA proposal and led the data analysis. All authors participated in different aspects of the analysis, interpretation, and preparation of this study for publication.

FUNDING

HN acknowledges support by the Israel Science Foundation grant 284/13. CC gratefully acknowledges support from the Swiss National Science Foundation Professorship grant PP00P2_138979/1. CC also acknowledges funding from the European Union's Horizon 2020 research and innovation programme under the Marie Sklodowska-Curie grant agreement No. 664931. RM acknowledges support by the Science and Technology Facilities Council (STFC) and the ERC Advanced Grant 695671 "QUENCH."

ACKNOWLEDGMENTS

We are grateful for the organizers of the "Quasars at All Cosmic Epochs" meeting for the opportunity to present our results in a stimulating and friendly environment. We thank K. Schawinski, L. Mayer, R. Teyssier, P. Capelo, M. Dotti, and D. Fiacconi for useful discussions during the preparation of the paper describing our results (T17). The work described here made use of the ALMA data set ADS/JAO.ALMA#2013.1.01153.S. ALMA is a partnership of ESO (representing its member states), NSF (USA) and NINS (Japan), together with NRC (Canada), NSC and ASIAA (Taiwan), and KASI (Republic of Korea), in cooperation with the Republic of Chile. The Joint ALMA Observatory is operated by ESO, AUI/NRAO and NAOJ.

REFERENCES

Aravena, M., Decarli, R., Walter, F., Bouwens, R. J., Oesch, P. A., Carilli, C. L., et al. (2016). ALMA spectroscopic survey in the hubble ultra deep field: Search for [CII] line and dust emission in 6 < z < 8 galaxies. *Astrophys. J.* 833:71. doi: 10.3847/1538-4357/833/1/71

Bañados, E., Venemans, B. P., Walter, F., Kurk, J., Overzier, R., and Ouchi, M. (2013). The galaxy environment of a QSO at z ˜ 5.7. *Astrophys. J.* 77:178. doi: 10.1088/0004-637X/773/2/178

Bouwens, R. J., Illingworth, G. D., Oesch, P. A., Trenti, M., Labbé, I., Bradley, L., et al. (2015). UV luminosity functions at redshifts z ∼ 4 to z ∼ 10: 10,000 galaxies from HST legacy fields. *Astrophys. J.* 803:34. doi: 10.1088/0004-637X/803/1/34

Chary, R.-R., and Elbaz, D. (2001). Interpreting the cosmic infrared background: constraints on the evolution of the dustenshrouded star formation rate. *Astrophys. J.* 556, 562–581. doi: 10.1086/321609

Costa, T., Sijacki, D., Trenti, M., and Haehnelt, M. G. (2014). The environment of bright QSOs at z ∼ 6: star-forming galaxies and X-ray emission. *Monthly Not. R. Astron. Soc.* 439, 2146–2174. doi: 10.1093/mnras/stu101

De Rosa, G., Decarli, R., Walter, F., Fan, X., Jiang, L., Kurk, J. D., et al. (2011). Evidence for non-evolving Fe II/Mg II ratios in rapidly accreting z ∼ 6 QSOs. *Astrophys. J.* 739:56. doi: 10.1088/0004-637X/739/2/56

Decarli, R., Walter, F., Venemans, B. P., Bañados, E., Bertoldi, F., Carilli, C. L., et al. (2017). Rapidly star-forming galaxies adjacent to quasars at redshifts exceeding 6. *Nature* 545:457. doi: 10.1038/nature22358

Dekel, A., Birnboim, Y., Engel, G., Freundlich, J., Goerdt, T., Mumcuoglu, M., et al. (2009). Cold streams in early massive hot haloes as the main mode of galaxy formation. *Nature* 457, 451–454. doi: 10.1038/nature07648

Di Matteo, T., Khandai, N., DeGraf, C., Feng, Y., Croft, R., Lopez, J., et al. (2012). Cold flows and the first quasars. *Astrophys. J.* 745:L29. doi: 10.1088/2041-8205/745/2/L29

Dubois, Y., Pichon, C., Haehnelt, M., Kimm, T., Slyz, A., Devriendt, J., et al. (2012). Feeding compact bulges and supermassive black holes with low angular momentum cosmic gas at high redshift. *Monthly Not. R. Astron. Soc.* 423, 3616–3630. doi: 10.1111/j.1365-2966.2012.21160.x

Hopkins, P. F., Hernquist, L., Cox, T. J., Di Matteo, T., Robertson B. E., and Springel, V. (2006). A unified, merger driven model of the origin of starbursts, quasars, the cosmic X ray background, supermassive black holes, and galaxy spheroids. *Astrophys. J. Suppl. Series* 163, 1–49. doi: 10.1086/499298

Husband, K., Bremer, M. N., Stanway, E. R., Davies, L. J. M., Lehnert, M. D., and Douglas, L. S. (2013). Are z ∼ 5 QSOs found in the most massive high redshift over-densities? *Monthly Not. R. Astron. Soc.* 432, 2869–2877. doi: 10.1093/mnras/stt642

Kim, S., Stiavelli, M., Trenti, M., Pavlovsky, C. M., Djorgovski, S. G., Scarlata, C., et al. (2009). The environments of high-redshift quasi-stellar objects. *Astrophys. J.* 695, 809–817. doi: 10.1088/0004-637X/695/2/809

Kurk, J. D., Walter, F., Fan, X., Jiang, L., Riechers, D. A., Rix, H., et al. (2007). Black hole masses and enrichment of z ∼ 6 SDSS quasars. *Astrophys. J.* 669, 32–44. doi: 10.1086/521596

Maiolino, R., Caselli, P., Nagao, T., Walmsley, M., De Breuck, C., and Meneghetti, M. (2009). Strong [CII] emission at high redshift. *Astron. Astrophys.* 500, L1–L4. doi: 10.1051/0004-6361/200912265

Mor, R., Netzer, H., Trakhtenbrot, B., Shemmer, O., and Lira, P. (2012). Extreme star formation in the host galaxies of the fastest growing supermassive black holes at z = 4.8. *Astrophys. J.* 749:L25. doi: 10.1088/2041-8205/749/2/L25

Natarajan, P. (2011). The formation and evolution of massive black hole seeds in the early Universe. *Bull. Astron. Soc. India* 39:145. doi: 10.1142/9789814374774_0013

Neri, R., Downes, D., Cox, P., and Walter, F. (2014). High-resolution C+ imaging of HDF850.1 reveals a merging galaxy at z = 5.185. *Astron. Astrophys.* 562:A35. doi: 10.1051/0004-6361/201322528

Netzer, H., Lani, C., Nordon, R., Trakhtenbrot, B., Lira, P., and Shemmer, O. (2016). Star formation black hole growth and dusty tori in the most luminous AGNs at z = 2–3.5. *Astrophys. J.* 819:123. doi: 10.3847/0004-637X/819/2/123

Netzer, H., Mor, R., Trakhtenbrot, B., Shemmer, O., and Lira, P. (2014). Star formation and black hole growth at z ≃ 4.8. *Astrophys. J.* 791:34. doi: 10.1088/0004-637X/791/1/34

Sanders, D. B., Soifer, B. T., Elias, J. H., Madore, B. F., Matthews, K., Neugebauer, G., et al. (1988). Ultraluminous infrared galaxies and the origin of quasars. *Astrophys. J.* 325:74. doi: 10.1086/165983

Simpson, C., Mortlock, D. J., Warren, S., Cantalupo, S., Hewett, P. C., McLure, R. J., et al. (2014). No excess of bright galaxies around the redshift 7.1 quasar ULAS J1120+0641. *Monthly Not. R. Astron. Soc.* 442, 3454–3461. doi: 10.1093/mnras/stu1116

Speagle, J. S., Steinhardt, C. L., Capak, P. L., and Silverman, J. D. (2014). A highly consistent framework for the evolution of the star-forming "mail sequence" from ∼ 0–6. *Astrophys. J. Suppl. Series* 214:15. doi: 10.1088/0067-0049/214/2/15

Stark, D. P. (2016). Galaxies in the first billion years after the big bang. *Annu. Rev. Astron. Astrophys.* 54, 761–803. doi: 10.1146/annurev-astro-081915-023417

Steinhardt, C. L., Speagle, J. S., Capak, P. L., Silverman, J. D., Carollo, C. M., Dunlop, J. S., et al. (2014). Star formation at $4 < z < 6$ from the *Spitzer* large area survey with hyper-suprime-Cam (SPLASH). *Astrophys. J.* 791:L25. doi: 10.1088/2041-8205/791/2/L25

Trakhtenbrot, B., Lira, P., Netzer, H., Cicone, C., Maiolino, R., and Shemmer, O. (2017). ALMA observations show major mergers among the host Galaxies of fast-growing, high-redshift, supermassive black holes. *Astrophys. J.* 836:8. doi: 10.3847/1538-4357/836/1/8

Trakhtenbrot, B., Netzer, H., Lira, P., and Shemmer, O. (2011). Black hole mass and growth rate at z ≃ = 4.8: a short episode of fast growth followed by short duty cycle activity. *Astrophys. J.* 730:7. doi: 10.1088/0004-637X/730/1/7

Venemans, B. P., Walter, F., Zschaechner, L., Decarli, R., Rosa, G. D., Findlay, J. R., et al. (2016). Bright [C II] and dust emission in three z < 6.6 quasar host Galaxies observed by ALMA. *Astrophys. J.* 816:37. doi: 10.3847/0004-637X/816/1/37

Volonteri, M. (2012). The formation and evolution of massive black holes. *Science* 337, 544–547. doi: 10.1126/science.1220843

Wagg, J., Wiklind, T., Carilli, C. L., Espada, D., Peck, A., Riechers, D., et al. (2012). [C II] Line emission in massive star-forming galaxies at $z = 4.7$. *Astrophys. J.* 752:L30. doi: 10.1088/2041-8205/752/2/L30

Wang, R., Wagg, J., Carilli, C. L., Walter, F., Lentati, L., Fan, X., et al. (2013). Star formation and gas kinematics of quasar host Galaxies at z∼6: new insights from ALMA. *Astrophys. J.* 773:24. doi: 10.1088/2041-8205/774/2/L24

Willott, C. J., Albert, L., Arzoumanian, D., Bergeron, J., Crampton, D., Delorme, P., et al. (2010). Eddington-limited accretion and the black hole mass function at redshift 6. *Astron. J.* 140, 546–560. doi: 10.1088/0004-6256/140/2/546

Willott, C. J., Bergeron, J., and Omont, A. (2015). Star formation rate and dynamical mass of 10^8 solar mass black hole host galaxies at redshift 6. *Astrophys. J.* 801:123. doi: 10.1088/0004-637X/801/2/123

Willott, C. J., Percival, W. J., McLure, R. J., Crampton, D., Hutchings, J. B., Jarvis, M. J., et al. (2005). Imaging of SDSS z > 6 quasar fields: gravitational lensing, companion galaxies, and the host dark matter halos. *Astrophys. J.* 626, 657–665. doi: 10.1086/430168

Conflict of Interest Statement: The authors declare that the research was conducted in the absence of any commercial or financial relationships that could be construed as a potential conflict of interest.

The reviewer DB and handling Editor declared their shared affiliation.

Copyright © 2017 Trakhtenbrot, Lira, Netzer, Cicone, Maiolino and Shemmer. This is an open-access article distributed under the terms of the Creative Commons Attribution License (CC BY). The use, distribution or reproduction in other forums is permitted, provided the original author(s) or licensor are credited and that the original publication in this journal is cited, in accordance with accepted academic practice. No use, distribution or reproduction is permitted which does not comply with these terms.

frontiers in Astronomy and Space Sciences

PERSPECTIVE
published: 21 December 2017
doi: 10.3389/fspas.2017.00061

Circum-Galactic Medium in the Halo of Quasars

Riccardo Ottolina[1], Renato Falomo[2], Aldo Treves[1], Michela Uslenghi[3], Jari K. Kotilainen[4], Riccardo Scarpa[5] and Emanuele Paolo Farina[6]*

[1] Dipartimento di Scienza e Alta Tecnologia (DISAT), Università degli Studi dell'Insubria, Como, Italy, [2] Osservatorio Astronomico di Padova (INAF), Padua, Italy, [3] Istituto di Astrofisica Spaziale e Fisica Cosmica di Milano (INAF), Milan, Italy, [4] Finnish Centre for Astronomy with ESO (FINCA), University of Turku, Turku, Finland, [5] Instituto de Astrofisica de Canarias, La Laguna, Spain, [6] Max-Planck-Institut für Astronomie, Heidelberg, Germany

The properties of circum-galactic gas in the halo of quasar host galaxies are investigated analyzing Mg II 2800 and C IV 1540 absorption-line systems along the line of sight close to quasars. We used optical spectroscopy of closely aligned pairs of quasars (projected distance $\leq$ 200 kpc, but at very different redshift) obtained at the VLT and Gran Telescopio Canarias to investigate the distribution of the absorbing gas for a sample of quasars at z $\sim$1. Absorption systems of EW $\geq$0.3 associated with the foreground quasars are revealed up to 200 kpc from the centre of the host galaxy, showing that the structure of the absorbing gas is patchy with a covering fraction quickly decreasing beyond 100 kpc. In this contribution we use optical and near-IR images obtained at VLT to investigate the relations between the properties of the circum-galactic medium of the host galaxies and of the large scale galaxy environments of the foreground quasars.

Keywords: quasar, quasar environment, quasar pair, quasar spectra, galaxy around quasar

OPEN ACCESS

Edited by:
Mauro D'Onofrio, Università degli Studi di Padova, Italy

Reviewed by:
José María Solanes, University of Barcelona, Spain
Ascensión Del Olmo, Instituto de Astrofísica de Andalucía (CSIC), Spain
Fabio La Franca, Università degli Studi Roma Tre, Italy

****Correspondence:***
Riccardo Ottolina
r.ottolina@uninsubria.it

Specialty section:
This article was submitted to Milky Way and Galaxies, a section of the journal Frontiers in Astronomy and Space Sciences

Received: *28 September 2017*
Accepted: *04 December 2017*
Published: *21 December 2017*

Citation:
Ottolina R, Falomo R, Treves A, Uslenghi M, Kotilainen JK, Scarpa R and Farina EP (2017) Circum-Galactic Medium in the Halo of Quasars. Front. Astron. Space Sci. 4:61. doi: 10.3389/fspas.2017.00061

1. INTRODUCTION

The standard model for the origin of the extreme luminosity of quasars considers that a supermassive black hole shines as a quasar when intense mass inflow takes place, possibly as a consequence of tidal forces in dissipative events (e.g., Di Matteo et al., 2005). In this scenario, the circum-galactic medium of quasar host galaxies is expected to be populated by streams, cool gas clouds and tidal debris, as commonly observed in interacting galaxies (e.g., Sulentic et al., 2001; Cortese et al., 2006). Moreover the gas of the circum-galactic medium could be metal enriched by supernova-driven winds triggered by starbursts events associated to the mergers or by quasar-driven outflows of gas (e.g., Steidel et al., 2010; Shen and Ménard, 2012).

One of the effective ways to study the circum-galactic medium of galaxies at high redshift is to investigate the absorption features that they imprint in the spectra of quasars. In particular, projected quasar pairs (**Figure 1** left) are ideal observational tools for this purpose, since the light of the very bright source in the background ($z \equiv z_B$) goes through the extended halo of the foreground ($z \equiv z_F < z_B$) object (e.g., Hennawi et al., 2006; Farina et al., 2013). This can be evidenced by absorption lines at the foreground redshift: an example is reported in **Figure 1** right.

In our previous works we studied 49 quasar pairs (Farina et al., 2013, 2014; Landoni et al., 2016). We used the optical spectroscopy of close pairs (projected distance $\leq$200 kpc) obtained at the ESO-VLT and Gran Telescopio Canarias (GTC) to investigate the distribution of the absorbing gas at 100-200 kpc projected distance from the quasar studying the presence of Mg II or C

IV absorption lines at the redshift of foreground quasar. In order to characterize the structure of circum-galactic medium of the foreground quasar host galaxy we estimated the covering fraction of Mg II or C IV as a function of the projected distance. We assumed a threshold in equivalent width of 0.3 Å, then we subdivided the projected distance in bins. For each bin we computed the covering fraction as the ratio between the number of systems with Mg II or C IV absorption lines greater than the threshold and the total number of observed systems. Our previous results (Farina et al., 2013, 2014; Landoni et al., 2016) indicate that 22 spectra exhibit absorption lines of foreground quasar in the background quasar: 15 Mg II and 7 C IV. We found that the detected Mg II absorption systems of EW >0.3 Å associated with the foreground quasars are revealed up to ∼200 kpc from the centre of the host galaxy. The structure of absorbing gas is patchy with covering fraction of the gas that quickly decreases beyond 100 kpc. This is illustrated in **Figure 2** left. A similar behavior is present in absorption systems with C IV doublet (**Figure 2** right).

In this paper we analyze optical and NIR images of foreground quasars in order to investigated their closed environments and their host galaxies.

2. SAMPLE AND OBSERVATIONS

The selection procedure of our quasar pair projected sample is reported in detail in Farina et al. (2013) and Farina et al. (2014). Here we summarize briefly the main criteria of our choice:

(i) visibility from telescope location;
(ii) foreground quasar redshift must be selected in order that Mg II doublet falls in GRISM wavelength range;

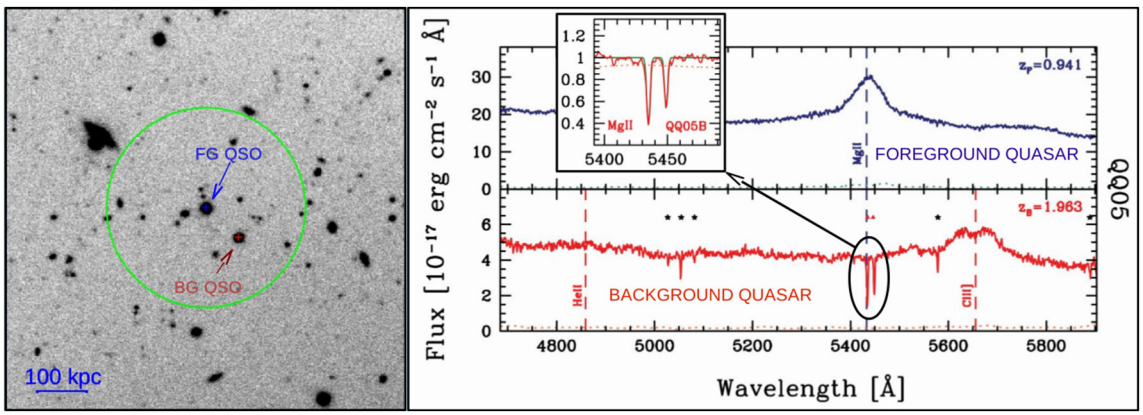

FIGURE 1 | Left: Image of projected quasar pair Q0059-2702. Blue and red arrows indicate the foreground quasar and the background one. Green circle shows the projected distance of 200 kpc from the foreground quasar. **Right**: VLT spectra of quasar pair Q0059-2702. The blue and red solid lines refer to foreground quasar and background quasar, respectively. The insert shows the zoom of Mg II absorptions at the same redshift of foreground quasar.

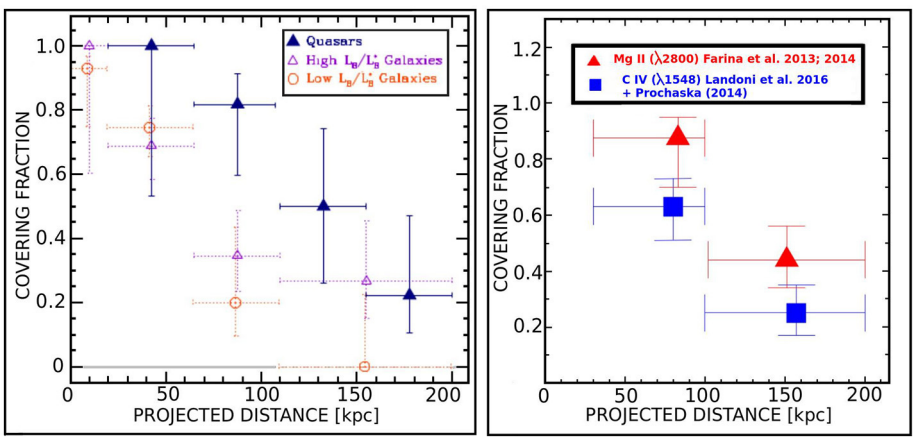

FIGURE 2 | Left: Comparison between quasars (Farina et al., 2014) and galaxies (Nielsen et al., 2013) of covering fraction of transversal absorption system of Mg II as a function of the projected distance. **Right**: Comparison of covering fraction of quasar halo for Mg II (red triangles) and C IV (blue squares) absorption lines. The covering fraction of Mg II is systematically higher than that of C IV.

(iii) projected distance at foreground redshift ≤200 kpc;
(iv) line-of-sight velocity difference ≥5,000 km s^{-1} to avoid physical pairs;
(v) background quasar must be brighter than $m_V \sim 21$ to ensure good spectra signal-to-noise ratio.

We acquired optical images at FORS2@VLT with the I BESS filter for the object with $z \leq 1$ and the Z GUNN filter otherwise, and near-IR images at HAWK-I@VLT with H filter for a total of 24 quasar projected pairs (4 targets have only optical images, 8 ones have only NIR images and 12 objects have images in both bands.). With this configuration we explore galaxies at the redshift of the target in the B band in the rest frame. For a subsample of object reported in **Table 1** we present here 8 deep high quality I-band images (seeing ∼0.5 arcsec).

3. ANALYSIS

We performed the analysis of optical images in order to characterize the close environment of foreground quasar. We used the software SEXTRACTOR (Bertin and Arnouts, 1996) to identify all objects in the frame over a given magnitude limit and to distinguish galaxy-like objects from star-like ones (galaxies have CLASS_STAR <0.5 and stars have CLASS_STAR >0.5). Then we evaluated the overdensity of galaxies around the foreground quasar calculating the ratio of number of galaxies per arcminute square to background estimated at distances greater than 500 kpc.

The near-IR images have been analyzed using the software package AIDA (Astronomical Image Decomposition Analysis,

TABLE 1 | List of targets observed in I band.

QSO_B (1)	z_B (2)	QSO_F (3)	z_F (4)	pd [kpc] (5)	Mg II (6)	Ovdens (7)
J003823.6−291259	2.699	J003823.74−291311.8	0.793	91	No	No
LQAC 015−026 011	1.963	J010204.12−264600.0	0.941	84	Yes	No
J013500.09−004113.4	1.259	J013458.77−004129.0	1.003	176	Yes	Yes
J014630.95+001531.6	1.019	J014630.14+001521.3	0.923	125	Yes	Yes
J021553.71+010953.9	2.215	J021552.53+011000.1	0.875	145	No	Yes
J022158.83−001052.5	3.213	J022158.77−001044.3	1.036	66	Yes	Yes
[HB89] 2225−403	2.398	J222850.49−400825.7	0.931	78	Yes	No
J225902.37+003221.7	1.456	J225902.87+003243.7	0.868	183	No	No

Column (1) and (3) give the name of background and foreground quasars respectively while (2) and (4) give their redshifts. Column (5) reports the projected distances at the redshift of the foreground quasar. Column (6) and (7) are labels for the presence of Mg II absorption lines and of an overdensity of galaxies around the foreground quasar.

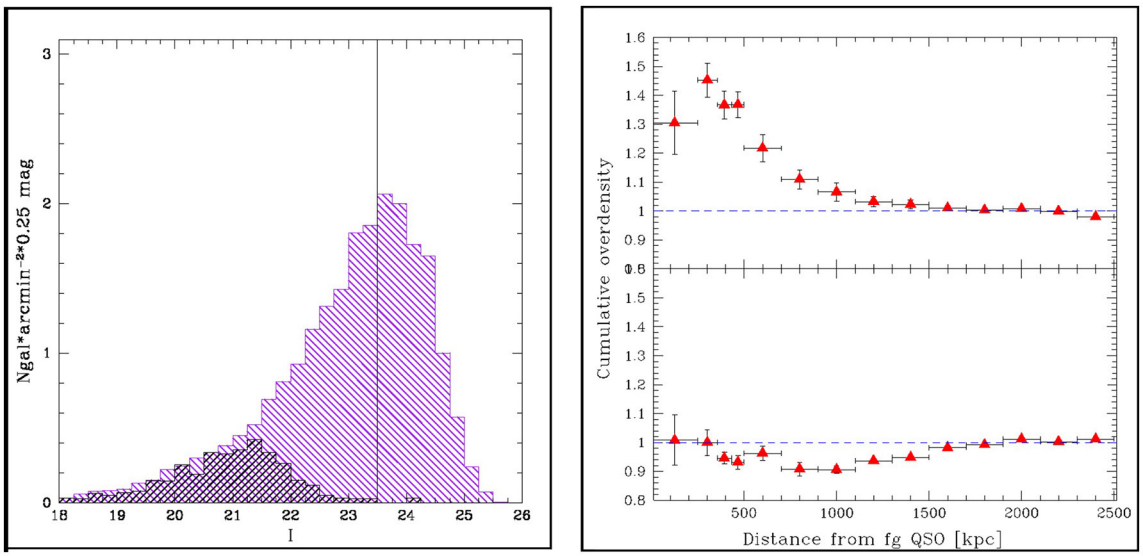

FIGURE 3 | Left: Average surface number density of galaxies vs. I magnitude of 8 quasar pair fields obtained at VLT FORS2. The vertical line marks the adopted threshold magnitude for the environment study. For comparison the black histogram shows the similar distribution based on the SDSS analysis of 5 fields.
Right: Average cumulative overdensity of galaxies around quasars (see **Table 1**). Only half of quasars exhibits a clear galaxy overdensity (upper panel) while the other half does not show any overdensity (lower panel).

Uslenghi and Falomo, 2008). From this analysis of the near-IR images we are able to characterize the properties of the foreground quasars host galaxy via 2-d model fitting, assuming that they are the result of the superposition of two components: the nucleus, described by the local PSF, and the host galaxy, modeled by a Sersic function convolved with the proper PSF.

4. PRELIMINARY RESULTS

Based on our deep optical images of quasars we are able to characterize the galaxy environment up to I $\sim$ 23.5 which is more than 2 magnitudes deeper than SDSS images (see **Figure 3** left). This allows to investigate the galaxy environment down to about 3 magnitude fainter than M^*. We find that for 4 cases there is a clear galaxy overdensity around the foreground quasar while in the another 4 cases there is no evidence that quasars live in a group of galaxies (see **Figure 3** and **Table 1**). In 3 quasars that exhibit overdensity there is also a detection of Mg II absorption systems at the same redshift of foreground quasar in the circum-galactic medium. In the cases of no galaxy overdensity Mg II absorption lines are detected in 2 objects. The small sample, investigated till now, does not permit us to draw firm conclusions on the relationship between galaxy environments and presence of cold gas in the intergalactic medium. We are completing the analysis of the full sample and extending it with other targets from ongoing observations at GTC.

Till now we analyzed 11 out of the 20 foreground quasars with NIR images. For 9 ($\sim$80%) the host galaxy is well resolved. In one case the detection of the host galaxy is marginal and only for one image no evidence of the host galaxy is found. The rest frame absolute magnitude in I band of the resolved host galaxies ranges from -22.5 to -24.9, with a median value of -23.7. These results are comparable to those reference to other quasars at similar redshift (Sanghvi et al., 2014).

AUTHOR CONTRIBUTIONS

RO provides the analysis of the environment. MU provides the analysis of NIR images. All other authors provide discussion of results and write the paper.

ACKNOWLEDGMENTS

EF acknowledge funding through the ERC grant "Cosmic Dawn."

REFERENCES

Bertin, E., and Arnouts, S. (1996). SExtractor: software for source extraction. *Astron. Astrophys. Suppl.* 117, 393–404. doi: 10.1051/aas:1996164.

Cortese, L., Gavazzi, G., Boselli, A., Franzetti, P., Kennicutt, R. C., O'Neil, K., et al. (2006). Witnessing galaxy preprocessing in the local Universe: the case of a star-bursting group falling into Abell 1367. *Astron. Astrophys.* 453, 847–861. doi: 10.1051/0004-6361:20064873

Di Matteo, T., Springel, V., and Hernquist, L. (2005). Energy input from quasars regulates the growth and activity of black holes and their host galaxies. *Nature* 433, 604–607. doi: 10.1038/nature03335

Farina, E. P., Falomo, R., Decarli, R., Treves, A., and Kotilainen, J. K. (2013). On the cool gaseous haloes of quasars. *Month. Notices R. Astron. Soc.* 429, 1267–1277. doi: 10.1093/mnras/sts410

Farina, E. P., Falomo, R., Scarpa, R., Decarli, R., Treves, A., and Kotilainen, J. K. (2014). The extent of the Mg II absorbing circumgalactic medium of quasars. *Month. Notices R. Astron. Soc.* 441, 886–899. doi: 10.1093/mnras/stu585

Hennawi, J. F., Prochaska, J. X., Burles, S., Strauss, M. A., Richards, G. T., Schlegel, D. J., et al. (2006). Quasars probing quasars. I. optically thick absorbers near luminous quasars. *Astrophys. J.* 651, 61–83. doi: 10.1086/507069

Landoni, M., Falomo, R., Treves, A., Scarpa, R., and Farina, E. P. (2016). Circumgalactic medium of quasars: C IV absorption systems. *Month. Notices R. Astron. Soc.* 457, 267–271. doi: 10.1093/mnras/stv2964

Nielsen, N. M., Churchill, C. W., and Kacprzak, G. G. (2013). MAGIICAT II. General characteristics of the Mg II absorbing circumgalactic medium. *Astrophys. J.* 776:115. doi: 10.1088/0004-637X/776/2/115

Sanghvi, J., Kotilainen, J. K., Falomo, R., Decarli, R., Karhunen, K., and Uslenghi, M. (2014). The black hole-host galaxy relation for very low mass quasars. *Month. Notices R. Astron. Soc.* 445, 1261–1268. doi: 10.1093/mnras/stu1822

Shen, Y., and Ménard, B. (2012). On the link between associated Mg II absorbers and star formation in quasar hosts. *Astrophys. J.* 748:131. doi: 10.1088/0004-637X/748/2/131

Steidel, C. C., Erb, D. K., Shapley, A. E., Pettini, M., Reddy, N., Bogosavljević, M., et al. (2010). The structure and kinematics of the circumgalactic medium from Far-ultraviolet spectra of z ˜= 2–3 galaxies. *Astrophys. J.* 717, 289–322. doi: 10.1088/0004-637X/717/1/289

Sulentic, J. W., Rosado, M., Dultzin-Hacyan, D., Verdes-Montenegro, L., Trinchieri, G., Xu, C., et al. (2001). A multiwavelength study of stephan's quintet. *Astron. J.* 122, 2993–3016. doi: 10.1086/324455

Uslenghi, M., and Falomo, R. (2008). "AIDA: astronomical image decomposition and analysis," in *Modelling and Simulation in Science*: Proceedings of the 6th International Workshop on Data Analysis in Astronomy "Livio Scarsi", eds V. D. Gesù, G. Lo Bosco, and M. C. Maccarone (Erice), 313–318.

Conflict of Interest Statement: The authors declare that the research was conducted in the absence of any commercial or financial relationships that could be construed as a potential conflict of interest.

Copyright © 2017 Ottolina, Falomo, Treves, Uslenghi, Kotilainen, Scarpa and Farina. This is an open-access article distributed under the terms of the Creative Commons Attribution License (CC BY). The use, distribution or reproduction in other forums is permitted, provided the original author(s) or licensor are credited and that the original publication in this journal is cited, in accordance with accepted academic practice. No use, distribution or reproduction is permitted which does not comply with these terms.

frontiers in Astronomy and Space Sciences

PERSPECTIVE
published: 08 August 2017
doi: 10.3389/fspas.2017.00009

A Catalog of Active Galactic Nuclei from the First 1.5 Gyr of the Universe

Krisztina Perger[1], Sándor Frey[2], Krisztina É. Gabányi[2] and L. Viktor Tóth[1]*

[1] Department of Astronomy, Eötvös Loránd University, Budapest, Hungary, [2] Konkoly Observatory, MTA Research Centre for Astronomy and Earth Sciences, Budapest, Hungary

Active galactic nuclei (AGN) are prominent astrophysical objects that can be observed throughout the whole Universe. To understand the underlying physical processes and the different appearance of AGN types, extensive samples are needed. Nowadays, various AGN catalogs are available at different wavebands. However, at the highest redshifts data are still relatively sparse. These data are required for examining AGN properties in the early Universe. This way we can compare the earliest AGN with those seen at lower redshifts, and can study their cosmological evolution. Additionally, because of their high luminosity, AGN may also be used as probes to test cosmological models. With the aim of constructing a complete sample of all known AGN at $z \geq 4$, we are currently compiling a photometric catalog from literature sources. We cross-match catalogs particularly at optical and radio wavebands, to build up a sample for detailed high-resolution radio interferometric studies. The continuously updated list now contains nearly 2,600 objects with known spectroscopic redshifts, optical magnitudes, and auxiliary information about observations at other wavebands. About 170 of them are known radio sources for which we collect existing radio interferometric data from the literature.

Keywords: quasars, active galactic nuclei, extragalactic astronomy, photometry, spectroscopy, catalogs

OPEN ACCESS

Edited by:
Mauro D'Onofrio, University of Padua, Italy

Reviewed by:
Giovanna Maria Stirpe, Osservatorio Astronomico di Bologna (INAF), Italy
Daniela Bettoni, Osservatorio Astronomico di Padova (INAF), Italy
Alenka Negrete, National Autonomous University of Mexico, Mexico

****Correspondence:***
Krisztina Perger
k.perger@astro.elte.hu

Specialty section:
This article was submitted to Milky Way and Galaxies, a section of the journal Frontiers in Astronomy and Space Sciences

Received: *22 June 2017*
Accepted: *21 July 2017*
Published: *08 August 2017*

Citation:
Perger K, Frey S, Gabányi KÉ and Tóth LV (2017) A Catalog of Active Galactic Nuclei from the First 1.5 Gyr of the Universe. Front. Astron. Space Sci. 4:9. doi: 10.3389/fspas.2017.00009

1. INTRODUCTION

Active galactic nuclei (AGN) have been extensively studied for more than half a century. The activity of AGN is believed to originate from material falling into an accreting supermassive black hole (SMBH) in the central region of the galaxy, as first proposed by Lynden-Bell (1969). Due to the accretion process, enormous amount of energy is released, which can be observed throughout the entire electromagnetic spectrum (e.g., Urry and Padovani, 1995). In the cases of radio-loud (jetted) AGN, strong radio emission is produced via synchrotron emission in a symmetric pair of jets emanating from the vicinity of the central SMBH (Blandford and Rees, 1974; Blandford and Königl, 1979). However, the formation and physical properties of AGN are not yet fully understood (e.g., Netzer, 2015).

The large variety of observed characteristics of AGN require sophisticated models to provide an adequate description of the underlying physics. To determine their properties satisfactorily, we need both low- and high-redshift populations of AGN, which requires statistically complete samples.

To date, several different AGN catalogs and samples exist at various wavebands (e.g., Constantin et al., 2009; Véron-Cetty and Véron, 2010; Shen et al., 2011; Kalfountzou et al., 2014; Secrest et al., 2015). We are currently compiling a catalog using extensive samples of AGN primarily discovered by optical observations in recent years, with the aim of constructing a complete sample of AGN at the earliest epochs of the Universe. Given the accelerating pace of data acquisition of

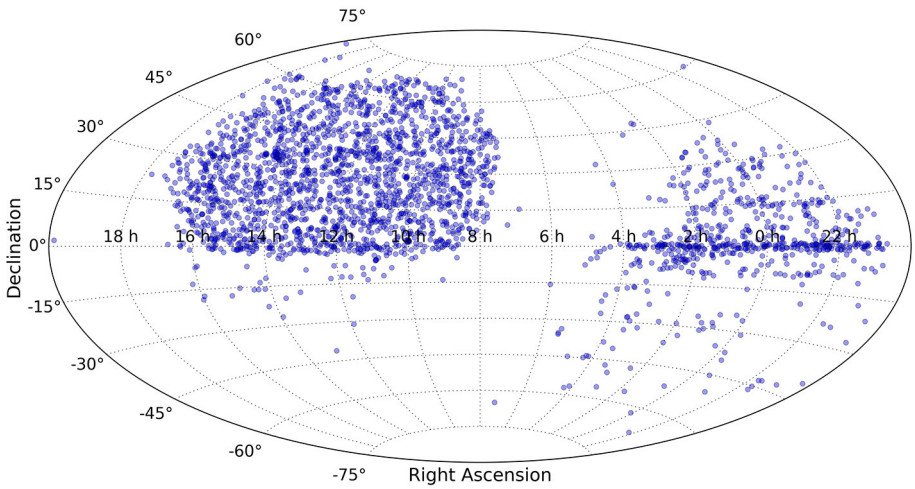

FIGURE 1 | Sky coverage of the sources at the current state of the catalog.

contemporary optical sky surveys, we intend to update and extend our catalog regularly.

To better understand the observable characteristics of AGN, we collected available data at radio wavebands as well, including flux densities from large radio surveys and interferometric observations of individual objects. Our catalog may facilitate several scientific studies. The future applications carry the opportunity to determine the luminosity function of AGN at the highest redshifts (e.g., Fan et al., 2004; Willott et al., 2010; Jiang et al., 2016). It can also provide sample for studies of galaxy environment and possible overdensities around high-redshift quasars (e.g., Orsi et al., 2016; Uchiyama et al., 2017). With supplementary UV data, it may become useful for cosmological studies, providing a sample where 'standard candles' can be selected from (e.g., Marziani and Sulentic, 2014). Likewise, using a sample of the most distant compact radio-emitting AGN, further constraints on the angular size–redshift relation could be obtained (e.g., Gurvits et al., 1999). Presumably, it will make the planning of interferometric observations for sufficiently bright radio sources simpler. Furthermore, it might aid in the selection of interesting individual objects for detailed analysis, and in examining the Galactic foreground in different wavebands.

To compile our sample of high-redshift AGN, we applied a somewhat arbitrary $z \geq 4$ threshold for redshifts. In this regime, the first AGN (QSO 0046–293) was discovered by Warren et al. (1987). Since then, the known number of sources at the earliest epochs of the Universe increased at a fast pace, primarily due to extensive all-sky surveys, e.g., the Sloan Digital Sky Survey (SDSS) (York et al., 2000; Eisenstein et al., 2011; Alam et al., 2015).

2. COMPILING THE CATALOG

We built the base of the catalog using 3 large samples of AGN: the quasars of the twelfth data release of SDSS (Jiang et al., 2016; Pâris et al., 2017), the high-redshift quasar sample (Bañados et al., 2016, and references therein) of the Panoramic Survey Telescope and Rapid Response System (Pan-STARRS, Chambers et al., 2016) Survey and the Half Million Quasars (HMQ) Catalog (Flesch, 2015). We filtered the HMQ and SDSS quasars for redshifts $z \geq 4$. Since sources in the Pan-STARRS high-redshift quasar sample had redshifts $z \geq 5.6$, no filtering was needed.

The bulk of the catalog was then constructed after cross-matching the three large samples above. First, HMQ and SDSS quasars were matched. To avoid duplicate entries, we were looking for SDSS-discovered objects in the HMQ sample. Based on the results of e.g., Barro et al. (2011) and Rimoldini et al. (2012), we applied a search radius of $1''$ and considered the objects within this radius identical if found in both catalogs. There were 2,363 objects in the HMQ catalog and 1,881 in the SDSS quasar sample at $z \geq 4$. All but 2 SDSS sources were also included in the HMQ sample. The match therefore resulted in 2,365 independent sources. Then the HMQ–SDSS sample was cross-matched with the Pan-STARRS quasar list, applying the same search radius of $1''$. This increased the number of unique sources to 2,470. The cross-matching and the concatenation of independent source lists were carried out using the `topcat` catalog editing software[1] (Taylor, 2005).

The resulting catalog contained the following properties: right ascension and declination (optical) coordinates, name, radio identification and X-ray identification names (when existing), redshift, optical magnitudes if known, and literature references regarding discovery and redshift data.

In the course of catalog updates, we added 121 new sources to the list. These were found in the literature (McMahon et al., 2002; Richards et al., 2009; Yi et al., 2014; Wang et al., 2016; Khorunzhev et al., 2017; Matsuoka et al., 2017; Reed et al., 2017; Tang et al., 2017; Tuccillo et al., 2017; Wang et al., 2017; Yang et al., 2017; Yi et al., 2017) but not contained in the 3 large catalogs

[1] http://www.starlink.ac.uk/topcat/

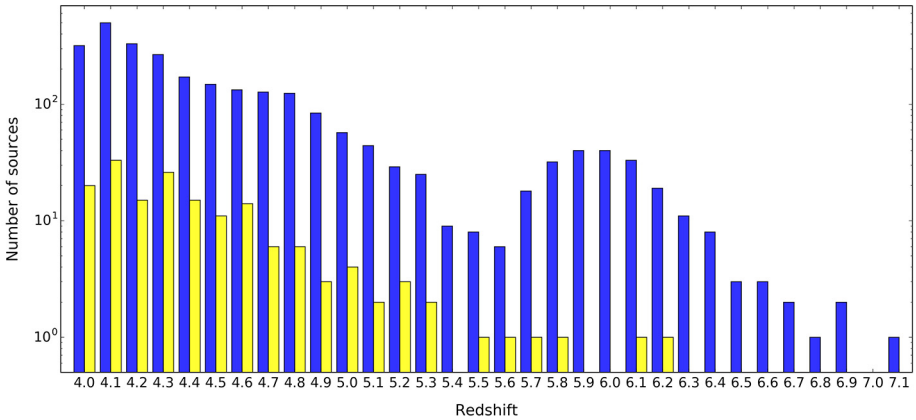

FIGURE 2 | Histogram of the redshift distribution of catalog entries, with a bin width of 0.1. Blue columns indicate all AGN in the sample, while yellow columns show the distribution of sources with available radio flux densities. From the total of 2,591 sources, 166 are detected in FIRST or (if out of FIRST coverage) in NVSS. Two thousand one hundred and forty-eight positions are covered by FIRST but radio sources not detected (brightness upper limit is available only). Two hundred and fifty two sources are outside the FIRST field and lack detection in NVSS, and 25 are outside the footprints of both surveys.

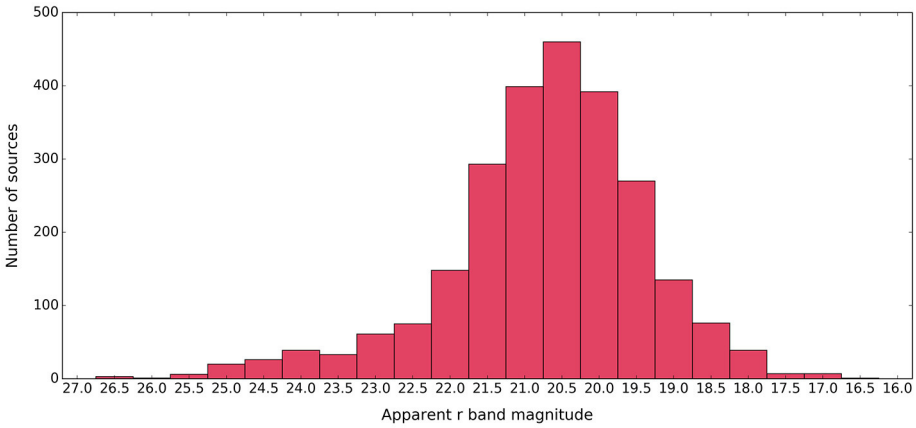

FIGURE 3 | Apparent red magnitude distribution of the high-redshift AGN. The histogram shows the 2,493 sources with available red magnitudes with a bin width of 0.5^m. Note that since most sources have photometry based on POSS plates, magnitudes might differ from SDSS magnitudes, up to $2^m - 3^m$.

that form the basis of our list. The sky coverage of the full sample is plotted in **Figure 1**.

To find radio counterparts, we searched for the catalog sources in the VLA Faint Images of the Radio Sky at Twenty-Centimeters (FIRST) Survey [2] (White et al., 1997) database with a 1.5″ radius, the same value that was applied by Ivezić et al. (2002). This resulted in 144 matches. We also marked those 2,148 positions which were covered by FIRST but there were no sources found above the detection limit (∼ 1 mJy), and those which were close to the field edge or lay outside FIRST coverage. Those which were outside the FIRST footprint, were also searched in the NRAO VLA Sky Survey (NVSS) catalog[3] (Condon et al., 1998), with a search radius of 10″ (Sadler et al., 2002). Positions outside the NVSS field or both survey footprints were also noted. Altogether 166 sources have radio flux densities measured in either FIRST or NVSS, both at 1.4 GHz. This is 6.5% of the 2,566 sources which were covered by either of the surveys. The redshift distribution of the full sample and of those sources with radio detection are plotted in **Figure 2**. The prominent "gap" visible between redshifts 5.3 and 5.6 and the excess in the 5.7–6.4 range arises mainly from the sample selection: the Pan-STARRS sample contained only quasars with $z \geq 5.6$. Moreover, the Pan-STARRS survey has a more extensive sky coverage than SDSS: the majority of independent Pan-STARRS quasars have redshifts between 5.7 and 6.4.

We added very long baseline interferometry (VLBI) flux densities for a total of 35 quasars (Paragi et al., 1999; Beasley et al., 2002; Frey et al., 2003, 2005, 2008, 2010, 2011; Fey et al., 2004; Momjian et al., 2004, 2005, 2008; Romani et al., 2004; Petrov et al., 2006, 2008; Helmboldt et al., 2007; Veres et al., 2010; Cheung et al., 2012; Frey et al., 2013; Cao et al., 2014, 2017; Parijskij et al., 2014; Frey et al., 2015; Gabányi et al., 2015; Coppejans et al., 2016; Wang et al., 2017; Zhang et al., 2017). We also marked sources

[2]http://sundog.stsci.edu
[3]http://www.cv.nrao.edu/nvss/

that have already been proposed for VLBI observations to our knowledge.

From the total of 2,591 AGN in the current version of our catalog, we have available red band optical magnitudes for 2,493 quasars. To illustrate this, the distribution of the r band magnitudes of these sources are shown in **Figure 3**. A descending trend can be seen at the faint end of the histogram due the selection effect casued by the limited sensitivity of the optical surveys. The histogram also shows that there are a couple of particularly bright sources in the sample. Given the high redshifts, these magnitudes would imply extremely high luminosities for these AGN. We therefore investigated this peculiarity by looking at individual objects in our catalog. We found that in some cases sources from the HMQ catalog where the photometry was based on Palomar Observatory Sky Survey (POSS) plates show significant difference from the values observed in SDSS, reaching up to $2^{\mathrm{m}} - 3^{\mathrm{m}}$. However, the original HMQ catalog contains a flag indicating the quality of the photometry. We plan to improve our catalog and make sure that only high-quality photometric data are listed in the next version.

3. SUMMARY

With the aim of creating a catalog which can be applied to a wide range of studies, we cross-matched and concatenated 3 large lists of AGN, taken from the SDSS twelfth data release, the Pan-STARRS first data release, and the HMQ catalog. We expanded this base catalog with numerous sources from the literature. The sample counts 2,591 sources at its current state, from which 166 AGN have available measured radio flux densities. Furthermore, 35 of them already have high-resolution VLBI imaging observations published in the literature. The current version of the catalog can be obtained on request by contacting the corresponding author. We intend to make the $z \geq 4$ AGN catalog publicly available in the near future.

AUTHOR CONTRIBUTIONS

KP compiled the catalog. All authors participated in defining the catalog content and the preparation of the manuscript.

FUNDING

This research was partly supported by the grants OTKA NN110333 and NN111016 received from the Hungarian National Research, Development and Innovation Office.

ACKNOWLEDGMENTS

KP thanks the organizers of the "Quasars at All Cosmic Epochs" conference for support. Funding for SDSS-III has been provided by the Alfred P. Sloan Foundation, the Participating Institutions, the National Science Foundation, and the U.S. Department of Energy Office of Science. The SDSS-III web site is http://www.sdss3.org/. The Pan-STARRS1 Surveys (PS1) and the PS1 public science archive have been made possible through contributions by the Institute for Astronomy, the University of Hawaii, the Pan-STARRS Project Office, the Max-Planck Society and its participating institutes, the Max Planck Institute for Astronomy, Heidelberg and the Max Planck Institute for Extraterrestrial Physics, Garching, The Johns Hopkins University, Durham University, the University of Edinburgh, the Queen's University Belfast, the Harvard-Smithsonian Center for Astrophysics, the Las Cumbres Observatory Global Telescope Network Incorporated, the National Central University of Taiwan, the Space Telescope Science Institute, the National Aeronautics and Space Administration under Grant No. NNX08AR22G issued through the Planetary Science Division of the NASA Science Mission Directorate, the National Science Foundation Grant No. AST-1238877, the University of Maryland, Eotvos Lorand University (ELTE), the Los Alamos National Laboratory, and the Gordon and Betty Moore Foundation.

REFERENCES

Alam, S., Albareti, F. D., Allende Prieto, C., Anders, F., Anderson, S. F., Anderton, T., et al. (2015). The eleventh and twelfth data releases of the Sloan Digital Sky Survey: final data from SDSS-III. *Astrophys. J.* 219:12. doi: 10.1088/0067-0049/219/1/12

Bañados, E., Venemans, B. P., Decarli, R., Farina, E. P., Mazzucchelli, C., Walter, F., et al. (2016). The Pan-STARRS1 distant $z > 5.6$ quasar survey: more than 100 quasars within the first Gyr of the Universe. *Astrophys. J.* 227:11. doi: 10.3847/0067-0049/227/1/11

Barro, G., Pérez-Gonz ález, P. G., Gallego, J., Ashby, M. L. N., Kajisawa, M., Miyazaki, S., et al. (2011). UV-to-FIR analysis of Spitzer/IRAC sources in the extended groth strip. I. Multi-wavelength photometry and spectral energy distributions. *Astrophys. J.* 193:13. doi: 10.1088/0067-0049/193/1/13

Beasley, A. J., Gordon, D., Peck, A. B., Petrov, L., MacMillan, D. S., Fomalont, E. B., et al. (2002). The VLBA Calibrator Survey-VCS1. *Astrophys. J.* 141:13. doi: 10.1086/339806

Blandford, R. D., and Königl, A. (1979). Relativistic jets as compact radio sources. *Astrophys. J.* 232:34. doi: 10.1086/157262

Blandford, R. D., and Rees, M. J. (1974). A "twin-exhaust" model for double radio sources. *Mon. Not. Roy. Astron. Soc.* 169:395. doi: 10.1093/mnras/169.3.395

Cao, H.-M., Frey, S., Gurvits, L. I., Yang, J., Hong, X.-Y., Paragi, Z., et al. (2014). VLBI observations of the radio quasar J2228+0110 at $z = 5.95$ and other field sources in multiple-phase-centre mode. *Astron. Astrophys.* 563:A111. doi: 10.1051/0004-6361/201323328

Cao, H.-M., Frey, S., Gabányi, K. É, Paragi, Z., Yang, J., Cseh, D., et al. (2017). VLBI observations of four radio quasars at $z > 4$: blazars or not? *Mon. Not. Roy. Astron. Soc.* 467:950. doi: 10.1093/mnras/stx160

Chambers, K. C., Magnier, E. A., Metcalfe, N., Flewelling, H. A., Huber, M. E., Waters, C. Z., et al. (2016). The Pan-STARRS1 Surveys. ArXiv eprint: 1612.05560

Cheung, C. C., Stawarz, Ł., Siemiginowska, A., Gobeille, D., Wardle, J. F. C., Harris, D. E., et al. (2012). Discovery of a Kiloparsec-scale X-Ray/Radio Jet in the $z = 4.72$ Quasar GB 1428+4217. *Astrophys. J.* 756:L20. doi: 10.1088/2041-8205/756/1/L20

Condon, J. J., Cotton, W. D., Greisen, E. W., Yin, Q. F., Perley, R. A., Taylor, G. B., et al. (1998). The NRAO VLA Sky Survey. *Astron. J.* 115:1693. doi: 10.1086/300337

Constantin, A., Green, P., Aldcroft, T., Kim, D.-W., Haggard, D., Barkhouse, W., et al. (2009). Probing the balance of AGN and star-forming activity in the local Universe with ChaMP. *Astrophys. J.* 705:1336. doi: 10.1088/0004-637X/705/2/1336

Coppejans, R., Frey, S., Cseh, D., Müller, C., Paragi, Z., Falcke, H., et al. (2016). On the nature of bright compact radio sources at $z > 4.5$. *Mon. Not. Roy. Astron. Soc.* 463:3260. doi: 10.1093/mnras/stw2236

Eisenstein, D. J., Weinberg, D. H., Agol, E., Aihara, H., Allende Prieto, C., Anderson, S. F., et al. (2011). SDSS-III: massive spectroscopic surveys of the distant Universe, the Milky Way, and Extra-Solar Planetary Systems. *Astron. J.* 142:72. doi: 10.1088/0004-6256/142/3/72

Fan, X., Hennawi, J. F., Richards, G. T., Strauss, M. A., Schneider, D. P., Donley, J. L., et al. (2004). A Survey of $z > 5.7$ Quasars in the Sloan Digital Sky Survey. III. Discovery of Five Additional Quasars. *Astron. J.* 128:515. doi: 10.1086/422434

Fey, A. L., Ma, C., Arias, E. F., Charlot, P. Feissel-Vernier, M., Gontier, A.-M., et al. (2004). The second extension of the international celestial reference frame: ICRF-EXT.1. *Astron. J.* 127:3587. doi: 10.1086/420998

Flesch, E. W. (2015). The Half Million Quasars (HMQ) Catalogue. *PASA* 32:10. doi: 10.1017/pasa.2015.10

Frey, S., Mosoni, L., Paragi, Z., and Gurvits, L. I. (2003). Radio structure of the most distant radio-detected quasar at the 10-mas scale. *Mon. Not. Roy. Astron. Soc.* 343:L20. doi: 10.1046/j.1365-8711.2003.06869.x

Frey, S., Paragi, Z., Mosoni, L., and Gurvits, L. I. (2005). High-resolution radio imaging of the most distant radio quasar SDSS J0836+0054. *Astron. Astrophys.* 436:L13. doi: 10.1051/0004-6361:200500112

Frey, S., Gurvits, L. I., Paragi, Z., and Gabányi, K. É. (2008). High-resolution double morphology of the most distant known radio quasar at $z = 6.12$. *Astron. Astrophys.* 484:L39. doi: 10.1051/0004-6361:200810040

Frey, S., Paragi, Z., Gurvits, L. I., Cseh, D., and Gabányi, K. É. (2010). High-resolution images of five radio quasars at early cosmological epochs. *Astron. Astrophys.* 524:A83. doi: 10.1051/0004-6361/201015554

Frey, S., Paragi, Z., Gurvits, L. I., Gabányi, K. É., and Cseh, D. (2011). Into the central 10 pc of the most distant known radio quasar. VLBI imaging observations of J1429+5447 at $z = 6.21$. *Astron. Astrophys.* 531:L5. doi: 10.1051/0004-6361/201117341

Frey, S., Fogasy, J. O., Paragi, Z., and Gurvits, L. I. (2013). On the Doppler boosting in the compact radio jet of the distant blazar J1026+2542 at $z = 5.3$. *Mon. Not. Roy. Astron. Soc.* 431:1314. doi: 10.1093/mnras/stt249

Frey, S., Paragi, Z., Fogasy, J. O., and Gurvits, L. I. (2015). The first estimate of radio jet proper motion at $z > 5$. *Mon. Not. Roy. Astron. Soc.* 446:2921. doi: 10.1093/mnras/stu2294

Gabányi, K. É., Cseh, D., Frey, S., Paragi, Z., Gurvits, L. I., An, T., et al. (2015). VLBI observation of the newly discovered $z = 5.18$ quasar SDSS J0131-0321. *Mon. Not. Roy. Astron. Soc.* 450:L57. doi: 10.1093/mnrasl/slv046

Gurvits, L. I., Kellermann, K. I., and Frey, S. (1999). The "angular size - redshift" relation for compact radio structures in quasars and radio galaxies. *Astron. Astrophys.* 342:378.

Helmboldt, J. F., Taylor, G. B., Tremblay, S., Fassnacht, C. D., Walker, R. C., Myers, S. T., et al. (2007). The VLBA Imaging and Polarimetry Survey at 5 GHz. *Astrophys. J.* 658:203. doi: 10.1086/511005

Ivezić, Ž., Menou, K., Knapp, G. R., Strauss, M. A., Lupton, R. H., Vanden Berk, D. E. et al. (2002). Optical and radio properties of extragalactic sources observed by the FIRST survey and the Sloan Digital Sky Survey. *Astron. J.* 124:2364. doi: 10.1086/344069

Jiang, L., McGreer, I. D., Fan, X., Strauss, M. A., Bañados, E., Becker, R. H., et al. (2016). The Final SDSS High-redshift Quasar Sample of 52 Quasars at $z > 5.7$. *Astrophys. J.* 833:222. doi: 10.3847/1538-4357/833/2/222

Kalfountzou, E., Civano, F., Elvis, M., Trichas, M., and Green, P. (2014). The largest X-ray-selected sample of z>3 AGNs: C-COSMOS and ChaMP. *Mon. Not. Roy. Astron. Soc.* 445:1430. doi: 10.1093/mnras/stu1745

Khorunzhev, G. A., Burenin, R. A., Sazonov, S. Y., Amvrosov, A. L., and Eselevich, M. V. (2017). Optical spectroscopy of candidates for quasars at $3 < z < 5.5$ from the XMM-newton X-ray survey. A distant X-ray quasar at $z = 5.08$. *Astr. L.* 43:135. doi: 10.1134/S1063773717030045

Lynden-Bell, D. (1969). Galactic Nuclei as Collapsed Old Quasars. *Nature* 223:690. doi: 10.1038/223690a0

Marziani, P., and Sulentic, J. W. (2014). Highly accreting quasars: sample definition and possible cosmological implications. *Mon. Not. Roy. Astron. Soc.* 442:1211. doi: 10.1093/mnras/stu951

Matsuoka, Y., Onoue, M., Kashikawa, N., Iwasawa, K., Strauss, M. A., Nagao, T., et al. (2017). Subaru High-z Exploration of Low-Luminosity Quasars (SHELLQs). II. Discovery of 32 Quasars and Luminous Galaxies at $5.7 < z < 6.8$. arXiv eprint:1704.05854

McMahon, R. G., White, R. L., Helfand, D. J., and Becker, R. H. (2002). Optical Counterparts for 70,000 Radio Sources: APM Identifications for the FIRST Radio Survey. *Astrophys. J.* 143:1. doi: 10.1086/342623

Momjian, E., Petric, A. O., and Carilli, C. L. (2004). VLBA Observations of $z > 4$ Radio-loud Quasars. *Astron. J.* 127:587. doi: 10.1086/381300

Momjian, E., Carilli, C. L., and Petric, A. O. (2005). Sensitive VLBI Observations of the $z = 4.7$ QSO BRI 1202-0725. *Astron. J.* 129:1809. doi: 10.1086/428598

Momjian, E., Carilli, C. L., and McGreer, I. D. (2008). Very Large Array and Very Long Baseline Array observations of the highest redshift radio-loud QSO J1427+3312 at $z = 6.12$. *Astron. J.* 136:344. doi: 10.1088/0004-6256/136/1/344

Netzer, H. (2015). Revisiting the Unified Model of Active Galactic Nuclei. *Annu. Rev. Astron. Astrophys.* 53:365. doi: 10.1146/annurev-astro-082214-122302

Orsi, Á. A., Fanidakis, N., Lacey, C. G., and Baugh, C. M. (2016). The environments of high-redshift radio galaxies and quasars: probes of protoclusters. *Mon. Not. Roy. Astron. Soc.* 456:3827. doi: 10.1093/mnras/stv2919

Paragi, Z., Frey, S., Gurvits, L. I., Kellermann, K. I., Schilizzi, R. T., McMahon, R. G., et al. (1999). VLBI imaging of extremely high redshift quasars at 5 GHz. *Astron. Astrophys.* 344:51.

Parijskij, Y. N., Thomasson, P., Kopylov, A. I., Zhelenkova, O. P., Muxlow, T. W. B., Beswick, R., et al. (2014). Observations of the $z = 4.514$ radio galaxy RC J0311+0507. *Mon. Not. Roy. Astron. Soc.* 439:2314. doi: 10.1093/mnras/stu047

Pâris, I., Petitjean, P., Ross, N. P., Myers, A. D., Aubourg, É., Streblyanska, A., et al. (2017). The Sloan Digital Sky Survey Quasar Catalog: Twelfth data release. *Astron. Astrophys.* 597:A25. doi: 10.1051/0004-6361/201527999

Petrov, L., Kovalev, Y. Y., Fomalont, E. B., and Gordon, D. (2006). The Fourth VLBA Calibrator Survey: VCS4. *Astron. J.* 131:1872. doi: 10.1086/499947

Petrov, L., Kovalev, Y. Y., Fomalont, E. B., and Gordon, D. (2008). The Sixth VLBA Calibrator Survey: VCS6. *Astron. J.* 136:580. doi: 10.1088/0004-6256/136/2/580

Reed, S. L., McMahon, R. G., Martini, P., Banerji, M., Auger, M., Hewett, P. C., et al. (2017). Eight new luminous $z > 6$ quasars selected via SED model fitting of VISTA, WISE and Dark Energy Survey Year 1 Observations. arXiv eprint:1701.04852

Richards, G. T., Myers, A. D., Gray, A. G., Riegel, R. N., Nichol, R. C., Brunner, R. J., et al. (2009). Efficient photometric selection of quasars from the Sloan Digital Sky Survey. II. ∼1,000,000 Quasars from Data Release 6. *Astrophys. J.* 180:67. doi: 10.1088/0067-0049/180/1/67

Rimoldini, L., Dubath, P., Süveges, M., López, M., Sarro, L. M., Blomme, J., et al. (2012). Automated classification of Hipparcos unsolved variables. *Mon. Not. Roy. Astron. Soc.* 427:2917. doi: 10.1111/j.1365-2966.2012.21752.x

Romani R. W., Sowards-Emmerd, D., Greenhill, L., and Michelson, P. (2004) Q0906+6930: The highest redshift blazar. *Astrophys. J.* 610:L9. doi: 10.1086/423201

Sadler, E. M., Jackson, C. A., Cannon, R. D., McIntyre, V. J., Murphy, T., Bland-Hawthorn, J., et al. (2002). Radio sources in the 2dF Galaxy Redshift Survey - II. Local radio luminosity functions for AGN and star-forming galaxies at 1.4 GHz. *Mon. Not. Roy. Astron. Soc.* 329:227. doi: 10.1046/j.1365-8711.2002.04998.x

Secrest, N. J., Dudik, R. P., Dorland, B. N., Zacharias, N., Makarov, V., Fey, A., et al. (2015). Identification of 1.4 Million Active Galactic Nuclei in the Mid-Infrared using WISE Data. *Astrophys. J.* 221:12. doi: 10.1088/0067-0049/221/1/12

Shen, Y., Richards, G. T., Strauss, M. A., Hall, P. B., Schneider, D. P., Snedden, S., et al. (2011). A Catalog of Quasar Properties from Sloan Digital Sky Survey Data Release 7. *Astrophys. J.* 194:45. doi: 10.1088/0067-0049/194/2/45

Tang, J., Goto, T., Ohyama, Y., Chen, W.-P., Walter, F., Venemans, B., et al. (2017). A quasar discovered at redshift 6.6 from Pan-STARRS1. *Mon. Not. Roy. Astron. Soc.* 466:4568. doi: 10.1093/mnras/stw3287

Taylor, M. B. (2005). "TOPCAT and STIL: Starlink Table/VOTable Processing Software," in *Astronomical Data Analysis Software and Systems, XIV ASP Conference Series* (Pasadena), 347:29.

Tuccillo, D., Bruni, G., DiPompeo, M. A., Brotherton, M. S., Pasetto, A., Kraus, A., et al. (2017). A multiwavelength continuum characterization of high-redshift broad absorption line quasars. *Mon. Not. Roy. Astron. Soc.* 467:4763. doi: 10.1093/mnras/stx333

Uchiyama, H., Toshikawa, J., Kashikawa, N., Overzier, R., Chiang, Y.-K., Tanaka, M., et al. (2017). Luminous quasars do not live in the most overdense regions of Galaxies at $z \sim 4$. arXiv eprint:1704.06050

Urry, C. M., and Padovani, P. (1995). Unified Schemes for Radio-Loud Active Galactic Nuclei. *PASP* 107:803. doi: 10.1086/133630

Veres, P., Frey, S. Paragi, Z., and Gurvits, L. I. (2010). Physical parameters of a relativistic jet at very high redshift: the case of the blazar J1430+4204. *Astron. Astrophys.* 521:A6. doi: 10.1051/0004-6361/201014957

Véron-Cetty, M. P., and Véron, P. (2010). A catalogue of quasars and active nuclei: 13th edition. *Astron. Astrophys.* 518A:10. doi: 10.1051/0004-6361/201014188

Wang, F., Wu, X., Fan, X., Yang, J., Yi, W., Bian, F., et al. (2016). A Survey of Luminous High-redshift Quasars with SDSS and WISE. I. Target Selection and Optical Spectroscopy. *Astrophys. J.* 819:24. doi: 10.3847/0004-637X/819/1/24

Wang, F., Fan, X., Yang, J., Wu, X.-B., Yang, Q., Bian, F., et al. (2017). First Discoveries of $z > 6$ Quasars with the DECam Legacy Survey and UKIRT Hemisphere Survey. *Astrophys. J.* 839:27. doi: 10.3847/1538-4357/aa689f

Wang, R., Momjian, E., Carilli, C. L., Wu, X.-B., Fan, X., Walter, F., et al. (2017). Milliarcsecond Imaging of the Radio Emission from the Quasar with the Most Massive Black Hole at Reionization. *Astrophys. J.* 835:L20. doi: 10.3847/2041-8213/835/2/L20

Warren, S. J., Hewett, P. C., Irwin, M. J., McMahon, R. G., Bridgeland, M. T., Bunclark, P. S., et al. (1987). First observation of a quasar with a redshift of 4. *Nature* 325:131. doi: 10.1038/325131a0

White, R. L., Becker, R. H., Helfand, D. J., and Gregg, M. D. (1997). A Catalog of 1.4 GHz Radio Sources from the FIRST Survey. *Astrophys. J.* 475:479. doi: 10.1086/303564

Willott, C. J., Delorme, P., Reylé, C., Albert, L., Bergeron, J., Crampton, D., et al. (2010). The Canada-France High-z Quasar Survey: Nine New Quasars and the Luminosity Function at Redshift 6. *Astron. J.* 139:906. doi: 10.1088/0004-6256/139/3/906

Yang, J., Fan, X., Wu, X., Wang, Fe., Bian, F.,, Yang, Q., et al. (2017). Discovery of 16 New $z \sim 5.5$ Quasars: Filling in the Redshift Gap of Quasar Color Selection. *Astron. J.* 153:184. doi: 10.3847/1538-3881/aa6577

Yi, W.-M., Wang, F., Wu, X.-B., Yang, J., Bai, J.-M., Fan, X., et al. (2014). SDSS J013127.34-032100.1: A Newly Discovered Radio-loud Quasar at $z = 5.18$ with Extremely High Luminosity. *Astrophys. J.* 795:L29. doi: 10.1088/2041-8205/795/2/L29

Yi, W., Green, R., Bai, J.-M., Wang, T., Grier, C. J., Trump, J. R., et al. (2017). The Physical Constraints on a New LoBAL QSO at $z = 4.82$. *Astrophys. J.* 838:135. doi: 10.3847/1538-4357/aa65d6

York, D. G., Adelman, J., Anderson, J. E. Jr., Anderson, S. F., Annis, J., Bahcall, N. A., et al. (2000). The Sloan Digital Sky Survey: technical summary. *Astron. J.* 120:1579. doi: 10.1086/301513

Zhang, Y., An, T., Frey, S., Gabányi, K. É., Paragi, Z., Gurvits, L. I., et al. (2017). J0906+6930: a radio-loud quasar in the early Universe. *Mon. Not. Roy. Astron. Soc.* 468:69. doi: 10.1093/mnras/stx392

Conflict of Interest Statement: The authors declare that the research was conducted in the absence of any commercial or financial relationships that could be construed as a potential conflict of interest.

Copyright © 2017 Perger, Frey, Gabányi and Tóth. This is an open-access article distributed under the terms of the Creative Commons Attribution License (CC BY). The use, distribution or reproduction in other forums is permitted, provided the original author(s) or licensor are credited and that the original publication in this journal is cited, in accordance with accepted academic practice. No use, distribution or reproduction is permitted which does not comply with these terms.

frontiers in Astronomy and Space Sciences

METHODS
published: 06 March 2018
doi: 10.3389/fspas.2018.00005

On the Selection of High-z Quasars Using LOFAR Observations

Edwin Retana-Montenegro and Huub Röttgering*

Leiden Observatory, Leiden University, Leiden, Netherlands

We present a method to identify candidate quasars which combines optical/infrared color selection with radio detections from the Low Frequency ARray (LOFAR) at 150 MHz. We apply this method in a region of 9 square degrees located in the Boötes field, with a wealth of multi-wavelength data. Our LOFAR imaging in the central region reaches a rms noise of $\sim 50\,\mu$Jy with a resolution of 5″. This is so deep that we also routinely detect, "radio-quiet" quasars. We use quasar spectroscopy from the literature to calculate the completeness and efficiency of our selection method. We conduct our analysis in two redshift intervals, $1 < z < 2$ and $2 < z < 3$. For objects at $1.0 < z < 2.0$, we identify 51% of the spectroscopic quasars, and 80% of our candidates are in the spectroscopic sample; while for objects at $2.0 < z < 3.0$ these numbers are 62 and 30%, respectively. We investigate the effect of the radio spectral index distribution on our selection of candidate quasars. For this purpose, we calculate the spectral index between 1,400 and 150 MHz, by combining our LOFAR-Boötes data with 1.4 GHz imaging of the Boötes field obtained with the Westerbork Synthesis Radio Telescope (WSRT), which has a rms noise of $\sigma \sim 28\,\mu$Jy with a resolution of $13'' \times 27''$. We find that 27% of the candidate quasars are detected at 1,400 MHz, and that these detected objects have a spectral index distribution with a median value of $\alpha = -0.73 \pm 0.07$. Using a flux density threshold of $S_{150MHz} = 1.50$ mJy, so that all the $\alpha > -1.0$ sources can be detected in the WSRT-Boötes map, we find that the spectral index distribution of the 21 quasars in the resulting sample is steeper than the general LOFAR-WSRT spectral index distribution with a median of $\alpha = -0.80 \pm 0.06$. As the upcoming LOFAR wide area surveys are much deeper than the traditional 1.4 GHz surveys like NVSS and FIRST, this indicates that LOFAR in combination with optical and infrared will be an excellent fishing ground to obtain large samples of quasars.

Keywords: quasars, active galactic nuclei, surveys, radio, extragalactic astronomy, photometry, spectroscopy

OPEN ACCESS

Edited by:
Paola Marziani, Osservatorio Astronomico di Padova (INAF), Italy

Reviewed by:
Andjelka Branislav Kovacevic, University of Belgrade, Serbia
Daniela Bettoni, Osservatorio Astronomico di Padova (INAF), Italy

****Correspondence:***
Edwin Retana-Montenegro
edwinretana@gmail.com; eretana@strw.leidenuniv.nl

Specialty section:
This article was submitted to Milky Way and Galaxies, a section of the journal Frontiers in Astronomy and Space Sciences

Received: *31 July 2017*
Accepted: *31 January 2018*
Published: *06 March 2018*

Citation:
Retana-Montenegro E and Röttgering H (2018) On the Selection of High-z Quasars Using LOFAR Observations. Front. Astron. Space Sci. 5:5. doi: 10.3389/fspas.2018.00005

1. INTRODUCTION

In recent years, large spectroscopically confirmed quasar samples have become available (Croom et al., 2005; Schneider et al., 2010; Pâris et al., 2017). These quasar samples enabled statistical studies related to many topics, including the relation between the black holes (BHs) and their host galaxies (Kauffmann et al., 2003), BH growth across cosmic time (McLure and Dunlop, 2004), and the quasar environments (Ross et al., 2009; Retana-Montenegro and Röttgering, 2017). With the next generation of wide-field surveys such as Pan-STARRS (Kaiser et al., 2002, 2010), Dark Energy Survey (DES, Flaugher, 2005), and the future Large Synoptic Survey Telescope (LSST, Tyson, 2002),

such studies will be extended to the fainter quasars. A challenge in properly exploiting these surveys is the identification of quasars without spectroscopic observations.

Quasar surveys historically made use of the ultraviolet-excess (UVX) of the typical quasar spectrum (Sandage et al., 1965; Richards et al., 2002). This translates into a set of optical and near-infrared color cuts chosen to separate quasars from stars. However, for $z > 2$ quasars this selection begins to fail as one approaches the flux limit, due to photometric errors broadening the stellar locus, and quasar and stellar color distributions blending. The necessity to increase the efficiency of quasar surveys has led to the development of new selection techniques (MacLeod et al., 2010b; Yèche et al., 2010; Bovy et al., 2011; Kirkpatrick et al., 2011; Palanque-Delabrouille et al., 2011).

A way to separate high-z quasars from stars is to complement optical/infrared color cuts with a radio detection. By imposing a radio detection the stellar contamination is reduced significantly, as radio stars are very rare (Kimball et al., 2009). This approach has been successful in discovering quasars that otherwise might have been missed using typical color selection (McGreer et al., 2009; Bañados et al., 2015) such as red and dusty quasars (Glikman et al., 2004, 2012, 2013) and rare high-z quasars (Hook et al., 2002; McGreer et al., 2006; Zeimann et al., 2011).

LOFAR is a new European radio interferometer operating at frequencies 15–240 MHz (van Haarlem et al., 2013) and represents a milestone in terms of radio survey speed compared to existing telescopes. The LOFAR Surveys Key Science Project aims to carry out a tiered survey. At Tier-1 level, the LOFAR Two-metre Sky Survey (LoTSS, Shimwell et al. 2017) aims to cover the whole northern sky down to $\sim$100 μJy rms. Deeper tiers cover smaller areas in fields with extensive multi-wavelength data (see Röttgering et al., 2011) with the LOFAR Boötes field the first of these deep fields to reach Tier-2 depth (Retana-Montenegro and Röttgering, in preparation). These surveys will open the low-frequency electromagnetic spectrum for exploration, allowing unprecedented studies of the radio population across cosmic time and opening up new parameter space for searches for rare, unusual objects such as high-z radio quasars in a systematic way. Perhaps, one of the most tantalizing prospects are the 21 cm absorption line measurements using LOFAR along sight lines toward $z > 6$ radio quasars.

One of the possibilities to increase the efficiency in the selection of quasars is by combining optical/infrared quasar selection techniques with LOFAR radio data. With its high sensitivity, LOFAR should detect significantly more quasars in comparison with previous shallower radio surveys. Here we describe a method to select candidate quasars that combines optical/infrared color cuts with LOFAR radio detection.

2. METHODS

2.1. Method Overview

Candidate quasars are selected by complementing optical and near-infrared color cuts with a LOFAR detection. The selection method is summarized in the following points:

- Optical color cuts to select Lyα break objects, and to separate quasars from stars.
- Mid-infrared color cuts to identify the presence of AGN-heated dust, and to reduce the contamination from low-z star-forming galaxies.
- Imposing a LOFAR 5σ detection. This point guarantees that stellar contamination in the sample is negligible.
- Fitting the UV/optical to MIR SEDs of the candidate quasars sample to quasar templates. This allows us to select the best candidates and further eliminate nonquasar contaminants from the sample.

2.2. Optical Selection

2.2.1. Selection of Lyα Break Objects

The use of color selection to identify high-z objects was first proposed more than four decades ago (e.g., Meier, 1976a,b). Since then this approach has been applied successfully to select quasars up to $z \gtrsim 6$ (Fan et al., 2001; Willott et al., 2007). The multi-color selection for finding high-z quasars usually employs at least 3 bands: one containing the Lyα emission line, one blueward (the dropout band), and one redward. This translates into a set of colors that can be to used to locate the Lyα emission line.

2.2.2. Separating Quasars and Stars

Although, quasars are starlike in appearance their radiation mechanisms are different to those of stellar sources. Stars have approximately single-temperature black-body spectral energy distributions (SEDs) (Bisnovatyi-Kogan, 2001), whereas energetic processes sculpt the distinctive power-law SEDs of quasars (Davidson and Netzer, 1979). These differences in the SEDs imply that stars and quasars occupy different regions in colorspace (Fan, 1999). Thus, in principle, optical color cuts can be chosen to reject the majority of stars.

2.3. Mid-Infrared Selection

Although, stellar contamination is reduced using the previous points, some contamination will still remain from other objects like compact low-z star-forming galaxies. These star-forming systems present optical red colors mimicking those of quasars, which is likely caused by a strong Balmer break or dust-extincted continuum. Here, we impose the color cuts proposed by Lacy et al. (2007) and Donley et al. (2012) to the Spitzer/IRAC photometry to reduce contamination by star-forming galaxies in our quasar sample.

2.4. LOFAR Detection

With increasing redshift the Lyα emission moves through and out of the blueward optical bands, resulting in quasars having similar colors to stars. Thus, a selection method based only on color cuts becomes less efficient at higher redshifts, as quasars occupy regions that overlap with those occupied by a significant fraction of stellar sources. This is worst at $2.2 < z < 3.0$, where the optical colors of quasars become indistinguishable from those of stars (Fan, 1999; Richards et al., 2002, 2006). An alternative approach to improve the quasar selection in these regions is the incorporation of information provided by radio surveys (Richards et al., 2002; Ross et al., 2012). The number

of radio stars with faint optical fluxes is very small (Kimball et al., 2009), therefore, by imposing a radio detection the stellar contamination becomes negligible in our sample.

2.5. Visual Inspection

We carry out a visual inspection of the imaging data for each candidate quasar. This process allows us to reject contaminants such as low-z galaxies and objects with photometry contaminated by nearby bright objects. We accept candidate quasars with the following characteristics: stellar optical morphology; no bright neighbors in close proximity; and no blending issues. The radio counterparts in the LOFAR map are also examined to reject artifacts or misclassified radio-lobes.

2.6. Fitting the UV/Optical to MIR Spectral Energy Distributions of the Candidate Quasar Sample

Our selection method exploits a variety of quasar observational properties to identify them in our survey data. We apply color cuts that diminish the fraction of stars and star-forming galaxies in our samples. However, these procedures do not completely eliminate confusion with other types of objects. Therefore, as a final confirmation we fit quasar templates to their SEDs. We build SEDs spanning from the optical/UV to the MIR range to identify the candidate quasars. These SEDs are fitted to the quasar templates from the AGN template library presented by Salvato et al. (2009).

The SED fits are inspected visually. We look for the following unequivocal features in the SEDs of quasars: (i) the strong break by absorption at 1215Å (rest-frame), (ii) the Lyα emission line, and (iii) a rising or flat power-law in the IRAC bands. We examine each SED to assess the overall quality of the fit. In this way, we are able to eliminate nonquasar contaminants.

3. RESULTS

3.1. Selecting Candidate Quasars in the NDWFS-Boötes Field

In this section, we apply the selection method using the Boötes ancillary data and our Tier-2 LOFAR catalog following the points aforementioned.

3.1.1. Data

The 9.2 deg^2 region in Boötes covered by the NOAO Deep Wide Field Survey (NDWFS, Jannuzi and Dey 1999) has optical data available on the U_{spec}, B_w, R, I, and Z bands. All these filters are standard except the U_{spec} and B_w, which have better efficiency and a more uniform wavelength coverage than the U-Bessel and B-Johnson filters, respectively. Additionally, the Boötes field has multi-wavelength coverage spanning from X-rays to radio wavelengths. In the X-rays and UV regimes, it has been observed with the Chandra (Kenter et al., 2005) and GALEX (Martin et al., 2003) satellites. At infrared wavelengths, it was part of the NEWFIRM survey (J,H,K bands; Autry et al., 2003) and Spitzer Deep, Wide-Field Survey (SDWFS) with IRAC (Ashby et al., 2009). Finally, in the radio regime, the Boötes region has been observed at 1.4 GHz with the VLA (Becker et al., 1995) and WSRT (de Vries et al., 2002), and at 150MHz with GMRT (Williams et al., 2013) and LOFAR (Williams et al., 2016). In this work, we use the deep 150 MHz LOFAR imaging presented by Retana-Montenegro and Röttgering (in preparation), with a noise level of $1\sigma\sim50\,\mu$Jy with a spatial resolution of $5''$. We use AB magnitudes for all bands in our analysis. We assume the convention $S_\nu \propto \nu^{-\alpha}$, where ν is the frequency, α is the spectral index, and S_ν is the flux density as function of frequency.

3.1.2. Candidate Quasars Selection

To test our quasar selection method, we utilize spectroscopy data from the AGES survey (Kochanek et al., 2012). While the spectroscopic sample spans the range $0 < z < 5.8$, we limit our selection to the intervals $1.0 \leq z \leq 2.0$ and $2.0 \leq z \leq 3.0$. The reason for using these two redshift intervals is twofold. First, quasars in these intervals provide a good test for our selection method. Secondly, there are more spectroscopically confirmed quasars for the redshift intervals considered as compared to those available at $z > 3.0$.

Quasars at $1.0 \leq z \leq 2.0$ are frequently selected using the excess of ultra-violet flux in the u-band, which results in a bluer u-g color as compared to that of stars with the same visual color (e.g., the g-r color) (Richards et al., 2002). However, the NDWFS-Boötes bandpass system (U_{spec},B_w,R,I,Z) does not include a g filter found in other photometric systems such as the SDSS filter set (u,g,r,i,z) (Fukugita et al., 1996). But instead the non-standard U_{spec} (λ_c = 3590Å, FWHM=540Å) and B_w (λ_c = 4111Å, FWHM=1275Å) filters had been used. The main disadvantage of the U_{spec} and B_w filter combination is the significant wavelength overlap between the two filters. This implies that quasars at $1.0 \leq z \leq 2.0$ can not be efficiently selected using their $U_{spec}-B_w$ colors.

To optimally define the color cuts for candidate quasars at $1.0 < z < 2.0$, we generate a library of synthetic quasar spectra following the procedure described in detail by Retana-Montenegro et al. (in preparation). These spectra are convolved with the NDWFS-Boötes filter curves to calculate the colors for the selection of $1.0 < z < 2.0$ quasars. Based on the colors derived, we adopt the color cuts shown by magenta lines in the first panel of **Figure 1**. These color cuts are:

$$y \geq 1.89 \times x - 1.0 \;\wedge\; y \leq 1.89 \times x + 1.20$$
$$\wedge\, y \geq -1.37 \times x - 1.20 \;\wedge\; y \leq -1.37 \times x + 3.38,$$

where $y = B_w - R$ and $x = U_{spec} - Z$.

Based on the colors obtained from simulated quasar spectra, we derive the color cuts to select $2.0 \leq z \leq 3.0$ quasars. The color cuts adopted for the selection are the following:

$$-0.35 \leq R - I \leq 0.75 \quad \text{and} \quad -0.35 \leq B_w - R \leq 1.2.$$

To reduce contamination from low-z star-forming galaxies in our quasar samples we adopt in both redshift bins the color cuts proposed by Donley et al. (2012):

$$w \geq 0.08 \wedge z \geq 0.15,$$
$$z \geq 1.21 \times w - 0.27 \;\wedge\; z \leq 1.21 \times w + 0.27$$

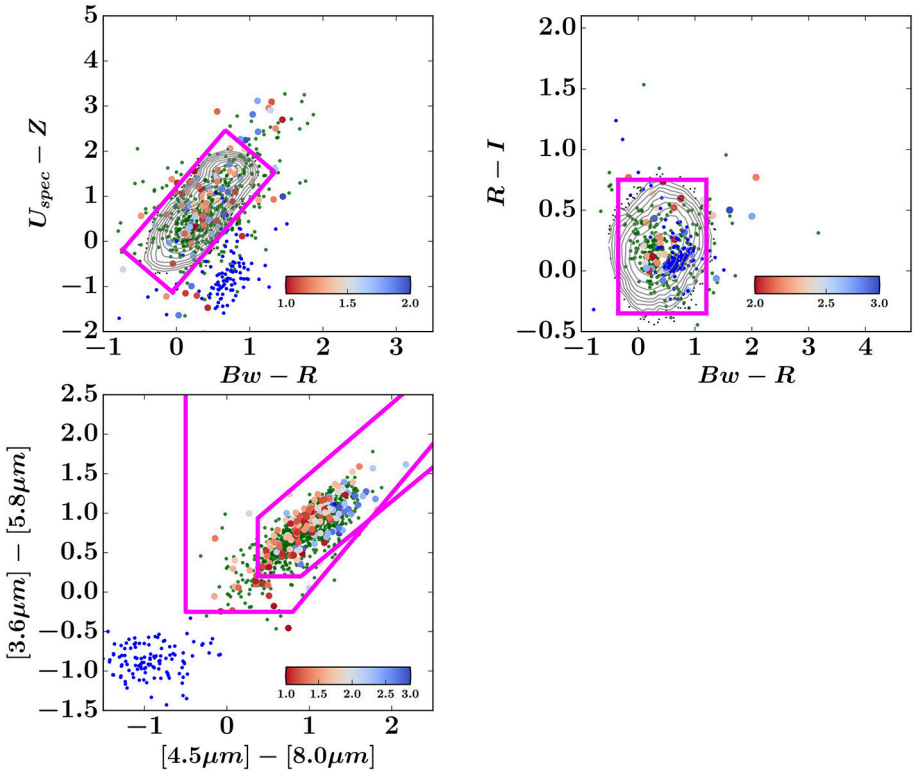

FIGURE 1 | Optical and mid-infrared colors for spectroscopic quasars in the Boötes field. The LOFAR detected quasars are plotted as redshift color-coded points according to the color bar at the lower right. The corresponding redshift bin is indicated by the colorbar legend. The dark green points represent spectroscopic quasars in the corresponding redshift that are undetected in our LOFAR observations, while the blue circles mark the location of stars. The solid magenta lines delimit the regions used to select the quasars in each color space. The gray contours denotes the density for 18,000 simulated quasars in the respective redshift bins.

and Lacy et al. (2007):

$$w > -0.1, z > -0.2,$$
$$z \leq 0.80 \times w + 0.5,$$

where $w = \log_{10}\left(\frac{S_{5.8\mu m}}{S_{3.6\mu m}}\right)$ and $z = \log_{10}\left(\frac{S_{8.0\mu m}}{S_{4.5\mu m}}\right)$.

Having defined the color cuts, the next task is to crossmatch the catalogs to find radio counterparts of the optical sources. We initially search for radio sources that lie within a radius of $2''$ from the optical source that fulfill our color cuts with a 5σ detection in our LOFAR catalog. For each one of these objects, we inspect its images in at least 4 bands. During this examination, we require that our candidate quasars are unresolved, not close to a bright neighbor and not blended. Additionally, we examine the morphology of the radio counterparts to prevent imaging artifacts or radio-lobes being incorrectly matched to optical sources. This examination of the radio maps ensures that only robust radio counterparts are matched to optical sources. Finally, we performed SED fitting to these sources with the photometric redshift code EAZY (Brammer et al., 2008). This allow us to assess the overall quality of the quasars photometry and to filter out contaminants from our sample. **Figure 2** shows two candidate quasars SEDs from our sample.

An important aspect to consider is the accuracy of the photometric redshifts. An inaccurate photometric redshift may cause the rejection of a quasar candidate. In **Figure 3**, we compare the EAZY z_{photo} and z_{spec} in the range $1.0 < z < 3.0$ for Boötes spectroscopic quasars with a signal-to-noise greater than 5σ. The objects that are catastrophic outliers (i.e., objects with a difference between the photometric and spectroscopic redshift larger than the 3σ uncertainty for the photometric redshift) based on the one-to-one relation are found using an iterative 3σ-clipped standard deviation. The fraction of catastrophic outliers is around 3.1%. After catastrophic outliers are eliminated, we compute the standard dispersion $\delta z = (z_{photo} - z_{spec})/(1 + z_{spec})$ (Ilbert et al., 2006), and the normalized median absolute deviation (NMAD), defined as $\mathrm{NMAD}(\delta z) = 1.48 \times \mathrm{Median}(\delta z)$ (Hoaglin et al., 1983). We find $\delta z = 0.15$ and $\mathrm{NMAD} = 0.12$. For comparison, Salvato et al. (2011) obtained more accurate photometric redshifts for COSMOS quasars with $\mathrm{NMAD} = 0.015$ using 30 bands, while Assef et al. (2010) found $\delta z = 0.18$ for point-source AGNs in Boötes. Therefore, we conclude that fraction of candidates quasars rejected with inaccurate z_{photo} is small in comparison with the total number of candidates in the final sample.

The optical and MIR colors of the spectroscopic quasars detected by LOFAR in the Boötes field are shown in

Figure 1. The colors of the spectroscopic quasars are generally consistent with the proposed color cuts. **Figure 4** shows the colors for the 154 candidate quasars selected using our method.

3.1.3. Performance of the Selection Method

In order to assess the performance of our selection method, we calculate the completeness and efficiency for our samples.

We define the completeness C as the number of spectroscopic quasars selected as candidates compared to the *total* number of spectroscopic quasars (Hatziminaoglou et al., 2000; MacLeod et al., 2010a):

$$C = \frac{\text{no. of selected spectroscopic quasars}}{\text{total no. of spectroscopic quasars}} \times 100.$$

Similarly, the efficiency E, i.e., the number of spectroscopic quasars selected as candidates compared to the number of objects selected as candidate quasars, is defined as:

$$E = \frac{\text{no. of selected spectroscopic quasars}}{\text{total no. of candidate quasars}} \times 100.$$

At $1.0 < z < 2.0$, our selection method identifies 59 of the 116 radio quasars with spectroscopic confirmation, resulting in a completeness of 51%. In the range $2.0 < z < 3.0$, 25 of 40 quasars pass our selection, which results in a completeness of 62%. For the entire redshift interval considered, we obtain a completeness of 54%.

With our method, we find 74 quasars candidates at $1.0 < z < 2.0$, which corresponds to an efficiency of 80%. In the range $2.0 < z < 3.0$, 84 candidate quasars are identified, which gives $E = 30\%$. For the full range, we find an efficiency equal to $E = 53\%$.

3.1.4. Effect of the Radio Spectral Index Distribution on the Candidate Quasar Selection

In this section, we investigate the effect of the radio spectral index distribution on our selection of candidate quasars. We therefore combine our LOFAR data with the deep 1.4 GHz radio survey of the Boötes field obtained using the Westerbork Synthesis Radio

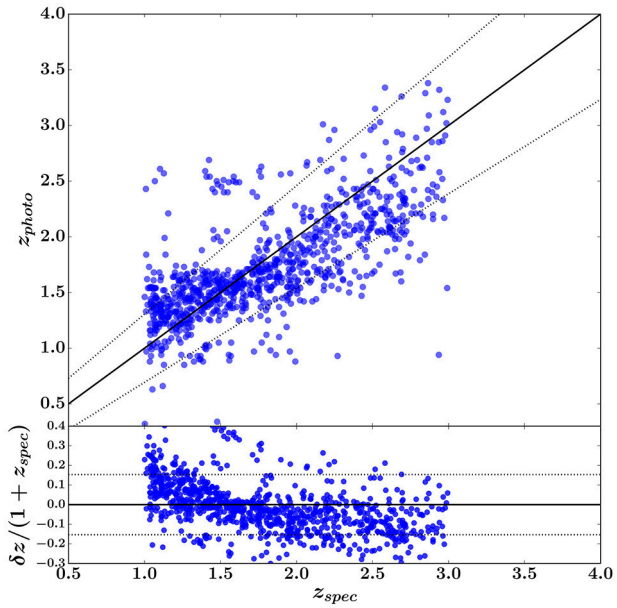

FIGURE 3 | (Top panel) Comparison between photometric and spectroscopic redshifts for 929 quasars in the Boötes field at $1.0 < z < 3.0$. The solid line represents the one-to-one $z_{phot} = z_{spec}$ relation, and the dotted lines correspond to $z_{phot} = z_{spec} \pm \sigma \times (1 + z_{spec})$. **(Bottom panel)** Standard dispersion between photometric and spectroscopic redshifts as function of the spectroscopic redshift. The solid and dotted lines are the same as in the top panel.

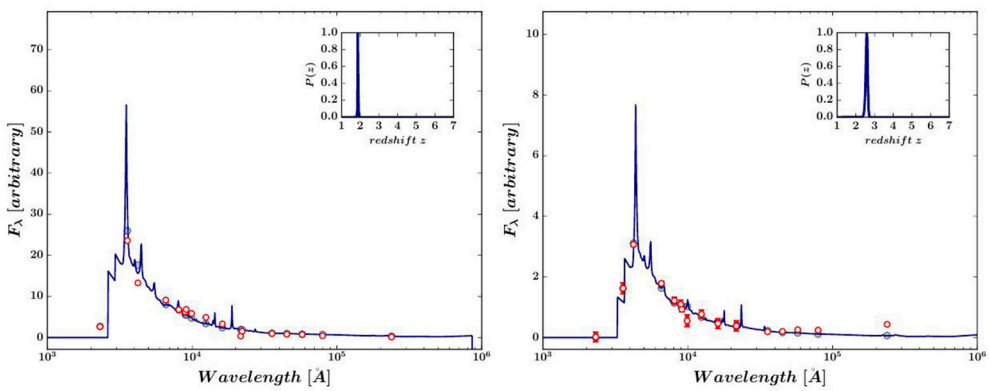

FIGURE 2 | Typical examples of the spectral energy distribution for two candidate quasars identified using our selection method. In each case the best-fit quasar template (as derived from the EAZY calculation) is also plotted. Red circles are the photometric points and the blue circles indicate the predicted photometry by the best-fit template. The phometric redhifts for objects are 1.87 and 2.57, respectively. The probability density distributions (PDFs) for each object are shown in the small inset. These PDFs strongly suggest that these objects are located at high-z. The Lyα line in the two candidate quasars is clearly identified as an abrupt break in the quasar SED between the NUV-GALEX band and U_{spec} and B_W filters, respectively.

Telescope (WSRT) telescope (de Vries et al., 2002). The WSRT-Boötes observations reach a rms noise of $1\sigma \sim 28\,\mu$Jy, with an angular resolution of $13'' \times 27''$. To compare the LOFAR and WSRT maps, we must take into account that there are incompleteness effects due to the different noise levels between the two observations. Therefore, we compare the LOFAR and WSRT observations using a flux density threshold of $S_{150MHz} =$ 1.5mJy. For a spectral index of -0.7 (Smolčić et al., 2017), this threshold is approximately equivalent to a noise level of 11σ in the WSRT-Boötes map, and ensures all the $\alpha > -1.0$ sources with a signal-to-noise $> 5\sigma$ will be detected in the WSRT-Boötes map. The spectral index distribution for the 1998 sources in the LOFAR-WSRT sample has a median of $\alpha = -0.65 \pm 0.016$.

Using these cuts, in the overlapping area between the LOFAR and WSRT maps, we find that 42 of 154 candidate quasars are detected at 1,400 MHz. The detected objects have a spectral index distribution with a median value of $\alpha = -0.73 \pm 0.07$ (see **Figure 5**). Using the flux density threshold of $S_{150MHz} \geq 1.50$ mJy, we find that the spectral index distribution of the 21 candidate quasars in this sample is steeper than the general LOFAR-WSRT spectral index distribution with a median of $\alpha = -0.80 \pm 0.06$. The 21 candidate quasars detected at $1,400MHz$ with $S_{150MHz} <$ 1.5 mJy are characterized by a steeper spectral index distribution compared to the LOFAR full sample with a median value of $\alpha = -0.71 \pm 0.05$. For the remaining 112 candidates undetected by WSRT, we derive an upper limit for their spectral indices assuming a 5σ WSRT detection ($S_{1.4GHz} = 0.140$ mJy). The median upper limit of the distribution of spectral indexes for these objects is $\alpha_{upp} < -0.75$. In the WSRT footprint, there are 70 of 139 spectroscopic quasars detected by WSRT. These detected quasars have a steeper distribution of spectral indices compared to the LOFAR-WSRT full sample with a median of $\alpha = -0.70 \pm 0.06$.

4. LIMITATIONS

The application of the selection method described in this work is dependent on the availability of LOFAR imaging and ancillary data. Fortunately, the dedicated LOFAR Tier-2 program selects extra-galactic fields with extensive multi-wavelength data to maximize the scientific exploitation of the LOFAR imaging. The ongoing LoTSS survey aims to map the observable northern sky, which has been observed previously in the optical (SDSS, York et al., 2000 and Pan-STARRS, Kaiser et al., 2002, 2010) and MIR (WISE, Wright et al., 2010) wavelengths. These LOFAR datasets will allow us to extend the identification of candidate quasars to a larger survey volume and to smaller regions with extensive multi-wavelength data.

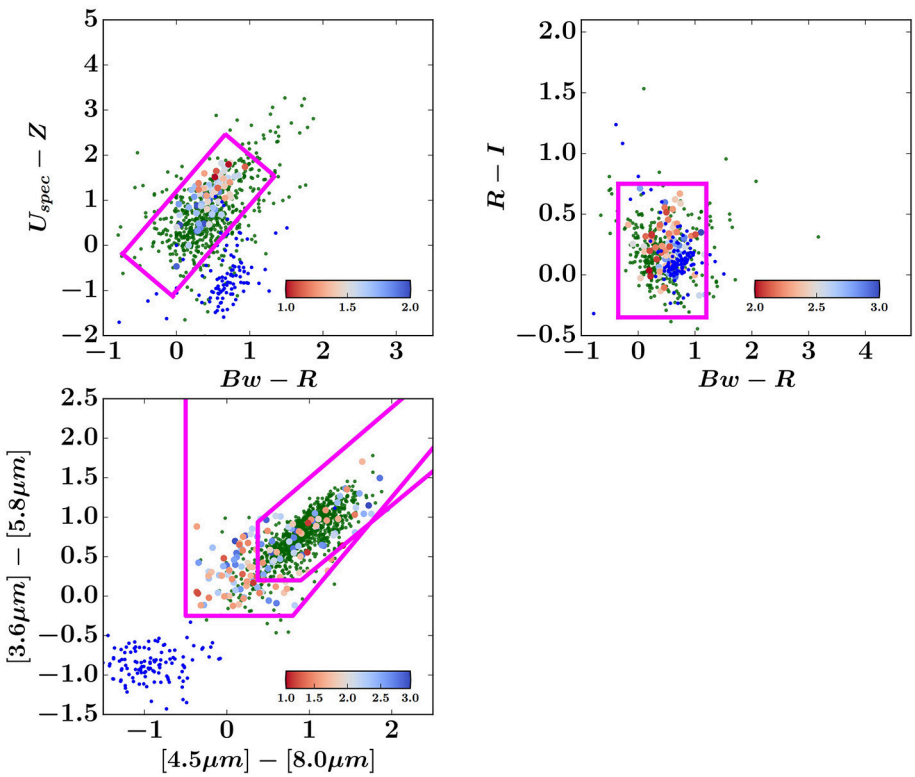

FIGURE 4 | Optical and mid-infrared colors for the candidate quasars identified within our selection regions (solid magenta lines). The color-scale indicates the photometric redshift for the candidate quasars. The dark green points represent all the spectroscopic quasars (both undetected and detected by LOFAR) in the Boötes region, while the blue circles mark the location of stars. The corresponding redshift bin is indicated by the colorbar legend.

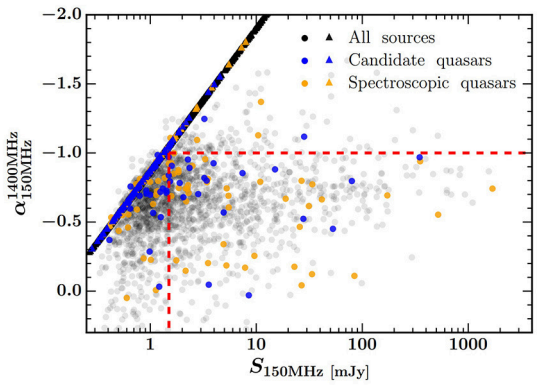

FIGURE 5 | The spectral index between 1,400 and 150 MHz for sources in the Boötes field as a function of the 150 MHz flux density. The candidate quasars, spectroscopic quasars, and all the sources in LOFAR catalog are shown by blue, orange and black markers, respectively. The circles denote 5σ detections in the LOFAR and WSRT catalogs, while the triangles indicate upper limits on the spectral indexes assuming a 5σ WSRT detection ($S_{1.4GHz} = 0.140$ mJy) for these objects. The red dashed lines indicate the region with $S_{150MHz} > 1.5$ mJy and $\alpha > -1.0$.

5. SUMMARY

We have examined the identification of high-z candidate quasars with LOFAR observations as an additional tool. The motivation for our method was to compile large samples of candidate quasars and to improve the efficiency of spectroscopic programs targeting these objects. Our selection method adopts color cuts between near-infrared and optical wavelengths to obtain a list of candidate quasars, while minimizing the contamination by stars and star-forming galaxies. Second, a LOFAR detection is required to further reduce the stellar contamination in our sample. We also carried out a visual inspection of candidate quasar SEDs to discard nonquasar contaminants. We used the LOFAR Tier-2 Boötes observations as an example of the application of our method and examined its completeness and efficiency in various redshift intervals. We also investigated the effect of the radio spectral index distribution on our selection of candidate quasars. For this purpose, we calculated the spectral index between 1,400 and 150 MHz, by combining our LOFAR data with WSRT-Boötes imaging. We found that the candidate quasars have a steep distribution of spectral indexes with a median value of $\alpha = -0.73 \pm 0.07$.

In conclusion, this work demonstrates that our selection method combining radio detections from LOFAR with optical/infrared color cuts will provide an excellent approach for obtaining large samples of quasars.

AUTHOR CONTRIBUTIONS

ER-M reduced the LOFAR Boötes data and carried out the source selection, as well as writing most of the text. HR contributed with ideas to the text writing.

FUNDING

ER-M acknowledges financial support from NWO Top project, No. 614.001.006. HR acknowledges support from the ERC Advanced Investigator program NewClusters 321271.

REFERENCES

Ashby, N. P., Stern, D., Brodwin, M., Griffith, R., Eisenhardt, P., Kozłowski, S., et al. (2009). The spitzer deep, wide-field survey. *Astrophys. J.* 701:428. doi: 10.1088/0004-637X/701/1/428

Assef, R. J., Kochanek, C. S., Brodwin, M., Cool, R., Forman, W., Gonzalez, A. H., et al. (2010). Low-resolution spectral templates for active galactic nuclei and galaxies from 0.03 to 30 μm. *Astrophys. J.* 713, 970–985. doi: 10.1088/0004-637X/713/2/970

Autry, R. G., Probst, R. G., Starr, B. M., Abdel-Gawad, K. M., Blakley, R. D., Daly, P. N., et al. (2003). Instrument design and performance for optical/infrared ground-based telescopes. *SPIE* 4841, 525–539. doi: 10.1117/12.460419

Bañados, E., Venemans, B. P., Morganson, E., Hodge, J., Decarli, R., Walter, F., et al. (2015). Constraining the radio-loud fraction of quasars at z ˜ 5.5. *Astrophys. J.* 804:118. doi: 10.1088/0004-637X/804/2/118

Becker, R. H., White, R. L., and Helfand, D. J. (1995). The FIRST survey: faint images of the radio sky at twenty centimeters. *Astrophys. J.* 450:559. doi: 10.1086/176166

Bisnovatyi-Kogan, G. S. (2001). *Stellar Physics. Vol.1: Fundamental Concepts and Stellar Equilibrium*. Astronomy and Astrophysics Library. (Trans.) A. Y. Blinov and M. Romanova. Berlin: Springer.

Bovy, J., Hennawi, J. F., Hogg, D. W., Myers, A. D., Kirkpatrick, J. A., Schlegel, D. F., et al. (2011). Think outside the color box: probabilistic target selection and the SDSS-XDQSO quasar targeting catalog. *Astrophys. J.* 729:141. doi: 10.1088/0004-637X/729/2/141

Brammer, G. B., van Dokkum, P. G., and Coppi, P. (2008). EAZY: a fast, public photometric redshift code. *Astrophys. J.* 686, 1503–1513. doi: 10.1086/591786

Croom, S. M., Boyle, B. J., Shanks, T., Smith, R. J., Miller, L., Outram, P. J., et al. (2005). Probing the radio loud/quiet AGN dichotomy with quasar clustering. *Month. Notices RAS* 356, 415–438. doi: 10.1111/j.1365-2966.2004.08379.x

Davidson, K., and Netzer, H. (1979). The emission lines of quasars and similar objects. *RevModPhys* 51, 715–766. doi: 10.1103/RevModPhys.51.715

de Vries, W. H., Morganti, R., Röttgering, H. J. A., Vermeulen, R., van Breugel, W., Rengelink, R., et al. (2002). Deep westerbork 1.4 GHz imaging of the bootes field *Astron. J.* 123, 1784–1800. doi: 10.1086/338906

Donley, J. L., Koekemoer, A. M., Brusa, M., Capak, P., Cardamone, C. N., Civano, F., et al. (2012). A new infrared color criterion for the selection of 0>z>7 AGNs: application to deep fields and implications for JWST surveys. *Astrophys. J.* 748:142.

Fan, X. (1999). Simulation of stellar objects in SDSS color space. *Astron. J.* 117, 2528–2551. doi: 10.1086/300848

Fan, X., Narayanan, V. K., Lupton, R. H., Strauss, M. A., Knapp, G. R., Becker, R. H., et al. (2001). A survey of z>5.8 quasars in the sloan digital sky survey. I. Discovery of three new quasars and the spatial density of luminous quasars at z=6. *Astrophys. J.* 122, 2833–2849. doi: 10.1086/324111

Flaugher, B. (2005). The dark energy survey. *IJMPA* 20, 3121–3123. doi: 10.1142/S0217751X05025917

Fukugita, M., Ichikawa, T., Gunn, J. E., Doi, M., Shimasaku, K., and Schneider, D. P. (1996). The sloan digital sky survey photometric system. *Astron. J.* 111:1748. doi: 10.1086/117915

Glikman, E., Gregg, M. D., Lacy, M., Helfand, D. J., Becker, R. H., and White, R. L. (2004). FIRST-2Mass sources below the APM detection threshold: a population of highly reddened quasars. *Astrophys. J.* 607, 60–75. doi: 10.1086/383305

Glikman, E., Urrutia, T., Lacy, M., Djorgovski, S. G., Mahabal, A., Myers, A. D., et al. (2012). FIRST-2MASS red quasars: transitional objects emerging from the dust. *Astrophys. J.* 757:51. doi: 10.1088/0004-637X/757/1/51

Glikman, E., Urrutia, T., Lacy, M., Djorgovski, S. G., Urry, M., Croom, S., et al. (2013). Dust reddened quasars in FIRST and UKIDSS: beyond the tip of the iceberg. *Astrophys. J.* 778:127. doi: 10.1088/0004-637X/778/2/127

Hatziminaoglou, E., Mathez, G., and Pelló, R. (2000). Quasar candidate multicolor selection technique: a different approach. *Astron. Astrophys.* 359, 9–17.

Hoaglin, D. C., Mosteller, F., and Tukey, J. W. (edS.). (1983). "Understanding robust and exploratory data analysis," in *Wiley Series in Probability and Mathematical Statistics*, (New York, NY: Wiley).

Hook, I. M., McMahon, R. G., Shaver, P. A., and Snellen, I. A. G. (2002). Discovery of radio-loud quasars with redshifts above 4 from the PMN sample. *Astron. Astrophys.* 391, 509–517. doi: 10.1051/0004-6361:20020869

Ilbert, O., Arnouts, S., McCracken, H. J., Bolzonella, M., Bertin, E., Le Fèvre, O., et al. (2006). Accurate photometric redshifts for the CFHT legacy survey calibrated using the VIMOS VLT deep survey. *Astron. Astrophys.* 457, 841–856. doi: 10.1051/0004-6361:20065138

Jannuzi, B. T., and Dey, A. (1999). Photometric redshifts and the detection of high redshift galaxies. *ASPCS* 191:111.

Kaiser, N., Aussel, H., Burke, B. E., Boesgaard, H., Chambers, K., Chun, M. R., et al. (2002). Pan-STARRS: a large synoptic survey telescope array. *Proc. SPIE* 4836, 154–164. doi: 10.1117/12.457365

Kaiser, N., Burgett, W., Chambers, K., Denneau, L., Heasley, J., Jedicke, R., et al. (2010). The pan-STARRS wide-field optical/NIR imaging survey. *Proc. SPIE* 7733. doi: 10.1117/12.859188

Kauffmann, G., Heckman, T. M., Tremonti, C., Brinchmann, J., Charlot, S., White, S. D. M., et al. (2003). The host galaxies of active galactic nuclei. *Month. Notices RAS* 346:1390. doi: 10.1111/j.1365-2966.2003.07154.x

Kenter, A., Murray, S. S., Forman, W. R., Jones, C., Green, P., Kochanek, C. S., et al. (2005). An X-ray survey of the NDWFS bootes field. II. The X-ray source catalog. *Astrophys. J. Suppl.* 161:9. doi: 10.1086/444379

Kimball, A. E., Knapp, G. R., Ivezić, Ž., West, A. A., Bochanski, J. J., Plotkin, R. M., et al. (2009). A sample of candidate radio stars in first and SDSS. *Astrophys. J.* 701, 535–546. doi: 10.1088/0004-637X/701/1/535

Kirkpatrick, J., Schlegel, D. J., Ross, N. P., Myers, A. D., Hennawi, J. F., Sheldon, E. S., et al. (2011). A simple likelihood method for quasar target selection. *Astrophys. J.* 743:2. doi: 10.1088/0004-637X/743/2/125

Kochanek, C. S., Eisenstein, D. J., Cool, R. J., Caldwell, N., Assef, R. J., Jannuzi, B. T., et al. (2012). AGES: the AGN and galaxy evolution survey. *Astrophys. J. Suppl.* 200:8. doi: 10.1088/0067-0049/200/1/8

Lacy, M., Petric, A. O., Sajina, A., Canalizo, G., Storrie-Lombardi, L. J., Armus, L., et al. (2007) Optical spectroscopy and X-ray detections of a sample of quasars and active galactic nuclei selected in the mid-infrared from two spitzer space telescope wide-area surveys. *Astron. J.* 133, 186–206. doi: 10.1086/509617

MacLeod, C. L., Brooks, K., Ivezic, Z., Kochanek, C. S., Gibson, R., Meisner, A., et al. (2010a). Quasar selection based on photometric variability. *Astrophys. J.* 728:16. doi: 10.1088/0004-637X/728/1/26

MacLeod, C. L., Ivezić, Ž., Kochanek, C. S., Kozłowski, S., Kelly, B., Bullock, E., et al. (2010b). Modeling the time variability of SDSS stripe 82 quasars as a damped random walk. *Astrophys. J.* 721:1014. doi: 10.1088/0004-637X/721/2/1014

Martin, C., Barlow, T., Barnhart, W., Bianchi, L., Blakkolb, B. K., Bruno, D., et al. (2003). The galaxy evolution explorer. *Proc. SPIE* 4854, 336–350. doi: 10.1117/12.460034

McGreer, I. D., Becker, R. H., Helfand, D. J., and White, R. L. (2006). Discovery of a z = 6.1 radio-loud quasar in the NOAO deep wide field survey. *Astrophys. J.* 652, 157–162. doi: 10.1086/507767

McGreer, I. D., Helfand, D. J., and White, R. L. (2009). Radio-selected quasars in the sloan digital sky survey. *Astron. J.* 138, 1925–1937. doi: 10.1088/0004-6256/138/6/1925

McLure, M. J., and Dunlop, J. S. (2004). The cosmological evolution of quasar black hole masses. *Month. Notices RAS* 352:1390. doi: 10.1111/j.1365-2966.2004.08034.x

Meier, D. L. (1976a). Have primeval galaxies been detected. *Astrophys. J.* 203, L103–L105. doi: 10.1086/182029

Meier, D. L. (1976b). The optical appearance of model primeval galaxies. *Astrophys. J.* 207, 343-350 doi: 10.1086/154500

Palanque-Delabrouille, N., Yeche, C. H., Myers, A. D., Petitjean, P., Ross, N. P., Sheldon, E., et al. (2011). Variability selected high-redshift quasars on SDSS Stripe 82. *Astron. Astrophys.* 530:A122. doi: 10.1051/0004-6361/201016254

Pâris, I., Petitjean, P., Ross, N. P., Myers, A. D., Aubourg, É., Streblyanska, A., et al. (2017). The sloan digital sky survey quasar catalog: twelfth data release. *Astrophys. J.* 597:A79. doi: 10.1051/0004-6361/201527999

Retana-Montenegro, E., and Röttgering, H. J. A. (2017). Probing the radio loud/quiet AGN dichotomy with quasar clustering *Astrophysics* 600:a197. doi: 10.1051/0004-6361/201526433

Richards, G. T., Fan, X., Newberg, H. J., Strauss, M. A., Vanden Berk, D. E., Schneider, D. P., et al. (2002). Spectroscopic target selection in the sloan digital sky survey: the quasar sample. *Astron. J.* 123:2945. doi: 10.1086/340187

Richards, G. T., Fan, X., Newberg, H. J., Strauss, M. A., Vande Berk, D. E., Schneider1, D. P., et al. (2006). Spectroscopic target selection in the sloan digital sky survey: the quasar sample. *Astron. J.* 131, 2766–2787. doi: 10.1086/503559

Ross, N. P., Myers, A. D., Sheldon, E. S., Yèche, C., Strauss, M. A., Bovy, J., et al. (2012). The SDSS-III baryon oscillation spectroscopic survey: quasar target selection for data release nine. *Astrophys. J.* 199:3. doi: 10.1088/0067-0049/199/1/3

Ross, N. P., Shen, Y., Strauss, M. A., Vanden Berk, D. E., Connolly, A. J., Richards, G. T., et al. (2009). Clustering of low-redshift (z <= 2.2) quasars from the sloan digital sky survey. *Astrophys. J.* 697:1634. doi: 10.1088/0004-637X/697/2/1634

Röttgering, H., Afonso, J., Barthel, P., Batejat, F., Best, P., Bonafede, A., et al. (2011). LOFAR and APERTIF surveys of the radio sky: probing shocks and magnetic fields in galaxy clusters. *J. Astrophys. Astron.* 32, 557–566. doi: 10.1007/s12036-011-9129-x

Salvato, M., Hasinger, G., Ilbert, O., Zamorani, G., Brusa, M., Scoville, N. Z., et al. (2009). Photometric redshift and classification for the XMM-COSMOS sources. *Astrophys. J.* 690, 1250–1263. doi: 10.1088/0004-637X/690/2/1250

Salvato, M., Ilbert, O., Hasinger, G., Rau, A., Civano, F., Zamorani, G., et al. (2011). Dissecting photometric redshift for active galactic nucleus using XMM- and chandra-COSMOS samples. *Astrophys. J.* 742:61. doi: 10.1088/0004-637X/742/2/61

Sandage, A., Véron, P., and Wyndham, J. D. (1965). Optical identification of new quasi-stellar radio sources. *Astrophys. J.* 142:1307. doi: 10.1086/148415

Schneider, D. P., Richards, G. T., Hall, P. B., Strauss, M. A., Anderson, S. F., Boroson, T. A., et al. (2010). The sloan digital sky survey quasar catalog. V. Seventh data release. *Astron. J.* 139:2360. doi: 10.1088/0004-6256/139/6/2360

Shimwell, T. W., Röttgering, H. J. A., Best, P. N., Williams, W. L., Dijkema, T. J., de Gasperin, F., et al. (2017). The LOFAR two-metre sky survey. I. Survey description and preliminary data release. *Astron. Astrophys.* 598:A104. doi: 10.1051/0004-6361/201629313

Smolčić, V., Novak, M., Bondi, M., Ciliegi, P., Mooley, K. P., Schinnerer, E., et al. (2017). The VLA-COSMOS 3 GHz large project: continuum data and source catalog release. *Astron. Astrophys.* 602:A1. doi: 10.1051/0004-6361/201628704

Tyson, J. A. (2002). Large synoptic survey telescope: overview. *Proc. SPIE* 4836, 10–20. doi: 10.1117/12.456772

van Haarlem, M. P., Wise, M. W., Gunst, A. W., Heald, G., McKean, J. P., Hessels, J. W. T., et al. (2013). LOFAR: the LOw-Frequency ARray. *Astron. Astrophys.* A2:556. doi: 10.1051/0004-6361/201220873

Williams, W., Intema, H. T., and Röttgering, H. J. A. (2013). T-RaMiSu: the two-meter radio mini survey. I. The Boötes field. *Astron. Astrophys.* 549:A55. doi: 10.1051/0004-6361/201220235

Williams, W., van Weeren, R. J., Röttgering, H. J. A., Best, P., Dijkema, T. J., de Gasperin, F., et al. (2016). LOFAR 150-MHz observations of the Boötes field: catalogue and source counts. *Month. Notices RAS* 460:2385. doi: 10.1093/mnras/stw1056

Willott, C. J., Philippe, P., Omont, A., Bergeron, J., Delfosse, X., Forveille, T., et al. (2007). Four quasars above redshift 6 discovered by the Canada-France high-z quasar survey. *Astrophys. J.* 134, 2435–2450. doi: 10.1086/522962

Wright, E. L., Eisenhardt, P. R. M., Mainzer, A. K., Ressler, M. E., Cutri, R. M., Jarrett, T., et al. (2010). The wide-field infrared survey explorer (WISE): mission description and initial on-orbit performance. *Astron. J.* 140, 1868–1881. doi: 10.1088/0004-6256/140/6/1868

York, D. G., Adelman, J., Anderson, J. E., Scott, F., Annis, J., Bahcall, N. A., et al. (2000). The sloan digital sky survey: technical summary. *Astron. J.* 120, 1579–1587. doi: 10.1086/301513

Yèche, N. P., Petitjean, P., Rich, J., Aubourg, E., Busca, N., Hamilton, J.-C., et al. (2010). Artificial neural networks for quasar selection and photometric redshift determination. *Astrophys. J.* 523:A14. doi: 10.1051/0004-6361/200913508

Zeimann, G. R., White, R. L., Becker, R. H., Hodge, J. A., Stanford, S. A., and Richards, G. T. (2011). Discovery of a radio-selected z ˜ 6 quasar. *Astrophys. J.* 746:57. doi: 10.1088/0004-637X/736/1/57

Conflict of Interest Statement: The authors declare that the research was conducted in the absence of any commercial or financial relationships that could be construed as a potential conflict of interest.

The reviewer, DB, and handling Editor declared their shared affiliation.

Copyright © 2018 Retana-Montenegro and Röttgering. This is an open-access article distributed under the terms of the Creative Commons Attribution License (CC BY). The use, distribution or reproduction in other forums is permitted, provided the original author(s) and the copyright owner are credited and that the original publication in this journal is cited, in accordance with accepted academic practice. No use, distribution or reproduction is permitted which does not comply with these terms.

frontiers in Astronomy and Space Sciences

PERSPECTIVE
published: 10 October 2017
doi: 10.3389/fspas.2017.00020

Phylogenetic Analyses of Quasars and Galaxies

Didier Fraix-Burnet[1]*, *Mauro D'Onofrio*[2] *and Paola Marziani*[3]

[1] Univ. Grenoble Alpes, CNRS, IPAG, Grenoble, France, [2] Osservatorio Astronomico di Padova (INAF), Padua, Italy, [3] Dipartimento di Fisica e Astronomia, Università di Padova, Padua, Italy

Phylogenetic approaches have proven to be useful in astrophysics. We have recently published a Maximum Parsimony (or cladistics) analysis on two samples of 215 and 85 low-z quasars ($z < 0.7$) which offer a satisfactory coverage of the Eigenvector 1-derived main sequence. Cladistics is not only able to group sources radiating at higher Eddington ratios, to separate radio-quiet (RQ) and radio-loud (RL) quasars and properly distinguishes core-dominated and lobe-dominated quasars, but it suggests a black hole mass threshold for powerful radio emission as already proposed elsewhere. An interesting interpretation from this work is that the phylogeny of quasars may be represented by the ontogeny of their central black hole, i.e. the increase of the black hole mass. However these exciting results are based on a small sample of low-z quasars, so that the work must be extended. We are here faced with two difficulties. The first one is the current lack of a larger sample with similar observables. The second one is the prohibitive computation time to perform a cladistic analysis on more that about one thousand objects. We show in this paper an experimental strategy on about 1,500 galaxies to get around this difficulty. Even if it not related to the quasar study, it is interesting by itself and opens new pathways to generalize the quasar findings.

Keywords: unsupervised classification, quasars, galaxies, multivariate analysis, phylogenetic methods

OPEN ACCESS

Edited by:
Sandor Mihaly Molnar, National Taiwan University, Taiwan

Reviewed by:
Milan S. Dimitrijevic, Astronomical Observatory, Serbia
Omaira González Martín, Instituto de Radioastronomía y Astrofísica, Mexico

***Correspondence:**
Didier Fraix-Burnet
didier.fraix-burnet@univ-grenoble-alpes.fr

Specialty section:
This article was submitted to Milky Way and Galaxies, a section of the journal Frontiers in Astronomy and Space Sciences

Received: *28 July 2017*
Accepted: *25 September 2017*
Published: *10 October 2017*

Citation:
Fraix-Burnet D, D'Onofrio M and Marziani P (2017) Phylogenetic Analyses of Quasars and Galaxies. Front. Astron. Space Sci. 4:20. doi: 10.3389/fspas.2017.00020

1. INTRODUCTION: ASTROCLADISTICS

Astrocladistics[1] (Fraix-Burnet et al., 2006a,b,c; Fraix-Burnet, 2016, 2017; Rampazzo et al., 2016, and references therein) aims at introducing phylogenetic tools in astrophysics.

These tools try to establish the relationships between the species by minimizing the total evolutionary cost depicted on a phylogenetic tree. The most general and the simplest to implement technique is Maximum Parsimony, also known as cladistics, and is based on the parameters, and not on distances between the objects. The trees that result from cladistic analysis should not be interpreted as genealogic trees: here, as the trees do not indicate ancestor or descendant objects, each quasar supposedly represents a species (i.e., a class). In this phylogenetic sense, the trees can be rooted according to a parameter that may have an evolutionary meaning.

The phylogenetic tools are devised to take the evolution of object populations into account. They do not rely on similarities, derived from the computation of distances, but on the fact that diversity is gained through evolution and speciation. For instance, similarity techniques (like most statistical clustering and classification or phenetic tools) tend to find hyperspheres in the parameter

[1] https://astrocladistics.org

space, while phylogenetic tools are able to detect evolutionary paths as can be shown on stellar evolutionary tracks (Fraix-Burnet, 2017). Many applications have been published on many kinds of astrophysical objects (Fraix-Burnet et al., 2009, 2010, 2012; Cardone and Fraix-Burnet, 2013; Fraix-Burnet and Davoust, 2015; Jofre et al., 2017; Holt et al., submitted).

Phylogenetic approaches represent the relationships using trees or networks, the first ones being simpler to read. From these evolutionary schemes, it is possible to gather objects into groups that supposedly share the same common ancestor species (monophyletic groups). These groups appear as sub-structures (i.e. bunches of branches) in the tree, their exact number depending on the desired level of details in their physical interpretation.

In this paper, we summarize an exciting cladistic analysis of low-z quasars and illustrate a possible approach to extend such study on much larger samples.

2. A CLADISTIC ANALYSIS OF A LOW-Z QUASAR SAMPLE

This analysis is published in Fraix-Burnet et al. (2017). Two samples of low-redshift ($z \leq 0.7$) quasars are used: one with 215 objects presented by Marziani et al. (2003), and another one made of 85 quasars cross-matched with (Sulentic et al., 2007) have measurements of the CIV line. These two samples are modest in size but have good quality measurements of emission lines (H_β, FeII, [OIII], CIV...). For the cladistic analysis, the 215 and 85 object samples have, respectively 7 and 11 parameters.

With such relatively small samples, the cladistic analysis is relatively easy, and allows for extensive test of its reliability through kinds of bootstrap approaches. The most parsimonious tree in **Figure 1** shows the 85 quasars at the leaves (ends of the branches). Bunches of branches that appear to depart from the main trunk are colored to define groups of quasars that hypothetically may share similar evolutionary histories.

To understand and interpret this tree, it is necessary to look at the properties of the groups, for instance using boxplots (**Figure 2**). The tree (**Figure 1**) is arbitrarily presented with the group having the lowest black hole mass is at the top. The groups on the boxplots are then ordered from the top of the tree to the bottom.

It is striking to note that the black hole mass increases nearly regularly toward the bottom of the tree. Since the black hole mass (MBH) can only grow as a function of quasar evolution and cosmic time, the ontogeny of black holes is represented by their monotonic increase in mass. Considering that MBH provides a sort of arrow of time of nuclear activity, a phylogenetic interpretation of the tree becomes possible if the cladistic tree is rooted on black hole mass.

Considering other properties, the cladistic tree is thus consistent with the more massive radio-quiet Population B sources (disk dominated, lower Eddingon ratio) at low-z appearing as a more evolved counterpart of Population A (wind dominated sources, higher Eddington ratio) to which the local Narrow-Line Seyfert 1s belong.

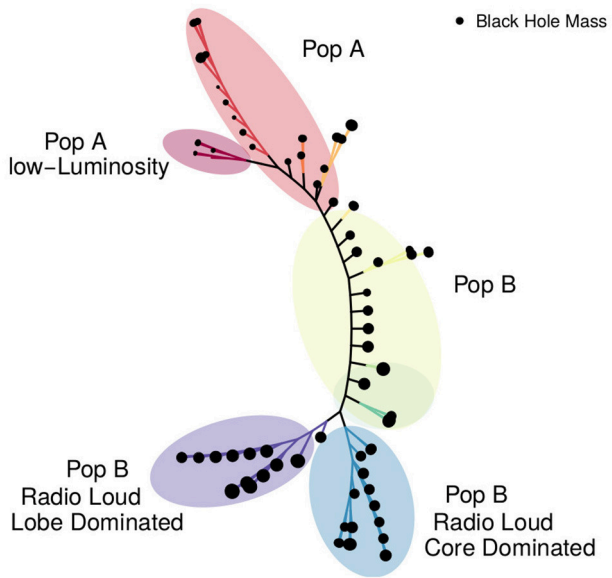

FIGURE 1 | The cladistics tree of 85 quasars. The tree representation is unrooted, but the low black hole masses (MBH) are at the top. We identify ten groups corresponding to bunches of branches and colored as in **Figure 2**. The colored ellipsoidal regions indicates well-known categories of quasars and encompass several of our groups.

The core-dominated and lobe-dominated Radio Loud (RL) sources are in two distinct groups at the bottom of the tree, indicating they are monophyletic groups. Quite interestingly, these powerful RL sources appear in our low-z sample only above a mass threshold.

In conclusion, the quasar sample studied in Fraix-Burnet et al. (2017) contains a population of massive quasars which are more evolved and a population of less-massive quasars that are radiating at a higher L/Ledd. While L/Ledd remains the physical factor governing E1 (Marziani et al., 2001; Sulentic et al., 2011; Sulentic and Marziani, 2015), high-MBH quasars may have resembled low-MBH quasars in an earlier stage of their evolution.

The cladistic analysis is thus able to recover well-known classes of quasars, but more importantly brings a unique insight on their phylogeny. However, this picture is only valid for the low-z sample studied, and no generalization to the entire quasar population is possible. But the results are sufficiently exciting to justify extensions of this work to other samples. Two directions are foreseen, both requiring higher-z quasar populations, to better depict the quasar evolution. Firstly, it would be interesting to study a sample within a constrained redshift range at another epoch of the Universe to check whether the evolution of the properties of quasars is similar. Secondly, the relationships between quasar populations in a larger redshift range would give a clearer picture of the global evolution of the black hole mass and the different properties like the radio loudness or the disk/wind dichotomy.

Unfortunately, data are either not existing or of insufficient quality which requires dedicated surveys with large-collecting

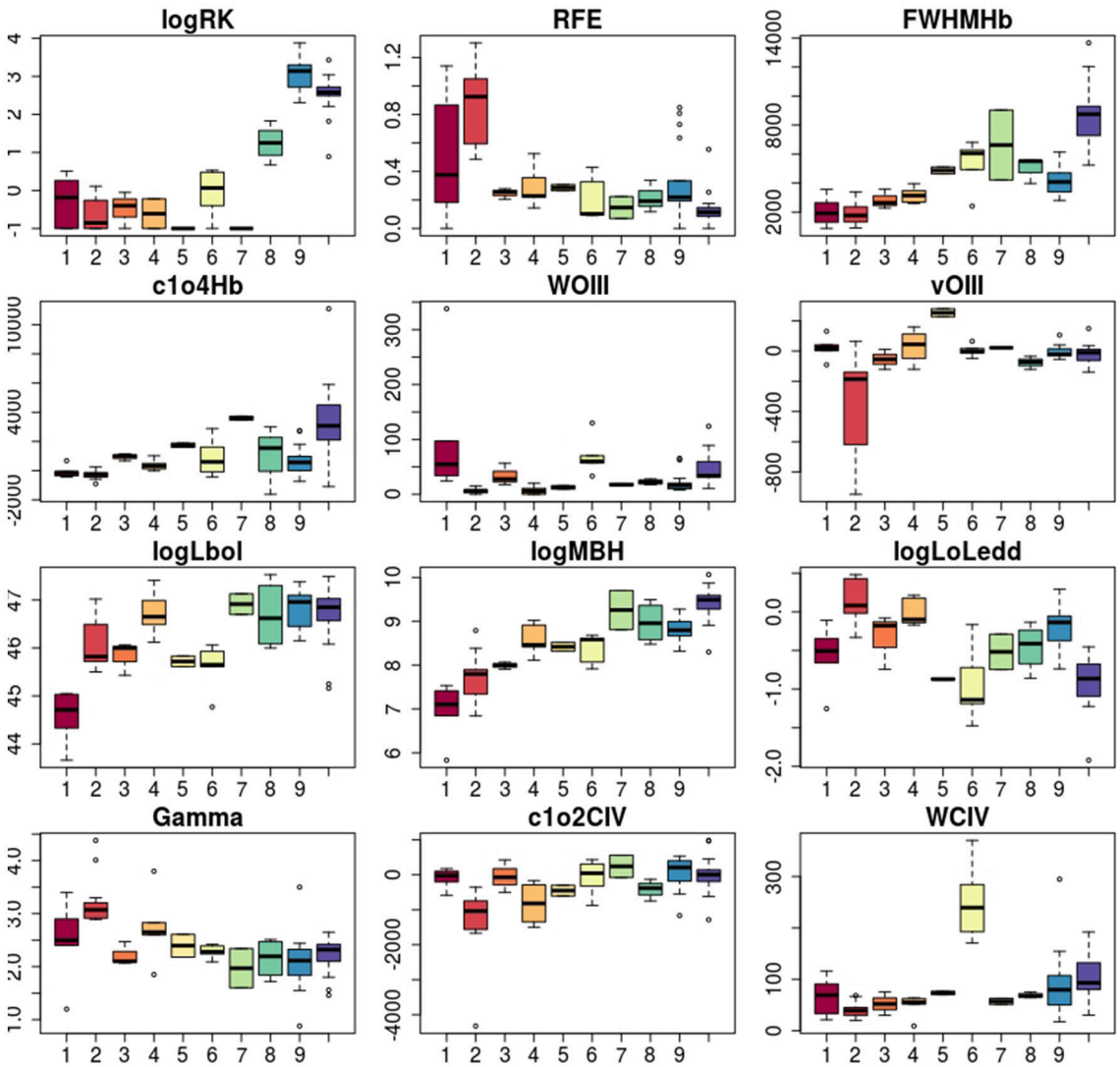

FIGURE 2 | Boxplots for the groups in the 85 quasar sample as defined on the tree in **Figure 1**. The parameters shown are: the radio loudness parameter (RK), the intensity ratio between Feλ4570 and Hβ (RFE), the Full Width at Half-intensity Maximum (FWHMHb) and the line centroid displacement at quarter maximum (c1o4Hb) of the Hβ line, the equivalent width (WOIII) and the peak shift (vOIII) of the [OIII]λ5007 line, the bolometric luminosity (Lbol), the Black Hole Mass (MBH), the Eddington ratio L/L_{edd} (LoLedd), the soft X-ray photon index (Gamma), the centroid displacement at half maximum (c1o2CIV) and the equivalent width of the CIVλ1549 line (WCIV).

area telescopes to match the luminosity range of low-z quasars that remain almost unobserved at intermediate-to-high redshift (Sulentic et al., 2014). In addition, the cladistic technique is very demanding in computing resources. Basically, all possible trees made of the objects must be built to select the most parsimonious one in terms of evolutionary complexity. There are heuristic tricks to avoid this thorough quest, but still a cladistic analysis is practically not feasible with more than about a thousand objects.

Another approach is required. Since we do not have a big quasar sample, we present in the following a tentative strategy on a different sample made of galaxies, as an example of potential applications of cladistics to large samples of sources.

3. A CLADISTIC ANALYSIS OF LOW-L ELGS IN CLUSTER

3.1. Sample

The WINGS survey (Fasano et al., 2006) is an imaging and spectroscopic study of the brightest X-ray clusters at redshift $0.04 < z < 0.07$ selected from the ROSAT all sky survey. The sample for this analysis has 1,494 galaxies belonging to several clusters, and eleven parameters have been used for the cladistic analysis itself: B-V, logRe, surface brightness, Hβ, D4000, Mass, Sersic index n (measures the degree of curvature of the Sersic profile describing how the intensity of a galaxy varies with distance from its center), Hα/NII, Gband, Mg, and Na.

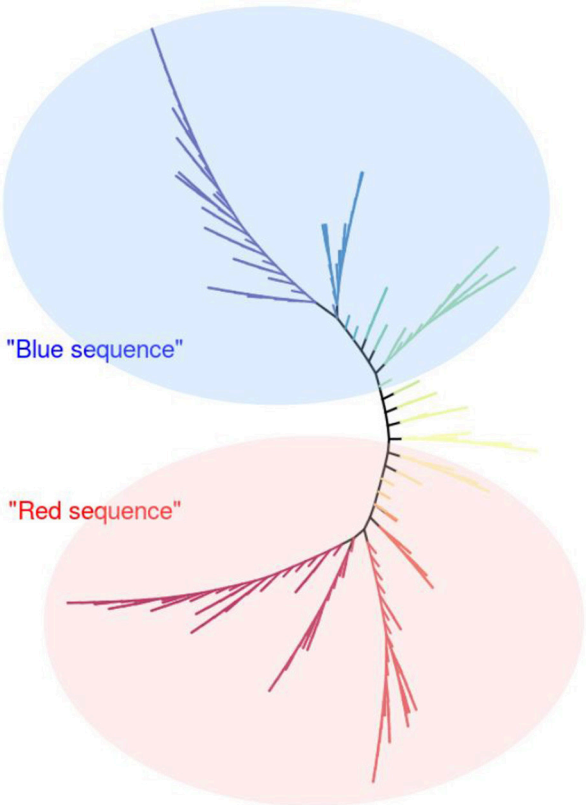

FIGURE 3 | The cladistics tree of 300 pre-clusters of the WINGS sample of 1,494 galaxies. The tree representation is unrooted, but the lower masses are at the top. The colors of the branches correspond to the groups and are the same as in **Figure 4**.

3.2. Pre-Clustering

Phylogenetic methods are intended to find relationships between classes (species) of objects. But there is no multivariate classification of galaxies (Fraix-Burnet et al., 2015). This would be however useful since it is easier and physically more relevant to study different types of objects rather than millions of individuals. This dimension reduction is also necessary in the era of the huge databases brought by current and future telescopes.

This multivariate classification is one objective of astrocladistics. However, we are limited by the size of the samples to study. There are other phylogenetic techniques that tackle this problem efficiently, but they are based on distances, and most often adapted for the specific evolutionary processes of living organisms and their traits (e.g., Saitou and Nei, 1987; Gascuel and Steel, 2006). Some work should be done to assess their applicability to astrophysics. There are also many statistical tools for unsupervised classification (or clustering, De et al., 2013), but they gather objects according to their similarities, not to their evolutionary relationships.

We will discuss this big issue with possible solutions in another paper (Fraix-Burnet in prep.), and here show the results of a first approach we have implemented.

The idea behind this approach is rather intuitive: we are looking for structures in the parameter space, structures that both gather and relate the objects of our sample. Since we have too many of these objects, we try to reduce the resolution of our data by replacing very close (similar) objects into meta-objects that we call pre-clusters. These pre-clusters take the median properties of their components. In other words, we postulate that there may be some redundancies in our data. Then we can perform the cladistic analysis on these pre-clusters that can subsequently gathered into groups from the tree.

This idea is also mentioned by Murtagh and Legendre (2014) that recommends to perform a pre-clustering using a hierarchical classification method (that builds a hierarchy of clusters, Fraix-Burnet et al., 2015) for the k-means analysis (a partitioning method, MacQueen, 1967; Fraix-Burnet et al., 2015). While for our problem many pre-clustering algorithms could a priori be used, we here choose the hierarchical clustering one. Note that this technique requires a huge amount of CPU time with very large samples.

The number of pre-clusters is arbitrary. Obviously it should not be too low otherwise we probably mix together different kinds of objects. It cannot be too high either because of the limitation of the cladistics analysis. We have found that 300 pre-clusters is here a good choice compromise because the cladistic analaysis takes only a few hours allowing many runs to test this strategy.

3.3. Results

The tree (**Figure 3**) is obtained with the 300 pre-clusters. Each leave (ending branch) of the tree is thus one pre-cluster. We have gathered these pre-clusters depending on the substructures of the tree, and the groups are represented by different colors. Each group of galaxies thus corresponds either to a single branch or to a bunch of branches on the tree.

The boxplots (**Figure 4**) show the statistics of several parameters for each of the groups. The order of the groups is arbitrary and has been chosen to underline the increase of the mass. On the tree in **Figure 3** this parameter increases from top to bottom.

The color progression from blue to red grossly matches the increase in mass of galaxies, as well as other clear trends as visible on the boxplots. Interestingly, the morphological type decreases along the tree downward, and possibly the distance to the cluster center as well even though the in-group scatters are large.

Sometimes, some groups stand out from these trends in some parameters, such as the group 6 for the mass or group 12 for Mg. These groups will be further investigated since they could be either the results of some weird data or, more interestingly, a new peculiar species of galaxies that could lead us to a better understanding of the evolution of galaxies than simply redder colors or larger masses.

The WINGS sample galaxies belong to X-ray brights clusters, which are rather evolved systems, predominantly close to a state of viral equilibrium. We find that most of the groups have a representant in all the clusters, or conversely all clusters span the entire tree. Despite the low statistics in some of the clusters, this would indicate that the classification scheme depicted on the tree

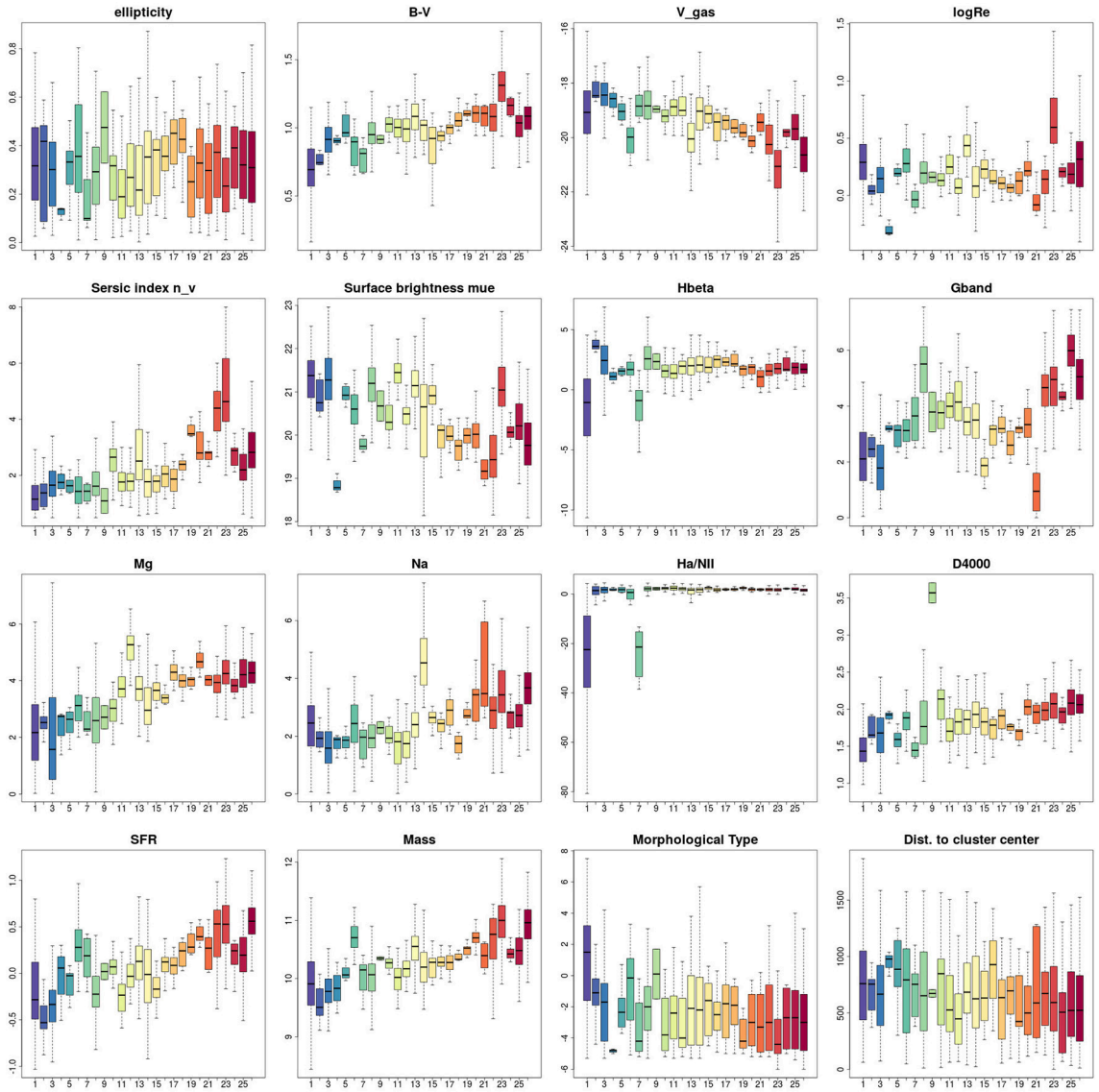

FIGURE 4 | Boxplots for the groups in the WINGS sample as defined on the tree in **Figure 3**.

in **Figure 3** could be well of general validity for galaxies at low redshift.

We have also analyzed a control sample of 497 higher redshift field galaxies. It is impossible to root the tree such that the boxplots show as many monotonic trends as for the cluster sample above, indicating that the field galaxies of our sample may not possess a "common ancestor," that is they could be made of two distinct populations with different origins. Another possibility is that their evolution is more complex, but the sample is probably too small to conclude in this direction. The fact that the cluster sample of low-redshift galaxies is compatible with a common ancestor can be due to: (i) the general influence of clusters on galaxy evolution, (ii) time smoothing out somewhat the different origins of these galaxies, (iii) a lower diversity by a sort of volume selection effect.

4. CONCLUSION

Categorizing quasars or galaxies is usually made through a handful of properties at most. Multivariate clustering is still rare (Fraix-Burnet et al., 2015), but only phylogenetic tools like cladistics provide relationships that emerge from the data. Here (Fraix-Burnet et al., 2017), the quasar sample is small and relatively well contained in redshift, so probably in diversity. Indeed, the diversity of the quasar sample (which is exclusively low-z, $z \lesssim 0.7$) can be organized along a 1D sequence, the eigenvector-1 main sequence.

To extend this study to larger samples at higher redshifts, we present a possible strategy to perform the same kind of analysis by performing a pre-clustering using a hierarchical clustering technique, followed by a cladistic analysis on the pre-clusters.

This is applied on a galaxy samples due to the current lack of larger samples of quasars with similar parameters as above.

Even though this diversity is much larger for the WINGS galaxy sample, our proposed strategy successfully establishes a phylogenetic scheme that points to several evolutive properties (like color, mass, metallicity but also D4000 and the Sersic index n) characterizing a level of diversification (or evolution). Some of these evolutive correlations are very probably not causal, unlike the quasar evolution with MBH.

Some caution is necessary when interpreting the cladograms presented here. One should not conclude that every quasar or every galaxy follows some linear evolution along the tree. There are bunches of branches (sub-structures of the trees) that could suggest some dead ends, or the lack of more ancestral objects. For instance, starting from the low luminosity Pop A quasars (group 1), how to understand the branch of more luminous Pop A quasars (group 2)? Regarding WINGS galaxies, the true ancestors of the objects studied here are at higher redshifts: where the connection to the presented trees would take place? This is impossible to answer these questions without further pursuing the present work.

AUTHOR CONTRIBUTIONS

The contributions is mainly as follows: DF performed the cladistic analyses, MD and PM worked on the WINGS project and gathered the sample. PM also provided the quasar sample. All three authors equally participated to the elaboration of the documents.

REFERENCES

Cardone, V. F., and Fraix-Burnet, D. (2013). Hints for families of grbs improving the hubble diagram. *Mon. Not. R. Astron. Soc.* 434, 1930–1938. doi: 10.1093/mnras/stt1122

De, T., Chattopadhyay, T., and Chattopadhyay, A. K. (2013). Comparison among clustering and classification techniques on the basis of galaxy data. *Calcutta Stat. Assoc. Bull.* 65, 257–260. doi: 10.1177/0008068320130110

Fasano, G., Marmo, C., Varela, J., D'Onofrio, M., Poggianti, B. M., Moles, M., et al. (2006). Wings: a wide-field nearby galaxy-cluster survey. i. optical imaging. *Astron. Astrophys.* 445, 805–817. doi: 10.1051/0004-6361:20053816

Fraix-Burnet, D. (2016). "Concepts of classification and taxonomy phylogenetic classification," in *Statistics for Astrophysics: Clustering and Classification*, Vol. 77 (Paris: EAS Publications Series; EDP Sciences), 221–257.

Fraix-Burnet, D. (2017). *Phylogenetic Tools in Astrophysics*. John Wiley & Sons, Ltd.

Fraix-Burnet, D., Chattopadhyay, T., Chattopadhyay, A. K., Davoust, E., and Thuillard, M. (2012). A six-parameter space to describe galaxy diversification. *Astron. Astrophys.* 545:A80. doi: 10.1051/0004-6361/201218769

Fraix-Burnet, D., Choler, P., and Douzery, E. (2006a). Towards a phylogenetic analysis of galaxy evolution : a case study with the dwarf galaxies of the local group. *Astron. Astrophys.* 455, 845–851. doi: 10.1051/0004-6361:20065098

Fraix-Burnet, D., Choler, P., Douzery, E., and Verhamme, A. (2006b). Astrocladistics: a phylogenetic analysis of galaxy evolution I. Character evolutions and galaxy histories. *J. Classif.* 23, 31–56. doi: 10.1007/s00357-006-0003-5

Fraix-Burnet, D., and Davoust, E. (2015). Stellar populations in ω centauri: a multivariate analysis. *Mon. Not. R. Astron. Soc.* 450, 3431–3441. doi: 10.1093/mnras/stv791

Fraix-Burnet, D., Davoust, E., and Charbonnel, C. (2009). The environment of formation as a second parameter for globular cluster classification. *Mon. Not. R. Astron. Soc.* 398, 1706–1714. doi: 10.1111/j.1365-2966.2009.15235.x

Fraix-Burnet, D., Douzery, E., Choler, P., and Verhamme, A. (2006c). Astrocladistics: a phylogenetic analysis of galaxy evolution II. Formation and diversification of galaxies. *J. Classif.* 23, 57–78. doi: 10.1007/s00357-006-0004-4

Fraix-Burnet, D., Dugué, M., Chattopadhyay, T., Chattopadhyay, A. K., and Davoust, E. (2010). Structures in the fundamental plane of early-type galaxies. *Mon. Not. R. Astron. Soc.* 407, 2207–2222. doi: 10.1111/j.1365-2966.2010.17097.x

Fraix-Burnet, D., Marziani, P., 'Onofrio, M. D., and Dultzin, D. (2017). The phylogeny of quasars and the ontogeny of their central black holes. *Front. Astron. Space Sci*, 4:1. doi: 10.3389/fspas.2017.00001

Fraix-Burnet, D., Thuillard, M., and Chattopadhyay, A. K. (2015). Multivariate approaches to classification in extragalactic astronomy. *Front. Astron. Space Sci.* 2:3. doi: 10.3389/fspas.2015.00003

Gascuel, O., and Steel, M. (2006). Neighbor-joining revealed. *Mol. Biol. Evol.* 23, 1997–2000. doi: 10.1093/molbev/msl072

Jofre, P., Das, P., Bertranpetit, J., and Foley, R. (2017). Cosmic phylogeny: reconstructing the chemical history of the solar neighbourhood with an evolutionary tree. *ArXiv e-prints* 467, 1140–1153. Submitted to MNRAS doi: 10.1093/mnras/stx075

MacQueen, J. B. (1967). "Some methods for classification and analysis of multivariate observations" in *Proceedings of 5th Berkeley Symposium on Mathematical Statistics and Probability* (Berkeley, CA: University of California Press), 281–297.

Marziani, P., Sulentic, J. W., Zamanov, R., Calvani, M., Dultzin-Hacyan, D., Bachev, R., et al. (2003). An optical spectroscopic atlas of low-redshift active galactic nuclei. *Astrophys. J. Suppl. Ser.* 145:199. doi: 10.1086/346025

Marziani, P., Sulentic, J. W., Zwitter, T., Dultzin-Hacyan, D., and Calvani, M. (2001). Searching for the physical drivers of the eigenvector 1 correlation space. *Astrophys. J.* 558, 553–560. doi: 10.1086/322286

Murtagh, F., and Legendre, P. (2014). Ward's hierarchical agglomerative clustering method: which algorithms implement ward's criterion? *J. Classif.* 31, 274–295. doi: 10.1007/s00357-014-9161-z

Rampazzo, R., Mauro, D., Simone, Z., Debra, M. E., Eija, L., Pierre, A., et al. (2016). "Family traits of galaxies: from the tuning fork to a physical classification in a multi-wavelength context," in *From the Realm of the Nebulae to Populations of Galaxies. Dialogues on a Century of Research, 1st Edn, Vol. 435, Astrophysics and Space Science Library* (Springer International Publishing), 189–242, 243–380.

Saitou, N., and Nei, M. (1987). The neighbor-joining method: a new method for reconstructing phylogenetic trees. *Mol. Biol. Evol.* 4, 406–425.

Sulentic, J., and Marziani, P. (2015). Quasars in the 4d eigenvector 1 context: a stroll down memory lane. *Front. Astron. Space Sci.* 2:6. doi: 10.3389/fspas.2015.00006

Sulentic, J., Marziani, P., and Zamfir, S. (2011). The case for two quasar populations. *Balt. Astron.* 20, 427–434. doi: 10.1515/astro-2017-0314

Sulentic, J. W., Bachev, R., Marziani, P., Negrete, C. A., and Dultzin, D. (2007). C iv 1549 as an eigenvector 1 parameter for active galactic nuclei. *Astrophys. J.* 666:757. doi: 10.1086/519916

Sulentic, J. W., Marziani, P., del Olmo, A., Dultzin, D., Perea, J., and Alenka Negrete, C. (2014). Gtc spectra of z $\simeq$ 2.3 quasars: comparison with local luminosity analogs. *Astron. Astrophys.* 570:A96. doi: 10.1051/0004-6361/201423975

Conflict of Interest Statement: The authors declare that the research was conducted in the absence of any commercial or financial relationships that could be construed as a potential conflict of interest.

Copyright © 2017 Fraix-Burnet, D'Onofrio and Marziani. This is an open-access article distributed under the terms of the Creative Commons Attribution License (CC BY). The use, distribution or reproduction in other forums is permitted, provided the original author(s) or licensor are credited and that the original publication in this journal is cited, in accordance with accepted academic practice. No use, distribution or reproduction is permitted which does not comply with these terms.

frontiers in Astronomy and Space Sciences

PERSPECTIVE
published: 13 November 2017
doi: 10.3389/fspas.2017.00037

Catalog of 3 < z < 5.5 Quasar Candidates Selected among XMM-Newton Sources and Its Spectroscopic Verification

Georgii Khorunzhev[1], Sergey Sazonov[1], Rodion Burenin[1] and Maxim Eselevich[2]*

[1] *High Energy Astrophysics, Space Research Institute, Russian Academy of Sciences, Moscow, Russia,* [2] *Laboratory of Infrared Methods in Astrophysics, Institute of Solar-Terrestrial Physics, Russian Academy of Sciences, Irkutsk, Russia*

We have compiled a catalog of 903 quasar candidates (including known quasars) at $3 < z < 5.5$ selected among X-ray sources from the XMM-Newton serendipitous survey (3XMM-DR4 catalog). We used photometric SDSS, 2MASS, and WISE data to select the objects. The surface number density of objects in our sample exceeds that in the SDSS spectroscopic quasar sample at the same redshifts by a factor of 1.5. We have performed spectroscopic observations of a subsample of new quasar candidates using a new low- and medium-resolution spectrograph at the 1.6-m AZT-33IK telescope (Mondy, Russia) and demonstrated that the purity of these candidates is about 65%. We have discovered one of the most distant ($z = 5.08$) X-ray selected quasars.

Keywords: active galactic nuclei, quasars, X-ray surveys, photometric redshifts, spectroscopy, XMM-Newton, SDSS

OPEN ACCESS

Edited by:
Mauro D'Onofrio,
Università degli Studi di Padova, Italy

Reviewed by:
Paola Severgnini,
Brera Astronomical Observatory, Italy
Fabio La Franca,
Università degli Studi Roma Tre, Italy

****Correspondence:***
Georgii Khorunzhev
horge@iki.rssi.ru

Specialty section:
This article was submitted to Milky Way and Galaxies, a section of the journal Frontiers in Astronomy and Space Sciences

Received: *31 August 2017*
Accepted: *24 October 2017*
Published: *13 November 2017*

Citation:
Khorunzhev G, Sazonov S, Burenin R and Eselevich M (2017) Catalog of 3 < z < 5.5 Quasar Candidates Selected among XMM-Newton Sources and Its Spectroscopic Verification. Front. Astron. Space Sci. 4:37. doi: 10.3389/fspas.2017.00037

1. INTRODUCTION

Searching for quasars at $z > 3$ is one of the key elements of studying the growth history of supermassive black holes and the evolution of massive galaxies in the Universe. For this purpose, multiwavelength observations of a large number of quasars are needed. Particularly valuable are X-ray observations: the intensive X-ray emission is directly connected with powerful processes of accretion onto the black hole. In order to improve our fairly poor knowledge of the evolution of the X-ray luminosity function of quasars at $z > 3$, larger X-ray samples of distant quasars are needed.

We have made an attempt to obtain a large sample of luminous X-ray quasars at $z > 3$ in the fields of the serendipitous XMM-Newton 3XMM-DR4 (Watson et al., 2009) survey at Galactic latitudes $|b| > 20°$ using photometric data from SDSS (Eisenstein et al., 2011), 2MASS (Skrutskie et al., 2006) and WISE (Wright et al., 2010). The 3XMM-DR4/SDSS overlapping area is ∼300 sq. deg, exceeding by several times the areas covered by known samples of distant X-ray quasars such as Champ (Kalfountzou et al., 2014) and XMM-XXL (north) (Menzel et al., 2016). The sample of Kalfountzou et al. (2014) covers ≈33 sq. deg and includes 87 X-ray selected optically bright (detected by SDSS) quasars. Half of them have photometric redshifts only. The spectroscopic program of (Menzel et al., 2016) has revealed 61 X-ray objects at $z_{\rm spec} > 3$ in a 18 sq. deg subfield of XMM-XXL (north). Our sample thus provides an opportunity to study a population of rare high-luminosity, distant quasars and complements recent studies of less luminous high-redshift quasars conducted using deep small-area surveys (e.g., Onoue et al., 2017; Ricci et al., 2017; Vito et al., 2017).

It should be noted that SDSS spectroscopic data provide redshift measurements for 33 thousand optically selected quasars at $z_{\rm spec} > 3$ (Alam et al., 2015) over 11,000 sq. deg in the sky. However,

existing wide-area X-ray surveys are too shallow to study these objects. It is only the forthcoming all-sky X-ray survey by eROSITA aboard the Spektrum-Roentgen-Gamma observatory (Pavlinsky et al., 2011; Merloni et al., 2012) that will be capable of finding X-ray counterparts for a substantial fraction of known quasars at $z_{\rm spec} > 3$.

Based on broadband photometry, we obtained photometric redshift estimates ($z_{\rm phot}$) and compiled a catalog of 903 candidates for distant quasars with $z_{\rm phot} > 2.75$ (Khorunzhev et al., 2016). The catalog includes 515 known quasars (with spectroscopic redshifts, of which 266 are at $z_{\rm spec} > 3$) and 388 new quasar candidates. Most (80%) of the spectroscopic redshifts have been obtained by SDSS (Alam et al., 2015). The remaining $z_{\rm spec}$ have been gathered from various sources (Flesch, 2015). The new quasar candidates selected by $z_{\rm phot}$ constitute a substantial addition to the spectroscopic sample. Thus, if most of these candidates prove to be quasars at $z > 3$, the existing 3XMM-DR4/SDSS sample of distant quasars will be enhanced by a factor of ∼1.5.

Spectroscopic verification is necessary to determine the accuracy of our $z_{\rm phot}$ estimates and assess the purity of our selection of quasar candidates. We have thus started a spectroscopy identification program for the new quasar candidates (Khorunzhev et al., 2017). Some initial results of this program are reported below.

2. SAMPLE SELECTION

K16 considered point SDSS sources at Galactic latitudes $|b| > 20°$ that have an X-ray counterpart in 3XMM-DR4[1]. In addition, we used near- (2MASS) and medium-infrared (WISE) photometry if available. To keep sources with reliable photometry and to get rid of M-dwarfs, we applied the following condition:

$$\delta m_{z'} < 0.2 \;\&\; i' - z' < 0.6\,, \tag{1}$$

where i' and z' are the PSF magnitudes in the appropriate SDSS bands and $\delta m_{z'} < 0.2$ is the corresponding error. This is a well-known technique (e.g., Richards et al., 2002; Wu et al., 2012; Skrzypek et al., 2015) for separating M-dwarfs from distant quasars. Stars have $i' - z' > 0.8$, while quasars have $i' - z' < 0.4$. This color remains approximately constant up to a redshift of ≈5.5, until the Lyα line passes from i' to z'. The color of quasars then becomes $i' - z' \approx 2$.

We then performed a broadband energy distribution fitting using the EAZY software (Brammer et al., 2008) to obtain photometric redshift estimates. We made two fitting iterations for each object using libraries of quasar (by various authors) and star (Pickles, 1998) templates. Those objects with

$$\chi^2_{star}/\chi^2_{qso} > 1 \;\&\; z_{phot} > 2.75, \tag{2}$$

finally constituted our catalog of 903 candidates for distant quasars selected by photometric redshift. At the same time, our procedure missed 63 known quasars at $z_{\rm spec} > 3$ (see **Figure 1**). Note that we lowered the threshold of selection from $z_{\rm phot} = 3.0$ to 2.75 to achieve reasonable selection completeness at $z \sim 3$.

The completeness of our catalog in the investigated fields relative to existing spectroscopic catalogs of quasars (SDSS DR12 Alam et al. 2015 and *The Half Million Quasars* Flesch 2015) with $z_{\rm spec} > 3$ is about 80%. The normalized median absolute deviation of photometric redshift estimates for the spectroscopically confirmed quasars ($\Delta z = |z_{\rm spec} - z_{\rm phot}|$) is $\sigma_{\Delta z/(1+z_{\rm spec})} = 0.07$, while the catastrophic outlier fraction is $\eta = 9\%$ (when $\Delta z/(1 + z_{\rm spec}) > 0.2$).

3. SPECTROSCOPIC VERIFICATION

We have performed a quasi-random spectroscopic survey of quasar candidates from the *K16* catalog at the 1.6-m AZT-33IK telescope (Kamus et al., 2002; Denisenko et al., 2009) equipped with the low- and medium-resolution ADAM spectrograph (Afanasiev et al., 2016; Burenin et al., 2016). A number of additional observations were conducted with the SCORPIO I (Afanasiev and Moiseev, 2005) spectrograph at the 6-m BTA telescope.

3.1. Observations at the AZT-33IK Telescope

The AZT-33IK telescope is located at the Sayan Solar Observatory of the Institute of Solar-Terrestrial Physics, the Siberian branch

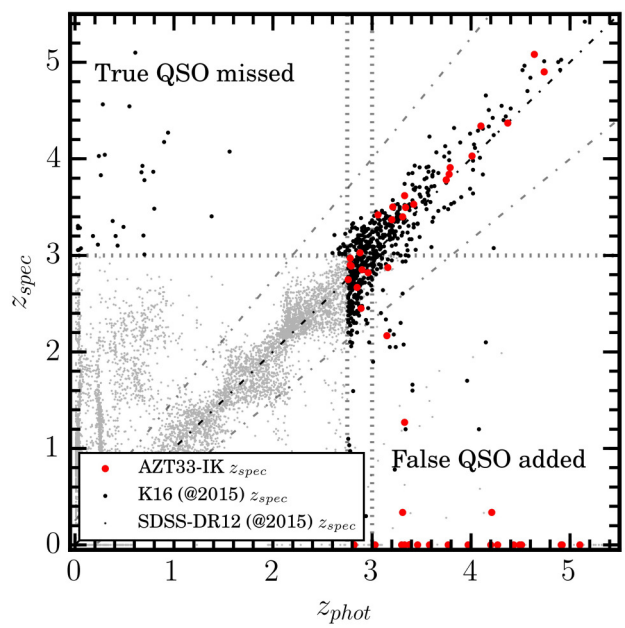

FIGURE 1 | Scatter plot of $z_{\rm spec}$ relative to $z_{\rm phot}$ for point objects (having an error $\delta z'_{psf} < 0.2$ and spectroscopic SDSS redshift $z_{\rm spec} < 5.5$). Light gray dots denote all SDSS sources. Black symbols are *K16* objects with known redshift at the time of catalog compilation. Red symbols are objects whose spectra were obtained afterwards at AZT-33IK. The dash–dotted lines limit the area of $z_{\rm phot}$ catastrophic outliers. The vertical dotted line at $z_{\rm phot} = 2.75$ denotes the *K16* low $z_{\rm phot}$ boundary of selection. The horizontal dotted line ($z_{\rm spec} = 3.0$) denotes our target $z_{\rm spec}$ boundary for distant quasars.

[1]http://heasarc.gsfc.nasa.gov/W3Browse/xmm-newton/xmmssc.html

of the Russian Academy of Sciences, and has a primary mirror diameter of 1.6 m. The low- and medium-resolution ADAM spectrograph was produced at the Special Astrophysical Observatory of the Russian Academy of Sciences and was installed on AZT-33IK in 2015. The quantum efficiency of the entire system (telescope mirror, spectrograph, grating and CCD array) reaches 50% (Burenin et al., 2016). The ADAM spectrograph allows the spectra of objects with an apparent magnitude R $\sim$ 19.5 to be taken with an exposure time of half an hour. If necessary and under good weather conditions, a magnitude I $\sim$ 21 can be reached with an exposure time of two hours.

By now, we have obtained the spectroscopic redshifts for 48 quasar candidates, i.e more than 10% of such objects in the *K16* catalog. Approximately 60% of the observed objects proved to be quasars at $z_{\rm spec} \gtrsim 2.5$, of which 16 have $z_{\rm spec} > 3$. We found 4 new spectroscopically confirmed quasars at $z_{\rm spec} > 4$, of which one, *3XMM J125329.4+305539* is at $z_{\rm spec} = 5.08$.

3.2. Discovery of a Quasar at $z = 5.08$

3XMM J125329.4+305539 was first reported (Khorunzhev et al., 2016) as a probable quasar at $z_{\rm phot} = 4.64$ in the *K16* catalog, and there was no information about this source in other photometric catalogs of quasar candidates[2]. Its SDSS apparent magnitude is $i' \simeq 21.0$. Its 0.5–2 keV flux is 1.5×10^{-15} erg/s/cm^2 and the corresponding X-ray luminosity is 4×10^{44} erg/s (without *k*-correction).

Apart from this source, there are only 3 optically bright (i.e., with reliable SDSS photometry) X-ray quasars at $z_{\rm spec} > 5.0$, which are not XMM-Newton observational targets, in the *3XMM-DR4* catalog. Thus, *3XMM J125329.4+305539* is one of the brightest and most distant X-ray quasars at $z_{\rm spec} > 5.0$ suitable for constructing the X-ray luminosity function at such redshifts.

3.3. Purity and Selection Completeness

We can estimate the purity of the *K16* catalog using the obtained quasi-random spectroscopic sample. Consider the following photometric redshift intervals: $2.75 \leq z_{\rm phot} < 4$, $4 \leq z_{\rm phot} < 5$ and $5 \leq z_{\rm phot} < 5.5$. By purity we mean the ratio of the number of true quasars ($|z_{\rm phot} - z_{\rm spec}|/(1 + z_{\rm spec}) < 0.2$) to that of all objects with available spectra. Here, the value 0.2 reflects the scatter (3 standard deviations) of $z_{\rm phot}$ relative to $z_{\rm spec}$ for all of the known and spectroscopically confirmed quasars in the *K16* catalog. The purity of the spectroscopic sample calculated in this way is shown in **Figure 2** (circles).

For comparison, the arrows in **Figure 2** indicate the lower limit on the purity of the *K16* catalog estimated at the time of its compilation (before our AZT-33IK observations). This limit was deduced as the ratio of the number of true quasars with known spectroscopic redshifts and $|z_{\rm phot} - z_{\rm spec}|/(1 + z_{\rm spec}) < 0.2$ to the total number of objects in the catalog. Recall that the new candidates without spectroscopic redshifts accounted for about 40% of the *K16* catalog.

[2]http://vizier.u-strasbg.fr

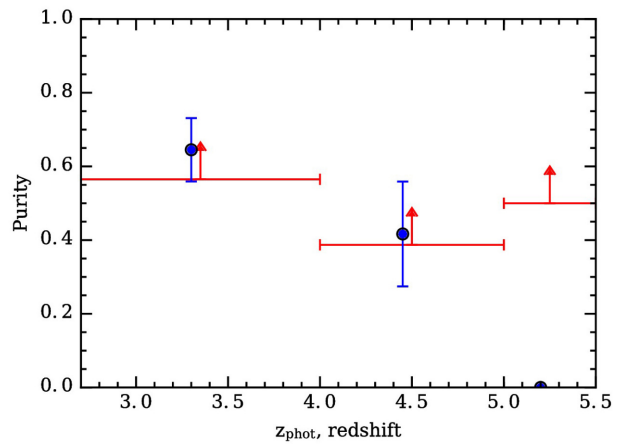

FIGURE 2 | Circles with Poissonian errorbars indicate the purity of the quasar candidates whose spectra have been taken at AZT-33IK or BTA. The arrows indicate the estimated lower limit for the purity of the *K16* catalog relative to the objects with known (from literature or SDSS) spectroscopic redshifts.

Based on these preliminary results, we can expect $\sim$250 quasars at $z \gtrsim 3$ to be firmly identified upon completion of the spectroscopy of all new quasar candidates from the *K16* catalog. This would significantly increase the sample of known distant X-ray quasars.

4. CONCLUSION

The obtained spectra of dosens of quasars at $z \sim 3$ and especially the discovery of one of the most distant X-ray selected quasars (*3XMM J125329.4+305539*) at $z_{\rm spec} = 5.08$ demonstrate that the AZT-33IK telescope of the Sayan Solar Observatory equipped with the new ADAM spectrograph is well suited for identification of distant quasars. This telescope is planned to be one of the instruments employed for optical support of the upcoming all-sky X-ray survey by the Spektrum-Roentgen-Gamma observatory (with its eROSITA and ART-XC telescopes, Pavlinsky et al., 2011; Merloni et al., 2012).

We have demonstrated that the existing sample of distant X-ray quasars can be substationally increased using publicly available X-ray (XMM-Newton) and optical photometry (SDSS) data, complemented by a relatively low-cost spectroscopic identification program.

We are continuing our spectroscopic verification program for *K16* candidates using the AZT-33IK and BTA telescopes and intend to obtain a complete spectroscopic sample at least for brighter X-ray sources from the *K16* catalog.

AUTHOR CONTRIBUTIONS

GK provided key contributions to the compilation of the catalog, spectroscopic observations, data analysis and writing of this paper. SS supervised the research at all stages. RB contributed to the aquisition and processing of spectroscopic data. ME organized spectroscopic observations at AZT-33IK.

FUNDING

The observations at the 6-m BTA telescope were financially supported by the Ministry of Education and Science of the Russian Federation (contract no. 14.619.21.0004, project identifier RFMEFI61914X0004).

ACKNOWLEDGMENTS

This research was partially supported by the Program of the President of the Russian Federation for support of leading scientific schools (grant NSh-10222.2016.2).

This research is based on observations obtained with XMM-Newton, an ESA science mission with instruments and contributions directly funded by ESA Member States and NASA. Also, we used SDSS-III, 2MASS, WISE data. Funding for SDSS-III has been provided by the Alfred P. Sloan Foundation, the Participating Institutions, the National Science Foundation, and the U.S. Department of Energy Office of Science. The Two Micron All Sky Survey is a joint project of the University of Massachusetts and the Infrared Processing and Analysis Center/California Institute of Technology, funded by the National Aeronautics and Space Administration and the National Science Foundation. The Wide-field Infrared Survey Explorer is a joint project of the University of California, Los Angeles, and the Jet Propulsion Laboratory/California Institute of Technology, funded by the National Aeronautics and Space Administration.

REFERENCES

Afanasiev, V. L., Dodonov, S. N., Amirkhanyan, V. R., and Moiseev, A. V. (2016). ADAM low- and medium-resolution spectrograph for 1.6-m AZT-33IK telescope. *Astrophys. Bull.* 71, 479–488. doi: 10.1134/S1990341316040118

Afanasiev, V. L., and Moiseev, A. V. (2005). The SCORPIO Universal Focal Reducer of the 6-m Telescope. *Astron. Lett.* 31, 194–204. doi: 10.1134/1.1883351

Alam, S., Albareti, F. D., Allende Prieto, C., Anders, F., Anderson, S. F., Anderton, T., et al. (2015). The eleventh and twelfth data releases of the sloan digital sky survey: final data from SDSS-III. *Astrophys. J. Suppl. Ser.* 219:12. doi: 10.1088/0067-0049/219/1/12

Brammer, G., van Dokkum, P., and Coppi, P. (2008). EAZY: a fast, public photometric redshift code. *Astrophysics* 686, 1503–1513. doi: 10.1086/591786

Burenin, R. A., Amvrosov, A. L., Eselevich, M. V., Grigor'ev, V. M., Aref'ev, V. A., Vorob'ev, V. S., et al. (2016). Observational capabilities of the new medium- and low-resolution spectrograph at the 1.6-m telescope of the Sayan Observatory. *Astron. Lett.* 42, 295–306. doi: 10.1134/S1063773716050017

Denisenko, S. A., Kamus, S. F., Pimenov, Y. D., Tergoev, V. I., and Papushev, P. G. (2009). The AZT-33VM fast, wide-aperture telescope . *J. Opt. Technol.* 76, 629–631. doi: 10.1364/JOT.76.000629

Eisenstein, D. J., Weinberg, D. H., Agol, E., Aihara, H., Allende Prieto, C., Anderson, S. F., et al. (2011). SDSS-III: Massive Spectroscopic Surveys of the Distant Universe, the Milky Way, and Extra-Solar Planetary Systems. *Astron. J.* 142:72. doi: 10.1088/0004-6256/142/3/72

Flesch, E. W. (2015). The Half Million Quasars (HMQ) Catalogue. *Publ. Astron. Soc. Aust.* 32:e010. doi: 10.1017/pasa.2015.10

Kalfountzou, E., Civano, F., Elvis, M., Trichas, M., and Green, P. (2014). The largest X-ray-selected sample of z>3 AGNs: C-COSMOS and ChaMP. *Month. Notices R. Astron. Soc.* 445, 1430–1448. doi: 10.1093/mnras/stu1745

Kamus, S. F., Denisenko, S. A., Lipin, N. A., Tergoev, V. I., Papushev, P. G., Druzhinin, S. A., et al. (2002). The AZT-33VM fast, wide-aperture telescope . *J. Opt. Technol.* 69:674. doi: 10.1364/JOT.69.000674

Khorunzhev, G., Burenin, R., Mescheryakov, A., and Sazonov, S. (2016). Catalog of candidates for quasars at $3 < z < 5.5$ selected among X-Ray sources from the 3XMM-DR4 survey of the XMM-Newton observatory. *Astron. Lett.* 42, 277–294. doi: 10.1134/S1063773716050042

Khorunzhev, G. A., Burenin, R. A., Sazonov, S. Y., Amvrosov, A. L., and Eselevich, M. V. (2017). Optical spectroscopy of candidates for quasars at $3 < z < 5.5$ from the XMM-newton X-ray survey. A distant X-ray quasar at z = 5.08. *Astron. Lett.* 43, 135–145. doi: 10.1134/S1063773717030045

Menzel, M.-L., Merloni, A., Georgakakis, A., Salvato, M., Aubourg, E., Brandt, W. N., et al. (2016). A spectroscopic survey of X-ray-selected AGNs in the northern XMM-XXL field. *Month. Notices R. Astron. Soc.* 457, 110–132. doi: 10.1093/mnras/stv2749

Merloni, A., Predehl, P., Becker, W., Böhringer, H., Boller, T., Brunner, H., et al. (2012). eROSITA Science Book: Mapping the Structure of the Energetic Universe. *ArXiv e-prints*.

Onoue, M., Kashikawa, N., Willott, C. J., Hibon, P., Im, M., Furusawa, H., et al. (2017). Minor Contribution of Quasars to Ionizing Photon Budget at $z \sim 6$: Update on Quasar Luminosity Function at the Faint End with Subaru/Suprime-Cam. *Astrophys. J. Lett.* 847:L15. doi: 10.3847/2041-8213/aa8cc6

Pavlinsky, M., Akimov, V., Levin, V., Lapshov, I., Tkachenko, A., Semena, N., et al. (2011). "The ART-XC instrument on board the SRG mission," in *Society of Photo-Optical Instrumentation Engineers (SPIE) Conference Series, Vol. 8147 of Proc. SPIE* (San Diego, CA), 814706.

Pickles, A. J. (1998). A Stellar Spectral Flux Library: 1150-25000 Å. *PASP* 110, 863–878.

Ricci, F., Marchesi, S., Shankar, F., La Franca, F., and Civano, F. (2017). Constraining the UV emissivity of AGN throughout cosmic time via X-ray surveys. *Month. Notices R. Astron. Soc.* 465, 1915–1925. doi: 10.1093/mnras/stw2909

Richards, G. T., Fan, X., Newberg, H. J., Strauss, M. A., Vanden Berk, D. E., et al. (2002). Spectroscopic target selection in the sloan digital sky survey: the quasar sample. *Astron. J.* 123, 2945–2975. doi: 10.1086/340187

Skrutskie, M. F., Cutri, R. M., Stiening, R., Weinberg, M. D., Schneider, S., Carpenter, J. M., et al. (2006). The two micron all sky survey (2MASS). 131, 1163–1183. doi: 10.1086/498708

Skrzypek, N., Warren, S. J., Faherty, J. K., Mortlock, D. J., Burgasser, A. J., and Hewett, P. C. (2015). Photometric brown-dwarf classification. I. A method to identify and accurately classify large samples of brown dwarfs without spectroscopy. *Astron. Astrophys.* 574:A78. doi: 10.1051/0004-6361/201424570

Vito, F., Brandt, W. N., Yang, G., Gilli, R., Luo, B., Vignali, C., et al. (2017). High-redshift AGN in the Chandra Deep Fields: the obscured fraction and space density of the sub-L_* population. *ArXiv e-prints*.

Watson, M. G., Schröder, A. C., Fyfe, D., Page, C. G., Lamer, G., Mateos, S., et al. (2009). The XMM-Newton serendipitous survey. V. The Second XMM-Newton serendipitous source catalogue. *Astron. Astrophys.* 493, 339–373. doi: 10.1051/0004-6361:200810534

Wright, E. L., Eisenhardt, P. R. M., Mainzer, A. K., Ressler, M. E., Cutri, R. M., Jarrett, T., et al. (2010). The wide-field infrared survey explorer (WISE): mission description and initial on-orbit performance. 140, 1868–1881. doi: 10.1088/0004-6256/140/6/1868

Wu, X.-B., Hao, G., Jia, Z., Zhang, Y., and Peng, N. (2012). SDSS Quasars in the WISE Preliminary Data Release and Quasar Candidate Selection with Optical/Infrared Colors. *Astron. J.* 144:49. doi: 10.1088/0004-6256/144/2/49

Conflict of Interest Statement: The authors declare that the research was conducted in the absence of any commercial or financial relationships that could be construed as a potential conflict of interest.

Copyright © 2017 Khorunzhev, Sazonov, Burenin and Eselevich. This is an open-access article distributed under the terms of the Creative Commons Attribution License (CC BY). The use, distribution or reproduction in other forums is permitted, provided the original author(s) or licensor are credited and that the original publication in this journal is cited, in accordance with accepted academic practice. No use, distribution or reproduction is permitted which does not comply with these terms.

frontiers in Astronomy and Space Sciences

ORIGINAL RESEARCH
published: 08 January 2018
doi: 10.3389/fspas.2017.00068

A Hubble Diagram for Quasars

Susanna Bisogni[1,2]*, *Guido Risaliti*[2,3] *and Elisabeta Lusso*[4]

[1] Harvard-Smithsonian Center for Astrophysics, Cambridge, MA, United States, [2] INAF, Osservatorio Astrofisico di Arcetri, Firenze, Italy, [3] Dipartimento di Fisica e Astronomia, Università degli Studi di Firenze, Firenze, Italy, [4] Centre for Extragalactic Astronomy, Department of Physics, Durham University, Durham, United Kingdom

The cosmological model is at present not tested between the redshift of the farthest observed supernovae ($z \sim 1.4$) and that of the Cosmic Microwave Background ($z \sim$1,100). Here we introduce a new method to measure the cosmological parameters: we show that quasars can be used as "standard candles" by employing the non-linear relation between their intrinsic UV and X-ray emission as an absolute distance indicator. We built a sample of ∼1,900 quasars with available UV and X-ray observations, and produced a Hubble Diagram up to $z \sim 5$. The analysis of the quasar Hubble Diagram, when used in combination with supernovae, provides robust constraints on the matter and energy content in the cosmos. The application of this method to forthcoming, larger quasar samples, will also provide tight constraints on the dark energy equation of state and its possible evolution with time.

Keywords: cosmology: distance scale–cosmological parameters–observations, galaxies: active, quasars: general, X-ray: general, ultraviolet: general

OPEN ACCESS

Edited by:
Mauro D'Onofrio,
Università degli Studi di Padova, Italy

Reviewed by:
Fabio La Franca,
Università degli Studi Roma Tre, Italy
Alenka Negrete,
Universidad Nacional Autónoma de México, Mexico

***Correspondence:**
Susanna Bisogni
susanna.bisogni@cfa.harvard.edu

Specialty section:
This article was submitted to Milky Way and Galaxies, a section of the journal Frontiers in Astronomy and Space Sciences

Received: *12 November 2017*
Accepted: *19 December 2017*
Published: *08 January 2018*

Citation:
Bisogni S, Risaliti G and Lusso E (2018) A Hubble Diagram for Quasars. Front. Astron. Space Sci. 4:68. doi: 10.3389/fspas.2017.00068

1. INTRODUCTION

Quasars are among the brightest sources in the universe, by now observable up to redshift $z \sim 7$ (Mortlock et al., 2011). For this reason they have always been considered as potential candidates for extending the distance ladder in a redshift range well beyond the limit imposed by the supernovae ($z \sim 1.4$). Quasars, however, are known to be extremely variable, anisotropic sources and characterized by a wide range in luminosity. Unlike supernovae, an "easy" connection between a spectral (or time-dependent) feature and the luminosity is not available. In short, the use of quasars as standard candles is not obvious. The fundamental requirement needed to employ these sources for a cosmological purpose is being able to measure a "standard luminosity" from which infer the distance.

Several attempts have been made in this sense, using different relations involving quasars luminosity, such as the *Baldwin effect* (Baldwin, 1977; Korista et al., 1998), the Broad Line Region radius—luminosity relation (Watson et al., 2011; Kilerci Eser et al., 2015), the wavelength-dependent time delays in the emission variability of the accretion disc (Collier et al., 1999), the distribution of the linewidths as a function of the inclination of the BLR and of the quasar luminosity function (Rudge and Raine, 1999), the properties of highly accreting quasars (Wang et al., 2013; Marziani and Sulentic, 2014), the relation between the mass of the SuperMassive Black Hole and the X-ray variability (La Franca et al., 2014) among the others, or invoking the use of classic geometrical arguments, such as the measurement of the apparent size of the Broad Line Region (Elvis and Karovska, 2002), whose intrinsic dimension can be inferred from reverberation mapping monitoring (Blandford and McKee, 1982; Peterson, 1993). Most of these methods suffer from the high scatter in the observed relation or are limited by a poor statistics—generally imposed by the long times required by the observations. In order to make cosmology with quasars we need

to (1) have a measurement of their distance with a high precision, i.e., we need a luminosity-related relation with the smallest possible scatter; (2) make the most out of their large statistics, i.e., being able to apply the method to a large number of sources.

We recently proposed the relation between the luminosities in the X-rays (2 keV) and UV (2,500 Å) bands (Tananbaum et al., 1979; Zamorani et al., 1981; Steffen et al., 2006; Lusso et al., 2010; Young et al., 2010; Lusso and Risaliti, 2016, 2017) as a method to estimate quasars distances (Risaliti and Lusso, 2015). The method relies on the simple fact that the $L_X - L_{UV}$ relation is not linear. If we express it in terms of the fluxes, it becomes a function of the slope, the intercept, the intrinsic dispersion and the luminosity distance, i.e., a function of the cosmological parameters Ω_M and Ω_Λ. We can then use the fit to the relation or, equivalently, we can build the Hubble diagram for quasars, to infer information on the cosmological parameters. The obvious advantage of this method is that it only requires a measure of the two fluxes to be employed, therefore avoiding long-monitoring programs and allowing its application on a large number of sources up to high redshifts.

2. SAMPLE

In Risaliti and Lusso (2015) we presented the first Hubble diagram for a sample of ∼800 quasars for which 2 keV and 2,500 Å measures were available from the literature. We extended the Hubble diagram in a redshift range that was never explored before by any other cosmological probe (up to $z \sim 6$) and verified the excellent agreement between the distance moduli inferred with supernovae and those inferred with quasars in the common redshift range ($z = 0.01$–1.4).

The reliability and effectiveness of the method strongly depend, respectively, on the non-evolution of the relation with reshift and the dispersion in the relation, that, as already mentioned, directly affects the precision in distance estimates. This first sample, although properly treated to suit cosmological studies, can be improved in terms of homogeneity, quality and statistics of the data. In order to do that we selected a new sample of ∼8,000 objects for which X-rays and UV observations are available, crossmatching the SDSS Data Release 7 (Shen et al., 2011) and Data Release 12 (Pâris et al., 2017) catalogs with the 3XMM-DR5 (Rosen et al., 2016) catalog. The much higher statistics of this sample with respect to the previous one allows us to apply stronger quality cuts in order to significantly decrease the dispersion in the $L_X - L_{UV}$ relation and eventually to verify to a much higher extent the non-evolution of the relation with redshift.

2.1. The Dispersion in the $L_X - L_{UV}$ Relation

The $L_X - L_{UV}$ relation has been known to be characterized by a high dispersion (∼ 0.3–0.4 dex) that has deterred from using it as an absolute distance indicator. The observed dispersion, however, is the result of two distinct contributions: an intrinsic scatter in the relation, related to the still unknown physics involved, and

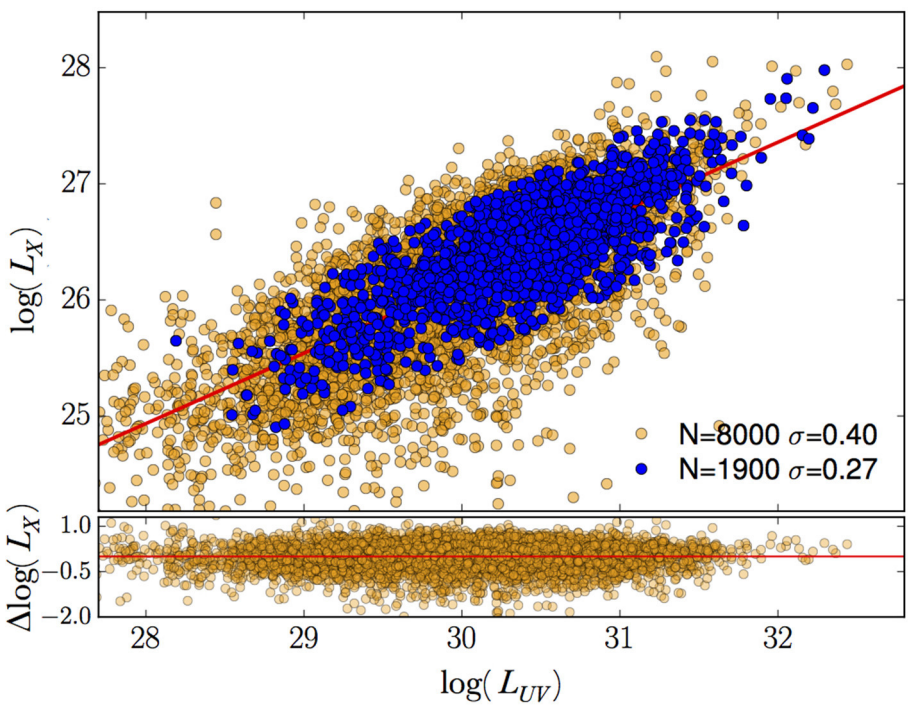

FIGURE 1 | Comparison between the relation obtained for the whole sample of quasars for which UV and X-ray observations are available (∼8,000) and for the sample cleaned by the observational issues that contribute to the observed dispersion (∼1,900). After the quality cuts are applied, the observed dispersion is decreased by ∼0.3 dex.

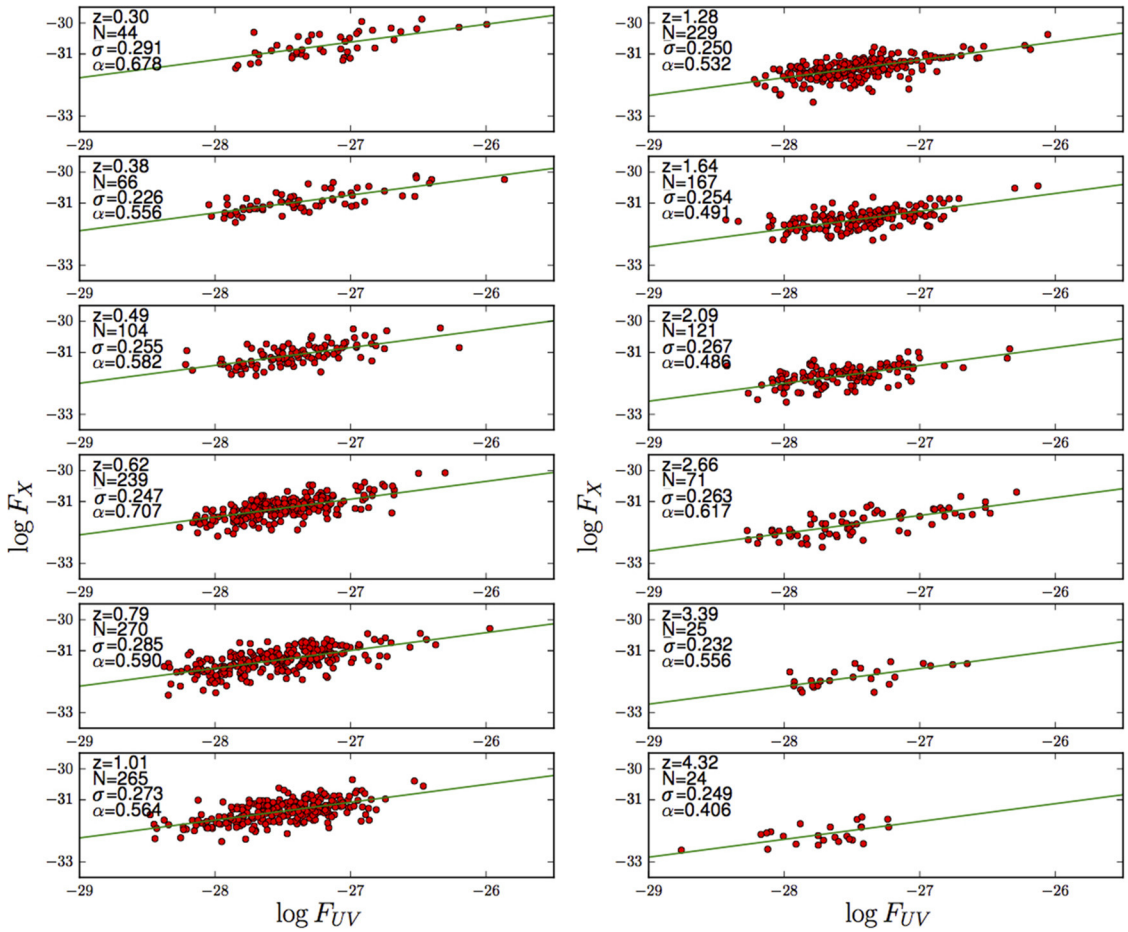

FIGURE 2 | Fits of the $F_X - F_{UV}$ in narrow redshift intervals. The distance differences among the objects in the same bin are small with respect to the dispersion of the relation, so we can use fluxes as proxies of the luminosities. In this way, the analysis is independent from the choice of a cosmological model. In each panel we report the median redshift, the number of objects N, the dispersion σ, and the best fit slope α of the relation.

an additional scatter due to observational issues. In Lusso and Risaliti (2016) and Lusso and Risaliti (2017) we demonstrated that a large part of the observed dispersion is ascribable to the latter contribution and, through the analysis of a smaller sample of high quality data and of sources with multiple observations available, that the magnitude of the *instrinsic dispersion* can be attested to be <0.20 dex. Removing the part of the observed dispersion related to observational issues makes the relation much tighter and our distance estimates much more precise. Significant efforts has then been made in this direction, once the major contributions to this "observational" scatter has been recognisee in the following issues:

1. Uncertainties in the measurement of the (2 keV) X-ray flux, which are, on average, a factor of 2 (unlike UV measurements that can be constrained with uncertainties lower than 10%),
2. Absorption in the spectrum in the UV and in the X-ray wavelength ranges (with the effect on the UV band being more severe and also less recognizable with respect to the one on the X-ray spectrum),
3. Variability of the source and non-simultaneity of the observation in the UV and X-ray bands,
4. Inclination effects affecting the intrinsic emission of the accretion disc,
5. Selection effects due to the flux limit in the surveys (the Eddington Bias, i.e., sources with an average flux below the detection threshold can be detected only while on a positive fluctuation).

By filtering the sample according to the quality of the X-ray measurements, the amount of intrinsic absorption in the source and the systematic effects due to the Eddington bias, we obtain a "clean" sample with a scatter in the relation reduced by ∼0.3 dex[1] (**Figure 1**). These criteria select a sample of ∼1,900 objects out of the initial ∼8,000 with a dispersion of ∼0.27 dex. Considering

[1] Since from the initial sample selection, jetted quasars and Broad Absorption Line quasars (BAL) were excluded. These sources are known, respectively, to have an additional contributions to the X-ray emission (with respect to the one coming from the hot corona) and to be heavily obscured.

that the dispersion in the $L_X - L_{UV}$ relation is propagated to the distance modulus and that the dispersion in the Hubble diagram for supernovae 1A is ∼0.07 at $z \sim 1$, this means that ∼15 quasars can provide the same cosmological information as one supernova at this redshift.

2.2. The Non-evolution of the $L_X - L_{UV}$ Relation with Redshift

For the relation to be used as a reliable method for distance estimates, we need to check its non-evolution with the redshift. We repeated the analysis performed in Risaliti and Lusso (2015) on the new, larger sample: we divided the sample in redshift bins and evaluated the relation within each one of them. The size of the redshift bin must fullfill two requirements: it has to be small enough so that differences in the luminosity distance within the same bin are negligible with respect to the intrinsic dispersion in the relation (the observed dispersion in each redshift bin is ∼0.25 dex on average), but large enough so that the number of sources within each bin makes this analysis meaningful. Moreover, if the differences in the luminosity distances are negligible, we can consider the relation between fluxes instead of luminosities, making this check independent from the assumed cosmological model.

The two requirements are met when the width of the redshift bin is $\Delta \log z = 0.08$. The whole redshift range spanned by quasars (with the exclusion of the range $z \cong 0.01$–0.3, for which a significant number of objects is not available) yields 12 redshift bins.

For each subsample in the 12 redshift bins, we fitted the X-tay to UV *fluxes* with the same log-linear relation adopted for the luminosities of the whole sample. The results of these fits for the slope parameter are shown in **Figure 2**. All the fits are consistent with $\alpha = 0.6$, with an average $< \alpha > = 0.56 \pm 0.08$.

3. THE HUBBLE DIAGRAM FOR QUASARS

The $L_X - L_{UV}$ relation has been used to estimate quasar distances and build a Hubble diagram of quasars. While slope of the relation can be obtained in a cosmology-independent way as described in the previous Section, its absolute calibration requires the comparison with other standard candles (analogously to the calibration of SN1a based on Cepheid stars). We obtained such a calibration by requiring an overlap of the Hubble diagram of SN1a and quasars in the overlapping redshift range, $z \sim 0.2$–1.4. The result is shown in **Figure 3**. The main interesting aspects of this work are the following:

1. The Hubble diagram of quasars perfectly overlap with the one of SN1a in the redshift range $z = 0.2$–1.4: the same cosmological model fits both the supernovae and quasars data, with no significant residuals beyond the expected Gaussian fluctuations (see inset of **Figure 3**). While the absolute calibration of quasars has been chosen in order to have such an agreement, the shape of the diagram has no free parameter once the slope of the relation has been fixed. Therefore, the match over the whole common redshift

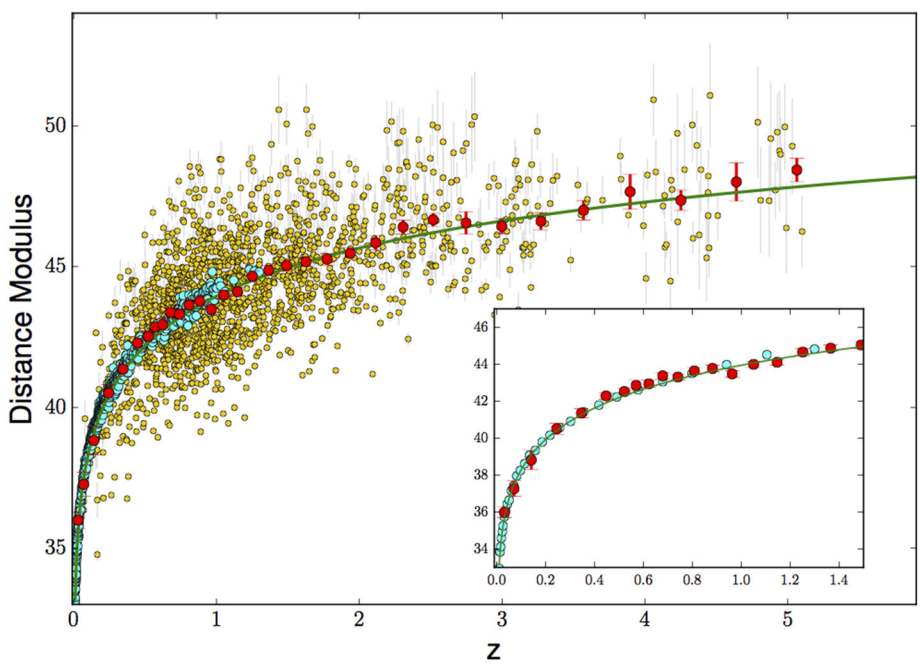

FIGURE 3 | Hubble diagram of quasars obtained with our "clean" sample and supernovae 1A. The orange points are single measurements for quasars, while the red points are quasar averages in small redshift bins. Type 1A supernovae are also plotted with cyan points (JLA sample, Betoule et al., 2014). The inset plot shows a zoom of the same diagram in the redshift range where supernova 1A and quasars overlap. In this case both red and cyan points are averages in small redshift bins for quasars and supernovae 1A respectively.

range is a strong confirmation of the reliability of our method.

2. There are a few hundred quasars at redshifts higher than $z = 1.4$, where no supernova has been observed. The Hubble diagram of these objects is a powerful check of the cosmological model, tracing the evolution of the Universe in the poorly investigated $z = 1.4$–6 redshift interval, the only other cosmological probes testing the expansion of the Universe above $z = 1.4$ being Gamma Ray Bursts (Ghirlanda et al., 2006) and Ly-α BAO at $z \sim 2.4$ (du Mas des Bourboux et al., 2017).
3. The average dispersion in the $\log(D_L)$-redshift relation is $\sigma \sim 0.27$ dex. This is a large improvement with respect to our first work based on literature samples ($\sigma \sim 0.35$) and also on our first Hubble diagram based on SDSS quasars ($\sigma \sim 0.30$, Risaliti and Lusso, 2017). This is due to our on-going refinement of both UV and X-ray flux measurements and sample selection. Our primary goal in the early phases of this new branch of observational cosmology is to obtain a clean sample, where biases and systematic effects are greatly reduced (a complete discussion of this point will be presented in a forthcoming paper, together with the results of the fits of the Hubble Diagram with several cosmological models). This comes at the expense of sample statistics: the final sample in **Figure 3** consists of "only" 1,900 objects, out of a parent sample of about 8,000 quasars. The main rejection criteria are: X-ray absorption, optical-UV reddening, poor quality of X-ray observations. In the future a more detailed spectral analysis of both the X-ray and optical/UV spectra will allow us to recover a large fraction of the rejected quasars, greatly enhancing the power of this method in constraining the cosmological parameters.

AUTHOR CONTRIBUTIONS

All authors listed have made a substantial, direct and intellectual contribution to the work, and approved it for publication.

FUNDING

Support for this work was provided by the National Aeronautics and Space Administration through Chandra Award Number AR7-18013 X issued by the Chandra X-ray Observatory Center, which is operated by the Smithsonian Astrophysical Observatory for and on behalf of the National Aeronautics Space Administration under contract NAS8-03060. EL is supported by a European Union COFUND/Durham Junior Research Fellowship (under EU grant agreement no. 609412).

REFERENCES

Baldwin, J. A. (1977). Luminosity indicators in the spectra of quasi-stellar objects. *Astrophys. J.* 214, 679–684. doi: 10.1086/155294

Betoule, M., Kessler, R., Guy, J., Mosher, J., Hardin, D., Biswas, R., et al. (2014). Improved cosmological constraints from a joint analysis of the SDSS-II and SNLS supernova samples. *Astron. Astrophys.* 568:A22. doi: 10.1051/0004-6361/201423413

Blandford, R. D., and McKee, C. F. (1982). Reverberation mapping of the emission line regions of Seyfert galaxies and quasars. *Astrophys. J.* 255, 419–439. doi: 10.1086/159843

Collier, S., Horne, K., Wanders, I., and Peterson, B. M. (1999). A new direct method for measuring the Hubble constant from reverberating accretion discs in active galaxies. *Month. Notices R. Astron. Soc.* 302, L24–L28. doi: 10.1046/j.1365-8711.1999.02250.x

du Mas des Bourboux, H., Le Goff, J.-M., Blomqvist, M., Busca, N. G., Guy, J., Rich, J., et al. (2017). Baryon acoustic oscillations from the complete SDSS-III Lyα-quasar cross-correlation function at $z = 2.4$. *ArXiv e-prints*.

Elvis, M., and Karovska, M. (2002). Quasar parallax: a method for determining direct geometrical distances to quasars. *Astrophys. J. Lett.* 581, L67–L70. doi: 10.1086/346015

Ghirlanda, G., Ghisellini, G., and Firmani, C. (2006). Gamma-ray bursts as standard candles to constrain the cosmological parameters. *New J. Phys.* 8:123. doi: 10.1088/1367-2630/8/7/123

Kilerci Eser, E., Vestergaard, M., Peterson, B. M., Denney, K. D., and Bentz, M. C. (2015). On the scatter in the radius-luminosity relationship for active galactic nuclei. *Astrophys. J.* 801:8. doi: 10.1088/0004-637X/801/1/8

Korista, K., Baldwin, J., and Ferland, G. (1998). Quasars as cosmological probes: the ionizing continuum, gas metallicity, and the W_λ-L relation. *Astrophys. J.* 507, 24–30. doi: 10.1086/306321

La Franca, F., Bianchi, S., Ponti, G., Branchini, E., and Matt, G. (2014). A new cosmological distance measure using active galactic nucleus X-ray variability. *Astrophys. J. Lett.* 787:L12. doi: 10.1088/2041-8205/787/1/L12

Lusso, E., Comastri, A., Vignali, C., Zamorani, G., Brusa, M., Gilli, R., et al. (2010). The X-ray to optical-UV luminosity ratio of X-ray selected type 1 AGN in XMM-COSMOS. *Astron. Astrophys.* 512:A34. doi: 10.1051/0004-6361/200913298

Lusso, E., and Risaliti, G. (2016). The tight relation between X-ray and ultraviolet luminosity of quasars. *Astrophys. J.* 819:154. doi: 10.3847/0004-637X/819/2/154

Lusso, E., and Risaliti, G. (2017). Quasars as standard candles. I. The physical relation between disc and coronal emission. *Astron. Astrophys.* 602:A79. doi: 10.1051/0004-6361/201630079

Marziani, P., and Sulentic, J. W. (2014). Highly accreting quasars: sample definition and possible cosmological implications. *Month. Notices R. Astron. Soc.* 442, 1211–1229. doi: 10.1093/mnras/stu951

Mortlock, D. J., Warren, S. J., Venemans, B. P., Patel, M., Hewett, P. C., McMahon, R. G., et al. (2011). A luminous quasar at a redshift of $z = 7.085$. *Nature* 474, 616–619. doi: 10.1038/nature10159

Pâris, I., Petitjean, P., Ross, N. P., Myers, A. D., Aubourg, É., Streblyanska, A., et al. (2017). The sloan digital sky survey quasar catalog: twelfth data release. *Astron. Astrophys.* 597:A79. doi: 10.1051/0004-6361/201527999

Peterson, B. M. (1993). Reverberation mapping of active galactic nuclei. *Publ. Astron. Soc. Pacific* 105, 247–268. doi: 10.1086/133140

Risaliti, G., and Lusso, E. (2015). A hubble diagram for quasars. *Astrophys. J.* 815:33. doi: 10.1088/0004-637X/815/1/33

Risaliti, G., and Lusso, E. (2017). Cosmology with AGN: can we use quasars as standard candles? *Astronomische Nachrichten* 338, 329–333. doi: 10.1002/asna.201713351

Rosen, S. R., Webb, N. A., Watson, M. G., Ballet, J., Barret, D., Braito, V., et al. (2016). The XMM-Newton serendipitous survey. VII. The third XMM-Newton serendipitous source catalogue. *Astron. Astrophys.* 590:A1. doi: 10.1051/0004-6361/201526416

Rudge, C. M., and Raine, D. J. (1999). Determining the cosmological parameters from the linewidths of active galaxies. *Month. Notices R. Astron. Soc.* 308, 1150–1158. doi: 10.1046/j.1365-8711.1999.02802.x

Shen, Y., Richards, G. T., Strauss, M. A., Hall, P. B., Schneider, D. P., Snedden, S., et al. (2011). A catalog of quasar properties from sloan digital sky survey data release 7. *Astrophys. J. Suppl.* 194:45. doi: 10.1088/0067-0049/194/2/45

Steffen, A. T., Strateva, I., Brandt, W. N., Alexander, D. M., Koekemoer, A. M., Lehmer, B. D., et al. (2006). The X-ray-to-optical properties of optically

selected active galaxies over wide luminosity and redshift ranges. *Astron. J.* 131, 2826–2842. doi: 10.1086/503627

Tananbaum, H., Avni, Y., Branduardi, G., Elvis, M., Fabbiano, G., Feigelson, E., et al. (1979). X-ray studies of quasars with the Einstein Observatory. *Astrophys. J. Lett.* 234, L9–L13. doi: 10.1086/183100

Wang, J. M., Du, P., Valls-Gabaud, D., Hu, C., and Netzer, H. (2013). Super-eddington accreting massive black holes as long-lived cosmological standards. *Phys. Rev. Lett.* 110:081301. doi: 10.1103/PhysRevLett.110.081301

Watson, D., Denney, K. D., Vestergaard, M., and Davis, T. M. (2011). A new cosmological distance measure using active galactic nuclei. *Astrophys. J. Lett.* 740:L49. doi: 10.1088/2041-8205/740/2/L49

Young, M., Elvis, M., and Risaliti, G. (2010). The X-ray energy dependence of the relation between optical and X-ray emission in quasars. *Astrophys. J.* 708, 1388–1397. doi: 10.1088/0004-637X/708/2/1388

Zamorani, G., Henry, J. P., Maccacaro, T., Tananbaum, H., Soltan, A., Avni, Y., et al. (1981). X-ray studies of quasars with the Einstein Observatory. II. *Astrophys. J.* 245, 357–374. doi: 10.1086/158815

Conflict of Interest Statement: The authors declare that the research was conducted in the absence of any commercial or financial relationships that could be construed as a potential conflict of interest.

Copyright © 2018 Bisogni, Risaliti and Lusso. This is an open-access article distributed under the terms of the Creative Commons Attribution License (CC BY). The use, distribution or reproduction in other forums is permitted, provided the original author(s) or licensor are credited and that the original publication in this journal is cited, in accordance with accepted academic practice. No use, distribution or reproduction is permitted which does not comply with these terms.

frontiers in Astronomy and Space Sciences

PERSPECTIVE
published: 15 December 2017
doi: 10.3389/fspas.2017.00059

Quasars as Cosmological Standard Candles

C. Alenka Negrete[1], Deborah Dultzin[2], Paola Marziani[3], Jack W. Sulentic[4], Donají Esparza-Arredondo[5], Mary L. Martínez-Aldama[4] and Ascensión Del Olmo[4]*

[1] CONACYT Research Fellow - Instituto de Astronomía, UNAM, Mexico City, Mexico, [2] Instituto de Astronomía, UNAM, Mexico City, Mexico, [3] INAF, Osservatorio Astronomico di Padova, Padua, Italy, [4] Instituto de Astrofísica de Andalucía, IAA-CSIC, Granada, Spain, [5] Instituto de Radioastronomía y Astrofísica, Morelia, Mexico

We propose the use of quasars with accretion rate near the Eddington ratio (extreme quasars) as standard candles. The selection criteria are based on the Eigenvector 1 (E1) formalism. Our first sample is a selection of 334 optical quasar spectra from the SDSS DR7 database with a S/N > 20. Using the E1, we define primary and secondary selection criteria in the optical spectral range. We show that it is possible to derive a redshift-independent estimate of luminosity for extreme Eddington ratio sources. Our results are consistent with concordance cosmology but we need to work with other spectral ranges to take into account the quasar orientation, among other constrains.

Keywords: quasars: general, quasars: emission lines, quasars: broad lines, quasar: extreme accretors, quasars: NLSy1

OPEN ACCESS

Edited by:
Gianluca Calcagni, Consejo Superior de Investigaciones Científicas (CSIC), Spain

Reviewed by:
Øyvind Geelmuyden Grøn, Oslo and Akershus University College, Norway
Zdenek Stuchlik, Silesian University in Opava, Czechia

****Correspondence:***
C. Alenka Negrete
alenka@astro.unam.mx

Specialty section:
This article was submitted to Cosmology, a section of the journal Frontiers in Astronomy and Space Sciences

Received: *23 August 2017*
Accepted: *27 November 2017*
Published: *15 December 2017*

Citation:
Negrete CA, Dultzin D, Marziani P, Sulentic JW, Esparza-Arredondo D, Martínez-Aldama ML and Del Olmo A (2017) Quasars as Cosmological Standard Candles. Front. Astron. Space Sci. 4:59. doi: 10.3389/fspas.2017.00059

1. INTRODUCTION

Active Galactic Nuclei (AGN or quasars) are among the most powerful objects in the Universe. They have been studied for more than 50 years. Their spectra and intrinsic properties, indicating intense nuclear activity, are widely diverse. In order to organize this diversity, Sulentic et al. (2000) proposed a parameter space, described by the Eigenvector 1 (E1, see e.g., Boroson and Green, 1992). The original E1 of Boroson and Green (1992) correlated the equivalent width (EW) of the low ionization line FeII between 4435 and 4685 Å, with the intensity peak of [OIII]λ5007. The parameter space proposed by Sulentic et al. (2000) correlates optical and X-Ray spectral parameters involving only broad lines: (1) the full width at half maximum of the broad component (BC) of Hβ FWHM(H$\beta_{\rm BC}$), (2) the ratio of the equivalent widths of FeII (described above) and H$\beta_{\rm BC}$, $R_{\rm FeII}$ = EW(FeII)/EW(H$\beta_{\rm BC}$), and (3) the photon index of the soft X-rays, Γ_{soft}. Subsequently, Sulentic et al. (2007) added the blue shifted component of CIVλ1549 a UV high ionization line, as a fourth dimension (4D) to the E1. This 4DE1 diagram for quasars is now understood to be driven mainly by the Eddington ratio ($L/L_{\rm Edd}$) and also by the BH mass (e.g., Marziani et al., 2001; Boroson, 2002; Ferland et al., 2009).

Sulentic et al. (2000) propose the presence of two main populations based on the optical plane (FWHM(H$\beta_{\rm BC}$) vs $R_{\rm FeII}$): Population A for quasars with FWHM(H$\beta_{\rm BC}$) < 4,000 km s^{-1}and Population B for those with FWHM(H$\beta_{\rm BC}$) > 4,000 km s^{-1} (Figure 1 of Sulentic et al., 2002). Their phenomenological study also shows that there are spectral characteristics that distinguish objects within the same population, especially those within Pop. A. For this reason, the optical plane of the E1 was subdivided into bins with ΔFWHM(H$\beta_{\rm BC}$) =4,000 km s^{-1}and $\Delta R_{\rm FeII}$ = 0.5. This created the bins A1, A2, A3, A4 defined as the $R_{\rm FeII}$ increases (Figure 1 of Sulentic et al., 2002). Thus, spectra belonging to the same bin are expected to have very similar characteristics.

In this article we will briefly illustrate how the scheme of Sulentic et al. (2000) may help solving one of the big challenges in cosmology, that is to measure distances in the Universe. The Hubble law can written as: v = c z = H D, where v is the recession velocity, and D is the proper distance. At low z, the factor H is constant and equal to H_0, the Hubble constant (e.g., Perlmutter et al., 1999). At higher z, H depends on both the cosmological model and the density parameter $\Omega = \Omega_M + \Omega_\Lambda$, where Ω_M is the density of matter and Ω_Λ is the energy density. So it is important to measure the cosmic matter density Ω_M in the distance range $1 < z < 4$. In this range, the effect of the cosmic matter density is believed to dominate over the repulsive effect of the cosmological constant.

There have been several works focused on measuring cosmological distances using different objects as standard candles. For example, cepheids, supernovae, extragalactic HII regions and clusters of galaxies (e.g., Perlmutter et al., 1999; Chávez et al., 2012, and references therein). These works have favored the model of a flat Universe ($\Omega_M + \Omega_\Lambda = 1$). At intermediate z, Terlevich et al. (2015) used 25 HII galaxies at z $\sim$ 2.3 to constrain Ω_M, however the dispersion obtained is larger than the one using supernovae. Another method to reach higher z ($\sim$3.5) involves the use of baryonic acoustic oscillations (BAOs) obtained from the database BigBOSS/DESI (Schlegel et al., 2011). Major surveys are tracking the BAOs as standard rulers. This is a technique that is fully independent from the classical discrete standard candles such as supernovae or HII regions.

In 2014, Marziani and Sulentic (2014) proposed the use of a specific type of quasars as standard candles. They studied objects that show extreme accretion near to the Eddington limit. In the super Eddington accretion regime, the geometrically and optically thick structure known as the "slim disk" is expected to develop (Abramowicz et al., 1988). Quasars hosting slim disks should radiate at a well defined limit because their luminosity is expected to saturate close to the Eddington luminosity even if the accretion rate becomes highly super-Eddington. We point out that there are works that analyze in full detail the structure of the accretion disk (AD) at different accretion regimes. Such an analysis implies varying thickness, optical depths and magnetic fields (Pugliese and Stuchlík, 2015, 2016). The black hole spin may also have an effect (Bardeen et al., 1972; Stuchlik, 1980). The spin is expected to play a role, not only by increasing the radiative efficiency, but also by displacing the Far UV peak toward shorter wavelength: the last stable inner radius is closer to the BH for a rotating black hole, implying a stronger FUV/soft X-ray emission with respect to the non rotating case. The detailed analysis of the AD structure and black hole spin however, goes beyond the scope of the present work. In the future we will consider different scenarios, including an analysis of the disk inclination. In conclusion, we propose that highly accreting quasars can be used as cosmological candles. The present work shows the results for an optical low redshift sample. An ultraviolet high-z sample (z $\sim$ 2.3) is discussed in the Martínez-Aldama et al., Submitted paper, also in this volume. All the computations were made considering $H_0 = 70\,\mathrm{km\,s^{-1}\,Mpc^{-1}}$ and a "concordance cosmology" with relative energy densities $\Omega_\Lambda = 0.72$ and $\Omega_M = 0.28$.

2. SAMPLE SELECTION

For our study, we used a sample of quasars chosen from the Sloan Digital Sky Survey Data Release 7 Shen et al. (2011), to identify the extreme accretors in the optical range at low redshift ($z < 0.8$). The identification of these quasars will follow the description of the E1 parameter space in the optical plane. That is, we isolated objects with $R_{\mathrm{FeII}} > 1$, belonging to Pops. A3, A4 and also some very extreme objects of Pop. A5 (with $R_{\mathrm{FeII}} > 2$).

We imposed the following filters to select only the objects with quality good enough to carry out our analysis:

1. $z < 0.8$ to cover the Hβ range, including the FeII blends around 4,570 and 5,260 Å.
2. S/N > 20 in the continuum at 5,100 Å.
3. $R_{\mathrm{FeII}} > 1$. To select objects with this condition, we performed automatic measurements using the IRAF task *splot* to estimate roughly the EW of FeII and Hβ.
4. No host galaxy contribution. The objects showing a strong contribution of the underlying galaxy were rejected.

This four criteria gave us a sample of 302 spectra.

3. METHODOLOGY

In order to isolate the "true" extreme accreting quasars, we made individual fits on the selected spectra using the *specfit* task of IRAF (Kriss, 1994). *Specfit* allows us to simultaneously fit all the components present in the spectrum: the underlying continuum, the FeII pseudo continuum and the emission lines. *Specfit* minimizes the χ^2 to find the best fit. The steps followed to accomplish identification, deblending, and measurement of the emission lines in each object are the following:

1. The continuum. We adopted a single power-law to describe the quasar continuum using the continuum windows around 4,430, 4,760, and 5,100 Å (see, e.g., Francis et al., 1991).
2. FeII template. We used the semi-empirical template by Marziani et al. (2009), obtained from a high resolution spectrum of I Zw 1, with a model of the FeII emission computed by a photoionization code in the range of Hβ.
3. Hβ broad emission line. For highly accreting Pop A objects, Hβ can be modeled with a sum of a Lorentzian profile in its rest frame plus a blue shifted gaussian (Marziani et al., 2009).
4. [OIII]$\lambda\lambda$4959,5007. We fitted this doublet with two Gaussians, considering: the ratio of theoretical intensities 1:3 (Dimitrijević et al., 2007), the same FWHM and the same line shift.

   Apart from these four parameters, in some cases it was necessary to add other emission lines. These extra emission lines could be strong and therefore obvious. In other cases, the emission lines are weak, but we can find and identify them in the residuals of the fit. These emission lines are:
5. Hβ narrow component, modeled similarly to [OIII]λ5007: with a Gaussian profile and with the same FWHM.
6. Hβ blue shifted component. This component would be associated with a non-virialized outflow in quasars with high

accretion rates (e.g., Marziani et al., 2013). We fitted this feature with a symmetric Gaussian.

7. [OIII]λλ4959,5007 semi broad component, also associated with outflows (Zamfir et al., 2010). It is characterized as being wider than the main component of [OIII]λλ4959,5007, and is generally shifted to the blue.
8. HeIIλ4686. In some objects it is detect as residual emission of the fit. We fitted it with a Gaussian component.

An example of the line fitting is shown in **Figure 1**. The upper panel shows the fit, and the lower panel under the fit shows the residuals. The upper abscissa is the rest frame wavelength in Å, the lower abscissa is in velocity units, and the ordinate is specific flux in arbitrary units. The vertical dashed lines are the rest frame for H$\beta_{\rm BC}$ and [OIII]λ5007. The purple long dashed line is the fit, solid black line is the H$\beta_{\rm BC}$. Grey lines are the [OIII]λλ4959,5007 narrow and semi broad components, the blue line is the Hβ blueshifted component. The green line is the FeII template.

4. EXTREME ACCRETORS AS STANDARD CANDLES

In order to isolate "true" extreme accreting quasars and avoid borderline/noisy objects, we impose tighter restrictions on the selected sample. On the one hand, we choose quasars with $R_{\rm FeII} > 1.2$, based on the typical $R_{\rm FeII}$ error at two sigma (one sigma is 0.1). On the other hand, we isolate only Pop. A objects, i.e., those ones with FWHM(H$\beta_{\rm BC}$) < 4,000 km s^{-1}. Finally, we selected objects with S/N strictly larger than 20.0 in the continuum. These restrictions, gave us an "extreme sample" of 117 objects. It is important to mention that in the beginning we were not able to impose these two conditions using the automatic measurements. The reason is that we would have introduced objects that are not extreme accretors, or reject some that really are extreme quasars.

As pointed out previously, the main hypothesis of Marziani and Sulentic (2014) to use extreme accretion quasars as standard candles is that they have the same intrinsic luminosity, or equivalently, similar physical conditions. The bolometric luminosity of a source radiating at the Eddington ratio $\lambda_{Edd} = L/L_{Edd}$ is proportional to the product λ_{Edd} times its black hole mass ($M_{\rm BH}$). If we consider virial motions,

$$L_{bol} = cte\,\lambda_{Edd}\,M_{BH} = cte\,\lambda_{Edd}\,f_s\,r_{BLR}\,(\delta v)^2\,G^{-1} erg\,s^{-1} \quad (1)$$

where cte = $10^{4.81}$, f_s is the structure factor, $r_{\rm BLR}$ is the the broad line region radius, δv is the virial velocity dispersion estimator and G the gravitational constant. There is a way to derive $r_{\rm BLR}$ independently of the quasar luminosity, based on the definition

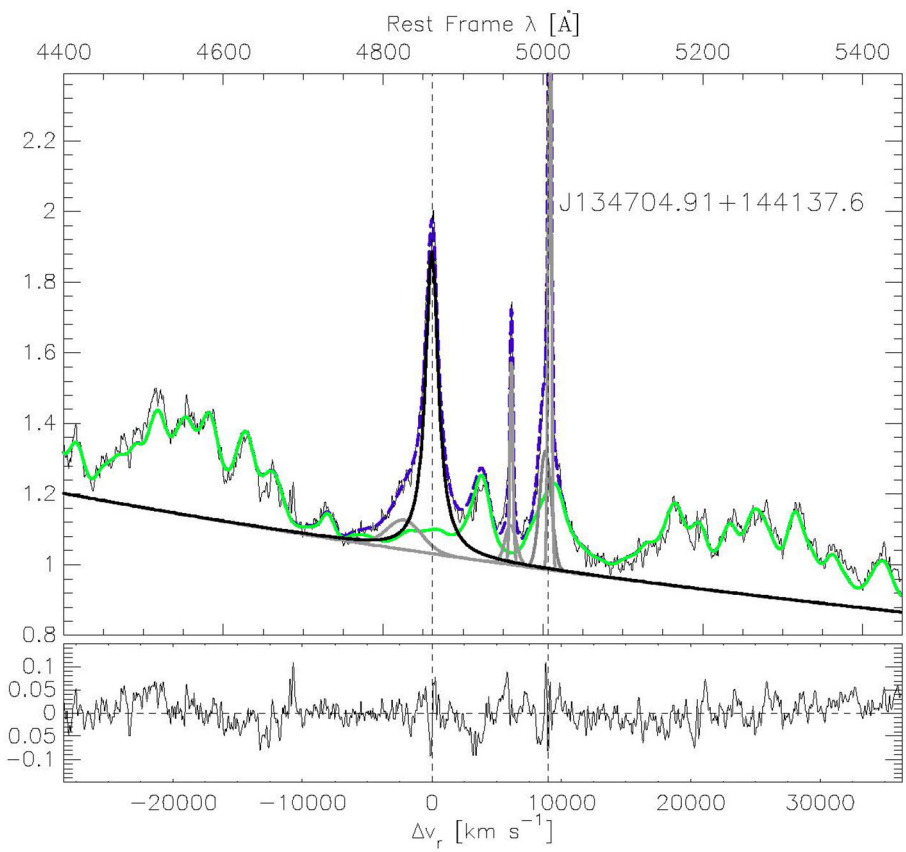

FIGURE 1 | Example of line decomposition for the quasar J134704.91+144137.6 using *specfit*. See text for description.

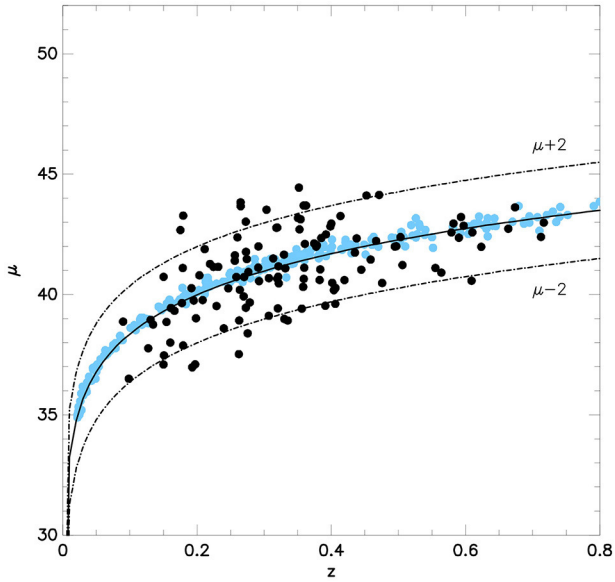

FIGURE 2 | Distance modulus of the "extreme sample" (black dots) and the Kessler et al. (2009) SDSS-II SN sample (cyan dots) with respect to the redshift. Solid curve is the expected distance modulus for the concordance cosmology, dash dotted lines are the distance modulus with a difference of ±2 in magnitude with respect to the solid curve.

of the ionization parameter U and described in detail in Negrete et al. (2012).

$$U = \frac{\phi}{4\,\pi\, n_H\, c\, r_{BLR}} \tag{2}$$

where $n_{\rm H}$ is the density, c is the light velocity and the number of ionizing photons $\phi = kL/h\nu_i$, with $k = 0.5$, ν_i the average frequency of the ionizing photons, and h the Planck constant. From Equation (2), $r_{\rm BLR}$ can be derived if we know the product of the ionization parameter times density

$$r_{BLR} = \left(\frac{kL}{4\,\pi\, n_H\, U\, c\, h\, \nu_i}\right)^{1/2}. \tag{3}$$

In Negrete et al. (2012) we showed that both, $n_{\rm H}$ and U, can be derived for individual objects using specific line ratios and CLOUDY photoionization models. In the case of the extreme accretors, we found a "typical" value of the product $n_{\rm H}{\rm U} = 10^{9.6}$ (see also Padovani and Rafanelli, 1988; Matsuoka et al., 2008). Inserting Equation 3 in Equation 1, we can derive a "virial luminosity" independent of redshift:

$$L(\nu) = 7.8X10^{44}\,\frac{\lambda^2_{Edd}\, k f_s^2\, \delta\nu^4}{h\,\nu_i\, n_H\, U}\; erg\, s^{-1}. \tag{4}$$

In order to prove the consistency of our luminosity z-independent estimates we calculate how the distance modulus depends on the redshift. The distance modulus is $\mu = 5\log(d_L/10{\rm pc})$. The luminous distance is $d_L = (L/4\pi f_\lambda)^{1/2}$, where $f_\lambda = BC\lambda f_\lambda/(1+z)^2$ is the continuum flux at $\lambda = 5{,}100$ Å, using the Bolometric Correction BC = 12.2 (Richards et al., 2006). The distance modulus can also be written as:

$$\mu = 2.5(logL(\nu) - logf_\lambda - 40.1). \tag{5}$$

Figure 2 shows the trend of our "extreme sample" in the distance modulus diagram (black points). We compare our results with a sample taken from the Sloan Digital Sky Survey (SDSS) II supernova (SN) survey (Kessler et al., 2009, cyan dots). The scatter of this Figure could be due to orientation. We found that the objects with broader FWHM(H$\beta_{\rm BC}$) are above the solid curve, while the narrower objects are placed below. This figure shows that the so called "virial luminosity" is in agreement with the concordance cosmology.

5. SUMMARY

We have shown that the 4DE1 proposed by Sulentic et al. (2000) is a very efficient diagram that organizes both observed and physical properties of broad line quasars. For low redshift objects ($z < 0.8$), we can use the optical parameter space, FWHM(H$\beta_{\rm BC}$) Vs. $R_{\rm FeII}$, to isolate the most extreme accreting quasars. The principal characteristics of these objects is that they are strong FeII emitters, i.e., they have $R_{\rm FeII} > 1$, and they have relatively narrow lines, with a FWHM(H$\beta_{\rm BC}$) $< 4{,}000$ km s^{-1}.

Based on the hypothesis that extreme accreting quasars should have the same intrinsic luminosity per unit mass, we test them as cosmological standard candles. Under several assumptions related to highly accreting objects, such as the physical conditions of the region close to the black hole, we computed a "virial luminosity" independent of z. With this luminosity we build the Hubble diagram which shows that the majority of the selected extreme quasars follow the trend of the distance modulus diagram.

In a forthcoming paper (Negrete et al., Submitted), we will give a detailed description of the selection of this sample, the methodology applied, a statistical analysis that includes the high-z sample, and the cosmological application to constrain Ω_M and Ω_Λ.

AUTHOR CONTRIBUTIONS

CN and DD wrote the paper. PM and JS contributed to the main idea of the paper. CN and DE-A made the fits and analyzed the sample. All the authors contributed to the discussion and revision of the paper.

FUNDING

DIPARTIMENTO DI FISICA E ASTRONOMIA, Università di Padova via Marzolo, 8, I-35131 Padova, Proceedings of the meeting "Quasars at all cosmic epoch", attn. Dr. Mauro D'Onofrio.

ACKNOWLEDGMENTS

CN and DD acknowledge support from grants IN107313 PAPIIT, DGAPA UNAM and CONACYT project 221398. CN acknowledge support from DGAPA-UNAM grants IN111514 and IN113417. DE-A and MM-A acknowledges the doctoral and postdoctoral grant from the CONACyT, respectively. MM-A and AD acknowledge financial support from Spanish Ministry for Economy and Competitiveness through grants AYA2013-42227-P and AYA2016-76682- C3-3-1-P.

REFERENCES

Abramowicz, M. A., Czerny, B., Lasota, J. P., and Szuszkiewicz, E. (1988). Slim accretion disks. *Astrophys. J.* 332, 646–658. doi: 10.1086/166683

Bardeen, J. M., Press, W. H., and Teukolsky, S. A. (1972). Rotating black holes: locally nonrotating frames, energy extraction, and scalar synchrotron radiation. *Astrophys. J.* 178, 347–370. doi: 10.1086/151796

Boroson, T. A. (2002). Black hole mass and eddington ratio as drivers for the observable properties of radio-loud and radio-quiet QSOs. *Astrophys. J.* 565, 78–85. doi: 10.1086/324486

Boroson, T. A., and Green, R. F. (1992). The emission-line properties of low-redshift quasi-stellar objects. *Astrophys. J. Suppl.* 80, 109–135. doi: 10.1086/191661

Chávez, R., Terlevich, E., Terlevich, R., Plionis, M., Bresolin, F., Basilakos, S., et al. (2012). Determining the Hubble constant using giant extragalactic H II regions and H II galaxies. *Month. Notices R. Astron. Soc.* 425, L56–L60. doi: 10.1111/j.1745-3933.2012.01299.x

Dimitrijević, M. S., Popović, L. Č., Kovačević, J., Dačić, M., and Ilić, D. (2007). The flux ratio of the [OIII] λλ5007, 4959 lines in AGN: comparison with theoretical calculations. *Month. Notices R. Astron. Soc.* 374, 1181–1184. doi: 10.1111/j.1365-2966.2006.11238.x

Ferland, G. J., Hu, C., Wang, J., Baldwin, J. A., Porter, R. L., van Hoof, P. A. M., et al. (2009). Implications of infalling Fe II-emitting clouds in active galactic nuclei: anisotropic properties. *Astrophys. J. Lett.* 707, L82–L86. doi: 10.1088/0004-637X/707/1/L82

Francis, P. J., Hewett, P. C., Foltz, C. B., Chaffee, F. H., Weymann, R. J., and Morris, S. L. (1991). A high signal-to-noise ratio composite quasar spectrum. *Astrophys. J.* 373, 465–470. doi: 10.1086/170066

Kessler, R., Becker, A. C., Cinabro, D., Vanderplas, J., Frieman, J. A., Marriner, J., et al. (2009). First-year sloan digital sky survey-II supernova results: hubble diagram and cosmological parameters. *Astrophys. J. Suppl.* 185, 32–84. doi: 10.1088/0067-0049/185/1/32

Kriss, G. (1994). Fitting models to UV and optical spectral data. *Astron. Data Anal. Softw. Syst.* 61, 437.

Marziani, P., and Sulentic, J. W. (2014). Highly accreting quasars: sample definition and possible cosmological implications. *Month. Notices R. Astron. Soc.* 442, 1211–1229. doi: 10.1093/mnras/stu951

Marziani, P., Sulentic, J. W., Plauchu-Frayn, I., and del Olmo, A. (2013). Low-ionization outflows in high eddington ratio quasars. *Astrophys. J.* 764:150. doi: 10.1088/0004-637X/764/2/150

Marziani, P., Sulentic, J. W., Stirpe, G. M., Zamfir, S., and Calvani, M. (2009). VLT/ISAAC spectra of the Hβ region in intermediate-redshift quasars. III. Hβ broad-line profile analysis and inferences about BLR structure. *Astron. Astrophys.* 495, 83–112. doi: 10.1051/0004-6361:200810764

Marziani, P., Sulentic, J. W., Zwitter, T., Dultzin-Hacyan, D., and Calvani, M. (2001). Searching for the physical drivers of the eigenvector 1 correlation space. *Astrophys. J.* 558, 553–560. doi: 10.1086/322286

Matsuoka, Y., Kawara, K., and Oyabu, S. (2008). Low-ionization emission regions in quasars: gas properties probed with broad O I and Ca II lines. *Astrophys. J.* 673, 62–68. doi: 10.1086/524193

Negrete, C. A., Dultzin, D., Marziani, P., and Sulentic, J. W. (2012). Broad-line region physical conditions in extreme population a quasars: a method to estimate central black hole mass at high redshift. *Astrophys. J.* 757:62. doi: 10.1088/0004-637X/757/1/62

Padovani, P., and Rafanelli, P. (1988). Mass-luminosity relationships and accretion rates for Seyfert 1 galaxies and quasars. *Astron. Astrophys.* 205, 53–70.

Perlmutter, S., Aldering, G., Goldhaber, G., Knop, R. A., Nugent, P., Castro, P. G., et al. (1999). Measurements of Ω and Λ from 42 High-redshift supernovae. *Astrophys. J.* 517, 565–586. doi: 10.1086/307221

Pugliese, D., and Stuchlík, Z. (2015). Ringed accretion disks: equilibrium configurations. *Astrophys. J. Suppl.* 221:25. doi: 10.1088/0067-0049/221/2/25

Pugliese, D., and Stuchlík, Z. (2016). Ringed accretion disks: instabilities. *Astrophys. J. Suppl.* 223:27. doi: 10.3847/0067-0049/223/2/27

Richards, G. T., Lacy, M., Storrie-Lombardi, L. J., Hall, P. B., Gallagher, S. C., Hines, D. C., et al. (2006). Spectral energy distributions and multiwavelength selection of type 1 quasars. *Astrophys. J. Suppl.* 166, 470–497. doi: 10.1086/506525

Schlegel, D., Abdalla, F., Abraham, T., Ahn, C., Allende Prieto, C., Annis, J., et al. (2011). The BigBOSS experiment. *ArXiv e-prints*

Shen, Y., Richards, G. T., Strauss, M. A., Hall, P. B., Schneider, D. P., Snedden, S., et al. (2011). A catalog of quasar properties from sloan digital sky survey data release 7. *Astrophys. J. Suppl.* 194:45. doi: 10.1088/0067-0049/194/2/45

Stuchlik, Z. (1980). Equatorial circular orbits and the motion of the shell of dust in the field of a rotating naked singularity. *Bull. Astron. Instit. Czechoslovakia* 31, 129–144.

Sulentic, J. W., Bachev, R., Marziani, P., Negrete, C. A., and Dultzin, D. (2007). C IV λ1549 as an eigenvector 1 parameter for active galactic nuclei. *Astrophys. J.* 666, 757–777. doi: 10.1086/519916

Sulentic, J. W., Marziani, P., and Dultzin-Hacyan, D. (2000). Phenomenology of Broad Emission Lines in Active Galactic Nuclei. *Annu. Rev. Astron. Astrophys.* 38, 521–571. doi: 10.1146/annurev.astro.38.1.521

Sulentic, J. W., Marziani, P., Zamanov, R., Bachev, R., Calvani, M., and Dultzin-Hacyan, D. (2002). Average quasar spectra in the context of eigenvector 1. *Astrophys. J. Lett.* 566, L71–L75. doi: 10.1086/339594

Terlevich, R., Terlevich, E., Melnick, J., Chávez, R., Plionis, M., Bresolin, F., et al. (2015). On the road to precision cosmology with high-redshift H II galaxies. *Month. Notices R. Astron. Soc.* 451, 3001–3010. doi: 10.1093/mnras/stv1128

Zamfir, S., Sulentic, J. W., Marziani, P., and Dultzin, D. (2010). Detailed characterization of Hβ emission line profile in low-z SDSS quasars. *Month. Notices R. Astron. Soc.* 403:1759. doi: 10.1111/j.1365-2966.2009.16236.x

Conflict of Interest Statement: The authors declare that the research was conducted in the absence of any commercial or financial relationships that could be construed as a potential conflict of interest.

Copyright © 2017 Negrete, Dultzin, Marziani, Sulentic, Esparza-Arredondo, Martínez-Aldama and Del Olmo. This is an open-access article distributed under the terms of the Creative Commons Attribution License (CC BY). The use, distribution or reproduction in other forums is permitted, provided the original author(s) or licensor are credited and that the original publication in this journal is cited, in accordance with accepted academic practice. No use, distribution or reproduction is permitted which does not comply with these terms.

frontiers in Astronomy and Space Sciences

ORIGINAL RESEARCH
published: 19 January 2018
doi: 10.3389/fspas.2017.00065

Highly Accreting Quasars at High Redshift

Mary L. Martínez-Aldama[1], Ascensión Del Olmo[1], Paola Marziani[2], Jack W. Sulentic[1], C. Alenka Negrete[3], Deborah Dultzin[4], Jaime Perea[1] and Mauro D'Onofrio[5]*

[1] Instituto de Astrofísica de Andalucía, IAA-CSIC, Granada, Spain, [2] INAF, Osservatorio Astronomico di Padova, Padova, Italy, [3] CONACYT Research Fellow, Instituto de Astronomía, Universidad Nacional Autónoma de México, Mexico City, Mexico, [4] Instituto de Astronomía, Universidad Nacional Autónoma de México, Mexico City, Mexico, [5] Dipartimento di Fisica Astronomia "Galileo Galilei", University of Padova, Padova, Italy

We present preliminary results of a spectroscopic analysis for a sample of type 1 highly accreting quasars ($L/L_{Edd} \sim 1.0$) at high redshift, $z \sim$2–3. The quasars were observed with the OSIRIS spectrograph on the GTC 10.4 m telescope located at the Observatorio del Roque de los Muchachos in La Palma. The highly accreting quasars were identified using the 4D Eigenvector 1 formalism, which is able to organize type 1 quasars over a broad range of redshift and luminosity. The kinematic and physical properties of the broad line region have been derived by fitting the profiles of strong UV emission lines such as AlIIIλ1860, SiIII]λ1892 and CIII]λ1909. The majority of our sources show strong blueshifts in the high-ionization lines and high Eddington ratios which are related with the productions of outflows. The importance of highly accreting quasars goes beyond a detailed understanding of their physics: their extreme Eddington ratio makes them candidates standard candles for cosmological studies.

Keywords: quasars: emission lines, quasar: UV spectrum, quasars: outflows, quasars: supermassive black holes, galaxy evolution: feedback

OPEN ACCESS

Edited by:
Fabio La Franca, Università degli Studi Roma Tre, Italy

Reviewed by:
Alessandra De Rosa, Istituto Nazionale di Astrofisica (INAF), Italy
Michele Perna, Osservatorio Astrofisico di Arcetri (INAF), Italy

****Correspondence:***
Mary L. Martínez-Aldama
maryloli@iaa.es

Specialty section:
This article was submitted to Milky Way and Galaxies, a section of the journal Frontiers in Astronomy and Space Sciences

Received: *27 September 2017*
Accepted: *12 December 2017*
Published: *19 January 2018*

Citation:
Martínez-Aldama ML, Del Olmo A, Marziani P, Sulentic JW, Negrete CA, Dultzin D, Perea J and D'Onofrio M (2018) Highly Accreting Quasars at High Redshift. Front. Astron. Space Sci. 4:65. doi: 10.3389/fspas.2017.00065

1. 4DE1 MAIN SEQUENCE

The 4D Eigenvector 1 (4DE1) formalism has been successful in arranging the type 1 AGN based on their spectral properties (Sulentic et al., 2000). Four observational parameters define four dimensions of the Eigenvector 1: the full width at half maximum (FWHM) of Hβ broad component (Hβ_{BC}), the strength of optical FeII blend at 4570Å described by the ratio $R_{FeII} = I(FeII)/I(H\beta_{BC})$, the velocity shift of the CIVλ1549 profile, and soft X-ray photon index (Γ_{soft}). The main correlation between these properties is provided by the optical parameters, FWHM(Hβ_{BC}) and the R_{FeII}, which define the 4DE1 optical plane.

Changes in the spectroscopic features at FWHM(Hβ) = 4,000 km s^{-1} causes the identification of two populations: A and B. Sources with FWHM(Hβ) $\leq$ 4,000 km s^{-1} are cataloged as population A. In this population the broad component (BC) of the low-ionization emission lines (LIL; ionization potential IP $\lesssim$ 20 eV) can be very well-model by a Lorentzian profile, for example in the case of Hβ emission. They also show a high intensity of FeII, large asymmetries in the high ionization lines (HIL; IP > 40 eV), like CIVλ1549, and an excess in the soft X-rays region. The majority of them are radio quiet sources. On the other hand, population B sources have a broader profile (FWHM; Hβ_{BC}) > 4,000 km s^{-1}). In this population the Hβ emission is redward asymmetric and it is modeled with two gaussian profiles. One of them corresponds to the BC located at the rest-frame, and the other is associated with a redshifted very broad component (VBC), which reaches widths

$\sim$10,000 km s^{-1}. The FeII intensity in these sources is weak and there is no large asymmetries in the HIL profiles. The domain at FWHM > 4,000 km s^{-1} is mostly populated by radio loud objects (Zamfir et al., 2010).

Along optical 4DE1 diagram we find different subpopulations (Sulentic et al., 2002), which are shown in the left panel of the **Figure 1**. Population A bins (A1, A2, A3, and A4) are based on the increment of the FeII intensity, $\Delta R_{FeII} = 0.5$. A1 sources have a lower contribution of FeII, than A4 sources. Whereas population B bins (B1, B1^{+}, B1^{++}, and B2) varying according to a width increment of ΔFWHM(Hβ_{BC}) = 4,000 km s^{-1}. For example, B1^{++} sources have a large width than the B1. Indeed, population B bins can be also defined in terms of the R_{FeII}, for example the B2 population has a $0.5 \leq R_{FeII} \leq 1.0$ and $4{,}000 \leq$ FWHM(Hβ_{BC}) $\leq$ 8,000 km s^{-1}.

Moving along the 4DE1 optical sequence, we find a well-organized variation of the physical properties like the black hole mass (M_{BH}), electronic density (n_H), ionization parameter (U) or dimensionless accretion rate ($\dot{m}$) (Marziani et al., 2001, 2010). For example, the most extreme B sources, the B1^{++}, have a high black hole mass and a small dimensionless accretion rate compared with the most extreme for the population A, the A4 population. Then, the 4DE1 could be considered as an evolution diagram for type 1 AGN, which could be driven by the Eddington ratio, L/L_{Edd} (Marziani et al., 2001; Shen and Ho, 2014; Fraix-Burnet et al., 2017). Updated results of the 4DE1 are found in Marziani et al. in this volume.

1.1. Extreme Radiating Sources along 4DE1

In each 4DE1 subpopulations we have identified specific properties. In this paper we focus on A3 and A4, which represent the 10% of the population A sources (Zamfir et al., 2010; Shen et al., 2011). In the optical range the main feature presented is the strong intensity of FeII at λ4570Å (Bachev et al., 2004), while in the UV the CIVλ1549 emission line frequently shows a blueshifted component with a shift respect to the rest-frame of $\Delta v_r < -1{,}000$ km s^{-1} (Sulentic et al., 2007).

A prototype A3 source at low redshift is I ZW 1 with $z \approx 0.0605$, $R_{FeII} = 1.3 \pm 0.1$, log $L/L_{Edd} \approx -0.11 \pm 0.17$; and a shift respect to the rest-frame of CIVλ1549 $\Delta v_r < -1{,}670 \pm 100$ km s^{-1} (Boroson and Green, 1992; Negrete et al., 2012; Marziani and Sulentic, 2014). Within 4DE1 formalism, A3 and A4 sources have been cataloged as xA by Marziani and Sulentic (2014). Left panel of **Figure 1** shows the area occupied by the xA sources in the 4DE1 optical plane.

Using optical and UV samples with around $\sim$60 sources in each spectral range (Bachev et al., 2004; Negrete et al., 2013; Marziani and Sulentic, 2014), we have recognized selection criteria to identify xA sources:

1. $R_{FeII} > 1$
2. AlIIIλ1860/SiIII]λ1892 ≥ 0.5
3. CIII]λ1909/SiIII]λ1892 ≤ 1.0

The optical criterion is commonly used in sources with low redshift ($z < 1.0$), while the UV one helps to identify xA sources at high redshift due to the limit of the detectors to observe the optical region. Both criteria are satisfied at the same time, they have been tested in a wide redshift range, $z = 0.4$–3.0 (Bachev et al., 2004; Negrete et al., 2013; Marziani and Sulentic, 2014).

Another important feature is the high Eddington ratio shown by the xA sources, $L/L_{Edd} > 0.2$ (Marziani and Sulentic, 2014). The high Eddington ratio reached could be associated with a slim disk, with a geometrically and optically thick structure. It could be formed in an advection-dominated accretion flow and

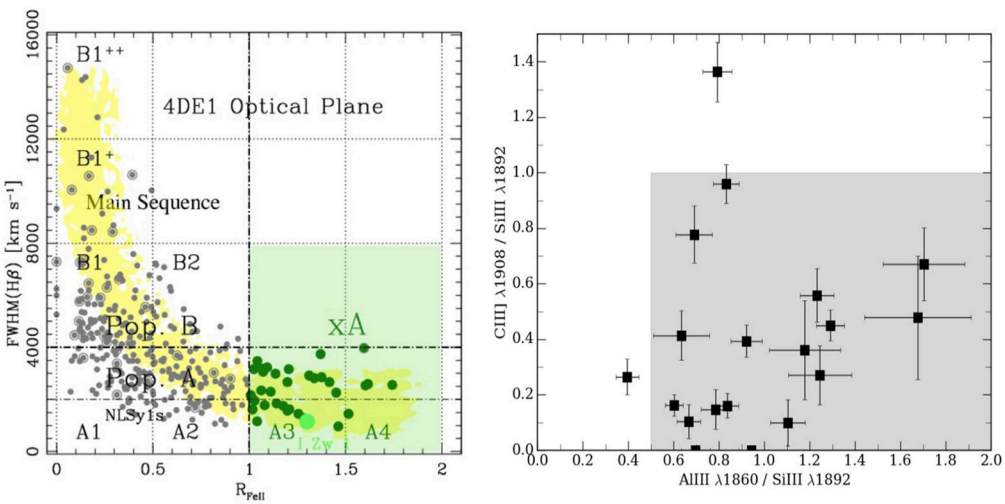

FIGURE 1 | (Left) 4DE1 Optical Plane. Data belong to a sample of 470 bright low-z QSOs from Zamfir et al. (2010). The plane is divided in bins according to Sulentic et al. (2002). xA sources (green dots) are located inside the green square defined by $R_{FeII} \geq 1$ and FWHM(Hβ_{BC}) $\leq$ 8,000 kms^{-1}. The greenyellow dot indicates the position of I Zw 1. Gray dots correspond to the rest of the population A and B. The yellow shadow marks the 4DE1 optical sequence. **(Right)** Distribution of the xA candidates sample (black squares) in the plane defined by the flux ratios Al III λ1860/Si III]λ1892 and C III]λ1909/Si III]λ1892 obtained from the measurements done with the GTC spectra. The gray area corresponds to the area occupied by the xA sources according to previous studies.

it could trigger the strong outflows observed in these objects (Abramowicz et al., 1988; Abramowicz and Straub, 2014). The strong relation between the high L/L_{Edd} and strong asymmetries observed in the xA sources points out that probably L/L_{Edd} is the driver of winds/outflows (Sulentic et al., 2017).

On the other hand, if the accretion rate is close the Eddington limit ($L/L_{Edd} = 1$), the dependency of the Eddington rates with the black holes mass is weak and then these sources can be used as standard candles, and help possibly determine cosmological parameters (Marziani and Sulentic, 2014; Wang et al., 2014).

With the purpose to analyze the behavior of xA objects, we observe a sample of 19 quasars in the UV region at high redshift using the GTC telescope. They were analyzed performing multicomponent fits (Section 2). We find a different behavior between the intermediate and high-ionization lines, which reveals the different structures presented in the the broad line region and their relation with the accretion disk (Section 3). In the Section 4 are presented our main results.

2. THE EXTREME ACCRETING SAMPLE

2.1. Sample Selection

With the purpose of analyzing the behavior of highly accreting sources, we observed a sample of 19 quasars with a redshift $2.05 < z < 2.98$. Marziani and Sulentic (2014) extracted spectra for ∼3,000 sources from SDSS DR6 with coverage of the 1900Å blend mainly composed by AlIIIλ1860, SiIII]λ1892 and CIII]λ1909 ($2.0 < z < 2.6$). They performed a multicomponent analysis considering the selection criteria previously described to select xA candidates. Some of these objects did not have the appropriated S/N > 15 to be included in their analysis, then they were observed with the Gran Telescopio de Canarias (GTC). The 19 objects presented in this work belong to a sample of 49 quasar. In the right panel of **Figure 1** is presented the distribution of our sample in the CIII]λ1909/SiIII]λ1892 vs. AlIIIλ1860/SiIII]λ1892 UV plane computed from the GTC spectra. They gray region indicates the zone were xA objects are located. The GTC spectra have a good S/N and verify the results previously obtained from the SDSS spectra analyzed by Marziani and Sulentic (2014).

The xA source candidates were observed with the OSIRIS spectrograph (Sánchez et al., 2012) mounted on the GTC, located at the Observatorio del Roque de los Muchachos in La Palma, Canary Islands, Spain. We used a slit of 0.6″ and according to redshift of the source, we use a R1000B or R1000R grisms with a spectral dispersion of 2.1 and 2.6 Å per pixel, respectively. The UV spectral range covers by our source at rest-frame is from 1150 to 2400 Å.

2.2. Data Reduction and Redshift Determination

The data reduction was done using the IRAF routines. Spectra were corrected by biases and flats field taken every night. The wavelength calibration was done using Hg+Ar and Ne arc lamps and the flux calibration was carried out using spectrophotometric standard stars. The spectra were corrected by telluric absorption and atmospheric differential refraction.

We have estimated the reddening of the sources, parametrized by the color excess E(B-V), by fitting its UV continuum with the template corresponding to the composite FIRST Bright Quasar Survey spectrum (FBQS; Brotherton et al., 2001) and excluding the regions of broad emission lines. To redden the template we used a Small Magellanic Cloud (SMC) extinction law (Gordon and Clayton, 1998; Gordon et al., 2003) with a RV = 3.07, as it is normally used as an appropriate reddening law in QSOs (York et al., 2006).

To perform the redshift correction, we apply an iterative measurements using three different methods to get a good approximation. The first two were done using isolated emission lines observed in our spectra, CII λ1335, OI λ1305 and SiIIλ1816. In the first one we model independently the line profiles using the MK1DSPEC routine to get a first approximation. In the second one we repeat the process, but employing the SPLOT task. In the third method we apply the last correction using the 1900Å blend lines: AlIIIλ1860 and SiIII]λ1892. Although these lines are blended with the CIII]λ1909 and some FeIII transitions, their high intensity permits a good approximation to the redshift.

2.3. Multicomponent Fits

In the UV range covered by our spectra we observe intermediate (IP ∼ 20–40 eV) and high-ionization lines (IP > 40 eV), which gives us the opportunity to analyze the behavior of different ionic species at the same time. In order to analyze the lines emitted in the covered spectral range, we perform multicomponent fits using the SPECFIT routine from IRAF (Kriss, 1994). This routine fits at the same time different kind of continuum, and emission/absorption lines. The best model is the one with the minimum χ^2 found for the global fit.

For the analysis we divided the observed spectral range in three zones, which are centered in the most important emission lines for our work:

- REGION 1: 1700–2200 Å, this range is dominated by the 1900Å blend which is composed by AlIIIλ1860, SiIII]λ1892, CIII]λ1909 and some FeIII transitions, and in the blue side are detected SiIIλ1816 and NIII]λ1750.
- REGION 2: 1450–1700 Å, the CIVλ1549 emission line dominates this zone and is accompanied by HeIIλ1640, OIII]1664 and AlII]λ1670.
- REGION 3: 1300–1450 Å, in this region the dominated emission is SiIVλ1397 + OIV]λ1402, which is accompanied by SiIIλ1304, OI λ1305 and CII λ1335.

The left panel of the **Figure 2** shows the spectrum of the quasar SDSSJ110022.53 + 484012.6 with $z = 2.08$ and $\log L_{Bol} = 46.17$ erg s^{-1}, as an example of the sources in our sample.

The main continuum source in the UV region is coming from the accretion disk (Malkan and Sargent, 1982; Malkan, 1983). A single powerlaw should be useful to model the observed spectral range, however due to the presence of intergalactic gas the continuum form can be flattened. In some cases we can fit with a single powerlaw or a linear continuum all the spectra range (1300–2200 Å). In the rest of the cases, we fit local continuums in three zones previously described. Details of the components fitted are explained in the next lines.

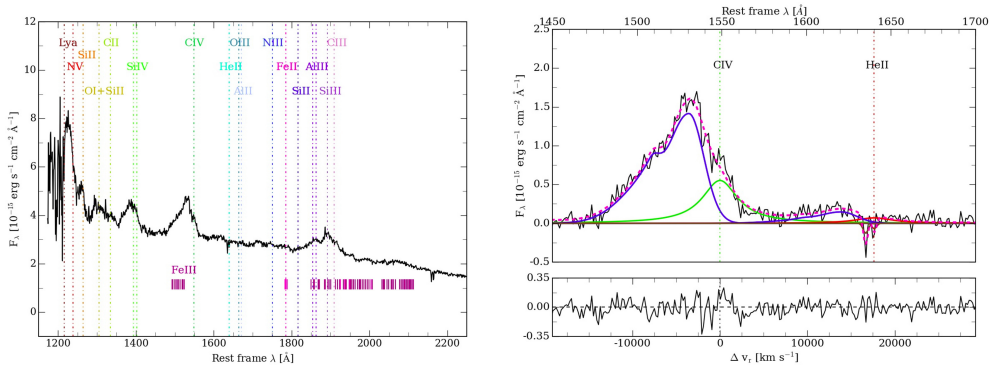

FIGURE 2 | (Left) SDSSJ110022.53+484012.6 spectrum before continuum subtraction. The vertical lines indicate the rest-frame of emission line in the observed spectral range. Small magenta vertical lines represent the FeIII contribution along the spectral range. **(Top right)** CIVλ1549 spectrum after continuum subtraction. Dashed magenta line indicates the fit to the whole spectrum. The green and red lines indicate the broad component of the CIVλ1549 and HeIIλ1640 respectively, while the blue ones represent the blueshifted component associated with each emission. The vertical lines mark the rest-frame of the CIV and HeII. The brown lines mark the absorption lines fitted. **(Bottom right)** Residual of the fit. In both panels, abscissae are rest-frame wavelength in Å and ordinates are rest-frame specific flux in units of 10^{-15} erg s^{-1} cm^{-2} Å^{-1}.

REGION 1. AlIIIλ1860, SiIII]λ1892 and CIII]λ1909 are intermediate-ionization lines (IIL) and according to Negrete et al. (2012) they can be well-modeled by Lorentzian profiles. The flux of the three lines vary freely. The FWHM associated with AlIII and SiIII] was taken equal, while the one of CIII] is free. The considerations about the FWHM of the lines are based on the physical properties where the lines are emitted, see Section 3.1. SiIIλ1816 and NIII]λ1750 were also modeled with Lorentzian profiles, and the flux and FWHM vary freely. All the Lorentzian profiles were fixed at the rest-frame.

The FeII has an important contribution around 1715 and 1785 Å. We tried to use the templates available in the literature (Bruhweiler and Verner, 2008; Mejía-Restrepo et al., 2016), however we can not reproduce the observed contribution. Therefore, we decided to fit isolated Gaussian profiles at 1715 and 1785 Å. The flux and FWHM vary freely.

The FeIII emission is an important contribution, mainly in the red side of the 1900Å blend. We modeled the emission of this ion with the Vestergaard and Wilkes (2001) template, and we include an extra component at 1914 Å such as Negrete et al. (2012) have done. However, around 2020 and 2080 Å we had to include extra gaussians to get a good fit. The flux and FWHM vary freely.

REGION 2. This zone is dominated by the high ionization line CIVλ1549. The broad component (BC) is modeled by a Lorentzian profile fixed at the rest-frame. The flux of the BC is free and the FWHM is the same that the shown by AlIIIλ1860 and SiIII]λ1892. In our sample all the CIVλ1549 profiles present a blueshifted asymmetry, to model it we used one or two blueshifted asymmetric gaussian profiles. The flux, FWHM, asymmetry and shift vary freely. Some of our objects are strongly affected by absorption lines, they were modeled using gaussian profiles without any constrain. Four object are Broad Absorption Lines (BAL) and 6 of them are mini-BAL. A wide analysis about this topic will be present in an upcoming paper.

HeIIλ1640 was modeled in a similar form that CIVλ1549, using a Lorentzian and skew Gaussians profiles for the BC and blueshifted components, respectively. The FWHM, shift and asymmetry were taken similar, but the flux varies freely. OIII]λ1664 and AlII]λ1670 were also modeled with Lorentzian profiles at the rest-frame, and the flux and FWHM vary freely.

REGION 3. This range is governed by the SiIVλ1397 + OIV]λ1402 blend. It is composed by two high-ionization lines. They are expected to shows a blueshifted, asymmetric profile. The broad component was modeled with the same conditions than CIVλ1549, but the flux is varying freely. In some cases the shift of the blueshifted lines were taken similar, but in other sources is independent due to the presence of absorption lines that affect the SIV profile.

An example a multicomponent fit for the CIV spectral range is shown in the right panel of the **Figure 2**. In a upcoming paper we will present the rest of the sample and a full analysis.

3. RESULTS

3.1. Intermediate-Ionization Lines

As the 4DE1 has found in previous samples, there is a significant change in properties shown by ionic species with different ionization potentials. We confirm this fact in the intermediate and high-ionization lines present in our sample. Intermediate-ionization lines AlIIIλ1860 and SiIII]λ1892 show symmetric profiles. Therefore the region where these lines are emitted is governed by virial motions. However, the quasar SDSSJ084036.16+235524.7 present a blueshifted component associated with the 1900Å blend with a centroid half maximum of $c(\frac{1}{2}) \sim -1{,}778$ km s^{-1}. A similar behavior, but in a extreme case is also presented by HE0359-3959, a high luminosity and redshift quasar, who present a blueshifted component of $c(\frac{1}{2}) \sim -6{,}000$ km s^{-1} (Martínez-Aldama et al., 2017). Then, the emitter region where the IIL are produced could be affected by radiation forces (Marziani et al., 2017).

In ∼35% of the sample the CIII]λ1909 shows intensity less than 20% compared with the ones observed in the AlIIIλ1860

and SiIII]λ1892. It indicates that either CIII] is not emitted by the same region or the ion is suppressed. The critical electronic density (n_e) of this semi-forbidden line is $n_e = 10^{10}$ cm^{-3} (Osterbrock and Ferland, 2006) and according to the models done by Negrete et al. (2013) AlIIIλ1860 and SiIII]λ1892 are emitted by regions with $n_H > 10^{11}$ cm^{-3}. It means that CIII]λ1909 is suppressed in this zone. On the other hand, the FWHM of CIII]λ1909 is lower than that shown by other lines, which points it out that the line is emitted in a external region than AlIIIλ1860 and SiIII]λ1892.

3.2. High-Ionization Lines

To measure the contribution of blueshifted components associated with high-ionization lines, we use the centroid at half intensity of the total profile, c(1/2). Left panel of **Figure 3** shows the distribution of the centroid c(1/2) for the most representative high-ionization line in our sample, the CIVλ1549 emission. We observe that ∼90% of our sample has blueshifts larger than −1,000 km s^{-1}, which reflects the presence of strong winds/outflows. A consistent trend is also found for blueshifted components of HeIIλ1640 and SiIVλ1397.

Two of the objects in the sample not satisfy the selection criteria, although these objects show xA properties. Therefore, they can be considered like borderline objects. These objects present a high contribution of CIII]λ1909, which could be related with a change in physical properties (primarily gas density) of the broad line region, as further discussed below.

Right panel of **Figure 3** shows the flux ratio between the flux associated with the blueshifted component and the total flux (Blue + BC) of the CIVλ1549 emission; $F(CIV_{Blue})/F(CIV_{Total})$. A relationship between the flux ratios and the centroid c(1/2) is clearly observed. If the contribution of the blue component is high, the centroid c(1/2) value also is. This relation has been previously found by Sulentic et al. (2017). Adding the information from Hβ and FeII they conclude that the blueshifted component has an important contribution: it is responsible for the blueshift and the additional broadening of the CIVλ1549 line to respect to the low-ionization line.

Sulentic et al. (2017) studied a sample of Population A and B sources. They clarify the different between the two populations. If we compared the behavior of their Population A object, we find only one xA source. There is a change from a spectroscopic behavior, which could be related with changes in the physical parameters of the broad line region as Negrete et al. (2012) and Martínez-Aldama et al. (2017) have found in these kind of objects high densities (n_H $\sim 10^{11-13}$ cm^{-3}) and low-ionization parameters (log U ~ -3), which enhanced the behavior of lines like AlIIIλ1860, and diminish the presence of lines like CIII]λ1909.

3.3. xA Sources and the Eddington Ratio

According to UV selection criteria at least 90% of our objects are highly accreting AGN. As we mentioned, one of the main important features is the presence of blueshifted components in all of our sources. In some cases the radiation forces reflected by prominent asymmetries are strong. In the **Figure 4** is presented the behavior of the centroid c(1/2) as a function of Eddington ratios. The Eddington ratios were computed via the mass black hole relation reported by Vestergaard and Peterson (2006) considering the FWHM of AlIIIλ1860 (Negrete et al., 2012), and the luminosity at 1350 Å. We present the estimations before and after the reddening correction. We have included two other samples with population A and B sources to compare the behavior of our data (Sulentic et al., 2004, 2006, 2007; Marziani et al., 2009; Marziani and Sulentic, 2014). The red dots correspond to population B sources, while the blue ones are population A; the blue diamonds indicate the sample presented in this paper. As we observe, population B objects of high luminosity show c(1/2) > −1,000 km s^{-1} and $L/L_{Edd} < 0.2$. Whereas the pop. A tends to have larger values and high L/L_{Edd}; even some of them

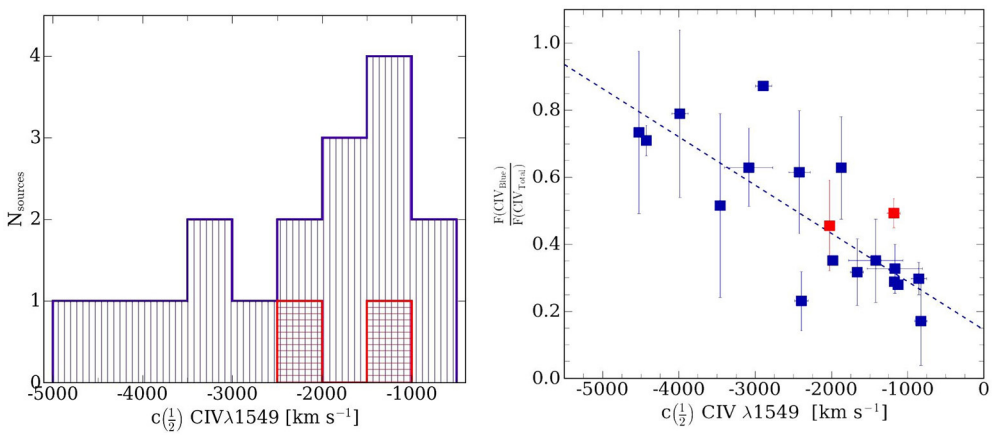

FIGURE 3 | (Left) Distribution of the centroid at half intensity, c(1/2), for the extreme radiating sample. Blue distribution indicates the sources that satisfied the criteria selection. Red distribution is the one associated with the borderline quasars. **(Right)** Relation between the centroid c(1/2) and the flux ratio of the blueshifted component respect to the total profile of CIVλ1549, $F(CIV_{Blue})/F(CIV_{Total})$. The color of the squares are the same that the left panel. The blue dashed line indicates the least-squares (LSQ) best fit.

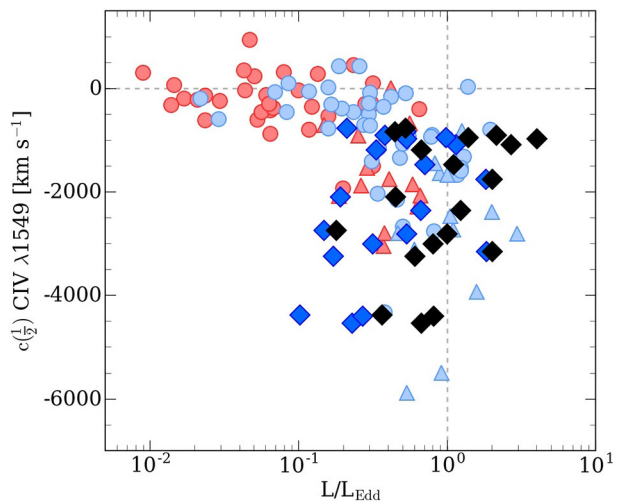

FIGURE 4 | Centroid at half intensity, c(1/2), as function of the Eddington ratio, L/L_{Edd}. The red dots correspond to the population B sources, while the blue ones indicate the population A sources. The highly accreting sample is indicated by blue and black diamonds, the first ones correspond before reddening correction, the second ones after. The origin of the rest of the data are indicated in the text. The black dashed horizontal line indicates c(1/2) = 0 km s^{-1} (any asymmetry), while the vertical corresponds to the L/L_{Edd} = 1.0.

are supper-Eddington sources, $L/L_{Edd} > 1$. Our sample covers very well the region described by the population A. It shows high asymmetries c(1/2) $< -1{,}000$ km s^{-1} and high Eddington ratios, $L/L_{Edd} > 0.2$. This result is in agreement with previous results (see Sulentic et al., 2017 and references therein).

It has been proposed that highly accreting sources host a geometrically and optically thick accretion disk called "slim" (Abramowicz et al., 1988; Elvis, 2000; Proga, 2007; Abramowicz and Straub, 2014). This structure in the inner region contains a narrow funnel, which produces anisotropy radiation that increases as the accretion rate (Sądowski et al., 2014; Wang et al., 2014).

If the accretion rate is close to the Eddington limit ($L/L_{Edd} = 1$), the dependency of the Eddington rates with the black holes mass is weak and then these sources could be used as standard candles to determine cosmological parameters (Marziani and Sulentic, 2014; Wang et al., 2014). From the observational point of view, our sample satisfies the conditions to host a slim disk, which could be associated with the observed behavior of the different ionic species in the BLR. In an upcoming paper we will discuss this issue in depth.

4. CONCLUSIONS

Based on the properties observed in our sample, like strong outflows in the high-ionization lines or high Eddington ratios, we proved that at least 90% of our sample is populated by highly accreting sources, which shows that the 4DE1 formalism is a good discriminator of the AGN class. In our sample we observe a different behavior for intermediate and high-ionization lines. The main features are observed in high-ionization lines, which are affected by strong outflow/winds. In some cases the intermediate-ionization lines, like AlIIIλ1860, are also affected by radiation forces. Centroid at half intensity values (c(1/2) $< -1{,}000$ km s^{-1}) indicate the presence of strong blueshifted, which lead to consider our sample populated by xA sources. On the other hand, the sample tends to show high Eddington ratios, which are related with the strong asymmetries of the high ionization lines.

AUTHOR CONTRIBUTIONS

MM-A: data reduction, multicomponents fits, analysis, writing, revision. AD: data reduction, analysis, revision. PM: analysis, revision. CN: analysis, revision. DD: writing, revision. JP: analysis, revision. JS: revision. MD: revision.

ACKNOWLEDGMENTS

MM-A acknowledge the postdoctoral grant from the CONACyT. MM-A and AD acknowledge financial support from Spanish Ministry for Economy and Competitiveness through grants AYA2013-42227-P and AYA2016-76682-C3-3-1-P.

REFERENCES

Abramowicz, M. A., Czerny, B., Lasota, J. P., and Szuszkiewicz, E. (1988). Slim accretion disks. *Astrophys. J.* 332, 646–658. doi: 10.1086/166683

Abramowicz, M. A., and Straub, O. (2014). Accretion discs. *Scholarpedia* 9:2408. doi: 10.4249/scholarpedia.2408

Bachev, R., Marziani, P., Sulentic, J. W., Zamanov, R., Calvani, M., and Dultzin-Hacyan, D. (2004). Average ultraviolet quasar spectra in the context of eigenvector 1: a baldwin effect governed by the eddington ratio? *Astrophys. J.* 617, 171–183. doi: 10.1086/425210

Boroson, T. A., and Green, R. F. (1992). The emission-line properties of low-redshift quasi-stellar objects. *Astrophys. J. Suppl.* 80, 109–135. doi: 10.1086/191661

Brotherton, M. S., Tran, H. D., Becker, R. H., Gregg, M. D., Laurent-Muehleisen, S. A., and White, R. L. (2001). Composite Spectra from the FIRST Bright Quasar Survey. *Astrophys. J.* 546, 775–781. doi: 10.1086/318309

Bruhweiler, F., and Verner, E. (2008). Modeling Fe II Emission and Revised Fe II (UV) empirical templates for the Seyfert 1 Galaxy I Zw 1. *Astrophys. J.* 675, 83–95. doi: 10.1086/525557

Elvis, M. (2000). A Structure for Quasars. *Astrophys. J.* 545, 63–76. doi: 10.1086/317778

Fraix-Burnet, D., Marziani, P., D'Onofrio, M., and Dultzin, D. (2017). The phylogeny of quasars and the ontogeny of their central black holes. *Front. Astron. Space Sci.* 4:1. doi: 10.3389/fspas.2017.00001

Gordon, K. D., and Clayton, G. C. (1998). Starburst-like dust extinction in the small magellanic cloud. *Astrophys. J.* 500, 816–824. doi: 10.1086/305774

Gordon, K. D., Clayton, G. C., Misselt, K. A., Landolt, A. U., and Wolff, M. J. (2003). A quantitative comparison of the small magellanic cloud, large magellanic cloud, and ilky way ultraviolet to near-infrared extinction curves. *Astrophys. J.* 594, 279–293. doi: 10.1086/376774

Kriss, G. (1994). "Fitting odels to UV and optical spectral data," in *Astronomical Data Analysis Software and Systems III, of Astronomical Society of the Pacific*

Conference Series, Vol. 61, eds D. R. Crabtree, R. J. Hanisch, and J. Barnes (San Francisco, CA: Astronomical Society of the Pacific), 437.

Malkan, M. A. (1983). The ultraviolet excess of luminous quasars. II - Evidence for massive accretion disks. *Astrophys. J.* 268, 582–590. doi: 10.1086/160981

Malkan, M. A., and Sargent, W. L. W. (1982). The ultraviolet excess of Seyfert 1 galaxies and quasars. *Astrophys. J.* 254, 22–37. doi: 10.1086/159701

Martínez-Aldama, M., Del Olmo, M., Marziani, P., Negrete, C., Dultzin, D., and Martínez-Carballo, M. A. (2017). HE0359-3959: an extremely radiating Quasar. *Front. Astron. Space Sci.* 4, 29–33. doi: 10.3389/fspas.2017.00029

Marziani, P., Del Olmo, A., Martínez-Aldama, M. L., Dultzin, D., Negrete, C., Bon, E., et al. (2017). Quasar black hole mass estimates from high-ionization lines: breaking a taboo? *Atoms* 5, 33–47. doi: 10.3390/atoms5030033

Marziani, P., and Sulentic, J. W. (2014). Highly accreting quasars: sample definition and possible cosmological implications. *Mon. Not. Roy. Astron. Soc.* 442, 1211–1229. doi: 10.1093/mnras/stu951

Marziani, P., Sulentic, J. W., Negrete, C. A., Dultzin, D., Zamfir, S., and Bachev, R. (2010). Broad-line region physical conditions along the quasar eigenvector 1 sequence. *Mon. Not. Roy. Astron. Soc.* 409, 1033–1048. doi: 10.1111/j.1365-2966.2010.17357.x

Marziani, P., Sulentic, J. W., Stirpe, G. M., Zamfir, S., and Calvani, M. (2009). VLT/ISAAC spectra of the Hβ region in intermediate-redshift quasars. III. Hβ broad-line profile analysis and inferences about BLR structure. *Astron. Astrophys.* 495, 83–112. doi: 10.1051/0004-6361:200810764

Marziani, P., Sulentic, J. W., Zwitter, T., Dultzin-Hacyan, D., and Calvani, M. (2001). Searching for the physical drivers of the eigenvector 1 correlation space. *Astrophys. J.* 558, 553–560. doi: 10.1086/322286

Mejía-Restrepo, J. E., Trakhtenbrot, B., Lira, P., Netzer, H., and Capellupo, D. M. (2016). Active galactic nuclei at z 1.5 - II. Black hole mass estimation by means of broad emission lines. *Mon. Not. Roy. Astron. Soc.* 460, 187–211. doi: 10.1093/mnras/stw568

Negrete, C. A., Dultzin, D., Marziani, P., and Sulentic, J. W. (2012). Broad-line egion physical conditions in extreme population A Quasars: a method to estimate central black hole mass at high redshift. *Astrophys. J.* 757:62. doi: 10.1088/0004-637X/757/1/62

Negrete, C. A., Dultzin, D., Marziani, P., and Sulentic, J. W. (2013). Reverberation and photoionization Estimates of the Broad-line Region Radius in low-z Quasars. *Astrophys. J.* 771:31. doi: 10.1088/0004-637X/771/1/31

Osterbrock, D. E., and Ferland, G. J. (2006). *Astrophysics of Gaseous Nebulae and Active Galactic Nuclei*. Sausalito, CA: University Science Books.

Proga, D. (2007). Dynamics of accretion flows irradiated by a Quasar. *Astrophys. J.* 66, 693–702. doi: 10.1086/515389

Sądowski, A., Narayan, R., McKinney, J. C., and Tchekhovskoy, A. (2014). Numerical simulations of super-critical black hole accretion flows in general relativity. *Mon. Not. Roy. Astron. Soc.* 439, 503–520. doi: 10.1093/mnras/stt2479

Sánchez, B., Aguiar-González, M., Barreto, R., Becerril, S., Bland-Hawthorn, J., Bongiovanni, A., et al. (2012). "OSIRIS tunable imager and spectrograph for the GTC: from design to commissioning," in *Proceedings of the SPIE Ground-based and Airborne Instrumentation for Astronomy IV*, Vol. 8446 (Bellingham, WA; Washington, DC: SPIE, Society of Photographic Instrumentation Engineers), 84464T.

Shen, Y., and Ho, L. C. (2014). The diversity of quasars unified by accretion and orientation. *Nature* 513, 210–213. doi: 10.1038/nature13712

Shen, Y., Richards, G. T., Strauss, M. A., Hall, P. B., Schneider, D. P., Snedden, S., et al. (2011). A catalog of quasar properties from sloan digital sky survey data Release 7. *Astrophys. J. Suppl.* 194:45. doi: 10.1088/0067-0049/194/2/45

Sulentic, J. W., Bachev, R., Marziani, P., Negrete, C. A., and Dultzin, D. (2007). C IV λ1549 as an eigenvector 1 parameter for active galactic nuclei. *Astrophys. J.* 666, 757–777. doi: 10.1086/519916

Sulentic, J. W., Del Olmo, A., Marziani, P., Martínez-Carballo, M. A., D'Onofrio, M., Oyabu, S., et al. (2017). What does CIV1549 tell us about the physical driver of the Eigenvector Quasar Sequence? *Astron. Astrophys.* arXiv:1708.03187

Sulentic, J. W., Marziani, P., and Dultzin-Hacyan, D. (2000). Phenomenology of broad emission ines in active galactic nuclei. *Annu. Rev. Astron. Astrophys.* 38, 521–571. doi: 10.1146/annurev.astro.38.1.521

Sulentic, J. W., Marziani, P., Zamanov, R., Bachev, R., Calvani, M., and Dultzin-Hacyan, D. (2002). Average uasar spectra in the context of eigenvector 1. *Astrophys. J.* 566, L71–L75. doi: 10.1086/339594

Sulentic, J. W., Repetto, P., Stirpe, G. M., Marziani, P., Dultzin-Hacyan, D., and Calvani, M. (2006). VLT/ISAAC spectra of the Hβ region in intermediate-redshift quasars. II. Black hole mass and Eddington ratio. *Astron. Astrophys.* 456, 929–939. doi: 10.1051/0004-6361:20054153

Sulentic, J. W., Stirpe, G. M., Marziani, P., Zamanov, R., Calvani, M., and Braito, V. (2004). VLT/ISAAC spectra of the Hβ region in intermediate redshift quasars. *Astron. Astrophys.* 423, 121–132. doi: 10.1051/0004-6361:20035912

Vestergaard, M., and Peterson, B. M. (2006). Determining central black hole masses in distant active galaxies and Quasars. II. Improved optical and UV scaling relationships. *Astrophys. J.* 641, 689–709. doi: 10.1086/500572

Vestergaard, M., and Wilkes, B. J. (2001). An empirical ultraviolet template for iron emission in quasars as derived from I Zwicky 1. *Astrophys. J. Suppl.* 134, 1–33. doi: 10.1086/320357

Wang, J.-M., Qiu, J., Du, P., and Ho, L. C. (2014). Self-shadowing effects of slim accretion disks in active galactic nuclei: the diverse appearance of the broad-line region. *Astrophys. J.* 797:65. doi: 10.1088/0004-637X/797/1/65

York, D. G., Khare, P., Vanden Berk, D., Kulkarni, V. P., Crotts, A. P. S., Lauroesch, J. T., et al. (2006). Average extinction curves and relative abundances for quasi-stellar object absorption-line systems at 1 <zabs <2. *Mon. Not. Roy. Astron. Soc.* 367, 945–978. doi: 10.1111/j.1365-2966.2005.10018.x

Zamfir, S., Sulentic, J. W., Marziani, P., and Dultzin, D. (2010). Detailed characterization of Hβ emission line profile in low-z SDSS quasars. *Mon. Not. Roy. Astron. Soc.* 403, 1759–1786. doi: 10.1111/j.1365-2966.2009.16236.x

Conflict of Interest Statement: The authors declare that the research was conducted in the absence of any commercial or financial relationships that could be construed as a potential conflict of interest.

Copyright © 2018 Martínez-Aldama, Del Olmo, Marziani, Sulentic, Negrete, Dultzin, Perea and D'Onofrio. This is an open-access article distributed under the terms of the Creative Commons Attribution License (CC BY). The use, distribution or reproduction in other forums is permitted, provided the original author(s) or licensor are credited and that the original publication in this journal is cited, in accordance with accepted academic practice. No use, distribution or reproduction is permitted which does not comply with these terms.

frontiers in Astronomy and Space Sciences

ORIGINAL RESEARCH
published: 28 November 2017
doi: 10.3389/fspas.2017.00029

HE0359-3959: An Extremely Radiating Quasar

M. L. Martínez-Aldama[1], A. Del Olmo[1], P. Marziani[2], C. A. Negrete[3], D. Dultzin[4] and M. A. Martínez-Carballo[1]*

[1] Instituto de Astrofísica de Andalucía, IAA-CSIC, Granada, Spain, [2] INAF, Osservatorio Astronomico di Padova, Padua, Italy, [3] CONACYT Research Fellow, Instituto de Astronomía, Universidad Nacional Autonoma de Mexico, Mexico City, Mexico, [4] Instituto de Astronomía, Universidad Nacional Autonoma de Mexico, Mexico City, Mexico

We present a multiwavelength spectral study of the quasar HE0359-3959, which has been identified as an extreme radiating source at intermediate redshift ($z = 1.5209$). Along the spectral range, the different ionic species give information about the substructures in the broad line region. The presence of a powerful outflow with an extreme blueshifted velocity of ∼–6,000 ± 500 km s^{-1} is shown in the Civλ1549 emission line. A prominent blueshifted component is also associated with the 1900Å blend, resembling the one observed in Civλ1549. We detect a strong contribution of very the low–ionization lines, FeII and Near-Infrared Ca II triplet. We find that the physical conditions for the low, intermediate, and high–ionization emission lines are different, which indicate that the emission lines are emitted in different zones of the broad line region. The asymmetries shown by the profiles reveal different forces over emitter zones. The high–ionization region is strongly dominated by radiation forces, which also affect the low and intermediate–ionization emitter region, commonly governed by virial motions. These results support the idea that highly radiating sources host a slim disk.

Keywords: quasars: emission lines, quasars: outflows, quasars: individuals HE0359-3959, quasars: supermassive black holes, galaxy evolution: feedback

OPEN ACCESS

Edited by:
Jirong Mao, Yunnan Observatories, National Astronomical Observatories (CAS), China

Reviewed by:
Andrea Marinucci, Roma Tre University, Italy
Milan S. Dimitrijevic, Astronomical Observatory, Serbia

****Correspondence:***
M. L. Martínez-Aldama
maryloli@iaa.es

Specialty section:
This article was submitted to Milky Way and Galaxies, a section of the journal Frontiers in Astronomy and Space Sciences

Received: *31 August 2017*
Accepted: *09 October 2017*
Published: *28 November 2017*

Citation:
Martínez-Aldama ML, Del Olmo A, Marziani P, Negrete CA, Dultzin D and Martínez-Carballo MA (2017) HE0359-3959: An Extremely Radiating Quasar. Front. Astron. Space Sci. 4:29. doi: 10.3389/fspas.2017.00029

1. EXTREME POPULATION A SOURCES ALONG THE 4DE1 MAIN SEQUENCE

The 4D Eigenvector 1 (4DE1) parameter space offers a formalism to distinguish and classify type 1 Active Galactic Nuclei (AGN) considering their spectral properties (Sulentic et al., 2000a,b). The Full Width at Half Maximum (FWHM) of Hβ broad component (H$\beta_{\rm BC}$), the strength of optical FeII blend at 4,570Å described by the ratio $R_{\rm FeII}$= I(FeII)/I(H$\beta_{\rm BC}$), the velocity shift of the CIVλ1549 profile, and soft X-ray photon index ($\Gamma_{\rm soft}$), provide four observationally independent dimensions of the Eigenvector 1. In the 4DE1 optical plane, the type 1 AGN occupy a well-defined sequence, driven mainly by the Eddington ratio, $L/L_{\rm Edd}$. Along this sequence we observe a variation of the physical parameters and orientation. Then, 4DE1 could be revealing an evolution sequence for type 1 AGN (Sulentic et al., 2000a; Marziani et al., 2010; Zamfir et al., 2010). For more information about the 4DE1 and update of results, see Marziani et al. in this volume.

Using the 4DE1 we identify two populations with different spectral features: A and B. Population A has a FWHM (H$\beta_{\rm BC}$) ≤4,000 km s^{-1}. It shows large blue asymmetries in the high-ionization lines like CIVλ1549, and it is majority populated by radio quiet sources. In contrast, population B shows a FWHM (H$\beta_{\rm BC}$)>4,000 km s^{-1} and it is mostly composed of radio-loud sources (Sulentic et al., 2002; Zamfir et al., 2010). Each population can be divided into small bins with ΔFWHM

($H\beta_{BC}$) = 4,000 km s^{-1} and ΔR_{FeII}= 0.5, defining subpopulations shown in the **Figure 1**. In this paper we focus in the subpopulation A3 and A4 (R_{FeII}> 1), which have been identified as highly radiating sources (xA, Marziani and Sulentic, 2014). These kind of sources show high Eddington ratios (L/L_{Edd}> 0.2) probably produced by a slim disk, which is geometrically and optically thick and it could be formed in an advection-dominated accretion flow (Abramowicz et al., 1988; Abramowicz and Straub, 2014) .

We have found selection criteria to identify the xA sources based on the 4DE1 formalism. In the optical region they show a R_{FeII} > 1 (high intensity of FeII) and in the UV range AlIIIλ1860/SiIII]λ1892 ≥ 0.5 and CIII]λ1909/SiIII]λ1892 ≤ 1.0 (Marziani and Sulentic, 2014). Also, they show strong blueshifted components associated with the high ionization lines, for example in CIVλ1549 emission line, indicating the presence of outflows. More details about the xA sources behavior can be found in Martínez-Aldama et al. of this volume.

1.1. HE0359-3959: An Extreme xA Source

In our extreme luminosity Hamburg-ESO sample (Marziani et al., 2009; Sulentic et al., 2017), we have identified four cases of highly radiating quasars that show an extreme behavior, i.e., a high Eddington ratio and a strong blue asymmetry [c(1/2)<−4,000 km s^{-1}; centroid at half intensity] in the CIVλ1549 profile (Sulentic et al., 2017). The most extreme case corresponds to the quasars HE0359-3959, with z = 1.5209, $\log(L_{bol})$ = 47.6 erg s^{-1} and a R_{FeII}= 1.12. It is cataloged as an A3 source (see **Figure 1**).

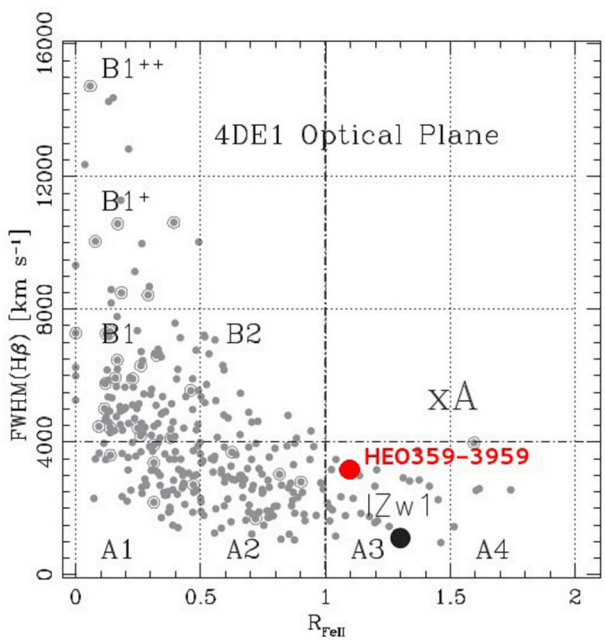

FIGURE 1 | 4DE1 Optical Plane reproduced from Marziani and Sulentic (2014). Gray points correspond to the sample of 470 bright low-z QSOs from Zamfir et al. (2010). The plane is divided in bins according to Sulentic et al. (2002). Extreme accretor population A sources (xA) are located in A3 and A4 bins. The black dot indicates the position of 1 Zw 1, the prototype of low-z xA sources. And, the red dot marks the location of HE0359-3959, an extreme xA source with high-z.

The aim of this paper is to analyze the spectral behavior of an extreme xA source, the quasar HE0359–3959. We performed multicomponent fits in a wide spectral range: UV, optical and Near–Infrared (Section 2); which gives us information about the dynamics and the physical conditions of the broad line region (BLR) (Section 3). In Section 4, we summarize the main results of our work.

2. OBSERVATIONS, DATA REDUCTION, AND MULTICOMPONENT FITTING

2.1. Observations and Data Reduction

Ultraviolet (UV), optical, and Near–Infrared spectra were observed with the Very Large Telescope (VLT-ESO). Optical and Near–Infrared spectra were obtained with the Infrared Spectrometer And Array Camera (ISAAC; decommissioned in 2013) using a slit of 0.6″. The near–infrared spectrum was observed in 2010 in the K band with a total exposure time of 1,120 s. The optical spectrum was observed in 2004 in the J band with a total exposure time of 3,600 s. For the ultraviolet spectrum we used the Focal Reducer and low dispersion Spectrograph (FORS1) and a slit of 1.0″ with a total exposure time of 1,440 s. It was observed in 2008. The data reduction was done using the IRAF package. The procedures followed are explained in Marziani et al. (2009), Martínez-Aldama et al. (2015), and Sulentic et al. (2017).

2.2. Multicomponent Fits

We perform multicomponent fits using SPECFIT, an IRAF routine (Kriss, 1994) to get the information of the most important emission lines. In each spectral range we fit a local continuum. The FWHM of all the broad components (BC) for Hβ, AlIIIλ1860, SiIII]λ1892, CIVλ1549, and SiIVλ1397 was taken equal. In the **Figure 2**, we present the multicomponents fits after continuum subtraction, for the CIVλ1549 and Ca II triplet range. The rest of the fits will be shown in an upcoming paper.

3. RESULTS

3.1. Multiwavelength Analysis

Low–ionization lines (LIL) have an ionization potential (IP) ≲20 eV. The Hβ line is the prototype of LIL. In population A3 and A4 sources Hβ has associated a blueshifted component (Bachev et al., 2004). In the case of HE0359-3959, the blueshifted component has a contribution to the total flux of ∼9%, and shows a centroid a half intensity of c(1/2)≈−500 ± 70 km s^{-1}.

The FeII (IP∼16 eV) has an important contribution in the optical and near–infrared regions. To reproduce it we used the templates modeled by Marziani et al. (2009) and Garcia-Rissmann et al. (2012) for the optical and near–infrared ranges, respectively. Several works have found (Persson, 1988; Ferland and Persson, 1989; Joly, 1989; Dultzin-Hacyan et al., 1999; Martínez-Aldama et al., 2015) a close relationship between the FeII and the NIR Ca II λ8498, λ 8542, and λ8662 Å triplet. This relation is very well appreciable in this object: as well as the optical

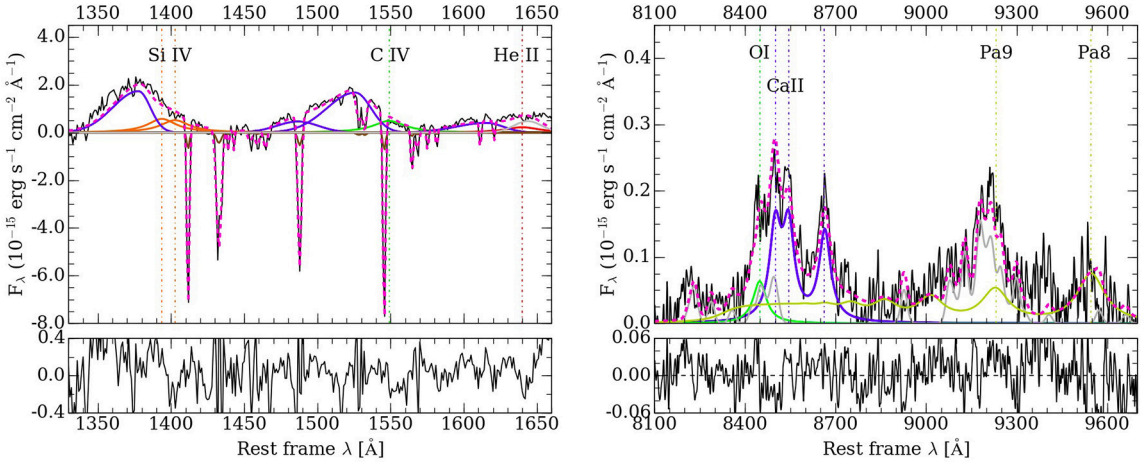

FIGURE 2 | Multicomponent analysis on the UV, optical and NIR spectra of HE0359-3959 after continuum subtraction. **(Top panels)**: In the left side is shown the UV spectrum, while in the right one is shown the near–infrared spectrum. The different components [broad (BC), BLUE, and narrow (NC)] in the line fitting are specified in each panel. Vertical lines indicate the rest-frame obtained through Hβ_{NC}. The gray line marks the FeII contribution. The vertical scale represents the relative flux in units of 10^{-15} erg s^{-1} cm^{-2} Å^{-1}. **(Bottom panel)**: Residuals of the fittings. The horizontal scale is the radial velocity shift in km s^{-1}. In all the panels the horizontal scale represents the rest–frame wavelength in Å.

FeII is strong, the NIR Ca II triplet also is. It is the first time where we observe the Ca II triplet lines isolated at high redshift. Strong intensities of both ions imply an extremely low-ionization degree ($U < 10^{-2}$; U: ionization parameter) and a high density ($n_H \sim 10^{11-13}$ cm^{-3}) (Baldwin et al., 2004; Matsuoka et al., 2007; Martínez-Aldama et al., 2015).

In the UV region, the 1900Å blend is formed by two intermediate–ionization lines (IIL; IP ∼ 20–40 eV), AlIIIλ1860 and SiIII]λ1892, which are accompanied by CIII]λ1909 and some FeIII transitions. In this blend we appreciate a blueshifted component. This component should be most likely associated with AlIIIλ1860. Respect to AlIIIλ1860, the blueshifted component has a contribution of the total profile of 60%. The centroid a half intensity is c(1/2)≈−3,200 ± 250 km s^{-1}, which indicates the presence of an outflow generated by radiation forces presented in the intermediate–ionization lines (Marziani et al., 2017). On the other hand, considering the high intensity of AlIIIλ1860, SiIII]λ1892, Ca II and FeII, it could suggest a possible chemical enrichment of the BLR (Juarez et al., 2009).

High ionization lines (HIL; IP > 40 eV), CIVλ1549, HeIIλ1640, and SiIVλ1397, show a prominent blueshifted component. We find that the blue component has a contribution of 76, 62, and 57% to the total flux of CIVλ1549, HeIIλ1640, and SiIVλ1397 , respectively. The CIVλ1549 reaches c(1/2) ∼−6,000 ± 500 km s^{-1}, while HeIIλ1640 and SiIVλ1397 c(1/2) ∼−4,000 ± 550 km s^{-1}. The velocities reached are ones of the highest found in the literature (Richards et al., 2011; Coatman et al., 2016; Sulentic et al., 2017). Then, it indicates that the full profile is dominated by an outflow and suggests the disk plus wind scenario (Gaskell, 1982; Richards et al., 2002, 2011).

3.2. Physical Properties of HE0359-3959

In order to study the physical properties of the quasar HE0359-3959, we built a grid of photoionization simulations using the CLOUDY code (Ferland et al., 1998, 2013). For our simulations we considerer a Mattews and Ferland continuum (Mathews and Ferland, 1987), a plane-parallel geometry, a metallicity 5Z⊙ with an overabundance of Al and Si with respect to carbon (by a factor of three), and a column density of $N_c = 10^{23}$ cm^{-2}. See Negrete et al. (2012) for more details. Our simulations span the density range 7.00 ≤ log (n_H) ≤ 14.00 and −4.5 ≤log (U) ≤0.00 for the ionization parameter, in intervals of 0.25 dex. More details about the CLOUDY simulations can be found in Negrete et al. (2014). Using the UV lines, we define three groups of diagnostic ratios::

- The flux ratio AlIIIλ1860/SiIII]λ1892 is a useful density diagnostic.
- The flux ratio SiIVλ1397/SiIII]λ1892 for the ionization parameter.
- The flux ratio CIVλ1549/SiIVλ1397 is mainly sensitive to the relatives abundances of C and Si.

In **Figure 3** is shown the result of the simulations. We obtained that the flux ratios are intersected in log(n_H) = 12.32 cm^{-3} and log(U) = −2.95. Compared to not highly radiating AGNs (Negrete et al., 2013), this source shows a high density and a low ionization parameter, which marks a different behavior in the BLR, probably causing by the slim disk hosted in these kind of sources. Taking into account the high intensity of AlIIIλ1860, FeII, and Ca II we conclude that effectively the low–ionization emitter zone has a high density and low–ionization parameter.

Negrete et al. (2012) proposed a new method to determine the size of the BLR (r_{BLR}) and the black hole mass (M_{BH}) based on the product $n_H \cdot U$ and independently of redshift. This method gives similar results to the obtained from the classical methods such as reverberation mapping at low–z (Negrete et al., 2014). Knowing the product of $n_H \cdot U$ obtained from the CLOUDY simulations, we compute the size of the BLR (r_{BLR}) and considering the

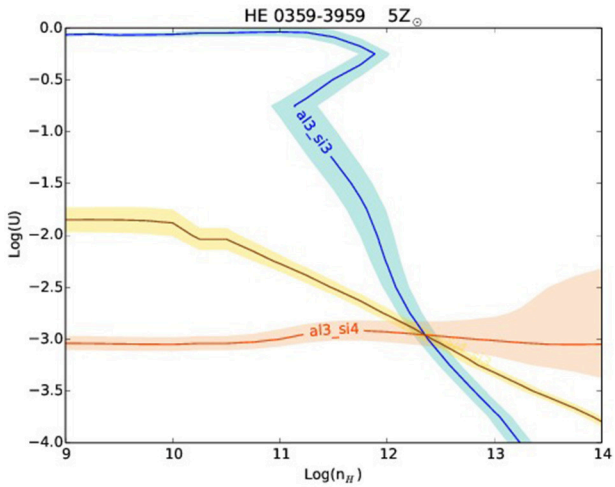

FIGURE 3 | Isocontors for HE0359-3959 with $5Z_{\odot}$ and an overabundance of Al and Si. The blue line indicates the flux ratio AlIIIλ1860/SiIII]λ1892, the yellow one indicates the ratio SiIVλ1397/SiIII]λ1892, and the orange corresponds to the AlIIIλ1860/SiIVλ1397. Shadows associated with each line indicate the error. The flux ratios are intersected in $n_H \cdot U = 9.27 \pm 0.39$.

FWHM of the broad components as the velocity dispersion, we can get the black hole mass (M_{BH}) and the Eddington ratio. The size of the BLR is $\log(r_{BLR}) = 18.37 \pm 0.04$ cm and the black hole mass is $\log(M_{BH}) = 9.52 \pm 0.41\ M_{\odot}$. These values are in agreement with the ones found for a large xA sample at high-redshift (Martínez-Aldama et al., in preparation).

The Eddington ratio for this source is $L/L_{Edd} = 0.74 \pm 0.11$. Considering that it shows a $c(1/2) \sim -6{,}000 \pm 500$ km s^{-1} for CIVλ1549, we confirm the directly proportional relation between $c(1/2)$ and L/L_{Edd}. Indicating that L/L_{Edd} could be the driver of the outflows (Sulentic et al., 2017).

4. CONCLUSIONS

The information given by the multiwavelength analysis indicates that in HE0359–3959 there is coexistence of substructures in the broad line region. Low and intermediate–ionization regions, where Hβ, AlIIIλ1860 and SiIII]λ1892 are emitted, are dense ($n_H \sim 10^{11-12}$ cm^{-3}) and optically thick ($U \sim 10^{-2.5}$). They are mainly governed by virial motions and the presence of a blueshifted component indicates the influence of radiation forces. On the other hand, according to Marziani et al. (2010) the high–ionization region is less dense ($n_H \sim 10^{10}$ cm^{-3}, $U \sim 10^{-1}$), pointing out a difference with the physical conditions shown by the low and intermediate–ionization lines.

High ionization lines are dominated by strong radiation forces, producing outflows in high–ionization lines like CIVλ1549, HeIIλ1640, and SiIVλ1397. The high Eddington ratio value suggests the presence of a slim optically thick disk which could be related to the extreme outflow properties observed in HE0359-3959. The presence of strong outflows has been related with the co–evolution of the active galactic nuclei and the host galaxy.

AUTHOR CONTRIBUTIONS

MLM-A and PM: Data reduction, multicomponents fits, analysis, writing, revision. AD: Analysis, reduction, writing, revision. CN: Analysis, photoionization models, revision. DD: Analysis, revision. MAM-C: Data reduction, multicomponents fits.

ACKNOWLEDGMENTS

MLM-A acknowledge the postdoctoral grant from the CONACyT. MLM-A, AD, and MAM-C acknowledge financial support from Spanish Ministry for Economy and Competitiveness through grants AYA2013-42227-P and AYA2016-76682-C3-3-1-P.

REFERENCES

Abramowicz, M. A., Czerny, B., Lasota, J. P., and Szuszkiewicz, E. (1988). Slim accretion disks. *Astrophys. J.* 332, 646–658.

Abramowicz, M. A., and Straub, O. (2014). Accretion discs. *Scholarpedia* 9:2408. doi: 10.4249/scholarpedia.2408

Bachev, R., Marziani, P., Sulentic, J. W., Zamanov, R., Calvani, M., and Dultzin-Hacyan, D. (2004). Average ultraviolet quasar spectra in the context of eigenvector 1: a baldwin effect governed by the eddington ratio? *Astrophys. J.* 617, 171–183. doi: 10.1086/425210

Baldwin, J. A., Ferland, G. J., Korista, K. T., Hamann, F., and LaCluyzé, A. (2004). The origin of Fe II emission in active galactic nuclei. *Astrophys. J.* 615, 610–624. doi: 10.1086/424683

Coatman, L., Hewett, P. C., Banerji, M., and Richards, G. T. (2016). C IV emission-line properties and systematic trends in quasar black hole mass estimates. *Mon. Not. R. Astron. Soc.* 461, 647–665. doi: 10.1093/mnras/stw1360

Dultzin-Hacyan, D., Taniguchi, Y., and Uranga, L. (1999). "Where is the Ca II triplet emitting region in AGN?," in *Structure and Kinematics of Quasar Broad Line Regions, Vol. 175, Astronomical Society of the Pacific Conference Series*, eds C. M. Gaskell, W. N. Brandt, M. Dietrich, D. Dultzin-Hacyan, and M. Eracleous (San Francisco, CA: Astronomical Society of the Pacific), 303.

Ferland, G. J., Korista, K. T., Verner, D. A., Ferguson, J. W., Kingdon, J. B., and Verner, E. M. (1998). CLOUDY 90: numerical simulation of plasmas and their spectra. *Publ. Astron. Soc. Pac.* 110, 761–778.

Ferland, G. J., and Persson, S. E. (1989). Implications of CA II emission for physical conditions in the broad-line region of active galactic nuclei. *Astrophys. J.* 347, 656–673.

Ferland, G. J., Porter, R. L., van Hoof, P. A. M., Williams, R. J. R., Abel, N. P., Lykins, M. L., et al. (2013). The 2013 release of cloudy. *RMxAA* 49, 137–163.

Garcia-Rissmann, A., Rodríguez-Ardila, A., Sigut, T. A. A., and Pradhan, A. K. (2012). A near-infrared template derived from I Zw 1 for the Fe II emission in active galaxies. *Astrophys. J.* 751:7. doi: 10.1088/0004-637X/751/1/7

Gaskell, C. M. (1982). A redshift difference between high and low ionization emission-line regions in QSOs - Evidence for radial motions. *Astrophys. J.* 263, 79–86.

Joly, M. (1989). Formation of CA II lines in active galactic nuclei. *Astron. Astrophys.* 208, 47–51.

Juarez, Y., Maiolino, R., Mujica, R., Pedani, M., Marinoni, S., Nagao, T., et al. (2009). The metallicity of the most distant quasars. *Astron. Astrophys.* 494, L25–L28.

Kriss, G. (1994). "Fitting models to UV and optical spectral data," in *Astronomical Data Analysis Software and Systems III, Vol. 61 Astronomical Society of the*

Pacific Conference Series, eds D. R. Crabtree, R. J. Hanisch, and J. Barnes (San Francisco, CA: Astronomical Society of the Pacific), 437.

Martínez-Aldama, M. L., Dultzin, D., Marziani, P., Sulentic, J. W., Bressan, A., Chen, Y., et al. (2015). O I and Ca II observations in intermediate redshift quasars. *Astrophys. J.* 217:3. doi: 10.1088/0067-0049/217/1/3

Marziani, P., Del Olmo, A., Martínez-Aldama, M. L., Dultzin, D., Negrete, C., Bon, E., et al. (2017). Quasar black hole mass estimates from high-ionization lines: breaking a taboo? *Atoms* 5, 33–47. doi: 10.3390/atoms5030033

Marziani, P., and Sulentic, J. W. (2014). Highly accreting quasars: sample definition and possible cosmological implications. *Mon. Not. R. Astron. Soc.* 442, 1211–1229. doi: 10.1093/mnras/stu951

Marziani, P., Sulentic, J. W., Negrete, C. A., Dultzin, D., Zamfir, S., and Bachev, R. (2010). Broad-line region physical conditions along the quasar eigenvector 1 sequence. *Mon. Not. R. Astron. Soc.* 409, 1033–1048. doi: 10.1111/j.1365-2966.2010.17357.x

Marziani, P., Sulentic, J. W., Stirpe, G. M., Zamfir, S., and Calvani, M. (2009). VLT/ISAAC spectra of the Hβ region in intermediate-redshift quasars. III. Hβ broad-line profile analysis and inferences about BLR structure. *Astron. Astrophys.* 495, 83–112. doi: 10.1051/0004-6361:200810764

Mathews, W. G., and Ferland, G. J. (1987). What heats the hot phase in active nuclei? *Astrophys. J.* 323, 456–467.

Matsuoka, Y., Oyabu, S., Tsuzuki, Y., and Kawara, K. (2007). Observations of O I and Ca II emission lines in Quasars: implications for the site of Fe II line emission. *Astrophys. J.* 663, 781–798. doi: 10.1086/518399

Negrete, C. A., Dultzin, D., Marziani, P., and Sulentic, J. W. (2012). Broad-line region physical conditions in extreme population a Quasars: a method to estimate central black hole mass at high redshift. *Astrophys. J.* 757:62. doi: 10.1088/0004-637X/757/1/62

Negrete, C. A., Dultzin, D., Marziani, P., and Sulentic, J. W. (2013). Reverberation and photoionization estimates of the broad-line region radius in low-z Quasars. *Astrophys. J.* 771:31. doi: 10.1088/0004-637X/771/1/31

Negrete, C. A., Dultzin, D., Marziani, P., and Sulentic, J. W. (2014). A new method to obtain the broad line region size of high redshift Quasars. *Astrophys. J.* 794:95. doi: 10.1088/0004-637X/794/1/95

Persson, S. E. (1988). Calcium infrared triplet emission in active galactic nuclei. *Astrophys. J.* 330, 751–765.

Richards, G. T., Kruczek, N. E., Gallagher, S. C., Hall, P. B., Hewett, P. C., Leighly, K. M., et al. (2011). Unification of luminous type 1 Quasars through C IV emission. *Astrophys. J.* 141, 167–183. doi: 10.1088/0004-6256/141/5/167

Richards, G. T., Vanden Berk, D. E., Reichard, T. A., Hall, P. B., Schneider, D. P., SubbaRao, M., et al. (2002). Broad emission-line shifts in Quasars: an orientation measure for radio-quiet quasars? *Astrophys. J.* 124, 1–17. doi: 10.1086/341167

Sulentic, J. W., Del Olmo, A., Marziani, P., Martínez-Carballo, M. A., D'Onofrio, M., Oyabu, S., et al. (2017). What does CIV1549 tell us about the physical driver of the Eigenvector Quasar Sequence? *Astron. Astrophys. arXiv:1708.03187*

Sulentic, J. W., Marziani, P., and Dultzin-Hacyan, D. (2000a). Phenomenology of broad emission lines in active galactic nuclei. *Annu. Rev. Astron. Astrophys.* 38, 521–571. doi: 10.1146/annurev.astro.38.1.521

Sulentic, J. W., Marziani, P., Zamanov, R., Bachev, R., Calvani, M., and Dultzin-Hacyan, D. (2002). Average quasar spectra in the context of eigenvector 1. *Astrophys. J.* 566, L71–L75. doi: 10.1086/339594

Sulentic, J. W., Zwitter, T., Marziani, P., and Dultzin-Hacyan, D. (2000b). Eigenvector 1: an optimal correlation space for active galactic nuclei. *Astrophys. J.* 536, L5–L9.

Zamfir, S., Sulentic, J. W., Marziani, P., and Dultzin, D. (2010). Detailed characterization of Hβ emission line profile in low-z SDSS quasars. *Mon. Not. R. Astron. Soc.* 403, 1759–1786. doi: 10.1111/j.1365-2966.2009.16236.x

Conflict of Interest Statement: The authors declare that the research was conducted in the absence of any commercial or financial relationships that could be construed as a potential conflict of interest.

Copyright © 2017 Martínez-Aldama, Del Olmo, Marziani, Negrete, Dultzin and Martínez-Carballo. This is an open-access article distributed under the terms of the Creative Commons Attribution License (CC BY). The use, distribution or reproduction in other forums is permitted, provided the original author(s) or licensor are credited and that the original publication in this journal is cited, in accordance with accepted academic practice. No use, distribution or reproduction is permitted which does not comply with these terms.

frontiers in Astronomy and Space Sciences

PERSPECTIVE
published: 09 May 2018
doi: 10.3389/fspas.2018.00010

Meeting Summary: A 2017 View of Active Galactic Nuclei

*Hagai Netzer**

School of Physics and Astronomy, Tel Aviv University, Tel Aviv, Israel

The topics covered in this summary review reflect the major areas discussed in the Padova meeting, in April 2017. They are divided into general categories: those areas where large progress has been made leading to a real new understanding (what we are doing "right"), and those where we are still in the dark (what we are doing "wrong"). The division reflects the status of the field as well as my subjective opinion.

Keywords: black holes, star formation, host galaxies, cosmology, accretion disks, reverberation mapping, AGN-feedback

OPEN ACCESS

Edited by:
Mauro D'Onofrio,
Università degli Studi di Padova, Italy

Reviewed by:
Luka C. Popovic,
Astronomical Observatory, Serbia
Gordon Richards,
Drexel University, United States

***Correspondence:**
Hagai Netzer
netzer@wise.tau.ac.il

Specialty section:
This article was submitted to Milky Way and Galaxies, a section of the journal Frontiers in Astronomy and Space Sciences

Received: *15 September 2017*
Accepted: *12 March 2018*
Published: *09 May 2018*

Citation:
Netzer H (2018) Meeting Summary: A 2017 View of Active Galactic Nuclei. Front. Astron. Space Sci. 5:10. doi: 10.3389/fspas.2018.00010

1. INTRODUCTION: "RIGHT" AND "WRONG" IN AGN STUDY

The topics covered in this meeting are very broad: from the central black hole (BH) and the accretion disk (AD), to the observations and physics of the broad line region (BLR), narrow line region (NLR), AGN-tori, AGN winds and feedback, the various types of AGN, the connection to the host galaxy and its star forming (SF) regions, and even AGN in a cosmological context. To summarize this huge area (usually divided into sub-areas and discussed in more specialized meetings) I chose to assess the quality of the observations presented here, and the complexity and reality of the associated models, by assigning to each one of the categories one of two "quality flags," either "right," or "wrong." These should not be understood in their every-day meaning. Rather, they reflect my personal view of where we have made big progress, and are starting to understand the big picture, and where we are probably missing some essential points, and hence may be proceeding in the wrong direction. Thus, the meaning of "we must be doing something wrong" used often in this review, means that in my opinion, we are missing some important ingredients either because we misunderstand the objects or phenomena we are studying, or because the work necessary to reach a real understanding is so complicated, or time-consuming, that it has not yet been done. Obviously there is no way to refer to all the talks and posters presented in the meeting, many of which represent excellent work. I only chose a small number of those that seem to represent the topics where "right" or "wrong," as defined here, are more clearly separable.

2. THE AGN FAMILY: NEW MULTI-WAVELENGTH OBSERVATIONS

2.1. Something Right: Systematic Study of LINERS, Seyferts, High Luminosity AGN and Objects Containing Disk-Like BLRs

There is rapid progress in obtaining improved observations of large and small AGN samples. The SDSS is leading this field because of the very large number of sources observed spectroscopically in this survey. However, smaller samples, especially those that are carefully selected in one wavelength band and then studied in others, provide valuable information in terms of being more complete. The COSMOS sample is one such sample, alongside with the older PG-Quasar sample, the new BAT sample, and more. Examples of this type were provided by Márquez et al. (2017, LINERs and Seyfert 2s) and Richards (2017, type-I AGN in the SDSS sample combined with a new division

into eigenvector groups), (Lusso and Risaliti, 2018) who provided a fresh look at X-ray sources and even some GAIA results that are going to contribute their part to the field in the near future (Angello, 2017). A somewhat different example, presented by Storchi-Bergmann et al. (2017), demonstrated the great advantage of looking at the rare group of double-hump broad line sources where studying a large sample in a very systematic way, leads to a new insight.

2.2. Something Wrong: A Complete Picture of Radio AGN

The clear and comprehensive review by Padovani (2017), as well as several talks on Blazars, only helped to demonstrate that we are still far from understanding many of these sources, their physics, variability and, most importantly, the connection (if any) between radio and optical-UV properties of many radio loud AGN. The Blazar field is perhaps the least understood and the new big observatories which help to extend their study to very high energies, and help to follow their variations in more detailed ways, seems to provide only incremental improvements over what was known 10 and 20 years ago. We must be doing something wrong in this area.

3. MAPPING AND MODELING THE BLR AND MEASURING BH MASS

3.1. Something Right: Reverberation Mapping in One and Two Dimensions

A giant leap forward in terms of 2D (location and kinematics) reverberation mapping (RM) of the BLR is the recent (2013–2014) study of NGC 5548 by HST and a host of ground-based telescopes. Despite being only one source, that may not be typical with respect to its very high X-ray luminosity compared with the optical-UV luminosity, this is a superb example of the power of well planned spectroscopic observations. The light-curves of different emission lines at various gas velocities are text-book examples which will likely provide the tool to solve some of the issues related to the physics of the BLR. The new information about time-dependent broad and narrow absorption lines, and the accretion disk itself, is equally exciting. Some examples of this were shown by Horne (2015) and Fausnaugh et al. (2017). The same group, now with the help of many others, is making plans to carry out a similar study of other AGN.

3.2. Something Right: The R-L Relationship and Single-Epoch Mass Measurements

Related to this is the impressive collection of sources (more than 70) where the emissivity weighted radius of the broad Hβ line has been measured through the correlated line and continuum variations, and variability may even be related to eigenvector 1 (Ilić et al., 2017; Bon et al., 2018). In some of the mapped sources, the Hβ line can be divided into several velocity bins allowing one to answer a simpler question of whether the BLR motion is mostly outflow, inflow, or closer to a bound rotational motion (Pancoast et al., 2014). Surprisingly, there is no single canonical dynamical pattern. Other important new results connect the Hβ emission region size to the Eddington ratio of the accreting BH.

New, long expected RM results applied to the most luminous AGN, at high redshift, were presented by Kaspi et al. (2017) and Lira et al. (2018). They show that the CIVλ1549 and Lyα emitting regions are much closer to the central BH compared with the Hβ emitting region, by a factor of $\sim$ 3. The two RM campaigns that finally answered this question took 10–15 years (!!) to complete—a good example showing what science can reveal when managing to convince large telescope TACs that some problems require more than a decade of observations. The other very good news in this area is the completion of VLT/GRAVITY that is capable of measuring, directly, BLR sizes in a small number of nearby type-I AGN.

Another idea, which is clearly becoming more visible due to the fact that more and more type-I AGN are studied, spectroscopically, in more and more detail, is the suggestion, by Marziani et al. (2018) that different locations in the eigenvector 1 plane hint to fundamentally different physics.

3.3. Something Wrong: Phase-Space Modeling of the BLR

Despite the impressive 2D RM maps of NGC 5548 presented in the meeting, and lower quality ones available for other sources, there is little if any progress in constructing consistent spatially and dynamically connected maps for the best studied source. We seem to be facing the same questions that were asked some 20 years ago, after the analysis of the very first optical-UV RM study of the same sources with ground based telescopes and the IUE satellite. This field is eagerly waiting for a more detailed models which will justify the huge resources invested in it.

Some good news in this area, not directly related to the mapping of the BLR, is a new model presented by Czerny et al. (2017), where the origin (and hence location) of the BLR clouds is the dusty outer parts of the central accretion disk. This and similar models can be tested by next generation 2D BLR models. Some other ideas that were proposed but never tested properly are related to the commonly assumed relationship $R_{BLR} \propto L^{\alpha}$ where R_{BLR} is the BLR radius estimated from RM campaign, L the monochromatic continuum at a chosen wavelength, and $\alpha = 0.5 \pm 0.1$. Is it possible, in view of the dependence on the Eddington ratio discovered recently, and hence the role of radiation pressure force, that an alternative approximation of the type $R_{BLR} = c_1 L^{\alpha} + c_2(L/M)$ will provide better BH mass estimates?

3.4. Better Calibration of BH Masses

While the commonly used single-epoch (SE) BH mass measurements is a substantial step forward, which is well recognized by the community, the field is still looking for a way to improve the calibration of these measurements, i.e., the factor f_{BLR} in the expression $M_{BH} = f_{BLR} R_{BLR} V_{BLR}^2/G$. The way used by most researchers is based on the well known $M_{BH} - \sigma*$ relationship which provides the calibration of f_{BLR} in the local universe, i.e., mostly for low luminosity AGN. A new promising method was presented by Mejía-Restrepo et al. (2018, paper presented by Lira). In this method, applied so far

to high luminosity, high redshift ($z \sim 1.5$) AGN, the observed FWHM of the broad lines can provide the desired calibration, i.e., $f_{BLR} \propto 1/FWHM(line)$.

4. ACCRETION DISKS AND DISK WINDS

4.1. Something Right: Thin Accretion Disk Models and the Optical-UV SED

After years of study it is now apparent that the optical-UV continuum of at lease some AGN, those with large BH mass ($10^8 - 10^9$ M_{sun}) and not too large Eddington ratio, can be adequately fitted by the canonical spectrum of a thin accretion disk. Apparently, the previous failure of such attempts was probably due to the lack of simultaneous observations that cover a large enough wavelength range.

4.2. Something Wrong: The Spectrum and Properties of Slim Accretion Disks

Despite heroic observational and theoretical efforts, slim accretion disks, those with an Eddingto ratio exceeding about 0.3, are not yet understood. The SED beyond the Lyman limit is not known observationally and there are clear discrepancies between theoretical predictions and the observed luminosity ratios of their NIR, extreme UV and X-ray radiation (Castelló-Mor et al., 2017).

4.3. Disk Winds: Right and Wrong

All theoretical slim disk models, as well as present-day (rather simplified) numerical simulations, show that strong disk winds must be present, especially close to the central BH. The amount of accreted energy carried out in such winds, and hence not by radiation, is not known and the geometry and velocity fields can only be guessed. On a slightly larger scale, there was a lot of discussion about dusty and dust-free winds as presented by Elitzur (e.g., Elitzur and Netzer, 2016). In fact, it is hard to imagine a disk with a strong magnetic field that does not show this component. One claim is that the outflowing BLR clouds, and even the dusty torus, are also related to such flows.

Unfortunately, so far we do not have a clear and convincing observational evidence for such winds. The dynamical studies of the BLR gas only show the signature of outflows in a handfull of sources and other observations show exactly the opposite. There are however a couple of new observations that can be interpreted as a signature of a wind. The first is the "polar dust" found in a couple of sources studied with various interferometers (Hönig, 2016). The second, which I consider to be one of the most amazing results presented in the meeting, is the study of a source which is microlensed by a foreground star (Hutsemékers et al., 2017). Reconstructing the lens magnification map, allows one to combine location and velocity in the lensed BLR. It shows that the Hα line profile is produced by a flat, rotating BLR while the CIVλ1549 line is probably produced in an outflowing polar gas. This way of probing the dynamics is extremely accurate but, unfortunately, can only be applied to a handful of lensed sources.

5. STAR FORMATION GALACTIC-SCALE WINDS MERGERS AND FEEDBACK

5.1. Something Right: Observational Evidence for Outflow and Mergers

In terms of new observations, and on-going effort, this topic is, arguably, the place where most observational effort has been made over the last few years. We have been presented with superb quality velocity maps, in different objects, showing large scale outward motion of ionized and molecular gas. The outflow can be associated with the vicinity of the BH (mostly X-ray outflows), the narrow line region, or even further away in the galaxy. Evidence comes from low redshift sources just "around the corner" and for redshift as large as 3–6. The available velocity maps are already of high quality and the coming new-generation IFU instruments, on JWST and several large ground-based telescopes, will no doubt provide even more detailed observations. ALMA is likely to play a role in proving, or disproving, the suggestion that many of the ionized outflow are associated with high mass-outflow rate molecular gas.

5.2. Something Wrong: Interpreting Outflow and Feedback

We are still in the dark regarding accurate measurements of mass outflow rates and hence the importance of AGN-feedback in quenching SF and in shaping the structure and evolution of the host galaxy. In ionized outflow, the main uncertainties are in those terms combining gas density and gas filling factor. The difficulty is due to poor observations (lack of outflow signature in several lines, not just the strongest ones) and the difficult estimate of the outflow filling factor. Molecular outflows are easier to model but questions about the production of CO lines in outflowing material still remain.

Present day feedback models are still not advanced enough to make clear and specific predictions about the galactic scale influence of the process. In particular, it is not very clear whether energy-conserved outflows, or momentum conserved outflows, are more important. One of them is associated with radiation pressure force mostly on dust grains. The other, with galactic scale shocked gas. Here, again, theory lags the observations, or perhaps more precisely, numerical simulations of galactic-scale shocks, and feedback, have a long way to go. The larger scale, cluster-size feedback, associated with powerful radio jets and X-ray cavities, is perhaps better understood (Morganti, 2017).

Related questions are the correlation of SF and AGN luminosity in low and high redshift sources. Here, again, we heard some conflicting results reflecting the large uncertainties in measuring SF rates, mostly in the FIR, and in correlating it with optical and X-ray observations. Thus Ichikawa et al. (2017) showed several samples where L(AGN)$\propto$L(SF) while according to Stanley et al. (2015), such a correlation does not exist in any redshift.

The presence of near companions can be interpreted as indication for merger that can trigger SF and speed up the

evolution of the system. The beautiful results presented by Fogasy et al. (2017), Kimball et al. (2015) and Trakhtenbrot et al. (2018) are quite amazing, given the redshift, size and brightness of the sources. However, they do not seem to be in agreement with each other, e.g., in relation to the question of which one is more FIR luminous, the AGN-host or the companion.

6. COSMOLOGY WITH AGN

6.1. Something Wrong: All AGN-Based Methods

Efforts to identify reliable tools based on AGN physics, that can help map the universe, and its expansion, at high redshift, and improve on the accuracy of present day measurements based on Type-Ia SNs, have not yet produced meaningful results. Some of these ideas have been mentioned in the meeting, e.g., the use of the observed luminosity of super-Eddington AGN, dust RM and its comparison with accurate IR interferometry (Hönig, 2016), the scaling of BLR density and ionization parameter (Negrete et al., 2017), or the relationship between X-ray and UV observations of type-I AGN (Lusso and Risaliti, 2018). Unfortunately, systematic uncertainties in all the methods, combined with a lack of understanding of some of the involved processes, prevent us from reducing the uncertainties of such methods to a trustable and useful level. We must be missing something very important in all these methods or, perhaps, AGN are simply not the tool to advance precision cosmology.

7. OPTIMISTIC SUMMARY

The approach followed in this summary review, of comparing things we understand ("we must be doing something right") with those we do not yet understand ("we must be doing something wrong") is useful since it allows us to produce an itemized list of topics, and hence specific goals, for future projects and meetings. Under the "right" header in this review I included: detailed and accurate new observations, larger and more complete samples, wider wavelength coverage, better spatial resolution, better time sampling, and more. The "wrong" category includes, in my opinion (and correct to 2017) topics like: understanding BH and galaxy evolution, simulating large scale baryonic processes like feedback, measuring mass outflow rates, understanding slim accretion disks and disk winds, proper modeling of the BLRs and dusty disk winds, and more. The common denominator is evident: We are making large and significant steps forward on the observational front but the theory, and the numerical simulations, lag behind. The optimistic view is that doing "wrong" is the first step for success. A nice summary of this idea is a clever quote from the writing of the late Susan Jeffers, a well known American psychologist and author, who once said: "If you haven't made any mistakes lately, you must be doing something wrong."

AUTHOR CONTRIBUTIONS

The author confirms being the sole contributor of this work and approved it for publication.

FUNDING

This research has been supported by the Israel Science Foundation grand 284/13.

ACKNOWLEDGMENTS

The information provided in this review is based on the excellent papers presented in this meeting, and the ideas and suggestions of my colleagues and students. The classification into the categories of right and wrong is entirely mine.

REFERENCES

Angello, A. (2017). Quasar lenses and galactic streams: outlier selection and Gaia multiplet detection. *Month. Notices R. Astron. Soc.* 471, 2013–2021. doi: 10.1093/mnras/stx1650

Bon, N., Bon, E., and Marziani, P. (2018). AGN broad line region variability in the context of eigenvector 1: case of NGC 5548. *Front. Astron. Space Sci.* 5:3. doi: 10.3389/fspas.2018.00003

Castelló-Mor, N., Kaspi, S., Netzer, H., Du, P., Hu, C., Ho, L. C., et al. (2017). Unveiling slim accretion disc in AGN through X-ray and Infrared observations. *Month. Notices R. Astron. Soc.* 467, 1209–1221. doi: 10.1093/mnras/stx153

Czerny, B., Li, Y.-R., Sredzinska, J., Hryniewicz, K., Panda, S., Wildy, C., et al. (2017). Self-consistent dynamical model of the broad line region. *Front. Astron. Space Sci.* 4:5. doi: 10.3389/fspas.2017.00005

Elitzur, M., and Netzer, H. (2016). Disc outflows and high-luminosity true type 2 AGN. *MNRAS* 459, 585–594. doi: 10.1093/mnras/stw657

Fausnaugh, M. M., Peterson, B. M., Starkey, D. A., and Horne, K. (2017). the AGN STORM Collaboration. Continuum reverberation mapping of AGN accretion disks. *Front. Astron. Space Sci.* 4:55. doi: 10.3389/fspas.2017.00055

Fogasy J., Knudsen K. K., Lagos, C. D. P., Drouart, G., and Gonzalez-perez, V. (2017). On the frequency of star-forming galaxies in the vicinity of powerful AGNs: the case of SMM J04135+10277. *Astron. Astrophys.* 597:123. doi: 10.1051/0004-6361/201628173

Hönig, S. F. (2016). Tori, discs, and winds: the first ten years of AGN interferometry. *Astrophys. Space Sc. L.* 439, 1–95. doi: 10.1007/978-3-319-39739-9_6

Horne, K. (2015). *AGN Space Telescope and Optical Reverberation Mapping Project. IV. Velocity-Delay Mapping of Broad Emission Lines in NGC 5548.* Available online at: http://adsabs.harvard.edu/abs/2015AAS...22510304H

Hutsemékers, D., Braibant, L., Sluse, D., Anguita, T., and Goosmann, R. (2017). New constraints on quasar broad absorption and emission line regions from gravitational microlensing. *Front. Astron. Space Sci.* 4:18. doi: 10.3389/fspas.2017.00018

Ilić, D., Shapovalova, A. I., Popovic, L. C., Chavushyan, V., Burenkov, A. N., Kollatschny, W., et al. (2017). Long-term monitoring of the broad-line region properties in a selected sample of AGN. *Front. Astron. Space Sci.* 4:12. doi: 10.3389/fspas.2017.00012

Ichikawa, K., Ricci, C., Ueda, Y., Matsuoka, K., Toba, Y., Kawamuro, T., et al. (2017). The complete infrared view of active galactic nuclei from the 70 month Swift/BAT catalog. *Astrophys. J.* 835:74. doi: 10.3847/1538-4357/835/1/74

Kaspi, S., Brandt, W. N., Maoz, D., Netzer, H., Schneider, D. P., and Shemmer, O. (2017). Reverberation mapping of high-luminosity quasars. *Front. Astron. Space Sci.* 4:31. doi: 10.3389/fspas.2017.00031

Kimball, A. E., Lacy, M., Lonsdale, C. J., and Macquart, J.-P. (2015). ALMA detection of a disc-dominated [C II] emission line at $z = 4.6$ in the luminous QSO J1554+1937. *MNRAS* 452, 88–98. doi: 10.1093/mnras/stv1160

Lira, P., Botti, I., Kaspi, S., and Netzer, H. (2018). Reverberation mapping of high-z, high-luminosity quasars. *Front Astron Space Sci.* 4:71. doi: 10.3389/fspas.2017.00071

Lusso, E., and Risaliti, G. (2018). The physical relation between disc and coronal emission in quasars. *Front. Astron. Space Sci.* 4:66. doi: 10.3389/fspas.2017.00066

Márquez, I., Masegosa, J., González-Martin, O., Hernández-Garcia, L., Povic, M., Netzer, H., et al. (2017). The AGN nature of LINER nuclear sources. *Front. Astron. Space Sci.* 4:34. doi: 10.3389/fspas.2017.00034

Marziani, P., Dultzin, D., Sulentic, J. W., Del Olmo, A., Negrete, C. A., Martinez-Aldama, M. L., et al. (2018). A main sequence for quasars. *Front. Astron. Space Sci.* 5:6. doi: 10.3389/fspas.2018.00006

Mejía-Restrepo, J. E., Lira, P., Netzer, H., Trakhtenbrot, B., and Capellupo, D. (2018). The virial factor and biases in single epoch black hole mass determinations. *Front. Astron. Space Sci.* 4:70. doi: 10.3389/fspas.2017.00070

Morganti, R. (2017). The many routes to AGN feedback. *Front. Astron. Space Sci.* 4:42. doi: 10.3389/fspas.2017.00042

Negrete, C. A., Dultzin, D., Marziani, P., Sulentic, J. W., Esparza-Arredondo, D., and Martĩnez-Aldama, M. L. (2017). Quasars as cosmological standard candles. *Front. Astron. Space Sci.* 4:59. doi: 10.3389/fspas.2017.00059

Padovani, P. (2017). Active galactic nuclei at all wavelengths and from all angles. *Front. Astron. Space Sci.* 4:35. doi: 10.3389/fspas.2017.00035

Pancoast, A., Brewer, B. J., Treu, T., Park, D., Barth, A. J., Bentz, M. C., et al. (2014). Modelling reverberation mapping data II. Dynamical modelling of the Lick AGN Monitoring Project 2008 data set. *Month. Notices R. Astron. Soc.* 445, 3073–3091. doi: 10.1093/mnras/stu1419

Richards, G. (2017). *Application of Independent Component Analysis to Legacy UV Quasar Spectra*. Available online at: http://adsabs.harvard.edu/abs/2017hst..prop15048R

Stanley, F., Harrison, C. M., Alexander, D. M., Swinbank, A. M., Aird, J. A., Del Moro, A., et al., (2015). A remarkably flat relationship between the average star formation rate and AGN luminosity for distant X-ray AGN. *MNRAS* 453, 591–604. doi: 10.1093/mnras/stv1678

Storchi-Bergmann, T., Schimoia, J. S., Peterson, B. M., Elvis, M., Denney, K. D., Eracleous, M., et al. (2017). Double-peaked profiles: ubiquitous signatures of disks in the broad emission lines of active galactic nuclei. 835:236. doi: 10.3847/1538-4357/835/2/236

Trakhtenbrot, B., Lira, P., Netzer, H., Cicone, C., Maiolino, R., and Shemmer, O. (2018). Fast-growing SMBHs in fast-growing galaxies, at high redshifts: the role of major mergers as revealed by ALMA. *arXiv e-print* arXiv:1801.01508.

Conflict of Interest Statement: The author declares that the research was conducted in the absence of any commercial or financial relationships that could be construed as a potential conflict of interest.

Copyright © 2018 Netzer. This is an open-access article distributed under the terms of the Creative Commons Attribution License (CC BY). The use, distribution or reproduction in other forums is permitted, provided the original author(s) and the copyright owner are credited and that the original publication in this journal is cited, in accordance with accepted academic practice. No use, distribution or reproduction is permitted which does not comply with these terms.

Advantages of publishing in Frontiers

OPEN ACCESS
Articles are free to read for greatest visibility and readership

FAST PUBLICATION
Around 90 days from submission to decision

HIGH QUALITY PEER-REVIEW
Rigorous, collaborative, and constructive peer-review

TRANSPARENT PEER-REVIEW
Editors and reviewers acknowledged by name on published articles

Frontiers
Avenue du Tribunal-Fédéral 34
1005 Lausanne | Switzerland

Visit us: www.frontiersin.org
Contact us: info@frontiersin.org | +41 21 510 17 00

REPRODUCIBILITY OF RESEARCH
Support open data and methods to enhance research reproducibility

DIGITAL PUBLISHING
Articles designed for optimal readership across devices

FOLLOW US
@frontiersin

IMPACT METRICS
Advanced article metrics track visibility across digital media

EXTENSIVE PROMOTION
Marketing and promotion of impactful research

LOOP RESEARCH NETWORK
Our network increases your article's readership